Thermodynamische Einschätzung der chemischen und elektrochemischen Stabilität von Siliziden der Übergangsmetalle der vierten Periode

Inauguraldissertation

zur

Erlangung des akademischen Grades eines

Doktors der Naturwissenschaften
(Dr. rer. nat.)

der

Mathematisch-Naturwissenschaftlichen Fakultät

der

Ernst-Moritz-Arndt-Universität Greifswald

vorgelegt von
Pawel Anatoljewitsch Nikolajtschuk
geboren am 17. Oktober 1985
in Kurgan, Union der Sozialistischen Sowjetrepubliken

Greifswald, 14. 06. 2018

Dekan: Prof. Dr. Werner Weitschies

1. Gutachter : Prof. Dr. Fritz Scholz

2. Gutachter: Prof. Dr. Su-Il Pyun

Tag der Promotion: 21. 01. 2019

Abstract:

The present work is a cumulative dissertation that covers the research work of the author at the Department of Analytical and Physical Chemistry of Chelyabinsk State University. It contains a short description of the study and a set of attached publications in peer-reviewed journals and conference proceedings.

The phase and chemical equilibria in binary systems Me – Si (where Me is the 4th-period transition metal) as well as Mo – Si, Mn – Ge and Fe – Ge at low temperatures were considered. The solid solubility of silicon in vanadium, chromium, manganese, iron, nickel, cobalt and copper and that of germanium in manganese and iron was estimated.

The phase equilibria in Me – Si – O, Mo – Si – O, Mn – Ge – O and Fe – Ge – O ternary systems at standard conditions were considered from a thermodynamic viewpoint. The atmospheric corrosion of transition metals silicides and manganese and iron germanides was discussed.

The chemical and electrochemical equilibria in Me – Si – H_2O, Mo – Si – H_2O, Mn – Ge – H_2O and Fe – Ge – H_2O systems were considered from a thermodynamic viewpoint. Pourbaix diagrams for some 4th-period transition metals and molybdenum, as well as for silicon, were revised. The potential – pH diagrams for Me – Si – H_2O, Mo – Si – H_2O, Mn – Ge – H_2O and Fe – Ge – H_2O systems were plotted in the first time. The corrosion-electrochemical behaviour of transition metals silicides and manganese and iron germanides in aqueous media was discussed.

The potential – pH diagrams for some siliceous brasses and bronzes (which are multicomponent alloys containing both transition metals and silicon) were plotted, and the corrosion of these alloys in aqueous media was discussed.

Method of estimation of corrosion-electrochemical behaviour of multicomponent alloys, which takes into account both thermodynamic and kinetic data and is based on mutual construction of equilibrium and polarisation potential – pH diagrams, was described. Its usage was illustrated in the example of the structural steel 20KT.

Kurzfassung:

Die vorliegende Schrift ist eine kumulative Dissertation, die die Forschungsarbeit des Autors am Lehrstuhl für Analytische und Physikalische Chemie der Staatuniversität Tscheljabinsk zusammenfast. Es enthält eine

kurze Beschreibung der Untersuchung und eine Reihe von beigefügten Veröffentlichungen in Peer-Review-Zeitschriften und Tagungsbänden.

Die Phasen- und chemischen Gleichgewichte in binären Systemen Me – Si (wobei Me das Übergangsmetall der 4. Periode ist) sowie Mo – Si, Mn – Ge und Fe – Ge bei niedrigen Temperaturen wurden berücksichtigt. Die Feststofflöslichkeit von Silizium in Vanadin, Chrom, Mangan, Eisen, Nickel, Kobalt und Kupfer und von Germanium in Mangan und Eisen wurde geschätzt.

Die Phasengleichgewichte in Dreistoffsystemen Me – Si – O, Mo – Si – O, Mn – Ge – O und Fe – Ge – O unter Standardbedingungen wurden unter thermodynamischen Standpunkt berücksichtigt. Die atmosphärische Korrosion von Übergangsmetallensiliziden und Mangan- und Eisengermaniden wurde diskutiert.

Die chemische und elektrochemische Gleichgewichte in Systemen Me – Si – H_2O, Mo – Si – H_2O, Mn – Ge – H_2O und Fe – Ge – H_2O wurden unter thermodynamischen Standpunkt berücksichtigt. Pourbaix-Diagramme für einige Übergangsmetalle der 4. Periode und Molybdän sowie für Silizium wurden revidiert. Die Potenzial – pH-Diagramme für die Systeme Me – Si – H_2O, Mo – Si – H_2O, Mn – Ge – H_2O und Fe – Ge – H_2O wurden zum ersten Mal geplottet. Das korrosionselektrochemische Verhalten von Übergangsmetallensiliziden und Mangan- und Eisengermaniden in wässrigen Medien wurde diskutiert.

Die Potenzial – pH-Diagramme für einige Siliziummessinge und -Bronzen (die Mehrkomponentenlegierungen enthält sowohl Übergangsmetalle als auch Silizium sind) wurde geplottet, und die Korrosion dieser Legierungen in wässrigen Medien wurde diskutiert.

Das Verfahren zur Abschätzung des korrosionselektrochemischen Verhaltens von Mehrkomponentenlegierungen, das sowohl thermodynamische als auch kinetische Daten berücksichtigt und auf der gegenseitigen Konstruktion von Gleichgewichts- und Polarisationspotential-pH-Diagrammen beruht, wurde beschrieben. Seine Verwendung wurde am Beispiel des Baustahls 20KT veranschaulicht.

Аннотация:

Настоящая работа представляет собой написанную по совокупности публикаций диссертацию, охватывающую исследовательскую работу автора на кафедре аналитической и физической химии Челябинского государственного университета. Она

содержит краткое описание исследования и набор прикреплённых публикаций в рецензируемых научных журналах и сборниках докладов конференций.

Рассмотрены фазовые и химические равновесия в двойных системах Me – Si (где Me – переходный металл четвёртого периода) а также Mo – Si, Mn – Ge и Fe – Ge при низких температурах. Оценена твердофазная растворимость кремния в ванадии, хроме, марганце, железе, никеле, кобальте и меди, а также германия в марганце и железе.

С термодинамической точки зрения рассмотрены фазовые равновесия в тройных системах Me – Si – O, Mo – Si – O, Mn – Ge – O и Fe – Ge – O при стандартных условиях. Обсуждена атмосферная коррозия силицидов переходных металлов и германидов марганца и железа.

С термодинамической точки зрения рассмотрены химические и электрохимические равновесия в системах Me – Si – H_2O, Mo – Si – H_2O, Mn – Ge – H_2O и Fe – Ge – H_2O. Уточнены диаграммы Пурбе для ряда переходных металлов 4 периода и молибдена, а также для кремния. Впервые построены диаграммы потенциал – pH для систем Me – Si – H_2O, Mo – Si – H_2O, Mn – Ge – H_2O и Fe – Ge – H_2O. Обсуждено коррозионно-электрохимическое поведение силицидов переходных металлов и германидов марганца и железа в водных средах.

Построены диаграммы потенциал – pH для некоторых кремнистых латуней и бронз (являющихся многокомпонентными сплавами, содержащими как переходные металлы, так и кремний) и обсуждена их коррозия в водных средах.

Описан метод оценки коррозионно-электрохимического поведения многокомпонентных сплавов, принимающий во внимание как термодинамические, так и кинетические данные, и основанный на одновременном построении равновесных и поляризационных диаграмм потенциал – pH. Его использование показано на примере конструкционной стали 20КТ.

Content

Foreword

The work is dedicated to one of the leading Russian scientists in the field of corrosion science and my supervisor, Aleksandr Georgievich Tyurin (in Russian: Александр Георгиевич Тюрин), who suddenly and unexpectedly passed away in 2015. The scientific biography of Prof. Dr. A. G. Tyurin and the overwiev of his publications was published in paper [Nikolaychuk, 2017]. The preprint of this paper is reproduced here with the permission from *Springer*. The Russian translation of this paper was published in [Николайчук, Бирюков, Працкова, 2016].

Aleksandr Georgievich Tyurin (1953 – 2015) and his Research in Corrosion Science

Pavel Anatolyevich Nikolaychuk

Čelâbinskij gosudarstvennyj universitet, Brat'ev Kaširinyh Street, 129, Chelyabinsk, 454001, Russian Federation
E-mail: npa@csu.ru

Abstract: This paper is a tribute to one of the leading Russian scientists in the field of corrosion science and my supervisor, Aleksandr Georgievich Tyurin, who suddenly and unexpectedly passed away in 2015. A short biographical note is given together with an outline of his contributions to corrosion and electrochemical science.

Keywords: Biography, chemical thermodynamics, metallurgy, deoxidisation of steels, corrosion science, potential–pH diagrams

Aleksandr Georgievich Tyurin[1] (see Figure 1) was born 7 May 1953 in Satka – a small town in the Chelyabinsk region of the Ural district of the Soviet Union. In 1970 he entered the Metallurgical faculty of Chelyabinsk Polytechnical Institute[2,3] (which is now South Ural State National Research University[4]). In 1975 he graduated from the institute with honours as an "Metallurgical engineer" with the specialisation "Physical and chemical research of the metallurgical processes". His name, along with names of the other graduates, who obtained the red diplomas[5], is still engraved on the Honourary Board in the entrance hall of the university main building.

From 1976 till 1978 he was employed as full-time postgraduate student in aspirantura[6] at Chelyabinsk Polytechnical Institute, where he studied under the supervision of doktor tehničeskih nauk[6] [Doctor of Technical Sciences][7] and Professor Gennadiy Georgievich Mikhaylov. The field of his research interest was a thermodynamic analysis of the deoxydisation processes of iron and steels – both by simple compouds [1–3] and by alloys based on calcium [4], barium [5–7] and aluminum [6, 7]. In 1979 he defended his Dissertation entitled "Termodinamika processov kompleksnogo raskisleniâ stali splavami, soderžaŝimi kal'cij i barij" ["Thermodynamics of the processes of complex deoxydisation of steels by the alloys containing calcium and barium"] [8] and obtained the degree of kandidat tehničeskih nauk[6] [Candidate of Technical Science]. After the defence, Tyurin continued his research at the Department of Physical Chemistry of the Metallurgical faculty of Chelyabinsk Polytechnical Institute in the chosen field.

Fig. 1. Aleksandr Georgievich Tyurin (1953 – 2015). The photo was made in 2013.

Later on his field of interest included not only the processes of deoxydisation, but also of desulphurisation of iron-based liquid melts using magnesium [9], manganese [10], and rare-earth metals [11, 12], as well as the processes of formation of non-metallic inclusions in steels [13, 14]. In 1982 he obtained his first academic rank "assistent"[6] [Assistant].

In 1984 Tyurin left Chelyabinsk Polytechnical Institute (although his collaboration with Prof. G. G. Mikhaylov continued till 1991 [15, 16]) and entered Ural (now – Russian) Scientific-Research Institute of Pipe Industry[8], where he was employed as seniour researcher in the Laboratory of Pipe Corrosion Testing until 1988. There he studied the corrosion resistance of steels used for pipe construction, and the structure of the oxide layers formed on these steels [17, 18]. The work in this field shifted his research interests from high-temperature metallic and oxide melts to low-temperature aqueous solutions. This was the time when he started to use and love the Pourbaix diagrams [19–21], which are one of the most concise ways of visualisation chemical and electrochemical equilibria in aqueous environments [22].

In 1987 he obtained the academic rank of "staršij naučnyj sotrudnik"[6] [Seniour Researcher], and in 1989 he travelled to Moscow to work in his doktorantura[6] at the Central Scientific-Research Institure of the Ferrous Metallurgy named after Ivan Pavlovich Bardin[9]. Tyurin's scientific advisor during his work on the dissertation of doktor nauk[6] was Prof. Boris Mikhaylovich Mogutnov, at that time, one of the leading specialists on thermodynamics of iron alloys in USSR [23]. However, the collapse of the Soviet Union and the subsequent economic crisis in the Russian Federation, which led to a serious reduction of the funding of research institutes, did not allow him to finish his dissertation studies. In 1991 Tyurin was forced to leave the doktorantura and returned to Chelyabinsk. Right at that time a Chemical faculty was founded at Chelyabinsk State University[10], and he was invited to the newly founded Department of Analytical and Physical Chemistry, where he worked right till his passing away.

After losing the possibility to conduct experimental work, he focused his attention on thermodynamic modelling of the electrochemical processes in aqueous environments. He used the Pourbaix diagrams for the description of not only the corrosion-electrochemical behaviour of metals and alloys [24], but also the processes of electrolytic deposition of titanium [25], gold and heavy metals [26] from a solution. The ninetieth years of the twentieth century were the period of active invasion of personal computers into the scientific life of academia. While even a few years before the Pourbaix diagrams were being plotted primarily for pure metals and very simple alloys only, the dissemination of personal computers and scientific graphing software allowed the scholars to perform more comprehensive calculations and to construct the diagrams for multicomponent systems. Tyurin was one of the first scholars in the world, who constructed Pourbaix diagrams for complex alloys; he developed an algorithm for this procedure [27]. Moreover, he proposed a new kind of expression for the excess Gibbs free energy of multicomponent solution [28], which (in his humble opinion) was more convenient than the analogous expressions proposed by Margules [29]

and Redlich and Kister [30], and can be employed together with both Hildebrand's theory of regular solutions [31] and Kozheurov's theory of ionic solutions [32]. Tyurin also made an attempt to substantiate the physical meaning of the parameters in his expression. He called his development „a generalised theory of «regular»[11] solutions" [33], and henceforth used it actively for the thermodynamic modelling of both molecular and ionic solutions.

Fig. 2. Aleksandr Georgievich Tyurin presents a report at the fifth session of the All-Russian conference «Современные проблемы коррозионно-электрохимической науки» ["The contemporary problems of a corrosion – electrochemical science"], dedicated to the 100th anniversary of academician Ya. M. Kolotyrkin, and describes the corrosion properties of the stainless steel 08Х15Н5Д2Т from the thermodynamic viewpoint (see Ref. [51]).

In 1994 Tyurin obtained the academic rank of "docent po kafedre"[6] [Associate Professor at the Department] and recommenced his work on the dissertation of doktor nauk, focusing the attention on the modelling of electrochemical behaviour of multicomponent systems. He plotted the Pourbaix diagrams and estimated the corrosion properties of the systems Fe – Sn [24], Fe – Cr [34], Fe – Ti [35], Fe – Ni [36], Fe – Mo [37], Fe – Cr – Si [38], Fe – Cu [39], Fe – Mn [40], Fe – C [41], Ni – Cr, Ni – Mo and Ni – Cr – Mo [42, 43], Ni – Ti [44], as well as iron, chromium, manganese and molybdenum carbides of the type $Me_{23}C_6$ [45, 46], non-metallic inclusions [47], hot and thermodiffusion zinc

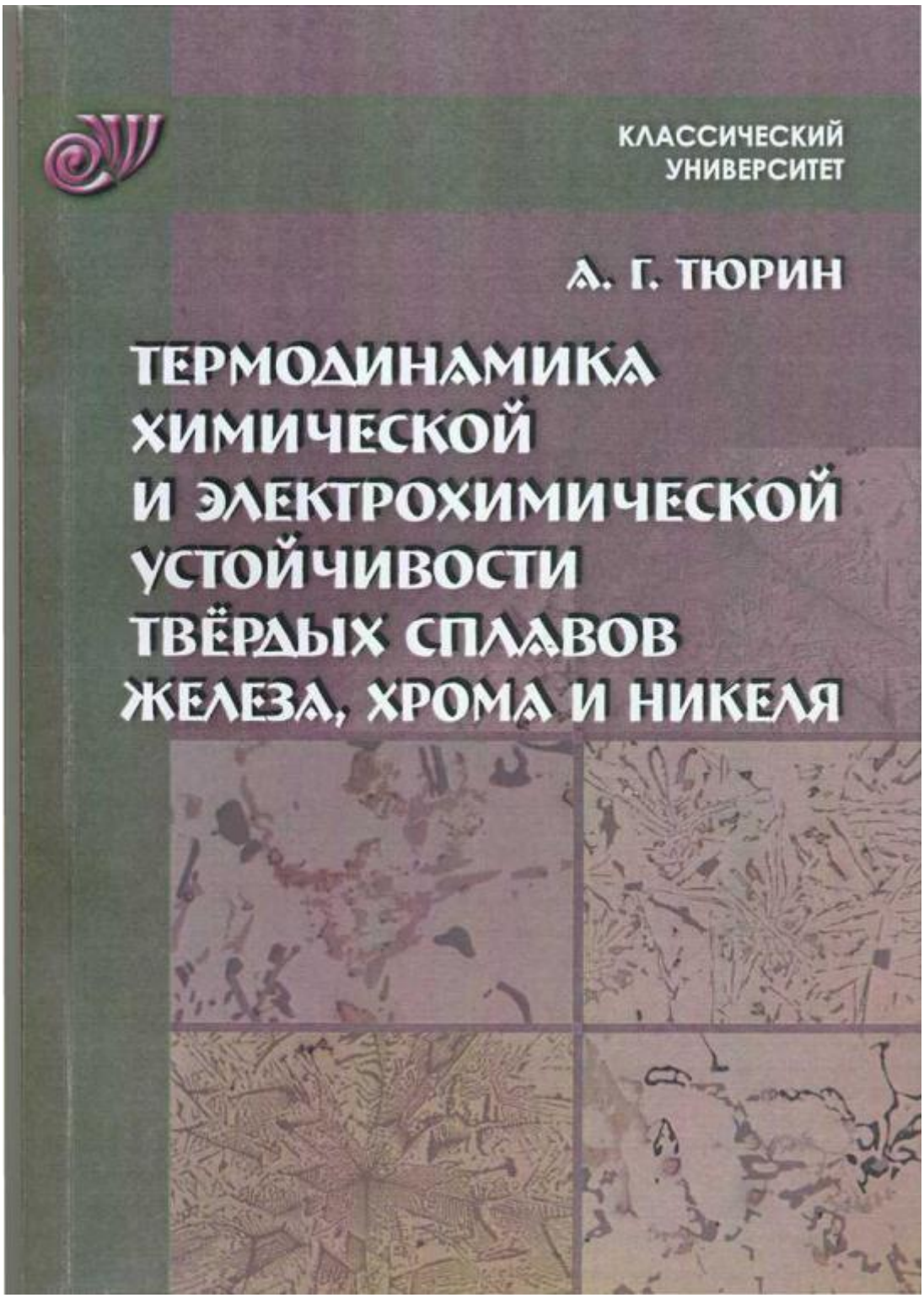

Fig. 3. Cover page of the monograph “Термодинамика химической и электрохимической устойчивости твёрдых сплавов железа, хрома и никеля” [“Thermodynamics of chemical and electrochemical stability of the solid alloys of iron, chromium and nickel”] written by A. G. Tyurin (see Ref. [56]).

coatings [48, 49], steels 08Х15Н5Д2Т[12] [50, 51] (see Figure 2) and 12Х18Н10Т[12]common and special brasses [53] and aluminium, siliceous and tin bronzes [54]. These studies became part of his dissertation entitled “Termodinamika himičeskoj i èlektrohimičeskoj ustojčivosti splavov”

["Thermodynamics of chemical and electrochemical stability of alloys"] [55] that was defended in 2008 and henceforth partially published in form of a monograph [56] (see Figure 3).

After the successful defence, Tyurin started to pay more attention to the work with students, and supervised his first aspirants. He had no own research group and no uniform research direction; instead of this he worked with each of his aspirants individually, and each of them set and solved his or her own research goals.

Svetlana Evgenyevna Pratskova was Tyurin's first aspirant. Together with her, he once again returned to the problem of thermodynamic modelling of high-temperature oxide melts. They performed a thermodynamic description of melts in the system Na^+, Ca^{2+}, Al^{3+} || O^{2-}, F^-, constructed the phase diagrams, estimated the thermodynamic functions of mixing and the excess thermodynamic functions of binary and ternary subsystems in this system [57–62], and provided a thermodynamic estimation of the sulphur-consuming ability of the slags in the system $CaO – CaF_2$ [63].

Aleksandr Igorevich Biryukov was the next aspirant of Tyurin. His work was devoted to the study of peculiarities of the corrosion-electrochemical behaviour of pure copper and steel Ст.3[13] in highly acidic sulphate environments. For the first time in his scientific work, Tyurin refrained from constructing potential–pH diagrams for pure aqueous environments, and from thermodynamic viewpoint, he took into account the fact that the composition of the corrosive media, in which the products are exploited, also affects the corrosion properties of materials. They plotted the Pourbaix diagrams for the systems "Cu – H_2SO_4 – H_2O" [64, 65] and "Steel Ст.3 – H_2SO_4 – H_2O" [66 – 68], and also performed experimental investigation of the corrosion properties of these materials in sulphuric media [65, 69].

The collaboration of Tyurin with Russian Scientific-Research Institute of Pipe Industry was also recommenced. Under his supervision at the base of the Laboratory of the corrosion testing the aspirants Irina Valeryevna Kostitsyna, Vladimir Pavlovich Parshukov, Dmitriy Andreevich Manannikov and Mariya Yuryevna Skryl'nik engaged in the thermodynamic modelling and the experimental investigation of the corrosion resistance of low-carbon pipe steels under the conditions of the elevated content of carbon dioxide [70, 71] and hydrogen sulphide [72, 73], under conditions of oil fields [74, 75], under conditions of microbial corrosion [76], and also under the influence of corrosion-active non-metallic inclusions in the materials [47, 77 – 79].

I was Tyurin's last aspirant, and my scientific interests were of purely theoretical nature. We collected reliable thermodynamic information on various aqueous species and revised the Pourbaix diagrams for cobalt [80], copper [81], zinc [82], molybdenum [83], silicon [84], iron [85], sulphur [86], titanium and nickel [87], mercury [88]. We estimated the corrosion properties of binary systems "metal – silicon" for a series of fourth period transition metals [80, 88 – 96], as well as of the siliceous brass ЛК80-3[14] [95] and the copper-nickel alloys МН19[15] and МНЖМц30-1-1[15] [97].

A. I. Biryukov, I. V. Kostitsina and S. E. Pratskova already defended their dissertations of kandidat nauk [98 – 100], whereas my dissertation and that by D. A. Manannikov are at the final stage of preparation.

Since 2010 Prof. Tyurin was a member of the Editorial Board of the journal "Butlerovskie soobŝeniâ" ["Butlerov Communications"].

In 2013 at the conference "X Meždunarodnoe Kurnakovskoe Soveŝanie po fiziko-himičeskomu analizu" ["X International Kurnakov Meeting on Physical and Chemical Analysis"], that was held in Samara State Technical University[16], Tyurin met Mikhail Viktorovich Vasekha, a docent from Murmansk State Technical University[17], and this acquaintanceship was the beginning of their further partnership. The field of research interests of Vasekha concerns the study of ferrous cake (a waste from copper-nickel production) and its peptisation, the development of sulphate method of its processing, as well as the study of the physical and chemical peculiarities of the processes in the sulphite solutions. Meeting with Tyurin allowed him to open for himself the thermodynamic analysis and the predictions based on potential–pH diagrams and to use it in his further studies. Tyurin acted as the official opponent at the defence of Vasekha's dissertation of doktor nauk entitled "Fiziko-himičeskie osnovy sul'fitnoj tehnologii železogidratnyh soedinenij" ["Physical and chemical fundamentals of the sulphite technology of the hydrate compounds of iron"] [101]. Their collaboration resulted in a few joint publications [102, 103].

The plans of the further research direction of Tyurin and his followers included expanding the range of the studied systems (particularly, to germanates of the fourth period transition metals [104 – 106]), the study of corrosion properties of the various alloys and metallic coatings, and, together with Vasekha, the application of thermodynamic analysis to various chemical technology processes. Tyurin also tried to develop a method of experimental confirmation of Pourbaix diagrams for multicomponent alloys [107 – 109]. Unfortunately, all these plans were not destined to materialise. In June 2015 Aleksandr Georgievich Tyurin suddenly and unexpectedly passed away due to cancer. His decease was a shocking hit for the scientific community of the South Ural. During his life he made a major contribution to the metallurgical and corrosion sciences, and the research direction, founded by him, will undoubtedly be developed even further in the works of his followers; many of his papers will be or are already published posthumously [102, 103, 105 – 111].

Acknowledgement

I am very grateful to Prof. Fritz Scholz from University of Greifswald[18], the Editor-in-Chief of *Journal of Solid State Electrochemistry* for his invitation to submit this article to this journal and for valuable discussion concerning the quality of this manuscript.

References[1]

1. Mikhaylov GG, Tyurin AG, Vilgel'm EM (1977). Termodinamičeskij analiz reakcij raskisleniâ železa alûminiem, margancem i uglerodom. In: Fiziko-himičeskie issledovaniâ metallurgičeskih processov: Mežvuzovskij sbornik. Sverdlovsk, Ural Polytechnical Institute named after S. M. Kirov[19] 5: 70 – 76.
2. Mikhaylov GG, Tyuria AG (1978). Termodinamičeskij analiz reakcij raskisleniâ železa bariem, kremniem i uglerodom. In: Voprosy proizvodstva i obrabotki stali: tematičeskij sbornik naučnyh trudov. Chelyabinsk, Chelyabinsk Polytechnical Institute 202: 7 – 12.
3. Mikhaylov GG, Tyurin AG (1978). Deoxidizing power of calcium and aluminum in liquid steel. Russian Metallurgy (Metally) 5: 13 – 16.
4. Mikhaylov GG, Tyurin AG (1979). Thermodynamics of steel deoxidation with calcium silicide. Russian Metallurgy (Metally) 2: 24 – 27.
5. Mikhaylov GG, Tyurin AG (1978). Termodinamika raskisleniâ stali silikobariem. Izvestiâ vysših učebnyh zavedenij. Čërnaâ metallurgiâ 12: 18 – 21.
6. Mikhaylov GG, Tyurin AG, Mizin VG, Dubrovin AS (1978). K voprosu raskisleniâ stali alûmobariem. Izvestiâ vysših učebnyh zavedenij. Čërnaâ metallurgiâ 5: 25 – 28.
7. Mikhaylov GG, Tyurin AG, Baybulenko EP (1980). Analysis of phase-equilibria in iron deoxidation by alumino-silicobarium. Russian Metallurgy (Metally) 5: 17 – 20.
8. Tyurin AG (1979). Termodinamika processov kompleksnogo raskisleniâ stali splavami, soderžaŝimi kal'cij i barij. Dissertation of kandidat tehničeskih nauk. Chelyabinsk, Chelyabinsk Polytichnical Institute.
9. Tyurin AG (1987). Deoxidation and desulfurization of cast-iron with magnesium. Russian Metallurgy (Metally) 4: 9 – 12.
10. Mikhaylov GG, Tyurin AG (1984). Deoxidation and desulfurization of steel with calcium, manganese and aluminum. Russian Metallurgy (Metally) 4: 7 – 12.
11. Tyurin AG, Mikhaylov GG (1983). Phase-equilibria during the interaction of cerium and aluminum with oxygen and sulfur in liquid-iron. Russian Metallurgy (Metally) 2: 22 – 25.
12. Tyurin AG, Mikhailov GG, Topchiy GI (1987). Refining ability of aluminum and rare earths in the iron-carbon melt. Soviet Materials Science Reviews 1(2): 145 – 152.
13. Tyurin AG, Mikhaylov GG, Shishkov VI (1982). Thermodynamic conditions for the formation of inclusions in Fe-Ce-Al-O metallic melts. Russian Metallurgy (Metally) 6: 31 – 34.
14. Tyurin AG, Mikhaylov GG (1986). Thermodynamic conditions for the modification of nonmetallic inclusions in steel by calcium and cerium. Russian Metallurgy (Metally) 1: 11 – 14.
15. Tyurin AG, Mikhaylov GG (1991). Thermodynamic features of the refining of steel on injection with silicocalcium powders. Russian Metallurgy (Metally) 1: 16 – 20.

16. Tyurin AG, Mikhaylov GG (1991). Thermodynamic analysis of the deoxidation of steel during blowing with barium compounds. Russian Metallurgy (Metally) 2: 12 – 15.
17. Tyurin AG, Berg BN, Zhivotovskii EA, Povolotskii VD (1985). Study of the oxidized layer on tubes of steel 08KH15N5D2T. Russian Metallurgy (Metally) 2: 163 – 167.
18. Tyurin AG, Povolotskii VD, Zhivotovskii EA, Berg BN (1985). A study of the surface-layer of the 08KH15N5D2T steel. Protection of Metals 22(4): 452 – 454.
19. Aleksandrov VN, Tyurin AG (1987). Effect of the structure of aqueous acid-solutions on the corrosive-electrochemical behavior of metals. Protection of Metals 23(6): 727 – 729.
20. Tyurin AG (1988). Chemical and electrochemical stability diagrams for aluminum coatings on iron. Protection of Metals 24(4): 547 – 549.
21. Tyurin AG, Yaseneva OYu, Aleksandrov VN, Samoylov VV (1988). O korozionno-èlektrohimičeskom povedenii alûmo-cinkovyh pokrytij v usloviâh holodnogo i gorâčego vodosnabženiâ. In: Diffuzionnoe nasyŝenie i pokrytie na metallah. Kiev, Naukova dumka 11 – 26.
22. Pourbaix MJN (1945). Thermodynamique des solutions aqueuses diluées: représentation graphique du rôle du pH et du potentiel. Dissertation. Meinema, Technical College of Delft[20].
23. Mogutnov BM, Tomilin IA, Shvartsman LA (1984). Termodinamika splavov železa. Moscow, Metallurgiâ.
24. Tyurin AG (1991). Equilibrium potential-pH diagram for the Fe-Sn-H_2O system. Soviet Electrochemistry 27(9): 1053 – 1055.
25. Tyurin AG (1990). Thermodynamic analysis of phase formation in electrolytic titanium deposition from aqueous-solutions. Soviet Electrochemistry 26(12): 1424 – 1430.
26. Myagkaya RV, Balykin VP, Tyurin AG, Finadeev SP (2001). Issledovanie termodinamičeskih uslovij i skorosti processa osaždeniâ iz rastvorov ionov tâželyh metallov i zolota gal'vanokoagulâcionnym metodom. Vestnik Čelâbinskogo gosudarstvennogo universiteta. Seriâ 4: Himiâ 1(2): 142 – 154.
27. Tyurin AG (2002). Modelirovanie diagramm pH-potencial mnogokomponentnyh smešannyh system. Himičeskij žurnal ural'skih universitetov 3: 148 – 161.
28. Tyurin, AG (1993). Thermodynamics of molecular and ionic-solutions. Russian Metallurgy (Metally) 2: 39 – 47.
29. Margules M (1895). Über die Zusammensetzung der gesättigten Dämpfe von Mischungen. Sitzungsberichte der Kaiserlichen Akademie der Wissenschaften. Mathematisch-Naturwissenschaftliche Classe. Abtheilung 2. Mathematik, Physik, Chemie, Physiologie, Meteorologie, physische Geographie und Astronomie 104: 1243 – 1278.
30. Redlich O, Kister AT (1948). Algebraic representation of thermodynamic properties and the classification of solutions. Industrial and Engineering Chemistry 40(2): 345 – 348.

31. Hildebrand JH (1927). A Quantitative Treatment of Deviations from Raoult's Law. Proceedings of the National Academy of Sciences of the United States of America 13(5): 267 – 272.
32. Kozheurov VA (1955). Termodinamika metallurgičeskih šlakov. Sverdlovsk, Metallurgizdat.
33. Tyurin AG (2004). Obobŝënnaâ teoriâ «regulârnyh» rastvorov In: Trudy XI Rossijskoj konferencii «Stroenie i svojstva metalličeskih i šlakovyh rasplavov». Tom 1. Fiziko-himičeskie modeli stroeniâ i metody modelirovaniâ svojstv rasplavov. Chelyabinsk, Izdatel'stvo Ûžno-Ural'skogo gosudarstvennogo universiteta 96 – 99.
34. Tyurin AG (1999). Thermodynamics of the chemical and electrochemical resistance of iron-chromium alloys. Protection of Metals 35(3): 215 – 220.
35. Tyurin AG (1999). Thermodynamic evaluation of the effect of titanium on the chemical and electrochemical resistance of alloys. Protection of Metals 35(4): 385 – 389.
36. Tyurin AG (2000). On the effect of nickel on the corrosion-electrochemical behavior of iron-nickel alloys. Protection of Metals 36(1): 61 – 68.
37. Tyurin AG (2003). Estimation of the effect of molybdenum on chemical and electrochemical stability of iron-based alloys. Protection of Metals 39(4): 367 – 373.
38. Tyurin AG (2004). Thermodynamic analysis of the silicon effect on chemical and electrochemical stability of iron-chromium alloys. Protection of Metals 40(1): 14 – 22.
39. Tyurin AG (2004). On the nature of the effect of copper on the corrosion resistance of iron. Protection of Metals 40(3): 232 – 239.
40. Tyurin AG (2005). A role of manganese in the corrosion and electrochemical behavior of stainless steels. Protection of Metals 41(1): 68 – 75.
41. Tyurin AG, Orda VV (2002). Termodinamičeskaâ ocenka vliâniâ ugleroda na himičeskuû i èlektrohimičeskuû ustojčivost' železouglerodistyh splavov. Himičeskij žurnal ural'skih universitetov 3: 162 – 166.
42. Tyurin AG (2003). Thermodynamic assessment of the effect of chromium and molybdenum on the passivability of nickel-base alloys. Protection of Metals 39(6): 568 – 574.
43. Tyurin AG, Markina NV (2009). Diagrams of chemical and electrochemical equilibriums of nickel-molybdenum and nickel-chromium-molybdenum alloys. Protection of Metals and Physical Chemistry of Surfaces 45(3): 361 – 368.
44. Tyurin AG (2004). Termodinamika himičeskoj i èlektrohimičeskoj ustojčivosti nikelida titana. Vestnik Čelâbinskogo gosudarstvennogo universiteta. Seriâ 4: Himiâ 1(3): 65 – 70.
45. Tyurin AG (2003). Diagrams of electrochemical equilibrium of $M_{23}C_6$ type carbides. Protection of Metals 39(5): 435 – 442.
46. Tyurin AG (2004). Diagrams of electrochemical equilibrium of $M_{23}C_6$ type carbides. ChemInform 35(19).

47. Tyurin AG, Pyshmintsev IYu, Kostitsyna IV, Zubkova IV (2007). Thermodynamics of chemical and electrochemical stability of corrosion active nonmetal inclusions. Protection of Metals 43(1): 34 – 44.
48. Tyurin AG (1996). Diagrammy himičeskoj i èlektrohimičeskoj ustojčivosti gorâčih metalličeskih pokrytij na nizkouglerodistoj stali. Vestnik Čelâbinskogo gosudarstvennogo universiteta. Seriâ 4: Himiâ 1(1): 81 – 92.
49. Tyurin AG, Galin RG (2005). Diagrams of chemical and electrochemical stability of thermal-diffusion zinc coatings. Protection of Metals 41(5): 472 – 478.
50. Tyurin AG (2001). Diagramma pH-potencial stali 08KH15N5D2T. Vestnik Čelâbinskogo gosudarstvennogo universiteta. Seriâ 4: Himiâ 1(2): 164 – 178.
51. Tyurin AG (2010). Termodinamika himičeskoj i èlektrohimičeskoj ustojčivosti splavov železa, hroma i nikelâ. In: Sbornik dokladov i tezisov Vserossijskoj konferencii «Sovremennye problemy korrozionno – èlektrohimičeskoj nauki», posvâŝënnoj 100-letiû so dnâ roždeniâ Â. M. Kolotyrkina. Moscow, Scientific-Research Physical and Chemical Institute named after L. Ya. Karpov[21] 1: 258 – 269.
52. Tyurin AG (2004). The diagram of electrochemical equilibrium of 12X18H10T steel. Protection of Metals 40(3): P. 240 – 248.
53. Tyurin AG., Shrainer AA (2007). Thermodynamics of chemical and electrochemical stability of brasses. Protection of Metals 43(3): 291 – 297.
54. Tyurin AG (2008). Thermodynamics of chemical and electrochemical stability of aluminum, silicon, and tin bronzes. Protection of Metals 44(3): 292 – 300.
55. Tyurin AG (2008). Termodinamika himičeskoj i èlektrohimičeskoj ustojčivosti splavov. Dissertation of doktor himičeskih nauk. Chelyabinsk, South Ural State University.
56. Tyurin AG (2012). Termodinamika himičeskoj i èlektrohimičeskoj ustojčivosti tvërdyh splavov železa, hroma i nikelâ. Chelyabinsk, Izdatel'stvo Čelâbinskogo gosudarstvennogo universiteta.
57. Tyurin AG, Annenkova MV, Pratskova SE (2008). Triangulâciâ sistemy NaF – Na_2O – Al_2O_3 – AlF_3 i fazovye ravnovesiâ s učastiem oksidno-ftoridnyh rasplavov. In: Komp'ûternoe modelirovanie fiziko-himičeskih svojstv stëkol i rasplavov: Trudy 9-go Rossijskogo seminara. Kurgan, Izdatel'stvo Kurganskogo gosudarstvennogo universiteta 40 – 42.
58. Pratskova SE, Tyurin AG, Nechaeva ES (2011). Modelirovanie termodinamičeskih svojstv kvazibinarov Na_2O-CaO-Al_2O_3. In: Trudy XIII rossijskoj konferencii «Stroenie i svojstva metalličeskih i šlakovyh rasplavov». Tom 3. Èksperimental'noe izučenie šlakovyh rasplavov, vzaimodejstvie metall-šlak. Yekaterinburg, UrORAN 8 – 11.
59. Tyurin AG, Pratskova SE (2012). Modelirovanie termodinamičeskih svojstv izvestkovo-glinozëmistyh rasplavov. Vestnik Ûžno-Ural'skogo gosudarstvennogo universiteta. Seriâ „Himiâ“ 7, 1(260): 29 – 34.
60. Tyurin AG, Pratskova SE (2013). K termodinamike oksidno-ftoridnyh rasplavov sistemy Ca^{2+}, Al^{3+} // O^{2-}, F^{-}. Vestnik Ûžno-Ural'skogo gosudarstvennogo universiteta. Seriâ „Himiâ“ 5(1): 23 – 27.

61. Pratskova SE, Tyurin AG (2013). Fazovye ravnovesiâ s učastiem oksidno-ftoridnyh rasplavov natriâ i alûminiâ. Butlerovskie soobŝeniâ 36(12): 163 – 167.
62. Tyurin AG, Pratskova SE (2014). Modelirovanie termodinamičeskih svojstv oksidno-ftoridnyh rasplavov sistemy Ca^{2+}, Al^{3+} // O^{2-}, F^{-}. Rasplavy 3: 73 – 84.
63. Pratskova SE, Tyurin AG (2015). Termodinamičeskaâ ocenka seropoglotitel'noj sposobnosti šlakov sistemy CaO – CaF_2. Butlerovskie soobŝeniâ 42(6): 86 – 90.
64. Tyurin AG, Biryukov AI (2013). Diagramma E – pH sistemy Cu – H_2SO_4 – H_2O. In: X Meždunarodnoe Kurnakovskoe soveŝanie po fiziko-himičeskomu analizu: sbornik trudov. Samara: Izdatel'stvo Samarskogo gosudarstvennogo tehničeskogo universiteta 2: 82 – 85.
65. Biryukov AI, Tyurin AG, Tronov AP (2015). Ob osobennostâh passivacii medi v sernokislyh rastvorah. Butlerovskie soobŝeniâ 42(6): 138 – 144.
66. Tyurin AG, Biryukov AI (2012). Diagramma èlektrohimičeskogo ravnovesiâ stali Ст.3 v sil'nokislyh sul'fatnyh rastvorah. Vestnik Kazanskogo tehnologičeskogo universiteta 15(16): 74 – 77.
67. Tyurin AG, Biryukov AI (2012). Diagramma èlektrohimičeskogo ravnovesiâ stali Ст.3 v sil'nokislyh rastvorah. Sviridovskie čteniâ: sbornik statej. Minsk, Izdatel'stvo Belorusskogo gosudarstvennogo universiteta 8: 160 – 167.
68. Tyurin AG, Biryukov AI (2013). Vliânie anionov na korrozionno-èlektrohimičeskoe povedenie stali Ст.3 v sul'fatnyh sredah. Soobŝenie 1. Termodinamika. Vestnik Ûžno-Ural'skogo gosudarstvennogo universiteta. Seriâ „Himiâ“ 5(3): 35 – 44.
69. Tyurin AG, Biryukov AI (2013). Vliânie anionov na korrozionno-èlektrohimičeskoe povedenie stali Ст.3 v sul'fatnyh sredah. Soobŝenie 2. Polârizacionnye izmereniâ. Vestnik Ûžno-Ural'skogo gosudarstvennogo universiteta. Seriâ „Himiâ“ 5(3): 45 – 50.
70. Pyshmitsev IYu, Kostitsyna IV, Biryukov AI, Manannikov DA, Parshukov VP (2011). Issledovanie korrozionnoj stojkosti hromistyh stalej v sredah s povyšennym soderžaniem uglekislogo gaza. Stal' 2: 90 – 92.
71. Kostitsyna IV, Tyurin AG, Parshukov VP, Biryukov AI (2012). Vliânie koncentracii hroma, temperatury i davleniâ CO_2 na korrozionnuû stojkost' nasosno-kompressornyh trub. Vestnik Ûžno-Ural'skogo gosudarstvennogo universiteta. Seriâ „Himiâ“ 8, 13(272): 30 – 37.
72. Tyurin AG, Kostitsyna IV, Manannikov DA, Parshukov VP (2011). Diagrammy himičeskoj i èlektrohimičeskoj ustojčivosti železouglerodistyh splavov v vodnyh sredah, soderžaŝih serovodorod. In: Fundamental'nye i prikladnye problemy nauki: materialy VI Meždunarodnogo simpoziuma. Moscow, RAN 2: 234 – 241.
73. Pyshmintsev IYu, Veselov IN, Kostitsyna IV (2006). O prognozirovanii sroka služby trub v serovodorodsoderžaŝih sredah. Territoriâ Neftegaz 9: 28 – 33.
74. Pyshmintsev IYu, Kostitsyna IV, Manannikov DA, Parshukov VP, Skryl’nik My, Zav’yalov VV (2012). Analiz korrozionnoj stojkosti neftegazoprovodnyh trub po rezul'tatam ispytanij na Samotlorskom mestoroždenii. Neftânoe hozâjstvo 3: 99 – 101.

75. Kostitsyna IV (2011). Issledovanie korrozionnoj stojkosti materialov nasosno-kompressornyh i neftegazoprovodnyh trub na mestorožděniâh OAO «Lukojl». Podbor materialov dlâ primeneniâ v korrozionno-aktivnyh sredah. Inženernaâ praktika 11–12: 18 – 21.
76. Kostitsyna IV, Parshukov VP, Biryukov AI, Tyurin AG (2011). Ocenka stojkosti uglerodistyh i nizkolegirovannyh stalej k bakterial'noj korrozii. Vestnik Ûžno-Ural'skogo gosudarstvennogo universiteta. Seriâ „Himiâ“ 5, 12(229): 54 – 57.
77. Pyshmintsev IYu, Kostitsyna IV, Manannikov DA, Parshukov VP (2010). Rol' nemetalličeskih vklûčenij v razvitii očagov lokal'noj korrozii trub iz uglerodistyh stalej. Problemy čërnoj metallurgii i materialovedeniâ 4: 49 – 53.
78. Pyshmintsev IYu, Kostitsyna IV, Manannikov DA, Parshukov VP (2010). Vliânie nemetalličeskih vklûčenij na stojkost' neftepromyslovyh truboprovodov k lokal'noj korrozii. Čërnaâ metallurgiâ 1(1321): 55 – 61.
79. Pyshmintsev IYu, Bityukov SM, Laev KA, Boryakova AN, Manannikov DA (2010). Issledovanie stalej klassa „superhrom“, prednaznačennyh dlâ izgotovleniâ korrozionnostojkih vysokopročnyh trub neftânogo sortamenta. Čërnaâ metallurgiâ 2(1322): 51 – 56.
80. Tyurin AG, Mosunova TV, Nikolaychuk PA (2010). Termodinamika himičeskoj i èlektrohimičeskoj ustojčivosti silicidov kobal'ta. Vestnik Ûžno-Ural'skogo gosudarstvennogo universiteta. Seriâ „Himiâ“ 3, 11(187): 52 – 60.
81. Nikolaychuk PA, Kanatyeva II, Tyurin AG (2010). Utočnënnaâ diagramma Purbe dlâ medi. In: Sovremennye problemy teoretičeskoj i èksperimental'noj himii: mežvuzovskij sbornik naučnyh trudov VII Vserossijskoj konferencii molodyh učënyh s meždunarodnym učastiem. Saratov: OOO Izdatel'stvo «KUBiK» 287 – 291.
82. Nikolaychuk PA, Tyurin AG (2011). Utočnënnaâ diagramma Purbe dlâ cinka. In: Sovremennye problemy teoretičeskoj i èksperimental'noj himii: mežvuzovskij sbornik naučnyh trudov VIII Vserossijskoj konferencii molodyh učënyh s meždunarodnym učastiem. Saratov: OOO Izdatel'stvo «KUBiK» 227 – 230.
83. Nikolaychuk PA, Tyurin AG (2011). Utočnënnaâ diagramma Purbe dlâ molibdena. Butlerovskie soobŝeniâ 24(2): 101 – 105.
84. Nikolaychuk PA (2014). The revised Pourbaix diagram for silicon. Silicon 6(2): 109 – 116.
85. Nikolaychuk PA (2015). The potential – pH diagram for Fe – H_2O system. In: Fundamental'nye i prikladnye issledovaniâ v oblasti himii i èkologii: materialy meždunarodnoj naučno-praktičeskoj konferencii studentov, aspirantov i molodyh učënyh. Kursk: ZAO “Universitetskaâ kniga” 80 – 83.
86. Nikolaychuk PA (2015). Das revidierte Pourbaix-Diagramm für Schwefel. In: Materialien zum wissenschaftlichen Seminar der Stipendiaten der Programme „Mikhail Lomonosov“ und „Immanuel Kant“. Moscow, Deutscher Akademischer Austausch Dienst und Ministerium für Bildung und Wissenschaft der RF 72 – 76.
87. Nikolaychuk PA, Tyurin AG (2012). Termodinamika himičekoj i èlektrohimičeskoj ustojčivosti sistem Me – Si (Me = Ti, Mo, Mn, Fe, Co, Ni, Cu,

Zn). In: Itogi dissertacionnyh issledovanij: Materialy IV Vserossijskogo konkursa molodyh učenyh. Moscow, RAN 1: 54 – 68.
88. Nikolaychuk PA (2016). Is calomel truly a poison and what happens when it enters the human stomach? A study from the thermodynamic viewpoint. Main Group Metal Chemistry 39(1 – 2): 41 – 47.
89. Nikolaychuk PA, Shalyapina TI, Tyurin AG, Mosunova TV (2010). Termodinamika himičeskoj i èlektrohimičeskoj ustojčivosti splavov sistemy Mn – Si. Vestnik Ûžno-Ural'skogo gosudarstvennogo universiteta. Seriâ „Himiâ“ 4, 31(207): 72 – 82.
90. Nikolaychuk PA, Tyurin AG (2011). Termodinamika himičeskoj i èlektrohimičeskoj ustojčivosti splavov sistemy Mo – Si. Butlerovskie soobŝeniâ 24(2): 95 – 100.
91. Nikolaychuk PA, Tyurin AG (2011). Termodinamika himičeskoj i èlektrohimičeskoj ustojčivosti splavov sistemy Ti – Si. Butlerovskie soobŝeniâ 24(2): 77 – 87.
92. Nikolaychuk PA, Tyurin AG (2011). Termodinamika himičeskoj i èlektrohimičeskoj ustojčivosti splavov sistemy Cu – Si. Butlerovskie soobŝeniâ 24(2): 88 – 94.
93. Nikolaychuk PA, Tyurin AG (2012). The estimation of Fe – Si system oxidation at 298 K in air and water environments. In: Physical Chemistry 2012: proceedings of the 11th International Conference on Fundamental and Applied Aspects of Physical Chemistry. Belgrade, Society of Physical Chemists of Serbia 1: 37 – 39.
94. Nikolaychuk PA, Tyurin AG (2013). Thermodynamic assessment of chemical and electrochemical stability of nickel – silicon system alloys. Corrosion Science 73: 237 – 244.
95. Nikolaychuk PA, Tyurin AG (2013). Thermodynamic Evaluation of Corrosion-Electrochemical Behaviour of Silicon Brass CuZn17Si3. Inorganic Materials 49(5): 457 – 467.
96. Nikolaychuk PA (2015). Thermodynamic evaluation of electrochemical stability of Me – Si systems (Me = 4th row transition metal). Žurnal Sibirskogo federal'nogo universiteta. Seriâ Himiâ 8(2): 160 – 180.
97. Nikolaychuk PA, Tyurin AG (2012). Thermodynamics of chemical and electrochemical stability of copper-nickel alloys. Protection of Metals and Physical Chemistry of Surfaces 48(4): 462 – 476.
98. Biryukov AI (2013). Osobennosti korrozionno-èlektrohimičeskogo povedeniâ stali Ст.3 i medi v sil'nokislyh sul'fatnyh rastvorah. Dissertation of kandidat himičeskih nauk. Chelyabinsk, South Ural State University.
99. Kostitsyna IV (2014). Korrozionnaâ stojkost' trubnyh stalej v agressivnyh sredah neftânyh i gazovyh mestoroždenij. Dissertation of kandidat himičeskih nauk. Chelyabinsk, South Ural State University.
100. Pratskova SE (2014). Modelirovanie termodinamičeskih svojstv rasplavov sistemy Na^+, Ca^{2+}, Al^{3+} // O^{2-}, F^-. Dissertation of kandidat himičeskih nauk. Chelyabinsk, South Ural State University.

101. Vasekha MV (2014). Fiziko-himičeskie osnovy sul'fitnoj tehnologii železogidratnyh soedinenij. Dissertation of doktor tehničeskih nauk. Sankt-Petersburg, Sankt-Petersburg State Technological Institute[22].
102. Tyurin AG, Vasekha MV, Biryukov AI (2016). Thermodynamic Fundamentals of Ferrous Cake Sulfitization. Russian Metallurgy (Metally) 3: 236 – 243.
103. Chalaya EA, Tyurin AG, Vasekha MV, Biryukov AI (2016). Sintez i svojstva dvojnogo sul'fita medi (I) – nikelâ (II). Žurnal obŝej himii. Accepted.
104. Tyurin AG, Kanatyeva II, Nikolaychuk PA (2013). Diagrammy himičeskoj i èlektrohimičeskoj ustojčivosti splavov sistemy Fe – Ge. In: X Meždunarodnoe Kurnakovskoe soveŝanie po fiziko-himičeskomu analizu: sbornik trudov. Samara: Izdatel'stvo Samarskogo gosudarstvennogo tehničeskogo universiteta 2: 85 – 90.
105. Tyurin AG, Nikolaychuk PA, Kanatyeva II (2015). Termodinamika himičeskoj i èlektrohimičeskoj ustojčivosti splavov sistemy Fe – Ge. Korroziâ: materialy, zaŝita, 12: 1 – 9.
106. Tyurin AG, Nikolaychuk PA, Kabardin AM (2016). Thermodynamic evaluation of the corrosion-electrochemical behaviour of manganese - germanium system alloys. Journal of Corrosion Science and Engineering 19(20): 1 – 38.
107. Tyurin AG, Manannikov DA, Parshukov VP, Antonova AV, Nikolaychuk PA (2016). Method of estimation of corrosion stability of multicomponent alloys using equilibrium and polarization potential – pH diagrams. Anti-Corrosion Methods and Materials. Accepted.
108. Tyurin AG, Manannikov DA, Parshukov VP, Nikolaychuk PA (2016). Korrozionno-èlektrohimičeskoe povedenie stali X13[12] v rastvore 5% NaCl + 0,5% CH_3COOH + CH_3COONa + CO_2. Journal of Corrosion Science and Engineering 19(27): 1 – 12.
109. Tyurin AG, Sharlay EV (2016). Termodinamičeskij analiz korrozionno-èlektrohimičeskogo povedeniâ amorfnogo splava 2HCP[23]. Vestnik Ûžno-Ural'skogo gosudarstvennogo universiteta. Seriâ “Himiâ”. Accepted.
110. Pratskova SE, Tyurin AG (2016). Modelirovanie kvazibinarov sistemy Na^+, Ca^{2+} // O^{2-}, F^-. Izvestiâ vysših učebnyh zavedenij. Seriâ: Himiâ i himičeskaâ tehnologiâ 59(1): 19 – 22.
111. Nikolaychuk PA, Kolpakova AS, Tyurin AG (2016). Termodinamičeskaâ ocenka korrozionno-èlektrohimičeskogo povedeniâ svincovoj latuni ЛС74-3[14]. Izvestiâ vysših učebnyh zavedenij. Cvetnaâ metallurgiâ. Accepted.

Notes:

[1] In most cases, the scientific transliteration of Cyrillic alphabet according to the International Standard ISO 9:1995 “Information and documentation – Transliteration of Cyrillic characters into Latin characters – Slavic and non-Slavic languages” was applied. This includes the terms related to the Russian and Soviet academic system and the titles of articles, books and conferences in the References section. The first exception is Russian names and surnames. If applicable, they

were written as in publications in English authored by these persons; otherwise, they were transliterated according to the rules of Federal Migration Service of Russian Federation for transliterating the names in visas and international passports. The second exception is Russian geographic names that were transliterated according to the rules issued by the United States Board of Geographical Names.

[2] The English translations of the names of universities and institutes are given in text. The original names are supplied in subsequent notes.

[3] The official Russian name of Chelyabinsk Polytechnical Institute was "Челябинский политехнический институт".

[4] The official Russian name of South Ural State National Research University is "Южно-Уральский государственный университет (национальный исследовательский университет)"

[5] In Russia and former the Soviet Union the university diplomas of the students with outstanding examination results have a red cover sheet and red pages background contrary to blue ones for the regular diplomas. This is why the diplomas with honours are called "the red diplomas".

[6] The academic system of Russia and the former Soviet Union is two-stage. See the detailed description at https://en.wikipedia.org/w/index.php?title=Academic_ranks_in_Russia&oldid=726904556. Particularly, "kandidat nauk" and "doktor nauk" are, respectively, the first and the second academic degrees; "assistent", "mladšij naučnyj sotrudnik", "docent" and "staršij naučnyj sotrudnik" are the academic ranks available for the holders of the degree "kandidat nauk", "professor" is the academic rank available for the holders of the degree "doktor nauk". The form of post-graduate education, in which the applicant pursues the degree of "kandidat nauk" is called "aspirantura" and the applicant himself is called "aspirant"; the form of post-graduate education, in which the applicant pursues the degree of "doktor nauk" is called "doktorantura" and the applicant himself is called "doktorant".

[7] The translations are given in the square brackets.

[8] The official Russian name of Ural Scientific-Research Institute of Pipe Industry was "Уральский научно-технический институт трубной промышленности". The official Russian name of its successor, Russian Scientific-Research Institute of Pipe Industry, is "Российский научно-технический институт трубной промышленности".

[9] The official Russian name of the Central Scientific-Research Institure of the Ferrous Metallurgy named after Ivan Pavlovich Bardin is "Центральный научно-исследовательский институт чёрной металлургии имени Ивана Павловича Бардина".

[10] The official Russian name of Chelyabinsk State University is "Челябинский государственный университет".

[11] Aleksandr Georgievich intentionally used the word "regular" in this term. In his opinion it meant that whereas all the equations, proposed by Hildebrand for regular solutions, are still applicable together with his theory, the implementation of his model could help to bypass the limitations of Hildebrand's theory.

[12] According to the Russian state standard “GOST 5632-2014 Legirovannye neržaveûŝie stali i splavy korrozionno-stojkie, žarostojkie i žaropročnye. Marki” [“Corrosion-resistant and heat-resistant alloyed stainless steels and alloys. Specifications”], the steel 08Х15Н5Д2Т contains (by weight %): C – 0.08, Cr – 14-16, Ni – 4-6, Cu – 2, Ti – 1, Fe – the rest. According to the same state standard, the steel 12Х18Н10Т contains (by weight %): C – 0.12, Cr – 17-19, Ni – 9-11, Ti – 1, Fe – the rest. The steel Х13 contains (by weight %): C – 0.5-0.7, Cr – 12-14, Mn – 0.25-0.80, Si – 0.2-0.5, Fe – the rest.

[13] According to the Russian state standard “GOST 380-2005 Stal' uglerodistaâ obyknovennogo kačestva. Marki” [“Common quality carbon steel. Specifications”], the steel Ст.3 contains (by weight %): C – 0.14-0.22, Si – 0.15-0.3, Mn – 0.4-0.65, Fe – the rest.

[14] According to the Russian state standard “GOST 15527-2004 Splavy medno-cinkovye (latuni), obrabatyvaemye davleniem. Marki” [“Copper-zinc alloys treated by pressure. Specifications”], the siliceous brass ЛК80-3 contains (by weight %): Cu – 79-81, Zn – 13.5-18.5, Si – 2.5-4. According to the same state standard, the leaded brass ЛС74-3 contains (by weight %): Cu – 72-75, Zn – 21.75-25.6, Pb – 2.4-3.

[15] According to the Russian state standard “GOST 492-2006 Nikel', splavy nikelevye i medno-nikelevye, obrabatyvaemye davleniem. Marki” [“Nickel, nickel alloys and copper-nickel alloys treated by pressure. Specifications”], the melchior МН19 contains (by weight %): Ni + Co – 18-20, Cu – the rest. According to the same state standard, the melchior МНЖМц30-1-1 contains (by weigth %): Ni + Co – 29-33, Fe – 0.5-1, Mn – 0.5-1, Cu – the rest. Melchiors are sometimes called “a German silver”.

[16] The official Russian name of Samara State Technical University is “Самарский государственный технический университет”.

[17] The official Russian name of Murmansk State Technical University is “Мурманский государственный технический университет”.

[18] The official German name of University of Greifswald is “Ernst-Moritz-Arndt-Universität Greifswald”.

[19] The official Russian name of Ural Polytechnical Institute named after Sergey Mironovich Kirov was “Уральский политехнический институт имени Сергея Мироновича Кирова”. Now its successor is Ural Federal University, and its official Russian name is “Уральский федеральный университет”.

[20] The official Dutch name of Technical College of Delft was “Technische Hogeschool Delft”. Now its successor is Delft University of Technology, and its official Dutch name is “Technische Universiteit Delft”.

[21] The official Russian name of Scientific-Research Physical and Chemical Institute named after L. Ya. Karpov is “Научно-исследовательский физико-химический институт имени Льва Яковлевича Карпова”.

[22] The official Russian name of Sankt-Petersburg State Technological Institute is “Санкт-Петербургский государственный технологический институт”.

[23] The soft magnetic amorphous alloy 2HCP is produced according to the Russian industry specifications “TU 14-123-149-2009 Lenta bystrozakalennaâ iz

magnitomâgkih amorfnyh splavov i magnitomâgkogo kompozicionnogo (nanokristalličeskogo) materiala" ["A rapidly hardened tape from the soft magnetic amorphous alloys and the soft magnetic composite (nanocrystallic) materials"]. It contains (by weight %): Si – 5.3, B – 3.2, Ni – 1.8, Fe – the rest.

1. General characteristics of fourth period transition metals silicides

Silicides are binary compounds of silicon with less electronegative elements, mainly metals. They are known for s-metals (except Be), most of d-elements (except Ag, Au, Zn, Cd and Hg) and all f-elements; p-metals do not form silicides. Non-metallic p-elements mostly form compounds with silicon, but these compounds should be considered as silicon carbides, borides, arsenides, selenides *et cetera*. By the chemical bond type silicides might be divided into three major groups, namely ionic-covalent, covalent and metal-like. The silicides of the highly electropositive elements, which atoms have outer s-electrons, refer to the first group; covalent silicides are formd by the elements, which atoms have outer sp-electrons, and metal-like — by transition metals, which atoms in isolated state have unfinished d- and f- electron shells [Бережной, 1958].

The silicides of 3d-transition metals differ in a variety of physical properties and exclusive broad range of technical applications [Chen, 2005]. Among these compounds there are high-conductive materials, semi-conductors and semi-metals, superconductors, magnetically ordered phases *et cetera*. Their crystal structures and thermodynamic properties are also very different [Schlesinger, 1990].

The specific physical and chemical properties of 3d-transition metals silicides lead to their diverse usage in technics. They are important ferroalloy manufacturing products (ferrosilicon, silicomanganese, sillicochromium *et cetera*) widely using in deoxidisation and alloying of steels, in reducing the oxides, as the source components for chemical syntheses and dressing pulps, in production of acid-resistant wares [Гельд, Сидоренко, 1971].

Metal silicides are crystal phases with metallic lustre, mostly of silverish-white or gray colour. Their crystal structure contains both Me — Si, Si — Si and Me — Me bonds. They do not form any interstitial phases. With silicon content increase the structures with silicon pairs, chains, layers and surfaces, and carcasses appear. Most silicides have a chemical compositions between Me_3Si and $MeSi_2$. The most common compositions are $MeSi_2$, Me_5Si_3, Me_3Si, Me_2Si_3 and Me_2Si, they are characterised by the most structural types variety. A few silicides with lesser silicon content is known. The copper silicide Cu_8Si has a minimal silicon content. In addition to aforementioned types, the following ones are observed mostly often:

Me_3Si_2, Me_5Si_4, MeSi and Me_3Si_5. Moreover, many transition metals silicides are the phases of variable composition.

s-Metals silicides are more infusible than corresponding metals, and transition metals silicides are less infusible than the metals. Usually the compounds with middle silicon content have the highest melting temperatures. Most metal-like silicides have the metallic conductivity. The highest silicides are often semiconductors. Some metal-like silicides have the superconductive properties, *exempli gratia* V_3Si with T_{crit} = 17 K. Alkaline and alkali-earth metals silicides are mostly semiconductors.

s- and d-Elements silicides are either weakly paramagnetic or diamagnetic. The silicides V_3Si, Cr_3Si and Mo_3Si are antiferromagnetics, the rare-earth metals silicides are either ferro- or antiferromagnetics.

Among the d-metals the 4th period elements form the maximal number of silicides (up to 6—7). While moving down, to heavier elements in each group, the number of silicides formed by the elements decreases [Murarka, 1983].

There are quite many ternary silicides known, and besides, they might be composed of metals that do not form binary silicides, *exempli gratia* Au_2EuSi_2. There are also ternary compounds containing transition metals, silicon and other non-metal, for example Mo_4Si_3C or V_5SiB_2.

The most common way of synthesis of the silicides is sintering or mutual melting of the pure substances. A self-propagating high temperature topochemical synthesis is also possible. Sometimes the synthesis is performed in a molten Al, Hg, Cu, Zn or other metal that allows to reduce the temperature drastically. After cooling, the silicides are divided from a solvent metal by chemical methods or, if from mercury, by sublimation. Some silicides might be obtained by reducing the metal oxides with elementary silicon or SiC, by reducing the mixtures of metal oxide with SiO_2 with C, Al or Mg. An electrochemical synthesis is also possible via electrolysis of sodium or potassium fluorosilicate melts with addition of corresponding metal oxide or salt, or of melts of corresponding metal silicate with addition of CaF_2, $CaCl_2$ or $CaCO_3$. Rarely used are the precipitation from the gas phase methods by reduction of mixtures of silicon chloride or bromide with metal by hydrogen or $SiHal_4$ over the metallic powder or heated wire.

Small silicide monocrystals might be grown by using chemical transport reactions with chlorine, bromine or iodine as the transporting agent. Large monocrystals are being grown by directed crystallisation or extrusion [Reader et al., 1993].

Many silicides are used as the refractory materials in chemical engineering for producing the reactor claddings, pumps, agitators and heat exchangers details. A formation of silicide layers on a surface of the metal is used to increase their heat resistance. Such coatings are used to protect Mo, Nb, Ta, W and their alloys from melting. Some silicides, especially disilicides of Cr, Mn, Co, Re and some other metals, are high-temperature semiconductors. Rare-earth metals silicides having a high thermal neutron capture cross section might be used as high-temperature neutron absorbers.

Silicides are used as the cermet and refractory alloys components, because they increase the metals resistance to oxidation. Particularly, the electric oven heaters that might work in oxidising atmospheres at the temperatures up to ~ 1700 °C are made of molybdenum silicide $MoSi_2$. Transition metals silicides do not react with water, are not or weakly soluble in both cold and hot acids, but are being decomposed by the alkalis. They are (especially, higher silicides) very resistant to atmospheric corrosion due to formation of the silicate layer (or, in the case of metals forming volatile oxides (Mo, Re, W), — the silica layer) on the surfaces [Самсонов, Дворина, Рудь, 1979].

2. Thermodynamic evaluation of chemical and electrochemical stability.

2.1. Phase equilibria in binary and multicomponent metallic systems

It is convenient to express the chemical composition of a metallic system in terms of mole fractions. Mole fraction (x) is the ratio of the amount of substance (n) of the given component i to the sum of the amounts of substances of all k components in the system:

$$x_i = \frac{n_i}{\sum_{j=1}^{k} n_j} \quad . \tag{1}$$

There are two ways to quantitatively express the non-ideality of a solution. The first method was proposed by G. N. Lewis [Lewis, 1899; Lewis, 1907; Lewis, 1908; Lewis, Randall, 1923], it is based on activities. Thermodynamic activity (a) is the „effective concentration" of the species taking into account the system non-ideality. It is related with the mole fraction through the activity coefficient (γ):

$$a_i = x_i \cdot \gamma_i \quad . \tag{2}$$

The mentioned reference state is „a pure component".

Thermodynamic activities are involved in the expression of equilibrium constant of any reaction (here ν are the corresponding stoichiometric coefficients of the reagents and products, gaseous substances are not included):

$$K = \frac{\prod_{j=1}^{\text{products}} a_j^{\nu_j}}{\prod_{l=1}^{\text{reagents}} a_l^{\nu_l}} \quad . \tag{3}$$

The second method was proposed by Scatchard [Scatchard, 1931; Scatchard, 1949; Scatchard, 1968; Scatchard, Raymond, 1938], it is based on excess thermodynamic properties. The excess thermodynamic property X^E is the difference between the property of the real system X at given conditions and the property of the hypothetical ideal system containing the same components X^{id} at the same conditions:

$$X^E = X - X^{id} \quad . \tag{4}$$

These two methods are related to each other through the equation:

$$\mu_i^E = R \cdot T \cdot \ln \gamma_i \, . \tag{5}$$

Combining equations, the following relation between the activities and excess chemical potentials of the components yields:

$$R \cdot T \cdot \ln a_i = R \cdot T \cdot \ln x_i + \mu_i^E \ . \tag{6}$$

The excess chemical potentials of the components are connected with the excess molar Gibbs energy of the system:

$$G^E = \sum_{i=1}^{k} \left(x_i \cdot \mu_i^E \right). \tag{7}$$

Therefore, the task of thermodynamic description of metallic systems relates to the task of finding the suitable expression for the excess molar Gibbs energy of the system.

Usually, the following expression for the excess molar Gibbs energy of multicomponent metallic system is employed [Kattner, 1997]:

$$G^E = \sum_{i=1}^{k-1} \sum_{j=i+1}^{k} \left(x_i \cdot x_j \cdot L_{ij} \right) + \sum_{i=1}^{k-2} \sum_{j=i+1}^{k-1} \sum_{l=j+1}^{k} \left(x_i \cdot x_j \cdot x_l \cdot L_{ijl} \right) + \ldots, \tag{8}$$

where L_{ij} are the binary interaction parameters, L_{ijl} are the ternary interaction parameters and so forth. These parameters are composition- and temperature-dependent. There are several models describing composition dependence [Renon, Prausnitz, 1968]. The most known and widely used are the following:

a) Regular solution model [Hildebrand, 1927; Hildebrand, 1929]: the parameter L_{ij} does not depend on composition and temperature;

b) Subregular solution model [Guggenheim, 1935; Аплатов, Падерин, 2009; Храпко, 2006; Храпко, 2011]: the parameter L_{ij} does not depend on composition, but depend on temperature;

c) Margules model [Margules, 1895]:

$$\begin{aligned} L_{ij} &= L_{ji}^{(1)} \cdot x_i + L_{ij}^{(1)} \cdot x_j + x_i \cdot x_j \cdot \left(L_{ji}^{(2)} \cdot x_i + L_{ij}^{(2)} \cdot x_j \right) + \ldots + \\ &+ \left(x_i \cdot x_j \right)^{m-1} \cdot \left(L_{ji}^{(m)} \cdot x_i + L_{ij}^{(m)} \cdot x_j \right); \end{aligned} \tag{9}$$

d) Redlich-Kister model [Redlich, Kister, 1948]:

$$L_{ij} = L_{ij}^{(0)} + L_{ij}^{(1)} \cdot \left(x_i - x_j \right) + L_{ij}^{(2)} \cdot \left(x_i - x_j \right)^2 + \ldots + L_{ij}^{(m)} \cdot \left(x_i - x_j \right)^m \ ; \tag{10}$$

e) van Laar model [Laar van, 1908a; Laar van, 1908b; Laar van, 1910; Laar van, 1913]:

$$L_{ij} = \frac{L_{ij}^{(1)} + L_{ji}^{(1)}}{L_{ij}^{(1)} \cdot x_i + L_{ji}^{(1)} \cdot x_j} \ ; \tag{11}$$

f) Tyurin model [Tyurin, 1993; Тюрин, 2012]:

$$L_{ij} = L_{ij}^{(1)} \cdot x_i + L_{ij}^{(2)} \cdot x_j + L_{ij}^{(3)} \cdot x_i \cdot x_j + L_{ij}^{(4)} \cdot x_i^2 + L_{ij}^{(5)} \cdot x_j^2 + \ldots \,. \qquad (12)$$

All parameters $L_{ij}^{(m)}$ in equations (9) through (12) might also be temperature-dependent. The temperature dependency is usually expressed in form of simple polynomials. Each of these models has multiple various extensions. There are also several methods of calculating the activities of multicomponent mixtures from the parameters of these models [Acree, 1992; Bale, Pelton, 1974; Bertrand, Acree, Burchfield, 1983; Blander, Pelton, 1987; Campbell, 1992; Chen, Kao, Chang, 1995; Cheng, Ganguly, 1994; Fei, Saxena, Eriksson, 1986; Ganguly, 2001; Harvig et al., 1971; Helffrich, Wood, 1989; Hillert, Staffansson, 1970; Hwang et al., 1991; Jackson, 1989; Keller, Capitani De, Abart, 2005; Marsh, 1977; Mukhopadhyay, Basu, Holdaway, 1993; Peng, 2010; Saulov, 2006; Wohl, 1946; Wohl, 1953; Zhang, Huang, Chang, 1997].

The estimation of component interaction parameters may be performed using the optimisation techniques based on global Gibbs energy minimisation (CALPHAD method [Campbell, 2012; Lukas, Fries, Sundman, 2007; Soustelle, 2015; Yaws, 1996; Карапетьянц, 1975; Морачевский, 1987]). This method was proposed by van Laar [Laar van, 1908a; Laar van, 1908b; Laar van, 1908c] and developed further by Kaufman [Kaufman, Bernstein, 1970]. Nowadays, several commercially available software packages allow their users to use this technique in estimating and predicting the thermodynamic properties of multicomponent mixtures of importance for chemical engineering. Other approaches, different from Gibbs energy minimisation, also exist.

When one need to consider only the particular single equilibrium, one can estimate the component interaction parameters that would be suitable only for this equilibrium and only within specified temperature interval. In the current study exactly this method is used to estimate solubilies at low temperatures.

If two different solutions with different crystal structures (α and β) are in equilibrium, it might be described by the equality of chemical potentials (μ) of each component (A and B) in both phases:

$$\begin{cases} \mu_A^{\alpha} = \mu_A^{\beta}; \\ \mu_B^{\alpha} = \mu_B^{\beta}. \end{cases} \qquad (13)$$

Expressions for chemical potentials of the component $i \in \{A; B\}$ in the phase $\chi \in \{\alpha; \beta\}$ are the following:

$$\mu_i^{\chi} = \mu_i^{\chi,o} + RT \ln x_i^{(\chi)} + \mu_i^{\chi,E}. \quad (14)$$

The standard chemical potentials (μ^o) of the same component i in different phases (χ and ω) are connected with each other through the Gibbs energy change of phase transition for this component:

$$\mu_i^{\omega,o} = \mu_i^{\chi,o} + \Delta_{tr} G_i^{\chi \to \omega}. \quad (15)$$

By solving the system of equations (13) through (15) the expressions for excess chemical potentials of components might be estimated.

If a solution is in equilibrium with any solid compound, the equilibrium is described by the reaction:

$$\nu_A \, A(\chi) + \nu_B \, B(\chi) \rightleftharpoons A_{\nu_A} B_{\nu_B} (s), \quad (16)$$

the equilibrium constant of which is related to the Gibbs energy of the reaction:

$$\Delta_r G_{(16)} = -R \cdot T \cdot \ln K_{(16)} = -R \cdot T \cdot \ln \frac{a_{A_{\nu_A} B_{\nu_B}}}{a_{A^{(\chi)}}^{\nu_A} \cdot a_{B^{(\chi)}}^{\nu_B}}. \quad (17)$$

If the compound $A_{\nu_A} B_{\nu_B}$ is pure, its activity $a_{A_{\nu_A} B_{\nu_B}}$ might be set equal to unity; the activities of the components A and B are expressed by equations derived from (6) through (12); the Gibbs energy of reaction might be calculated from thermochemical tables of reference data. The resulting equation might be then solved for the component interaction parameters.

2.2. $Me_1 - Me_2 - O$ ternary state diagrams and chemical stability

A chemical stability is the ability of a substance to resist the influence of environment. Particularly, it concerns the ability to resist oxidative effect of the atmospheric air.

The oxidation of any metal by oxygen might be described by the reaction:

$$\nu_{Me} \, Me \, (s) + \frac{\nu_O}{2} O_2 (g) \rightleftharpoons Me_{\nu_{Me}} O_{\nu_O} (s). \quad (18)$$

The equilibrium constant of the reaction is:

$$\Delta_r G_{(18)} = -R \cdot T \cdot \ln K_{(18)} = -R \cdot T \cdot \ln \frac{a_{Me_{\nu_{Me}} O_{\nu_O}}}{a_{Me}^{\nu_{Me}} \cdot P_{O_2}^{\frac{\nu_O}{2}}}. \quad (19)$$

If both metal and its oxide are pure, their thermodynamic activities might be set equal to unity, and the relationship between the Gibbs energy of reaction and equilibrium oxygen pressure might be expressed as:

$$\Delta_r G_{(18)} = -R \cdot T \cdot \ln K_{(18)} = \frac{\nu_O}{2} \cdot R \cdot T \cdot \ln P_{O_2}. \quad (20)$$

Thus, equilibrium oxygen pressure P_{O_2} is an important thermodynamic property that characterises the oxidation process.

The chemical stability of binary system could be visualised in form of a ternary state diagram. The method of plotting and describing three-component state diagrams for metal-oxygen-containing systems was developed in [Hubbard, Schlom, 1996; Третьяков, 1967; Тюрин, 2012]. A diagram consists of two ordinary orthogonal axes. The abscissa is the mole fraction of one metal compound in the binary metallic system. The ordinate is represented by system oxidation degree (y), which is the quantity of moles of atomic oxygen in system, corresponding to the one mole of metallic compounds:

$$y = \frac{n_{O_2}}{\sum_{\text{metals}} n_{Me}} = \frac{n_{O_2}}{n_{Me_1} + n_{Me_2}}. \quad (21)$$

A diagram is plotted at fixed temperature and pressure. According to Gibbs' phase rule [Gibbs, 1876a], when these two variables are fixed, maximum of three phases can coexist in three-component system. Any single compound (one-phase region) is depicted by any vertex within the diagram, a two-phase region is depicted by any tie-line between two nearest vertices, a three-phase region is depicted by any triangle and it corresponds to the invariant system condition. Crossing tie-lines isn't allowed, because the point of their intersection would correspond to four-phase region, which is impossible. Any phase of variable composition is depicted by line; any triangle, containing this line and filled with dotted lines, corresponds to monovariant system condition. Thus, this kind of state diagram has the same functionality as the ordinary barycentric triangle phase diagram [Finetti de, 1926; Gibbs, 1876b; Roozeboom, 1887; Roozeboom, 1899], but is simpler to plot and examine [Лаптев, 1992].

Let us consider a hypothetical Me_1 – Me_2 system, in which two metals are mutually insoluble in each other but form two intermetallides, $(Me_1)_2(Me_2)$ and $(Me_1)(Me_2)_3$. Let the metal Me_1 forms a variety of oxides, $(Me_1)O$, $(Me_1)_3O_4$, $(Me_1)_2O_3$ and $(Me_1)O_2$, and the metal Me_2 forms two oxides, $(Me_2)O_2$ and $(Me_2)_2O_5$. Oxides $(Me_1)O$ and $(Me_2)O_2$ might react forming a ternary compound $(Me_1)(Me_2)O_3$.

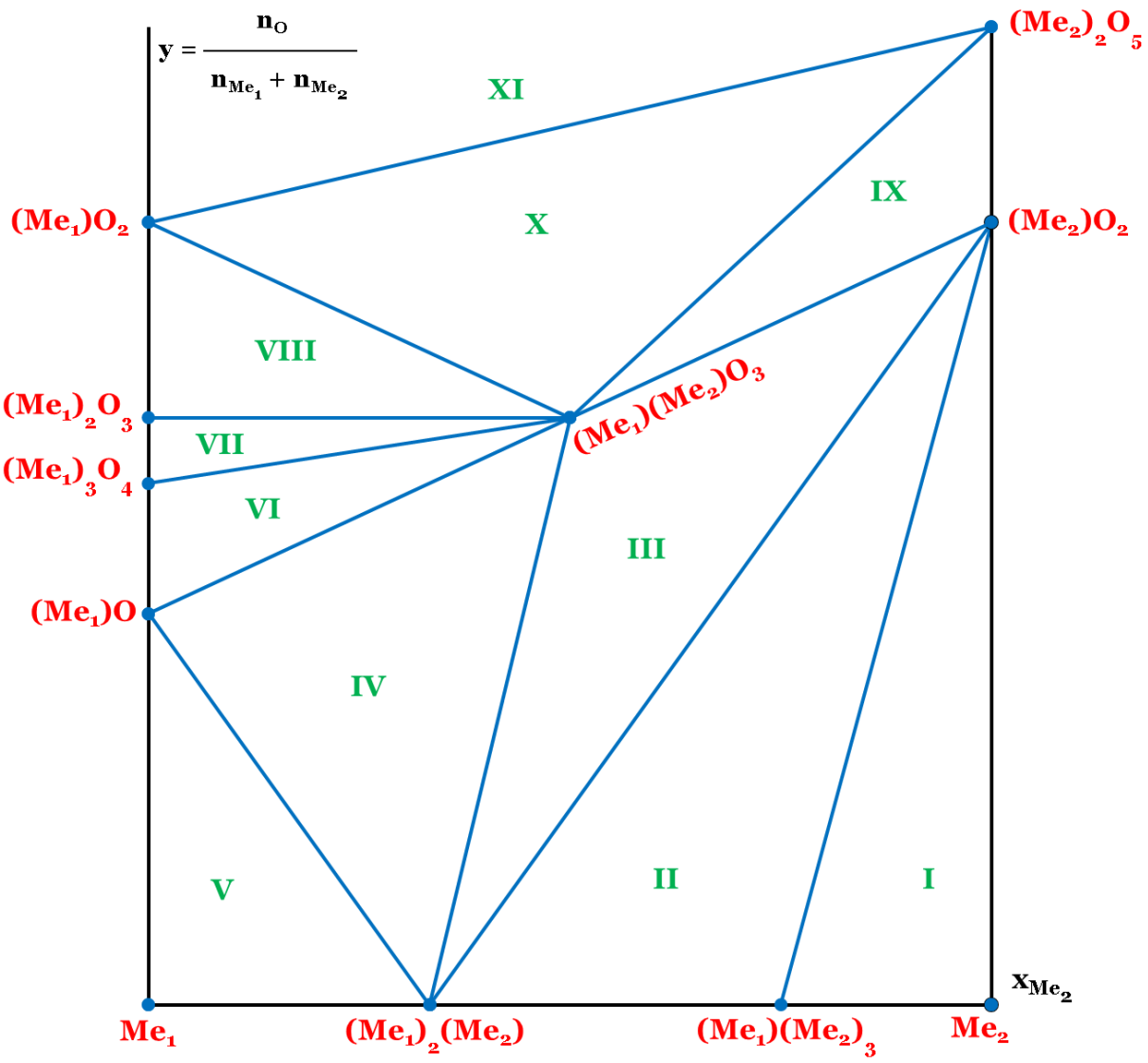

Fig. 1. The ternary state diagram for the hypothetic $Me_1 – Me_2 – O$ system.

Table 1. List of equilibria in the hypothetical $Me_1 – Me_2 – O$ ternary system in accordance with the state diagram presented in Figure 1.

No of domain in Fig. 1	Equilibrium phases	Reaction equation
I	$(Me_1)(Me_2)_3 – (Me_2) – (Me_2)O_2$	$(Me_2) + O_2\ (g) \rightleftharpoons (Me_2)O_2$
II	$(Me_1)_2(Me_2) – (Me_1)(Me_2)_3 – -(Me_2)O_2$	$2(Me_1)(Me_2)_3 + 5O_2\ (g) \rightleftharpoons \rightleftharpoons (Me_1)_2(Me_2) + 5(Me_2)O_2$
III	$(Me_1)_2(Me_2) – (Me_1)(Me_2)O_3 – -(Me_2)O_2$	$(Me_1)_2(Me_2) + (Me_2)O_2 + +2O_2\ (g) \rightleftharpoons 2(Me_1)(Me_2)O_3$

IV	$(Me_1)_2(Me_2)-(Me_1)O-$ $-(Me_1)(Me_2)O_3$	$(Me_1)_2(Me_2)+2O_2\,(g)\rightleftharpoons$ $\rightleftharpoons(Me_1)(Me_2)O_3+(Me_1)O$
V	$(Me_1)-(Me_1)_2(Me_2)-(Me_1)O$	$2(Me_1)+O_2\,(g)\rightleftharpoons 2\,(Me_1)O$
VI	$(Me_1)O-(Me_1)_3O_4-$ $-(Me_1)(Me_2)O_3$	$6\,(Me_1)O+O_2\,(g)\rightleftharpoons 2(Me_1)_3O_4$
VII	$(Me_1)_3O_4-(Me_1)_2O_3-$ $-(Me_1)(Me_2)O_3$	$4\,(Me_1)_3O_4+O_2\,(g)\rightleftharpoons 6(Me_1)_2O_3$
VIII	$(Me_1)_2O_3-(Me_1)O_2-$ $-(Me_1)(Me_2)O_3$	$2(Me_1)_2O_3+O_2\,(g)\rightleftharpoons 4(Me_1)O_2$
IX	$(Me_1)(Me_2)O_3-$ $-(Me_2)O_2-(Me_2)_2O_5$	$4(Me_2)O_2+O_2\,(g)\rightleftharpoons 2(Me_2)_2O_5$
X	$(Me_1)O_2-(Me_1)(Me_2)O_3-$ $-(Me_2)_2O_5$	$4(Me_1)(Me_2)O_3+3O_2\,(g)\rightleftharpoons$ $\rightleftharpoons 4(Me_1)O_2+2(Me_2)_2O_5$
XI	$(Me_1)O_2-(Me_2)_2O_5-O_2\,(g)$	–

An example of the ternary state diagram for the hypothetic Me_1 – Me_2 – O system is presented in Figure 1. Such diagrams are usually supplied with a list of equilibria corresponding to each of the domains in it with their respective thermodynamic characteristics. For the system from Figure 3, the hypothetical equilibria are listed in Table 1. It presents a scheme of the consecutive oxidation of Me_1 – Me_2 system by oxygen.

2.3. Chemical and electrochemical equilibria in aqueous solutions

In a general case, the process, which occurs at the *complex redox electrode* (according to the IUPAC nomenclature [Inczedy, Lengye, Ure, 1998]), can be characterised be the following half-reaction:

$$\nu_A A+\nu_B B+\nu_{H^+} H^+ +\nu_{e^-} e^- \rightleftharpoons \nu_C C+\nu_D D. \qquad (22)$$

Here, A and B are the source compounds; C and D are the products; ν_A, ν_B, ν_C, ν_D and ν_{H^+} are the stoichiometric coefficients, ν_{e^-} is the number of electrochemical equivalents [Faraday, 1834] in reaction (22).

The Gibbs energy [Gibbs, 1876a; Гиббс, 1950] of reaction (22) at the temperature T and the standard pressure, equal to 1 bar, is determined [Guggenheim, 1928] by the equation:

$$\Delta_r G_T = \Delta_r G_T^o - R \cdot T \cdot \ln \frac{a_C^{\nu_C} \cdot a_D^{\nu_D}}{a_A^{\nu_A} \cdot a_B^{\nu_B} \cdot a_{H^+}^{\nu_{H^+}}}, \quad (23)$$

where $\Delta_r G_T$ is the Gibbs energy of reaction, $J \cdot mol^{-1}$, $\Delta_r G_T^o$ is the standard Gibbs energy of reaction, $J \cdot mol^{-1}$, R = 8,314459848 $J \cdot mol^{-1} \cdot K^{-1}$ is the universal gas constant [Horstmann, 1873; Алымовъ, 1865; Менделѣевъ, 1874a; Менделѣевъ, 1874b; Менделѣевъ, 1906], T is the thermodynamic temperature, K [Thomson, 1843], a_i is the thermodynamic activity of i-th species [Lewis, 1908] (its dimension depends on the choice of the reference state [McNaught, Wilkinson, 1997]).

The relation between the Gibbs energy of half-reaction and the electrode potential is determined [Gibbs, 1889; Helmholtz, 1883; Scholz, 2010] by the basic equation of electrochemical thermodynamics:

$$\Delta_r G_T = -\nu_{e^-} \cdot F \cdot E_T. \quad (24)$$

After substitution of equation (24) into equation (23) the expression analogous to the Nernst [Nernst, 1887; Nernst, 1889a; Nernst, 1889b] and Peters [Peters, 1898] equations yields:

$$E_T = E_T^o + \frac{R \cdot T}{\nu_{e^-} \cdot F} \cdot \ln \frac{a_C^{\nu_C} \cdot a_D^{\nu_D}}{a_A^{\nu_A} \cdot a_B^{\nu_B} \cdot a_{H^+}^{\nu_{H^+}}}, \quad (25)$$

where E_T is the electrode potential at the temperature T, V, E_T^o is the standard electrode potential, V, F = 96485,3328959 $Cl \cdot mol^{-1}$ is the Faraday constant [Faraday, 1833; Faraday, 1834].

Because, according to the definition of pH [McCarty, Vitz, 2006; Sgambato et al., 2011a; Sgambato et al., 2011b; Sörensen, 1909; Sørensen, 1909a; Sørensen, 1909b]:

$$pH = -\lg a_{H^+}, \quad (26)$$

then, after substitution of equation (26) into equation (25) and changing the base of logarithms from natural to decimal ($\lg x = \ln x \cdot \ln 10$), the following expression yields:

$$E_T = E_T^o - \frac{\ln 10 \cdot \nu_{H^+} \cdot R \cdot T}{\nu_{e^-} \cdot F} \cdot pH + \frac{\ln 10 \cdot R \cdot T}{\nu_{e^-} \cdot F} \cdot \lg \frac{a_C^{\nu_C} \cdot a_D^{\nu_D}}{a_A^{\nu_A} \cdot a_B^{\nu_B}}. \quad (27)$$

The expression (27) evidences about that electrode potential is the function of pH and the values of the activities of reaction participants, $E_T = E_T(pH, a_i)$.

There are several papers and reference books collecting information on the standard electrode potentials of different chemical elements [Bard, Parsons, Jordan, 1985; Bethune de, Licht, Swendeman, 1959; Blackman, Gahan, 2014; Bratsch, 1989; Burgot, 2012; Charlot, Collumeau, Marchon, 1971; Dean, 1979; Dean, 1999; Hayes, Algie, 1993; Robinson, Stokes, 1959; Salvi, Bethune De, 1961; Speight, 2005; Vanýsek, 2012; Лурье, 2007; Справочник химика. Том третий. Химическое равновесие и кинетика. Свойства растворов. Электродные процессы, 1965; Справочник по электрохимии, 1981; Краткий справочник физико-химических величин, 2003].

Among with electrochemical reactions in solutions the purely chemical reactions may take place, which occur without participation of electrons ($\nu_{e^-} = 0$). For these reactions the equation (27) is not suitable. To calculate the dependency of pH on the activities of reaction participants at the equilibrium state an equation, analogous to the Henderson – Hasselbalch equation [Hasselbalch, 1917; Henderson, 1908a; Henderson, 1908b] is used, which is derived after substitution of equation (26) into equation (23) and accounting the condition $\Delta_r G_T = 0$:

$$\mathrm{pH} = \frac{\Delta_r G_T^o}{\ln 10 \cdot \nu_{H^+} \cdot R \cdot T} - \frac{1}{\nu_{H^+}} \cdot \lg \frac{a_C^{\nu_C} \cdot a_D^{\nu_D}}{a_A^{\nu_A} \cdot a_B^{\nu_B}}, \qquad (28)$$

The equations (27) and (28) are the master equations for thermodynamic calculations of chemical and electrochemical equilibria in aqueous environments.

2.4. Activity – pH diagrams

The ionic species in aqueous solutions tend to hydrolyse with alteration of pH [Baes Jr., Mesmer, 1976; Baes Jr., Mesmer, 1981]. For example, the ion of a hypothetical metal Me with the charge of +2 can be present in the following forms: Me^{2+} (aq), $MeOH^+$ (aq), $HMeO_2^-$(aq), MeO_2^{2-}(aq). The transition metals in their highest oxidation states can form a variety of anions. The polynuclear species with the general formula $\overset{(+z)}{Me}_x(OH)_y^{z\cdot x-y}$(aq) can also be present in a solution. The predominance of one or another species is determined by two factors: the solution pH and the total content of metal in solution (and, consequently, the activities of dissolved species). The diagram also considers any solid oxides or hydroxides of the same metal that can be precipitated.

The activity – pH diagram clearly depicts possible acid-base equilibria between various species of the same oxidation state in a (pH, a_i) space. In order to construct such a diagram one should first collect the data on Gibbs free energies of formation of all species of the same element, then write the equations of possible acid-base reactions in the system and calculate the Gibbs free energy changes that are associated with these reactions, then calculate a pH = pH(lg a_i) dependencies for each reaction in accordance with the equation (28), and, finally, plot the corresponding lines in a (pH, lg a_i) graph. Since the alteration of activity values can involve several orders-of-magnitude, the logarithmic scale on the corresponding axis is preferred.

For a hypothetical species, listed afore, the following equilibria can be considered:

$$MeO\,(s) + 2H^+\,(aq) \rightleftharpoons Me^{2+}(aq) + H_2O\,(l), \quad (29)$$

$$MeOH^+\,(aq) + H^+\,(aq) \rightleftharpoons Me^{2+}\,(aq) + H_2O\,(l), \quad (30)$$

$$MeO\,(s) + H^+\,(aq) \rightleftharpoons MeOH^+\,(aq), \quad (31)$$

$$HMeO_2^-\,(aq) + 2H^+\,(aq) \rightleftharpoons MeOH^+\,(aq) + H_2O\,(l), \quad (32)$$

$$HMeO_2^-\,(aq) + H^+\,(aq) \rightleftharpoons MeO\,(s) + H_2O\,(l). \quad (33)$$

$$MeO_2^{2-}\,(aq) + H^+\,(aq) \rightleftharpoons HMeO_2^-\,(aq). \quad (34)$$

$$MeO_2^{2-}\,(aq) + 2H^+\,(aq) \rightleftharpoons MeO\,(s) + H_2O\,(l). \quad (35)$$

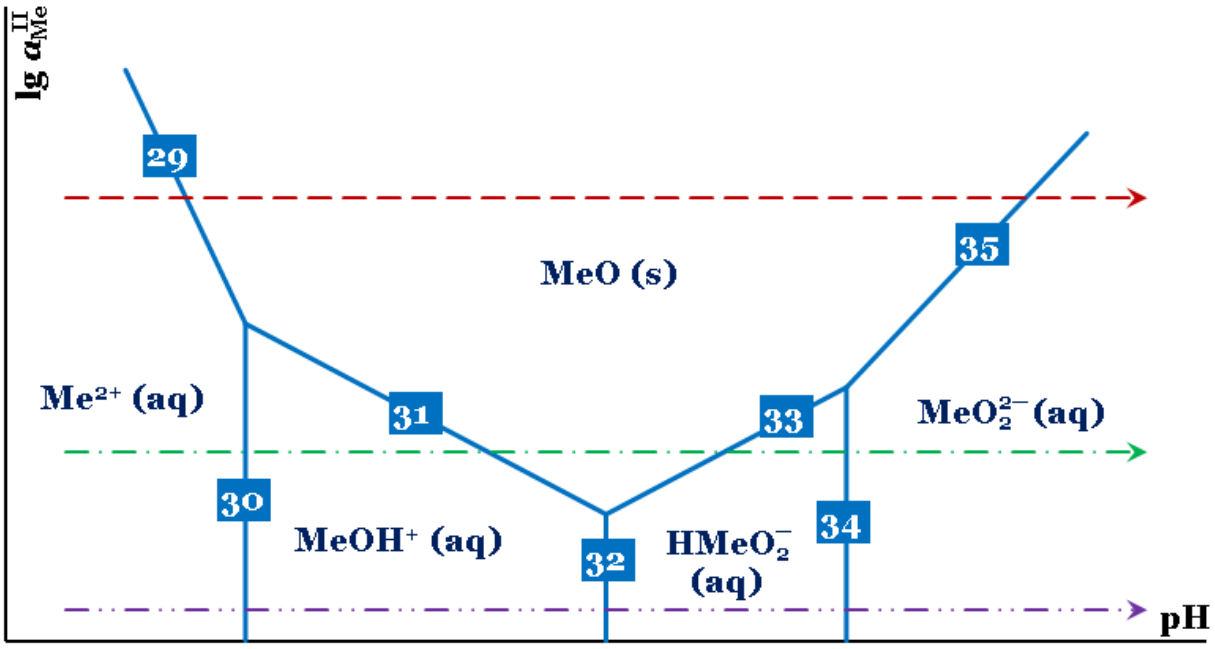

Fig. 2. The activity – pH diagram for (+2) species of a hypothetical metal Me.

A schematic activity – pH diagram for Me^{II} species that consider these equilibria is presented in Figure 2. The numbered solid lines in the diagram represent the pH – lg a_i dependencies of the equilibria in a solution. The numbers on the lines correspond to the numbers of equations, given afore. The fields in the diagram indicate the predominance of one or another species in the bordered domain of activities and pH. However, another species can also be present in this domain. Usually the quantitative estimations of content of the species in a solution are visualised by so called speciation diagrams that are outside the scope of this chapter.

The activity – pH diagram provides information of how the particular ion hydrolyses upon increase of pH at different values of the ion activities in a solution. This is illustrated by three horizontal arrowed lines in Figure 4. In concentrated solutions (at high values of activities) the metal exhibits the following sequence of transformations (represented by the dash line):

$$Me^{2+}\,(aq) \rightleftharpoons MeO\,(s) \rightleftharpoons MeO_2^{2-}\,(aq),$$

at intermediate values of activities the sequence is (represented by the dash-dot line):

$$Me^{2+}\,(aq) \rightleftharpoons MeOH^{+}\,(aq) \rightleftharpoons MeO\,(s) \rightleftharpoons HMeO_2^{-}\,(aq) \rightleftharpoons MeO_2^{2-}\,(aq),$$

and, in diluted solutions (at low values of activities) the sequence is (represented by the dash-two dots line) as follows:

$$Me^{2+}\,(aq) \rightleftharpoons MeOH^{+}\,(aq) \rightleftharpoons HMeO_2^{-}\,(aq) \rightleftharpoons MeO_2^{2-}\,(aq).$$

The information provided by the activity – pH diagrams is essential for plotting the potential – pH diagrams at various activities.

Recent applications of activity – pH diagrams include laboratory studies of water treatment [Akyol, Can, Bayramoglu, 2015; Jiang et al., 2002; Yilmaz, Boncukcuoğlu, Kocakerim, 2007], corrosion and stability of alloys in aqueous environments [Baker, Castle, 1992; Brandon et al., 2001; Cheng, Kelsall, 2007; Kelsall, 1991a; Kelsall, 1991b; Kelsall, Robbins, 1990; Krupp, Weiser, 1992; Kubal, Panacek, 1995; Zhou et al., 2011a], removal of the pollutants from the solution [Ang, Zhang, Bao, 2015; Aoudj et al., 2010; Aoudj et al., 2016; Brandon et al., 2003; Can et al., 2016; Carvalho de et al., 2015; Karakas et al., 2013; Missaoui et al., 2013; Parsa et al., 2011; Yilmaz et al., 2005; Yilmaz et al., 2008], photoelectrophoresis of semiconductors [Boxall, Kelsall, 1991; Brahmi et al., 2016; Cheraghi et al., 2015; Naje et al., 2015], in analytical chemistry [Marinakis, Kelsall, 1987], geochemistry [Abreli, Brearley, 2005; Brahmi et al., 2015; Janeczek et al., 2016; Phillipson, Romberger, 2004; Song, Ziyuan, 1991; Thiry, Galbois, Schmitt, 2006] *et cetera*.

2.5. Potential – pH diagrams and electrochemical stability

As the equations (27) and (28) show, every both the chemical and electrochemical equilibrium in an aqueous media might be visualised in the (E, pH, a_i) space. If the activities of all species in a solution are fixed and set to pre-determined values, all equilibria might be presented in a form of the conventional E – pH diagram, which is a graphic representation of equilibrium potential with respect to the standard hydrogen electrode (vertical axis) versus pH (horizontal axis) relations corresponding to the various equilibria between the different compounds of a given element under chosen thermodynamic conditions [Kiss, 1988; Thompson et al., 2011; Vernik, 1967; Сорокина, Зыкова, 2006].

The idea to represent the dependencies of electrochemical potential on pH graphically was proposed by the American chemist R. Clark [Clark, 1920; Clark, 1923; Clark, Cohen, 1923], then developed further by L. Michaelis [Michaelis, 1930], and finally crystallised in the form of diagrams of potential versus pH in the works of the Belgian electrochemist Marcel Pourbaix [Pourbaix, 1945]. This idea was then widely accepted, and the diagrams proposed by him are now called „*Pourbaix diagrams*".

The method and the algorithm of Pourbaix diagrams construction were published several times. Let us assume that the hypothetical metal Me from the previous section in addition to its aforementioned (+2)-state species has also such (+3)-state species as Me^{3+} (aq) and Me_2O_3 (s), and a (+5)-state anion MeO_3^-. Let the activities of ions in a solution are in the middle range, so the sequence of transformations, represented by dash-dot line in Figure 2 is realised. Then the following equilibria may occur in a solution:

a) Equilibria involving electrons but not involving H^+ species.
They are described by equation (27) and presented in potential – pH diagrams as horizontal lines. There are the following examples:

$$Me^{2+}(aq) + 2e^- \rightleftharpoons Me(s), \tag{36}$$

$$Me^{3+}(aq) + e^- \rightleftharpoons Me^{2+}(aq), \tag{37}$$

$$Me_2O_3(s) + H_2O(l) + 2e^- \rightleftharpoons 2HMeO_2^-(aq); \tag{38}$$

b) Equilibria involving H^+ species but not involving electrons.
They are described by equation (28) and presented in potential – pH diagrams as vertical lines. The examples are equations (30), (31), (33), (34), and the equilibrium:

$$Me_2O_3(s) + 6H^+(aq) \rightleftharpoons 2Me^{3+}(aq) + 3H_2O(l); \tag{39}$$

c) Equilibria involving both electrons and H+ species.
They are described by equation (27) and presented in potential – pH diagrams as sloped lines. There are the following examples:

$$MeOH^+(aq)+H^+(aq)+2e^- \rightleftharpoons Me(s)+H_2O(l), \quad (40)$$

$$MeO(s)+2H^+(aq)+2e^- \rightleftharpoons Me(s)+H_2O(l), \quad (41)$$

$$HMeO_2^-(aq)+3H^+(aq)+2e^- \rightleftharpoons Me(s)+2H_2O(l), \quad (42)$$

$$MeO_2^{2-}(aq)+4H^+(aq)+2e^- \rightleftharpoons Me(s)+2H_2O(l), \quad (43)$$

$$Me^{3+}(aq)+H_2O(l)+e^- \rightleftharpoons MeOH^+(aq)+H^+(aq), \quad (44)$$

$$Me^{3+}(aq)+H_2O(l)+e^- \rightleftharpoons MeO(s)+2H^+(aq), \quad (45)$$

$$Me_2O_3(s)+2H^+(aq)+2e^- \rightleftharpoons 2MeO(s)+H_2O(l), \quad (46)$$

$$Me_2O_3(s)+H_2O(l)+2e^- \rightleftharpoons 2MeO_2^{2-}(aq)+2H^+(aq), \quad (47)$$

$$MeO_3^-(aq)+6H^+(aq)+2e^- \rightleftharpoons Me^{3+}(aq)+3H_2O(l), \quad (48)$$

$$2MeO_3^-(aq)+6H^+(aq)+4e^- \rightleftharpoons Me_2O_3(s)+3H_2O(l), \quad (49)$$

$$MeO_3^-(aq)+2H^+(aq)+3e^- \rightleftharpoons MeO_2^{2-}(aq)+H_2O(l). \quad (50)$$

The resulting potential – pH diagram is presented in Figure 3. Again, the numbers on the lines correspond to the numbers of equations, given afore.

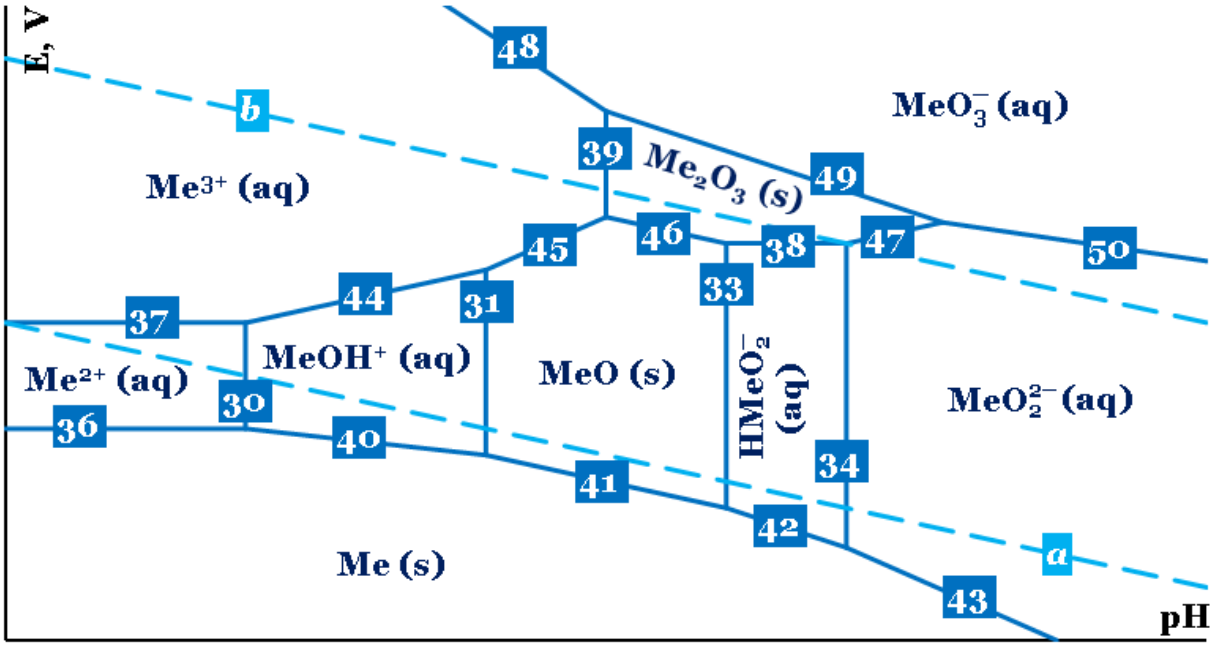

Fig. 3. The potential – pH diagram for a hypothetical metal Me.

According to the Gibbs' phase rule, no more than three different species could be present in equilibrium simultaneously. The lines, corresponding to three equilibria with the same species, always have the

intersection point, in which these three lines converge. At this intersection points, the system exhibits an invariant state. The examples in Figure 5 are the intersection points of the lines (30), (36) and (40); (33), (38) and (46); (47), (49) and (50), and others. Each line itself corresponds to the monovariant system state, where two adjacent species are present in equilibrium. The domains bordered by these lines present the areas of predominance of the certain species and represent the bivariant system conditions.

The lines in the diagram, corresponding to two equilibria independent from each other, could intersect. If the electrochemical cell is composed of these two reactions, the half-cell reaction depicted by the upper line corresponds to oxidiser, and the lower line – to reductor. The intersection point depicts the conditions where the reaction reverses (see Figure 4). This property allows using potential – pH diagrams in inorganic and analytical chemistry in order to choose a proper oxidiser or reductor in certain conditions.

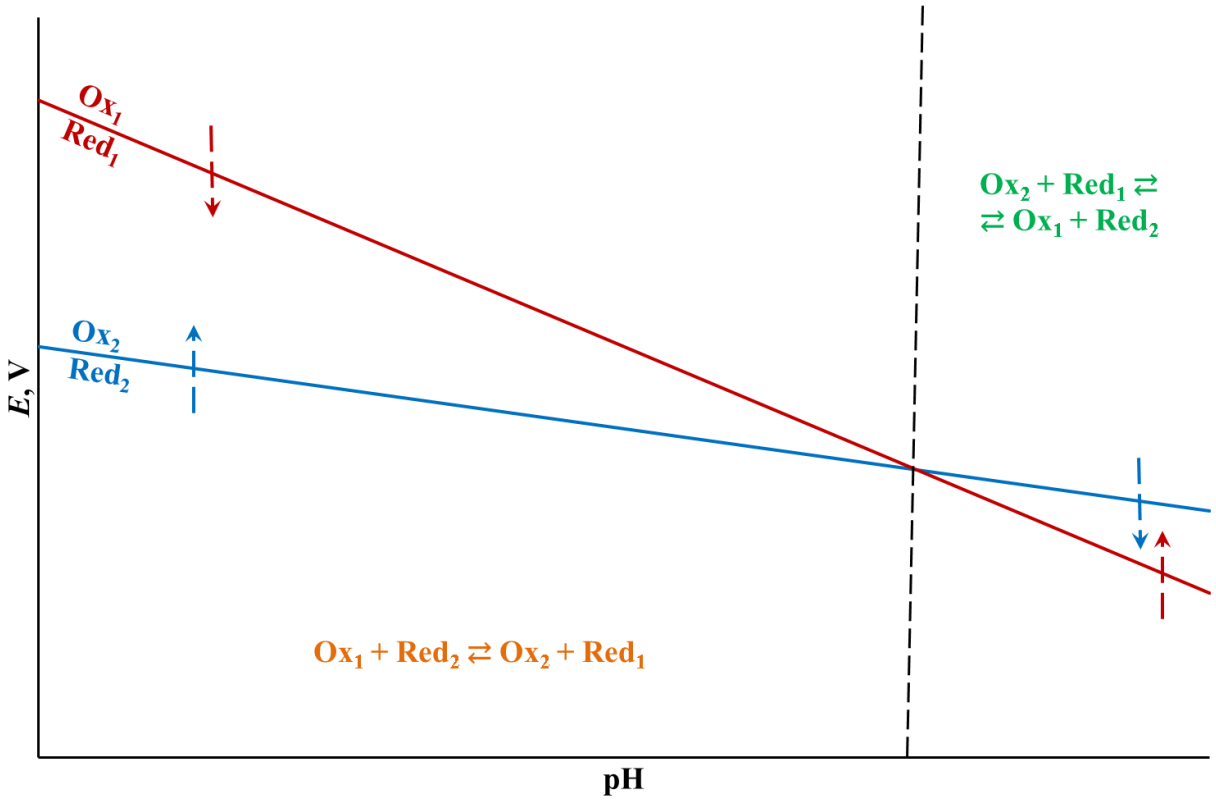

Fig. 4. Two independent equilibria in the (E, pH) space and the resulting cell reaction.

Pourbaix diagrams are widely used for thermodynamic estimation and prediction of a corrosion-electrochemical behaviour of metals, alloys and other compounds in aqueous environments. In this case the domain of

electrochemical stability of water has the great importance. This domain in Pourbaix diagrams is bordered by the lines corresponding to hydrogen and oxygen electrodes (lines *a* and *b* in Figure 3, respectively). These two lines are included in nearly all potential – pH diagrams. The equilibria corresponding to them are presented in Table 2. Usually, in order to estimate the domain of electrochemical stability of water in contact with atmospheric air, the electrode potentials of hydrogen and oxygen electrodes are calculated not in the standard but in atmospheric conditions.

Table 2. Equilibria corresponding to hydrogen and oxygen electrodes under atmospheric conditions.

Line	Electrode reaction	E, V (SHE)
a	$2H^+(aq)+2e^- \rightleftharpoons H_2(g);\ P_{H_2(g)}=5\cdot10^{-7}$ bar	$E=0{,}186-0{,}0591\cdot pH$
b	$O_2(g)+4H^+(aq)+4e^- \rightleftharpoons 2H_2O(l);$ $P_{O_2(g)}=0{,}21$ bar	$E=1{,}219-0{,}0591\cdot pH$

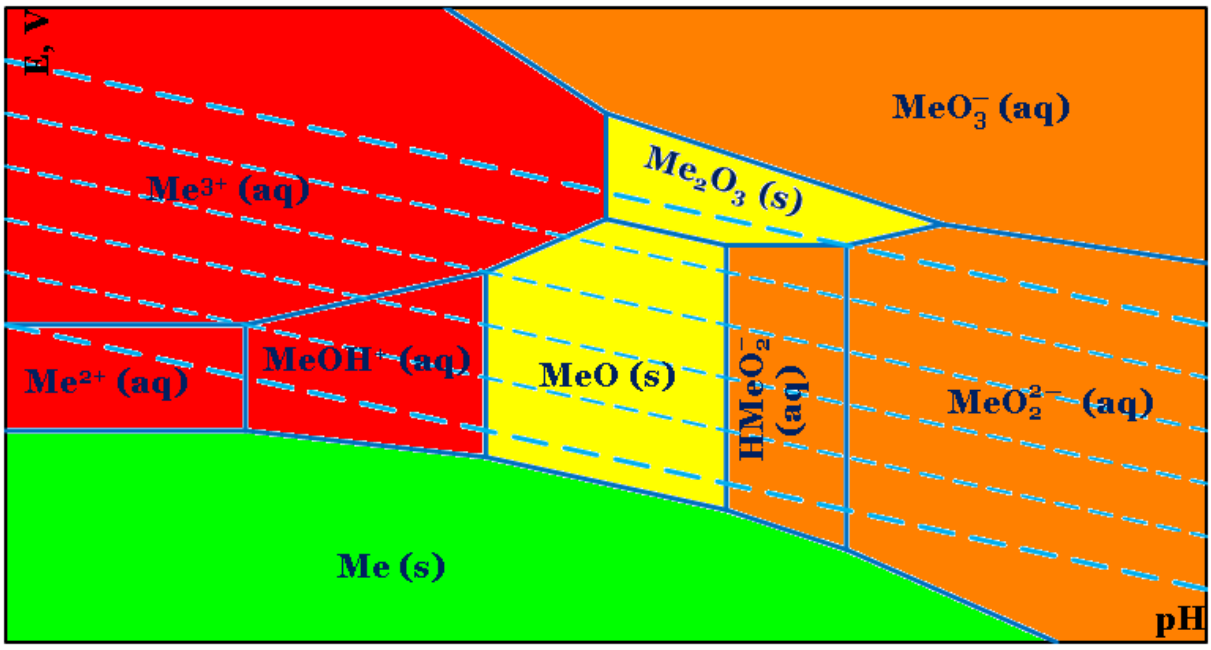

Fig. 5. Various corrosion-electrochemical behaviour of the hypothetical metal Me in the potential – pH diagram: – domain of immunity, – domain of active dissolution, – domain of passivity, – domain of transpassivity; – domain of water electrochemical stability.

Lines in Pourbaix diagrams border the areas of thermodynamic stability of certain species and determine the regions of various corrosion behaviour of materials [Anderko, 2010; Kaesche, 2003; McCafferty, 2010;

Revie, Uhlig, 2008; Schon, Heidendael, 1998; Uhlig's Corrosion Handbook, 2011]. There are four possible regions:

a) Domain of immunity. In this region all solid components of the system are immune (thermodynamically stable) to corrosion;

b) Domain of active dissolution. In this region various cations in a solution are thermodynamically stable. The material exhibits active dissolution;

c) Domain of passivity. In this region various solid oxides or hydroxides, hydrides, nitrides, sulphides or other solid products are thermodynamically stable. The protective layer consisting of these solid compounds is usually formed on the surface on the material, which prevents its further reaction. The material is passivated. If a multicomponent system is considered, some components in certain conditions might form an oxide layer, whereas for other ones the active dissolution might be thermodynamically favourable. In this case the overall behaviour of the system depends on the ability of the layer to prevent diffusion of the aggressive media through it. In a case, when diffusion is restrained, the material is passivated, otherwise, a selective dissolution of some components might occur;

d) Domain of transpassivity. In this region the protective layer is oxidised further with the formation of anions in a solution. The integrity of the passivation film is violated, and the pitting corrosion occurs.

The domains of various corrosion-electrochemical behaviour of the hypothetical metal Me are illustrated in Figure 7.

Pourbaix diagrams found the application in studying corrosion properties of pure metals, steels and alloys [Anderko, Sanders, Young, 1997; Banaś et al., 2007; Binder, Graff, 1995; Bombara, Baudo, Tamba, 1968; Craig, 2013; Davoodi et al., 2011; Davoodi, Babaiee, Pakshir, 2013; Delahay, Pourbaix, Rysselberghe, 1951; Dhawale, 1993; Du, Zhang, Pourbaix, 2001; Eggert, Weichert, 2004; Eklund, 1974; Graedel, 1992; Hazlewood, Singh, Hsieh, 2006; Hemmingsen, Fusek, Skavås, 2006; Hemmingsen, Lima, 1998; Henríquez, 2005; Hermansson, 2004; Horváth, Novák, 1964; Johansson, Vannerberg, 1981; Jones, Amy, 2000; Jones, Amy, 2002; Ko, Lichti, 2010; Larsen, Oil, Hilbert, 2014; Marcus, 1998; Marcus, 2011; Mattsson, 1961; McNeil, Jones, Little, 1991; McNeil, Little, 1999; McNeil, Mohr, 1992; McNeil, Mohr, 1993; Meyer et al., 1958; Minzari et al., 2011; Ning et al., 2014; Pourbaix, Aguiar, Clarinval, 1993; Pourbaix, 1987; Puigdomenech, Taxen, 2000; Rahmel, 1968; Refait et al., 2006; Salesse et al., 2007; Schmitt, 1991; Sequeira, Hocking, 1977; Sluys Van Der,

Emanuelson, 1986; Toedtemeir, Dandapani, Ghali, 1992; Tomio et al., 2014; Tyurin, Biryukov, 2012; Tyurin, Biryukov, 2013a; Tyurin et al., 2007; Tzvetkoff, Gencheva, 2003; White, Lichti, Bacon, 2000; Wiener et al., 2006; Modern Aspects of Electrochemistry No 10, 1975; Comprehensive Treatise of Electrochemistry. Volume 4: Electrochemical Materials Science, 1981], including corrosion in sulphuric media [Bombara, Baudo, Tamba, 1968; Dhawale, 1993; Du, Zhang, Pourbaix, 2001; Eklund, 1974; Hazlewood, Singh, Hsieh, 2006; Hemmingsen, Fusek, Skavås, 2006; Hemmingsen, Lima, 1998; McNeil, Mohr, 1992; Minzari et al., 2011; Puigdomenech, Taxen, 2000; Rahmel, 1968; Sequeira, Hocking, 1977; Sluys Van Der, Emanuelson, 1986; Toedtemeir, Dandapani, Ghali, 1992; Tyurin, Biryukov, 2012; Tyurin, Biryukov, 2013a], corrosion in presence of gaseous H_2S [Banaś et al., 2007; Davoodi et al., 2011; Davoodi, Babaiee, Pakshir, 2013; Meyer et al., 1958; Ning et al., 2014; Schmitt, 1991; Tomio et al., 2014; Tyurin et al., 2007; Wiener et al., 2006], atmospheric corrosion [Eggert, Weichert, 2004; Graedel, 1992; Hermansson, 2004; Johansson, Vannerberg, 1981], corrosion in geothermal and technological waters [Henríquez, 2005; Ko, Lichti, 2010; Larsen, Oil, Hilbert, 2014; Sluys Van Der, Emanuelson, 1986; White, Lichti, Bacon, 2000] and microbiologically influenced corrosion [Binder, Graff, 1995; Jones, Amy, 2000; Jones, Amy, 2002; McNeil, Jones, Little, 1991; McNeil, Little, 1999; Pourbaix, Aguiar, Clarinval, 1993; Refait et al., 2006]; in analytical chemistry [Bohn, Fenn, Moore, 1969; Buckley, Hamilton, Woods, 1987; Burgot, 2012; Dutta et al., 2009b; Hamilton, Woods, 1981; Lisak et al., 2010; Michałowska-Kaczmarczyk et al., 2015; Michałowska-Kaczmarczyk, Toporek, Michałowski, 2015; Mycroft et al., 1990; Sergeev, Shlyapunova, Pozdnyakova, 2007], in energy science and engineering [Bouroushian, 2010; Delahay, Pourbaix, Rysselberghe, 1951; Demir-Cakan et al., 2014; Holton, Stevenson, 2013; Pavlov, 2011; Prengaman, 2006; Sergeev, Shlyapunova, Pozdnyakova, 2007; Visco et al., 2014; Yokokawa et al., 2009; Yokokawa, Sakai, 1990], in studying processes of deposition of various sulphur-containing substances from solution [Ateya, AlKharafi, Al-Azab, 2003; Barnes, Kullerud, 1961; Chaparro, 2005; Hamilton, Woods, 1983; Mishra, 1989; Poisot-Díaz, González, Lapidus, 2008; Zhang, Singh, Muir, 2002], in geochemistry, mineral chemistry and environmental chemistry [Anderko, Shuler, 1997; Bohn, 1976; Brent Hiskey, Atluri, 2007; Brookins, 1986; Corry, 1985; Costa et al., 2009; Couture, Cappellen Van, 2011; Detournay et al., 1975; Dutta et al., 2009a; Firer, Friedler, Lahav, 2008; Fomchenko, Muravyov, 2014; Garrels, Naeser, 1958; Génin et al.,

1998; Génin et al., 2006; Génin et al., 1996; Huber, 1958; Hundal et al., 2012; Kelsall, Thompson, 1993; Kelsall, Thompson, Francis, 1993; KocabaĞ, 1992; Koch, 1975; Kounde, Raharinaivo, Olowe, 1989; Lichti, 2007; Livingston, 1991; Makgamatha, Mulaba-Bafubiandi, Adams, 2014; Molinero, Samper, 2006; Pourbaix, Pourbaix, 1992; Rodriguez-Freire et al., 2014; Sato, 1992; Seward, 1974; Simon, Génin, Refait, 1997; Thornber, 1975; Vitorge et al., 2007; W. Chesworth, A. Martínez Cortizas, E. García-Rodeja, 2006; Wang, Forssberg, Bolin, 1989; Woods, Young, Yoon, 1990; Woods, 1987; Zhang, 1994; Zhijian Wang et al., 2013; Thermodynamics in Geology, 1977], in studying processes of leaching of various compounds [Abbruzzese, 1990; Córdoba et al., 2008; Gök, 2014; Gudyanga et al., 1998; Hasab, Rashchi, Raygan, 2013; Mulaudzi, Mahlangu, 2009; Peters, 1976; Puente-Siller, Fuentes-Aceituno, Nava-Alonso, 2013; Rumpold, Antrekowitsch, 2012], in metallurgy [Anderson, Twidwell, 2008; Forsén, Aromaa, 2013; Larsen, Linkson, 1993; Majima, 1969; McCormick, Dayananda, Grace, 1975; Tan, Rolia, 1985; Tukel, Kelebek, Yalcin, 2010; Warren, Drouven, Price, 1984], in water treatment [Angelis de et al., 2010; Espinoza, Escudero, Tavera, 2012; Hem, 1972; Hem, Durum, 1973; Parent, Crabtree, Brudvig, 2013; Sanlı, Aytaç, Mat, 2014], in studying processes on phase boundaries and surfaces [Dewitt, Mesmaeker, 1983; Kalinkin et al., 2000; Marcus, Protopopoff, 1990; Marcus, Protopopoff, 1993; Marcus, Protopopoff, 1997a; Marcus, Protopopoff, 1997b; Pandit, Keswani, 2007; Protopopoff, Marcus, 2003; Protopopoff, Marcus, 2012], in chemical education [Angus, Angus, 1985; Angus, Zappia, 1987b; Campbell, Whiteker, 1969; Delahay, Pourbaix, Rysselberghe Van, 1950; El-Raghy, El-Demerdash, 1989; Hem, Stumm, 1961; Lewis, 1971a; Pourbaix et al., 1986; Yokokawa, Kawada, Makajuki D, 1989; Zappia, 1990; Zappia, Angus, Yung, 1989] and in other fields [Biernat, Robins, 1969; Biernat, Robins, 1972; Bouet, Brenet, 1963; Canut Le, Maximovitch, Dalard, 2004; Chen et al., 2002; Deschênes, Ghali, 1988; Escudero, Espinoza, Tavera, 2013; Fränzle, Markert, Wünschmann, 2005; Ghali, Toedtemeier, Dandapani, 1984; Hemmingsen, 1992; Herman et al., 1997; Hongyu, 1995; Horvath, Hackl, 1965; Kishimoto et al., 2010; Lasebikan et al., 2011; Macdonald, Hyne, 1979; Murray, Cubicciotti, 1983; Ness, 1967; Nila, González, 1995; Piet Lens, 2000; Pourbaix, Marquez Jacone, 1988; Pourbaix, 1984; Pourbaix, Zhang, 1988; Qingfeng et al., 1997; Qingfeng, Xiaoping, Xiulin, 2004; Robozerov, Zykov, Gavrikova, 2000; Sandström, Jalilehvand, Persson, 2002; Sheets et al., 2007; Smith, Miller, 1975; Sourisseau, Chauveau, Baroux, 2005; Stampler et al., 2008; Tunnicliffe, Mohammadi, Alfantazi,

2012; Tyurin, Biryukov, 2013b; Valenzuela, Valenzuela, Parga, 2013; Wadsley, 1992; Warner, Rice, Taylor, 1996; Young, Dahlgren, Robins, 2003; Zhou et al., 2011b].

2.6. Possible extensions of potential – pH diagrams

Classical potential – pH diagrams are the basis for many other types of diagrams [Anderko, Sanders, Young, 1997; Angus, Zappia, 1987a; Bryzgalin, 1989; Fishtik, 2006; Huang, 2016; Kurov, 2001; Kurov, 2013; Kurov, 2007; Lewis, 1971a; Liu, Zhang, 2001; Marcus, 1998; Rahmel, 1968; Rojas-Hernández et al., 1991; Tzvetkoff, Gencheva, 2003; Wong, 1980; Yokokawa, Sakai, 1990]. The complete overview of possible Pourbaix diagrams extensions falls outside the scope of this work. However, a few most common and obvious cases are considered here.

a) Non-stoichiometric compounds.

In accordance with the equations (27) and (28), all common chemical and electrochemical equilibria in aqueous solutions are presented at the (E; pH) surface as the straight lines. However, if any compound of variable composition with noticeable homogeneity range comes into play, equations (27) and (28) also become dependent on this variable composition, and the corresponding lines on the diagram become curved.

The examples of non-stoichiometry in Pourbaix diagrams are presented in Chapters 4, 13 and 14.

b) Active solution species.

Common Pourbaix diagrams present the chemical and electrochemical reactions of metals in pure water only. Only H^+ (aq), OH^- (aq) and H_2O (l) are considered as external species. However, these diagrams are of a purely academic interest only and have a little practical importance. When the potential – pH diagram is plotted in order to predict the corrosion-electrochemical behaviour of a metal in the specific aqueous environment, active solution species that could form various complexes and insoluble compounds with this metal should be considered [Salhi, 2005].

Usually, any complex potential – pH diagram is a superposition of many simple diagrams of corresponding system compounds. However, the equilibria related to the formation of various complex ions and insoluble precipitates should be added to this plot. Moreover, the possible oxidation and reduction of the complexation agent should not be forgotten, and the

formation of species with different oxidation state of the complexation agent should be also considered.

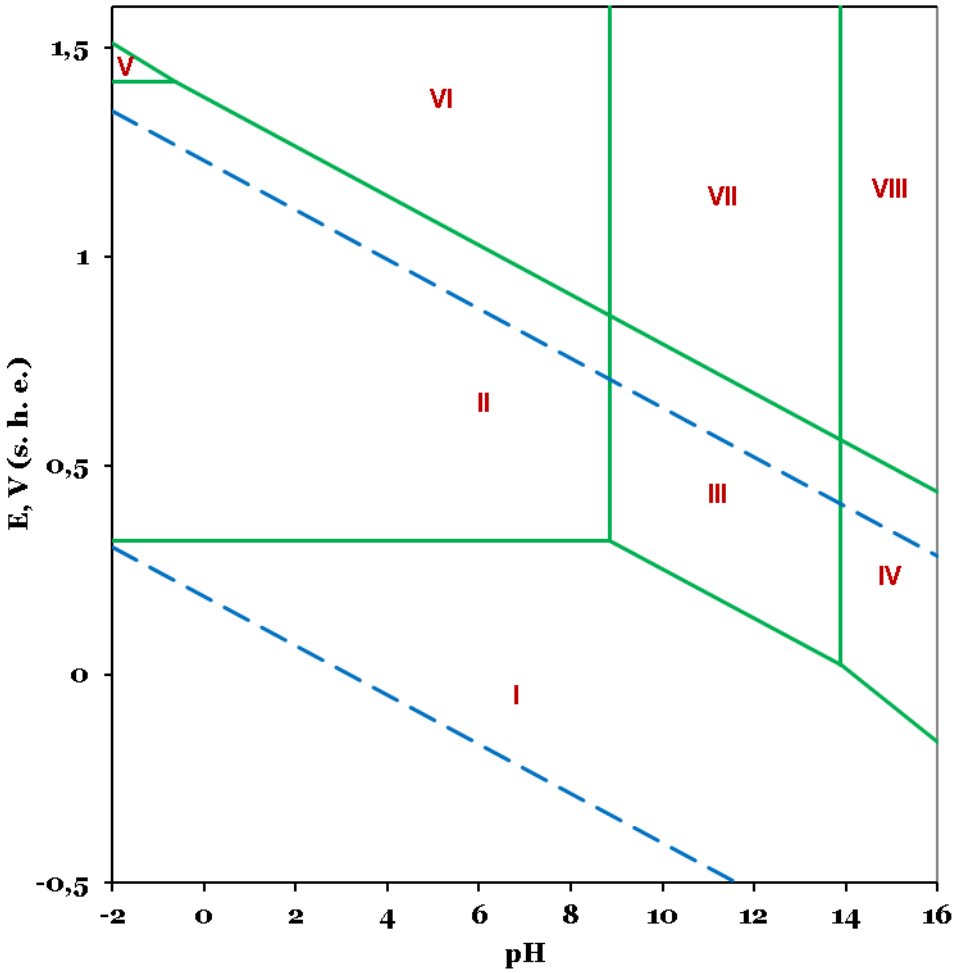

Fig. 6. The potential – pH diagram for Hg – Cl_2 – H_2O system. The domains of thermodynamic stability: I – Hg (l) + Cl^- (aq); II – Hg^{2+} (aq), $[HgCl]^+$ (aq), $[HgCl_2]$ (aq), $[HgCl_3]^-$ (aq), $[HgCl_4]^{2-}$ (aq), Cl^- (aq); III – $[Hg(OH)_2]$ (aq), Cl^- (aq); IV – $[Hg(OH)_3]^-$ (aq), Cl^- (aq); V – Hg^{2+} (aq), $[HgCl]^+$ (aq), $[HgCl_2]$ (aq), $[HgCl_3]^-$ (aq), $[HgCl_4]^{2-}$ (aq), Cl_2 (aq); VI – Hg^{2+} (aq), $[HgCl]^+$ (aq), $[HgCl_2]$ (aq), $[HgCl_3]^-$ (aq), $[HgCl_4]^{2-}$ (aq), ClO_4^- (aq); VII – $[Hg(OH)_2]$ (aq), ClO_4^- (aq); VIII – $[Hg(OH)_3]^-$ (aq), ClO_4^- (aq).

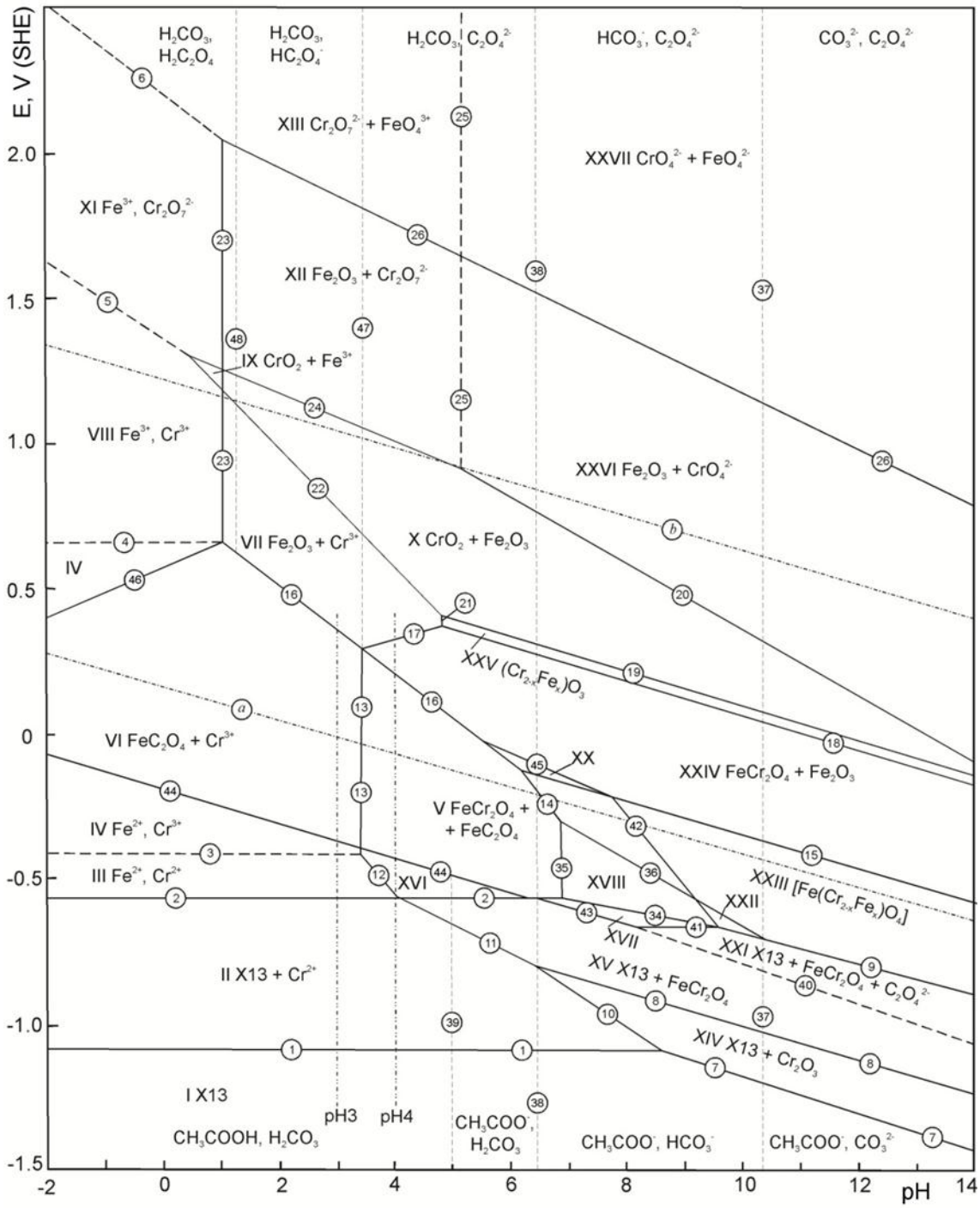

Fig. 7. The potential – pH diagram for steel X12 – CH_3COOH – CO_2 (g) – H_2O system.

As the first example, Figure 6 presents the potential – pH diagram of mercury in presence of chlorides. In addition to common mercuric and mercurious ions, the complex ions $[HgCl]^+$ (aq), $[HgCl_3]^-$ (aq) and $[HgCl_4]^{2-}$ (aq), as well as chlorate-ions and elemental chlorine were taken into consideration.

As the second example, Figure 7 presents the potential – pH diagram of chromium steel X13 in the presence of acetic acid and carbon dioxide. The diagram includes not only acetates, but also carbonates and oxalates as the possible products of oxidation and reduction.

c) Alloys.

The potential diagram for any alloy is usually also a superposition of many diagrams for its metallic components. However, an attention should be paid to some details. First, the activities of alloy components evidently differ from unity. This affects the position of some lines depicting equilibria with these metals. Next, the mixed oxides of two or more metals might exist in the system, and the corresponding equilibria should be also introduced. Last, the oxides of different metals might also have a mutual solubility that should also not be ignored.

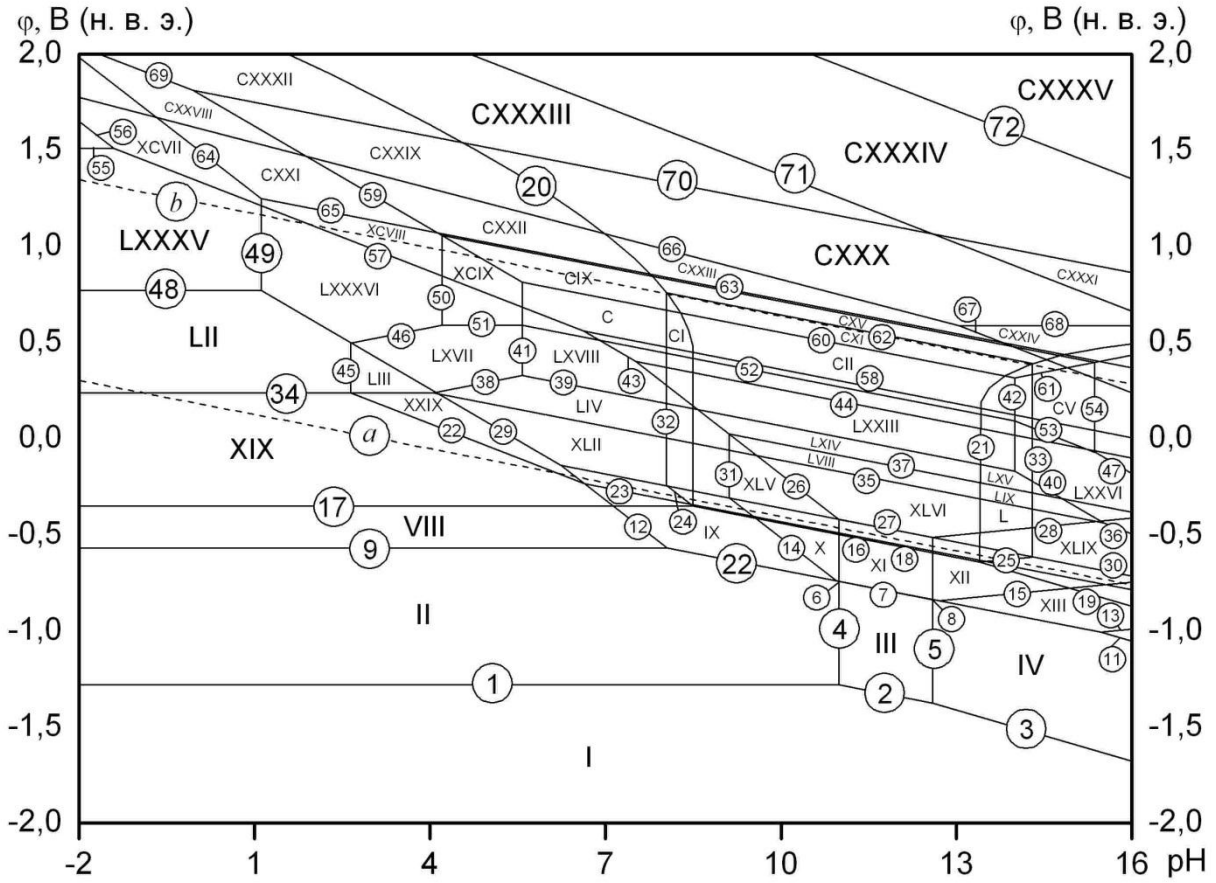

Fig. 8. The potential – pH diagram for melchior МНЖМц30–1–1 – H_2O system. The domains of thermodynamic stability are discussed in the attached publication.

As the example, Figure 8 presents the potential – pH diagram for a melchior МНЖМц30–1–1, containing (by weight) 30% nickel, 1% of iron,

1% of manganese and the rest of copper. Here the lines presenting the equilibria with metals are affected by the activities of these metals; the diagram takes into account the mixed oxides $NiFe_2O_4$, $MnFe_2O_4$, $CuFe_2O_4$ and $CuFeO_2$, and the solubility between Fe_3O_4, $NiFe_2O_4$, $MnFe_2O_4$ and $CuFe_2O_4$ and between $Fe2O_3$ and Mn_2O_3.

d) Third dimension in diagrams.

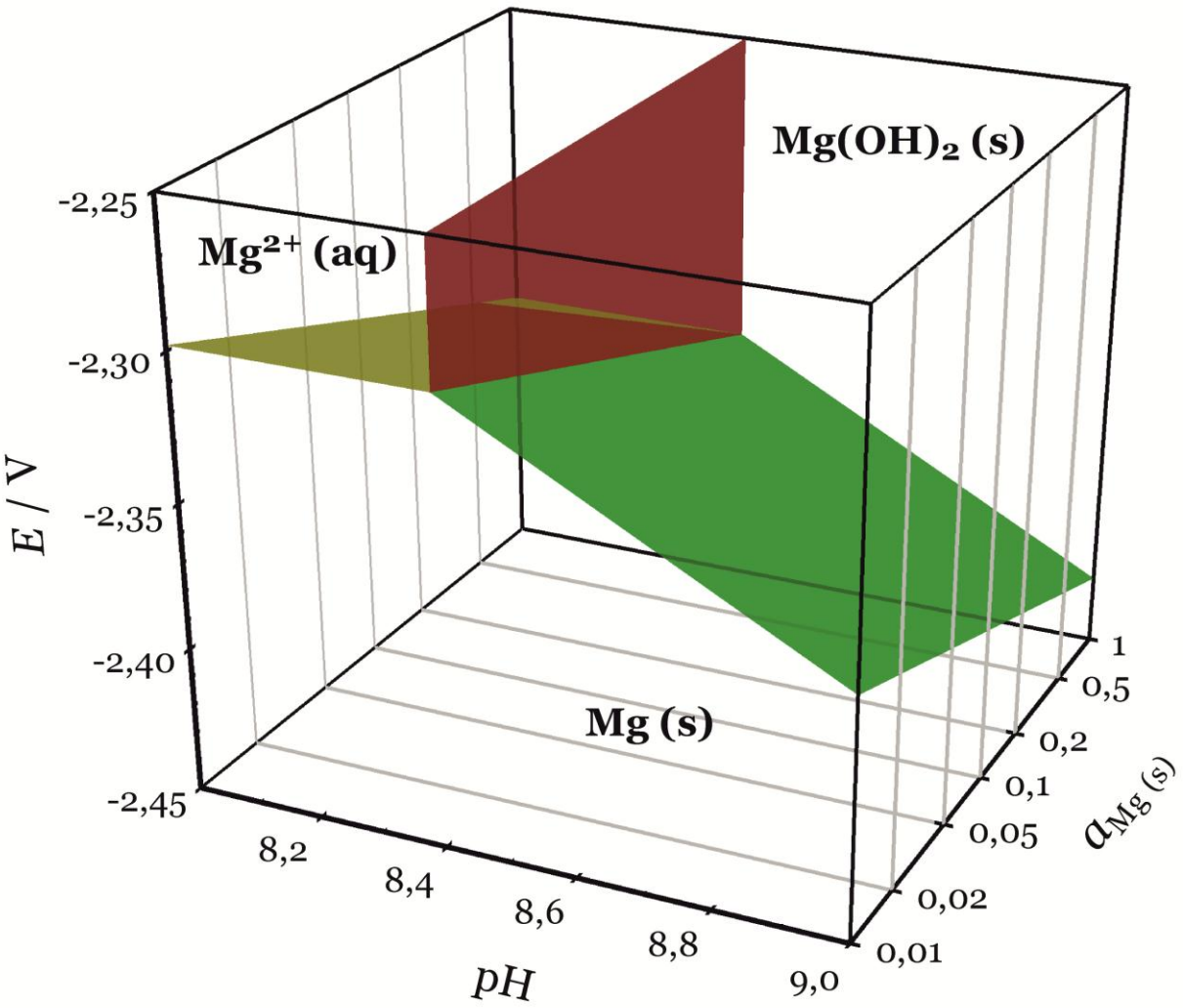

Fig. 9. The potential – pH diagram for Mg – H_2O system at the various activities of Mg (s).

As the equations (27) and (28) show, all equilibria in a solution depend on activities of aqueous species. Moreover, as it was demonstrated in the Section 2.4, the activities determine even the possible presence or absence of some species in the potential – pH diagram. Generally, both activity – pH and potential – pH diagrams are two-dimensional cross-sections of the three-dimensional (E; pH; a_i) space. It is, therefore, obvious

that several attempts to plot the complete three-dimensional (E; pH; a_i) diagrams were performed in the last six decades [Huang, 2016; Pesterfield et al., 2012; Sillen, 1952]. Most of these attempts, however, dealt only with the variation of activities of the aqueous species. The activities of solid species might (although, formally) also be varied in this type of diagrams, for instance, in order to show, how the metal in the metastable crystal structure or the metal from an alloy might affect the equilibria.

Exempli gratia, Figure 9 shows the three-dimensional Pourbaix diagram for magnesium, in which the activities of a solid magnesium are varied.

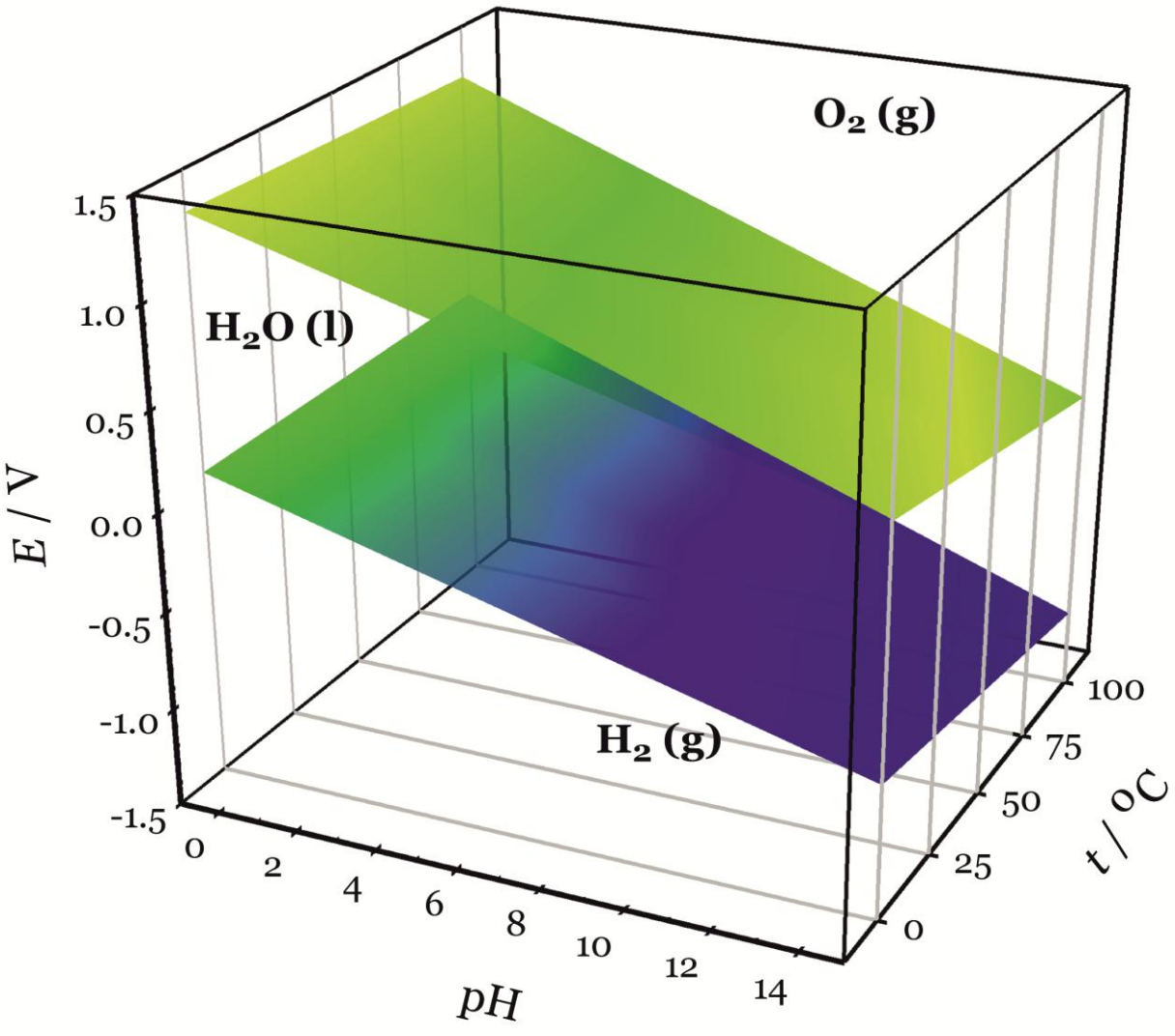

Fig. 10. The potential – pH diagram for water at various temperatures.

The E – pH – a_i diagram is not the only possible variant of applying the third axis in the Pourbaix plot. The dependence of half-cell reaction electrode potential on temperature is expressed as:

$$E_T^o = E_{298,15}^o + (T - 298,15) \cdot \left(\frac{dE^o}{dT}\right)_{298,15} + \frac{(T - 298,15)^2}{2} \cdot \left(\frac{d^2E^o}{dT^2}\right)_{298,15}, \quad (51)$$

where $\left(\frac{dE^o}{dT}\right)_{298,15}$ and $\left(\frac{d^2E^o}{dT^2}\right)_{298,15}$ are, respectively, the first and the second electrode potential temperature coefficients [Bethune de, Licht, Swendeman, 1959; Bratsch, 1989; Salvi, Bethune De, 1961]. Therefore the position and the slope of lines in Pourbaix diagram depend on temperature. This way the E – pH – T diagrams might be introduced. For example the E – pH – T diagram for H_2O over the temperature range of stability of liquid water is presented in Figure 10.

2.7. Existing books, databases and software for plotting potential – pH diagrams

Since Pourbaix published his first „Atlas of electrochemical equilibria in aqueous solutions“ [Pourbaix, 1966], a couple of other books, overviewing the potential – pH diagrams of pure metals, were published [Brookins, 1988; Schweitzer, Pesterfield, 2010]. Moreover, there are several online services and software packages that provide the opportunity to plot the potential – pH diagrams automatically. The following web databases of Pourbaix diagrams [Takeno, 2005] are known: SUPCRT [Johnson, Oelkers, Helgeson, 1992a; SUPCRT / Prediction Central], JNC-TDB [Japan Nuclear Cycle Organization Thermodynamic Database] and ChemEQL [ChemEQL,], SGTE [SGTE E-pH Web], LLNL (integrated into GWB software) [The Geochemist's Workbench (GWB)], PhreePlot [PhreePlot], ZZ-HATCHES [ZZ HATCHES-20, Database for radiochemical modelling], THERMEXPERT [THERMEXPERT – Potential – pH diagram generator], Materials Project website [Materials Project Pourbaix Diagrams] and HYDRA (integrated with MEDUSA software [Chemical Equilibrium Diagrams] and based on SOLGASWATER [Eriksson, 1979] and HALTAFALL [Ingri et al., 1967] databases).

However, all these services are some type of the „black box“ for the users. One could not see and control the calculations; one could not select and change the thermodynamic data; and one could not add new components into the system. Therefore, the information from these sources was taken into account in this study, but the dedicated software „*EpHDiagrPlot*“ was created and used for plotting the complex potential – pH diagrams. The description of this software is given in Appendix A.

Publications to chapter 2

Four papers are provided as the supplementary information to Section 2.6. The first one [Nikolaychuk, 2016b] presents the detailed description of chemical and electrochemical equilibria in the Hg – Cl_2 – H_2O system and complements the diagram presented in Figure 6. The preprint of this paper is presented with the permission from *De Gryuter*.

The second one [Manannikov, Parshukov, Nikolaychuk, 2017] presents the potential – pH diagram of X13 steel in acetic environments and complements the diagram presented in Figure 7. The preprint of this paper is presented with the permission from *Grupo Tchê Química*. The Russian translation of the second publication was posted as a preprint on the website of the *Journal of Corrosion Science and Engineering* [Тюрин et al., 2016]. These two papers explain how anions in a solution influence on potential – pH digarams.

The third paper [Николайчук, Тюрин, 2012a] presents the potential – pH diagrams of copper – nickel alloys, explains how Pourbaix diagrams of multicomponents alloys could be constructed, and complements Figure 8. The preprint of this paper is presented with the permission from *Nauka / Interperiodica*. The English version of this paper was published in [Nikolaychuk, Tyurin, 2012a].

The last paper [Nikolaychuk, 2014b] presents the third axis in Pourbaix diagrams and complements Figures 9 and 10. The preprint of this paper is presented with the permission from *American Chemical Society*.

Is calomel truly a poison and what happens when it enters the human stomach?

A study from the thermodynamic viewpoint

Pavel Anatolyevich Nikolaychuk

Department of Analytical and Physical Chemistry, Chelyabinsk State University

Bratyev Kashirinykh Street, 129. Chelyabinsk. 454001. Russian Federation.

E-mail: npa@csu.ru.

Abstract: The chemical and electrochemical equilibria involving mercurous and mercuric chlorides in the conditions, corresponding to the human stomach environment, were studied from the point of view of chemical thermodynamics. The Gibbs free energies of formation of the various mercury and chlorine compounds, the equilibrium constants and the electrode potentials of reactions involving these compounds at 37 ºC were calculated. The potential – pH diagrams of Hg_2^{2+} – H_2O, Cl^- – H_2O and Hg_2^{2+} – Cl^- – H_2O systems were plotted. The question of how toxic is calomel when ingested, was discussed.

Keywords: calomel; mercury chlorides; human stomach; Pourbaix diagram; toxicity.

Running Title: What happens if calomel enters the human stomach?

Introduction

In his recent paper entitled „Mercury(I) chloride *in vivo* oxidation: a thermodynamic study“ Mousavi (2015) discussed the medical usage and the toxicity of mercurous and mercuric chlorides. He raised the hypothesis that when calomel enters the stomach, it will almost entirely be converted to $HgCl_2$. Then he presented the thermodynamic calculations that in the author's opinion „prove“ this hypothesis and assumed that Napoleon's death could had been caused by administering calomel into his body. Later he published another paper (Burke et al., 2015), in which he assumed the responsibility of the calomel ingestion for another historical death.

Unfortunately, the thermodynamic calculations performed by Mousavi (2015) are very tenuous and his conclusions are crude and premature. In fact, he only calculated the equilibrium constant for the reaction $2Hg_2^{2+}(aq) + 4H^+(aq) + O_2(g) \rightarrow 4Hg^{2+}(aq) + 2H_2O(l)$ at 37ºC using the van't Hoff isochore equation (van't Hoff, 1884), observed that it has the order-of-magnitude of 10^{19} and concluded that calomel in the human stomach would be completely converted to $HgCl_2$. However, such hypotheses can not be based only on the analysis of a single reaction! At least the possible side reactions and the alternative products of mercury (I) oxidation should be taken into consideration. The influence of concentration of the species on equilibrium conditions should also not be ignored. Therefore, this study aims to perform the more rigorous thermodynamic analysis of the mercury (I) oxidation in human stomach and to extend the approach given by Mousavi (2015).

Results and discussion

Thermodynamic data on aqueous mercury and chlorine compounds

Mercury in an aqueous environment can form the following species: Hg (aq), $Hg_2^{2+}(aq)$, Hg^{2+} (aq), $HgOH^+$ (aq), $Hg(OH)_2$ (aq) and $Hg(OH)_3^-(aq)$. The aqueous

species of chlorine are the following: Cl^- (aq), HCl (aq), Cl_2 (aq), ClO^- (aq), HClO (aq), ClO_2^- (aq), $HClO_2$ (aq), ClO_2 (aq), ClO_3^- (aq), $HClO_3$ (aq), ClO_4^- (aq) and $HClO_4$ (aq). Mercury (II) can form not only the chloride $HgCl_2$ (aq), but also the cation $HgCl^+$ (aq) and the anions $HgCl_3^-$ (aq) and $HgCl_4^{2-}$ (aq). In addition, the solid Hg_2Cl_2 and HgO, the liquid Hg and H_2O, the gaseous H_2, O_2 and Cl_2 and the aqueous H^+ and OH^- can be present in the system (Schweitzer and Pesterfield, 2010).

The average temperature inside the stomach is equal to the human core body temperature of 37.6°C (Cagnacci, 1997; Houdas and Ring, 2013). The gastric fluid consists primarily of HCl (Prout, 1824; Davies, 1951), which average concentration is about 0.5% or 0.14 mol l^{-1} (MacLean and Griffiths, 1928; Ash, 2011). Sodium and potassium chlorides are also present in the gastric fluid (Hollander, 1952; Torosov, 1966), which raises the average concentration of chloride ions in the stomach up to 0.2 mol l^{-1} (Lee, Code and Scholer, 1955; Strong, Cameron and Riddell, 1960; Mößeler et al., 2010). The gastric gas present in the stomach includes up to 16% of oxygen (Dunn and Thompson, 1923; Kanner and Lapidot, 2001; Forth and Adam, 2001) and no more than $3 \cdot 10^{-6}$ % of hydrogen (Borgeskov et al., 1966; Urita et al., 2006).

The standard Gibbs energies and the standard enthalpies of formation of aforementioned mercury and chlorine compounds were collected from various sources (Wagman et al., 1982; Bard, Parsons and Jordan, 1985; Chase et al., 1998; Speight, 2005; Schweitzer and Pesterfield, 2010). Since the difference between the human core body temperature (310.75 K) and the reference temperature (298.15 K) is small, the enthalpies and entropies of formation may be treated as constant and independent of temperature, and the Gibbs energies of formation of compounds may be calculated according to Helmholtz – Gibbs equation (Helmholtz, 1882 and 1883) as follows:

$$\Delta_f G_{310.75} = \Delta_f H_{298.15} - 310.75 \cdot \Delta_f S_{298.15} = \Delta_f H_{298.15} - 310.75 \cdot \frac{\Delta_f H_{298.15} - \Delta_f G_{298.15}}{298.15} \quad (1).$$

The calculated values of $\Delta_f G_{310.75}$ are listed in Table 1.

Table 1. The Gibbs energies of formation of compounds in Hg_2^{2+} – Cl^- – H_2O system at 310.75 K and 1 bar.

Compound	$\Delta_f G_{310.75}$, J mol^{-1}	Compound	$\Delta_f G_{310.75}$, J mol^{-1}
Hg (l)	0	Cl_2 (g)	0
Hg (aq)	39370	Cl_2 (aq)	8220
Hg^{2+} (aq)	164120	ClO^- (aq)	42880
Hg_2^{2+} (aq)	152720	ClO_2 (aq)	122010
HgO (s)	–57050	ClO_2^- (aq)	20740
$HgOH^+$ (aq)	–50940	ClO_3^- (aq)	–3890
$Hg(OH)_2$ (aq)	–271400	ClO_4^- (aq)	–3410
$Hg(OH)_3^-$ (aq)	–427200	HCl (aq)	–129710
$HgCl^+$ (aq)	–4830	HClO (aq)	–78170
$HgCl_2$ (aq)	–171380	$HClO_2$ (aq)	8340
$HgCl_3^-$ (aq)	–305740	O_2 (g)	0
$HgCl_4^{2-}$ (aq)	–442270	H_2 (g)	0
Hg_2Cl_2 (s)	–208440	OH^- (aq)	–154150
Cl^- (aq)	–129710	H_2O (l)	–235070

The ionic strength of the intestinal solution is determined by the concentration of the chlorides, and the assumption was made that it is equal to 0.2 mol l^{-1}. The activity coefficient of the chloride ion was calculated according to the extended Debye – Hückel equation (Debye and Hückel, 1923). The values of the effective radii of the ions were taken from the paper of Kielland (1937) and the value of dielectric constant of water at

310.75 K needed for calculation of the parameters in Debye – Hückel equation was collected from the papers of Coolidge (1899), Wyman (1930) and Malmberg and Maryott (1956). The calculated value of the activity coefficient equals 0.610, leading to $a_{\mathrm{Cl}^-\,(\mathrm{aq})} = 0.122$ mol l^{-1}. The concentration of mercurous ions in the stomach is determined by the maximum solubility of solid calomel at 310.75 K and equals $1.2 \cdot 10^{-6}$ mol l^{-1}. At such a low concentrations the solution can be treated as the ideal one, and the activity is assumed equal to concentration. Since the concentrations of the other mercury and chlorine ions that can be formed from $\mathrm{Hg_2^{2+}}$ (produced by calomel) and $\mathrm{Cl^-}$ (from the gastric fluid) can not exceed the concentrations of these two ions, the assumption was made and used in further calculations that the activities of all chlorine ions are equal to 0.1 mol l^{-1}, and the activities of all mercury ions except those, containing both mercury and chlorine, are equal to 10^{-6} mol l^{-1}. Liquid mercury is a pure substance and its activity is equal to unity.

The equilibria, involving mercuric and chloride ions

The interaction of $\mathrm{Hg^{2+}}$ with $\mathrm{Cl^-}$ may result in the following reactions:

$$\mathrm{Hg^{2+}\,(aq) + Cl^-\,(aq) \rightleftharpoons HgCl^+\,(aq)} \quad (2),$$

$$\mathrm{HgCl^+\,(aq) + Cl^-\,(aq) \rightleftharpoons HgCl_2\,(aq)} \quad (3),$$

$$\mathrm{HgCl_2\,(aq) + Cl^-\,(aq) \rightleftharpoons HgCl_3^-\,(aq)} \quad (4),$$

$$\mathrm{HgCl_3^-\,(aq) + Cl^-\,(aq) \rightleftharpoons HgCl_4^{2-}\,(aq)} \quad (5).$$

The values of equilibrium constants of the reactions (2) – (5) at 310.75 K were calculated from the values of the Gibbs energies of formation of compounds using van't Hoff isotherm equation (van't Hoff, 1884). The following values were obtained: $K_{(2)}$ = 3944847 l mol^{-1}, $K_{(3)}$ = 1554731 l mol^{-1}, $K_{(4)}$ = 6.0433 l mol^{-1} and $K_{(5)}$ = 14.0301 l mol^{-1}. The values of thermodynamic activities of the ions are related to each other with the expressions of equilibrium constants and the equation of the material balance:

$$\frac{a_{HgCl^+\,(aq)}}{a_{Hg^{2+}\,(aq)} \cdot a_{Cl^-\,(aq)}} = 3944847\ \text{mol l}^{-1} \quad (6),$$

$$\frac{a_{HgCl_2\,(aq)}}{a_{HgCl^+\,(aq)} \cdot a_{Cl^-\,(aq)}} = 1554731\ \text{mol l}^{-1} \quad (7),$$

$$\frac{a_{HgCl_3^-\,(aq)}}{a_{HgCl_2\,(aq)} \cdot a_{Cl^-\,(aq)}} = 6.0433\ \text{mol l}^{-1} \quad (8),$$

$$\frac{a_{HgCl_4^{2-}\,(aq)}}{a_{HgCl_3^-\,(aq)} \cdot a_{Cl^-\,(aq)}} = 14.0301\ \text{mol l}^{-1} \quad (9),$$

$$a_{Hg^{2+}\,(aq)} + a_{HgCl^+\,(aq)} + a_{HgCl_2\,(aq)} + a_{HgCl_3^-\,(aq)} + a_{HgCl_4^{2-}\,(aq)} = 10^{-6}\ \text{l mol}^{-1} \quad (10).$$

After substituting the condition a_{Cl^-} = 0.1 mol l^{-1} into the equations (6) – (10) they transfer to the system of five equations with five variables, which have the unambiguous solution: $a_{Hg^{2+}\,(aq)} = 6.649 \cdot 10^{-18}$ mol l^{-1}, $a_{HgCl^+\,(aq)} = 2.623 \cdot 10^{-12}$ mol l^{-1}, $a_{HgCl_2\,(aq)} = 4.078 \cdot 10^{-7}$ mol l^{-1}, $a_{HgCl_3^-\,(aq)} = 2.464 \cdot 10^{-7}$ mol l^{-1} and $a_{HgCl_4^{2-}\,(aq)} = 3.458 \cdot 10^{-7}$ mol l^{-1}.

When the mercuric and the chloride ions coexist in a solution, the predominant forms of their existence are neutral $HgCl_2$ and the anions $HgCl_3^-$ and $HgCl_4^{2-}$ with approximately equal ratio between them. The cationic forms Hg^{2+} and $HgCl^+$ exist in a much smaller degree.

The equilibria in Hg_2^{2+} – H_2O and Cl^- – H_2O systems

The most compact way of presentation of the chemical and electrochemical equilibria in the aqueous redox systems is the potential – pH diagram, initially proposed by Pourbaix (1947 and 1963); Delahay, Pourbaix and van Rysselberghe (1950). The procedure of constructing the Pourbaix diagrams was described in detail several times; the most recent description was made by Schweitzer and Pesterfield (2010). The equations of electrochemical equilibria can be calculated using the Nernst equation (Nernst, 1887 and 1889), and the expression similar to Hendersson – Hasselbalch

equation (Hendersson, 1908; Hasselbalch, 1916) is used for calculating pH (Sørensen,1909a and 1909b) of chemical equilibria. The values of the Gibbs energies of formation of compounds from Table 1 were used in calculations.

The potential – pH diagram of Hg_2^{2+} – H_2O system at 310.75 K, 1 bar and $a_{[Hg]\,(aq)} = 10^{-6}$ mol l^{-1} is presented at Figure 1, and the potential – pH diagram of Cl^- – H_2O system at 310.75 K, 1 bar and $a_{[Cl](aq)} = 0.1$ mol l^{-1} is presented at Figure 2. The calculated characteristics of the chemical and electrochemical equilibria are listed in Table 2.

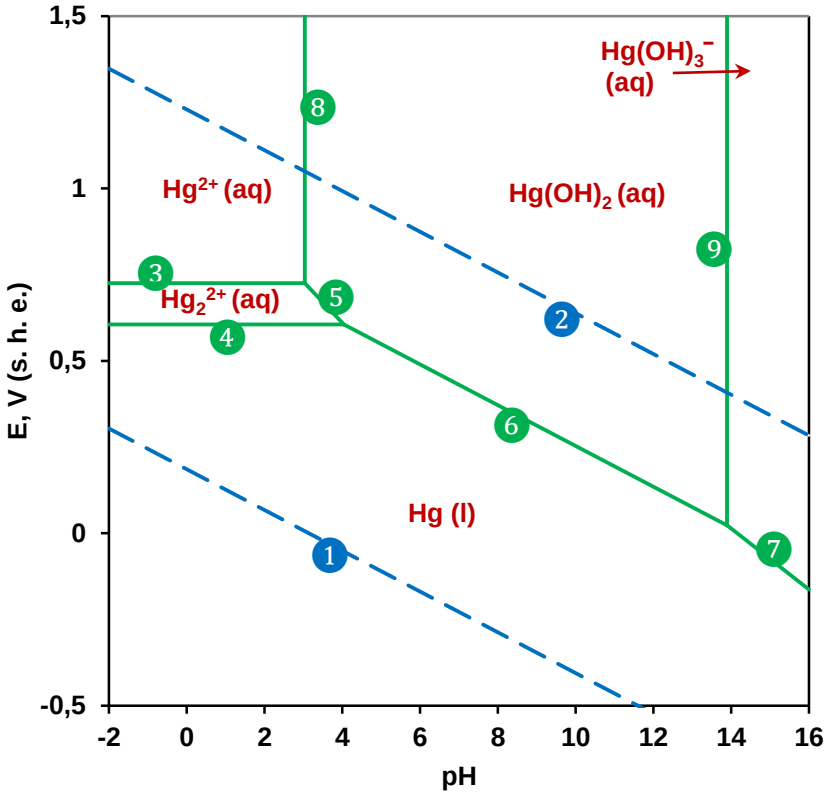

Figure 1. The potential – pH diagram of Hg_2^{2+} – H_2O system at 310.75 K and 1 bar

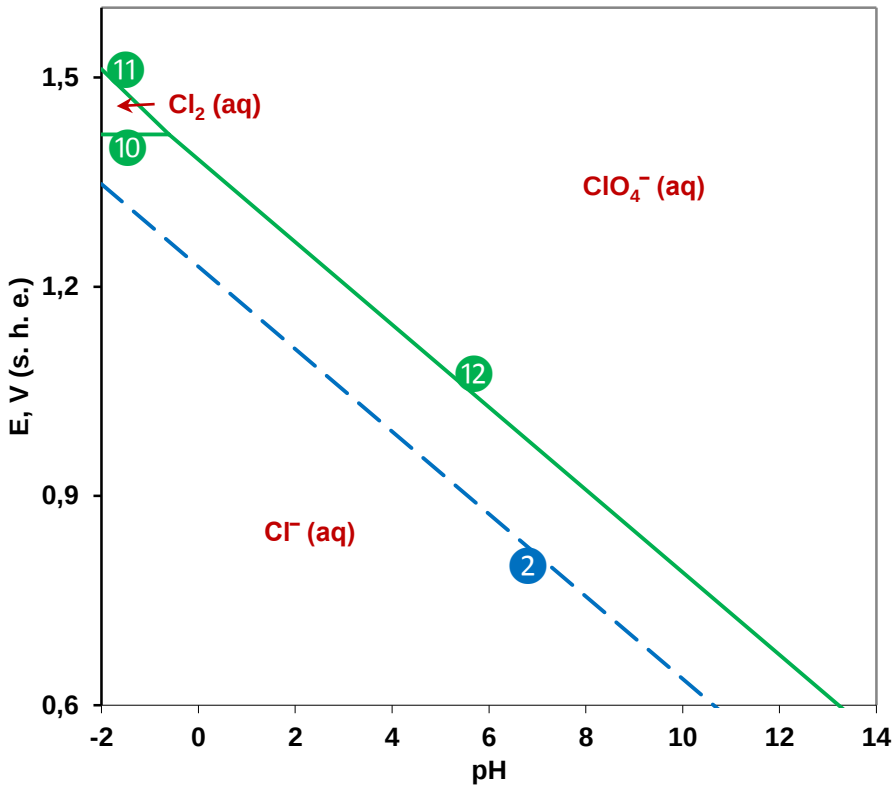

Figure 2. The potential – pH diagram of Cl^- – H_2O system at 310.75 K and 1 bar

The Pourbaix diagram for mercury shows that it can form both the mercurous and mercuric cations or be oxidised to aqueous $Hg(OH)_2$ or $Hg(OH)_3^-$, while aqueous $HgOH^+$ and solid HgO are thermodynamically unstable. The diagram for chlorine indicates that the only stable forms of chlorine in solution are the chloride- and the perchlorate-ion and the aqueous elemental chlorine.

The equilibria in Hg_2^{2+} – Cl^- – H_2O system

The method of constructing the potential – pH diagrams of the multielement systems is described by Thompson et al. (2011). The diagram of Hg_2^{2+} – Cl^- – H_2O system was constructed using the diagrams of Hg_2^{2+} – H_2O and Cl^- – H_2O systems and the data on the equilibria in Hg^{2+} – Cl^- system and presented at Figure 3. The calculated characteristics of the chemical and electrochemical equilibria are listed in

Table 2. The thermodynamic characteristics of basic chemical and electrochemical equilibria in Hg_2^{2+} – H_2O, Cl^- – H_2O and Hg_2^{2+} – Cl^- – H_2O systems at 310.75 K and 1 bar.

Line at Figures 1 – 3	Equilibrium reaction	Activities (a, mol l^{-1}) or partial pressures (p, bar) of the components	E, V (s. h. e.) or pH of the solution
1	$2H^+\,(aq) + 2e^- \rightleftharpoons H_2\,(g)$	$p_{H_2\,(g)} = 3 \cdot 10^{-6}$	$E = 0.170 - 0.0309 \cdot pH$
2	$O_2\,(g) + 4H^+\,(aq) + 4e^- \rightleftharpoons 2H_2O\,(l)$	$p_{O_2\,(g)} = 0.16;\ a_{H_2O\,(l)} = 1$	$E = 1.206 - 0.0309 \cdot pH$
3	$2Hg^{2+}\,(aq) + 2e^- \rightleftharpoons Hg_2^{2+}\,(aq)$	$a_{Hg^{2+}\,(aq)} = 10^{-6};\ a_{Hg_2^{2+}\,(aq)} = 10^{-6}$	$E = 0.725$
4	$Hg_2^{2+}\,(aq) + 2e^- \rightleftharpoons 2Hg\,(l)$	$a_{Hg_2^{2+}\,(aq)} = 10^{-6};\ a_{Hg\,(l)} = 1$	$E = 0.606$
5	$2Hg(OH)_2\,(aq) + 4H^+\,(aq) + 2e^- \rightleftharpoons Hg_2^{2+}\,(aq) + 4H_2O\,(l)$	$a_{Hg(OH)_2\,(aq)} = 10^{-6};\ a_{Hg_2^{2+}\,(aq)} = 10^{-6};$ $a_{H_2O\,(l)} = 1$	$E = 1.083 - 0.1234 \cdot pH$
6	$Hg(OH)_2\,(aq) + 2H^+\,(aq) + 2e^- \rightleftharpoons Hg\,(l) + 2H_2O\,(l)$	$a_{Hg(OH)_2\,(aq)} = 10^{-6};\ a_{Hg\,(l)} = 1;$ $a_{H_2O\,(l)} = 1$	$E = 0.845 - 0.0617 \cdot pH$
7	$Hg(OH)_3^-\,(aq) + 3H^+\,(aq) + 2e^- \rightleftharpoons Hg\,(l) + 3H_2O\,(l)$	$a_{Hg(OH)_3^-\,(aq)} = 10^{-6};\ a_{Hg\,(l)} = 1;$	$E = 1.256 - 0.0926 \cdot pH$

		$a_{H_2O\,(l)} = 1$	
8	$Hg(OH)_2\,(aq) + 2H^+\,(aq) \rightleftharpoons Hg^{2+}\,(aq) + 2H_2O\,(l)$	$a_{Hg(OH)_2\,(aq)} = 10^{-6};\ a_{Hg^{2+}\,(aq)} = 10^{-6};$ $a_{H_2O\,(l)} = 1$	$pH = 2.909$
9	$Hg(OH)_3^-\,(aq) + H^+\,(aq) \rightleftharpoons Hg(OH)_2\,(aq) + H_2O\,(l)$	$a_{Hg(OH)_3^-\,(aq)} = 10^{-6};$ $a_{Hg(OH)_2\,(aq)} = 10^{-6};\ a_{H_2O\,(l)} = 1$	$pH = 13.320$
10	$Cl_2\,(aq) + 2e^- \rightleftharpoons 2Cl^-\,(aq)$	$a_{Cl_2\,(aq)} = 0.1;\ a_{Cl^-\,(aq)} = 0.1$	$E = 1.418$
11	$2ClO_4^-\,(aq) + 16H^+\,(aq) + 14e^- \rightleftharpoons Cl_2\,(aq) + 8H_2O\,(l)$	$a_{ClO_4^-\,(aq)} = 0.1;\ a_{Cl_2\,(aq)} = 0.1;$ $a_{H_2O\,(l)} = 1$	$E = 1.377 - 0.0705 \cdot pH$
12	$ClO_4^-\,(aq) + 8H^+\,(aq) + 8e^- \rightleftharpoons Cl^-\,(aq) + 4H_2O\,(l)$	$a_{ClO_4^-\,(aq)} = 0.1;\ a_{Cl^-\,(aq)} = 0.1;$ $a_{H_2O\,(l)} = 1$	$E = 1.382 - 0.0617 \cdot pH$
13	$\begin{cases} Hg^{2+}\,(aq) + 2e^- \rightleftharpoons Hg\,(l) \\ HgCl^+\,(aq) + 2e^- \rightleftharpoons Hg\,(l) + Cl^-\,(aq) \\ HgCl_2\,(aq) + 2e^- \rightleftharpoons Hg\,(l) + 2Cl^-\,(aq) \\ HgCl_3^-\,(aq) + 2e^- \rightleftharpoons Hg\,(l) + 3Cl^-\,(aq) \\ HgCl_4^{2-}\,(aq) + 2e^- \rightleftharpoons Hg\,(l) + 4Cl^-\,(aq) \end{cases}$	$a_{Hg^{2+}\,(aq)} = 6.649 \cdot 10^{-18};$ $a_{HgCl^+\,(aq)} = 2.623 \cdot 10^{-12}\ ;$ $a_{HgCl_2\,(aq)} = 4.078 \cdot 10^{-7}\ ;$	$E = 0.321$

		$a_{HgCl_3^-\,(aq)} = 2.464 \cdot 10^{-7}$; $a_{HgCl_4^{2-}\,(aq)} = 3.458 \cdot 10^{-7}$; $a_{Cl^-\,(aq)} = 0.1$; $a_{Hg\,(l)} = 1$	
14	$\begin{cases} Hg(OH)_2\,(aq) + 2H^+\,(aq) \rightleftharpoons Hg^{2+}\,(aq) + 2H_2O\,(l) \\ Hg(OH)_2\,(aq) + 2H^+\,(aq) + Cl^-(aq) \rightleftharpoons HgCl^+\,(aq) + 2H_2O\,(l) \\ Hg(OH)_2\,(aq) + 2H^+\,(aq) + 2Cl^-\,(aq) \rightleftharpoons HgCl_2\,(aq) + 2H_2O\,(l) \\ Hg(OH)_2\,(aq) + 2H^+\,(aq) + 3Cl^-\,(aq) \rightleftharpoons HgCl_3^-\,(aq) + 2H_2O\,(l) \\ Hg(OH)_2\,(aq) + 2H^+\,(aq) + 4Cl^-\,(aq) \rightleftharpoons HgCl_4^{2-}\,(aq) + 2H_2O\,(l) \end{cases}$	$a_{Hg^{2+}\,(aq)} = 6.649 \cdot 10^{-18}$; $a_{HgCl^+\,(aq)} = 2.623 \cdot 10^{-12}$; $a_{HgCl_2\,(aq)} = 4.078 \cdot 10^{-7}$; $a_{HgCl_3^-\,(aq)} = 2.464 \cdot 10^{-7}$; $a_{HgCl_4^{2-}\,(aq)} = 3.458 \cdot 10^{-7}$; $a_{Cl^-\,(aq)} = 0.1$; $a_{Hg(OH)_2\,(aq)} = 10^{-6}$; $a_{H_2O\,(l)} = 1$	$pH = 8.496$

Table 2. The diagram shows that both the solid Hg_2Cl_2 and the aqueous Hg_2^{2+} have no domains of thermodynamic stability in presence of the chloride ions.

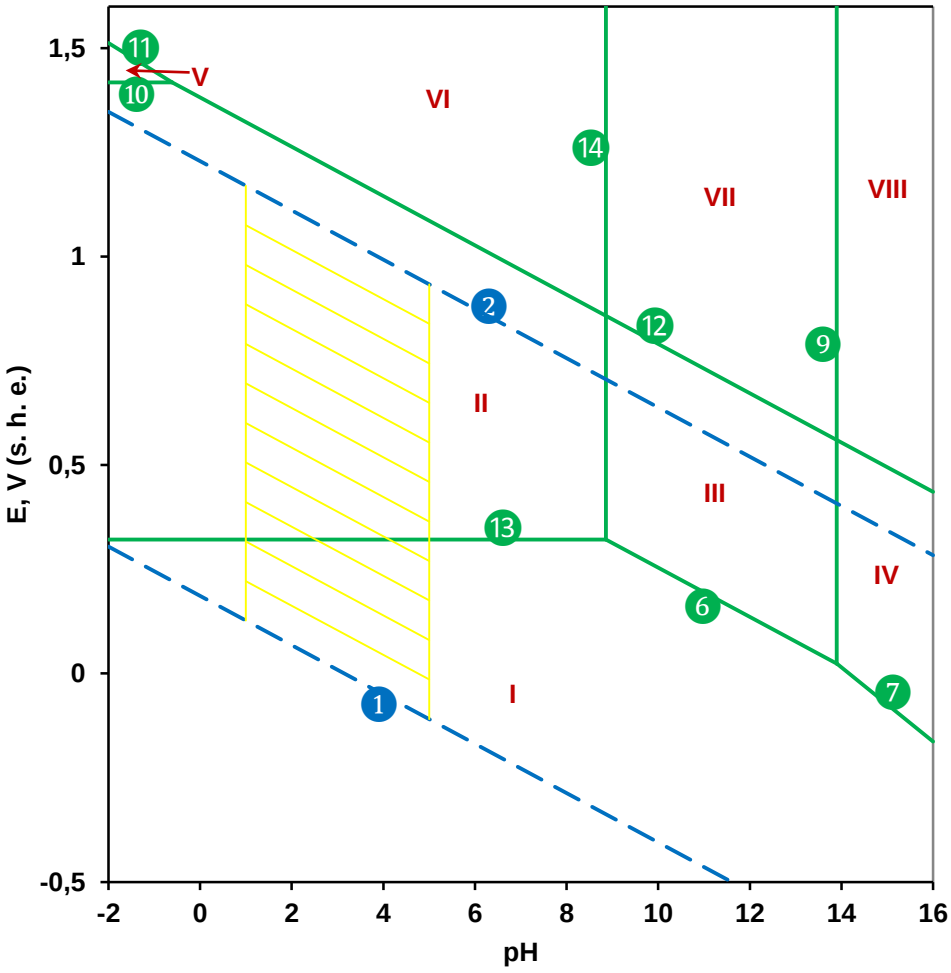

Figure 3. The potential – pH diagram of Hg_2^{2+} – Cl^- – H_2O system at 310.75 K and 1 bar. The domains of thermodynamic stability: I – Hg (l) + Cl^- (aq); II – Hg^{2+} (aq), $HgCl^+$ (aq), $HgCl_2$ (aq), $HgCl_3^-$ (aq), $HgCl_4^{2-}$ (aq), Cl^- (aq); III – $Hg(OH)_2$ (aq), Cl^- (aq); IV – $Hg(OH)_3^-$ (aq), Cl^- (aq); V – Hg^{2+} (aq), $HgCl^+$ (aq), $HgCl_2$ (aq), $HgCl_3^-$ (aq), $HgCl_4^{2-}$ (aq), Cl_2 (aq); VI – Hg^{2+} (aq), $HgCl^+$ (aq), $HgCl_2$ (aq), $HgCl_3^-$ (aq), $HgCl_4^{2-}$ (aq), ClO_4^- (aq); VII – $Hg(OH)_2$ (aq), ClO_4^- (aq); VIII – $Hg(OH)_3^-$ (aq), ClO_4^- (aq).

The dashed lines at the Figures 1 through 3, described by the equations 1 and 2 in Table 2, represent the equilibria corresponding to the hydrogen and the oxygen

electrodes in the human stomach environment. The domain between these lines corresponds to the area of the electrochemical stability of water.

Conclusion

The acidity in a human stomach varies from pH ≈ 1 to pH ≈ 5 depending on time of a day and the condition of the digestive tract (Kong and Singh, 2008a, 2008b and 2009; Beasley et al., 2015). This variety of environments is depicted at Figure 3 as the hatched area. As can be seen, either the mixture of Hg^{2+} (aq), $HgCl^{+}$ (aq), $HgCl_2$ (aq), $HgCl_3^-$ (aq), $HgCl_4^{2-}$ (aq) or the liquid mercury is thermodynamically stable in the gastric fluid environment depending on the equilibrium potential in the system. Therefore, the hypothesis raised by Mousavi (2015) is only a partial case. When the solid calomel enters the stomach, it will be oxidised to the various mercury (II) and chloride complexes or will be reduced to the liquid metallic mercury. Since the solubility of calomel is low, most probably only the small part of it dissolves and forms the mercuric compounds and the rest of it reduces to the metal. The liquid mercury is however relatively harmless (Saunders, 2008; Schmidt, 2013) because it quickly passes through the intestinal tract towards the rectum due to its high density. In the 18th and 19th centuries both solid calomel and liquid mercury were extensively used as the purgatives (Geffner and Sandler, 1980; Saunders, 2008). Moreover, calomel was used in medicine since the Dark Ages and till the 20th century very widely (Blair et al., 1720; Clay, 1841; Harrison, 1847; Jones, 1888; Beatty, 1899; Patwardhan et al, 2005; Clarkson and Magos, 2006; Schmid, 2008; Bachour, 2015; Gerke, 2015; Preckel, 2015; Sébastia, 2015; Thomann, 2015; Trambaiolo, 2015; Walker, 2015; Wujastik, 2015a and 2015b), and another mercury compound, cinnabar (HgS), which behaviour in the intestinal tract is very similar to that of calomel (Liu et al., 2008; Lu et al., 2011), is still widely used in traditional Chinese medicine (Wong and Koh, 1986; Chi et al., 1993; Espinoza, Mann

and Bleasdell, 1995; Bleasdell et al, 1996; Ernst and Coon, 2001; Wong, 2004; Liu et al., 2008; Lu et al., 2011; Zhang et al., 2012). If it had provided a significant lethal effect, it would have caused mass deaths and thus would been withdrawn from the medical usage very quickly. Indeed the mercury is extremely toxic in large doses (Kang-Yum and Oranski, 1992; Chan and Critchley, 1996; Ernst, 1998 and 2002; Langford and Ferner, 1999; Davis, 2000; Broussard et al., 2002; Clarkson and Magos, 2006; Wong, 2008; Byard, 2010; Keil, Berger-Ritchie and McMillin, 2011; Wu et al., 2013; Yu et al., 2015) and the modern medicine does not use it, however, the accurate and careful ingestion of calomel, as the patients did it two centuries ago, is not harmful.

An implication of calomel in the Napoleon's death is also questionable. Several studies of the specimens obtained from his hairs (Forshufvud, Smith and Wassén, 1964; Weider and Fournier, 1999 and 2000; Corso, Hindmarch and Stritto, 2000; Lin and Henkelmann, 2003; Keynes, 1994 and 2004; Lin, Alber and Henkelmann, 2004; Mari et al., 2004; Kinzt, Ginet and Cirimele, 2006) indicate that arsenicals rather than mercurials are most likely responsible for it. Probably, Mousavi (2015) overestimates the decisive effect of ingesting calomel on the poisoning and murdering in the history.

References

Ash, M. The Role of HCL In Gastric Function And Health. *Clinical Education*. **2011**. Available at http://www.clinicaleducation.org/resources/reviews/the-role-of-hcl-in-gastric-function-and-health (access date - 05. 02. 2016).

Bard, A. J.; Parsons, R.; Jordan, J. Standard potentials in aqueous solutions; New York: Marcel Dekker Inc., **1985**.

Bachour, N. *Healing with Mercury*: The Uses of Mercury in Arabic Medical Literature. *Asiatische Studien – Études Asiatiques: Zeitschrift der Schweizerischen Asiengesellschaft – Revue de la Société Suisse-Asie*. **2015**, *69(4)*, 831 – 866.

Beasley, D. E.; Koltz, A. M.; Lambert, J. E.; Fierer, N.; Dunn, R. R. The Evolution of Stomach Acidity and Its Relevance to the Human Microbiome. *PLoS ONE*. **2015**, *10(7)*, Article e0134116, 1 – 12. DOI:10.1371/journal.pone.0134116.

Beatty, W. Mercury in diseases of the heart. *Transactions of the Royal Academy of Medicine in Ireland*. **1899**, *17(1)*, 34 – 44.

Blair, P.; Jackson, J.; Bell, E.; Browne, C.; Anthone, G. A Discourse concerning a Method of Discovering the Virtues of Plants by Their External Structure. By the Same. *Philosophical Transactions of the Royal Society of London*. **1720 – 1721**, *31*, 30 – 38.

Bleasdell, B.; Espinoza, E. O.; Cox, M.; Mann, M. J.; DeKorte, S. Toxic metals in selected traditional Chinese medicinals. *Journal of Forensic Science*. **1996**, *41(3)*, 453 – 456.

Borgeskov, S.; Lockwood, K.; Bertelsen, S.; Hasner, E. Simultaneous pressure and hydrogen ion measurements in the esophagus and stomach. A preliminary report. *Acta Chirurgica Scandinavica. Supplementum*. **1966**, *356B*, 105 – 112.

Broussard, L. A.; Hammett-Stabler, C. A.; Winecker, R. E.; Ropero-Miller, J. D. The Toxicology of Mercury. *Lab Medicine*. **2002**, *33(8)*, 614 – 625.

Burke, N.; Golas, M.; Raafat, C. L.; Mousavi, A. A forensic hypothesis for the mystery of al-Hasan's death in the 7th century: Mercury(I) chloride intoxication. *Medicine, Science and the Law*. **2015**, published ahead of print; DOI: 10.1177/0025802415601456.

Byard, R. W. A Review of the Potential Forensic Significance of Traditional Herbal Medicines. *Journal of Forensic Sciences*. **2010**, *55(1)*, 89 – 92.

Cagnacci, A.; Kräuchi, K.; Wirz-Justice, A.; Volpe, A. Homeostatic versus Circadian Effects of Melatonin on Core Body Temperature in Humans. *Journal of Biological Rhythms*. **1997**, *12(6)*, 509 – 517.

Chan, T. Y.; Critchley, J. A. Usage and adverse effects of Chinese herbal medicines. *Human & experimental toxicology*. **1996**, *15(1)*, 5 – 12.

Chase, M. W. Jr.; Davies, C. A.; Downey, J. R. Jr.; Frurip, D. J.; McDonald, R. A.; Syverud, A. N. JANAF – NIST Thermochemical Tables. 4th Edition. *Journal of Physical and Chemical Reference Data*. **1998**. Monograph 9. Available online at http://kinetics.nist.gov/janaf/janaf4pdf.html (access date - 05. 02. 2016).

Chi, Y. W.; Chen, S. L.; Yang, M. H.; Hwang, R. C.; Chu, M. L. Heavy metals in traditional Chinese medicine: ba-pao-neu-hwang-san. *Zhonghua Minguo Xiao er ke yi xue hui za zhi*. **1993**, *34(3)*, 181 – 190.

Clarkson, T. W.; Magos, L. The Toxicology of Mercury and Its Chemical Compounds. *Critical Reviews in Toxicology*. **2006**, *36(8)*, 609 – 662.

Clay, C. On the exhibition of small doses of mercury in effecting ptyalism. *The Lancet*. **1841**, *2(938)*, 751 – 753.

Coolidge, W. D. Dielektrische Untersuchungen und elektrische Drahtwellen. *Wiedemann's Annalen der Physik und Chemie*. **1899**, *69(9)*, 123 – 166.

Corso, P. F.; Hindmarsh, J. T.; Stritto, F. D. The death of Napoleon. *The American Journal of Forensic Medicine and Pathology*. **2000**, *21(3)*, 300 – 303.

Davies, R. E. The mechanism of hydrochloric production by the stomach. *Biological Reviews*. **1951**, *26(1)*, 87 – 120.

Davis, L. E. Unregulated potions still cause mercury poisoning. *Western Journal of Medicine*. **2000**, *173(1)*, 19.

Debye, P.; Hückel, E. Zur Theorie der Elektrolyte. I. Gefrierpunktserniedrigung und verwandte Erscheinungen. *Physikalische Zeitschrift*. **1923**, *24*, 185 – 206.

Delahay, P.; Pourbaix, M.; van Rysselberghe, P. Potential – pH diagrams. *Journal of Chemical Education*. **1950**, *27(12)*, 683 – 688.

Dunn, A. D.; Thompson, W. The carbon dioxid and oxygen content of stomach gas in normal persons. *Archives of Internal Medicine*. **1923**, *31(1)*, 1 – 8.

Ernst, E. Harmless Herbs? A Review of the Recent Literature. *The American Journal of Medicine*. **1998**, *104(2)*, 170 – 178.

Ernst, E. Toxic heavy metals and undeclared drugs in Asian herbal medicines. *Trends in Pharmacological Sciences*. **2002**, *23(3)*, 136 – 139.

Ernst, E.; Coon, J. T. Heavy metals in traditional Chinese medicines: a systematic review. *Clinical Pharmacology & Therapeutics*. **2001**, *70(6)*, 497 – 504.

Espinoza, E. O.; Mann, M.-J.; Bleasdell, B. Arsenic and Mercury in Traditional Chinese Herbal Balls. *The New England Journal of Medicine*. **1995**, *333*, 803 – 804.

Forshufvud, S.; Smith, H.; Wassén, A. Napoleon's illness 1816–1821 in the light of activation analyses of hairs from various dates. *Archiv für Toxikologie*. **1964**, *20(4)*, 210 – 219.

Forth, W; Adam, O. Uptake of oxygen from the intestine – experiments with rabbits. *European Journal of Medical Research*. **2001**, *6(1)*, 488 – 492.

Geffner, M. E.; Sandler, A. Oral metallic mercury. A folk medicine remedy for gastroenteritis. *Clinical Pediatrics*. **1980**, *19(6)*, 435 – 437.

Gerke, B. Biographies and Knowledge Transmission of Mercury Processing in Twentieth Century Tibet. *Asiatische Studien – Études Asiatiques: Zeitschrift der Schweizerischen Asiengesellschaft – Revue de la Société Suisse-Asie*. **2015**, *69(4)*, 867 – 899.

Harrison, J. B. Mercury as a Remedy. *The Boston Medical and Surgical Journal*. **1847**, *36(5)*, 101 – 102.

Hasselbalch, K. A. Die Berechnung der Wasserstoffzahl des Blutes aus der freien und gebundenen Kohlensäure desselben, und die Sauerstoffbindung des Blutes als Funktion der Wasserstoffzahl. *Biochemische Zeitschrift. Beiträge zur chemischen Physiologie und Pathologie*. **1917**, *78(1 – 2)*, 112 – 144.

Helmholtz, H. Die Thermodynamik chemischer Vorgänge. *Sitzungsberichte der Königlich Preußischen Akademie der Wissenschaften zu Berlin*. **1882**, 22 – 39, 825 – 836; **1883**, 647 – 665.

Henderson, L. J. Concerning the relationship between the strength of acids and their capacity to preserve neutrality. *American Journal of Physiology*. **1908**, *21(2)*, 173 – 179.

Hollander, F. Gastric secretion of electrolytes. *Federation Proceedings*. **1952**, *11(3)*, 706 – 714.

Houdas, Y.; Ring, E. F. J. Human Body Temperature: Its Measurement and Regulation; Amsterdam: Springer Science & Business Media, **2013**.

Jones, T. Mercury As A Diuretic. *The British Medical Journal*. **1888**, *2(1447)*, 660 – 663.

Kang-Yum, E.; Oranski, S. H. Chinese patent medicine as a potential source of mercury poisoning. *Veterinary and Human Toxicology*. **1992**, *34(3)*, 235 – 238.

Kanner, J.; Lapidot, T. The stomach as a bioreactor: dietary lipid peroxidation in the gastric fluid and the effects of plant-derived antioxidants. *Free Radical Biology and Medicine*. **2001**, *31(11)*, 1388 – 1395.

Keil, D. E.; Berger-Ritchie, J.; McMillin, G. A. Testing for toxic elements: a focus on arsenic, cadmium, lead, and mercury. *Laboratory Medicine*. **2011**, *42(12)*, 735 –742.

Keynes, M. Did Napoleon die from arsenical poisoning? *The Lancet*. **1994**, *2(8917)*, 276.

Keynes, M. The death of Napoleon. *Journal of the Royal Society of Medicine*. **2004**, *97(10)*, 507 – 508.

Kielland, J. Individual Activity Coefficients of Ions in Aqueous Solutions. *Journal of the American Chemical Society*. **1937**, *59(9)*, 1675 – 1678.

Kintz, P.; Ginet, M.; Cirimele, V. Multi-element screening by ICP-MS of two specimens of Napoleon's hair. *Journal of analytical toxicology*. **2006**, *30(8)*, 621 – 623.

Kong, F.; Singh, R. P. A Model Stomach System to Investigate Disintegration Kinetics of Solid Foods during Gastric Digestion. *Journal of Food Science*. **2008b**, *73(5)*, E202 – E210.

Kong, F.; Singh, R. P. Disintegration of Solid Foods in Human Stomach. *Journal of Food Science*. **2008a**, *73(5)*, R67 – R80.

Kong, F.; Singh, R. P. Modes of Disintegration of Solid Foods in Simulated Gastric Environment. *Food Biophysics*. **2009**, *4(3)*, 180 – 190.

Langford, N.; Ferner, R. Toxicity of mercury. *Journal of Human Hypertension*. **1999**, *13(10)*, 651 – 656.

Lee, P. R.; Code, C. F.; Scholer, J. F. The influence of varying concentrations of sodium chloride on the rate of absorption of water from the stomach and small bowel of human beings. *Gastroenterology*. **1955**, *29(6)*, 1008.

Lin, X.; Henkelmann, R. Contents of arsenic, mercury and other trace elements in Napoleon's hair determined by INAA using the k0-method. *Journal of Radioanalytical and Nuclear Chemistry*. **2003**, *257(3)*, 615 – 620.

Lin, X.; Alber, D.; Henkelmann, R. Elemental contents in Napoleon's hair cut before and after his death: did Napoleon die of arsenic poisoning? *Analytical and Bioanalytical Chemistry*. **2004**, *379(2)*, 218 – 220.

Liu, J.; Shi, J.-Z.; Yu, L.-M.; Goyer, R. A.; Waalkes, M. P. Mercury in Traditional Medicines: Is Cinnabar Toxicologically Similar to Common Mercurials? *Experimental Biology and Medicine*. **2008**, *233(7)*, 810 – 817.

Lu, Y.-F.; Wu, Q.; Yan, J.-W.; Shi, J.-Z.; Liu, J.; Shi, J.-S. Realgar, cinnabar and An-Gong-Niu-Huang Wan are much less chronically nephrotoxic than common arsenicals and mercurial. *Experimental Biology and Medicine*. **2011**, *236(2)*, 233 – 239.

MacLean, H.; Griffiths, W. J. The factors influencing the concentration of hydrochloric acid during gastric digestion. *The Journal of Physiology*. **1928**, *65(1)*, 63 – 76.

Malmberg, C. G.; Maryott, A. A. Dielectric Constant of Water from 0º to 100º C. *Journal of Research of the National Bureau of Standards*. **1956**, *56(1)*, 1 – 8.

Mari, F.; Bertol, E.; Fineschi, V.; Karch, S. B. Channelling the Emperor: what really killed Napoleon? *Journal of the Royal Society of Medicine*. **2004**, *97(8)*, 397 – 399.

Mößeler, A.; Köttendorf, S.; Liesner, V. G.; Kamphues, J. Impact of diets' physical form (particle size; meal/pelleted) on the stomach content (dry matter content, pH, chloride concentration) of pigs. *Livestock Science*. **2010**, *134(1 – 3)*, 146 – 148.

Mousavi, A. Mercury(I) chloride *in vivo* oxidation: a thermodynamic study. *Main Group Metals Chemistry*. **2015**, *38(3 – 4)*, 121 – 124.

Nernst, W. Über die electromotorischen Kräfte, welche durch den Magnetismus in von einem Wärmestrome durchflossenen Metallplatten geweckt werden. *Wiedemann's Annalen der Physik und Chemie*. **1887**, *31(8)*, 760 – 789.

Nernst, W. Zur Theorie umkehrbarer galvanischer Elemente. *Sitzungsberichte der Königlich Preußichen Akademie der Wissenschaften zu Berlin*, **1889**, *1889(1)*, 83 – 98.

Patwardhan, B.; Warude, D.; Pushpangadan, P.; Bhatt, N. Ayurveda and Traditional Chinese Medicine: A Comparative Overview. *Evidence-Based Complementary and Alternative Medicine*. **2005**, *2(4)*, 465 – 473.

Pourbaix, M. Atlas d''equilibres 'electrochimiques. Publication de Centre belge d''etude de la corrosion ''Cebelcor''. Gauthier-Villars, **1963**.

Pourbaix, M. J. N. Thermodynamique des solutions aqueuses diluées: représentation graphique du rôle du pH et du potentiel. Dissertation. Technische hoogeschool de Delft, Meinema, **1945**.

Preckel, C. Cinnabar, Calomel and the Art of *kushtasāzī*: Mercurial Preparations in Unani Medicine. *Asiatische Studien – Études Asiatiques: Zeitschrift der Schweizerischen Asiengesellschaft – Revue de la Société Suisse-Asie*. **2015**, *69(4)*, 901 – 932.

Prout, W. On the Nature of the Acid and Saline Matters Usually Existing in the Stomachs of Animals. *Philosophical Transactions of the Royal Society of London*. **1824**, *114*, 45 – 49.

Saunders, M. Not All Mercury Is Equal. *Chemical & Engineering News*, **2008**, *86(35)*, 6.

Schmid, J. Beautiful Black Poison: The History of Calomel as Medicine in America. *Wise Traditions in Food, Farming and the Healing Arts*. **2008**, *9(2)*, 17 – 31.

Schmidt, F. Just how dangerous is mercury, anyway? *Deutsche Welle*. 15. 01. 2013. Abailable online at http://dw.com/p/17KFn (access date - 05. 02. 2016).

Schweitzer, G. K.; Pesterfield, L. L. The aqueous chemistry of the elements; Oxford: Oxford University Press, **2010**.

Sébastia, B. Preserving Identity or Promoting Safety? The Issue of Mercury in Siddha Medicine: A Brake on the Crossing of Frontiers. *Asiatische Studien – Études Asiatiques: Zeitschrift der Schweizerischen Asiengesellschaft – Revue de la Société Suisse-Asie*. **2015**, *69(4)*, 933 – 969.

Sørensen, S. P. L. Enzymstudier II. Om Maalingen og Betydningen af Brintionkoncentrationen ved enzymatiske Processer. *Meddelelser fra Carlsberg Laboratoriet*, **1909b**, *8*, 1 – 153, 313 – 317.

Sørensen, S. P. L. Études enzymatiques. II. Sur la mesure et l'importance de la concentration des ions hydrogène dans les réactions enzymatiques. *Comptes rendus des travaux du laboratoire Carlsberg*. **1909a**, *8*, 1 – 162.

Speight, J. Lange's Handbook of Chemistry. 16th Edition; New York: McGraw-Hill Education, **2005**.

Strong, J. A.; Cameron, D.; Riddell, M. J. The electrolyte concentration of human gastric secretion. *Quarterly Journal of Experimental Physiology and Cognate Medical Sciences*. **1960**, *45(1)*, 1 – 11.

Thomann, J. Early Persian Medical Works on Antisyphilitic Mercury Medicines. *Asiatische Studien – Études Asiatiques: Zeitschrift der Schweizerischen Asiengesellschaft – Revue de la Société Suisse-Asie*. **2015**, *69(4)*, 971 – 996.

Thompson, W. T.; Kaye, M. H.; Bale, C. W.; Pelton, A. D. Pourbaix Diagrams for Multielement Systems. In *Uhlig's corrosion handbook*. Wiley, **2011**, 103 – 110.

Torosov, T. M. Analysis of the chloride-secreting function of the stomach in experimental animals and in man. *Bulletin of Experimental Biology and Medicine*. **1966**, *62(5)*, 1227 – 1229.

Trambaiolo, D. Antisyphilitic Mercury Drugs in Early Modern China and Japan. *Asiatische Studien – Études Asiatiques: Zeitschrift der Schweizerischen Asiengesellschaft – Revue de la Société Suisse-Asie*. **2015**, *69(4)*, 997 – 1016.

Urita, Y.; Ishihara, S.; Akimoto, T.; Kato, H.; Hara, N.; Honda, Y.; Nagai, Y.; Nakanishi, K.; Shimada. N.; Sugimoto, M.; Miki, K. Hydrogen and methane gases are frequently detected in the stomach. *World Journal of Gastroenterology*. **2006**, *12(9)*, 3088 – 3091.

van't Hoff, M. J. H. Études de dynamique chimique. *Recueil des Travaux Chimiques des Pays-Bas*. **1884**, *3(10)*, 333 – 336.

Wagman, D. D.; Evans, W. H.; Parker, V. B.; Schumm, R. H.; Halow, I. B.; Sylvia, M.; Churney, K. L.; Nuttal, R. L. The NBS tables of chemical thermodynamic properties. Selected values for inorganic and C_1 and C_2 organic substances in SI units. *Journal of Physical and Chemical Reference Data*. **1982**, *11*, Supplement 2.

Walker, T. Medicinal Mercury in Early Modern Portuguese Records: Recipes and Methods from Eighteenth-Century Medical Guidebooks. *Asiatische Studien – Études Asiatiques: Zeitschrift der Schweizerischen Asiengesellschaft – Revue de la Société Suisse-Asie*. **2015**, *69(4)*, 1017 – 1042.

Weider, B.; Fournier, J. H. Activation analyses of authenticated hairs of Napoleon Bonaparte confirm arsenic poisoning. *The American Journal of Forensic Medicine and Pathology*. **1999**, *20(4)*, 378 – 382.

Weider, B.; Fournier, J. H. The Death of Napoleon. *The American Journal of Forensic Medicine and Pathology*. **2000**, *21(3)*, 303 – 305.

Wong, H. C. G. Mercury and Chinese herbal medicine. *British Columbia Medical Journal*. **2004**, *46*, 442.

Wong, H. C. G. Side-effects of CAM/Chinese herbal meds. *British Columbia Medical Journal*. **2008**, *50(2)*, 59.

Wong, M. K.; Koh, L. L. Mercury, lead, and other heavy metals in Chinese medicines. *Biological Trace Element Research*. **1986**, *10(2)*, 91 – 97.

Wu, M.-L.; Deng, J.-F.; Lin, K.-P.; Tsai, W.-J. Lead, Mercury, and Arsenic Poisoning Due to Topical Use of Traditional Chinese Medicines. *The American Journal of Medicine*. **2013**, *126(5)*, 451 – 454.

Wujastik, D. Mercury as an Antisyphilitic in Ayurvedic Medicine. *Asiatische Studien – Études Asiatiques: Zeitschrift der Schweizerischen Asiengesellschaft – Revue de la Société Suisse-Asie*. **2015**, *69(4)*, 1043 – 1067.

Wujastik, D. Histories of Mercury in Medicine across Asia and Beyond. *Asiatische Studien – Études Asiatiques: Zeitschrift der Schweizerischen Asiengesellschaft – Revue de la Société Suisse-Asie*. **2015**, *69(4)*, 819 – 830.

Wyman, J. Jr. Measurements of the Dielectric Constants of Conducting Media. *Physical Review*. **1930**, *35(6)*, 623 – 634.

Yu, W.-H.; Zhang, N.; Qi, J.-F.; Sun, C.; Wang, Y. H.; Liu, M. Arsenic and Mercury Containing Traditional Chinese Medicine (Realgar and Cinnabar) Strongly Inhibit Organic Anion Transporters, Oat1 and Oat3, *In Vivo* in Mice. *BioMed Research International*. **2015**, *2015*, Article ID 863971, 1 – 7. DOI: 10.1155/2015/863971.

Zhang, L.; Yan, J.; Liu, X.; Ye, Z.; Yang, X.; Meyboom, R.; Chan, K.; Shaw, D.; Duez, P. Pharmacovigilance practice and risk control of Traditional Chinese Medicine drugs in China: current status and future perspective. *Journal of ethnopharmacology*. **2012**, *140(3)*, 519 – 525.

INVESTIGAÇÃO EXPERIMENTAL E TEÓRICA DAS PROPRIEDADES DE CORROSÃO DO AÇO X13 NO ÁCIDO ACÉTICO A 20 E 80 °C

EXPERIMENTAL AND THEORETICAL INVESTIGATION OF THE CORROSION PROPERTIES OF STEEL X13 IN THE ACETIC ACID AT 20 AND 80 °C

MANANNIKOV, Dmitrii Andreevich[1,2]; PARSHUKOV, Vladimir Pavlovich[1,2]; NIKOLAYCHUK, Pavel Anatolyevich[2,*]

[1] Laboratoriâ korrozionnyh ispytanij, Rossijskij naučno-issledovatel'skij institut trubnoj promyšlennosti, Novorossijskaâ, 30, zip code 454139, Chelyabinsk, Russian Federation
(phone: +7 351 225 02 22 8802)

[2] Kafedra analitičeskoj i fizičeskoj himii, Čelâbinskij gosudarstvennyj universitet, Brat'ev Kaširinyh, 129, zip code 454001, Chelyabinsk, Russian Federation
(phone: +7 351 799 70 69)

** Corresponding author*
e-mail: npa@csu.ru

Received 12 June 2000; received in revised form 30 November 2000; accepted 14 December 2000

RESUMO

As curvas de polarização de X13 aço inoxidável numa atmosfera de 5% de NaCl + 0,5% de CH_3COOH + CH_3COONa + CO_2 (P_{CO_2} = 0.1 MPa) em solução pH 3 e 4 e as temperaturas de 20 e 80 ° C. Foram obtidos pelo método potenciostática. As características corrosão eletroquímica do aço nesses ambientes foram medidos. Os diagramas de aço sistemas X13-CH_3COOH-CO_2-H2O potencial de pH foram construídos e o comportamento de corrosão do aço foi determinada utilizando esses diagramas. A passivação do aço pode proceder devido à formação da camada ($FeCr_2O_4$) fase de cromite de ferro e de oxalato de ferro (FeC_2O_4) polylayer.

Palavras-chave O aço inoxidável X13, ambientes de ácido acético, curvas de polarização, o potencial - diagrama de pH.

ABSTRACT

Polarisation curves of stainless steel X13 in a 5% NaCl + 0.5% CH_3COOH + CH_3COONa + CO_2 (P_{CO_2} = 0.1 MPa) solution at pH 3 and 4 and temperatures 20 and 80 °C were obtained by the potentiostatic method. The corrosion-electrochemical characteristics of the steel in these environments were measured. The potential–pH diagrams of steel X13–CH_3COOH–CO_2–H_2O systems were constructed and the corrosion behaviour of the steel was determined using these diagrams. The passivation of the steel may proceed due to the formation of iron chromite ($FeCr_2O_4$) phase layer and of iron oxalate (FeC_2O_4) polylayer.

Keywords: Stainless steel X13, acetic acid environments, polarisation curves, potential – pH diagram.

INTRODUCTION

Acetic acid is widely used in various branches of industry, and the study of corrosion of the metallic equipment in the acetic media is an important task (Davis, 2000; Schweitzer, 2006). Numerous studies on the corrosion of various metals and alloys in the acetic media were conducted in the past years (Malakhova *et al*., 1995; Nickel Institute, 2016;. Onuchukwu and Oppong-Boachie, 1986; Thirumalaikumar and Jegannathan, 2011; Hassan and Fahmy, 2008; Rafiquee *et al*., 2007; Ansari and Quraishi, 2011; Allahkaram *et al*., 2011; Veloz and González, 2002; Amri *et al*., 2008; Tétreault *et al*., 1998; Rocca *et al*., 2004; Turnbull *et al*., 2003; Lou and Singh, 2010; Singer *et al*., 2011). This study aims the investigation of the corrosion properties of the stainless steel X13.

Steel X13 is an instrumental stainless steel produced in accordance with the Russian State Standard GOST 5632–72. It is designed for usage in weakly aggressive environments. This steel grade is analogous to such steel grades as UNS S42000 (USA), ASTM 420–SS2303 (EU), SUS420J1 (Japan) or 2Cr13 (China) (Database of Steel and Alloy, 2016). The average composition of steel X13 is presented in Table 1.

MATERIALS AND METHODS

Sample preparation

The cylindrical samples made of steel X13, 9.5 mm in diameter and 5 mm in height with the small hole in the cylinder base for binding current-conductible parts were used. The working surface of the samples was approximately equal to 2.7 cm^2. Before the polarisation tests the samples were polished and degreased in acetone.

Reagents of analytical quality were used. Analytical balance with maximum uncertainty of ±0.0001 g was used for taking weights. pH-meter with maximum uncertainty of ±0.01 pH unit was used to control solution pH. The solutions for polarisation measurements were prepared in accordance with NACE/ASTM TM0169 G0031 12A Standard Guide for Laboratory Immersion Corrosion Testing of Metals: 1 L of the solution containing (by weight) 5 % NaCl and 0.5 % CH_3COOH was saturated by CO_2 at P_{CO_2} = 0.1 MPa, after that 100 ml of the 100 g/mL Na_2CO_3 solution was added, and then pH was adjusted to the necessary value by adding hydrochloric acid.

Polarisation measurements

The polarisation measurements were performed in the potentiodynamic mode using the potentiostat Gamry Series G750 in the standard three-electrode thermostated cell. A saturated calomel electrode was used as the reference electrode. The temperature of the solution was maintained at 20±2 ºC or 80±2ºC. IR drop was minimised by using and accurately positioning the Luggine capillary.

The potential of dissolution of steel X13 was preliminary determined. For this the potential on steel was measured without external polarisation during at least one hour, taking E_{corr} as the potential at the end of exposure with the condition that potential change in the last 30 minutes was no more than ±30 mV. After that the sample was cathodically polarized at the potential of –1.1 V (SHE) for 10 minutes and potentiodynamic curve was registered with potential sweep rate of 0.1 mV/s. The experiment was repeated until three polarisation curves compatible with each other were obtained for each solution. The potential with respect to the standard hydrogen electrode was calculated taking into account the temperature dependency of the potential of a saturated calomel electrode.

Construction of potential – pH diagrams

The method of plotting the potential – pH diagrams of multielement systems and the application of these diagrams to the thermodynamic study of the corrosion processes is described in detail elsewhere (Thompson *et al*. 2011).

RESULTS AND DISCUSSION

The polarisation curves

The polarisation curves of steel X13 in a solution containing 5% NaCl + 0.5% CH_3COOH + CH_3COONa + CO_2 at 20 ºC are presented in Figure 1, and at 80 ºC – in Figure 2.

From the anodic branches of polarisation curves the following quantities were determined: passivation potential (E_p), pitting formation

potential (E_{pit}), the size of the passivity region ($\Delta E = E_{pit} - E_p$), the pitting resistance index ($\Delta E_{pit} = E_{pit} - E_{corr}$) (Freiman *et al*. 1986), the Tafel slope of the active corrosion region of the curve (b_a) and the corrosion rate in the passive state (i_p). The results are presented in Table 2.

The experimental data show that at elevated temperature both the passivity region size and the pitting resistance index substantially decrease, which indicates lesser stability of metal and higher probability of pitting formation at higher temperatures. Lowering pH of the test media from 4 to 3 also causes the narrowing of the passivity region size and the increase of the corrosion rate. A very high value of the corrosion rate in the passivity state region at 20 ºC and pH 3 indicates the change of the passivation mechanism.

The visual inspection of the samples after electrochemical tests is presented in Figure 3. Pittings are present on all samples, and moreover, the number of local corrosion damage nuclei is significantly larger at pH 3. The surface of the samples tested at pH 4 is generally brilliant and for the samples tested at pH 3 it becomes dull. It shows that whereas at pH 4 the test media inflicts only local damage to the surface of the steel, at pH 3 the anodic dissolution occurs not only in pittings but also over the entire surface.

Thermodynamic evaluation of the corrosion properties of steel

The steel X13 has the crystal structure of ferrite (a Fe-based solid solution with body centered cubic lattice). The thermodynamic description of this solid solution was performed using the quasi-regular solution model (Chen, 1988) using the data from Kaufman and Nesor (1973). The calculated thermodynamic activities of iron and chromium in the steel are the following: at 20 °C $a_{Fe\ (bcc)} \approx 0.99$ and $a_{Cr\ (bcc)} \approx 114.3$; and at 80 °C $a_{Fe\ (bcc)} \approx 0.99$ and $a_{Cr\ (bcc)} \approx 31.1$. The activities of chromium exceed unity, which is proved by the phase diagram of Fe – Cr system (Kaufman and Nesor, 1973) and indicates that at low temperatures steel X13 is metastable.

The basic chemical and electrochemical equilibria of the steel X13 in acetic media along with the temperature dependencies of the Gibbs free energies of reactions are listed in Table 3. Since the studied temperature interval is relatively narrow, the temperature dependencies of the Gibbs free energies are approximated as linear functions of temperature. The parameters of temperature relationships were calculated from the data of Tyurin (1999), Lee (1981), Belyaev *et al*. (1984) and Saltykov *et al*. (2004).

The duration of single electrochemical test was ~4 hours, from which 1.5 hours was the duration of corrosion potential measurements and 2.5 hours was the duration of polarisation curve registration. It was estimated from the corrosion rate values listed in Table 2 that the average content of iron and chromium in a solution after four-hour exposure has the order-of-magnitude of 10^{-4} mol/L. The potential – pH diagram of steel X13 – CH_3COOH (~0,1 mol/L) – CO_2 (~ 10^{-4} mol/L) – H_2O system at 20 °C, P=1 bar (air) and the activities of iron and chromium ions in solution ~10^{-4} mol/L is presented in Figure 4, and at 80 °C – in Figure 5. Thermodynamic calculations show that at pH 3 and 4 and potentials from –0.6V to +0.3 V (SHE) the passivation of steel is determined by the formation of iron chromite ($FeCr_2O_4$) or iron oxalate (FeC_2O_4) on its surface. At pH 4 iron chromite forms a protective layer on the steel surface both at ambient and elevated temperatures, whereas at pH 3 the situation is different. At 80 °C $FeCr_2O_4$ remains thermodynamically stable, but at 20 °C it decomposes and the protective layer consists from iron oxalate. Thermodynamic calculations explain the unusually high value of the corrosion rate at pH 3 and 20 °C in Table 2. The protective effect of iron chromite is very well known (Reformatskaya *et al*., 2004), and it is significantly stronger than that of iron oxalate (Saltykov *et al*., 2004). At lower pH, however, the strength and the protective function of the iron chromite layer decreases, and the iron oxalate layer is not able to fully resist the destructive influence of the aggressive components of the environment, and the steel is affected by overall corrosion. In these conditions rising the temperature can shift the border of thermodynamic stability of iron chromite and slow down the dissolution of steel.

CONCLUSIONS

1. The corrosion-electrochemical behaviour of steel X13 in a solution containing by weight 5% NaCl + 0.5% CH_3COOH + CH_3COONa + CO_2 (P_{CO_2} =0,1 MPa) at pH 3 and 4

and temperatures 20 and 80 °C was studied by the potentiodynamic method. The values of the potentials of corrosion (E_{corr}), passivation (E_p) and pitting formation (E_{pit}) as well as corrosion rate in the passive state (i_p) were determined. The anomaly in the temperature dependency of the corrosion rate at pH 3 was revealed.

2. The thermodynamic evaluation of the corrosion properties of steel X13 in a solution containing by weight 5% NaCl + 0.5% CH_3COOH + CH_3COONa + CO_2 (P_{CO_2} =0,1 MPa) at pH 3 and 4 and temperatures 20 and 80 °C was performed. The potential – pH diagrams of steel X13 – CH_3COOH (~0,1 mol/L) – CO_2 (~ 10^{-4} mol/L) – H_2O were plotted.

3. It is shown that the passivation of steel X13 in the studied range of pH and temperatures can be provided by the formation of the iron chromite or iron oxalate layers on its surface.

4. The changing of the nature of the protective layer at pH 3 from FeC_2O_4 at 20 °C to $FeCr_2O_4$ at 80 °C lowers the corrosion rate 3 times. The increase of temperature of the environment can be used for retaining the passivation state of the steel in acetic environments

REFERENCES:

P. A. Schweitzer. Fundamentals of Metallic Corrosion: Atmospheric and Media Corrosion of Metals. CRC Press, 2006. 752 p.

J. R. Davis. Corrosion: Understanding the Basics. ASM International, 2000. 563 p.

É. K. Malakhova, A. N. Kuzyukov, A. V. Meshcheryakov. Corrosion resistance of zirconium alloys in acetic acid media. *Chemical and Petroleum Engineering*, 1995, 31(3), 183 – 185.

Corrosion Resistance of Nickel-containing Alloys in Organic Acids and Related Substances. Nickel Institute. 64 p. URL: https://www.nickelinstitute.org/~/media/Files/TechnicalLiterature/CorrosionResistanceofNickel_ContainingAlloysinOrganicAcidsandRelatedCompounds_1285_.ashx. (Accessed October 2016)

A. I. Onuchukwu, F. K. Oppong-Boachie. The corrosion behaviour of aluminum alloy AA1060 in p-quinone and acetic acid media. *Corrosion Science*, 1986, 26(11), 919 – 926.

M. Thirumalaikumar, S. Jegannathan. Inhibition Effects of Nitrones on the Corrosion of Mild Steel in Organic Acid Media. *Portugaliae Electrochimica Acta*, 2011, 29(1), 1 – 8.

H. H. Hassan, K. Fahmy. Pitting Corrosion of Tin by Acetate Anion in Acidic Media. *International Journal of Electrochemical Science*, 2008, 3, 29 – 43.

M. Z. A. Rafiquee, S. Khan, N. Saxena, M. A. Quraishi. Influence of Some Thiadiazole Derivatives on Corrosion Inhibition of Mild Steel in Formic and Acetic Acid Media. *Portugaliae Electrochimica Acta*, 2007, 25, 419 – 434.

F. A. Ansari, M. A. Quraishi. Inhibitive Effect of Some Gemini Surfactants as Corrosion Inhibitors for Mild Steel in Acetic Acid Media. *Arabian Journal for Science and Engineering*, 2011, 36(1), 11 – 20.

S. R. Allahkaram, M. Honarvar Nazari, S. Mamaghani, A. Zarebidaki. Characterization and corrosion behavior of electroless Ni–P/nano-SiC coating inside the CO_2 containing media in the presence of acetic acid. *Materials & Design*, 2011, 32(2), 750 – 755.

M. A. Veloz, I. González. Electrochemical study of carbon steel corrosion in buffered acetic acid solutions with chlorides and H_2S. *Electrochimica Acta*, 2002, 48(2), 135 – 144.

J. Amri, E. Gulbrandsen, R. P. Nogueira. The effect of acetic acid on the pit propagation in CO_2 corrosion of carbon steel. *Electrochemistry Communications*, 2008, 10(2), 200 – 203.

J. Tétreault, J. Sirois, E. Stamatopoulou. Studies of lead corrosion in acetic acid environments. *Studies in Conservation*, 1998, 43(1), 17 – 32.

E. Rocca, C. Rapin, F. Mirambet. Inhibition treatment of the corrosion of lead artefacts in atmospheric conditions and by acetic acid vapour: use of sodium decanoate. *Corrosion Science*, 2004, 46(3), 653 – 665.

A. Turnbull, M. Ryan, A. Willetts, S. Zhou. Corrosion and electrochemical behaviour of 316L stainless steel in acetic acid solutions. Corrosion Science, 2003, 45(5), 1051 – 1072.

X. Lou, P. M. Singh. Role of water, acetic acid and chloride on corrosion and pitting behaviour of carbon steel in fuel-grade ethanol. *Corrosion Scie*nce, 2010, 52(7), 2303 – 2315.

M. Singer, A. Camacho, B. Brown, S. Nešić. Sour Top-of-the-Line Corrosion in the Presence of Acetic Acid. *Corrosion*, 2011, 67(8), 085003-1 – 085003-16.

Database of Steel and Alloy. URL: http://splav-kharkov.com/mat_start.php?name_id=7#1. (Accessed October 2016).

M. T. Thompson, M. H. Kaye, C. W. Bale, A. D. Pelton. Pourbaix Diagrams for Multielement Systems. In: Uhlig's corrosion handbook. Wiley, 2011. P. 103 – 110.

L. I. Freiman, Ya. Flis, M. Prazhak, L. Garts, B.

Narovska, R. Bartonichek, M. M. Kristal', R. L. Baru, S. N. Mandzhagaladze, S. A. Glazkova, Ya. Tlamsa, I. I. Reformatskaya, D. I. Starosvetskii, A. R. Basman, T. P. Markova. Standartization of methods of accelerated tests of stainless steel of its resistance to pitting corrosion. Electrochemical tests. *Protection of Metals*, 1986, 22(2), 149 – 164.

L.-R. Chen. Quasiregular model and phase equilibrium diagram of a binary system. *Physica status solidi (a) – applications and materials science*, 1988, 110(1), K19 – K24.

L. Kaufman, H. Nesor. Calculation of the binary phase diagrams of iron, chromium, nickel and cobalt. *Zeitschrift für Metallkunde*, 1973, 64, 249 – 257.

A. G. Tyurin. Thermodynamics of the chemical and electrochemical resistance of iron-chromium alloys. *Protection of Metals*, 1999, 35(3), 215 – 220.

J. B. Lee. Elevated temperature potential – pH diagrams for the Cr-H_2O, Ti-H_2O, Mo-H_2O and Pt-H_2O systems. *Corrosion*, 1981, 37(8), 467 – 481.

V. P. Belyaev, I. V. Parputs, V. L. Artem'ev, A. M. Sukhotin. Potential – pH diagram and passivity of iron in hot alkaline solutions. *Protection of Metals*, 1984, 20(6), 692 – 696.

S. N. Saltykov, G. V. Makarov, E. L. Toroptseva, Ya. B. Filatova. Anodic behavior of white iron phases in oxalic media. *Protection of Metals*, 2004, 40(1), 56 – 61.

I. I. Reformatskaya, A. N. Podobaev, E. V. Trofimova, T. I. Ashcheulova. Developing concepts of chromium functions in the passivation and pitting of Fe-Cr alloys. *Protection of Metals*, 2004, 40(3), 207 – 213.

Table 1. *The average chemical composition of steel X13*

Composition of the element, weight %												
C	Si	Mn	P	S	Cr	Ni	Cu	Mo	Al	Ti	V	W
0.15	0.41	0.35	0.010	0.002	12.5	0.16	0.07	0.007	0.016	0.001	0.021	0.001

Table 2. *The corrosion-electrochemical characteristics of steel X13 in a 5% NaCl + 0,5% CH_3COOH + CH_3COONa + CO_2 solution*

Conditions	**E_{corr}, mV**	**E_p, mV**	**E_{pit}, mV**	**ΔE, mV**	**ΔE_{pit}, mV**	**b_a**	**i_p, mA/cm^2 (mm/year)**
t = 20 °C, pH 4	–345	–260	–30	230	315	0.072	0.005 (0.04)
t = 20 °C, pH 3	–360	–210	–30	180	330	0.135	0.111 (0.86)
t = 80 °C, pH 4	–380	–315	–240	75	140	0.060	0.018 (0.14)
t = 80 °C, pH 3	–390	–330	–295	35	95	0.035	0.046 (0.36)

Table 3. *The Gibbs free energies of the basic chemical and electrochemical reactions in Fe – Cr – CH_3COOH – CO_2 system*

No of line at Figs. 4 and 5	Electrode reaction	$\Delta_r G^o_T = f(T)$, J/mol
a	$2H^+ + 2e = H_2$	0
b	$O_2 + 4H^+ + 4e = 2H_2O$	$-571620 + 326.5 \cdot T$
1	$Cr^{2+} + 2e = Cr$ (bcc, ferrite)	$206230 - 100.9 \cdot T$
2	$Fe^{2+} + 2e = Fe$ (bcc, ferrite)	$87930 - 10.0 \cdot T$
3	$Cr^{3+} + e = Cr^{2+}$	$108010 - 230.5 \cdot T$
4	$Fe^{3+} + e = Fe^{2+}$	$-21330 - 178.1 \cdot T$
5	$Cr_2O_7^{2-} + 14H^+ + 6e = 2Cr^{3+} + 7H_2O$	$-987830 + 731.2 \cdot T$
6	$FeO_4^{2-} + 8H^+ + 3e = Fe^{3+} + 4H_2O$	$-710120 + 246.0 \cdot T$
7	$Cr_2O_3 + 6H^+ + 6e = 2Cr(bcc) + 3H_2O$	$426190 - 301.5 \cdot T$
8	$FeCr_2O_4 + 2H^+ + 2e = Fe(bcc) + Cr_2O_3 + H_2O$	$102760 - 74.2 \cdot T$
9	$Fe_3O_4 + 8H^+ + 8e = 3Fe(bcc) + 4H_2O$	$179450 - 382.0 \cdot T$
10	$Cr_2O_3 + 6H^+ + 2e = 2Cr^{2+} + 3H_2O$	$14110 - 99.8 \cdot T$
11	$FeCr_2O_4 + 8H^+ + 4e = Fe(bcc) + Cr^{2+} + 4H_2O$	$140030 - 251.0 \cdot T$
12	$FeCr_2O_4 + 8H^+ + 2e = Fe^{2+} + Cr^{2+} + 4H_2O$	$8040 - 93.0 \cdot T$
13	$FeCr_2O_4 + 8H^+ = Fe^{2+} + 2Cr^{3+} + 4H_2O$	$195810 - 372.7 \cdot T$
14	$Fe_3O_4 + 8H^+ + 2e = 3Fe^{2+} + 4H_2O$	$-211330 + 92.0 \cdot T$
15	$3Fe_2O_3 + 2H^+ + 2e = 2Fe_3O_4 + H_2O$	$87550 - 142.3 \cdot T$
16	$Fe_2O_3 + 6H^+ + 2e = 2Fe^{2+} + 3H_2O$	$-180070 + 144.8 \cdot T$
17	$Fe_2O_3 + 4Cr^{3+} + 5H_2O + 2e = 2FeCr_2O_4 + 10H^+$	$357550 - 876.1 \cdot T$
18	$2Cr_2O_3 + Fe_2O_3 + 2H^+ + 2e = 2FeCr_2O_4 + H_2O$	$-83080 - 153.8 \cdot T$
19	$2CrO_2 + 2H^+ + 2e = Cr_2O_3 + H_2O$	$-101640 - 96.7 \cdot T$
20	$CrO_4^{2-} + 4H^+ + 2e = CrO_2 + 2H_2O$	$-277260 - 125.1 \cdot T$
21	$Cr_2O_3 + 6H^+ = 2Cr^{3+} + 3H_2O$	$-201760 + 361.1 \cdot T$
22	$CrO_2 + 4H^+ + e = Cr^{3+} + 2H_2O$	$-151710 + 132.5 \cdot T$
23	$Fe_2O_3 + 6H^+ = 2Fe^{3+} + 3H_2O$	$-99340 + 370.1 \cdot T$
24	$Cr_2O_7^{2-} + 6H^+ + 4e = 2CrO_2 + 3H_2O$	$-494760 - 169.7 \cdot T$
25	$Cr_2O_7^{2-} + H_2O = 2CrO_4^{2-} + 2H^+$	$30 + 273.3 \cdot T$
26	$2FeO_4^{2-} + 10H^+ + 6e = Fe_2O_3 + 5H_2O$	$-1122400 - 546.2 \cdot T$
27	$2CrO_2^- + 6H^+ = Cr_2O_3 + 3H_2O$	$-215640 - 26.3 \cdot T$
28	$CrO_4^{2-} + 4H^+ + 3e = CrO_2^- + 2H_2O$	$-232340 - 138.5 \cdot T$
29	$4CrO_2^- + Fe_2O_3 + 6H^+ + 2e = 2FeCr_2O_4 + 3H_2O$	$-511230 - 216.3 \cdot T$
30	$Fe_3O_4 + 2H_2O + 2e = 3HFeO_2^- + H^+$	$409090 - 194.9 \cdot T$
31	$HFeO_2^- + 3H^+ + 2e = Fe(\alpha) + 4H_2O$	$-34880 + 202.2 \cdot T$
32	$FeCr_2O_4 + 2e = 2CrO_2^- + Fe(bcc)$	$317350 - 445.0 \cdot T$
33	$CrO_2^- + 4H^+ + 3e = Cr(\alpha) + 2H_2O$	$69510 + 180.0 \cdot T$
34	$FeCO_3 + H^+ + 2e = Fe(\alpha) + HCO_3^-$	$94950 - 26.8 \cdot T$
35	$Fe^{2+} + H_2CO_3 = FeCO_3 + 2H^+$	$19840 + 114.2 \cdot T$
36	$Fe_3O_4 + 3HCO_3^- + 5H^+ + 2e = 3FeCO_3 + 4H_2O$	$-148700 - 141.8 \cdot T$
37	$HCO_3^- = CO_3^{2-} + H^+$	$14640 + 148.6 \cdot T$
38	$H_2CO_3 = HCO_3^- + H^+$	$7740 + 97.4 \cdot T$
39	$CH_3COOH = CH_3COO^- + H^+$	$-420 + 92.5 \cdot T$
40	$C_2O_4^{2-} + 7H^+ + 6e = CH_3COO^- + 2H_2O$	$113340 - 183.3 \cdot T$
41	$FeC_2O_4 + 2e = Fe(bcc) + C_2O_4^{2-}$	$-58380 + 646.4 \cdot T$
42	$Fe_3O_4 + 3C_2O_4^{2-} + 8H^+ + 2e = 3FeC_2O_4 + 4H_2O$	$-217180 - 345.5 \cdot T$
43	$FeC_2O_4 + 7H^+ + 8e = Fe(bcc) + CH_3COO^- + 2H_2O$	$73890 + 411.7 \cdot T$
44	$FeC_2O_4 + 8H^+ + 6e = Fe^{2+} + CH_3COOH + 2H_2O$	$-106320 + 607.8 \cdot T$
45	$Fe_2O_3 + C_2O_4^{2-} + 6H^+ + 4e = FeC_2O_4 + 3H_2O$	$-122650 - 193.1 \cdot T$
46	$Fe^{3+} + H_2C_2O_4 + e = FeC_2O_4 + 2H^+$	$-7160 - 305.5 \cdot T$
47	$HC_2O_4^- = C_2O_4^{2-} + H^+$	$-6570 + 35.4 \cdot T$
48	$H_2C_2O_4 = HC_2O_4^- + H^+$	$-3140 + 35.4 \cdot T$

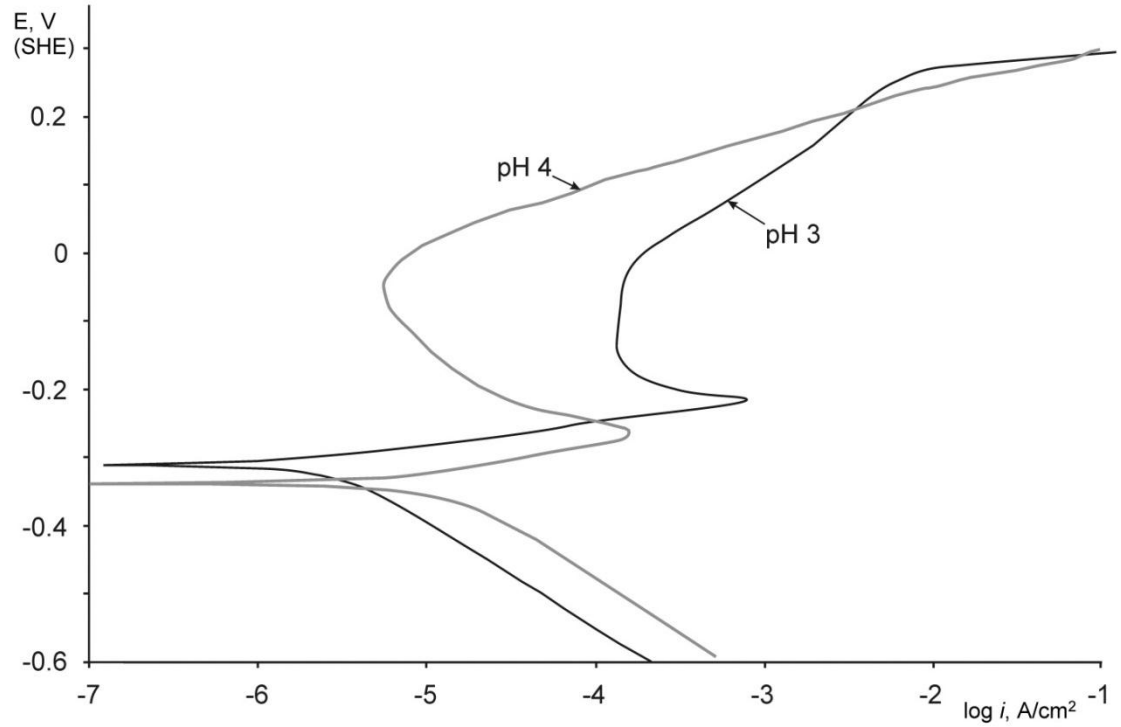

Figure 1. *The polarisation curves of steel X13 in a solution containing 5% NaCl + 0.5% CH_3COOH + CH_3COONa + CO_2 at 20 °C.*

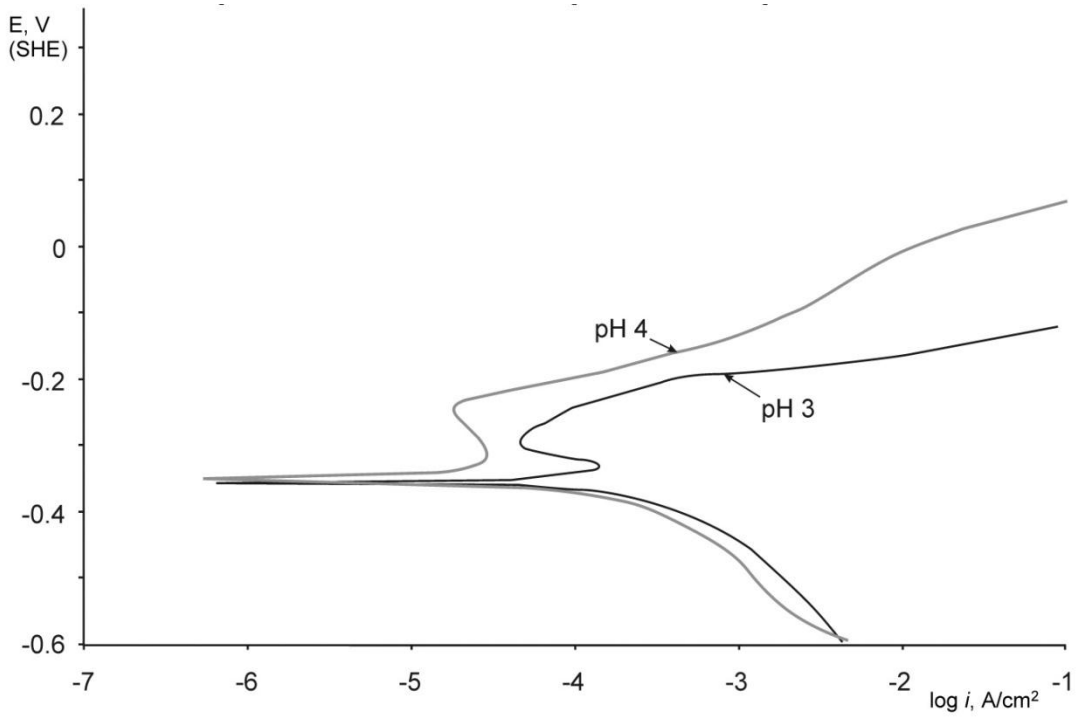

Figure 2. *The polarisation curves of steel X13 in a solution containing 5% NaCl + 0.5% CH_3COOH + CH_3COONa + CO_2 at 80 °C.*

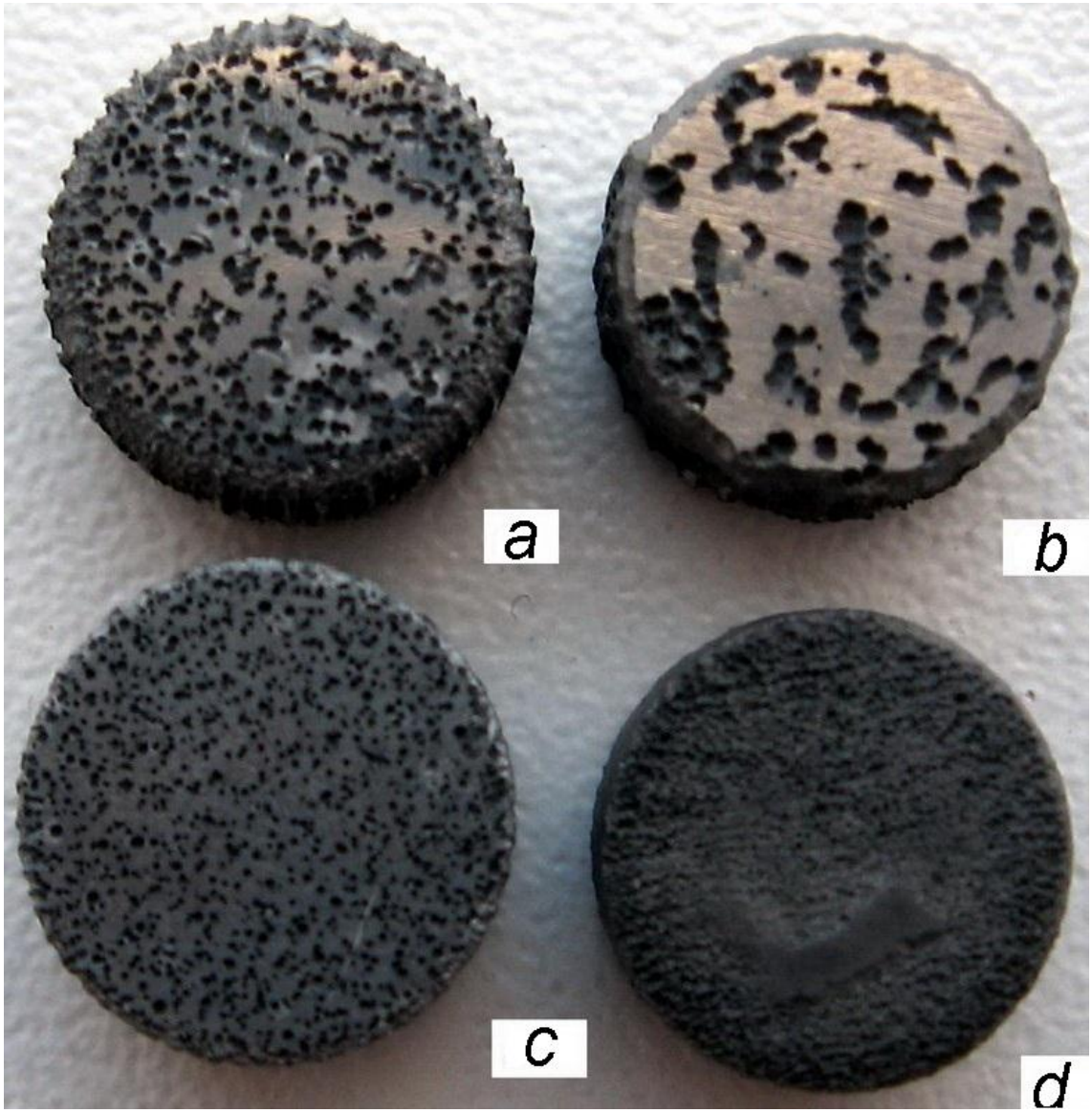

Figure 3. *The view of the samples of X13 steel after electrochemical test in various conditions: a – 20 °C, pH 4; b – 80 °C, pH 4; c – 20 °C, pH 3; d – 80 °C, pH 3.*

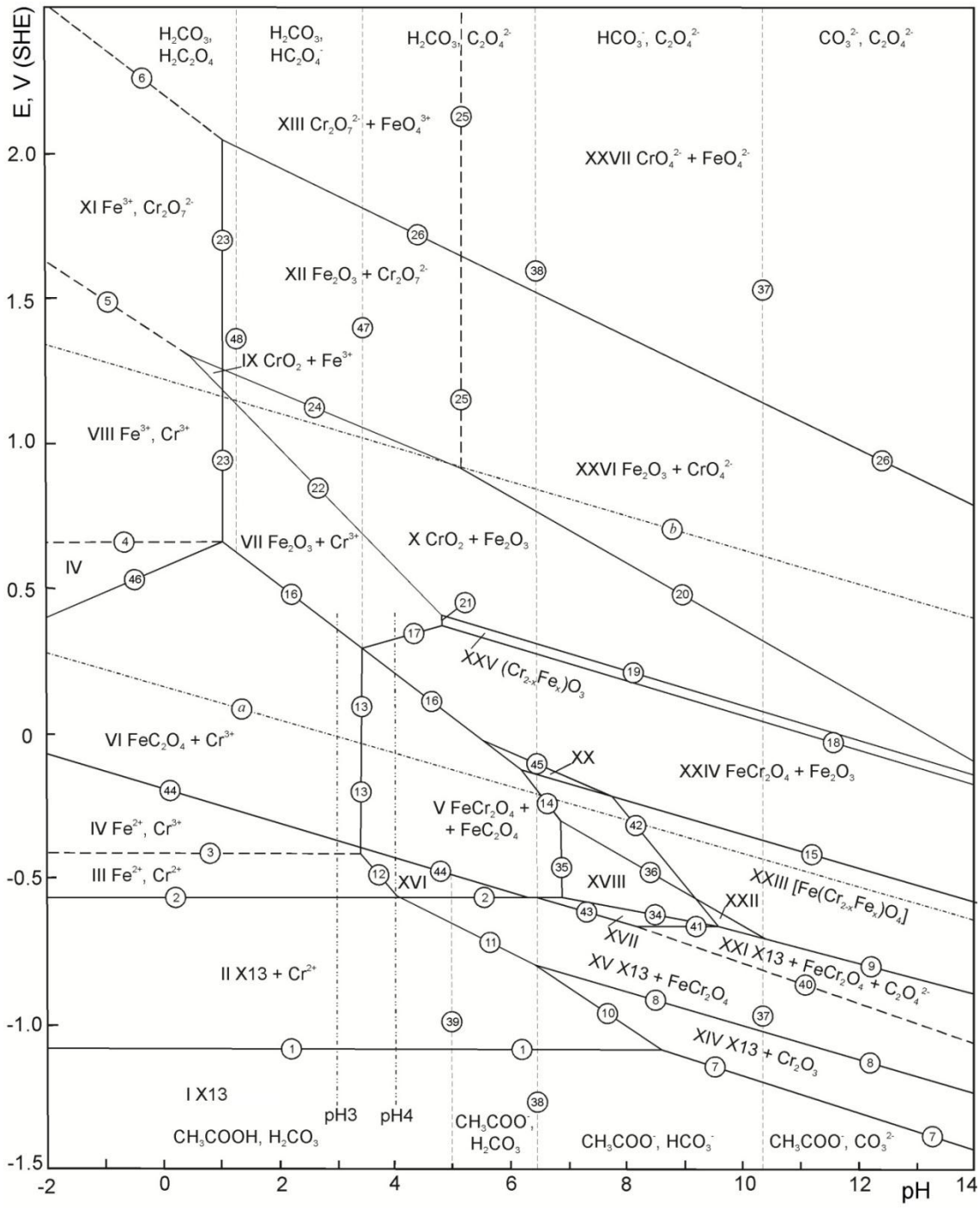

Figure 4. *The potential – pH diagram of steel X13 – CH_3COOH (~0,1 mol/L) – CO_2 (~ 10^{-4} mol/L) – H_2O system at 20 °C, P=1 bar (air) and the activities of iron and chromium ions ~10^{-4} mol/L (unhydrated form of the oxides).*

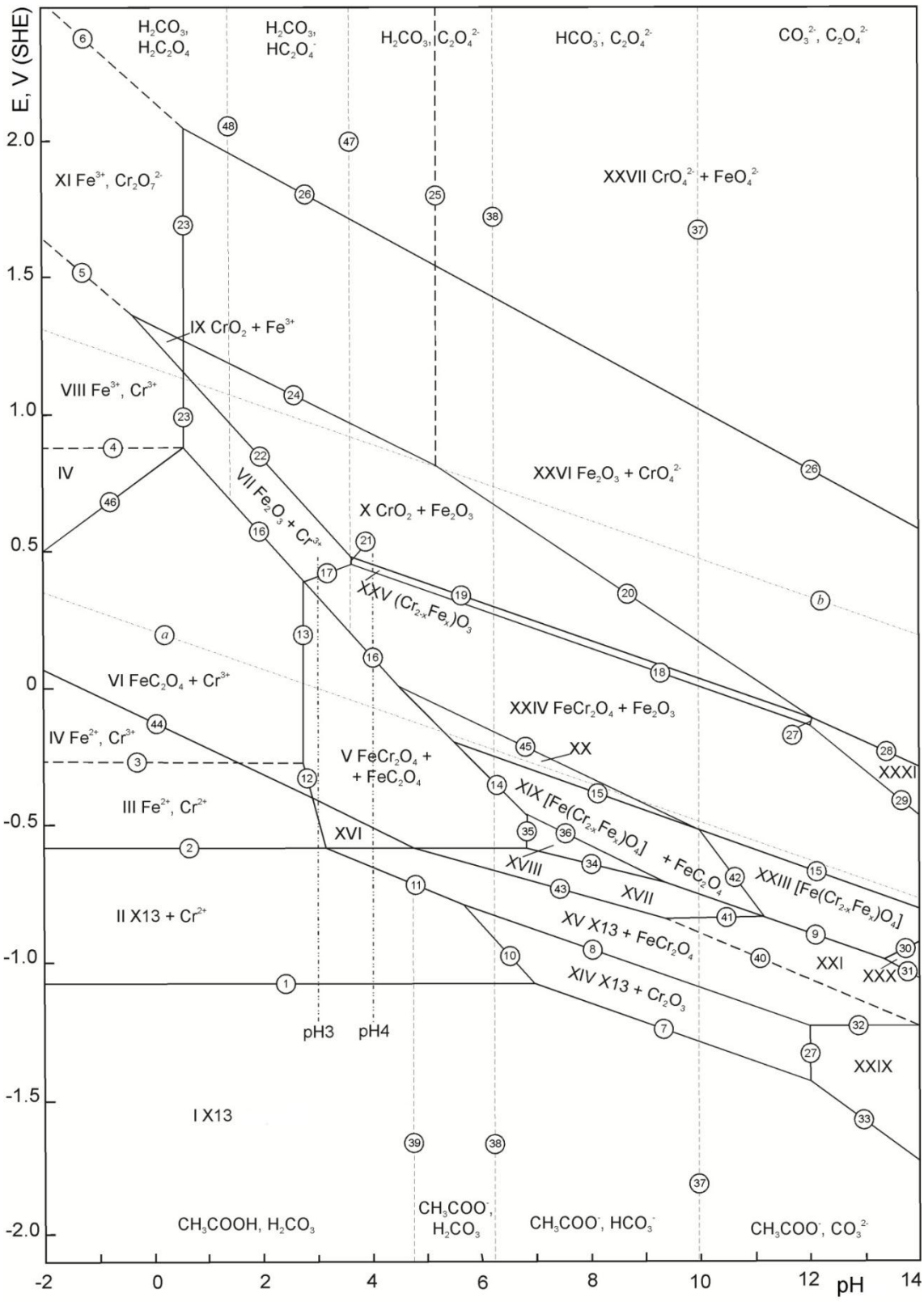

Figure 5. *The potential – pH diagram of steel X13 – CH_3COOH (~0,1 mol/L) – CO_2 (~ 10^{-4} mol/L) – H_2O system at 80 °C, P=1 bar (air) and the activities of iron and chromium ions ~10^{-4} mol/L (unhydrated form of the oxides).*

This is an article preprint. The title, abstract and figures and tables are translated into English.

УДК 620.193:669.14

ТЕРМОДИНАМИКА ХИМИЧЕСКОЙ И ЭЛЕКТРОХИМИЧЕСКОЙ УСТОЙЧИВОСТИ МЕДНО-НИКЕЛЕВЫХ СПЛАВОВ

THERMODYNAMICS OF CHEMICAL AND ELECTROCHEMICAL STABILITY OF COPPER-NICKEL ALLOYS

© П. А. Николайчук, А. Г. Тюрин
Челябинский государственный университет
454021 Челябинск, ул. Братьев Кашириных, 129
E-mail: npa@csu.ru, tag@csu.ru ; тел. (3512) 799 – 70 – 69
Поступила в редакцию

В рамках модели раствора замещения описаны термодинамические свойства твёрдых растворов системы Cu – Ni в области расслоения. Построены сечения фазовой диаграммы Cu – Ni – O и диаграммы потенциал – pH систем мельхиор МН19 – H_2O и мельхиор МНЖМц30-1-1 – H_2O при 25˚C и 1 бар. Оценена область гомогенности фазы NiO_x в равновесии с атмосферным кислородом при различных температурах. Анализируются термодинамические особенности коррозионно-электрохимического поведения медно-никелевых сплавов.

The thermodynamic properties of the solid solution of Cu – Ni system in the miscibility gap region were described in terms of substitution solution model. The cross-section of the Cu – Ni – O state diagram and the potential – pH diagrams for the systems melchior MH19 – H_2O and melchior МНЖМц30-1-1 – H_2O at 25˚C and 1 bar were plotted. The homogeneity range of the phase NiO_x in equilibrium with atmospheric oxygen at different temperatures was estimated. The corrosion-electrochemical behaviour of copper-nickel alloys was analysed.

В группу медно-никелевых сплавов входят такие сплавы на основе меди, в которых никель является основным легирующим компонентом, оказывающим решающее влияние на их свойства [1, 2]. Среди различных марок [3] медно-никелевых сплавов можно выделить группу мельхиоров [4] (англ. “cupronickel” [5]) – конструкционных сплавов,

обладающих повышенной коррозионной стойкостью [1, 5]. Изделия из них работают в агрессивных коррозионных условиях [5]: морской воде, водяном паре, растворах на основе гидроксида натрия и других, поэтому широко исследуется их коррозионно-электрохимическое поведение [6 – 10]. В работе выполнен термодинамический анализ химической устойчивости медно-никелевых сплавов и электрохимической устойчивости мельхиоров МН19 и МНЖМц30-1-1.

Структуры двойных сплавов системы Cu – Ni хорошо изучены [11, 12]. При высоких температурах металлы неограниченно растворяются друг в друге с образованием твёрдых растворов с решёткой г. ц. к. Однако, при температурах ниже 342˚С гомогенная система распадается на две фазы: α-фазу – твёрдый раствор на основе меди и γ-фазу – твёрдый раствор на основе никеля. Обе фазы имеют структуру матрицы, т. е. решётку г. ц. к. Однако, литературные данные о координатах купола расслаивания [11 – 14] рознятся довольно сильно: так, при 25˚С область расслоения простирается по одним данным [12, 13] от ~10 до ~95 ат. % Ni, а по другим [11, 12, 14] – от ~25 ат. % Ni до практически чистого никеля. Даже в рамках различных баз данных проекта FactSage Web Phase Diagrams [12] приводятся различные варианты. По мнению авторов, более достоверным является положение купола расслаивания, изложенное в [11, 14] и некоторых базах данных проекта [12].

Имеющиеся в литературе варианты термодинамического описания α-фазы системы Cu – Ni непригодны для расчётов термодинамических свойств исследуемых мельхиоров, поскольку они либо основываются на неверных координатах купола расслаивания [13], либо используют [15] модель подрешёток (описанную в [16]), что затрудняет применение термодинамических данных по бинарной системе для описания свойств многокомпонентных систем. Поэтому для системы Cu – Ni был проведён собственный расчёт термодинамических функций твёрдого раствора.

Избыточную энергию Гиббса G^E [17] α-фазы систем Cu – Ni и Cu – Ni – Fe – Mn описывали в рамках модели раствора замещения [18]:

$$G^E = \sum_{i=1}^{n-1} \sum_{j=i+1}^{n} x_i \cdot x_j \cdot Q_{ij} \qquad (1),$$

где n – число компонентов (равное двум для мельхиора МН19 и четырём для сплава МНЖМц30-1-1). Температурно-концентрационную зависимость параметров Q_{ij} представляли следующим образом [19]:

$$Q_{ij}(x_i, x_j, T) = (x_i \cdot Q_{ij}^{(1)}(T) + x_j \cdot Q_{ij}^{(2)}(T)) \qquad (2).$$

Расчёт зависимостей $Q_{12} = f(T)$ для системы Cu – Ni производился на основании условия равенства химических потенциалов компонентов α- и γ-фаз:

$$\begin{cases} \mu_{Cu}^{o,\alpha} + R \cdot T \cdot \ln x_{Cu}^{\alpha} + \mu_{Cu}^{E,\alpha} = \mu_{Cu}^{o,\gamma} + R \cdot T \cdot \ln x_{Cu}^{\gamma} + \mu_{Cu}^{E,\gamma} \\ \mu_{Ni}^{o,\alpha} + R \cdot T \cdot \ln x_{Ni}^{\alpha} + \mu_{Ni}^{E,\alpha} = \mu_{Ni}^{o,\gamma} + R \cdot T \cdot \ln x_{Ni}^{\gamma} + \mu_{Ni}^{E,\gamma} \end{cases} \quad (3),$$

после чего, для проверки корректности вычислений, производился расчёт купола расслаивания по найденным выражениям для избыточной энергии Гиббса с помощью программы PhDi [20].

Аналогичные зависимости параметров Q_{ij} других компонентов сплава МНЖМц30-1-1 взяты из литературы [19, 21] и сведены в табл. 1. Составы исследуемых сплавов и рассчитанные термодинамические активности компонентов α-фаз (Cu) при 25˚C представлены в табл. 2.

Table 1.The parameters in equation (2) for the excess Gibbs energy of the α-phase

Binary system	Indices i, j	$Q_{ij}^{(1)}(T), \frac{Дж}{моль}$	$Q_{ij}^{(2)}(T), \frac{Дж}{моль}$	Ref.
Cu – Ni	1, 2	$76{,}81 \cdot T - 39250$	$-51{,}09 \cdot T + 39360$	*
Cu – Fe	1, 3	37800	37800	[19]
Cu – Mn	1, 4	$27 \cdot T - 7390$	$27 \cdot T - 7390$	[21]
Ni – Fe	2, 3	$-1{,}04 \cdot 10^5 \cdot T^3 - -2{,}440 \cdot 10^{-2} \cdot T^2 - -34810$	$1{,}63 \cdot 10^6 \cdot T^3 - -3{,}821 \cdot 10^{-3} \cdot T^2 + +2092$	[19]
Ni – Mn	2, 4	$10{,}878 \cdot T - 64434$	$10{,}878 \cdot T - 51882$	[19]
Fe – Mn	3, 4	$16{,}987 \cdot T - 18870$	$16{,}987 \cdot T - 18870$	[19]

* estimated in present study.

Table 2. The composition and the thermodynamic activities of the components of α-phase (Cu) in the melchiors МН19 and МНЖМц30-1-1 at 25˚C

Alloy	Component of α-phase	Solid solution composition		Thermodynamic activity
		weight. %	molar fraction	
МН19	Cu	81	0,7965	0,405
	Ni	19	0,2035	0,21
МНЖМц 30-1-1	Cu	68	0,6604	0,22
	Ni	30	0,3173	0,27
	Fe	1	0,0111	2,01
	Mn	1	0,0112	0,18

Активность железа в твёрдом растворе на основе меди для сплава МНЖМц30-1-1 больше единицы (стандартное состояние – чистый компонент с решёткой г. ц. к.), что свидетельствует о неравновесности системы. Это обусловлено очень низкой растворимостью железа в меди [22]. Избыточная фаза железа, выделяясь из α-фазы мельхиора, обеспечивает дисперсионное упрочнение сплава [1].

Для того, чтобы построить термодинамическую модель процессов окисления мельхиоров, необходимо сначала рассмотреть равновесия их отдельных компонентов с кислородом.

В системе Cu – O широко известны два оксида [11, 12] – Cu_2O и CuO. Однако, в настоящее время показано, что медь может образовывать и соединение Cu_2O_3 [23, 24]. Кроме того, в литературе имеются многочисленные свидетельства о возможности образования сложных оксидов нескольких металлов, в состав которых входят слои, состоящие из CuO_2 [25 – 32]. Поэтому также проведено прогнозирование термодинамических свойств чистого диоксида меди.

В системе Ni – O между моноксидом никеля NiO и его высшими оксидами (Ni_2O_3, NiO_2) образуется непрерывный ряд твёрдых растворов [33, 34], что соответствует фазе переменного состава NiO_x. В различных работах [33, 35 – 37] показано, что содержание избыточного кислорода в нестехиометрическом оксиде никеля существенно зависит от метода его получения и температуры синтеза. Известные результаты экспериментального определения величины индекса “x” в формуле NiO_x от температуры представлены на рис. 1.

В системе Fe – O при 25˚C существуют оксиды Fe_3O_4 и Fe_2O_3 [11, 12]. Несмотря на то, что стандартная энергия Гиббса образования оксида FeO отрицательна ($\Delta_f G^o_{298}(FeO) = -244300\ ^{Дж}/_{моль}$ по данным [38]), он термодинамически неустойчив при данной температуре [39, 40], поскольку самопроизвольно разлагается:

$$4FeO = Fe + Fe_3O_4;\ \Delta_r G^o_{298} = -36960\ ^{Дж}/_{моль} \qquad (4).$$

Поскольку в сильноокислительных средах возможно образование феррат-ионов [40], а окисление Fe^{+3} до Fe^{+6} должно протекать через промежуточную форму Fe^{+4}, то процесс образования оксида FeO_2 также включён в термодинамическую модель окисления мельхиора МНЖМц30-1-1.

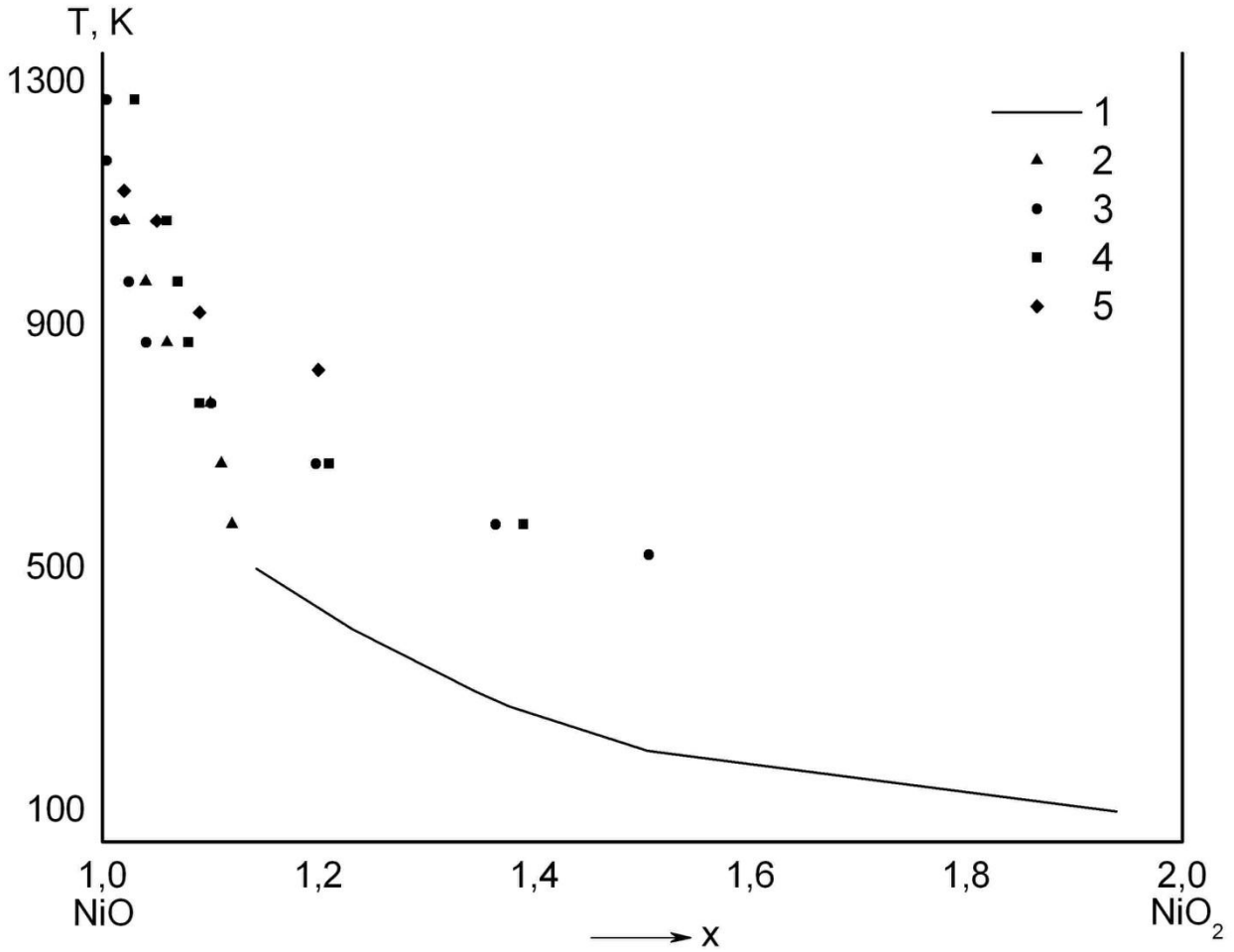

Fig. 1. The possible non-stoichiometry domain of the phase NiO_x at different temperatures in equilibrium with atmospheric ari (at P_{O_2} = 0,21 bar): 1 – calculated by Gorichev's method [66, 67]; 2 – data from [35]; 3 – data from [36], the sample was obtained from $2NiCO_3 \cdot 3Ni(OH)_2 \cdot 4H_2O$; 4 – data from [36], the sample was obtained from $Ni(NO_3)_2 \cdot 6H_2O$; 5 – data from [37], the sample was obtained from $Ni(NO_3)_2 \cdot 6H_2O$.

В системе Mn – O при 25˚C существуют оксиды MnO, Mn_3O_4, Mn_2O_3 и MnO_2 [11, 12]. Для образования оксида Mn_2O_7 в стандартных условиях требуется равновесное давление кислорода, значительно превышающее давление кислорода в атмосфере ($P_{O_2} = 2{,}2 \cdot 10^{78}$ бар [41]), либо сильноокислительные условия [40].

Кроме того, при составлении термодинамической картины окисления мельхиоров необходимо учитывать возможность образования простых и смешанных шпинелей (двойных оксидов переменного состава на основе железа, никеля, марганца и меди) [39, 42]. Так в системе Cu – Fe – O образуется множество ферритов меди, среди которых наиболее стабильны $CuFeO_2$ и $CuFe_2O_4$ [19, 22, 39, 42 – 47], в системе Ni – Fe – O образуется соединение $NiFe_2O4$ [19, 39, 42, 48 – 50], в системе Mn – Fe – O существуют

соединения $MnFe_2O4$ [39, 42, 51] и $FeMn_2O_4$ [42], в системе Ni – Mn – O сообщается о синтезе соединений $NiMnO_3$ и $NiMn_2O_4$ [42, 52], в системе Cu – Mn – O возможно образование $CuMn_2O_4$ [42].

Значения стандартных энергий Гиббса образования простых и смешанных оксидов из элементов [23, 38, 39, 43, 47, 53 – 62] собраны в табл. 3. Для большинства соединений величины, представленные в различных источниках, сопоставимы друг с другом в пределах их погрешностей. В этом случае для дальнейших расчётов использованы усреднённые значения $\Delta_f G^o_{298}$. Серьёзные расхождения между термодинамическими данными различных авторов наблюдаются для ферритов меди $CuFeO_2$ и $CuFe_2O_4$. Для оценки применимости этих величин использовано следующее допущение: для того, чтобы ферриты меди были термодинамически устойчивыми в стандартных условиях, необходимо, чтобы для реакций их разложения на простые оксиды:

$$2CuFeO_2 = Cu_2O + Fe_2O_3 \quad (5),$$

$$CuFe_2O_4 = CuO + Fe_2O_3 \quad (6),$$

выполнялось условие $\Delta_r G^o_{298} > 0$. После подстановки в это выражение значений стандартных энергий Гиббса образования оксидов меди и железа, получаются следующие условия стабильности ферритов меди, которые были использованы для выбора данных, используемых в дальнейших расчётах:

$$\begin{aligned} &2\Delta_f G^o_{298}(CuFeO_2) < \Delta_f G^o_{298}(Cu_2O) + \Delta_f G^o_{298}(Fe_2O_3); \\ &\Delta_f G^o_{298}(CuFeO_2) < -445\ 000\ {}^{Дж}/_{моль} \end{aligned} \quad (7).$$

$$\begin{aligned} &\Delta_f G^o_{298}(CuFe_2O_4) < \Delta_f G^o_{298}(CuO) + \Delta_f G^o_{298}(Fe_2O_3); \\ &\Delta_f G^o_{298}(CuFe_2O_4) < -870\ 000\ {}^{Дж}/_{моль} \end{aligned} \quad (8).$$

Следуя этому же принципу, можно показать, что соединения $NiMn_2O_4$ и $CuMn_2O_4$, несмотря на отрицательную величину их стандартной энергии Гиббса образования [38], термодинамически неустойчивы в стандартных условиях и разлагаются на простые оксиды по реакциям:

$$NiMn_2O_4 = NiO + Mn_2O_3;\ \Delta_r G^o_{298} = -77\ 160\ {}^{Дж}/_{моль} \quad (9),$$

$$CuMn_2O_4 = CuO + Mn_2O_3;\ \Delta_r G^o_{298} = -7\ 620\ {}^{Дж}/_{моль} \quad (10).$$

поэтому эти соединения не были включены в термодинамическую модель окисления мельхиоров.

Вышеперечисленные простые и двойные оксиды, имеющие степень окисленности [19], равную ${}^4/_3$, могут образовывать друг с другом твёрдые растворы [19, 22, 39, 43, 45, 46, 48, 49, 51, 63 – 65]. Феррит $CuFeO_2$ не растворяется в шпинелях [39]. Кроме того,

непрерывный ряд твёрдых растворов существует между полуторными оксидами Fe_2O_3 и Mn_2O_3 [19, 39, 63]. Данных о взаимной растворимости Fe_2O_3 и Cu_2O_3 в литературе нет.

Table 3. The standard Gibbs energies of formation of the compounds from elements

Compound	Reference	$-\Delta_f G^o_{298}$, Дж/моль	Compound	Reference	$-\Delta_f G^o_{298}$, Дж/моль
Cu_2O	[53]	147848	NiO	[53]	211430
	[38]	150548		[38]	211600
	[54]	147886		[55]	214828
	[55]	144340		[56]	211617
	[56]	147935		[59]	211700
	[57]	145520		[60]	211585
	[58]	148140		[61]	211100
	[43]	146363		[57]	208373
CuO	[53]	127890		[58]	210635
	[38]	129365	NiO_x	*	см. (11)
	[54]	128292	MnO	[53]	362770
	[55]	127750		[38]	363326
	[56]	127920		[55]	362965
	[57]	124229		[56]	362946
Cu_2O_3	[23]	279480	Mn_3O_4	[53]	1281955
CuO_2	*	90000		[38]	1282885
Fe_3O_4	[53]	1026182		[55]	1281092
	[38]	1014163		[56]	1283468
	[54]	1017438		[57]	1279258
	[55]	1019112	Mn_2O_3	[53]	879280
	[56]	1015391		[38]	879865
	[57]	1007561		[55]	894079
Fe_2O_3	[53]	743800		[56]	881205
	[38]	740337		[57]	881505
	[54]	743523	MnO_2	[53]	465370
	[55]	741613		[38]	466662
	[56]	742413		[55]	474167
	[57]	739991		[56]	465217
FeO_2	*	360000	$CuFe_2O_4$	[53]	887480
$NiFe_2O_4$	[53]	958600		[38]	852675
	[38]	956935		[62]	871437
	[39]	966596		[43]	859951
$MnFe_2O_4$	[38]	1125075		[47]	1011724
$CuMn_2O_4$	[38]	1001610		[39]	877050
$NiMn_2O_4$	[38]	1014305	$CuFeO_2$	[53]	478300
				[38]	479540
				[62]	485627
				[43]	454217
				[47]	539454

Для предполагаемых оксидов CuO_2, FeO_2, а также для фазы NiO_x термодинамические функции образования были оценены с помощью метода И. Г. Горичева [66], модифицированного авторами [41, 67]. Кроме того, в предположении о том, что термодинамические свойства однотипных соединений изменяются монотонно в пределах одного периода [68] была выведена приближённая функциональная зависимость между порядковым номером d-элемента 4 периода и стандартной энергией Гиббса образования его оксида типа MeO_2 [69]. На основании этой зависимости также была проведена независимая оценка термодинамических функций оксидов CuO_2, FeO_2 и NiO_2. Результаты оценок также приведены в табл. 3. Для фазы переменного состава NiO_x получена следующая зависимость:

$$\Delta_f G^o_{298}(NiO_x) = 155912 \cdot x^2 - 367342 \cdot x, \ {}^{Дж}/_{моль} \qquad (11).$$

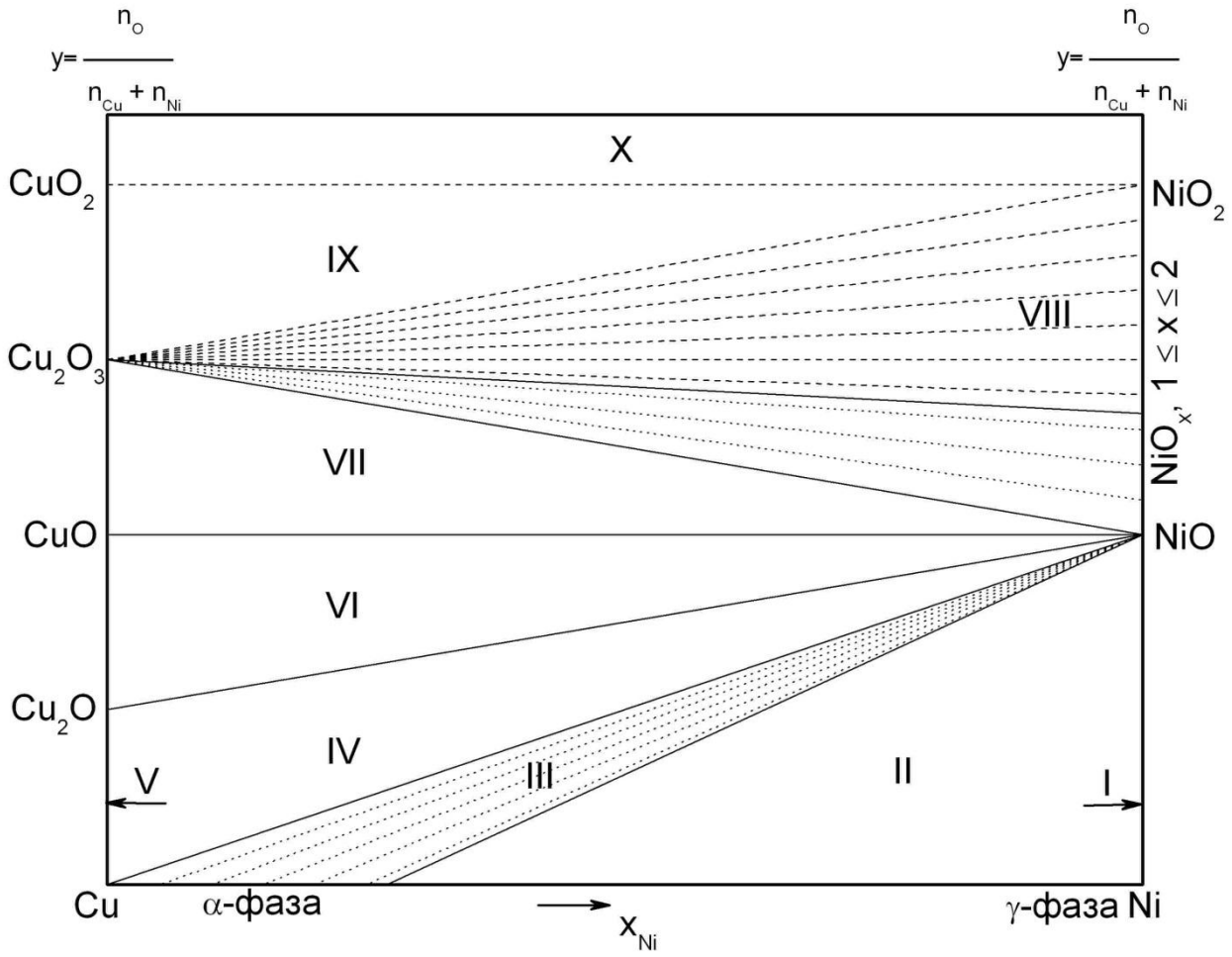

Fig. 2. The state diagram of the Cu – Ni – O system at 25˚C and air pressure of 1 bar.

Проведена термодинамическая оценка зависимости величины “x” в формуле NiO_x от температуры в области низких температур в равновесии с атмосферным воздухом (при P_{O_2} = 0,21 бар). Результаты оценки нанесены на рис. 1. При 25˚C в равновесии с

кислородом воздуха находится фаза состава $NiO_{1,344}$. Оценить корректность этих расчётов не представляется возможным, поскольку экспериментальные данные для выбранного интервала температур отсутствуют.

Table 4. The characteristics of the invariant conditions in the Cu – Ni – O system at 25˚C and 1 bar.

No of domain in Fig. 2	Invariant condition	Reaction equation	P_{O_2}, бар
I	γ-фаза (Ni) + NiO	$2Ni\ (\gamma) + O_2 = 2NiO$	–
II	γ-фаза (Ni) + α-фаза (Cu) + NiO $x_{Ni(\gamma)} \approx 1;\ x_{Cu(\gamma)} = 1{,}4 \cdot 10^{-5};$ $x_{Ni(\alpha)} = 0{,}277;\ x_{Cu(\alpha)} = 0{,}723;$ $a_{Ni(\gamma)} = a_{Ni(\alpha)} = 0{,}998;$ $a_{Cu(\gamma)} = a_{Cu(\alpha)} = 0{,}244$	$3Ni\ (\gamma) + O_2 =$ $= Ni\ (\alpha) + 2NiO$	$7{,}5 \cdot 10^{-75}$
III	α-фаза (Cu) + NiO	$2Ni\ (\alpha) + O_2 = 2NiO$	–
IV	α-фаза (Cu) + NiO + Cu_2O $x_{Ni(\alpha)} = 5{,}4 \cdot 10^{-9};\ x_{Cu(\alpha)} \approx 1;$ $a_{Ni(\alpha)} = 4{,}2 \cdot 10^{-21};\ a_{Cu(\alpha)} = 0{,}999$	$\begin{cases} 2Ni(\alpha) + O_2 = 2NiO \\ 4Cu(\alpha) + O_2 = 2Cu_2O \end{cases}$	$3{,}3 \cdot 10^{-54}$
V	α-фаза (Cu) + Cu_2O	$4Cu\ (\alpha) + O_2 = 2Cu_2O$	–
VI	Cu_2O + CuO + NiO	$2Cu_2O + O2 = 4CuO$	$2{,}2 \cdot 10^{-39}$
VII	CuO + Cu_2O_3 + NiO	$4CuO + O2 = 2Cu_2O_3$	$1{,}4 \cdot 10^{-6}$
VIII	Cu_2O_3 + NiO_x $(1 \le x \le 2)$ а) x = 1,344 б) x = 2	$2NiO + (x-1)O_2 = 2NiO_x$	см. * 0,21 $1{,}5 \cdot 10^{35}$
IX	Cu_2O_3 + CuO_2 + NiO_2	$2Cu_2O_3 + O2 = 4CuO_2$	$1{,}5 \cdot 10^{39}$
X	CuO_2 + NiO_2 + $\{O_2\}$	–	–

* $\ln P_{O_2}\,[\text{бар}] = 125{,}79 \cdot (x+1) - 296{,}37$

Фазовая диаграмма системы Cu – Ni – O при 25˚C и давлении воздуха 1 бар приведена на рис. 2. Рассчитанные характеристики состояний системы представлены в табл. 4. Несмотря на то, что оксид Cu_2O_3 термодинамически устойчив в нормальных условиях, он не образует отдельную фазу [24], поэтому окисление медно-никелевых сплавов на воздухе должно завершиться образованием CuO и NiO_x. Как показывают расчёты, химическая устойчивость медно-никелевых сплавов на воздухе определяется содержанием в них никеля. При его содержании в поверхностном слое сплава выше 10^{-7} мол. % единственным продуктом окисления может быть NiO_x $(1 \le x \le 1{,}344)$.

Для построения термодинамической модели окисления сплавов МН19 и МНЖМц30-1-1 в водных средах удобно использовать диаграммы электрохимического равновесия (потенциал – pH) [70 – 72], которые наиболее наглядно отображают возможные химические и электрохимические равновесия в системе. Методика построения и анализа подобных диаграмм подробно изложена в [19]. В качестве продуктов окисления наряду с вышеперечисленными оксидами нужно учитывать и возможные ионы, которые могут образоваться в растворе. Ранее были построены диаграммы электрохимического равновесия систем Cu – H_2O [73], Fe – Cu – H_2O [22], Fe – Ni – H_2O [48], Fe – Mn – H_2O [63].

Первичную информацию о продуктах окисления в системах "металл – вода" для компонентов сплавов можно получить из различных баз данных диаграмм потенциал – pH [74 – 83]. Наиболее полно эта информация собрана и обобщена в обзоре [84]. Однако, приводимые варианты диаграмм являются полуколичественными, информация в аналитическом виде либо отсутствует, либо находится в ограниченном доступе, отсутствует возможность внесения новых исходных данных и учёта равновесий с фазами переменного состава. Всё это делает невозможным применение указанных ресурсов для построения диаграмм электрохимического равновесия сложных сплавов, ограничивая их применение лишь данными о возможных формах нахождения компонентов сплавов в растворе. В данной работе построение диаграмм потенциал – pH осуществлялось с использованием собственных программных разработок авторов.

Любые оксиды или кислородсодержащие ионы в растворе могут находиться как в негидратированной, так и в гидратированной формах [70]. Переход от первой ко второй форме протекает через ряд промежуточных состояний. Наиболее устойчивой в термодинамическом плане являются негидратированная форма [85], поэтому гидроксиды металлов и другие, указанные на диаграммах [74 – 84] частицы – $CuOH^+$, $Cu_2(OH)_2^{2+}$, $Cu(OH)_4^{2-}$, $FeOH^+$, $FeOOH$, $FeOH^{2+}$, $Fe(OH)_2^+$, $Fe(OH)_3^-$, $Fe(OH)_4^-$, $Fe_2(OH)_2^{4+}$, $Fe_3(OH)_4^{5+}$, $NiOH^+$, $NiOOH$, $Ni(OH)_3^-$, $Ni(OH)_4^{2-}$, Ni_2OH^{3+}, $Ni_4(OH)_4^{4+}$, $MnOH^+$, $MnOOH$, $MnOH^{2+}$, $Mn(OH)_3^-$, $Mn(OH)_4^{2-}$, $Mn_2(OH)_3^+$, Mn_2OH^{3+} – не принимаются во внимание в дальнейших расчётах. Возможность образования гидрида никеля Ni_2H [8 – 10, 73] также не учитывается, поскольку для него отсутствует надёжная термодинамическая информация.

При расчёте химических и электрохимических равновесий с участием ионов использованы справочные данные [62, 70, 86].

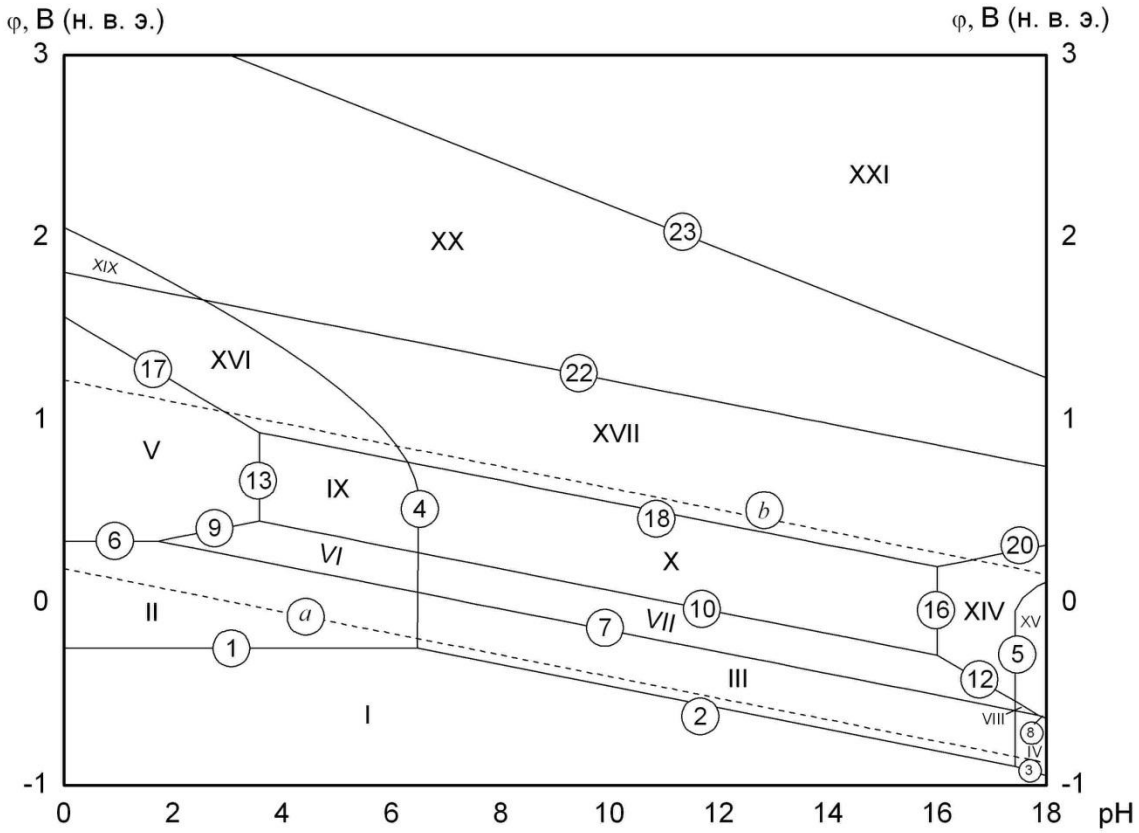

Fig. 3. The potential – pH diagram of the system melchior MH19 (α-phase) – H_2O at 25˚C, air pressure of 1 bar and $a_i = 1$ моль/л (undydrated form of the oxides).

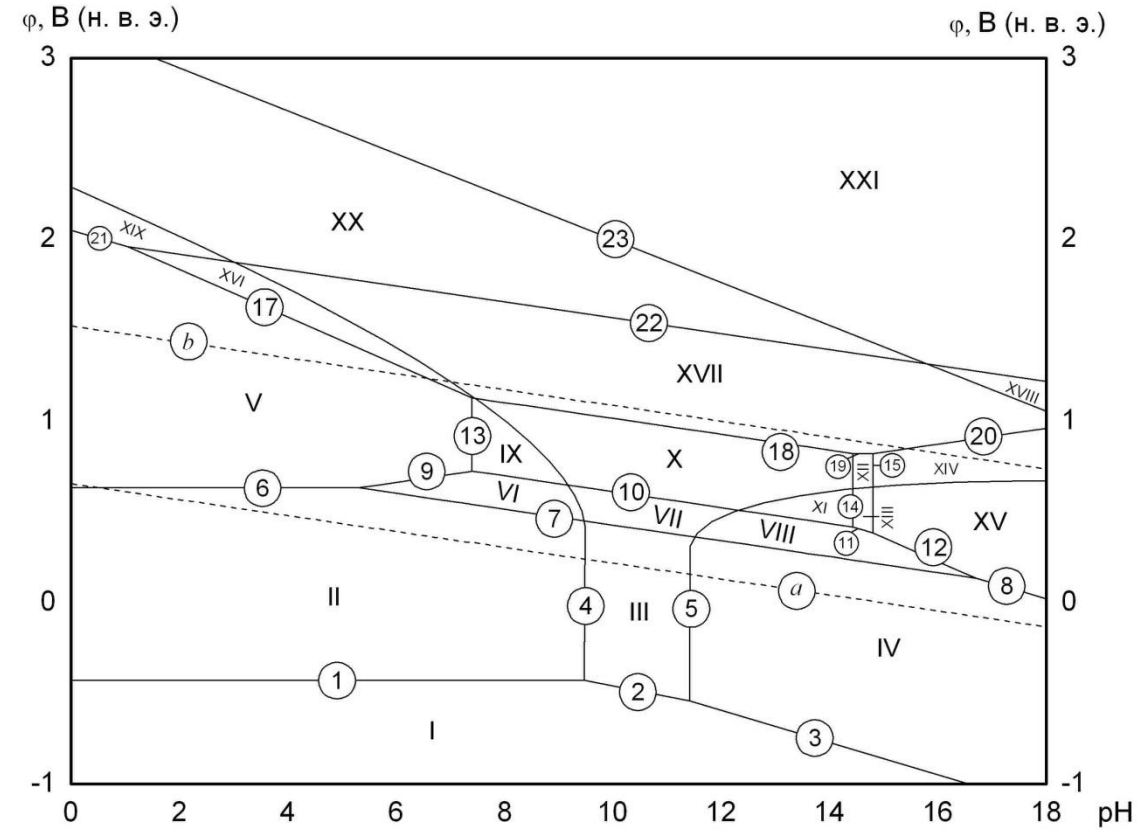

Fig. 4. The potential – pH diagram of the system melchior MH19 (α-phase) – H_2O at 25˚C, air pressure of 1 bar and $a_i = 10^{-6}$ моль/л (unhydrated form of the oxides).

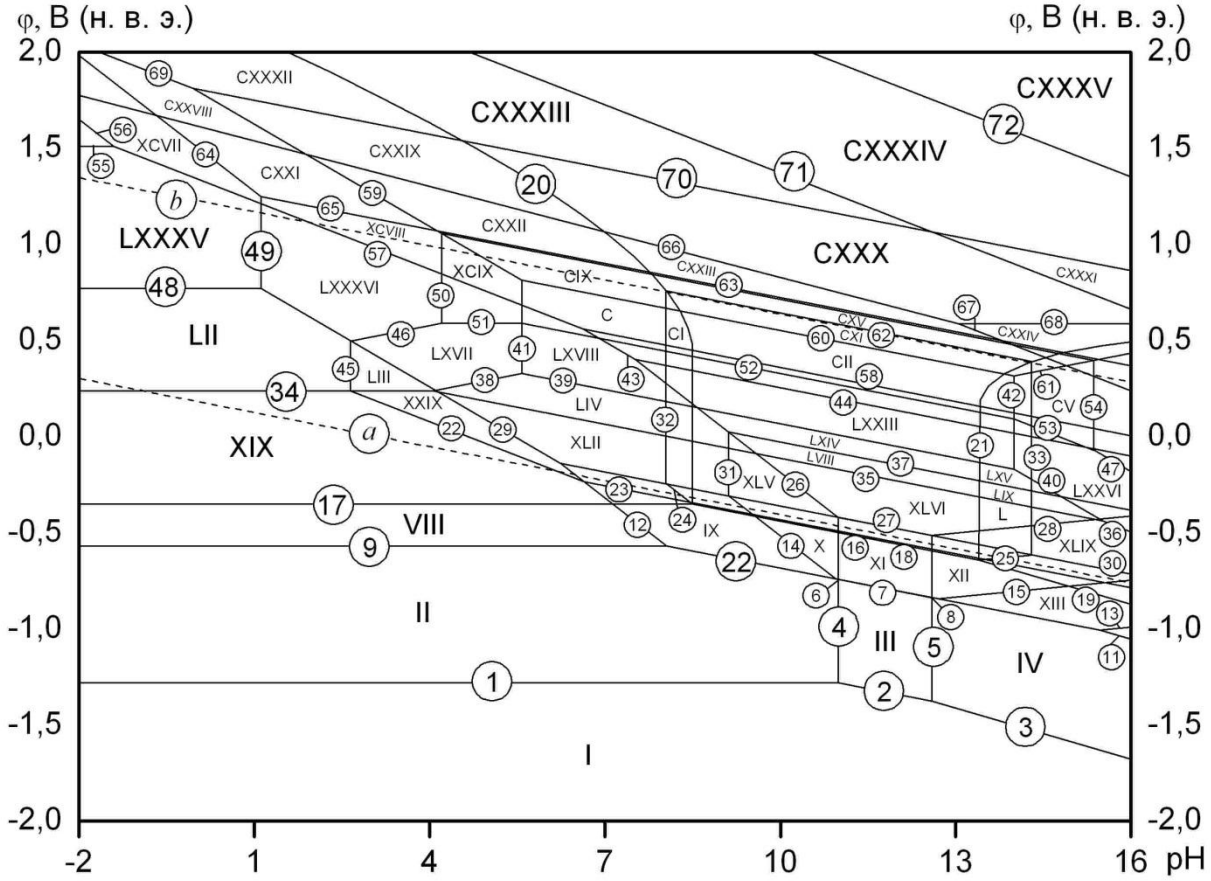

Fig. 5. The potential – pH diagram of the system melchior МНЖМц30-1-1 (α-phase) – H_2O at 25˚C, air pressure of 1 bar and $a_i = 10^{-4}$ моль/л (unhydrated form of the oxides).

Table 5. The basic chemical and electrochemical equilibria in the system alloy МН19 – H_2O at 25˚C and air pressure of 1 bar

No of line in Figs.. 3 and 4	Electrode reaction	Equilibrium potential (V, s. h. e.) or solution pH
a	$2H^+ + 2e^- = H_2(г); P_{H_2} = 5 \cdot 10^{-7}$ бар	$0{,}186 - 0{,}0591 \cdot pH$
b	$O_2(г) + 4H^+ + 4e^- = 2H_2O; P_{O_2} = 0{,}21$ бар	$1{,}219 - 0{,}0591 \cdot pH$
1	$Ni^{2+} + 2e^- = Ni(\alpha); a_{Ni(\alpha)} = 0{,}21$	$-0{,}230 + 0{,}0295 \cdot \lg a_{Ni^{2+}}$
2	$NiO + 2H^+ + 2e^- = Ni(\alpha) + H_2O; a_{Ni(\alpha)} = 0{,}21$	$0{,}154 - 0{,}0591 \cdot pH$
3	$HNiO_2^- + 3H^+ + 2e^- = Ni(\alpha) + 2H_2O;$ $a_{Ni(\alpha)} = 0{,}21$	$0{,}668 - 0{,}0887 \cdot pH + 0{,}0295 \cdot \lg a_{HNiO_2^-}$
4	$NiO_x + 2xH^+ + 2(x-1)e^- = Ni^{2+} + xH_2O$	$\frac{0{,}808 \cdot x^2 - 0{,}674 \cdot x + 0{,}250}{x-1} -$ $- \frac{0{,}0591 \cdot x}{x-1} \cdot pH - \frac{0{,}0295}{x-1} \cdot lg\, a_{Ni^{2+}}$

5	$HNiO_2^- + (3-2x)H^+ + 2(1-x)e^- = NiO_x + (2-x)H_2O$	$\frac{-0{,}808\cdot x^2 + 0{,}674\cdot x + 0{,}648}{1-x} - \frac{0{,}0295\cdot(3-2\cdot x)}{1-x}\cdot pH + \frac{0{,}0295}{1-x}\cdot lg\, a_{HNiO_2^-}$
6	$Cu^{2+} + 2e^- = Cu(\alpha); a_{Cu(\alpha)} = 0{,}405$	$0{,}342 + 0{,}0295\cdot \lg a_{Cu^{2+}}$
7	$Cu_2O + 2H^+ + 2e^- = 2Cu(\alpha) + H_2O;$ $a_{Cu(\alpha)} = 0{,}405$	$0{,}448 - 0{,}0591\cdot pH$
8	$CuO_2^{2-} + 4H^+ + 2e^- = Cu(\alpha) + 2H_2O;$ $a_{Cu(\alpha)} = 0{,}405$	$1{,}499 - 0{,}1182\cdot pH + 0{,}0295\cdot \lg a_{CuO_2^{2-}}$
9	$2Cu^{2+} + H_2O + 2e^- = Cu_2O + 2H^+$	$0{,}235 + 0{,}0591\cdot pH + 0{,}0591\cdot \lg a_{Cu^{2+}}$
10	$2CuO + 2H^+ + 2e^- = Cu_2O + H_2O$	$0{,}658 - 0{,}0591\cdot pH$
11	$2HCuO_2^- + 4H^+ + 2e^- = Cu_2O + 3H_2O$	$1{,}771 - 0{,}1182\cdot pH + 0{,}0591\cdot \lg a_{HCuO_2^-}$
12	$2CuO_2^{2-} + 6H^+ + 2e^- = Cu_2O + 3H_2O$	$2{,}549 - 0{,}1773\cdot pH + 0{,}0591\cdot \lg a_{CuO_2^{2-}}$
13	$CuO + 2H^+ = Cu^{2+} + H_2O$	$pH = 3{,}58 - 0{,}5\cdot \lg a_{Cu^{2+}}$
14	$HCuO_2^- + H^+ = CuO + H_2O$	$pH = 18{,}83 + \lg a_{HCuO_2^-}$
15	$CuO_2^{2-} + H^+ = HCuO_2^-$	$pH = 13{,}16 + \lg \frac{a_{CuO_2^{2-}}}{a_{HCuO_2^-}}$
16	$CuO_2^{2-} + 2H^+ = CuO + H_2O$	$pH = 15{,}99 + 0{,}5\cdot \lg a_{CuO_2^{2-}}$
17	$Cu_2O_3 + 6H^+ + 2e^- = 2Cu^{2+} + 3H_2O$	$1{,}566 - 0{,}1773\cdot pH - 0{,}0591\cdot \lg a_{Cu^{2+}}$
18	$Cu_2O_3 + 2H^+ + 2e^- = 2CuO + H_2O$	$1{,}143 - 0{,}0591\cdot pH$
19	$Cu_2O_3 + H_2O + 2e^- = 2HCuO_2^-$	$0{,}030 - 0{,}0591\cdot \lg a_{HCuO_2^-}$
20	$Cu_2O_3 + H_2O + 2e^- = 2CuO_2^{2-} + 2H^+$	$-0{,}748 + 0{,}0591\cdot pH - 0{,}0591\cdot \lg a_{CuO_2^{2-}}$
21	$CuO_2 + 4H^+ + 2e^- = Cu^{2+} + 2H_2O$	$1{,}687 - 0{,}1182\cdot pH - 0{,}0295\cdot \lg a_{Cu^{2+}}$
22	$2CuO_2 + 2H^+ + 2e^- = Cu_2O_3 + H_2O$	$1{,}809 - 0{,}0591\cdot pH$
23	$NiO_4^{2-} + 4H^+ + 2e^- = NiO_2 + 2H_2O$	$3{,}360 - 0{,}1182\cdot pH + 0{,}0295\cdot \lg a_{NiO_4^{2-}}$

Table 6. The basic chemical and electrochemical equilibria in the system alloy МНЖМц30-1-1 – H_2O at 25˚C and air pressure of 1 bar

No of line in Fig. 5	Electrode reaction	Equilibrium potential (V, s. h. e.) or solution pH
a	$2H^+ + 2e^- = H_2(г); P_{H_2} = 5\cdot 10^{-7}$ бар	$0{,}186 - 0{,}0591\cdot pH$
b	$O_2(г) + 4H^+ + 4e^- = 2H_2O; P_{O_2} = 0{,}21$бар	$1{,}219 - 0{,}0591\cdot pH$
1	$Mn^{2+} + 2e^- = Mn(\alpha); a_{Mn(\alpha)} = 0{,}18$	$-1{,}163 + 0{,}0295\cdot \lg a_{Mn^{2+}}$
2	$MnO + 2H^+ + 2e^- = Mn(\alpha) + H_2O;$ $a_{Mn(\alpha)} = 0{,}18$	$-0{,}631 - 0{,}0591\cdot pH$

3	$HMnO_2^- + 3H^+ + 2e^- = Mn(\alpha) + 2H_2O$; $a_{Mn(\alpha)} = 0{,}18$	$-0{,}141 - 0{,}0887 \cdot pH + 0{,}0295 \cdot \lg a_{HMnO_2^-}$
4	$MnO + 2H^+ = Mn^{2+} + H_2O$	$pH = 8{,}99 - 0{,}5 \cdot \lg a_{Mn^{2+}}$
5	$HMnO_2^- + H^+ = MnO + H_2O$	$pH = 16{,}58 + \lg a_{HMnO_2^-}$
6	$MnFe_2O_4 + 8H^+ + 6e^- =$ $= Mn^{2+} + 2Fe(\alpha) + 4H_2O; a_{Fe(\alpha)} = 2{,}01$	$0{,}085 - 0{,}0788 \cdot pH - 0{,}00985 \cdot \lg a_{Mn^{2+}}$
7	$MnFe_2O_4 + 6H^+ + 6e^- =$ $= MnO + 2Fe(\alpha) + 3H_2O; a_{Fe(\alpha)} = 2{,}01$	$-0{,}0924 - 0{,}0591 \cdot pH$
8	$MnFe_2O_4 + 5H^+ + 6e^- =$ $= HMnO_2^- + 2Fe(\alpha) + 2H_2O; a_{Fe(\alpha)} = 2{,}01$	$-0{,}256 - 0{,}0492 \cdot pH - 0{,}00985 \cdot \lg a_{HMnO_2^-}$
9	$Fe^{2+} + 2e^- = Fe(\alpha); a_{Fe(\alpha)} = 2{,}01$	$-0{,}449 + 0{,}0295 \cdot \lg a_{Fe^{2+}}$
10	$Fe_3O_4 + 8H^+ + 8e^- = 3Fe(\alpha) + 4H_2O$; $a_{Fe(\alpha)} = 2{,}01$	$-0{,}0912 - 0{,}0591 \cdot pH$
11	$HFeO_2^- + 3H^+ + 2e^- = Fe(\alpha) + 2H_2O$; $a_{Fe(\alpha)} = 2{,}01$	$0{,}484 - 0{,}0887 \cdot pH + 0{,}0295 \cdot \lg a_{HFeO_2^-}$
12	$Fe_3O_4 + 8H^+ + 2e^- = 3Fe^{2+} + 4H_2O$	$0{,}982 - 0{,}2364 \cdot pH - 0{,}0887 \cdot \lg a_{Fe^{2+}}$
13	$Fe_3O_4 + 2H_2O + 2e^- = 3HFeO_2^- + H^+$	$-1{,}817 + 0{,}0295 \cdot pH - 0{,}0887 \cdot \lg a_{HFeO_2^-}$
14	$3MnFe_2O_4 + 8H^+ + 2e^- =$ $= 3Mn^{2+} + 2Fe_3O_4 + 4H_2O$	$1{,}493 - 0{,}2364 \cdot pH - 0{,}0887 \cdot \lg a_{Mn^{2+}}$
15	$3MnFe_2O_4 + 2H_2O + 2e^- =$ $= 3HMnO_2^- + 2Fe_3O_4 + H^+$	$-1{,}573 + 0{,}0295 \cdot pH - 0{,}0887 \cdot \lg a_{HMnO_2^-}$
16	$3NiFe_2O_4 + 8H^+ + 8e^- =$ $= 3Ni(\alpha) + 2Fe_3O_4 + 4H_2O; a_{Ni(\alpha)} = 0{,}27$	$0{,}15058 - 0{,}0591 \cdot pH$
17	$Ni^{2+} + 2e^- = Ni(\alpha); a_{Ni(\alpha)} = 0{,}27$	$-0{,}233 + 0{,}0295 \cdot \lg a_{Ni^{2+}}$
18	$NiO + 2H^+ + 2e^- = Ni(\alpha) + H_2O$; $a_{Ni(\alpha)} = 0{,}27$	$0{,}15059 - 0{,}0591 \cdot pH$
19	$HNiO_2^- + 3H^+ + 2e^- = Ni(\alpha) + 2H_2O$; $a_{Ni(\alpha)} = 0{,}27$	$0{,}665 - 0{,}0887 \cdot pH + 0{,}0295 \cdot \lg a_{HMnO_2^-}$
20	$NiO_x + 2xH^+ + 2(x-1)e^- = Ni^{2+} + xH_2O$	$\frac{0{,}808 \cdot x^2 - 0{,}674 \cdot x + 0{,}250}{x-1} -$ $- \frac{0{,}0591 \cdot x}{x-1} \cdot pH - \frac{0{,}0295}{x-1} \cdot lg\, a_{Ni^{2+}}$
21	$HNiO_2^- + (3-2x)H^+ + 2(1-x)e^- =$ $= NiO_x + (2-x)H_2O$	$\frac{-0{,}808 \cdot x^2 + 0{,}674 \cdot x + 0{,}648}{1-x} -$ $- \frac{0{,}0295 \cdot (3-2 \cdot x)}{1-x} \cdot pH + \frac{0{,}0295}{1-x} \cdot lg\, a_{HNiO_2^-}$
22	$CuFeO_2 + 4H^+ + 2e^- =$ $= Cu(\alpha) + Fe^{2+} + 2H_2O; a_{Cu(\alpha)} = 0{,}22$	$0{,}433 - 0{,}1182 \cdot pH - 0{,}0295 \cdot \lg a_{Fe^{2+}}$

23	$3CuFeO_2 + 4H^+ + 4e^- =$ $= 3Cu(\alpha) + Fe_3O_4 + 2H_2O; a_{Cu(\alpha)} = 0,22$	$0,159 - 0,0591 \cdot pH$
24	$3NiFe_2O_4 + 8H^+ + 2e^- =$ $= 3Ni^{2+} + 2Fe_3O_4 + 4H_2O$	$1,302 - 0,2364 \cdot pH - 0,0887 \cdot \lg a_{Ni^{2+}}$
25	$3NiFe_2O_4 + 2H_2O + 2e^- =$ $= 3HNiO_2^- + 2Fe_3O_4 + H^+$	$-1,392 + 0,0295 \cdot pH - 0,0887 \cdot \lg a_{HNiO_2^-}$
26	$Mn_3O_4 + 8H^+ + 2e^- = 3Mn^{2+} + 4H_2O$	$1,825 - 0,2364 \cdot pH - 0,0887 \cdot \lg a_{Mn^{2+}}$
27	$Mn_3O_4 + 2H^+ + 2e^- = 3MnO + H_2O$	$0,2298 - 0,0591 \cdot pH$
28	$Mn_3O_4 + 2H_2O + 2e^- = 3HMnO_2^- + H^+$	$-1,241 + 0,0295 \cdot pH - 0,0887 \cdot \lg a_{HMnO_2^-}$
29	$Fe_2O_3 + 6H^+ + 2e^- = 2Fe^{2+} + 3H_2O$	$0,732 - 0,1773 \cdot pH - 0,0591 \cdot \lg a_{Fe^{2+}}$
30	$3Fe_2O_3 + 2H^+ + 2e^- = 2Fe_3O_4 + H_2O$	$0,2308 - 0,0591 \cdot pH$
31	$MnFe_2O_4 + 2H^+ = Mn^{2+} + Fe_2O_3 + H_2O$	$pH = 7,11 - 0,5 \cdot \lg a_{Mn^{2+}}$
32	$NiFe_2O_4 + 2H^+ = Ni^{2+} + Fe_2O_3 + H_2O$	$pH = 6,04 - 0,5 \cdot \lg a_{Ni^{2+}}$
33	$HNiO_2^- + Fe_2O_3 + H^+ = NiFe_2O_4 + H_2O$	$pH = 18,30 + \lg a_{HNiO_2^-}$
34	$Cu^{2+} + 2e^- = Cu(\alpha); a_{Cu(\alpha)} = 0,22$	$0,356 + 0,0295 \cdot \lg a_{Cu^{2+}}$
35	$Cu_2O + 2H^+ + 2e^- = 2Cu(\alpha) + H_2O;$ $a_{Cu(\alpha)} = 0,22$	$0,478 - 0,0591 \cdot pH$
36	$CuO_2^{2-} + 4H^+ + 2e^- = Cu(\alpha) + 2H_2O;$ $a_{Cu(\alpha)} = 0,22$	$1,513 - 0,1182 \cdot pH + 0,0295 \cdot \lg a_{CuO_2^{2-}}$
37	$3Fe_2O_3 + Mn_3O_4 + 2H^+ + 2e^- =$ $= 3MnFe_2O_4 + H_2O$	$0,563 - 0,0591 \cdot pH$
38	$2Cu^{2+} + H_2O + 2e^- = Cu_2O + 2H^+$	$0,235 + 0,0591 \cdot pH + 0,0591 \cdot \lg a_{Cu^{2+}}$
39	$2CuO + 2H^+ + 2e^- = Cu_2O + H_2O$	$0,658 - 0,0591 \cdot pH$
40	$2CuO_2^{2-} + 6H^+ + 2e^- = Cu_2O + 3H_2O$	$2,549 - 0,1773 \cdot pH + 0,0591 \cdot \lg a_{CuO_2^{2-}}$
41	$CuO + 2H^+ = Cu^{2+} + H_2O$	$pH = 3,58 - 0,5 \cdot \lg a_{Cu^{2+}}$
42	$CuO_2^{2-} + 2H^+ = CuO + H_2O$	$pH = 15,99 + 0,5 \cdot \lg a_{CuO_2^{2-}}$
43	$Mn_2O_3 + 6H^+ + 2e^- = 2Mn^{2+} + 3H_2O$	$1,499 - 0,1773 \cdot pH - 0,0591 \cdot \lg a_{Mn^{2+}}$
44	$3Mn_2O_3 + 2H^+ + 2e^- = 2Mn_3O_4 + H_2O$	$0,847 - 0,0591 \cdot pH$
45	$CuFeO_2 + 4H^+ = Cu^{2+} + Fe^{2+} + 2H_2O$	$pH = 0,65 - 0,25 \cdot \lg (a_{Cu^{2+}} \cdot a_{Fe^{2+}})$
46	$2Cu^{2+} + Fe_2O_3 + H_2O + 2e^- =$ $= 2CuFeO_2 + 2H^+$	$0,578 + 0,0591 \cdot pH + 0,0591 \cdot \lg a_{Cu^{2+}}$
47	$2CuO_2^{2-} + Fe_2O_3 + 6H^+ + 2e^- =$ $= 2CuFeO_2 + 3H_2O$	$2,892 - 0,1773 \cdot pH + 0,0591 \cdot \lg a_{CuO_2^{2-}}$
48	$Fe^{3+} + e^- = Fe^{2+}$	$0,771 + 0,0591 \cdot \lg \frac{a_{Fe^{3+}}}{a_{Fe^{2+}}}$
49	$Fe_2O_3 + 6H^+ = 2Fe^{3+} + 3H_2O$	$pH = -0,221 - 0,333 \cdot \lg a_{Fe^{3+}}$
50	$CuFe_2O_4 + 2H^+ = Cu^{2+} + Fe_2O_3 + H_2O$	$pH = 2,20 - 0,5 \cdot \lg a_{Cu^{2+}}$
51	$CuFe_2O_4 + Cu^{2+} + 2e^- = 2CuFeO_2$	$0,708 + 0,0295 \cdot \lg a_{Cu^{2+}}$

52	$CuFe_2O_4 + CuO + 2H^+ + 2e^- = 2CuFeO_2 + H_2O$	$0{,}920 - 0{,}0591 \cdot pH$
53	$CuFe_2O_4 + CuO_2^- + 4H^+ + 2e^- = 2CuFeO_2 + 2H_2O$	$1{,}865 - 0{,}1182 \cdot pH + 0{,}0295 \cdot \lg a_{CuO_2^-}$
54	$CuO_2^- + Fe_2O_3 + 2H^+ = CuFe_2O_4 + H_2O$	$pH = 17{,}37 + 0{,}5 \cdot \lg a_{CuO_2^-}$
55	$Mn^{3+} + e^- = Mn^{2+}$	$1{,}510 + 0{,}0591 \cdot \lg \frac{a_{Mn^{3+}}}{a_{Mn^{2+}}}$
56	$MnO_2 + 4H^+ + e^- = Mn^{3+} + 2H_2O$	$0{,}941 - 0{,}2364 \cdot pH - 0{,}0591 \cdot \lg a_{Mn^{3+}}$
57	$MnO_2 + 4H^+ + 2e^- = Mn^{2+} + 2H_2O$	$1{,}226 - 0{,}1182 \cdot pH - 0{,}0295 \cdot \lg a_{Mn^{2+}}$
58	$2MnO_2 + 2H^+ + 2e^- = Mn_2O_3 + H_2O$	$0{,}952 - 0{,}0591 \cdot pH$
59	$Cu_2O_3 + 6H^+ + 2e^- = 2Cu^{2+} + 3H_2O$	$1{,}566 - 0{,}1773 \cdot pH - 0{,}0591 \cdot \lg a_{Cu^{2+}}$
60	$Cu_2O_3 + 2H^+ + 2e^- = 2CuO + H_2O$	$1{,}143 - 0{,}0591 \cdot pH$
61	$Cu_2O_3 + H_2O + 2e^- = 2CuO_2^{2-} + 2H^+$	$-0{,}748 + 0{,}0591 \cdot pH - 0{,}0591 \cdot \lg a_{CuO_2^{2-}}$
62	$NiO_{1,223} + Fe_2O_3 + 0{,}446H^+ + 0{,}446e^- = NiFe_2O_4 + 0{,}223H_2O$	$1{,}254 - 0{,}0591 \cdot pH$
63	$Cu_2O_3 + 2Fe_2O_3 + 2H^+ + 2e^- = 2CuFe_2O_4 + H_2O$	$1{,}306 - 0{,}0591 \cdot pH$
64	$FeO_2 + 4H^+ + e^- = Fe^{3+} + 2H_2O$	$1{,}276 - 0{,}2364 \cdot pH - 0{,}0591 \cdot \lg a_{Fe^{3+}}$
65	$2FeO_2 + 2H^+ + 2e^- = Fe_2O_3 + H_2O$	$1{,}315 - 0{,}0591 \cdot pH$
66	$MnO_4^- + 4H^+ + 3e^- = MnO_2 + 2H_2O$	$1{,}695 - 0{,}0788 \cdot pH + 0{,}0197 \cdot \lg a_{MnO_4^-}$
67	$MnO_4^{2-} + 4H^+ + 2e^- = MnO_2 + 2H_2O$	$2{,}249 - 0{,}1182 \cdot pH + 0{,}0295 \cdot \lg a_{MnO_4^{2-}}$
68	$MnO_4^- + e^- = MnO_4^{2-}$	$0{,}588 + 0{,}0591 \cdot \lg \frac{a_{MnO_4^-}}{a_{MnO_4^{2-}}}$
69	$CuO_2 + 4H^+ + 2e^- = Cu^{2+} + 2H_2O$	$1{,}687 - 0{,}1182 \cdot pH - 0{,}0295 \cdot \lg a_{Cu^{2+}}$
70	$2CuO_2 + 2H^+ + 2e^- = Cu_2O_3 + H_2O$	$1{,}809 - 0{,}0591 \cdot pH$
71	$FeO_4^{2-} + 4H^+ + 2e^- = FeO_2 + 2H_2O$	$2{,}673 - 0{,}1182 \cdot pH + 0{,}0295 \cdot \lg a_{FeO_4^{2-}}$
72	$NiO_4^{2-} + 4H^+ + 2e^- = NiO_2 + 2H_2O$	$3{,}360 - 0{,}1182 \cdot pH + 0{,}0295 \cdot \lg a_{NiO_4^{2-}}$

Диаграммы электрохимического равновесия мельхиоров МН19 и МНЖМц30-1-1 приведены на рис. 3 – 5. Для сплава МН19 диаграмма потенциал – pH построена при активностях ионов в растворе, равных 1 и 10^{-6} моль/л. Различия в виде диаграмм, построенных при разных активностях, связаны с термодинамической неустойчивостью ионов $HCuO_2^-$ при высоких концентрациях [73]. Для сплава МНЖМц30-1-1 диаграмма построена при активностях ионов, равных 10^{-4} моль/л. Результаты расчётов химических и электрохимических равновесий в системах приведены в табл. 5 и 6.

На диаграмме потенциал – pH системы мельхиор МН19 (α-фаза) – H_2O при 25˚С (рис. 3 и 4) можно выделить 21 область преобладания различных фаз:

I – мельхиор МН19 (α-фаза); II – α-фаза + Ni^{2+}; III – α-фаза + NiO_x; IV – α-фаза + $HNiO_2^-$;

V – Cu^{2+}, Ni^{2+}; VI – Cu_2O + Ni^{2+}; VII – Cu_2O + NiO_x; VIII – Cu_2O + $HNiO_2^-$; IX – CuO + Ni^{2+};

X – CuO + NiO_x; XI – CuO + $HNiO_2^-$; XII – $HCuO_2^-$ + NiO_x; XIII – $HCuO_2^-$, $HNiO_2^-$;

XIV – CuO_2^{2-} + NiO_x; XV – CuO_2^{2-}, $HNiO_2^-$; XVI – Cu_2O_3 + Ni^{2+}; XVII – Cu_2O_3 + NiO_x;

XVIII – Cu_2O_3 + NiO_4^{2-}; XIX – CuO_2 + Ni^{2+}; XX – CuO_2 + NiO_x; XXI – CuO_2 + NiO_4^{2-}.

Область I – это область термодинамической устойчивости (иммунности) сплава, области II – IV – области селективной коррозии никеля, область V соответствует общей коррозии. В областях XVIII и XXI никель находится в транспассивном состоянии, а в областях III, VI – XII, XIV, XVI – XXI сплав подвергается оксидной пассивации.

Как и на чистом никеле [48], пассивационная плёнка на сплаве однородна и представляет собой фазу NiO_x (область III, негидратированная форма оксидов). При гидратации она переходит в оксигидраты $Ni(OH)_2$ и NiOOH [87]. С ростом активности (концентрации) ионов Ni^{2+} и $HNiO_2^-$ в водном растворе поле оксидной пассивации сплава расширяется и при $a_i \geq 10^{-2}$ моль/л занимает всю область нейтральных и щелочных сред. Увеличение окислительно-восстановительного потенциала системы смещает границу активно-пассивного перехода в сплаве в кислую область. Это соответствует данным экспериментов [6 – 9].

На диаграмме потенциал – pH системы мельхиор МНЖМц30-1-1 (α-фаза) – H_2O при 25˚С (рис. 5) можно выделить 135 областей преобладания различных фаз:

I – мельхиор МНЖМц30-1-1 (α-фаза);

II – α-фаза + Mn^{2+};

III – α-фаза + MnO;

IV – α-фаза + $HMnO_2^-$;

V – α-фаза + $MnFe_2O_4$ + Mn^{2+};

VI – α-фаза + $MnFe_2O_4$ + MnO;

VII – α-фаза + $MnFe_2O_4$ + $HMnO_2^-$;

VIII – α-фаза + Mn^{2+}, Fe^{2+};

IX – α-фаза + Fe_3O_4 + Mn^{2+};

X – α-фаза + (Fe, Mn)Fe_2O_4 + Mn^{2+};

XI – α-фаза + (Fe, Mn)Fe_2O_4 + MnO;

XII – α-фаза + (Fe, Mn)Fe_2O_4 + $HMnO_2^-$;

XIII – α-фаза + Fe_3O_4 + $HMnO_2^-$;

XIV – α-фаза + $HMnO_2^-$, $HFeO_2^-$;

XV – α-фаза + (Fe, Ni)Fe_2O_4 + Mn^{2+};

XVI – α-фаза + (Fe, Ni, Mn)Fe_2O_4 + Mn^{2+};

XVII – α-фаза + (Fe, Ni, Mn)Fe_2O_4 + MnO;

XVIII – α-фаза + (Fe, Ni, Mn)Fe_2O_4 + $HMnO_2^-$;

XIX – α-фаза + Mn^{2+}, Fe^{2+}, Ni^{2+};

XX – α-фаза + Fe_3O_4 + Mn^{2+}, Ni^{2+};

XXI – α-фаза + (Fe, Ni)Fe_2O_4 + Mn^{2+}, Ni^{2+};

XXII – α-фаза + NiO_x + (Fe, Ni)Fe_2O_4 + Mn^{2+};

XXIII – α-фаза + NiO_x + (Fe, Ni, Mn)Fe_2O_4 + Mn^{2+};

XXIV – α-фаза + NiO_x + (Fe, Ni, Mn)Fe_2O_4 + MnO;

XXV – α-фаза + NiO_x + (Fe, Ni, Mn)Fe_2O_4 + $HMnO_2^-$;

XXVI – α-фаза + (Fe, Ni, Mn)Fe_2O_4 + $HMnO_2^-$, $HNiO_2^-$;

XXVII – α-фаза + (Fe, Mn)Fe_2O_4 + $HMnO_2^-$, $HNiO_2^-$;

XXVIII – α-фаза + Fe_3O_4 + $HMnO_2^-$, $HNiO_2^-$;

XXIX – α-фаза + $CuFeO_2$ + Mn^{2+}, Fe^{2+}, Ni^{2+};

XXX – α-фаза + Fe_3O_4 + $CuFeO_2$ + Mn^{2+}, Ni^{2+};

XXXI – α-фаза + $CuFeO_2$ + (Fe, Ni)Fe_2O_4 + Mn^{2+}, Ni^{2+};

XXXII – α-фаза + NiO_x + $CuFeO_2$ + (Fe, Ni)Fe_2O_4 + Mn^{2+};

XXXIII – α-фаза + NiO_x + $CuFeO_2$ + (Fe, Ni, Mn)Fe_2O_4 + Mn^{2+};

XXXIV – α-фаза + NiO_x + $CuFeO_2$ + (Fe, Ni, Mn)Fe_2O_4 + MnO;

XXXV – α-фаза + NiO_x + $CuFeO_2$ + (Fe, Ni, Mn)Fe_2O_4 + $HMnO_2^-$;

XXXVI – α-фаза + $CuFeO_2$ + (Fe, Ni, Mn)Fe_2O_4 + $HMnO_2^-$, $HNiO_2^-$;

XXXVII – α-фаза + $CuFeO_2$ + (Fe, Mn)Fe_2O_4 + $HMnO_2^-$, $HNiO_2^-$;

XXXVIII – α-фаза + Fe_3O_4 + $CuFeO_2$ + $HMnO_2^-$, $HNiO_2^-$;

XXXIX – α-фаза + NiO_x + $CuFeO_2$ + (Fe, Ni, Mn)(Fe, Mn)$_2O_4$ + Mn^{2+};

XL – α-фаза + NiO_x + $CuFeO_2$ + (Fe, Ni, Mn)(Fe, Mn)$_2O_4$;

XLI – α-фаза + NiO_x + $CuFeO_2$ + (Fe, Ni, Mn)(Fe, Mn)$_2O_4$ + $HMnO_2^-$;

XLII – α-фаза + Fe_2O_3 + $CuFeO_2$ + Mn^{2+}, Ni^{2+};

XLIII – α-фаза + Fe_2O_3 + $CuFeO_2$ + $NiFe_2O_4$ + Mn^{2+}, Ni^{2+};

XLIV – α-фаза + NiO_x + Fe_2O_3 + $CuFeO_2$ + $NiFe_2O_4$ + Mn^{2+};

XLV – α-фаза + NiO_x + Fe_2O_3 + $CuFeO_2$ + $(Ni, Mn)Fe_2O_4$ + Mn^{2+};

XLVI – α-фаза + NiO_x + Fe_2O_3 + $CuFeO_2$ + $(Ni, Mn)(Fe, Mn)_2O_4$;

XLVII – α-фаза + NiO_x + Fe_2O_3 + $CuFeO_2$ + $(Ni, Mn)Fe_2O_4$ + $HMnO_2^-$;

XLVIII – α-фаза + Fe_2O_3 + $CuFeO_2$ + $(Ni, Mn)Fe_2O_4$ + $HMnO_2^-$, $HNiO_2^-$;

XLIX – α-фаза + Fe_2O_3 + $CuFeO_2$ + $MnFe_2O_4$ + $HMnO_2^-$, $HNiO_2^-$;

L – α-фаза + Fe_2O_3 + $CuFeO_2$ + $(Ni, Mn)(Fe, Mn)_2O_4$ + $HNiO_2^-$;

LI – α-фаза + Fe_2O_3 + $CuFeO_2$ + $Mn(Fe, Mn)_2O_4$ + $HNiO_2^-$;

LII – Mn^{2+}, Fe^{2+}, Ni^{2+}, Cu^{2+};

LIII – $CuFeO_2$ + Mn^{2+}, Fe^{2+}, Ni^{2+}, Cu^{2+};

LIV – Cu_2O + Fe_2O_3 + $CuFeO_2$ + Mn^{2+}, Ni^{2+};

LV – Cu_2O + Fe_2O_3 + $CuFeO_2$ + $NiFe_2O_4$ + Mn^{2+}, Ni^{2+};

LVI – Cu_2O + NiO_x + Fe_2O_3 + $CuFeO_2$ + $NiFe_2O_4$ + Mn^{2+};

LVII – Cu_2O + NiO_x + Fe_2O_3 + $CuFeO_2$ + $(Ni, Mn)Fe_2O_4$ + Mn^{2+};

LVIII – Cu_2O + NiO_x + Fe_2O_3 + $CuFeO_2$ + $(Ni, Mn)(Fe, Mn)_2O_4$;

LIX – Cu_2O + Fe_2O_3 + $CuFeO_2$ + $(Ni, Mn)(Fe, Mn)_2O_4$+ $HNiO_2^-$;

LX – Cu_2O + Fe_2O_3 + $CuFeO_2$ + $Mn(Fe, Mn)_2O_4$ + $HNiO_2^-$;

LXI – Cu_2O + Fe_2O_3 + $CuFeO_2$ + $MnFe_2O_4$ + $HMnO_2^-$, $HNiO_2^-$;

LXII – Fe_2O_3 + $CuFeO_2$ + $MnFe_2O_4$ + $HMnO_2^-$, $HNiO_2^-$, CuO_2^{2-};

LXIII – Fe_2O_3 + Mn_3O_4 + $CuFeO_2$ + $MnFe_2O_4$ + $HNiO_2^-$, CuO_2^{2-};

LXIV – Cu_2O + NiO_x + Fe_2O_3 + $CuFeO_2$ + $(Ni, Mn)(Fe, Mn)_2O_4$;

LXV – Cu_2O + Fe_2O_3 + $CuFeO_2$ + $(Ni, Mn)(Fe, Mn)_2O_4$ + $HNiO_2^-$;

LXVI – Cu_2O + Fe_2O_3 + Mn_3O_4 + $CuFeO_2$ + $HNiO_2^-$;

LXVII – Fe_2O_3 + $CuFeO_2$ + Mn^{2+}, Ni^{2+}, Cu^{2+};

LXVIII – CuO + Fe_2O_3 + $CuFeO_2$ + Mn^{2+}, Ni^{2+};

LXIX – CuO + Fe_2O_3 + $CuFeO_2$ + $NiFe_2O_4$ + Mn^{2+}, Ni^{2+};

LXX – CuO + NiO_x + Fe_2O_3 + $CuFeO_2$ + $NiFe_2O_4$ + Mn^{2+};

LXXI – CuO + Fe_2O_3 + Mn_3O_4 + $CuFeO_2$ + Ni^{2+};

LXXII – CuO + Fe_2O_3 + $CuFeO_2$ + $(Ni, Mn)(Fe, Mn)_2O_4$ + Ni^{2+};

LXXIII – CuO + NiO_x + Fe_2O_3 + $CuFeO_2$ + $(Ni, Mn)(Fe, Mn)_2O_4$;

LXXIV – CuO + Fe_2O_3 + $CuFeO_2$ + $(Ni, Mn)(Fe, Mn)_2O_4$ + $HNiO_2^-$;

LXXV – Fe_2O_3 + $CuFeO_2$ + $(Ni, Mn)(Fe, Mn)_2O_4$ + $HNiO_2^-$, CuO_2^{2-};

LXXVI – Fe_2O_3 + Mn_3O_4 + $CuFeO_2$ + $HNiO_2^-$, CuO_2^{2-};

LXXVII – Fe_2O_3 + (Cu, Mn)$(Fe, Mn)_2O_4$ + $HNiO_2^-$, CuO_2^{2-};

LXXVIII – Fe_2O_3 + Mn_3O_4 + $HNiO_2^-$, CuO_2^{2-};

LXXIX – CuO + $(Fe, Mn)_2O_3$ + $CuFeO_2$ + Ni^{2+};

LXXX – CuO + $(Fe, Mn)_2O_3$ + $CuFeO_2$ + $NiFe_2O_4$ + Ni^{2+};

LXXXI – CuO + NiO_x + $(Fe, Mn)_2O_3$ + $CuFeO_2$ + $NiFe_2O_4$;

LXXXII – CuO + $(Fe, Mn)_2O_3$ + $CuFeO_2$ + $NiFe_2O_4$ + $HNiO_2^-$;

LXXXIII – $(Fe, Mn)_2O_3$ + $CuFeO_2$ + $NiFe_2O_4$ + $HNiO_2^-$, CuO_2^{2-};

LXXXIV – $(Fe, Mn)_2O_3$ + $CuFeO_2$ + $HNiO_2^-$, CuO_2^{2-};

LXXXV – Mn^{2+}, Fe^{3+}, Ni^{2+}, Cu^{2+};

LXXXVI – Fe_2O_3 + Mn^{2+}, Ni^{2+}, Cu^{2+};

LXXXVII – Fe_2O_3 + $CuFe_2O_4$ + Mn^{2+}, Ni^{2+}, Cu^{2+};

LXXXVIII – CuO + Fe_2O_3 + $CuFe_2O_4$ + Mn^{2+}, Ni^{2+};

LXXXIX – CuO + $(Fe, Mn)_2O_3$ + $CuFe_2O_4$ + Ni^{2+};

XC – CuO + $(Fe, Mn)_2O_3$ + $(Cu, Ni)Fe_2O_4$ + Ni^{2+};

XCI – CuO + NiO_x + $(Fe, Mn)_2O_3$ + $(Cu, Ni)Fe_2O_4$;

XCII – CuO + $(Fe, Mn)_2O_3$ + $(Cu, Ni)Fe_2O_4$ + $HNiO_2^-$;

XCIII – $(Fe, Mn)_2O_3$ + $(Cu, Ni)Fe_2O_4$ + $HNiO_2^-$, CuO_2^{2-};

XCIV – $(Fe, Mn)_2O_3$ + $CuFe_2O_4$ + $HNiO_2^-$, CuO_2^{2-};

XCV – $(Fe, Mn)_2O_3$ + $HNiO_2^-$, CuO_2^{2-};

XCVI – Mn^{2+}, Fe^{3+}, Ni^{2+}, Cu^{2+};

XCVII – MnO_2 + Fe^{3+}, Ni^{2+}, Cu^{2+};

XCVIII – Fe_2O_3 + MnO_2 + Ni^{2+}, Cu^{2+};

XCIX – Fe_2O_3 + $CuFe_2O_4$ + MnO_2 + Ni^{2+}, Cu^{2+};

C – CuO + Fe_2O_3 + $CuFe_2O_4$ + MnO_2 + Ni^{2+};

CI – CuO + Fe_2O_3 + MnO_2 + $(Cu, Ni)Fe_2O_4$ + Ni^{2+};

CII – CuO + NiO_x + Fe_2O_3 + MnO_2 + $(Cu, Ni)Fe_2O_4$;

CIII – CuO + Fe_2O_3 + MnO_2 + $(Cu, Ni)Fe_2O_4$ + $HNiO_2^-$;

CIV – Fe_2O_3 + MnO_2 + $(Cu, Ni)Fe_2O_4$ + $HNiO_2^-$, CuO_2^{2-};

CV – Fe_2O_3 + MnO_2 + $CuFe_2O_4$ + $HNiO_2^-$, CuO_2^{2-};

CVI – Fe_2O_3 + MnO_2 + $HNiO_2^-$, CuO_2^{2-};

CVII – Fe_2O_3 + $CuFe_2O_4$ + $HNiO_2^-$, CuO_2^{2-}, MnO_4^{2-};

CVIII – Fe_2O_3 + $HNiO_2^-$, CuO_2^{2-}, MnO_4^{2-};

CIX – $Cu_2O_3 + Fe_2O_3 + CuFe_2O_4 + MnO_2 + Ni^{2+}$;

CX – $Cu_2O_3 + Fe_2O_3 + MnO_2 + (Cu, Ni)Fe_2O_4 + Ni^{2+}$;

CXI – $Cu_2O_3 + NiO_x + Fe_2O_3 + MnO_2 + (Cu, Ni)Fe_2O_4$;

CXII – $Cu_2O_3 + Fe_2O_3 + MnO_2 + (Cu, Ni)Fe_2O_4 + HNiO_2^-$;

CXIII – $Cu_2O_3 + Fe_2O_3 + MnO_2 + CuFe_2O_4 + HNiO_2^-$;

CXIV – $Cu_2O_3 + Fe_2O_3 + CuFe_2O_4 + HNiO_2^-, MnO_4^{2-}$;

CXV – $Cu_2O_3 + NiO_x + Fe_2O_3 + MnO_2 + CuFe_2O_4$;

CXVI – $Cu_2O_3 + NiO_x + Fe_2O_3 + CuFe_2O_4 + MnO_4^{2-}$;

CXVII – $Cu_2O_3 + Fe_2O_3 + MnO_2 + Ni^{2+}$;

CXVIII – $Cu_2O_3 + NiO_x + Fe_2O_3 + MnO_2$;

CXIX – $Cu_2O_3 + NiO_x + Fe_2O_3 + MnO_4^{2-}$;

CXX – $Cu_2O_3 + Fe_2O_3 + HNiO_2^-, MnO_4^{2-}$;

CXXI – $FeO_2 + MnO_2 + Ni^{2+}, Cu^{2+}$;

CXXII – $Cu_2O_3 + FeO_2 + MnO_2 + Ni^{2+}$;

CXXIII – $Cu_2O_3 + NiO_x + FeO_2 + MnO_2$;

CXXIV – $Cu_2O_3 + NiO_x + FeO_2 + MnO_4^{2-}$;

CXXV – $Cu_2O_3 + FeO_2 + HNiO_2^-, MnO_4^{2-}$;

CXXVI – $FeO_2 + HNiO_2^-, CuO_2^{2-}, MnO_4^{2-}$;

CXXVII – $Fe^{3+}, Ni^{2+}, Cu^{2+}, MnO_4^-$;

CXXVIII – $FeO_2 + Ni^{2+}, Cu^{2+}, MnO_4^-$;

CXXIX – $Cu_2O_3 + FeO_2 + Ni^{2+}, MnO_4^-$;

CXXX – $Cu_2O_3 + NiO_x + FeO_2 + MnO_4^-$;

CXXXI – $Cu_2O_3 + NiO_x + FeO_4^{2-}, MnO_4^-$;

CXXXII – $CuO_2 + FeO_2 + Ni^{2+}, MnO_4^-$;

CXXXIII – $CuO_2 + NiO_x + FeO_2 + MnO_4^-$;

CXXXIV – $CuO_2 + NiO_x + FeO_4^{2-}, MnO_4^-$;

CXXXV – $CuO_2 + NiO_4^{2-}, FeO_4^{2-}, MnO_4^-$;

Как следует из диаграмм электрохимического равновесия (рис. 3 – 5), сплав МНЖМц30-1-1 в коррозионно-электрохимическом плане существенно отличается от сплава МН19. Область иммунности мельхиора МНЖМц30-1-1 более чем на 1В смещена в катодную область по сравнению с МН19. Переход его в транспассивное состояние за счёт

образования манганат-ионов (MnO_4^-) происходит на 2В ниже, чем у МН19. За счёт образования ферритов меди и никеля уменьшается область активного растворения сплава МНЖМц30-1-1, это подтверждается также авторами работ [88, 89], в которых также построены диаграммы потенциал – pH для ферритов. Таким образом, благотворное влияние легирующей добавки железа на стойкость медно-никелевых сплавов является результатом участия железа в образовании защитных плёнок. Марганец, наоборот, снижает коррозионную стойкость сплава за счёт селективной коррозии (области II – IV), поэтому его содержание в медно-никелевых сплавах не должно превышать 1 мас. % [90].

Первичная пассивация сплава МНЖМц30-1-1, например, в растворах гидроксида натрия [9] при потенциалах, соответствующих области электрохимической устойчивости воды может протекать по схеме (см. рис. 5):

I

α-фаза + MnO →

II

→ α-фаза + MnO + (Fe, Ni)Fe_2O_4 →

III

→ α-фаза + MnO + (Fe, Ni)Fe_2O_4 + $CuFeO_2$ + NiO_x.

Общее содержание марганца и железа в сплаве таково, что процессы пассивации α-фазы должны протекать до III стадии: простых (MnO) и двойных оксидов марганца и железа недостаточно для образования сплошной пассивирующей плёнки, и процесс завершается с образованием защитной плёнки фазы NiO_x. Поэтому химическая и электрохимическая устойчивость медно-никелевых сплавов определяется в целом химической и электрохимической устойчивостью никеля. Оксиды марганца и железа могут входить во внутренний подслой плёнки оксидов никеля (NiO_x) лишь в виде локальных участков.

ВЫВОДЫ

1. Построена фазовая диаграмма системы Cu – Ni – O при 25˚C и 1 бар. Химическая устойчивость медно-никелевых сплавов на воздухе определяется только никелем: единственным продуктом окисления сплавов выступает оксидная фаза NiO_x, где $1 \leq x \leq 1{,}344$.

2. Построены диаграммы потенциал – pH систем мельхиор МН19 – H_2O и мельхиор МНЖМц30-1-1 – H_2O при 25˚C. Пассивационная плёнка на сплавах однородна и представляет собой также фазу NiO_x (негидратированная форма оксидов). Оксиды марганца (MnO) и железа ($CuFeO_2$, (Fe, Ni)Fe_2O_4) могут локально входить во внутренний

подслой защитной плёнки NiO_x и таким образом влиять на коррозионную стойкость мельхиора МНЖМц30-1-1.

СПИСОК ЛИТЕРАТУРЫ

1. Смирягин, А. П. Промышленные цветные металлы и сплавы. – М.: Металлургиздат, 1974. – 559 с.
2. Новиков, И. И. Меди сплавы // Краткая химическая энциклопедия / под ред. И. Л. Кнунянц. – М.: Советская энциклопедия, 1964. – Т. 3. – С. 70.
3. Медно-никелевый сплав. Марки // Марочник стали и сплавов. – URL: <http://www.splav.kharkov.com/choose_mat.php?class_id=61>.
4. Мельхиоры // Справочник химика. – URL: <http://chem100.ru/text.php?t=131b>.
5. Cupronickel. – URL: < http://en.wikipedia.org/wiki/Cupronickel >.
6. Червяков, В. И. Коррозионное поведение медно-никелевых сплавов в нейтральных хлоридных сульфидсодержащих растворах / В. И. Червяков, Г. Н. Маркосьян, А. П. Пчельников // Защита металлов, 2004. – Т. 40. – № 2. – С. 123 – 127.
7. Кузнецов, Ю. И. Некоторые особенности локальной депассивации бинарных сплавов / Ю. И. Кузнецов, М. В. Рылкина // Защита металлов, 2004. – Т. 40. – № 5. – С. 505 – 512.
8. Маркосьян, Г. Н. Коррозия гидридов никеля и сплава Cu30Ni в кислородсодержащих растворах / Г. Н. Маркосьян, Д. С. Сирота, А. П. Пчельников // Защита металлов, 2005. – Т. 41. – № 4. – С. 390 – 394.
9. Сирота, Д. С. Электрохимическое поведение α-фазы системы Cu30Ni – H в растворах гидроксида натрия / Д. С. Сирота, А. П. Пчельников // Защита металлов, 2005. – Т. 41. – № 6. – С. 652 – 655.
10. Сирота, Д. С. Электрохимическое поведение β-фазы системы Cu30Ni – H в растворах гидроксида натрия / Д. С. Сирота, А. П. Пчельников // Защита металлов, 2005. – Т. 41. – № 6. – С. 598 – 601.
11. Диаграммы состояния двойных металлических систем: Справочник / Под ред. Лякишева Н. П. М.: Машиностроение, 1997. Т. 2. С. 283 – 286.
12. Phase diagram – Web // FactSage Database. – URL: <http://www.crct.polymtl.ca/fact/documentation>.
13. Sabine an Mey. Thermodynamic re-evaluation of the Cu – Ni system // CALPHAD, 1992. – Vol. 16. – № 3. – P. 255 – 260.
14. Straumal, B. B. et al. Deformation-driven formation of equilibrium phases in the Cu – Ni alloys // Journal of Material Science, 2011. – DOI: 10.1007/s10853-011-5805-0.

15. Servant, C. Thermodynamic assessment of the Cu – Fe – Ni system / C. Servant, B. Sundman and O. Lyon // CALPHAD, 2001. – Vol. 25. – № 1. – P. 79 – 95.
16. Sundman, B. A regular solution model for phases with several components and sublattices suitable for computer applications / B. Sundman and J. Ågren // Journal of Physical Chemistry of Solids, 1981. – Vol. 42. – P. 297 – 301.
17. Лаптев, Д. М. Термодинамика металлургических растворов: монография. – Челябинск: Металлургия, 1992. – 352 с.
18. Михайлов, Г. Г. Термодинамика металлургических процессов и систем: монография / Г. Г. Михайлов, Б. И. Леонович, Ю. С. Кузнецов. – М.: Изд. Дом МИСиС, 2009. – 520 с.
19. Тюрин А. Г. Термодинамика химической и электрохимической устойчивости твёрдых сплавов железа, хрома и никеля: монография. – Челябинск: Изд-во ЧелГУ, 2011. – 241 с.
20. Программа PhDi // Лаборатория химической термодинамики химического факультета МГУ им. М. В. Ломоносова. – URL: <http://td.chem.msu.ru/?page_id=4>.
21. Тюрин, А. Г Термодинамика химической и электрохимической устойчивости латуней / А. Г. Тюрин, А. А. Шрейнер // Защита металлов, 2007. – Т. 43. – № 3. – С. 313 – 319.
22. Тюрин, А. Г. О природе влияния меди на коррозионную стойкость железа // Защита металлов, 2004. – Т. 40. – № 3. – С. 256 – 262.
23. Моисеев, Г. К. Температурные зависимости приведённой энергии Гиббса некоторых неорганических веществ: альтернативный банк данных ASTRA. OWN / Г. К. Моисеев, Н. А. Ватолин, Л. А. Маршук, Н. П. Ильиных. – Екатеринбург: УрОРАН, 1997. – 230 с.
24. Шарлай, Е. В. Особенности электрохимического поведения системы медь – раствор гидроксида калия в области температур 295 – 320 К: автореф. дисс. канд. хим. наук. – Челябинск: Изд-во ЮурГУ, 2008. – 19 с.
25. Gernot Goll. Metal-oxide superconductors // Springer Tracts in Modern Physics, 2006. – Vol. 214/2006. Unconventional superconductors. – P. 121 – 151.
26. Захаров, А. Ю. Барическая зависимость температуры Нееля T_N в $LaCu_2O_4$ /А. Ю. Захаров, В. Я. Митрофанов, А. Е. Никифоров // Оксиды. Физико-химические свойства. Сборник трудов V Всероссийской научной конференции. – Екатеринбург, 2000. – С. 181 – 184.
27. Панов, Ю. Д. Локальные эффекты анизотропного давления в сверхпроводящих CuO_2-плоскостях / Ю. Д. Панов, Е. В. Зенков, А. С. Москвин // Оксиды. Физико-

химические свойства. Сборник трудов V Всероссийской научной конференции. – Екатеринбург, 2000. – С. 366 – 369.

28. Gaojie, Xu. Effect of oxygen-deficiency of CuO_2 plane on the structure, magnetism, and transport properties / Xu Gaojie, Pu Qirong, Zhang Zengming, Ding Zejun // Journal of Superconductivity, 2001. – Vol. 14. – № 4. – P. 509 – 517.
29. Teplov, M. A. Inhomogeneity of charge and spin distribution in CuO_2 layers of high-T_c superconductors: NQR/NMR studies of 1-2-3 compounds / M. A. Teplov, O. N. Bakharev, A. V. Dooglav, A. V. Egorov, I. R. Mukhamedshin, et al. // Journal of Superconductivity, 1999. – Vol. 12. – № 1. – P. 113 – 115.
30. El-Tantawy, Y. A. The passivation of dilute Cu(Hg) in alkaline solutions / Y.A. El-Tantawy, A.E. El-Kholy, T.S.E. Kasem // Corrosion Science, 1978. – Vol. 18. – № 12. – P. 1065 – 1073.
31. Muroi, M. Charge distribution in triple-layered copper oxide superconductors / Michihito Muroi, Robert Street // Physica C: Superconductivity, 1995. – Vol. 248. – № 3 – 4. – P. 290 – 310.
32. Tokura, Y. Material overview of high-T_c oxides // Physica C: Superconductivity, 1991. – Vol. 185 – 189. – Part 1, 1. – P. 174 – 179.
33. Третьяков, Ю. Д. Химия нестехиометрических окислов: монография. – М.: Изд-во Моск. гос. ун-та, 1974. – 364 с.
34. Морачевский, А. Г. Термодинамика системы никель – кислорода / А. Г. Морачевский, Л. Ш. Цемехман, Л. Б. Цымбулов // Термодинамика систем и процессов в металлургии никеля и меди. Вып. 12. – СПб.: Изд-во Политехн. ун-та, 2008. – 148 с.
35. Богацкий, Д. П. Физико-химическое исследование структуры и свойств кислородных соединений никеля / Д. П. Богацкий, И. А. Минеева // Журнал общей химии, 1959. – Т. 29. – № 4. – С. 1382 – 1390.
36. Широков, Ю. Г. Некоторые магнитные свойства закиси никеля / Ю. Г. Широков, И. П. Кириллов // Известия вузов. Химия и химическая технология, 1961. – № 4. – С. 599 – 603.
37. Gmelins Handbuch der anorganischen Chemie. 8 Auflage. Nickel. Teil B. Lieferung 2. – Vienheim: Verlag Chemie, 1966. – S. 376 – 389.
38. Термические константы веществ: база данных – URL: <http://www.chem.msu.su/cgi-bin/tkv.pl?show=welcome.html>.
39. Третьяков, Ю. Д. Термодинамика ферритов: монография. – Л.: Химия, 1967. – 305 с.

40. Cotton, F. Advanced Inorganic Chemistry / F. Cotton, G. Wilkinson. – New York – London – Sydney – Toronto: John Wiley & Sons, 1972. – 1147 p.
41. Николайчук, П. А. Термодинамика химической и электрохимической устойчивости сплавов системы Mn – Si / П. А. Николайчук, Т. И. Шаляпина, А. Г. Тюрин, Т. В. Мосунова // Вестник ЮурГУ. Серия «Химия», 2010. – № 31 (207). – Вып. 4. – С. 72 – 82.
42. Navrotsky, A. Thermodynamics of formation of simple spinels / A. Navrotsky and O. J. Kleppa // Journal of Inorganic and Nuclear Chemistry, 1968. – Vol. 30. – P. 479 – 498.
43. Jacob, K. T. Activities in the spinel solid solution, phase equilibria and thermodynamic properties of ternary phases in the system Cu – Fe – O / K. T. Jacob, K. Fitzner and C. B. Alcock // Metallurgical Transactions B, 1977. – Vol. 8. – № 3. – P. 451 – 460.
44. Kulkarni, A. D. The thermodynamic studies of liquid copper alloys by electromotive force method. Part I. The Cu – O, Cu – Fe – O and Cu – Fe systems // Metallurgical Transactions, 1973. – Vol. 4. – № 7. – P. 1713 – 1721.
45. Samadashvili, I. Dzh. Thermodynamic functions of $Cu_{1-x}Zn_xFe_2O_4$ ferrite solid solutions from 300 to 900 K / I. Dzh. Samadashvili, V. S. Vararashvili, T. E. Machaladze, T. A. Pavlenishvili // Inorganic Materials, 2002. – Vol. 38. – № 11. – P. 1186 – 1188.
46. Gollai, A. V. The thermodynamic properties of spinel solutions in the Fe – Cu – O system / A. V. Gollai, A. A. Lykasov, M. S. Pavlovskaya, S. V. Buldygin // Russian Journal of Physical Chemistry, 2006. – Vol. 80. – № 11. – P. 1770 – 1772.
47. Khvan, V. A. et al. Thermodynamic assessment of the Cu – Fe – O system // Journal of Phase Equilibria and Diffusion, 2011. – Vol. 32. – № 6. – P. 498 – 511.
48. Тюрин, А. Г. О влиянии никеля на корроизонно-электрохимическое поведение легированных им сплавов железа // Защита металлов, 2000. – Т. 36. – № 1. – С. 67 – 74.
49. Katayama, Iwao. Thermodynamic study of spinel type solid solutions of the Fe_3O_4 – $NiFe_2O_4$ system by the E. M. F. method / Iwao Katayama, Yasuaki Watanabe, Zensaku Kozuka // Materials Transaction. The Japan Institute of Metals, 1979. – Vol. 20. – № 10. – P. 593 – 596. – URL: < http://www.jim.or.jp/journal/e/pdf3/20/10/593.pdf >.
50. Schneider, F. Thermodynamic Investigation of the system Ni – Fe – O / F. Schneider, H. Schmalzried // Zeitschrift für Physikalische Chemie Neue Folge, 1990. – Bd. 166. – S. 1 – 18.
51. Kjellqvist, L. Thermodynamic assessment of the Fe – Mn – O system // Lina Kjellqvist, Malln Selleby // Journal of Phase Equilibria and Diffusion, 2010. – Vol. 31. – № 2. – P. 113 – 134.

52. Yang, Bo et al. Preparation of nickel-manganese composite oxide by room temperature solid state reaction-calcining decomposition // Chinese Journal of Nonferrous Metals, 2007. – Vol. 17. – № 10. – P. 1705 – 1710.
53. Рузинов, Л. П. Равновесные превращения металлургических реакций: справочник / Л. П. Рузинов, Б. С. Гуляницкий. – М.: Металлургия, 1975. – 416 с.
54. JANAF Thermochemical Tables. Third Edition. // J. Phys. Chem. Ref. Data, 1985. – Vol. 14. – Suppl. 1.
55. Верягин, У. Д. et al. Термодинамические свойства неорганических веществ: справочник / под ред. А. П. Зефирова. – М.: Атомиздат, 1965. – 461 с.
56. Pankratz, L. B. Thermodynamic data for mineral technology: handbook. Bulletin 677 / L. B. Pankratz, J. M. Stuve, M. A. Gokcen. – Bureau of Mines USA, 1984. – 355 p.
57. Charette, G. G. Thermodynamic properties of the oxides of Fe, Ni, Pb, Cu, and Mn, by EMF measurements / G. G. Charette, S. N. Flengas // Journal of Electrochemical Society. Electrochemical Science, 1968. – Vol. 115. – № 8. – P. 796 – 804.
58. Hugh, St. C. Thermodynamic data from redox reactions at high temperatures. I. An experimental and theoretical assessment of the electrochemical method using stabilized zirconia electrolytes, with revised values for the Fe – "FeO", Co – CoO, Ni – NiO and Cu – Cu_2O oxygen buffers, and new data for the W – WO_2 buffer / Hugh St. C. O'Neill, Mark I. Pownceby // Contributions to Mineralogy and Petrology, 1993. – Vol. 114. – № 3. – P. 296 – 314.
59. Уикс, К. Е. Термодинамические свойства 65 элементов, их окислов, галогенидов, карбидов и нитридов / пер. с англ. / К. Е. Уикс, Ф. Е. Блок. – М.: Металлургия, 1965. – 240 с.
60. Elliott, G. F. Thermochemistry for steelmaking. Volume 1 / G. F. Elliott, M. Gleiser. – London: Pergamon Press, 1960. – 296 p.
61. Robie, A. Thermodynamic properties of minerals and related substances at 298,15 K and 1 bar (10^5 pascals) pressure and at higher temperatures. US geological survey bulletin 2131 / A. Robie, B. S. Hemingway. – Washington: United States government printing office, 1995. – 461 p.
62. Ball, J. W. User's manual for WATEQ4F with revised thermodynamic data base and test cases for calculating speciation of major, trace and redox elements in natural waters / J. W. Ball, D. K. Nordstrom. – US geological survey. Open-file report 91 – 183. – URL: <http://wwwbrr.cr.usgs.gov/projects/GWC_chemtherm/pubs/wq4fdoc.pdf>.
63. Тюрин, А. Г. Роль марганца в коррозионно-электрохимическом поведении нержавеющих сталей // Защита металлов, 2005. – Т. 41. – № 1. – С. 74 – 81.

64. Katkov, A. E. Spinel phase relations in the Fe_3O_4 – $CuFe_2O_4$ system / A. E. Katkov, A. A. Lykasov // Inorganic Materials, 2003. – Vol. 39. – № 2. – P. 171 – 174.
65. Park, B. H. Thermodynamic properties of $NiCr_2O4$ – $NiFe_2O_4$ spinel solid solutions / Bong-Hoon Park, Dong-Su Kim // Bulletin of Korean Chemical Society, 1999. – Vol. 20. – № 8. – P. 939 – 942.
66. Жук, Н. П. Курс теории коррозии и защиты металлов: учеб. пособие для вузов. – 2-е изд., стереотип. (перепеч. с изд. 1976 г.). – М: ООО ТИД "Альянс", 2006. – 472 с.
67. Nikolaychuk, P. A. Method of estimating the standard Gibbs energies of formation of binary compounds // Abstracts of the XVIII International Conference on Chemical Thermodynamics in Russia: Vol. 2. – Samara: Samara State Technical University, 2011. – P. 16 – 17.
68. Киреев, В. А. Методы практических расчётов в термодинамике химических реакций. – М.: Химия, 1970. – 520 с.
69. Nikolaychuk P. A., Tyurin A. G. The analysis of standard Gibbs energies of formation of MeO_2 type oxides of fourth period d-elements // Abstracts of the XVIII International Conference on Chemical Thermodynamics in Russia: Vol. 2. – Samara: Samara State Technical University, 2011. – P. 17 – 18.
70. Справочник химика / под ред. Б. П. Никольского. – М.–Л.: Химия, 1964. – Т. 3. – 1008 с.
71. Киш, Л. Кинетика электрохимического растворения металлов / пер. с англ. Е. В. Овсянниковой; под ред. А. М. Скундина. – М: Мир, 1990. – 272 с.
72. Pourbaix diagrams / Substances & Technologies. – URL: <http://www.substech.com/dokuwiki/doku.php?id=pourbaix_diagrams>.
73. Николайчук П. А., Тюрин А. Г., Канатьева И. И. Уточнённая диаграмма Пурбе для меди // Современные проблемы теоретической и экспериментальной химии: Межвузовский сборник научных трудов VII Всероссийской конференции молодых учёных с международным участием. Саратов: ООО Издательство "КУБиК", 2010. – С. 287 – 291.
74. FactSage EpH-Web. – URL: <http://www.sgte.org/ephweb.php>.
75. THERMEXPERT – Potential – pH diagram generator / Argentum Solutions, Inc. – URL: <http://www.argentumsolutions.com/cgi-bin/thermexpert>.
76. SUPCRT / Prediction Central. – URL: <http://www.predcent.org/download/supcrt>.
77. Johnson, J. W. SUPCRT92: A software package for calculating the standard molal thermodynamic properties of minerals, gases, aqueous species, and reactions from 1 to

5000 bar and 0 to 1000°C / J. W. Johnson, E. H. Oelkers, H. C. Helgeson // Computers & Geosciences, 1992. – Vol. 16. – № 7. – P. 899 – 947.

78. The Geochemist's Workbench (GWB). – Rockware: Earth Science and GIS Software. – URL: <http://www.rockware.com/product/overview.php?id=132>.
79. JNC-TDB. – Japan Nuclear Cycle Organization. – URL: <http://migrationdb.jnc.go.jp>.
80. ZZ-HATCHES 19: Database for radiochemical modeling / Nuclear Energy Agency. – URL: <http://www.oecd-nea.org/tools/abstract/detail/nea-1210>.
81. PHREEQC-2: A Computer Program for speciation, batch-reaction, one-dimensional transport, and inverse geochemical calculations / USGS. – URL: <http://wwwbrr.cr.usgs.gov/projects/GWC_coupled/phreeqc>.
82. Eriksson, Gunnar. An algorithm for the computation of aqueous multicomponent, multiphase equilibria // Analytica Chimica Acta, 1979. – Vol. 112. – № 4. – P. 375 – 383.
83. SOLGASWATER program. – URL: <http://158.227.5.164/Chemical_Diagrams/html/ISP_Solgaswater.htm>.
84. Atlas of Eh-pH diagrams: Intercomparison of thermodynamic databases / Geological survey of Japan. Open file report № 419. – National Institute of Advanced Industrial Science and Technology, 2005. – URL: <www.gsj.jp/GDB/openfile/files/no0419/openfile419e.pdf>.
85. Тюрин, А. Г. Термодинамика химической и электрохимической устойчивости сплавов: автореф. дисс. д. х. н. – Челябинск: Изд-во ЧелГУ, 2008. – 40 с.
86. Справочник по электрохимии / под ред. А. М. Сухотина. – Л.: Химия, 1981. – 488 с.
87. Silverman, D. C. Revised EMF – pH diagram for nickel // Corrosion, 1981. – Vol. 37. – № 9. – P. 546 – 548.
88. Beverskog, B. Pourbaix diagrams for the ternary system of iron-chromium-nickel / B. Beverskog, I. Puigdomenech // Corrosion, 1999. – Vol. 55. - № 11. – P. 1077 – 1087.
89. Glasby, G. P. E_H, pH diagrams for Mn, Fe, Co, Ni, Cu and As under seawater conditions: application of two new types of E_H, pH diagrams to the study of specific problems in marine geochemistry / G. P. Glasby, H. D. Schulz // Aquatic Geochemistry, 1999. – Vol. 5. – № 3. – P. 227 – 248.
90. Улиг, Г. Г. Коррозия и борьба с ней. Введение в коррозионную науку и технику / Г. Г. Улиг, Р. У. Реви / пер. с англ.; под ред. А. М. Сухотина. – Л.: Химия, 1989. – 456 с.

The Third Dimension in Pourbaix Diagrams: A Further Extension

Pavel Anatolyevich Nikolaychuk*

Department of Analytical and Physical Chemistry, Chelyabinsk State University, Chelyabinsk, 454001, Russian Federation

ABSTRACT
Clarification is provided regarding the third axis in E – pH – M diagram. The other variants of three dimensional Pourbaix diagram are proposed.

KEYWORDS
Second-year Undergraduate, Upper-Division Undergraduate, Physical Chemistry, Computer-Based Learning, Aqueous Solution Chemistry, Electrochemistry, Metals, Oxidation / Reduction, Thermodynamics.

Recently the concept of 3D Pourbaix diagram was introduced.[1] Two issues from this paper can be discussed further.
The potential associated with a half-reaction

$$a\mathrm{A} + b\mathrm{B} + m\mathrm{H}^+ + n\mathrm{e}^- = c\mathrm{C} + d\mathrm{D} \qquad (1)$$

in nonstandard conditions is determined by the Nernst equation[2]

$$E = E^o - \frac{RT}{nF}\ln\frac{a_{\mathrm{C}}^c \cdot a_{\mathrm{D}}^d}{a_{\mathrm{A}}^a \cdot a_{\mathrm{B}}^b \cdot a_{\mathrm{H}^+}^m} \qquad (2)$$

assuming $-\log a_{\mathrm{H}^+} = \mathrm{pH}$, the generalized equation that represents any line on E – pH diagram can be derived

$$E = E^o - \frac{\ln\ 10 \cdot R \cdot T}{n \cdot F}\log\frac{a_{\mathrm{C}}^c \cdot a_{\mathrm{D}}^d}{a_{\mathrm{A}}^a \cdot a_{\mathrm{B}}^b} - \frac{\ln\ 10 \cdot R \cdot T \cdot m}{n \cdot F}\mathrm{pH} \qquad (3)$$

where a_i is the thermodynamic activity of component i, other variables are the same as in Ref. 2. The activity units depend on the reference state of compounds. They are equal to molarities only for species in water solution.[2] Thus E – pH – M diagram presented by the authors of Ref. 1 is only a particular case of E – pH – a_i diagram in which varied parameters are the activities of ions in solution. It would be more correct in educational term to change the titles of the third axis in diagrams from Ref. 1 from molarities of the species to their activities.
Another case in which E – pH – a_i diagram can be applied is if the half-reaction involves gases (which fugacities may vary) or impure solid species (which activities may vary). As the example, the E – pH – a diagram for Mg – H_2O system is presented at Figure 1. Magnesium is the lightest structural metal, therefore its alloys are widely using as the components of modern cars and high-performance vehicles, in aerospace industry, as orthopedic biomaterials, as components in lenses.[3] The corrosion resistance of such alloys is studied very widely.[4] Therefore, the E – pH – $a_{\mathrm{Mg\ (s)}}$ diagram is the relevant example demonstrating how the electrochemical properties of magnesium depend on its activity in alloys. The expressions for electrode potentials of corresponding half-cell reactions are listed in Table 1. The activity of solid magnesium is variable; the activities of other species are set equal to unity. The values of standard Gibbs energies of formation of magnesium species are taken from Ref. 1. The compounds of monovalent magnesium and magnesium hydrides, which are present at the complete E – pH diagram for Mg,[5] are not taken into account.

Table 1. Basic chemical and electrochemical equilibria in Mg – H_2O system at 298.15 K and unity activities of all species except Mg (s).

Half-cell reaction	*Electrode potential / V or solution pH*
$Mg^{2+}(aq) + 2e^- = Mg(s)$	$E = -2.357 - 0.0295 \cdot \log a_{Mg(s)}$
$Mg(OH)_2(s) + 2H^+ + 2e^- = Mg(s) + 2H_2O(l)$	$E = -1.860 - 0.0591 \cdot pH - 0.0295 \cdot \log a_{Mg(s)}$
$Mg(OH)_2(s) + 2H^+ = Mg^{2+}(aq) + 2H_2O(l)$	$pH = 8.394$

(A)

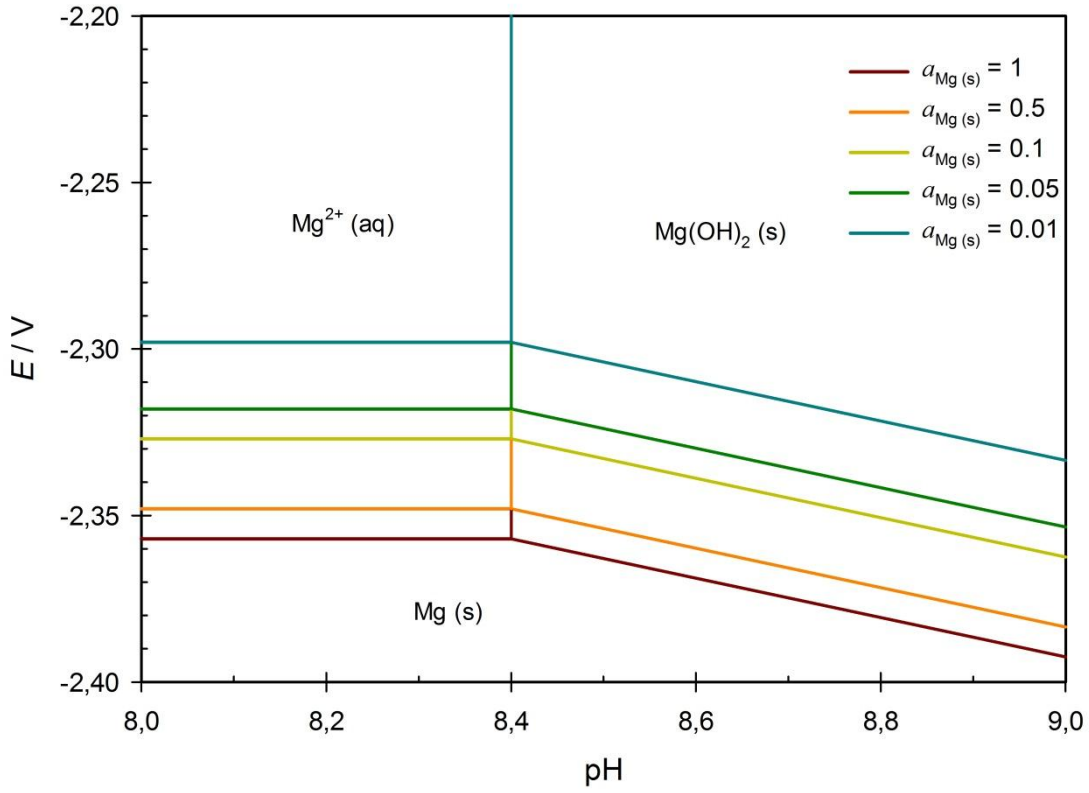

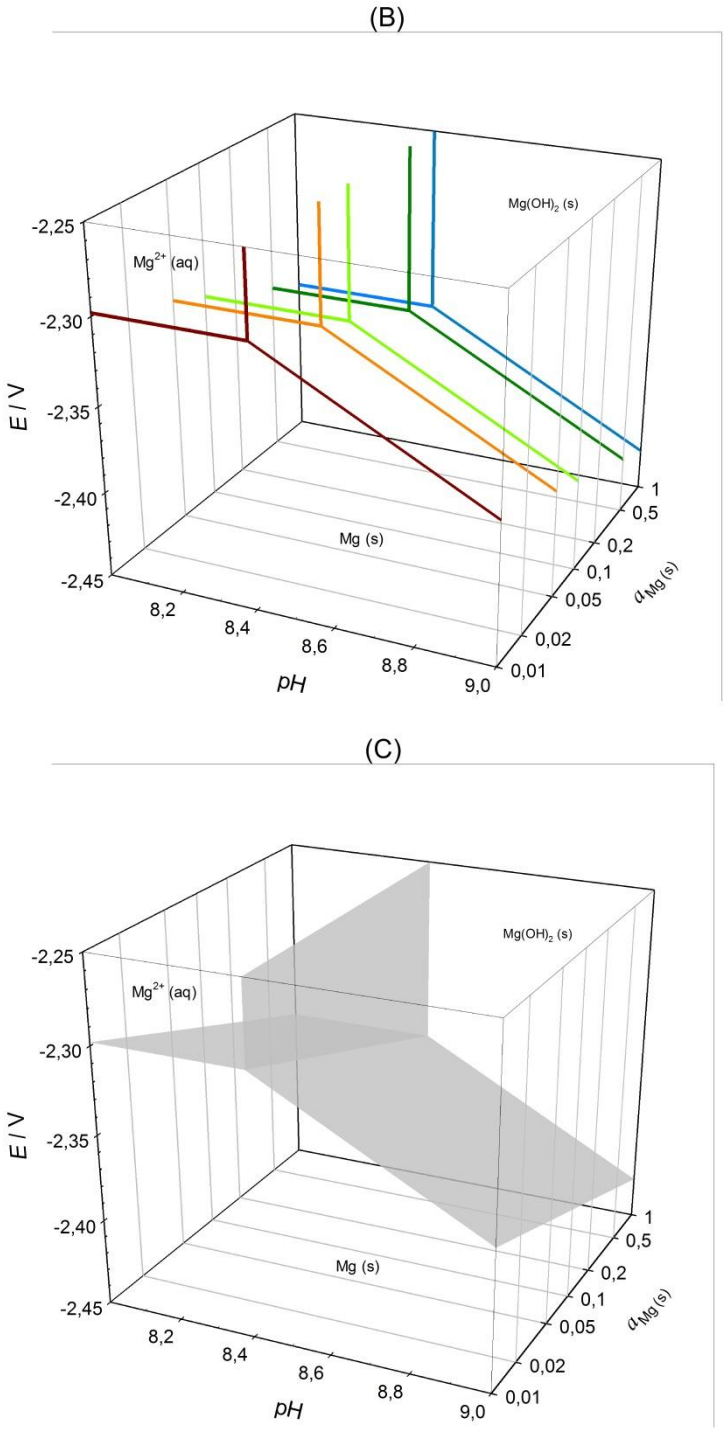

Figure 1. E – pH diagram for Mg – H_2O system: (A) two-dimensional, (B) three-dimensional using individual curves and (C) three-dimensional using surfaces. The activities of all species except Mg (s) are set equal to unity.

The E – pH – a_i diagram is not the only possible variant of applying the third axis in the Pourbaix plot. According to Refs. 6 and 7, the dependence of half-cell reaction electrode potential on temperature is expressed as

$$E_T^o = E_{298}^o + (T - 298.15) \cdot (\frac{dE^o}{dT})_{298} + 0.5(T - 298.15)^2 \cdot (\frac{d^2E^o}{dT^2})_{298} \qquad (4)$$

Therefore the position and the slope of lines in Pourbaix diagram depend on temperature. This way the E – pH – T diagrams can be introduced. For example the E – pH – T diagram for H_2O over the temperature range of stability of liquid water is presented at Figure 2. The expressions for electrode potentials of corresponding half-cell reactions in form of Equation (4) are listed in

Table 2. The values of the first ($(\frac{dE^o}{dT})_{298}$) and the second ($(\frac{d^2E^o}{dT^2})_{298}$) temperature coefficients were obtained from Refs. 6 and 7.

Table 2. Electrode potentials of hydrogen and oxygen electrodes with respect to temperature. The activities of all species are set equal to unity.

Half-cell reaction	*Electrode potential / V*
$2H^+(aq) + 2e^- = H_2(g)$	$E = 0.0000 + 0\cdot(T - 298.15) + 0\cdot(T - 298.15)^2 - -1.9842\cdot10^{-4}\cdot T\cdot pH$
$O_2(g) + 4H^+(aq) + 4e^- = = 2H_2O\ (l)$	$E = 1.2291 - 8.456\cdot10^{-4}\cdot(T - 298.15) + 2.7625\cdot10^{-7}\cdot(T - 298.15)^2 - -1.9842\cdot10^{-4}\cdot T\cdot pH$

(A)

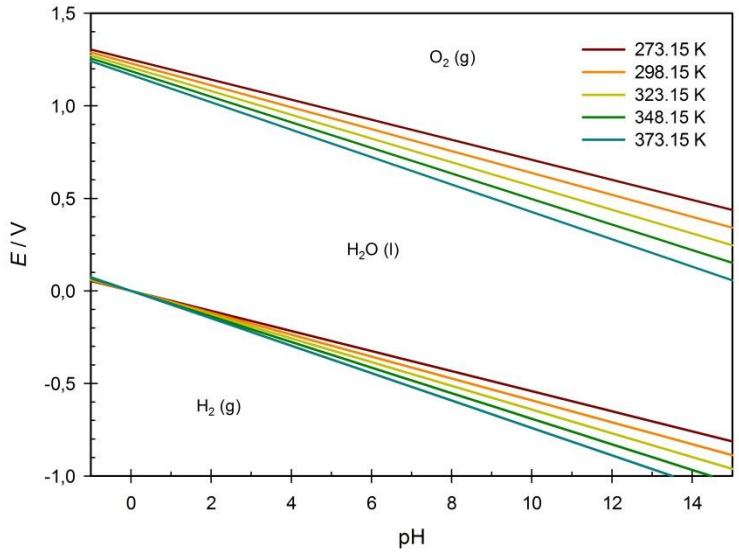

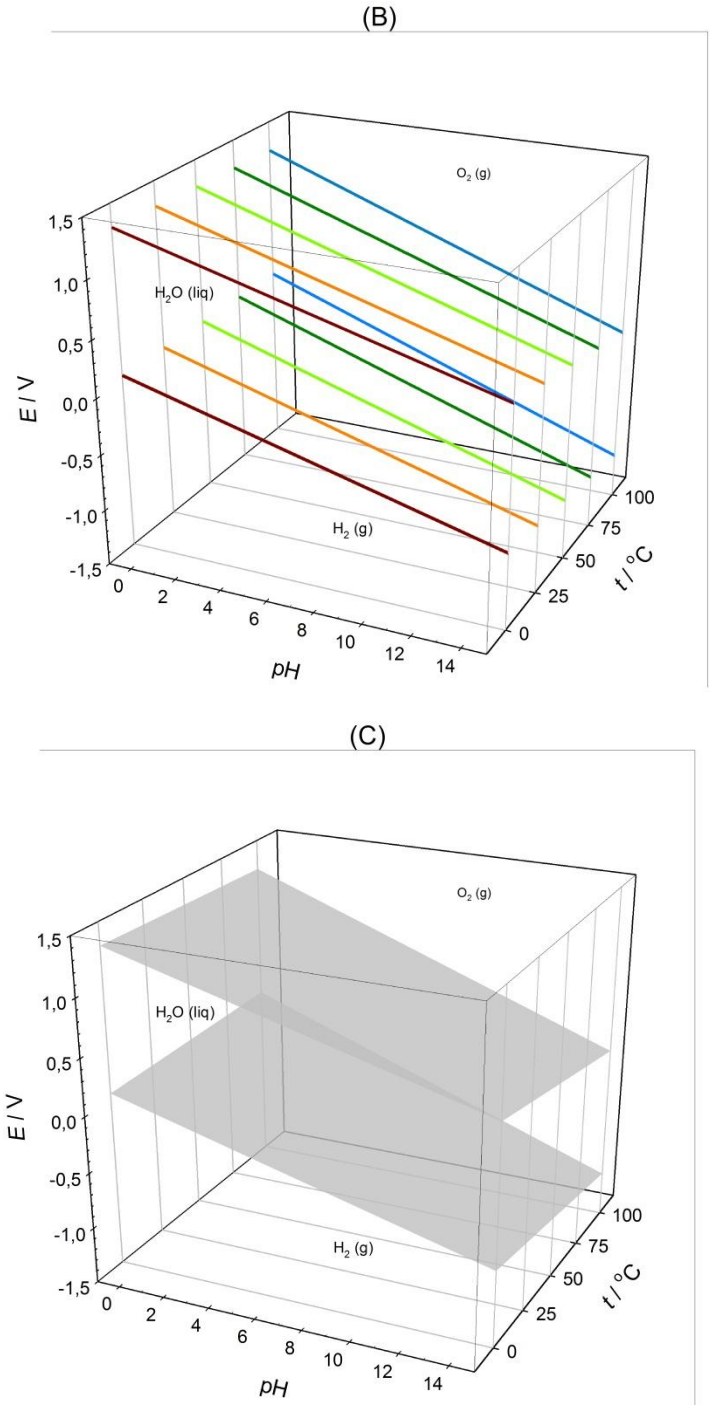

Figure 2. E – pH diagram for H_2O at various temperatures: (A) two-dimensional, (B) three-dimensional using individual curves and (C) three-dimensional using surfaces. Temperature axis is calibrated in degrees Celsius for convenience. The activities of all species are set equal to unity.

Moreover, the standard Gibbs energy change associated with a half-cell reaction is linked with its standard electrode potential according to the equation.

$$E_T^o = -n \cdot F \cdot \Delta_r G_T^o \qquad (5)$$

The standard Gibbs energies of formation of some metals and other compounds may depend on pressure.[8,9]

$$\Delta_f G(T, p) = \frac{A \cdot e^{a_0 \cdot T + \frac{a_1 \cdot T^2}{2} + \frac{a_2 \cdot T^3}{3} + \frac{a_3}{T}}}{(K_0 + K_1 \cdot T + K_2 \cdot T^2) \cdot (n-1)} \cdot ((1 + n \cdot p \cdot (K_0 + K_1 \cdot T + K_2 \cdot T^2))^{1-\frac{1}{n}} - 1) \quad (6)$$

Where A, a_0, a_1, a_2, a_3, K_0, K_1, K_2 and n are constants for the particular compound and phase. This results in dependence on pressure of standard Gibbs energy of reactions involving these compounds and consequently of corresponding standard electrode potentials. This way the E – pH – p diagrams can be introduced. This can be important because the next generation of nuclear power plants will use supercritical water as working fluid[10] and plotting Pourbaix diagrams at elevated pressures and temperatures may be required to predict the corrosion properties of boilers and pipes in such power plants. In addition, E – pH – T and E – pH – p diagrams can be used in modeling of chemical and electrochemical processes in geothermal reservoirs.

AUTHOR INFORMATION

Corresponding Author

*E-mail: npa@csu.ru

Notes

The author declares no competing financial interest.

REFERENCES

1. Pesterfield L. L.; Maddox J. B.; Crocker M. S.; Schweitzer G. K. Pourbaix (E–pH-M) Diagrams in Three Dimensions. *J. Chem. Educ.* **2012,** *89* (7), 191–199.
2. Bratsch S. G. Standard Electrode Potentials and Temperature Coefficients in Water at 298.15K. *J. Phys. Chem. Ref. Data* **1989,** *18*(1), 1–21.
3. Polmear I. J. Magnesium Alloys and Applications. *Mater. Sci. Technol.* **1994,** *10*(1), 1–16.
4. Makar G. L.; Kruger J. Corrosion of Magnesium. *Int. Mater. Rev.* **1993,** *38*(3), 138–153.
5. Perrault G. G. The Potential–pH Diagram of the Magnesium–Water System. *Electroanal. Chem. Interfac. Electrochem.* **1974,** *51*, 107–119.
6. deBethune A. J.; Licht T. S.; Swendeman N. The Temperature Coefficient of Electrode Potentials. The Isothermal and Thermal Coefficients – The Standard Ionic Entropy of Electrochemical Transport of the Hydrogen Ion. *J. Electrochem. Soc.* **1959,** *106*(7), 616–625.
7. Salvi G. R.; deBethune A. J. The Temperature Coefficient of Electrode Potentials. II. The Second Isothermal Temperature Coefficient. *J. Electrochem. Soc.* **1961,** *108*(7), 672–676.
8. Dinscale A. T. SGTE Data for Pure Elements. *CALPHAD* **1991,** *15*(4), 317–425.
9. Guillermet A. F.; Gustafson P; Hillert M. The Representation of Thermodynamic Properties at High Pressures. *J. Phys. Chem. Solids* **1985,** *46*(12), 1427–1429.
10. Pioro I.; Mokry S.; Peiman W.; Saltanov E.; Grande L. Application of Supercritical Fluids in Power Engineering. In *Proceedings of the 10th International Symposium on Supercritical Fluids (ISSF-2012), May 13 -16, 2012, San Francisco, USA.*
http://issf2012.com/handouts/documents/109_004.pdf (Accessed Dec 2013).

3. Estimation of Gibbs energies of formation of various compounds

The Gibbs energy of reaction that is needed for calculations of electrode potentials and equilibrium constants might be calculated from the values of the Gibbs energies of formation of reagents and products [Карапетьянц, 1975; Лаптев, 1992]:

$$\Delta_r G^o_T = \sum_{i=1}^{\text{products}} \left(\nu_i \cdot \Delta_f G^o_{T,i}\right) - \sum_{j=1}^{\text{reagents}} \left(\nu_j \cdot \Delta_f G^o_{T,j}\right). \quad (52)$$

The Gibbs energies of formation might be estimated in the different ways.

3.1. From the reference data on standard enthalpies of formation and absolute standard entropies

Many reference books contain information on standard enthalpies of formation and absolute standard entropies of several compounds. Using these data, the standard Gibbs energies of formation might be easily calculated.

The standard entropy of formation is the entropy change associated with the reaction of formation of compounds from elements in their thermodynamically stable states at the given conditions. *Exempli gratia*, for the reaction (16) the standard entropy of formation of the compound $A_{\nu_A}B_{\nu_B}$ might be calculated as [Лаптев, 1992]:

$$\Delta_f S^o_{298,15,\,A_{\nu_A}B_{\nu_B}} = S^o_{298,15,\,A_{\nu_A}B_{\nu_B}} - \nu_A \cdot S^o_{298,15,\,A} - \nu_B \cdot S^o_{298,15,\,B}. \quad (53)$$

The standard Gibbs energies of formation might be then calculated according to the Helmholtz – Gibbs equation:

$$\Delta_f G^o_{298,15} = \Delta_f H^o_{298,15} - 298,15 \cdot \Delta_f S^o_{298,15}. \quad (54)$$

The standard entropies and Gibbs energies of formation of charged species in a water solution could not be calculated in this way, because the reference state of the electrons, involved in their formation reaction, is not specified and the absolute standard entropy of the electrons is not determined. Therefore, thermodynamic properties of charged species in a solution are calculated indirectly, using standard reaction properties [Dolejs, 2013; Sedlbauer, O'Connell, Wood, 2000]. For instance, for a hypothetical ion Me^{3+} (aq) the standard entropy and Gibbs energy of formation might be estimated from the reaction:

$$2Me^{3+}\,(aq) + 3H_2\,(g) \rightleftharpoons 2Me\,(s) + 6H^+(aq) \quad (55)$$

as

$$\Delta_f S^o_{298,15,\,Me^{3+}\,(aq)} = \Delta_f S^o_{298,15,\,Me\,(s)} + 3\cdot\Delta_f S^o_{298,15,\,H^+(aq)} - \\ -\frac{3}{2}\cdot\Delta_f S^o_{298,15,\,H_2\,(g)} - \frac{1}{2}\cdot\Delta_r S^o_{298,15,\,(54)}, \quad (56)$$

$$\Delta_f G^o_{298,15,\,Me^{3+}\,(aq)} = \Delta_f G^o_{298,15,\,Me\,(s)} + 3\cdot\Delta_f G^o_{298,15,\,H^+(aq)} - \\ -\frac{3}{2}\cdot\Delta_f G^o_{298,15,\,H_2\,(g)} - \frac{1}{2}\cdot\Delta_r G^o_{298,15,\,(54)}. \quad (57)$$

The respective standard entropy and Gibbs energy of reaction might be estimated independently by equation (24) from measured electromotive force of this reaction and its temperature coefficients.

Table 3 presents the data on standard enthalpies of formation and standard absolute entropies of several transition metals oxides, silicides and silicates, as well as on phase transition and melting temperatures (T_{tr}, T_m) and enthalpies ($\Delta_{tr}H$, $\Delta_m H$). All data were collected from the textbook [Рузинов, Гуляницкий, 1975].

Table 3. Standard enthalpies of formation, standard absolute entropies, phase transition temperatures and enthalpies, melting temperatures and enthalpies of some transition metals and their oxides, silicides and silicates.

Compound		$-\Delta_f H^o_{298,15}$, $\frac{kcal}{mol}$	$S^o_{298,15}$, $\frac{cal}{mol\cdot K}$	T_{tr}, K	$\Delta_{tr}H$, $\frac{kcal}{mol}$	T_m, K	$\Delta_m H$, $\frac{kcal}{mol}$
Co	cr	0	7,18±0,1	713	0,06	1768	3,9±0,1
				1393	0,07		
Co_2Si	cr	27,6±2,0	10,3	–	–	1603	16,5±1,5
CoSi	cr	24,0±2,0	10,36±0,4	–	–	1738	16,0±1,0
$CoSi_2$	cr	24,6±2,0	15,4±0,8	–	–	1600	24,0±0,3
Co_2SiO_4	cr	337,2±1,5	37,9±1,0	–	–	1688	–
CoO	cr	57,1±0,5	12,65±0,1	1258	–	2078	12
Co_3O_4	cr	216,3±3,0	24,5±0,2	–	–	1240_p	–
Fe	cr	0	6,49±0,03	1033	1,22	1810	3,301±0,07
				1185	0,218±0,003		
				1667	0,265±0,050		
Fe_3Si	cr	22,4±0,6	24,8	835	–	1813	13,62
				1323	–		
Fe_5Si_3	cr	46±3	50,1	363	–	1373_p	$4,69_p$
		54,6		1098	–		
				1303	–		
FeSi	cr	19,2±1,5	12,0±1,5	–	–	1678	16,4
		18,3±1,0	11,0±0,4			1693	
$FeSi_2$	cr	19,4±1,8	13,3	–	–	1238_p	–

Fe_3Si_2	cr	43,2±7,2	49,8	–	–	–	–
Fe_2SiO_4	cr	352,9±2,4	34,7±0,5	–	–	1493	22,0±1,0
$FeSiO_3$	cr	285,6±0,7	22,449	–	–	–	–
FeO	cr	63,3±1,0	14,52	–	–	1650	5,75
							7,40
$Fe_{0,947}O$	cr	63,2±0,3	14,05±3,2	–	–	1651_p	7,4±0,2
Fe_3O_4	cr	267,9±0,2	36,2±0,6	866	0	1867	33,0±2,0
			34,95±0,1	851			
Fe_2O_3	cr	197,3±0,3	20,9±0,1	953	0,16	1735_p	–
				1053	0		
	am	164,5	–	–	–	–	–
α-Mn	cr	0	7,60±0,1	980	0,53	1517	2,88
				1360	0,51		3,50
				1410	0,45		
β-Mn	cr	–	8,22	–	–	–	–
γ-Mn	cr	−0,37	8,56	–	–	–	–
Mn_3Si	cr	25,7±2,6	24,78	950	1,09	1305	10,4
Mn_5Si_3	cr	65,4±3,6	57,0	–	–	1573	39,5
MnSi	cr	19,0±0,5	10,84	–	–	1543	14,3
$MnSi_{1,7}$	cr	22,0±0,7	11,04	–	–	1433	23,9
Mn_2SiO_4	cr	413,58	36,9	–	–	1618_p	$26,15_p$
		423,5±1,9					
$MnSiO_3$	cr	315,7	21,3±0,2	–	–	1543_p	$8,0_p$
	am	307,2	–	–	–	–	–
MnO	cr	92,0±0,5	14,3±0,2	–	–	2148	13,0±1,5
						2058	
Mn_3O_4	cr	331,4±1,0	36,8±0,8	1445	5,0±0,3	1838	39,0
Mn_2O_3	cr	228,7±1,2	26,4±0,5	873	–	1620_p	–
$MnMnO_4$	cr	284,73	–	–	–	–	–
MnO_2	cr	124,3±0,5	12,7±0,1	523	–	–	–
	am	120,1	–	–	–	1120_p	–
Mn_2O_7	l	174,1±2,5	–	–	–	–	–
Mo	cr	0	6,83±0,1	–	–	2873	9,861±0,79
						2890	8,32±0,07
Mo_3Si	cr	24,6±5,0	25,4±0,3	–	–	2303_p	–
Mo_3Si_2	cr	46,8±3,0	–	–	–	–	–
Mo_5Si_3	cr	68	–	–	–	2453	–
		72±7					
$MoSi_2$	cr	31,4±3,5	–	–	–	2303	–
MoO	g	−92,5±15	56,9±2	–	–	–	–
Mo_2O_3	cr	99,9	–	–	–	–	–
MoO_2	cr	140,8±0,2	11,95±2	–	–	2200	16
Mo_4O_{11}	cr	680,3±2,5	–	–	–	–	–
MoO_3	cr	178,2±0,5	18,6±0,3	–	–	1068	12,55±0,4

Ni	cr	0	7,12±0,05	631	0,14±0,02	1728	4,461±0,37
Ni_3Si	cr	35,5±3,0	–	1313 1398	–	1431_p	–
Ni_5Si_2	cr	75,0±6,0	–	–	–	1555	–
Ni_2Si	cr	33,6±3,0	–	1487	1,425	1591	12,0±0,6
Ni_3Si_2	cr	53,5±4,0	–	–	–	1118_p	–
NiSi	cr	20,5±2,0	11,2±0,5	–	–	1265	10,6±0,6
$NiSi_2$	cr	20,7±2,0	15,77	–	–	1245	–
Ni_2SiO_4	cr	341,7±2,0	26,5±5,0	–	–	–	–
NiO	cr	57,24±0,13	9,1±0,1	565	–	2228	12,1
Ni_2O_3	cr	117,0	–	–	–	–	–
O_2	g	–	49,005±0,008	–	–	–	–
Si	cr	0	4,50±0,02	–	–	1683 1688	11,9±0,2
	am	–1,0	–	–	–	–	–
SiO	am	102,7±5	11,1±1,5	–	–	–	–
SiO_2	cr [1*]	217,72±0,34	10,0±0,1	846	0,15	–	–
	cr [2*]	–	–	1140	0,12	1883 1696	2,04 1,8±0,2
	cr [3*]	216,4	10,4±0,2	390 436 509	0,07 0,04 0,05	1953	2,15
	cr [4*]	217,08±0,37	10,2±0,1	515 543	0,31±0,05	–	–
	cr [5*]	216,417	11,963	–	–	2001 1996	1,84 2,29±0,5
	cr [6*]	216,51±0,37	9,65±0,05 8,6±0,7	–	–	–	–
	cr [7*]	205,91±0,45	6,64±0,05	–	–	–	–
	ст	215,48±0,36	–	–	–	–	–
	am	214,35±0,36	11,2	–	–	–	–
	[*1] – hexagonal modification, α-quartz; [*2] – hexagonal modification, β-quartz; [*3] – hexagonal modification, α-tridimite; [*4] – tetragonal modification, α-cristobalite; [*5] – cubic modification, β-cristobalite; [*6] – monoclinic modification, coesite; [*7] – tetragonal modification, stishovite.						
H_2SiO_3	cr	284,0±0,4	32	–	–	–	–
H_4SiO_4	cr	353,5±0,4	46	–	–	–	–
$H_2Si_2O_5$	cr	498,3±0,5	46	–	–	–	–
$H_6Si_2O_7$	cr	638,0	79	–	–	–	–
Ti	cr	0	7,325±0,02	1155	1,00	1933 1943	3,16±0,02 4,1±0,1 4,45
Ti_5Si_3	cr	138,7±8,0 138	50,32	–	–	2403	–
TiSi	cr	31,0±2,0	14,2	–	–	1843_p	–

$TiSi_2$	cr	32,3±2,0	19,1	–	–	1743	–
α-TiO	cr	124,19±1	12,2	1264	0,82±0,2	–	–
β-TiO	cr	123,872	12,372	–	–	2023	13
Ti_2O_3	cr	363,49±2	18,83±0,2	473	0,22±0,05	2112	26,4
Ti_3O_5	cr	587,75±3,0 586,9±1,5	30,9±0,3	450	2,81	2047	33
TiO_2	cr [1*]	223,0±1 224,21±0,5	11,93±0,07	918 1264	0 0,82±0,2	–	–
	cr [2*]	225,8±1 225,5±1,0	12,04±0,04	–	–	2143	16
	cr [3*]	225,1	–	–	–	–	–
	am	210	–	–	–	–	–
	[*1] – anatase; [*2] – rutile; [*3] – brookite.						

3.2. From the data on reduced thermodynamic potentials

Reduced thermodynamic potential of any compound is the quantity, determined according to the equation:

$$\Phi_T^{'} = \frac{\Delta_f G_T^o - H_o^o}{T}\ , \tag{58}$$

where H_0^o is the enthalpy of a compound at 0K [Elliott, Gleiser, 1960].

The standard Gibbs energy of any reaction (including formation of the compound from the elements) might be calculated according to the equation:

$$\Delta_r G_T^o = \Delta_r H_{298,15}^o + T\cdot\left(\sum_{i=1}^{\text{products}}\left(\nu_i\cdot\Phi_{T,i}^{'}\right) - \sum_{j=1}^{\text{reagents}}\left(\nu_j\cdot\Phi_{T,j}^{'}\right)\right) -$$

$$-\sum_{i=1}^{\text{products}}\left(\nu_i\cdot\left(\Delta_f H_{298,i}^o - H_{0,i}^o\right)\right) - \sum_{j=1}^{\text{reagents}}\left(\nu_j\cdot\left(\Delta_f H_{298,j}^o - H_{0,j}^o\right)\right)\ . \tag{59}$$

The thermodynamic potential values at various temperatures for many compounds, calculated on the basis of statistical thermodynamics, might be found in reference books. The values for manganese and iron silicides and silicates were presented by the authors of book [Моисеев et al., 1997] in form of the temperature dependence:

$$\Phi_T^{'} = \varphi_1 + \varphi_2\cdot\ln x + \frac{\varphi_3}{x^2} + \frac{\varphi_4}{x} + \varphi_5\cdot x + \varphi_6\cdot x^2,\ {}^{cal}/_{mol\cdot K}\ , \tag{60}$$

where

$$x = \frac{T}{10^4}, K \ . \tag{61}$$

The parameters are presented in Table 4.

3.3. Miedema's and Eastman's methods

The standard enthalpies of formation and the standard absolute entropies of intermetallic compounds usually are not present in common reference books. In this case some predictive methods might be implemented in order to estimate these quantities [Смитлз, 1980].

A very powerful method of estimation of the standard enthalpies of formation of intermetallic compounds was proposed by A. R. Miedema [Debski, Debski, Gasior, 2014; Miedema, 1973a; Miedema, 1973b; Niessen et al., 1983; Zhang et al., 2016; Zhang et al., 2017]. He stated that for intermetallides two factors contribute to the value of $\Delta_f H^o_{298,15}$. The first factor is negative and is determined by the equalising of chemical potentials of electrons in the atomic cells of different kinds, and by the charge transfer. It is directly proportional to the squared difference of atoms electronegativities, which are determined, according to him, as the work functions of pure compounds. The nature of the second (positive) factor is that electron density should vary continuously at the transfer to the different kind of atomic cell.

The expression was proposed as follows:

$$\Delta_f H^o_{298,15} = \varphi \cdot P \cdot \left(-(\Delta\Phi)^2 + Q \cdot \left(\Delta n_{WS}^{\frac{1}{3}} \right)^2 - R \right) + \Delta_{tr} H, \ {kJ}/{g-atom}, \tag{62}$$

where

$$\Delta\Phi = \Phi_A - \Phi_B, \tag{63}$$

$$\Delta n_{WS}^{\frac{1}{3}} = n_{WS,A}^{\frac{1}{3}} - n_{WS,B}^{\frac{1}{3}}, \tag{64}$$

$$\varphi = f \cdot g, \tag{65}$$

$$g = \frac{2 \cdot (x_A \cdot V_A^{\frac{2}{3}} + x_B \cdot V_B^{\frac{2}{3}})}{n_{WS,A}^{-\frac{1}{3}} + n_{WS,B}^{-\frac{1}{3}}}, \tag{66}$$

$$f = x_{s,A} \cdot x_{s,B} \cdot \left(8 \cdot \left(x_{s,A} \cdot x_{s,B} \right)^2 + 1 \right), \tag{67}$$

Table 4. The parameters in the equation (60) for some compounds.

Compound	Temperature interval, K	φ_1, $cal/mol \cdot K$	φ_2, $cal/mol \cdot K$	φ_3, $cal \cdot K/mol$	φ_4, cal/mol	φ_5, $cal/mol \cdot K^2$	φ_6, $cal/mol \cdot K^3$
FeSi	298 – 1683	36,4357	10,59	−0,000098	0,144066	17,95	0
$FeSi_2$	298 – 1493	48,6711	14,56	0	0,212093	20,5	0
Fe_5Si_3	298 – 1373	149,629	42,14	−0,000049	0,527282	106,1	0
Fe_3Si	298 – 830	61,4232	17,04	0,000018	0,187329	104,4	0
Mn_2SiO_4	298 – 1620	128,976	38,0201	−0,00372	0,863356	23,303	0
$MnSiO_3$	298 – 1559	83,075	26,4201	−0,00308	0,668259	19,403	0
MnSi	298 – 1543	39,111	11,7901	−0,000765	0,23024	15,253	0
Mn_5Si_3	298 – 1573	170,771	48,1301	−0,00234	0,76479	64,703	0
Mn_3Si	298 – 950	79,852	24,1101	−0,00176	0,478389	62,25	0
$MnSi_2$	298 – 1433	54,403	17,2001	−0,00156	0,394149	5,503	0

$$\begin{cases} x_{s,A} = \dfrac{x_A \cdot V_A^{\frac{2}{3}}}{x_A \cdot V_A^{\frac{2}{3}} + x_B \cdot V_B^{\frac{2}{3}}}; \\ x_{s,B} = \dfrac{x_B \cdot V_B^{\frac{2}{3}}}{x_A \cdot V_A^{\frac{2}{3}} + x_B \cdot V_B^{\frac{2}{3}}}. \end{cases} \quad (68)$$

Here Φ is the electronegativity, $n_{WS}^{\frac{1}{3}}$ is the electronic density at the boundaries of the dissimilar Wigner-Seitz atomic cells, φ is the function depending on intermetallide composition, x_S is the surface mole fraction of the element, V is the molar volume of the pure element, P, R and Q are the model empirical parameters, $\Delta_{tr}H$ is the enthalpy of transition of the element to the metallic crystal structure (which is applicable for silicon, carbon and nitrogen, which reference states at the standard conditions differ from metallic).

The parameters of the Miedema's model for 4th period transition metals and for silicon are listed in Table 5.

Table 5. Miedema's model parameters for some elements.

Element	Φ	$V^{\frac{2}{3}}$	$n_{WS}^{\frac{1}{3}}$	P	Q	R	$\Delta_{tr}H$, $kJ/g-atom$
Sc	3,25	6,1	1,27	14,2	9,4	0	0
Ti	3,65	4,8	1,47	14,2	9,4	0	0
V	4,25	4,1	1,64	14,2	9,4	0	0
Cr	4,65	3,7	1,73	14,2	9,4	0	0
Mo	4,65	4,4	1,77	14,2	9,4	0	0
Mn	4,45	3,8	1,61	14,2	9,4	0	0
Fe	4,93	3,7	1,77	14,2	9,4	0	0
Co	5,10	3,5	1,75	14,2	9,4	0	0
Ni	5,20	3,5	1,75	14,2	9,4	0	0
Cu	4,55	3,7	1,47	14,2	9,4	0	0
Zn	4,10	4,4	1,32	14,2	9,4	0	0
Si	4,70	4,2	1,50	12,3	9,4	2,1	35,5

The method of estimation of the standard absolute entropies of intermetallic compounds was proposed by Eastman [Eastman, 1923]:

$$S^{o}_{298,15} = \frac{3}{2} \cdot R \cdot \ln A_{av} + R \cdot \ln V_{av} - \frac{3}{2} \cdot R \cdot \ln T_{dec} + a, \ J/g-atom \cdot K, \quad (69)$$

where A_{av}, $^{g}/_{mol}$ is the average atomic mass of the compound (*id est*, its molar mass divided to the total number of atoms), V_{av}, $^{cm^3}/_{mol}$ is its average atomic volume (*id est*, its average atomic mass divided to the compound density), T_{dec}, K is the temperature of compound decomposition (either via congruent or incongruent transition), $a = 52{,}3$ $^{J}/_{g-atom \cdot K}$ is the constant.

Formulae (62) and (69) give the results related to 1 g–atom of intermetallic compound. To convert it to the common molar values, one should multiply the resulting values by the number of atoms in the compound molecule.

3.4. Kireev's method

Sometimes, when information about thermodynamic properties of necessary substances is incomplete or missing at all, it is appropriate to use the computational methods in order to determine such unknown properties.

Thermodynamic properties of the various compounds of the same kind vary periodically with the change of element atomic number. V. A. Kireev proposed [Киреев, 1970] that an approximate relationship exists between the standard Gibbs energies of formation of similar compounds of transition metals and the atomic number of elements forming these compounds. Various kinds of dependencies might be tried to fit the existing data and then be used for predictions. Most likely, however, logarithmic or semi-logarithmic dependencies have the highest approximation rates.

Particularly, it applies to the thermodynamic properties of oxides [Парфёнова, Гаркушин, Медовщикова, 2000]. The dependence of standard Gibbs energies of formation of MeO_2-type oxides of 4th period d-elements on metals nucleus charge (z_{Me}) was analysed. In order to determine the correlative equation between these variables, the attempt was performed to use various kinds of functional relationships using a least squares technique [Adrain, 1808; Mortimer, 2013; Trefall, Nordö, 1959]:

$$-\Delta_f G^{o}_{298,15,\,MeO_2} = f(z_{Me}),$$

$$-\Delta_f G^{o}_{298,15,\,MeO_2} = f(\lg z_{Me}),$$

$$\lg\left(-\Delta_f G^{o}_{298,15,\,MeO_2}\right) = f(z_{Me}),$$

$\lg\left(-\Delta_f G^{o}_{298,15,\,MeO_2}\right) = f\left(\lg z_{Me}\right)$ and

$$\frac{-\Delta_f G^{o}_{298,15,\,MeO_2}}{z_{Me}} = f\left(z_{Me}\right).$$

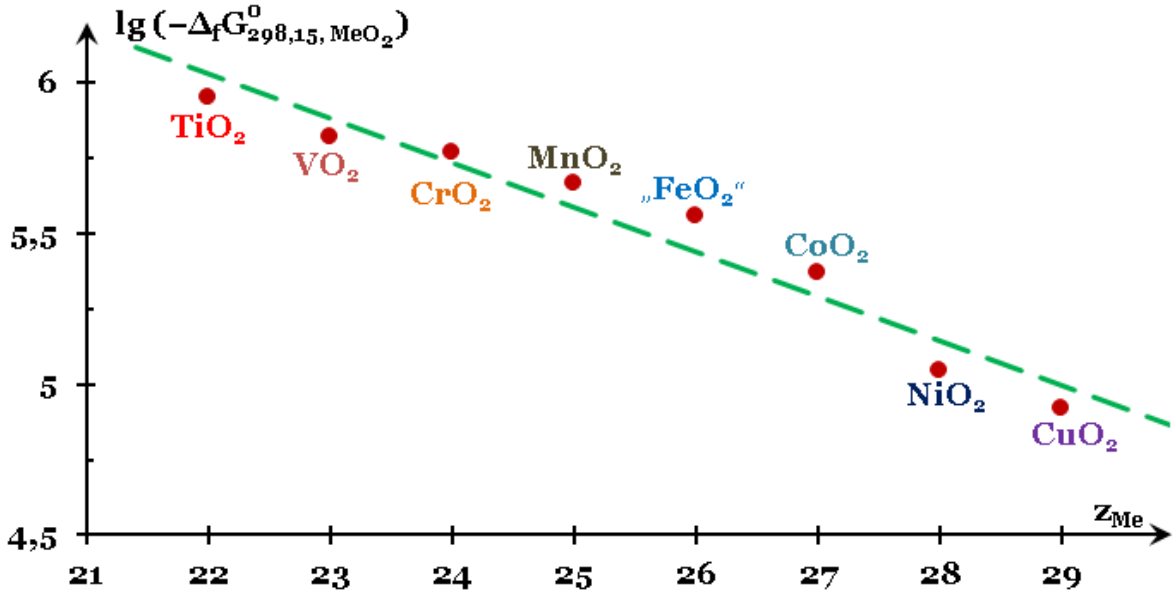

Fig. 11. The correlation of $\lg\left(-\Delta_f G^{o}_{298,15,\,MeO_2}\right)$ versus z_{Me} according to equation (70).

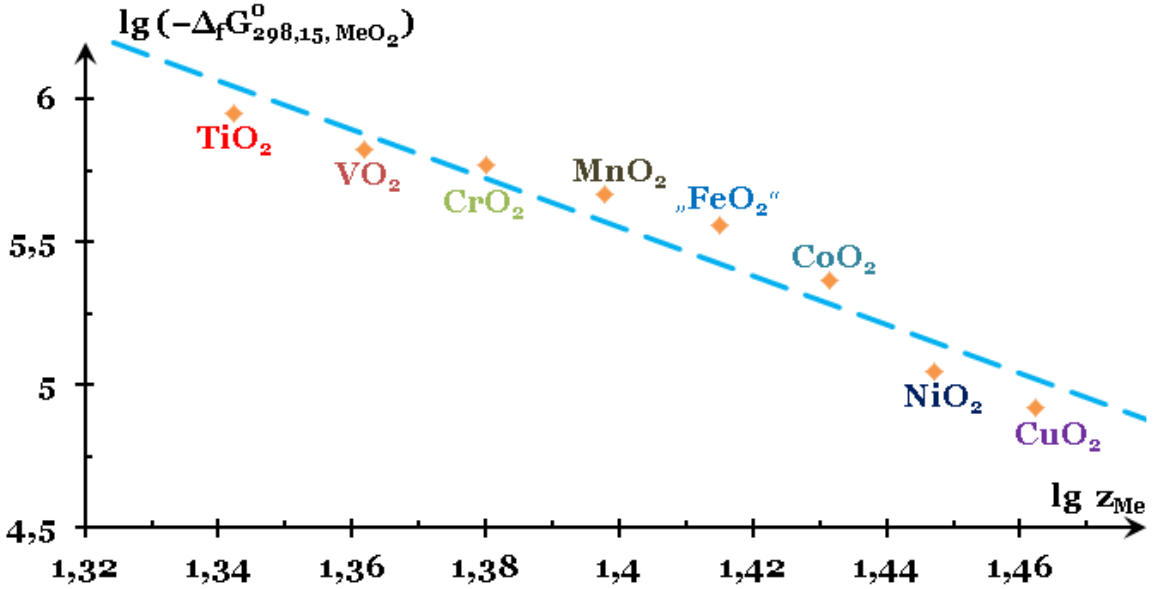

Fig. 12. The correlation of $\lg\left(-\Delta_f G^{o}_{298,15,\,MeO_2}\right)$ versus $\lg z_{Me}$ according to equation (71).

From all these dependencies only the third one and the fourth one provided a good level of data approximation. The following relations were

established, the calculations on which gave a convergence between the results (see Figures 11 and 12):

$$\lg\left(-\Delta_f G^{o}_{298,15,\,MeO_2}\right) = -0,1472 \cdot z_{Me} + 9,2569,\ {}^{J}/_{mol};\ R^2 = 0,9448, \qquad (70)$$

$$\lg\left(-\Delta_f G^{o}_{298,15,\,MeO_2}\right) = -8,5173 \cdot \lg z_{Me} + 17,4776,\ {}^{J}/_{mol};\ R^2 = 0,9280. \qquad (71)$$

The obtained analytical relations might be used to verify the reference data and to predict the thermodynamic properties of those substances, for which they could not be determined experimentally (CrO_2, FeO_2, NiO_2, CuO_2, ZnO_2). Thus, the results of calculations according to aforementioned equation for iron, chromium and nickel dioxides are in good agreement with the independent estimates, made by Tyurin [Тюрин, 2012] using methods of I. G. Gorichev, A. F. Kapustinskiy and M. Ch. Karapet'yantz.

Further implementations of the Kireev's method are presented in Chapters 4 and 11.

3.5. Gorichev's method

It was found by I. G. Gorichev [Gorichev, Klyushin, 1971; Жук, 2006], that an approximate functional relationship exist between the reduced chemical potential of oxygen atoms in metal oxide and system's degree of oxidation, $\Delta_f G^{o}_{298,15,\,Me_{\frac{1}{x}}O} = f(x)$. He assumed this relationship is linear and, basing on this assumption and using Waring–Lagrange interpolation formula [Lagrange, 1812; Waring, 1779], derived the equation, which allowed estimation of an unknown standard Gibbs energy of formation of metal oxide MeO_x according to available data on the Gibbs energies of formation of two other oxides of the same metal – namely, MeO_i and MeO_j:

$$\frac{\Delta_f G^{o}_{298,15,\,MeO_x}}{x} = \frac{\Delta_f G^{o}_{298,15,\,MeO_i}}{i} - \left(\frac{\Delta_f G^{o}_{298,15,\,MeO_i}}{i} - \frac{\Delta_f G^{o}_{298,15,\,MeO_j}}{j}\right) \cdot \frac{i-x}{i-j}. \qquad (72)$$

A similar relationship might be valid not only for oxides, but also for some other binary compounds with polar covalent bond (sulphides, carbides, nitrides, silicides, *et cetera*). However, attempts to apply this equation to predict the unknown thermodynamic properties of certain compounds in various systems showed that linear nature of this relationship was obeyed not strictly. Therefore, the formula (72) was modified in such a way, that the interpolation could be based on the reliable

thermodynamic data on several compounds, assuming the polynomial nature of aforementioned relationship. A modified variant of the calculation formula appears as follows:

$$\Delta_f G^o_{T,\,Me_{\nu_{Me,x}}A_{\nu_{A,x}}} = \nu_{A,x} \times$$
$$\times \sum_{i=1}^{n} \left(\frac{\Delta_f G^o_{T,\,Me_{\nu_{Me,i}}A_{\nu_{A,i}}}}{\nu_{A,i}} \cdot \prod_{j \neq i} \frac{\nu_{Me,i} \cdot \left(\nu_{Me,j} \cdot \nu_{A,x} - \nu_{Me,x} \cdot \nu_{A,j} \right)}{\nu_{Me,x} \cdot \left(\nu_{Me,j} \cdot \nu_{A,i} - \nu_{Me,i} \cdot \nu_{A,j} \right)} \right), \quad (73)$$

where n is a number of Gibbs energies of formation of binary compounds, accepted as a reliable initial data; $Me_{\nu_{Me,i}}A_{\nu_{A,i}}$ – formulae of these binary compounds (Me – metal atom, A – more electronegative element atom, $\nu_{Me,i}$ and $\nu_{A,i}$ – indices for Me and A atoms in compound, respectively); $Me_{\nu_{Me,x}}A_{\nu_{A,x}}$ – formula of the compound, Gibbs energy of formation of which is to be estimated, $\nu_{Me,x}$ and $\nu_{A,x}$ – indices for the Me and A atoms in it.

While doing calculations by formula (73), as opposed to calculations by formula (72), there is no necessity to convert thermodynamic data according to 1 gram-atom of metal.

The proposed method can be successfully used to estimate the thermodynamic properties of compounds, for which the experimental information is missing.

3.6. ΔO^{2-} method

The method of estimating the Gibbs energies of formation of metal oxides, hydroxides and silicates was proposed by Y. Tardy and R. M. Garrels [Tardy, Garrels, 1974; Tardy, Garrels, 1976; Tardy, Garrels, 1977]. It is based on the quantity of ΔO^{2-} that can be calculated for any metal Me in the oxidation state +x as follows:

$$\Delta O^{2-}_{\substack{(+x)\\Me}} = \Delta_f G^o_{298,15,\,MeO_{\frac{x}{2}}} - \Delta_f G^o_{298,15,\,Me^{x+}}. \quad (74)$$

Actually, this quantity equals the Gibbs energy change in the following reaction:

$$Me^{x+}(aq) + \frac{x}{4} O_2\,(g) + x e^- \rightleftharpoons MeO_{\frac{x}{2}}\,(s). \quad (75)$$

The authors analysed the data on Gibbs energies of formation of oxides, hydroxides and aqueous cations for several metals and derived the following linear regression [Tardy, Garrels, 1976]:

$$\Delta\text{hydroxide}_{\underset{\text{Me}}{(+x)}} = \Delta_f G^o_{298,15,\ \text{Me(OH)}_x} - \Delta_f G^o_{298,15,\ \text{MeO}_{\frac{x}{2}}} - \frac{x}{2}\,\Delta_f G^o_{298,15,\ \text{H}_2\text{O (ice)}}, \qquad (76)$$

$$\Delta\text{hydroxide}_{\underset{\text{Me}}{(+x)}} = -0,21\cdot\left(\Delta O^{2-}_{\underset{\text{Me}}{(+x)}} + 53\right), \qquad (77)$$

if all quantities in equation (77) are expressed in $\frac{\text{kcal}}{\text{mol}}$.

Equations (74), (76) and (77) might be implemented to estimate the values of the Gibbs energies of formation for hydroxides, oxides and aqueous cations that are normally not stable in the standard conditions (*exempli gratia*, for the aqueous cation Si^{4+}).

The Gibbs energies of formation of silicates might be estimated as follows [Tardy, Garrels, 1977]:

$$\Delta\text{silicate}_{\underset{\text{Me}}{(+x)}} = \Delta_f G^o_{298,15,\ \text{silicate}} - \sum_{\text{oxides}} \Delta_f G^o_{298,15,\ \text{oxide}}, \qquad (78)$$

$$\Delta\text{silicate}_{\underset{\text{Me}}{(+x)}} = -1,01\cdot\frac{n_{\text{Me}}\cdot n_{\text{Si}}}{n_{\text{Me}} + n_{\text{Si}}}\cdot\left(\Delta O^{2-}_{\underset{\text{Me}}{(+x)}} - \Delta O^{2-}_{\underset{\text{Si}}{(+4)}}\right). \qquad (79)$$

where n_{Me} and n_{Si} are, correspondingly, the numbers of oxygen atoms required to balance the metal cation and the silicon in the silicate formula.

3.7. Dependence of Gibbs energies of formation on temperature

The dependence of the enthalpy of formation of any compound on temperature is determined by the Kirchhoff equation [Kirchhoff, 1858; Kirchhoff, 1882]:

$$\left(\frac{d\Delta_f H^o_T}{dT}\right)_P = \Delta C_p, \qquad (80)$$

from which follows that

$$\Delta_f H^o_T = \Delta_f H^o_{298,15} + \int_{298,15}^{T} \Delta C_p dT. \qquad (81)$$

The dependency of absolute entropy on temperature is given by the expression that follows from the second law of thermodynamics:

$$S_T^o = S_{298,15}^o + \int_{298,15}^{T} \frac{\Delta C_p}{T} dT . \qquad (82)$$

Here C_p is the isobaric heat capacity that is a function of temperature. ΔC_p is a function that depends on heat capacities of all reaction participants. For the reaction (16) it is determined by the expression:

$$\Delta C_{p,(16)} = C_{p,A_{\nu_A}B_{\nu_B}} - \nu_A \cdot C_{p,A} - \nu_B \cdot C_{p,B} . \qquad (83)$$

The dependency of heat capacities on temperature might be expressed in form of polynomial series:

$$C_p = \frac{a_{-2}}{T^2} + \frac{a_{-1}}{T} + a_o + a_1 \cdot T + a_2 \cdot T^2 + a_3 \cdot T^3 + \ldots , \qquad (84)$$

where the parameters a_i are adjusted to fit the experimental dependencies.

Equations (81) and (82) are suitable only if a given substance does not exhibit any phase transitions in the considered temperature interval. Otherwise, the calculations should be performed for every phase and temperature interval separately. *Exempli gratia*, if the thermodynamically stable phase in the standard state is χ, then the substance exhibits a solid phase transition to the phase ω at the temperature T_{tr}, and then it melts at the temperature T_m, than the enthalpy of formation of liquid substance at the temperature T might be expressed as:

$$\begin{aligned} \Delta_f H_T^{(l)} = \Delta_f H_{298,15}^{o,(\chi)} + \int_{298,15}^{T_{tr}} \Delta C_p^{(\chi)} dT + \Delta_{tr} H_{T_{tr}}^{(\chi\to\omega)} + \\ + \int_{T_{tr}}^{T_m} \Delta C_p^{(\omega)} dT + \Delta_m H_{T_m}^{(\omega\to l)} + \int_{T_m}^{T} \Delta C_p^{(l)} dT \end{aligned} , \qquad (85)$$

$$\begin{aligned} S_T^{(l)} = S_{298,15}^{o,(\chi)} + \int_{298,15}^{T_{tr}} \frac{\Delta C_p^{(\chi)}}{T} dT + \frac{\Delta_{tr} H_{T_{tr}}^{(\chi\to\omega)}}{T_{tr}} + \\ + \int_{T_{tr}}^{T_m} \frac{\Delta C_p^{(\omega)}}{T} dT + \frac{\Delta_m H_{T_m}^{(\omega\to l)}}{T_m} + \int_{T_m}^{T} \frac{\Delta C_p^{(l)}}{T} dT \end{aligned} , \qquad (86)$$

Here $\Delta_{tr}H_{T_{tr}}$ and $\Delta_m H_{T_m}$ are, respectively, the enthalpies of phase transition and melting; $\Delta_{tr}S_{T_{tr}} \cong \frac{\Delta_{tr}H_{T_{tr}}}{T_{tr}}$ and $\Delta_m S_{T_m} \cong \frac{\Delta_m H_{T_m}}{T_m}$ – the corresponding entropies of phase transition and melting.

When the enthalpy of formation and absolute entropy at the desired temperature are calculated, the Gibbs energy of formation might be calculated straightforwardly by equation (54).

Table 6 presents the data on temperature dependencies of heat capacities of several transition metals oxides, silicides and silicates [Рузинов, Гуляницкий, 1975]. Using the data from Tables 3 and 6 together, one might calculate the Gibbs energies of formation of these compounds at any temperature.

Table 6. Temperature dependencies of heat capacities of some transition metals and their oxides, silicides and silicates.

Compound		$C_p = a_0 + a_1 \cdot 10^{-3} \cdot T + a_{-2} \cdot 10^5 \cdot T^{-2}$, $\frac{cal}{mol \cdot K}$			Temperature interval, K
		a_0	a_1	a_{-2}	
α-Co	cr	4,74	4,00	–	298 – 713
β-Co	cr	3,30	5,86	–	713 – 1393
γ-Co	cr	9,60	–	–	1393 – 1765
Co_2Si	cr	17,04	6,40	–0,9	298 – 1603
	l	32,67	–	–	1603 – 1800
CoSi	cr	9,82	2,85	–1,36	298 – 1738
	l	20,9	–	–	1738+
$CoSi_2$	cr	17,12	3,61	–2,27	298 – 1600
	l	27,7	–	–	1600+
CoO	cr	11,54	2,04	0,40	298 – 1800
	l	15,5	–	–	–
Co_3O_4	cr	30,84	17,08	–5,72	298 – 1000
α-Fe	cr	4,18	5,92	–	273 – 1033
β-Fe	cr	9,0	–	–	1033 – 1185
γ-Fe	cr	1,84	4,66	–	1185 – 1667
δ-Fe	cr	10,5	–	–	1667 – 1809
Fe_3Si	cr	17,04	20,88	0,035	298 – 800
Fe_5Si_3	cr	42,14	21,22	–0,98	298 – 1303
FeSi	cr	10,59	3,59	–0,195	298 – 1673
	l	19,50	–	–	1673 – 1925
$FeSi_2$	cr	14,56	4,11	–	298 – 1233
Fe_2SiO_4	cr	35,61	9,36	–6,70	298 – 1493
	l	57,5	–	–	1493 – 1724
$FeSiO_3$	cr	37,84	4,06	–6,5	–

FeO	cr	12,38	1,62	−0,38	298 – 1200
	l	16,3	–	–	$1650_{п}$ – 3600
$Fe_{0,947}O$	cr	11,66	2,00	−0,67	298 – $1651_{п}$
	l	16,30	–	–	$1651_{п}$ – 1800
α-Fe_3O_4	cr	21,88	48,2	–	298 – 866
β-Fe_3O_4	cr	48,00	–	–	866 – 1867
α-Fe_2O_3	cr	23,49	18,60	−3,55	298 – 954
β-Fe_2O_3	cr	36,0	–	–	954 – 1054
γ-Fe_2O_3	cr	31,70	1,76	–	1054 – 1735
α-Mn	cr	5,16	3,81	–	298 – 991
		5,704	3,38	−0,375	298 – 991
β-Mn	cr	8,33	0,66	–	991 – 1373
γ-Mn	cr	10,70	–	–	1373 – 409
		6,03	3,56	−0,443	298 – 1409
δ-Mn	cr	11,30	–	–	1409 – 1517
Mn_3Si	cr	24,13	12,45	−3,52	298 – 950
		0,848	24,78	113,9	950 – 1343
	l	38,7	–	–	1343+
Mn_5Si_3	cr	48,95	11,20	−4,91	298 – 1573
	l	77,9	–	–	1573+
MnSi	cr	11,21	4,00	−1,02	298 – 1543
	l	18,9	–	–	1543+
$MnSi_{1,7}$	cr	17,2	1,10	−3,12	298 – 1433
	l	26,8	–	–	1433+
Mn_2SiO_4	cr	29,4	12,6	–	298 – 1618
		37,62	5,95	−6,86	298 – 1618
		34,38	11,25	−3,92	298 – 1618
$MnSiO_3$	cr	26,42	3,88	−6,16	298 – 1298
MnO	cr	11,11	1,94	−0,88	298 – 1800
	l	13,5	–	–	–
α-Mn_3O_4	cr	34,64	10,82	−2,20	298 – 1445
β-Mn_3O_4	cr	50,20	–	–	1445 – 1800
Mn_3O_4	l	49,0	–	–	–
Mn_2O_3	cr	24,73	8,38	−3,23	298 – 1350
MnO_2	cr	16,60	2,44	−3,88	298 – 780
Mo	cr	5,77	0,28	–	300 – 2500 $+0{,}54\cdot10^{-6}\cdot T^2$
		5,19	1,658	–	298 – 2890

		5,308	1,503	–	$1900 - 2890 + 2030 \cdot 10^7 \cdot T^{-2} \times \times \exp\left(-\frac{200,4 \cdot 10^2}{T}\right)$
Mo_3Si	cr	21,98	4,58	−1,0	298 – 1450
		−1,25	17,70	45,29	1200 – 2200
Mo_5Si_3	cr	48,53	6,48	−17,60	1200 – 2200
$MoSi_2$	cr	15,75	3,24	−1,08	298 – 1200
		6,30	8,66	17,86	1200 – 2200
MoO_2	cr	14,11	5,82	−2,18	298 – 2000
	l	23	–	–	–
MoO_3	cr	20,07	5,90	−3,68	298 – 1074
	l	30,342	–	–	1074+
α-Ni	cr	7,80	0,47	−1,345	298 – 631
β-Ni	cr	7,10	1,00	−2,23	631 – 1728
Ni_2Si	cr	17,49	3,81	−1,83	298 – 1591
	l	26,91	–	–	1591 – 1800
NiSi	cr	12,86	0,90	−2,29	298 – 1265
	l	19,1	–	–	1265+
$NiSi_2$	cr	17,94	2,64	−2,59	298 – 1245
	l	25,7	–	–	1245+
Ni_2SO_4	cr	36,64	5,49	–	298 – 1570
α-NiO	cr	−4,99	37,58	3,89	298 – 525
β-NiO	cr	13,88	–	–	525 – 565
γ-NiO	cr	11,18	2,02	–	565 – 1800
O_2	g	7,16	1,00	−0,40	298 – 3000
Si	cr	5,72	0,59	−0,99	298 – 1688
	l	6,50	–	–	1688 – 3552
SiO	g	7,70	0,74	−0,70	298 – 2000
SiO_2	cr [1*]	11,22	8,20	−2,70	298 – 846
	cr [2*]	14,41	1,94	–	846 – 1883
	cr [3*]	4,28	21,06	–	298 – 515
	cr [4*]	14,40	2,04	–	515 – 2001
	cr [5*]	3,27	24,80	–	298 – 390
	cr [6*]	13,64	2,64	–	390 – 1953
	glass	13,38	3,68	−3,45	298 – 2000
	[*1] – α-quartz; [*2] – β-quartz; [*3] – α-cristobalite; [*4] – β-cristobalite; [*5] – α-tridimite; [*6] – β-tridimite				

α-Ti	cr	6,226	1,444	−0,617	298 – 1120
		5,28	2,4	–	298 – 1155
β-Ti	cr	4,34	2,2	–	1155 – 1941
TiSi	cr	15,42	6,45	–	298 – 1350
Ti_5Si_3	cr	58,22	5,74	−26,46	298 – 1200
$TiSi_2$	cr	14,94	8,32	−4,55	298 – 1180
α-TiO	cr	10,57	3,60	−1,86	298 – 1264
β-TiO	cr	11,85	3,00	–	1264 – 2023
TiO	l	16,00	–	–	2023+
α-Ti_2O_3	cr	17,5	65,5	–	298 – 473
β-Ti_2O_3	cr	34,68	1,30	−10,20	473 – 2112
Ti_2O_3	l	37,60	–	–	2112 – 3300
α-Ti_3O_5	cr	35,47	20,58	–	298 – 450
β-Ti_3O_5	cr	41,60	8,0	–	450 – 2173
Ti_3O_5	l	56,0	–	–	2173+
TiO_2	cr [1*]	17,83	0,50	−4,23	298 – 1300
	cr [2*]	17,97	0,28	−4,35	298 – 1800
	l	21,00	–	–	2143+
	[*1] – anatase; [*2] – rutile.				

The dependency of reduced thermodynamic potentials on temperature is also presented in many reference books.

3.8. Dependence of Gibbs energies of formation on pressure

The problem of prediction and estimation of thermodynamic properties of substances and reactions at elevated pressures faces the researchers and engineers for a long time, and the first attempts to solve it relate to the fiftieths years of the past century. Knowledge of the thermodynamic properties of aqueous species at elevated temperatures and pressures allows plotting potential – pH diagrams and studying the corrosion properties of materials in geothermal reservoirs, deep marine environments and industrial autoclaves [Cook, Olive, 2012; Kaufman et al., 2009; Lewis, 1971b; Yagi, 2011; 夏大海, Luo, 2015].

The standard Gibbs energies of formation of some metals and other solid compounds might depend on pressure as follows [Dinsdale, 1991]:

$$\Delta_f G_{T,p} = \frac{A \cdot e^{a_0 \cdot T + \frac{a_1 \cdot T^2}{2} + \frac{a_2 \cdot T^3}{3} + \frac{a_3}{T}}}{\left(K_0 + K_1 \cdot T + K_2 \cdot T^2\right) \cdot (n-1)} \times$$
$$\times \left(\left(1 + n \cdot p \cdot \left(K_0 + K_1 \cdot T + K_2 \cdot T^2\right)\right)^{1-\frac{1}{n}} - 1 \right), \quad (87)$$

where A, a_0, a_1, a_2, a_3, K_0, K_1, K_2 and n are model parameters for the particular compound and phase.

For estimation of the Gibbs energies of formation of ions and other species in an aqueous solution several models were proposed to the present time [Dolejs, 2013]. The most widely known is the Helgesson – Kirkham – Flowers model [Haas, Shock, Sassani, 1995; Helgeson, 1969; Helgeson, Kirkham, 1974a; Helgeson, Kirkham, 1974b; Helgeson, Kirkham, 1976; Helgeson, Kirkham, Flowers, 1981; Johnson, Oelkers, Helgeson, 1992b; Shock et al., 1992; Shock et al., 1997a; Shock, Helgeson, 1988; Sverjensky, Shock, Helgeson, 1997; Tanger, 1986; Tanger, Helgeson, 1988]. It is based on the estimations of heat capacities and molar volumes of compounds:

$$\Delta_f G_{T,p} = \Delta_f G_{T_{ref}, p_{ref}} + \int_{T_{ref}}^{T} C_p dT - S_{T_{ref}} \cdot \left(T - T_{ref}\right) -$$
$$-T \cdot \int_{T_{ref}}^{T} \frac{C_p}{T} dT + \int_{p_{ref}}^{p} V dp + \Delta_B G_{T,p} - \Delta_B G_{T_{ref}, p_{ref}}. \quad (88)$$

The heat capacity and the molar volume of system are expressed as:

$$V = a_1 + a_2 \cdot \frac{1}{p + \Psi} + a_3 \cdot \frac{1}{T - \Theta} + a_4 \cdot \frac{1}{(T - \Theta)^2}, \quad (89)$$

$$C_p = c_1 + c_2 \cdot \frac{1}{(T - \Theta)^2}. \quad (90)$$

Here a_1, a_2, a_3, a_4, c_1 and c_2 are model parameters, Ψ = 2600 bar and Θ = 228 K are constants, $\Delta_B G$ is the Gibbs energy of solvation, which is determined by Born equation:

$$\Delta_B G = \omega \cdot \left(\frac{1}{\varepsilon} - 1\right), \quad (91)$$

where ε is the dielectric constant of water and ω is the Born constant for a particular species in a solution. The dependence of the water dielectric constant on temperature and pressure was described by several authors [Johnson, Norton, 1991; Malmberg, Maryott, 1956; Uematsu, Frank, 1980; Wasserman, Wood, Brodhol, 1995].

The Helgesson – Kirkham – Flowers model was, among other usages, included into several commercial engineering software packages, such as *ThermoCalc*® [Andersson et al., 2002] or *FactSage*®. The broadness of its usage might be explained by a very extensive model parameters database [Oelkers et al., 1995; Plyasunov, Shock, 2001; Pokrovskii, Helgeson, 1997; Sassani, Shock, 1990; Sassani, Shock, 1992; Schulte, Shock, 1993; Shock et al., 1997b; Shock, Helgeson, 1989; Shock, Helgeson, 1990; Shock, Helgeson, Sverjensky, 1989; Shock, Koretsky, 1993; Shock, McKinnon, 1993]. However, this model has a significant limitation that the density of water must be higher than 0,35 $^{g}/_{ml}$, therefore, the model gives unsatisfactory predictions in the near-critical region of water, where its density does not exceed 0,18 $^{g}/_{ml}$.

There are some other models that have no such restrictions [Bryzgalin, 1989; Djamali, Cobble, 2009; Majer, Sedlbauer, Wood, 2004; Sedlbauer, O'Connell, Wood, 2000; Wasserman, Wood, Davies, 1995; Zotov, Keppler, 2002]. This is, for instance, a method based on the pressure dependency of water density (ρ_w) and thermal expansion coefficient (α_w), proposed by Anderson [Anderson, 1995]:

$$\Delta_r G_{T,p} = \Delta_r G_{T_{ref},p_{ref}} - \Delta_r S_{T_{ref},p_{ref}} \cdot (T - T_{ref}) + \\ + \frac{\Delta_r C_{p,\,T_{ref},p_{ref}}}{T_{ref} \cdot \left(\frac{\partial \alpha_w}{\partial T}\right)_{T_{ref},p_{ref}}} \cdot \left(\alpha_{w,T_{ref},p_{ref}} \cdot (T - T_{ref}) + \ln \frac{\rho_{w,\,T,p}}{\rho_{w,\,T_{ref},p_{ref}}} \right). \quad (92)$$

This model was revised and developed further by Holland and Powell [Holland, Powell, 1998; Holland, Powell, 2011]:

$$\Delta_f G_{T,\,p} = \Delta_f H_{T_{ref},\,p_{ref}} - T \cdot S_{T_{ref},\,p_{ref}} + p \cdot V_{T_{ref},\,p_{ref}} + b \cdot \left(T_{ref} \cdot T - \frac{T_{ref}^2}{2} - \frac{T^2}{2} \right) + \\ + \frac{C_{p,\,T_{ref},\,p_{ref}}}{T_{ref} \cdot \left(\frac{\partial \alpha_w}{\partial T}\right)_{T_{ref},\,p_{ref}}} \cdot \left(\alpha_{w,T_{ref},\,p_{ref}} \cdot (T - T_{ref}) - \kappa_{w,T_{ref},\,p_{ref}} \cdot p + \frac{T}{T'} \cdot \ln \frac{\rho_{w,T,p}}{\rho_{w,T_{ref},p_{ref}}} \right). \quad (93)$$

Here κ_w is the isobaric compressibility of water and b is the model parameter for certain aqueous species.

The model proposed by Walther determines the equilibrium constant of any isocoulombic chemical reaction through the sum of contributions of both electrostatic and non-electrostatic interactions between the ions in a solution, and expresses it through the dependency of the dielectric constant of water on temperature and pressure [Walther, 1992]:

$$\lg K_{T,p} = \frac{T_{ref}}{T} \cdot \lg K_{T_{ref},p_{ref}} + \\ + \frac{\left|z^{+}_{eff} \cdot z^{-}_{eff}\right| \cdot e^2 \cdot N_A}{4\pi \cdot \varepsilon_o \cdot r_{eff} \cdot R \cdot T \cdot \ln 10} \cdot \left(\frac{1}{\varepsilon_{T,p}} - \frac{1}{\varepsilon_{T_{ref},p_{ref}}} \right) - \sum_i \left(\nu_i \cdot \lg \rho_{T,p} \right), \quad (94)$$

or, in parameterised form:

$$\lg K_{T,p} = a_1 + a_2 \cdot p + \frac{a_3 + a_4 \cdot p}{\varepsilon_{T,p} \cdot T \cdot 10^5}, \quad (95)$$

where a_1, a_2, a_3 and a_4 are the model parameters.

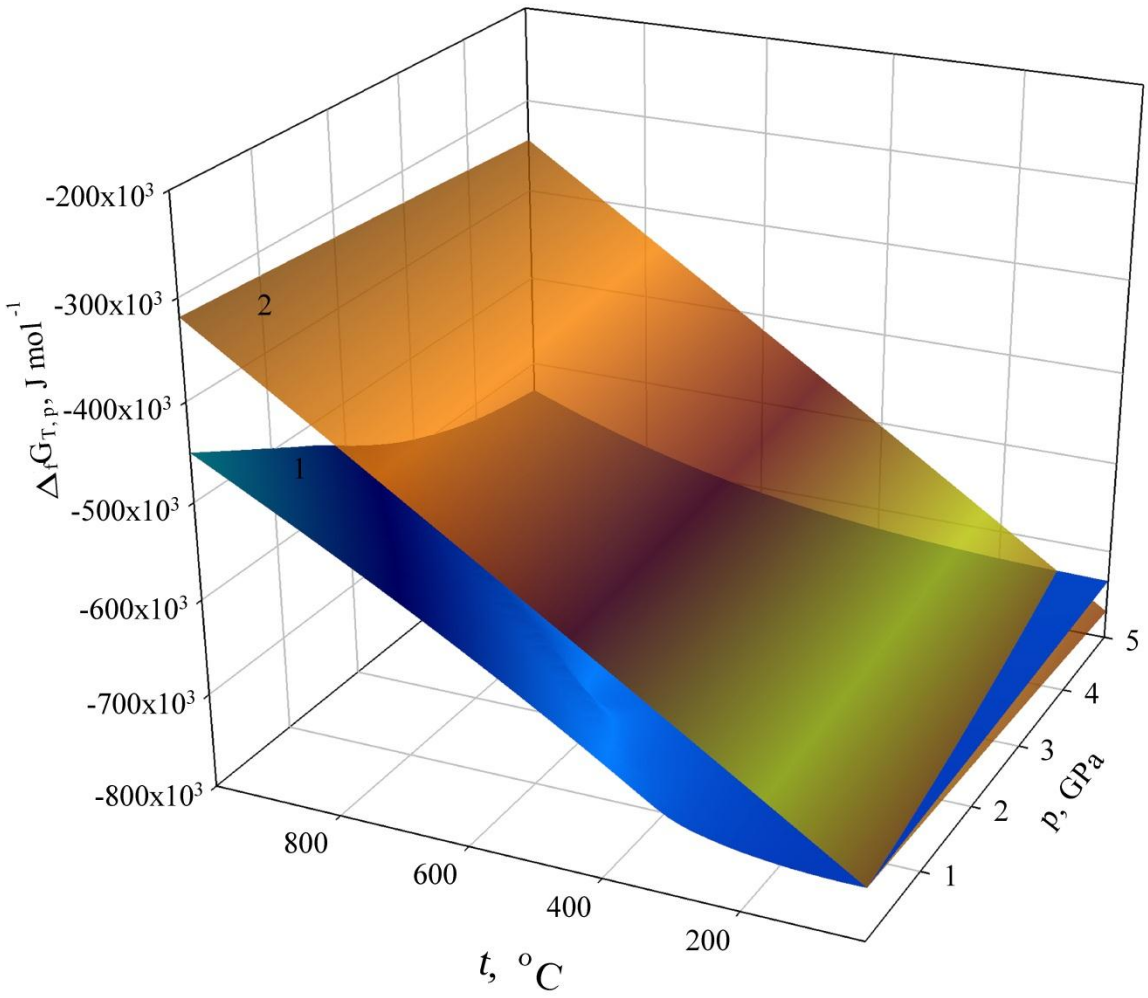

Fig. 13. The dependency of the Gibbs energy of formation of the aqueous sulphate-ion on temperature and pressure predicted by: 1 – the Helgesson – Kirkham – Flowers model; 2 – the Anderson model.

Unfortunately, the Gibbs energies of formation of various ions in an aqueous solution at the different temperatures and pressures predicted by

various models are not consistent with each other. *Exempli gratia*, Figures 13 and 14 demonstrate the temperature and pressure dependencies of the Gibbs energies of formation of the aqueous sulphate- and chloride-ions, respectively, calculated according to the different models.

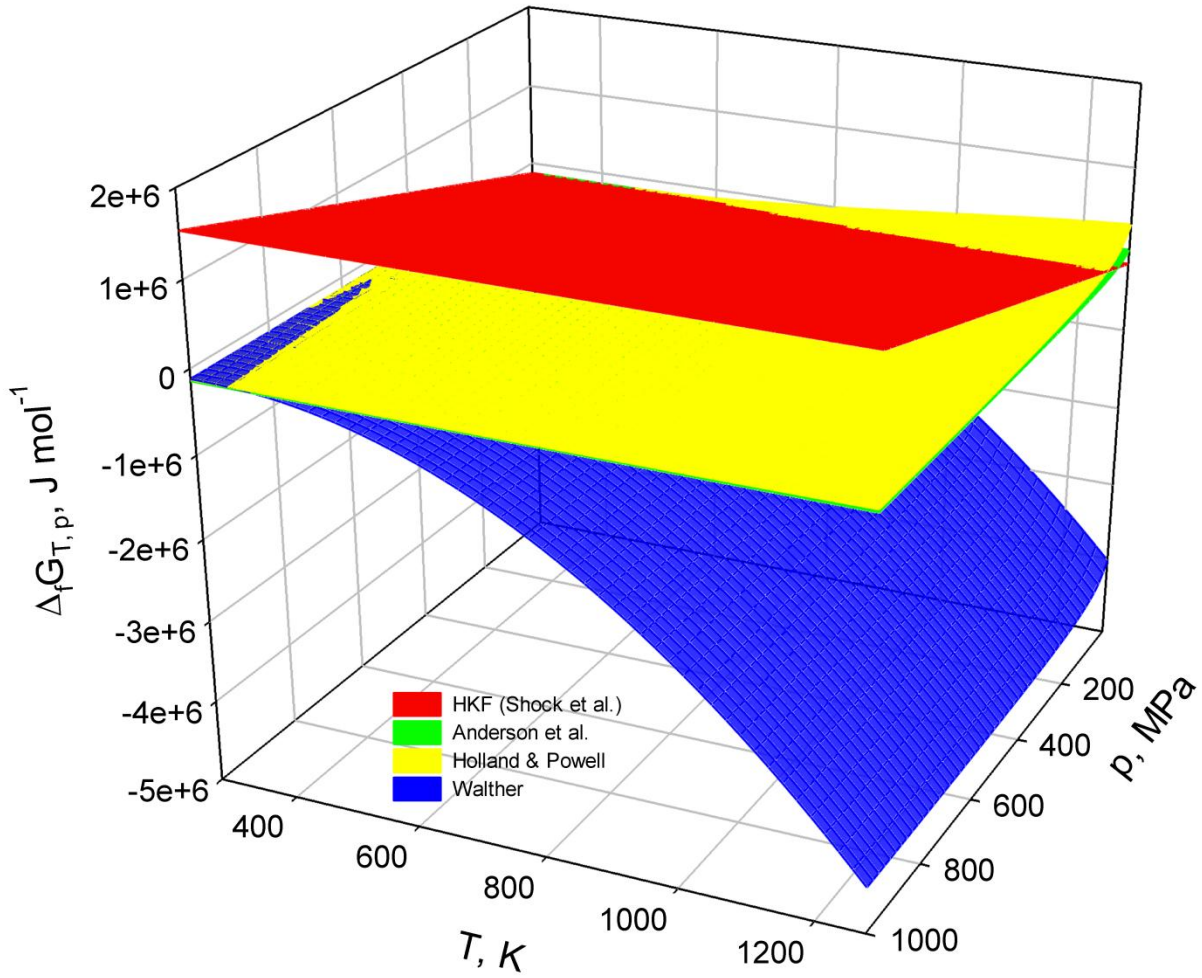

Fig. 14. The dependency of the Gibbs energy of formation of the aqueous chloride-ion on temperature and pressure predicted by: – the Helgesson – Kirkham – Flowers model, – the Anderson model, – the Holland – Powell model, – the Walther model.

Although the predicted values are similar for the small deviations from the standard conditions, the values from various models diverge more and more significantly with the temperature and pressure increase. The question, which model gives the most accurate predictions, is still open for discussion.

Publications to chapter 3

The content of this chapter is partially published in three conference papers. Actually, they resemble the content of Sections 3.4 [Nikolaychuk, Tyurin, 2011a], 3.5 [Nikolaychuk, Tyurin, 2011b] and 3.8 [Николайчук, 2015].

METHOD OF ESTIMATING THE STANDARD GIBBS ENERGIES OF FORMATION OF BINARY COMPOUNDS

Nikolaychuk P.A., Tyurin A.G.

Chelyabinsk State University, Russia, Chelyabinsk,
Brat'ev Kashirinykh st. 129. npa@csu.ru, tag@csu.ru

It was found by I. G. Gorichev [1], that an approximate functional relationship exist between the reduced chemical potential of oxygen atoms in metal oxide and system degree of oxidations $\Delta_f G^o_{298}(Me_{1/x}O) = f(x)$. He assumed such relationship as linear and, basing on this assumption and using Lagrange interpolation formula, derived the equation, which allows estimating the unknown standard Gibbs energy of formation of metal oxide MeO_x according to available data on the thermodynamic formation functions of two other oxides of this metal – MeO_i and MeO_j:

$$\frac{\Delta_f G^o_{298}(MeO_x)}{x} = \frac{\Delta_f G^o_{298}(MeO_i)}{i} - \left(\frac{\Delta_f G^o_{298}(MeO_i)}{i} - \frac{\Delta_f G^o_{298}(MeO_j)}{j}\right) \cdot \frac{i-x}{i-j} \quad (1).$$

A similar relationship is valid not only for oxides, but also for some other binary compounds with polar covalent bond (sulfides, carbides, nitrides, silicides, etc.).

However, attempts to apply this equation to predict the unknown thermodynamic properties of certain compounds in various systems showed, that linear nature of this relationship holds far from always. Therefore, the formula (1) was modified in this study in such a way, that the interpolation can be based on the reliable thermodynamic data on several compounds, assuming the polynomial nature of above-mentioned relationship.

A modified variant of the calculation formula appears as follows:

$$\Delta_f G^o_{298}(M_{a_x} A_{b_x}) = b_x \cdot \sum_{i=1}^{n} \left(\frac{\Delta_f G^o_{298}(M_{a_i} A_{b_i})}{b_i} \cdot \prod_{j \neq i} \frac{a_i \cdot (a_j \cdot b_x - a_x \cdot b_j)}{a_x \cdot (a_j \cdot b_i - a_i \cdot b_j)} \right) \quad (2).$$

Where n – number of Gibbs energies of formation of binary compounds, accepted as a reliable initial data; $M_{a_i} A_{b_i}$ – formulae of these binary compounds (M – metal atom, A – more electronegative element atom, a_i and b_i – indices for the M and A atoms in compound, respectively); $M_{a_x} A_{b_x}$ – formula of the compound, Gibbs energy of formation of which is to be estimated, a_x и b_x – indices for the M and A atoms in it.

While doing calculations by formula (2), as opposed to calculations by formula (1), there is no necessity to convert thermodynamic data according to 1 gram-atom of metal.

The proposed method can be successfully used to estimate the thermodynamic properties of compounds, for which the experimental information is missing.

References

[1] Жук, Н.П. Курс теории коррозии и защиты металлов: учеб. пособие для вузов [Текст]. – 2-е изд., стереотип. (перепеч. с изд. 1976 г.). – М: ООО ТИД "Альянс", 2006. – 472 с.

THE ANALYSIS OF STANDARD GIBBS ENERGIES OF FORMATION OF MeO_2 TYPE OXIDES OF FOURTH PERIOD d-ELEMENTS

Nikolaychuk P.A., Tyurin A.G.

Chelyabinsk State University, Russia, Chelyabinsk,
Brat'ev Kashirinykh st. 129. npa@csu.ru, tag@csu.ru

Almost always, when considering a new task, a problem reveals, that information about thermodynamic properties of necessary substances is incomplete or missing at all. It's appropriate to use the computational methods in order to determine such unknown properties.

Thermodynamic properties of the various compounds of the same type vary periodically with the change of element atomic number [1]. Particularly, it applies to the thermodynamic properties of oxides [2].

The dependence of standard Gibbs energies of formation of MeO_2 type oxides of 4th period d-elements on metals nuclear charge is analyzed. In order to determine the correlative equation between these variables, the attempt is made to use various kinds of functional relationships: $-\Delta_f G^o_{298}(MeO_2) = f(z)$, $-\Delta_f G^o_{298}(MeO_2) = f(\lg z)$, $\lg(-\Delta_f G^o_{298}(MeO_2)) = f(z)$, $\lg(-\Delta_f G^o_{298}(MeO_2)) = f(\lg z)$ and $-\frac{\Delta_f G^o_{298}(MeO_2)}{z} = f(z)$. From all these dependencies only the third one and the fourth one provide a good level of data approximation. The following relations are established, the calculations on which give a convergence between the results:

$$\lg(-\Delta_f G^o_{298}(MeO_2), J/mole) = -0{,}1472 \cdot z + 9{,}2569;\ R^2 = 0{,}9448.$$

$$\lg(-\Delta_f G^o_{298}(MeO_2), J/mole) = -8{,}5173 \cdot \lg z + 17{,}4776;\ R^2 = 0{,}9280$$

The obtained analytical relations can be used to match the reference data and to predict thermodynamic properties of those substances, for which they couldn't be established experimentally (CrO_2, FeO_2, NiO_2, CuO_2, ZnO_2). Thus,

the results of calculations according to above-mentioned equation for iron, chromium and nickel oxides are in good agreement with independent estimates, made by author of paper [3] using methods of I.G. Gorichev, A.F. Kapustinskiy and M. Ch. Karapet'yantz.

References

[1] Киреев В. А. Методы практических расчётов в термодинамике химических реакций. М.: Химия, 1970. С. 520.
[2] Парфёнова С. И., Гаркушин И. К., Медовщикова Л. А. Анализ термодинамических свойств элементов на группы периодической системы // Оксиды. Физико-химические свойства: сб. трудов V Всероссийской науч. Конференции. Екатеринбург, 2000. С. 374 – 377.
[3] Тюрин А. Г. Термодинамика химической и электрохимической устойчивости сплавов: автореф. дисс…. д-ра хим. наук. Челябинск: Изд-во ЧелГУ, 2008. 40 с.

THERMODYNAMICAL ANALYSIS OF MANGANESE SILICIDES CORROSION-ELECTROCHEMICAL BEHAVIOUR

Nikolaychuk P.A., Shalyapina T.I., Tyurin A.G.

Chelyabinsk State University, Russia, Chelyabinsk,
Brat'ev Kashirinykh st. 129, npa@csu.ru, tag@csu.ru

The phase and chemical equilibria in Mn – Si system are considered [1]. There are seven intermetallic phases in it at 25˚C: $Mn_{11}Si_{19}$, MnSi, Mn_5Si_3, Mn_5Si_2, Mn_3Si and two phases of various composition – ν(Mn_9Si_2) and R(Mn_6Si). In addition, formation of the solid solution of silicon in α-manganese with cubic lattice (α-phase) is possible. The excessive Gibbs energy of this solution is described in terms of one-parameter approximation of generalized theory of "regular" solutions [2]. The dependence of model parameter on temperature is as follows: $Q_{12}(Mn-Si) = -219292 + 211{,}95 \cdot T, \, J/mole$. The maximum solid solubility of Si in α-Mn at 25˚C amounts slightly more than 4 atomic percent. The Gibbs energy of phase transition of silicon into cubic lattice is estimated: $\Delta_{tr}G^{o}_{T}(Si(diamond) \rightarrow Si(cubic)) = 92048 - 174{,}66 \cdot T, \, J/mole$. The coordination of thermodynamical properties of manganese silicides is performed. In cases, where published thermodynamical data are missing, the evaluation of Gibbs energies of formation is performed, according to Gorichev's method modified variant.

The equilibrium of Mn – Si system with oxygen is considered. The Mn – Si – O state diagram at 25˚C and air pressure of 1 bar is plotted. This diagram takes into consideration all manganese and silicon oxides, as well as silicates

О МЕТОДАХ РАСЧЁТА ЗАВИСИМОСТИ ЭНЕРГИИ ГИББСА ОБРАЗОВАНИЯ ИОНОВ В ВОДНЫХ СРЕДАХ ОТ ДАВЛЕНИЯ И ТЕМПЕРАТУРЫ

П. А. Николайчук[1,2]

[1]*Челябинский государственный университет*
[2]*Universität zu Köln*

E-Mail: npa@csu.ru. Тел.: +7 (351) 799 – 70 – 69.

Основной термодинамической характеристикой любого электродного процесса

$$a\,\mathrm{A}+b\,\mathrm{B}+m\,\mathrm{H}^{+}+n\,\mathrm{e}^{-} \rightleftharpoons c\,\mathrm{C}+d\,\mathrm{D}$$

является электродный потенциал, являющийся функцией температуры раствора, внешнего давления и термодинамических активностей компонентов – участников электродной реакции в растворе:

$$E = f(T,\ p,\ a_i)\,.$$

Связь электродного потенциала с энергией Гиббса реакции выражается основным уравнением электрохимической термодинамики:

$$E(T,\ p) = -\frac{\Delta_r G(T,p)}{n\cdot F}$$

В свою очередь, энергия Гиббса реакции определяется через энергии Гиббса образования участников реакции и их термодинамические активности

$$\Delta_r G(T,p) = c\Delta_f G_{\mathrm{C}}(T,p) + d\Delta_f G_{\mathrm{D}}(T,p) - a\Delta_f G_{\mathrm{A}}(T,p) - b\Delta_f G_{\mathrm{B}}(T,p) + \frac{a_{\mathrm{C}}^{c}\cdot a_{\mathrm{D}}^{d}}{a_{\mathrm{A}}^{a}\cdot a_{\mathrm{B}}^{b}\cdot a_{\mathrm{H^+}}^{m}}$$

Таким образом, для того, чтобы с точки зрения термодинамики описывать электродные процессы, необходимо знать зависимости энергий Гиббса образования возможных участников реакции от температуры и давления.

Проблема прогнозирования термодинамических свойств веществ и реакций при повышенных давлениях стоит перед исследователями достаточно давно, и первые попытки её решения относятся к 50-м годам прошлого века. В настоящее время различными исследователями предложено множество моделей и подходов [1]. Наиболее широкое распространение получила модель Хельгессона – Киркхама – Флауэрса [2, 3]. Их метод основан на оценке зависимости теплоёмкости и молярного объёма раствора:

$$\Delta_f G_{T,p} = \Delta_f G_{T_{\mathrm{ref}},p_{\mathrm{ref}}} + \int_{T_{\mathrm{ref}}}^{T} C_p dT - S_{T_{\mathrm{ref}}}\cdot\left(T - T_{\mathrm{ref}}\right) - T\cdot\int_{T_{\mathrm{ref}}}^{T}\frac{C_p}{T}dT + \int_{p_{\mathrm{ref}}}^{p} V dp + \Delta_B G_{T,p} - \Delta_B G_{T_{\mathrm{ref}},p_{\mathrm{ref}}}$$

Теплоёмкость и молярный объём системы выражаются следующими параметрами модели

$$V = a_1 + a_2\cdot\frac{1}{p+\Psi} + a_3\cdot\frac{1}{T-\Theta} + a_4\cdot\frac{1}{\left(T-\Theta\right)^2},\ C_p = c_1 + c_2\cdot\frac{1}{\left(T-\Theta\right)^2}$$

Рис. 1. показывает зависимость энергии Гиббса образования иона железа (II) от температуры и давления в рамках этой модели. Модель Хельгессона-Киркхама-Флауэрса широко используется, в том числе в таких коммерческих программных продуктах, как ThermoCalc или FactSage. Широта её применения объясняется наличием огромной базы данных параметров модели [4]. Однако существенным ограничением применения этой модели является то, что она не работает в условиях, когда плотность воды превышает 0,35 г/мл. Поэтому модель даёт неудовлетворительные результаты в области сверхкритических состояний воды, где её плотность не превышает 0,18 г/мл.

Существуют другие модели, позволяющие обойти эту проблему. Это, например, метод, применённый впервые Андерсоном и основанный на зависимости от давления плотности и коэффициента термического расширения растворителя [5]:

$$\Delta_r G_{T,p} = \Delta_r G_{T_{\text{ref}},p_{\text{ref}}} - \Delta_r S_{T_{\text{ref}},p_{\text{ref}}} \cdot (T - T_{\text{ref}}) + \frac{\Delta_r C_{p,\ T_{\text{ref}},p_{\text{ref}}}}{T_{\text{ref}} \cdot \left(\frac{\partial \alpha_w}{\partial T}\right)_{T_{\text{ref}},p_{\text{ref}}}} \cdot \left(\alpha_{w,T_{\text{ref}},p_{\text{ref}}} \cdot (T - T_{\text{ref}}) + \ln \frac{\rho_{w,T,\text{p}}}{\rho_{w,T_{\text{ref}},p_{\text{ref}}}} \right)$$

Или электростатическая модель, определяющая константу равновесия реакций, как сумму вкладов электростатических и неэлектростатических взаимодействий между частицами в растворах и выражающая её через зависимость диэлектрической проницаемости среды от температуры и давления [6]:

$$\lg \mathrm{K}_{T,p} = \frac{T_{\text{ref}}}{T} \cdot \lg K_{T_{\text{ref}},p_{\text{ref}}} + \frac{\left| z^+_{\text{eff}} \cdot z^-_{\text{eff}} \right| \cdot e^2 \cdot N_A}{4\pi \cdot \varepsilon_0 \cdot r_{\text{eff}} \cdot R \cdot T \cdot \ln 10} \cdot \left(\frac{1}{\varepsilon_{T,p}} - \frac{1}{\varepsilon_{T_{\text{ref}},p_{\text{ref}}}} \right) - \sum_i \left(\nu_i \cdot \lg \rho_{T,p} \right)$$

После подстановки в уравнение параметров модели получается зависимость:

$$\lg \mathrm{K}_{T,p} = a_1 + a_2 \cdot p + \frac{a_3 + a_4 \cdot p}{\varepsilon_{T,p} \cdot T \cdot 10^5}$$

Похожий принцип заложен в основу модели Джамали-Коббла [7]:

$$\Delta_r G = \Delta G_{nel} + \Delta_B G + \Delta_{ss} G, \text{ где}$$

$$\Delta_B G = + \frac{e^2 \cdot N_A}{2 r_B} \cdot \left(\frac{1}{\varepsilon_{T,p}} - 1 \right) \text{ и } \Delta_{ss} G = \nu \cdot R \cdot T \cdot \ln \frac{m_0 \cdot \rho \cdot R \cdot T}{1000 \cdot P_0}$$

Ещё два метода оценки, основанные на зависимости плотности растворителя, предложены Сэдлбауэром, О'Коннелом и Вудом [8]:

$$\Delta_r G_{T,p} = R \cdot T \cdot \ln \frac{p}{p_{\text{ref}}} + \int_p^{p_{\text{ref}}} \left(V_{aq} - \frac{R \cdot T}{p} \right) dP - d \cdot R \cdot T \cdot \ln \frac{R \cdot T \cdot \rho_{w,p,T}}{p_{\text{ref}} \cdot M_w} + \Delta_{\text{cor}} G$$

и Холландом и Повеллом [9]::

$$\Delta_f G_{T,p} = \Delta_f H_{T_{\text{ref}},p_{\text{ref}}} - T \cdot S_{T_{\text{ref}},p_{\text{ref}}} + p \cdot V_{T_{\text{ref}},p_{\text{ref}}} + b \cdot \left(T_{\text{ref}} \cdot T - \frac{T_{\text{ref}}^2}{2} - \frac{T^2}{2} \right) +$$

$$+ \frac{C_{p,\ T_{\text{ref}},p_{\text{ref}}}}{T_{\text{ref}} \cdot \left(\frac{\partial \alpha_w}{\partial T}\right)_{T_{\text{ref}},p_{\text{ref}}}} \cdot \left(\alpha_{w,T_{\text{ref}},p_{\text{ref}}} \cdot (T - T_{\text{ref}}) - \kappa_{T_{\text{ref}},p_{\text{ref}}} \cdot p + \frac{T}{T'} \cdot \ln \frac{\rho_{w,T,\text{p}}}{\rho_{w,T_{\text{ref}},p_{\text{ref}}}} \right)$$

Результаты предсказания, рассчитанные различными методами, порой отличаются очень сильно. Например, на **рис. 2** показан результат сравнения оценки энергии образования сульфат-ионов от давления и температуры моделями Хельгессона – Киркхама – Флауэрса [2, 3] и Андерсона [5]. Целью работы является сравнение предсказательной способности указанных выше методов оценки.

СПИСОК ЛИТЕРАТУРЫ

1. *Dolejš D.* // Rev. Mineral. Geochemistry. 2013. Vol. 76. No. 1. P. 35–79.
2. *Johnson J.W. et al.* // Comput. Geosci. 1992. Vol. 18. No. 7. P. 899–947.
3. *Shock E.L. et al.* // Geochim. Cosmochim. Acta. 1988. Vol. 52. No. 8. P. 2009–2036.
4. *Oelkers E.H. et al.* // J. Phys. Chem. Ref. Data. 1995. Vol. 24. No. 4. P. 1401–1560.
5. *Anderson G. M.* // Geochim. Cosmochim. Acta. 1995. Vol. 59. No. 11. P. 2155–2161.
6. *Walther J. V.* // J. Metamorph. Geol. 1995. Vol. 10. No. 6. P. 789–797.
7. *Djamali E., Cobble J. W.* // J. Phys. Chem. B. 2009. Vol. 113. No. 8. P. 2398–2403.
8. *Sedlbauer J. et al.* // Chem. Geol. 2000. Vol. 163. No. 1–4. P. 43–63.
9. *Holland T. J. B. et al.* // J. Metamorph. Geol. 2011. Vol. 29. No. 3. P. 333–383.

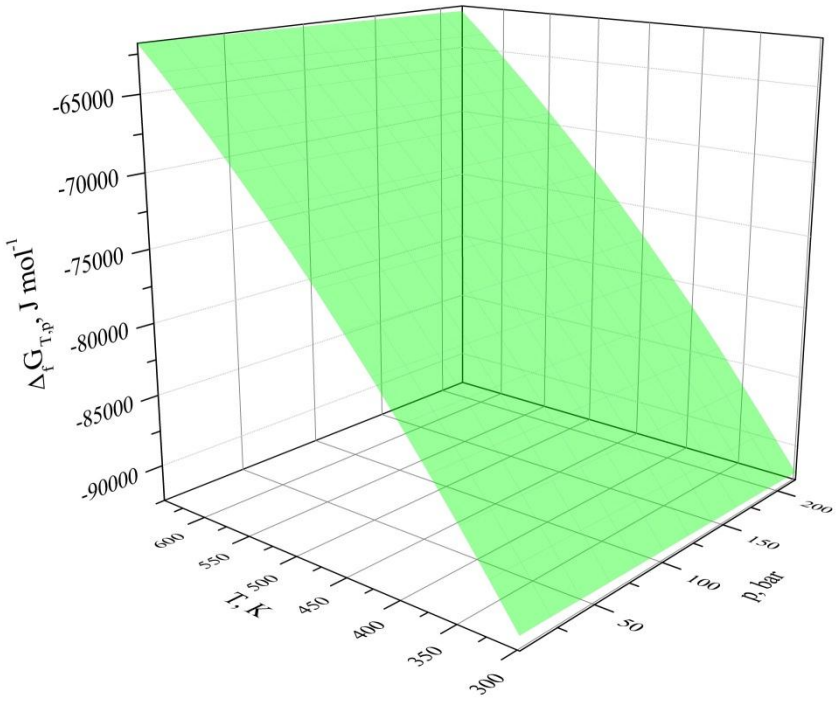

Рис. 1. Зависимость энергии Гиббса образования ионов Fe^{2+} от давления и температуры в докритической области воды в соответствии с моделью Хельгессона – Киркхама – Флауэрса [2, 3].

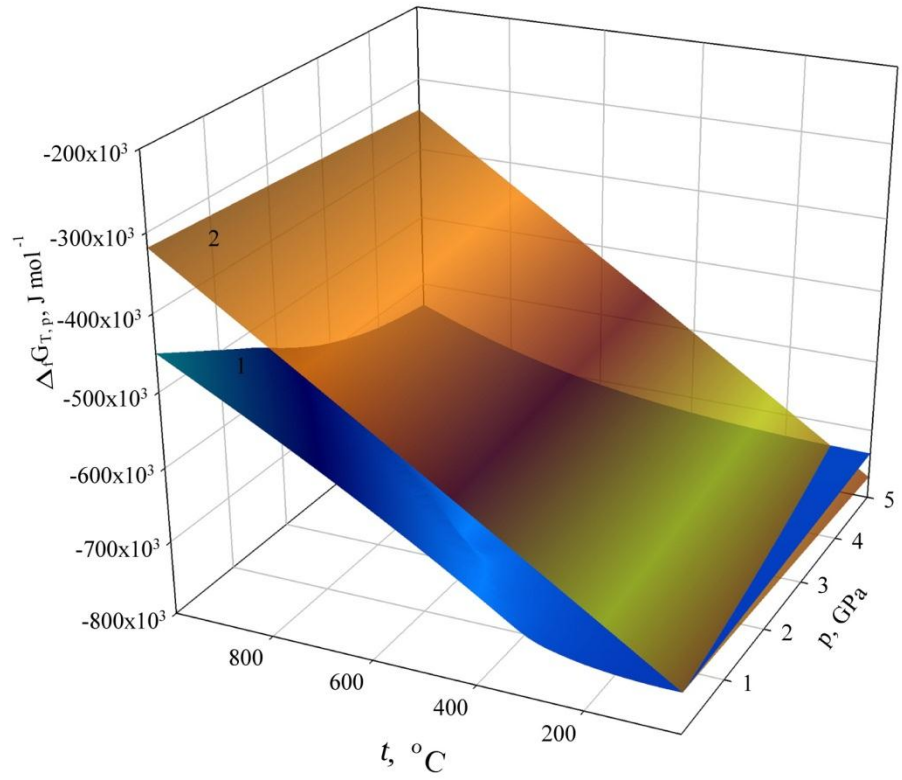

Рис. 2. Зависимость энергии Гиббса образования ионов SO_4^{2-} от давления и температуры в до- и сверхкритических областях воды в соответствии с моделями: (1) Хельгессона – Киркхама – Флауэрса [2, 3] и (2) Андерсона [5].

4. Sc – Si system
4.1. Scandium silicides

The phase diagram of the Sc – Si system is presented in Figure 15.

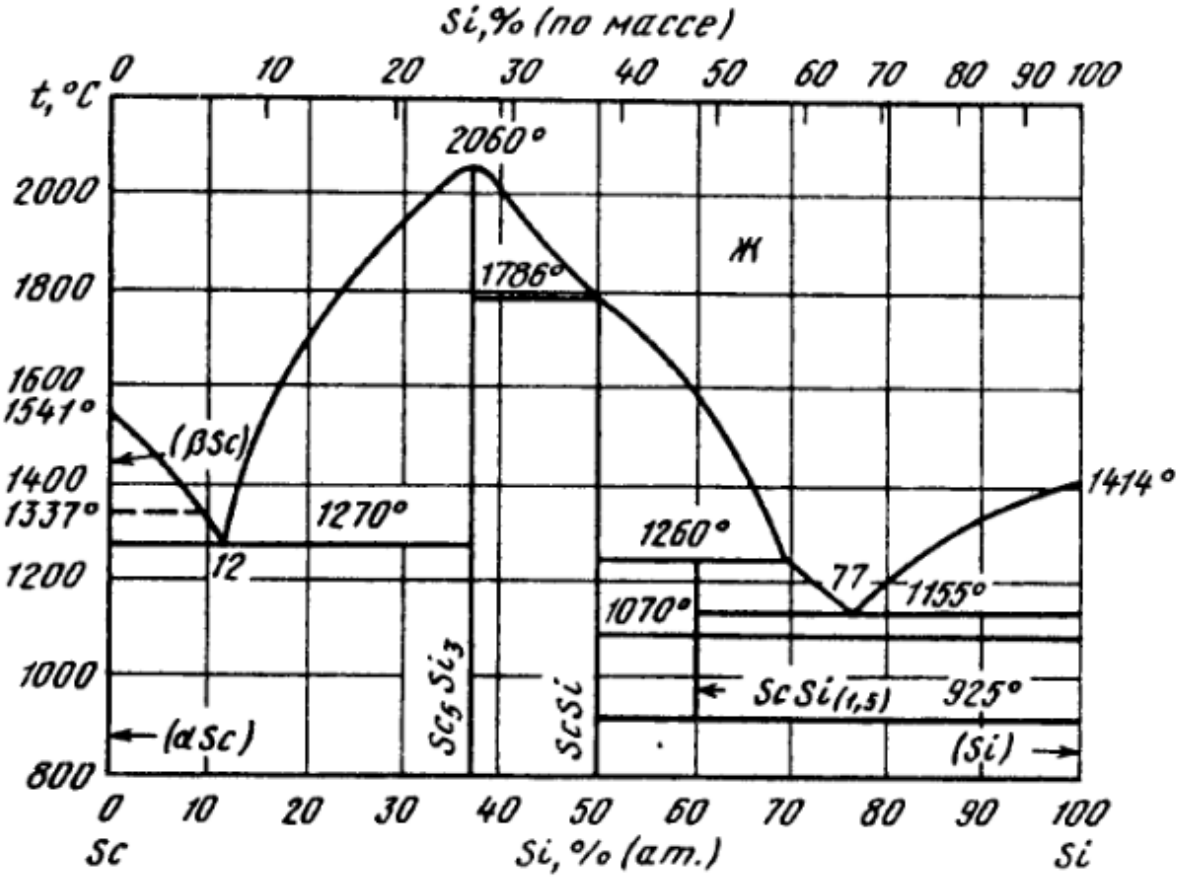

Fig. 15. The phase diagram of the Sc – Si system [Диаграммы состояния двойных металлических систем: справочник, 2001].

According to it, two scandium silicides – Sc_5Si_3 and ScSi – exist is system at standard conditions. The third silicide, Sc_2Si_3, exists only at elevated temperatures. All silicides are stoichiometric compounds without any noticeable homogeneity ranges. There are no data on solid solubility of Si in (hcp-Sc) and Sc in (diamond-Si); it is vanishingly small and the components can be treated as insoluble in each other. The standard Gibbs energies of formation of scandium silicides were taken from [Lukashenko, Polotskaya, Sidorko, 1992] and are presented in Table 7.

Table 7. The standard Gibbs energies of formation of scandium silicides.

Compound	$-\Delta_f G^\circ_{298,15}$, J·mol^{-1}
Sc_5Si_3	801 700
ScSi	225 800

4.2. Equilibira in Sc – Si – O system

Scandium can form only one oxide, Sc_2O_3. Its standard Gibbs energy of formation was obtained from [Horovitz et al., 1975] and is presented in the attached publication. Some scandium silicates exist at elevated temperatures [Hong et al., 2009] but only thorvertite ($Sc_2Si_2O_7$) remains stable at 298,15 K. The standard Gibbs energy of formation of this compound was estimated according to ΔO^{2-} method and it equals $\Delta_f G^o_{298,15,\,Sc_2Si_2O_7} = -3\,498\,500\ J \cdot mol^{-1}$. It seems that chemical affinity of scandium to oxygen is greater, than that of silicon, and it oxidizes more easily. The oxidation of Sc – Si system in air environments ends with formation of Sc_2O_3 and $Sc_2Si_2O_7$ in scandium-rich region and of $Sc_2Si_2O_7$ and SiO_2 in silicon-rich region. The state diagram of the Sc – Si – O system is presented in Figure 16. The equilibria are listed in Table 8.

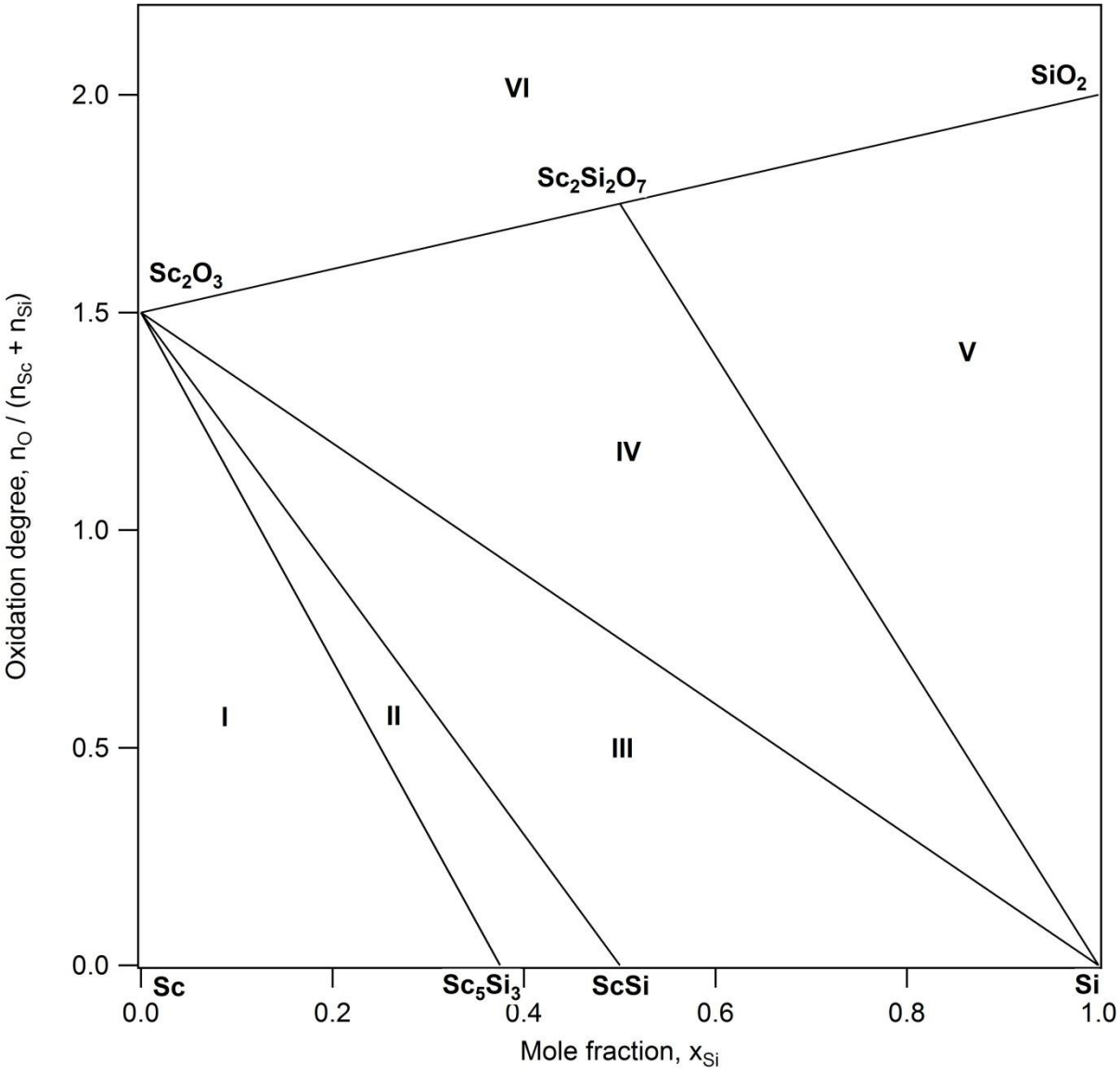

Fig. 16. The state diagram of the Sc – Si – O system.

Table 8. List of equilibria in the Sc – Si – O ternary system in accordance with the state diagram presented in Figure 16.

No of domain in Fig. 16	Equilibrium phases	Reaction equation	P_{O_2}, bar
I	$Sc\,(hcp) - Sc_5Si_3 - Sc_2O_3$	$4Sc + 3O_2\ (g) \rightleftharpoons 2Sc_2O_3$	$2{,}4 \cdot 10^{-213}$
II	$Sc_5Si_3 - ScSi - Sc_2O_3$	$2Sc_5Si_3 + 3O_2\ (g) \rightleftharpoons 6ScSi + 2Sc_2O_3$	$8{,}2 \cdot 10^{-199}$
III	$ScSi - Si\ (dia) - Sc_2O_3$	$4ScSi + 3O_2\ (g) \rightleftharpoons 4Si + 2Sc_2O_3$	$1{,}4 \cdot 10^{-160}$
IV	$Si\ (dia) - Sc_2O_3 - Sc_2Si_2O_7$	$Sc_2O_3 + 2Si + 2O_2\ (g) \rightleftharpoons Sc_2Si_2O_7$	$7{,}1 \cdot 10^{-148}$
V	$Si\ (dia) - Sc_2Si_2O_7 - SiO_2$	$Si + O_2\ (g) \rightleftharpoons SiO_2$	$7{,}7 \cdot 10^{-142}$
VI	$Sc_2O_3 - Sc_2Si_2O_7 - O_2\ (g)$ or $Sc_2Si_2O_7 - SiO_2 - O_2\ (g)$	–	–

4.3. Potential – pH diagram of Sc – H_2O system

In aqueous acidic environments scandium exists in form of the cation Sc^{3+} (aq), which with increase of the basicity of the solution can be hydrolysed to $ScOH^{2+}$ (aq), $Sc(OH)_2^+$(aq) or $Sc(OH)_4^-$(aq) [Baes Jr., Mesmer, 1976; Schweitzer, Pesterfield, 2010]. The polynuclear complexes $Sc_2(OH)_2^{4+}$ and $Sc_3(OH)_5^{4+}$ could also be formed.

However, the calculations show that for the environments, in which the activities exceed 10^{-7} M and which are of the most importance for applied chemistry, only an unhydrolysed cation Sc^{3+} is thermodynamically stable. The details are presented in the attached publication.

The potential – pH diagram also predicts that both the aqueous scandium and its oxide would oxidise directly to scandium hydride, ScH_2 (s), rather than to elemental scandium. The potential – pH diagram for scandium at 25 °C, air pressure of 1 bar and the activities of scandium species in a solution of 1 mol l^{-1} is presented in Figure 17 without (*a*) and with (*b*) consideration of scandium hydride.

a)

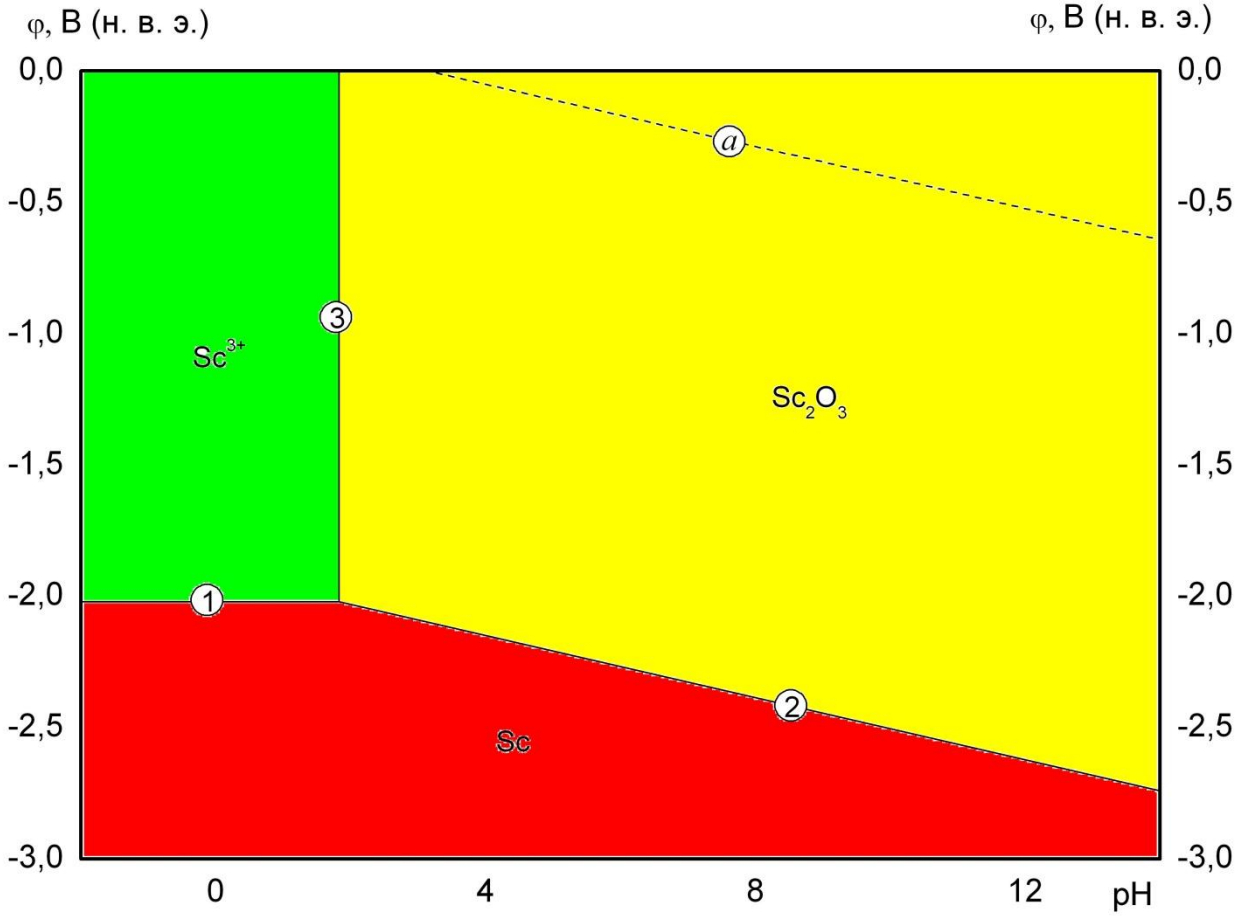

b)

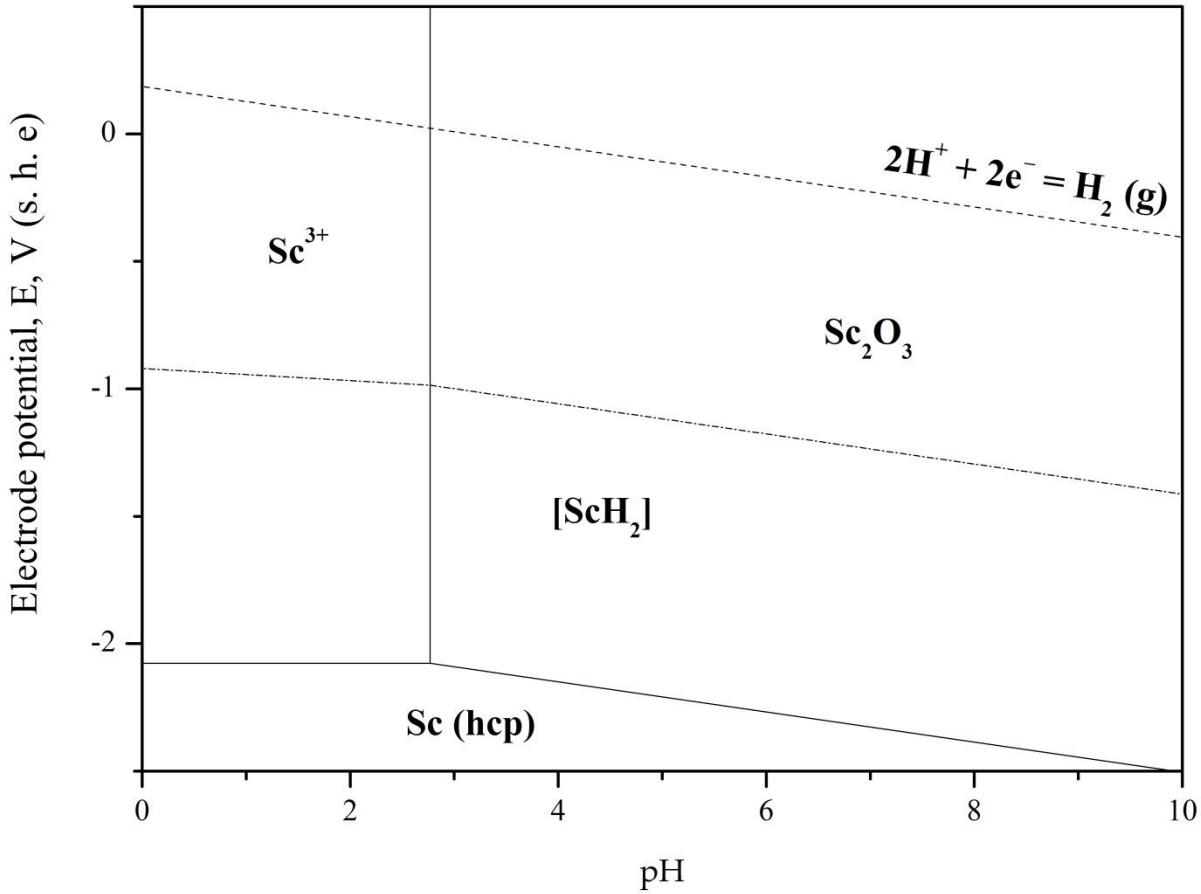

Fig. 17. The potential – pH diagram of the Sc – H_2O system at 25 °C, air pressure of 1 bar and the activities of scandium species in a solution of 1 M without (*a*) and with (*b*) consideration of scandium hydride.

4.4. Potential – pH diagram of Si – H_2O system

Silicon might form three different uncharged species in an aqueous media, namely, silicon dioxide SiO_2 (aq), metasilicic acid H_2SiO_3 (aq), and orthosilicic acid H_4SiO_4 (aq) [Smith, Martell, 1976]. All three species coexist in a solution simultaneously in the ratio 1 : 2 600 000 : 2 900 000, but the latter one slightly predominates.

Several both mono- and polynuclear silicate-ions might be formed. The calculations show that the ions $H_3SiO_4^-$ (aq) and $H_2SiO_4^{2-}$ (aq) are the most thermodynamically stable. Therefore, only orthosilicic acid and its ions will be considered in all consequent calculations. The detailed analysis and the resulting potential – pH diagrams for Si – H_2O system are presented in the attached publication.

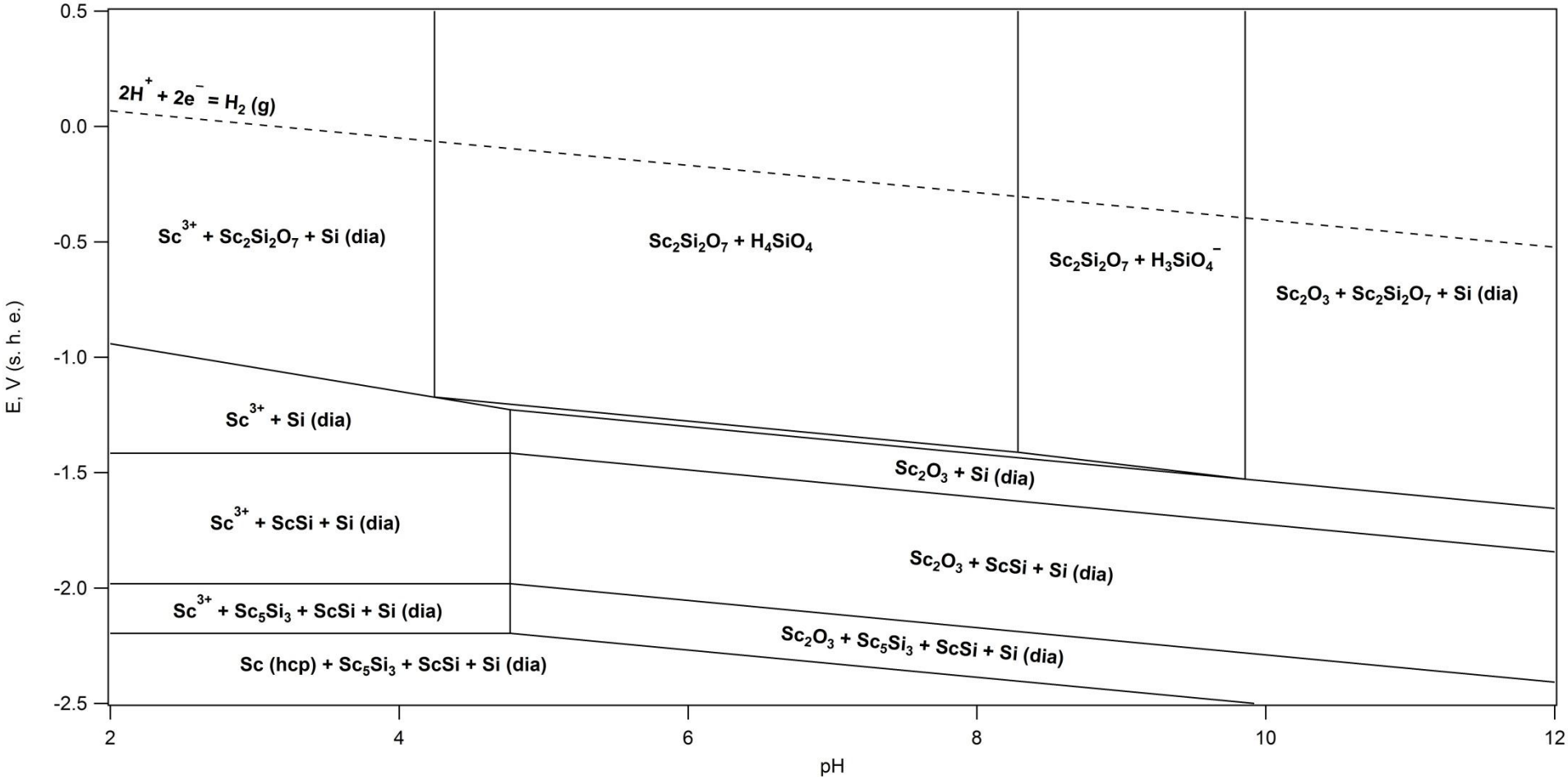

Fig. 18. The potential – pH diagram of the Sc – Si – H_2O system at 25 °C, air pressure of 1 bar and the activities of species in a solution of 1 M.

4.5. Potential – pH diagram of Sc – Si – H_2O system

The potential – pH diagram of Sc – Si – H_2O system is plotted at temperature of 25 °C, air pressure of 1 bar and activities of ions in solutions, equal to 1 mol l^{-1} and presented in Figure 18.

Thermodynamic stability of Sc – Si system in air and water environments is determined by the composition of the system. In very acidic environments scandium dissolves forming a Sc^{3+} (aq) cation, and silicon forms a surface layer from (depending on the silicon content in the system) either scandium silicate $Sc_2Si_2O_7$ or silicon dioxide. In neutral and alkaline environments the composition of the protective layer on the surface depends on silicon content. It might consist from Sc_2O_3 + $Sc_2Si_2O_7$ if the silicon content is low; or from $Sc_2Si_2O_7$ + SiO_2 if the silicon content is high. In strongly alkaline environments silicon forms the soluble orthosilicates, and the protective layer on the surface consists from scandium sesquioxide only.

Publications to chapter 4

The content of this chaptes was published in two papers. The first paper [Nikolaychuk, 2014a] presents the potential – pH diagram for silicon. The preprint of this paper is presented with the permisson from *Springer*. The second paper [Nikolaychuk, 2016a] presents the potential – pH diagram for scandium. The preprint of this paper is presented with the permission from *Belgorodskij gosudarstvennyj nacional'nyj issledovatel'skij universitet*.

The Revised Pourbaix Diagram for Silicon

Pavel Anatolyevich Nikolaychuk

Chelyabinsk State University, Brat'ev Kashirinykh Street, 129, Chelyabinsk, Russian Federation, E–mail: npa@csu.ru

Abstract:

Thermodynamic properties of silicon species in aqueous solution are collected. The chemical and electrochemical equilibria between various forms of Si(IV) are considered. Basic chemical and electrochemical equilibria for silicon are calculated. The potential – pH diagram for Si – H_2O system is revised.

Keywords:

Silicic acids, silicate ions, chemical and electrochemical equilibria, Pourbaix diagram.

1. Introduction.

A Pourbaix diagram, also known as a potential – pH diagram, is a graphic representation of equilibrium potential with respect to the standard hydrogen electrode (vertical axis) versus pH (horizontal axis) relations corresponding to the various equilibria between the different compounds of a given element under standard thermodynamic conditions (usually at 298 K, air pressure of 1 bar and fixed concentrations of ions in solution). Pourbaix diagrams have proved to be very useful in corrosion as well as in many other fields, such as industrial electrolysis, plating, electrowinning and electrorefining of metals, primary and secondary electric cells, water treatment and hydrometallurgy [1]. Pourbaix diagram for silicon can be applied in major variety of fields as electrochemical modeling of formation of porous silicon [2], silicon chemical polishing [3], electroluminescence [4], measuring of silicon oxide thickness [5]. Moreover, the knowledge of chemical and electrochemical equilibria in Si – H_2O system is necessary when plotting Pourbaix diagrams for complex materials containing silicon like metals silicides [6], siliceous brasses [7], nuclear waste glasses [8] or refractory castables [9].

However, despite almost five decades past since Pourbaix diagrams for silicon was firstly introduced [10], there is still no single opinion about the form of the diagram and compounds present on it. Different researchers consider different silicon species to be thermodynamically stable in water solution. According to [10], the only stable uncharged form of Si (IV) is SiO_2 (aq) and with increase of pH it transforms to $HSiO_3^-$ and then to SiO_3^{2-}. The diagram presented in study [11] was plotted without

considering ionic species, but it was stated that the equilibrium uncharged form depends on silicon concentration in solution; it is SiO_2 if $C_{[Si]} = 10^{-3}$ M and H_4SiO_4 if $C_{[Si]} = 10^{-6}$ M. There are many thermodynamic databases containing potential – pH diagrams for pure elements [12 – 16] and they also propose different forms of existence of Si(IV) in solution. The SUPCRT database [12] considers SiO_2 as uncharged compound but rejects the existence of SiO_3^{2-}, proposing only the transformation $SiO_2(aq)|HSiO_3^-$. The GWB database [13] states that there are ions $H_3SiO_4^-$and $H_2SiO_4^{2-}$instead of $HSiO_3^-$and $SiO_3^{2-}$and proposes the sequence of equilibria $SiO_2(aq)|H_3SiO_4^-, H_3SiO_4^-|H_2SiO_4^{2-}$. The databases JNC–TDB [14] and ZZ–HATCHES [15] use H_4SiO_4 (aq) instead of SiO_2 (aq) as stable uncharged form of Si (IV) and propose the equilibria $H_4SiO_4(aq)|H_3SiO_4^-, H_3SiO_4^-|H_2SiO_4^{2-}$. And finally the FACTSAGE database [16] states that the only stable ionic specie in Si – H_2O system is $H_7SiO_6^-$and propose the equilibrium $H_4SiO_4(aq)|H_7SiO_6^-$. Unfortunately, information presented in databases [12 – 16] is available only in semi-quantitative form without giving analytical expressions for lines on the diagrams and without references to data used in calculations. This makes it not possible to verify the relevance of these diagrams. In addition, silicon hydrides SiH_4 and Si_2H_6 are present on Pourbaix diagrams provided in [10, 15, 16] but not present on diagrams from another sources.

As can be seen, there is no convergence between the results provided in different sources. This study makes attempt to bring the available points of view on Pourbaix diagram for silicon together. The aim of this study is to collect thermodynamic information about various silicon aqueous species, determine which of them are the most thermodynamically stable, calculate characteristics of chemical and electrochemical equilibria in Si – H_2O system and revise potential – pH diagram for silicon.

2. Thermodynamic properties of silicon species.

Silicon in aqueous media can form a variety of polysilicic acids with general formula $[SiO_x(OH)_{4-2x}]_n$[17 – 19]. Only few of them are obtained in form of pure substances: metasilicic acid (H_2SiO_3), orthosilicic acid (H_4SiO_4), pyrosilicic acid ($H_6Si_2O_7$), disilicic acid ($H_2Si_2O_5$) and other are present as mixtures. Consequently, a variety of silicate ions can be formed in solution.

The values of standard Gibbs energies of formation for silicon species are collected from various sources [20 – 27] and summarized in Table 1. If more than one value is present for any species, the values, used in further calculations, are additionally marked. In addition, data on other thermodynamic properties in aqueous solutions were used to verify these standard Gibbs energies of formation.

For the reaction on silicon electrode$SiO_2(aq) + 4H^+ + 4e^- = Si(diamond) + 2H_2O(liq)$the standard equilibrium potential is $E^o_{298}(s.h.e.) = -0.857V$[28 – 30] which gives the value of $\Delta_f G^o_{298}(SiO_2(aq)) = -805100 Jmol^{-1}$that substantially (by

5%) differs from values presented in Table 1 for $\Delta_f G^o_{298}(SiO_2(s))$.

For the reaction $SiO_3^{2-} + 3H_2O(liq) + 4e^- = Si(diamond) + 6OH^-$the standard equilibrium potential is $E^o_{298}(s.h.e.) = -1.697V$[28 – 30] which confirms the value of $\Delta_f G^o_{298}(SiO_3^{2-}) = -887000 Jmol^{-1}$from Table 1.

Table 1. The standard Gibbs energies of formation for silicon species.

Compound	Reference state	$\Delta_f G^o_{298}$, kJmol^{-1}	Reference
SiO_2	s, am	–850.733	[22]
	s, am	–844.174	[23]
	s, am	–850.70	[24]
	aq	–805.1[c]	[29][a]
H_4SiO_4	s	–1305.094	[20]
	s	–1309.181	[21]
	s	–1333.024	[22]
	s	–1330.893	[23]
	s	–1332.90	[24]
	aq	–1316.495[c]	[25]
$H_2Si_2O_5$	s	–1939.543	[23]
	s	–1943.40	[24]
	s	–1943.059	[25]
$H_6Si_2O_7$	s	–2426.39	[23]
	s	–2425.70	[24]
	s	–2425.974	[25]
H_2SiO_3	s	–1092.087	[23]
	aq	–1079.40[c]	[24]
	aq	–1079.015	[25]
H_8SiO_6	s	–1790.90	[24]
H_2O	liq	–237.245	[27]
	liq	–237.14[c]	[24]
OH^-	aq	–230.03	[24]
$HSiO_3^-$	aq	–955.46	[26]
SiO_3^{2-}	aq	–887.00	[26]
$H_3SiO_4^-$	aq	–1223.40[c]	[26]
	aq	–1223.32	[31][b]
$H_2SiO_4^{2-}$	aq	–1152.70	[26]
	aq	–1148.65[c]	[31][b]
$H_4Si_4O_{12}^{4-}$	aq	–3969.80	[26]
$H_6Si_4O_{12}^{2-}$	aq	–4079.80	[26]
$H_4Si_2O_7^{2-}$	aq	–2211.20	[26]

$H_7SiO_6^-$	aq	–1734.50[c]	[24]
	aq	–1409.430[c]	[25]
SiH_4	g	56.90	[24]
	g	57.182	[27]
	g	56.795	[25]
	g	56.902	[22]
Si_2H_6	g	127.30	[24]
	g	126.05	[27]
	g	127.085	[25]
	s	126.156[c]	
	g	127.193	[22]

[a] Calculated from standard electrode potential of silicon electrode

[b] Calculated from equilibrium constant of reaction $H_2SiO_4^{2-} + H^+ = H_3SiO_4^-$

[c] Value, used in Pourbaix diagram calculation

The equilibrium constant for reaction $H_3SiO_4^- + H^+ = SiO_2(aq) + 2H_2O(liq)$equals $10^{-9.82}$ [31]. Using the previously calculated value of $\Delta_f G^o_{298}(SiO_2(aq))$it gives $\Delta_f G^o_{298}(H_3SiO_4^-) = -1223320 Jmol^{-1}$which is well compatible with value from Table 1. For the reaction $H_2SiO_4^{2-} + H^+ = H_3SiO_4^-$equilibrium constant equals $10^{-13.10}$ [31] and it leads to the value of $\Delta_f G^o_{298}(H_2SiO_4^{2-}) = -1148650 Jmol^{-1}$which slightly deviates from value presented in Table 1.

As can be seen, the differences between standard Gibbs energies of formation of solid and aqueous forms of SiO_2, H_2SiO_3 and H_4SiO_4 are substantial. Therefore, other silicic acids were excluded from further consideration, because they only have data referred to solid state and using these data to describe their properties in aqueous state leads to serious uncertainties.

3. Equilibria, concerning silicic acids.

The activity coefficients of all aqueous species were set equal to unity in all calculations, therefore all equations with activity terms were rewritten using concentration terms.

The following system of equilibria between uncharged silicon aqueous species was considered:

$$\begin{cases} SiO_2(aq) + H_2O(liq) = H_2SiO_3(aq), pK_1 = -6.43, \\ SiO_2(aq) + 2H_2O(liq) = H_4SiO_4(aq), pK_2 = -6.47 \end{cases} \quad (1).$$

If equilibrium concentrations of species are denoted as C_{SiO_2}, $C_{H_2SiO_3}$ and $C_{H_4SiO_4}$respectively and $C_{[Si]}$ is total concentration of all these forms in solution then the following system can be derived:

$$\begin{cases} \frac{C_{H_2SiO_3}}{C_{SiO_2}} = 10^{6.43}, \\ \frac{C_{H_4SiO_4}}{C_{SiO_2}} = 10^{6.47}, \\ C_{SiO_2} + C_{H_2SiO_3} + C_{H_4SiO_4} = C_{[Si]} \end{cases} \quad (2).$$

Solving this system leads to the following dependencies:

$$\begin{cases} C_{H_4SiO_4} = \frac{2951209}{5581477} \cdot C_{[Si]}, \\ C_{H_2SiO_3} = \frac{2630267}{5581477} \cdot C_{[Si]}, \\ C_{SiO_2} = \frac{1}{5581477} \cdot C_{[Si]} \end{cases} \quad (3).$$

All three forms exist in equilibrium and can participate in chemical and electrochemical reactions. The Gibbs energies, equilibrium constants and equilibrium potentials of these reactions will be the same if estimated equilibrium concentrations from equation (3) are used in calculations.

As the example, the following reactions are considered:

$$SiO_2(aq) + 4H^+ + 4e^- = Si(diamond) + 2H_2O(liq),$$
$$E = -0.857 - 0.0591 \cdot pH + 0.0148 \cdot \log C_{SiO_2(aq)} \quad (4),$$

$$H_2SiO_3(aq) + 4H^+ + 4e^- = Si(diamond) + 3H_2O(liq),$$
$$E = -0.952 - 0.0591 \cdot pH + 0.0148 \cdot \log C_{H_2SiO_3(aq)} \quad (5),$$

$$H_4SiO_4(aq) + 4H^+ + 4e^- = Si(diamond) + 4H_2O(liq),$$
$$E = -0.951 - 0.0591 \cdot pH + 0.0148 \cdot \log C_{H_4SiO_4(aq)} \quad (6).$$

If $C_{[Si]}$ is assumed to be equal to unity and corresponding equilibrium concentrations of silicon species from equation (3) are substituted into equations (4) – (6), the equilibrium potentials become equal to each other, $E = -0.956 - 0.0591 \cdot pH$. This can be applied to other reactions involving aqueous uncharged silicon species. By means of convention, only one of these three species is considered in further calculations.

It was reported by Treguer et al. [32] that in natural oceanic waters silicon exist primarily in form of orthosilicic acid. Oceanic water has the values of pH and equilibrium potential where silicate ions are not formed. Therefore, only reactions with this form are considered in further calculations.

4. Equilibria, concerning silicon hydrides.

The reactions of possible electrochemical reduction of silicon and orthosilicic acid to silicon hydrides were considered:

$$Si(diamond) + 4H^+ + 4e^- = SiH_4(g),$$
$$E = -0.147 - 0.0591 \cdot pH - 0.0148 \cdot \log p_{SiH_4} \quad (7),$$

$$H_4SiO_4(aq) + 8H^+ + 8e^- = SiH_4(g) + 4H_2O(liq),$$
$$E = -0.550 - 0.0591 \cdot pH - 0.0074 \cdot \log\frac{p_{SiH_4}}{C_{H_4SiO_4(aq)}} \quad (8),$$

The domain of stability of Si (diamond) on Pourbaix diagram exists if line of reaction (7) is located below line of reaction (6) and line of reaction (8) is located between the lines of reactions (6) and (7). It appears if the inequality $E_{(6)}>E_{(8)}>E_{(7)}$ is obeyed. Solving it leads to condition of $\log p_{SiH_4} > 54.5$. If this condition fails then there is no domain of stability of silicon itself because H_4SiO_4 would reduce directly to silane as Ti_2O_3 reduces directly to TiH_2 in the Pourbaix diagram for titanium [33]. By analogy, the following equations with disilane can be written:

$$2Si(diamond) + 6H^+ + 6e^- = Si_2H_6(g),$$
$$E = -0.220 - 0.0591 \cdot pH - 0.0099 \cdot \log p_{Si_2H_6} \quad (9),$$

$$2H_4SiO_4(aq) + 14H^+ + 14e^- = Si_2H_6(g) + 8H_2O,$$
$$E = -0.639 - 0.0591 \cdot pH - 0.0042 \cdot \log\frac{p_{Si_2H_6}}{C^2_{H_4SiO_4(aq)}} \quad (10).$$

Again, it can be shown solving the inequality $E_{(6)}>E_{(10)}>E_{(9)}$ that if $\log p_{Si_2H_6} < 74.7$there would be no domain of silicon stability.

There are no evidences in literature that gaseous silicon hydrides can be obtained electrochemically from water solutions of silicon species. Thermodynamic predictions are not proven experimentally. Therefore, gaseous silicon hydrides were simply excluded from consideration. However, according to [15, 16] solid Si_2H_6 is present on potential – pH diagrams for silicon and corresponding equilibria related to it were not rejected.

5. Equilibria, concerning silicate ions.

The equilibria between aqueous H_4SiO_4 and various silicate ions were considered. The corresponding equations are presented in Table 2.

Table 2. Basic chemical and electrochemical equilibria in Si – H_2O system at 298 K and air pressure of 1 bar.

No. of line at Figures 1 – 3	Electrode reaction	Equilibrium potential (s. h. e.) or solution pH
a	$2H^+ + 2e^- = H_2(g), P_{H_2} = 0.21bar$	$E = 0.186 - 0.0591 \cdot pH$
1	$H_2SiO_4^{2-} + 2H^+ = H_4SiO_4(aq)$	$pH = 14.71 + 0.5 \cdot \log\frac{C_{H_2SiO_4^{2-}}}{C_{H_4SiO_4(aq)}}$
2	$H_3SiO_4^- + H^+ = H_4SiO_4(aq)$	$pH = 16.31 + \log\frac{C_{H_3SiO_4^-}}{C_{H_4SiO_4(aq)}}$

3	$H_2SiO_4^{2-} + H^+ = H_3SiO_4^-$	$pH = 13.10 + \log\frac{C_{H_2SiO_4^{2-}}}{C_{H_3SiO_4^-}}$
4	$SiO_3^{2-} + H_2O(liq) + 2H^+ = H_4SiO_4(aq)$	$pH = 16.85 + 0.5 \cdot \log\frac{C_{SiO_3^{2-}}}{C_{H_4SiO_4(aq)}}$
5	$HSiO_3^- + H_2O(liq) + H^+ = H_4SiO_4(aq)$	$pH = 21.69 + \log\frac{C_{HSiO_3^-}}{C_{H_4SiO_4(aq)}}$
6	$SiO_3^{2-} + H^+ = HSiO_3^-$	$pH = 12.00 + \log\frac{C_{SiO_3^{2-}}}{C_{HSiO_3^-}}$
7	$H_4Si_2O_7^{2-} + H_2O(liq) + 2H^+ = 2H_4SiO_4(aq)$	$pH = 16.17 + 0.5 \cdot \log\frac{C_{H_4Si_2O_7^{2-}}}{C^2_{H_4SiO_4(aq)}}$
8	$H_4Si_4O_{12}^{4-} + 4H_2O(liq) + 4H^+ = 4H_4SiO_4(aq)$	$pH = 15.21 + 0.25 \cdot \log\frac{C_{H_4Si_4O_{12}^{4-}}}{C^4_{H_4SiO_4(aq)}}$
9	$H_6Si_4O_{12}^{2-} + 4H_2O(liq) + 2H^+ = 4H_4SiO_4(aq)$	$pH = 20.78 + 0.5 \cdot \log\frac{C_{H_6Si_4O_{12}^{2-}}}{C^4_{H_4SiO_4(aq)}}$
10	$H_7SiO_6^- + H^+ = H_4SiO_4(aq) + 2H_2O(liq)$	$pH = 9.87 + \log\frac{C_{H_7SiO_6^-}}{C_{H_4SiO_4(aq)}}$
11	$H_4SiO_4(aq) + 4H^+ + 4e^- = Si(diamond) + 4H_2O(liq)$	$E = -0.952 - 0.0591 \cdot pH - -0.0148 \cdot \log C_{H_4SiO_4(aq)}$
12	$H_3SiO_4^- + 5H^+ + 4e^- = Si(diamond) + 4H_2O(liq)$	$E = -0.711 - 0.0739 \cdot pH - -0.0148 \cdot \log C_{H_3SiO_4^-}$
13	$H_2SiO_4^{2-} + 6H^+ + 4e^- = Si(diamond) + 4H_2O(liq)$	$E = -0.518 - 0.0887 \cdot pH - -0.0148 \cdot \log C_{H_2SiO_4^{2-}}$
14	$H_7SiO_6^- + 5H^+ + 4e^- = Si(diamond) + 6H_2O(liq)$	$E = -0.806 - 0.0739 \cdot pH - -0.0148 \cdot \log C_{H_7SiO_6^-}$
15	$2H_4SiO_4(aq) + 14H^+ + 14e^- = Si_2H_6(s) + 8H_2O(liq)$	$E = -0.638 - 0.0591 \cdot pH - -0.0084 \cdot \log C_{H_4SiO_4(aq)}$
16	$2H_3SiO_4^- + 16H^+ + 14e^- = Si_2H_6(s) + 8H_2O(liq)$	$E = -0.500 - 0.0675 \cdot pH - -0.0084 \cdot \log C_{H_3SiO_4^-}$
17	$2H_2SiO_4^{2-} + 18H^+ + 14e^- = Si_2H_6(s) + 8H_2O(liq)$	$E = -0.389 - 0.0760 \cdot pH - -0.0084 \cdot \log C_{H_2SiO_4^{2-}}$
18	$2H_7SiO_6^- + 16H^+ + 14e^- = Si_2H_6(s) + 12H_2O(liq)$	$E = -0.554 - 0.0675 \cdot pH - -0.0084 \cdot \log C_{H_7SiO_6^-}$

There are two values of $\Delta_f G^o_{298}(H_7SiO_6^-)$in Table 1 [24, 25]. Since differences between them are huge and it is not clear, which value is more reliable than the other one, both of them were used in calculations. The characteristics of equilibria involving $H_7SiO_6^-$presented in Table 2 are calculated using data from NBS tables [24]. The value from FactSage database [25] makes this ion thermodynamically unstable with respect to other ions.

The concentration – pH diagram for various Si (IV) compounds was plotted. It is presented at Figure 1. Solid lines at Figure 1 represent equilibria involving $H_2SiO_4^{2-}$and $H_3SiO_4^-$which are thermodynamically stable. The point of intersection of lines 1, 2 and 3 ($\log C_{[Si]} = -3.46$) determines region of stability of $H_3SiO_4^-$; it is stable only if concentrations are lower than this value. Equilibria involving other ions which become metastable in presence of $H_2SiO_4^{2-}$and $H_3SiO_4^-$are represented by dash lines. The dash–dot line represent equilibrium with $H_7SiO_6^-$with Gibbs energy of formation calculated from NBS tables [24].

This way, the scheme of consecutive transformation of various forms of Si (IV) with alteration of pH depends on that which value of $\Delta_f G^o_{298}(H_7SiO_6^-)$is more reliable. If this is the value from NBS tables [24] then the scheme would be the following: $H_4SiO_4(aq)|H_7SiO_6^-$. If this is the value from FactSage database [25] then the scheme would be $H_4SiO_4(aq)|H_2SiO_4^{2-}$in concentrated solutions (if $\log C_{[Si]} > -3.46$) and $H_4SiO_4(aq)\,|/H_3SiO_4^-, H_3SiO_4^-|H_2SiO_4^{2-}$in more diluted solutions (if $\log C_{[Si]} < -3.46$).

In accordance with this assumption the potential – pH diagrams for Si–H_2O system are plotted at 298 K, air pressure of 1 bar and concentrations of silicon species in solutions, equal to 10^{-3} M (Figure 2) and 10^{-6} M (Figure 3).

Solid lines at the diagrams allocate the domains of stability of silicon, orthosilicic acid, $H_2SiO_4^{2-}$and $H_3SiO_4^-$. If $H_7SiO_6^-$is assumed to be stable, its domain of stability is bordered by dash lines. Additionally, if the hypothesis of electrochemical formation of solid Si_2H_6 is not rejected, its domain of its stability is bordered by dash–dot lines (if considered in equilibrium with $H_2SiO_4^{2-}$and $H_3SiO_4^-$) or dash–two dots line (if considered in equilibrium with $H_7SiO_6^-$).

The dot line marked by "*a*" at Figures 2 and 3 represents potential of hydrogen electrode under the pressure of 1 bar.

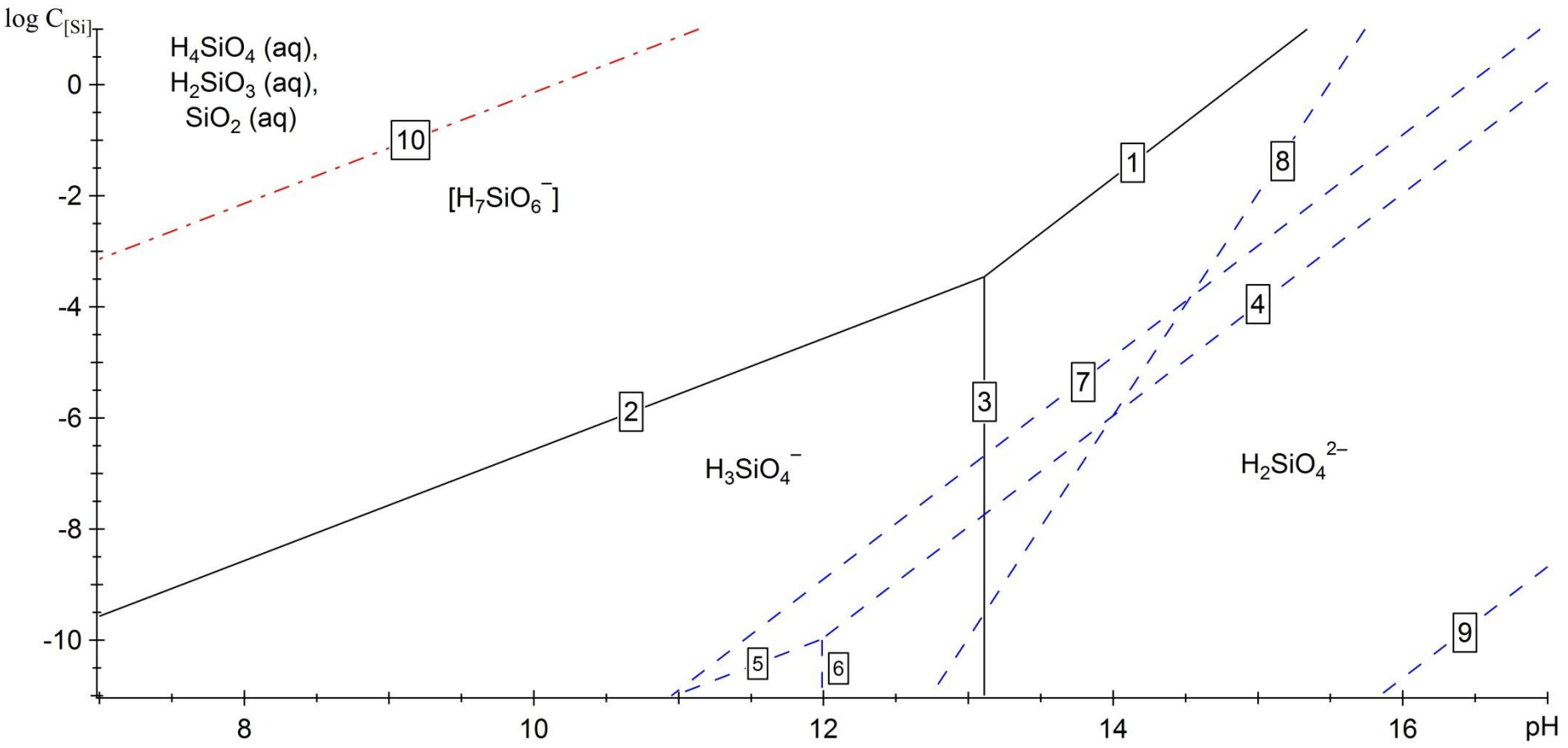

Figure 1. The concentration – pH diagram for various forms of Si (IV).

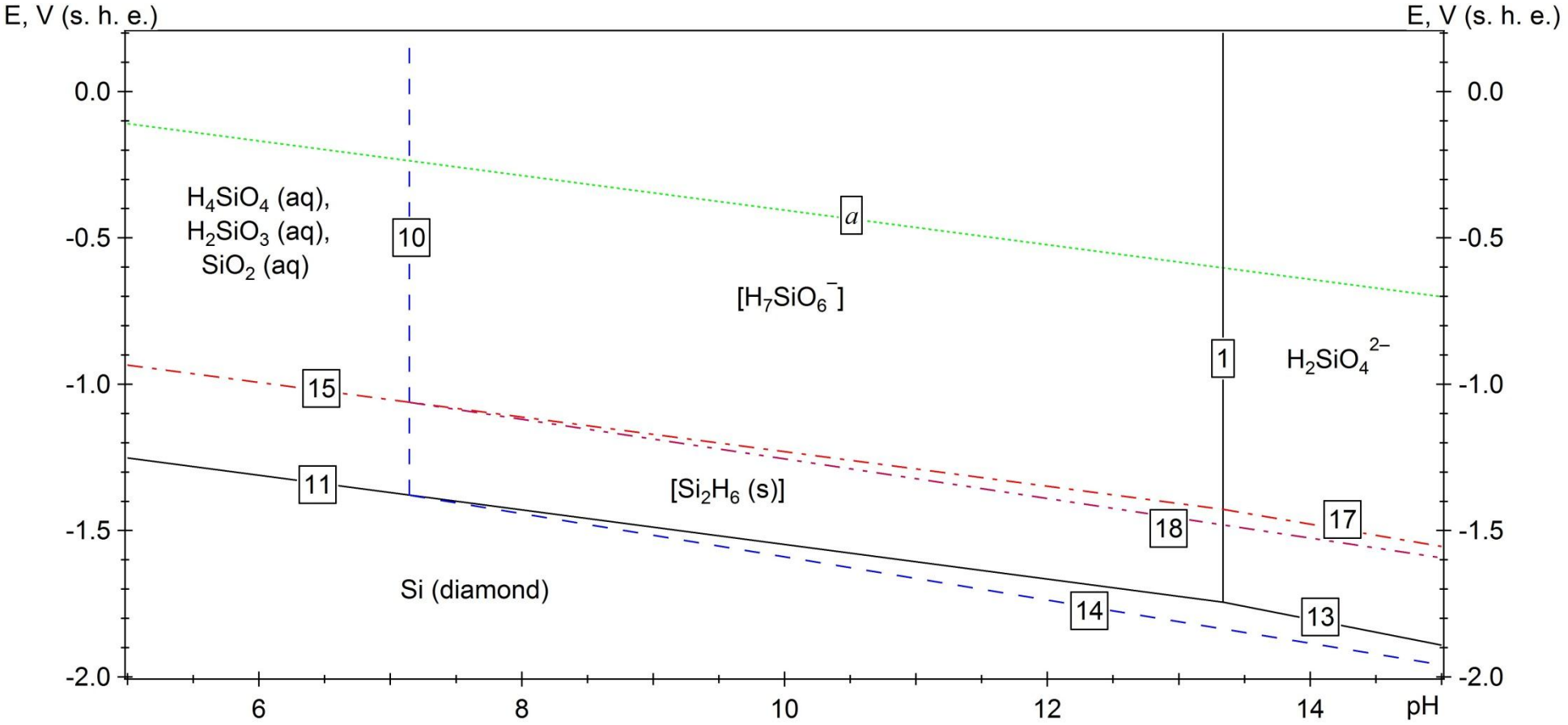

Figure 2. The potential – pH diagram of Si – H_2O system at 298 K, air pressure of 1 bar and $C_{[Si]} = 10^{-3}$ M.

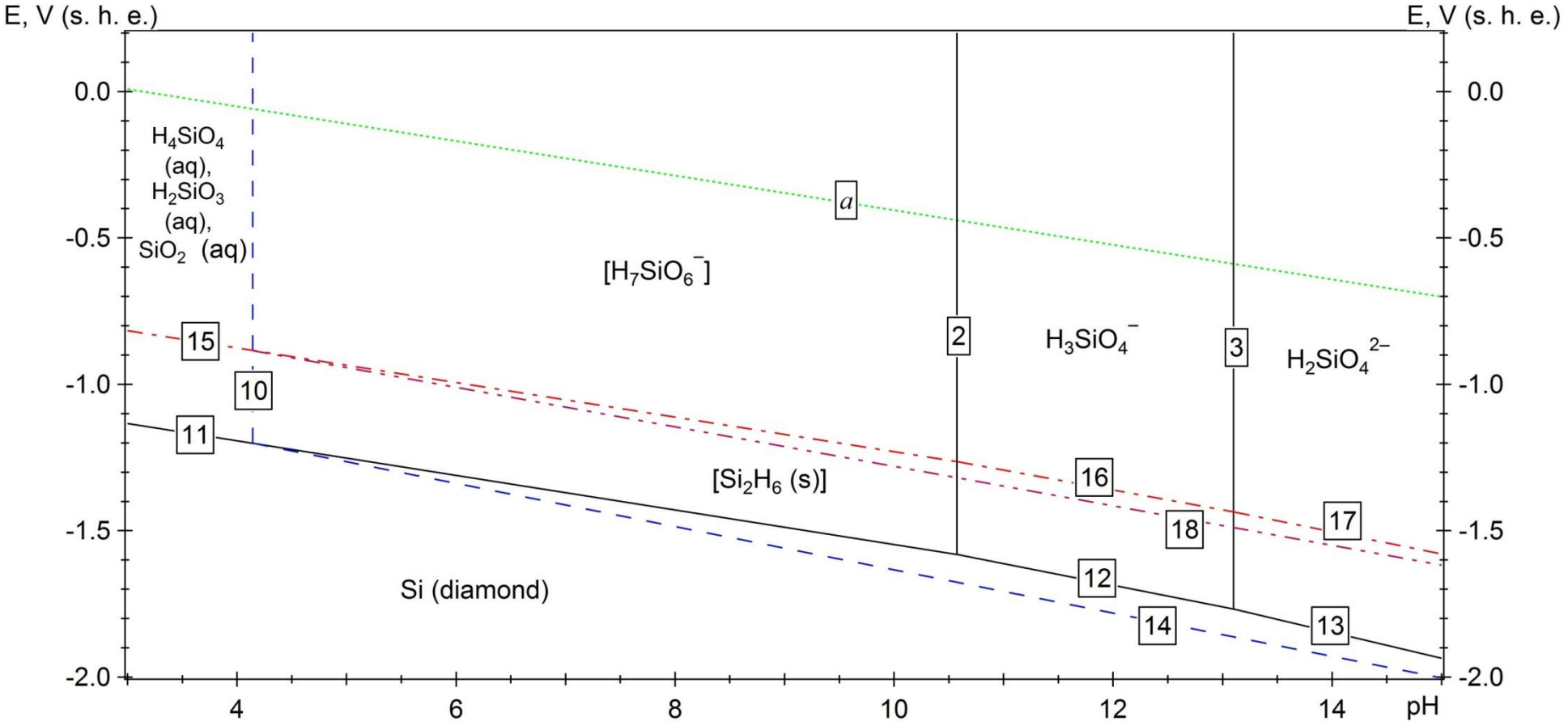

Figure 3. The potential – pH diagram of Si – H_2O system at 298 K, air pressure of 1 bar and $C_{[Si]} = 10^{-6}$ M.

6. Discussion.

Contrary to the Pourbaix diagrams for silicon available in thermodynamic databases, this study provides it in quantitative form and supplies all the lines presented on the diagram with their equations. The data on the standard Gibbs energies of formation of various species in Si – O – H system are collected, analyzed and the values used for further calculations are chosen. Thermodynamic equations of basic chemical and electrochemical equilibria in Si – H_2O system are recalculated using these values.

It was shown that it is not correct to consider SiO_2 (aq) or H_4SiO_4 (aq) as single thermodynamically stable uncharged form of Si (IV). Instead of this all three forms (SiO_2 (aq), H_2SiO_3 (aq) and H_4SiO_4 (aq)) are present in equilibrium with each other and they can simultaneously transform into other species if pH or equilibrium potential of the environment changes. However, by means of convention and since equilibrium concentration of H_4SiO_4 (aq) is higher than that of SiO_2 (aq) or H_2SiO_3 (aq) all chemical and electrochemical reactions can be written using only this form.

The equilibria between charged forms of Si (IV) are also considered. It was shown that $H_2SiO_4^{2-}$ and $H_3SiO_4^-$ are most thermodynamically stable ions if $H_7SiO_6^-$ is not taken into account. Unfortunately, there are not enough reliable thermodynamic data on $H_7SiO_6^-$ and the question about its domain of stability is still open for discussion.

Although thermodynamic calculations show that there is no domain of stability of pure silicon and H_4SiO_4 is reduced to gaseous SiH_4, there are no experimental confirmations of this. Probably, this reaction is complicated by something that thermodynamics cannot handle and therefore cannot be observed. The reduction of H_4SiO_4 to solid Si_2H_6 is also thermodynamically possible but this reaction was also not confirmed by experiments. Again, due to lack of reliable information about its standard Gibbs energies of formation the question about domain of stability of Si_2H_6 (s) is open for discussion.

Despite this the presented information can be useful for developing potential – pH diagrams of complex systems containing silicon.

References:

[1]. Kish L (1988) Kinetics of Electrochemical Metal Dissolution. Budapest: Akademiai Kiado.

[2]. Ronkel F, Schultze JW (2000) Electrochemical Aspects of Porous Silicon Formation. Journal of Porous Materials 7(1 – 3): 11 – 16.

[3]. Estrangat E, Tang G, Liang H, Jahonmir S, Pei P, Martin JM (2004) Experimental investigation on mechanisms of silicon chemical mechanical polishing. Journal of Electronic Materials 33(4): 334 – 339.

[4]. Halimaoui A, Oules C, Bomchil G, Bsiesy A, Gaspard F, Herino R, Ligeon M, Muller F (1991) Electroluminescence in the visible range during anodic oxidation of porous silicon films. Applied Physics Letters 59(3): 304 – 306.

[5]. Kahn H, Deeb C, Chasiotis I, Heuer AH (2005) Anodic Oxidation During MEMS Processing of Silicon and Polysilicon: Native Oxides Can Be Thicker Than You Think. Journal of Microelectromechanical Systems 14(5): 914 – 923.
[6]. Ketsall GH, Williams RA (1991) Electrochemical Behavior of Ferrosilicides (Fe_xSi) in Neutral and Alkaline Aqueous Electrolytes. I. Thermodynamics of Fe – Si – H_2O Systems at 298 K. Journal of Electrochemical Society 138(4): 931 – 940.
[7]. Nikolaychuk PA, Tyurin AG (2013) Thermodynamic evaluation of corrosion-electrochemical behaviour of silicon brass CuZn17Si3. Inorganic Materials 49(5): 457 – 467.
[8]. Jantzen CM (1992) Nuclear Waste Glass Durability: I, Predicting Environmental Response from Thermodynamic (Pourbaix) Diagrams. Journal of American Ceramic Society 75(9): 2433 – 2448.
[9]. Domiciano VG, Garcia JR, Pandalfelli VC (2005) Hydration Resistance of Silicon Powder in High-Carbon-Containing Refractory Castables. American Ceramic Society Bulletin 84(10): 31 – 36.
[10]. Pourbaix M (1966) Atlas of Electrochemical Equilibria in Aqueous Solutions. Pergamon Press Ltd.: Oxford.
[11]. Osseo–Asare K, Wei D (1996) Dissolution Windows for Wet Chemical Processing of Silicon and Silicon Dioxide: Potential–pH Diagrams for the Si–F–H_2O System. Journal of Electrochemical Society 143(2): 749 – 751.

[12]. SUPCRT / Prediction Central. – URL: <http://www.predcent.org/download/supcrt.html> (Access Date – 19. V. 2013).

[13]. The Geochemist's Workbench (GWB). – Rockware: Earth Science and GIS Software. – URL: <http://www.rockware.com/product/overview.php?id=132> (Access Date – 19. V. 2013).

[14]. JNC–TDB. – Japan Nuclear Cycle Organization. – URL: <http://migrationdb.jnc.go.jp> (Access Date – 19. V. 2013).

[15]. ZZ–HATCHES 19: Database for radiochemical modeling / Nuclear Energy Agency. – URL: <http://www.oecd–nea.org/tools/abstract/detail/nea–1210> (Access Date – 19. V. 2013).

[16]. FactSage EpH–Web. – URL: <http://www.sgte.org/ephweb.php> (Access Date – 19. V. 2013).

[17]. Cotton F, Wilkinson G (1972) Advanced Inorganic Chemistry. New York – London – Sydney – Toronto: John Wiley & Sons.

[18]. Iler RK (1979) The Chemistry of Silica. New York: Wiley.

[19]. Martin KR (2007) The chemistry of silica and its potential health benefits. Journal of Nutrition, Health & Aging 11(2): 94 – 98.

[20] Hurst VJ, Kunkle AC (1985) Dehydroxylation, Rehydroxylation and Stabiliby of Kaolinite. Clays and Clay Minerals 33(1): 1 – 14.

[21]. Gunnarsson I, Amorsson S (1999) New data on the standard Gibbs energy of

H_4SiO_4 and its effect on silicate solubility In: Geochemistry of the Earth's Surface: Proceedings of the 5th international symposium, Reykjavik, 16-20 August 1999. P. 449 – 452.

[22] Dean JA (1979) Lange's Handbook of Chemistry, 12th ed.; McGraw-Hill: New York. P. 9-4–9-94.

[23] Ruzinov LP, Gulyanitskiy BS (1975) Ravnovesnye prevrashcheniya metallurgicheskikh reaktsiy (Equilibrium Transformations of Metallurgic Reactions). Moscow: Metallurgiya [In Russian].

[24] Wagman DD, Evans WH, Parker VB, Schumm RH, Halow I, Bailey SM, Churney KL, Nuttall RL (1982) Journal of Physical and Chemical Reference Data. Vol. 11. Suppl. 2.

[25] FactSage Compound–Web. – URL: <http://www.sgte.org/ephweb.php> (Access Date – 19. V. 2013).

[26] Bard AJ, Parsons R, Jordan J (1985) Standard Potentials in Aqueous Solution. New York: Marcel Dekker, Inc.

[27] Thermal Constants of Substances: Database. – URL: <http://www.chem.msu.su/cgi-bin/tkv.pl?show=welcome.html> (Access Date – 19. V. 2013).

[28]. Hayes PC, Algie SH (1993) Process Principles in Minerals and Materials Production. Brisbane: Hayes Publishing Co.

[29] Vanýsek P (2012) Electrochemical Series. In: CRC Handbook on Chemistry and Physics. 93rd Edition. Chemical Rubber Company.

[30] Atkins PW, Overton TL, Rourke JR, Weller MT, Armstrong FA (2010) Inorganic Chemistry. Fifth Edition. Oxford University Press.

[31]. Walther JV (2005) Essentials of Geochemistry. Second Edition. Jones & Bartlett Learning.

[32] Treguer P, Nelson DM, Van Bennekom AJ, DeMaster DJ, Leynaert A, Queguiner B (1995) The silica balance in the world ocean: A Reestimate. Science 268: 375 – 379.

[33] Ketsall GH, Robbins DJ (1990) Thermodynamics of Ti–H_2O–F (–Fe) Systems at 298 K. Journal of Electroanalytical Chemistry and Interfacial Electrochemistry 283(1–2): 135 – 137.

УДК 544.3:544.4

The revised potential–pH diagram of Sc – H_2O system

Pavel Anatolyevich Nikolaychuk

Čelâbinskij gosudarstvennyj universitet, Bratyev Kashirinykh Street, 129, Chelyabinsk, 454001, Russian Federation. E-mail: npa@csu.ru.

Résumé: The thermodynamic data on the standard Gibbs energies of formation of scandium solid and aqueous species were collected and systematised. The speciation diagram for the dimerisation reaction $2ScOH^{2+}\ (aq) \rightleftharpoons Sc_2(OH)_2^{4+}\ (aq)$ was plotted. The equilibria between various hydrolysed scandium (III) species in an aqueous solution were discussed. The potential–pH diagram of system Sc – H_2O at 25°C, air pressure of 1 bar and various activities of ions in a solution were plotted. The influence of possible electrochemical formation of scandium hydride and the effect of non-stoichiometry of scandium sesquioxide on the corrosion-electrochemical properties of scandium were discussed.

Key Words: scandium, scandium oxide, scandium hydride, scandium nitride, non-stoichiometry, scandium aqueous species, speciation diagram, activity – pH diagram, potential – pH diagram, corrosion-electrochemical behaviour.

1. Introduction

An interest to the chemistry of scandium significantly increased in the last five decades. With the development of microelectronics, air- and spacecraft engineering, hydrogen energetics and other high-technology branches of industry scandium began to attract an attention of researchers. Various scandium compounds are widely employed for the development of high-temperature ceramics, quantum-mechanical amplifiers, lasers, luminophores, emission materials, dielectrics, solid electrolytes, halogen projectors, catalysts, filters for quasimonochromatic rays of neutrons, emitters of β–particles *et cetěra*. Scandium-based alloys have a series of valuable properties, including thermal and mechanical stability, corrosion and radiation resistance [Horovitz et al., 1975; Комиссарова, 2001]. The aqueous chemistry and the corrosion-electrochemical behaviour of scandium are very similar to that of aluminum [Brookins, 1988; Rayner-Canham, 2013; Schweitzer, Pesterfield, 2010]. The potential – pH diagram for scandium found its application in studying of pitting behaviour of alloys [Santamaria, Muratore, Quarto Di, 2013; Wloka, Virtanen, 2007] and characterisation of scandium inorganic compounds [Wang et al., 2013]. However, the existing variants of Pourbaix diagram for scandium [Brookins, 1988; Pourbaix, 1966; Schweitzer, Pesterfield, 2010; Takeno, 2005] take into account only Sc (hcp), Sc^{3+} (aq), $ScOH^{2+}$ (aq) and Sc_2O_3 (bcc) and do not consider another scandium aqueous species, including the polimerised forms. The goal of this study is to collect the reliable data on the Gibbs energies of formation of the various scandium aqueous species, consider the speciation of Sc (III) species and revise the potential – pH diagram of Sc – H_2O system.

2. Thermodynamic data on scandium solid and aqueous species

According to the phase diagram of Sc – O system [Kuprashvili, Naumkin, Savitskii, 1969; Predel, 1998; Купрашвили, Наумкин, Савицкий, 1969; Диаграммы состояния двойных металлических систем: справочник, 2001], only one stable oxide – Sc_2O_3 – exists in the system at 298 K. It has the crystal structure of body centered cube. It was reported earlier [Dufek, Brožek, Petrů, 1969; Dufek, Petrů, Brožek, 1967; Petrů, Brožek, Dufek, 1970] about the existence of scandium monoxide, ScO (s), which can be obtained by reduction of Sc_2O_3 by silicon, but the subsequent studies and the thermodynamic calculations [Work, Eick, 1972; Юдин et al., 1976] disproved this report. Upon interaction with hydrogen scandium form two hydrides, namely, ScH_2 (s) and ScH_3 (s) [Bashkin, Ponyatovskii, Kost, 1978; Horovitz et al., 1975; Jerosch-Herold, Torgeson, Barnes, 1997; Kobayashi, Takei, 1978; Kobayashi, Takei, 1980; Switendick, 1989; Комиссарова, 2001]. In aqueous acidic environments scandium exists in form of the cation Sc^{3+} (aq), which with increase of the basicity of the solution can be hydrolysed to $ScOH^{2+}$ (aq), $Sc(OH)_2^+$ (aq) or $Sc(OH)_4^-$ (aq) [Baes Jr., Mesmer,

1976; Schweitzer, Pesterfield, 2010]. The hydroxide $Sc(OH)_3$ (s) can be precipitated from a solution, but it is unstable relative to the oxide [Travers, Dellien, Hepler, 1976].

Table 1 summarises the standard Gibbs energies of formation of various scandium species. In the case when only the standard enthalpies of formation and the standard entropies of the species were present in literature [Bommer, Hohmann, 1941; Huber et al., 1963], the standard entropy of pure scandium were taken from [Gerstein, 1971] and used in calculations of the standard Gibbs energies. The standard Gibbs energy of formation of scandium (III) hydroxide was estimated from the value of the solubility product of $Sc(OH)_3$ (s) [Aksel'rud, 1963; Feitknecht, Schindler, 1963; Moeller, Kremers, 1945; Oka, 1938; Wood, Samson, 2006]. The standard Gibbs energies of formation of various scandium hydroxocations were estimated from the values of hydrolysis constants [Akalin, Özer, 1971; Antonovich, Nazarenko, 1968; Aveston, 1966; Biedermann et al., 1956; Cole et al., 1969; Haas, Shock, Sassani, 1995; Kilpatrick, Pokras, 1953; Kilpatrick, Pokras, 1954; Komissarova, Prutkova, Pushkina, 1971; Lindqvist-Reis, Persson, Sandström, 2006; Marques et al., 1997; Paul, 1962; Sekine, Hasegawa, 1966; Siqueira et al., 1995; Türkel, Aydin, Özer, 1999; Wu et al., 2004; Жук, 1954]. The values chosen for further calculations are marked in Italic.

Table 1. The standard Gibbs energies of formation of various scandium species.
Таблица 1. Стандартные энергии Гиббса образования различных соединений скандия.

Compound	Reference state	$-\Delta_f G^o_{298}$, $J \cdot mol^{-1}$	Reference
Sc	s, hexagonal close packed	0	By convention
ScN	s, cubic	253 250	[Alimarin, Yung-Schaing, 1961; Комиссарова, 2001]
		253 150	[Gschneider Jr., 1961; Horovitz et al., 1975]
		283 800	[Pankratz, Stuve, Gokcen, 1984]
ScH_2	s, face centered cubic	149 280	[Термические константы веществ, 2007]
		157 170	[Lieberman, Wahlbeck, 1965; Комиссарова, 2001]
		157 300	[Horovitz et al., 1975]
Sc_2O_3	s, body centered cubic	1 819 360	[Brookins, 1988; Wagman et al., 1982]
		1 819 410	[Speight, 2005]
		1 819 460	[Horovitz et al., 1975]
		1 804 110	[Pankratz, Stuve, Gokcen, 1984]
		1 804 250	[Верягин et al., 1965]
		1 819 320	[Рузинов, Гуляницкий, 1975; Progress in the Science and Technology of the Rare Earths, 2013]
		1 819 200	[Schweitzer, Pesterfield, 2010]
		1 818 930	[Термические константы веществ, 2007]
		1 802 030	[Jichang, Ke'ren, 1984; Комиссарова, 2001]
		1 819 380	[Travers, Dellien, Hepler, 1976]
		1 819 370	[Robie, Hemingway, Fisher, 1979]
$Sc(OH)_3$	s, body centered cubic	1 233 300	[Brookins, 1988; Wagman et al., 1982]
		1 233 230	[Рузинов, Гуляницкий, 1975]
		1 233 400	[Schweitzer, Pesterfield, 2010]
		1 232 980	[Horovitz et al., 1975]
		1 226 000	[Travers, Dellien, Hepler, 1976]
		1 055 830	[Термические константы веществ, 2007]
ScO(OH)	s	1 007 200	[Baes Jr., Mesmer, 1976]
Sc^{3+}	aq	586 600	[Brookins, 1988; Schweitzer, Pesterfield, 2010; Wagman et al., 1982]
		586 200	[Schweitzer, Pesterfield, 2010]
		583 890	[Термические константы веществ, 2007]
		586 650	[Travers, Dellien, Hepler, 1976]

$ScOH^{2+}$	aq	801 200	[Brookins, 1988; Speight, 2005; Wagman et al., 1982]
		799 000	[Schweitzer, Pesterfield, 2010]
		799 220	[Travers, Dellien, Hepler, 1976]
		799 200	[Baes Jr., Mesmer, 1976]
		794 120	[Термические константы веществ, 2007]
$Sc(OH)_2^+$	aq	1 005 400	[Schweitzer, Pesterfield, 2010]
		1 005 500	[Baes Jr., Mesmer, 1976]
$Sc(OH)_4^-$	aq	1 370 800	[Brookins, 1988]
		1 380 700	[Schweitzer, Pesterfield, 2010]
		1 386 750	[Baes Jr., Mesmer, 1976]
$Sc_2(OH)_2^{4+}$	aq	1 649 750	[Термические константы веществ, 2007]
		1 613 200	[Baes Jr., Mesmer, 1976]
$Sc_3(OH)_4^{5+}$	aq	2 626 500	[Термические константы веществ, 2007]
$Sc_3(OH)_5^{4+}$	aq	2 838 220	[Термические константы веществ, 2007]
		2 852 200	[Baes Jr., Mesmer, 1976]

3. The equilibria involving various scandium (III) compounds

3.1. The oxide, the oxyhydrate and the hydroxide

The following reactions involving the oxide, the oxyhydrate and the hydroxide of scandium (III) can be considered:

$$Sc_2O_3\,(s) + H_2O\,(l) \rightleftharpoons 2ScO(OH)\,(s)\,, \quad (1)$$

$$ScO(OH)\,(s) + H_2O\,(l) \rightleftharpoons Sc(OH)_3\,(s)\,, \quad (2)$$

$$Sc_2O_3\,(s) + 3H_2O\,(l) \rightleftharpoons 2Sc(OH)_3\,(s)\,. \quad (3)$$

The Gibbs energy changes in the reactions (1), (2) and (3) are calculated using the values from Table 1, and the following values are obtained: $\Delta_r G^o_{298}(1) = 41\,940\ \mathrm{J\cdot mol^{-1}}$, $\Delta_r G^o_{298}(2) = 10\,940\ \mathrm{J\cdot mol^{-1}}$ and $\Delta_r G^o_{298}(3) = 63\,820\ \mathrm{J\cdot mol^{-1}}$. The calculations show that scandium sesquioxide is the most thermodynamically stable compound, and it does not tend to be hydrolysed.

3.2. The polymerisation of aqueous $ScOH^{2+}$

The ion $ScOH^{2+}$ (aq) can form a dimer according to the reaction:

$$2ScOH^{2+}\ (aq) \rightleftharpoons Sc_2(OH)_2^{4+}\ (aq)\,. \quad (4)$$

The Gibbs energy change in the reaction (4) from the data of Table 1 is $\Delta_r G^o_{298}(4) = -15\,200\ \mathrm{J\cdot mol^{-1}}$, and the equilibrium constant is $K_{(4)} = 461.62\ \mathrm{l\cdot mol^{-1}}$. The ratio of activities of monomeric and dimeric forms is determined by the following system of equations:

$$\begin{cases} K_{(4)} = \dfrac{a_{Sc_2(OH)_2^{4+}\,(aq)}}{a^2_{ScOH^{2+}\,(aq)}}; \\ a_{[Sc]} = a_{ScOH^{2+}\,(aq)} + 2\cdot a_{Sc_2(OH)_2^{4+}\,(aq)}. \end{cases} \quad (5)$$

Here $a_{[Sc]}$ is the total activity of dissolved scandium in a solution. The dependency of activities of monomeric and dimeric forms on the total activity of dissolved scandium is illustrated by Figure 1. Here curves *1* and *2* show the dependencies of the "activity fractions" $\dfrac{a_{ScOH^{2+}(aq)}}{a_{ScOH^{2+}(aq)} + a_{Sc_2(OH)_2^{4+}(aq)}}$ and $\dfrac{a_{Sc_2(OH)_2^{4+}(aq)}}{a_{ScOH^{2+}(aq)} + a_{Sc_2(OH)_2^{4+}(aq)}}$ on $a_{[Sc]}$, and curve *3* determines the ratio $\dfrac{a_{ScOH^{2+}(aq)}}{a_{Sc_2(OH)_2^{4+}(aq)}}$.

The dimeric form predominates in concentrated solutions. At $a_{[Sc]}$ = 1 M the ratio $\frac{a_{ScOH^{2+}(aq)}}{a_{Sc_2(OH)_2^{4+}(aq)}} = 0.067$. With decrease of the total content of dissolved scandium this ratio begins to grow. The activities of monomeric and dimeric forms become equal at lg $a_{[Sc]}$ = −2.15, and in more diluted solution the monomeric form predominates. At $a_{[Sc]}$ = 10^{-3} M the ratio $\frac{a_{ScOH^{2+}(aq)}}{a_{Sc_2(OH)_2^{4+}(aq)}} = 3.43$ and at $a_{[Sc]}$ = 10^{-6} M $\frac{a_{ScOH^{2+}(aq)}}{a_{Sc_2(OH)_2^{4+}(aq)}} = 2170$.

3.3. The aqueous scandium (III) species

The relative stability of other scandium (III) hydroxocomplexes depends on both pH and the activities of species in a solution. This dependence is illustrated in Figure 2.

The cation Sc^{3+} exhibits the following consecutive reactions with increase of pH depending on the activities:

lg $a_{[Sc]}$ > −7.14: $Sc^{3+}(aq) \rightarrow Sc_2O_3(s) \rightarrow Sc(OH)_4^-(aq)$;

−7.14 > lg $a_{[Sc]}$ > −9.38: $Sc^{3+}(aq) \rightarrow ScOH^{2+}(aq),\ Sc_2(OH)_2^{4+}(aq) \rightarrow Sc_2O_3(s) \rightarrow Sc(OH)_4^-(aq)$;

−9.38 > lg $a_{[Sc]}$ > −12.66: $Sc^{3+}(aq) \rightarrow ScOH^{2+}(aq),\ Sc_2(OH)_2^{4+}(aq) \rightarrow Sc(OH)_2^+(aq) \rightarrow Sc_2O_3(s) \rightarrow Sc(OH)_4^-(aq)$;

log $a_{[Sc]}$ < −12.66: $Sc^{3+}(aq) \rightarrow ScOH^{2+}(aq),\ Sc_2(OH)_2^{4+}(aq) \rightarrow Sc(OH)_2^+(aq) \rightarrow Sc(OH)_4^-(aq)$.

Accordingly, the cation $Sc_3(OH)_5^{4+}$ has no domain of thermodynamic stability.

4. The potential – pH diagram

In accordance with Figure 2 the sequence of equilibria involving various scandium ions differs with alteration of activities of dissolved species in a solution. This also affects the potential – pH diagrams. The diagrams at various activities of ions in solutions from 10^{-6} M to 10^{-15} M are shown at Figures 3 through 6. The calculations show that for the environments, in which the activities exceed 10^{-6} M and which are of the most importance for applied chemistry, the diagrams are in good agreement with the previously published ones [Brookins, 1988; Pourbaix, 1966; Schweitzer, Pesterfield, 2010; Takeno, 2005]. The diagrams at the activities lower than 10^{-10} M currently have no practical implementation; however they are presented in order to show the influence of the thermodynamic activities on the presence or absence of the domains of thermodynamic stability of certain phases. Probably the thermodynamic prediction of the electrochemical properties of solutions at super-low activities of ions in solutions may become practically important in the future due to developing of analytical techniques and the tendency of decreasing the detection limit of substances in a solution.

The corrosion-electrochemical behaviour of scandium is very similar to that of aluminum. In the highly acidic environments (at pH < 4) scandium exhibits the active dissolution with formation of Sc^{3+} (aq). At higher pH values the protective layer consisting of Sc_2O_3 (s) is formed on the metal surface. However, in very diluted solutions, where $a_{[Sc]} < 10^{-7}$ M, the hydrolysed aqueous scandium species begin to predominate, and the domain of scandium passivity is rapidly narrowed.

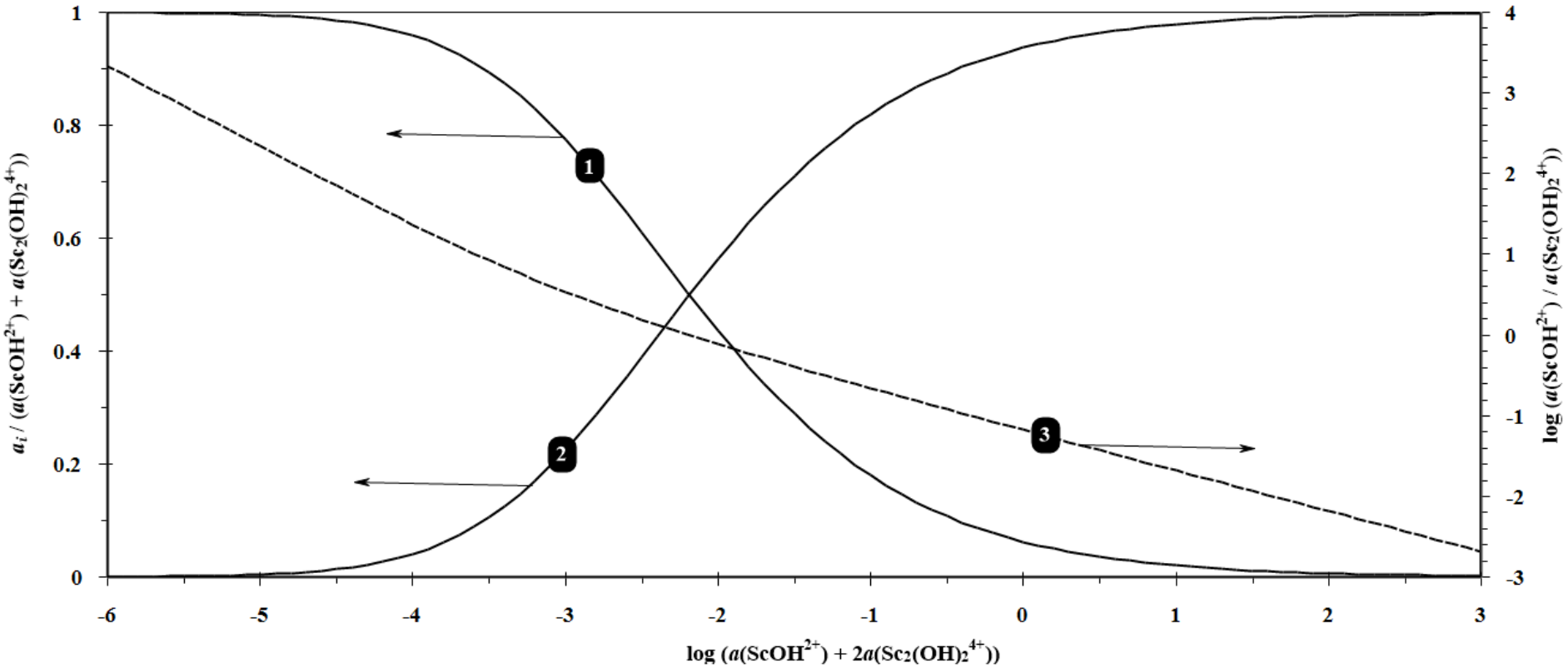

Fig. 1. The speciation diagram of the scandium (III)⇄ hydroxocations in a solution, $2ScOH^{2+}(aq) \rightleftharpoons Sc_2OH_2^{4+}(aq)$:

1 – $\dfrac{a_{ScOH^{2+}(aq)}}{a_{ScOH^{2+}(aq)} + a_{Sc_2(OH)_2^{4+}(aq)}} = f\left(\lg\left(a_{ScOH^{2+}(aq)} + 2 \cdot a_{Sc_2OH_2^{4+}(aq)}\right)\right)$, left axis;

2 – $\dfrac{a_{Sc_2(OH)_2^{4+}(aq)}}{a_{ScOH^{2+}(aq)} + a_{Sc_2(OH)_2^{4+}(aq)}} = f\left(\lg\left(a_{ScOH^{2+}(aq)} + 2 \cdot a_{Sc_2OH_2^{4+}(aq)}\right)\right)$, left axis;

3 – $\lg\dfrac{a_{ScOH^{2+}(aq)}}{a_{Sc_2(OH)_2^{4+}(aq)}} = f\left(\lg\left(a_{ScOH^{2+}(aq)} + 2 \cdot a_{Sc_2OH_2^{4+}(aq)}\right)\right)$, right axis.

Рис. 1. Диаграмма распределения гидроксокатионов скандия (III) в растворе, $2ScOH^{2+}(aq) \rightleftharpoons Sc_2OH_2^{4+}(aq)$:

1 – $\frac{a_{ScOH^{2+}(aq)}}{a_{ScOH^{2+}(aq)} + a_{Sc_2(OH)_2^{4+}(aq)}} = f\left(\lg\left(a_{ScOH^{2+}(aq)} + 2 \cdot a_{Sc_2OH_2^{4+}(aq)}\right)\right)$, левая ось;

2 – $\frac{a_{Sc_2(OH)_2^{4+}(aq)}}{a_{ScOH^{2+}(aq)} + a_{Sc_2(OH)_2^{4+}(aq)}} = f\left(\lg\left(a_{ScOH^{2+}(aq)} + 2 \cdot a_{Sc_2OH_2^{4+}(aq)}\right)\right)$, левая ось;

3 – $\lg\frac{a_{ScOH^{2+}(aq)}}{a_{Sc_2(OH)_2^{4+}(aq)}} = f\left(\lg\left(a_{ScOH^{2+}(aq)} + 2 \cdot a_{Sc_2OH_2^{4+}(aq)}\right)\right)$, правая ось.

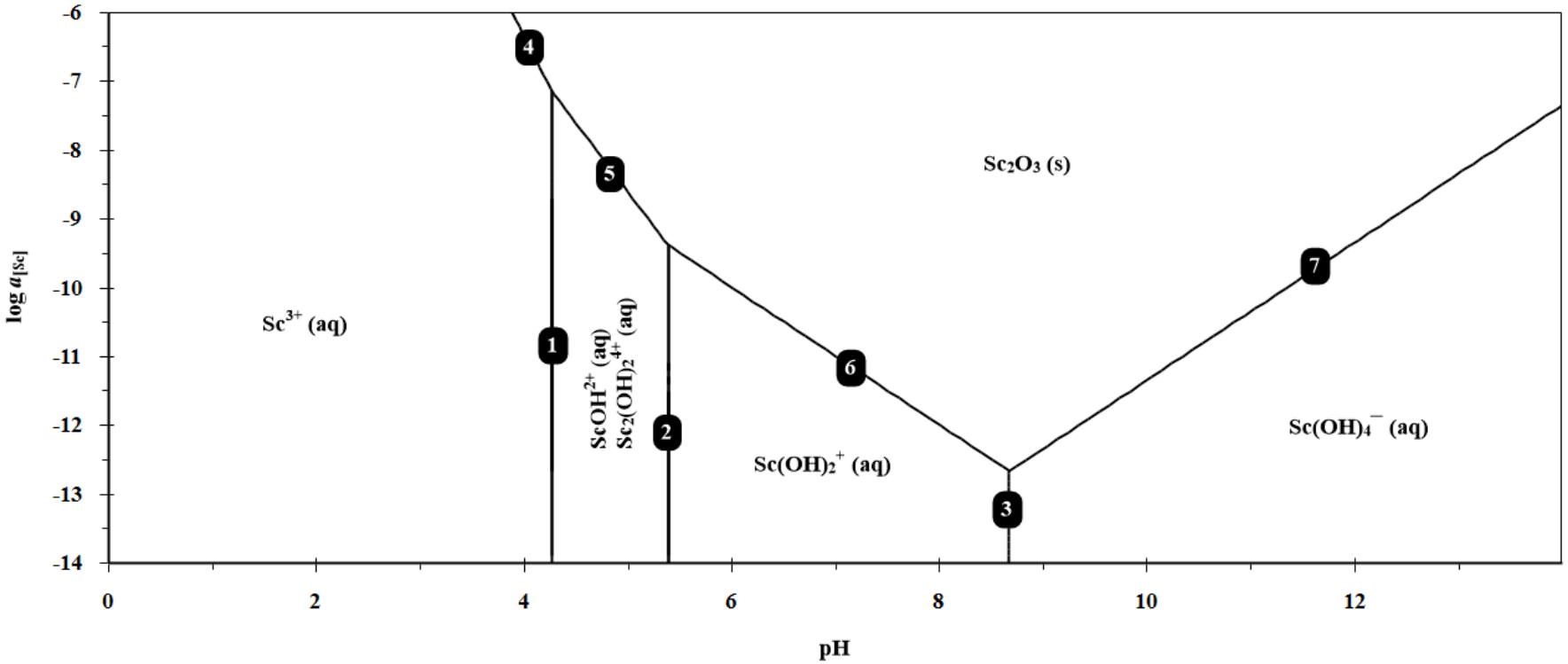

Fig. 2. The activity – pH diagram for Sc (III) species.
Рис. 2. Диаграмма активность – pH для соединений Sc (III).

5. The influence of scandium hydride and nitride

In addition to the oxide passivation, scandium can exhibit either hydride or nitride passivation. The layer of scandium hydride can be formed due to electrochemical reduction of water and interaction of metallic scandium with the forming hydrogen. When scandium is exposed in a natural water that stays in equilibrium with atmospheric air, the possible electrochemical formation of scandium nitride due to reduction of the atmospheric nitrogen should also be considered.

Using the data from Table 1 the potentials of reduction of Sc_2O_3 (s) to metallic scandium, scandium hydride and scandium nitride were calculated:

$$Sc_2O_3\ (s) + 6H^+ + 6e^- \rightleftharpoons 2Sc\ (hcp) + 3H_2O\ (l);\ E^o_{298} = -1{,}914\ V, \quad (6)$$

$$Sc_2O_3\ (s) + 10H^+ + 10e^- \rightleftharpoons 2ScH_2\ (s) + 3H_2O\ (l);\ E^o_{298} = -0{,}822\ V, \quad (7)$$

$$Sc_2O_3\ (s) + N_2(g) + 6H^+ + 6e^- \rightleftharpoons 2ScN\ (s) + 3H_2O\ (l),\ P_{N_2\ (g)} = 0.79\ bar;\ E^o_{298} = -1{,}040\ V, \quad (8)$$

It follows from the equations (6), (7) and (8) that both metallic scandium and scandium nitride become thermodynamically unstable in presence of scandium hydride, and that scandium oxide is electrochemically reduced directly to ScH_2 (s). Therefore, the potential – pH diagram for scandium with consideration of scandium hydride ScH_2 (s) were calculated and presented in Figures 7 through 10. The domain of hydride passivation of scandium is present at these diagrams instead of the domain of thermodynamic stability of pure scandium. However, all the reactions involving dissolution of both metallic scandium and its hydride, occur below the potential of the standard hydrogen electrode, and therefore, do not affect the corrosion-electrochemical properties of scandium in the domain of electrochemical stability of water.

The basic chemical and electrochemical equilibria in Sc – H_2O system are listed in Table 2.

6. The influence of non-stoichiometry of scandium sesquioxide

It was reported [Arkharov, Kichigina, 1966; Horovitz et al., 1975; Young Jr., Sienko, 1972] that scandium sesquioxide has a considerable degree of homogeneity Sc_2O_x, $2{,}89 \leqslant x < 3$.

The standard Gibbs free energy of formation of Sc_2O_x can be estimated according to the Gorichev's method [Gorichev, Klyushin, 1971] based on Waring – Lagrange interpolation polynomial [Lagrange, 1812; Meijering, 2002; Waring, 1779]. However, the implementation of this method requires reliable data on at least two different oxides of the same metal with different oxidation states. As only data on Sc_2O_3 (s) are available in literature, the standard Gibbs energy of formation of ScO (s) should be estimated.

V. A. Kireev proposed [Киреев, 1970] that an approximate relationship exists between the standard Gibbs energies of formation of similar compounds of transition metals and the atomic number of elements forming these compounds. Using this method, the standard Gibbs energy of formation of hypothetical scandium monoxide ScO (s) was estimated basing on the data on the standard Gibbs
energies of formation of TiO (s), VO (s), MnO (s) and ZnO (s) taken from [Wagman et al., 1982]. The following relationship was found:

$$\frac{\Delta_f G^o_{298}\ (MeO)}{z_{Me}} = -233{,}4 \cdot z^2_{Me} + 13500 \cdot z_{Me} - 205550,\ J \cdot mol^{-1}, \quad (9)$$

where $21 \leqslant z_{Me} \leqslant 30$ is the atomic number of metal. The dependence is illustrated in Figure 11.

From this relationship the standard Gibbs energy of formation of ScO (s) was found to be equal to $\Delta_f G^o_{298}\ (ScO) \cong -525550\ J \cdot mol^{-1}$. Using this value and that of Sc_2O_3 (s) from Table 1, the standard Gibbs energy of formation of non-stoichiometric scandium oxide was estimated by the following relationship:

$$\Delta_f G^o_{298}\ (Sc_2O_x) = -80900 \cdot x^2 - 363700 \cdot x,\ J \cdot mol^{-1};\ 2{,}89 \leqslant x < 3\ . \quad (10)$$

The hypothetical potential – pH diagram of Sc – H_2O system at 298 K, air pressure of 1 bar and activities of ions in solutions a_i = 10^{-6} M taking into consideration the non-stoichiometry of scandium sesquioxide is presented in Figure 12. Thermodynamic prediction shows that the domain of thermodynamic stability of Sc_2O_x decreases with decrease of x.

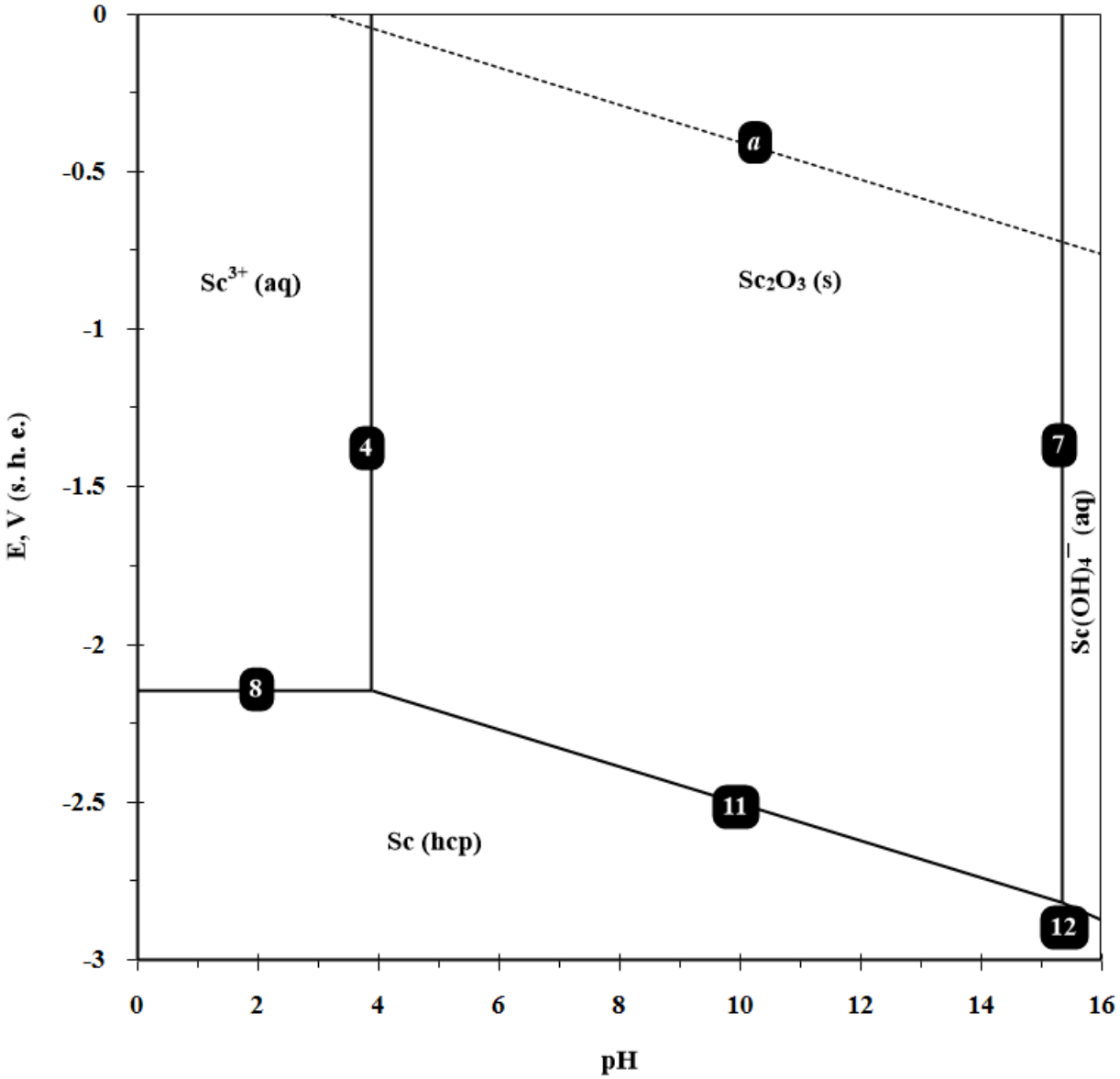

Fig. 3. The potential – pH diagram of Sc – H_2O system at 298 K, air pressure of 1 bar and activities of ions in solutions $a_i = 10^{-6}$ M.

Рис. 3. Диаграмма потенциал – pH системы Sc – H_2O при 298 K, давлении воздуха 1 бар и активностях ионов в растворе $a_i = 10^{-6}$ M.

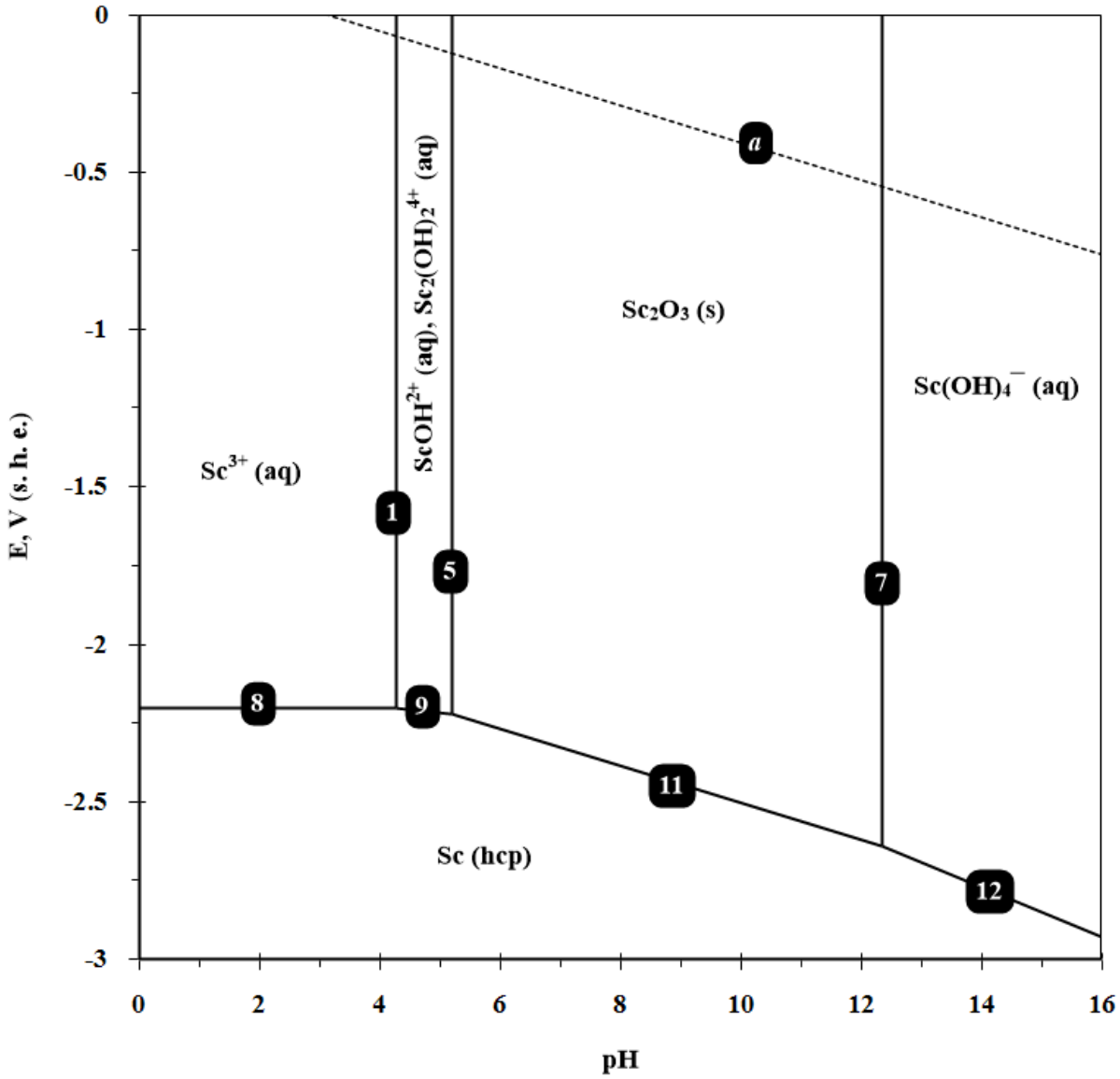

Fig. 4. The potential – pH diagram of Sc – H_2O system at 298 K, air pressure of 1 bar and activities of ions in solutions $a_i = 10^{-9}$ M.

Рис. 4. Диаграмма потенциал – pH системы Sc – H_2O при 298 K, давлении воздуха 1 бар и активностях ионов в растворе $a_i = 10^{-9}$ M.

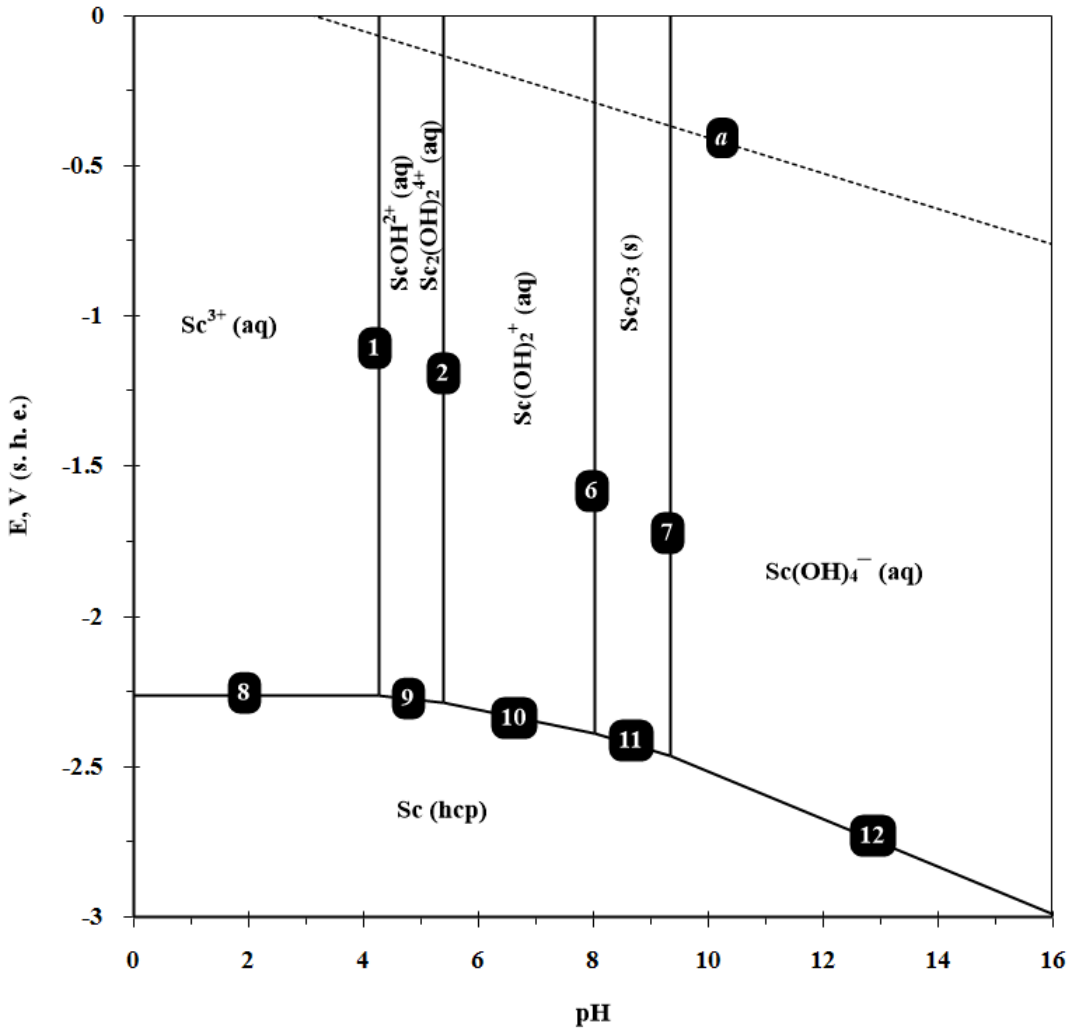

Fig. 5. The potential – pH diagram of Sc – H_2O system at 298 K, air pressure of 1 bar and activities of ions in solutions $a_i = 10^{-12}$ M.

Рис. 5. Диаграмма потенциал – pH системы Sc – H_2O при 298 K, давлении воздуха 1 бар и активностях ионов в растворе $a_i = 10^{-12}$ M.

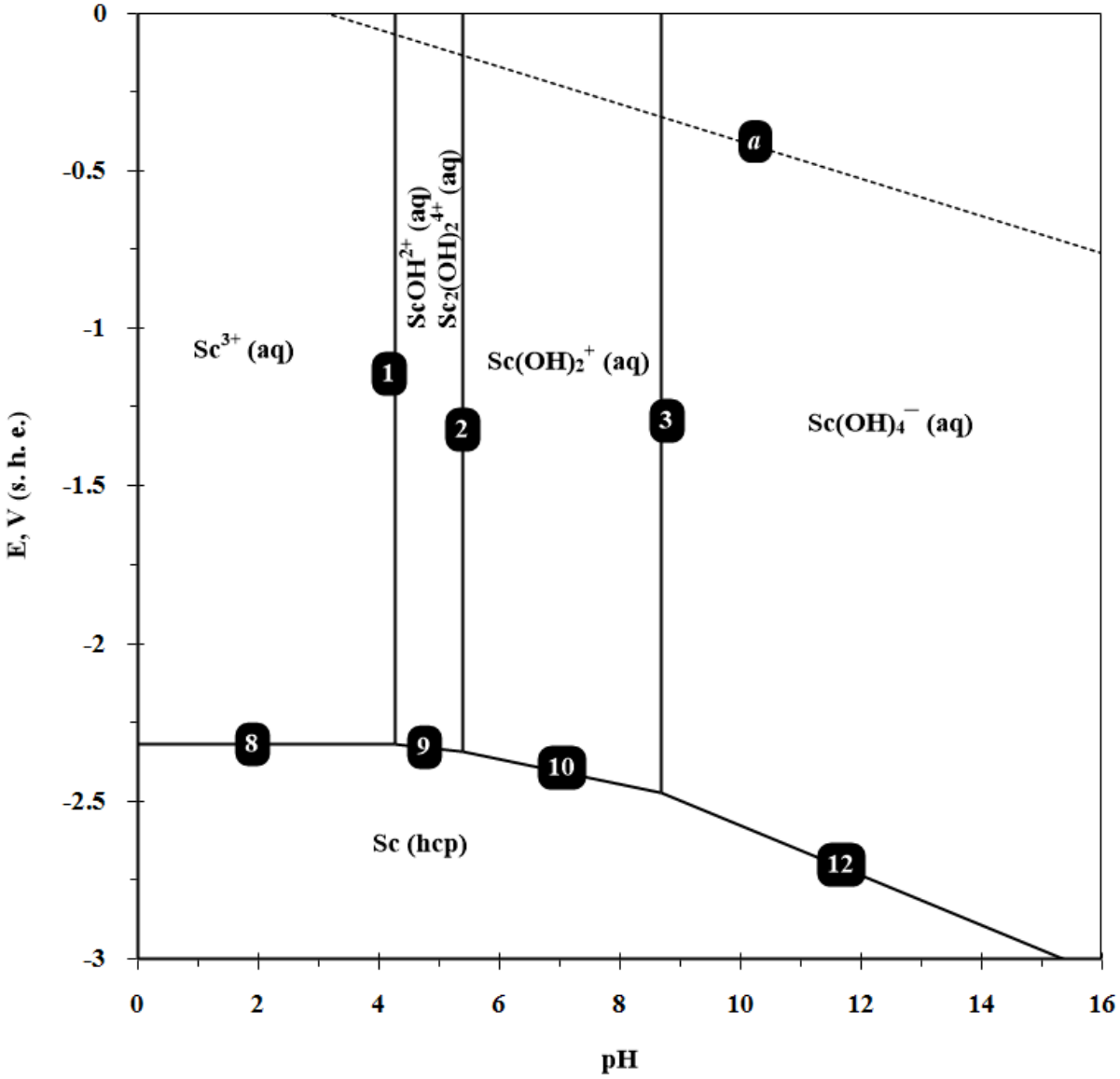

Fig. 6. The potential – pH diagram of Sc – H_2O system at 298 K, air pressure of 1 bar and activities of ions in solutions $a_i = 10^{-15}$ M.

Рис. 6. Диаграмма потенциал – pH системы Sc – H_2O при 298 K, давлении воздуха 1 бар и активностях ионов в растворе $a_i = 10^{-15}$ M.

Table 2. Basic chemical and electrochemical equilibria in Sc – H_2O system at 298 K and air pressure of 1 bar.

Таблица 2. Основные химические и электрохимические равновесия в системе Sc – H_2O при 298 K и давлении воздуха 1 bar.

No of line in Figures 2–10 and 12	Electrode reaction	E, V (s. h. e.) or pH of the solution
a	$2H^+(aq)+2e^- \rightleftharpoons H_2(g); P_{H_2(g)} = 5\cdot10^{-7}$ bar	$E = 0.186 - 0.0591\cdot pH$
1	$\begin{cases} ScOH^{2+}(aq)+H^+(aq) \rightleftharpoons Sc^{3+}(aq)+H_2O(l); \\ Sc_2(OH)_2^{4+}(aq)+2H^+(aq) \rightleftharpoons 2Sc^{3+}(aq)+2H_2O(l) \end{cases}$	$pH = 4{,}266 + \lg\frac{a_{ScOH^{2+}(aq)}}{a_{Sc^{3+}(aq)}} = 2{,}934 + 0{,}5\cdot\lg\frac{a_{Sc_2(OH)_2^{4+}(aq)}}{a^2_{Sc^{3+}(aq)}}$
2	$\begin{cases} Sc(OH)_2^+(aq)+H^+(aq) \rightleftharpoons ScOH^{2+}(aq)+H_2O(l); \\ 2Sc(OH)_2^+(aq)+2H^+(aq) \rightleftharpoons Sc_2(OH)_2^{4+}(aq)+2H_2O(l) \end{cases}$	$pH = 5{,}387 + \lg\frac{a_{Sc(OH)_2^+(aq)}}{a_{ScOH^{2+}(aq)}} = 6{,}719 + 0{,}5\cdot\lg\frac{a^2_{Sc(OH)_2^+(aq)}}{a_{Sc_2(OH)_2^{4+}(aq)}}$
3	$Sc(OH)_4^-(aq)+2H^+(aq) \rightleftharpoons Sc(OH)_2^+(aq)+2H_2O(l)$	$pH = 8{,}673 + 0{,}5\cdot\lg\frac{a_{Sc(OH)_4^-(aq)}}{a_{Sc(OH)_2^+(aq)}}$
4	$Sc_2O_3(s)+6H^+(aq) \rightleftharpoons 2Sc^{3+}(aq)+3H_2O(l)$	$pH = 1{,}887 - \frac{1}{3}\cdot\lg a_{Sc^{3+}(aq)}$
5	$\begin{cases} Sc_2O_3(s)+4H^+(aq) \rightleftharpoons 2ScOH^{2+}(aq)+H_2O(l); \\ Sc_2O_3(s)+4H^+(aq) \rightleftharpoons Sc_2(OH)_2^{4+}(aq)+H_2O(l) \end{cases}$	$pH = 0{,}698 - 0{,}5\cdot\lg a_{ScOH^{2+}(aq)} = 1{,}364 - 0{,}25\cdot\lg a_{Sc_2(OH)_2^{4+}(aq)}$
6	$Sc_2O_3(s)+H_2O(l)+2H^+(aq) \rightleftharpoons 2Sc(OH)_2^+(aq)$	$pH = -3{,}991 - \lg a_{Sc(OH)_2^+(aq)}$
7	$2Sc(OH)_4^-(aq)+2H^+(aq) \rightleftharpoons Sc_2O_3(s)+5H_2O(l)$	$pH = 21{,}337 + \lg a_{Sc(OH)_4^-(aq)}$
8	$Sc^{3+}(aq)+3e^- \rightleftharpoons Sc(hcp)$	$E = -2{,}025 + 0{,}0197\cdot\lg a_{Sc^{3+}(aq)}$
9	$\begin{cases} ScOH^{2+}(aq)+H^+(aq)+3e^- \rightleftharpoons Sc(hcp)+H_2O(l); \\ Sc_2(OH)_2^{4+}(aq)+2H^+(aq)+6e^- \rightleftharpoons 2Sc(hcp)+2H_2O(l) \end{cases}$	$E = -1{,}941 - 0{,}0197\cdot pH + 0{,}0197\cdot\lg a_{ScOH^{2+}(aq)} = -1{,}967 - 0{,}0197\cdot pH + 0{,}0099\cdot\lg a_{Sc_2(OH)_2^{4+}(aq)}$
10	$Sc(OH)_2^+(aq)+2H^+(aq)+3e^- \rightleftharpoons Sc(hcp)+2H_2O(l)$	$E = -1{,}835 - 0{,}0394\cdot pH + 0{,}0197\cdot\lg a_{Sc(OH)_2^+(aq)}$
11	$Sc_2O_3(s)+6H^+(aq)+6e^- \rightleftharpoons 2Sc(hcp)+3H_2O(l)$	$E = -1{,}914 - 0{,}0591\cdot pH$
12	$Sc(OH)_4^-(aq)+4H^+(aq)+3e^- \rightleftharpoons Sc(hcp)+4H_2O(l)$	$E = -1{,}493 - 0{,}0788\cdot pH + 0{,}0197\cdot\lg a_{Sc(OH)_4^-(aq)}$
13	$Sc^{3+}(aq)+2H^+(aq)+5e^- \rightleftharpoons ScH_2(s)$	$E = -0{,}889 - 0{,}0236\cdot pH + 0{,}0118\cdot\lg a_{Sc^{3+}(aq)}$

14	$\begin{cases} ScOH^{2+}\ (aq)+3H^{+}(aq)+5e^{-} \rightleftharpoons ScH_2\ (s)+H_2O\ (l); \\ Sc_2(OH)_2^{4+}\ (aq)+6H^{+}(aq)+10e^{-} \rightleftharpoons 2ScH_2\ (s)+2H_2O\ (l) \end{cases}$	$E=-0,839-0,0355\cdot pH+0,0118\cdot \lg a_{ScOH^{2+}\ (aq)}=-0,855-0,0355\cdot pH+0,0059\cdot \lg a_{Sc_2(OH)_2^{4+}(aq)}$
15	$Sc(OH)_2^{+}\ (aq)+4H^{+}(aq)+5e^{-} \rightleftharpoons ScH_2\ (s)+2H_2O\ (l)$	$E=-0,775-0,0473\cdot pH+0,0118\cdot \lg a_{Sc(OH)_2^{+}(aq)}$
16	$Sc_2O_3\ (s)+10H^{+}(aq)+10e^{-} \rightleftharpoons 2ScH_2\ (s)+3H_2O\ (l)$	$E=-0,822-0,0591\cdot pH$
17	$Sc(OH)_4^{-}\ (aq)+6H^{+}(aq)+5e^{-} \rightleftharpoons ScH_2\ (s)+4H_2O\ (l)$	$E=-0,570-0,0790\cdot pH+0,0118\cdot \lg a_{Sc(OH)_4^{-}(aq)}$
18	$2Sc^{3+}(aq)+xH_2O\ (l)+(6-2\cdot x)e^{-} \rightleftharpoons Sc_2O_x\ (s)+2\cdot xH^{+}(aq);$ $2,89 \leqslant x < 3$	$E=\frac{-0,419\cdot x^2-0,656\cdot x+6,076}{x-3}-\frac{0,0591\cdot x}{x-3}\cdot pH-\frac{0,0591}{x-3}\cdot \lg a_{Sc^{3+}(aq)}$
19	$Sc_2O_x\ (s)+2\cdot x\ H^{+}(aq)+2\cdot x\ e^{-} \rightleftharpoons 2Sc\ (hcp)+x\ H_2O\ (l);$ $2,89 \leqslant x < 3$	$E=-0,419\cdot x-0,656-0,0591\cdot pH$
20	$2Sc(OH)_4^{-}(aq)+(8-2\cdot x)H^{+}(aq)+(6-2\cdot x)e^{-} \rightleftharpoons$ $\rightleftharpoons Sc_2O_x\ (s)+(8-x)\ H_2O\ (l);\ 2,89 \leqslant x < 3$	$E=\frac{-0,419\cdot x^2-0,656\cdot x+4,495}{x-3}-\frac{0,0591\cdot (x-4)}{x-3}\cdot pH-\frac{0,0591}{x-3}\cdot \lg a_{Sc(OH)_4^{-}(aq)}$

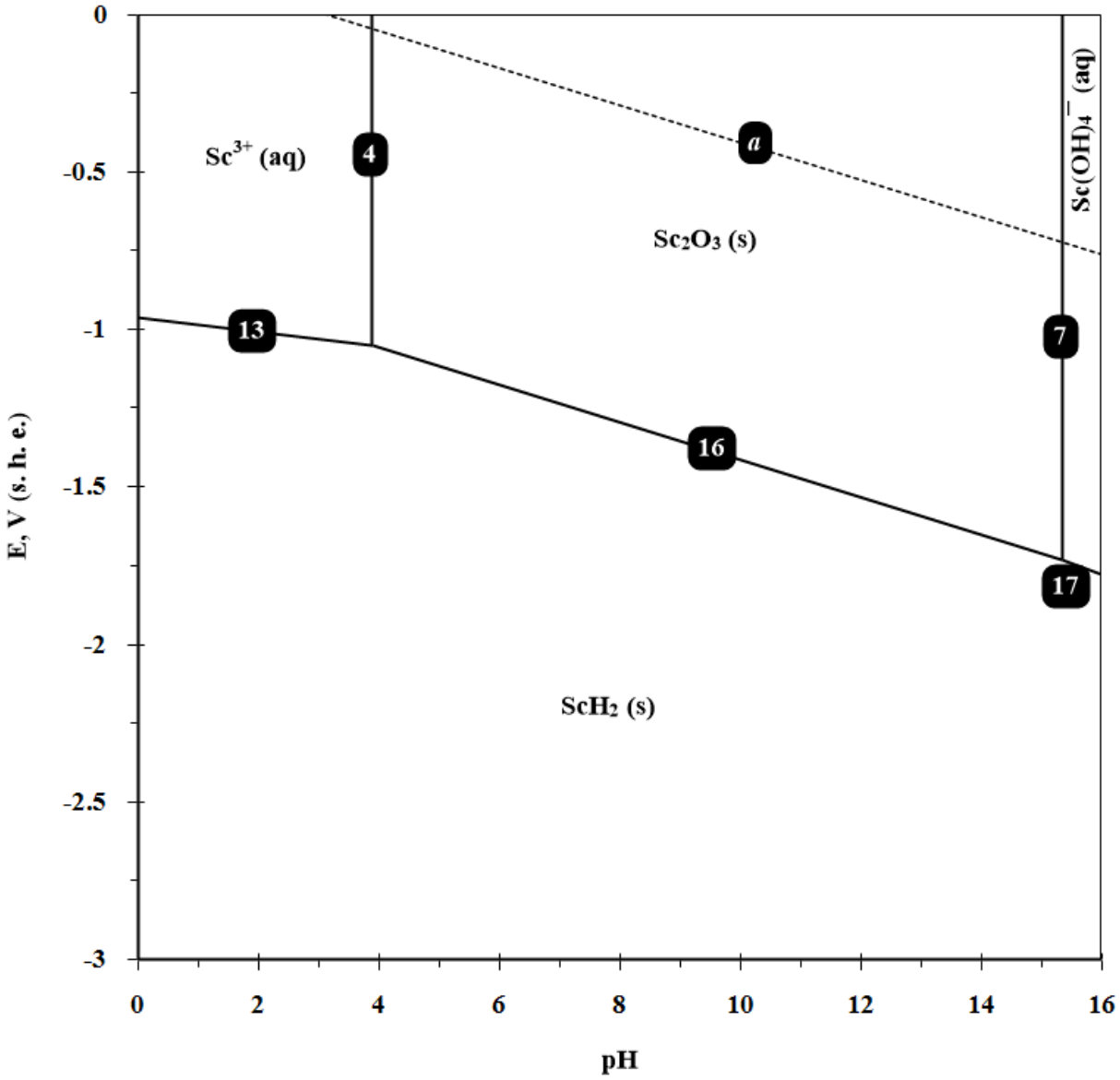

Fig. 7. The potential – pH diagram of Sc – H_2O system at 298 K, air pressure of 1 bar and activities of ions in solutions $a_i = 10^{-6}$ M with consideration of scandium hydride.
Рис. 7. Диаграмма потенциал – pH системы Sc – H_2O при 298 K, давлении воздуха 1 бар и активностях ионов в растворе $a_i = 10^{-6}$ М с учётом гидрида скандия.

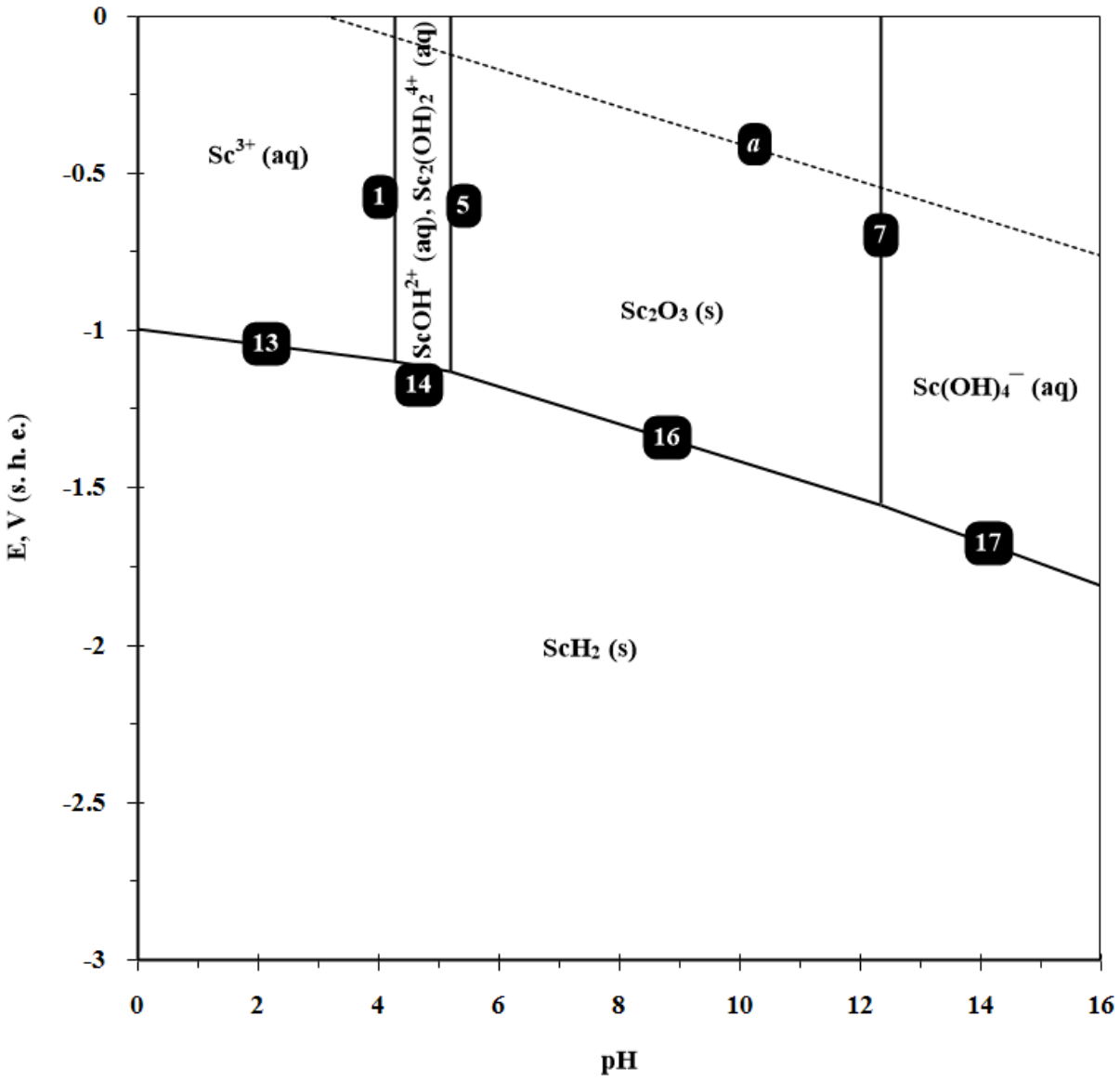

Fig. 8. The potential – pH diagram of Sc – H_2O system at 298 K, air pressure of 1 bar and activities of ions in solutions $a_i = 10^{-9}$ M with consideration of scandium hydride.
Рис. 8. Диаграмма потенциал – pH системы Sc – H_2O при 298 K, давлении воздуха 1 бар и активностях ионов в растворе $a_i = 10^{-9}$ M с учётом гидрида скандия.

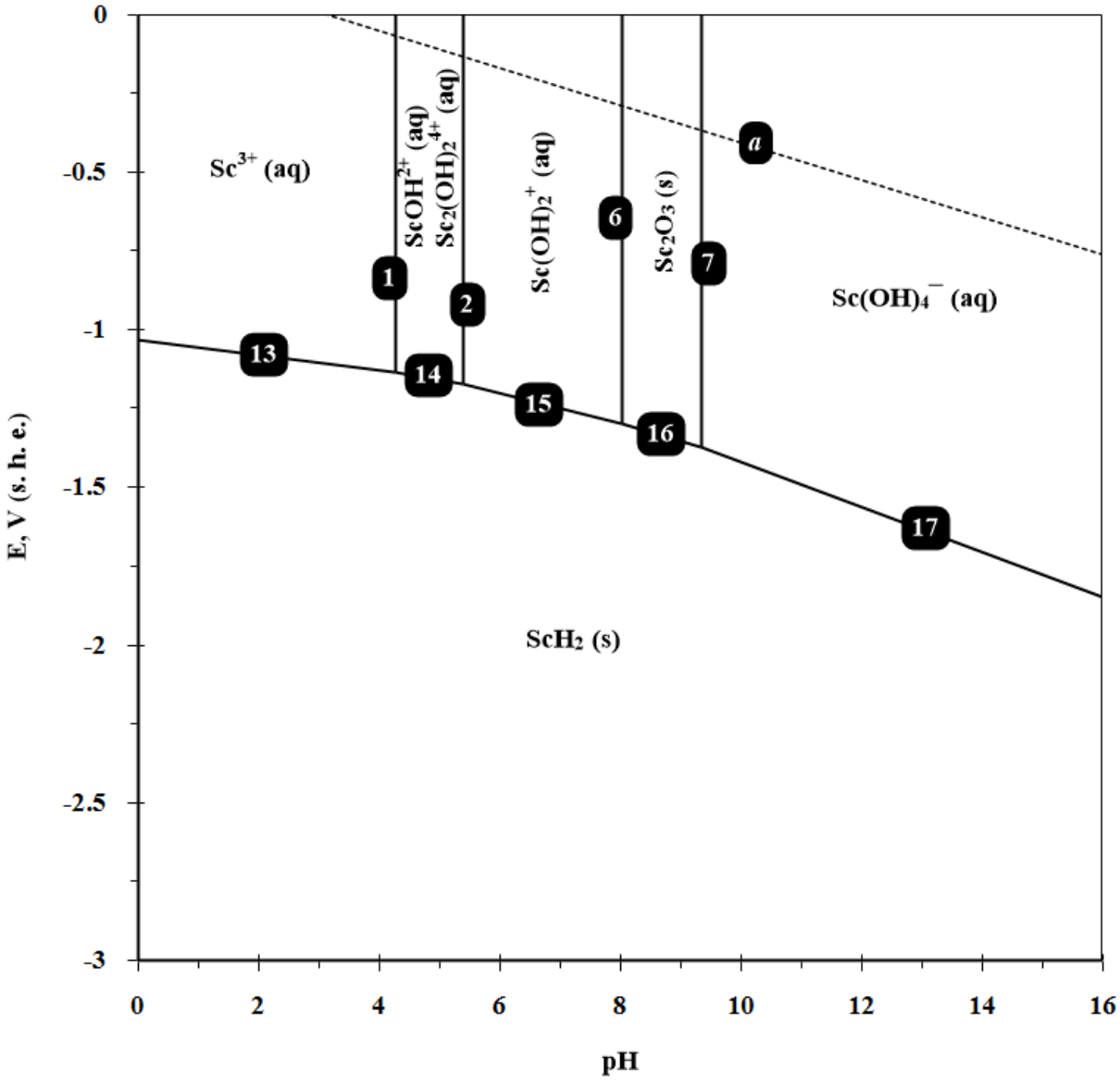

Fig. 9. The potential – pH diagram of Sc – H_2O system at 298 K, air pressure of 1 bar and activities of ions in solutions $a_i = 10^{-12}$ M with consideration of scandium hydride.
Рис. 9. Диаграмма потенциал – pH системы Sc – H_2O при 298 K, давлении воздуха 1 бар и активностях ионов в растворе $a_i = 10^{-12}$ М с учётом гидрида скандия.

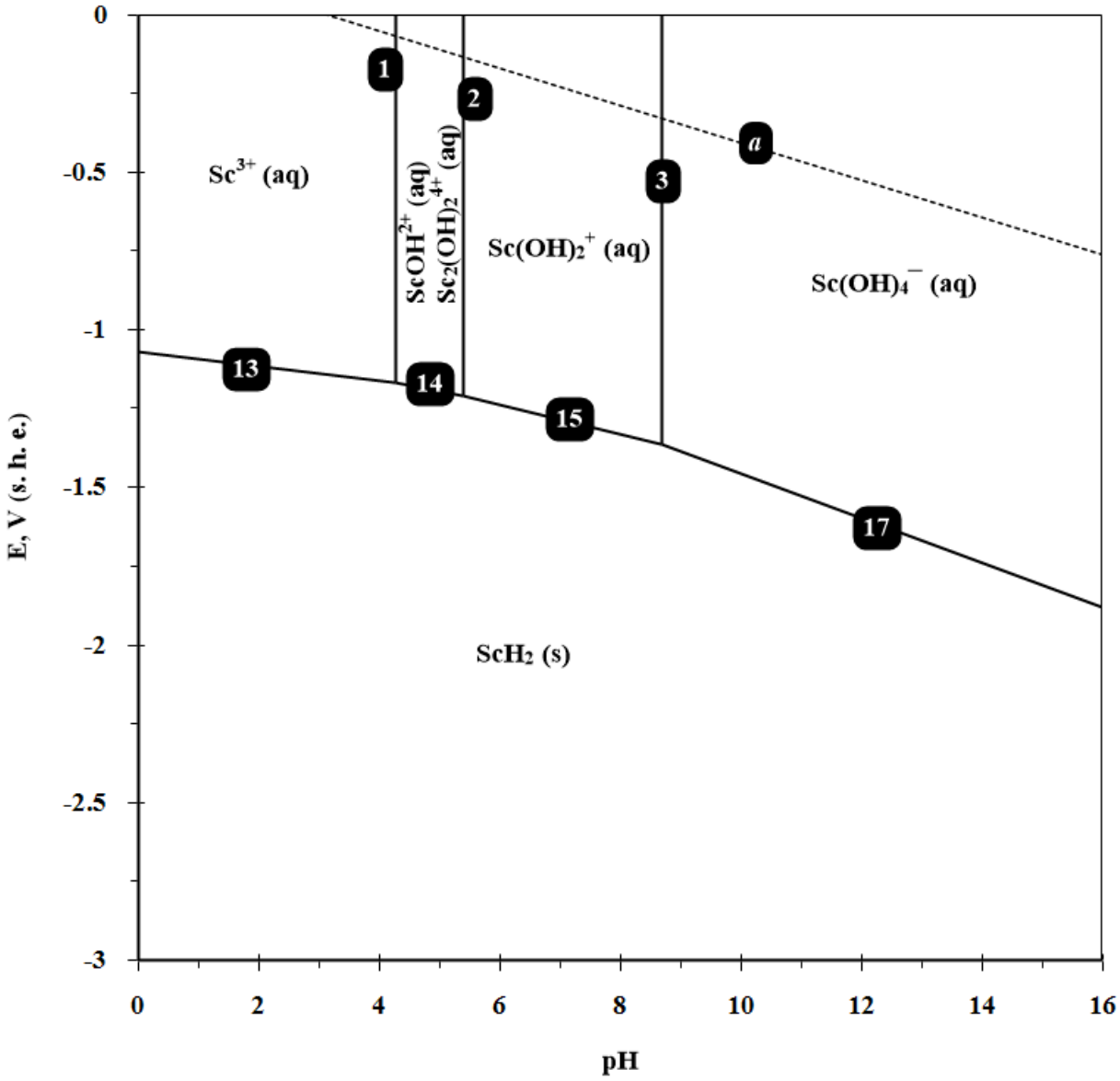

Fig. 10. The potential – pH diagram of Sc – H_2O system at 298 K, air pressure of 1 bar and activities of ions in solutions $a_i = 10^{-15}$ M with consideration of scandium hydride.
Рис. 10. Диаграмма потенциал – pH системы Sc – H_2O при 298 K, давлении воздуха 1 бар и активностях ионов в растворе $a_i = 10^{-15}$ M с учётом гидрида скандия.

7. Conclusions

The dimerisation of the ion $ScOH^{2+}$ (aq) was considered, and it was shown that the dimeric form predominates in concentrated solutions, whereas the monomeric form predominates in diluted media. The polynuclear ions $Sc_3(OH)_4^{5+}$ (aq) and $Sc_3(OH)_5^{4+}$ (aq) have no domains of thermodynamic stability.

The revised potential – pH diagrams of Sc – H_2O system presented in this study, take into account the possible formation of various hydrolysed scandium species with alteration of the activities of ions in a solution. For the solutions with moderate content of scandium these diagrams are consistent with the previously published ones.

The corrosion properties of scandium are similar to that of aluminum; in most environments the passivation layer on the surface of metal consists of Sc_2O_3 (s). The possible formation of scandium hydride ScH_2 (s) shifts the borders of scandium active dissolution, but does not affect its properties in the domain

of electrochemical stability of water. The scandium nitride ScN (s) is not thermodynamically stable in aqueous solutions in presence of pure scandium and scandium hydride.

An attempt to estimate the corrosion properties of non-stoichiometric scandium oxide Sc_2O_x ($2{,}89 \leqslant x < 3$) was performed. Using Kireev's method the standard Gibbs energy of formation of ScO (s) was estimated and then, using Gorichev's method the dependency of $\Delta_f G^\circ_{298}(Sc_2O_x)$ on x was also estimated. Thermodynamic prediction shows that with increase of the degree of homogeneity of Sc_2O_x its domain of passivity in the potential – pH diagram narrows.

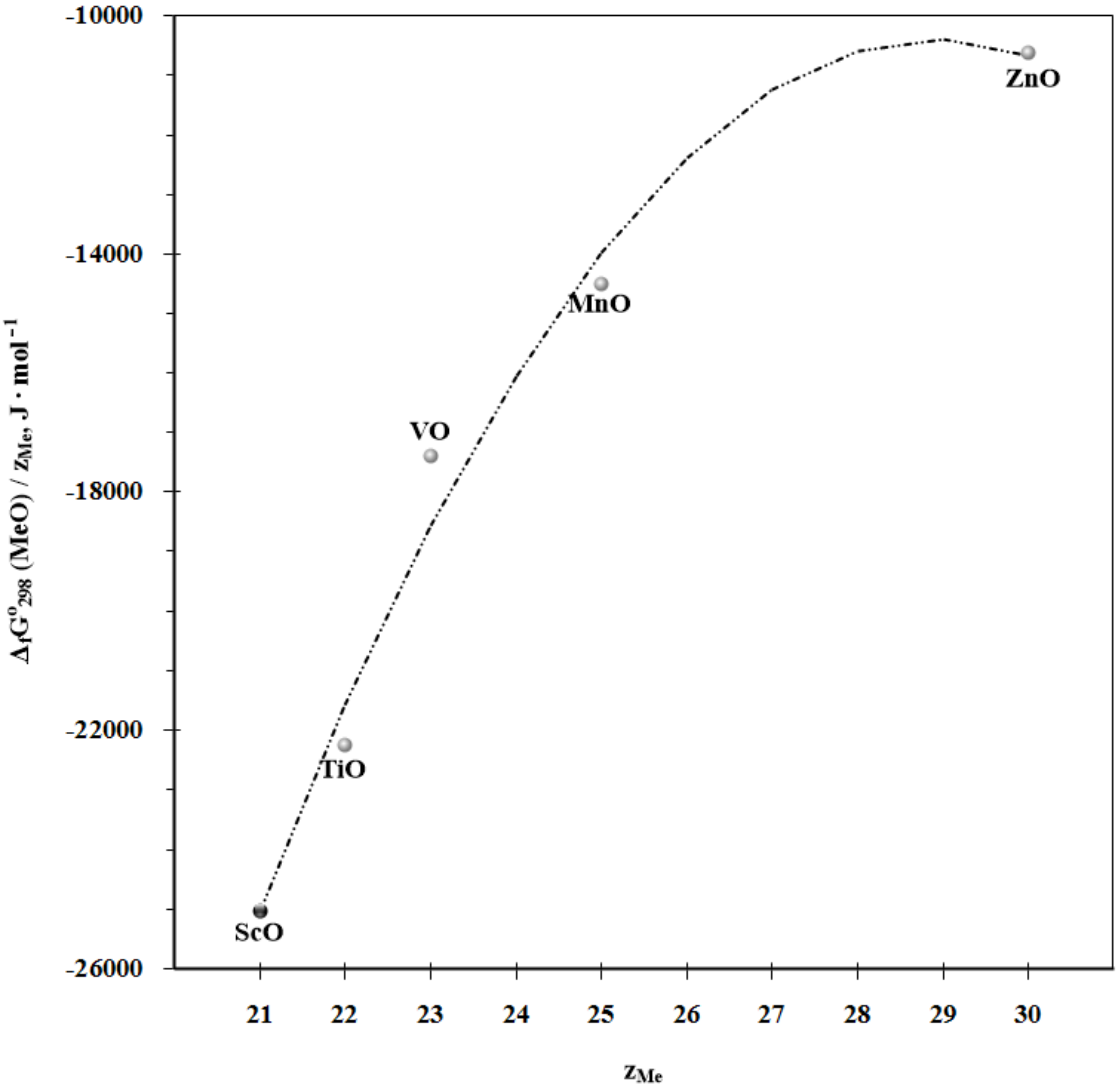

Fig. 11. The relationship between the standard Gibbs energies of formation of some transition metals monoxides and the atomic numbers of metals.

Рис. 11. Зависимость между стандартными энергиями Гиббса образования моноксидов некоторых переходных металлов и атомными номерами металлов.

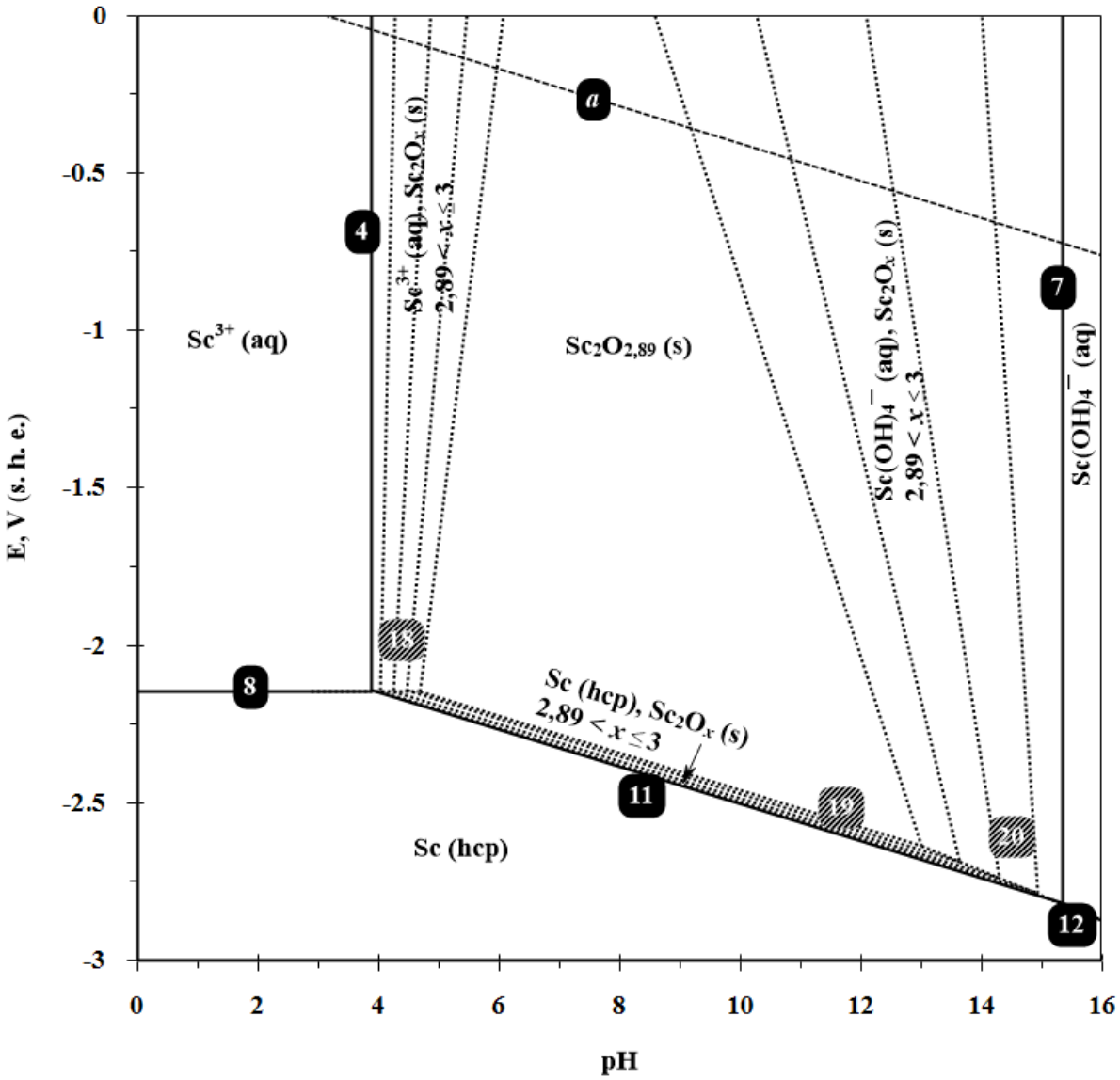

Fig. 12. The hypothetical potential – pH diagram of Sc – H_2O system at 298 K, air pressure of 1 bar and activities of ions in solutions $a_i = 10^{-6}$ M with consideration of non-stoichiometry of scandium sesquioxide.

Рис. 12. Гипотетическая диаграмма потенциал – pH системы Sc – H_2O при 298 K, давлении воздуха 1 бар и активностях ионов в растворе $a_i = 10^{-6}$ M с учётом нестехиометрии сесквиоксида скандия.

References

Список литературы

1. Akalin S., Özer U.Y. 1971. Hydrolysis of Sc_{aq}^{3+} and the stabilities of scandium (III)-Tiron chelates in aqueous solution. Journal of Inorganic and Nuclear Chemistry. 33(12): 4171–4180.

2. Aksel'rud N. V. 1963. Hydroxide chlorides and hydroxides of elements of the scandium subgroup and of the lanthanides. Russian Chemical Reviews. 32(7): 353–366.

3. Alimarin I.P., Yung-Schaing T. 1961. Separation and determination of scandium using N-benzoylphenylhydroxylamine. Talanta. 8(5): 317–321.

4. Antonovich V.P., Nazarenko V.A. 1968. Spectrophotometric determination of the hydrolysis constants of scandium ions. Russian Journal of Inorganic Chemistry. 13(7): 940 – 941.

5. Arkharov V.I., Kichigina Z.P. 1966. Surface Interactions between Metals and Gases. New York: Consultants Bureau. 101 – 103.

6. Aveston J. 1966. Hydrolysis of scandium(III): ultracentrifugation and acidity measurements Journal of Chemical Society A: Inorganic, Physical, Theoretical. 1599 – 1601.
7. Baes Jr. C.F., Mesmer R.E. 1976. The Hydrolysis of Cations. New York: Wiley. 254 p.
8. Bashkin I.O., Ponyatovskii E.G., Kost M.E. 1978. Phase Transformations in Hydrides of Rare-Earth Metals under Pressure. II. The Sc-H and Yb-H Systems under High Hydrogen Pressure. Physica Status Solidi. 87(1): 369–372.
9. Biedermann G. et al. 1956. Studies on the Hydrolysis of Metal Ions. 18. The Scandium Ion, Sc^{3+}. Acta Chemica Scandinavica. 10: 1327–1339.
10. Bommer H., Hohmann E. 1941. Zur Thermochemie der seltenen Erden. I. Die Lösungswärmen der Metalle der seltenen Erden. Zeitschrift für Anorganische und Allgemeine Chemie. 248(4): 357–372 (In German).
11. Brookins D.G. 1988. E_h - pH Diagrams for Geochemistry. Berlin, Heidelberg: Springer-Verlag. 183 p.
12. Cole D.L. et al. 1969. Kinetics of aqueous scandium(III) perchlorate hydrolysis and dimerization. Inorganic Chemistry. 8(3): 682–685.
13. Diagrammy sostoâniâ dvojnyh metalličeskih sistem: spravočnik. 2001. Editor N. P. Lyakishev. Moscow: Mašinostroenie. 872 p (In Russian).
14. Dufek V., Brožek V., Petrů F. 1969. Zur Existenz des Seandiummonoxides. Monatshefte für Chemie. 100(5): 1628–1630 (In German).
15. Dufek V., Petrů F., Brožek V. 1967. Über Sauerstoff-haltige Verbindungen vom Strukturtyp B1 der ersten vier Übergangsmetalle. Monatshefte für Chemie. 98(6): 2424–2430 (In German).
16. Feitknecht W., Schindler P. 1963. Solubility constants of metal oxides, metal hydroxides and metal hydroxide salts in aqueous solution. Pure and Applied Chemistry. 6(2): 125 – 206.
17. Gerstein B.C. 1971. Heat Capacity of Scandium from 6 to 350 °K. .Journal of Chemical Physics. 54(11): 4723–4737.
18. Gorichev I.G., Klyushin N.G. 1971. Dependence of standard electrode potentials and free-energies of some oxides on their stoichiometric composition. Russian Journal of Physical Chemistry A. Focus on Chemistry. 45(4): 615.
19. Gschneider Jr. K.A. 1961. Rare Earth Alloys: A Critical Review of the Alloy Systems of the Rare Earth, Scandium, and Yttrium Metals. New Jersey: Van Nostrand. 449 p.
20. Haas J.R., Shock E.L., Sassani D.C. 1995. Rare earth elements in hydrothermal systems: Estimates of standard partial molal thermodynamic properties of aqueous complexes of the rare earth elements at high pressures and temperatures. Geochimica et Cosmochimica Acta. 59(21): 4329–4350.
21. Horovitz C.T. et al. 1975. Scandium: Its Occurrence, Chemistry Physics, Metallurgy, Biology and Technology. London: Academic Press. 614 p.
22. Huber E.J. et al. 1963. The heat of formation of scandium oxide. Journal of Physical Chemistry. 67(8): 1731–1733.
23. Jerosch-Herold M., Torgeson D.., Barnes R.. 1997. Systematics of the anomalous high-temperature ^{45}Sc spin–lattice relaxation in scandium hydrides and deuterides. Journal of Alloys and Compounds. 1997. 253-254: 441–444.
24. Jichang B., Ke'ren H. 1984. Shi er wan ji liu suan na cun zai xia zuo duo yuan luo he wu xian se fan ying de yan jiu. Hua xue shi ji. 6(2): 118 – 119 (In Chinese).
25. Kilpatrick M., Pokras L. 1953. Acid Dissociation of the Aquoscandium Ions. Journal of Electrochemical Society. 100(2): 85 – 92.
26. Kilpatrick M., Pokras L. 1954. The Acid Dissociation of the Aquoscandium Ions. Journal of Electrochemical Society. 101(1): 39 – 43.
27. Kireev V. A.. 1970. Metody praktičeskih rasčëtov v termodinamike himičeskih reakcij. Moscow: Himiâ. 520 p (In Russian).
28. Kobayashi T., Takei H. 1978. Chemical vapor deposition of scandium hydride. Journal of Crystal Growth. 45: 29–36.
29. Kobayashi T., Takei H. 1980. Chemical vapour deposition of scandium metal. Journal of the Less Common Metals. 70(2): 243–252.
30. Komissarova L. N. 2001. Neorganičeskaâ i analitičeskaâ himiâ skandiâ. Moscow: Èditorial URSS. 512 p (In Russian).
31. Komissarova L.N., Prutkova N.M., Pushkina G.Y. 1971. Stability of hydroxo-ions of scandium in aqueous solution. Russian Journal of Inorganic Chemistry. 16(7): 954 – 956.

32. Kuprashvili I.S., Naumkin O.P., Savitskii E.M. 1969. Phase diagram of the Scandium - Oxygen system. Inorganic Materials. 5(12): 1809 – 1813.
33. Lieberman M.L., Wahlbeck P.G. 1965. The Thermodynamics of the Scandium-Hydrogen System. Journal of Physical Chemistry. 69(10): 3514–3519.
34. Lindqvist-Reis P., Persson I., Sandström M. 2006. The hydration of the scandium (III) ion in aqueous solution and crystalline hydrates studied by XAFS spectroscopy, large-angle X-ray scattering and crystallography. Dalton Transactions. 32: 3868–3878.
35. Marques R.N. et al. 1997. Complexation of some trivalent lanthanides, scandium(III) and thorium(IV) by benzylidenepyruvates in aqueous solution. Journal of Alloys and Compounds. 249(1–2): 102–105.
36. Meijering E. 2002. A chronology of interpolation: from ancient astronomy to modern signal and image processing. Proceedings of the Institute of Electrical and Electronic Engineers. 90(3): 319–342.
37. Moeller T., Kremers H.E. 1945. The Basicity Characteristics of Scandium, Yttrium, and the Rare Earth Elements. Chemical Reviews. 57(1): 97–159.
38. Oka Y. 1938. Bunseki kagaku ni okeru kiso-teki han'nō no kenkyū. Watashi kinzoku ion to kasei sōda no han'nō. Nippon Kagaku Kaishi. 59(8): 971–1013 (In Japanese).
39. Pankratz L.B., Stuve J.M., Gokcen M.A. 1984. Thermodynamic Data for Mineral Technology. USA: Bureau of Mines. 360 p.
40. Paul A.D.1962. The chloride and bromide complexing of scandium (III) and yttrium (III) in aqueous solution. Journal of Physical Chemistry. 66(7): 1248–1252.
41. Petrů F., Brožek V., Dufek V. 1970. Contribution to the chemistry of the rarer elements. LXI. Contribution to the study of the structure of scandium monoxide. Collection of Czechoslovak Chemical Communications. 35(4): 1041–1046.
42. Pourbaix M. 1974. Atlas of Electrochemical Equilibria in Aqueous Solutions. Oxford: Pergamon Press.
43. Predel B. 1998. O-Sc (Oxygen-Scandium). Ni-Np–Pt-Zr. Berlin/Heidelberg: Springer-Verlag. 1–2.
44. Progress in the Science and Technology of the Rare Earths. 2013. Editor L. Eyring. Amsterdam: Elsevier. 540 p.
45. Rayner-Canham G. 2013. Periodic patterns: the Group (n) and Group (n + 10) linkage. Foundation of Chemistry. 15(2): 229–237.
46. Robie R.A., Hemingway B.S., Fisher J.R.1979. Thermodynamic Properties of Minerals and Related Substances at 298.15 K and 1 Bar (10^5 Pascals) Pressure and at Higher Temperatures. Washington: U. S. Government Printing Office. 2nd edition. 464 p.
47. Ruzinov L. P., Gulyanitskii B. S. 1975. Ravnovesnye prevraŝeniâ metallurgičeskih reakcij. Moscow: Metallurgiâ. 417 p (In Russian).
48. Santamaria M., Muratore F., Quarto F. Di. 2013. Growth and Characterization of Anodic Films on Scandium. Journal of Electrochemical Society. 161(1): C36–C41.
49. Schweitzer G.K., Pesterfield L.L. 2010. The Aqueous Chemistry of the Elements. Oxford: Oxford University Press. 447 p.
50. Sekine T., Hasegawa Y. 1966. Studies of Scandium in Various Solutions. I. An Ion-Exchange Study of Scandium(III) Chloride and Nitrate Complexes. Bulletion of Chemical Society of Japan. 39(2): 240–243.
51. Siqueira O.S. et al. 1995. Complexation of some trivalent lanthanides, scandium(III) and thorium(IV) by benzylidenepyruvates and cinnamylidenepyruvate in aqueous solution. Journal of Alloys and Compounds. 225(1-2): 267–270.
52. Speight J.G. 2005. Lange's Handbook of Chemistry. New York: McGraw-Hill. 16th edition.
53. Switendick A.C. 1989. Electronic Structure and Properties of Scandium, Titanium, and Yttrium Hydride Systems. Zeitschrift für Physikalische Chemie. 163(Part 2): 527.
54. Takeno N. 2005. Atlas of E_h–pH Diagrams. Intercomparison of Thermodynamic Databases. Open File Report No. 419.
55. Termičeskie konstanty veŝestv. Available at: http://www.chem.msu.ru/cgi-bin/tkv.pl?show=welcome.html. Access date – 27. 08. 2016 (In Russian).
56. Travers J.G., Dellien I., Hepler L.G. 1976. Scandium: Thermodynamic properties, chemical equilibria, and standard potentials. Thermochimica Acta. 15(1): 89–104.
57. Türkel N., Aydin R., Özer U. 1999. Stabilities of complexes of Scandium (III) and Yttrium (III) with salicylic acid. Turkish Journal of Chemistry 23(3): 249 – 256.
58. Veryagin U. D. et al. 1965. Termodinamičeskie svojstva neorganičeskih veŝestv: spravočnik. Editor A. P. Zefirov. Moscow: Atomizdat, 461 p (In Russian).

59. Wagman D.D. et al. 1982. The NBS tables of chemical thermodynamic properties. Selected values for inorganic and C_1 and C_2 organic substances in SI units. Journal of Physical and Chemical Reference Data. 11(Supplement 2).
60. Wang W. et al. 2013. $[Sc_2(\mu\text{-}OH)_2(H_2O)_6(NO_3)_2](NO_3)_2$: Aqueous Synthesis and Characterization. Inorganic Chemistry. 52(4): 1807–1811.
the Royal Society of London. 69: 59–67.
61. Wloka J., Virtanen S. 2007. Influence of scandium on the pitting behaviour of Al–Zn–Mg–Cu alloys. Acta Materialia. 55(19): 6666–6672.
62. Wood S.A., Samson I.M. 2006. The aqueous geochemistry of gallium, germanium, indium and scandium. Ore Geology Reviews. 28(1): 57–102.
63. Work D.E., Eick H.A. 1972. On the preparation of condensed ScO. Journal of the Less Common Metals. 26(3): 413–416.
64. Wu D. et al. 2004. Solvent extraction of scandium(III), yttrium(III), lanthanum(III) and gadolinium(III) using Cyanex 302 in heptane from hydrochloric acid solutions. Journal of Alloys and Compounds. 374(1-2): 442–446.
65. Young Jr. J.E., Sienko M.J. 1972. Plasma-synthesized substoichiometric scandium oxide. Solid State Chemistry. Proceedings of the 5th Materials Research Symposium. Editors R.S. Roth, S.J. Schneider. National Bureau of Standards (U.S.). 385 – 395.
66. Yudin B. F. et al. 1976. Žurnal prikladnoj himii. 49: 776 – 780 (In Russian).
67. Zhuk N. P. 1954. Termodinamicheskie postoyannye trudnorastvorimykh v vode galogenidov, sulfidov, okislov i gidratov okislov metallov Žurnal fizičeskoj himii. 28(8): 1523 – 1527 (In Russian).

Уточнённая диаграмма потенциал–pH системы Sc – H_2O

Павел Анатольевич Николайчук

Кафедра аналитической и физической химии, Челябинский государственный университет, Челябинск, 454001, ул. Братьев Кашириных, 129, Российская Федерация. E-mail: npa@csu.ru.

Аннотация: Собраны и систематизированы термодинамические данные о стандартных энергия Гиббса образования различных соединений скандия в твёрдом состоянии и в водном растворе. Построена диаграмма распределения для реакции $2ScOH^{2+}\,(aq) \rightleftharpoons Sc_2(OH)_2^{4+}\,(aq)$. Обсуждены равновесия между различными гидратированными формами скандия (III) в водном растворе. Построены диаграммы потенциал–pH системы Sc – H_2O при 25°C, давлении воздуха 1 бар и различных активностях ионов в растворе. Обсуждено возможное влияние электрохимического образования гидрида скандия и нестехиометрии сесквиоксида скандия на коррозионно-электрохимические свойства скандия.

Ключевые слова: скандий, оксид скандия, гидрид скандия, нитрид скандия, нестехиометрия, водные соединения скандия, диаграмма распределения, диаграмма активность – pH, диаграмма потенциал – pH, коррозионно-электрохимическое поведение.

5. Ti – Si system
5.1. Titanium silicides

Titanium silicides are used as cathodes in vacuum arc during the synthesis of superhard nanocrystal coatings [Korosteleva, Pribytkov, Gurskikh, 2009]. They reveal high corrosion resistance in both reducing and oxidizing environments and can be characterized by stability of the passive state [Jiang, Dai, Middleton, 2011].

The following silicides exist in Ti – Si system at 25˚C [Du et al., 2000; Racault, Langlais, Bernard, 1994]: Ti_3Si, Ti_5Si_3, Ti_5Si_4, TiSi and $TiSi_2$. It was reported [Bandyopadhyay, 2004] about the compounds Ti_3Si_4 and Ti_6Si_5, however, there are no confirmations of their existence in other literature. The silicide Ti_5Si_3 have wide homogeneity range at elevated temperature, but it can be considered as stoichiometric compound at 25˚C; other silicides do not have any homogeneity ranges. The maximum solid solubility of Si in (hcp-Ti) equals ~3.3 atomic percents at 1000˚C and only ~0.7 at. % at 800˚C, therefore it is vanishingly small at standard temperature and thus might be neglected. The solubility of Ti in (diamond-Si) is about 10^{-17} at. % at 1100˚C [Miki, Morita, Sano, 1997; Yoshikawa et al., 2010]. The values of standard Gibbs energies of formation of titanium silicides were taken from [Vahlas, Chevalier, Blanquet, 1989]. The phase diagram of the Ti – Si system is presented in Figure 19.

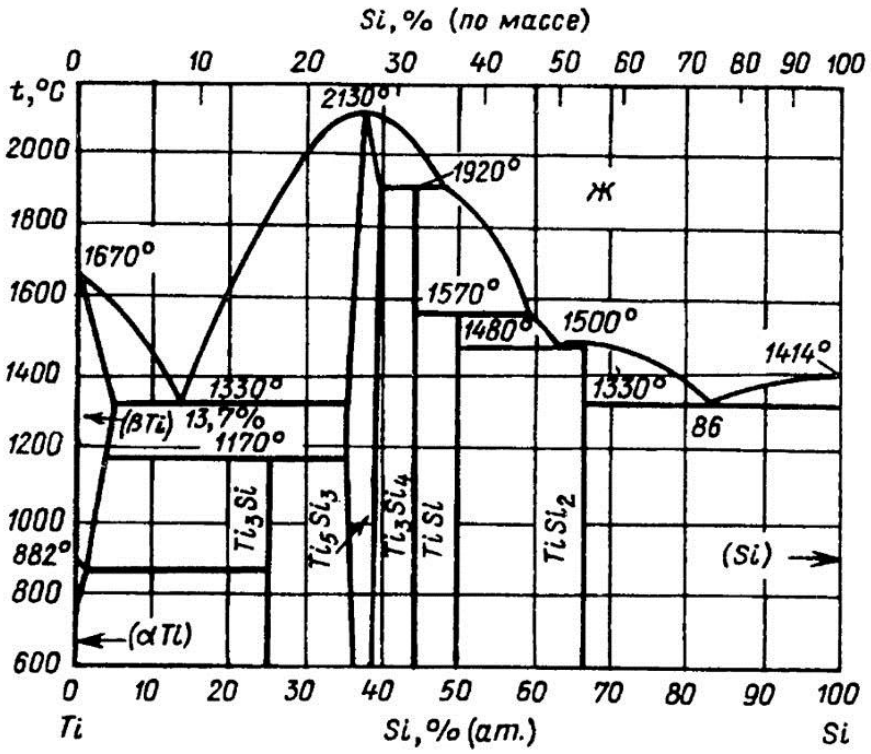

Fig. 19. The phase diagram of the Ti – Si system [Диаграммы состояния двойных металлических систем: справочник, 2001].

5.2. Equilibira in Ti – Si – O system

The phase diagram of Ti – O system reveals a large number of titanium oxides and suboxides at 25 °C – Ti_6O, Ti_3O, Ti_2O, Ti_3O_2, TiO, Ti_2O_3, Ti_3O_5, Magnéli phases [Andersson, Magnéli, 1956; Arif et al., 2017; Liborio, Harrison, 2008; Padilha et al., 2014; Tang, Zhou, Zhang, 2012] Ti_nO_{2n-1} ($4 \leqslant n \leqslant 10$), TiO_2. There are no compounds in binary TiO_2 – SiO_2 system [Ricker, Hummel, 1951]. The standard Gibbs energies of formation of titanium oxides were taken from [Robie, Hemingway, Fisher, 1979; Термические константы веществ, 2007], and the values for some lower oxides were estimated using the Gorichev's method according to the equation:

$$\Delta_f G^{o}_{298}(Ti_{\frac{1}{x}}O) = 19380 \cdot x^2 + 1055{,}7 \cdot x - 517941,\ {}^{J}\!/_{mol}\ . \qquad (96)$$

The state diagram of the Ti – Si – O system and the thermodynamic characteristics of the equilibria are presented in the attached publication.

5.3. Potential – pH diagram of Ti – H_2O system

Titanium could form the cations Ti^{3+} and TiO^{2+} in an aqueous solution. No titanate-anions could be formed [Atkins et al., 2010; Cotton, Wilkinson, 1971]. The potential – pH diagram for Ti – H_2O system at 25 °C, air pressure of 1 bar and activities of ions in a solution 1 M, taking into account all the aforementioned titanium oxides and cations, is presented in Figure 20.

There are, however, some experimental evidences that titanium in an aqueous media could be electrochemically reduced to the titanium hydride TiH_2. Moreover, the titanium nitride TiN is thermodynamically very stable, and could be formed from aqueous titanium species and atmospheric nitrogen.

Thermodynamic calculations show that in presence of titanium nitride and hydride all titanium oxides except TiO_2 become thermodynamically unstable. The potential – pH diagram for Ti – H_2O system at 25 °C, air pressure of 1 bar and activities of ions in a solution 1 M, taking into account titanium hydride and nitride, is presented in Figure 21.

In any case, all the equilibria involving either lower titanium oxides, or titanium hydride and nitride, take place below the line, corresponding to the hydrogen electrode. It implies that in the domain of electrochemical stability of water the only thermodynamically stable solid product would be

TiO_2. It should also be noted that the predominance domain of titanium cations is very narrow and lies at very low pH values. Consequently, in nearly all aqueous environments titanium forms a protective oxide layer on its surface.

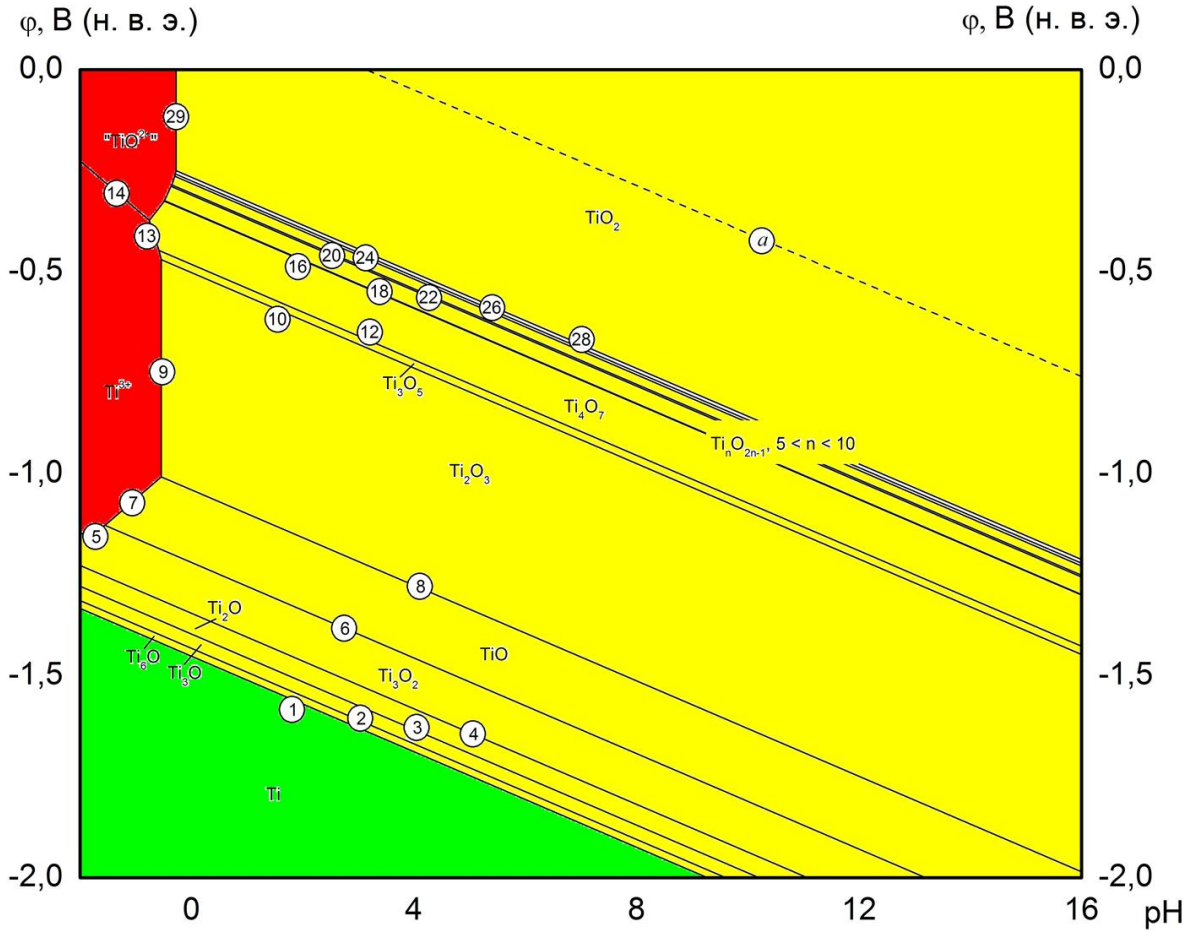

Fig. 20. The potential – pH diagram of the Ti – H_2O system at 25 °C, air pressure of 1 bar and the activities of titanium species in a solution of 1 M without consideration of titanium hydride and nitride.

5.4. Potential – pH diagram of Ti – Si – H_2O system

The potential – pH diagram of Ti – Si – H_2O system is presented in the attached publication.

The calculations show that the presence of titanium hydride and nitride changes the mechanism and the order of titanium silicides oxidation. As can be seen, the full decomposition of titanium silicides to components is the thermodynamically unprofitable process. The presence of silicon in the system can stabilise titanium and prevent it from formation of hydride and further oxidation. This could be explained by a high strength of Ti – Si covalent bonds [Jiang, Dai, Middleton, 2011].

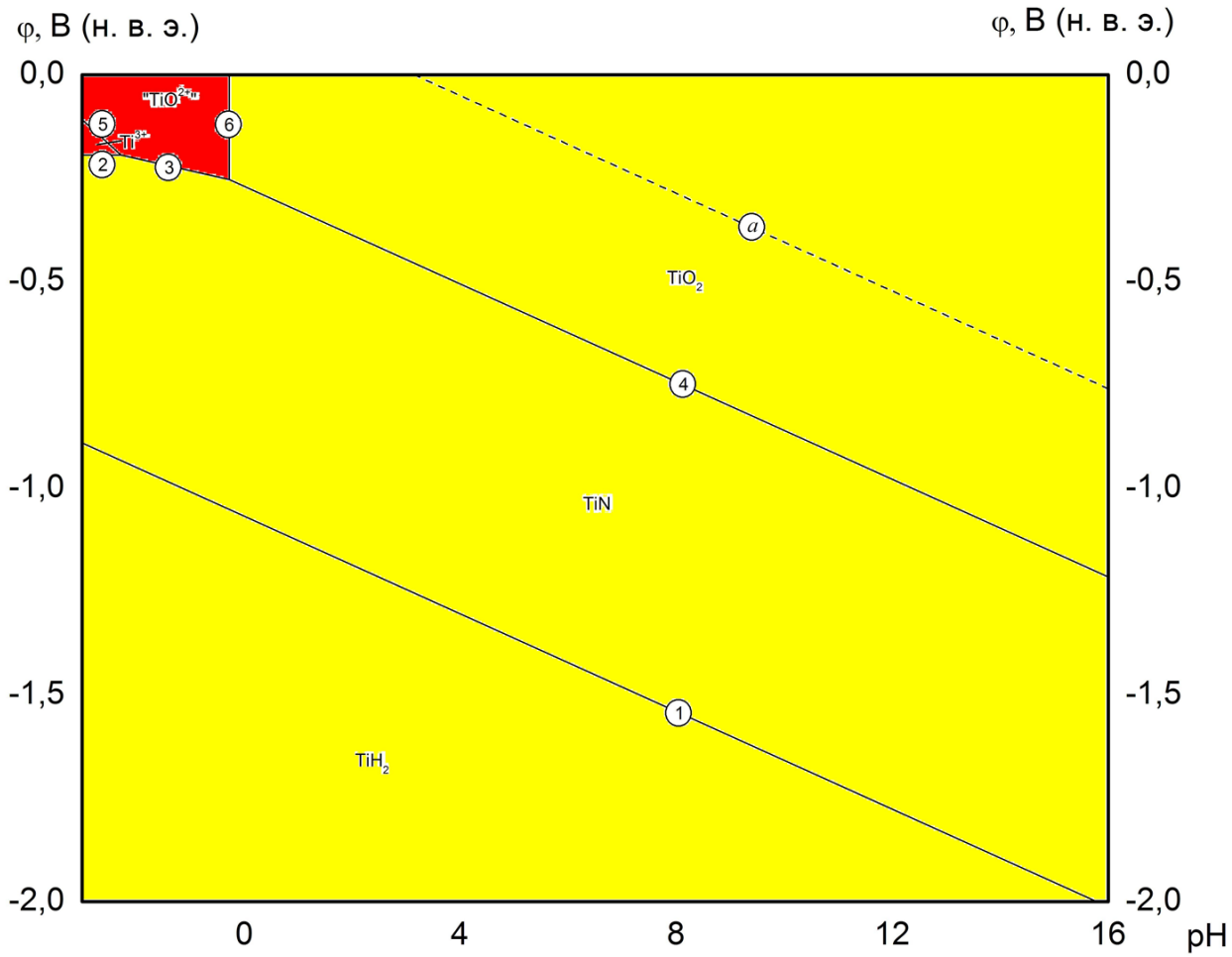

Fig. 21. The potential – pH diagram of the Ti – H_2O system at 25 °C, air pressure of 1 bar and the activities of scandium species in a solution of 1 M with consideration of titanium hydride and nitride.

Publications to chapter 5

This chapter was published in paper [Николайчук, Тюрин, 2011a]. The paper was translated into English with the permission of *Butlerovskoe Nasledie* and posted as a preprint at the website of *Research Gate* (DOI 10.13140/2.1.2738.4003). This English version is presented below.

УДК 541.1:620.193.01:669.14

Thermodynamics of Chemical and Electrochemical Stability of the Ti – Si System Alloys

© **Pavel Anatolyevich Nikolaychuk** [+] and **Aleksandr Georgievich Tyurin***
Department of Analytical and Physical Chemistry. Chelyabinsk State University. Brat'ev Kashirinykh Street, 129,Chelyabinks, 454026, Russia. Phone:+7 (351)799-70-69.
E-mail:npa@csu.ru, tag@csu.ru.

*Supervisor; [+]Corresponding author

Keywords: *titanium silicides, low temperature oxidation, chemical stability, diagram of electrochemical equilibria, electrochemical stability.*

Abstract

A phase diagram of Ti – Si – O system and a potential – pH diagram of Ti – Si – H_2O at 25˚C, air pressure of 1 bar and activities of ions in solution equal to 1 mole/l, with and without consideration of titanium hydride and titanium nitride formation, are plotted. The corrosion-electrochemical behaviour of Ti – Si system alloys is considered from the thermodynamic point of view.

Introduction

Interest in titanium-silicon alloys is increasing in recent years, because they, having lightness, high durability, excellent electrical conductivity and stability at elevated temperatures, are successfully used as sputtering targets (cathodes) in vacuum arc and magnetron synthesis of superhard ion-plasma nanocrystalline coatings [1]. There is evidence about establishing electrical nanochains for modern electronics on the basis of titanium silicides [2]. Moreover, it is shown in papers [3, 4], that titanium silicides (and especially disilicide $TiSi_2$) are perspective courrosion-resistance materials, which can be used in both reducing and oxidizing environments. Their high tendency to passivation and stability of the passive state are revealed.

Undoubtedly, the consideration of thermodynamics features of the corrosion-electrochemical behaviour of the Ti–Si system alloys represents a particular scientific interest.

Experimental Procedure

The binary subsystems of the Ti–Si–O system are to be considered in order to obtain the basic information, needed for calculations and thermodynamic modelling.

The Ti–Si phase diagram [5-9] assumes the existence of the following compounds in it at 25 °C: Ti_3Si, Ti_5Si_3, Ti_5Si_4, TiSi and $TiSi_2$. Also, paper [6] indicates the existence in system of the Ti_3Si_4 silicide , as well as paper [8] – the Ti_6Si_5 silicide. These data are obviously unreliable, as they have no confirmations

in other studies. The Ti_5Si_3 silicide has a wide range of nonstoichiometry at high temperatures, but it can be treated as daltonide at room temperature. Other silicides also don't have areas of nonstoichiometry.

All data about maximum solid solubility of silicon in fcc-titanium at various temperatures [6] are summarized in table 1.

Table 1. Maximum solid solubility of Si in fcc-Ti at various temperatures

Temperature, °C	800	1000	1200
Solubility of Si in (Ti), atomic %	~0,7	~3,35	~5

It can be argued, based on presented data that at 25 °C the possible solubility of silicon in titanium can be neglected. The solid solubility of titanium in silicon, according to [10], amounts less than 10^{-11} atomic % at 1100 °C, also it can be ignored too.

Only one stable oxide – SiO_2 – exists in Si–O system [6, 7] at 25 °C The value of $\Delta_f G^o_{298}(SiO_2) = -805067$ J/mole is taken from handbook [11], because this value is compatible with the experimentally measured standard potential of the silicon electrode ($SiO_2 + 4H^+ + 4e^- = Si(diamond) + 2H_2O$, $\varphi^o_{298} = -0{,}857$ V).

The Ti–O phase diagram [6] implies the presence in system at 298 K the large number of oxides and suboxides – Ti_6O, Ti_3O, Ti_2O, TiO, Ti_2O_3, Ti_3O_5, Magnelli phases Ti_nO_{2n-1} ($4 \le n \le 10$), TiO_2. There are no intermediate compounds (silicates) between TiO_2 and SiO_2 [12].

All data on the standard Gibbs energies of formation of the above-mentioned compounds from elements, which are available in different studies [5, 13-15], are summarized in table 2.

Table 2. The values of standard Gibbs energy of formation ($-\Delta_f G^o_{298}$, J/mole) of compounds from elements

Reference / Compound	[5]	[13]	[14]	[15]	*
Ti_3Si	252536	–	–	–	–
Ti_5Si_3	580032	580620	–	–	–
Ti_5Si_4	641123	–	–	–	–
TiSi	136025	132680	–	–	–
$TiSi_2$	168901	138620	–	–	–
Ti_6O	–	–	–	–	517227
Ti_3O	–	–	–	–	515436
Ti_2O	–	–	–	–	512568
TiO	–	495200	496598	513278	–
Ti_2O_3	–	1435300	1431049	1433829	–
Ti_3O_5	–	2316400	2313668	2317293	–

Ti_4O_7	–	–	3194960	3213016	–
Ti_5O_9	–	–	4070107	–	–
Ti_6O_{11}	–	–	4943446	–	–
Ti_7O_{13}	–	–	5818910	–	–
Ti_8O_{15}	–	–	6689563	–	–
Ti_9O_{17}	–	–	7565521	–	–
$Ti_{10}O_{19}$	–	–	8439839	–	–
TiO_2	–	890100	888610	889406	–
TiH_2	–	80500	88437	105073	–
TiN	–	307800	294370	308930	–

There are no published data on the thermodynamical characteristics of the titanium suboxides Ti_6O, Ti_3O и Ti_2O. In order to evaluate it, the assumption, made by I. G. Gorichev, is used, about the existence of an approximate functional relationship between the standard Gibbs energy of formation of the $Me_{1/x}O$ oxide and the value of x [16]. The parameters of this relationship for the titanium – oxygen system are determined, based on the thermodynamic properties of the other titanium oxides (see figure 1). The estimated values of $\Delta_f G^o_{298}$ for Ti_6O, Ti_3O and Ti_2O suboxides are shown in table. 2 in column, marked by *.

According to [16], titanium can form only Ti^{3+} ions in aqueous environments. The Ti^{2+} and Ti^{4+} ions don't be formed. Titanium (IV) can also form titanyl cation "TiO^{2+}". This cation doesn't exist in such a monomeric form, instead of it the oligomers are formed, which are based on a chain, consisting of –Ti–O–Ti – bonds. Despite many metals titanates are known, these compounds don't contain the fragments of the anionic nature and are, in essence, mixed oxides of titanium and other metal. Therefore, titanate ions doesn't exist in solution.

Silicon can be present in aqueous solutions in form of ortho-silicate ions SiO_3^{2-}. Data on the electrode equilibria, involving above-mentioned ions, are taken from [11] or calculated, using thermodynamic properties, presented in [14].

The method of calculating and plotting the Ti–Si–O state diagram and potential – pH diagram of the Ti–Si–H_2O system is described in paper [18].

Results and Discussion

The Ti–Si–O state diagram at 25 ^oC is shown at figure 2. The characteristics of the system invariant conditions are represented in table 3. It should be noted that all substances, involved in all these equilibria, are pure, and thus the mole fractions and activities of all components are set equal to unity.

Diagram analysis shows, that chemical affinity of titanium to oxygen is higher, than that of silicon. This means that titanium from alloys should be oxidized in air in the first order. The equilibrium oxygen pressure, needed for complete oxidation of titanium and silicon to their highest oxides – $6.7 \cdot 10^{-102}$ bar – is much lower, than partial pressure of oxygen in air at 25 ^oC. This implies that the oxidation of the titanium-silicon alloys in air, upon reaching equilibrium conditions, should be completed by forming TiO_2 and SiO_2 oxides. The specific

composition of the oxide film on alloy surface will strongly depend on silicon percentage in alloys.

Basic chemical and electrochemical equilibria in Ti–Si–H_2O system at standard conditions are shown in table 4. The potential–pH diagram of the system is presented at figure 3.

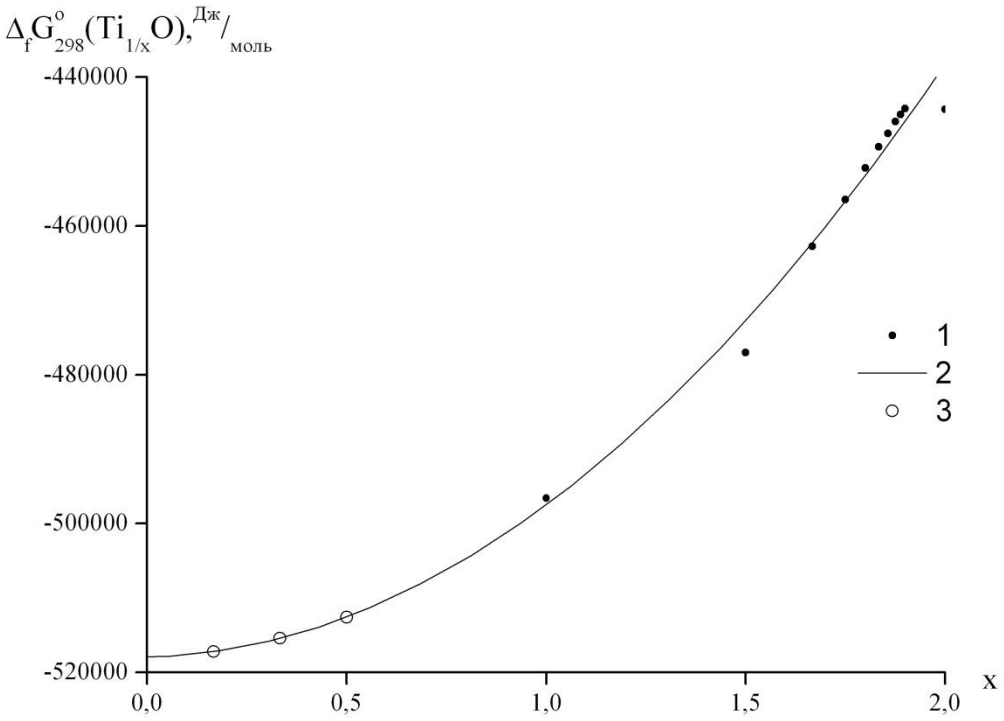

Figure 1. The relationship between standard Gibbs energy of formation of titanium oxides from elements and system's degree of oxidation: 1 – available thermodynamical properties of titanium oxides; 2 – the function, approximating these data, using the lesser squares method ($\Delta_f G^o_{298}(Ti_{1/x}O) = 19380 \cdot x^2 + 1055.7 \cdot x - 517941 \text{ J/mole}, R^2 = 0.9745$); 3 – the characteristics of Ti_6O, Ti_3O и Ti_2O, evaluated on the basis of this function

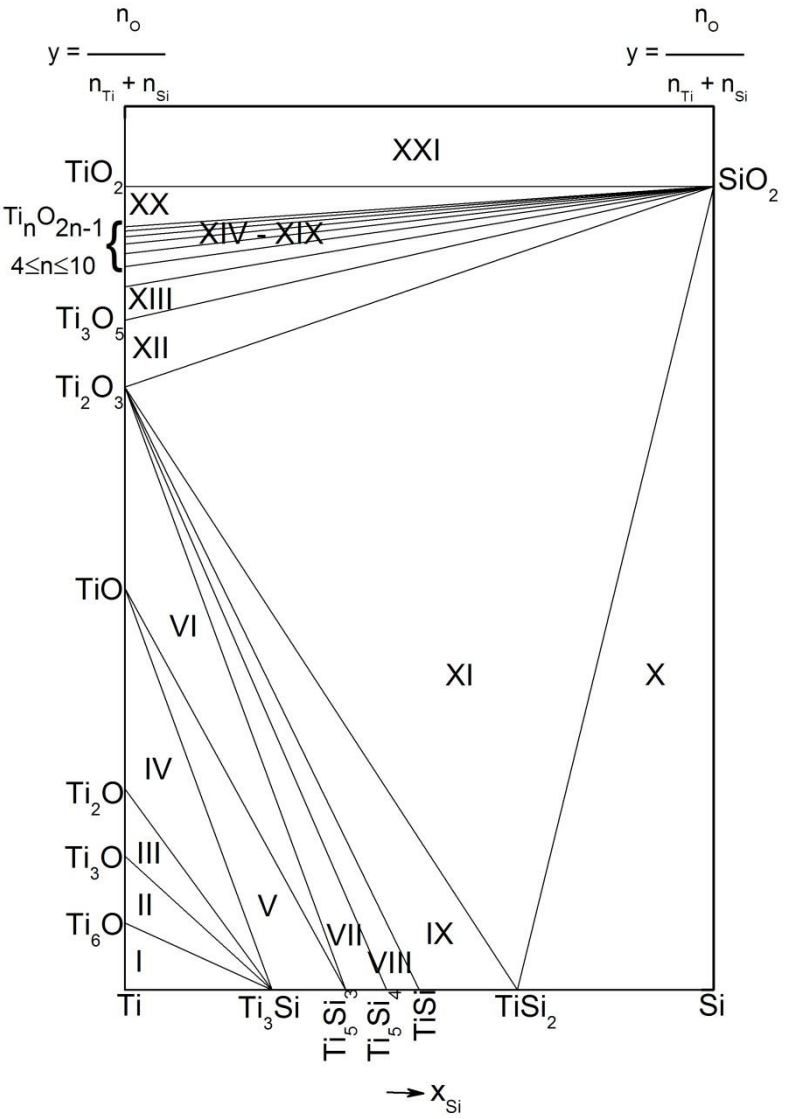

Figure 2. The Ti–Si–O state diagram at 25 °C

Table 3. The characteristics of the Ti–Si–O system invariant conditions at temperature 25 °C

№ of domain	System condition	Reaction equation	P_{O_2}, bar
I	$Ti – Ti_6O – Ti_3Si$	$12Ti + O_2 = 2Ti_6O$	$4{,}8\cdot10^{-182}$
II	$Ti_6O – Ti_3O – Ti_3Si$	$2Ti_6O + O_2 = 4Ti_3O$	$8{,}6\cdot10^{-181}$
III	$Ti_3O – Ti_2O – Ti_3Si$	$4Ti_3O + O_2 = 6Ti_2O$	$2{,}1\cdot10^{-178}$
IV	$Ti_2O – TiO – Ti_3Si$	$2Ti_2O + O_2 = 4TiO$	$3{,}2\cdot10^{-169}$
V	$Ti_3Si – Ti_5Si_3 – TiO$	$3Ti_3Si + 2O_2 = Ti_5Si_3 + 4TiO$	$2{,}9\cdot10^{-159}$
VI	$TiO – Ti_2O_3 – TiSi$	$4TiO + O_2 = 2Ti_2O_3$	$3{,}2\cdot10^{-154}$
VII	$Ti_5Si_3 – Ti_5Si_4 – Ti_2O_3$	$16Ti_5Si_3 + 15O_2 = 12Ti_5Si_4 + 10Ti_2O_3$	$2{,}1\cdot10^{-149}$

VIII	$Ti_5Si_4 – TiSi – Ti_2O_3$	$4Ti_5Si_4 + 3O_2 = 16TiSi + 2Ti_2O_3$	$2{,}8\cdot10^{-145}$
IX	$TiSi – TiSi_2 – Ti_2O_3$	$8TiSi + 3O_2 = 4TiSi_2 + 2Ti_2O_3$	$7{,}6\cdot10^{-144}$
X	$Si – SiO_2 – TiSi_2$	$Si + O_2 = SiO_2$	$7{,}7\cdot10^{-142}$
XI	$TiSi_2 – Ti_2O_3 – SiO_2$	$4TiSi_2 + 11O_2 = 8SiO_2 + 2Ti_2O_3$	$3{,}4\cdot10^{-138}$
XII	$Ti_2O_3 – Ti_3O_5 – SiO_2$	$6Ti_2O_3 + O_2 = 4Ti_3O_5$	$7{,}0\cdot10^{-118}$
XIII	$Ti_3O_5 – Ti_4O_7 – SiO_2$	$8Ti_3O_5 + O_2 = 6Ti_4O_7$	$1{,}7\cdot10^{-116}$
XIV	$Ti_4O_7 – Ti_5O_9 – SiO_2$	$10Ti_4O_7 + O_2 = 8Ti_5O_9$	$7{,}2\cdot10^{-108}$
XV	$Ti_5O_9 – Ti_6O_{11} – SiO_2$	$12Ti_5O_9 + O_2 = 10Ti_6O_{11}$	$9{,}0\cdot10^{-108}$
XVI	$Ti_6O_{11} – Ti_7O_{13} – SiO_2$	$14Ti_6O_{11} + O_2 = 12Ti_7O_{13}$	$7{,}3\cdot10^{-105}$
XVII	$Ti_7O_{13} – Ti_8O_{15} – SiO_2$	$16Ti_7O_{13} + O_2 = 14Ti_8O_{15}$	$1{,}4\cdot10^{-104}$
XVIII	$Ti_8O_{15} – Ti_9O_{17} – SiO_2$	$18Ti_8O_{15} + O_2 = 16Ti_9O_{17}$	$5{,}6\cdot10^{-103}$
XIX	$Ti_9O_{17} – Ti_{10}O_{19} – SiO_2$	$20Ti_9O_{17} + O_2 = 18Ti_{10}O_{19}$	$1{,}6\cdot10^{-102}$
XX	$Ti_{10}O_{19} – TiO_2 – SiO_2$	$2Ti_{10}O_{19} + O_2 = 20TiO_2$	$6{,}7\cdot10^{-102}$
XXI	$TiO_2 – SiO_2 – \{O_2\}$	–	–

Table 4. Basic chemical and electrochemical equilibria in Ti–Si–H_2O system at temperature 25 ^oC and air pressure of 1 bar without regard to titanium hydride and nitride.

№ of line at figure 3	Electrode reaction	Equilibrium potential, V (s. h. e.) or solution pH
a	$2H^+ + 2e^- = H_2; P_{H_2} \approx 5\cdot10^{-7}$ бар	$0{,}186 - 0{,}0591pH$
1	$Ti_6O + 2H^+ + 2e^- = 6Ti + H_2O$	$-1{,}451 - 0{,}0591pH$
2	$2Ti_3O + 2H^+ + 2e^- = Ti_6O + H_2O$	$-1{,}432 - 0{,}0591pH$
3	$3Ti_2O + 2H^+ + 2e^- = 2Ti_3O + H_2O$	$-1{,}397 - 0{,}0591pH$
4	$2Ti^{3+} + H_2O + 4e^- = Ti_2O + 2H^+$	$-1{,}103 + 0{,}0295pH + 0{,}0295\cdot\lg a_{Ti^{3+}}$
5	$2TiO + 2H^+ + 2e^- = Ti_2O + H_2O$	$-1{,}261 - 0{,}0591pH$
6	$Ti^{3+} + H_2O + e^- = TiO + 2H^+$	$-0{,}944 + 0{,}1182pH + 0{,}0591\cdot\lg a_{Ti^{3+}}$
7	$Ti_5Si_3 + 4Ti^{3+} + 12e^- = 3Ti_3Si$	$-1{,}057 + 0{,}0197\cdot\lg a_{Ti^{3+}}$
8	$Ti_5Si_3 + 4TiO + 8H^+ + 8e^- = 3Ti_3Si + 4H_2O$	$-1{,}114 - 0{,}0591pH$
9	$Ti_2O_3 + 2H^+ + 2e^- = 2TiO + H_2O$	$-1{,}040 - 0{,}0591pH$
10	$Ti_2O_3 + 6H^+ = 2Ti^{3+} + 3H_2O$	$pH = -0{,}540 - 0{,}333\cdot\lg a_{Ti^{3+}}$
11	$3Ti_5Si_4 + 5Ti^{3+} + 15e^- = 4Ti_5Si_3$	$-0{,}937 + 0{,}0197\cdot\lg a_{Ti^{3+}}$
12	$6Ti_5Si_4 + 5Ti_2O_3 + 30H^+ + 30e^- = 8Ti_5Si_3 + 15H_2O$	$-0{,}968 - 0{,}0591pH$
13	$4TiSi + Ti^{3+} + 3e^- = Ti_5Si_4$	$-0{,}876 + 0{,}0197\cdot\lg a_{Ti^{3+}}$
14	$8TiSi + Ti_2O_3 + 6H^+ + 6e^- = 2Ti_5Si_4 + 3H_2O$	$-0{,}907 - 0{,}0591pH$

15	$TiSi_2 + Ti^{3+} + 3e^- = 2TiSi$	$-0{,}854 + 0{,}0197 \cdot \lg a_{Ti^{3+}}$
16	$2TiSi_2 + Ti_2O_3 + 6H^+ + 6e^- = 4TiSi + 3H_2O$	$-0{,}886 - 0{,}0591pH$
17	$SiO_2 + 4H^+ + 4e^- = Si + 2H_2O$	$-0{,}857 - 0{,}0591pH$
18	$SiO_3^{2-} + 6H^+ + 4e^- = Si + 3H_2O$	$-0{,}444 - 0{,}0887pH + 0{,}0148 \cdot \lg a_{SiO_3^{2-}}$
19	$SiO_3^{2-} + 2H^+ = SiO_2 + 2H_2O$	$pH = 13{,}94 + 0{,}5 \cdot \lg a_{SiO_3^{2-}}$
20	$2SiO_2 + Ti^{3+} + 8H^+ + 11e^- = TiSi_2 + 4H_2O$	$-0{,}794 - 0{,}0430pH + 0{,}0054 \cdot \lg a_{Ti^{3+}}$
21	$4SiO_2 + Ti_2O_3 + 22H^+ + 22e^- = 2TiSi_2 + 11H_2O$	$-0{,}803 - 0{,}0591pH$
22	$4SiO_3^{2-} + Ti_2O_3 + 30H^+ + 22e^- = 2TiSi_2 + 15H_2O$	$-0{,}503 - 0{,}0806pH + 0{,}0107 \cdot \lg a_{SiO_3^{2-}}$
23	$2Ti_3O_5 + 2H^+ + 2e^- = 3Ti_2O_3 + H_2O$	$-0{,}502 - 0{,}0591pH$
24	$Ti_3O_5 + 10H^+ + e^- = 3Ti^{3+} + 5H_2O$	$-0{,}790 - 0{,}5914pH - 0{,}1773 \cdot \lg a_{Ti^{3+}}$
25	$3Ti_4O_7 + 2H^+ + 2e^- = 4Ti_3O_5 + H_2O$	$-0{,}482 - 0{,}0591pH$
26	$Ti_4O_7 + 14H^+ + 2e^- = 4Ti^{3+} + 7H_2O$	$-0{,}687 - 0{,}4137pH - 0{,}1182 \cdot \lg a_{Ti^{3+}}$
27	$"TiO^{2+}" + 2H^+ + e^- = Ti^{3+} + H_2O$	$-0{,}463 - 0{,}1182pH + 0{,}0591 \cdot \lg \frac{a_{"TiO^{2+}"}}{a_{Ti^{3+}}}$
28	$4"TiO^{2+}" + 3H_2O + 2e^- = Ti_4O_7 + 6H^+$	$-0{,}239 + 0{,}1773pH + 0{,}1182 \cdot \lg a_{"TiO^{2+}"}$
29	$4Ti_5O_9 + 2H^+ + 2e^- = 5Ti_4O_7 + H_2O$	$-0{,}354 - 0{,}0591pH$
30	$5"TiO^{2+}" + 4H_2O + 2e^- = Ti_5O_9 + 8H^+$	$-0{,}210 + 0{,}2364pH + 0{,}1478 \cdot \lg a_{"TiO^{2+}"}$
31	$5Ti_6O_{11} + 2H^+ + 2e^- = 6Ti_5O_9 + H_2O$	$-0{,}353 - 0{,}0591pH$
32	$6"TiO^{2+}" + 5H_2O + 2e^- = Ti_6O_{11} + 10H^+$	$-0{,}181 + 0{,}2955pH + 0{,}1773 \cdot \lg a_{"TiO^{2+}"}$
33	$6Ti_7O_{13} + 2H^+ + 2e^- = 7Ti_6O_{11} + H_2O$	$-0{,}310 - 0{,}0591pH$
34	$7"TiO^{2+}" + 6H_2O + 2e^- = Ti_7O_{13} + 12H^+$	$-0{,}160 + 0{,}3546pH + 0{,}2069 \cdot \lg a_{"TiO^{2+}"}$
35	$7Ti_8O_{15} + 2H^+ + 2e^- = 8Ti_7O_{13} + H_2O$	$-0{,}306 - 0{,}0591pH$
36	$8"TiO^{2+}" + 7H_2O + 2e^- = Ti_8O_{15} + 14H^+$	$-0{,}139 + 0{,}4137pH + 0{,}2364 \cdot \lg a_{"TiO^{2+}"}$
37	$8Ti_9O_{17} + 2H^+ + 2e^- = 9Ti_8O_{15} + H_2O$	$-0{,}282 - 0{,}0591pH$
38	$9"TiO^{2+}" + 8H_2O + 2e^- = Ti_9O_{17} + 16H^+$	$-0{,}121 + 0{,}4728pH + 0{,}2660 \cdot \lg a_{"TiO^{2+}"}$
39	$9Ti_{10}O_{19} + 2H^+ + 2e^- = 10Ti_9O_{17} + H_2O$	$-0{,}275 - 0{,}0591pH$
40	$10"TiO^{2+}" + 9H_2O + 2e^- = Ti_{10}O_{19} + 18H^+$	$-0{,}104 + 0{,}5319pH + 0{,}2955 \cdot \lg a_{"TiO^{2+}"}$
41	$10TiO_2 + 2H^+ + 2e^- = Ti_{10}O_{19} + H_2O$	$-0{,}266 - 0{,}0591pH$
42	$TiO_2 + 2H^+ = "TiO^{2+}" + H_2O$	$pH = -0{,}274 - 0{,}5 \cdot \lg a_{"TiO^{2+}"}$

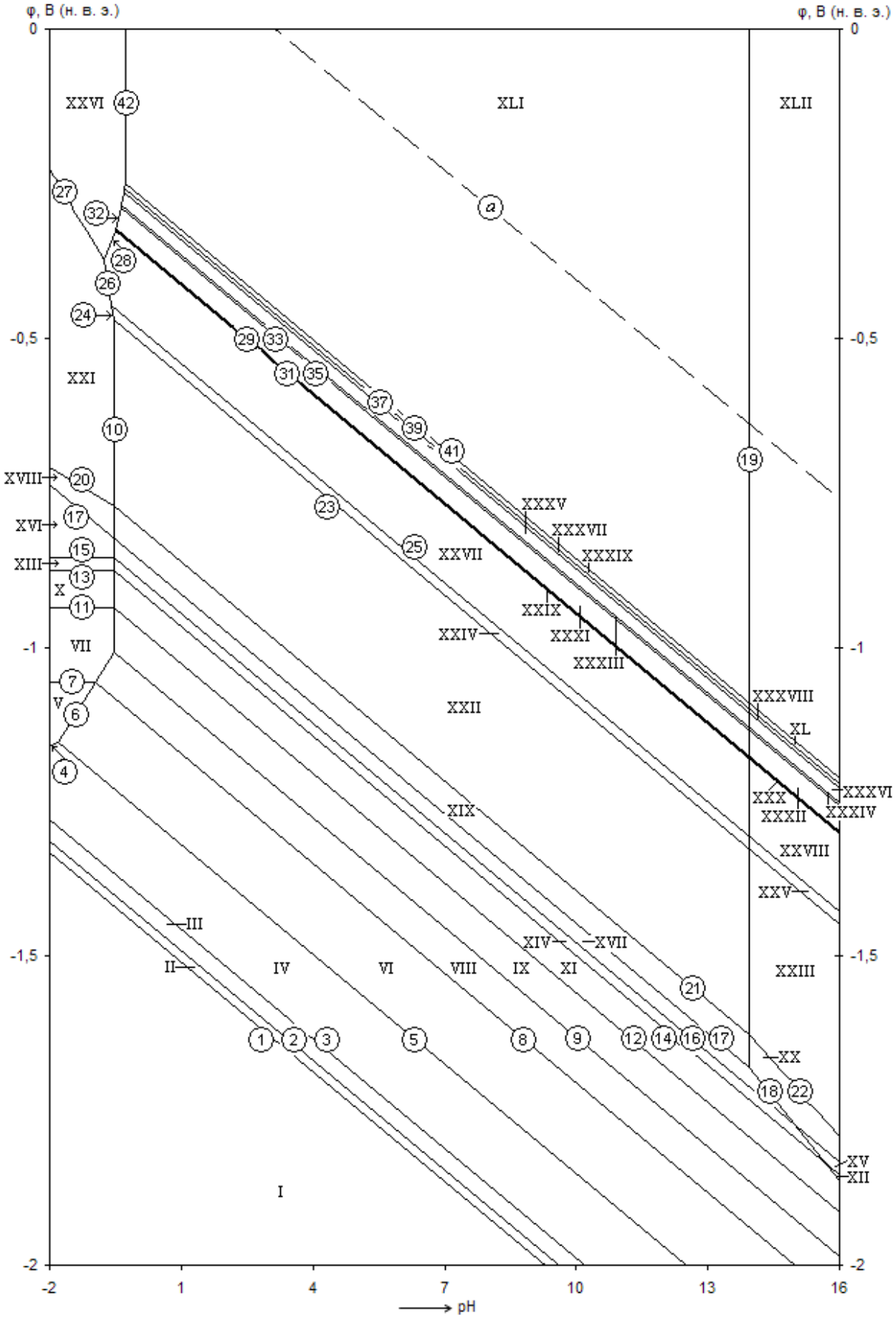

Figure 3. The hypothetical potential – pH diagram of the Ti–Si–H_2O system at 25 ^{o}C, air pressure of 1 bar and $a_i = 1$ mole/l (unhydrated from of oxides, without regard to titanium hydride and nitride)

42 domains of the thermodynamical stability of certain phases can be depicted at this diagram (see figure 3): I – Ti + Ti_3Si + Ti_5Si_3 + Ti_5Si_4 + TiSi + $TiSi_2$ + Si; II – Ti_6O + Ti_3Si + Ti_5Si_3 + Ti_5Si_4 + TiSi + $TiSi_2$ + Si; III – Ti_3O + Ti_3Si + Ti_5Si_3 + Ti_5Si_4 + TiSi + $TiSi_2$ + Si; IV – Ti_2O + Ti_3Si + Ti_5Si_3 + Ti_5Si_4 + TiSi + $TiSi_2$ + Si; V – Ti^{3+} + Ti_3Si + Ti_5Si_3 + Ti_5Si_4 + TiSi + $TiSi_2$ + Si; VI – TiO + Ti_3Si + Ti_5Si_3 + Ti_5Si_4 + TiSi + $TiSi_2$ + Si; VII – Ti^{3+} + Ti_5Si_3 + Ti_5Si_4 + TiSi + $TiSi_2$ + Si; VIII – TiO + Ti_5Si_3 + Ti_5Si_4 + TiSi + $TiSi_2$ + Si; IX – Ti_2O_3 + Ti_5Si_3 + Ti_5Si_4 + TiSi + $TiSi_2$ + Si; X – Ti^{3+} + Ti_5Si_4 + TiSi + $TiSi_2$ + Si; XI – Ti_2O_3 + Ti_5Si_4 + TiSi + $TiSi_2$ + Si; XII – Ti_2O_3 + Ti_5Si_4 + TiSi + $TiSi_2$ + SiO_3^{2-}; XIII – Ti^{3+} + TiSi + $TiSi_2$ + Si; XIV – Ti_2O_3 + TiSi + $TiSi_2$ + Si; XV – Ti_2O_3 + TiSi + $TiSi_2$ + SiO_3^{2-}; XVI – Ti^{3+} + $TiSi_2$ + Si; XVII – Ti_2O_3 + $TiSi_2$ + Si; XVIII – Ti^{3+} + $TiSi_2$ + SiO_2; XIX – Ti_2O_3 + $TiSi_2$ + SiO_2; XX – Ti_2O_3 + $TiSi_2$ + SiO_3^{2-}; XXI – Ti^{3+} + SiO_2; XXII – Ti_2O_3 + SiO_2; XXIII – Ti_2O_3 + SiO_3^{2-}; XXIV – Ti_3O_5 + SiO_2; XXV – Ti_3O_5 + SiO_3^{2-}; XXVI – "TiO^{2+}" + SiO_2; XXVII – Ti_4O_7 + SiO_2; XXVIII – Ti_4O_7 + SiO_3^{2-}; XXIX – Ti_5O_9 + SiO_2; XXX – Ti_5O_9 + SiO_3^{2-}; XXXI – Ti_6O_{11} + SiO_2; XXXII – Ti_6O_{11} + SiO_3^{2-}; XXXIII – Ti_7O_{13} + SiO_2; XXXIV – Ti_7O_{13} + SiO_3^{2-}; XXXV – Ti_8O_{15} + SiO_2; XXXVI – Ti_8O_{15} + SiO_3^{2-}; XXXVII – Ti_9O_{17} + SiO_2; XXXVIII – Ti_9O_{17} + SiO_3^{2-}; XXXIX – $Ti_{10}O_{19}$ + SiO_2; XL – $Ti_{10}O_{19}$ + SiO_3^{2-}; XLI – TiO_2 + SiO_2; XLII – TiO_2 + SiO_3^{2-}.

Domain I is the domain of system proposed immunity (or thermodynamical stability).

Domains V, VII, X, XIII, XVI, XVIII, XXI and XXVI correspond to titanium selective corrosion, in which it actively passes into solution in form of Ti^{3+} or "TiO^{2+}" cations.

All other domains correspond to system equilibrium conditions, at which the passivation oxide film (which can include silicon dioxide and one of the titanium oxides) is formed on the surface on alloys.

Line *a* at the diagram correspond to the hydrogen electrode work. The domain of electrochemical stability of water lies above this line.

As seen from figure 3, titanium has very narrow area of active dissolution, because the cations of titanium and titanyl exist only in strongly acidic environments. In addition, all lines of chemical and electrochemical equilibria, determining titanium corrosion-electrochemical behaviour, are located below line *a* at the diagram. This means, that in real environments (which lie in the domain of electrochemical stability of water and are characterized by much higher stationary potentials values) the TiO_2 and SiO_2 oxides are thermodynamically stable phases, which confirms the conclusion, made in study [3], about ease of formation and stability of Ti–Si system passive state.

Despite the potential – pH diagram, presented at figure 3, completely corresponds to Ti–Si–O state diagram, it doesn't reflect the true nature of titanium silicides corrosion-electrochemical behaviour in aqueous environments, and represents its hypothetical model only. This is due to the fact, that titanium has

high chemical affinity not only to oxygen, but also to hydrogen and nitrogen. Therefore, it's necessary to take into account the reaction products of titanium with them (titanium hydride TiH_2 and titanium nitride TiN, respectively) in thermodynamical modelling.

It's proved at the present time [19], that oxidation of titanium in aqueous environments proceeds through consecutive formation and decomposition of titanium hydride TiH_2. Therefore, thermodynamical analysis of the Ti–Si–H_2O system, considering titanium hydride, is also performed. The corresponding potential – pH diagram is shown at figure 4. Basic chemical and electrochemical equilibria in the system are listed in table 5. In thes case, lines 15-34 at figure 4 completely correspond to lines 23-42 at figure 3. 35 domains of the prevalence of different phases can be depicted at the diagram (see figure 4):: I – TiH_2 + Ti_3Si + Ti_5Si_3 + Ti_5Si_4 + TiSi + $TiSi_2$ + Si; II – TiH_2 + Ti_3Si + Ti_5Si_3 + Ti_5Si_4 + TiSi + $TiSi_2$ + SiO_2; III – TiH_2 + Ti_3Si + Ti_5Si_3 + Ti_5Si_4 + TiSi + $TiSi_2$ + SiO_3^{2-}; IV – TiH_2 + Ti_3Si + Ti_5Si_3 + Ti_5Si_4 + TiSi + SiO_2; V – TiH_2 + Ti_3Si + Ti_5Si_3 + Ti_5Si_4 + TiSi + SiO_3^{2-}; VI – TiH_2 + Ti_3Si + Ti_5Si_3 + Ti_5Si_4 + SiO_2; VII – TiH_2 + Ti_3Si + Ti_5Si_3 + Ti_5Si_4 + SiO_3^{2-}; VIII – TiH_2 + Ti_3Si + Ti_5Si_3 + SiO_2; IX – TiH_2 + Ti_3Si + Ti_5Si_3 + SiO_3^{2-}; X – TiH_2 + Ti_3Si + SiO_3^{2-}; XI – Ti^{3+} + Ti_3Si + Ti_5Si_3 + SiO_2; XII – Ti_2O_3 + Ti_3Si + Ti_5Si_3 + SiO_2; XIII – Ti_2O_3 + Ti_3Si + Ti_5Si_3 + SiO_3^{2-}; XIV – Ti^{3+} + Ti_3Si

Table 5. Basic chemical and electrochemical equilibria in Ti–Si–H_2O system at temperature 25 °C and air pressure of 1 bar, considering titanium hydride, but without regard to titanium nitride.

№ of line at figure 4	Electrode reaction	Equilibrium potential, V (s. h. e.) or solution pH
a	$2H^+ + 2e^- = H_2; P_{H_2} \approx 5\cdot10^{-7}$ бар	$0{,}186 - 0{,}0591pH$
1	$SiO_2 + 4H^+ + 4e^- = Si + 2H_2O$	$-0{,}857 - 0{,}0591pH$
2	$SiO_3^{2-} + 6H^+ + 4e^- = Si + 3H_2O$	$-0{,}444 - 0{,}0887pH + 0{,}0148\cdot\lg a_{SiO_3^{2-}}$
3	$SiO_3^{2-} + 2H^+ = SiO_2 + 2H_2O$	$pH = 13{,}94 + 0{,}5\cdot\lg a_{SiO_3^{2-}}$
4	$TiSi + SiO_2 + 4H^+ + 4e^- = TiSi_2 + 2H_2O$	$-0{,}771 - 0{,}0591pH$
5	$TiSi + SiO_3^{2-} + 6H^+ + 4e^- = TiSi_2 + 3H_2O$	$-0{,}359 - 0{,}0887pH + 0{,}0148\cdot\lg a_{SiO_3^{2-}}$
6	$Ti_5Si_4 + SiO_2 + 4H^+ + 4e^- = 5TiSi + 2H_2O$	$-0{,}755 - 0{,}0591pH$
7	$Ti_5Si_4 + SiO_3^{2-} + 6H^+ + 4e^- = 5TiSi + 3H_2O$	$-0{,}343 - 0{,}0887pH + 0{,}0148\cdot\lg a_{SiO_3^{2-}}$
8	$Ti_5Si_3 + SiO_2 + 4H^+ + 4e^- = Ti_5Si_4 + 2H_2O$	$-0{,}698 - 0{,}0591pH$
9	$Ti_5Si_3 + SiO_3^{2-} + 6H^+ + 4e^- = Ti_5Si_4 + 3H_2O$	$-0{,}286 - 0{,}0887pH + 0{,}0148\cdot\lg a_{SiO_3^{2-}}$
10	$Ti^{3+} + 2H^+ + 5e^- = TiH_2$	$-0{,}543 - 0{,}0236pH + 0{,}0118\cdot\lg a_{Ti^{3+}}$
11	$Ti_2O_3 + 10H^+ + 10e^- = 2TiH_2 + 3H_2O$	$-0{,}562 - 0{,}0591pH$

12	$Ti_2O_3 + 6H^+ = 2Ti^{3+} + 3H_2O$	$pH = -0{,}540 - 0{,}333 \cdot \lg a_{Ti^{3+}}$
13	$5Ti_3Si + 4SiO_2 + 16H^+ + 16e^- = 3Ti_5Si_3 + 8H_2O$	$-0{,}547 - 0{,}0591pH$
14	$5Ti_3Si + 4SiO_3^{2-} + 24H^+ + 16e^- = 3Ti_5Si_3 + 12H_2O$	$-0{,}135 - 0{,}0887pH + 0{,}0148 \cdot \lg a_{SiO_3^{2-}}$
15	$2Ti_3O_5 + 2H^+ + 2e^- = 3Ti_2O_3 + H_2O$	$-0{,}502 - 0{,}0591pH$
16	$Ti_3O_5 + 10H^+ + e^- = 3Ti^{3+} + 5H_2O$	$-0{,}790 - 0{,}5914pH - 0{,}1773 \cdot \lg a_{Ti^{3+}}$
17	$3Ti_4O_7 + 2H^+ + 2e^- = 4Ti_3O_5 + H_2O$	$-0{,}482 - 0{,}0591pH$
18	$Ti_4O_7 + 14H^+ + 2e^- = 4Ti^{3+} + 7H_2O$	$-0{,}687 - 0{,}4137pH - 0{,}1182 \cdot \lg a_{Ti^{3+}}$
19	$"TiO^{2+}" + 2H^+ + e^- = Ti^{3+} + H_2O$	$-0{,}463 - 0{,}1182pH + 0{,}0591 \cdot \lg \frac{a_{"TiO^{2+}"}}{a_{Ti^{3+}}}$
20	$4"TiO^{2+}" + 3H_2O + 2e^- = Ti_4O_7 + 6H^+$	$-0{,}239 + 0{,}1773pH + 0{,}1182 \cdot \lg a_{"TiO^{2+}"}$
21	$4Ti_5O_9 + 2H^+ + 2e^- = 5Ti_4O_7 + H_2O$	$-0{,}354 - 0{,}0591pH$
22	$5"TiO^{2+}" + 4H_2O + 2e^- = Ti_5O_9 + 8H^+$	$-0{,}210 + 0{,}2364pH + 0{,}1478 \cdot \lg a_{"TiO^{2+}"}$
23	$5Ti_6O_{11} + 2H^+ + 2e^- = 6Ti_5O_9 + H_2O$	$-0{,}353 - 0{,}0591pH$
24	$6"TiO^{2+}" + 5H_2O + 2e^- = Ti_6O_{11} + 10H^+$	$-0{,}181 + 0{,}2955pH + 0{,}1773 \cdot \lg a_{"TiO^{2+}"}$
25	$6Ti_7O_{13} + 2H^+ + 2e^- = 7Ti_6O_{11} + H_2O$	$-0{,}310 - 0{,}0591pH$
26	$7"TiO^{2+}" + 6H_2O + 2e^- = Ti_7O_{13} + 12H^+$	$-0{,}160 + 0{,}3546pH + 0{,}2069 \cdot \lg a_{"TiO^{2+}"}$
27	$7Ti_8O_{15} + 2H^+ + 2e^- = 8Ti_7O_{13} + H_2O$	$-0{,}306 - 0{,}0591pH$
28	$8"TiO^{2+}" + 7H_2O + 2e^- = Ti_8O_{15} + 14H^+$	$-0{,}139 + 0{,}4137pH + 0{,}2364 \cdot \lg a_{"TiO^{2+}"}$
29	$8Ti_9O_{17} + 2H^+ + 2e^- = 9Ti_8O_{15} + H_2O$	$-0{,}282 - 0{,}0591pH$
30	$9"TiO^{2+}" + 8H_2O + 2e^- = Ti_9O_{17} + 16H^+$	$-0{,}121 + 0{,}4728pH + 0{,}2660 \cdot \lg a_{"TiO^{2+}"}$
31	$9Ti_{10}O_{19} + 2H^+ + 2e^- = 10Ti_9O_{17} + H_2O$	$-0{,}275 - 0{,}0591pH$
32	$10"TiO^{2+}" + 9H_2O + 2e^- = Ti_{10}O_{19} + 18H^+$	$-0{,}104 + 0{,}5319pH + 0{,}2955 \cdot \lg a_{"TiO^{2+}"}$
33	$10TiO_2 + 2H^+ + 2e^- = Ti_{10}O_{19} + H_2O$	$-0{,}266 - 0{,}0591pH$
34	$TiO_2 + 2H^+ = "TiO^{2+}" + H_2O$	$pH = -0{,}274 - 0{,}5 \cdot \lg a_{"TiO^{2+}"}$

+ SiO_2; XV – Ti_2O_3 + Ti_3Si + SiO_2; XVI – Ti_2O_3 + Ti_3Si + SiO_3^{2-}; XVII – Ti_3O_5 + Ti_3Si + SiO_2; XVIII – Ti_3O_5 + Ti_3Si + SiO_3^{2-}; XIX – "TiO^{2+}" + Ti_3Si + SiO_2; XX – Ti_4O_7 + Ti_3Si + SiO_2; XXI – Ti_4O_7 + Ti_3Si + SiO_3^{2-}; XXII – Ti_5O_9 + Ti_3Si + SiO_2; XXIII – Ti_5O_9 + Ti_3Si + SiO_3^{2-}; XXIV – Ti_6O_{11} + Ti_3Si + SiO_2; XXV – Ti_6O_{11} + Ti_3Si + SiO_3^{2-}; XXVI – Ti_7O_{13} + Ti_3Si + SiO_2; XXVII – Ti_7O_{13} + Ti_3Si + SiO_3^{2-}; XXVIII – Ti_8O_{15} + Ti_3Si + SiO_2; XXIX – Ti_8O_{15} + Ti_3Si + SiO_3^{2-}; XXX – Ti_9O_{17} + Ti_3Si + SiO_2; XXXI – Ti_9O_{17} + Ti_3Si + SiO_3^{2-}; XXXII – $Ti_{10}O_{19}$ + Ti_3Si + SiO_2; XXXIII – $Ti_{10}O_{19}$ + Ti_3Si + SiO_3^{2-}; XXXIV – TiO_2 + Ti_3Si + SiO_2; XXXV – TiO_2 + Ti_3Si + SiO_3^{2-}.

In the presence of titanium hydride all of the lower titanium oxides up to Ti_2O_3 are thermodynamically unstable. There is no domain of thermodynamical stability of pure titanium and all domains below lines 10 and 11 at figure 4 correspond to TiH_2 formation (there are domains of titanium hydride passivation).

Variant of the Ti–Si system electrochemical equilibrium diagram, which also takes into account the possibility of electrochemical formation of titanium nitride TiN, is shown at figure 5. Chemical and electrochemical equilibria in system are represented in table 6.

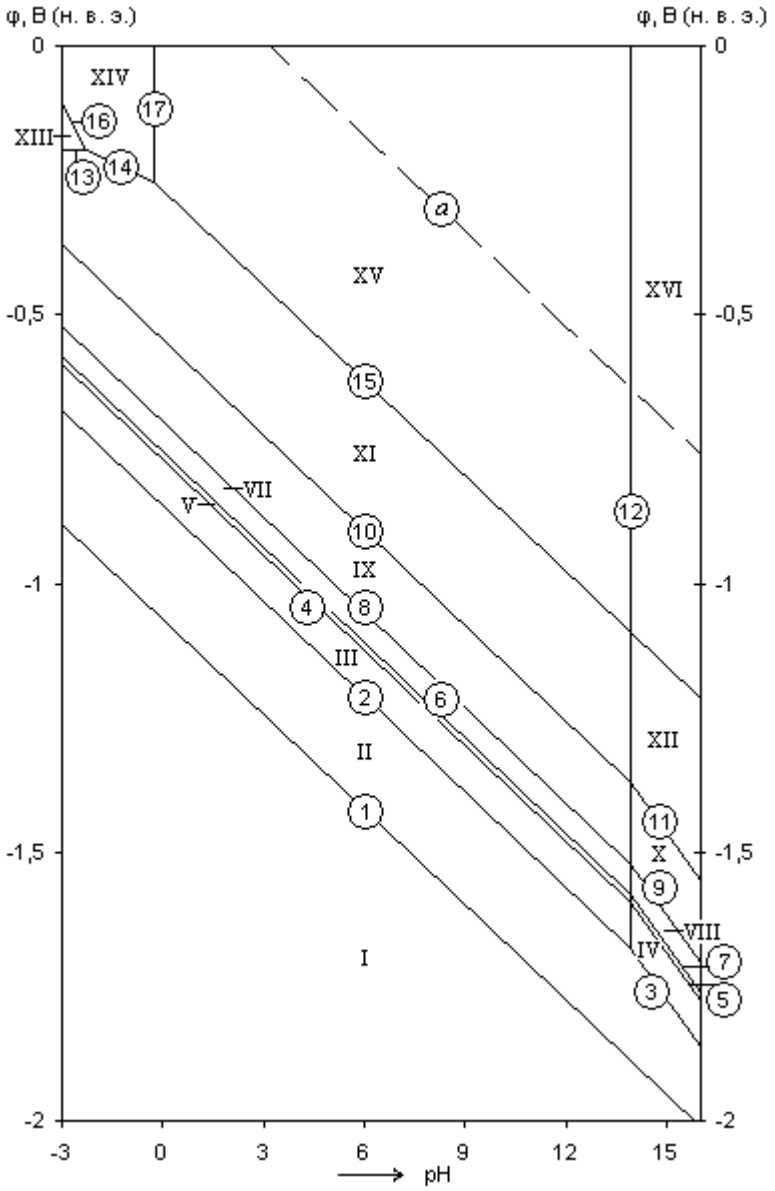

Figure 5. The potential – pH diagram of the Ti–Si–H_2O system at 25 ^oC, air pressure of 1 bar and $a_i = 1$ mole/l (unhydrated form of oxides, considering titanium hydride and nitride).

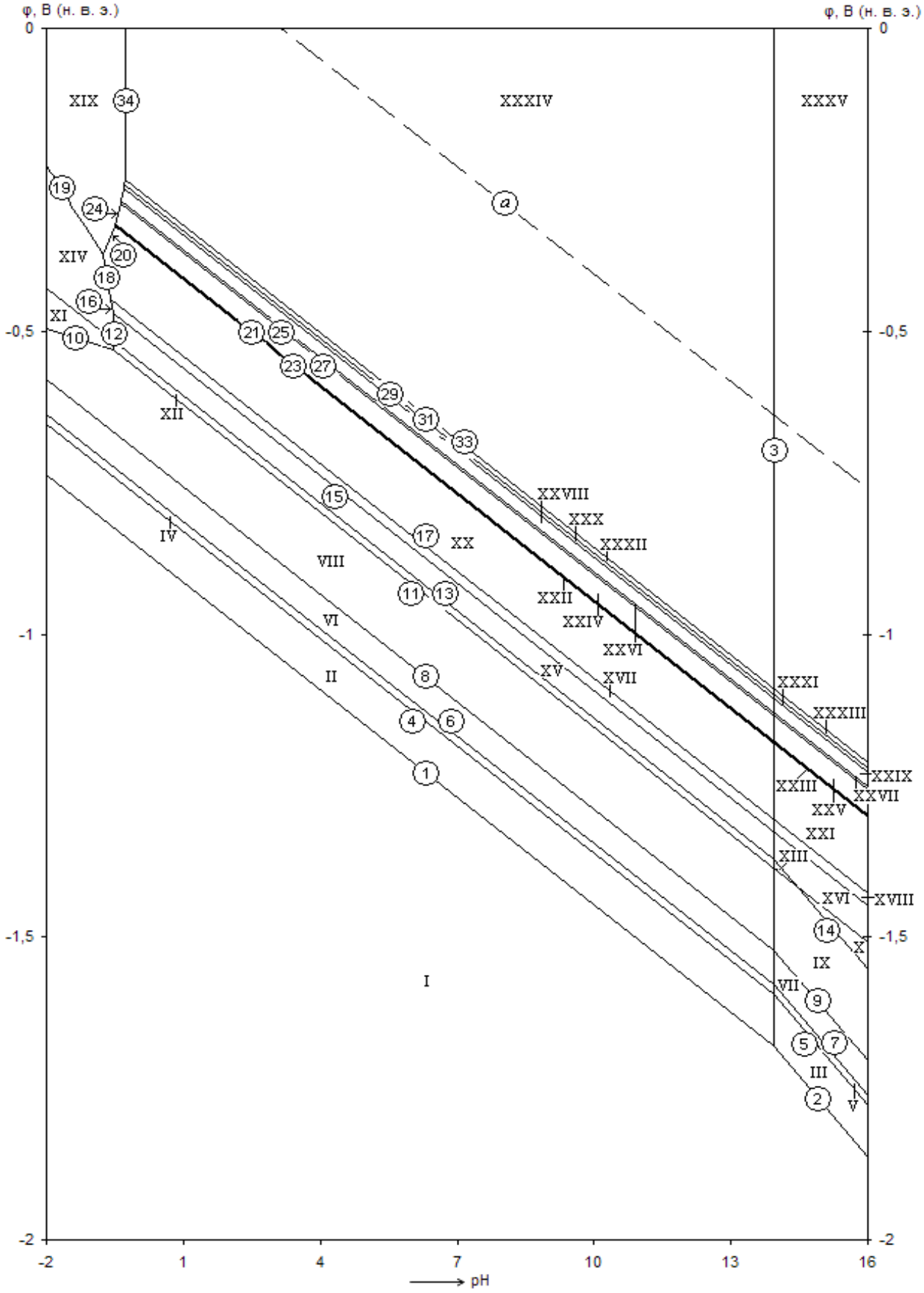

Figure 4. The hypothetical potential – pH diagram of the Ti–Si–H_2O system at 25 ^oC, air pressure of 1 bar and $a_i = 1$ mole/l (unhydrated form of oxides, considering titanium hydride, but without regard to titanium nitride).

Table 6. Basic chemical and electrochemical equilibria in Ti–Si–H_2O system at temperature 25 ^oC and air pressure of 1 bar, considering titanium hydride and nitride

№ of line at figure 5	Electrode reaction	Equilibrium potential, V (s. h. e.) or solution pH
a	$2H^+ + 2e^- = H_2; P_{H_2} \approx 5 \cdot 10^{-7}$ бар	$0{,}186 - 0{,}0591pH$
1	$2TiN + 4H^+ + 4e^- = 2TiH_2 + N_2; P_{N_2} \approx 0{,}79$ бар	$-1{,}066 - 0{,}0591pH$
2	$SiO_2 + 4H^+ + 4e^- = Si + 2H_2O$	$-0{,}857 - 0{,}0591pH$
3	$SiO_3^{2-} + 6H^+ + 4e^- = Si + 3H_2O$	$-0{,}444 - 0{,}0887pH + 0{,}0148 \cdot \lg a_{SiO_3^{2-}}$
4	$TiSi + SiO_2 + 4H^+ + 4e^- = TiSi_2 + 2H_2O$	$-0{,}771 - 0{,}0591pH$
5	$TiSi + SiO_3^{2-} + 6H^+ + 4e^- = TiSi_2 + 3H_2O$	$-0{,}359 - 0{,}0887pH + 0{,}0148 \cdot \lg a_{SiO_3^{2-}}$
6	$Ti_5Si_4 + SiO_2 + 4H^+ + 4e^- = 5TiSi + 2H_2O$	$-0{,}755 - 0{,}0591pH$
7	$Ti_5Si_4 + SiO_3^{2-} + 6H^+ + 4e^- = 5TiSi + 3H_2O$	$-0{,}343 - 0{,}0887pH + 0{,}0148 \cdot \lg a_{SiO_3^{2-}}$
8	$Ti_5Si_3 + SiO_2 + 4H^+ + 4e^- = Ti_5Si_4 + 2H_2O$	$-0{,}698 - 0{,}0591pH$
9	$Ti_5Si_3 + SiO_3^{2-} + 6H^+ + 4e^- = Ti_5Si_4 + 3H_2O$	$-0{,}286 - 0{,}0887pH + 0{,}0148 \cdot \lg a_{SiO_3^{2-}}$
10	$5Ti_3Si + 4SiO_2 + 16H^+ + 16e^- = 3Ti_5Si_3 + 8H_2O$	$-0{,}547 - 0{,}0591pH$
11	$5Ti_3Si + 4SiO_3^{2-} + 24H^+ + 16e^- = 3Ti_5Si_3 + 12H_2O$	$-0{,}135 - 0{,}0887pH + 0{,}0148 \cdot \lg a_{SiO_3^{2-}}$
12	$SiO_3^{2-} + 2H^+ = SiO_2 + 2H_2O$	$pH = 13{,}94 + 0{,}5 \cdot \lg a_{SiO_3^{2-}}$
13	$2Ti^{3+} + N_2 + 6e^- = 2TiN; P_{N_2} \approx 0{,}79$ бар	$-0{,}195 + 0{,}0197 \cdot \lg a_{Ti^{3+}}$
14	$2"TiO^{2+}" + N_2 + 4H^+ + 8e^- = 2TiN + 2H_2O;$ $P_{N_2} \approx 0{,}79$ бар	$-0{,}262 - 0{,}0295pH + 0{,}0148 \cdot \lg a_{"TiO^{2+}"}$
15	$2TiO_2 + N_2 + 8H^+ + 8e^- = 2TiN + 4H_2O; P_{N_2} \approx 0{,}79$ бар	$-0{,}270 - 0{,}0591pH$
16	$"TiO^{2+}" + 2H^+ + e^- = Ti^{3+} + H_2O$	$-0{,}463 - 0{,}1182pH + 0{,}0591 \cdot \lg \frac{a_{"TiO^{2+}"}}{a_{Ti^{3+}}}$
17	$TiO_2 + 2H^+ = "TiO^{2+}" + H_2O$	$pH = -0{,}274 - 0{,}5 \cdot \lg a_{"TiO^{2+}"}$

16 domains of the prevalence of different phases can be depicted at the diagram (see figure 5):: I – TiH_2 + Ti_3Si + Ti_5Si_3 + Ti_5Si_4 + TiSi + $TiSi_2$ + Si; II – TiN + Ti_3Si + Ti_5Si_3 + Ti_5Si_4 + TiSi + $TiSi_2$ + Si; III – TiN + Ti_3Si + Ti_5Si_3 + Ti_5Si_4 + TiSi + $TiSi_2$ + SiO_2; IV – TiN + Ti_3Si + Ti_5Si_3 + Ti_5Si_4 + TiSi + $TiSi_2$ + SiO_3^{2-}; V – TiN + Ti_3Si + Ti_5Si_3 + Ti_5Si_4 + TiSi + SiO_2; VI – TiN + Ti_3Si + Ti_5Si_3 + Ti_5Si_4 + TiSi + SiO_3^{2-}; VII – TiN + Ti_3Si + Ti_5Si_3 + Ti_5Si_4 + SiO_2; VIII – TiN + Ti_3Si + Ti_5Si_3 + Ti_5Si_4 + SiO_3^{2-}; IX – TiN + Ti_3Si + Ti_5Si_3 + SiO_2; X – TiN + Ti_3Si + Ti_5Si_3 + SiO_3^{2-}; XI – TiN + Ti_3Si + SiO_2; XII – TiN + Ti_3Si + SiO_3^{2-}; XIII – Ti^{3+} +

$Ti_3Si + SiO_2$; XIV – "TiO^{2+}" + $Ti_3Si + SiO_2$; XV – $TiO_2 + Ti_3Si + SiO_2$; XVI – $TiO_2 + Ti_3Si + SiO_3^{2-}$.

Domains I and II are domains of hydride and nitride passivation of titanium, respectively, domains III-XII correspond to titanium silicides consecutive oxidation, domains XIII and XIV are domains of titanium selective dissolution, domains XV and XVI correspond to TiO_2 oxide formation conditions.

As seen from the diagram, all of titanium oxides, except the highest one, become thermodynamically unstable in presence of titanium nitride. Moreover, presence of titanium hydride and nitride in system significantly affects the mechanism and order of oxidation of its silicides. As seen from figures 4 and 5, complete decomposition of titanium silicides on the components is thermodynamically unfavourable process. The presence of silicon in the system is able to stabilize the titanium and keep it from hydride formation and further oxidation. The authors of [3] associate this fact to the high strength of the Ti–Si covalent bonds.

The conclusions, which are made in this study and based on thermodynamical analysis, don't contradict with experimental researches data. The corrosion-electrochemical behaviour in acidic environments have been studied: for Ti_5Si_3, TiSi and $TiSi_2$ silicides in study [3], and for titanium-silicon alloys, containing from 2.5 up to 11% silicon (by weight) – in study [4]. In both papers it's shown, that passivation film on alloys is mixed and consists of TiO_2 and SiO_2 oxides. No trails of titanium oxides with a lower oxidation degree were found, which indirectly confirms titanium oxidation mechanism via hydride and nitride formation. A more detailed study of the oxide film, that have been performed by authors of [4], allowed to detect the Ti–Si and Ti–O–Si bonds in it (as well as Ti^{3+} and Ti^{2+} ions), which confirms the thermodynamical conclusions about the stabilizing influence of silicon on titanium..

Conclusions

1. The Ti–Si–O state diagram and potential – pH diagram of Ti–Si–H_2O system at 25 ^oC, air pressure of 1 bar and activities of ions in solutions, equal to 1 mole/l with and without consideration of titanium hydride and nitride are calculated and plotted.
2. The thermodynamical analysis of chemical and electrochemical stability of titanium – silicon alloys is performed. Positive influence on silicon at titanium corrosion properties is shown.

References

[1] E. N. Korosteleva, G. A. Pribytkov and A. V. Gurskikh. Bulk changes and structurization in solid-phase sintering of titanium-silicon powder mixtures. *Powder Metallurgy and Metal Ceramics*. **2009**. Vol. 48. № 1-2. P. 8 – 12.

[2] Нанокабели из силицида титана. Нанотехнологическое сообщество «Нанометр» – URL: <http://www.nanometer.ru/2008/07/16/nanoelektronika_53560.html>.

[3] Колотыркин В. И., Княжева В. М. [et al.] Коррозионно-электрохимическое поведение силицидов титана в растворах кислот. *Защита металлов*. **1992**. Т. 28. № 4. С. 545 – 551.
[4] Zhonglin Jiang, Xin Dai and Hugh Middleton. Effect of silicon on corrosion resistance of Ti–Si alloys. *Materials Science and Engineering B.* **2011**. Vol. 176. P. 79 – 86.
[5] C. Vahlas, P. Y. Chevalier, and E. Blanquet. A Thermodynamic evaluation of four Si-M (M = Mo, Ta, Ti, W) binary systems. *CALPHAD*. **1989**. Vol. 13. № 3. P. 273 – 292.
[6] Диаграммы состояния двойных металлических систем: справочник / под ред. Н. П. Лякишева. М.: Машиностроение, **2000**. Т. 3. Кн. 1. С. 449 – 452.
[7] FactSage Databases: база данных фазовых диаграмм. – URL: <http://www.crct.polymtl.ca/fact/documentation>.
[8] Debashis Bandyopadhyay. The Ti-Si-C system (Titanium-Silicon-Carbon). *Journal of Phase Equilibria and Diffusion*. **2004**. Vol. 25. № 5. P. 415 – 420.
[9] Yong Du, Julius C. Schuster, Hans J. Seifert and Fritz Aldinger. Experimental investigation and thermodynamic calculation of the Titanium–Silicon–Carbon system. *Journal of the American Ceramic Society*. **2000**. Vol. 83. № 1. P. 197 – 203.
[10] Takeshi Yoshikawa, Kazuki Morita, Sakiko Kawanishi and Toshihiro Tanaka. Thermodynamics of impurity elements in solid silicon. *Journal of Alloys and Compounds*. **2010**. Vol. 490. P. 31 – 41.
[11] Справочник по электрохимии / под ред. А. М. Сухотина. Л.: Химия, **1981**. 488 с.
[12] Диаграммы состояния силикатных систем: справочник / Торопов Н. А., Борзаковский В. П. [et al.]. М. – Л.: Наука, **1965**. Вып. 2. 372 с.
[13] Рузинов Л. П, Гуляницкий Б. С. Равновесные превращения металлургических реакций М.: Металлургия, **1975**. 416 с.
[14] Термические константы веществ: база данных. – URL: <http://www.chem.msu.su/cgi-bin/tkv.pl?show=welcome.html>
[15] JANAF Thermochemical Tables. Third Edition. *J. Phys. Chem. Ref. Data*. **1985**..Vol. 14. Suppl. 1.
[16] Жук Н. П. Курс теории коррозии и защиты металлов: учеб. пособие для вузов: 2-е изд., стереотип. (перепеч. с изд. 1976 г.). М: ООО ТИД "Альянс". **2006**. 472 с.
[17] F. Cotton and G. Wilkinson. Advanced Inorganic Chemistry. Third Edition. New York – London – Sydney – Toronto: John Wiley & Sons. 1972. P. 807 – 818.
[18] Тюрин А. Г. Термодинамика химической и электрохимической устойчивости сплавов: учебное пособие. В 2 ч. Ч. 2. Низкотемпературное окисление. Челябинск: Изд-во Челяб. гос. ун-та, **2004**. 91 с.
[19] Тюрин А. Г. Термодинамический анализ образования фаз в процессах электролитического осаждения титана из водных растворов. *Электрохимия*. **1990**. Вып. 26. № 12. С. 1599 – 1605.

6. V – Si system
6.1. Vanadium silicides

The phase diagram of the V – Si system is presented in Figure 22.

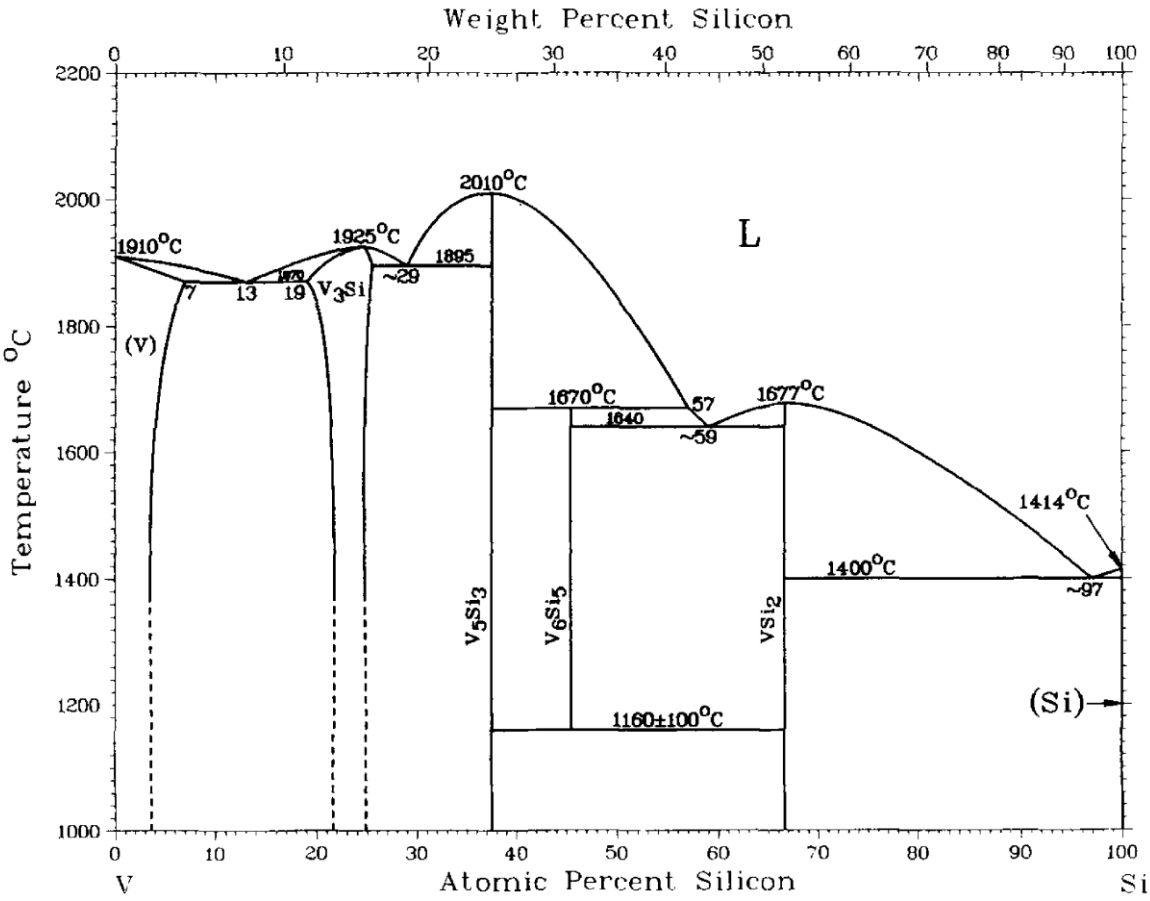

Fig. 22. The phase diagram of the V – Si system [Smith, 1985].

Four vanadium silicides, namely V_3Si, V_5Si_3, V_6Si_5 and VSi_2, exist in the system; however, the silicide V_6Si_5 is stable only at elevated temperatures [Okamoto, 2010; Smith, 1981; Smith, 1985; Storms, Myers, 1984; Zhang et al., 2008]. The compounds V_5Si_3, V_6Si_5 and VSi_2 are stoichiometric, whereas V_3Si has the noticeable homogeneity range at elevated temperatures. However, the broadness of this homogeneity range quickly lowers with the temperature decrease: it is ~5 at. % wide at 1800 °C, and only ~1 at. % wide at 1000 °C. Therefore, in the present study the silicide V_3Si is treated as the stoichiometric compound at 25 °C.

The standard Gibbs energies of formation of vanadium silicides are presented in Table 9.

Table 9. The standard Gibbs energies of formation of vanadium silicides.

Compound	$-\Delta_f G^o_{298,15}$, $J \cdot mol^{-1}$	Reference
V_3Si	168 400	[Zhang et al., 2008]
V_5Si_3	459 300	[Smith, 1985]
VSi_2	119 300	[Zhang et al., 2008]

The maximum solid solubility of silicon in vanadium with body-centered cubic crystal structure at 25 °C might be estimated according to the equilibrium:

$$3\,V\,(bcc) + Si\,(bcc) \rightleftharpoons V_3Si\,(s). \qquad (97)$$

The Gibbs energy of reaction (97) consists of two terms:

$$\Delta_r G^o_{298,15,\,(97)} = \Delta_f G^o_{298,15,\,V_3Si} - \Delta_{tr} G^o_{298,15,\,Si(diamond \rightarrow bcc)}. \qquad (98)$$

According to the reference book [Dinsdale, 1991], $\Delta_{tr} G^o_{298,15,\,Si(diamond \rightarrow bcc)} = 40\,300 \dfrac{J}{mol}$. The excess Gibbs energy of the bcc-solid solution of silicon in vanadium at 25 °C is expressed as [Zhang et al., 2008]:

$$G^E_{298,15,\,V-Si\,(bcc)} = -187\,180 \cdot x_{Si} \cdot (1 - x_{Si}), \ \frac{J}{mol}. \qquad (99)$$

The Gibbs energy of reaction (97) is related to the thermodynamic activities of silicon and vanadium in the solid solution as follows:

$$\Delta_r G^o_{298,15,\,(97)} = -2478{,}9562 \cdot \ln \frac{a_{V_3Si\,(s)}}{a^3_{V\,(bcc)} \cdot a_{Si\,(bcc)}} = \qquad (100)$$
$$= 7436{,}8686 \cdot \ln a_{V\,(bcc)} + 2478{,}9562 \cdot \ln a_{Si\,(bcc)}$$

Differentiating equation (99) with respect to the mole fractions of vanadium and silicon and applying equation (6) yields the following expressions for the activities of the solid solution components:

$$2478{,}9562 \cdot \ln a_{V\,(bcc)} = 2478{,}9562 \cdot \ln (1 - x_{Si}) - 187\,180 \cdot x^2_{Si}, \qquad (101)$$

$$2478{,}9562 \cdot \ln a_{Si\,(bcc)} = 2478{,}9562 \cdot \ln x_{Si} - 187\,180 \cdot (1 - x_{Si})^2. \qquad (102)$$

Substituting the equations (98), (101) and (102) into the equation (100) and solving it for the silicon mole fraction gives the maximum solid solubility of silicon at 25 °C: $x_{Si} = 1{,}657 \cdot 10^{-4}$. The activities of the solid solution components are equal to $a_{V\,(bcc)} = 0{,}9826$ and $a_{Si\,(bcc)} = 7{,}245 \cdot 10^{-35}$.

6.2. Equilibira in V – Si – O system

The phase diagram of V – O system is rich with various oxides. The following ones are thermodynamically stable at 25 °C: VO, V_2O_3, V_3O_5, Magnéli phases [Magnéli, 1978; Schwingenschlögl, Eyert, 2004] V_nO_{2n-1} ($4 \leqslant n \leqslant 8$), VO_2, V_6O_{13}, V_3O_7 and V_2O_5. No vanadium silicates are known at the standard conditions [Spear, Gilles, Schäfer, 1968]. The standard Gibbs energies of formation of almost all vanadium oxides (except VO_2, V_3O_7 and V_2O_5) were taken from [Термические константы веществ, 2007]; the values for these three exceptions were taken from [Chase Jr. et al., 1985].

The state diagram of the V – Si – O system is presented in Figure 23. The equilibria are listed in Table 10.

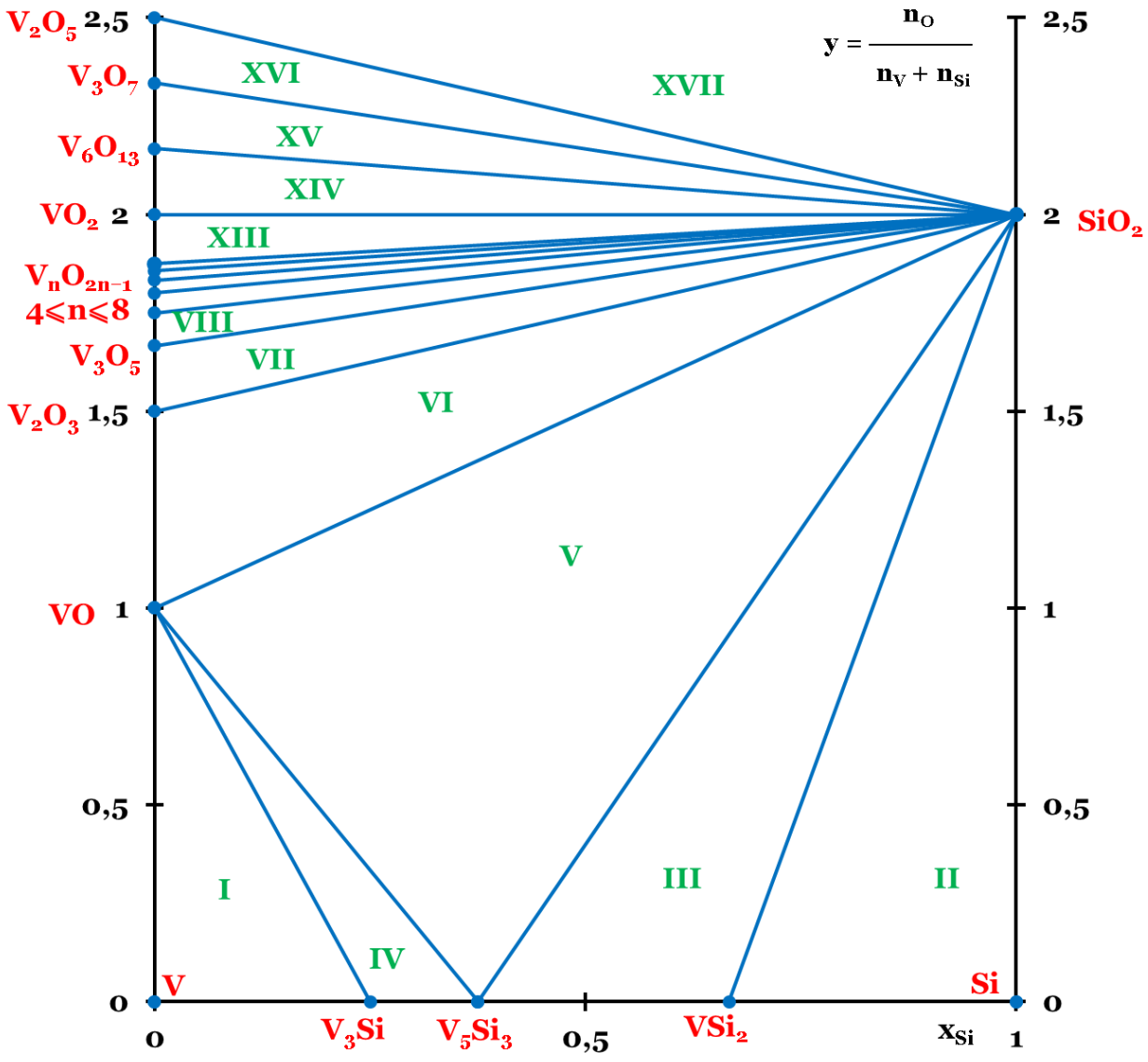

Fig. 23. The state diagram of the V – Si – O system.

Table 10. List of equilibria in the V – Si – O ternary system according to the state diagram presented in Figure 23.

No of domain in Fig. 23	Equilibrium phases	Reaction equation	P_{O_2}, bar
I	$V(bcc) - V_3Si - VO$	$2V(bcc) + O_2\ (g) \rightleftharpoons 2VO;\ a_{V(bcc)} = 0{,}9826$	$7{,}4 \cdot 10^{-142}$
II	$Si\ (dia) - VSi_2 - SiO_2$	$Si\ (dia) + O_2\ (g) \rightleftharpoons SiO_2$	$7{,}7 \cdot 10^{-142}$
III	$VSi_2 - V_5Si_3 - SiO_2$	$5VSi_2 + 7O_2\ (g) \rightleftharpoons V_5Si_3 + 7SiO_2$	$2{,}1 \cdot 10^{-138}$
IV	$V_3Si - V_5Si_3 - VO$	$3V_3Si + 2O_2\ (g) \rightleftharpoons V_5Si_3 + 4VO$	$7{,}6 \cdot 10^{-138}$
V	$V_5Si_3 - VO - SiO_2$	$2V_5Si_3 + 11O_2\ (g) \rightleftharpoons 10VO + 6SiO_2$	$3{,}2 \cdot 10^{-127}$
VI	$VO - V_2O_3 - SiO_2$	$4VO + O_2\ (g) \rightleftharpoons 2V_2O_3$	$4{,}5 \cdot 10^{-111}$
VII	$V_2O_3 - V_3O_5 - SiO_2$	$6V_2O_3 + O_2\ (g) \rightleftharpoons 4V_3O_5$	$4{,}6 \cdot 10^{-91}$
VIII	$V_3O_5 - V_4O_7 - SiO_2$	$8V_3O_5 + O_2\ (g) \rightleftharpoons 6V_4O_7$	$1{,}1 \cdot 10^{-68}$
IX	$V_4O_7 - V_5O_9 - SiO_2$	$10V_4O_7 + O_2\ (g) \rightleftharpoons 8V_5O_9$	$5{,}5 \cdot 10^{-59}$
X	$V_5O_9 - V_6O_{11} - SiO_2$	$12V_5O_9 + O_2\ (g) \rightleftharpoons 10V_6O_{11}$	$9{,}7 \cdot 10^{-58}$
XI	$V_6O_{11} - V_7O_{13} - SiO_2$	$14V_6O_{11} + O_2\ (g) \rightleftharpoons 12V_7O_{13}$	$2{,}2 \cdot 10^{-54}$
XII	$V_7O_{13} - V_8O_{15} - SiO_2$	$16V_7O_{13} + O_2\ (g) \rightleftharpoons 14V_8O_{15}$	$1{,}1 \cdot 10^{-52}$
XIII	$V_8O_{15} - VO_2 - SiO_2$	$2V_8O_{15} + O_2\ (g) \rightleftharpoons 16VO_2$	$5{,}6 \cdot 10^{-51}$
XIV	$VO_2 - V_6O_{13} - SiO_2$	$12VO_2 + O_2\ (g) \rightleftharpoons 2V_6O_{13}$	$3{,}4 \cdot 10^{-47}$
XV	$V_6O_{13} - V_3O_7 - SiO_2$	$2V_6O_{13} + O_2\ (g) \rightleftharpoons 4V_3O_7$	$1{,}3 \cdot 10^{-44}$
XVI	$V_3O_7 - V_2O_5 - SiO_2$	$4V_3O_7 + O_2\ (g) \rightleftharpoons 6V_2O_5$	$1{,}6 \cdot 10^{-21}$
XVII	$V_2O_5 - SiO_2 - O_2\ (g)$	–	–

6.3. Potential – pH diagram of V – H_2O system

In aqueous environments vanadium might form four different cations – V^{2+} (aq), V^{3+} (aq), VO^{2+} (aq) and VO_2^+ (aq). Vanadium (V) forms several anions. The simplest vanadate is VO_4^{3-} (aq), however, it tends to polimerise. Several isopolyvanadates, both hydrolysed and unhydrolysed, might exist in a solution, the data on them are often contradictory, and there is still no single opinion about it [Pope, Dale, 1968; Ropp, Carroll, 1977; Sadiq, 1988; Музгин et al., 1981]. Several variations of the potential – pH diagram for vanadium containing different aqueous species exist in the literature [Evans, Garrels, 1958; Kelsall, Thompson, Francis, 1993; Post, Robins, 1976; 曾英, 马旻锐, 2009].

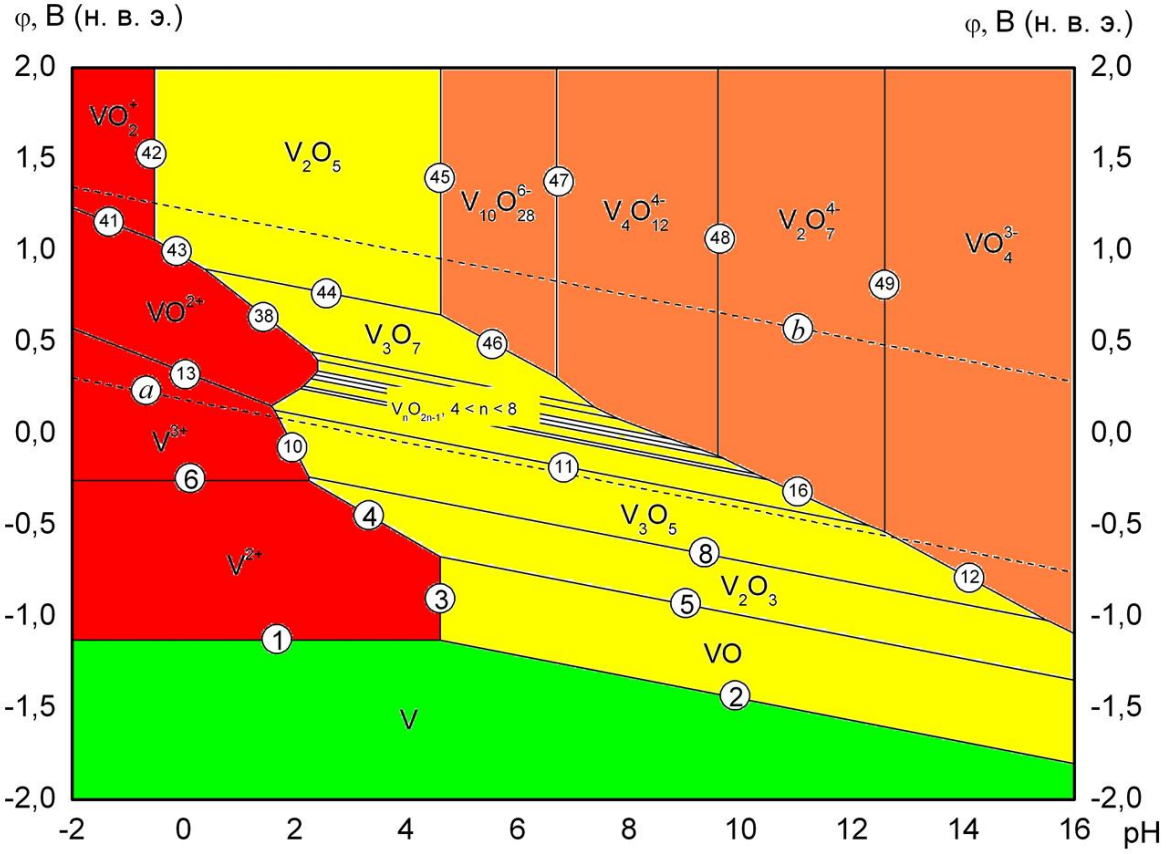

Fig. 24. The potential – pH diagram of the V – H_2O system at 25 °C, air pressure of 1 bar and the activities of vanadium species in a solution of 1 M.

In this study only those species were considered that were presented in each of these publications. The following vanadates were chosen for consideration: VO_4^{3-} (aq), $V_2O_7^{4-}$ (aq), $V_4O_{12}^{4-}$ (aq) and $V_{10}O_{28}^{6-}$ (aq). The standard Gibbs energies of formation of aqueous vanadium species were

taken from [Kelsall, Thompson, Francis, 1993]. No vanadium hydrides are known [Griffiths, Pryde, Righini-Brand, 1972].

The potential – pH diagram for vanadium taking into account the aforementioned vanadium oxides and aqueous species is presented in Figure 24.

6.4. Potential – pH diagram of V – Si – H_2O system

The potential – pH diagram of the V – Si – H_2O system at 25 °C, air pressure of 1 bar and the activities of species in a solution of 1 mol l^{-1} is presented in Figure 25. As can be seen, the upper part of the diagram is a simple superposition of the potential – pH diagrams of vanadium and silicon. The equilibria involving vanadium silicides occur far below the domain of water electrochemical stability. The cross section of the potential – pH diagram in the region of thermodynamic stability of vanadium silicides is presented in Figure 26. The following domains of thermodynamic stability of certain phases might be depicted:

I – VO + V_3Si + V_5Si_3 + VSi_2 + Si (diamond);

II – V (bcc) + V_3Si + V_5Si_3 + VSi_2 + $H_2SiO_4^{2-}$;

III – V^{2+} + V_3Si + V_5Si_3 + VSi_2 + Si (diamond);

IV – V^{2+} + V_3Si + V_5Si_3 + VSi_2 + H_4SiO_4;

V – VO + V_3Si + V_5Si_3 + VSi_2 + H_4SiO_4;

VI – VO + V_3Si + V_5Si_3 + VSi_2 + $H_2SiO_4^{2-}$;

VII – V^{2+} + V_3Si + V_5Si_3 + Si (diamond);

VIII – V^{2+} + V_3Si + V_5Si_3 + H_4SiO_4;

IX – VO + V_5Si_3 + VSi_2 + H_4SiO_4;

X – VO + V_5Si_3 + VSi_2 + $H_2SiO_4^{2-}$;

XI – V^{2+} + V_5Si_3 + H_4SiO_4;

XII – VO + V_5Si_3 + H_4SiO_4;

XIII – VO + V_5Si_3 + $H_2SiO_4^{2-}$;

XIV – V^{2+} + H_4SiO_4;

XV – VO + H_4SiO_4;

XVI – VO + $H_2SiO_4^{2-}$.

The diagrams show that silicon has a little impact on the corrosion-electrochemical behaviour of the V – Si system. The passivity domain of vanadium is also quite narrow. If the silicon content in the system is enough, H_4SiO_4 would be the only product that could prevent the dissolution of silicides.

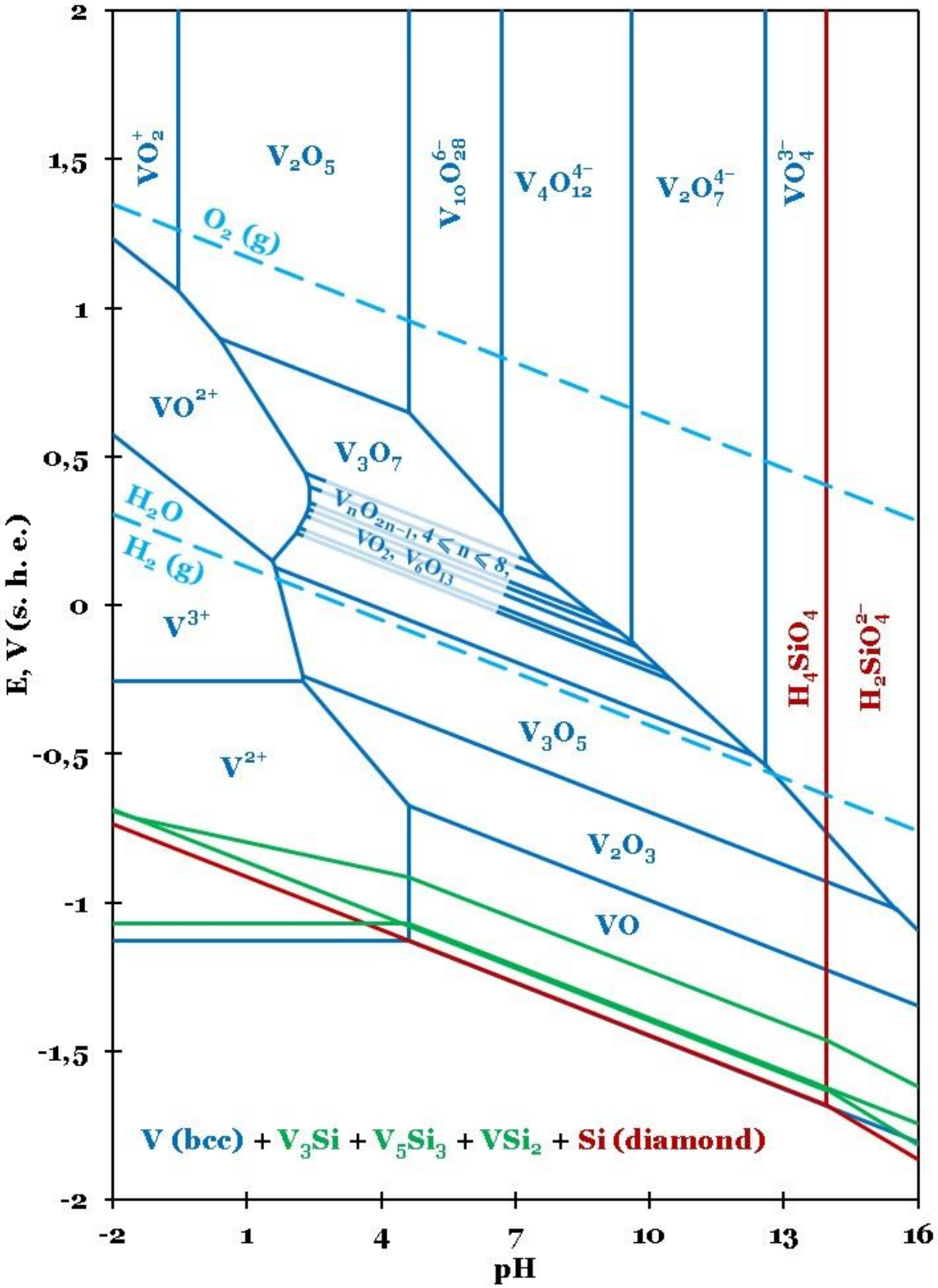

Fig. 25. The potential – pH diagram of the V – Si – H_2O system at 25 °C, air pressure of 1 bar and the activities of species in a solution of 1 M.

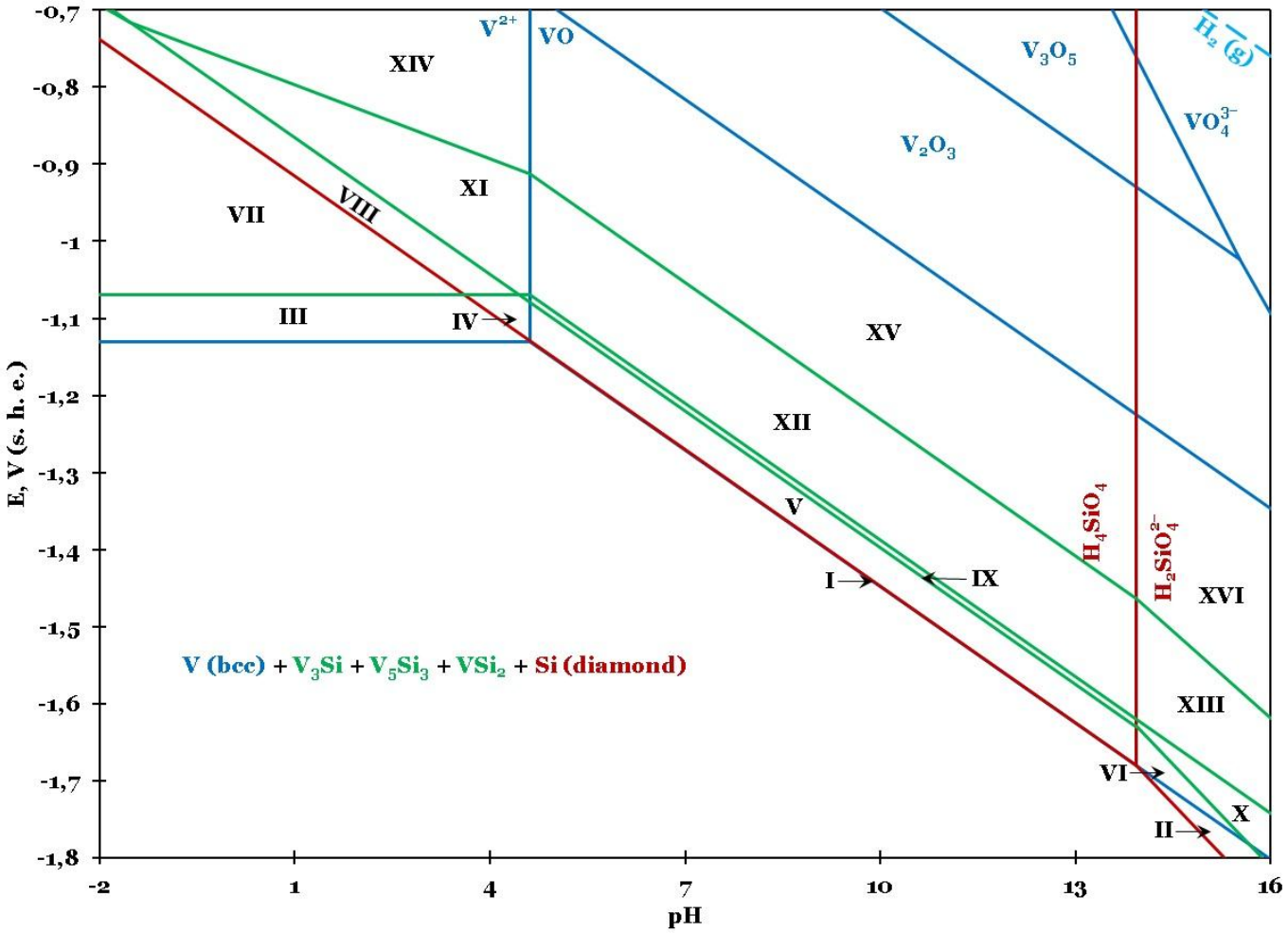

Fig. 26. The cross-section of the potential – pH diagram for the V – Si – H_2O system in the region of thermodynamic stability of vanadium silicides. The domains of thermodynamic stability are discussed in text.

Publications to chapter 6

The content of this chapter was not published yet.

7. Cr – Si system

The chemical and electrochemical stability of the Cr – Si system was already assessed earlier [Tyurin, 2004]. However, that study did not take into account all features of the system and relied on the outdated thermodynamic information. Therefore, a new assessment was performed.

7.1. Chromium silicides

The phase diagram of the Cr – Si system is presented in Figure 27.

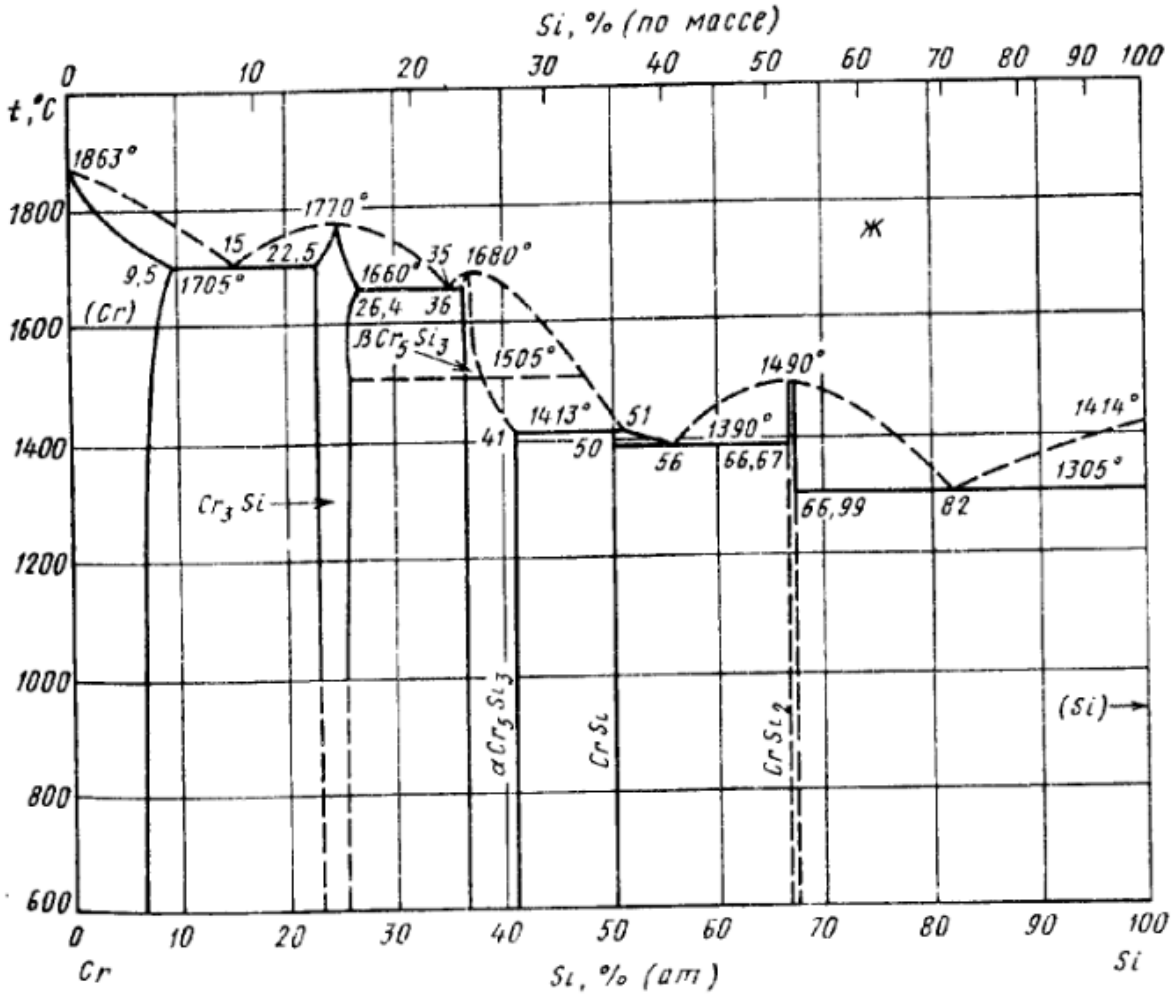

Fig. 27. The phase diagram of the Cr – Si system [Диаграммы состояния двойных металлических систем: справочник, 2001].

The nature of chromium – silicon alloys was studied several times till the beginning of the XX century. Herewith, the results of early studies were very diverse and, sometimes, contradictory to each other. The existence of several chromium silicides (Cr_3Si, Cr_2Si, Cr_3Si_2, Cr_5Si_3, CrSi, Cr_2Si_3, $CrSi_2$, Cr_2Si_7) was reported, but in the present time only four silicides (namely,

Cr_3Si, Cr_5Si_3, CrSi and $CrSi_2$), as well as the solid solution of silicon in bcc-chromium were reliably identified [Chen, Du, Schuster, 2009; Coughanowr, Ansara, Lukas, 1994; Cui, Jung, 2017; Du, Schuster, 2000; Gokhale, Abbaschian, 1987; Okamoto, 1997; Okamoto, 2001; Predel, 1994; Свечников, Кочержинский, Юлко, 1964]. The silicides Cr_3Si and $CrSi_2$ are not stoichiometric and have a homogeneity ranges.

Silicon forms a substitution solid solution in chromium. The solid solubility is (by weight) ~2,5 % at 750 °C, ~3,5 % at 1000 °C, ~4,5 % at 1550 °C and ~5,5 % at the eutectic temperature [Диаграммы состояния двойных металлических систем: справочник, 2001].

The standard Gibbs energies of formation of chromium silicides according to paper [Chen, Du, Schuster, 2009] are presented in Table 11.

Table 11. The standard Gibbs energies of formation of chromium silicides [Chen, Du, Schuster, 2009].

Compound	$-\Delta_f G^{o}_{298,15}$, $J \cdot mol^{-1}$
Cr_3Si	124 400
Cr_5Si_3	320 100
CrSi	76 400
$CrSi_2$	99 700

The maximum solid solubility of silicon in chromium with body-centered cubic crystal structure at 25 °C might be estimated according to the equilibrium:

$$3\,Cr\,(bcc) + Si\,(bcc) \rightleftharpoons Cr_3Si\,(s). \qquad (103)$$

The excess Gibbs energy of the bcc-solid solution of silicon in chromium at 25 °C is expressed as:

$$G^{E}_{298,15,\,Cr-Si\,(bcc)} = -x_{Si} \cdot (1 - x_{Si}) \cdot (98\,400 \cdot x_{Si} + 28\,800),\ \frac{J}{mol}. \qquad (104)$$

The maximum solid solubility of silicon in chromium at 25 °C was estimated totally analogous to that how the maximum solid solubility of silicon in vanadium were estimated in Section 6.1; the calculated value is $x_{Si} = 7{,}198 \cdot 10^{-6}$. The activities of the solid solution components are equal to $a_{Cr\,(bcc)} = 0{,}9999$ and $a_{Si\,(bcc)} = 1{,}4152 \cdot 10^{-29}$.

7.2. Equilibira in Cr – Si – O system

The phase diagram of Cr – O reveals three common chromium oxides, namely, Cr_2O_3, CrO_2 and CrO_3. However, in addition to these ones, other oxygen compounds of chromium exist in the system, although they are of lesser importance.

The thermal decomposition of CrO_3 to Cr_2O_3 proceeds through several intermediate steps [Chamberland, 1977; Fukunaga, Saito, 1968; Goto, Kitamura, 1962; Kubota, 1961; Mittal et al., 2014; White, Roy, 1975; Wilhelmi et al., 1968]. Different compositions were proposed for these intermediate phases, including Cr_2O_5, Cr_3O_8, Cr_5O_{12}, Cr_6O_{15} and Cr_8O_{21}. It was later found that Cr_2O_5 and Cr_6O_{15} were the various proposed formulae for the one phase, as well as Cr_3O_8 and Cr_8O_{21}. Moreover, Cr_5O_{12}, Cr_6O_{15} and Cr_8O_{21} are, in fact, chromium chromates and dichromates, correspondingly, $Cr_2(CrO_4)_3$, $Cr_2(CrO_4)_2(Cr_2O_7)$ and $Cr_2(Cr_2O_7)_3$.

By reduction of Cr_2O_3 by H_3PO_2 or by thermal decomposition of $Cr(CO)_6$ the chromium (II) oxide, CrO, might be obtained [Holleman, Wiberg, Wiberg, 2001]. It is readily oxidised by the atmosphere. By reduction of Cr_2O_3 by other metals or by reaction of chromium with water steam in the presence of hydrogen at higher temperatures the unstable oxide Cr_3O might be obtained [Диаграммы состояния двойных металлических систем: справочник, 2001].

The phase Cr_3O_4, which existence was proposed earlier, is stable only in presence of iron, and is actually a solid solution of Cr_3O_4 and $FeCr_2O_4$, rather than a pure phase [Диаграммы состояния двойных металлических систем: справочник, 2001].

A single ternary compound exist in the Cr – Si – O system, it is chromium metasilicate, Cr_2SiO_4 [Dollase, Seifert, O'Neill, 1994; Miletich et al., 1999; Акимов, Сенин, Рощин, 2013].

The standard Gibbs energies of formation are available in reference books only for Cr_2O_3 and CrO_3. Using the values from [Wagman et al., 1982], the standard Gibbs energies of formation of other chromium oxides were estimated according to the Gorichev's method. The following equation was obtained:

$$3 \cdot \Delta_f G^o_{298,15,\ CrO_x} = 363\,400 \cdot x^2 - 1\,603\,200 \cdot x. \qquad (105)$$

The standard Gibbs energy of formation of Cr_2SiO_4 was estimated according to ΔO^{2-} method and equals $\Delta_f G^o_{298,15,\ Cr_2SiO_4} = -1\,687\,200\ J \cdot mol^{-1}$.

The state diagram of the Cr – Si – O system including only the most important compounds is presented in Figure 28; the corresponding equilibria are listed in Table 12. The hypothetical state diagram taking into account all known chromium oxides and chromium silicate is presented in Figure 29; the corresponding equilibria are listed in Table 13.

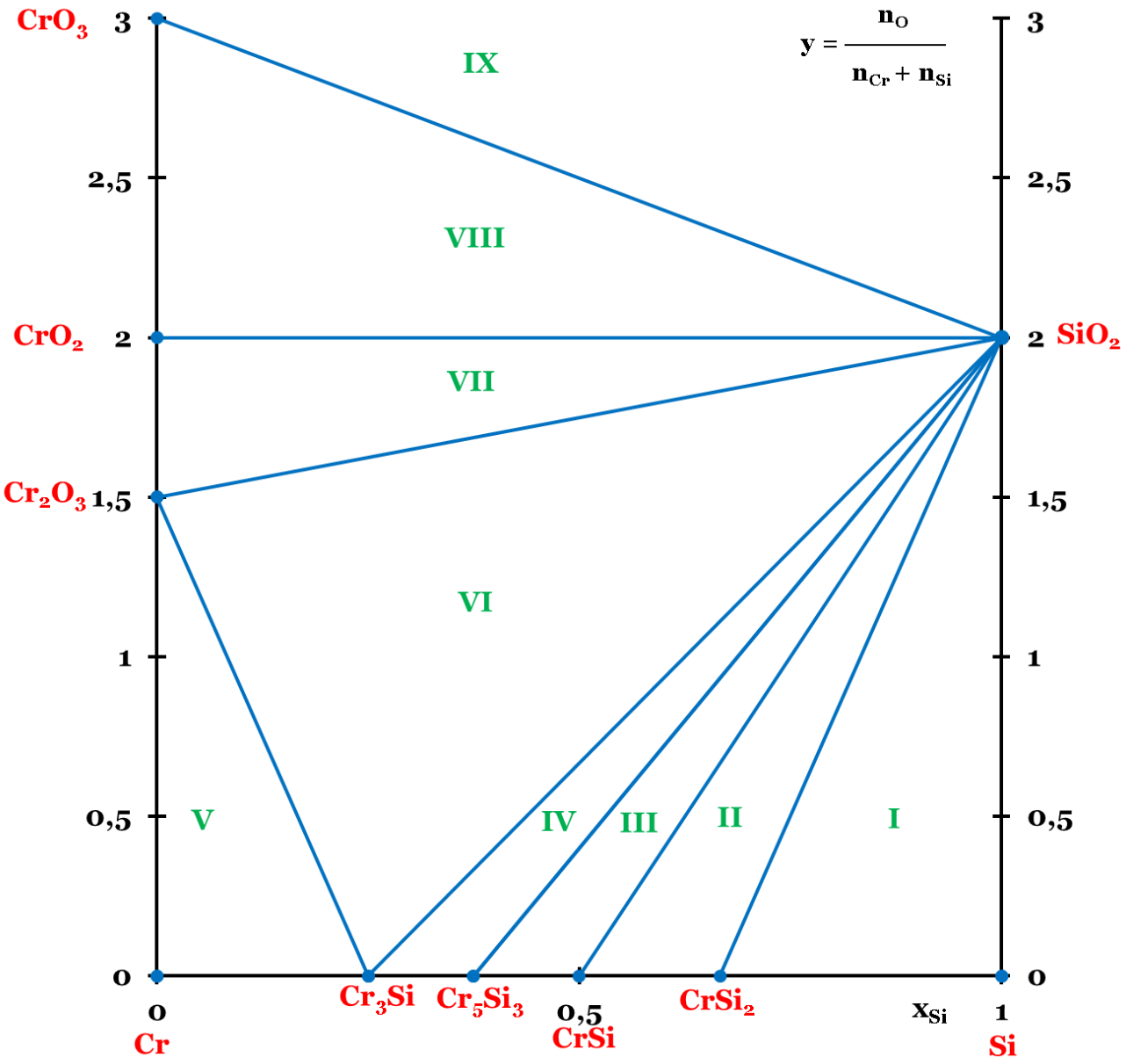

Fig. 28. The state diagram of the Cr – Si – O system with only the most important chromium oxides.

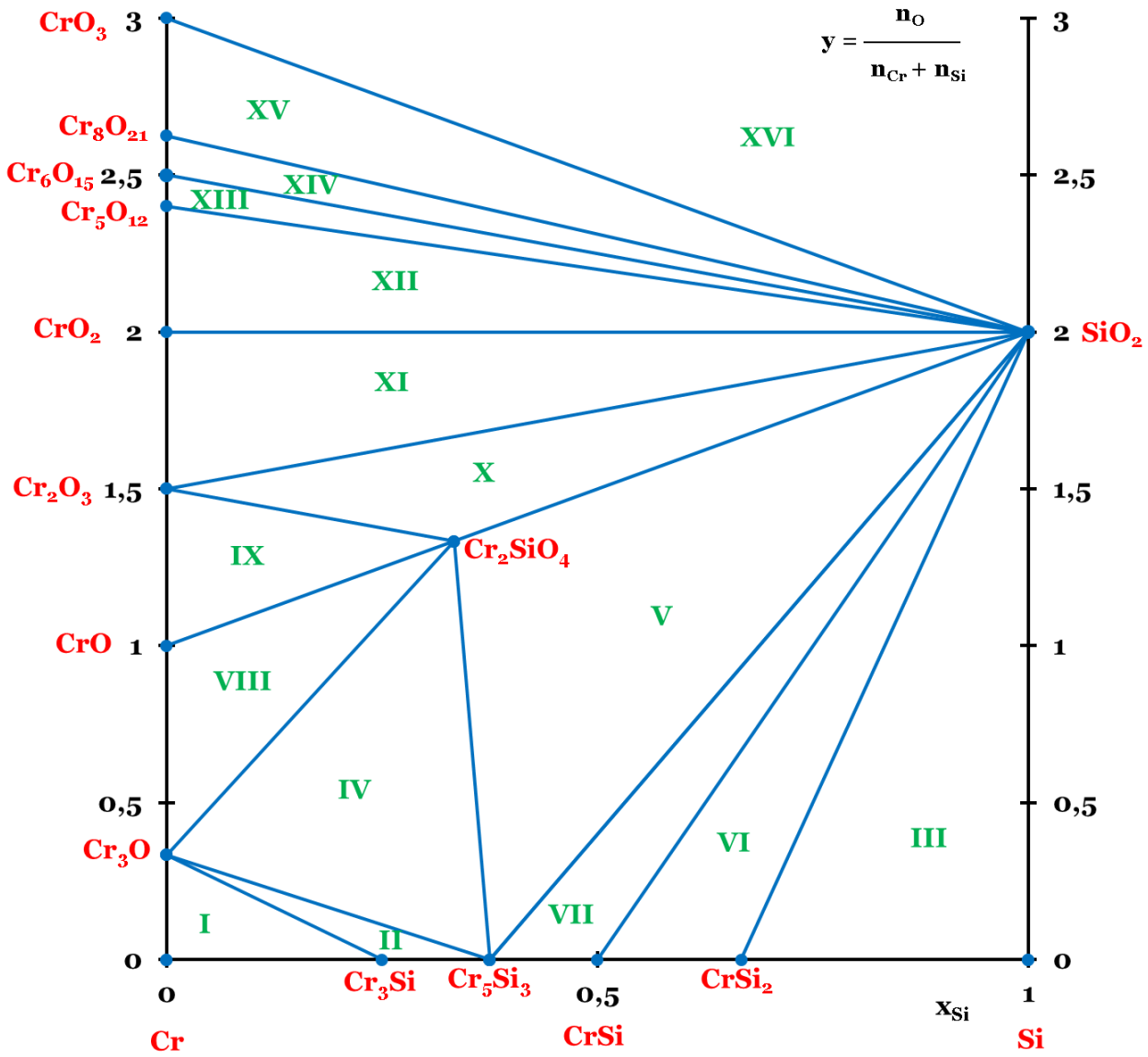

Fig. 29. The hypothetical state diagram of the Cr – Si – O system taking into account all possible chromium oxides and chromium silicate.

Table 12. List of equilibria in the Cr – Si – O ternary system according to the state diagram presented in Figure 28.

No of domain in Fig. 28	Equilibrium phases	Reaction equation	P_{O_2}, bar
I	$Si\,(dia) - CrSi_2 - SiO_2$	$Si\,(dia) + O_2\,(g) \rightleftharpoons SiO_2$	$7{,}7 \cdot 10^{-142}$
II	$CrSi_2 - CrSi - SiO_2$	$CrSi_2 + O_2\,(g) \rightleftharpoons CrSi + SiO_2$	$9{,}5 \cdot 10^{-138}$
III	$CrSi - Cr_5Si_3 - SiO_2$	$5CrSi + 2O_2\,(g) \rightleftharpoons Cr_5Si_3 + 2SiO_2$	$2{,}0 \cdot 10^{-136}$
IV	$Cr_5Si_3 - Cr_3Si - SiO_2$	$3Cr_5Si_3 + 4O_2\,(g) \rightleftharpoons 5Cr_3Si + 4SiO_2$	$5{,}2 \cdot 10^{-127}$
V	$Cr\,(bcc) - Cr_3Si - Cr_2O_3$	$4Cr\,(bcc) + 3O_2\,(g) \rightleftharpoons 2Cr_2O_3;\ a_{Cr\,(bcc)} = 0{,}9999$	$2{,}3 \cdot 10^{-124}$
VI	$Cr_3Si - Cr_2O_3 - SiO_2$	$4Cr_3Si + 13O_2\,(g) \rightleftharpoons 6Cr_2O_3 + 4SiO_2$	$4{,}9 \cdot 10^{-123}$
VII	$Cr_2O_3 - CrO_2 - SiO_2$	$2Cr_2O_3 + O_2\,(g) \rightleftharpoons 4CrO_2$	$1{,}9 \cdot 10^{-39}$
VIII	$CrO_2 - CrO_3 - SiO_2$	$2CrO_2 + O_2\,(g) \rightleftharpoons 2CrO_3$	$9{,}7 \cdot 10^{24}$
IX	$CrO_3 - SiO_2 - O_2\,(g)$	–	–

Table 13. List of equilibria in the Cr – Si – O ternary system according to the state diagram presented in Figure 29.

No of domain in Fig. 29	Equilibrium phases	Reaction equation	P_{O_2}, bar
I	$Cr(bcc) - Cr_3Si - Cr_3O$	$6Cr(bcc) + O_2\ (g) \rightleftharpoons 2Cr_3O;\ a_{Cr(bcc)} = 0{,}9999$	$6{,}5 \cdot 10^{-174}$
II	$Cr_3Si - Cr_5Si_3 - Cr_3O$	$18Cr_3Si + 4O_2\ (g) \rightleftharpoons 6Cr_5Si_3 + 8Cr_3O$	$5{,}6 \cdot 10^{-160}$
III	$Si\ (dia) - CrSi_2 - SiO_2$	$Si\ (dia) + O_2\ (g) \rightleftharpoons SiO_2$	$7{,}7 \cdot 10^{-142}$
IV	$Cr_5Si_3 - Cr_3O - Cr_2SiO_4$	$6Cr_5Si_3 + 2Cr_3O + 35O_2\ (g) \rightleftharpoons 18Cr_2SiO_4$	$3{,}0 \cdot 10^{-138}$
V	$Cr_5Si_3 - Cr_2SiO_4 - SiO_2$	$2Cr_5Si_3 + 11O_2\ (g) \rightleftharpoons 5Cr_2SiO_4 + SiO_2$	$8{,}9 \cdot 10^{-138}$
VI	$CrSi_2 - CrSi - SiO_2$	$CrSi_2 + O_2\ (g) \rightleftharpoons CrSi + SiO_2$	$9{,}5 \cdot 10^{-138}$
VII	$CrSi - Cr_5Si_3 - SiO_2$	$5CrSi + 2O_2\ (g) \rightleftharpoons Cr_5Si_3 + 2SiO_2$	$2{,}0 \cdot 10^{-136}$
VIII	$Cr_3O - CrO - Cr_2SiO_4$	$2Cr_3O + 2O_2\ (g) \rightleftharpoons 6CrO$	$1{,}9 \cdot 10^{-131}$
IX	$CrO - Cr_2O_3 - Cr_2SiO_4$	$4CrO + O_2\ (g) \rightleftharpoons 2Cr_2O_3$	$6{,}7 \cdot 10^{-82}$
X	$Cr_2O_3 - Cr_2SiO_4 - SiO_2$	$2Cr_2SiO_4 + O_2\ (g) \rightleftharpoons 2Cr_2O_3 + 2SiO_2$	$2{,}0 \cdot 10^{-62}$
XI	$Cr_2O_3 - CrO_2 - SiO_2$	$2Cr_2O_3 + O_2\ (g) \rightleftharpoons 4CrO_2$	$1{,}9 \cdot 10^{-39}$
XII	$CrO_2 - Cr_5O_{12} - SiO_2$	$5CrO_2 + O_2\ (g) \rightleftharpoons Cr_5O_{12}$	0,322
XIII	$Cr_5O_{12} - Cr_6O_{15} - SiO_2$	$12Cr_5O_{12} + 3O_2\ (g) \rightleftharpoons 10Cr_6O_{15}$	$5{,}5 \cdot 10^{20}$
XIV	$Cr_6O_{15} - Cr_8O_{21} - SiO_2$	$8Cr_6O_{15} + 3O_2\ (g) \rightleftharpoons 6Cr_8O_{21}$	$2{,}0 \cdot 10^{30}$
XV	$Cr_8O_{21} - CrO_3 - SiO_2$	$2Cr_8O_{21} + 3O_2\ (g) \rightleftharpoons 16CrO_3$	$3{,}4 \cdot 10^{-51}$
XVI	$CrO_3 - SiO_2 - O_2\ (g)$	–	–

7.3. Potential – pH diagram of Cr – H_2O system

Chromium might exist in an aqueous solution in three different oxidation states: +2, +3 and +6. The first two of them are represented by the cations Cr^{2+} (aq) and Cr^{3+} (aq), respectively. The last one is represented by the various chromate species: CrO_4^{2-} (aq) , $HCrO_4^-$ (aq), H_2CrO_4 (aq) and $Cr_2O_7^{2-}$ (aq). The Gibbs energies of formation of these species were taken from [Ball, Nordstrom, 1998]. There is no chromium hydrides known [Baranowski, 1972; Katsura, 1992; Venkatraman, Neumann, 1991].

The activity – pH diagram for chromium (VI) species is presented in Figure 30.

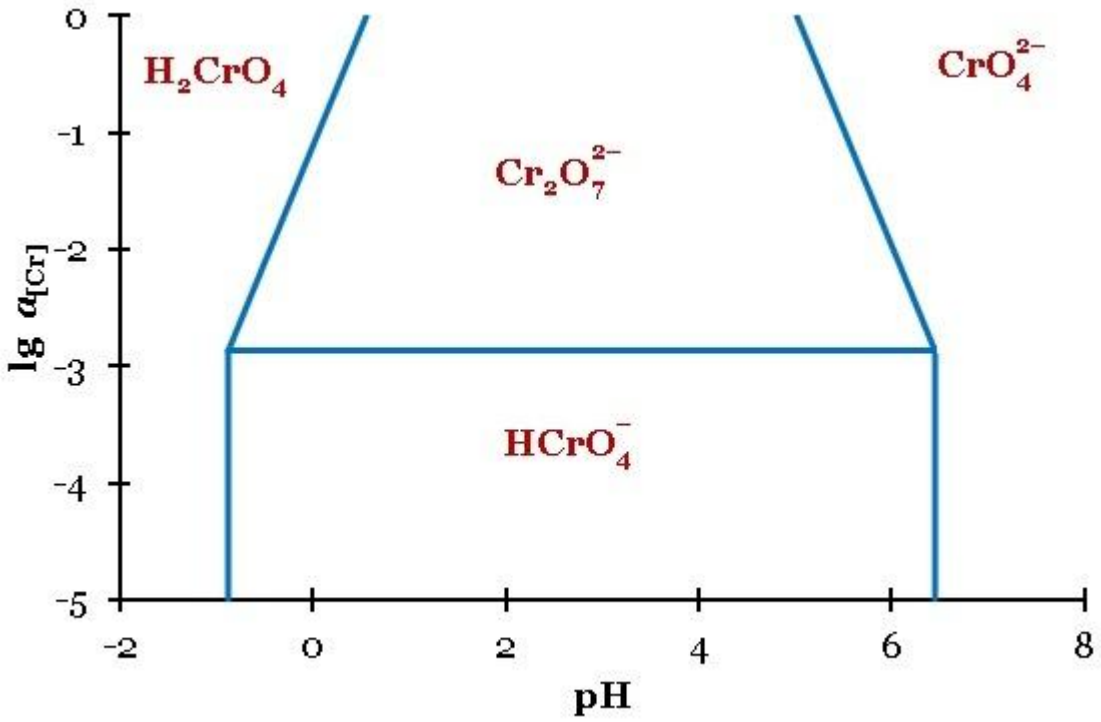

Fig. 30. The activity – pH diagram for chromium (IV) aqueous species.

As could be seen from the diagram, the dichromate-ion $Cr_2O_7^{2-}$ (aq) is thermodynamically stable in concentrated solutions (if lg $a_{[Cr]} > -2{,}866$) only, whereas in more diluted solutions (if lg $a_{[Cr]} < -2{,}866$) the hydrochromate-ion $HCrO_4^-$ (aq) is stable.

The potential – pH diagram of Cr – H_2O system is presented in Figures 31 through 33. In the Figures 31 and 32 only the most common chromium species are presented, in accordance with the published Pourbaix diagrams of chromium [Beverskog, Puigdomenech, 1997; You et

al., 2010]. Figure 31 presents the diagram at the activities of chromium species 1 mol·l^{-1}, and Figure 32 – at 10^{-6} mol·l^{-1}.

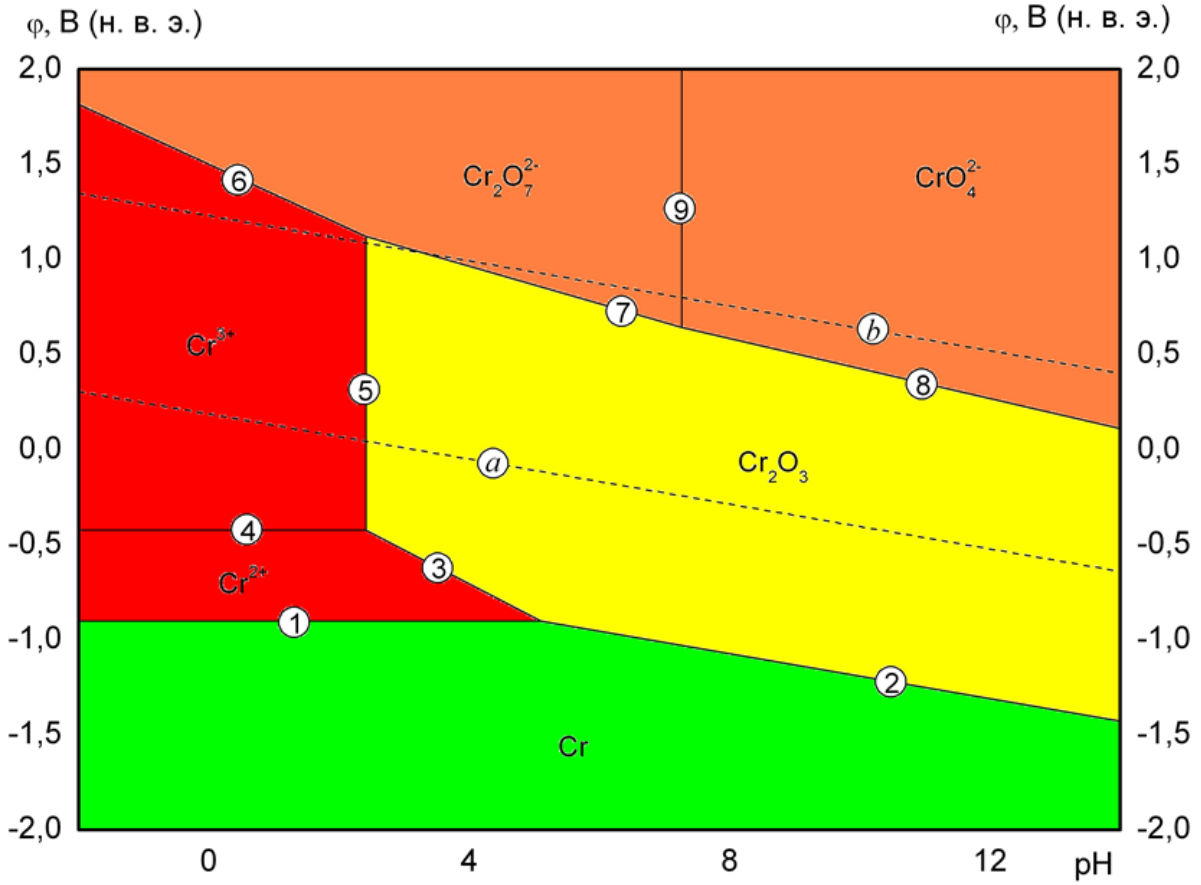

Fig. 31. The potential – pH diagram of the Cr – H_2O system at 25 °C, air pressure of 1 bar and the activities of chromium species in a solution of 1 M.

Figure 33 presents a hypothetical potential – pH diagram for chromium that takes into consideration all known oxygen compounds of chromium. The diagram was plotted at 25 °C, air pressure of 1 bar and the activities of chromium species in a solution equal to 1 mol·l^{-1}.

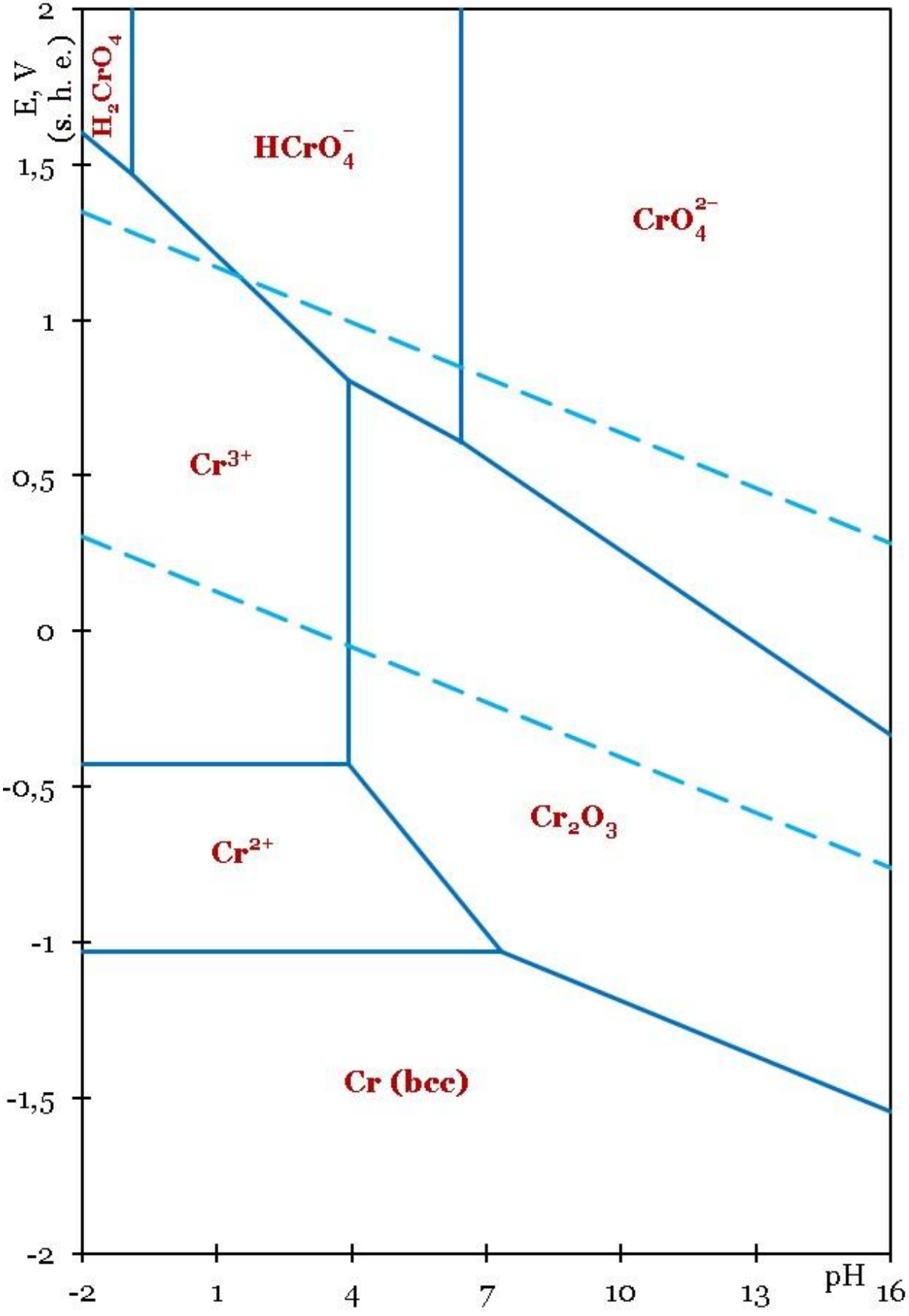

Fig. 32. The potential – pH diagram of the Cr – H_2O system at 25 °C, air pressure of 1 bar and the activities of species in a solution of 10^{-6} M.

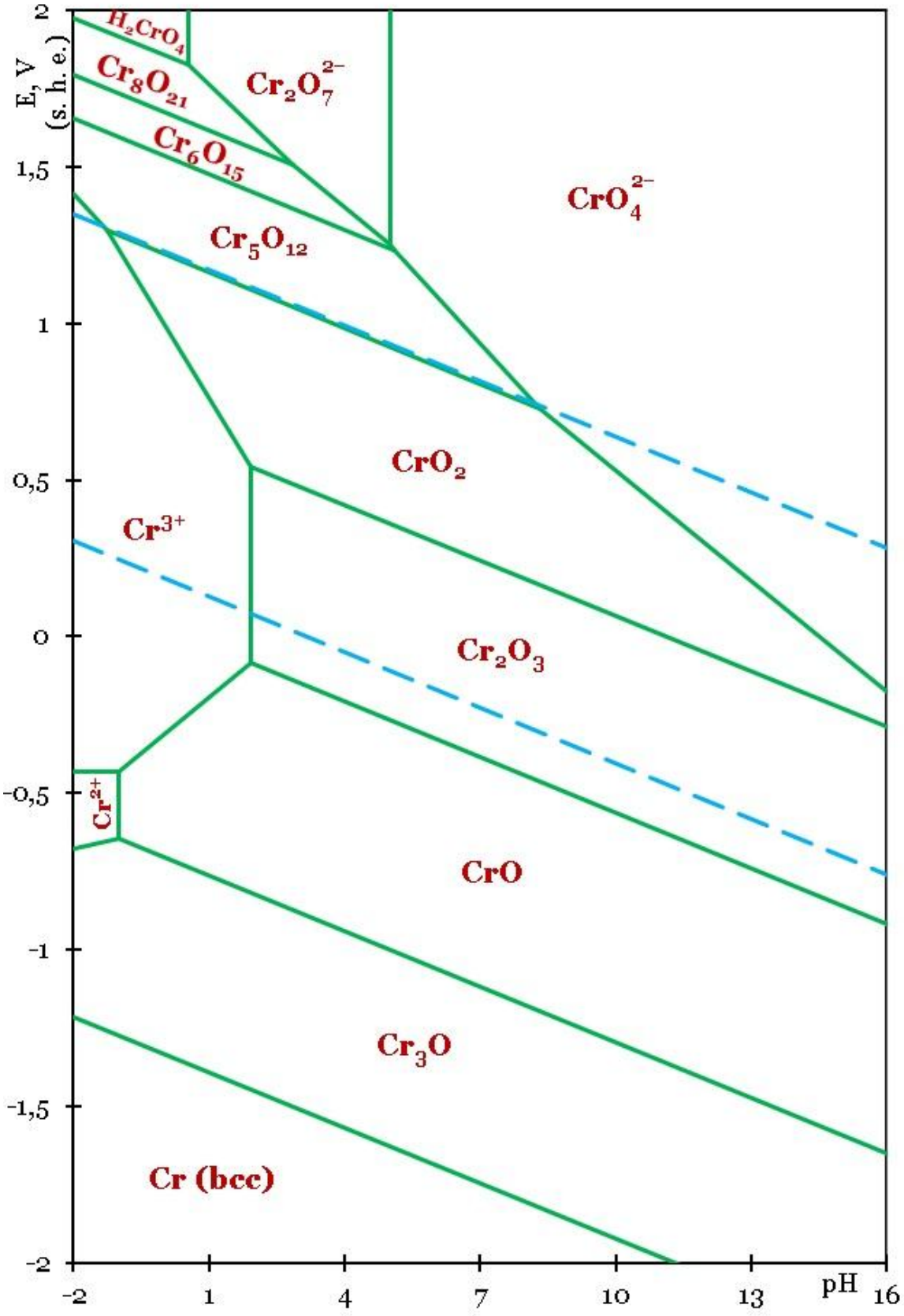

Fig. 33. The hypothetical potential – pH diagram of the Cr – H_2O system at 25 °C, air pressure of 1 bar and the activities of chromium species in a solution of 1 M with consideration of all known oxygen compounds of chromium.

7.4. Potential – pH diagram of Cr – Si – H_2O system

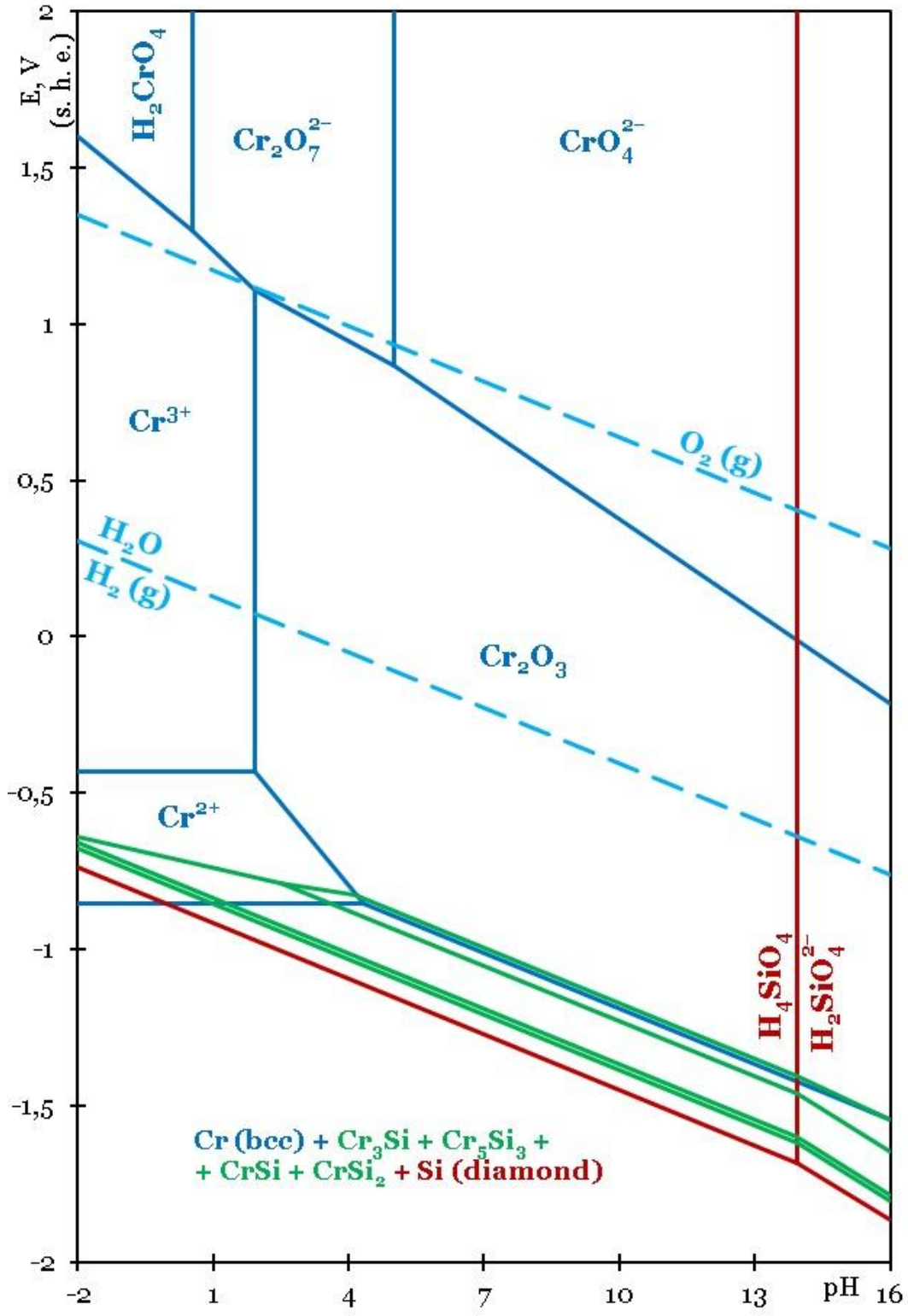

Fig. 34. The potential – pH diagram of the Cr – Si – H_2O system at 25 °C, air pressure of 1 bar and the activities of species in a solution of 1 M showing only the most important chromium oxides and without consideration of chromium silicate

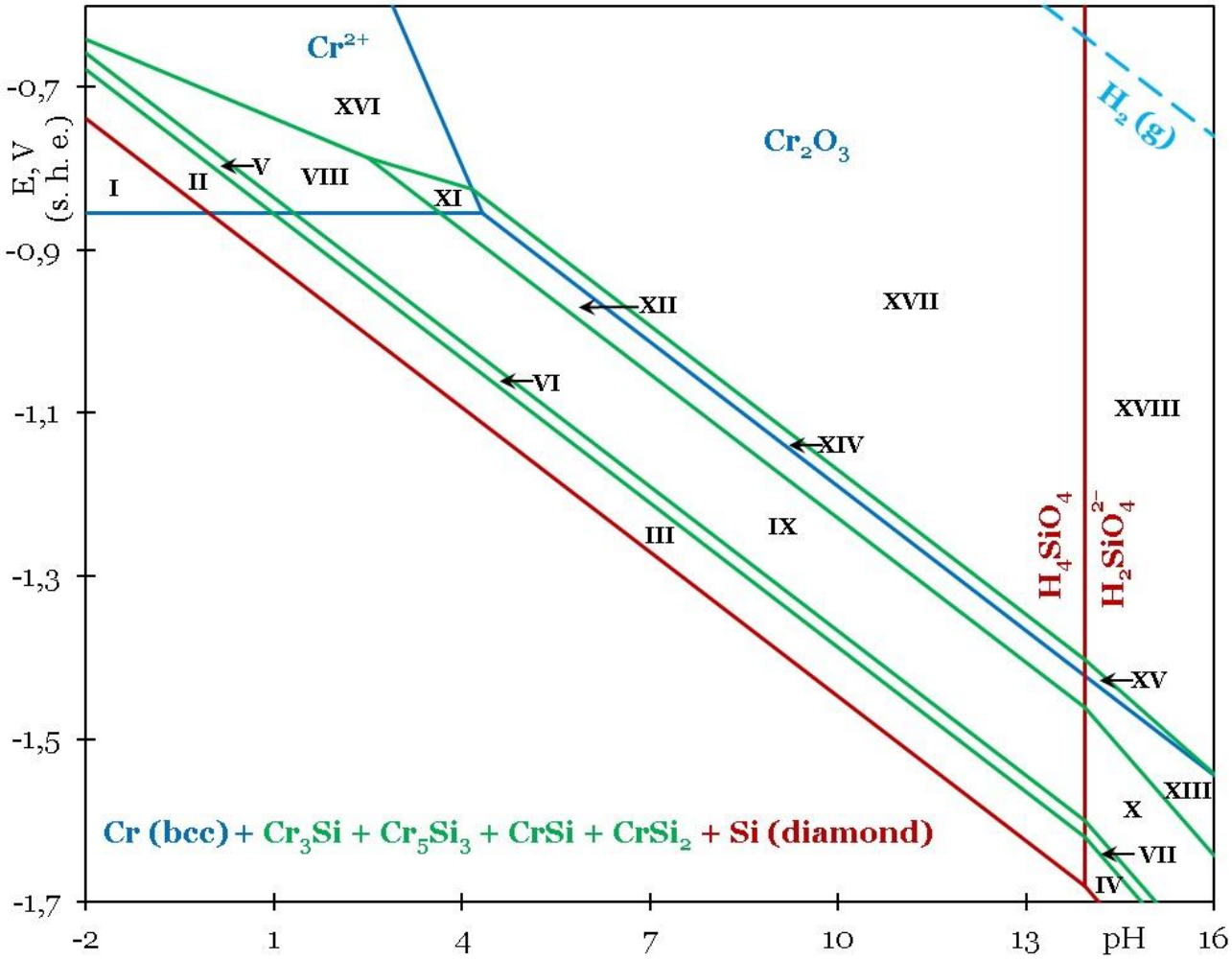

Fig. 35. The cross-section of the potential – pH diagram for the Cr – Si – H_2O system from Figure 34 in the region of thermodynamic stability of chromium silicides. The domains of thermodynamic stability are discussed in text.

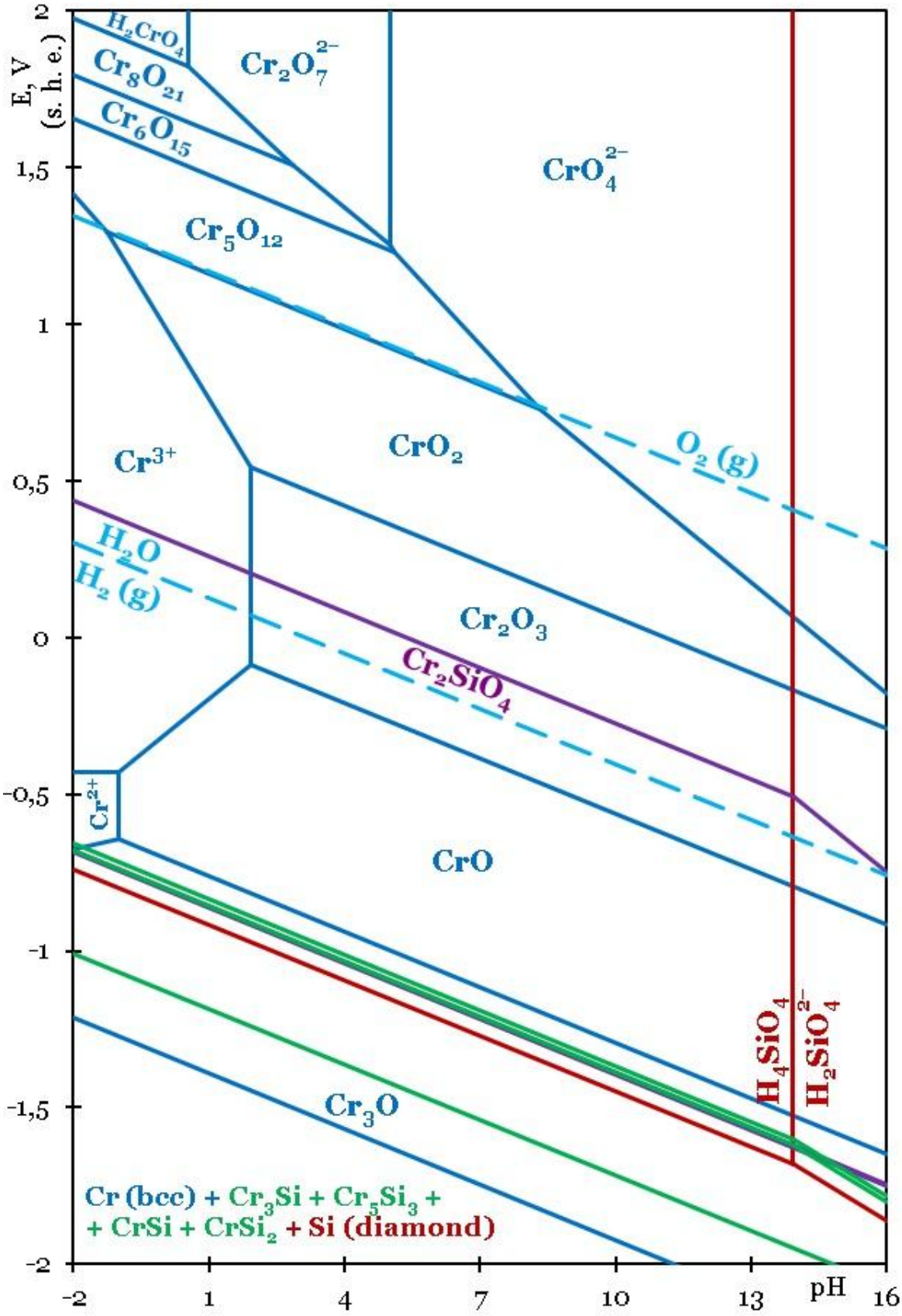

Fig. 36. The potential – pH diagram of the Cr – Si – H_2O system at 25 °C, air pressure of 1 bar and the activities of species in a solution of 1 M with consideration of all chromium oxides and chromium silicate

a)

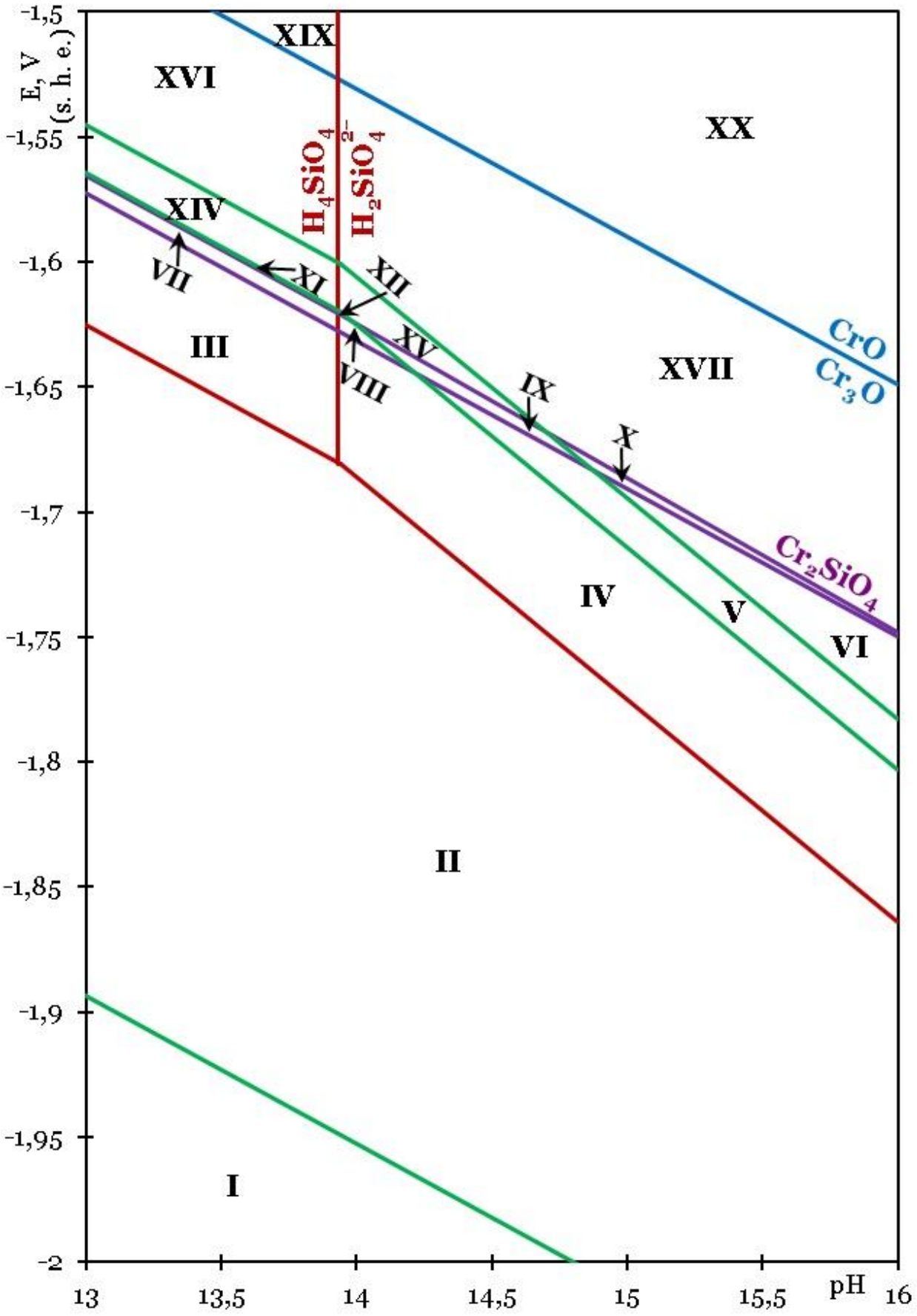
E, V (s. h. e.)
-1,5
-1,55
-1,6
-1,65
-1,7
-1,75
-1,8
-1,85
-1,9
-1,95
-2
13
13,5
14
14,5
15
15,5
16
pH
XIX
XVI
XX
XIV
XII
XI
VII
III
VIII
XV
IX
XVII
X
IV
V
VI
II
I
H_4SiO_4
$H_2SiO_4^{2-}$
CrO
Cr_3O
Cr_2SiO_4

b)

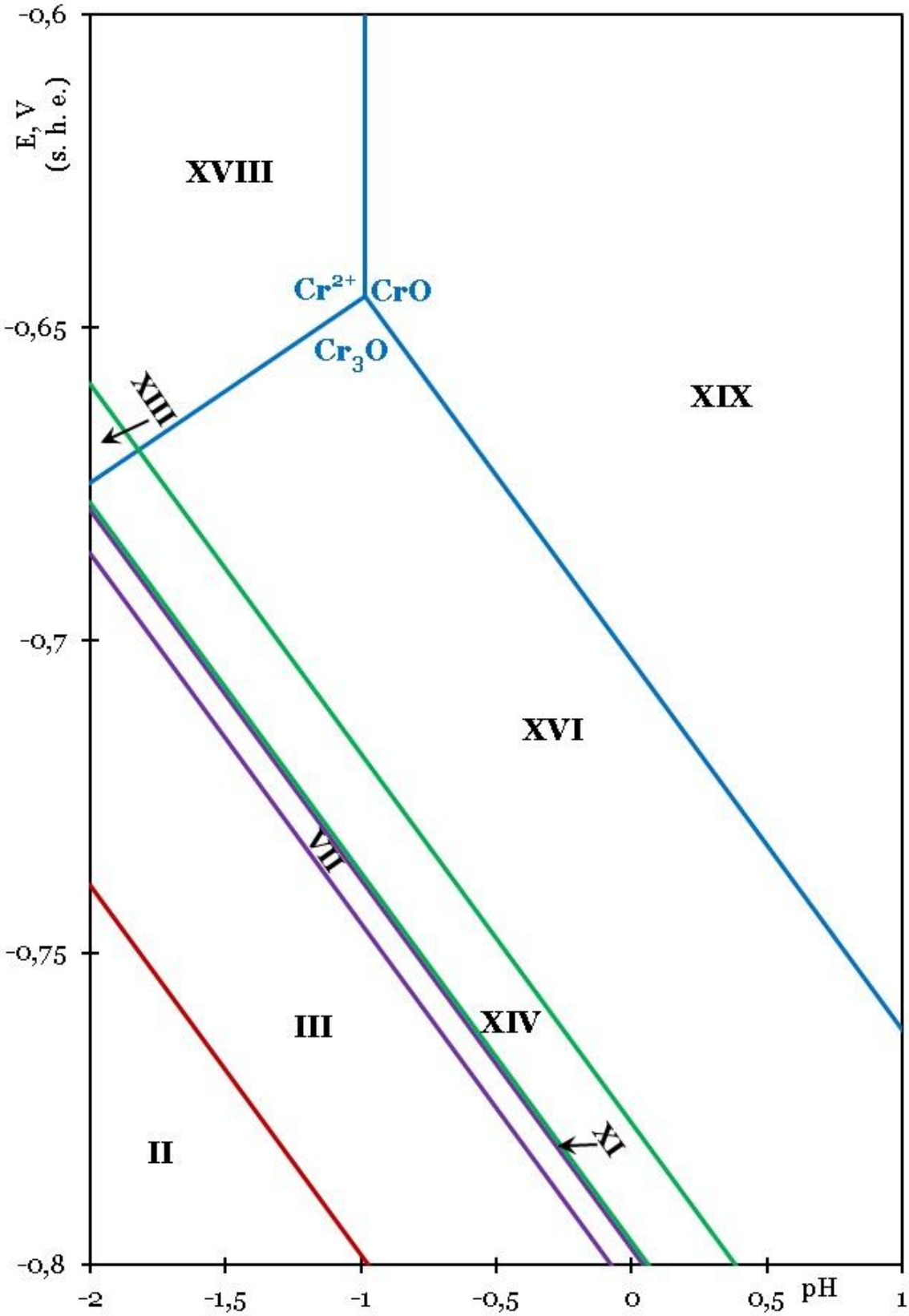

Fig. 37. The cross-section of the potential – pH diagram for the Cr – Si – H_2O system from Figure 36 in the region of thermodynamic stability of chromium silicides and: *a*) $H_2SiO_4^{2-}$ anion, *b*) Cr^{2+} cation. The domains of thermodynamic stability are discussed in text.

The potential – pH diagram of the Cr – Si – H_2O system at 25 °C, air pressure of 1 bar and the activities of species in a solution of 1 mol l^{-1} that takes into account only the most important chromium oxides and does not consider chromium silicate is presented in Figure 34. The upper part of the diagram is a simple superposition of the potential – pH diagrams of chromium and silicon. The equilibria involving chromium silicides occur far below the domain of water electrochemical stability. The cross section of the potential – pH diagram in the region of thermodynamic stability of chromium silicides is presented in Figure 35. The following domains of thermodynamic stability of certain phases might be depicted:

I – Cr^{2+} + Cr_3Si + Cr_5Si_3 + CrSi + $CrSi_2$ + Si (diamond);

II – Cr^{2+} + Cr_3Si + Cr_5Si_3 + CrSi + $CrSi_2$ + H_4SiO_4;

III – Cr (bcc) + Cr_3Si + Cr_5Si_3 + CrSi + $CrSi_2$ + H_4SiO_4;

IV – Cr (bcc) + Cr_3Si + Cr_5Si_3 + CrSi + $CrSi_2$ + $H_2SiO_4^{2-}$;

V – Cr^{2+} + Cr_3Si + Cr_5Si_3 + CrSi + H_4SiO_4;

VI – Cr (bcc) + Cr_3Si + Cr_5Si_3 + CrSi + H_4SiO_4;

VII – Cr (bcc) + Cr_3Si + Cr_5Si_3 + CrSi + $H_2SiO_4^{2-}$;

VIII – Cr^{2+} + Cr_3Si + Cr_5Si_3 + H_4SiO_4;

IX – Cr (bcc) + Cr_3Si + Cr_5Si_3 + H_4SiO_4;

X – Cr (bcc) + Cr_3Si + Cr_5Si_3 + $H_2SiO_4^{2-}$;

XI – Cr^{2+} + Cr_3Si + H_4SiO_4;

XII – Cr (bcc) + Cr_3Si + H_4SiO_4;

XIII – Cr (bcc) + Cr_3Si + $H_2SiO_4^{2-}$;

XIV – Cr_2O_3 + Cr_3Si + H_4SiO_4;

XV – Cr_2O_3 + Cr_3Si + $H_2SiO_4^{2-}$;

XVI – Cr^{2+} + H_4SiO_4;

XVII – Cr_2O_3 + H_4SiO_4;

XVIII – Cr_2O_3 + $H_2SiO_4^{2-}$.

Figure 36 shows the potential – pH diagram of the Cr – Si – H_2O system at 25 °C, air pressure of 1 bar and the activities of species in a solution of 1 mol l^{-1} that takes into account all chromium oxides as well as chromium silicate. Again, the upper part of the diagram is a superposition of the potential – pH diagrams of chromium and silicon. The cross section of the potential – pH diagram in the region of thermodynamic stability of chromium silicides is presented in Figure 37. The diagram presents the following domains of thermodynamic stability of certain phases:

I – Cr_3O + Cr_3Si + Cr_5Si_3 + CrSi + $CrSi_2$ + Si (diamond);

II – $Cr_3O + Cr_5Si_3 + CrSi + CrSi_2 + Si$ (diamond);
III – $Cr_3O + Cr_5Si_3 + CrSi + CrSi_2 + H_4SiO_4$;
IV – $Cr_3O + Cr_5Si_3 + CrSi + CrSi_2 + H_2SiO_4^{2-}$;
V – $Cr_3O + Cr_5Si_3 + CrSi + H_2SiO_4^{2-}$;
VI – $Cr_3O + Cr_5Si_3 + H_2SiO_4^{2-}$;
VII – $Cr_3O + Cr_5Si_3 + CrSi + CrSi_2 + Cr_2SiO_4 + H_4SiO_4$;
VIII – $Cr_3O + Cr_5Si_3 + CrSi + CrSi_2 + Cr_2SiO_4 + H_2SiO_4^{2-}$;
IX – $Cr_3O + Cr_5Si_3 + CrSi + Cr_2SiO_4 + H_2SiO_4^{2-}$;
X – $Cr_3O + Cr_5Si_3 + Cr_2SiO_4 + H_2SiO_4^{2-}$;
XI – $Cr_3O + CrSi + CrSi_2 + Cr_2SiO_4 + H_4SiO_4$;
XII – $Cr_3O + CrSi + CrSi_2 + Cr_2SiO_4 + H_2SiO_4^{2-}$;
XIII – $Cr^{2+} + CrSi + Cr_2SiO_4 + H_4SiO_4$;
XIV – $Cr_3O + CrSi + Cr_2SiO_4 + H_4SiO_4$;
XV – $Cr_3O + CrSi + Cr_2SiO_4 + H_2SiO_4^{2-}$;
XVI – $Cr_3O + Cr_5Si_3 + Cr_2SiO_4 + H_4SiO_4$;
XVII – $Cr_3O + Cr_5Si_3 + Cr_2SiO_4 + H_2SiO_4^{2-}$;
XVIII – $Cr^{2+} + Cr_5Si_3 + Cr_2SiO_4 + H_4SiO_4$;
XIX – $CrO + Cr_5Si_3 + Cr_2SiO_4 + H_4SiO_4$;
XX – $CrO + Cr_5Si_3 + Cr_2SiO_4 + H_2SiO_4^{2-}$.

The presence of chromium silicate significantly changes the order and the mechanism of chromium silicides oxidation both in air and aqueous environments. The full decomposition of all chromium silicides to chromium and silicon oxides becomes thermodynamically unfavourable. This confirms the conclusion made by Tyurin [Tyurin, 2004] that chromium silicates themselves provide a passivity layer on the chromium – silicon alloys.

However, the oxidation scheme of Cr – Si system taking into consideration all chromium oxides and chromium silicate presented in this study is still open for discussion due to lack of reliable data on the Gibbs energies of formation for uncommon chromium oxides and Cr_2SiO_4.

Publications to chapter 7

The content of this chapter was not published yet.

8. Mo – Si system

Molybdenum does not belong to 3d-metals. However, it is the only metal amongst all 4d-metals that is of importance in metallurgy. Molybdenum is used as the alloying element in both ferrous and non-ferrous metallurgy, it is a component of many structural steels and alloys. Molybdenum silicides are used for making high-temperature thermocouples for measuring temperatures in air up to 1700˚C, electric resistance heaters, working without protective atmosphere, for creating materials to be used in oxidizing environments. Therefore, this system was included into consideration.

8.1. Molybdenum silicides

The phase diagram of Mo – Si system [Gokhale, Abbaschian, 1991; Nunes, Coelho, Ramos, 2001; Okamoto, 2011] is presented in Figure 38. It assumes the existence of molybdenum silicides Mo_3Si, Mo_5Si_3 and $MoSi_2$. All these compounds do not have any ranges of nonstoichiometry. The maximum solid solubility of Si in (fcc-Mo) equals ~2.5 atomic percents at 1500˚C and do not exceeds 1 at. % at 1300˚C [Диаграммы состояния двойных металлических систем: справочник, 2001], therefore it is vanishingly small at standard temperature and thus can be neglected. The values of standard Gibbs energies of formation of molybdenum silicides were taken from [Okamoto, 2011; Vahlas, Chevalier, Blanquet, 1989].

8.2. Equilibira in Mo – Si – O system

Molybdenum forms stable oxides MoO_2, Mo_4O_{11}, Mo_8O_{23}, Mo_9O_{26}, MoO_3 and a variety of metastable phases ($Mo_{17}O_{47}$, Mo_5O_{14}, $Mo_{18}O_{52}$) [Диаграммы состояния двойных металлических систем: справочник, 2001]. The oxides Mo_4O_{11}, Mo_8O_{23} and Mo_9O_{26} are Magnéli phases [Magnéli, 1950; Magnéli et al., 1952; Magnéli, 1978]. Metastable compounds were not taken into account in thermodynamic calculations.

There is no data about the existence of molybdenum silicates. The standard Gibbs energies of formation of molybdenum oxides were taken from [Chase Jr. et al., 1985].

The state diagram of the Mo – Si – O system and the list of equilibria in the Mo – Si – O ternary system are presented in the attached publication.

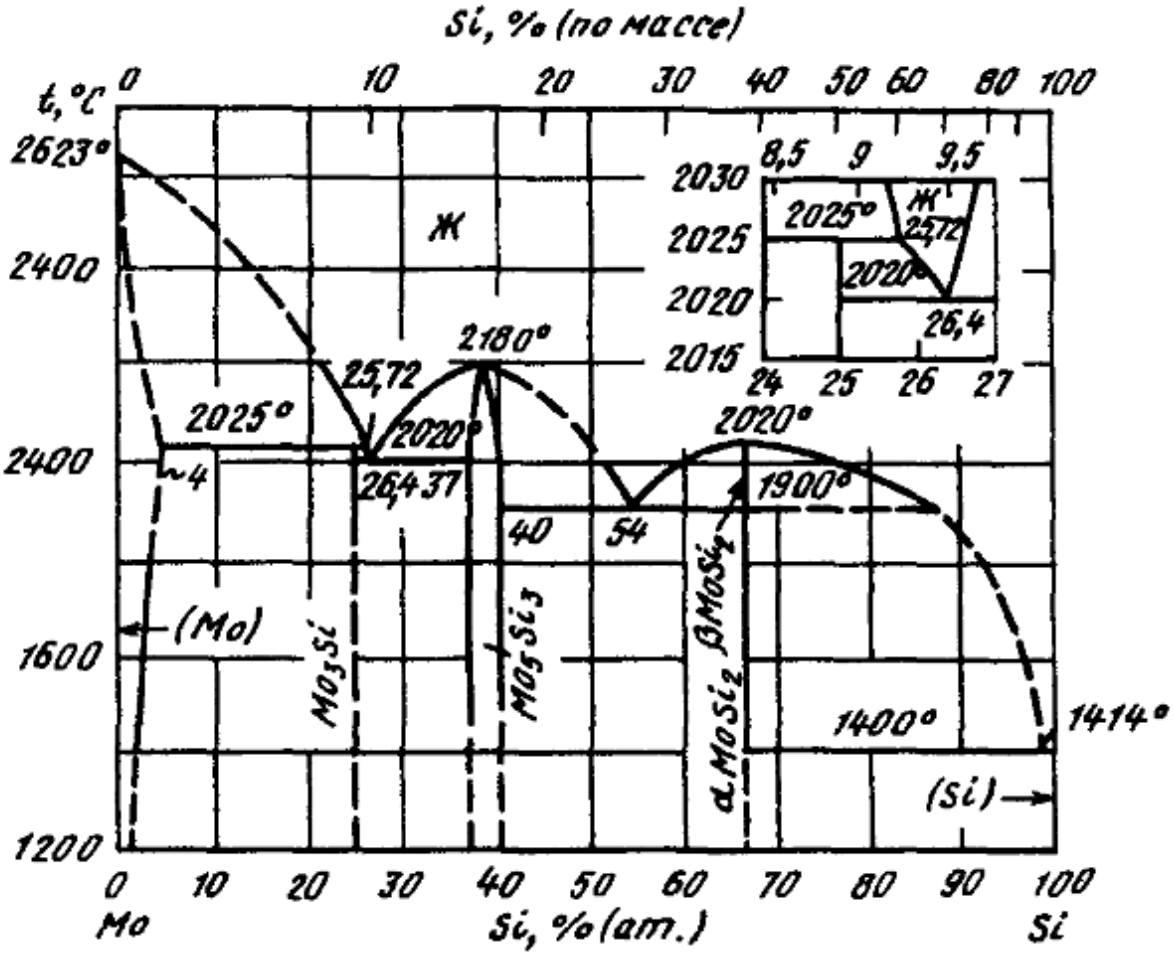

Fig. 38. The phase diagram of the Mo – Si system [Диаграммы состояния двойных металлических систем: справочник, 2001].

8.3. Potential – pH diagram of Mo – H_2O system

In an aqueous solution molybdenium forms the cations Mo^{3+} and MoO_2^{2+}, and could be oxidized to various isopolymolybdate-anions with oxidation degree +6 [Cotton, Wilkinson, 1971; Keulks et al., 1974; Mahadevaiah, Venkataramani, Jai Prakash, 2007; Tytko, Glemser, 1976]. According to [Сибиркин, Замятин, Чурбанов, 2008], the following anions are most stable in a solution: $H_2Mo_8O_{26}^{2-}$, $HMo_8O_{26}^{3-}$, $Mo_8O_{26}^{4-}$, $H_2Mo_7O_{24}^{4-}$, $Mo_7O_{24}^{6-}$ and MoO_4^{2-}. The values of the standard Gibbs energies of formation for molybdate-anions were calculated according to data from the Pourbaix diagram for molybdenum [Lee, 1981].

The potential – pH diagram for molybdenum is presented in the attached publication.

8.4. Potential – pH diagram of Mo – Si – H_2O system

The potential – pH diagram of Mo – Si – H_2O system is presented in the attached publication.

As could be seen from the diagram, molybdenum has a very narrow domain of active dissolution, because the cations Mo^{3+} and MoO_2^{2+} exist only in strongly acidic environments. However, the domain of oxide passivation of molybdenum is also quite small, and, when the environment becomes more alkaline, the domain of transpassivity (which contains all possible isopolymolybdates) becomes broader. Generally, the electrochemical stability of molybdenum-silicon alloys is completely determined by the silicon content in them. If it is enough to form a continuous passivation film from H_4SiO_4 on the alloy surface, then the active oxidation of molybdenum is prevented.

Publications to chapter 8

The content of this chapter is published in two papers. The first paper [Николайчук, Тюрин, 2011b] presents the revised potential – pH diagram for molybdenum. The second one [Николайчук, Тюрин, 2011c] presents the potential – pH diagram for Mo – Si – H_2O system. Both papers were translated into English with the permission of *Butlerovskoe Nasledie* and posted as preprints at the website of *Research Gate* (DOIs, correspondingly, 10.13140/2.1.2853.0883 and 10.13140/2.1.4901.0887). Thess English versions are presented below.

Публикация доступна для обсуждения в интернет как материал "Всероссийской рабочей химической конференции "*Бутлеровское наследие-2011*". http://butlerov.com/bh-2011/
Поступила в редакцию 13 января 2011 г. УДК 541.1:620.193.01:669.14.

The Revised Pourbaix Diagram for Molybdenum

© **Pavel Anatolyevich Nikolaychuk** [+] and **Aleksandr Georgievich Tyurin***
Department of Analytical and Physical Chemistry. Chelyabinsk State University. Brat'ev Kashirinykh Street, 129,Chelyabinks, 454026, Russia. Phone:+7 (351)799-70-69.
E-mail:npa@csu.ru, tag@csu.ru.

*Supervisor; [+]Corresponding author

Keywords: *molybdenum, diagram of electrochemical equilibria, Pourbaix diagram.*

Abstract

A revised equilibrium potential – pH diagram for molybdenum is plotted. A thermodynamic analysis of its corrosion – electrochemical behaviour in aqueous environments is performed.

Introduction

The potential – pH diagrams are the best carriers of the thermodynamical information about the corrosion – electrochemical behaviour of one or another system is aqueous environments. Plotting and analyzing such diagrams is the important task of theoretical electrochemistry.

The known variants of molybdenum potential – pH diagram [1-4] are incomplete, because they don't represent a whole variety of phases, as shown at Mo–O phase diagram [5]. In addition, they don't consider the possibility of forming many forms of molybdates in solution. In this paper the attempt is made to address these deficiencies and to revise the Pourbaix diagram for molybdenum.

Experimental Procedure

The phase diagram of Mo – O system [5] assumes, that a number of stable (MoO_2, Mo_4O_{11}, Mo_8O_{23}, Mo_9O_{26}, MoO_3) and metastable ($Mo_{17}O_{47}$, Mo_5O_{14}, $Mo_{18}O_{52}$) phases exist in it at 298 K. Metastable phases are usually not taking into account in thermodynamic modeling. Thermodynamic properties of molybdenum stable oxides are given in [6 – 8]. They are presented in table 1.

Table 1. Standard Gibbs energies of formation of molybdenum oxides from elements

Oxide	MoO_2	Mo_4O_{11}	Mo_8O_{23}	Mo_9O_{26}	MoO_3
Reference	[6, 7]	[8]	[8]	[8]	[7, 8]
$-\Delta_f G^o_{298}$, J/mole	533200	2546500	5221500	5890100	668100

There is no single opinion about the forms of molybdates presence in solution [9-19]. There is often contradictory information on the various ions (MoO_4^{2-} [9-19], $HMoO_4^-$, $Mo_2O_7^{2-}$, $HMo_2O_7^-$, $Mo_3O_{10}^{2-}$ [9], $Mo_3O_{11}^{4-}$ [12], $Mo_4O_{13}^{2-}$ [9, 13], $Mo_6O_{21}^{6-}$ [12-14, 16], $Mo_7O_{24}^{6-}$ [9-11, 14-19], $Mo_8O_{26}^{4-}$ [10, 11, 13, 15, 16, 19], $Mo_{12}O_{40}^{8-}$ [9], $H_2Mo_{12}O_{40}^{6-}$, $Mo_{12}O_{41}^{10-}$ [13, 14], $H_7Mo_{12}O_{41}^{3-}$ [18]), conditions of their existence in solution, as well as the possible stepwise polymolybdate-ions protonation. These issues are most completely considered in paper [19], which sets two main trends – monotonic increase in the number of molybdenum atoms in isopolyanions with decreasing pH, and decrease in the ratio of the ion charge to the number of molybdenum atoms in molybdates. Also, the own experimental researches are performed in this study, indicating the following molybdenum (VI) isopolyanions mutual transition scheme:

$$MoO_4^{2-} \Leftrightarrow Mo_7O_{24}^{6-} \Leftrightarrow H_2Mo_7O_{24}^{4-} \Leftrightarrow Mo_8O_{26}^{4-} \Leftrightarrow HMo_8O_{26}^{3-} \Leftrightarrow H_2Mo_8O_{26}^{2-} \Leftrightarrow MoO_3 \cdot H_2O.$$

These results are similar to the data, considered in paper [15], as well they confirm the suggestion, contained in study [10], about lack of evidences on the formation of anions with less than seven molybdenum atoms, if its further polymerization in molybdates is possible. That's why the data of [19] are set as the basis in potential – pH diagram thermodynamic modelling in area of molybdate ions existence.

In addition, the textbooks [9, 10, 18] contain information about possibility of molybdenyl cations MoO_2^{2+} formation in acidic environments. The value of its standard Gibbs energy of formation is available in [7] ($\Delta_f G^o_{298}(MoO_2^{2+}) = -408776\ ^{J}/_{mole}$), which allows this cation to be also involved into thermodynamical analysis.

The data about standard electrode potentials from handbook [20] are also used in calculations.

Method of potential – pH diagrams calculating and plotting is described in [4].

Results and Discussion

Basic chemical and electrochemical equilibria in the Mo – H_2O system at standard conditions are represented in table 2. The system potential – pH diagram is shown at figure 1. The cross sections of this diagram in enlarged scale are shown at figure 2.

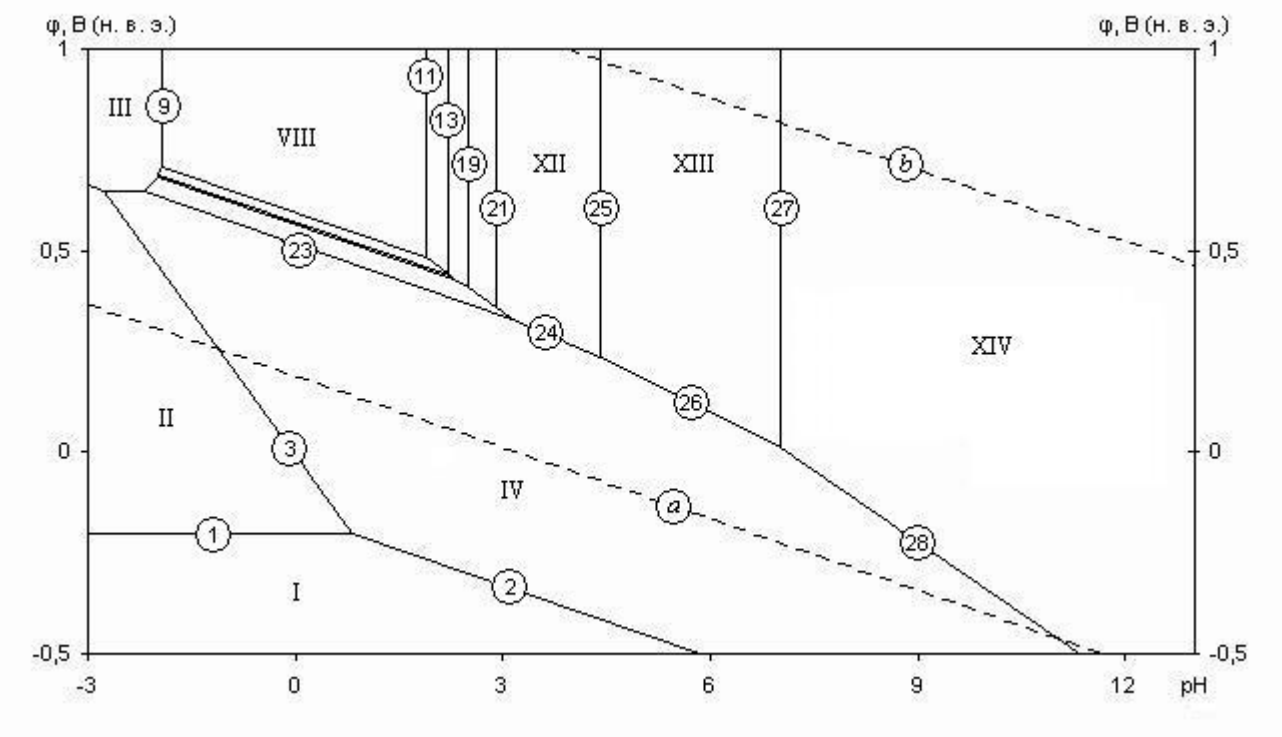

Figure 1. The potential – pH diagram of Mo – H_2O system at 25˚C, air pressure of 1 bar and $a_i = 1\ ^{mole}/_{l}$ (unhydrated form of oxides)

Only unhydrated form of oxides, as the most stable, is considered while plotting the diagram. According to [9, 10], molybdenum doesn't form hydroxides, and possible hydrated forms of oxides are only $MoO_2(OH)_2$ and $MoO_3 \cdot H_2O$ (or H_2MoO_4), which are not taken into account, since they are metastable.

14 domains of stability of certain phases can be depicted at the diagram: I – Mo; II – Mo^{3+}; III – MoO_2^{2+}; IV – MoO_2; V – Mo_4O_{11}; VI – Mo_8O_{23}; VII – Mo_90_{26}; VIII – MoO_3; IX – $H_2Mo_8O_{26}^{2-}$; X – $HMo_8O_{26}^{3-}$; XI – $Mo_8O_{26}^{4-}$; XII – $H_2Mo_7O_{24}^{4-}$; XIII – $Mo_7O_{24}^{6-}$; XIV – MoO_4^{2-}.

Domain I is the domain of molybdenum immunity (or thermodynamic stability).

Domains II and III are the domains of molybdenum active corrosion, in which it passes into solution in form of respectively Mo^{3+} or MoO_2^{2+} cations.

Oxide phases become thermodynamically stable at values of potentials and pH, corresponding to domains IV–VIII. A protective oxide film forms on the metal surface, which prevents further oxidation. There are domains of molybdenum passivity. The specific composition of the oxide layer will vary, depending on environmental conditions. Domains IX-XIV are domains of molybdenum

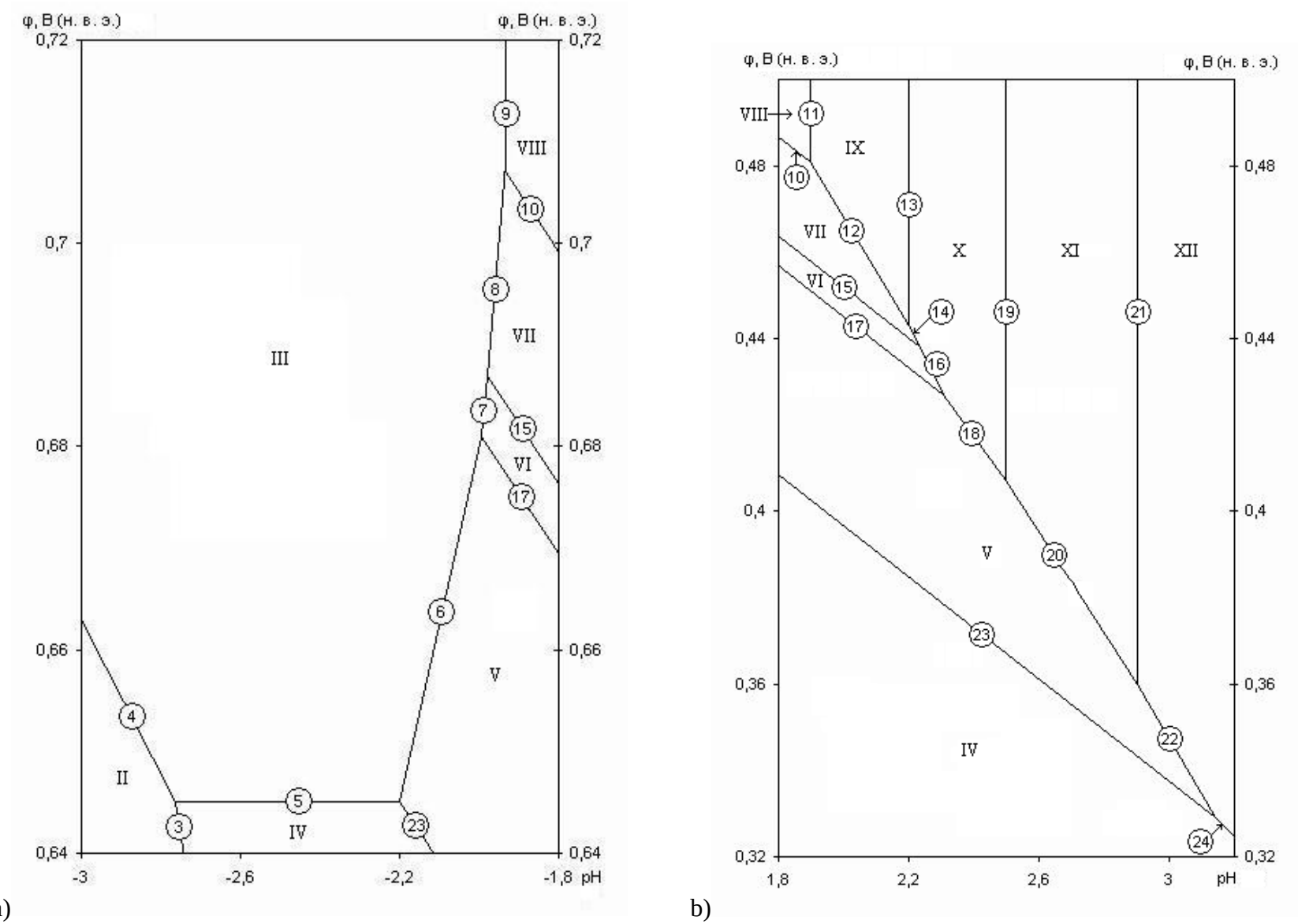

a) b)

Figure 2. The cross sections of the Mo–H_2O system potential – pH diagram in areas of existence of: a) molybdenyl cation; b) molybdate ions and molybdenum oxides.

Table 2. Basic chemical and electrochemical equilibria in the Mo –H_2O system at temperature 25˚C and air pressure of 1 bar

№ of line	Electrode reaction	Equilibrium potential, V (s. h. e.) or solution pH
a	$2H^+ + 2e^- = H_2; P_{H_2} \approx 5\cdot 10^{-7}$ bar	$0.186 - 0.0591pH$
b	$O_2 + 4H^+ + 4e^- = 2H_2O; P_{O_2} \approx 0.21$bar	$1.219 - 0.0591pH$
1	$Mo^{3+} + 3e^- = Mo$	$-0.200 + 0.0197\cdot \lg a_{Mo^{3+}}$
2	$MoO_2 + 4H^+ + 4e^- = Mo + 2H_2O$	$-0.152 - 0.0591pH$
3	$MoO_2 + 4H^+ + e^- = Mo^{3+} + 2H_2O$	$-0.008 - 0.2364pH - 0.0591\cdot \lg a_{Mo^{3+}}$
4	$MoO_2^{2+} + 4H^+ + 3e^- = Mo^{3+} + 2H_2O$	$0.427 - 0.0788pH + 0.0197\cdot \lg \frac{a_{MoO_2^{2+}}}{a_{Mo^{3+}}}$
5	$MoO_2^{2+} + 2e^- = MoO_2$	$0.645 + 0.0295\cdot \lg a_{MoO_2^{2+}}$
6	$4MoO_2^{2+} + 3H_2O + 2e^- = Mo_4O_{11} + 6H^+$	$1.035 + 0.1773pH + 0.1182\cdot \lg a_{MoO_2^{2+}}$
7	$8MoO_2^{2+} + 7H_2O + 2e^- = Mo_8O_{23} + 14H^+$	$1.506 + 0.4137pH + 0.2364\cdot \lg a_{MoO_2^{2+}}$
8	$9MoO_2^{2+} + 8H_2O + 2e^- = Mo_9O_{26} + 16H^+$	$1.623 + 0.4728pH + 0.2660\cdot \lg a_{MoO_2^{2+}}$
9	$MoO_3 + 2H^+ = MoO_2^{2+} + H_2O$	$pH = -1.935 - 0.5\cdot \lg a_{MoO_2^{2+}}$
10	$9MoO_3 + 2H^+ + 2e^- = Mo_9O_{26} + H_2O$	$0.593 - 0.0591pH$
11	$H_2Mo_8O_{26}^{2-} + 2H^+ = 8MoO_3 + 2H_2O$	$pH = 1.9 + 0.5\cdot \lg a_{H_2Mo_8O_{26}^{2-}}$
12	$9H_2Mo_8O_{26}^{2-} + 34H^+ + 16e^- = 8Mo_9O_{26} + 26H_2O$	$0.719 - 0.1256pH + 0.0332\cdot \lg a_{H_2Mo_8O_{26}^{2-}}$
13	$HMo_8O_{26}^{3-} + H^+ = H_2Mo_8O_{26}^{2-}$	$pH = 2.2 + \lg \frac{a_{HMo_8O_{26}^{3-}}}{a_{H_2Mo_8O_{26}^{2-}}}$
14	$9HMo_8O_{26}^{3-} + 43H^+ + 16e^- = 8Mo_9O_{26} + 26H_2O$	$0.793 - 0.1588pH + 0.0332\cdot \lg a_{HMo_8O_{26}^{3-}}$
15	$8Mo_9O_{26} + 2H^+ + 2e^- = 9Mo_8O_{23} + H_2O$	$0.570 - 0.0591pH$
16	$HMo_8O_{26}^{3-} + 5H^+ + 2e^- = Mo_8O_{23} + 3H_2O$	$0.768 - 0.1478pH + 0.0295\cdot \lg a_{HMo_8O_{26}^{3-}}$
17	$Mo_8O_{23} + 2H^+ + 2e^- = 2Mo_4O_{11} + H_2O$	$0.564 - 0.0591pH$
18	$HMo_8O_{26}^{3-} + 7H^+ + 4e^- = 2Mo_4O_{11} + 4H_2O$	$0.666 - 0.1034pH + 0.0148\cdot \lg a_{HMo_8O_{26}^{3-}}$
19	$Mo_8O_{26}^{4-} + H^+ = HMo_8O_{26}^{3-}$	$pH = 2.5 + \lg \frac{a_{Mo_8O_{26}^{4-}}}{a_{HMo_8O_{26}^{3-}}}$
20	$Mo_8O_{26}^{4-} + 8H^+ + 4e^- = 2Mo_4O_{11} + 4H_2O$	$0.703 - 0.1182pH + 0.0148\cdot \lg a_{Mo_8O_{26}^{4-}}$
21	$8H_2Mo_7O_{24}^{4-} + 4H^+ = 7Mo_8O_{24}^{4-} + 10H_2O$	$pH = 2.9 + 0.25\cdot \lg \frac{a^8_{H_2Mo_7O_{24}^{4-}}}{a^7_{Mo_8O_{26}^{4-}}}$
22	$4H_2Mo_7O_{24}^{4-} + 30H^+ + 14e^- = 7Mo_4O_{11} + 19H_2O$	$0.727 - 0.1266pH + 0.0169\cdot \lg a_{H_2Mo_7O_{24}^{4-}}$
23	$Mo_4O_{11} + 6H^+ + 6e^- = 4MoO_2 + 3H_2O$	$0.515 - 0.0591pH$
24	$H_2Mo_7O_{24}^{4-} + 18H^+ + 14e^- = 7MoO_2 + 10H_2O$	$0.568 - 0.0760pH + 0.0042\cdot \lg a_{H_2Mo_7O_{24}^{4-}}$
25	$Mo_7O_{24}^{6-} + 2H^+ = H_2Mo_7O_{24}^{4-}$	$pH = 4.4 + 0.5\cdot \lg \frac{a_{Mo_7O_{24}^{6-}}}{a_{H_2Mo_7O_{24}^{4-}}}$
26	$Mo_7O_{24}^{6-} + 20H^+ + 14e^- = 7MoO_2 + 10H_2O$	$0.605 - 0.0844pH + 0.0042\cdot \lg a_{Mo_7O_{24}^{6-}}$
27	$7MoO_4^{2-} + 8H^+ = Mo_7O_{24}^{6-} + 4H_2O$	$pH = 7.008 + 0.125\cdot \lg \frac{a^7_{MoO_4^-}}{a_{Mo_7O_{24}^{6-}}}$
28	$MoO_4^{2-} + 4H^+ + 2e^- = MoO_2 + 2H_2O$	$0.842 - 0.1182pH + 0.0295\cdot \lg a_{MoO_4^-}$

transpassivity, in which further oxidation of oxide film occurs, and it passes into solution in form of anions.

Lines *a* and *b* in the diagram correspond to the work of the hydrogen and oxygen electrodes, respectively. Domain of potentials and pH, which lies between them, corresponds to the electrochemical stability of water.

The following conclusions can be drawn from analyzing the potential – pH diagram. Molybdenum has a very narrow area of active dissolution, as the cations of molybdenum and molybdenyl exist only in strongly acidic environments. However, the domain of its passivity (on the potentials) is also quite small, and the more alkaline the environment is, the broader the domain of transpassivity becomes, that restricts the use of molybdenum in strongly alkaline environments.

Conclusions

3. The potential – pH diagram for molybdenum is revised. This diagram, in contrast to the previous ones, completely corresponds to the latest variant of the Mo – O phase diagram and also reflects the possibility of forming polymolybdate ions in solution.
4. A thermodynamical analysis of molybdenum corrosion – electrochemical behaviour features in aqueous solutions is performed.

References

1. B. P. Nikol'skiy. Spravochnik khimika [In Russian] (Handbook on Chemistry). *Moscow - Leningrad.: Khimiya*. **1964**. Vol.3. 1008p.
2. Lee J. B. Elevated temperature potential – pH diagrams for the Cr – H_2O, Mo – H_2O, Ti – H_2O and Pt – H_2O systems. *Corrosion (USA)*. **1981**. Vol.37. №8. P.467-480.
3. V. V. Batrakov, I. G. Gorichev, N. M. Simonova. Anodnoye povedeniye molibdena v sulfatnykh rastvorakh [In Russian]. *Zashchita Metallov*. **1993**. Vol.29. No 4. P.554-559.
4. A. G. Tyurin. Termodinamika khimicheskoy i elektrokhimicheskoy ustoychivosti splavov [In Russian] (Thermodynamics of the chemical and electrochemical stability of alloys). In 2 parts. Part. 2. *Chelyabinsk:Publishing center of Chelyabinsk State University*. **2004**. 91p.
5. N. P. Lyakishev. Diagrammy sostoyaniya dvoynykh metallicheskikh sistem: spravochnik [In Russian] (Phase diagrams of binary metallic systems: textbook). *Moscow: Mashinostroyeniye.* **2000**. Vol.3. Book No.1. P.449-452.
6. L. P. Ruzinov, B. S. Gulyanitckiy. Ravnovesnyye prevrashcheniya metallurgicheskikh reaktciy [In Russian] (Equilibrium transformations in metallurgical reactions) *Moscow: Metallurgiya.* **1975**. 416p.
7. Termicheskiye konstanty veshchestv: database [In Russian] (Thermal constants of the substances). URL: <http://www.chem.msu.su/cgi-bin/tkv.pl?show=welcome.html>
8. JANAF Thermochemical Tables. Third Edition. *J. Phys. Chem. Ref. Data*. **1985**. Vol.14. Suppl.1.
9. V. A. Novozhenov. Vvedeniye v neorganicheskuyu khimiyu [In Russian] (Introduction to inorganic chemistry). *Barnaul: Publishing House of Altay State University*. **2001**. P.518. URL: <http://www.chem.asu.ru/ncd/novogenov>
10. F. Cotton and G. Wilkinson. Advanced Inorganic Chemistry. Third Edition. *New York – London – Sydney – Toronto: John Wiley & Sons*. **1972**. P.951.
11. N. Mahadevaiah, B. Venkataramani, and B. S. Jai Prakash. Restrictive Entry of Aqueous Molybdate Species into Surfactant Modified Montmorillonite – A Breakthrough Curve Study. URL: <http://www.chemsite.ru/abstract_17798.html>
12. A. I. Busev. Analiticheskaya khimiya molibdena [In Russian] (Analytical chemistry of molybdenum). *Moscow.: Publishing House of USSR Academy of Science*. **1962**. 301p.
13. K. A. Bol'shakov. Khimiya i tekhnologiya redkikh i rasseyannykh elementov [In Russian] (Chemistry and technology of rare and scattered elements). *Moscow.:Vysshaya shkola*. **1976**. Part III. 320p.
14. R. Ripan, I. Chetyanu. Neorganicheskaya khimiya [In Russian] (Inorganic chemistry). *Moscow.:Mir*. **1972**. Vol.2. 871p.
15. Keulks G.W., Hall J.L., Chellian D., et al. *J. Catal.* **1974**. Vol.34. No.1. P.79-97.
16. N. Ya. Turova. Neorganicheskaya khimiya v tablitsakh [In Russian] (Inorganic chemistry in tables). *Moscow.:Vysshyy tekhnicheskiy kolledzh RAN*. **1999**. 140p.

17. Yu. D. Tretyakov [et al.] Neorganicheskaya khimiya. Khimiya elementov [In Russian] (Inorganic chemistry. Chemistry of elements). *Moscow.:Publishing House of Moscow State University*. **2007**. Vol.1. 537p.
18. G. Remi. Kurs neorganicheskoy khimii [In Russian] (Lectures on inorganic chemistry). *Moscow.:Mir*. **1966**. Vol.2. 836p.
19. A. A. Sibirkin, O. A. Zamyatov., M. F. Churbanov. Vzaimnoye prevrashcheniye izopolisoyedineniy molibdena (VI) v vodnom rastvore [In Russian] (The mutual transformations of molybdenum (VI) isopolycompounds in aqueous solution). *Vestnik Nizhegorodskogo Universiteta imeni N. I. Lobachevskogo*. **2008**. No 5. P.45-51.
20. Spravochnik po elektrokhimii [In Russian] (Textbook on Electrochemistry). Editor A. M. Sukhotin. *Leningrad: Khimiya.* **1981**. 488p.

Публикация доступна для обсуждения в интернет как материал "Всероссийской рабочей химической конференции "*Бутлеровское наследие-2011*". http://butlerov.com/bh-2011/
Поступила в редакцию 13 января 2011 г. УДК 541.1:620.193.01:669.14.

Thermodynamics of Chemical and Electrochemical Stability of the Mo – Si System Alloys

© **Pavel Anatolyevich Nikolaychuk** [+] and **Aleksandr Georgievich Tyurin***
Department of Analytical and Physical Chemistry. Chelyabinsk State University. Brat'ev Kashirinykh Street, 129,Chelyabinks, 454026, Russia. Phone:+7 (351)799-70-69.
E-mail:npa@csu.ru, tag@csu.ru.

*Supervisor; [+]Corresponding author

Keywords: *molybdenum silicides, low temperature oxidation, chemical stability, diagram of electrochemical equilibria, electrochemical stability.*

Abstract

A phase diagram of Mo – Si – O system and a potential – pH diagram of Mo – Si – H_2O at 25˚C, air pressure of 1 bar and activities of ions in solution equal to 1 mole/l are plotted. The corrosion-electrochemical behaviour of Mo – Si system alloys is considered from the thermodynamic point of view.

Introduction

In recent years, there is growing evidence about the perspective of using some metal-like transition metals compounds (including silicides) as a new corrosion- and wear-resistant coatings and protective materials [1]. However, the available literature data on the silicides refer, to a greater extent, to the metals used in ferroalloy production. The iron triad metals silicides are studied most thoroughly. Studying the properties of other metals silicides such as molybdenum silicides also undoubtedly represents scientific and practical interest.

Molybdenum silicides are used for making high-temperature thermocouples for measuring temperatures in air up to 1700˚C, electric resistance heaters, working without protective atmosphere [2], for creating materials to be used in oxidizing environments [3]. Using materials based on molybdenum silicides in liquid environments is also perspective. Therefore, the thermodynamic analysis of chemical and electrochemical stability of molybdenum – silicon alloys is an important task of theoretical and applied electrochemistry.

Experimental Procedure

It is necessary to analyze the phase diagrams of binary subsystems of the Mo - Si – O system to obtain the basic data needed for calculations and thermodynamic analysis.

Following compounds – Mo_3Si, Mo_5Si_3 and $MoSi_2$ – exist in Mo – Si system at 25˚C according to its phase diagram [4-6]. These compounds don't have any homogeneity range at this condition. There are data on the solid solubility of silicon in bcc-molybdenum at different temperatures [4, 5], which are summarized in table 1.

Table 1. Maximum solid solubility of silicon in molybdenum at different temperatures

Temperature, ˚C	1316	1371	1427	1820	2025
Solubility of Si in (Mo), at. %	0.727	1.09	2.52	3.59	~ 4

The assumption based on these data can be made, that at 25˚C possible solubility of silicon in molybdenum can be neglected. The solubility of molybdenum in silicon at this temperature is also vanishingly small.

The available data on molybdenum silicides thermodynamic properties are contradictory [4, 7 – 10]. All of them are presented in table 2. However, only enthalpies of formation for Mo_5Si_3 and $MoSi_2$ are available in papers [7, 8]. In this case, values of absolute entropy of these silicides, required to calculate the standard Gibbs energy, are evaluated according to Eastman formulae [11].

Table 2. Standard Gibbs energies of formation ($-\Delta_f G^o_{298}$, J/mole) of compounds from elements

Compound \ Reference	[4]	[7]	[8]	[9]	[10]	[12]
Mo_3Si	116900	103447	102143	116880	119450	–
Mo_5Si_3	311984	249958*	251184*	–	305095	–
$MoSi_2$	131325	117955*	105390*	131340	142080	–
MoO_2	–	534440	533238	–	–	532011
Mo_4O_{11}	–	–	–	–	–	2546532
Mo_8O_{23}	–	–	–	–	–	5221596
Mo_9O_{26}	–	–	–	–	–	5890149
MoO_3	–	668680	668117	–	–	668079

* Contains only $\Delta_f H^o_{298}$; value of S^o_{298} is evaluated according to Eastman formulae.

Only one oxide – SiO_2 – exist in Si – O system at 25˚C [5, 6]. The value of $\Delta_f G^o_{298}(SiO_2) = -805067$ J/mole is taken from [15], because this value is compatible with the experimentally measured standard potential of the silicon electrode ($SiO_2 + 4H^+ + 4e^- = Si(diamond) + 2H_2O$, $\varphi^o_{298} = -0{,}857$ V).

The phase diagram of Mo – O system [5] assumes, that a number of stable (MoO_2, Mo_4O_{11}, Mo_8O_{23}, Mo_9O_{26}, MoO_3) and metastable ($Mo_{17}O_{47}$, Mo_5O_{14}, $Mo_{18}O_{52}$) phases exist in it at 298 K. Metastable phases are usually not taking into account in thermodynamic modeling. Thermodynamic properties of molybdenum oxides, available in [7, 8, 12], are also presented in table 2. There are no intermediate compounds (silicates) between molybdenum and silicon oxides [13].

In addition, in liquid environments silicon dioxide can be oxidized to silicates, and molybdenum trioxide – to molybdates. Information about most likely forms of molybdates presence in solution is summarized in [14], where also the potential – pH diagram of pure molybdenum is plotted. Data on the characteristics of electrochemical equilibria with the participation of other ions are taken from handbook [15].

Method of calculating and plotting the Mo – Si – O state diagram and potential – pH diagram of Mo – Si – H_2O system is described in [16].

Results and Discussion

The state diagram of Mo – Si – O system at 25˚C is shown in figure 1. System invariant conditions characteristics are presented in table 3. It should be noted that all substances, involved in all these equilibria, are pure, and thus the mole fractions and activities of all components are set equal to unity.

As can be seen from the diagram, the chemical affinity of silicon to oxygen is much higher than that of molybdenum. The consequence is that silicon, containing in molybdenum–silicon alloys, should be oxidized in first order. However, the equilibrium pressure of oxygen required for oxidation of molybdenum from alloy to its highest oxide is much lower than the pressure of oxygen in air at standard conditions. This means that the oxidation of the Mo – Si alloys in the air must proceed completely and end with the formation of an oxide film, consisting of MoO_3 and SiO_2. The specific composition of the oxide film should vary strongly, depending on the silicon content in the alloy. If ti si sufficient to form the continuous film of SiO_2, then molybdenum should remain passivated and do not oxidize at all. Otherwise, the various molybdenum oxides should be included into the composition of the oxide film.

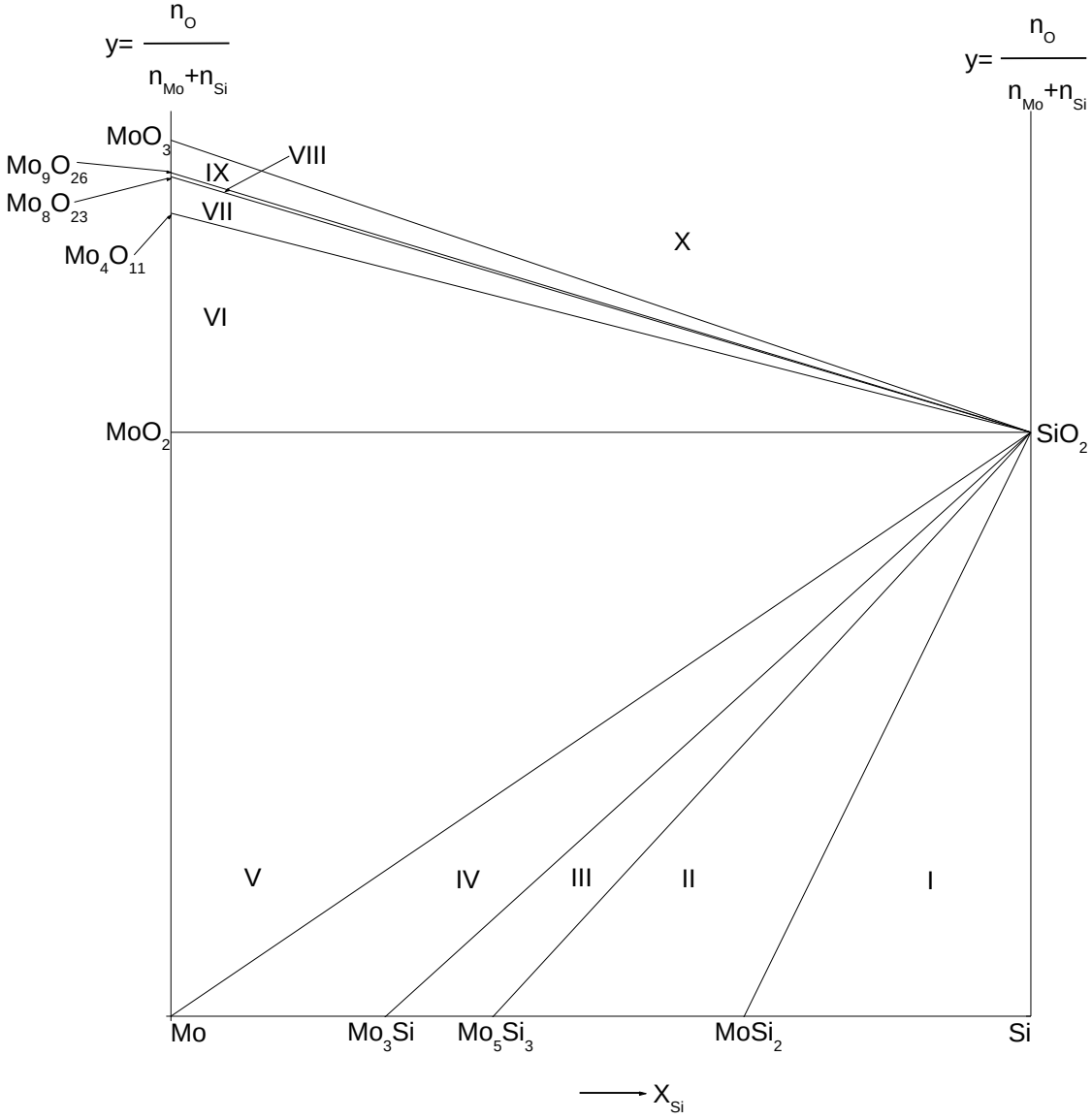

Figure 1. The state diagram of Mo – Si – O system at 25˚C

Table 3. Invariant conditions of Mo – Si – H_2O system characteristics at temperature 25˚C

№ of domain	System condition	Reaction equation	P_{O_2}, bar
I	$MoSi_2 – Si – SiO_2$	$Si + O_2 = SiO_2$	$7.7 \cdot 10^{-142}$
II	$Mo_5Si_3 – MoSi_2 – SiO_2$	$5MoSi_2 + 7O_2 = Mo_5Si_3 + 7SiO_2$	$3.3 \cdot 10^{-133}$
III	$Mo_3Si – Mo_5Si_3 – SiO_2$	$3Mo_5Si_3 + 4O_2 = 5Mo_3Si + 4SiO_2$	$1.9 \cdot 10^{-126}$
IV	$Mo – Mo_3Si – SiO_2$	$Mo_3Si + O_2 = 3Mo + SiO_2$	$2.4 \cdot 10^{-121}$
V	$Mo – MoO_2 – SiO_2$	$Mo + O_2 = MoO_2$	$3.5 \cdot 10^{-94}$
VI	$MoO_2 – Mo_4O_{11} – SiO_2$	$8MoO_2 + 3O_2 = 2Mo_4O_{11}$	$4.5 \cdot 10^{-49}$
VII	$Mo_4O_{11} – Mo_8O_{23} – SiO_2$	$4Mo_4O_{11} + O_2 = 2Mo_8O_{23}$	$9.0 \cdot 10^{-46}$
VIII	$Mo_8O_{23} – Mo_9O_{26} – SiO_2$	$18Mo_8O_{23} + O_2 = 16Mo_9O_{26}$	$2.3 \cdot 10^{-45}$
IX	$Mo_9O_{26} – MoO_3 – SiO_2$	$2Mo_9O_{26} + O_2 = 18MoO_3$	$8.9 \cdot 10^{-44}$
X	$MoO_3 – SiO_2 – \{O_2\}$	—	—

Basic chemical and electrochemical equilibrium in the Mo – Si – H_2O system at standard conditions are represented in table 4. The system potential – pH diagram is shown at figure 2.

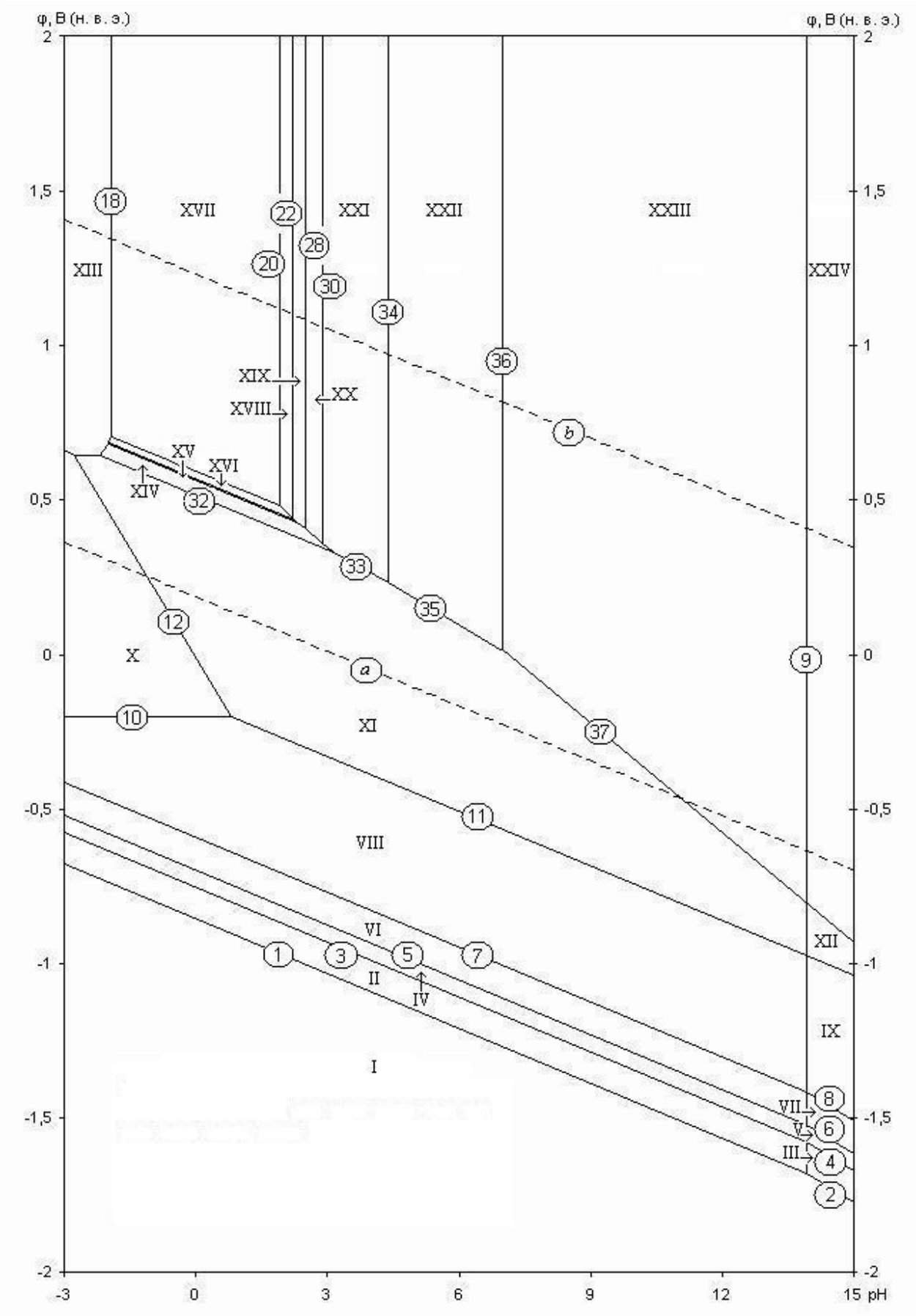

Figure 2. The potential – pH diagram of Mo – Si – H_2O system at 25˚C, air pressure of 1 bar and $a_i = 1^{\text{mole}}/_{\text{l}}$ (unhydrated form of oxides)

24 domains can be depicted at the diagram (see figure 2), each of which represents a thermodynamic stability of certain phases: I – Mo + Mo_3Si + Mo_5Si_3 + $MoSi_2$ + Si ; II – Mo + Mo_3Si + Mo_5Si_3 + $MoSi_2$ + SiO_2 ; III – Mo + Mo_3Si + Mo_5Si_3 + $MoSi_2$ + SiO_3^{2-} ; IV – Mo + Mo_3Si + Mo_5Si_3 + SiO_2 ; V – Mo + Mo_3Si + Mo_5Si_3 + SiO_3^{2-} ; VI – Mo + Mo_3Si + SiO_2 ; VII – Mo + Mo_3Si + SiO_3^{2-} ; VIII – Mo + SiO_2 ; IX – Mo + SiO_3^{2-} ; X – Mo^{3+} + SiO_2 ; XI – MoO_2 + SiO_2 ; XII – MoO_2 + SiO_3^{2-} ; XIII – MoO_2^{2+} + SiO_2 ; XIV – Mo_4O_{11} + SiO_2 ; XV – Mo_8O_{23} + SiO_2 ; XVI – Mo_9O_{26} + SiO_2 ; XVII – MoO_3 + SiO_2 ; XVIII – $H_2Mo_8O_{26}^{2-}$ + SiO_2 ; XIX – $HMo_8O_{26}^{3-}$ + SiO_2 ; XX – $Mo_8O_{26}^{4-}$ + SiO_2 ; XXI – $H_2Mo_7O_{24}^{4-}$ + SiO_2 ; XXII – $Mo_7O_{24}^{6-}$ + SiO_2 ; XXIII – MoO_4^{2-} + SiO_2 ; XXIV – MoO_4^{2-}, SiO_3^{2-}.

Table 4. Basic chemical and electrochemical equilibrium in the Mo – Si – H_2O system at temperature 25°C and air pressure of 1 bar

No of line	Electrode reaction	Equilibrium potential, V (s. h. e.) or pH of the solution
a	$2H^+ + 2e^- = H_2; P_{H_2} \approx 5\cdot10^{-7}$ бар	$0.186 - 0.0591pH$
b	$O_2 + 4H^+ + 4e^- = 2H_2O; P_{O_2} \approx 0{,}21$бар	$1.219 - 0.0591pH$
1	$SiO_2 + 4H^+ + 4e^- = Si + 2H_2O$	$-0.857 - 0.0591pH$
2	$SiO_3^{2-} + 6H^+ + 4e^- = Si + 3H_2O$	$-0.444 - 0.0887pH + 0.0148\cdot\lg a_{SiO_3^{2-}}$
3	$7SiO_2 + Mo_5Si_3 + 28H^+ + 28e^- = 5MoSi_2 + 14H_2O$	$-0.729 - 0.0591pH$
4	$7SiO_3^{2-} + Mo_5Si_3 + 42H^+ + 28e^- = 5MoSi_2 + 21H_2O$	$-0.317 - 0.0887pH + 0.0148\cdot\lg a_{SiO_3^{2-}}$
5	$4SiO_2 + 5Mo_3Si + 16H^+ + 16e^- = 3Mo_5Si_3 + 8H_2O$	$-0.629 - 0.0591pH$
6	$4SiO_3^{2-} + 5Mo_3Si + 24H^+ + 16e^- = 3Mo_5Si_3 + 12H_2O$	$-0.217 - 0.0887pH + 0.0148\cdot\lg a_{SiO_3^{2-}}$
7	$SiO_2 + 3Mo + 4H^+ + 4e^- = Mo_3Si + 2H_2O$	$-0.554 - 0.0591pH$
8	$SiO_3^{2-} + 3Mo + 4H^+ + 4e^- = Mo_3Si + 2H_2O$	$-0.141 - 0.0887pH + 0.0148\cdot\lg a_{SiO_3^{2-}}$
9	$SiO_3^{2-} + 2H^+ = SiO_2 + 2H_2O$	$pH = 13.94 + 0.5\cdot\lg a_{SiO_3^{2-}}$
10	$Mo^{3+} + 3e^- = Mo$	$-0.200 + 0.0197\cdot\lg a_{Mo^{3+}}$
11	$MoO_2 + 4H^+ + 4e^- = Mo + 2H_2O$	$-0.152 - 0.0591pH$
12	$MoO_2 + 4H^+ + e^- = Mo^{3+} + 2H_2O$	$-0.008 - 0.2364pH - 0.0591\cdot\lg a_{Mo^{3+}}$
13	$MoO_2^{2+} + 4H^+ + 3e^- = Mo^{3+} + 2H_2O$	$0.427 - 0.0788pH + 0.0197\cdot\lg\frac{a_{MoO_2^{2+}}}{a_{Mo^{3+}}}$
14	$MoO_2^{2+} + 2e^- = MoO_2$	$0.645 + 0.0295\cdot\lg a_{MoO_2^{2+}}$
15	$4MoO_2^{2+} + 3H_2O + 2e^- = Mo_4O_{11} + 6H^+$	$1.035 + 0.1773pH + 0.1182\cdot\lg a_{MoO_2^{2+}}$
16	$8MoO_2^{2+} + 7H_2O + 2e^- = Mo_8O_{23} + 14H^+$	$1.506 + 0.4137pH + 0.2364\cdot\lg a_{MoO_2^{2+}}$
17	$9MoO_2^{2+} + 8H_2O + 2e^- = Mo_9O_{26} + 16H^+$	$1.623 + 0.4728pH + 0.2660\cdot\lg a_{MoO_2^{2+}}$
18	$MoO_3 + 2H^+ = MoO_2^{2+} + H_2O$	$pH = -1.935 - 0.5\cdot\lg a_{MoO_2^{2+}}$
19	$9MoO_3 + 2H^+ + 2e^- = Mo_9O_{26} + H_2O$	$0.593 - 0.0591pH$
20	$H_2Mo_8O_{26}^{2-} + 2H^+ = 8MoO_3 + 2H_2O$	$pH = 1.9 + 0.5\cdot\lg a_{H_2Mo_8O_{26}^{2-}}$
21	$9H_2Mo_8O_{26}^{2-} + 34H^+ + 16e^- = 8Mo_9O_{26} + 26H_2O$	$0.719 - 0.1256pH + 0.0332\cdot\lg a_{H_2Mo_8O_{26}^{2-}}$
22	$HMo_8O_{26}^{3-} + H^+ = H_2Mo_8O_{26}^{2-}$	$pH = 2.2 + \lg\frac{a_{HMo_8O_{26}^{3-}}}{a_{H_2Mo_8O_{26}^{2-}}}$
23	$9HMo_8O_{26}^{3-} + 43H^+ + 16e^- = 8Mo_9O_{26} + 26H_2O$	$0.793 - 0.1588pH + 0.0332\cdot\lg a_{HMo_8O_{26}^{3-}}$
24	$8Mo_9O_{26} + 2H^+ + 2e^- = 9Mo_8O_{23} + H_2O$	$0.570 - 0.0591pH$
25	$HMo_8O_{26}^{3-} + 5H^+ + 2e^- = Mo_8O_{23} + 3H_2O$	$0.768 - 0.1478pH + 0.0295\cdot\lg a_{HMo_8O_{26}^{3-}}$
26	$Mo_8O_{23} + 2H^+ + 2e^- = 2Mo_4O_{11} + H_2O$	$0.564 - 0.0591pH$
27	$HMo_8O_{26}^{3-} + 7H^+ + 4e^- = 2Mo_4O_{11} + 4H_2O$	$0.666 - 0.1034pH + 0.0148\cdot\lg a_{HMo_8O_{26}^{3-}}$

28	$Mo_8O_{26}^{4-} + H^+ = HMo_8O_{26}^{3-}$	$pH\ 2.5 + \lg \frac{a_{Mo_8O_{26}^{4-}}}{a_{HMo_8O_{26}^{3-}}}$
29	$Mo_8O_{26}^{4-} + 8H^+ + 4e^- = 2Mo_4O_{11} + 4H_2O$	$0.703 - 0.1182pH + 0.0148 \cdot \lg a_{Mo_8O_{26}^{4-}}$
30	$8H_2Mo_7O_{24}^{4-} + 4H^+ = 7Mo_8O_{24}^{4-} + 10H_2O$	$pH = 2.9 + 0.25 \cdot \lg \frac{a^8_{H_2Mo_7O_{24}^{4-}}}{a^7_{Mo_8O_{26}^{4-}}}$
31	$4H_2Mo_7O_{24}^{4-} + 30H^+ + 14e^- = 7Mo_4O_{11} + 19H_2O$	$0.727 - 0.1266pH + 0.0169 \cdot \lg a_{H_2Mo_7O_{24}^{4-}}$
32	$Mo_4O_{11} + 6H^+ + 6e^- = 4MoO_2 + 3H_2O$	$0.515 - 0.0591pH$
33	$H_2Mo_7O_{24}^{4-} + 18H^+ + 14e^- = 7MoO_2 + 10H_2O$	$0.568 - 0.0760pH + 0.0042 \cdot \lg a_{H_2Mo_7O_{24}^{4-}}$
34	$Mo_7O_{24}^{6-} + 2H^+ = H_2Mo_7O_{24}^{4-}$	$pH = 4.4 + 0.5 \cdot \lg \frac{a_{Mo_7O_{24}^{6-}}}{a_{H_2Mo_7O_{24}^{4-}}}$
35	$Mo_7O_{24}^{6-} + 20H^+ + 14e^- = 7MoO_2 + 10H_2O$	$0.605 - 0.0844pH + 0.0042 \cdot \lg a_{Mo_7O_{24}^{6-}}$
36	$7MoO_4^{2-} + 8H^+ = Mo_7O_{24}^{6-} + 4H_2O$	$pH = 7.008 + 0.125 \cdot \lg \frac{a^7_{MoO_4^-}}{a_{Mo_7O_{24}^{6-}}}$
37	$MoO_4^{2-} + 4H^+ + 2e^- = MoO_2 + 2H_2O$	$0.842 - 0.1182pH + 0.0295 \cdot \lg a_{MoO_4^-}$

Domain I corresponds to system immunity (or thermodynamic stability), all system components should not corrode at these solution pH and equilibrium potentials.

The selective oxidation of silicon from alloy occurs at domains II – IX. This results in consecutive formation of phases, increasingly rich in molybdenum, up to pure metal, and the excess silicon oxidizes to silica (at domains II, IV, VI, VIII) or, in highly alkaline environments, to metasilicate ions.

Domains X and XIII correspond to molybdenum selective corrosion, in which it actively passes into solution in form of respectively Mo^{3+} or MoO_2^{2+} cations.

If values of potentials and pH correspond to domains XI, XII, XIV – XVII, then thermodynamic conditions for the oxidation of molybdenum to one of its oxide are created. There are domains of molybdenum passivation of alloys. Domains XVIII – XXIV are domains of molybdenum transpassivity of alloys: the oxide film exposes further oxidation and partially passes into solution in form of one of the molybdate ions.

Lines *a* and *b* in the diagram correspond to the work of the hydrogen and oxygen electrodes, respectively. Domain of potentials and pH, which lies between them, corresponds to the electrochemical stability of water.

As seen from figure 2, molybdenum has a very narrow area of active dissolution, as the cations of molybdenum and molybdenyl exist only in strongly acidic environments. However, the domain of its passivity (on the potentials) is also quite small, and the more alkaline the environment is, the broader the domain of transpassivity becomes. Generally, the electrochemical stability of the molybdtnum-silicon alloys is also entirely determined by silicon content in it. Despite the fact, that the oxidation of the alloy silicon component begins earlier (on the potentials) than the oxidation of molybdenum, the SiO_2 oxide film is much more resistant in chemical and electrochemical terms, than the molybdenum oxides film. If the silicon percentage in the alloy is sufficient to form on its surface a continuous film of silica, than molybdenum active oxidation should not occur in all. In this case, one or another molybdenum oxide should be included into the passivity film only in the form of local inclusions.

Conclusions:

5. A phase diagram of Mo – Si – O system and a potential – pH diagram of Mo – Si – H_2O at 25˚C, air pressure of 1 bar and activities of ions in solution equal to 1 mole/l are plotted. Basic equilibria in Mo – Si – O and Mo – Si – H_2O systems at these conditions are calculated.
6. The thermodynamic analysis of chemical and electrochemical stability of Mo – Si system alloys is performed. It is proved, that the stability is determined by silicon content in alloys.

References

1. A. B. Shein. Elektrokhimiya silitcidov i germanidov perekhodnykh metallov [In Russian] (Electrochemistry of transition metals silicides and germanides) *Perm:Publishing House of Perm State University.* **2009**. 269p.
2. Silicides: Material Sciences Laboratory. URL: < http://lm-sgc.ru/silycidi.htm>.

3. A composite heat-resistant material: Russian Federation patent No 2154122 from 10.08.2000 [In Russian]. URL:<http://ru-patent.info/21/50-54/2154122.html>.
4. A.B Gokhale and G.J Abbaschian. The Mo-Si (Molybdenum-Silicon) system. *Journal of Phase Equilibria*, **1991**. Vol.12. No.4. P.493-498.
5. N. P. Lyakishev. Diagrammy sostoyaniya dvoynykh metallicheskikh sistem: spravochnik [In Russian] (Phase diagrams of binary metallic systems: textbook). *Moscow: Mashinostroyeniye*. **2000**. Vol.3. Book No.1. P.449-452.
6. FactSage Databases: phase diagrams database. URL: <http://www.crct.polymtl.ca/fact/documentation>.
7. L. P. Ruzinov, B. S. Gulyanitckiy. Ravnovesnyye prevrashcheniya metallurgicheskikh reaktciy [In Russian] (Equilibrium transformations in metallurgical reactions) *Moscow: Metallurgiya.* **1975**. 416p.
8. Termicheskiye konstanty veshchestv: database [In Russian] (Thermal constants of the substances). URL: <http://www.chem.msu.su/cgi-bin/tkv.pl?show=welcome.html>
9. B. M. Mogutnov, I. A. Tomilin, L. A. Shwarzman. Termodinamika splavov zheleza [In Russian] (Thermodynamics of iron alloys). *Moscow.: Metallurgiya.* **1984**. 208p.
10. C. Vahlas, P.Y. Chevalier, and E. Blanquet. A Thermodynamic evaluation of four Si-M (M = Mo, Ta, Ti, W) binary systems. *CALPHAD*. **1989**. Vol.13. No.3. P.273-292.
11. A. G. Tyurin. Termodinamicheskiy analiz obrazovaniya faz v protcessakh elektroliticheskogo osazhdeniya titana iz vodnykh rastvorov [In Russian]. (Thermodynamic analysis of phase formation during the titanium electrochemical sedimentation process). *Elektrokhimiya*. **1990**. Vol.26. No.12. P.1599-1605.
12. JANAF Thermochemical Tables. Third Edition. *J. Phys. Chem. Ref. Data*. **1985**. Vol.14. Suppl.1.
13. N. A. Toropov, V. P. Borzakovskiy [et al.] Diagrammy sostoyaniya silikatnykh sistem: spravochnik [In Russian] (Phase diagrams of silicate systems). *Moscow-Leningrad.: Nauka*. **1965**. Issue No.2. 372p.
14. P. A. Nikolaychuk, A. G. Tyurin. The revised Pourbaix diagram for molybdenum. *Butlerov Communications.* **2011**. Vol.24. No 2. P.101-105.
15. Spravochnik po elektrokhimii [In Russian] (Textbook on Electrochemistry). Editor A. M. Sukhotin. *Leningrad: Khimiya.* **1981**. 488p.
16. A. G. Tyurin. Termodinamika khimicheskoy i elektrokhimicheskoy ustoychivosti splavov [In Russian] (Thermodynamics of the chemical and electrochemical stability of alloys). In 2 parts. Part. 2. *Chelyabinsk:Publishing center of Chelyabinsk State University*. **2004**. 91p.

9. Mn– Si system
9.1. Manganese silicides

Manganese doped by silicon is used in manufacturing of rail and structural steels, in metallurgy as the deoxidizer, as the dopant to alloys based on aluminum, magnesium and copper.

For a long time the phase diagrams taking into account only four manganese silicides (Mn_3Si, Mn_5Si_3, MnSi and $MnSi_2$) were proposed. However, by more meticulous investigation of alloys both rich of manganese and of silicon, the number and the composition of silicides, and the phase diagram of the Mn – Si system were revised (see Figure 39).

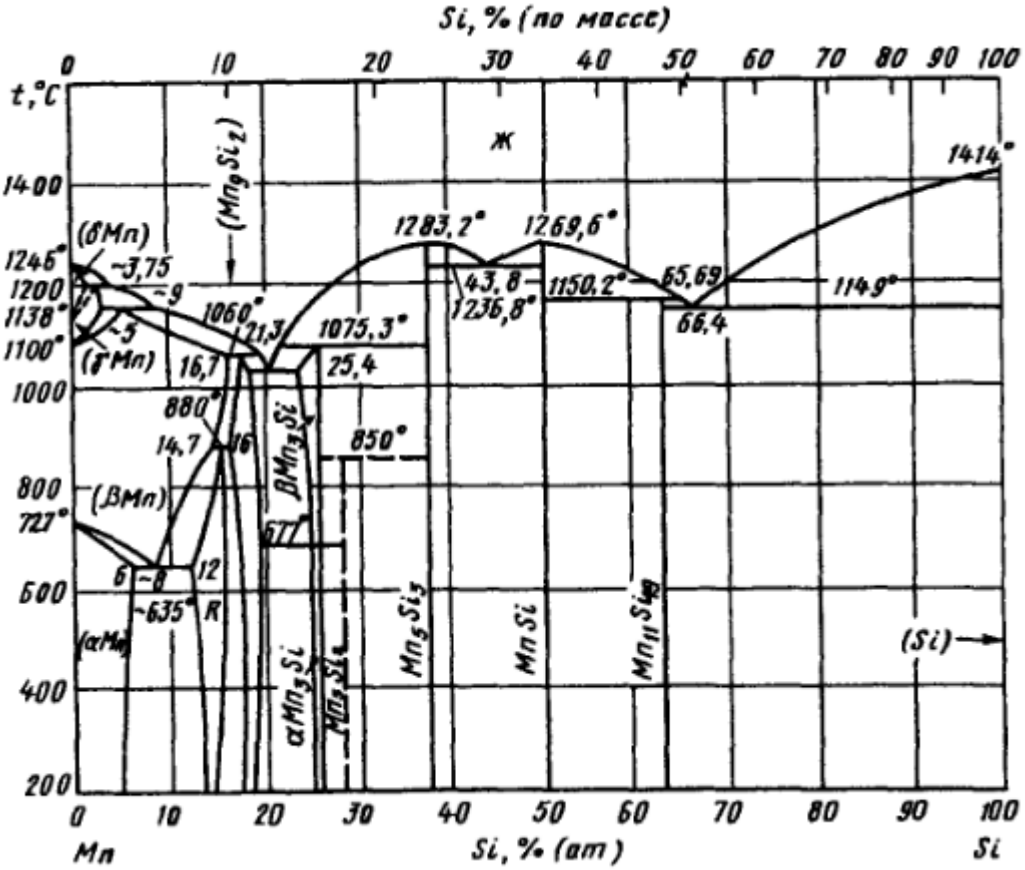

Fig. 39. The phase diagram of the Mn – Si system [Диаграммы состояния двойных металлических систем: справочник, 2001].

There are seven intermetallic phases in Mn – Si system: $Mn_{11}Si_{19}$, MnSi, Mn_5Si_3, Mn_5Si_2, Mn_3Si, ν-phase (Mn_9Si_2) and R-phase (Mn_6Si) [Chakraborti, Lukas, 1989; Chevalier, Fischer, Rivet, 1995; Du et al., 2004; Kanibolotskii, Lesnyak, 2006; Miettinen, 2003b]. The first five silicides are stoichiometric phases. ν-phase has a narrow homogeneity range at elevated temperatures but can be considered as stoichiometric compound at

standard conditions. R-phase has a noticeable homogeneity range at 25°C. Moreover, a solid solution of Si in (cubic-Mn) can be formed (α-phase). According to [Артюх et al., 1988], R-phase in equilibrium with α-phase has the composition of $Mn_{0.85}Si_{0.15}$. Several studies were devoted to investigations of the highest manganese silicide, and the authors did not meet a single opinion on its composition and properties. It was stated that the highest manganese silicide at elevated temperatures has a homogeneity range of $MnSi_{1,70}$ – $MnSi_{1,75}$ [Гельд, Сидоренко, 1971].

There were studies devoted to the thermodynamic description of the Mn – Si system that proposed the different models for both α- and R-phases. These models were implemented to estimate the maximum solid solubility of silicon in manganese at the room temperature.

a) α-phase was treated as the bcc solid solution and described in terms of quasiregular solution model [Guggenheim, 1935], and R-phase was described as $Mn_{26}Si_3(Mn, Si)_{24}$ in terms of sublattice model. The comparison between the calculated data on α ⇌ R equilibrium and the phase diagram is presented in Figure 40.

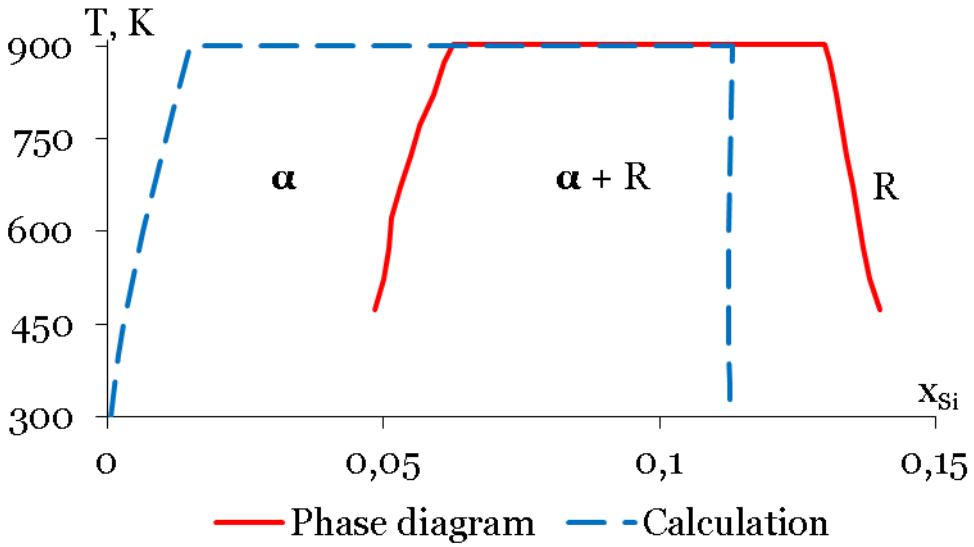

Fig. 40. The comparison between the calculated data on α ⇌ R phase equilibrium according to [Chakraborti, Lukas, 1989] and the phase diagram.

b) α-phase was treated as the bcc solid solution and described in terms of quasiregular solution model, and R-phase was described as the stoichiometric compound Mn_6Si. The comparison between the calculated data on α ⇌ R equilibrium and the phase diagram is presented in Figure 41.

c) α-phase was treated as the cbcc solid solution and described in terms of substitution solution model using the Redlich-Kister equation for

the excess Gibbs energy, and R-phase was described as the stoichiometric compound $Mn_{0,85}Si_{0,15}$. The comparison between the calculated data on α ⇌ R equilibrium and the phase diagram is presented in Figure 42.

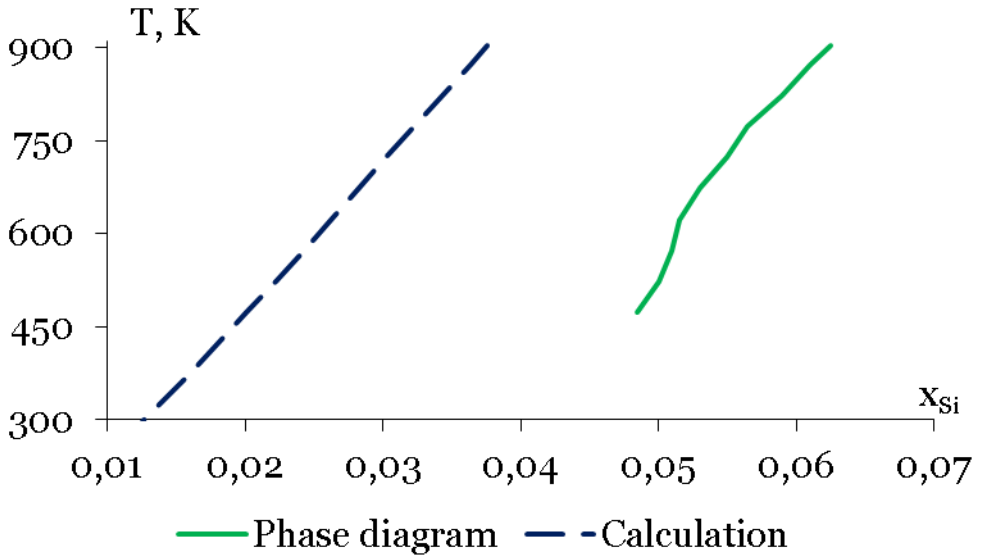

Fig. 41. The comparison between the calculated data on α ⇌ R phase equilibrium according to [Chakraborti, Lukas, 1989] and the phase diagram.

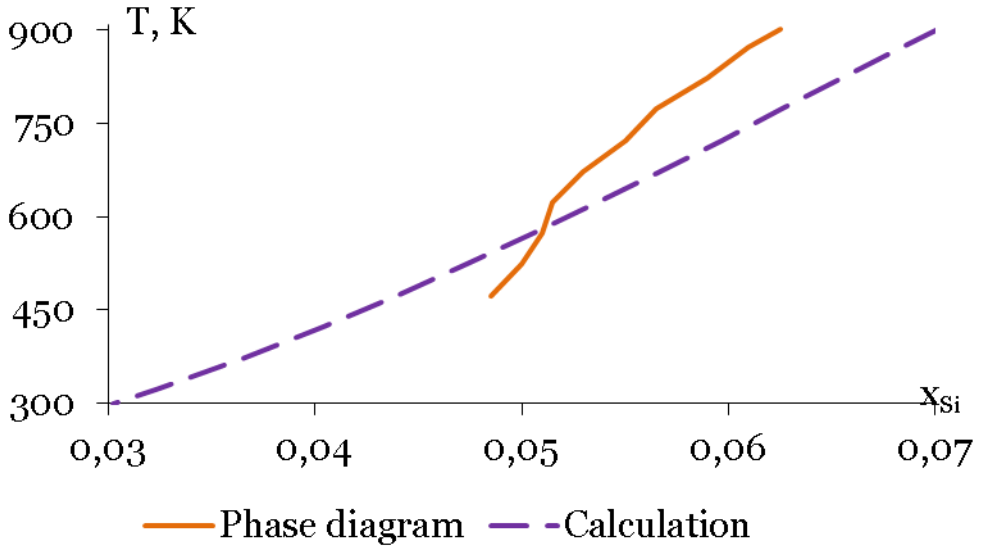

Fig. 42. The comparison between the calculated data on α ⇌ R phase equilibrium according to [Chevalier, Fischer, Rivet, 1995] and the phase diagram.

As could be seen, the existing thermodynamic models do not reproduce the α ⇌ R phase equilibrium in the low-temperature region. This is why the new model was developed, in which α-phase was treated as the cbcc solid solution and described in terms of quasiregular solution model,

and R-phase was described as the stoichiometric compound $Mn_{0,85}Si_{0,15}$. More details are presented in the attached publication. Calculated solid solubility of Si in cbcc-Mn at 25˚C equals 4.56 at. %. Thermodynamic activities of solid solution compounds are the following: $a_{Mn(\alpha)} = 0.83$, $a_{Si(\alpha)} = 3.8 \cdot 10^{-28}$.

The solid solubility of Mn in diamond-Si is about 10^{-14} at. % at 1100˚C [Yoshikawa et al., 2010]. The standard Gibbs energies of formation of manganese silicides were collected from various sources [Chakraborti, Lukas, 1989; Chevalier, Fischer, Rivet, 1995; Miettinen, 2003b; Артюх et al., 1988; Верягин et al., 1965; Рузинов, Гуляницкий, 1975; Рябин, Остроумов, Свит, 1977; Термические константы веществ, 2007].

9.2. Equilibira in Mn – Si – O system

Manganese forms the oxides MnO, Mn_3O_4, Mn_2O_3, MnO_2 and Mn_2O_7 though the last one is not stable in water solutions. There are two manganese silicates at 25˚C, namely, $MnSiO_3$ and Mn_2SiO_4 [Glasser, 1958]. The compound Mn_7SiO_{12} exist only at elevated temperatures [Huang, Rosén, 1994].

The state diagram of the Mn – Si – O system is presented in Figure 43. More details, including the standard Gibbs energies of formation of manganese oxides and silicates, are provided in the attached publication.

9.3. Potential – pH diagram of Mn – H_2O system

The following manganese ions exist in an aqueous solution: Mn^{2+}, Mn^{3+}, $HMnO_2^-$, MnO_4^{2-} and MnO_4^-. The values of the standard Gibbs energies of formation of these ions, and the activity – pH diagram for Mn (II) species are presented in the attached publication.

The potential – pH diagram of the Mn – H_2O system at 25 °C, air pressure of 1 bar and the activities of manganese species in a solution of 1 1 $mol \cdot l^{-1}$ is presented in Figure 44, and the diagram at the activities of manganese species of 10^{-6} $mol \cdot l^{-1}$ is presented in Figure 45.

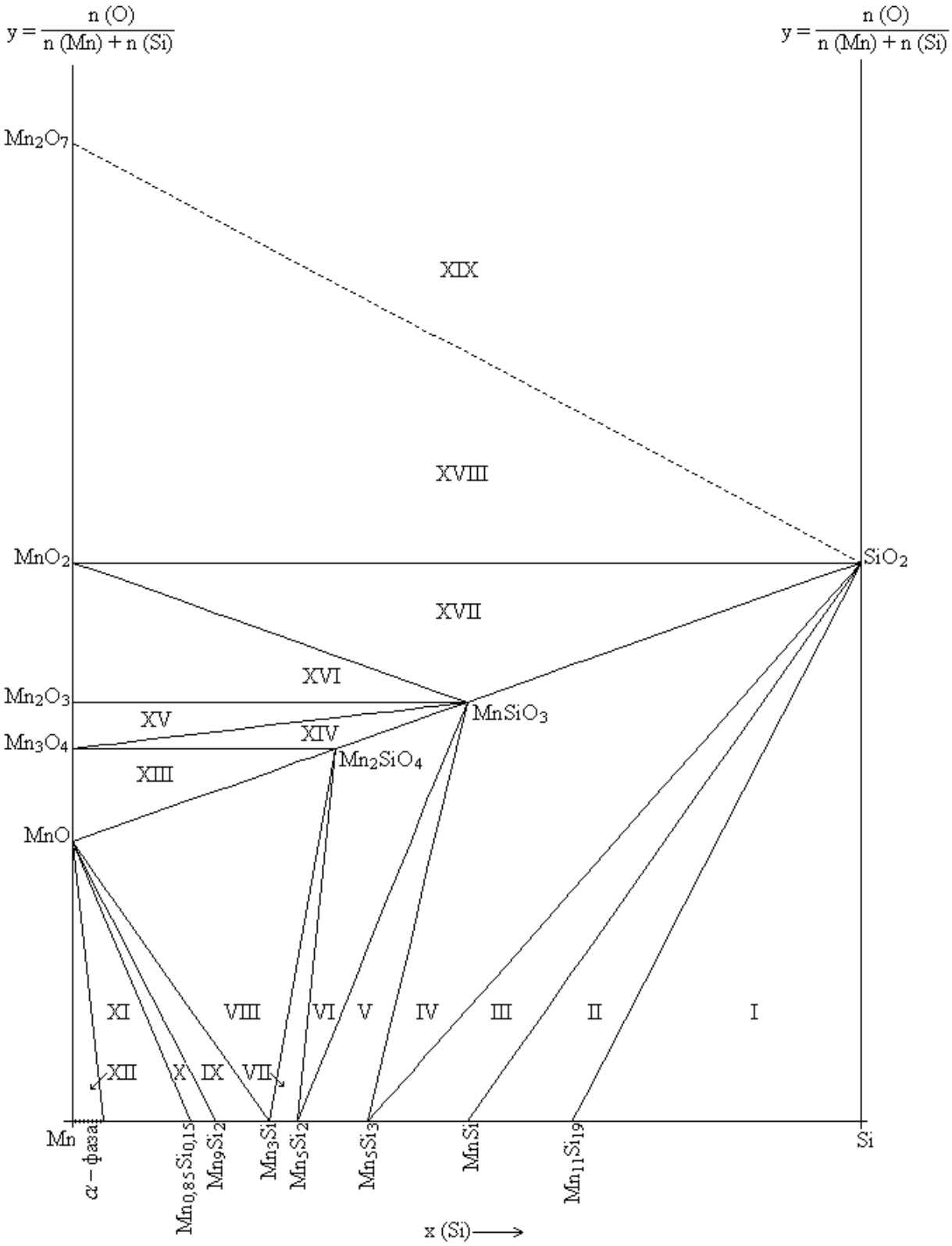

Fig. 43. The state diagram of the Mn – Si – O system.

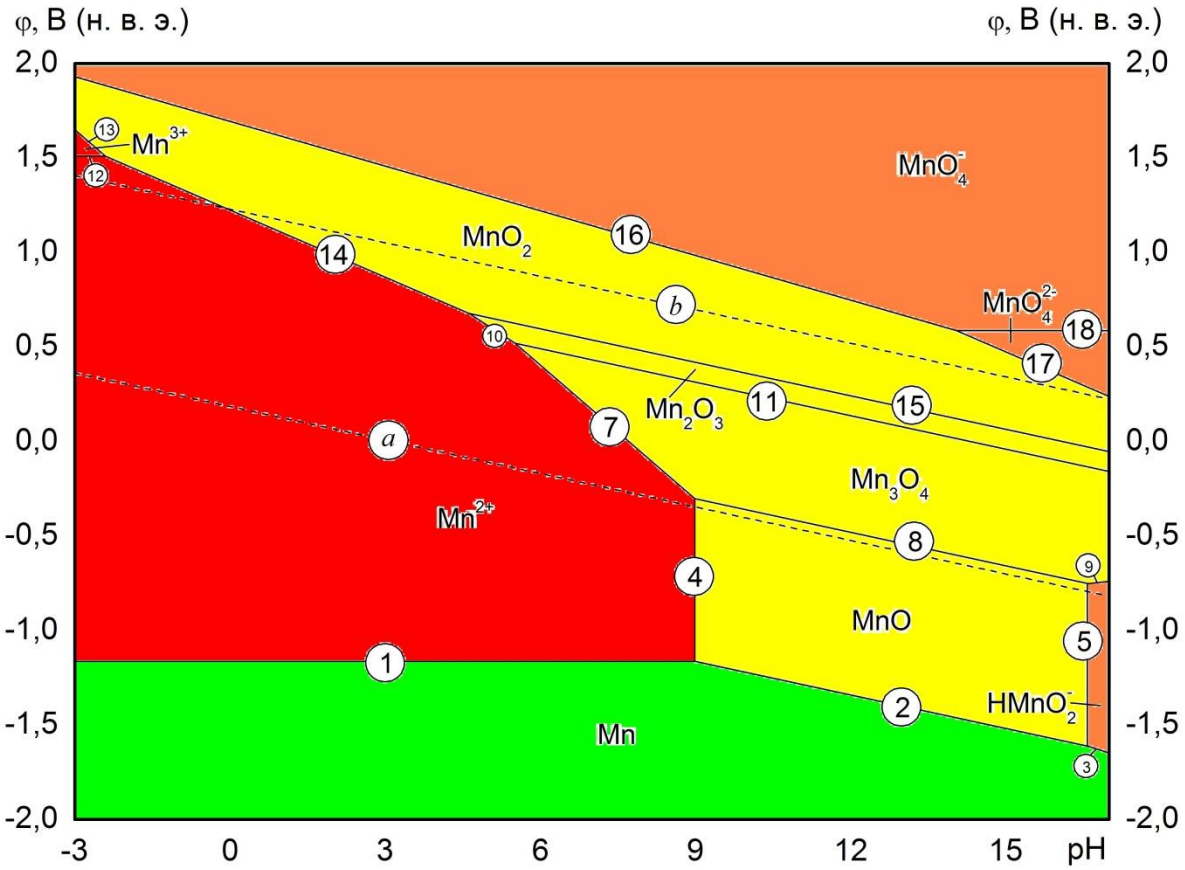

Fig. 44. The potential – pH diagram of the Mn – H_2O system at 25 °C, air pressure of 1 bar and the activities of manganese species in a solution of 1 mol·l^{-1}.

9.4. Potential – pH diagram of Mn – Si – H_2O system

The potential – pH diagram of Mn – Si – H_2O system at 25 °C, air pressure of 1 bar and the activities of species in a solution of 1 mol·l^{-1} is presented in Figure 46. The cross-section of this diagram in the region of thermodynamic stability of *a*) manganese silicides and *b*) silicate-ions is presented in Figure 47.

The corrosion-electrochemical behavior of manganese-silicon alloys is determined by the acidity of environment and the value of equilibrium potential. In acidic environments the selective corrosion of manganese takes place and it forms the cations Mn^{2+} and silicon from alloy is oxidized to silicic acid. In neutral and alkaline environments oxidation can end with formation of passivation film consisting of silicates Mn_2SiO_4 or $MnSiO_3$.

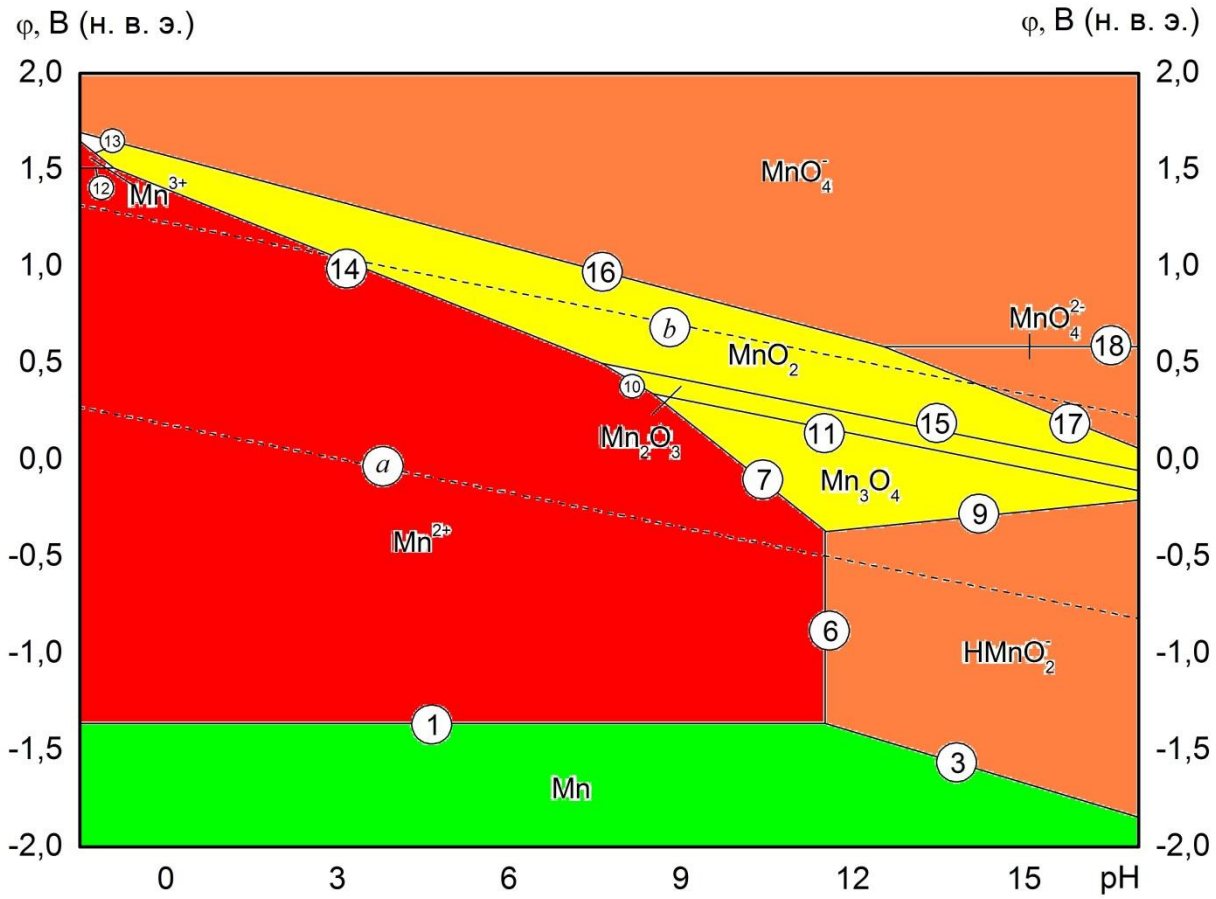

Fig. 45. The potential – pH diagram of the Mn – H_2O system at 25 °C, air pressure of 1 bar and the activities of manganese species in a solution of 10^{-6} mol·l^{-1}.

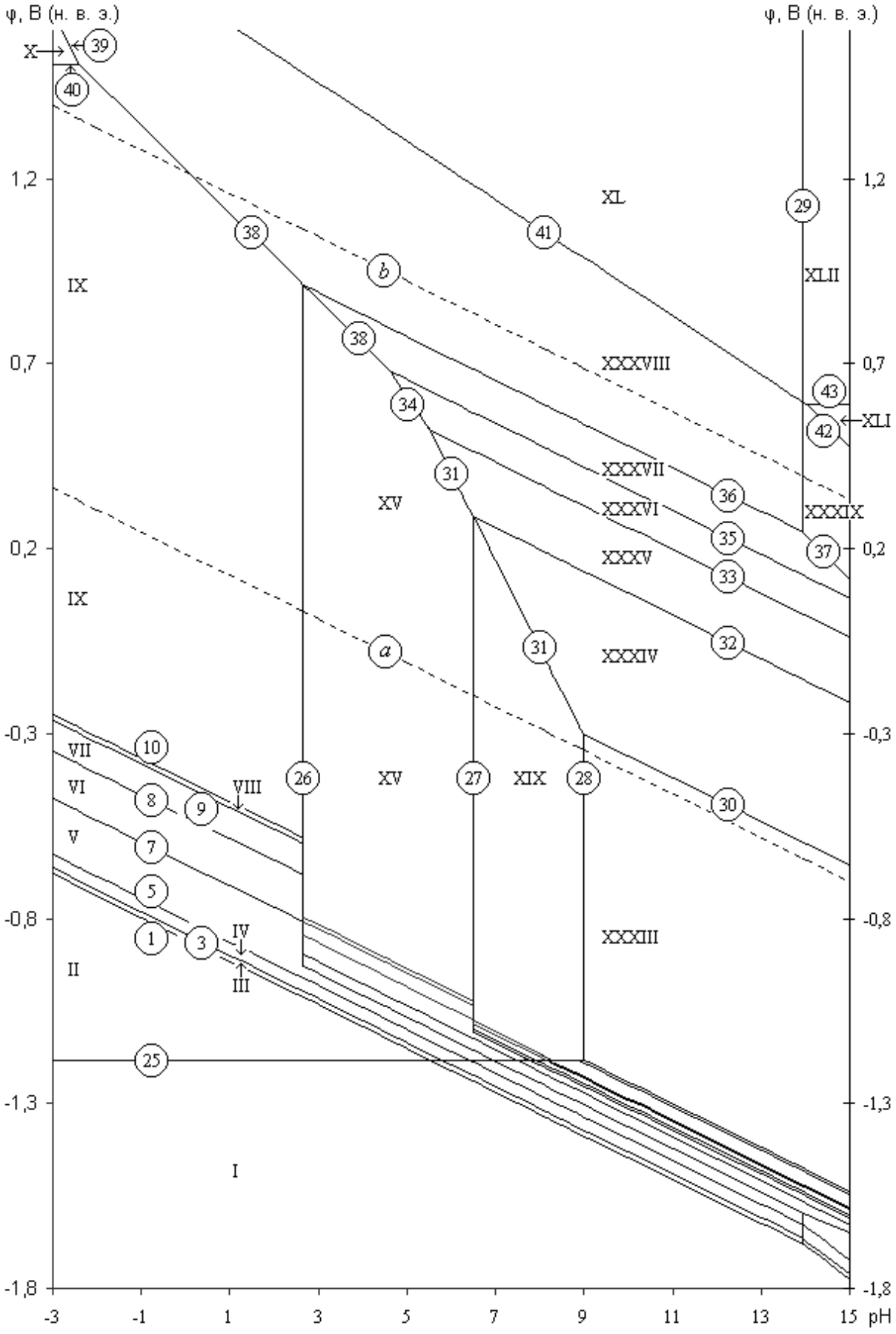

Fig. 46. The potential – pH diagram of the Mn –Si – H_2O system at 25 °C, air pressure of 1 bar and the activities of species in a solution of 1 M.

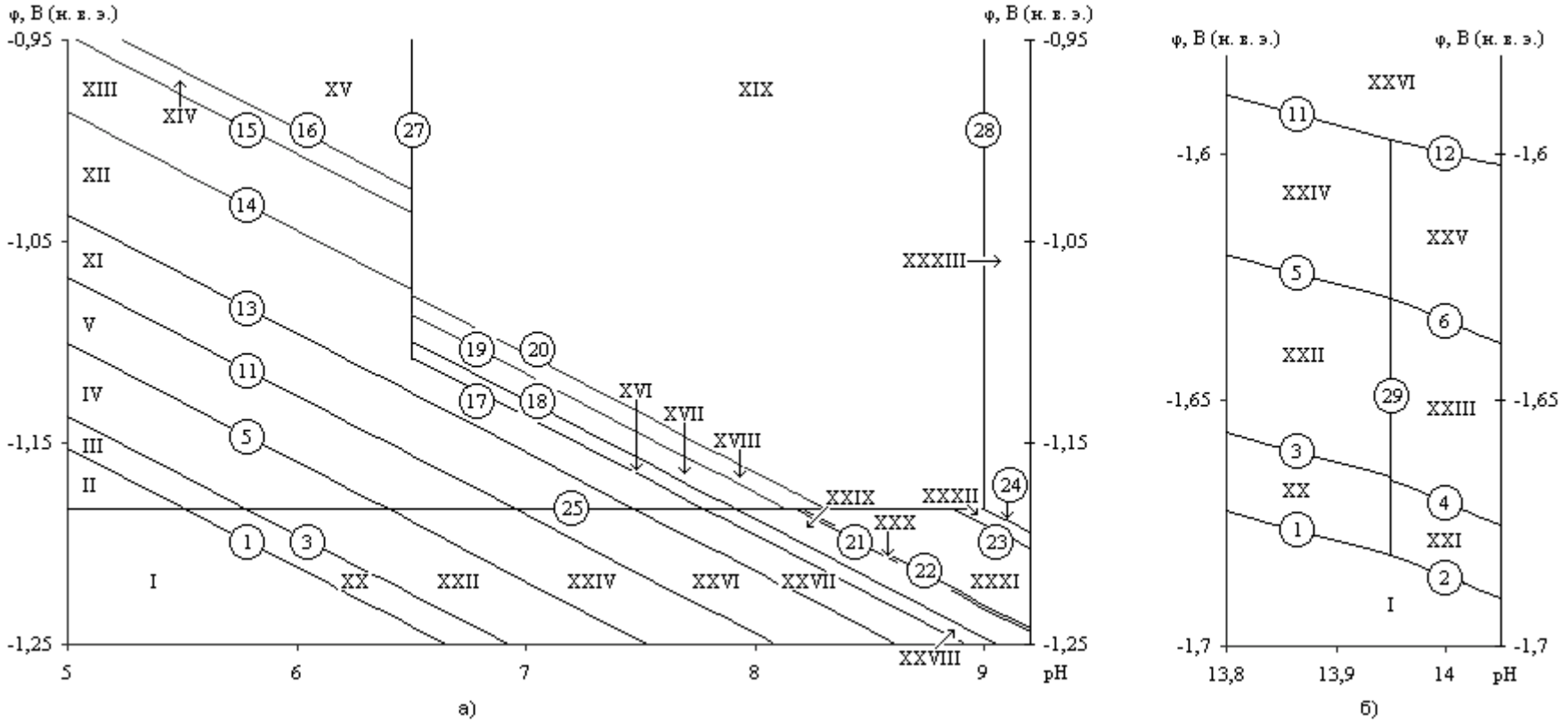

Fig. 47. The cross-section of the potential – pH diagram of the Mn –Si – H_2O system from Figure 46 in the in the region of thermodynamic stability of *a*) manganese silicides and *b*) silicate-ions.

Publications to chapter 9

The potential – pH diagram of Mn – H_2O system was published in conference paper [Nikolaychuk, 2015a].

The potential – pH diagram of Mn – Si – H_2O system was published in paper [Николайчук et al., 2010]. The Russian preprint of this paper with the title, abstract, figures and tables translated into English is presented below with the permission from *Ûžno-Ural'skij gosudarstvennyj universitet (nacional'nyj issledovatel'skij universitet)*.

УДК 544.653:544.016:544.313.2.031

THE POTENTIAL – pH DIAGRAM FOR Mn – H_2O SYSTEM

P. A. Nikolaychuk

Chelyabinsk State University, Chelyabinsk, Russia. E-mail: npa@csu.ru

Thermodynamic information on aqueous manganese species is systematized. The reactions between various species are discussed. The activity – pH diagram for Mn^{II} species and the revised potential – pH diagrams of Mn – H_2O system at 25ºC, 1 bar and $a_{[Mn]}$ = 1 mol l^{-1} and $a_{[Mn]}$ = 10^{-6} mol l^{-1} are plotted.

Since Pourbaix diagrams were firstly introduced, several papers concerning potential – pH diagrams for pure elements were published. However, even the diagrams presented in the most recent books [1–3] aren't consistent with each other and contain various species. This paper aims to collect and analyze available data on Gibbs energies of formation of manganese species and revise the diagram.

Elemental manganese has the simple cubic lattice at standard conditions. Five manganese oxides with oxidation degrees ranging from II to VII are known: MnO, Mn_3O_4, Mn_2O_3, MnO_2 and Mn_2O_7 [4]. However, Mn_2O_7 is extremely unstable in water solution and decomposes spontaneously according to equation Mn_2O_7 (s) + H_2O (l) $\rightarrow 2\,MnO_4^-$ (aq) + $2H^+$ (aq) [3].

In aqueous solution manganese forms a variety of unhydrolyzed and hydrolyzed species with oxidation degrees II (Mn^{2+}, $MnOH^+$, $HMnO_2^-$), III (Mn^{3+}), VI (MnO_4^{2-}) and VII (MnO_4^-). There is no available thermodynamic information on $MnOH^{2+}$, $Mn(OH)_3^-$ and $Mn(OH)_4^{2-}$. Polymerized species like $Mn_2(OH)_3^+$ and Mn_2OH^{3+} and oxyhydrate MnOOH aren't considered. The standard Gibbs energies of formation used in calculations are presented in Table 1. The value of $\Delta_f G^o_{298}$ ($HMnO_2^-$) was calculated according to data on standard electrode potentials collected from various reference textbooks [7 – 10].

However, since the data from the various sources weren't consistent with each other, the averaged value was calculated.

Table 1. The standard Gibbs energies of formation of manganese species.

Compound	$\Delta_f G^o_{298}$, J mol^{-1}	Reference	Compound	$\Delta_f G^o_{298}$, J mol^{-1}	Reference
MnO (s)	–362 800	[5, 6]	Mn^{3+} (aq)	–85 000	[3, 6]
Mn_3O_4 (s)	–1 283 000	[5, 6]	$MnOH^+$ (aq)	–405 000	[6]
Mn_2O_3 (s)	–878 900	[5, 6]	$HMnO_2^-$ (aq)	–506 000	[7 – 10]
MnO_2 (s)	–465 000	[5, 6]	MnO_4^{2-} (aq)	–503 700	[3, 6]
Mn^{2+} (aq)	–228 400	[3, 6]	MnO_4^- (aq)	–447 300	[3, 6]

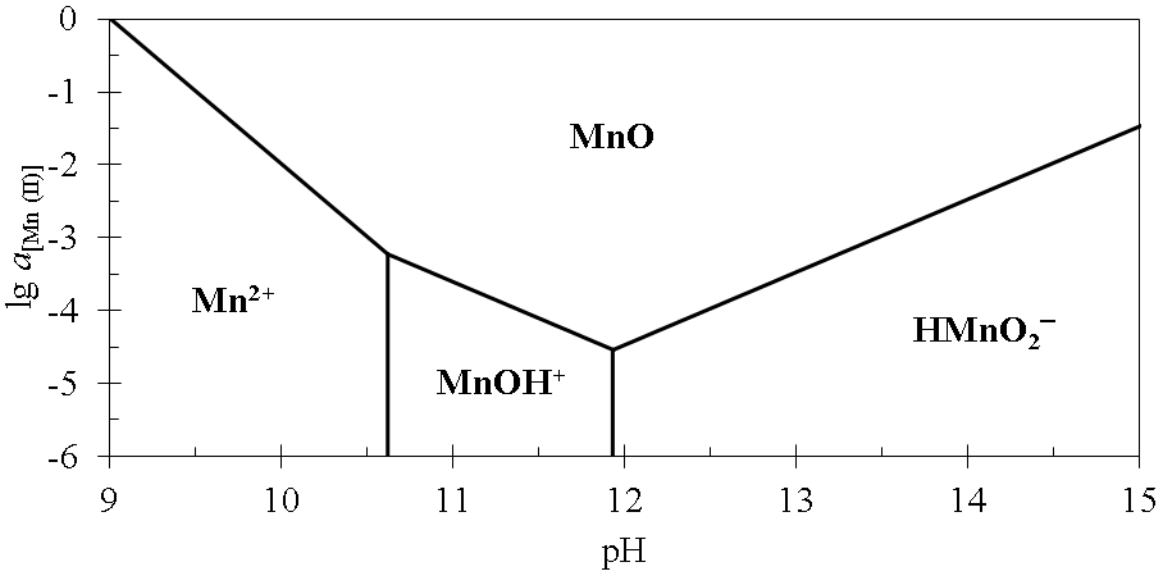

Figure 1. The activity – pH diagram for Mn^{II} species.

Figure 1 shows the predominance diagram of Mn^{II} species. The following order of oxidation is possible depending on ion activities:

lg $a_{[Mn]}$ > –3,224: Mn^{2+} (aq) → MnO (s) → $HMnO_2^-$ (aq);

–3,224 > lg $a_{[Mn]}$ > –4,54: Mn^{2+} (aq) → $MnOH^+$ (aq) → MnO (s) → → $HMnO_2^-$ (aq);

lg $a_{[Mn]}$ < —4,54: Mn^{2+} (aq) → $MnOH^+$ (aq) → $HMnO_2^-$ (aq).

Calculations show that in diluted media, when $a_{[Mn]} < 10^{-5}$ mol l^{-1}, the domain of stability of MnO vanishes and $MnOH^+$ is oxidized directly to $HMnO_2^-$.

The potential – pH diagrams of Mn – H_2O system plotted at 25ºC, air pressure of 1 bar and activities of ions in solution, equal to 1 and 10^{-6} mol l^{-1} are shown at Figures 2 and 3, respectively.

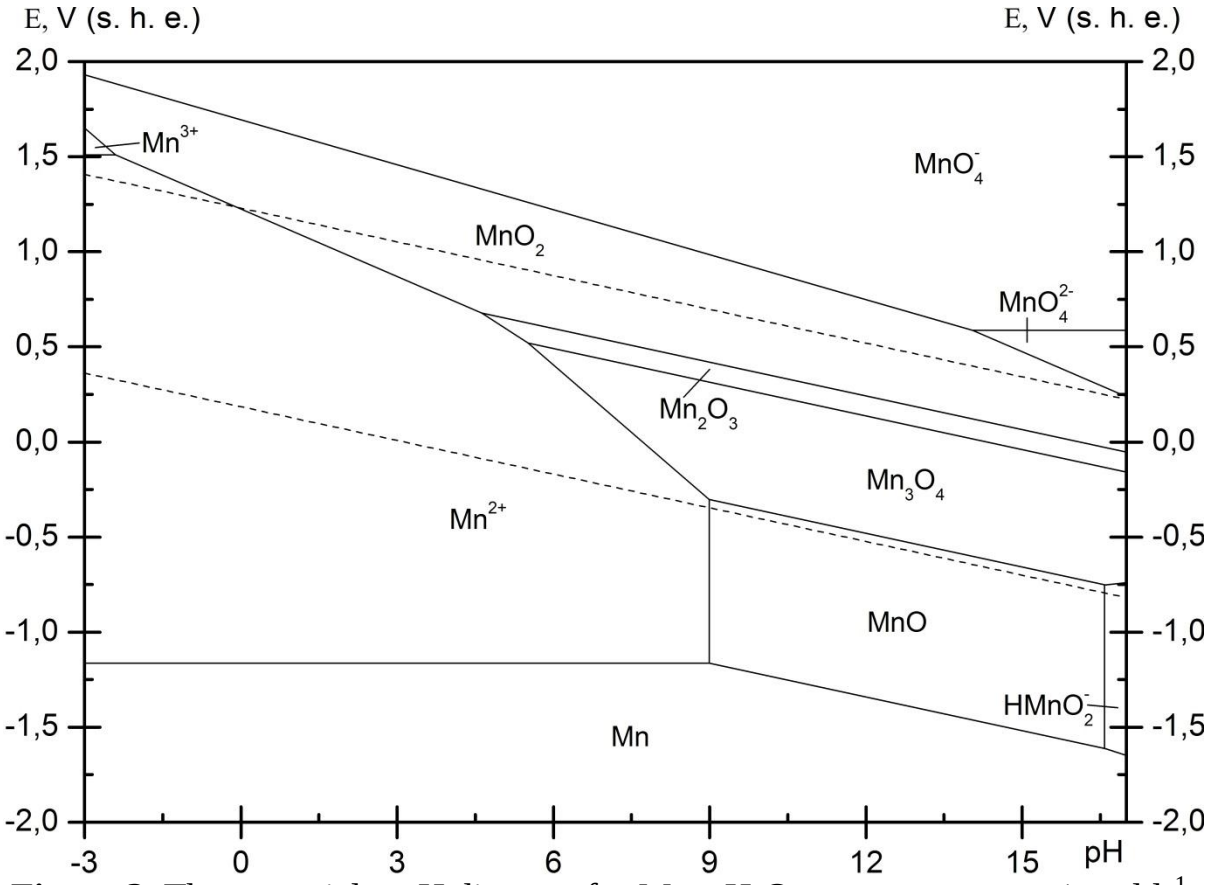

Figure 2. The potential – pH diagram for Mn – H_2O system at $a_{[Mn]}$ = 1 mol l^{-1}.

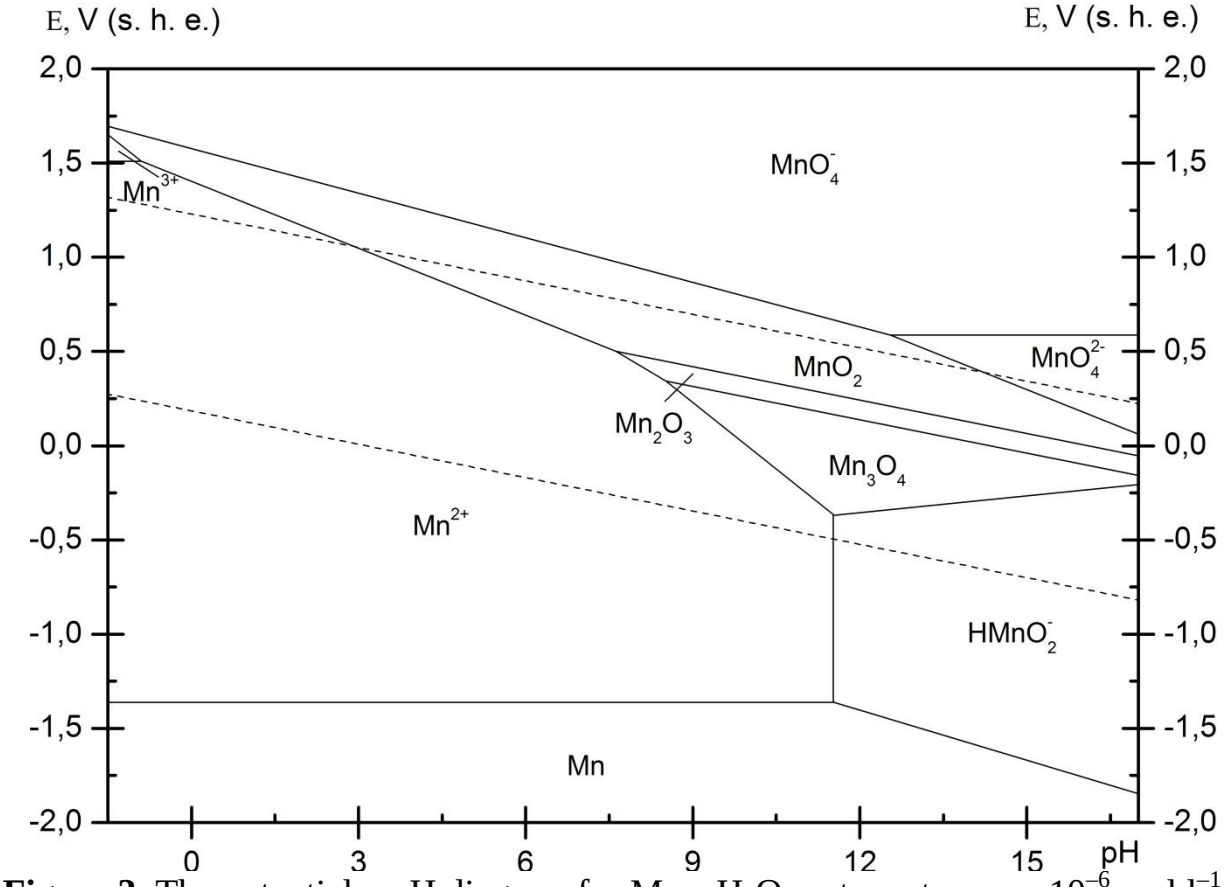

Figure 3. The potential – pH diagram for Mn – H_2O system at $a_{[Mn]}$ = 10^{-6} mol l^{-1}.

Figure 2 shows the diagram with the domain of thermodynamic stability of MnO, while Figure 3 presents a diagram without it.

Dashed lines represent the hydrogen and oxygen electrodes and border the domain of electrochemical stability of water at atmospheric conditions.

REFERENCES:

1. Atlas of Eh-pH diagrams: Intercomparison of thermodynamic databases. Open file report № 419. National Institute of Advanced Industrial Science and Technology, 2005.
2. Brookins, D. G. Eh-pH diagrams for geochemistry. Berlin: Springer, 1987.
3. Schweitzer, G. K., Pesterfield, L. L. The aqueous chemistry oft he elements. Oxford: Oxford University Press, 2010.
4. Phase diagram – Web. FactSage Database.
5. Chase, M. W. Jr et al. JANAF thermochemical tables. Third edition. Journal of Physical and Chemical Reference Data, 1985. Vol. 14. Suppl. 1.
6. Wagman, D. D. et al. The NBS tables of chemical thermodynamic properties. Selected values for inorganic and C_1 and C_2 organic substances in SI units. Journal of Physical and Chemical Reference Data, 1982. Vol. 11. Suppl. 2.
7. Garrels, R. M., Christ, Ch. L. Solutions, minerals, and equilibria. New York: Harper & Row, 1965.
8. Bard, A. J., Parsons, R., Jordan, J. Standard potentials in aqueous solutions. New York: Marcel Dekker Inc., 1985.
9. Speight, J. Lange's Handbook of Chemistry, 16th Edition. New York: McGraw-Hill Education, 2005.
10. Vanýsek, P. Electrochemical Series. In: CRC Handbook of Chemistry and Physics, 95th Edition; Ed. W. M. Haynes. CRC Press, 2014.

УДК 541.1:620.193.01:669.14

ТЕРМОДИНАМИКА ХИМИЧЕСКОЙ И ЭЛЕКТРОХИМИЧЕСКОЙ УСТОЙЧИВОСТИ СПЛАВОВ СИСТЕМЫ Mn – Si

П. А. Николайчук, Т. И. Шаляпина, А. Г. Тюрин, Т. В. Мосунова

Проведён термодинамический анализ химических и фазовых равновесий в системе Mn – Si. Построены фазовая диаграмма Mn – Si – O и диаграмма потенциал – pH системы Mn – Si – H_2O при 25˚C. С точки зрения термодинамики проанализированы процессы низкотемпературного окисления марганец-кремниевых сплавов на воздухе и в водных средах.

Ключевые слова: силициды марганца, низкотемпературное окисление, химическая устойчивость, коррозионно-электрохимическое поведение, диаграммы потенциал – pH, электрохимическая устойчивость.

THERMODYNAMICS OF CHEMICAL AND ELECTROCHEMICAL STABILITY OF Mn – Si SYSTEM ALLOYS

P. A. Nikolaychuk, T. I. Shalyapina, A. G. Tyurin, T. V. Mosunova

The thermodynamical analysis of chemical and phase equilibria in Mn – Si system is performed. The Mn – Si – O phase diagram and the potential – pH diagram of Mn – Si – H_2O system at 25˚C are plotted. The processes of low temperature oxidation of manganese-silicon alloys in air and water environments are analyzed from the point of view of thermodynamics.

Keywords: manganese silicides, low temperature oxidation, chemical stability, corrosion-electrochemical behaviour, potential – pH diagrams, electrochemical stability.

Введение

Марганец в сплаве с кремнием используется в производстве рельсовой и конструкционной стали, им легируют сплавы на основе алюминия, магния и меди. Силикомарганец – ферросплав, основные компоненты которого – это железо, кремний и марганец – используется при выплавке стали как раскислитель и легирующая присадка [1].

Известно [2], что сплавы кремния с переходными металлами, в том числе и с марганцем, обладают необычным комплексом магнитных, электрических, механических свойств, а также высоким химическим сопротивлением, и поэтому являются перспективными электродными материалами. Однако указанные свойства сильно различаются в зависимости от природы металлического компонента и его содержания в сплаве. Имеющиеся экспериментальные данные об электрохимическом поведении силицидов марганца [3] не охватывают весь возможный ряд силицидов и все возможные среды. Поэтому анализ коррозионно-электрохимического поведения сплавов марганца с кремнием различного состава представляет безусловный интерес. Кроме того, понимание термодинамических аспектов электрохимической устойчивости системы Mn – Si важно для дальнейшего изучения более сложных систем, например, системы Fe – Mn – Si.

Цель данного исследования – с точки зрения термодинамики рассмотреть вопрос электрохимической стойкости марганец-кремниевых сплавов в водных средах различного состава. В ходе решения этой задачи необходимо сначала разобраться с химическими и фазовыми равновесиями в системе Mn – Si и с механизмом окисления марганец-кремниевых сплавов кислородом воздуха.

Химические и фазовые равновесия в системе Mn – Si

Из анализа фазовой диаграммы состояния системы Mn – Si [4] следует, что при температуре 25˚C в системе существует семь интерметаллических фаз: $Mn_{11}Si_{19}$, MnSi, Mn_5Si_3, Mn_5Si_2, Mn_3Si и две фазы переменного состава – ν(Mn_9Si_2) и R(Mn_6Si). Кроме того, возможно образование твёрдого раствора кремния в α-марганце с кубической решёткой (α-фаза). Область нестехиометрии ν-фазы очень мала, поэтому при термодинамическом моделировании она будет считаться чистым силицидом Mn_9Si_2. По данным [5] R-фаза в точке, соответствующей равновесию с α-фазой имеет состав $Mn_{0,85}Si_{0,15}$.

В литературе [5 – 9] имеется множество справочных данных об энергиях Гиббса образования силицидов марганца (см. табл. 1). Эти данные часто противоречивы, а для некоторых соединений они и вовсе отсутствуют. Поэтому появляется необходимость в проведении термодинамической оценки недостающих величин. Такая оценка была проведена с использованием формул Миедемы [8] и Истмена [10], а также с помощью метода Горичева [11]. При этом интерполяционная формула Лагранжа, используемая в этом методе, была модифицирована авторами таким образом, чтобы в качестве исходных данных в ней можно было использовать энергии Гиббса образования нескольких (а не только двух, как в оригинале) соединений. Модифицированный вариант расчётной формулы выглядит следующим образом:

$$\Delta_f G^o_{298}(M_{a_x}A_{b_x}) = b_x \cdot \sum_{i=1}^{n}\left(\frac{\Delta_f G^o_{298}(M_{a_i}A_{b_i})}{b_i} \cdot \prod_{j\neq i}\frac{a_i\cdot(a_j\cdot b_x - a_x\cdot b_j)}{a_x\cdot(a_j\cdot b_i - a_i\cdot b_j)}\right) \quad (1).$$

Здесь n – количество энергий Гиббса образования бинарных соединений, принимаемых в качестве достоверных исходных данных; $M_{a_i}A_{b_i}$ – формулы этих соединений (M – металл, A – атом более электроотрицательного элемента, a_i и b_i – индексы при атомах M и A в соединении, соответственно); $M_{a_x}A_{b_x}$ – формула соединения, энергию Гиббса образования которого нужно оценить, a_x и b_x – индексы при атомах M и A в нём.

В качестве исходных данных для расчётов по формуле (1) были выбраны энергии Гиббса образования силицидов $Mn_{11}Si_{19}$, MnSi, Mn_5Si_3 и Mn_3Si из [7], как наиболее достоверные, по мнению авторов.

Результаты расчётов с использованием обоих методов также приведены в табл. 1. При этом результаты расчётов по формулам Миедемы и Истмена следует считать недостоверными, поскольку они слишком сильно отличаются от данных других источников.

Для термодинамического описания равновесия R-фазы с α-фазой рассмотрена реакция образования силицида $Mn_{0,85}Si_{0,15}$ из компонентов твёрдого раствора кремния в марганце:

$$0{,}85\,Mn(\alpha) + 0{,}15\,Si(\alpha) \rightarrow R\,(Mn_{0,85}Si_{0,15}) \quad (2),$$

которая может быть получена путём комбинирования следующих реакций:

$$0{,}85\,Mn(\alpha) + 0{,}15\,Si(\text{алмаз}) \rightarrow R\,(Mn_{0,85}Si_{0,15}) \quad (3),$$

$$Si(\text{алмаз}) \rightarrow Si(\alpha) \quad (4).$$

Table 1

The reference data on the standard Gibbs energies of formation of compounds from elements

The standard Gibbs energy of formation of the compound ($\Delta_f G^o_{298}$), $^J/_{mol}$									Reference
$Mn_{11}Si_{19}$	MnSi	Mn_5Si_3	Mn_5Si_2	Mn_3Si	Mn_9Si_2	$Mn_{0,85}Si_{0,15}$	$MnSiO_3$	Mn_2SiO_4	
–954878	–77932	–280518	–	–104397	–	–	–1240827	–1629818 –1671327	[6]
–892500	–76701	–278892	–	–107758	–	–	–1240552	–1632190	[7]
–	–59290	–207480	–	–72260	–	–	–	–	[8]
–	–92612	–343444	–	–141997	–	–	–1347490	–1779298	[9]
–998905 –965780 –947780 –935780 –758780 –344780 –997960 –979960 –967960 –790960 –376960	–78200 –76500 –68100 –93900 –74700 –62100 –78280 –95680 –69880 –76480 –63880	–284920 –273120 –257120 –230720 –317120 –243520 –280520 –264520 –238120 –324520 –250920	–	–103240 –104500 –107300 –134100 –144100 –104380 –107180 –133980 –143980	–222880	–16850	–	–	[5]
–281944	–48107	–158711	–74502	–23546	87218	6045	–	–	*
–892500	–76701	–278892	–207269	–107758	–230761	–17823	–	–	**
–892500	–76701	–343444	–265000	–133500	–240000	–17800	–1240552	–1632190	***

The standard Gibbs energy of formation of the compound ($\Delta_f G^o_{298}$), $^J/_{mol}$						Reference
MnO	Mn_3O_4	Mn_2O_3	MnO_2	Mn_2O_7	SiO_2	
–362770	–1281955	–879280	–465370	–262940	–851279	[6]
–363326	–1282885	–879865	–466662	–	–854243	[7]
–	–	–	–	–	–805067	[15]
–363326	–1282885	–879865	–466662	–262940	–805067	***

* – calculated according to Miedema [8] and Eastman [10] equations,

** – calculated according to Gorichev's method [11] using equation (1),

*** – data used in further calculations.

$\Delta_r G_T^o$ реакции (3) – это, фактически, величина, равная $\Delta_f G_T^o(Mn_{0,85}Si_{0,15})$. По данным [5] она выражается уравнением $\Delta_f G_T^o(Mn_{0,85}Si_{0,15}) = -16700 - 0{,}5 \cdot T, ^{Дж}/_{моль}$. Однако, с учётом того, что по выполненным расчётам $\Delta_f G_{298}^o(Mn_{0,85}Si_{0,15}) = -17823 ^{Дж}/_{моль}$, это выражение было скорректировано:

$$\Delta_r G_T^o(3) = \Delta_f G_T^o(Mn_{0,85}Si_{0,15}) = -17700 - 0{,}5 \cdot T, ^{Дж}/_{моль} \quad (5).$$

$\Delta_r G_T^o$ реакции (4) есть энергия Гиббса фазового перехода кремния из кристаллической решётки алмаза в кубическую кристаллическую решётку. В литературе не имеется данных об этой величине, поэтому был предположен линейный характер её зависимости от температуры:

$$\Delta_r G_T^o(4) = \Delta_{tr} G_T^o(Si(алмаз) \rightarrow Si(\alpha)) = a \cdot T + b, ^{Дж}/_{моль} \quad (6).$$

Энергия Гиббса реакции (2) может быть выражена через энергии Гиббса реакций (3) и (4):

$$\Delta G_T^o(2) = \Delta G_T^o(3) - 0{,}15\Delta G_T^o(4) = (-0{,}5 - 0{,}15 \cdot a) \cdot T + (-17700 - 0{,}15 \cdot b) \quad (7).$$

Если принять R-фазу как чистое вещество $Mn_{0,85}Si_{0,15}$ ($a_{R(Mn_{0,85}Si_{0,15})} = 1$), то, согласно уравнению изотермы химической реакции:

$$\Delta_r G_T^o(2) = -RT \cdot \ln K_p(2) = -RT \cdot \ln \frac{1}{a_{Mn(\alpha)}^{0,85} \cdot a_{Si(\alpha)}^{0,15}} = 0{,}85RT \cdot \ln a_{Mn(\alpha)} + 0{,}15RT \cdot \ln a_{Si(\alpha)} \quad (8).$$

Активности компонентов α-фазы рассчитываются в рамках однопараметрического приближения обобщённой теории "регулярных" растворов [12]:

$$RT \cdot \ln a_{Mn(\alpha)} = RT \cdot \ln x_{Mn(\alpha)} + x_{Si(\alpha)}^2 \cdot Q_{12}(T) \quad (9),$$

$$RT \cdot \ln a_{Si(\alpha)} = RT \cdot \ln x_{Si(\alpha)} + x_{Mn(\alpha)}^2 \cdot Q_{12}(T) \quad (10),$$

где x – мольная доля, $Q_{12}(T)$ – энергия смешения компонентов раствора. Авторами предположен линейный характер её зависимости от температуры:

$$Q_{12}(T) = c \cdot T + d, ^{Дж}/_{моль} \quad (11).$$

После подстановки в уравнение (8) выражений (7), (9), (10) и (11) и учёта того факта, что в твёрдом растворе $x_{Mn(\alpha)} = 1 - x_{Si(\alpha)}$, получается окончательное выражение:

$$0{,}15 \cdot a \cdot T + 0{,}15 \cdot b + c \cdot (0{,}85x_{Si(\alpha)}^2 + 0{,}15 \cdot (1 - x_{Si(\alpha)})^2) \cdot T +$$
$$+ d \cdot (+0{,}85x_{Si(\alpha)}^2 + 0{,}15 \cdot (1 - x_{Si(\alpha)})^2) +$$
$$+17700 + 0{,}5 \cdot T + 0{,}85RT \cdot \ln(1 - x_{Si(\alpha)}) + 0{,}15RT \cdot \ln x_{Si(\alpha)} = 0 \quad (12).$$

Задача сводится к определению неизвестных параметров *a*, *b*, *c*, *d* уравнения (12). Необходимые для расчёта значения мольных долей кремния в точках, отвечающих равновесию твёрдого раствора с R-фазой, сняты с диаграммы состояния системы Mn – Si [4] и представлены в табл. 2.

Table 2

The silicon mole fractions corresponding to the equilibrium of α-phase with R-phase at different temperatures [4]

T, K	473	523	573	623	673	723	773	823	873	903
$x_{Si(\alpha)}$	0,0485	0,0500	0,0510	0,0515	0,0530	0,0550	0,0565	0,0590	0,0610	0,0625

После подстановки данных табл. 2 в уравнение (12) получена система из 10 уравнений с 4 неизвестными (*a*, *b*, *c*, *d*). В литературе [8] имеются данные об энергиях Гиббса фазовых переходов кремния из решётки алмаза в решётки г. ц. к., о. ц. к. и г. п. у. В предположении, что при нормальной температуре энергия Гиббса фазового перехода кремния из решётки алмаза в

кубическую решётку должна быть сравнимой с этими величинами и составлять приблизительно 40 $^{кДж}/_{моль}$, в систему было введено дополнительное одиннадцатое уравнение: $298 \cdot a + b = 40000, ^{Дж}/_{моль}$.

С помощью метода наименьших квадратов [13] из полученной системы составлена система нормальных уравнений, содержащая 4 уравнения с 4 неизвестными. Данная система была решена методом Крамера [14]. Получены следующие результаты ($^{Дж}/_{моль}$): a = –174,66; b = 92049; c = 211,95; d = –219292. Таким образом, проведена термодинамическая оценка температурных зависимостей энергии смешения компонентов твёрдого раствора Mn – Si и энергии Гиббса фазового перехода кремния из кристаллической решётки алмаза в кубическую решётку:

$$\Delta_{tr}G_T^o(\text{Si(алмаз)} \rightarrow \text{Si}(\alpha)) = 92048 - 174{,}66 \cdot T, ^{Дж}/_{моль} \quad (13),$$

$$Q_{12}(\text{Mn–Si}) = -219292 + 211{,}95 \cdot T, ^{Дж}/_{моль} \quad (14).$$

Для того, чтобы определить мольную долю кремния в твёрдом растворе, отвечающую равновесию α-фазы с R-фазой, при комнатной температуре, уравнение (12) было решено относительно $x_{Si(\alpha)}$ при известных значениях параметров a, b, c, d и условии T = 298 K. Найденный корень уравнения $x_{Si(\alpha)} = 0{,}0456$. Активности компонентов твёрдого раствора в этой точке рассчитаны по формулам (9) и (10): $a_{Mn(\alpha)} = 0{,}8321, a_{Si(\alpha)} = 3{,}835 \cdot 10^{-28}$. Таким образом, можно прийти к заключению, что в области низких температур (вплоть до комнатной) кремний практически не растворяется в марганце.

Химическая устойчивость

В соответствии с видом диаграммы состояния системы Mn – O [4] возможно существование следующих оксидов марганца: MnO, Mn_3O_4, Mn_2O_3, MnO_2 и Mn_2O_7. Кремний образует только один оксид SiO_2. Также марганец и кремний могут образовывать смешанные оксиды (силикаты марганца) $MnO \cdot SiO_2 (MnSiO_3)$ и $2MnO \cdot SiO_2 (Mn_2SiO_4)$. Стандартные энергии Гиббса образования вышеперечисленных веществ, имеющиеся в различных источниках [6, 7, 9, 15], представлены в табл. 1. Для оксидов и силикатов марганца авторы считают наиболее достоверными данные из базы [7], для кремнезёма – величину из справочника [15], поскольку именно это значение $\Delta_f G_{298}^o$ согласовано с экспериментально измеренным стандартным потенциалом кремниевого электрода ($SiO_2 + 4H^+ + 4e^- = \text{Si(алмаз)} + 2H_2O; \varphi_{298}^o = -0{,}857\,\text{В}$).

Для того, чтобы построить фазовую диаграмму Mn – Si – O, необходимо разобраться с механизмом окисления марганец-кремниевых сплавов и подобрать последовательность равновесий, реализуемых в системе, таким образом, чтобы для каждой следующей реакции равновесное давление кислорода в газовой фазе было больше, чем для предыдущей. Было обнаружено, что полученные из [7] и рассчитанные термодинамические характеристики силицидов марганца не позволяют сделать это корректно. Поэтому было принято решение произвести корректировку энергий Гиббса образования некоторых соединений в пределах доверительных интервалов их возможных справочных значений. Окончательно откорректированные и использованные во всех дальнейших расчётах данные представлены в табл. 1 в строке ***. Фазовая диаграмма Mn – Si – O при 25˚C изображена на рис. 1. Рассчитанные характеристики трёхфазных равновесий системы представлены в табл. 3.

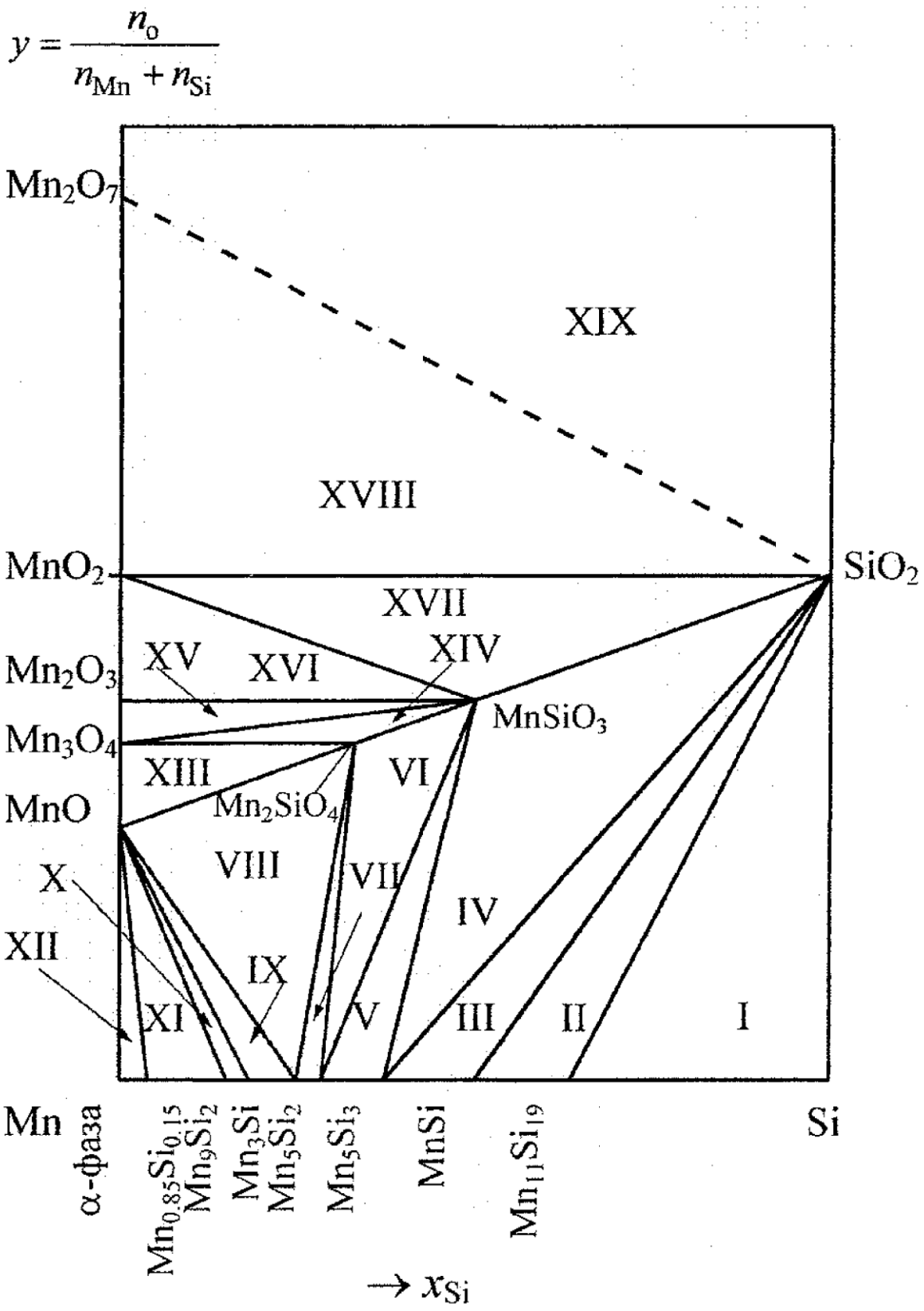

Fig. 1. The Mn – Si – O system state diagram at 25˚C

Электрохимическая устойчивость

Основные химические и электрохимические равновесия в системе Mn – Si – H_2O при 25˚C и 1 атм. (воздух) представлены в табл. 4. Для расчёта термодинамических характеристик равновесий с участием ионов в растворе использована информация о стандартных электродных потенциалах из справочника [15].

Диаграмма потенциал – pH системы Mn – Si – H_2O при 25˚C, 1 атм. (воздух) и активностях ионов в растворе $a_i = 1$ моль/л изображена на рис. 2. На рис. 3 в увеличенном масштабе изображены сечения этой диаграммы в областях существования силицидов марганца.

На диаграмме электрохимического равновесия системы Mn – Si – H_2O (рис. 2, 3) можно выделить 42 области термодинамической устойчивости различных фаз: I – α-фаза (Mn) + R-фаза ($Mn_{0,85}Si_{0,15}$) + ν-фаза (Mn_9Si_2) + Mn_3Si + Mn_5Si_2 + Mn_5Si_3 + MnSi + $Mn_{11}Si_{19}$ + Si; II – Mn^{2+} + $Mn_{0,85}Si_{0,15}$ + Mn_9Si_2 + Mn_3Si + Mn_5Si_2 + Mn_5Si_3 + MnSi + $Mn_{11}Si_{19}$ + Si; III – Mn^{2+} + $Mn_{0,85}Si_{0,15}$ + Mn_9Si_2 + Mn_3Si + Mn_5Si_2 + Mn_5Si_3 + MnSi + $Mn_{11}Si_{19}$ + SiO_2; IV – Mn^{2+} + $Mn_{0,85}Si_{0,15}$ + Mn_9Si_2 + Mn_3Si + Mn_5Si_2 + Mn_5Si_3 + MnSi + SiO_2; V – Mn^{2+} + $Mn_{0,85}Si_{0,15}$ + Mn_9Si_2 + Mn_3Si + Mn_5Si_2 + Mn_5Si_3 + SiO_2; VI – Mn^{2+} + $Mn_{0,85}Si_{0,15}$ + Mn_9Si_2 + Mn_3Si + Mn_5Si_2 + SiO_2; VII – Mn^{2+} + $Mn_{0,85}Si_{0,15}$ + Mn_9Si_2 + Mn_3Si + SiO_2; VIII – Mn^{2+} + $Mn_{0,85}Si_{0,15}$ + Mn_9Si_2 + SiO_2; IX – Mn^{2+} + $Mn_{0,85}Si_{0,15}$ + SiO_2; X – Mn^{3+} + $Mn_{0,85}Si_{0,15}$ + SiO_2; XI – Mn^{2+} + $Mn_{0,85}Si_{0,15}$ + Mn_9Si_2 + Mn_3Si + Mn_5Si_2 + Mn_5Si_3 + $MnSiO_3$; XII – Mn^{2+} + $Mn_{0,85}Si_{0,15}$ + Mn_9Si_2 + Mn_3Si + Mn_5Si_2 + $MnSiO_3$; XIII – Mn^{2+} + $Mn_{0,85}Si_{0,15}$ + Mn_9Si_2 + Mn_3Si + $MnSiO_3$; XIV – Mn^{2+} + $Mn_{0,85}Si_{0,15}$ + Mn_9Si_2 + $MnSiO_3$; XV – Mn^{2+} + $Mn_{0,85}Si_{0,15}$ + $MnSiO_3$; XVI – Mn^{2+} + $Mn_{0,85}Si_{0,15}$ + Mn_9Si_2 + Mn_3Si + Mn_5Si_2 + Mn_2SiO_4; XVII – Mn^{2+} + $Mn_{0,85}Si_{0,15}$ + Mn_9Si_2 + Mn_3Si + Mn_2SiO_4; XVIII – Mn^{2+} + $Mn_{0,85}Si_{0,15}$ + Mn_9Si_2 + Mn_2SiO_4; XIX – Mn^{2+} + $Mn_{0,85}Si_{0,15}$ + Mn_2SiO_4; XX – α + $Mn_{0,85}Si_{0,15}$ + Mn_9Si_2 + Mn_3Si + Mn_5Si_2 + Mn_5Si_3 + MnSi + $Mn_{11}Si_{19}$ + SiO_2; XXI – α + $Mn_{0,85}Si_{0,15}$ + Mn_9Si_2 + Mn_3Si + Mn_5Si_2 + Mn_5Si_3 + MnSi + $Mn_{11}Si_{19}$ + SiO_3^{2-}; XXII – α + $Mn_{0,85}Si_{0,15}$ + Mn_9Si_2 + Mn_3Si + Mn_5Si_2 + Mn_5Si_3 + MnSi + SiO_2; XXIII – α + $Mn_{0,85}Si_{0,15}$ + Mn_9Si_2 + Mn_3Si + Mn_5Si_2 + Mn_5Si_3 + MnSi + SiO_3^{2-}; XXIV – α + $Mn_{0,85}Si_{0,15}$ + Mn_9Si_2 + Mn_3Si + Mn_5Si_2 + Mn_5Si_3 + SiO_2; XXV – α + $Mn_{0,85}Si_{0,15}$ + Mn_9Si_2 + Mn_3Si + Mn_5Si_2 + Mn_5Si_3 + SiO_3^{2-}; XXVI – α + $Mn_{0,85}Si_{0,15}$ + Mn_9Si_2 + Mn_3Si + Mn_5Si_2 + Mn_5Si_3 + $MnSiO_3$; XXVII – α + $Mn_{0,85}Si_{0,15}$ + Mn_9Si_2 + Mn_3Si + Mn_5Si_2 + $MnSiO_3$; XXVIII – α + $Mn_{0,85}Si_{0,15}$ + Mn_9Si_2 + Mn_3Si + Mn_5Si_2 + Mn_2SiO_4; XXIX – α + $Mn_{0,85}Si_{0,15}$ + Mn_9Si_2 + Mn_3Si + Mn_2SiO_4; XXX – α + $Mn_{0,85}Si_{0,15}$ + Mn_9Si_2 + Mn_3Si + Mn_2SiO_4 + MnO; XXXI – α + $Mn_{0,85}Si_{0,15}$ + Mn_9Si_2 + Mn_2SiO_4 + MnO; XXXII – α + $Mn_{0,85}Si_{0,15}$ + Mn_2SiO_4 + MnO; XXXIII – $Mn_{0,85}Si_{0,15}$ + Mn_2SiO_4 + MnO; XXXIV – $Mn_{0,85}Si_{0,15}$ + Mn_2SiO_4 + Mn_3O_4; XXXV – $Mn_{0,85}Si_{0,15}$ + $MnSiO_3$ + Mn_3O_4; XXXVI – $Mn_{0,85}Si_{0,15}$ + $MnSiO_3$ + Mn_2O_3; XXXVII – $Mn_{0,85}Si_{0,15}$ + $MnSiO_3$ + MnO_2; XXXVIII – $Mn_{0,85}Si_{0,15}$ + MnO_2 + SiO_2; XXXIX – $Mn_{0,85}Si_{0,15}$ + MnO_2 + SiO_3^{2-}; XL – $Mn_{0,85}Si_{0,15}$ + SiO_2 + MnO_4^-; XLI – $Mn_{0,85}Si_{0,15}$ + MnO_4^{2-}, SiO_3^{2-}; XLII – $Mn_{0,85}Si_{0,15}$ + MnO_4^-, SiO_3^{2-}.

Обсуждение результатов

Анализируя фазовую диаграмму Mn – Si – O, можно прийти к следующим выводам: окисление марганец-кремниевых сплавов начинается при давлениях кислорода в газовой фазе выше $7{,}70 \cdot 10^{-142}$ атм. Поскольку для окисления MnO_2 до Mn_2O_7 необходимо давление кислорода, равное $2{,}18 \cdot 10^{78}$атм., то окисление на воздухе ($P_{O_2} = 0{,}21$ атм.) должно завершиться образованием оксидов MnO_2 и SiO_2. Однако, поскольку в реальных условиях термодинамическое

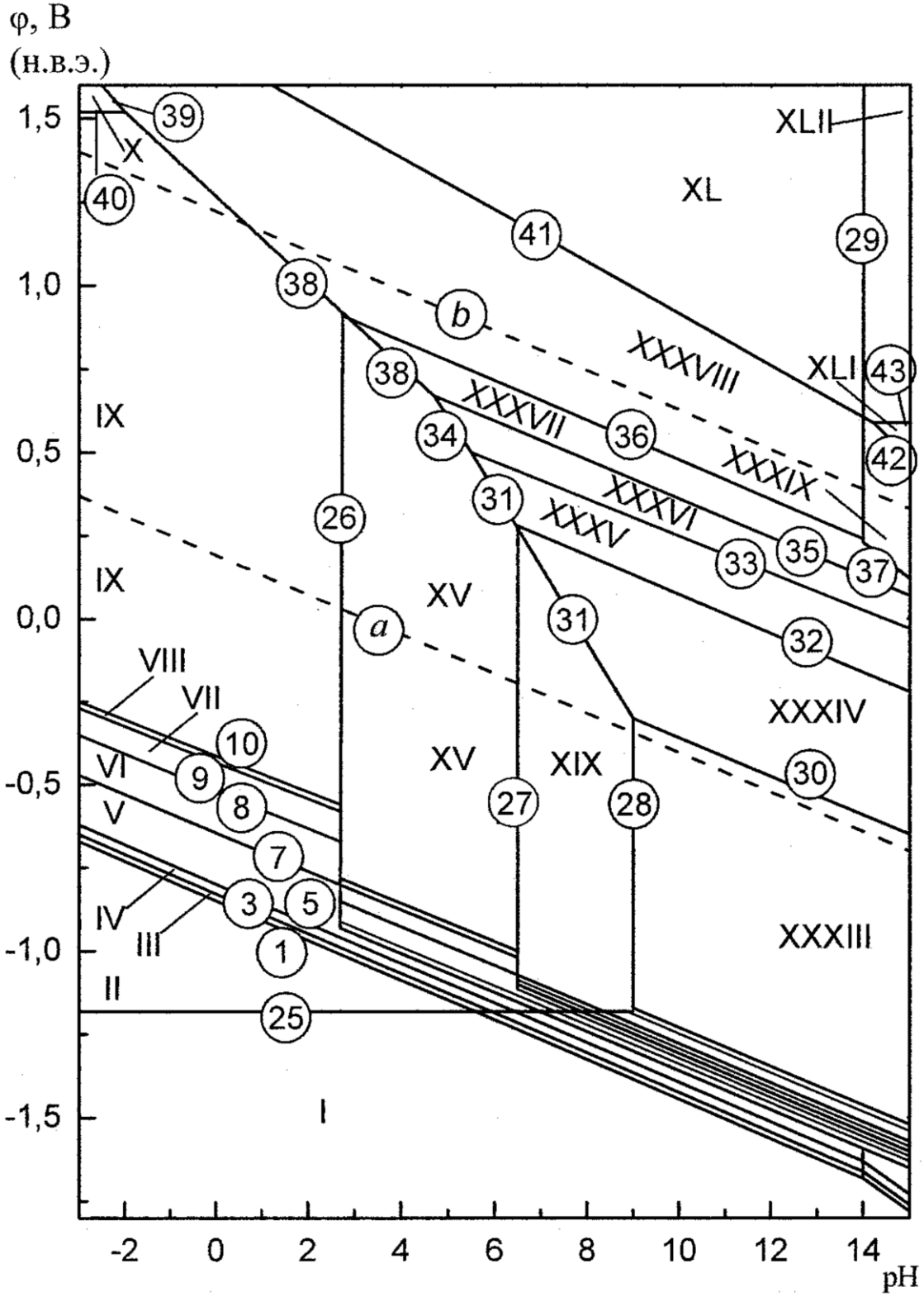

Fig. 2. The potential – pH diagram of the Mn – Si – H_2O system at 25˚C, 1 bar (air) and $a_i = 1$ моль/л

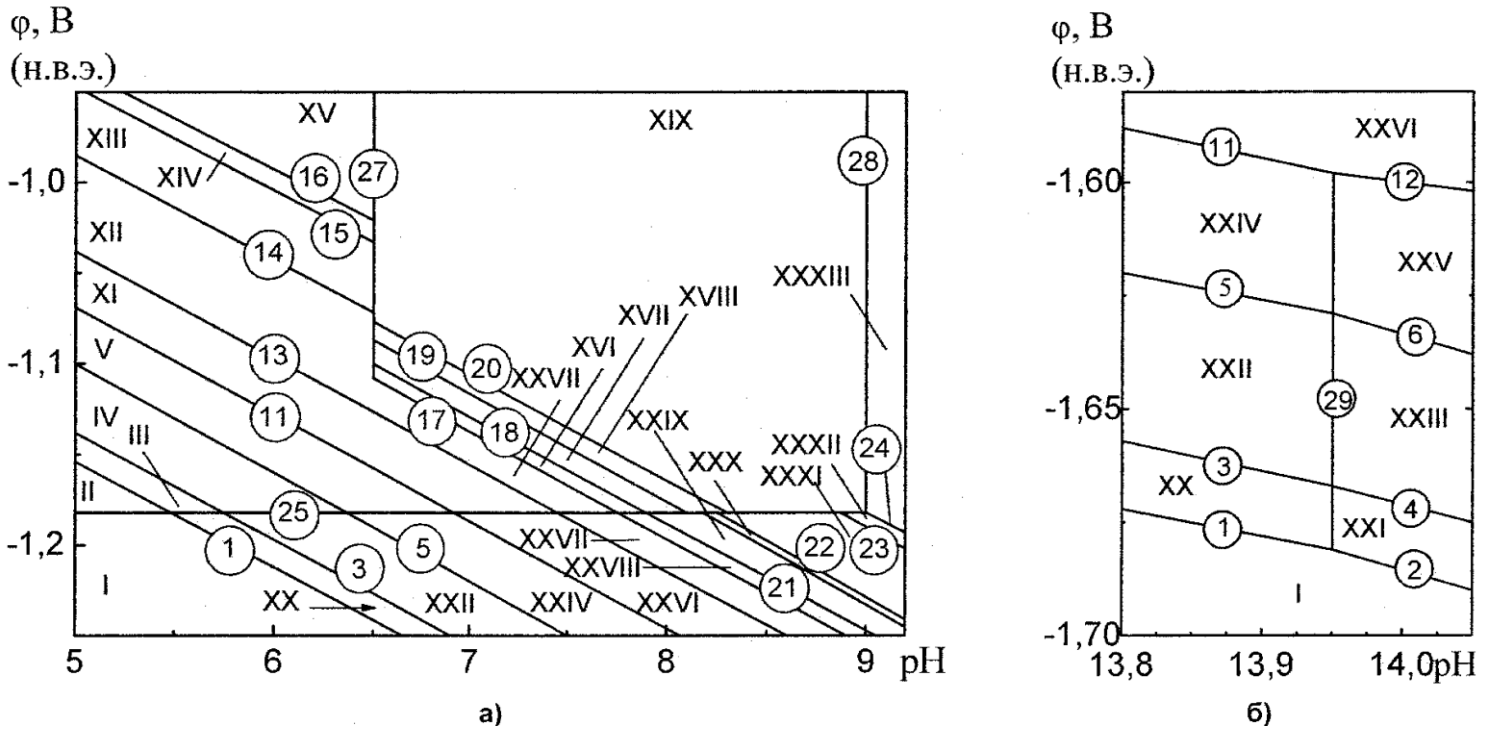

Fig. 3. The cross-section of the potential – pH diagram of the Mn – Si – H_2O system at 25°C, 1 bar (air) and $a_i = 1$ моль/л in the domains of existence of: a) manganese silicides; b) ions SiO_3^{2-}.

Table 3

The characteristics of the invariant states in the Mn – Si – O system at 25°C

No of domain	Equilibrium	Reaction equation	P_{O_2}, bar.	Equilibrium composition of phases
I	Si(алмаз) – $Mn_{11}Si_{19}$ – SiO_2	Si(алмаз) + O_2 = SiO_2	$7{,}70 \cdot 10^{-142}$	$x_{Si} = 1; x_{Mn_{11}Si_{19}} = 1; x_{SiO_2} = 1$
II	$Mn_{11}Si_{19}$ – MnSi – SiO_2	$Mn_{11}Si_{19}$ + $8O_2$ = 11MnSi + $8SiO_2$	$9{,}02 \cdot 10^{-141}$	$x_{Mn_{11}Si_{19}} = 1; x_{MnSi} = 1; x_{SiO_2} = 1$
III	MnSi – Mn_5Si_3 – SiO_2	5MnSi + $2O_2$ = Mn_5Si_3 + $2SiO_2$	$2{,}50 \cdot 10^{-138}$	$x_{MnSi} = 1; x_{Mn_5Si_3} = 1; x_{SiO_2} = 1$
IV	Mn5Si3 – $MnSiO_3$ – SiO_2	$2Mn_5Si_3$ + $4SiO_2$ + $11O_2$ = $10MnSiO_3$	$3{,}81 \cdot 10^{-136}$	$x_{Mn_5Si_3} = 1; x_{MnSiO_3} = 1; x_{SiO_2} = 1$
V	Mn_5Si_3 – Mn_5Si_2 – $MnSiO_3$	$6Mn_5Si_3$ + $15O_2$ = $4Mn_5Si_2$ + $10MnSiO_3$	$5{,}36 \cdot 10^{-134}$	$x_{Mn_5Si_3} = 1; x_{Mn_5Si_2} = 1; x_{MnSiO_3} = 1$
VI	Mn_5Si_2 – $MnSiO_3$ – Mn_2SiO_4	$2Mn_5Si_2$ + $2MnSiO_3$ + $9O_2$ = $6Mn_2SiO_4$	$8{,}22 \cdot 10^{-133}$	$x_{Mn_5Si_2} = 1; x_{MnSiO_3} = 1; x_{Mn_2SiO_4} = 1$
VII	Mn_5Si_2 – Mn_3Si – Mn_2SiO_4	Mn_5Si_2 + $2O_2$ = Mn_3Si + Mn_2SiO_4	$3{,}01 \cdot 10^{-132}$	$x_{Mn_5Si_2} = 1; x_{Mn_3Si} = 1; x_{Mn_2SiO_4} = 1$
VIII	Mn_3Si – Mn_2SiO_4 – MnO	$2Mn_3Si$ + $5O_2$ = $2Mn_2SiO_4$ + 2MnO	$2{,}81 \cdot 10^{-131}$	$x_{Mn_3Si} = 1; x_{Mn_2SiO_4} = 1; x_{MnO} = 1$
IX	Mn_9Si_2 – Mn_3Si – MnO	$2Mn_9Si_2$ + $3O_2$ = $4Mn_3Si$ + 6MnO	$2{,}99 \cdot 10^{-131}$	$x_{Mn_9Si_2} = 1; x_{Mn_3Si} = 1; x_{MnO} = 1$
X	$Mn_{0,85}Si_{0,15}$ – Mn_9Si_2 – MnO	$80Mn_{0,85}Si_{0,15}$ + $7O_2$ = $6Mn_9Si_2$ + 4MnO	$1{,}70 \cdot 10^{-128}$	$x_{Mn_{0,85}Si_{0,15}} = 1; x_{Mn_9Si_2} = 1; x_{MnO} = 1$
XI	α – $Mn_{0,85}Si_{0,15}$ – MnO	2Mn(α) + O_2 = 2MnO	$3{,}52 \cdot 10^{-128}$	$x_{Mn(\alpha)} = 0{,}9544;$ $x_{Mn_{0,85}Si_{0,15}} = 1; x_{MnO} = 1$
XII	α – MnO			
XIII	MnO – Mn_3O_4 – Mn_2SiO_4	6MnO + O_2 = $2Mn_3O_4$	$2{,}36 \cdot 10^{-68}$	$x_{MnO} = 1; x_{Mn_3O_4} = 1; x_{Mn_2SiO_4} = 1$
XIV	Mn_3O_4 – Mn_2SiO_4 – $MnSiO_3$	$6Mn_2SiO_4$ + O_2 = $6MnSiO_3$ + $2Mn_3O_4$	$1{,}41 \cdot 10^{-38}$	$x_{Mn_3O_4} = 1; x_{MnSiO_3} = 1; x_{Mn_2SiO_4} = 1$
XV	Mn_3O_4 – Mn_2O_3 – $MnSiO_3$	$4Mn_3O_4$ + O_2 = $6Mn_2O_3$	$1{,}32 \cdot 10^{-26}$	$x_{Mn_3O_4} = 1; x_{Mn_2O_3} = 1; x_{MnSiO_3} = 1$

Ending of Table 3

No of domain	Equilibrium	Reaction equation	P_{O_2}, bar.	Equilibrium composition of phases
XVI	$Mn_2O_3 - MnO_2 - MnSiO_3$	$2Mn_2O_3 + O_2 = 4MnO_2$	$1{,}82 \cdot 10^{-19}$	$x_{Mn_2O_3} = 1; x_{MnO_2} = 1; x_{MnSiO_3} = 1$
XVII	$MnO_2 - MnSiO_3 - SiO_2$	$2MnSiO_3 + O_2 = 2MnO_2 + 2SiO_2$	$1{,}18 \cdot 10^{-11}$	$x_{MnO_2} = 1; x_{MnSiO_3} = 1; x_{SiO_2} = 1$
XVIII	$MnO_2 - Mn_2O_7 - SiO_2$	$4MnO_2 + 3O_2 = 2Mn_2O_7$	$2{,}18 \cdot 10^{78}$	$x_{MnO_2} = 1; x_{Mn_2O_7} = 1; x_{SiO_2} = 1$
XIX	$Mn_2O_7 - SiO_2 - \{O_2\}$	–	–	–

Table 4

Basic chemical and electrochemical equilibria in the Mn – Si – H_2O system at 25°C and 1 bar (air)

No of line	Electrode reaction	Equilibrium potential, V (s. h. e.) or pH of the solution
a	$2H^+ + 2e^- = H_2; P_{H_2} \approx 5 \cdot 10^{-7}$ атм.	$0{,}186 - 0{,}0591pH$
b	$O_2 + 4H^+ + 4e^- = 2H_2O; P_{O_2} \approx 0{,}21$ атм.	$1{,}219 - 0{,}0591pH$
1	$SiO_2 + 4H^+ + 4e^- = Si + 2H_2O$	$-0{,}857 - 0{,}0591pH$
2	$SiO_3^{2-} + 6H^+ + 4e^- = Si + 3H_2O$	$-0{,}444 - 0{,}08865pH + 0{,}0148 \lg a_{SiO_3^{2-}}$
3	$8SiO_2 + 11MnSi + 32H^+ + 32e^- = Mn_{11}Si_{19} + 16H_2O$	$-0{,}841 - 0{,}0591pH$
4	$8SiO_3^{2-} + 11MnSi + 48H^+ + 32e^- = Mn_{11}Si_{19} + 24H_2O$	$-0{,}429 - 0{,}08865pH + 0{,}0148 \lg a_{SiO_3^{2-}}$
5	$2SiO_2 + Mn_5Si_3 + 8H^+ + 8e^- = 5MnSi + 4H_2O$	$-0{,}805 - 0{,}0591pH$
6	$2SiO_3^{2-} + Mn_5Si_3 + 12H^+ + 8e^- = 5MnSi + 6H_2O$	$-0{,}392 - 0{,}08865pH + 0{,}0148 \lg a_{SiO_3^{2-}}$
7	$SiO_2 + Mn_5Si_2 + 4H^+ + 4e^- = Mn_5Si_3 + 2H_2O$	$-0{,}653 - 0{,}0591pH$
8	$SiO_2 + 5Mn_3Si + 4H^+ + 4e^- = 3Mn_5Si_2 + 2H_2O$	$-0{,}526 - 0{,}0591pH$
9	$SiO_2 + Mn_9Si_2 + 4H^+ + 4e^- = 3Mn_3Si + 2H_2O$	$-0{,}441 - 0{,}0591pH$

Continuation of Table 4

No of line	Electrode reaction	Equilibrium potential, V (s. h. e.) or pH of the solution
10	$7SiO_2 + 180Mn_{0,85}Si_{0,15} + 28H^+ + 28e^- = 17Mn_9Si_2 + 14H_2O$	$-0,426 - 0,0591pH$
11	$5MnSiO_3 + 22H^+ + 22e^- = Mn_5Si_3 + 2SiO_2 + 11H_2O$	$-0,772 - 0,0591pH$
12	$5MnSiO_3 + 18H^+ + 22e^- = Mn_5Si_3 + 2SiO_3^{2-} + 9H_2O$	$-0,922 - 0,04835pH - 0,00537 \lg a_{SiO_3^{2-}}$
13	$5MnSiO_3 + 2Mn_5Si_2 + 30H^+ + 30e^- = 3Mn_5Si_3 + 15H_2O$	$-0,741 - 0,0591pH$
14	$MnSiO_3 + 3Mn_3Si + 6H^+ + 6e^- = 2Mn_5Si_2 + 3H_2O$	$-0,690 - 0,0591pH$
15	$3MnSiO_3 + 2Mn_9Si_2 + 18H^+ + 18e^- = 7Mn_3Si + 9H_2O$	$-0,652 - 0,0591pH$
16	$MnSiO_3 + 20Mn_{0,85}Si_{0,15} + 6H^+ + 6e^- = 2Mn_9Si_2 + 3H_2O$	$-0,644 - 0,0591pH$
17	$3Mn_2SiO_4 + 18H^+ + 18e^- = Mn_5Si_2 + MnSiO_3 + 9H_2O$	$-0,723 - 0,0591pH$
18	$Mn_2SiO_4 + Mn_3Si + 8H^+ + 8e^- = Mn_5Si_2 + 4H_2O$	$-0,715 - 0,0591pH$
19	$3Mn_2SiO_4 + Mn_9Si_2 + 24H^+ + 24e^- = 5Mn_3Si + 12H_2O$	$-0,701 - 0,0591pH$
20	$7Mn_2SiO_4 + 100Mn_{0,85}Si_{0,15} + 56H^+ + 56e^- = 11Mn_9Si_2 + 28H_2O$	$-0,696 - 0,0591pH$
21	$Mn_2SiO_4 + MnO + 10H^+ + 10e^- = Mn_3Si + 5H_2O$	$-0,7004 - 0,0591pH$
22	$3MnO + 2Mn_3Si + 6H^+ + 6e^- = Mn_9Si_2 + 3H_2O$	$-0,7000 - 0,0591pH$
23	$7MnO + 3Mn_9Si_2 + 14H^+ + 14e^- = 40Mn_{0,85}Si_{0,15} + 7H_2O$	$-0,659 - 0,0591pH$
24	$MnO + 2H^+ + 2e^- = Mn(\alpha) + H_2O; a_{Mn(\alpha)} = 0,8321$	$-0,651 - 0,0591pH$
25	$Mn^{2+} + 2e^- = Mn(\alpha); a_{Mn(\alpha)} = 0,8321$	$-1,183 + 0,02955 \lg a_{Mn^{2+}}$
26	$MnSiO_3 + 2H^+ = Mn^{2+} + SiO_2 + H_2O$	$pH = 2,66 - 0,5 \lg a_{Mn^{2+}}$
27	$Mn_2SiO_4 + 2H^+ = Mn^{2+} + MnSiO_3 + H_2O$	$pH = 6,51 - 0,5 \lg a_{Mn^{2+}}$
28	$MnO + 2H^+ = Mn^{2+} + H_2O$	$pH = 8,99 - 0,5 \lg a_{Mn^{2+}}$
29	$SiO_3^{2-} + 2H^+ = SiO_2 + H_2O$	$pH = 13,94 + 0,5 \lg a_{SiO_3^{2-}}$
30	$Mn_3O_4 + 2H^+ + 2e^- = 3MnO + H_2O$	$0,230 - 0,0591pH$

Ending of Table 4

No of line	Electrode reaction	Equilibrium potential, V (s. h. e.) or pH of the solution
31	$Mn_3O_4 + 8H^+ + 2e^- = 3Mn^{2+} + 4H_2O$	$1{,}825 - 0{,}2364\,pH - 0{,}08865 \lg a_{Mn^{2+}}$
32	$Mn_3O_4 + 3MnSiO_3 + 2H^+ + 2e^- = 3Mn_2SiO_4 + H_2O$	$0{,}670 - 0{,}0591\,pH$
33	$3Mn_2O_3 + 2H^+ + 2e^- = 2Mn_3O_4 + H_2O$	$0{,}847 - 0{,}0591\,pH$
34	$Mn_2O_3 + 6H^+ + 2e^- = 2Mn^{2+} + 3H_2O$	$1{,}499 - 0{,}1773\,pH - 0{,}0591 \lg a_{Mn^{2+}}$
35	$2MnO_2 + 2H^+ + 2e^- = Mn_2O_3 + H_2O$	$0{,}952 - 0{,}0591\,pH$
36	$MnO_2 + SiO_2 + 2H^+ + 2e^- = MnSiO_3 + H_2O$	$1{,}068 - 0{,}0591\,pH$
37	$MnO_2 + SiO_3^{2-} + 4H^+ + 2e^- = MnSiO_3 + 2H_2O$	$1{,}892 - 0{,}1182\,pH + 0{,}02955 \lg a_{SiO_3^{2-}}$
38	$MnO_2 + 4H^+ + 2e^- = Mn^{2+} + 2H_2O$	$1{,}226 - 0{,}1182\,pH - 0{,}02955 \lg a_{Mn^{2+}}$
39	$MnO_2 + 4H^+ + e^- = Mn^{3+} + 2H_2O$	$0{,}941 - 0{,}2364\,pH - 0{,}02955 \lg a_{Mn^{3+}}$
40	$Mn^{3+} + e^- = Mn^{2+}$	$1{,}510 + 0{,}0591 \lg \dfrac{a_{Mn^{3+}}}{a_{Mn^{2+}}}$
41	$MnO_4^- + 4H^+ + 3e^- = MnO_2 + 2H_2O$	$1{,}695 - 0{,}0788\,pH + 0{,}0197 \lg a_{MnO_4^-}$
42	$MnO_4^{2-} + 4H^+ + 2e^- = MnO_2 + 2H_2O$	$2{,}249 - 0{,}1182\,pH + 0{,}02955 \lg a_{MnO_4^{2-}}$
43	$MnO_4^- + e^- = MnO_4^{2-}$	$0{,}588 + 0{,}0591 \lg \dfrac{a_{MnO_4^-}}{a_{MnO_4^{2-}}}$

равновесие недостижимо, оксидная плёнка на сплавах может содержать и другие оксиды, а также силикаты марганца. Её конкретный состав будет очень сильно зависеть от содержания кремния в сплаве. Так, если кремния в сплаве не более 25 ат. % (его недостаточно для образования силицида Mn_3Si и силицидов с более высоким содержанием кремния), то наиболее вероятными продуктами окисления будут оксиды марганца и Mn_2SiO_4. При увеличении содержания кремния в сплаве возможно образование в составе оксидной плёнки $MnSiO_3$ и SiO_2.

Коррозионно-электрохимическое поведение марганец-кремниевых сплавов будет определяться кислотностью среды и установившимся в ней значением стационарного потенциала. В кислых средах будет наблюдаться селективная коррозия марганца, и переход его в раствор в виде катионов Mn^{2+} (области II – IX на рис. 2, 3), а кремниевая составляющая сплава будет окисляться до SiO_2 (в работе [3] это подтверждено экспериментально). В нейтральных и щелочных средах, в зависимости от содержания кремния в системе и конкретных условий, окисление может заканчиваться образованием силикатов Mn_2SiO_4 или $MnSiO_3$. Защитная плёнка из этих силикатов является более стойкой в химическом и электрохимическом плане, нежели SiO_2, поскольку она не окисляется до SiO_3^{2-}.

Наличие множества различных справочных данных и необходимость оценивания и корректировки некоторых термодинамических величин не позволяют говорить о том, что предложенная авторами работы картина окисления марганец-кремниевых сплавов является окончательной и безусловно верной. Теория не даёт однозначного ответа по поводу некоторых конкретных равновесий, особенно в областях существования низших силицидов марганца. Несмотря на это, общие закономерности коррозионно-электрохимического поведения системы Mn – Si выявлены, показано, что химическая и электрохимическая устойчивость марганец-кремниевых сплавов выше, чем таковая для чистых марганца и кремния, и что конкретный состав продуктов окисления определяется содержанием обоих компонентов в сплаве.

Выводы

1. С точки зрения термодинамики рассмотрены химические и фазовые равновесия в системе Mn – Si при 25˚C. Проведено согласование и прогнозирование термодинамических свойств компонентов системы, проведена оценка предельной растворимости кремния в марганце при комнатной температуре.
2. Построена фазовая диаграмма Mn – Si – O при 25˚C. Рассчитаны характеристики трёхфазных равновесий системы, показано, что химическая устойчивость сплавов системы Mn – Si определяется содержанием в сплаве обоих компонентов.
3. Построена диаграмма потенциал – pH системы Mn – Si – H_2O при 25˚C, 1 атм. (воздух) и $a_i = 1$ моль/л. Показано, что в кислых средах первичная пассивационная плёнка на сплавах Mn – Si представляет собой чистый кремнезём. В нейтральных и щелочных средах она в зависимости от содержания кремния в сплавах может состоять как из чистых оксидов марганца и кремния, так и из силикатов марганца.

Литература

1. Силикомарганец: Большая Советская энциклопедия [Электронный ресурс]. – URL:<http://slovari.yandex.ru/dict/bse/article/00070/96500.htm> (дата обращения – 27. VIII. 2010 г.)
2. Гельд, П. В. Силициды переходных металлов четвёртого периода [Текст] / П. В. Гельд, Ф. А. Сидоренко. – М.: Металлургия, 1971. – 582 с.

3. Шеин, А. Б. Электрохимическое поведение силицидов марганца в растворе серной кислоты [Текст] / А. Б. Шеин, Е. Н. Зубова // Защита металлов. – 2005. – Т. 41. – № 3. – С. 258 – 266.
4. Диаграммы состояния двойных металлических систем: справочник [Текст] / под ред. Н. П. Лякишева. – М.: Машиностроение, 2000. – Т. 3. – Кн. 1. – С. 361, 383, 698.
5. Физическая химия неорганических материалов. В 3 т. Т. 1. Термодинамика интерметаллидов и фазовые равновесия в металлических системах [Текст] / В. Н. Ерёменко [et al.]. – Киев: Наукова думка, 1988. – 365 с.
6. Рузинов, Л. П. Равновесные превращения металлургических реакций [Текст] / Л. П. Рузинов, Б. С. Гуляницкий. – М.: Металлургия, 1975. – 416 с..
7. Термические константы веществ: база данных [Электронный ресурс] / руководители проекта В. С. Иориш, В. С. Юнгман. – URL: <http://www.chem.msu.su/cgi-bin/tkv.pl?show=welcome.html> (дата обращения – 27. VIII. 2010 г.)
8. Термодинамика сплавов железа [Текст] / Б. М. Могутнов, И. А. Томилин, Л. А. Шварцман. – М.: Металлургия, 1984. – 208 с.
9. Температурные зависимости приведённой энергии Гиббса некоторых неорганических веществ: альтернативный банк данных ASTRA. OWN [Текст] / Г. К. Моисеев, Н. А. Ватолин, Л. А. Маршук, Н. И. Ильиных. – Екатеринбург: УрОРАН, 1997. – 230 с.
10. Тюрин, А. Г. Термодинамический анализ образования фаз в процессах электролитического осаждения титана из водных растворов [Текст] // Электрохимия. – 1990. – Вып. 26. – № 12. – С. 1599 – 1605.
11. Жук, Н. П. Курс теории коррозии и защиты металлов: учеб. пособие для вузов [Текст]. – 2-е изд., стереотип. (перепеч. с изд. 1976 г.). – М: ООО ТИД “Альянс”, 2006. – 472 с.
12. Тюрин, А. Г. Термодинамика химической и электрохимической устойчивости сплавов: учеб. пособие: Ч. 1. Общие принципы. Высокотемпературное окисление [Текст]. – Челябинск: Изд-во Челяб. гос. ун-та, 2004. – 86 с.
13. Метод наименьших квадратов: энциклопедический проект «Наука» [Электронный ресурс]. – URL:< http://ru.science.wikia.com/wiki/Метод_наименьших_квадратов> (дата обращения – 27. VIII. 2010 г.)
14. Метод Крамера: математическая энциклопедия [Электронный ресурс]. – URL:<http://dic.academic.ru/dic.nsf/ruwiki/149541> (дата обращения – 27. VIII. 2010 г.)
15. Справочник по электрохимии [Текст] / под ред. А. М. Сухотина. – Л.: Химия, 1981. – 488 с.

10. Mn – Ge system
10.1. Manganese germanides

Manganese germanides have some unusual magnetic and thermoelectric properties [Aoyama et al., 2005; Cho et al., 2002; Duman et al., 2007; Ohoyama, 1961] and are of interest for the chemical industry.

The phase diagram of the Mn – Ge system [Arras et al., 2011; Berche, Tedenac, Jund, 2014; Gokhale, Abbaschian, 1990; Predel, 1996; Диаграммы состояния двойных металлических систем: справочник, 2001] is presented in Figure 48.

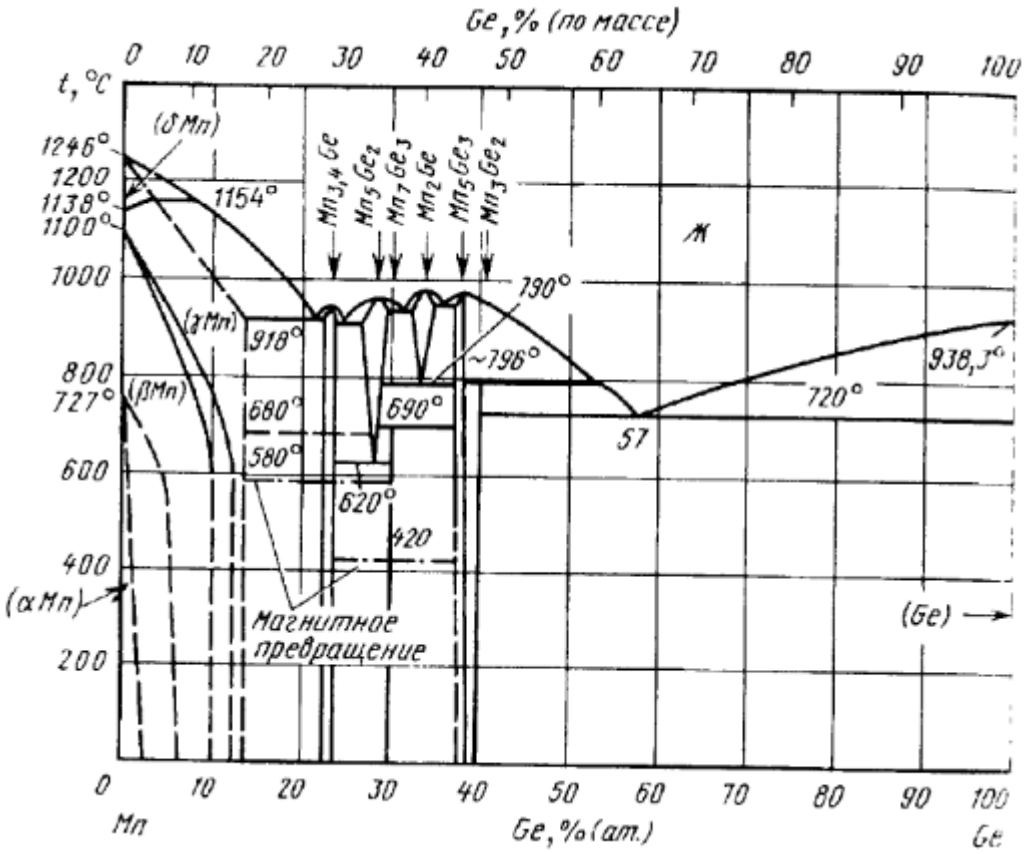

Fig. 48. The phase diagram of the Mn – Ge system [Диаграммы состояния двойных металлических систем: справочник, 2001].

Four compounds of the stoichiometric composition, namely $Mn_{3,4}Ge$, Mn_7Ge_3, Mn_5Ge_3, $Mn_{11}Ge_8$, two solid solutions of germanium in manganese (β-phase with cubic lattice and γ-phase with fcc lattice, pure α-Mn with cbcc lattice and pure germanium with diamond lattice exist in the system at 25 °C. The solubility of germanium α-Mn and of manganese in diamond-Ge is vanishingly small at 25 °C.

The thermodynamic properties of both solid solutions of germanium in manganese were modelled in terms of substitution solution model using the Redlich-Kister polynomials for the excess Gibbs energy of the solution. The standard Gibbs energies of formation of manganese germanides were estimated according to the equation presented in the textbook. More details could be found in the attached publication.

10.2. Equilibira in Mn – Ge – O system

Manganese oxides were discussed in Section 9.2, and germanium forms only two oxides, GeO and GeO_2. Moreover, germanium (II) oxide is thermodynamically unstable with respect to pure germanium and germanium (IV) oxide.

The existence of two manganese germanates, namely, Mn_2GeO_4 and $MnGeO_3$, was reported [Takayama, 1981]. The standard Gibbs energies of formation of these germanates were estimated using Kireev's method. It was found, that $MnGeO_3$ is thermodynamically unstable with respect to manganese and germanium oxides.

More details, including the state diagram of the Mn – Ge – O system and the list of equilibria in it, are provided in the attached publication.

10.3. Potential – pH diagram of Ge – H_2O system

In an aqueous solution germanium might form the cation Ge^{2+} and the anions $HGeO_3^-$ and GeO_3^{2-}. However, the calculations show that these aqueous germanium species have their domains of thermodynamic stability only in much diluted solutions. In concentrated and moderately diluted solutions the only oxidation product of germanium is GeO_2.

The potential – pH diagram of Ge – H_2O system at 25 °C, air pressure of 1 bar and the activities of germanium species of 1 $mol \cdot l^{-1}$ is presented in Figure 49.

10.4. Potential – pH diagram of Mn – Ge – H_2O system

The potential – pH diagram of Mn – Ge – H_2O system is presented in the attached publication.

Because germanium dioxide is thermodynamically stable in a wide interval of potentials and pH, it is very suitable for the passivation layer

formation. If the germanium content in the system is not high enough to form a continuous layer of GeO_2 on the surface, the passivation layer might consist of manganese germanate Mn_2GeO_4.

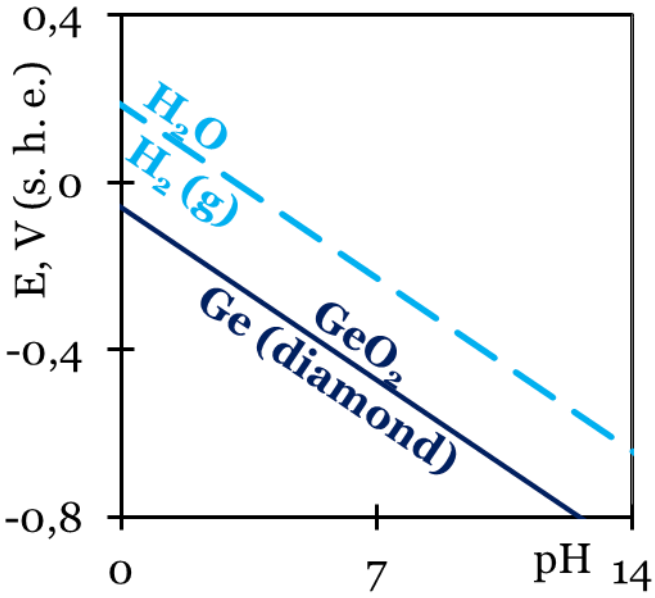

Fig. 49. The potential – pH diagram of the Ge – H_2O system at 25 °C, air pressure of 1 bar and the activities of germanium species in a solution of 1 M.

Publications to chapter 10

The content of this chapter was published as a preprint [Тюрин, Николайчук, Кабардин, 2016] at the website of *Journal of Corrosion Science and Engineering*. This Russian preprint with title, abstract, figures and tables translated into English is presented below.

УДК 620.193:669.14

ТЕРМОДИНАМИЧЕСКАЯ ОЦЕНКА КОРРОЗИОННО-ЭЛЕКТРОХИМИЧЕСКОГО ПОВЕДЕНИЯ СПЛАВОВ СИСТЕМЫ МАРГАНЕЦ – ГЕРМАНИЙ

А. Г. Тюрин, П. А. Николайчук, А. М. Кабардин

Кафедра аналитической и физической химии,
ФГБОУ ВПО «Челябинский государственный университет»,
ул. Братьев Кашириных, 129, 454001,Челябинск, Россия,
E-Mail: npa@csu.ru.

Аннотация: Описаны термодинамические свойства β- и γ- твёрдых металлических растворов системы Mn – Ge в области низких температур. Оценены стандартные энергии Гиббса образования германидов и германатов марганца $Mn_{3,4}Ge$, Mn_7Ge_3, Mn_5Ge_3, $Mn_{11}Ge_8$, $MnGeO_3$ и Mn_2GeO_4. Построены фазовая диаграмма системы Mn – Ge – O и диаграмма потенциал – pH системы Mn – Ge – H_2O при 25°C и 1 бар. Обсуждаются термодинамические особенности коррозионно-электрохимического поведения системы Mn – Ge.

Ключевые слова: германиды марганца, система Mn – Ge, диаграмма состояния системы Mn – Ge – O, диаграмма потенциал – pH системы Mn – Ge – H_2O, химическая и электрохимическая устойчивость.

UDC 620.193:669.14

THERMODYNAMIC EVALUATION OF THE CORROSION-ELECTROCHEMICAL BEHAVIOUR OF MANGANESE – GERMANIUM SYSTEM ALLOYS

A.G. Tyurin, P. A. Nikolaychuk, A. M. Kabardin

Department of Analytical and Physical Chemistry,

Chelyabinsk State University,

Bratyev Kashirinykh Street, 129, 454001,Chelyabinsk, Russia,

E-Mail: npa@csu.ru.

Abstract: The thermodynamic properties of β- and γ- solid metallic solutions of the Mn – Ge system at the low temperatures were described. The standard Gibbs energies of formation of manganese germanides and germanates $Mn_{3.4}Ge$, Mn_7Ge_3, Mn_5Ge_3, $Mn_{11}Ge_8$, $MnGeO_3$ and Mn_2GeO_4 were estimated. The state diagram of the Mn – Ge – O system and the potential – pH diagram of the Mn – Ge – H_2O system at 25°C and 1 bar were plotted. The thermodynamic features of the corrosion-electrochemical behaviour of the Mn – Ge system alloys were discussed.

Keywords: manganese germanides, Mn – Ge system, Mn – Ge – O system state diagram, potential – pH diagram of Mn – Ge – H_2O system, chemical and electrochemical stability.

1. ВВЕДЕНИЕ

Задача оптимизации коррозионных потерь материалов, эксплуатируемых в различных агрессивных средах, до сих пор остаётся чрезвычайно актуальной Одним из перспективных направлений коррозиологии является поиск новых материалов, обладающих уникальными физико-химическими свойствами и функциональными характеристиками. Примерами таких материалов могут служить металлоподобные интерметаллические соединения переходных металлов [1], в частности, германиды марганца. Германиды марганца обладают необычными магнитными [2 – 4] и термоэлектрическими [5] свойствами и представляют интерес для промышленности. Поэтому исследование их коррозионно-электрохимических свойств является важной научной задачей. Электрохимия интерметаллических и металлоподобных соединений является теоретической основой таких технологических процессов, как электрорафинирование металлов, электрохимическая размерная обработка, получение скелетных катализаторов. Анодные реакции на данных соединениях представляют собой один из парциальных коррозионных процессов, который определяют характер их коррозионного поражения

Сплавы германия и марганца представляют собой практически неисследованные в коррозионно-электрохимическом плане объекты, несмотря на то, что электрохимическое поведение германидов марганца в различных электролитах изучается [6, 7]. Однако результаты теоретических исследований коррозионных свойств марганец-германиевых сплавов могут существенно дополнить и расширить имеющийся материал. Технология производства материалов системы Mn – Ge требует информации об этих материалах, а также о других формах существования марганца и германия в рудах чёрных и цветных металлов. Цель данной работы – в рамках термодинамической теории провести описание коррозионно-электрохимического поведения сплавов системы Mn – Ge.

2. МОДЕЛИРОВАНИЕ ФАЗОВЫХ И ХИМИЧЕСКИХ РАВНОВЕСИЙ В СИСТЕМЕ Mn – Ge

Фазовая диаграмма системы Mn – Ge представлена в работах [8 – 11]. В системе при 25°C существуют четыре соединения стехиометрического состава ($Mn_{3,4}Ge$, Mn_7Ge_3, Mn_5Ge_3, $Mn_{11}Ge_8$), два твёрдых раствора германия в марганце (β-фаза с кубической (cub_A13) решёткой и γ-фаза с гранецентрироавнной кубической (fcc_A1) решёткой), чистый α-Mn с кластерной объёмноцентрированной (cbcc_A12) решёткой и чистый германий с

решёткой алмаза (dia_A4). Растворимость германия в α-марганце и марганца в германии с решёткой алмаза при 25°C пренебрежимо мала.

2.1. Расчёт равновесия α-фазы с β-фазой

Это равновесие описывается условием равенства химических потенциалов марганца в обеих фазах. Если выразить избыточный химический потенциал марганца в β-фазе с использованием степенных рядов Редлиха – Кистера [12], это условие преобразуется к следующему:

$$\Delta\mu_{1(\alpha\to\beta)} = \Delta\mu^{0}_{1(\alpha\to\beta)} + R\cdot T\cdot \ln x_{1(\beta)} + \\ + x^{2}_{2(\beta)}\cdot(L^{(0)}_{12(\beta)} + L^{(1)}_{12(\beta)}\cdot(1-4x_{1(\beta)})\cdot T),\ \text{Дж}/\text{моль}. \qquad (1)$$

Обозначения компонентов: 1 – Mn, 2 – Ge, $L^{(0)}_{12}$ и $L^{(1)}_{12}$ – параметры в уравнении Редлиха – Кистера. Выражение для мольной энергии Гиббса перехода чистого марганца из α- в β-фазу получено из базы данных NASA [13]:

$$\Delta\mu^{0}_{1(\alpha\to\beta)} = -2{,}2714\cdot T + 2226,\ \text{Дж}/\text{моль}. \qquad (2)$$

По результатам моделирования равновесия путём решения уравнений (1) и (2) получены следующие значения параметров:

$$L^{(0)}_{12(\beta)} = -367670,\ \text{Дж}/\text{моль}, \qquad (3)$$

$$L^{(1)}_{12(\beta)} = -58{,}564,\ \text{Дж}/\text{моль}\cdot\text{К}. \qquad (4)$$

2.2. Расчёт равновесия β-фазы с γ-фазой

Это равновесие описывается условием равенства химических потенциалов и марганца и германия в обеих фазах:

$$\Delta\mu_{1\,(\beta\to\gamma)} = \Delta\mu^{0}_{1\,(\beta\to\gamma)} + R\cdot T\cdot \ln\left(x_{1(\gamma)}/x_{1(\beta)}\right) + \\ + x^{2}_{2(\gamma)}\cdot\left(L^{(0)}_{12(\gamma)} + L^{(1)}_{12(\gamma)}\cdot(1-4x_{1(\gamma)})\cdot T\right) - \\ - x^{2}_{2(\beta)}\cdot\left(L^{(0)}_{12(\beta)} + L^{(1)}_{12(\beta)}\cdot(1-4x_{1(\beta)})\cdot T\right),\ Дж/моль, \qquad (5)$$

$$\Delta\mu_{2\,(\beta\to\gamma)} = \Delta\mu^{0}_{2\,(\beta\to\gamma)} + R\cdot T\cdot \ln\left(x_{2(\gamma)}/x_{2(\beta)}\right) + \\ + x^{2}_{1(\gamma)}\cdot\left(L^{(0)}_{12(\gamma)} + L^{(1)}_{12(\gamma)}\cdot(4x_{2(\gamma)}-1)\cdot T\right) - \\ - x^{2}_{1(\beta)}\cdot\left(L^{(0)}_{12(\beta)} + L^{(1)}_{12(\beta)}\cdot(4x_{2(\beta)}-1)\cdot T\right),\ Дж/моль. \qquad (6)$$

Выражение для мольной энергии Гиббса перехода из β- в γ-фазу для чистого марганца имеется в базе данных NASA [13]:

$$\Delta\mu^{0}_{1(\beta\to\gamma)} = -1{,}5597\cdot T + 2123,\ Дж/моль, \qquad (7)$$

а энергия Гиббса фазового перехода германия и значения параметров уравнения Редлиха – Кистера для γ-фазы были получены при моделировании равновесия путём решения уравнений (5) – (7):

$$\Delta\mu^{0}_{2(\beta\to\gamma)} = -3{,}6718\cdot T + 76510,\ Дж/моль, \qquad (8)$$

$$L^{(0)}_{12(\gamma)} = -470980,\ Дж/моль, \qquad (9)$$

$$L^{(1)}_{12(\beta)} = -74{,}779,\ Дж/моль\cdot К. \qquad (10)$$

2.3. Оценка энергий Гиббса образования германидов марганца

Согласно справочнику [14], в общем виде энергия Гиббса образования германидов марганца по реакции

$$x\,\mathrm{Mn}\ (a) + y\ \mathrm{Ge}\ (\text{алмаз}) \rightarrow \mathrm{Mn}_x\mathrm{Ge}_y \qquad (11)$$

может быть представлена уравнением

$$\Delta_f G_T^0(\mathrm{Mn}_x\mathrm{Ge}_y) = x \cdot y \cdot (A \cdot x + B \cdot y), \qquad (12)$$

в котором A и B – некоторые зависящие от температуры параметры. Для нахождения их значений использованы данные о средних энтальпиях и энтропиях образования некоторых германидов марганца в интервале температур 700 – 1300°C [14], представленные в таблице 1.

Таблица 1.

Средние энтальпии и энтропии образования интерметаллидов состава Mn_xGe_y в интервале температур 700 – 1300°C [14]

Table 1.

The average enthalpies and entropies of formation of intermetallides of a composition Mn_xGe_y in the temperature interval 700 – 1300°C [14]

x	y	$\Delta_f H_T^0$, Дж/моль	$\Delta_f S_T^0$, Дж/моль·К
0,57895	0,42105	-16200	5,9
0,625	0,375	-17900	5,6
0,71429	0,28571	-15400	5,5
0,76471	0,23529	-14200	4,5

На основании данных таблицы 1 было получено следующее регрессионное уравнение для энергий Гиббса образования интерметаллидов:

$$\Delta_f G_T^0(Mn_xGe_y) = x \cdot y \cdot ((-28{,}674 \cdot T - 92529) \cdot x + \\ +(-17{,}639 \cdot T - 37442) \cdot y),\ \text{Дж}/\text{моль}. \quad (13)$$

В таблице 2 представлены значения стандартных энергий Гиббса образования германидов марганца, оценённые по уравнению (13).

Таблица 2.

Стандартные энергии Гиббса образования германидов марганца

Table 2.

The standard Gibbs energies of formation of manganese germanides

No	Intermetallide		$\Delta_f G_{298,15}^0$, Дж/моль
1	$Mn_{3,4}Ge$	$Mn_{0,77273}Ge_{0,22727}$	-15420
2	Mn_7Ge_3	$Mn_{0,7}Ge_{0,3}$	-17550
3	Mn_5Ge_3	$Mn_{0,625}Ge_{0,375}$	-19570
4	$Mn_{11}Ge_8$	$Mn_{0,57895}Ge_{0,42105}$	-18650

2.4. Расчёт равновесия γ-фазы с $Mn_{3,4}Ge$

Это равновесие описывается следующей реакцией:

$$3,4Mn_{(\gamma)} + Ge_{(\gamma)} \rightarrow Mn_{3,4}Ge, \qquad (14)$$

или, в пересчёте на 1 моль интерметаллида

$$0,77273\ Mn_{(\gamma)} + 0,22727\ Ge_{(\gamma)} \rightarrow Mn_{0,77273}Ge_{0,22727}. \qquad (15)$$

В соответствии с уравнением изотермы химической реакции [15]:

$$\begin{aligned}
&\Delta_r G_T = -R \cdot T \cdot \ln K = -0,77273 \cdot R \cdot T \cdot \ln a_{1(\gamma)} - \\
&-0,22727 \cdot R \cdot T \cdot \ln a_{2(\gamma)} = -0,77273 \times \\
&\times (R \cdot T \cdot \ln x_{1(\gamma)} + x_{2(\gamma)}^2 \cdot (L_{12(\gamma)}^{(0)} + L_{12(\gamma)}^{(1)} \cdot (1 - 4x_{1(\gamma)}) \cdot T)) - \\
&-0,22727 \cdot (R \cdot T \cdot \ln x_{2(\gamma)} + x_{1(\gamma)}^2 \times \\
&\times (L_{12(\gamma)}^{(0)} + L_{12(\gamma)}^{(1)} \cdot (4x_{2(\gamma)} - 1) \cdot T)),\ {Дж}/{моль}.
\end{aligned} \qquad (16)$$

Энергия Гиббса реакции (15) может быть вычислена с использованием энергии образования $Mn_{0,77273}Ge_{0,22727}$ и энергий Гиббса фазовых переходов марганца и германия в γ-фазу:

$$\begin{aligned}
&\Delta_r G_T = \Delta_f G_T^0(Mn_{0,77273}Ge_{0,22727}) - \\
&-0,77273\Delta\mu_{1(\alpha\rightarrow\gamma)}^0 - 0,22727\Delta\mu_{2\,(\text{алмаз}\rightarrow\gamma)}^0.
\end{aligned} \qquad (17)$$

Зависимость энергии Гиббса образования германида марганца $Mn_{0,77273}Ge_{0,22727}$ от температуры, в соответствии с уравнением (13), такова:

$$\Delta_f G_T^0(Mn_{0,77273}Ge_{0,22727}) = -4,5954 \cdot T - 14051,\ {Дж}/{моль}. \qquad (18)$$

Энергия Гиббса фазового перехода марганца из α-фазы в γ-фазу может быть оценена по справочным данным [13]:

$$\Delta\mu^0_{1(\alpha\to\gamma)} = \Delta\mu^0_{1(\alpha\to\beta)} + \Delta\mu^0_{1(\beta\to\gamma)} = -3,8311\cdot T + 4349,\ {}^{Дж}/_{моль}. \qquad (19)$$

При моделировании равновесия с использованием уравнений (16) – (19) оценена зависимость энергии Гиббса перехода германия из кристаллической решётки алмаза в γ-фазу:

$$\Delta\mu^0_{2(алмаз\to\gamma)} = -18,3687\cdot T + 307370,\ {}^{Дж}/_{моль}. \qquad (20)$$

2.5. Построение фазовой диаграммы системы Mn – Ge в области низких температур

С использованием оцененных термодинамических параметров фаз и энергий Гиббса фазовых переходов произведён расчёт линий фазовых равновесий в системе. Результаты вычисления фазовой диаграммы представлены на рисунках 1а и 1б. Линии на рисунках показывают результаты моделирования, а точки – данные, снятые с диаграммы состояния.

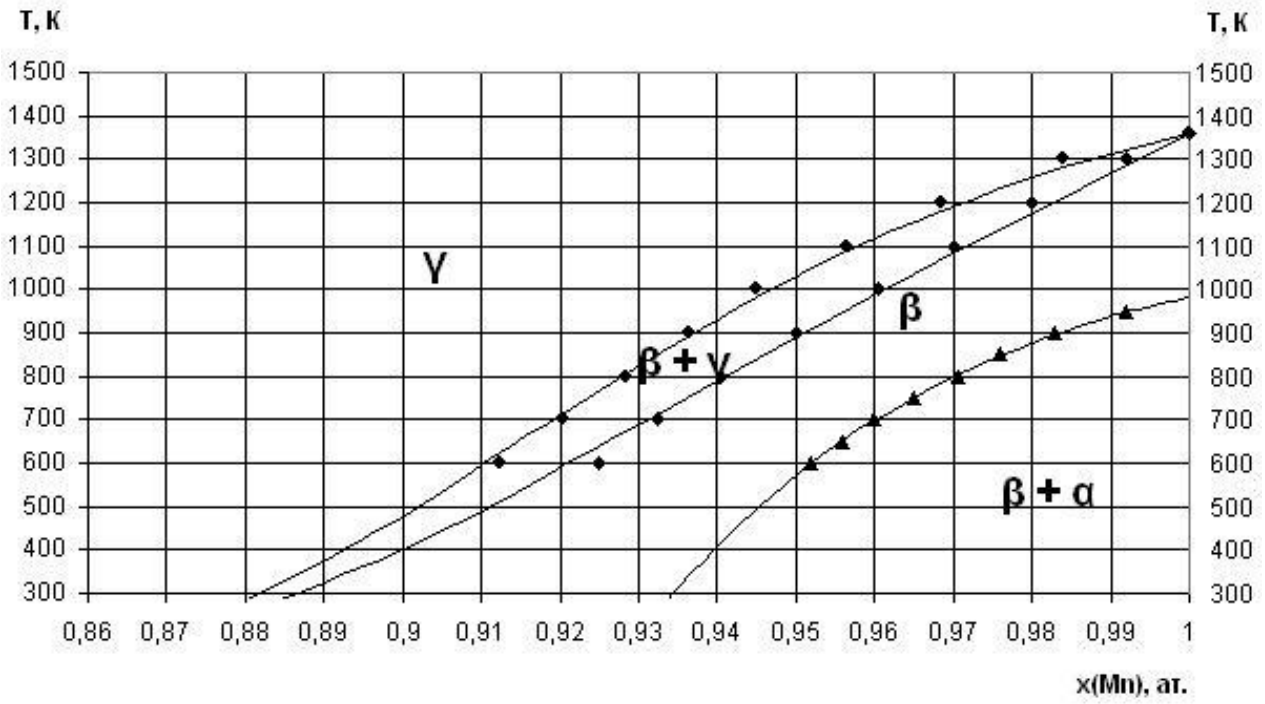

Рис. 1а. Расчётная фазовая диаграмма системы Mn – Ge, $0{,}86 \leqslant x_1 \leqslant 1$.

Fig. 1a. The calculated phase diagram of the Mn – Ge system, $0{,}86 \leqslant x_1 \leqslant 1$.

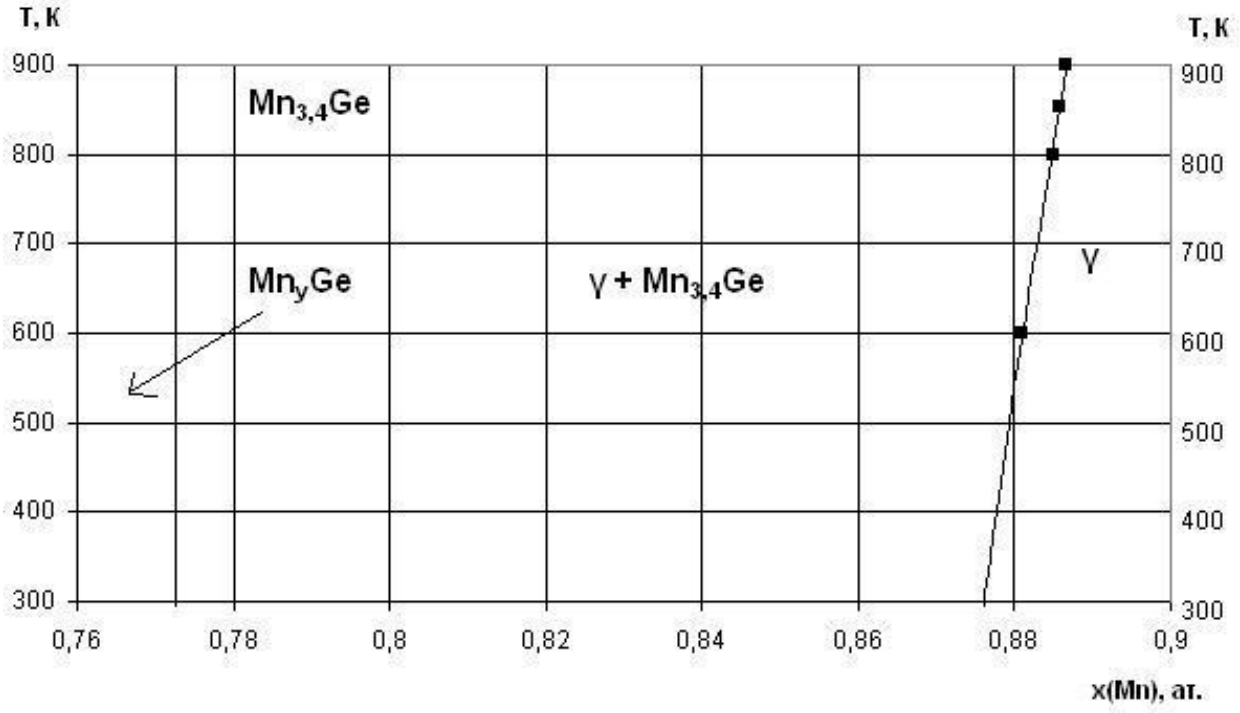

Рис. 1б. Расчётная фазовая диаграмма системы Mn – Ge, $0{,}76 \leqslant x_1 \leqslant 0{,}9$.

Fig. 1b. The calculated phase diagram of the Mn – Ge system, $0{,}76 \leqslant x_1 \leqslant 0{,}9$.

2.6. Функция стабильности фаз переменного состава

Функция стабильности бинарной смеси в общем виде определяется выражением

$$\Psi = 1 + x_1 \cdot \frac{\partial \ln \gamma_1}{\partial x_1} = 1 + x_2 \cdot \frac{\partial \ln \gamma_2}{\partial x_2}, \qquad (21)$$

где γ_i – коэффициент активности соответствующего компонента *i*.

Для раствора замещения, избыточная энергия которого выражается степенными рядами Редлиха-Кистера, выражение преобразуется к виду

$$\Psi = 1 + 2x_1 \cdot x_2 \cdot \frac{2x_1 \cdot L_{12}^{(1)} \cdot T - (L_{12}^{(0)} + (4x_2 - 1) \cdot L_{12}^{(1)} \cdot T)}{R \cdot T}. \qquad (22)$$

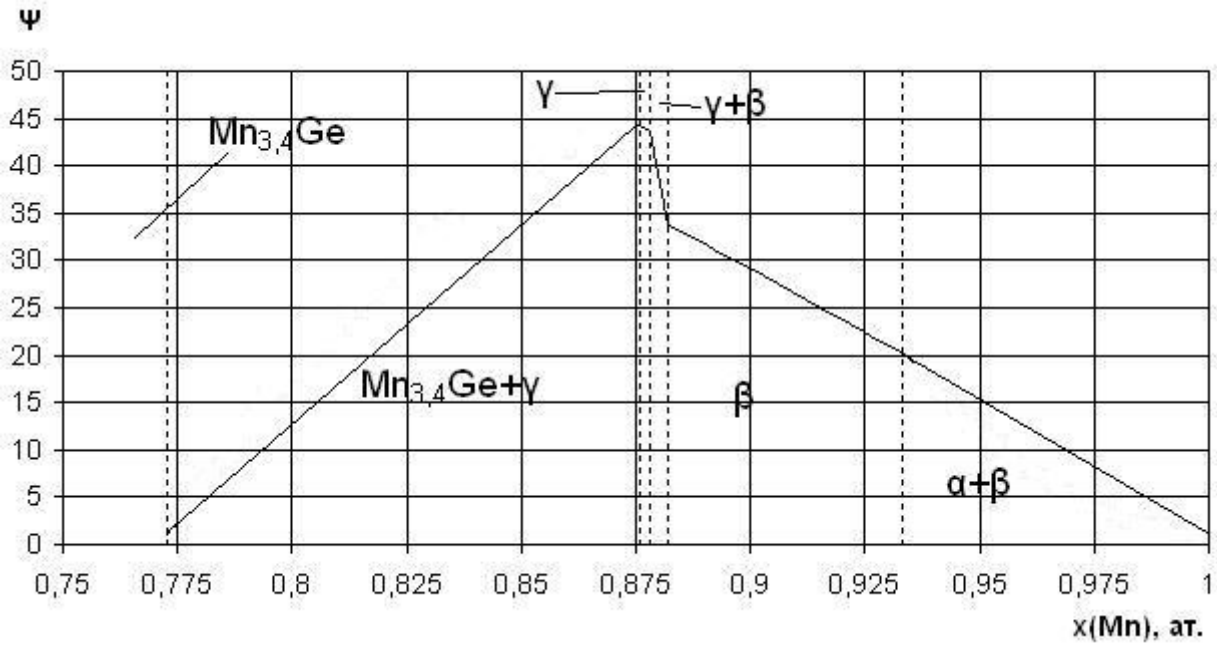

Рис. 2. Зависимость функции стабильности системы Mn – Ge от состава раствора.

Fig. 2. The dependence of the stability function of the Mn – Ge system on the solution composition.

2.7. Активности компонентов твёрдых растворов системы Mn – Ge

Активности компонентов β-фазы и γ-фазы зависят от состава и температуры следующим образом:

$$a_1 = x_1 \cdot \exp\left(\frac{x_2^2 \cdot \left(L_{12}^{(0)} + (1 - 4x_1) \cdot T \cdot L_{12}^{(1)} \right)}{R \cdot T} \right), \qquad (22)$$

$$a_2 = x_2 \cdot \exp\left(\frac{x_1^2 \cdot \left(L_{12}^{(0)} + (4x_2 - 1) \cdot T \cdot L_{12}^{(1)} \right)}{RT} \right). \qquad (23)$$

Зависимость активности марганца от состава раствора при 25°C показана на рисунке 3. Активность германия в рассматриваемом диапазоне концентраций близка к нулю.

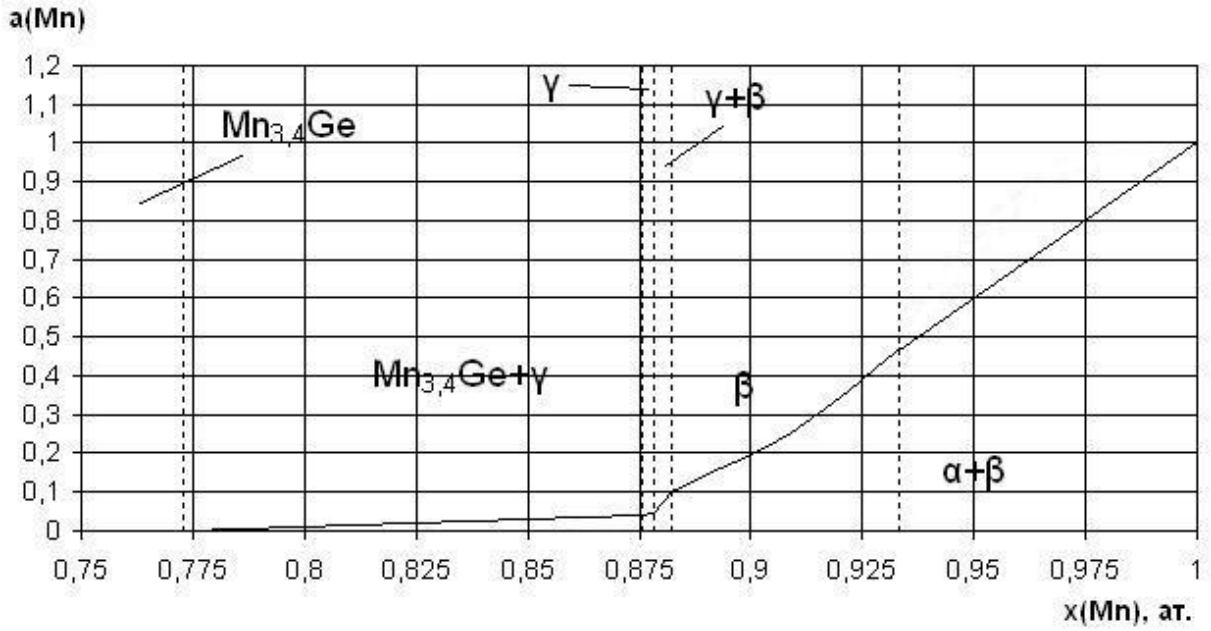

Рис. 3. Зависимость активности марганца от состава раствора при 25°C.

Fig. 3. The dependence of manganese activity on the solution composition at 25°C.

3. ФАЗОВЫЕ РАВНОВЕСИЯ В СИСТЕМЕ Mn – Ge – O. ХИМИЧЕСКАЯ УСТОЙЧИВОСТЬ

В системе Mn – O при 25°C термодинамически устойчивы оксиды марганца MnO, Mn_3O_4, Mn_2O_3 и MnO_2, а в системе Ge – O образуется один оксид, GeO_2 [8]. Стандартные энергии Гиббса образования оксидов марганца и германия заимствованы из справочника [16]. В тройной системе Mn – Ge – O возможно образование германатов марганца $MnGeO_3$ и Mn_2GeO_4 [17], данных о стандартных энергиях Гиббса образования которых в литературе нет.

3.1. Оценка термодинамической устойчивости германатов марганца

Для того, чтобы оценить стандартные энергии Гиббса образования германатов марганца, было использовано допущение о том, что энергии Гиббса образования однотипных (похожих по составу) веществ A и B приближённо подчиняются следующей закономерности [18]:

$$\Delta_f G^0_{298,15}(A) = a \cdot \Delta_f G^0_{298,15}(B). \qquad (24)$$

Данную закономерность не рекомендуется экстраполировать на другие температуры из-за больших разниц в теплоёмкостях веществ при низких температурах (параметр a в таком случае заметно зависит от температуры), но можно использовать при постоянной температуре 298,15 K. С её помощью стандартные

энергии Гиббса образования $MnGeO_3$ и Mn_2GeO_4 можно оценить следующим образом:

$$\frac{\Delta_f G^0_{298,15}(Mn_2GeO_4)}{\Delta_f G^0_{298,15}(Mn_2SiO_4)} = \frac{\Delta_f G^0_{298,15}(Fe_2GeO_4)}{\Delta_f G^0_{298,15}(Fe_2SiO_4)}, \quad (25)$$

$$\frac{\Delta_f G^0_{298,15}(MnGeO_3)}{\Delta_f G^0_{298,15}(Mn_2GeO_4)} = \frac{\Delta_f G^0_{298,15}(MnSiO_3)}{\Delta_f G^0_{298,15}(Mn_2SiO_4)}. \quad (26)$$

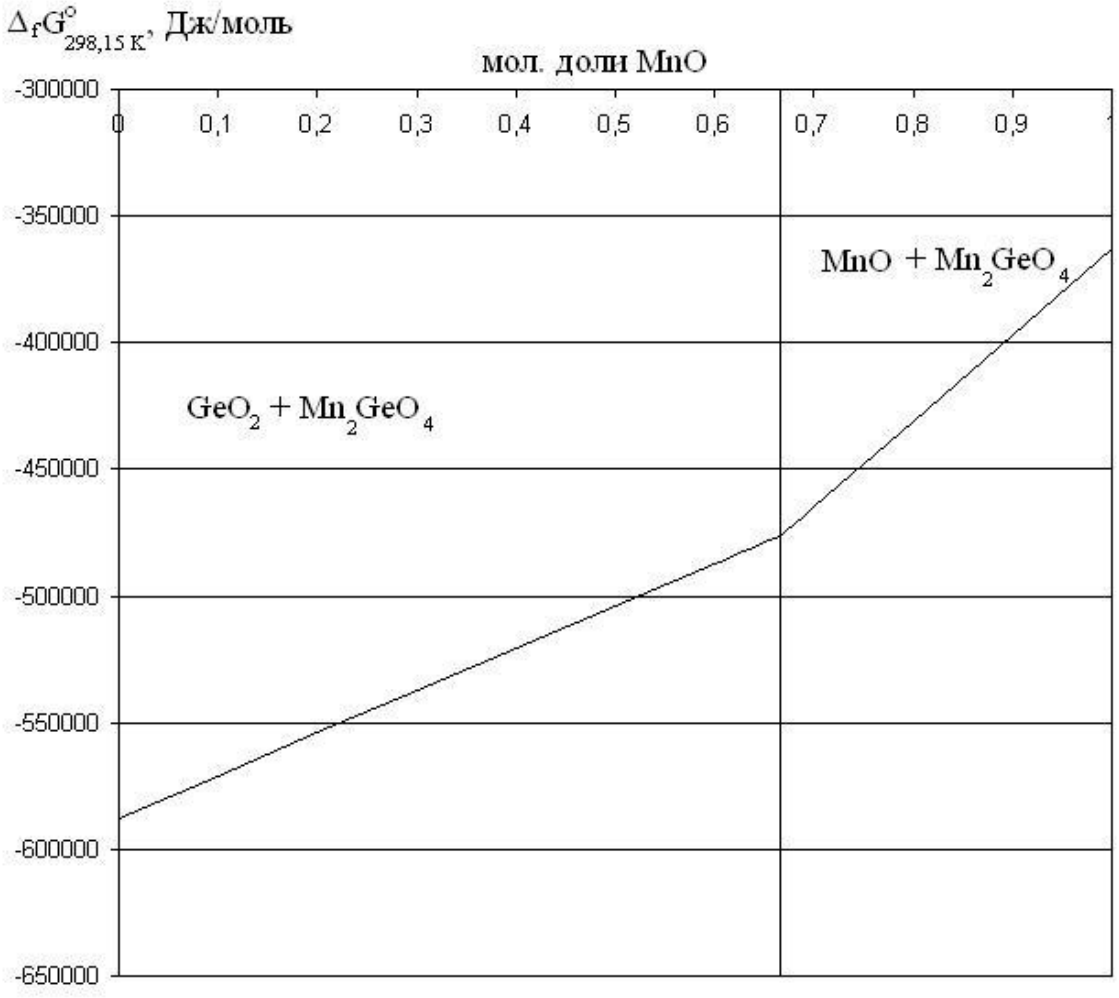

Рис. 4. Зависимость $\Delta_f G^0_{298,15}$ наиболее устойчивых наборов равновесных фаз от компонентного состава системы MnO – GeO_2.

Fig. 4. The dependence of $\Delta_f G^0_{298,15}$ of the components of the MnO – GeO_2 system on its compositon.

Необходимые для оценки данные о стандартных энергиях Гиббса образования соединений Mn_2SiO_4, $MnSiO_3$, Fe_2SiO_4 и Fe_2GeO_4 взяты из работ [19 – 21]. По результатам оценки получены следующие значения:

$$\Delta_f G^0_{298,15}\,(Mn_2GeO_4) = -1428300\ {Дж}/{моль},\qquad (27)$$

$$\Delta_f G^0_{298,15}\,(MnGeO_3) = -995800\ {Дж}/{моль}.\qquad (28)$$

По данным работы [17], растворимость $MnGeO_3$ в Mn_2O_3 даже при 900°C составляет всего 0,32 мол. %, поэтому при комнатной температуре ей можно пренебречь.

Для того, чтобы узнать, какие германаты марганца наиболее устойчивы при температуре 298,15 К, был рассмотрен разрез MnO – GeO_2. Путём варьирования компонентного состава системы и минимизации стандартной энергии Гиббса образования компонентов, были определены наиболее устойчивые соединения. Результат оценки показан на рисунке 4.

Рисунок 4 показывает, что германат $MnGeO_3$ при 25°C термодинамически неустойчив при любом составе системы.

3.2. Диаграмма состояния системы Mn – Ge – O при 25°C

Диаграмма состояния системы Mn – Ge – O при 25°C показана на рисунке 5. По оси абсцисс отложена мольная доля германия в

двойной системе Mn – Ge, а по оси ординат – степень окисленности системы $y = \frac{n_O}{n_{Mn} + n_{Ge}}$.

На диаграмме показаны следующие инвариантные равновесия, реализуемые в системе:

I. α-Mn – β-фаза – MnO;

II. γ-фаза – β-фаза – MnO;

III. γ-фаза – $Mn_{3,4}Ge$ – MnO;

IV. Mn_7Ge_3 – $Mn_{3,4}Ge$ – MnO;

V. Mn_5Ge_3 – Mn_7Ge_3 – MnO;

VI. Mn_5Ge_3 – MnO – Mn_2GeO_4;

VII. $Mn_{11}Ge_8$ – Mn_5Ge_3 – Mn_2GeO_4;

VIII. Ge – $Mn_{11}Ge_8$ – Mn_2GeO_4;

IX. Ge – GeO_2 – Mn_2GeO_4;

X. MnO – Mn_3O_4 – Mn_2GeO_4;

XI. Mn_3O_4 – Mn_2O_3 – Mn_2GeO_4;

XII. Mn_2O_3 – MnO_2 – Mn_2GeO_4;

XIII. MnO_2 – Mn_2GeO_4 – GeO_2.

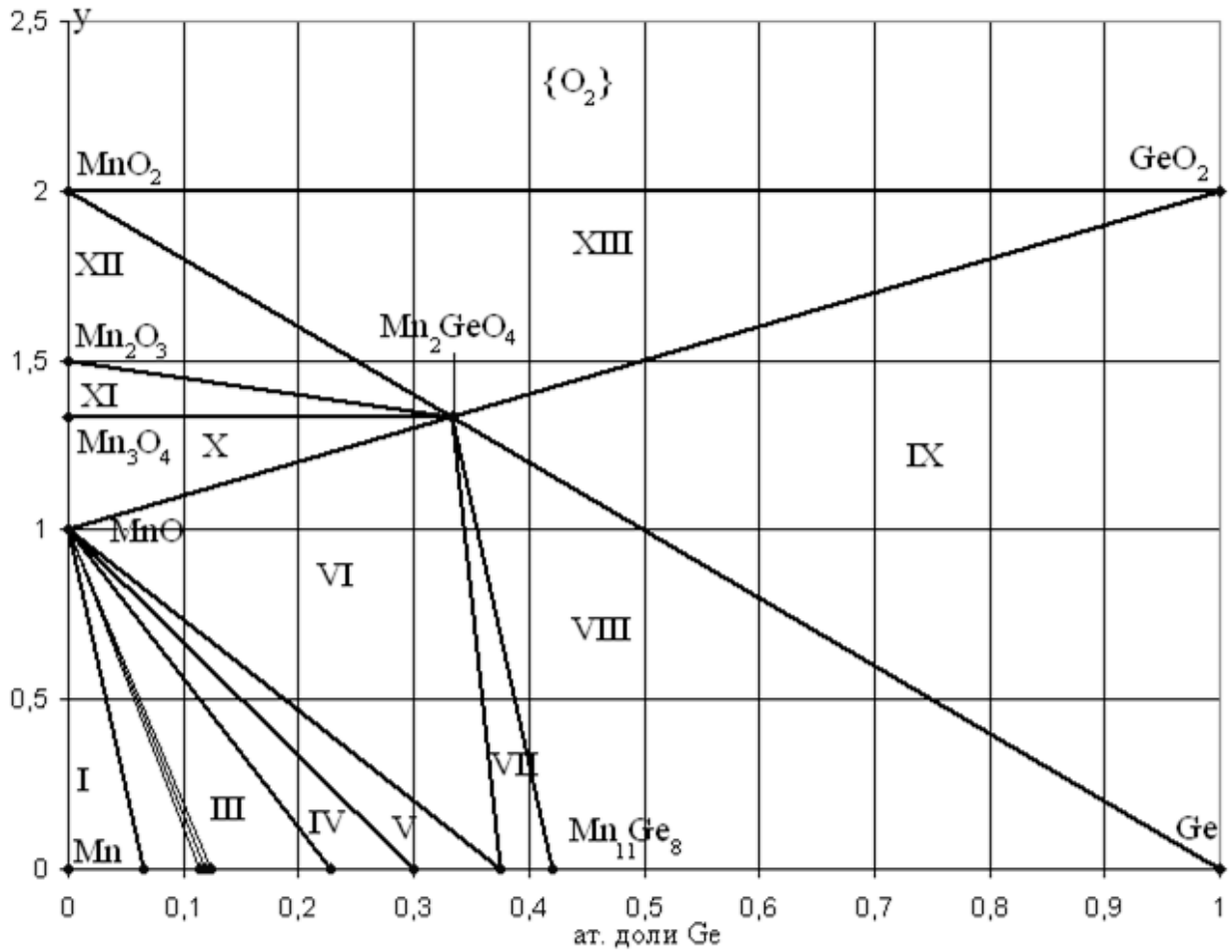

Рис. 5. Диаграмма состояния системы Mn – Ge при 25°C и 1 бар.

Fig. 5. The state diagram of the Mn – Ge system at 25°C and 1 bar.

Термодинамические характеристики инвариантных состояний в системе приведены в таблице 3.

Расчёты показывают, что окисление германидов марганца и сплавов системы Mn – Ge кислородом воздуха приводит к образованию на его поверхности оксидов MnO_2 и GeO_2, а также германата марганца Mn_2GeO_4. Конкретный состав пассивирующей плёнки на металле будет определяться содержанием германия в сплавах.

Таблица 3.

Характеристики инвариантных состояний системы Mn – Ge – O при 25°C.

Table 3.

Characteristics of the Mn – Ge – O system invariant conditions at 25°C.

Phase equilibrium	$p(O_2)$, bar	Solid phases composition
I. α-Mn – β-фаза – MnO	$7{,}00 \cdot 10^{-128}$	x(α-Mn) =1; x(MnO)=1; x(β-Mn)=0,93431
II. MnO – β-фаза – γ-фаза	$7{,}41 \cdot 10^{-127}$	x(MnO)=1; x(β-Mn)=0,88636; x(γ-Mn)=0,88154
III. $Mn_{3,4}Ge$ – MnO – γ-фаза	$1{,}22 \cdot 10^{-126}$	$x(Mn_{3,4}Ge)$=1; x(MnO)=1; x(γ-Mn)=0,87565
IV. $Mn_{3,4}Ge$ – Mn_7Ge_3 – MnO	$8{,}31 \cdot 10^{-125}$	$x(Mn_{3,4}Ge)$=1; $x(Mn_7Ge_3)$=1; x(MnO)=1
V. Mn_7Ge_3 – Mn_5Ge_3 – MnO	$1{,}45 \cdot 10^{-124}$	$x(Mn_5Ge_3)$=1; $x(Mn_7Ge_3)$=1; x(MnO)=1
VI. Mn_5Ge_3 – MnO – Mn_2GeO_4	$1{,}14 \cdot 10^{-120}$	$x(Mn_5Ge_3)$=1; $x(Mn_2GeO_4)$=1; x(MnO)=1
VII. Mn_5Ge_3 – $Mn_{11}Ge_8$ – Mn_2GeO_4	$1{,}77 \cdot 10^{-120}$	$x(Mn_5Ge_3)$=1; $x(Mn_2GeO_4)$=1; $x(Mn_{11}Ge_8)$=1

VIII. $Ge - Mn_{11}Ge_8 - Mn_2GeO_4$	$3{,}38 \cdot 10^{-120}$	$x(Ge)=1;\ x(Mn_{11}Ge_8)=1;\ x(Mn_2GeO_4)=1$
IX. $Ge - GeO_2 - Mn_2GeO_4$	$1{,}15 \cdot 10^{-103}$	$x(Ge)=1;\ x(GeO_2)=1;\ x(Mn_2GeO_4)=1$
X. $MnO - Mn_3O_4 - Mn_2GeO_4$	$7{,}08 \cdot 10^{-69}$	$x(Mn_3O_4)=1;\ x(MnO)=1;\ x(Mn_2GeO_4)=1$
XI. $Mn_3O_4 - Mn_2O_3 - Mn_2GeO_4$	$1{,}14 \cdot 10^{-27}$	$x(Mn_3O_4)=1;\ x(Mn_2O_3)=1;\ x(Mn_2GeO_4)=1$
XII. $Mn_2O_3 - MnO_2 - Mn_2GeO_4$	$6{,}25 \cdot 10^{-18}$	$x(MnO_2)=1;\ x(Mn_2O_3)=1;\ x(Mn_2GeO_4)=1$
XIII. $MnO_2 - Mn_2GeO_4 - GeO_2$	$2{,}10 \cdot 10^{-16}$	$x(MnO_2)=1;\ x(Mn_2GeO_4)=1;\ x(GeO_2)=1$

4. ЭЛЕКТРОХИМИЧЕСКАЯ УСТОЙЧИВОСТЬ.

Термодинамические характеристики основных химических и электрохимических равновесий в системе Mn – Ge – H_2O при 25°C и давлении воздуха 1 бар рассчитаны по результатам фазовых равновесий в системе Mn – Ge – O и данным о стандартных электродных потенциалах [22, 23] и константах основности гидроксидов марганца [24] и представлены в таблице 4. На основании этих расчётов построена диаграмма электрохимического

равновесия (потенциал – pH) марганецгерманиевых сплавов при 25°C, давлении 1 бар и активностях ионов в растворе, равных 1, 10^{-3} и 10^{-6} моль/л (стандартное состояние – гипотетический одномолярный раствор), которая изображена на рисунках 6а – 6в. Рисунок 6г детализирует область активного растворения марганца на диаграмме.

Таблица 4.

Основные химические и электрохимические равновесия в системе Mn – Ge – H_2O при 25°C и 1 бар.

Table 4.

The basic chemical and electrochemical equilibria in the Mn – Ge – H_2O system at 25°C and 1 bar.

No	Electrode reaction	Equilibrium potential, V (s. h. e.) or pH of the solution
a	$2H^+ + 2e = H_2; p(H_2) = 10^{-7}$ бар	φ = 0,20706 – 0,059159pH
b	$O_2 + 4H^+ + 4e = 2H_2O;\ p(O_2) = 0,21$ бар	φ = 1,2086 – 0,059159pH
1	$Mn^{2+} + 2e = Mn_{(a)}$	φ = – 1,18 + 0,029580lg $a_{Mn^{2+}}$ $x_{Mn(a)} = 1$
2	$Mn(OH)_2 + 2H^+ + 2e = Mn_{(a)} + 2H_2O$	φ = – 0,74001 – 0,059159pH $x_{Mn(a)} = 1$

3	$\left[Mn(OH)_4\right]^{2-} + 4H^+ + 2e = Mn_{(\alpha)} + 4H_2O$	$\varphi = 0{,}24870 - 0{,}11832pH +$ $+ 0{,}029580 \lg a_{\left[Mn(OH)_4\right]^{2-}}$ $\ln a_{Mn(\alpha)} = 0;$ $\ln a_{Mn(\beta)} = -0{,}62476$
4	$0{,}3579Mn^{2+} + 7{,}4417Mn_{(\gamma)} + 0{,}7158e =$ $= 7{,}7996Mn_{(\beta)}$	$\varphi = -1{,}1648 + 0{,}029580 \lg a_{Mn^{2+}}$ $\ln a_{Mn(\beta)} = -1{,}8045;$ $\ln a_{Mn(\gamma)} = -2{,}4734$
5	$0{,}3579Mn(OH)_2 + 7{,}4417Mn_{(\gamma)} +$ $+0{,}7158H^+ + 0{,}7158e =$ $= 7{,}7996Mn_{(\beta)} + 0{,}7158H_2O$	$\varphi = -0{,}72485 - 0{,}059159pH$ $\ln a_{Mn(\beta)} = -1{,}8045;$ $\ln a_{Mn(\gamma)} = -2{,}4734$
6	$0{,}3579\left[Mn(OH)_4\right]^{2-} + 7{,}4417Mn_{(\gamma)} +$ $+1{,}4316H^+ + 0{,}7158e =$ $= 7{,}7996Mn_{(\beta)} + 1{,}4316H_2O$	$\varphi = 0{,}26385 - 0{,}11832pH +$ $+ 0{,}029580 \lg a_{\left[Mn(OH)_4\right]^{2-}}$ $\ln a_{Mn(\beta)} = -1{,}8045;$ $\ln a_{Mn(\gamma)} = -2{,}4734$
7	$3{,}6421Mn^{2+} + Mn_{3,4}Ge +$ $+7{,}2842e = 7{,}0421Mn_{(\gamma)} + Ge_{(\gamma)}$	$\varphi = -1{,}1616 + 0{,}029580 \lg a_{Mn^{2+}}$ $\ln a_{Mn(\gamma)} = -20{,}959;$ $\ln a_{Ge(\gamma)} = -144{,}30$
8	$3{,}6421Mn(OH)_2 + Mn_{3,4}Ge +$ $+7{,}2842H^+ + 7{,}2842e =$ $= 7{,}0421Mn_{(\gamma)} + Ge_{(\gamma)} + 7{,}2842H_2O$	$\varphi = -0{,}72166 - 0{,}059159pH$ $\ln a_{Mn(\gamma)} = -20{,}959;$ $\ln a_{Ge(\gamma)} = -144{,}30$
9	$3{,}6421\left[Mn(OH)_4\right]^{2-} + Mn_{3,4}Ge +$ $+14{,}5684H^+ + 7{,}2842e =$ $= 7{,}0421Mn_{(\gamma)} + Ge_{(\gamma)} + 14{,}5684H_2O$	$\varphi = 0{,}26705 - 0{,}11832pH +$ $+ 0{,}029580 \lg a_{\left[Mn(OH)_4\right]^{2-}}$

		$\ln a_{Mn(\gamma)} = -20{,}959;$ $\ln a_{Ge(\gamma)} = -144{,}30$
10	$3{,}2Mn^{2+} + Mn_7Ge_3 + 6{,}4e = 3Mn_{3,4}Ge$	$\varphi = -1{,}1345 + 0{,}029580\lg a_{Mn^{2+}}$
11	$3{,}2Mn(OH)_2 + Mn_7Ge_3 + 6{,}4H^+ + +6{,}4e = 3Mn_{3,4}Ge + 6{,}4H_2O$	$\varphi = -0{,}69455 - 0{,}059159pH$
12	$3{,}2\left[Mn(OH)_4\right]^{2-} + Mn_7Ge_3 + 12{,}8H^+ + +6{,}4e = 3Mn_{3,4}Ge + 6{,}4H_2O$	$\varphi = 0{,}29416 - 0{,}11832pH + + 0{,}029580\lg a_{\left[Mn(OH)_4\right]^{2-}}$
13	$2Mn^{2+} + Mn_5Ge_3 + 4e = Mn_7Ge_3$	$\varphi = -1{,}1310 + 0{,}029580\lg a_{Mn^{2+}}$
14	$2Mn(OH)_2 + Mn_5Ge_3 + 4H^+ + +4e = Mn_7Ge_3 + 4H_2O$	$\varphi = -0{,}69096 - 0{,}059159pH$
15	$2\left[Mn(OH)_4\right]^{2-} + Mn_5Ge_3 + 8H^+ + +4e = Mn_7Ge_3 + 8H_2O$	$\varphi = 0{,}29774 - 0{,}11832pH + + 0{,}029580\lg a_{\left[Mn(OH)_4\right]^{2-}}$
16	$7Mn^{2+} + 3Mn_{11}Ge_8 + 14e = 8Mn_5Ge_3$	$\varphi = -1{,}0397 + 0{,}029580\lg a_{Mn^{2+}}$
17	$7Mn(OH)_2 + 3Mn_{11}Ge_8 + 14H^+ + +14e = 8Mn_5Ge_3 + 14H_2O$	$\varphi = -0{,}59969 - 0{,}059159pH$
18	$7\left[Mn(OH)_4\right]^{2-} + 3Mn_{11}Ge_8 + 28H^+ + +14e = 8Mn_5Ge_3 + 28H_2O$	$\varphi = 0{,}38902 - 0{,}11832pH + + 0{,}029580\lg a_{\left[Mn(OH)_4\right]^{2-}}$
19	$11Mn^{2+} + 8Ge + 22e = Mn_{11}Ge_8$	$\varphi = -1{,}0131 + 0{,}029580\lg a_{Mn^{2+}}$
20	$11Mn(OH)_2 + 8Ge + 22H^+ + +22e = Mn_{11}Ge_8 + 22H_2O$	$\varphi = -0{,}57309 - 0{,}059159pH$
21	$11\left[Mn(OH)_4\right]^{2-} + 8Ge + 44H^+ + +22e = Mn_{11}Ge_8 + 44H_2O$	$\varphi = 0{,}41562 - 0{,}11832pH + + 0{,}029580\lg a_{\left[Mn(OH)_4\right]^{2-}}$

22	$Mn^{2+} + 2H_2O = Mn(OH)_2 + 2H^+$	$pH = 7{,}4374 - 0{,}5\lg a_{Mn^{2+}}$
23	$Mn(OH)_2 + 2H_2O = \left[Mn(OH)_4\right]^{2-} + 2H^+$	$pH = 16{,}713 + 0{,}5\lg a_{Mn^{2+}}$
24	$Mn_2GeO_4 + 8H^+ + 4e = $ $= 2Mn^{2+} + Ge + 4H_2O$	$\varphi = -0{,}063453 - 0{,}11832pH -$ $- 0{,}029580\lg a_{Mn^{2+}}$ $\ln a_{Ge(A)} = 0$
25	$Mn_2GeO_4 + 4H^+ + 4e = $ $= 2Mn(OH)_2 + Ge$	$\varphi = -0{,}50344 - 0{,}059159pH$ $\ln a_{Ge(A)} = 0$
26	$Mn_2GeO_4 + 4H_2O + 4e = $ $= 2\left[Mn(OH)_4\right]^{2-} + Ge$	$\varphi = -1{,}4922 -$ $- 0{,}029580\lg a_{\left[Mn(OH)_4\right]^{2-}}$ $\ln a_{Ge(A)} = 0$
27	$GeO_2 + 4H^+ + 4e = Ge + 2H_2O$	$\varphi = -0{,}29380 - 0{,}059159pH$ $\ln a_{Ge(A)} = 0$
28	$GeO_2 + H_2O = HGeO_3^- + H^+$	$pH = 20{,}222 + \lg a_{HGeO_3^-}$
29	$2Mn^{2+} + GeO_2 + 2H_2O = $ $= Mn_2GeO_4 + 4H^+$	$pH = 3{,}8936 - 0{,}5\lg a_{Mn^{2+}}$
30	$Mn_3O_4 + 2H^+ + 2e = 3Mn(OH)_2 + H_2O$	$\varphi = 0{,}48505 - 0{,}059159pH$
31	$Mn_3O_4 + 8H_2O + 2e = $ $= 3\left[Mn(OH)_4\right]^{2-} + 4H^+$	$\varphi = -2{,}4811 + 0{,}11832pH -$ $- 0{,}088738\lg a_{\left[Mn(OH)_4\right]^{2-}}$
32	$Mn_3O_4 + 8H^+ + 2e = 3Mn^{2+} + 4H_2O$	$\varphi = 1{,}8050 - 0{,}23664pH -$ $- 0{,}088738\lg a_{Mn^{3+}}$
33	$3Mn_2O_3 + 2H^+ + 2e = 2Mn_3O_4 + H_2O$	$\varphi = 0{,}83018 - 0{,}059159pH$

34	$Mn_2O_3 + 5H_2O + 2e = 2\left[Mn(OH)_4\right]^{2-} + 2H^+$	$\varphi = -1{,}3773 + 0{,}059159pH - 0{,}059159\lg a_{\left[Mn(OH)_4\right]^{2-}}$
35	$2MnO_2 + 2H^+ + 2e = Mn_2O_3 + H_2O$	$\varphi = 0{,}97424 - 0{,}059159pH$
36	$Mn_2O_3 + 6H^+ + 2e = 2Mn^{2+} + 3H_2O$	$\varphi = 1{,}4801 - 0{,}17748pH - 0{,}059159\lg a_{Mn^{2+}}$
37	$Mn_2O_3 + HGeO_3^- + 3H^+ + 2e = Mn_2GeO_4 + 2H_2O$	$\varphi = 1{,}6176 - 0{,}088738pH + 0{,}029580\lg a_{HGeO_3^-}$
38	$2MnO_2 + HGeO_3^- + 5H^+ + 4e = Mn_2GeO_4 + 3H_2O$	$\varphi = 1{,}2959 - 0{,}73949pH + 0{,}014790\lg a_{HGeO_3^-}$
39	$2MnO_2 + GeO_2 + 4H^+ + 4e = Mn_2GeO_4 + 2H_2O$	$\varphi = 0{,}99681 - 0{,}059159pH$
40	$MnO_2 + 4H^+ + 2e = Mn^{2+} + 2H_2O$	$\varphi = 1{,}2272 - 0{,}11832pH - 0{,}029580\lg a_{Mn^{2+}}$
41	$MnO_4^{3-} + 4H^+ + e = MnO_2 + 2H_2O$	$\varphi = 4{,}2377 - 0{,}23664pH + 0{,}059159\lg a_{MnO_4^{3-}}$
42	$MnO_4^{2-} + e = MnO_4^{3-}$	$\varphi = 0{,}3 + 0{,}059159\lg \frac{a_{MnO_4^{2-}}}{a_{MnO_4^{3-}}}$
43	$MnO_4^{2-} + 4H^+ + 2e = MnO_2 + 2H_2O$	$\varphi = 2{,}2688 - 0{,}11832pH + 0{,}029580\lg a_{MnO_4^{2-}}$
44	$MnO_4^- + e = MnO_4^{2-}$	$\varphi = 0{,}558 + 0{,}059159\lg \frac{a_{MnO_4^-}}{a_{MnO_4^{2-}}}$

45	$MnO_4^- + 4H^+ + 3e = MnO_2 + 2H_2O$	$\varphi = 1{,}6986 - 0{,}078879pH + + 0{,}019720\lg a_{MnO_4^-}$
46	$Mn^{3+} + e = Mn^{2+}$	$\varphi = 1{,}51 + 0{,}059159\lg \frac{a_{Mn^{3+}}}{a_{Mn^{2+}}}$
47	$MnO_2 + 4H^+ + e = Mn^{3+} + 2H_2O$	$\varphi = 0{,}94432 - 0{,}23664pH - - 0{,}059159\lg a_{Mn^{3+}}$
48	$MnO_4^- + 8H^+ + 4e = Mn^{3+} + 4H_2O$	$\varphi = 1{,}51 - 0{,}11832pH + + 0{,}059159\lg \frac{a_{MnO_4^-}}{a_{Mn^{3+}}}$

На диаграммах, представленных на рисунках 6а – 6г, можно выделить 38 областей термодинамической устойчивости различных фаз системы:

I. $Mn_{(\alpha)} + \beta + \gamma + Mn_{3,4}Ge + Mn_7Ge_3 + Mn_5Ge_3 + Mn_{11}Ge_8 + Ge_{(алмаз)}$;

II. $\beta + \gamma + Mn_{3,4}Ge + Mn_7Ge_3 + Mn_5Ge_3 + Mn_{11}Ge_8 + Ge_{(алмаз)} + Mn^{2+}$;

III. $\beta + \gamma + Mn_{3,4}Ge + Mn_7Ge_3 + Mn_5Ge_3 + Mn_{11}Ge_8 + Ge_{(алмаз)} + Mn(OH)_2$;

IV. $\beta + \gamma + Mn_{3,4}Ge + Mn_7Ge_3 + Mn_5Ge_3 + Mn_{11}Ge_8 + Ge_{(алмаз)} + \left[Mn(OH)_4\right]^{2-}$;

V. $\gamma + Mn_{3,4}Ge + Mn_7Ge_3 + Mn_5Ge_3 + Mn_{11}Ge_8 + Ge_{(алмаз)} + Mn^{2+}$;

VI. $\gamma + Mn_{3,4}Ge + Mn_7Ge_3 + Mn_5Ge_3 + Mn_{11}Ge_8 + Ge_{(алмаз)} + Mn(OH)_2$;

VII. $\gamma + Mn_{3,4}Ge + Mn_7Ge_3 + Mn_5Ge_3 + Mn_{11}Ge_8 + Ge_{(алмаз)} + \left[Mn(OH)_4\right]^{2-}$;

VIII. $Mn_{3,4}Ge + Mn_7Ge_3 + Mn_5Ge_3 + Mn_{11}Ge_8 + Ge_{(алмаз)} + Mn^{2+}$;

IX. $Mn_{3,4}Ge + Mn_7Ge_3 + Mn_5Ge_3 + Mn_{11}Ge_8 + Ge_{(алмаз)} + Mn(OH)_2$;

X. $Mn_{3,4}Ge + Mn_7Ge_3 + Mn_5Ge_3 + Mn_{11}Ge_8 + Ge_{(алмаз)} + \left[Mn(OH)_4\right]^{2-}$;

XI. $Mn_7Ge_3 + Mn_5Ge_3 + Mn_{11}Ge_8 + Ge_{(алмаз)} + Mn^{2+}$;

XII. $Mn_7Ge_3 + Mn_5Ge_3 + Mn_{11}Ge_8 + Ge_{(алмаз)} + Mn(OH)_2$;

XIII. $Mn_7Ge_3 + Mn_5Ge_3 + Mn_{11}Ge_8 + Ge_{(алмаз)} + \left[Mn(OH)_4\right]^{2-}$;

XIV. $Mn_5Ge_3 + Mn_{11}Ge_8 + Ge_{(алмаз)} + Mn^{2+}$;

XV. $Mn_5Ge_3 + Mn_{11}Ge_8 + Ge_{(алмаз)} + Mn(OH)_2$;

XVI. $Mn_5Ge_3 + Mn_{11}Ge_8 + Ge_{(адмах)} + \left[Mn(OH)_4\right]^{2-}$;

XVII. $Mn_{11}Ge_8 + Ge_{(алмаз)} + Mn^{2+}$;

XVIII. $Mn_{11}Ge_8 + Ge_{(алмаз)} + Mn(OH)_2$;

XIX. $Mn_{11}Ge_8 + Ge_{(алмаз)} + \left[Mn(OH)_4\right]^{2-}$;

XX. $Ge_{(алмаз)} + Mn^{2+}$;

XXI. $Ge_{(алмаз)} + Mn(OH)_2$;

XXII. $Ge_{(алмаз)} + \left[Mn(OH)_4\right]^{2-}$;

XXIII. $GeO_2 + Mn^{2+}$;

XXIV. $Mn_2GeO_4 + Mn^{2+}$;

XXV. $Mn_2GeO_4 + Mn(OH)_2$;

XXVI. $Mn_2GeO_4 + \left[Mn(OH)_4\right]^{2-}$;

XXVII. $Mn_2GeO_4 + Mn_3O_4$;

XXVIII. $Mn_2GeO_4 + Mn_2O_3$;

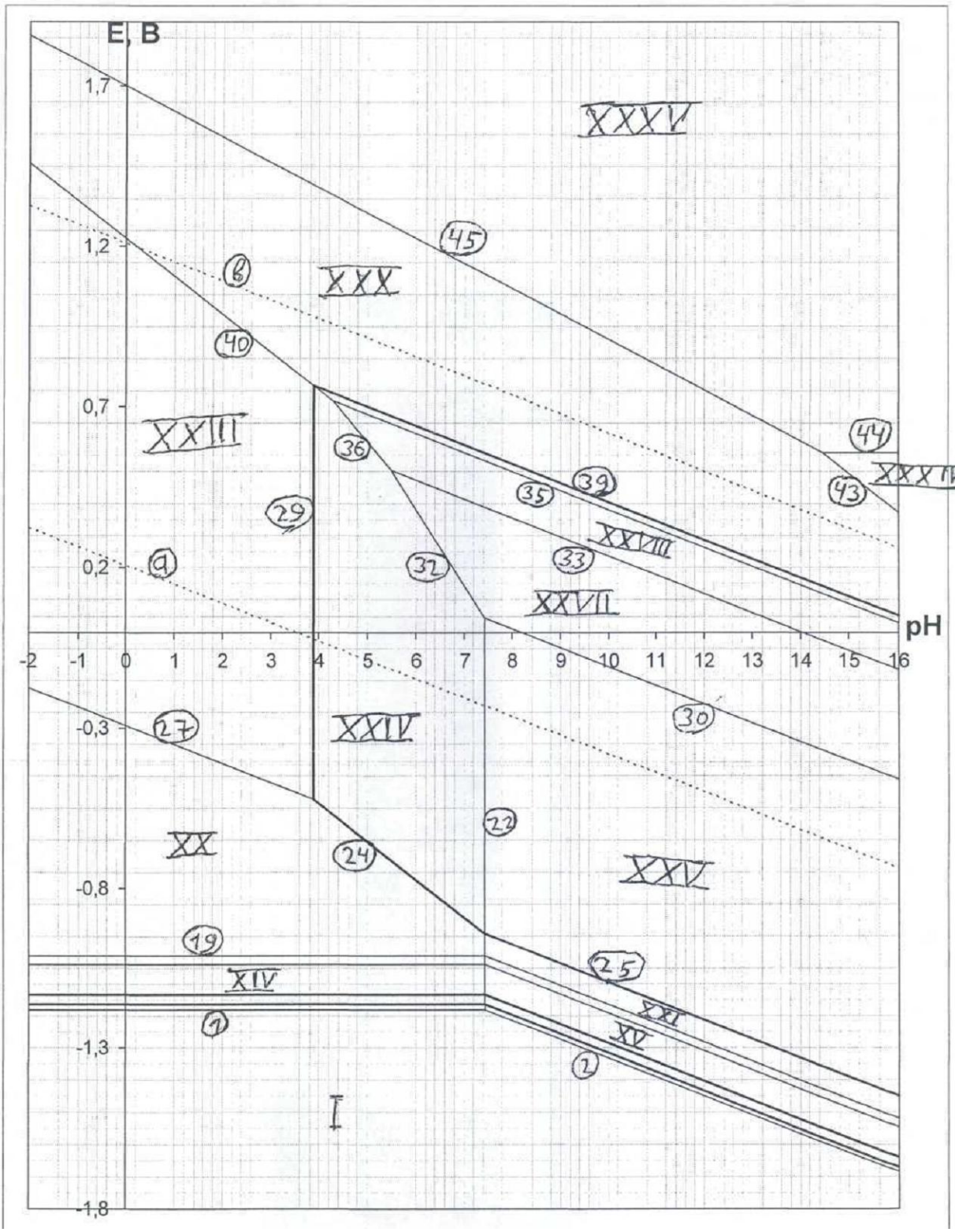

Рис. 6а. Диаграмма потенциал – pH системы Mn – Ge – H_2O при 25°C, 1 бар и 1 моль/л.

Fig. 6a. The potential – pH diagram of the Mn – Ge – H_2O system at 25°C, 1 bar and 1 mol/l.

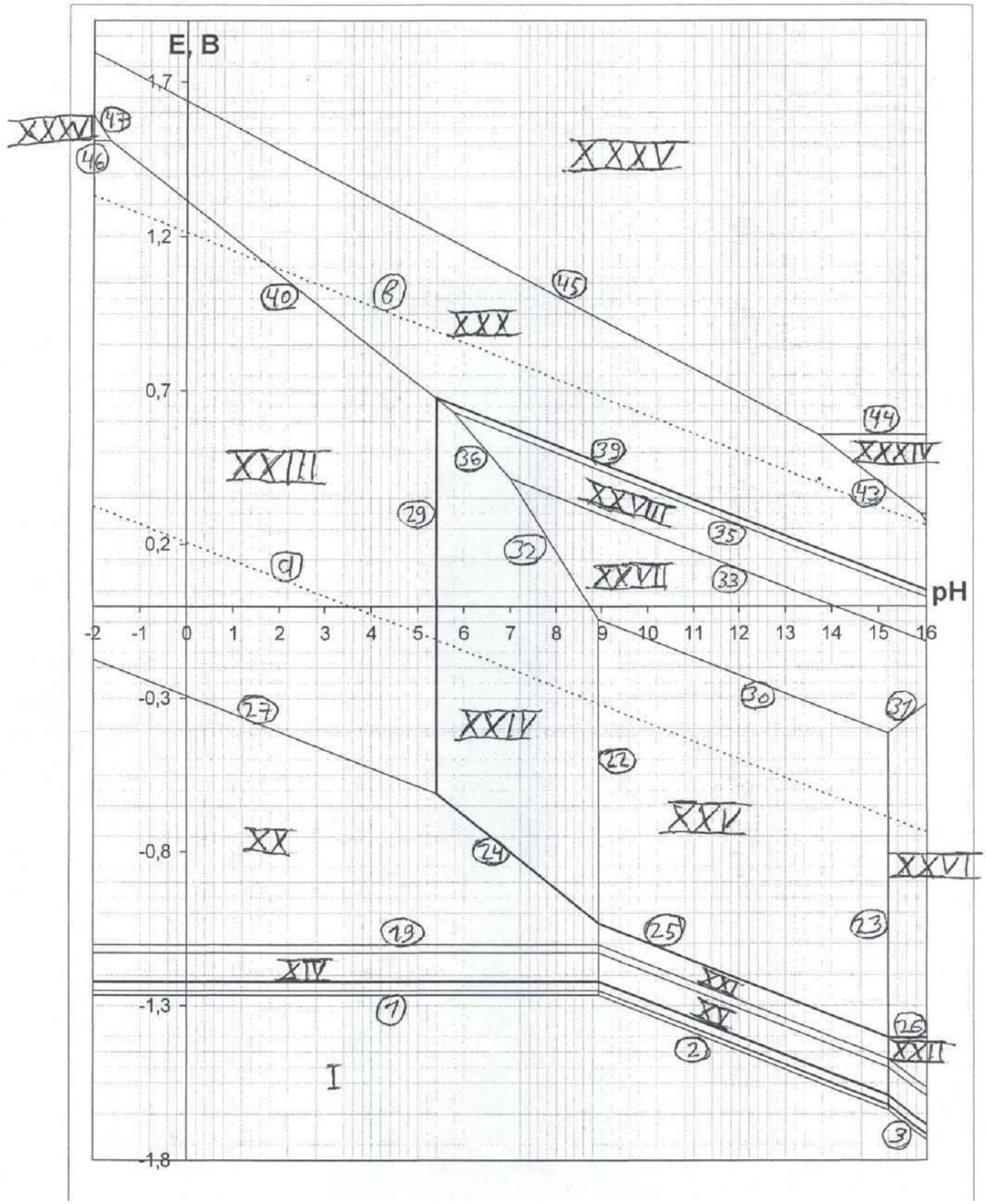

Рис. 6б. Диаграмма потенциал – pH системы Mn – Ge – H_2O при 25°C, 1 бар и 10^{-3} моль/л.

Fig. 6b. The potential – pH diagram of the Mn – Ge – H_2O system at 25°C, 1 bar and 10^{-3} mol/l.

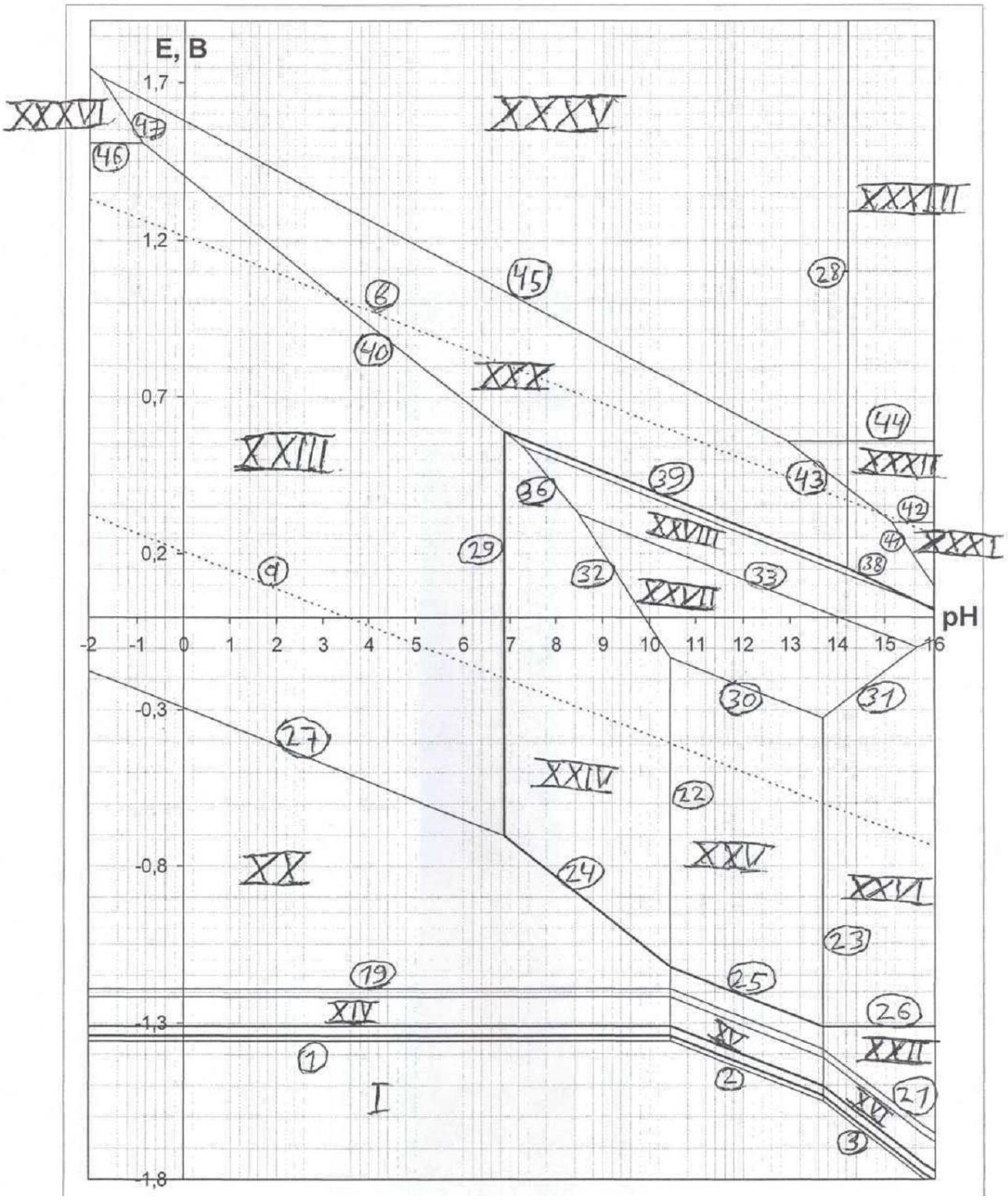

Рис. 6в. Диаграмма потенциал – pH системы Mn – Ge – H_2O при 25°C, 1 бар и 10^{-6} моль/л.

Fig. 6c. The potential – pH diagram of the Mn – Ge – H_2O system at 25°C, 1 bar and 10^{-6} mol/l.

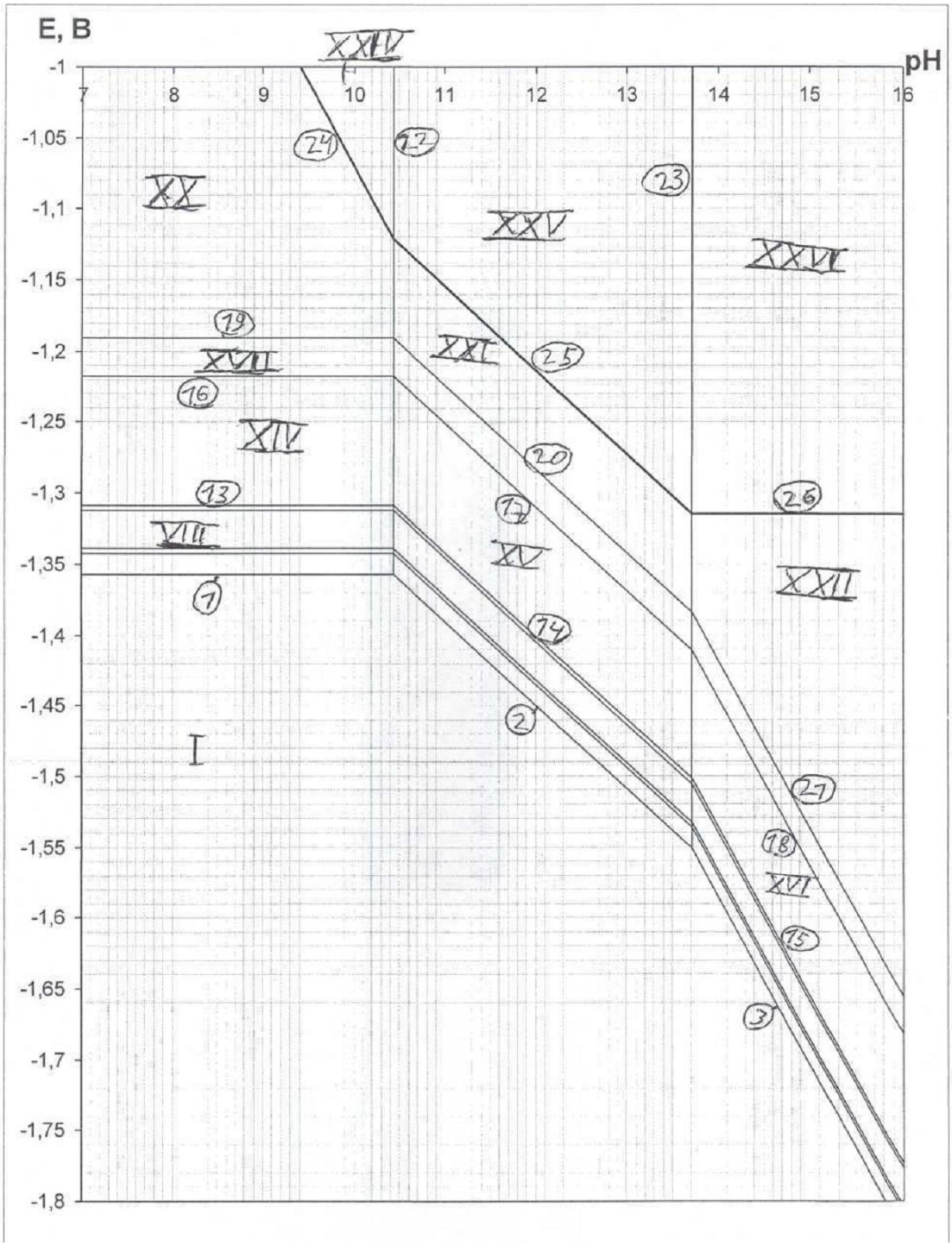

Рис. 6г. Сечение диаграммы потенциал – pH системы Mn – Ge – H_2O при 25°C, 1 бар и 10^{-6} моль/л в области активного растворения германидов марганца.

Fig. 6d. The potential – pH diagram of the Mn – Ge – H_2O system at 25°C, 1 bar and 10^{-6} mol/l in the area of the active dissolution of manganese germanides.

XXIX. $Mn_2GeO_4 + MnO_2$;

XXX. $GeO_2 + MnO_2$;

XXXI. $HGeO_3^- + MnO_4^{3-}$;

XXXII. $HGeO_3^- + MnO_4^{2-}$;

XXXIII. $HGeO_3^- + MnO_4^-$;

XXXIV. $GeO_2 + MnO_4^{2-}$;

XXXV. $GeO_2 + MnO_4^-$;

XXXVI. $GeO_2 + Mn^{3+}$;

XXXVII. $HGeO_3^- + Mn_2O_3$;

XXXVIII. $HGeO_3^- + MnO_2$.

Область I – это область иммунности всех возможных структурных составляющих системы марганец-германий (двух твёрдых растворов замещения, четырёх интерметаллидов, марганца и германия в виде чистых простых веществ). В областях II – XII протекает селективное превращение марганца. Вид образующегося продукта при этом зависит от pH, концентрации и ионной силы раствора (Mn^{2+}, $Mn(OH)_2$, $[Mn(OH)_4]^{2-}$). Соответственно, превращение марганца в ионы приводит к его растворению, а в гидроксид – к образованию пассивационной плёнки, затормаживающей дальнейшую коррозию. При этом $Mn(OH)_2$ термодинамически более устойчив соответствующего оксида MnO. В областях XXIV – XXIX наблюдается общая коррозия сплавов с образованием пассивационной плёнки Mn_2GeO_4. В областях XXXIV –XXXVI и

XXIII происходит общая коррозия сплавов с растворением марганца и окисления германия до GeO_2 (оксидная пассивация сплавов плёнкой диоксида германия). В областях XXXVII и XXXVIII происходит общая коррозия сплавов с растворением германия и образования пассивационной плёнки оксидов марганца. В области XXX происходит общая коррозия сплавов с образованием диоксидов марганца и германия. В областях XXXI – XXXIII происходит полное растворение всех материалов.

5. ВЫВОДЫ

1. Проведена оценка стандартных энергий Гиббса образования германидов и германатов марганца $Mn_{3,4}Ge$, Mn_7Ge_3, Mn_5Ge_3, $Mn_{11}Ge_8$, $MnGeO_3$ и Mn_2GeO_4.
2. В рамках модели растворов замещения описаны термодинамические свойства β- и γ-твёрдых металлических растворов системы Mn – Ge и оценены значения энергий Гиббса фазовых переходов чистых германия и марганца в γ-фазу. Показаны отрицательные отклонения твёрдых растворов от идеальности.
3. Рассчитаны сечения фазовых диаграмм Mn – Ge и Mn – Ge – O при 25°C.
4. Рассчитана диаграмма потенциал – pH системы Mn – Ge – H_2O при 25°C, 1 бар и различных активностях ионов в растворе.

Рассмотрены термодинамические особенности коррозионно-электрохимического поведения германия и железа в сплавах при различных электродных потенциалах и pH растворов.

СПИСОК ЛИТЕРАТУРЫ

REFERENCES

1. Княжева В. М., Бабич, С. Г., Колотыркин В. И., Кожевников В. Б. Металлоподобные соединения переходных металлов – новый класс коррозионностойких материалов и покрытий // Защита металлов, 1991. Т. 27. № 4. С. 603 – 616.

Knyazheva V. M., Babich S. G., Kolotyrkin V. I., Kozhevnikova V. B. Metallopodobnye soyedineniya perekhodnykh metallov – novyi klass korrozionnostoikikh materialov i pokrytii [Metal-like transition metals compounds – a new class of corrosion-resistant materials and coatings] // Zashchita metallov, 1991. Vol. 27. No. 4. P. 603 – 616 [In Russian].

2. Ohoyama T. X-ray and Magnetic Studies of the Manganese-Germanium System // Journal of the Physical Society of Japan, 1961. Vol. 16. No 10. P. 1995 – 2002.

3. Durman E., Acel M., Dincer I., Elmali A., Elerman Y. Competing magnetic interactions in rare-earth manganese silicides and germanides // Journal of Magnetism and Magnetic Materials, 2007. Vol. 309. No 1. P. 40 – 53.

4. Cho S., Choi S., Hong S. C., Kim Y., Ketterson J. B., Kim B.-J., Kim Y. C., Jung Y.-H. Ferromagnetism in Mn-doped Ge // Physical Review B, 2002. Vol. 66. No 3. Article 033303. P. 1 – 3.

5. Aoyama I., Fedorov M. I., Zaitsev V. K., Solomkin F. Yu., Eremin E. S., Samunin A. Yu., Mikoujima M., Sano S., Tsuji T. Effects of Ge Doping on Micromorphology of MnSi in $MnSi_{\sim 1.7}$ and on Their Thermoelectric Transport Properties // Japanese Journal of Applied Physics, 2005. Vol. 44. Part 1. No 12. P. 8562 – 8570.

6. Шеин А. Б. Электрохимия силицидов и германидов переходных металлов: монография. Пермь: Изд-во Пермского гос. ун-та, 2009. 257 с.

Shein A. B. Elektrokhimiya silitcidov i germanidov perekhodnykh metallov: monografiya [The electrochemistry oft he silicides and germanides of transition metals: a monograph]. Perm: Izdatel'stvo Permskogo gos. un-ta, 2009. 257 p [In Russian].

7. Шеин А. Б. Коррозионно-электрохимическое поведение Mn_5Si_3, Mn_5Ge_3 и $Mn_5(Ge_{1-x}Si_x)_3$ в сернокислом электролите // Ползуновский вестник, 2009. № 3. С. 247 – 252.

Shein A. B. Korrozionno-elektrokhimicheskoye povedeniye Mn_5Si_3, Mn_5Ge_3 i $Mn_5(Ge_{1-x}Si_x)_3$ v sernokislom elektrolite [The corrosion-electrochemical behaviour of Mn_5Si_3, Mn_5Ge_3 and $Mn_5(Ge_{1-x}Si_x)_3$ in the sulphuric acid electrolyte] // Polzunovskii Vestnik, 2009. No 3. P. 247 – 252 [In Russian].

8. Диаграммы состояния двойных металлических систем: справ. изд. В 3 т. Т. 2; под. ред. Н. П. Лякишева. М.: Машиностроение, 1997. 1024 с.

Diagrammy sostoyaniya dvoinykh metallicheskikh system: sprav. izd [Phase diagrams of binary metallic systems: a handbook]. In 3 volumes. Vol. 2; Ed. Lyakishev N. P. Moscow: Mashinostroyeniye, 1997. 1024 p [In Russian].

9. Berche A., Tedenac J. C., Jund P. Thermodynamic modeling of the germanium – manganese system // Intermetallics, 2014. Vol. 47. P. 23 – 30.

10. Arras E., Caliste D., Deutsch T., Lançon F., Pochet P. Phase diagram, structure, and magnetic properties of the Ge-Mn system: A first-principles study // Physical Review B, 2011. Vol. 83. No 17. Article 174103. P. 1 – 12.

11. Gokhale A. B., Abbaschian R. The Ge-Mn (Germanium-Manganese) system // Bulletin of Alloy Phase Diagrams, 1990. Vol. 11. No 5. P. 460 – 468.

12. Redlich O., Kister A. T. Algebraic representation of thermodynamic properties and the classification of solutions // Industrial and Engineering Chemistry, 1948. Vol. 40. No 2. P. 345 – 348.

13. NASA Thermo Build Database.

URL: http://www.grc.nasa.gov/WWW/CEAWeb/ceaThermoBuild.htm.

Accessed 10 March 2016.

14. Физическая химия неорганических материалов. В 3 т.; под общ. ред. В. Н. Ерёменко. Киев: Наукова думка, 1988. Т. 1: Термодинамика интерметаллидов и фазовые равновесия в металлических системах / Л. В. Артюх, Ю. И. Буянов, Т. Я. Великанова et al. С. 9 – 70. Fizicheskaya khimiya neorganicheskikh materialov [Physical Chemistry of Inorganic Materials]. In 3 Volumes. Ed. Eryomenko V. N. Kiev: Naukova dumka, 1988. Vol. 1. Termodinamika intermetallidov i fazovyye ravnovesiya v metallicheskikh sistemakh [Thermodynamics of intermetallides and phase equilibria in metallic systems] / Artyukh L. V., Buyanov Yu. I., Velikanova T. Ya et al.. P. 9 – 70 [In Russian].

15. van't Hoff, M. J. H. Études de dynamique chimique [Studies on chemical dynamics] // Recueil des Travaux Chimiques des Pays-Bas, 1884. Vol. 3. No 10. P. 333 – 336 [In French].

16. Волков А. И., Жарский И. М. Термодинамические характеристики веществ: справочник. Минск: Букмастер, 2014. 288 с. Volkov A. I., Zharskiy I. M. Termodinamicheskiye kharakteristiki veshchestv: spravochnik [Thermodynamic Properties of the Substances: A Handbook]. Minsk: Bukmaster, 2014. 288 p [In Russian].

17. Takayama E. The system GeO_2 – MnO – Mn_2O_3 at 900°C // Journal of Solid State Chemistry, 1981. Vol. 39. No 1. P. 133 – 134.

18. Киреев В. А. Курс физической химии. Изд. 3-е. М.: Химия, 1975. 776 с.

Kireev V. A. Kurs fizicheskoi khimii [A Course of Physical Chemistry]. 3rd Edn. Moscow: Khimiya, 1975. 776 p [In Russian].

19. Николайчук П. А., Шаляпина Т. И., Тюрин А. Г., Мосукова Т. В. Термодинамика химической и электрохимической устойчивости сплавов системы Mn – Si // Вестник Южно-Уральского государственного университета. Серия "Химия", 2010. Вып. 4. № 31 (207). С. 72 – 82.

Nikolaychuk P. A., Shalyapina T. I., Tyurin A. G., Mosunova T. V. Termodinamika khimicheskoi i elektrokhimicheskoi ustoichivosti splavov sistemy Mn – Si [Thermodynamics of Chemical and Electrochemical Stability of Mn – Si system Alloys] // Vestnik Yuzhno-Ural'skogo gosudarstvennogo universiteta. Seriya "Khimiya", 2010. Issue 4. No 31(207). P. 72 – 82 [In Russian].

20. Тюрин А. Г. Термодинамика химической и электрохимической устойчивости твёрдых сплавов железа, хрома и никеля. Челябинск: Издательство Челябинского государственного университета, 2012. 241 с.

Tyurin A. G. Termodinamika khimicheskoi i elektrokhimicheskoi ustoichivosti tvyordykh splavov zheleza, khroma i nikelya [Thermodynamics of Chemical and Electrochemical Stability of the Solid Iron, Chromium and Nickel Alloys]. Chelyabinsk: Izdatel'stvo Chelyabinskogo gosudarstvennogo universiteta, 2012. 241 p [In Russian].

21. Тюрин А. Г., Николайчук П. А., Канатьева И. И. Термодинамика химической и электрохимической устойчивости сплавов системы Fe – Ge // Коррозия: материалы, защита, 2015. № 12. С. 1 – 9.

Tyurin A. G., Nikolaychuk P. A., Kanatyeva I. I. Termodinamika khimicheskoi I elektrokhimicheskoi ustoichivosti splavov sistemy Fe – Ge [Thermodynamics of Chemical and Electrochemical Stability of Fe – Ge system Alloys] // Korroziya: materialy, zashchita, 2015.No 12. P. 1 – 9 [In Russian].

22. Справочник по электрохимии; под ред. Сухотина А. М. Л.: Химия, 1981. 488 с.

Spravochnik po elektrokhimii [Handbook on Electrochemistry]; Ed. Sukhotin A. M. Leningrad: Khimiya, 1981. 488 p [In Russian].

23. Speight J. Lange's Handbook of Chemistry, 16th Edition. New York: McGraw-Hill Education, 2005. 1623 p.

24. Лурье Ю. Ю. Справочник по аналитической химии. Изд. 6-е. М.: Химия, 1989. 448 с.

Lur'e Yu. Yu. Spravochnik po analiticheskoi khimii [Handbook on Analytical Chemistry]. 6th Edn. Moscow: Khimiya, 1989. 488 p [In Russian].

11. Fe – Si system

Iron – silicon is a very important binary system for metallurgy. Iron silicides are perspective materials; they are well-known for their unusual magnetic, optical and thermodynamic properties [Paschen et al., 1997]. Iron-silicon alloys could be found in Earth's core [Lin, 2002], they are using in technology as thin films [Lau et al., 1975] and nanowires [Hu, Odom, Lieber, 1999]. Moreover, many important ternary and multicomponent systems, including Fe – Si binary system are of great interest to the researches. The Fe – Si system was therefore studied very thoroughly. The chemical and electrochemical stability of the Fe – Si system was already assessed earlier [Tyurin, 2004]. However, that study did not take into account all features of the system and relied on the outdated thermodynamic information. Therefore, a new assessment was performed.

11.1. Iron silicides

According to the Fe – Si phase diagram (see Figure 50), several intermetallic phases exist in system, namely Fe_3Si_7, $FeSi_2$, FeSi, Fe_5Si_3 and Fe_2Si. But only $FeSi_2$ and FeSi are thermodynamically stable at standard conditions. FeSi has a narrow homogeneity range [Patrin et al., 2006], from $FeSi_{0.961}$ to $FeSi_{1.033}$, which does not depend on temperature. The solid solubility of Si in (bcc-Fe) is equal to about 25 atomic percent at ambient temperatures, and silicon could form three types of solutions. The first one is the disordered phase, in which only short range ordering exists (α-phase), two others have long range atomic ordering: α_2-phase and α_1-phase. Additionally, a miscibility gap exists between α_2 and α_1 phases. Moreover, a fully ordered α_1-phase is often treated as independent compound Fe_3Si [Gude, Mehrer, 1997]. Upon a rapid cooling of the system from the temperatures of 1100 °C and higher, the solubility of Fe in (diamond-Si) might achieve 4 atomic % [Miki, Morita, Sano, 1997; Morita, Miki, 2003; Struthers, 1956]. Upon a cooling from lower temperatures no solubility is detected.

Several authors presented the different thermodynamic models for the system. Figure 51 compares the solubility of silicon in α-phase calculated using these models with the phase diagram. The expression for the excess Gibbs energy of α-phase was taken from [Kaufman, 1979] because this expression gives the most satisfactory convergence between

the phase diagram data and the calculations. The activities of the components of solid solution corresponding to maximum silicon solubility in α_1-phase are the following: $a_{Fe(\alpha_1)} = 0.473$ and $a_{Si(\alpha_1)} = 5.5 \cdot 10^{-20}$ meaning strong negative deviations from ideal behaviour. The solid solubility of silicon in disordered α-phase at 25°C is about ~11 at. %. The activities of the components in this solution are equal to $a_{Fe(\alpha)} = 0.13$, $a_{Si(\alpha)} = 5.0 \cdot 10^{-20}$. The standard Gibbs energies of formation of iron silicides were collected from [Acker et al., 1999b; Dean, 1979; Dean, 1999; Kaufman, 1979; Lacaze, Sundman, 1991; Lee, Lee, Lee, 1987; Speight, 2005; Термические константы веществ, 2007]. More details are provided in the attached publication.

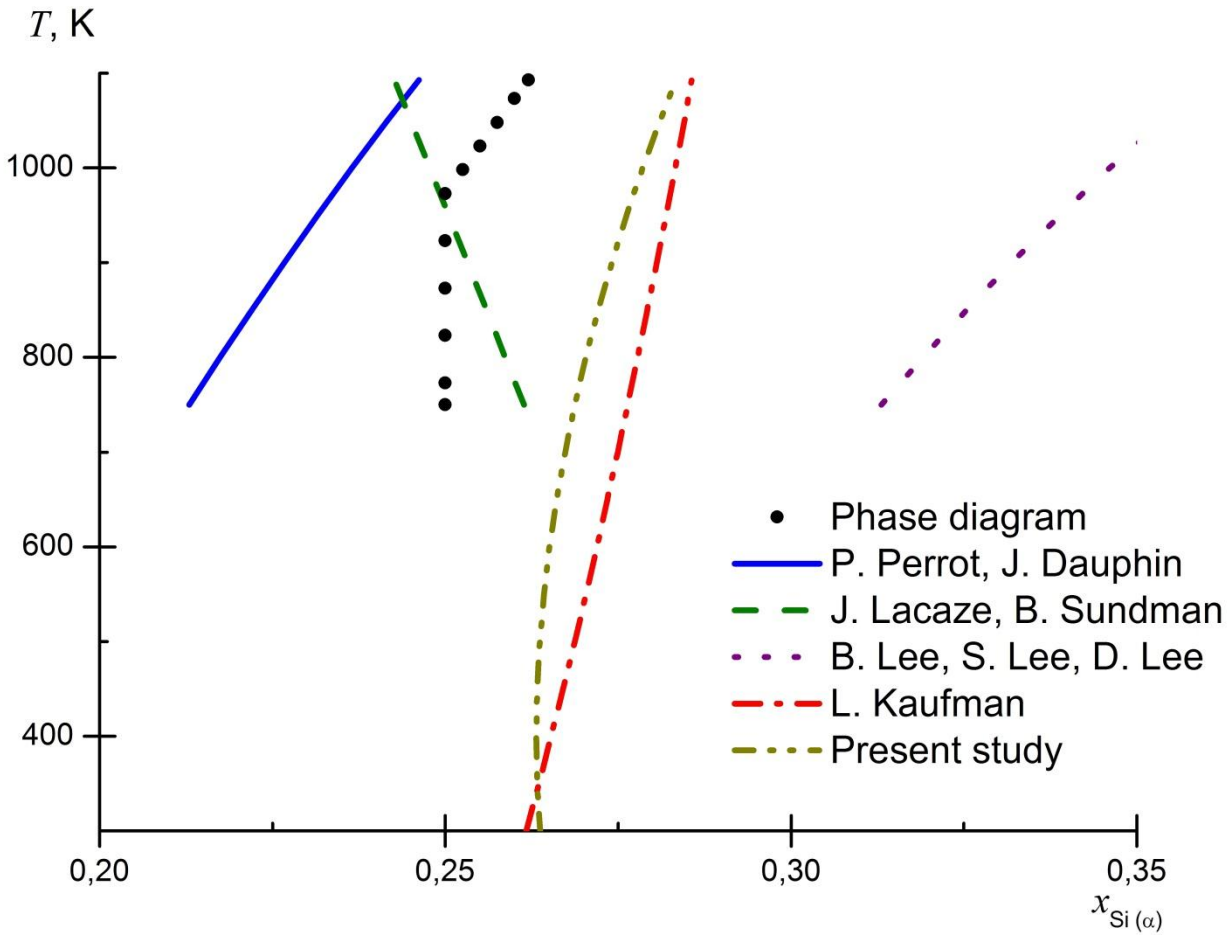

Fig. 51. The solid solubility of Si in (α-Fe) calculated by different models.

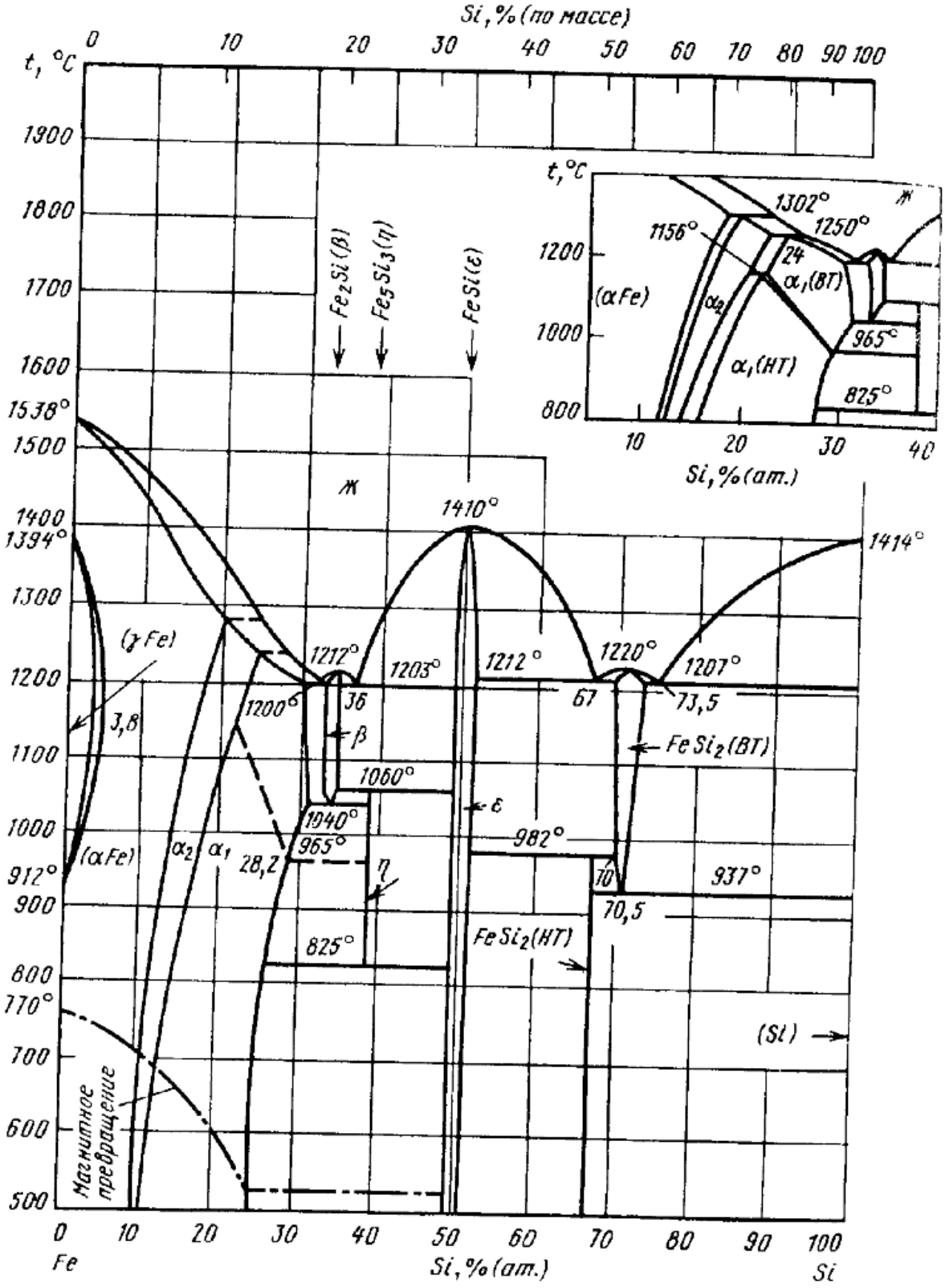

Fig. 50. The phase diagram of the Fe – Si system [Диаграммы состояния двойных металлических систем: справочник, 2001].

11.2. Equilibira in Fe – Si – O system

Iron could form the following oxides: FeO, Fe_3O_4 and Fe_2O_3. However, FeO is not thermodynamically stable at temperatures below 570˚C [Kaufman, 1979]. Fe_3O_4 and Fe_2O_3 have noticeable homogeneity ranges at elevated temperatures but they are stoichiometric compounds at 25˚C. Only one ternary compound exists in Fe – Si – O system, and it is Fe_2SiO_4 [Navrotsky, 1971]. Another compound, $FeSiO_3$, exists only at elevated temperatures and pressures [Fabrichnaya, Sundman, 1997]. A solid solution of Fe_3O_4 in Fe_2SiO_4 can be formed [Лыкасов, Кимяшов, 2010] and its maximum solubility at 25˚C equals $6.85 \cdot 10^{-5}$ atomic %. In addition, up to $1.54 \cdot 10^{-3}$ atomic % of SiO_2 can be dissolved in Fe_2O_3 [Лыкасов, Кимяшов, 2010]. The values of standard Gibbs energies of formation of iron oxides were obtained from [Charette, Flengas, 1968; Chase Jr. et al., 1985; Термические константы веществ, 2007], the values for Fe_2SiO_4 were obtained from [Jacobs, Jong de, Oonk, 2001; Navrotsky, 1971; Yong et al., 2007].

It was known, that Fe (IV) could be present in the mixed oxides such as Ba_2FeO_4 or K_4FeO_4 in the form of layers with the composition of FeO_2 [Cotton, Wilkinson, 1971; 周震涛, 廖宗友, 2003]. It was already hypothesised earlier, that iron (IV) oxide might exist, and the attempts to build an iron oxidation thermodynamic model with its participation were made [Klyushin, Gorichev, Malov, 1973]. Therefore, a prediction of the thermodynamic properties of the compound „FeO_2“ is made using Kireev's and Gorichev's methods.

More details, including the state diagram of the Fe – Si – O system and the list of equilibria in it, are provided in the attached publication. It was shown that the hypothetical compound „FeO_2“ would not be thermodynamically stable at the atmospheric conditions.

11.3. Potential – pH diagram of Fe – H_2O system

Iron could form ferrous (Fe^{2+}) and ferric (Fe^{3+}) cations, as well as ferrate-anions (FeO_4^{2-}) in concentrated water solutions.

The potential – pH diagram of Fe – H_2O system at 25 °C, air pressure of 1 bar and the activities of iron species of 1 mol·l^{-1} is presented in Figure 52.

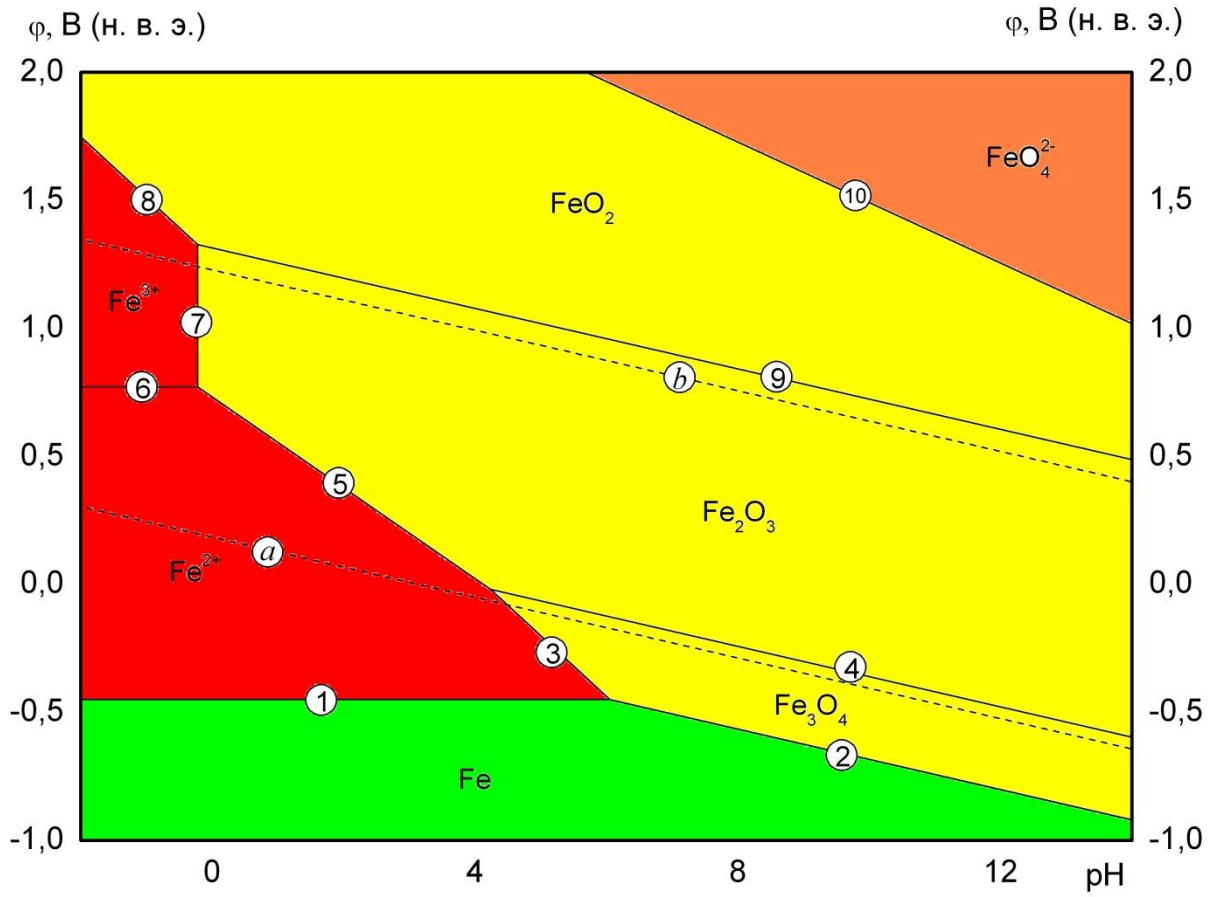

Fig. 52. The potential – pH diagram of Fe – H_2O system at 25 °C, air pressure of 1 bar and the activities of iron species in a solution of 1 M.

In diluted aqueous solutions in addition to the previous ones the anions $HFeO_2^-$ and FeO_2^{2-} might be formed, and the cations might be hydrolised. The potential – pH diagram of Fe – H_2O system at 25 °C, air pressure of 1 bar and the activities of iron species of 10^{-6} mol·l^{-1} taking into account these species is presented in the attached publication.

11.4. Potential – pH diagram of Fe – Si – H_2O system

The potential – pH diagram of Fe – Si – H_2O system is presented in the attached publication.

The calculations show that iron silicate plays a minor role in the corrosion-electrochemical behaviour of Fe – Si system alloys, because it is not thermodynamically stable in the domain of thermodynamic stability of water. The specific composition of oxide layer on Fe – Si alloys depends on their composition. Silicon is oxidised in the first order, but if its content in

alloy is insufficient to form a continuous passiviation layer, Fe_2O_3 could also be involved in its formation. Even Fe_2SiO_4 might be presented in in protective film in form of local inclusions due to the kinetic factors and the unreachability of true equilibrium.

Publications to chapter 11

The potential – pH diagram of Fe – H_2O system was published in the conference paper [Nikolaychuk, 2015b]. The potential – pH diagram of Fe – Si – H_2O system was published in another conference paper [Nikolaychuk, Tyurin, 2012b]. The extended version of this paper was submitted to peer-reviewed journal, but rejected for publication. The draft of this manuscript is also presented below.

УДК 544.653:544.016:544.313.2.031

THE POTENTIAL – pH DIAGRAM FOR Fe – H_2O SYSTEM

P. A. Nikolaychuk

Chelyabinsk State University, Chelyabinsk, Russia. E-mail: npa@csu.ru

Thermodynamic information on aqueous iron species is systematized. The reactions between various species are discussed. The activity – pH diagram for Fe^{III} species and the revised potential – pH diagram of Fe – H_2O system at 25ºC, 1 bar and $a_{[Fe]} = 10^{-6}$ mol l^{-1} are plotted.

Aqueous chemistry of iron is studied very widely. Several papers were focused on plotting a Pourbaix diagram for iron. However, the diagrams presented in various sources [1–3] aren't consistent with each other. This paper aims to collect and analyze available data on Gibbs energies of formation of iron species and revise the diagram.

Elemental iron has bcc lattice at standard conditions. Iron forms two well-known oxides, Fe_3O_4 and Fe_2O_3 [4]. Iron monoxide FeO is thermodynamically unstable and decomposes spontaneously according to the reaction 4FeO (s) → Fe (bcc) + Fe_3O_4 (s). Since iron can form mixed oxides with oxidation state equal to IV [5], it is interesting to make thermodynamic prediction of oxidation properties of hypothetical compound "FeO_2". The standard Gibbs energy of formation of "FeO_2" was estimated using methods proposed earlier [6,7]. In aqueous solution iron forms a variety of unhydrolyzed and hydrolyzed species with oxidation degrees II (Fe^{2+}, $FeOH^+$, $HFeO_2^-$, FeO_2^{2-}), III (Fe^{3+}, $FeOH^{2+}$, $Fe(OH)_2^+$, $Fe(OH)_4^-$) and VI (FeO_4^{2-}). Polymerized species like $Fe_2(OH)_2^{4+}$ and $Fe_3(OH)_4^{5+}$ and oxyhydrate FeOOH aren't considered. The standard Gibbs energies of formation used in calculations are presented in Table 1.

Calculations show that domains of thermodynamic stability of Fe^{II} species with respect to pH don't depend on activities of ions in solution. However, in diluted media, when $a_{[Fe]} < 10^{-8}$ mol l^{-1}, the domain of stability of Fe_3O_4 vanishes and $FeOH^+$ is oxidized directly to $HFeO_2^-$.

Table 1. The standard Gibbs energies of formation of iron species.

Compound	$\Delta_f G^o_{298}$, J mol^{-1}	Reference	Compound	$\Delta_f G^o_{298}$, J mol^{-1}	Reference
Fe_3O_4 (s)	–1 014 160	[8,9]	$FeOH^{2+}$(aq)	–244 800	[3]
Fe_2O_3 (s)	–742 200	[8,9]	$Fe(OH)_2^+$(aq)	–427 800	[3]
"FeO_2" (s)	–360 000	[6,7]	$Fe(OH)_4^-$(aq)	–842 200	[10]
Fe^{2+} (aq)	–86 600	[3]	$HFeO_2^-$(aq)	–405 800	[3]
Fe^{3+} (aq)	–12 100	[3]	FeO_2^{2-}(aq)	–295 300	[9]
$FeOH^+$ (aq)	–290 000	[3]	FeO_4^{2-}(aq)	–352 300	[3]

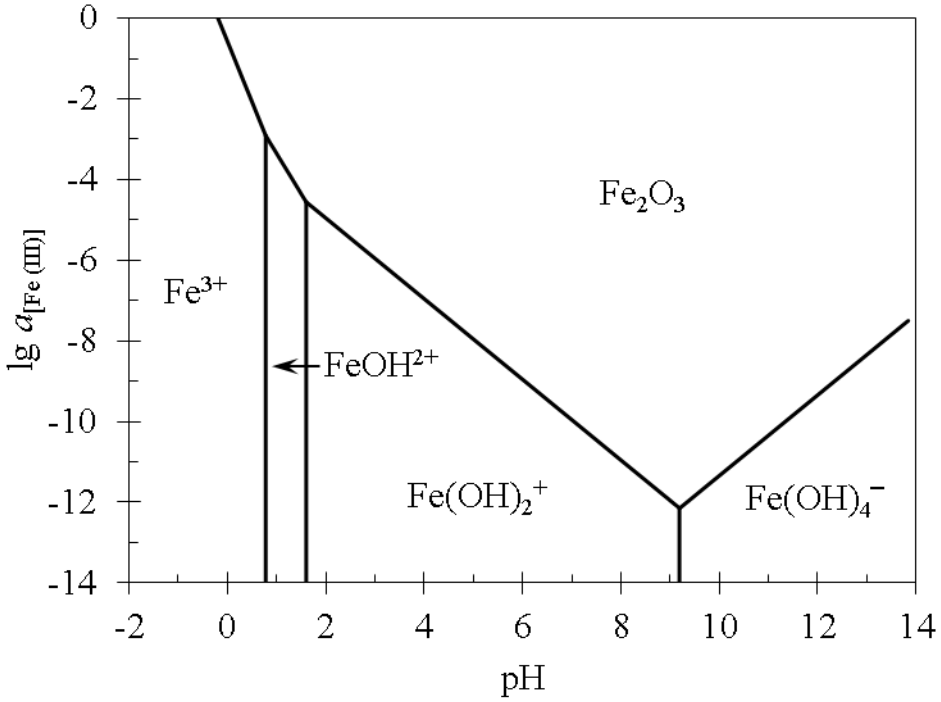

Figure 1. The activity – pH diagram for Fe^{III} species.

Figure 1 shows the predominance diagram of Fe^{III} species. The following order of oxidation is possible depending on ion activities:

lg $a_{[Fe]} > -2{,}91$: $Fe^{3+}(aq) \rightarrow Fe_2O_3(s) \rightarrow Fe(OH)_4^-(aq)$;

$-2{,}91 >$ lg $a_{[Fe]} > -4{,}56$: $Fe^{3+}(aq) \rightarrow FeOH^{2+}(aq) \rightarrow Fe_2O_3(s) \rightarrow \rightarrow Fe(OH)_4^-(aq)$;

$-4{,}56 >$ lg $a_{[Fe]} > -12{,}15$: $Fe^{3+}(aq) \rightarrow FeOH^{2+}(aq) \rightarrow Fe(OH)_2^+(aq) \rightarrow \rightarrow Fe_2O_3(s) \rightarrow Fe(OH)_4^-(aq)$;

lg $a_{[Fe]} < -12{,}15$: $Fe^{3+}(aq) \rightarrow FeOH^{2+}(aq) \rightarrow Fe(OH)_2^+(aq) \rightarrow \rightarrow Fe(OH)_4^-(aq)$.

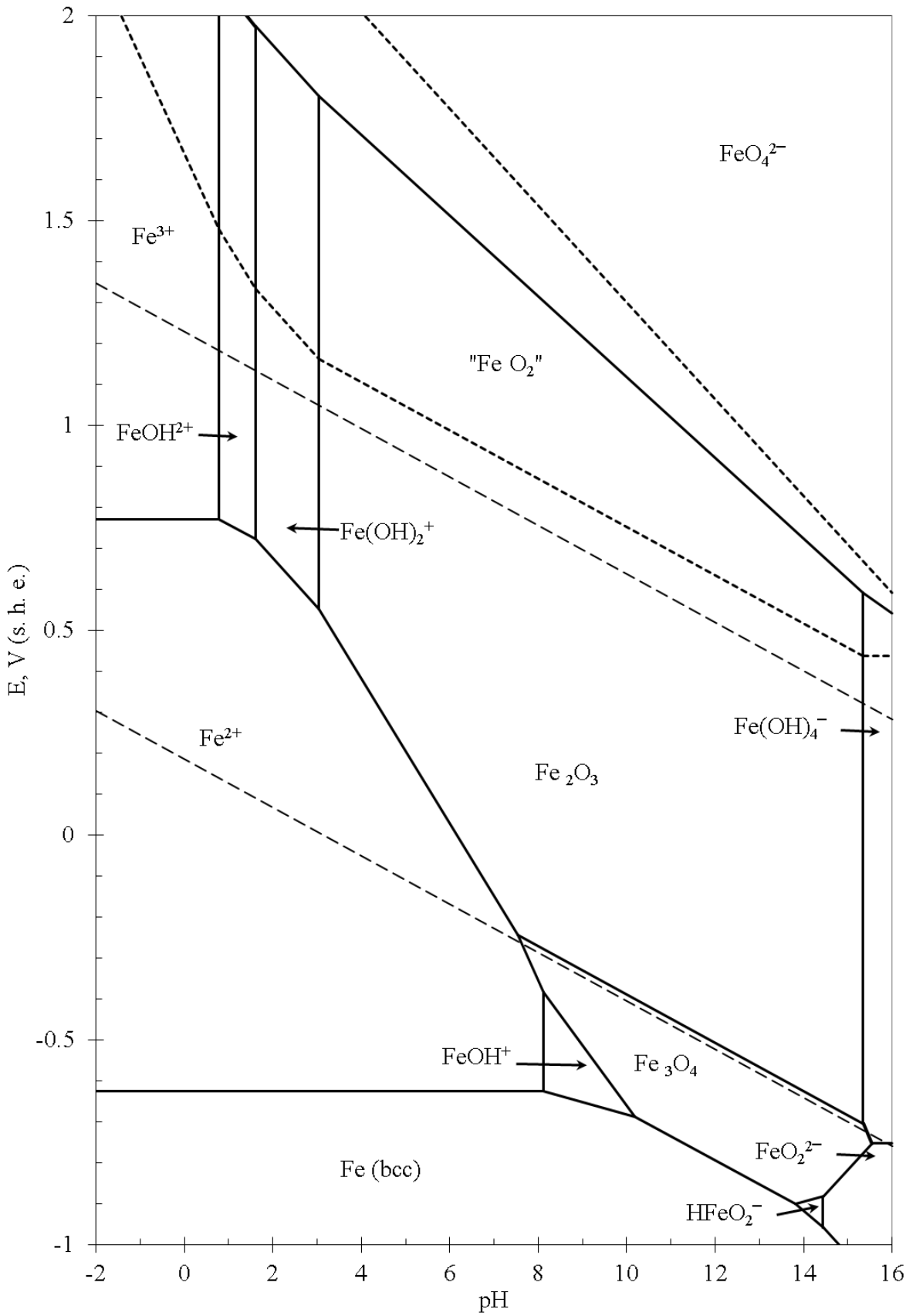

Figure 2. The potential – pH diagram for Fe – H_2O system.

In very diluted solutions the domain of stability of solid Fe_2O_3 also vanishes. Calculations show that among all Fe^{VI} species only FeO_4^{2-} is thermodynamically stable. The revised potential – pH diagram of Fe – H_2O system at 25ºC, 1 bar and $a_{[Fe]} = 10^{-6}$ mol l^{-1} is presented at Figure 2. Dashed lines represent the hydrogen and oxygen electrodes and border the domain of electrochemical stability of water at atmospheric conditions. Dotted lines border the hypothetical domain of stability of "FeO_2". It isn't thermodynamically stable at standard conditions and doesn't form a separate oxide layer.

REFERENCES:

1. Atlas of Eh-pH diagrams: Intercomparison of thermodynamic databases. Open file report № 419. National Institute of Advanced Industrial Science and Technology, 2005.
2. Brookins, D. G. Eh-pH diagrams for geochemistry. Berlin: Springer, 1987.
3. Schweitzer, G. K., Pesterfield, L. L. The aqueous chemistry of the elements. Oxford: Oxford University Press, 2010.
4. Phase diagram – Web. FactSage Database.
5. Cotton, F. A., Wilkinson, G. Advanced inorganic chemistry. A comprehensive test. New York: Wiley, 1965.
6. Nikolaychuk, P. A., Tyurin, A. G. Method of estimating the standard Gibbs energies of formation of binary compounds. Abstracts of the XVIII International Conference on Chemical Thermodynamics in Russia (RCCT-2011). Vol. 2. Samara: Samara State Technical University, 2011. P. 16 – 17.
7. Nikolaychuk, P. A., Tyurin, A. G. The analysis of standard Gibbs energies of formation of MeO_2 type oxides of fourth period d-elements. Abstracts of the XVIII International Conference on Chemical Thermodynamics in Russia (RCCT-2011). Vol. 2. Samara: Samara State Technical University, 2011. P. 17 – 18.
8. Chase, M. W. Jr et al. JANAF thermochemical tables. Third edition. Journal of Physical and Chemical Reference Data, 1985. Vol. 14. Suppl. 1.
9. Wagman, D. D. et al. The NBS tables of chemical thermodynamic properties. Selected values for inorganic and C_1 and C_2 organic substances in SI units. Journal of Physical and Chemical Reference Data, 1982. Vol. 11. Suppl. 2.
10. Bard, A. J., Parsons, R., Jordan, J. Standard potentials in aqueous solutions. New York: Marcel Dekker Inc., 1985.

THE ESTIMATION OF Fe – Si SYSTEM OXIDATION AT 298 K IN AIR AND WATER ENVIRONMENTS

P. A. Nikolaychuk and A. G. Tyurin

Department of Analytical and Physical Chemistry, Chelyabinsk State University, Chelyabinsk, Russian Federation, npa@csu.ru, tag@csu.ru

Abstract

Thermodynamic description of systems Fe – Si, Fe – Si – O and Fe – Si – H_2O at standard conditions is performed. The Fe – Si – O system state diagram and potential – pH diagram of Fe – Si – H_2O system are plotted. Thermodynamic features of chemical and electrochemical stability of iron silicides are analyzed.

Introduction

Fe – Si is important binary system, and the thermodynamic features of its oxidation and corrosion processes were modeled many times [1-3]. However, these studies do not cover all possible chemical and electrochemical equilibria in system. The purpose of this study is to make revision of previous researches and take into account all uncounted thermodynamic properties.

Results and Discussion

The Fe – Si phase diagram [4] assumes, that two stable iron silicides, FeSi and $FeSi_2$, exist in system at standard temperature. FeSi has a small homogeneity range, from $FeSi_{0,961}$ to $FeSi_{1,033}$. Maximum solid solubility of Si in α-Fe is equal to about 25 atomic percent. It corresponds to fully ordered α_2-phase, and this solution composition is often considered as subsilicide "Fe_3Si" [5]. Thermodynamic properties of α-phase are described in terms of substitution solution model. The comparison between different approaches [6-8] is performed with and without considering "Fe_3Si" phase existence. The activities of iron and silicon in "saturated" solid solution are equal to 0,473 and $5{,}5\cdot10^{-20}$ respectively, meaning strong negative deviations from ideal behaviour. There are a lot of different thermodynamic data on various iron silicides, which often do not agree with each other. The revision and estimation of these data is performed and the correct values are chosen. The standard Gibbs energy of formation of nonstoichiometric $FeSi_x$ compound is estimated by a following equation:

$$\Delta_f G^o_{298}(FeSi_x) = 34100\cdot x^2 - 107800\cdot x,\ J/mol \quad (1).$$

In order to describe chemical resistance of Fe-Si system alloys to corrosion in oxygen environments the consecutive scheme of oxidation reactions is considered, the Fe-Si-O state diagram is plotted (see fig. 1) and the characteristics of system conditions are calculated. There is an experimental approval that there is a solid solubility of SiO_2 in Fe_2O_3 and Fe_3O_4 in Fe_2SiO_4 at elevated temperatures [9]. Using these data and according to strictly regular solution model the energy of mixing (Q_{12}) and the Gibbs energies of phase transitions of SiO_2 from diamond lattice to the lattice of Fe_2O_3 and of Fe_3O_4 from magnetite lattice to the lattice of Fe_2SiO_4 are estimated to be the following:

$$Q_{SiO_2-Fe_2O_3} = 8740\ J/mol,\ Q_{Fe_3O_4-Fe_2SiO_4} = 25200\ J/mol \quad (2),$$

$$\Delta_{tr}G^o_T(SiO_2, diamond \rightarrow (SiO_2)_{Fe_2O_3}) = 2{,}621\cdot T + 6557,\ J/mol \quad (3),$$

$$\Delta_{tr}G^o_T(Fe_3O_4, magnetite \rightarrow (Fe_3O_4)_{Fe_2SiO_4}) = 0{,}235\cdot T - 1523,\ J/mol \quad (4),$$

The solubility of SiO_2 in Fe_2O_3 is estimated equal to $1{,}54\cdot10^{-3}$ mole percent at 298 K. The activities of the components are $a_{SiO_2} = 0{,}0541$ and $a_{Fe_2O_3} = 0{,}998$. The solubility of Fe_3O_4 in Fe_2SiO_4 is equal to

$6{,}85\cdot10^{-5}$ mole percent and $a_{Fe_3O_4} = 0{,}00233$, $a_{Fe_2SiO_4} \approx 1$. The small positive deviations from ideal behaviour for both these solutions are revealed.

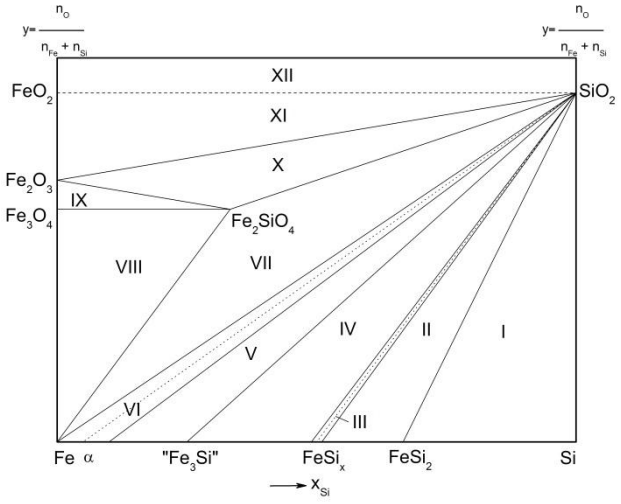

Fig. 1. Fe-Si-O system state diagram at 298 K

Domains at the diagram (fig. 1) correspond to the following system states: I – $FeSi_2$ – Si – SiO_2, II – $FeSi_{1,033}$ – $FeSi_2$ – SiO_2, III – $FeSi_x$ – SiO_2, IV – "Fe_3Si" – $FeSi_{0,961}$ – SiO_2, V – α_1 – SiO_2, VI – α – SiO_2, VII – α – Fe_2SiO_4 – SiO_2, VIII – α – (Fe_3O_4, Fe_2SiO_4), IX – (Fe_3O_4, Fe_2SiO_4) – Fe_2O_3, X – (Fe_2O_3, SiO_2) – Fe_2SiO_4, XI – Fe_2O_3 – FeO_2 – SiO_2, XII – FeO_2 – SiO_2 – $\{O_2\}$.

The standard Gibbs energy of formation of metastable iron dioxide is estimated to be equal to about –360000 $^{J}/_{mol}$. The calculations show, that equilibrium oxygen pressure, needed for FeO_2 formation, exceeds $6\cdot10^5$ bar. Thus it can not be formed in air environments at standard conditions.

The best way to describe thermodynamic features of electrochemical stability of Fe-Si system in liquid environments is to plot the diagram of electrochemical equilibrium (potential-pH) [10]. It was plotted at 298 K, air pressure of 1 bar and activities of ions in solution, equal to 1 $^{mol}/_{l}$ (see fig. 2). Thermodynamic properties of basic chemical and electrochemical equilibria in Fe-Si-H_2O system are calculated.

21 domains of various phases can be depicted at the diagram (fig. 2):

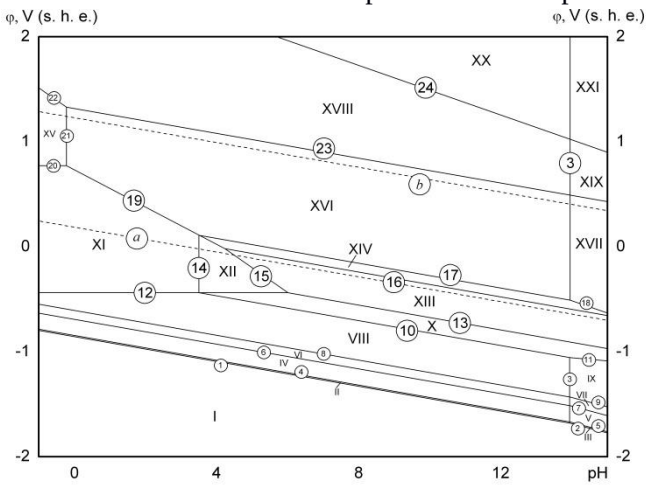

Fig. 2. The potential – pH diagram of Fe-Si-H_2O system at 298 K, air pressure of 1 bar and activities of ions, equal to 1 $^{mol}/_{l}$ (unhydrated form of the oxides).

I – α-phase (bcc) + "Fe_3Si" + $FeSi_x$ + $FeSi_2$ + Si; II – α + "Fe_3Si" + $FeSi_x$ + $FeSi_2$ + SiO_2; III – α + "Fe_3Si" + $FeSi_x$ + $FeSi_2$ + SiO_3^{2-}; IV – α + "Fe_3Si" + $FeSi_x$ + SiO_2; V – α + "Fe_3Si" + $FeSi_x$ + SiO_3^{2-}; VI – α + α_1 + SiO_2; VII – α + α_1 + SiO_3^{2-}; VIII – α + SiO_2; IX – α + SiO_3^{2-}; X – α + Fe_2SiO_4; XI – Fe^{2+} + SiO_2; XII – Fe^{2+} + Fe_2SiO_4; XIII – Fe_3O_4 + (Fe_3O_4, Fe_2SiO_4); XIV – Fe_2O_3 + Fe_2SiO_4; XV – Fe^{3+} + SiO_2; XVI – (SiO_2, Fe_2O_3) + SiO_2; XVII – Fe_2O_3 + SiO_3^{2-}; XVIII – "FeO_2" + SiO_2; XIX – "FeO_2" + SiO_3^{2-}; XX – FeO_4^{2-} + SiO_2; XXI – FeO_4^{2-}, SiO_3^{2-}.

The primary passivation film on the Fe-Si system alloys in the area of water electrochemical stability (between the lines *a* and *b* on fig. 2, corresponding to hydrogen and oxygen electrodes, respectively) consists of Fe_2O_3 and SiO_2. Its specific composition depends on silicon content in the system.

Conclusions

The Fe – Si – O system state diagram and the potential – pH diagram of Fe – Si – H_2O system at 298 K and 1 bar are revised to take into account all uncounted thermodynamic properties of these systems. Thermodynamic description of chemical and electrochemical stability of iron silicides is performed.

References

[1] A. Atkinson. Corrosion Science, 1982, **22(2)**, 87-102.
[2] G. Kelsall et al. Journal of the Electrochemical Society, 1991, **138(4)**, 931-940.
[3] A. Tyurin. Protection of Metals, 2004, **40(1)**, 14-22.
[4] Phase diagram – Web, http://www.crct.polymtl.ca/fact/documentation.
[5] A. Gude. Philosophical Magazine A, 2006, **76(1)**, 1-29.
[6] L. Kaufman. CALPHAD, 1979, **3(1)**, 45-76.
[7] B. Lee et al. CALPHAD, 1987, **11(2)**, 253-270.
[8] J. Lacaze. Metallurgical Transactions A, 1991, **22**, 2211-2223.
[9] A. Lykasov et al. Butlerov Communications, 2010, **21(7)**, 42-49.
[10] Pourbaix diagrams / Substances & Technologies, http://www.substech.com/dokuwiki/doku.php?id=pourbaix_diagrams.

THERMODYNAMIC ASSESSMENT OF CHEMICAL AND ELECTROCHEMICAL STABILITY OF IRON SILICIDES

Pavel Anatolyevich Nikolaychuk and **Aleksandr Georgievich Tyurin**
Chelyabinsk State University, Brat'ev Kashirinykh Street, 129, Chelyabinsk, Russian Federation.
E-mail: npa@csu.ru, tag@csu.ru

Abstract:

Phase and chemical euqilibria in Fe – Si system at 298 K are considered. The comparison between available thermodynamic information on the solid solution, of silicon in bcc-iron at low temperatures is performed with and without consideration of α-phase ordering. The possible maximum solid solubility of Si in bcc-Fe at 298 K is estimated. The thermodynamic activities of the components in this "saturated" solution are calculated.

The state diagram of Fe – Si – O system at 298 K is plotted and the characteristics of their invariant conditions are calculated. The potential – pH diagram of the Fe – Si – H_2O system at 298 K, air pressure of 1 bar and activities of ions in solution, equal to 1 mol/l is plotted. Basic chemical and electrochemical equilibria in this system are considered.

The thermodynamic analysis of chemical and electrochemical stability of Fe – Si system alloys is made.

1. Introduction.

Iron–silicon is a very important binary system. Reliable information on the thermodynamic properties and phase equilibria in Fe – Si alloys is needed for calculation of the technological quantities for various metallurgical processes. Iron silicides are perspective materials, including metalloid conductors [1], semiconductors [2, 3] and amorphous materials [4], they are well-known for their unusual magnetic, optical and thermodynamic properties [5 – 7]. Iron-silicon alloys can be found in Earth's core [8], they are using in technology as thin films [9] and nanowires [2, 10]. Moreover, many important ternary and multicomponent systems, including Fe - Si binary system, such as Ni – Fe – Si [11], Al – Fe – Si [12 – 14], Fe – Mn – Si [15, 16], Cu – Fe – Si [17, 18], Cr – Fe – Si [19], Fe – Zn – Si [20 – 22], Fe – Si – C [23 – 26], Fe – Si – O [27, 28], Fe – Si – B [29, 30], Al – Ca – Fe – Si [31] and others, are of great interest to the researches. The alloys and compounds, based on Fe – Si system can be used as corrosion-resistant materials and coatings. The experimental investigations of iron silicides corrosion properties are very intensive; it will be discussed further in section 5. But the theoretical studying of this issue is also important scientific task. One of the methods to describe the oxidation of silicides both in oxygen-containing gaseous environments (chemical stability) and in water environments (electrochemical stability) is the thermodynamic modelling. The previous investigations of thermodynamic features of Fe – Si system corrosion and oxidation properties [32, 33] don't cover all possible chemical and electrochemical equilibria in system. The purpose of this study is to make revision of previous researches and take into account all uncounted thermodynamic properties. Unlike to many other published papers, which correspond to high temperatures, the present study devoted to thermodynamic description of Fe – Si system at standard temperature only.

2. Phase and chemical equilibria in Fe – Si system at the temperature of 298 K.

2. 1. Comparison of previous thermodynamic descriptions.

According to the Fe – Si phase diagram [34 – 35], several intermetallic phases exist in system: Fe_3Si_7, $FeSi_2$, FeSi, Fe_5Si_3 and Fe_2Si. But only $FeSi_2$ and FeSi are thermodynamically stable at standard conditions. FeSi has a narrow homogeneity range [7, 34], from $FeSi_{0,961}$ to $FeSi_{1,033}$, which doesn't depend on temperature. Pure silicon exist in diamond modification (the Strukturbericht symbol is A4), and the solid solubility of iron in it is negligibly small and can be

ignored. Iron exists in face centered cubic (fcc) and body centered cubic (bcc) modifications, but only the bcc one is stable at 298 K, it is called α-Fe. The solid solubility of Si in α-Fe is equal to about 25 atomic percent and silicon can form three types of solutions. The first one is the disordered phase, in which only short range ordering exist (α-phase, the Strukturbericht symbol is A2), two others have long range atomic ordering – α_2-phase, the Strukturbericht symbol is B2 and α_1-phase, the Strukturbericht symbol is DO_3. The crystallographic features and lattice parameters of these phases were described many times [36 – 38]. Additionally, a miscibility gap exists between α_2 and α_1 phases. The magnetic transformation, which occurs in α-phase, corresponds to elevated temperatures and inflicts no effect on Fe – Si system thermodynamic properties at standard temperature. The Gibbs energy of the magnetic ordering is considered in studies [26, 38] and isn't taken into account in present study.

However, there is no single and clear opinion about phase boundaries between α, α_2 and α_1 phases at low temperatures. Experimental data [39 – 41] are available only for high temperatures, all studies, considering Fe – Si phase diagram [34 – 38], provide reliable information about phase boundaries at the diagram for the temperatures, exceeding 500ºC. The attempts of thermodynamic extrapolation of phase diagram below 500ºC are often contradictory. Some studies [34, 36] notice, that $\alpha - \alpha_2 - \alpha_1$ transformations take place at silicon concentration in solution, slightly more, than 10 atomic percent. On the other hand, the authors of [38] provide the following relation between the temperatures of phase transition from A2 phase to B2 (T_{A2-B2}) and from B2 phase to DO_3 (T_{B2-DO_3}) and mole fraction of silicon in solid solution (x):

$$T_{A2-B2} = x\cdot(1-x)\cdot(-4293{,}3\cdot(1-2x)^3 - 112{,}5\cdot(1-2x)^2 + 2515{,}2\cdot(1-2x) + 9825{,}6) \quad (1),$$

$$T_{B2-DO_3} = x\cdot(1-2x)\cdot(134\cdot(1-4x)^3 - 4291{,}1\cdot(1-4x)^2 - 2306{,}2\cdot(1-4x) + 12024) \quad (2),$$

where temperatures T_{A2-B2} and T_{B2-DO_3} are given in Kelvins, mole fraction x is dimensionless. These equations are written to fit the experimental data of [39], but they can be solved in relation to x at the transition temperatures set to 298 K, this solution gives x = 0,036 for A2 – B2 transition and x = 0,045 for B2 – DO_3 transition. Moreover, there is no information about the exact position of miscibility gap between α_2 and α_1 phases. And finally, authors of [42] declare, that there is no B2 phase either at low temperatures!

Most of researches, concerning thermodynamic assessment of ternary and multicomponent systems [12, 13, 15 – 18, 20, 22, 24, 25, 28 – 31], refer to thermodynamic information about Fe – Si binary system, provided in few descriptions [23, 38, 43]. Additionally, the authors of [20] provide their own thermodynamic description of Fe – Si α-phase. All of these descriptions don't take into account long range ordering transformations in α-phase completely. The authors of [20, 43] simply ignore it; the authors of [23] consider only α_2-phase using two-sublattice model [44], but give the analytical expression for the excess Gibbs energy G^E [45] without considering α_2-phase; the authors of [38] give analytical expressions for the atomic ordering Gibbs energy for both α_2 and α_1 phases, but also offer a single equation for the excess Gibbs energy for all types of solid solutions, without contribution of atomic ordering on it. All of these descriptions treat FeSi as the stoichiometric phase, without considering its homogeneity range.

Since in all above-mentioned studies [20, 23, 38, 43] the thermodynamic properties of bcc solid solution are estimated, concerning all possible equilibria with α-phase involved, especially in high-temperature region, the estimated parameters values provide minimal deviations of calculated whole Fe – Si phase diagram from the experimental one, but these deviations are still significant, when only one single equilibrium is taken into account. In present study only the equilibrium of α-phase with FeSi compound is important in order to estimate maximum silicon solid solubility in α-Fe at 298 K. Thus the comparison between all available descriptions is performed, in order to choose one of them, which provides better agreement of calculated and experimental data on this single equilibrium. So, at the temperatures below 820ºC

[34, 36] at the Fe-rich side on Fe – Si system, the following reaction occurs between α-phase (bcc solid solution) and FeSi compound:

$$\mathrm{Fe}\ (\alpha) + \mathrm{Si}\ (\alpha) = \mathrm{FeSi} \qquad (3).$$

It can be described using the following equation:

$$\Delta_r G_T^o = -RT \cdot \ln\ K_p = -RT \cdot \ln \frac{1}{a_{\mathrm{Fe}(\alpha)} \cdot a_{\mathrm{Si}(\alpha)}} = RT \cdot \ln a_{\mathrm{Fe}(\alpha)} + RT \cdot \ln a_{\mathrm{Si}(\alpha)} \qquad (4),$$

where $\Delta_r G_T^o$ is the Gibbs energy change of reaction (3), $^{\mathrm{J}}/_{\mathrm{mol}}$, K_p is an equilibrium constant of this reaction, $R = 8{,}3144\ ^{\mathrm{j}}/_{\mathrm{mol \cdot K}}$ is a universal gas constant, T is a temperature in Kelvins, $a_{\mathrm{Fe}(\alpha)}$ and $a_{\mathrm{Si}(\alpha)}$ are, respectively, thermodynamic activities of iron and silicon in α-phase (reference state – pure component with bcc lattice), which is in equilibrium with FeSi. Here and further in the text, unless it is specially noticed, all compounds, including silicides, oxides and silicates, are treated as pure substances, and their activities are set to unity. The analytical expressions of $a_{\mathrm{Fe}(\alpha)}$ and $a_{\mathrm{Si}(\alpha)}$ are linked with expression for the excess Gibbs energy $\mathrm{G^E}$ of α-phase:

$$RT \cdot \ln a_{i(\alpha)} = RT \cdot \ln\ x_{i(\alpha)} + \mu_{i(\alpha)}^{\mathrm{E}} \qquad (5),$$

where $i(\alpha)$ denotes any α-phase component (Fe or Si), $x_{i(\alpha)}$ is the mole fraction of the component i and $\mu_{i(\alpha)}^{\mathrm{E}}$ is an excess chemical potential of the component, that can be determined as the partial derivative of excess Gibbs energy $\mathrm{G^E}$ by number of moles of this component [45]. Thus, the analytical expression of $\mathrm{G}_\alpha^{\mathrm{E}} = \mathrm{f}\,(x_{\mathrm{Fe}(\alpha)}, x_{\mathrm{Si}(\alpha)}, T)$ is needed to solve equation (4).

In paper [43] the following equations are proposed for the Gibbs energy change of reaction (3) and for the excess Gibbs energy of α-phase:

$$\Delta_r G_T^o\ (3) = 27{,}572T - 123010,\ ^{\mathrm{J}}/_{\mathrm{mol}} \qquad (6),$$

$$G_\alpha^E = x(1-x) \cdot ((1-x) \cdot (7{,}95T - 129704) + x \cdot (136{,}82T - 297064)),\ ^{\mathrm{J}}/_{\mathrm{mol}} \qquad (7).$$

Here x denotes silicon mole fraction in the solid solution.

The authors of [20] also use equation (6) for Gibbs energy change of reaction (3), but offer the description of $\mathrm{G}_\alpha^{\mathrm{E}}$ according to Redlich-Kister power series [46]:

$$\begin{aligned} G_\alpha^E = {} & x(1-x) \cdot ((34{,}81T - 156900) + (1-2x) \cdot (-0{,}41T - 33470) + \\ & + (1-2x)^2 \cdot (-11{,}08T + 35780) + (1-2x)^3 \cdot (-6{,}92T - 28800)),\ ^{\mathrm{J}}/_{\mathrm{mol}} \end{aligned} \qquad (8).$$

Another set of parameters is proposed by the authors of paper [38]. They consider reaction of FeSi formation in the following form:

$$\mathrm{Fe}\ (\gamma) + \mathrm{Si}\ (\mathrm{diamond}) = \mathrm{FeSi} \qquad (9),$$

and give the value of Gibbs energy change in reaction (9) by the equation

$$\Delta_r G_T^o\ (9) = 10{,}2906T - 86421{,}72,\ ^{\mathrm{J}}/_{\mathrm{mol}} \qquad (10).$$

Additionally, they consider reactions of phase transitions of iron and silicon:

$$\mathrm{Fe}\ (\gamma) = \mathrm{Fe}\ (\alpha) \qquad (11),$$

$$\mathrm{Si}\ (\mathrm{diamond}) = \mathrm{Si}\ (\alpha) \qquad (12),$$

and give the values of Gibbs energies of these transitions:

$$\Delta_r G_T^o\ (11) = \Delta_{tr} G_T^o\ (\mathrm{Fe}_{\gamma \to \alpha}) = -6{,}4 \cdot 10^{-4} T^2 - 8{,}282T + 1{,}15T \cdot \ln\ T + 1462{,}4,\ ^{\mathrm{J}}/_{\mathrm{mol}} \qquad (13),$$

$$\Delta_r G_T^o\ (12) = \Delta_{tr} G_T^o\ (\mathrm{Si}_{\mathrm{diamond} \to \alpha}) = -19{,}54T + 44350,\ ^{\mathrm{J}}/_{\mathrm{mol}} \qquad (14).$$

Obviously, the Gibbs energy of reaction (3) can be calculated according to Hess' law:

$$\Delta_r G_T^o\ (3) = \Delta_r G_T^o\ (9) - \Delta_r G_T^o\ (11) - \Delta_r G_T^o\ (12) \qquad (15).$$

The equation for excess Gibbs energy $\mathrm{G}_\alpha^{\mathrm{E}}$ is also written according to Redlich-Kister formalism:

$$G_\alpha^E = x(1-x) \cdot ((13{,}7306T - 129038) - 39244 \cdot (1-2x)),\ ^{\mathrm{J}}/_{\mathrm{mol}} \qquad (16).$$

And, finally, the authors of [23] give another set of parameters. They consider formation of FeSi from the elements in their standard reference states at low temperatures:

$$\mathrm{Fe}\ (\alpha) + \mathrm{Si}\ (\mathrm{diamond}) = \mathrm{FeSi} \qquad (17),$$

giving the value of Gibbs energy of reaction (17) by the equation

$$\Delta_r G_T^o\ (17) = 4{,}44T - 72761{,}2,\ \text{J/mol} \qquad (18).$$

This time, the Gibbs energy of reaction (3) can be gained in the following way:

$$\Delta_r G_T^o\ (3) = \Delta_r G_T^o\ (17) - \Delta_r G_T^o\ (12) \qquad (19),$$

but, instead of using Gibbs energy change of reaction (12), proposed in [38] and listed in equation (14), the authors of [23] use the value, obtained from database [47]:

$$\Delta_r G_T^o\ (12) = \Delta_{tr} G_T^o\ (\mathrm{Si}_{\mathrm{diamond}\to\alpha}) = -22{,}5T + 47000,\ \text{J/mol} \qquad (20).$$

And the excess Gibbs energy $\mathrm{G}_\alpha^{\mathrm{E}}$ is presented in the following form:

$$G_\alpha^E = x(1-x)\cdot((46{,}48T - 111236) - 92352\cdot(1-2x) + 62240\cdot(1-2x)^2),\ \text{J/mol} \qquad (21).$$

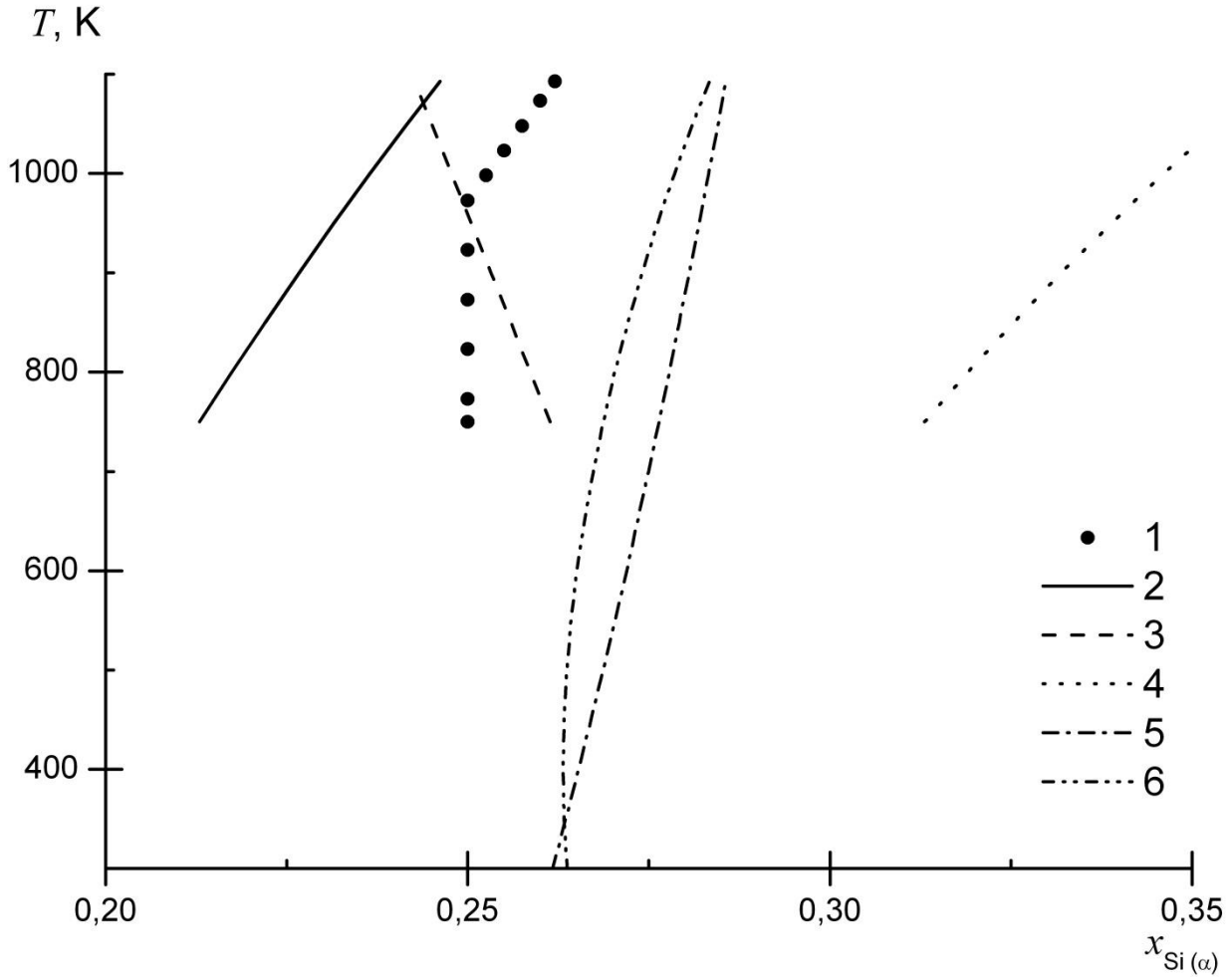

Figure 1. Maximum solid solubility of Si in α-Fe at various temperatures: *1* – experimental values, obtained from Fe – Si phase diagram [34, 35]; *2* – calculated according to data of [20] using equations (4), (6) and (8); *3* – calculated according to data of [23] using equations (4), (18), (20) and (21); *4* – calculated according to data of [38] using equations (4), (10), (13), (14) and (16); *5* – calculated according to data of [43] using equations (4), (6) and (7); *6* – calculated in present study using equations (7), (20), (25) and (27).

After substituting these parameters values into equation (4), only two variables remain in it: *T* and *x*. Solving this equation gives the position of line on the Fe – Si phase diagram that corresponds to maximum silicon solid solubility. The solutions, obtained with all of above-

mentioned parameters sets, compared with values, obtained from currently accepted Fe – Si phase diagram [34, 35], are presented at figure 1. As can be seen, the best convergence between the experimental and calculated lines is achieved when using parameters from paper [43]. This allows to extrapolate this calculated equilibrium line down to the standard temperature. The estimated silicon maximum solid solubility at 298 corresponds to $x = 0{,}262$.

2.2. Considering the nonstoichiometry of FeSi compound.

The next step is to extend this thermodynamic description by taking into account the nonstoichiometry of FeSi compound. There are no thermodynamic properties of nonstoichiometric FeSi in literature; therefore it is necessary to predict it. The authors of [48] notice, that an approximate functional relationship exist between the reduced chemical potential of oxygen atoms in metal oxide and system oxidation degree: $\Delta_f G_T^o(\mathrm{Me}_{1/x}\mathrm{O}) = f(x)$. The assumption is made by in paper [49], that similar relationship is valid not only for oxides, but also for some other binary compounds with polar covalent bond (sulfides, carbides, nitrides, silicides, etc.). They derived the following interpolation formula for the Gibbs energy of formation of binary compounds:

$$\Delta_f G_T^o(M_{a_x}A_{b_x}) = b_x \cdot \sum_{i=1}^{n}\left(\frac{\Delta_f G_T^o(M_{a_i}A_{b_i})}{b_i} \cdot \prod_{j\neq i}\frac{a_i \cdot (a_j \cdot b_x - a_x \cdot b_j)}{a_x \cdot (a_j \cdot b_i - a_i \cdot b_j)}\right) \qquad (22),$$

where n is a number of Gibbs energies of formation of binary compounds, accepted as a reliable initial data; $M_{a_i}A_{b_i}$ – formulae of these binary compounds (M – metal atom, A – more electronegative element atom,, a_i and b_i – indices for M and A atoms in compound, respectively); $M_{a_x}A_{b_x}$ – formula of the compound, Gibbs energy of formation of which is to be estimated, a_x and b_x – indices for the M and A atoms in it.

Despite only FeSi and $FeSi_2$ are stable compounds in the Fe – Si system at standard temperature, the information about the standard Gibbs energies of formation ($\Delta_f G_{298}^o$) for other iron silicides is also presented in literature. The data from [23, 38, 43, 50 – 57] are summarized in table 1.

Compound / Reference	$\Delta_f G_{298}^o$, J/mol					
	Fe_3Si	Fe_2Si	Fe_5Si_3	FeSi	Fe_3Si_7	$FeSi_2$
[23]	–	–74421	–240500	–71438	–199231	–79038
[38]	–	–75414	–252822	–83355	–	–83764
[43]	–	–	–	–76266	–251934	–
[50]	–94765	–	–233643	–76587	–179307	–78447
[51]	–84592	–	–197639	–76579	–198495	–73291
[52]	–83740	–	–244510	–81600	–	–80390
[53]	–94605	–	–	–73223	–	–78357
[54]	–	–	–	–73765	–	–79660
[55]	–	–92064	–	–76028	–	–92593
[56]	–103200	–	–	–78600	–	–91800
[57]	–124656	–	–306841	–94056	–	–97762
*	–95850	–90180	–260340	–73180	–194900	–78360

* Calculated according to formula (25).

Table 1. Standard Gibbs energies of formation of iron silicides (referred to bcc Fe and diamond Si).

As can be seen from table 1, there is no convergence between the results, given in various papers. The differences are often significant. Only the data for FeSi and $FeSi_2$ agree satisfactory with each others. The most reliable information on standard Gibbs energies of formation of these two silicides is obtained from paper [54], because it was determined within the temperature range of $10\ \text{K} \le T \le 400\ \text{K}$ by means of adiabatic low-temperature calorimetry, while the data from some other papers involve extrapolations of thermodynamic properties from high-temperature region down to the standard temperature. From all studies, containing dependencies of $\Delta_f G_T^o\ (\text{FeSi, FeSi}_2) = f(T)$ [23, 38, 50, 52, 53, 55, 57], only those from study [53] satisfactory agree with values from paper [54]. In this case, the decision is made to use only data for FeSi and $FeSi_2$ from [53] in estimation of nonstoichiometric $FeSi_x$ unknown thermodynamic properties. The values in [53] are tabulated in temperature range of $298\ \text{K} \le T \le 1200\ \text{K}$, and the approximation of them gives the following equations:

$$\Delta_f G_T^o\ (\text{FeSi}) = 0{,}0051T^2 - 2{,}8429T - 72785,\ \text{J/mol} \qquad (23),$$

$$\Delta_f G_T^o\ (\text{FeSi}_2) = 0{,}0072T^2 + 4{,}4465T - 80321,\ \text{J/mol} \qquad (24).$$

Substituting equations (23) and (24) into equation (22) leads to the following equation for the Gibbs energy of formation of $FeSi_x$ phase:

$$\Delta_f G_T^o\ (\text{FeSi}_x) = x^2 \cdot (-0{,}0015T^2 + 5{,}06615T + 32624{,}5) + x \cdot (0{,}0066T^2 - 7{,}90905T - 105409{,}5),\ \text{J/mol} \qquad (25).$$

Here x is an index in formula $FeSi_x$. In order to verify formula (25), the values of $\Delta_f G_{298}^o$ for all iron silicides are estimated, according to it. They are placed in table 1 in column, marked by * and agree more or less satisfactory with values, presented in literature. Thus, this formula can be used for further calculations. It gives the following results at standard temperature: $\Delta_f G_{298}^o(\text{FeSi}_{0,961}) = -71600\ \text{J/mol}$ and $\Delta_f G_{298}^o(\text{FeSi}_{1,033}) = -74430\ \text{J/mol}$.

Now, the equations (3) and (4) can be replaced with the following ones:

$$\text{Fe}\ (\alpha) + 0{,}961\ \text{Si}\ (\alpha) = \text{FeSi}_{0,961} \qquad (26).$$

$$\Delta_r G_T^o = -RT \cdot \ln \frac{1}{a_{\text{Fe}(\alpha)} \cdot a_{\text{Si}(\alpha)}^{0,961}} = RT \cdot \ln a_{\text{Fe}(\alpha)} + 0{,}961RT \cdot \ln a_{\text{Si}(\alpha)} \qquad (27).$$

The Gibbs energy of formation of $FeSi_{0,961}$, acquired by setting x = 0,961 in equation (25), however, refers to standard element reference states:

$$\text{Fe}\ (\alpha) + 0{,}961\ \text{Si}\ (\text{diamond}) = \text{FeSi}_{0,961} \qquad (28),$$

and have to be combined with the reaction (12) according to Hess' law:

$$\Delta_r G_T^o\ (26) = \Delta_r G_T^o\ (28) - 0{,}961 \cdot \Delta_r G_T^o\ (12) \qquad (29).$$

The expression of silicon Gibbs energy of transition in reaction (12) is taken from equation (20), and previously chosen expression for excess Gibbs energy G_α^E from [43] (equation (7)) is used. The result of solving equation (27) is also depicted in figure 1 (line *6*) and is very good compatible with values, calculated without considering $FeSi_x$ nonstoichiometry (line *5*) and experimental phase diagram (line *1*). The estimated silicon maximum solid solubility at 298 K corresponds to x = 0,264, the activities of this "saturated" solid solution components are equal to $a_{\text{Fe}(\alpha)} = 0{,}114$ and $a_{\text{Si}(\alpha)} = 7{,}2 \cdot 10^{-20}$, meaning strong negative deviations from ideal behaviour.

2. 3. Considering subsilicide "Fe_3Si" and α-phase ordering.

Also, an attempt is performed to take into account atomic ordering in α-phase. But, unlike to previous descriptions [23, 38], the completely another way is chosen. It is well known [36 – 38], that α_1-phase, in which full ordering occurs, corresponds to alloy composition of $Fe_{0,75}Si_{0,25}$. Since the line of maximum silicon solid solubility in α-Fe, depicted in experimental Fe – Si

phase diagram [34, 35] stands exactly on this alloy composition at low temperatures, it is possible to treat this fully ordered α_1-phase as the independent compound "Fe_3Si". There are several evidences in literature [4, 9, 16, 20, 23, 30, 36, 55, 56, 58 – 60], considering Fe_3Si as low-temperature subsilicide, moreover, even its standard Gibbs energy of formation is estimated in [50 – 53, 56, 57].

Usually, if the temperature is fixed, the next sequence of phase transitions is observed, when moving at the Fe-rich side of Fe – Si phase diagram in the direction of silicon concentration increase: $\alpha \mid \alpha_2 \mid \alpha_2 + \alpha_1 \mid \alpha_1 \mid \alpha_1 + FeSi_{0,961}$ and so on. However, following the suggestion of authors of [42], that there is no α_2-phase at low temperatures, the sequence of phase transitions reduces to $\alpha \mid \alpha_1 \mid \alpha_1 + FeSi_{0,961}$. When fully ordered α_1-phase is treated as the independent compound "Fe_3Si", the α_1 phase region can be described as the mixture of disordered α-phase and "Fe_3Si". Then the sequence of phase transitions becomes the following: $\alpha \mid \alpha +$ "Fe_3Si" | "Fe_3Si" + $FeSi_{0,961}$. This assumption is certainly a simplification, but it allows avoiding addition of special parameters in the equations for the α-phase Gibbs energies to describe its ordering, as it was done in papers [23, 38].

Instead of equations (3) and (4), describing the line of silicon maximum solid solubility in α-Fe, the next ones can be written now:

$$3\ \mathrm{Fe}\ (\alpha) + \mathrm{Si}\ (\alpha) = \text{"}\mathrm{Fe_3Si}\text{"} \qquad (30).$$

$$\Delta_r G_T^o = -RT \cdot \ln \frac{1}{a_{\mathrm{Fe}(\alpha)}^3 \cdot a_{\mathrm{Si}(\alpha)}} = 3RT \cdot \ln a_{\mathrm{Fe}(\alpha)} + RT \cdot \ln a_{\mathrm{Si}(\alpha)} \qquad (31).$$

Again the comparison between all available thermodynamic data for α-phase [20, 23, 38, 43] is performed, in order to choose one, which provides better description of this equilibrium. The procedure is similar to that, described in section 2. 1., and thus the calculations are omitted. It is found, that parameters from paper [23] are the best choice at this time. They are used to extrapolate equilibrium (30) down to the temperature of 298 K. The estimated silicon maximum solid solubility at 298 K corresponds to $x = 0{,}112$, the activities of solid solution components are equal to $a_{\mathrm{Fe}(\alpha)} = 0{,}473$ and $a_{\mathrm{Si}(\alpha)} = 5{,}5 \cdot 10^{-20}$, and deviations of this solution from ideal behaviour are negative.

3. The chemical stability of iron silicides.

3. 1. Phase and chemical equilibria in Fe – Si – O system at the temperature of 298 K.

The chemical stability of any alloy or compound is the ability to resist the chemical influence of natural environment, particularly, the oxidation by atmospheric oxygen [61, 62]. The thermodynamic features of Fe – Si system chemical stability can be clearly described by plotting Fe – Si – O system state diagram and considering equilibria in this system. But prior to plotting a diagram, the primary information about possible oxides in binary Fe – O and Si – O [34] systems, as well as about possible ternary compounds [63], must be taken into consideration.

Only one stable oxide – SiO_2 – exists in Si – O system. There are also many values of its Gibbs energy of formation available in literature [50 – 53]. However, since electrochemical formation of silicon dioxide is to be considered (see section 4), the value is chosen that corresponds to experimentally determined potential of the silicon electrode [64]:

$$\mathrm{SiO_2} + 4\mathrm{H^+} + 4\mathrm{e^-} = \mathrm{Si\ (diamond)} + 2\mathrm{H_2O};\ \varphi^o_{298} = -0{,}857\ \mathrm{V} \qquad (32),$$

which leads to a following equation:

$$\mathrm{Si\ (diamond)} + \mathrm{O_2} = \mathrm{SiO_2};\ \Delta_r \mathrm{G}^o_{298} = -805067\ {}^{\mathrm{J}}\!/_{\mathrm{mol}} \qquad (33).$$

In system Fe – O at 25˚C two oxides are stable, Fe_3O_4 and Fe_2O_3 [34, 35]. Despite the fact, that standard Gibbs energy of formation of the iron monoxide FeO is negative ($\Delta_f G^o_{298}(\mathrm{FeO}) = -244300\ {}^{\mathrm{J}}\!/_{\mathrm{mol}}$ according to [51]), it is thermodynamically unstable at standard temperature [62, 65], because decomposes spontaneously according to reaction

$$4\ FeO = Fe(\alpha) + Fe_3O_4;\ \Delta_r G^o_{298} = -36960\ \text{J/mol} \qquad (34).$$

It is known [65], that some mixed metal oxides exist, containing FeO_2 layers. They are, for example, Ba_2FeO_4 and $SrFe_2O_4$, which can be introduced as $2BaO \cdot FeO_2$ and $2SrO \cdot FeO_2$ respectively. Moreover, the formation of ferrate-ions is possible in highly oxidizing environments [65] and the electrochemical oxidation of Fe^{+3} state to Fe^{+6} one can't proceed in one step, because iron can't lose three electrons at once [66]. Therefore, intermediate Fe^{+4} state exists in solution undoubtedly. All this make to consider "FeO_2" as an independent metastable compound in Fe – O system and involve it into iron oxidation scheme. The standard Gibbs energy of formation for FeO_2 is estimated by two independent methods. The first one is the same as previously used for estimation of $FeSi_x$ phase thermodynamic properties [48, 49]. The reliable initial data, used for calculations, are the values of $\Delta_f G^o_{298}$ for Fe_3O_4 and Fe_2O_3. The second method depends on the assumption that thermodynamic properties of the various compounds of the same type vary periodically with change of element atomic number [67]. The authors of [68] have considered the dependence of standard Gibbs energies of formation of MeO_2-type oxides of fourth period d-elements on metals nuclear charge. The results of two these estimations agree to each other within the ranges of uncertainties, provided by methods, and give the averaged value of $\Delta_f G^o_{298}$ ("FeO_2") $= -360000$ J/mol.

Information about thermodynamic functions of other iron oxides [50 – 53, 69, 70] is listed in table 2.

Reference / Compound	$\Delta_f G^o_{298}$, J/mol					
	[50]	[51]	[52]	[53]	[69]	[70]
Fe_3O_4	–1026182	–1014163	–1019112	–1015391	–1017438	–1007561
Fe_2O_3	–743800	–740337	–741613	–742413	–743523	–739991

Table 2. Standard Gibbs energies of formation of iron oxides (referred to bcc Fe and gaseous O_2).

A single ternary compound exist in Fe – Si – O system at standard temperature and pressure, it is iron orthosilicate (or fayalite) Fe_2SiO_4 [63]. Another compound, ferrosilite $FeSiO_3$, is formed only at elevated temperatures or very high pressures [28]. Fayalite exists in two forms: α-Fe_2SiO_4, which has olivine crystal structure and γ-Fe_2SiO_4, which has spinel crystal structure [71, 72]. Only α-Fe_2SiO_4 is thermodynamically stable at standard conditions. The values of standard Gibbs energies of formation of α-Fe_2SiO_4 [28, 50 – 53, 71, 73, 74] are summarized in table 3.

Reference	[28]	[50]	[51]	[52]
$\Delta_f G^o_{298}$, J/mol	–1378035	–1375934	–1377004	–1347064
Reference	[53]	[71]	[73]	[74]
$\Delta_f G^o_{298}$, J/mol	–1380890	–1313750	–1379160	–1379188

Table 3. Standard Gibbs energies of formation of iron silicate Fe_2SiO_4 (referred to bcc Fe, diamond Si and gaseous O_2).

In addition to iron silicates of known composition and structure, there are notifications [75, 76] that some silicates have unknown and complex composition and structure. One of the possible explanations of this fact is related with the ability of Fe_3O_4 to form a solid solution with Fe_2SiO_4, observed by the authors of [77 – 79]. Moreover, they observed a solid solubility of SiO_2

in Fe_2O_3. The information of solid solubility of these compounds at various temperatures [79] is presented in table 4.

System $Fe_3O_4 - Fe_2SiO_4$			System $SiO_2 - Fe_2O_3$		
Temperature, K	Solid solubility in		Temperature, K	Solid solubility in	
	mass %	atomic %		mass %	atomic %
1073	20,2	19,9	1073	7,7	18,2
1173	26,2	20,5	1173	9,3	21,4
1273	31,7	24,7	1273	10,9	24,5

Table 4. The experimentally measured [79] solid solubility of Fe_3O_4 in Fe_2SiO_4 and SiO_2 in Fe_2O_3 at various temperatures.

The estimation of maximum solid solubility at 298 K is performed using thermodynamic modelling. The equilibrium between pure Fe_3O_4 (magnetite) and its solid solution in fayalite

$$Fe_3O_4\ (\text{magnetite}) = Fe_3O_4[\text{in } Fe_2SiO_4] \quad (35)$$

can be characterized with the equality of chemical potentials (μ) of Fe_3O_4 in both phases [45]:

$$\mu_{Fe_3O_4\ (\text{magnetite})} = \mu_{Fe_3O_4[\text{in } Fe_2SiO_4]} \quad (36).$$

Since magnetite is treated as pure substance at standard conditions, its chemical potential equals the standard chemical potential

$$\mu_{Fe_3O_4\ (\text{magnetite})} = \mu^{o}_{Fe_3O_4\ (\text{magnetite})} \quad (37).$$

and chemical potential of Fe_3O_4 in solution is represented by the sum of three terms:

$$\mu_{Fe_3O_4[\text{in } Fe_2SiO_4]} = \mu^{o}_{Fe_3O_4[\text{in } Fe_2SiO_4]} + RT \cdot \ln\ x_{Fe_3O_4[\text{in } Fe_2SiO_4]} + \mu^{E}_{Fe_3O_4[\text{in } Fe_2SiO_4]} \quad (38),$$

where $\mu^{o}_{Fe_3O_4[\text{in } Fe_2SiO_4]}$ is standard chemical potential of Fe_3O_4, referred to the lattice of solvent compound, Fe_2SiO_4; $\mu^{E}_{Fe_3O_4[\text{in } Fe_2SiO_4]}$ is its excess chemical potential and $x_{Fe_3O_4[\text{in } Fe_2SiO_4]}$ is the mole fractions of Fe_3O_4 corresponding to maximum solubility at the temperature *T*. The difference between standard chemical potentials of Fe_3O_4 in magnetite lattice and in lattice of solid solution is equal to molar Gibbs energy of transition of Fe_3O_4 from pure component to solution:

$$\Delta_{tr}G^{o}_{T}(Fe_3O_4\ (\text{magnetite}) \rightarrow Fe_3O_4[\text{in } Fe_2SiO_4]) = \mu^{o}_{Fe_3O_4[\text{in } Fe_2SiO_4]} - \mu^{o}_{Fe_3O_4\ (\text{magnetite})} \quad (39),$$

$$\Delta_{tr}G^{o}_{T}(Fe_3O_4\ (\text{magnetite}) \rightarrow Fe_3O_4[\text{in } Fe_2SiO_4]) = \Delta_{tr}H^{o}_{T} - T \cdot \Delta_{tr}S^{o}_{T} \quad (40).$$

Only the simplest thermodynamic models with minimal number of parameters can be employed to describe the excess chemical potentials of solutions components. This is because the lack of experimental data. The strictly regular solution model [80] is used, and according to it:

$$\mu^{E}_{Fe_3O_4[\text{in } Fe_2SiO_4]} = (1 - x_{Fe_3O_4[\text{in } Fe_2SiO_4]})^2 \cdot L_{Fe_3O_4,\ Fe_2SiO_4} \quad (41).$$

where $L_{Fe_3O_4,\ Fe_2SiO_4}$ is the energy of mixing of compounds in solution, which isn't depend on temperature.

Substituting equations (37) through (41) into equation (36) gives the following expression:

$$\Delta_{tr}H^{o}_{T} - T \cdot \Delta_{tr}S^{o}_{T} + RT \cdot \ln\ x_{Fe_3O_4[\text{in } Fe_2SiO_4]} + (1 - x_{Fe_3O_4[\text{in } Fe_2SiO_4]})^2 \cdot L_{Fe_3O_4,\ Fe_2SiO_4} = 0 \quad (42).$$

Substituting data on *T* and $x_{Fe_3O_4[\text{in } Fe_2SiO_4]}$ from table 4 into equation (42) gives the system of three linear equations with three variables. This system is solved according to Cramer's method [81]. As the result, the following parameters values are estimated

$$\Delta_{tr}G^{o}_{T}(Fe_3O_4\ (\text{magnetite}) \rightarrow Fe_3O_4[\text{in } Fe_2SiO_4]) = 0{,}235T - 1523,\ J/mol \quad (43),$$

$$L_{Fe_3O_4,\ Fe_2SiO_4} = 25216\ J/mol \quad (44).$$

Then, with calculated parameters values, equation (42) can be solved relatively to $x_{Fe_3O_4[\text{in } Fe_2SiO_4]}$ at the temperature T = 298 K. The calculated solid solubility of Fe_3O_4 in Fe_2SiO_4 at standard temperature is $x_{Fe_3O_4[\text{in } Fe_2SiO_4]} = 6{,}85 \cdot 10^{-5}$. The activities of solid solution components (reference state – pure component with fayalite lattice) are $a_{Fe_3O_4} = 0{,}00233$ and $a_{Fe_2SiO_4} \approx 1$.

The equilibrium between pure SiO_2 (quartz) and its solid solution in hematite

$$SiO_2\ (\text{quartz}) = SiO_2[\text{in } Fe_2O_3] \qquad (45)$$

can be described in a similar way that the previous one. The parameters are the molar Gibbs energy of phase transition of SiO_2 from the lattice of pure compound (quartz) to the lattice of solution (hematite)

$$\Delta_{tr}G_T^o(SiO_2\ (\text{quartz}) \rightarrow SiO_2[\text{in } Fe_2O_3]) = \Delta_{tr}H_T^o - T \cdot \Delta_{tr}S_T^o \qquad (46)$$

and the energy of mixing in strictly regular solution of SiO_2 and Fe_2O_3

$$\mu^E_{SiO_2[\text{in } Fe_2O_3]} = (1 - x_{SiO_2[\text{in } Fe_2O_3]})^2 \cdot L_{SiO_2,\,Fe_2O_3} \qquad (47).$$

The resulting equation for thermodynamic calculations is similar to equation (42):

$$\Delta_{tr}H_T^o - T \cdot \Delta_{tr}S_T^o + RT \cdot \ln x_{SiO_2[\text{in } Fe_2O_3]} + (1 - x_{SiO_2[\text{in } Fe_2O_3]})^2 \cdot L_{SiO_2,\,Fe_2O_3} = 0 \qquad (48).$$

The results of solving equation (48) are the following:

$$\Delta_{tr}G_T^o(SiO_2\ (\text{quartz}) \rightarrow SiO_2[\text{in } Fe_2O_3]) = 2{,}621T + 6557,\ ^{J}/_{mol} \qquad (49),$$

$$L_{SiO_2,\,Fe_2O_3} = 8740\ ^{J}/_{mol} \qquad (50).$$

The calculated solid solubility of SiO_2 in Fe_2O_3 at standard temperature is $x_{SiO_2[\text{in } Fe_2O_3]} = 1{,}54 \cdot 10^{-3}$. The activities of solid solution components (reference state – pure component with hematite lattice) are $a_{SiO_2} = 0{,}0541$ and $a_{Fe_2O_3} = 0{,}998$.

Both solid solutions reveal small positive deviations from ideal behaviour. Calculated solid solubility at standard temperature in both cases is vanishingly small. It inflicts no effect on crystal structure and composition of iron silicate.

3. 2. The Fe – Si – O system state diagram.

The method of plotting and describing three-component state diagrams for metal-oxygen-containing systems was developed in [61, 62]. A diagram consists of two ordinary orthogonal axes. The abscissa is the mole fraction of one metal compound in binary system; in present study abscissa is represented by silicon mole fraction x_{Si}, assuming $x_{Fe} = 1 - x_{Si}$. The ordinate is represented by system oxidation degree (y), which is the quantity of moles of atomic oxygen in system, corresponding to the one mole of metallic compounds; in present study it is determined as

$$y = \frac{n_O}{n_{Fe} + n_{Si}} \qquad (51).$$

A diagram is plotted at fixed temperature and pressure. According to Gibbs' phase rule [45], when these two variables are fixed, maximum of three phases can coexist in three-component system. Any single compound (one-phase region) is depicted by any vertex within the diagram, a two-phase region is depicted by any tie-line between two nearest vertices, a three-phase region is depicted by any triangle and it corresponds to invariant system condition. Crossing tie-lines isn't allowed, because the point of their intersection would correspond to four-phase region, which is impossible. Any phase of variable composition is depicted by line; any triangle, containing this line and filled with dotted lines, corresponds to monovariant system condition. Thus, this kind of state diagram has the same functionality as the ordinary triangle phase diagram (which, for example, are plotted for some Metal – Si – O systems by the authors of [82]), but is simpler to plot and examine.

While any Fe – Si system compound is oxidizing, all equilibria with oxygen (from thermodynamic point of view) take place in multiple stages, one after the other. Since the

chemical affinity of silicon to oxygen in much higher, than that of iron [61], silicon from iron silicides has to be oxidized in the first order, and the consecutive formation of phases, more and more rich of iron has to be observed. Along with this, the equilibrium oxygen pressure is to increase from the previous stage to the next one. The equilibrium oxygen pressure for each system condition is calculated according to the laws of chemical equilibrium as it is shown in [61].

The Fe – Si – O state diagram is plotted in two variants. The first one doesn't take into account the formation of "Fe_3Si" compound and α-phase ordering (as discussed earlier in section 2. 3.). It is shown at figure 2. The second variant of the diagram takes into account formation of "Fe_3Si" compound. It is shown at figure 3. The appropriate characteristics of system conditions for the both diagram variants are represented in table 5.

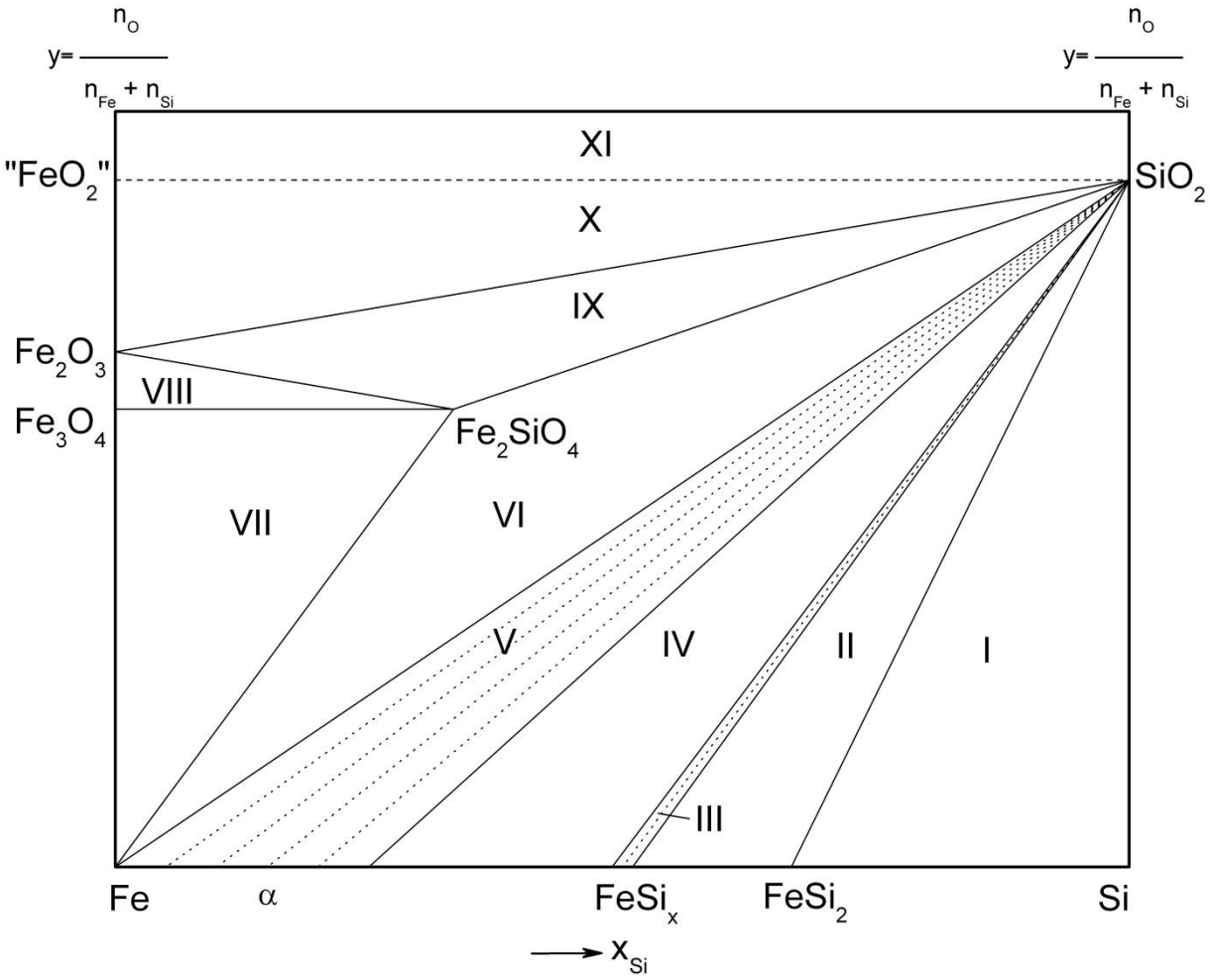

Figure 2. The Fe – Si – O state diagram at 298 K without consideration of "Fe_3Si".

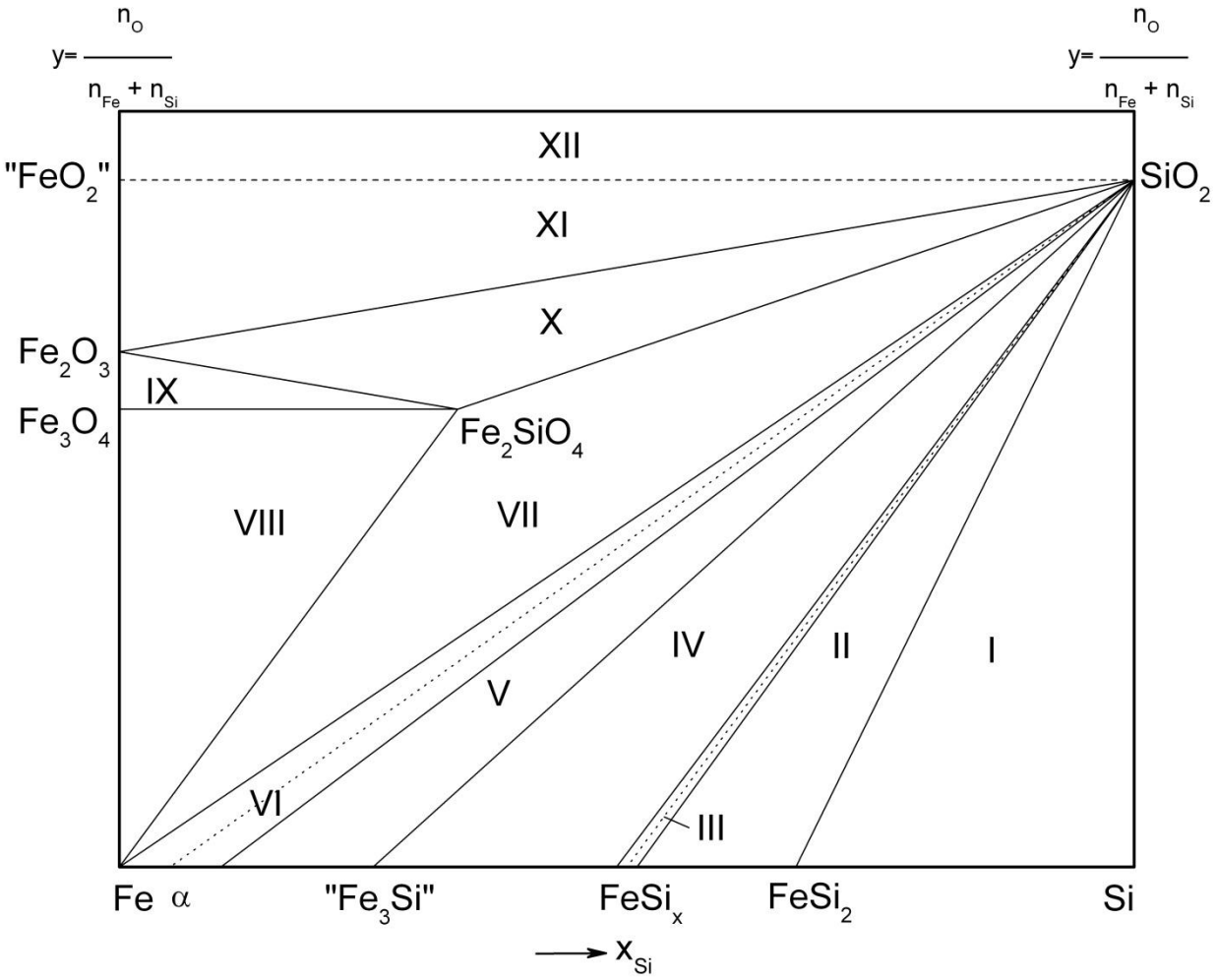

Figure 3. The Fe – Si – O state diagram at 298 K with consideration of "Fe_3Si".

No. of domain at		System condition	Reaction equation	P_{O_2}, bar
figure 2	figure 3			
I	I	$FeSi_2$ – Si (diamond) – SiO_2	Si (diamond) + O_2 = SiO_2	$7{,}7 \cdot 10^{-142}$
II	II	$FeSi_{1,033}$ – $FeSi_2$ – SiO_2	$FeSi_2$ + 0,967 O_2 = = $FeSi_{1,033}$ + 0,967 SiO_2	$4{,}5 \cdot 10^{-141}$
III	III	$FeSi_x$ – SiO_2 ($0{,}961 \le x \le 1{,}033$)	$FeSi_n + (n-m)\ O_2 =$ $= FeSi_m + (n-m)\ SiO_2$ ($0{,}961 \le m,\ n \le 1{,}033,\ m < n$)	–
IV	–	α-phase (Fe) – $FeSi_{0,961}$ – SiO_2	$FeSi_{0,961}$ + 0,961 O_2 = = Fe (α) + 0,961 SiO_2 $x_{Si(\alpha)} = 0{,}264$; $a_{Si} = 7{,}2 \cdot 10^{-20}$; $a_{Fe} = 0{,}114$	$1{,}1 \cdot 10^{-129}$
–	IV	"Fe_3Si" – $FeSi_{0,961}$ – SiO_2	$3FeSi_{0,961}$ + 1,883 O_2 = = "Fe_3Si" + 1,883 SiO_2	$1{,}1 \cdot 10^{-130}$
–	V	α-phase (Fe) – "Fe_3Si" – SiO_2	"Fe3Si" + O_2 = 3Fe (α) + SiO_2 $x_{Si(\alpha)} = 0{,}112$; $a_{Si} = 5{,}5 \cdot 10^{-20}$; $a_{Fe} = 0{,}473$	$6{,}4 \cdot 10^{-126}$

V	VI	α-phase (Fe) – SiO_2	Si (α) + O_2 = SiO_2	–
VI	VII	α-phase (Fe) – Fe_2SiO_4 – SiO_2	2Fe (α) + Si (α) + $2O_2$ = Fe_2SiO_4 Si (α) + O_2 = SiO_2 $x_{Si(\alpha)} = 1{,}1 \cdot 10^{-27}$; $a_{Si} = 5{,}3 \cdot 10^{-50}$; $a_{Fe} \approx 1$	$1{,}3 \cdot 10^{-99}$
VII	VIII	α-phase (Fe) – Fe_3O_4 – [Fe_3O_4, Fe_2SiO_4]	3Fe (α) + $2O_2$ = Fe_3O_4 (magnetite) 2Fe (α) + Si (α) + $2O_2$ = Fe_2SiO_4 Fe_3O_4 (magnetite) = = Fe_3O_4 [in Fe_2SiO_4] $x_{Si(\alpha)} = 1{,}02 \cdot 10^{-47}$; $a_{Si} = 4{,}9 \cdot 10^{-70}$; $a_{Fe} \approx 1$; $x_{Fe_3O_4[\text{in } Fe_2SiO_4]} = 6{,}85 \cdot 10^{-5}$; $a_{Fe_3O_4} = 0{,}00233$; $a_{Fe_2SiO_4} \approx 1$	$1{,}3 \cdot 10^{-89}$
VIII	IX	Fe_3O_4 – Fe_2O_3 – [Fe_3O_4, Fe_2SiO_4]	Fe_3O_4 [in Fe_2SiO_4] = Fe_3O_4 (magnetite) $4Fe_3O_4$ (magnetite) + O_2 = = 6 Fe_2O_3	$2{,}8 \cdot 10^{-68}$
IX	X	[SiO_2, Fe_2O_3] – Fe_2SiO_4 – SiO_2	$2Fe_2SiO_4$ + O_2 = $2Fe_2O_3$ + $2SiO_2$ (quartz) SiO_2 (quartz) = SiO_2 [in Fe_2O_3] $x_{SiO_2[\text{in } Fe_2O_3]} = 1{,}54 \cdot 10^{-3}$; $a_{Fe_3O_4} = 0{,}0541$; $a_{Fe_2O_3} = 0{,}998$	$1{,}8 \cdot 10^{-62}$
X	XI	[SiO_2, Fe_2O_3] – "FeO_2" – SiO_2	SiO_2 [in Fe_2O_3] = SiO_2 (quartz) $2Fe_2O_3$ + O_2 = 4"FeO_2"	$6{,}0 \cdot 10^{5}$
XI	XII	"FeO_2" – SiO_2 – {O_2}	–	–

Table 5. The characteristics of the Fe – Si – O system conditions at 298 K.

At domain III, reaction between $FeSi_{1,033}$ phase and oxygen takes place with selective oxidation of silicon. As the result, some silicon oxidizes to SiO_2 and *x* index in $FeSi_x$ formula decreases, unless $FeSi_{0,961}$ composition is reached. The similar situation occurs at domain V at figure 2 and domain VI at figure 3, where α-phase reacts with oxygen. Silicon from solid solution oxidizes to SiO_2 and the new solution composition, more and more rich of iron, forms. Both these system conditions are monovariant, therefore equilibrium oxygen pressure changes during reaction and there is no exact value presented in table 5 for these equilibria.

At domain VII at figure 2 and domain VIII at figure 3 both components of α-phase are oxidized, and simultaneous formation of Fe_3O_4 and Fe_2SiO_4 takes place. A very small amount of magnetite dissolves in fayalite until the maximum solid solubility is reached. The remaining magnetite forms an independent phase. At the next stage (domains VIII and IX at figures 2 and 3, respectively) magnetite phase oxidizes to hematite. This causes the equilibrium (35) to shift in opposite direction; Fe_3O_4 from solid solution transforms back to magnetite and then oxidizes. A similar situation occurs with the second solid solution. At domain IX at figure 2 and domain X at figure 3 the simultaneous formation of Fe_2O_3 and SiO_2 from Fe_2SiO_4 takes place. A small amount of silicon dioxide dissolves in hematite and the remaining SiO_2 forms a separate phase. At the next stage (domains X and XI at figures 2 and 3, respectively) hematite phase oxidizes to "FeO_2", the equilibrium (45) shifts in opposite direction and SiO_2 from solution transforms back

to quartz phase. All these phase transitions don't involve oxygen and cause no influence on equilibrium oxygen pressure at corresponding stages.

4. Chemical and electrochemical equilibria in Fe – Si – H_2O system at standard conditions and the electrochemical stability of iron silicides.

In order to develop thermodynamic model of Fe – Si alloys oxidation in liquid environments, it is convenient to use the diagrams of electrochemical equilibrium (potential – pH dependencies) [61, 83, 84], that most clearly show the possible chemical and electrochemical equilibria in system. Method of plotting such diagrams was in detail described several times [83, 84] and the application of potential – pH diagrams to multicomponent and multiphase equilibria was proposed by the author of [85[. Along the above mentioned oxides, the possible ions, which can be formed in solution, have to be considered as the oxidation products. These ions are Fe^{2+}, Fe^{3+}, FeO_4^{2-} and SiO_3^{2-}. The $HFeO_2^-$ ion, mentioned in paper [86], can be formed only in strongly alkaline environments (pH > 14) and very dilute solutions ($a_i < 10^{-6}$ $^{mol}/_{l}$), therefore they aren't taken into consideration in present study. The primary information about the Fe – H_2O and Si – H_2O potential – pH diagrams and the thermodynamic properties of the electrochemical reactions, involving ions, can be obtained from textbooks [64, 87], papers [88 – 90] and databases [91 – 99]. The potential – pH diagram for Fe – Si – H_2O system was previously plotted in studies [33, 100], but both these diagrams don't take into account all phases in Fe – Si system.

Any oxides or oxygen-containing ions in solution can exist in unhydrated or in hydrated form. The transition from the first form to the second one proceeds through the series of intermediate conditions. The unhydrated form is most thermodynamically stable, therefore metal hydroxides and other particles like $FeOH^+$, $FeOOH$, $FeOH^{2+}$, $Fe(OH)_2^+$, $Fe(OH)_3^-$, $Fe(OH)_4^-$, $Fe_2(OH)_2^{4+}$, $Fe_3(OH)_4^{5+}$, H_4SiO_4, H_8SiO_6, $H_2Si_2O_5$, $H_6Si_2O_7$, $HSi(OH)_6^-$, $H_2SiO_4^{2-}$, $H_3SiO_4^-$, $H_4(H_2SiO_4)_4^{4-}$, $H_6(H_2SiO_4)_4^{2-}$, $SiO_2(OH)^{2-}$, $SiO(OH)_3^-$, $Si_2O_3(OH)_4^{2-}$ and others, noticed in [51, 64, 87 – 100], aren't taken into consideration.

The potential – pH diagram of Fe – Si – H_2O system at 25˚C, air pressure of 1 bar and activities of ions in solutions (standard reference state – hypothetical one molar solution), equal to 1 $^{mol}/_{l}$ without consideration of "Fe_3Si" is represented at figure 4. The characteristics of basic chemical and electrochemical equilibria in system are summarized in table 6.

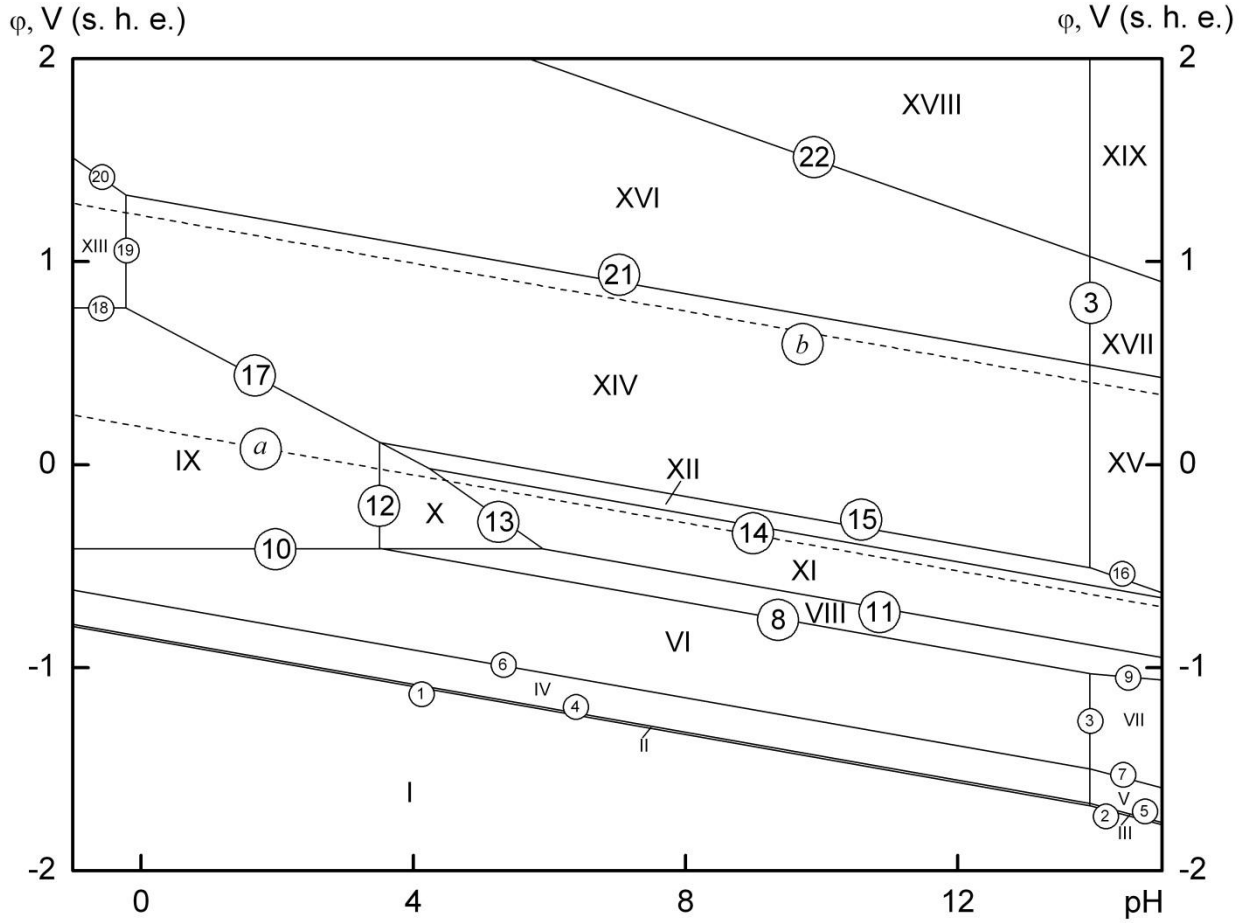

Figure 4. The potential – pH diagram of the Fe – Si – H_2O system at 298 K, air pressure of 1 bar and activities of ions in solutions, equal to 1 $^{mol}/_{l}$ (unhydrated form of oxides, without consideration of "Fe_3Si" compound).

No. of line at figure 4	Electrode reaction	Equilibrium potential, V (s. h. e.) or solution pH
a	$2H^+ + 2e^- = H_2; P_{H_2} = 5 \cdot 10^{-7}$ bar	$0{,}186 - 0{,}0591 \cdot pH$
b	$O_2 + 4H^+ + 4e^- = 2H_2O; P_{O_2} = 0{,}21$ bar	$1{,}219 - 0{,}0591 \cdot pH$
1	$SiO_2 + 4H^+ + 4e^- = Si\ (diamond) + 2H_2O$	$-0{,}857 - 0{,}0591 \cdot pH$
2	$SiO_3^{2-} + 6H^+ + 4e^- = Si(diamond) + 3H_2O$	$-0{,}444 - 0{,}0887 \cdot pH + 0{,}0148 \cdot \lg a_{SiO_3^{2-}}$
3	$SiO_3^{2-} + 2H^+ = SiO_2 + 2H_2O$	$pH = 13{,}94 + 0{,}5 \cdot \lg a_{SiO_3^{2-}}$
4	$FeSi_{1{,}033} + 0{,}967\ SiO_2 + 3{,}868\ H^+ + 3{,}868\ e^- = FeSi_2 + 1{,}934\ H_2O$	$-0{,}845 - 0{,}0591 \cdot pH$
5	$FeSi_{1{,}033} + 0{,}967\ SiO_3^{2-} + 5{,}802\ H^+ + 3{,}868\ e^- = FeSi_2 + 2{,}901\ H_2O$	$-0{,}433 - 0{,}0887 \cdot pH + 0{,}0148 \cdot \lg a_{SiO_3^{2-}}$
6	$Fe\ (\alpha) + 0{,}961\ SiO_2 + 3{,}844\ H^+ + 3{,}844\ e^- = FeSi_{0{,}961} + 1{,}922\ H_2O; a_{Fe(\alpha)} = 0{,}114$	$-0{,}677 - 0{,}0591 \cdot pH$

7	$\mathrm{Fe}\,(\alpha) + 0{,}961\ \mathrm{SiO_3^{2-}} + 5{,}766\ \mathrm{H^+} + 3{,}844\ \mathrm{e^-} = \mathrm{FeSi_{0{,}961}} + 2{,}883\ \mathrm{H_2O};\ a_{\mathrm{Fe}(\alpha)} = 0{,}114$	$-0{,}264 - 0{,}0887 \cdot \mathrm{pH} + 0{,}0148 \cdot \lg a_{\mathrm{SiO_3^{2-}}}$
8	$\mathrm{Fe_2SiO_4} + 4\mathrm{H^+} + 4\mathrm{e^-} = 2\mathrm{Fe}(\alpha) + \mathrm{SiO_2} + 2\mathrm{H_2O};\ a_{\mathrm{Fe}(\alpha)} = 0{,}114$	$-0{,}205 - 0{,}0591 \cdot \mathrm{pH}$
9	$\mathrm{Fe_2SiO_4} + 2\mathrm{H^+} + 4\mathrm{e^-} = 2\mathrm{Fe}(\alpha) + \mathrm{SiO_3^{2-}} + \mathrm{H_2O};\ a_{\mathrm{Fe}(\alpha)} = 0{,}114$	$-0{,}617 - 0{,}0295 \cdot \mathrm{pH} - 0{,}0148 \cdot \lg a_{\mathrm{SiO_3^{2-}}}$
10	$\mathrm{Fe^{2+}} + 2\mathrm{e^-} = \mathrm{Fe}(\alpha);\ a_{\mathrm{Fe}(\alpha)} = 0{,}114$	$-0{,}412 + 0{,}0295 \cdot \lg a_{\mathrm{Fe^{2+}}}$
11	$\mathrm{Fe_3O_4} + 8\mathrm{H^+} + 8\mathrm{e^-} = 3\mathrm{Fe}(\alpha) + 4\mathrm{H_2O};\ a_{\mathrm{Fe}(\alpha)} = 0{,}114$	$-0{,}064 - 0{,}0591 \cdot \mathrm{pH}$
12	$\mathrm{Fe_2SiO_4} + 4\mathrm{H^+} = 2\mathrm{Fe^{2+}} + \mathrm{SiO_2} + 2\mathrm{H_2O}$	$\mathrm{pH} = 3{,}508 - 0{,}5 \cdot \lg a_{\mathrm{Fe^{2+}}}$
13	$\mathrm{Fe_3O_4} + 8\mathrm{H^+} + 2\mathrm{e^-} = 3\mathrm{Fe^{2+}} + 4\mathrm{H_2O}$	$0{,}982 - 0{,}2364 \cdot \mathrm{pH} - 0{,}0887 \cdot \lg a_{\mathrm{Fe^{2+}}}$
14	$3\mathrm{Fe_2O_3} + 2\mathrm{H^+} + 2\mathrm{e^-} = 2\mathrm{Fe_3O_4} + \mathrm{H_2O}$	$0{,}231 - 0{,}0591 \cdot \mathrm{pH}$
15	$\mathrm{Fe_2O_3} + \mathrm{SiO_2} + 2\mathrm{H^+} + 2\mathrm{e^-} = \mathrm{Fe_2SiO_4} + \mathrm{H_2O}$	$0{,}317 - 0{,}0591 \cdot \mathrm{pH}$
16	$\mathrm{Fe_2O_3} + \mathrm{SiO_3^{2-}} + 4\mathrm{H^+} + 2\mathrm{e^-} = \mathrm{Fe_2SiO_4} + 2\mathrm{H_2O}$	$1{,}141 - 0{,}1182 \cdot \mathrm{pH} + 0{,}0295 \cdot \lg a_{\mathrm{SiO_3^{2-}}}$
17	$\mathrm{Fe_2O_3} + 6\mathrm{H^+} + 2\mathrm{e^-} = 2\mathrm{Fe^{2+}} + 3\mathrm{H_2O}$	$0{,}732 - 0{,}1773 \cdot \mathrm{pH} - 0{,}0591 \cdot \lg a_{\mathrm{Fe^{2+}}}$
18	$\mathrm{Fe^{3+}} + \mathrm{e^-} = \mathrm{Fe^{2+}}$	$0{,}771 + 0{,}0591 \cdot \lg \dfrac{a_{\mathrm{Fe^{3+}}}}{a_{\mathrm{Fe^{2+}}}}$
19	$\mathrm{Fe_2O_3} + 6\mathrm{H^+} = 2\mathrm{Fe^{3+}} + 3\mathrm{H_2O}$	$\mathrm{pH} = -0{,}221 - 0{,}333 \cdot \lg a_{\mathrm{Fe^{3+}}}$
20	$\text{"}\mathrm{FeO_2}\text{"} + 4\mathrm{H^+} + \mathrm{e^-} = \mathrm{Fe^{3+}} + 2\mathrm{H_2O}$	$1{,}276 - 0{,}2364 \cdot \mathrm{pH} - 0{,}0591 \cdot \lg a_{\mathrm{Fe^{3+}}}$
21	$2\ \text{"}\mathrm{FeO_2}\text{"} + 2\mathrm{H^+} + 2\mathrm{e^-} = \mathrm{Fe_2O_3} + \mathrm{H_2O}$	$1{,}315 - 0{,}0591 \cdot \mathrm{pH}$
22	$\mathrm{FeO_4^{2-}} + 4\mathrm{H^+} + 2\mathrm{e^-} = \text{"}\mathrm{FeO_2}\text{"} + 2\mathrm{H_2O}$	$2{,}673 - 0{,}1182 \cdot \mathrm{pH} + 0{,}0295 \cdot \lg a_{\mathrm{FeO_4^{2-}}}$

Table 6. Basic chemical and electrochemical equilibria in the Fe – Si – H_2O system at 298 K and air pressure of 1 bar, without consideration of "Fe_3Si" compound.

19 domains of thermodynamic stability of certain phases can be depicted at the presented diagram (figure 4):
I – α-phase (bcc) + $FeSi_x$ + $FeSi_2$ + Si (diamond);
II – α-phase (bcc) + $FeSi_x$ + $FeSi_2$ + SiO_2;
III – α-phase (bcc) + $FeSi_x$ + $FeSi_2$ + SiO_3^{2-};
IV – α-phase (bcc) + $FeSi_x$ + SiO_2;
V – α-phase (bcc) + $FeSi_x$ + SiO_3^{2-};
VI – α-phase (bcc) + SiO_2;
VII – α-phase (bcc) + SiO_3^{2-};
VIII – α-phase (bcc) + Fe_2SiO_4;
IX – Fe^{2+} + SiO_2;
X – Fe^{2+} + Fe_2SiO_4;
XI – Fe_3O_4 (magnetite) + [Fe_3O_4, Fe_2SiO_4] (fayalite);
XII – Fe_2O_3 + Fe_2SiO_4;
XIII – Fe^{3+} + SiO_2;
XIV – [SiO_2, Fe_2O_3] (hematite) + SiO_2 (quartz);
XV – Fe_2O_3 + SiO_3^{2-};

XVI – “FeO_2” + SiO_2;

XVII – “FeO_2” + SiO_3^{2-};

XVIII – FeO_4^{2-} + SiO_2;

XIX – FeO_4^{2-}, SiO_3^{2-}.

Domain I is the domain of thermodynamic stability, where all components of Fe – Si system remain immune to corrosion. At the domains from II to VII the consecutive decomposition of iron silicides takes place. Domains IX, X and XIII are the domains of active corrosion, where iron dissolves from alloys and passes into solution in form of cations Fe^{2+} or Fe^{3+}. Domains II, IV, VI, VIII, XI, XII, XIV and XVI are the domains of passivity, where the protective oxide film, consisting of simple oxides of iron or silicon or iron silicate, is formed on the alloy surface and prevent further oxidation. Domains III, V, VII, XV, XVII, XVIII and XIX are the domains of transpassivity, where the oxides from passivation layer oxidize further and pass into solution in form of anions, which violates the integrity of the protective film.

The potential – pH diagram of Fe – Si – H_2O system at 25˚C, air pressure of 1 bar and activities of ions in solutions, equal to 1 $^{mol}/_{l}$, considering “Fe_3Si”, is represented at figure 5. The characteristics of appropriate chemical and electrochemical equilibria in system are summarized in table 7.

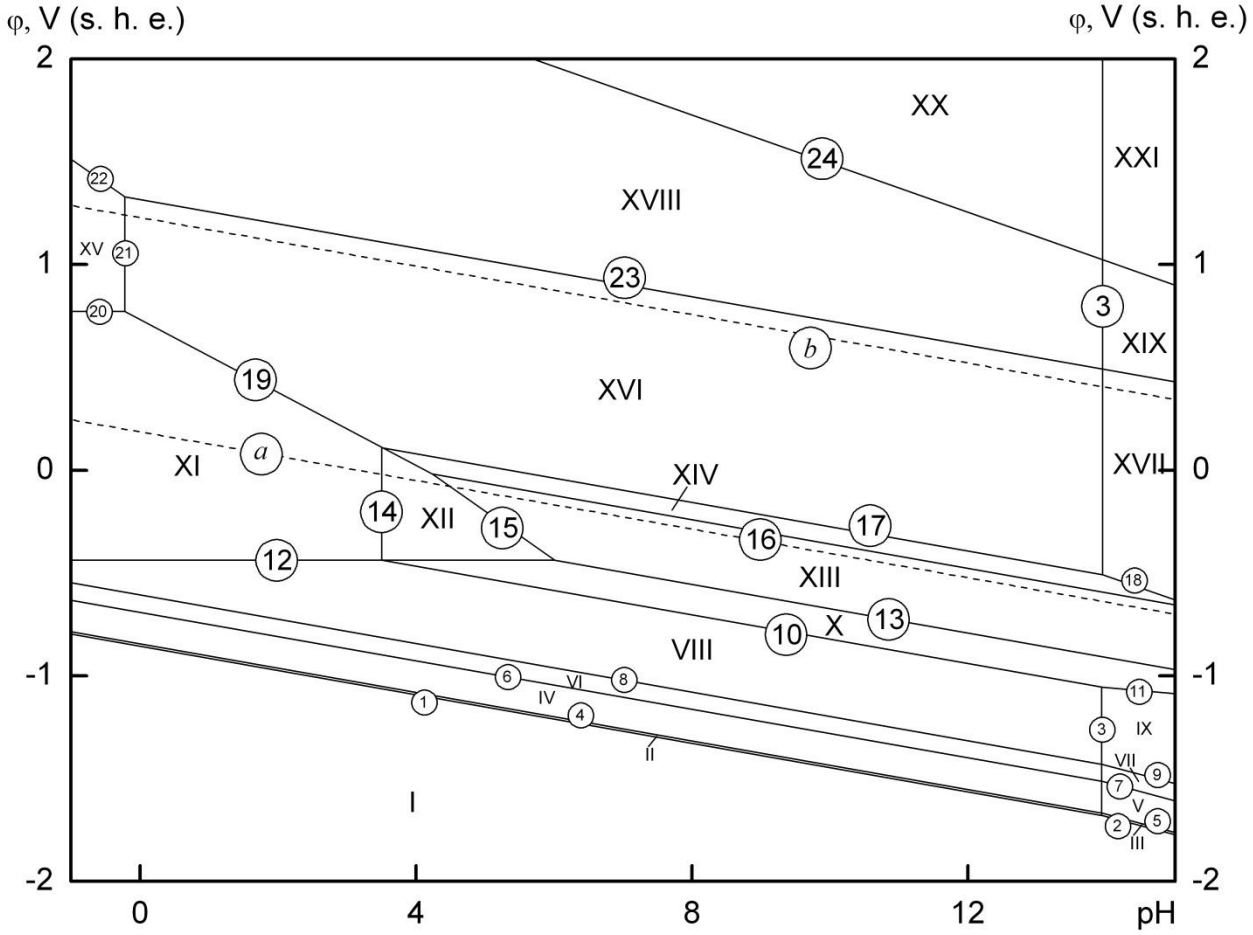

Figure 5. The potential – pH diagram of the Fe – Si – H_2O system at 298 K, air pressure of 1 bar and activities of ions in solutions, equal to 1 $^{mol}/_{l}$ (unhydrated form of oxides, considering “Fe_3Si” compound).

No. of line at figure 5	Electrode reaction	Equilibrium potential, V (s. h. e.) or solution pH
a	$2H^+ + 2e^- = H_2; P_{H_2} = 5 \cdot 10^{-7}$ bar	$0{,}186 - 0{,}0591 \cdot pH$
b	$O_2 + 4H^+ + 4e^- = 2H_2O; P_{O_2} = 0{,}21$bar	$1{,}219 - 0{,}0591 \cdot pH$
1	$SiO_2 + 4H^+ + 4e^- = Si\ (diamond) + 2H_2O$	$-0{,}857 - 0{,}0591 \cdot pH$
2	$SiO_3^{2-} + 6H^+ + 4e^- = Si(diamond) + 3H_2O$	$-0{,}444 - 0{,}0887 \cdot pH + 0{,}0148 \cdot \lg a_{SiO_3^{2-}}$
3	$SiO_3^{2-} + 2H^+ = SiO_2 + 2H_2O$	$pH = 13{,}94 + 0{,}5 \cdot \lg a_{SiO_3^{2-}}$
4	$FeSi_{1,033} + 0{,}967\ SiO_2 + 3{,}868\ H^+ + 3{,}868\ e^- = FeSi_2 + 1{,}934\ H_2O$	$-0{,}845 - 0{,}0591 \cdot pH$
5	$FeSi_{1,033} + 0{,}967\ SiO_3^{2-} + 5{,}802\ H^+ + 3{,}868\ e^- = FeSi_2 + 2{,}901\ H_2O$	$-0{,}433 - 0{,}0887 \cdot pH + 0{,}0148 \cdot \lg a_{SiO_3^{2-}}$
6	$"Fe_3Si" + 1{,}883\ SiO_2 + 7{,}532\ H^+ + 7{,}532\ e^- = 3FeSi_{0,961} + 3{,}766\ H_2O$	$-0{,}692 - 0{,}0591 \cdot pH$
7	$"Fe_3Si" + 1{,}883\ SiO_3^{2-} + 11{,}298\ H^+ + 7{,}532\ e^- = FeSi_{0,961} + 5{,}649\ H_2O$	$-0{,}279 - 0{,}0887 \cdot pH + 0{,}0148 \cdot \lg a_{SiO_3^{2-}}$
8	$3Fe\ (\alpha) + SiO_2 + 4H^+ + 4e^- = "Fe_3Si" + 2H_2O; a_{Fe(\alpha)} = 0{,}456$	$-0{,}622 - 0{,}0591 \cdot pH$
9	$3Fe\ (\alpha) + SiO_3^{2-} + 6H^+ + 4e^- = "Fe_3Si" + 3H_2O; a_{Fe(\alpha)} = 0{,}456$	$-0{,}210 - 0{,}0887 \cdot pH + 0{,}0148 \cdot \lg a_{SiO_3^{2-}}$
10	$Fe_2SiO_4 + 4H^+ + 4e^- = 2Fe(\alpha) + SiO_2 + 2H_2O;$ $a_{Fe(\alpha)} = 0{,}456$	$-0{,}222 - 0{,}0591 \cdot pH$
11	$Fe_2SiO_4 + 2H^+ + 4e^- = 2Fe(\alpha) + SiO_3^{2-} + H_2O;$ $a_{Fe(\alpha)} = 0{,}456$	$-0{,}635 - 0{,}0295 \cdot pH - 0{,}0148 \cdot \lg a_{SiO_3^{2-}}$
12	$Fe^{2+} + 2e^- = Fe(\alpha); a_{Fe(\alpha)} = 0{,}456$	$-0{,}430 + 0{,}0295 \cdot \lg a_{Fe^{2+}}$
13	$Fe_3O_4 + 8H^+ + 8e^- = 3Fe(\alpha) + 4H_2O;$ $a_{Fe(\alpha)} = 0{,}456$	$-0{,}077 - 0{,}0591 \cdot pH$
14	$Fe_2SiO_4 + 4H^+ = 2Fe^{2+} + SiO_2 + 2H_2O$	$pH = 3{,}508 - 0{,}5 \cdot \lg a_{Fe^{2+}}$
15	$Fe_3O_4 + 8H^+ + 2e^- = 3Fe^{2+} + 4H_2O$	$0{,}982 - 0{,}2364 \cdot pH - 0{,}0887 \cdot \lg a_{Fe^{2+}}$
16	$3Fe_2O_3 + 2H^+ + 2e^- = 2Fe_3O_4 + H_2O$	$0{,}231 - 0{,}0591 \cdot pH$
17	$Fe_2O_3 + SiO_2 + 2H^+ + 2e^- = Fe_2SiO_4 + H_2O$	$0{,}317 - 0{,}0591 \cdot pH$
18	$Fe_2O_3 + SiO_3^{2-} + 4H^+ + 2e^- = Fe_2SiO_4 + 2H_2O$	$1{,}141 - 0{,}1182 \cdot pH + 0{,}0295 \cdot \lg a_{SiO_3^{2-}}$
19	$Fe_2O_3 + 6H^+ + 2e^- = 2Fe^{2+} + 3H_2O$	$0{,}732 - 0{,}1773 \cdot pH - 0{,}0591 \cdot \lg a_{Fe^{2+}}$
20	$Fe^{3+} + e^- = Fe^{2+}$	$0{,}771 + 0{,}0591 \cdot \lg \dfrac{a_{Fe^{3+}}}{a_{Fe^{2+}}}$
21	$Fe_2O_3 + 6H^+ = 2Fe^{3+} + 3H_2O$	$pH = -0{,}221 - 0{,}333 \cdot \lg a_{Fe^{3+}}$

22	$"FeO_2"+4H^+ + e^- = Fe^{3+} + 2H_2O$	$1{,}276 - 0{,}2364 \cdot pH - 0{,}0591 \cdot \lg a_{Fe^{3+}}$
23	$2\ "FeO_2"+2H^+ + 2e^- = Fe_2O_3 + H_2O$	$1{,}315 - 0{,}0591 \cdot pH$
24	$FeO_4^{2-} + 4H^+ + 2e^- = "FeO_2"+2H_2O$	$2{,}673 - 0{,}1182 \cdot pH + 0{,}0295 \cdot \lg a_{FeO_4^{2-}}$

Table 7. Basic chemical and electrochemical equilibria in the Fe – Si – H_2O system at 298 K and air pressure of 1 bar, considering "Fe_3Si" compound.

The diagram at figure 5 contains 21 domain of thermodynamic stability of certain phases:
I – α-phase (bcc) + "Fe_3Si" + $FeSi_x$ + $FeSi_2$ + Si (diamond);
II – α-phase (bcc) + "Fe_3Si" + $FeSi_x$ + $FeSi_2$ + SiO_2;
III – α-phase (bcc) + "Fe_3Si" + $FeSi_x$ + $FeSi_2$ + SiO_3^{2-};
IV – α-phase (bcc) + "Fe_3Si" + $FeSi_x$ + SiO_2;
V – α-phase (bcc) + "Fe_3Si" + $FeSi_x$ + SiO_3^{2-};
VI – α-phase (bcc) + "Fe_3Si" + SiO_2;
VII – α-phase (bcc) + "Fe_3Si" + SiO_3^{2-};
VIII – α-phase (bcc) + SiO_2;
IX – α-phase (bcc) + SiO_3^{2-};
X – α-phase (bcc) + Fe_2SiO_4;
XI – Fe^{2+} + SiO_2;
XII – Fe^{2+} + Fe_2SiO_4;
XIII – Fe_3O_4 (magnetite) + [Fe_3O_4, Fe_2SiO_4] (fayalite);
XIV – Fe_2O_3 + Fe_2SiO_4;
XV – Fe^{3+} + SiO_2;
XVI – [SiO_2, Fe_2O_3] (hematite) + SiO_2 (quartz);
XVII – Fe_2O_3 + SiO_3^{2-};
XVIII – "FeO_2" + SiO_2;
XIX – "FeO_2" + SiO_3^{2-};
XX – FeO_4^{2-} + SiO_2;
XXI – FeO_4^{2-}, SiO_3^{2-}.

There are minor differences between the diagrams at figures 4 and 5, related with existence of "Fe_3Si" phase. The equilibria, involving α-Fe (lines 8 through 11 at figure 4 and lines 10 through 13 at figure 5) differ by 0,02V due to different activities of iron in solid solutions. The equilibria, involving oxide phases (lines 12 – 22 and 14 – 24, respectively) are completely the same. Consequently, the classification of domains at figure 5 is very similar to these, presented for figure 4. In addition to domains I through V at figure 4 there are two extra domains, VI and VII at figure 5, which correspond to "Fe_3Si" compound stability. Domains VI through XIX at figure 4 and domains VIII through XXI at figure 5 are identical and represent the same areas of active corrosion, passivity and transpassivity.

Along with electrochemical oxidation to oxides or anions, the electrochemical reduction of metal compounds to their hydrides can occur in water environments. Therefore, possible formation of iron and silicon hydrides is taken into consideration. It is well known, that iron hydride exist within the Earth's core at high pressures and temperatures [101, 102]. But its synthesis at standard temperature was also studied by the authors of [102, 103]. Iron hydride has hcp structure and the variable composition FeH_x $\{0 < x \le 1\}$ [102, 103]. Index "x" strongly depends on the sample synthesis conditions, for example, $FeH_{0,3}$ – $FeH_{0,4}$ was reported in [102] and the variety from $FeH_{0,1}$ to $FeH_{0,8}$ in [103]. There are a few studies of iron hydride thermodynamic properties [104, 105] since its standard Gibbs energy of formation can't be

determined directly. The authors of [104] have performed an estimation of this value, referred to stoichiometric compound “FeH”. The result of their estimation is the following:

$$\Delta_f G^o_{298}(\text{"FeH"}) = 23500\ {}^{J}/_{\text{mol}} \quad (52).$$

Silicon hydrides SiH_2, SiH_4 and Si_2H_6 can be produced only at 120ºC, they resist any chemical influence of water environments (unless there are no fluoride ions in solution) and can’t be formed electrochemically [65]. Therefore, only equilibria, involving iron hydride are considered in present study.

Calculations show, that “Fe_3Si” compound isn’t thermodynamically stable in presence of iron hydride. Therefore, it isn’t taken into consideration, and the first variant of Fe – Si system potential – pH diagram, presented at figure 4, is modify in order to consider possible electrochemical formation of iron hydride.

The potential – pH diagram of Fe – Si – H_2O system at 25˚C, air pressure of 1 bar and activities of ions in solutions, equal to 1 ${}^{\text{mol}}/_{\text{l}}$, with consideration of “FeH”, is represented at figure 6. The characteristics of appropriate chemical and electrochemical equilibria in system are summarized in table 8.

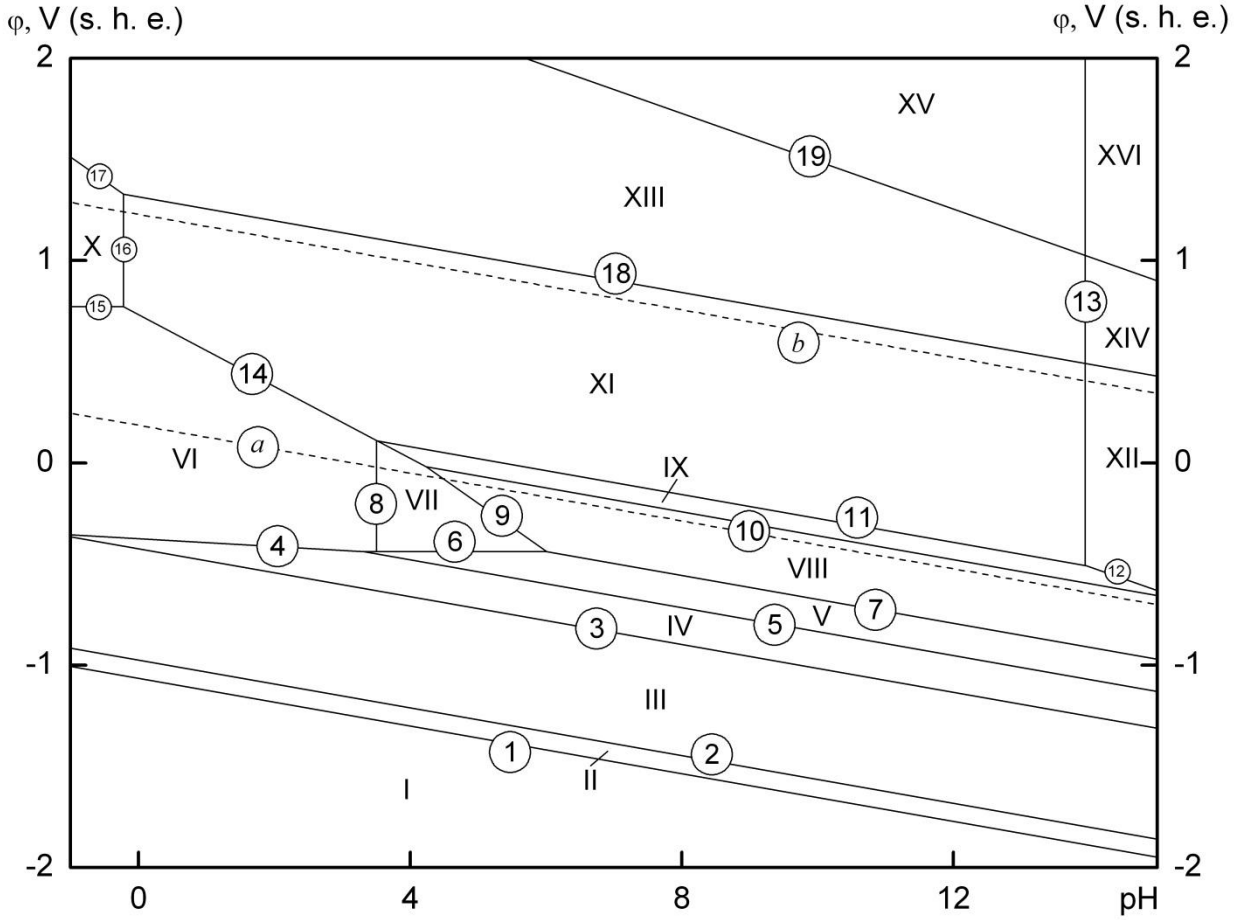

Figure 6. The potential – pH diagram of the Fe – Si – H_2O system at 298 K, air pressure of 1 bar and activities of ions in solutions, equal to 1 ${}^{\text{mol}}/_{\text{l}}$ (unhydrated form of oxides, considering “FeH” compound).

No. of line at figure 6	Electrode reaction	Equilibrium potential, V (s. h. e.) or solution pH
a	$2H^+ + 2e^- = H_2; P_{H_2} = 5 \cdot 10^{-7}$ бар	$0{,}186 - 0{,}0591 \cdot pH$
b	$O_2 + 4H^+ + 4e^- = 2H_2O; P_{O_2} = 0{,}21$бар	$1{,}219 - 0{,}0591 \cdot pH$
1	$FeSi_2 + H^+ + e^- = "FeH" + 2Si$ (diamond)	$-1{,}064 - 0{,}0591 \cdot pH$
2	$2\ FeSi_{1{,}033} + 0{,}967\ H^+ + 0{,}967\ e^- = 0{,}967\ "FeH" + 1{,}033\ FeSi_2$	$-0{,}974 - 0{,}0591 \cdot pH$
3	$0{,}961\ Fe_2SiO_4 + 8{,}61\ H^+ + 8{,}61\ e^- = FeSi_{0{,}961} + 0{,}922\ "FeH" + 3{,}844\ H_2O$	$-0{,}426 - 0{,}0591 \cdot pH$
4	$Fe^{2+} + H^+ + 3e^- = "FeH"$	$-0{,}375 - 0{,}0197 \cdot pH + 0{,}0197 \cdot \lg a_{Fe^{2+}}$
5	$Fe(\alpha) + H^+ + e^- = "FeH"; a_{Fe(\alpha)} = 0{,}114$	$-0{,}299 - 0{,}0591 \cdot pH$
6	$Fe^{2+} + 2e^- = Fe(\alpha); a_{Fe(\alpha)} = 0{,}114$	$-0{,}412 + 0{,}0295 \cdot \lg a_{Fe^{2+}}$
7	$Fe_3O_4 + 8H^+ + 8e^- = 3Fe(\alpha) + 4H_2O;$ $a_{Fe(\alpha)} = 0{,}114$	$-0{,}064 - 0{,}0591 \cdot pH$
8	$Fe_2SiO_4 + 4H^+ = 2Fe^{2+} + SiO_2 + 2H_2O$	$pH = 3{,}508 - 0{,}5 \cdot \lg a_{Fe^{2+}}$
9	$Fe_3O_4 + 8H^+ + 2e^- = 3Fe^{2+} + 4H_2O$	$0{,}982 - 0{,}2364 \cdot pH - 0{,}0887 \cdot \lg a_{Fe^{2+}}$
10	$3Fe_2O_3 + 2H^+ + 2e^- = 2Fe_3O_4 + H_2O$	$0{,}231 - 0{,}0591 \cdot pH$
11	$Fe_2O_3 + SiO_2 + 2H^+ + 2e^- = Fe_2SiO_4 + H_2O$	$0{,}317 - 0{,}0591 \cdot pH$
12	$Fe_2O_3 + SiO_3^{2-} + 4H^+ + 2e^- = Fe_2SiO_4 + 2H_2O$	$1{,}141 - 0{,}1182 \cdot pH + 0{,}0295 \cdot \lg a_{SiO_3^{2-}}$
13	$SiO_3^{2-} + 2H^+ = SiO_2 + 2H_2O$	$pH = 13{,}94 + 0{,}5 \cdot \lg a_{SiO_3^{2-}}$
14	$Fe_2O_3 + 6H^+ + 2e^- = 2Fe^{2+} + 3H_2O$	$0{,}732 - 0{,}1773 \cdot pH - 0{,}0591 \cdot \lg a_{Fe^{2+}}$
15	$Fe^{3+} + e^- = Fe^{2+}$	$0{,}771 + 0{,}0591 \cdot \lg \frac{a_{Fe^{3+}}}{a_{Fe^{2+}}}$
16	$Fe_2O_3 + 6H^+ = 2Fe^{3+} + 3H_2O$	$pH = -0{,}221 - 0{,}333 \cdot \lg a_{Fe^{3+}}$
17	$"FeO_2" + 4H^+ + e^- = Fe^{3+} + 2H_2O$	$1{,}276 - 0{,}2364 \cdot pH - 0{,}0591 \cdot \lg a_{Fe^{3+}}$
18	$2\ "FeO_2" + 2H^+ + 2e^- = Fe_2O_3 + H_2O$	$1{,}315 - 0{,}0591 \cdot pH$
19	$FeO_4^{2-} + 4H^+ + 2e^- = "FeO_2" + 2H_2O$	$2{,}673 - 0{,}1182 \cdot pH + 0{,}0295 \cdot \lg a_{FeO_4^{2-}}$

Table 8. Basic chemical and electrochemical equilibria in the Fe – Si – H_2O system at 298 K and air pressure of 1 bar, considering "FeH" compound.

Presence of "FeH" changes and simplifies the scheme of iron silicides decomposition; there are only 16 domains of thermodynamic stability of certain phases:
I – "FeH" + $FeSi_x$ + $FeSi_2$ + Si (diamond);
II – "FeH" + $FeSi_x$ + $FeSi_2$;
III – "FeH" + $FeSi_x$;
IV – "FeH" + Fe_2SiO_4;
V – α-phase (bcc) + Fe_2SiO_4;
VI – Fe^{2+} + SiO_2;

VII – Fe^{2+} + Fe_2SiO_4;
VIII – Fe_3O_4 (magnetite) + [Fe_3O_4, Fe_2SiO_4] (fayalite);
IX – Fe_2O_3 + Fe_2SiO_4;
X – Fe^{3+} + SiO_2;
XI – [SiO_2, Fe_2O_3] (hematite) + SiO_2 (quartz);
XII – Fe_2O_3 + SiO_3^{2-};
XIII – FeO_2 + SiO_2;
XIV – FeO_2 + SiO_3^{2-};
XV – FeO_4^{2-} + SiO_2;
XVI – FeO_4^{2-}, SiO_3^{2-}.

According to calculations, silicon dioxide and iron hydride can't coexist. Another scheme of iron silicides oxidation is presented (lines 1 – 5 at the diagram), without formation of SiO_2 and SiO_3^{2-}. Instead of domains I through VII at figure 4 only another domains I through IV are depicted at figure 6. These domains can be also classified as domains of passivity of Fe – Si alloy components, where the passivation film consists of iron hydride instead of any oxides. The conssideration of "FeH" doesn't affect all equilibria, which take place in Fe – Si – H_2O system after Fe_2SiO_4 was formed. Lines 6 through 19 and domains V through XVI at figure 6 are identical to lines 10 through 22 and domains VIII through XIX at figure 4.

5. Results and discussion.

Partial pressure of oxygen in atmospheric air is equal to 0,21 bar at standard conditions. This means, that all equilibria in Fe – Si – O system, for which equilibrium oxygen pressure is lesser than 0,21 bar, take place in air environments. Table 5 shows, that oxidation of Fe – Si system alloys ends with formation of Fe_2O_3 and SiO_2 (domains IX and X at figures 2 and 3, respectively) and this agrees with information given in [65]. Small part of SiO_2 can dissolve in Fe_2O_3, while other part forms independent quartz phase. Further oxidation of iron to "FeO_2" doesn't occur, because equilibrium oxygen pressure is $6 \cdot 10^5$ bar. This equilibrium is shown by dashed line at figures 2 and 3. Iron (IV) oxide can be formed only as the part of mixed metals oxide, but it can probably be an independent compound in strongly oxidizing media with very high oxygen pressure.

The specific composition of oxide layer on Fe – Si alloys depends on their composition. Silicon oxidizes in the first order, but if its content in alloy is insufficient to form a continious passiviation layer, Fe_2O_3 can also be involved in its formation. Even Fe_2SiO_4 can be presented in in protective film in form of local inclusions due to the kinetic factors and unreachability of the true equilibrium.

The oxidation features of iron-silicon alloys with variable silicon content in them were studied experimentally several times [106 – 114], however, these studies correspond to high temperatures (800 – 1100ºC). It was found [111, 113, 114], that due to a very low diffusibility of iron through a silica film, the oxidation rate of Fe – Si alloys is much lower, than that of pure iron and typical Cr_2O_3-forming alloy Fe-26Cr. Oxidation rate becomes slower and slower with increasing silicon content in alloy if it exceeds ~5 weight percent [113]. It is related with the minimum silicon concentration, sufficient to develop and maintain a continuous SiO_2 layer on alloy surface [112]. Theoretical studies [32] predict that this minimum concentration is precisely 5 weight percent at the temperatures of 400 – 1000 K. For the alloys composition with lesser silicon content [107 – 110, 114], the presence of Fe_2O_3, Fe_3O_4 and Fe_2SiO_4 is also detected in oxide layer. The primary passivation film, consisting of SiO_2, can, however, decompose, if a significant amount of CO_2 is presented in atmosphere [108 – 112].

When analysing Fe – Si alloys electrochemical oxidation, it is important to pay attention in lines *a* and *b* at the potential – pH diagrams. They correspond to hydrogen and oxygen

electrodes, respectively. The area between these two lines corresponds to water electrochemical stability and has the most importance while studying the corrosion processes. At the diagrams, presented at figures 4 – 6, the area of water electrochemical stability is the same, regardless of considering or not considering some compounds. In strongly acidic environments (pH < 3) iron oxidizes to Fe^{2+} or Fe^{3+} cations, and only in very alkaline environments (pH > 14) silicate ions can be produced. The most part of this area is occupied by the domain of thermodynamic stability of Fe_2O_3 + SiO_2, which correspond to a very large passivity region. The author of [33] declares that there are three stages of oxidation process, involving SiO_2, Fe_2SiO_4 and iron oxides. This is a doubtful suggestion, because, in contrast to some other transition metals silicates [115 – 117], iron silicate has a very narrow field of thermodynamic stability and plays a minor role in Fe – Si alloys corrosion-electrochemical behaviour in area of water stability. Moreover, Fe_2SiO_4 is treated as metastable compound in water environments and excluded from considerations in study [100]. The conclusions, made earlier for chemical stability of iron silicides, about passivation film, containing of Fe_2O_3 and SiO_2, are valid also for electrochemical corrosion.

However, the aspects of electrochemical behaviour of Fe – Si system outside the area of water stability aren't so clear. In studies [33, 100] the compound "FeO_2" isn't considered, and Fe_2O_3 oxidizes directly to FeO_4^{2-} ions. Instead of reaction, represented by line 22, 24 and 19 at figures 4, 5 and 6, respectively, the following equilibrium is given:

$$2FeO_4^{2-} + 10H^+ + 6e^- = Fe_2O_3 + 5H_2O;\ \varphi = 2{,}220 - 0{,}0985 \cdot pH + 0{,}0197 \cdot \lg a_{FeO_4^{2-}},\ V \qquad (53).$$

The comparison between these two equilibria allows assuming, that "FeO_2" is definitely a metastable particle, an intermediate state between Fe^{+3} and Fe^{+6}. There is no possibility to approve or disprove this, because the stationary potentials, needed to form electrochemically a separate phase of "FeO_2" are very hard to achieve.

The equilibria, involving iron hydride, "FeH", have also predictive nature. There is no data in literature on electrochemical formation of hydride that can verify these calculations, which are very approximate, because thermodynamic properties of "FeH" are just estimated, rather than directly determined. The consecutive schemes of decomposition of iron silicides with and without iron hydride vary from each other essentially, so the exact mechanism of these processes remains open for discussion.

Corrosion properties of Fe – Si systems were studied very intensive, including corrosion rate measurements and polarization tests on various iron silicides [118 – 129], particularly in acidic [118 – 122] and alkaline [127 – 129] environments, corrosion studies of Fe – Si solid solutions [130], studies of oxidation products [131 – 133] and the corrosion properties of multicomponent alloys, coatings, films and other complicated wares, including iron-silicon system [134 – 140]. Thermodyanmic calculations, performed in present study, don't contradict to experimental data, presented in these papers. For all iron silicides, in which silicon content is high enough, in acidic electrolytes, iron selectively dissolves from the silicide sublattice forming cations, while silicon remains on the surface and forms a SiO_2 film, which has a high electrochemical resistance (certainly, if there is no fluoride-ions in solution). Later, the process is limited by the diffusion of metal atoms from the bulk of the silicide toward the surface layer and the diffusion of oxidized metal through the film of hydrated silicon hydroxide. In alkaline electrolytes, the solubility of silicon and silicon dioxide sharply increases, and the mechanism of the anodic process is determined by the formation of protective films composed of Fe_3O_4 and FeOOH. The films passivate the surface and make the silicides stable against alkalis. The minimal silicon concentration, which allows forming protective SiO_2 films in acids for Fe – Si containing alloys, is about 5 weight percent.

Despite due to lack of reliable information thermodynamic theory still can't give a single and clear answer to the all aspects of chemical and electrochemical stability of Fe – Si system alloys, basic regularities are revealed and analyzed. Thermodynamic description can successfully complement and broaden the results of corrosion experiments.

Conclusions.

1. Thermodynamic properties of Fe – Si system at 298 K are analyzed, the comparison between available thermodynamic description is performed with and without considering metastable "Fe_3Si" compound.

2. The Fe – Si – O state diagram and the potential – pH diagrams of Fe – Si – H_2O system at 298 K, air pressure of 1 bar and activities of ions in solution, equal to 1 $^{mol}/_{l}$ with and without consideration of "Fe_3Si" and "FeH" are plotted. The invariant conditions of Fe – Si – O system and basic chemical and electrochemical equilibria in Fe – Si – H_2O system are calculated.

3. Thermodynamic analysis of chemical and electrochemical stability of iron – silicon system alloys is performed. The positive influence of silicon on iron corrosion properties is revealed.

References:

1. А. Б. Шеин. Электрохимия силицидов и германидов переходных металлов [In Russian] (A. B. Shein Electrochemistry of transition metals silicides and germanides). Perm: Publishing House of Perm State University, **2009**.

2. Alfredo M. Morales and Charles M. Lieber. A Laser Ablation Method for the Synthesis of Crystalline Semiconductor Nanowires \\ *Science*, **1998**. Vol. 279. P. 208 – 211.

3. M. Milosavljević, G. Shao, N. Bibić, C. N. McKinty, C. Jeynes [et al.]. Amorphous-iron disilicide: A promising semiconductor // *Applied Physics Letters*, **2001**. Vol. 79. No. 10. P. 1438 – 1440.

4. Thomas Novet and David C. Johnson. New Synthetic Approach to Extended Solids: Selective Synthesis of Iron Silicides via the Amorphous State // *Journal of the American Chemical Society*, **1991**. Vol. 113. No. 9. P. 3398 – 3403.

5. D. Mandrus, J. L. Sarrao, A. Migliori, J. D. Thompson and Z. Fisk. Thermodynamics of FeSi // *Physical Review B*, **1995**. Vol. 51. No. 8. P. 4763 – 4767.

6. S. Paschen [et al.]. Low-temperature transport, thermodynamic and optical properties of FeSi // *Physical Review B*, **1997**. Vol. 56. No. 20. P. 12916 – 12930.

7. G. S. Patrin [et al.]. Nonstoichiometry and Low-Temperature Magnetic Properties of FeSi Crystals // *Physics of the Solid State*, **2006**. Vol. 48. No. 4. P. 700 – 704.

8. Jung-FuLin, DionL.Heinz, AndrewJ.Campbell, JamesM.Devine, GuoyinShen. Iron-Silicon Alloy in Earth's Core? // *Science*, **2002**. Vol. 295. P. 313 – 315.

9. S. S. Lau, J. S.-Y. Feng, J. O. Olowolafe and M.-A. Nicolet. Iron Silicide Thin Film Formation at Low Temperatures // *Thin Solid Films*, **1975**. Vol. 25. P. 415 – 422.

10. Jiangtao Hu, Teri Wang Odom and Charles M. Lieber. Chemistry and Physics in One Dimension: Synthesis and Properties of Nanowires and Nanotubes // *Accounts of Chemical Research*, **1999**. Vol. 32. No. 5. P. 435 – 445.

11. V. Raghavan. Fe-Ni-Si (Iron-Nickel-Silicon) // *Journal of Phase Equilibria*, **2003**. Vol. 24. No. 3. P. 269 – 271.

12. Yong Du, Julius Clemens Schuster [et al.]. A thermodynamic description of the Al – Fe – Si system over the whole composition and temperature ranges via a hybrid approach of CALPHAD and key experiments // *Intermetallics*, **2008**. Vol. 16. P. 554 – 570.

13. Zi-Kui Liu and Y. Austin Chang. Thermodynamic Assessment of the Al-Fe-Si System // *Metallurgical and Materials Transactions A*, **1999**. Vol. 30A. P. 1081 – 1095.

14. V. Raghavan. Al-Fe-Si (Aluminium-Iron-Silicon) // *Journal of Phase Equilibria*, **2002**. Vol. 22. No. 4. P. 362 – 366.

15. Annika Forsberg and John Ågren. Thermodynamics, Phase Equilibria and Martensitic Transformation in Fe-Mn-Si Alloys // *Materials Research Society Symposium Proceedings*, **1992**. Vol. 246. P. 289 – 295.

16. Annika Forsberg and John Ågren. Thermodynamic Evaluation of the Fe-Mn-Si System and the γ/ε Martensitic Transformation // *Journal of Phase Equilibria*, **1993**. Vol. 14. No. 3. P. 354 – 363.
17. M. Hino, T. Nagasaka and T. Washizu. Phase Diagram of Fe-Cu-Si Ternary System above 1523 K // *Journal of Phase Equilibria*, **1999**. Vol. 20. No. 3. P. 179 – 186.
18. Jingrui Zhao, Lijun Zhang [et al.]. Experimental Investigation and Thermodynamic Reassessment of the Cu-Fe-Si System // *Metallurgical and Materials Transactions A*, **2009**. Vol. 40A. P. 1811 – 1825.
19. V. Raghavan. Cr-Fe-Si (Chromium-Iron-Silicon) // *Journal of Phase Equilibria*, **2003**. Vol. 24. No. 3. P. 265 – 266.
20. P. Perrot and J. Y. Dauphin. Calculation of the Fe-Zn-Si Phase Diagram between 773 and 1173 K // *CALPHAD*, **1988**. Vol. 12. No. 1. P. 33 – 40.
21. Xuping Su, Nai-Yong Tang and Jim M. Toguri. 450ºC Isothermal Section Of the Fe-Zn-Si Ternary Phase Diagram // *Canadian Metallurgical Quarterly*, **2001**. Vol. 40. No. 3. P. 377 – 384.
22. Xuping Su, Fucheng Yin, Zhi Li, Nai-Yong Tang, Manxiu Zhao. Thermodynamic calculation of the Fe–Zn–Si system // *Journal of Alloys and Compounds*, **2005**. Vol. 396. P. 156 – 163.
23. Jacques Lacaze and Bo Sundman. An Assessment of the Fe-C-Si System // *Metallurgical and Materials Transactions A*, **1991**. Vol. 22A. P. 2211 – 2223.
24. Tsuguyasu Wada, Harue Wada, John F. Elliott and John Chipman. Thermodynamics of the FCC Fe-Mn-C and Fe-Si-C Alloys // *Metallurgical and Materials Transactions*, **1972**. Vol. 3. P. 1657 – 1662.
25. Jyrki Miettinen. Reassessed Thermodynamic Solution Phase Data for Ternary Fe-Si-C System // *CALPHAD*, **1998**. Vol. 22. No. 2. P. 231 – 256.
26. N. G. Shaposhnikov and B. M. Mogutnov. Paraequilibria in the Fe–Si–C System and Their Relation to the Bainite Transformation in Steels // *Russian Metallurgy (Metally)*, **2008**. Vol. 2008. No. 2. P. 174 – 179.
27. J. Myers and H. P. Eugster. The System Fe-Si-O: Oxygen Buffer Calibrations to 1,500K // *Contribution to Mineralogy and Petrology*, **1983**. Vol. 82. P. 75 – 90.
28. O. B. Fabrichnaya and B. Sundman. The assessmeut of thermodynamic parameters in the Fe-O and Fe-Si-O systems // *Geochimica et Cosmochimica Acta*, **1997**. Vol. 61. No. 21. P. 4539 – 4555.
29. Tatsuya Tokunaga, Hiroshi Ohtani, Mitsuhiro Hasebe. Thermodynamic evaluation of the phase equilibria and glass-forming ability of the Fe–Si–B system // *Computer Coupling of Phase Diagrams and Thermochemistry*, **2004**. Vol. 28. P. 354 – 362.
30. A. I. Zaitsev and N. E. Zaitseva. Thermodynamic Study of Liquid Fe–Si–B Alloys: The Effect of Ternary Associated Groups on Transformation of the Alloy into the Amorphous State // *Doklady Physical Chemistry*, **2002**. Vol. 384. Nos. 4 – 6. P. 126 – 130.
31. J. C. Anglezio, C. Servant and I. Ansara. Contribution to the Experimental and Thermodynamic Assessment of the Al – Ca – Fe – Si system – I. Al – Ca – Fe, Al – Ca – Si, Al – Fe – Si and Ca – Fe – Si systems // *CALPHAD*, **1994**. Vol. 18. No. 3. P. 273 – 309.
32. A. Atkinson. A theoretical analysis of the oxidation of Fe – Si alloys // *Corrosion Science*, **1982**. Vol. 22. No. 2. P. 87 – 102.
33. A. G. Tyurin. Thermodynamic evaluation of silicon influence on chemical and electrochemical stability of iron-chromium alloys // *Protection of Metals*, **2004**. Vol. 40. No. 1. P. 14 – 22.
34. Диаграммы состояния двойных металлических систем: справочник / под. ред. Н. П. Лякишева [In Russian] (Phase Diagrams of Binary Metallic Systems / Editor N. P. Lyakishev.) Moscow: Mashinostroenie, **1997**. Vol. 2. P. 551 – 554.
35. Phase diagram – Web. FactSage Database. – URL: <http://www.crct.polymtl.ca/fact/documentation> (Access Date – 14. VII. 2012).

36. A. Gude and H. Mehrer. Diffusion in the $D0_3$-type intermetallic phase Fe_3Si // *Philosophical Magazine A*, **1997**. Vol. 76. No. 1. P. 1 – 29.
37. L. Haggstrom, L. Grinas, R. Wappling and S. Devanarayanan. Mössbauer Study of Ordering in FeSi Alloys // *Physica Scripta*, **1973**. Vol. 7. P. 125 – 131.
38. Byeong-joo Lee, Seh Kwang Lee and Dong Nyung Lee. Formulation of the A2/B2/$D0_3$ Atomic Ordering Energy and a Thermodynamic Analysis of the Fe-Si System // *CALPHAD*, **1987**. Vol. 11. No. 2. P. 253 – 270.
39. H. Sakao and J. F. Elliott. Thermodynamics of Dilute bcc Fe-Si Alloys // *Metallurgical and Materials Transactions A*, **1975**. Vol. 6A. P. 1849 – 1851.
40. J. Chipman, J. C. Fulton, N. Gokcen and G. R. Caskey, Jr. Activity of Silicon in Liquid Fe-Si and Fe-C-Si Alloys // *Acta Metallurgica*, **1954**. Vol. 2. P. 439 – 450.
41. R. J. Fruehan. The Thermodynamic Properties of Liquid Fe-Si Alloys // *Metallurgical Transactions*, **1970**. Vol. 1. P. 865 – 870.
42. K. Hilfrich [et al.]. Revision of the Fe-Si phase diagram: No B2-phase for 7.6 at.% $\leq c_{Si} \leq$ 10.2 at.% // *Scripta Metallurgica et Materialia*, **1990**. Vol. 24. No. 1. P. 39 – 44.
43. Larry Kaufman. Coupled Phase Diagrams and Thermochemical Data for Transition Metal Binary System – VI // *CALPHAD*, **1979**. Vol. 3. No. 1. P. 45 – 76.
44. B. Sundman and J. Ågren. A regular solution model for phases with several components and sublattices suitable for computer applications // *Journal of Physical Chemistry of Solids*, **1981**. Vol. 42. P. 297 – 301.
45. Д. М. Лаптев. Термодинамика металлургических растворов [In Russian] (D. M. Laptev. Thermodynamics of Metallurgical Solutions). Chelyabinsk: Metallurgija, **1992**.
46. Otto Redlich and A. T. Kister. Algebraic representation of thermodynamic properties and the classification of solutions // *Industrial and Engineering Chemistry*, **1948**. Vol. 40. No. 2. P. 345 – 348.
47. A. T. Dinsdale. SGTE Data for Pure Elements // *CALPHAD*, **1991**. Vol. 15. No. 4. P. 317 – 425.
48. Н. П. Жук. Курс теории коррозии и защиты металлов: учебное пособие для вузов [In Russian] (N. P. Zhuk. Textbook on the Theory of Corrosion and Metal Protection. University Course). Moscow: Al'yans, **2006**.
49. P. A. Nikolaychuk, A. G. Tyurin Method of estimating the standard Gibbs energies of formation of binary compounds // *Abstracts of the XVIII International Conference on Chemical Thermodynamics in Russia (RCCT-2011)*. Samara, **2011**. Vol. 2. P. 16 – 17.
50. Л. П. Рузинов, Б. С. Гуляницкий. Равновесные превращения металлургических реакций: справочник [In Russian] (L. P. Ruzinov, B. S. Gulyanitskii. Equilibrium Transformations in Metallurgical Reactions: Handbook). Moscow: Metallurgiya, **1975**.
51. Thermal Constants of Substances: Database. – URL: <http://www.chem.msu.su/cgi-bin/tkv.pl?show=welcome.html> (Access Date – 22. VI. 2012).
52. У. Д. Верягин et al. Термодинамические свойства неорганических веществ: справочник / под ред. А. П. Зефирова [In Russian] (U. D. Veryagin et al. Thermodynamic Properties of Inorganic Substances: Handbook. Editor A. P. Zefirov). Moscow: Atomizdat, **1965**.
53. L. B. Pankratz, J. M. Stuve, M. A. Gokcen. Thermodynamic Data for Mineral Technology: Handbook. Bureau of Mines, USA, **1984**.
54. J. Acker, K. Bohmhammel, G. J. K. van den Berg, J. C. van Miltenburg and Ch. Kloc. Thermodynamic properties of iron silicides FeSi and α-$FeSi_2$ // *Journal of Chemical Termodynamics*, **1999**. Vol. 31. P. 1523 – 1536.
55. A. I. Zaitsev, M. A. Zemchenko and B. M. Mogutnov. Thermodynamic properties of iron silicides and phase equilibria in (1 - x)Si + xFe} // *Journal of Chemical Termodynamics*, **1991**. Vol. 23. P. 933 – 940.
56. Mark E. Schlesinger. Thermodynamics of Solid Transition-Metal Silicides // *Chemical Reviews*, **1990**. Vol. 90. No. 4. P. 607 – 628.

57. Г. К. Моисеев, Н. А. Ватолин, Л. А. Маршук, Н. И. Ильиных. Температурные зависимости приведённой энергии Гиббса некоторых неорганических веществ: альтернативный банк данных ASTRA. OWN [In Russian] (G. K. Moiseev, N. A. Vatolin, L. A. Marshuk, N. I. Ilyinykh. Temperature Dependencies of the Reduced Gibbs Energy of Some Inorganic Compounds: An ASTRA. OWN Alternative Databank). Yekaterinburg: Ural Branch of RAS, **1997**.
58. E. Gaffet, N. Malhouroux and M. Abdellaoui. Far from equilibrium phase transition induced by solid-state reaction in the Fe-Si system // *Journal of Alloys and Compounds*, **1993**. Vol. 194. P. 339 – 360.
59. A. C. Swintendick. A Theoretical Model for Site Preference of Transition Metal Solutes in Fe_3Si // *Solid State Communications*, **1976**. Vol. 19. P. 511 – 515.
60. 陈安合, 杨学民, 林伟刚. 生物质燃烧过程中Cl及碱金属逸出的化学热力学平衡分析 [In Chinese] (An-he Chen, Xue-min Yang, Wei-gang Lin. Thermodynamic Equilibrium Analysis on Release Characteristics of Chlorine and Alkali Metals during Combustion of Biomass Residues) // *Chinese Journal of Process Engineering*, **2007**. Vol. 7. No. 5. P. 989 – 998.
61. А. Г. Тюрин. Термодинамика химической и электрохимической устойчивости твёрдых сплавов железа, хрома и никеля [In Russian] (A. G. Tyurin. Thermodynamics of the Chemical and Electrochemical Stability of Solid Iron, Chromium, and Nickel Alloys). Chelyabinsk: Publishing House of Chelyabinsk State University, **2011**.
62. Ю. Д. Третьяков. Термодинамика ферритов [In Russian] (Yu. D. Tret'yakov. Thermodynamics of the Ferrites). Leningrad: Khimiya, **1967**.
63. Н. А. Торопов, В. П. Борзаковский. Диаграммы состояния силикатных систем [In Russian] (N. A. Toropov, V. P. Borzakovskiy. Phase Diagrams of Silicate Systems). Vol. 2. Leningrad: Khimiya, **1965**.
64. Справочник по электрохимии / под ред. А. М. Сухотина [In Russian] (Handbook of Electrochemistry. Editor A. M. Sukhotin). Leningrad: Khimiya, **1981**.
65. F. Cotton, G. Wilkinson. Advanced Inorganic Chemistry. New York – London – Sydney – Toronto: John Wiley & Sons, **1972**.
66. V. S. Protsenko and F. I. Danilov. Multistep electrochemical reactions involving transport of intermediates between the near-electrode layer and the bulk solution: A kinetics analysis based on theory of generalized variables (theory of similarity) // *Russian Journal of Electrochemistry*, **2005**. Vol. 41. No. 1. P. 108 – 112.
67. В. А. Киреев. Методы практических расчётов в термодинамике химических реакций [In Russian] (V. A. Kireev. The Methods of Practical Calculations in Thermodynamics of Chemical Reactions). Moscow: Khimiya, **1970**.
68. P. A. Nikolaychuk, A. G. Tyurin. The analysis of standard Gibbs energies of formation of MeO_2 type oxides of fourth period d-elements // *Abstracts of the XVIII International Conference on Chemical Thermodynamics in Russia (RCCT-2011)*. Samara, **2011**. Vol. 2. P. 17 – 18.
69. JANAF Thermochemical Tables. Third Edition. // *Journal of Physical and Chemical Reference Data*, **1985**. Vol. 14. Supplement 1.
70. G. G. Charette, S. N. Flengas. Thermodynamic properties of the oxides of Fe, Ni, Pb, Cu, and Mn, by EMF measurements // *Journal of Electrochemical Society. Electrochemical Science*, **1968**. Vol. 115. No. 8. P. 796 – 804.
71. A. Navrotsky. Thermodynamics of Formation of the Silicates and Germanates of some Divalent Transition Metals and of Magnesium // *Journal of Inorganic and Nuclear Chemistry*, **1971**. Vol. 33. P. 4035 – 4050.
72. William A. Bassett and Li-Chung Ming. Disproportionation of Fe_2SiO_4 to $2FeO+SiO_2$ at Pressures up to 250 kbar and Temperatures up to 3000°C // *Physics of the Earth and Planetary Interiors*, **1972**. Vol. 6. P. 154 – 160.
73. Michel H. G. Jacobs, Bernard H. W. S. de Jong and Harry A. J. Oonk. The Gibbs energy formulation of α, γ and liquid Fe_2SiO_4 using Grover, Getting and Kennedy's empirical relation

between volume and bulk modulus // *Geochimica et Cosmochimica Acta*, **2001**. Vol. 65. No. 22. P. 4231 – 4242.
74. Wenjun Yong, E. Dachs, A. C. Withers, E. J. Essene. Heat capacity of γ-Fe_2SiO_4 between 5 and 303 K and derived thermodynamic properties // *Physical Chemistry of Minerals*, **2007**. Vol. 34. P. 121 – 127.
75. G. M. Bancroft, A. G. Maddock, R. G. Burns. Application of the Mössbauer effect to silicate mineralogy – I. Iron silicates of known crystal structure // *Geochimica et Cosmochimica Acta*, **1967**. Vol. 31. P. 2219 – 2246.
76. G. M. Bancroft, R. G. Burns, A. J. Stone. Application of the Mössbauer effect to silicate mineralogy – II. Iron silicates of unknown and complex crystal structure // *Geochimica et Cosmochimica Acta*, **1968**. Vol. 32. P. 547 – 559.
77. А. А. Кимяшов, М. В. Евтушенко, С. В. Штин, А. А. Лыкасов. Фазовые равновесия в системе Fe – Fe_3O_4 – Fe_2SiO_4 [In Russian] (A. A. Kimyashov, M. V. Evtushenko, S. V. Shtin, A. A. Lykasov. Phase Equilibria in the System Fe – Fe_3O_4 – Fe_2SiO_4) // *Vestnik YUUrGU. Serija Metallurgija*, **2010**. Vol. 189. No. 13. P. 10 – 14.
78. А. А. Лыкасов, А. А. Кимяшов. Условия фазовых равновесий в системе Fe – Si – O в интервале температур 1100 – 1300 K [In Russian] {A. A. Lykasov, A. A. Kimyashov. The Conditions of Phase Equilibria in Fe – Si – O System at Temperature Interval of 1100 – 1300 K} // *Butlerov Communications*, **2010**. Vol. 21. No. 7. P. 42 – 49.
79. A. A. Kimyashov. Phase Equilibria in Systems Fe – Al – O and Fe – Si – O at Temperature Interval of 1100 – 1300 K. Dissertation thesis. Chelyabinsk: South Ural State University, **2010**.
80. А. В. Аплатов, С. Н. Падерин. Термодинамические модели жидких многокомпонентных металлических растворов [In Russian] (A. V. Aplatov, S. N. Paderin. Thermodynamic Models of Liquid Multicomponent Metallic Solutions) // *Elektrometallurgiya*, **2009**. No. 9. P. 28 – 36.
81. Cramer's Rule – Cramer's Method of solving a system of linear equations. URL: < http://2000clicks.com/mathhelp/MatrixCramersRule.aspx> (Access Date – 2. 8. 2012).
82. K. J. Hubbard and D. G. Schlom. Thermodynamic stability of binary oxides in contact with silicon // *Journal of Materials Research*, **1996**. Vol. 11. No. 11. P. 2757 – 2776.
83. L. Kish. Kinetics of Electrochemical Metal Dissolution. Budapest: Akademiai Kiado, **1988**.
84. Pourbaix diagrams / Substances & Technologies. – URL: <http://www.substech.com/dokuwiki/doku.php?id=pourbaix_diagrams> (Access Date – 22. VI. 2012).
85. Gunnar Eriksson. An algorithm for the computation of aqueous multicomponent, multiphase equilibria // *Analytica Chimica Acta*, **1979**. Vol. 112. No. 4. P. 375 – 383.
86. P. A. Nikolaychuk, A. G. Tyurin Thermodynamics of Chemical and Electrochemical Stability of Copper-Nickel Alloys // *Protection of Metals and Physical Chemistry of Surfaces*, **2012**. Vol. 48. No. 4. P. 462 – 476.
87. Справочник химика / под ред. Б. П. Никольского [In Russian]. (Chemist's Handbook. Editor B. P. Nikol'skii). Moscow: Khimiya, **1964**. Vol. 3.
88. J. W. Ball, D. K. Nordstrom. User's manual for WATEQ4F with revised thermodynamic data base and test cases for calculating speciation of major, trace and redox elements in natural waters. US geological survey. Open-file report 91-183. – URL: <http://wwwbrr.cr.usgs.gov/projects/GWC_chemtherm/pubs/wq4fdoc.pdf> (Access Date – 22. VI. 2012).
89. J. W. Johnson, E. H. Oelkers, H. C. Helgeson. SUPCRT92: A software package for calculating the standard molal thermodynamic properties of minerals, gases, aqueous species, and reactions from 1 to 5000 bar and 0 to 1000°C // *Computers & Geosciences*, **1992**. Vol. 16. No. 7. P. 899 – 947.

90. G. P. Glasby, H. D. Schulz. E_H, pH diagrams for Mn, Fe, Co, Ni, Cu and As under seawater conditions: application of two new types of E_H, pH diagrams to the study of specific problems in marine geochemistry // *Aquatic Geochemistry*, **1999**. Vol. 5. No. 3. P. 227 – 248.
91. FactSage EpH-Web. – URL: <http://www.sgte.org/ephweb.php> (Access Date – 22. VI. 2012).
92. THERMEXPERT – Potential – pH diagram generator / Argentum Solutions, Inc. – URL: <http://www.argentumsolutions.com/cgi-bin/thermexpert> (Access Date – 22. VI. 2012).
93. SUPCRT / Prediction Central. – URL: <http://www.predcent.org/download/supcrt.html> (Access Date – 22. VI. 2012).
94. The Geochemist's Workbench (GWB). – Rockware: Earth Science and GIS Software. – URL: <http://www.rockware.com/product/overview.php?id=132> (Access Date – 22. VI. 2012).
95. JNC-TDB. – Japan Nuclear Cycle Organization. – URL: <http://migrationdb.jnc.go.jp> (Access Date – 18. XII. 2011).
96. ZZ-HATCHES 19: Database for radiochemical modeling / Nuclear Energy Agency. – URL: <http://www.oecd-nea.org/tools/abstract/detail/nea-1210> (Access Date – 22. VI. 2012).
97. PHREEQC-2: A Computer Program for speciation, batch-reaction, one-dimensional transport, and inverse geochemical calculations / USGS. – URL: <http://wwwbrr.cr.usgs.gov/projects/GWC_coupled/phreeqc> (Access Date – 22. VI. 2012).
98. SOLGASWATER program. – URL: <http://158.227.5.164/Chemical_Diagrams/html/ISP_Solgaswater.htm> (Access Date – 22. VI. 2012).
99. Atlas of Eh-pH diagrams: Intercomparison of thermodynamic databases. Geological survey of Japan. Open file report № 419. National Institute of Advanced Industrial Science and Technology, 2005. – URL: <www.gsj.jp/GDB/openfile/files/no0419/openfile419e.pdf> (Access Date – 22. VI. 2012).
100. G. H. Kelsall and R. A. Williams. Electrochemical Behavior of Ferrosilicides (Fe_xSi) in Neutral and Alkaline Aqueous Electrolytes. I. Thermodynamics of Fe-Si-H_2O Systems at 298 K // *Journal of the Electrochemical Society*, **1991**. Vol. 138. No. 4. P. 931 – 940.
101. Toshihiro Suzuki, Syun-iti Akimoto, Yuh Fukai. The system iron-enstatite-water at high pressures and temperatures – formation of iron hydride and some geophysical implications // *Physics of the Earth and Planetary Interiors*, **1984**. Vol. 36 P. 135 – 144.
102. Takehiko Yagi and Takahiro Hishinuma. Iron hydride formed by the reaction of iron, silicate, and water: Implications for the light element of the Earth's core // *Geophysical Research Letters*, **1995**. Vol. 22. No. 14. P. 1933 – 1936.
103. J. V. Badding, R. J. Hemley, H. K. Mao. High-Pressure Chemistry of Hydrogen in Metals: In Situ Study of Iron Hydride // *Science*, **1991**. Vol. 253. P. 421 – 424.
104. M. Tkacz. Thermodynamic properties of iron hydride // *Journal of Alloys and Compounds*, **2002**. Vols. 330 – 332. P. 25 – 28.
105. Masahiro Katsura. Thermodynamics of nitride and hydride formation by the reaction of metals with flowing NH_3 // *Journal of Alloys and Compounds*, **1992**. Vol. 182. P. 91 – 102.
106. 椙 山 正 孝, 山 忠 行. Fe – Si および Fe－Si－Al 合金の高温酸化被膜 [In Japanese] (Masataka Sugiyama and Tadayuki Nakayama. On Oxide Films of Fe – Si and Fe－Si－Al Alloys at High Temperature) // Journal of the Japanese Institute of Metals, 1959. Vol. 23. P. 534 – 538.
107. C. W. Tuck. Non-protective and Protective Scaling of a Commercial $1^3/_4$ % Alloy in the Range 800ºC – 1000ºC // *Corrosion Science*, **1965**. Vol. 5. No. 631 – 643.
108. R. Logani and W. W. Smeltzer. Kinetics of Wustite-Fayalite Scale Formation on Iron-Silicon Alloys // *Oxidation of Metals*, **1969**. Vol. 1. No. 1. P. 3 – 21.
109. R. C. Logani, W. W. Smeltzer. The Development of the Wustite-Fayalite Scale on an Iron-l.5 wt. % Silicon Alloy at 1000ºC // *Oxidation of Metals*, **1971**. Vol. 3. No. 1. P. 15 – 32.

110. R. C. Logani, W. W. Smeltzer. The Growth of Wustite-Fayalite Nodules on an Iron-l.5 wt. % Silicon Alloy Exposed to Carbon Dioxide-Carbon Monoxide Atmospheres // *Oxidation of Metals*, **1971**. Vol. 3. No. 3. P. 279 – 290.
111. I. Svedung and N.-G. Vannerberg. The influence of silicon on the oxidation properties of iron // *Corrosion Science*, **1974**. Vol. 14. P. 391 – 399.
112. P. T. Moseley, G. Tappin, G. C. Rivière. The oxidation of Dilute Iron – Silicon Alloys ([Si] ≤1%) in Carbon Dioxide // *Corrosion Science*, **1982**. Vol. 22. No. 2. P. 69 – 86.
113. T. Adachi and G. H. Meier. Oxidation of Iron-Silicon Alloys // *Oxidation of Metals*, **1987**. Vol. 27. Nos. 5 – 6. P. 347 – 366.
114. T. Ban, K. Bohnenkamp and H.-J. Engell. The Formation of Protective Films of Iron – Silicon Alloys // *Corrosion Science*, **1979**. Vol. 19. P. 283 – 293.
115. А. Г. Тюрин, Т. В. Мосунова, П. А. Николайчук. Термодинамика химической и электрохимической устойчивости силицидов кобальта [in Russian] {A. G. Tyurin, T. V. Mosunova, P. A. Nikolaychuk. Thermodynamics of Chemical and Electrochemical Stability of Cobalt Silicides) // *Vestnik YUUrGU. Serija Khimija*, **2010**. Vol. 3. No. 11 (187). P. 52 – 60.
116. П. А. Николайчук, Т. И. Шаляпина, А. Г. Тюрин, Т. В. Мосунова. Термодинамика химической и электрохимической устойчивости сплавов системы Mn – Si [in Russian] {P. A. Nikolaychuk, T. I. Shalyapina, A. G. Tyurin, T. V. Mosunova. Thermodynamics of Chemical and Electrochemical Stability of Mn – Si System Alloys) // Vestnik YUUrGU. Serija Khimija, **2010**. Vol. 4. No. 31 (207). P. 72 – 82.
117. П. А. Николайчук, А. Г. Тюрин. Термодинамика химической и электрохимической устойчивости сплавов системы Cu – Si [in Russian] {P. A. Nikolaychuk, A. G. Tyurin. Thermodynamics of Chemical and Electrochemical Stability of Cu – Si System Alloys) // *Butlerov Communications*, **2011**. Vol. 24. No. 2. P. 84 – 94.
118. E. S. Greiner, J. S. Marsh and B. Stoughton. The Alloys of Iron and Silicon. New York and London: McGraw – Hill Book Company, **1933**.
119. W. B. Crow, J. R. Myers, J. V. Jeffreys. Anodic Polarization Behaviour of Fe-Si Alloys in Sulfuric Acid Solutions // *Corrosion*, **1972**. Vol. 28. No. 3. P. 77 – 82.
120. Р. Г. Аитов, А. Б. Шеин. Коррозионно-электрохимическое поведение силицидов железа различного состава в кислотах [In Russian] (R. G. Aitov, A. B. Shein. The Corrosion – Electrochemical Behaviour of Iron Silicides of Various Compositions in Acids) // *Zashchita Metallov*. **1993**. Vol. 29. No. 6. P. 895 – 899.
121. Р. Г. Аитов, А. Б. Шеин. Влияние фторид-ионов на анодное поведение силицидов железа, никеля и кобальта [In Russian] (R. G. Aitov, A. B. Shein. The Influence of Fluoride-Ions on Anodic Behaviour of Iron, Cobalt and Nickel Silicides) // *Zashchita Metallov*. **1994**. Vol. 30. No. 4. P. 439 – 440.
122. A. B. Shein and O. V. Kanaeva. Anodic Dissolution of the (100) and (110) Faces of Iron Monosilicide in a Sulfuric Acid Electrolyte // *Russian Journal of Electrochemistry*, **2000**. Vol. 36. No. 8. P. 913 – 915.
123. А. Б. Шеин. Электрохимическое поведение эвтектических сплавов силицидов и германидов металлов подгруппы железа с кремнием и германием [In Russian] (A. B. Shein. Electrochemical Behaviour of the Eutectic Alloys of Iron, Cobalt and Nickel Silicides and Germanides with Silicon and Germanium) // *Zashchita Metallov*. **1998**. Vol. 34. No. 1. P. 25 – 28.
124. A. B. Shein. Effect of the Metal Component on Anodic Dissolvability of Iron, Cobalt and Nickel Silicides // *Protection of Metals*, **2001**. Vol. 37. No. 3. P. 281 – 283.
125. V. S. Povroznik and A. B. Shein. Environmental and Inherent Factors That Affect Hydrogen Cathodic Evolution on Silicides of the Iron Family Metals // *Protection of Metals*, **2007**. Vol. 43. No. 2. P. 203 – 207.

126. A. B. Shein. Corrosion–Electrochemical Behavior of Iron Family Silicides in Various Electrolytes // *Protection of Metals and Physical Chemistry of Surfaces*, **2010**. Vol. 46. No. 4. P. 479 – 488.
127. G. H. Kelsall and R. A. Williams. Electrochemical Behavior of Ferrosilicides (Fe_xSi) in Neutral and Alkaline Aqueous Electrolytes. II. Fe_xSi Electrochemical Kinetics and Corrosion Behavior // *Journal of the Electrochemical Society*, **1991**. Vol. 138. No. 4. P. 941 – 951.
128. I. L. Rakityanskaya and A. B. Shein. Anodic Behavior of Iron, Cobalt and Nickel Silicides in Alkaline Electrolytes // *Russian Journal of Electrochemistry*, **2006**. Vol. 42. No. 11. P. 1208 – 1212.
129. A. B. Shein, I. L. Rakityanskaya and S. F. Lomaeva. Anodic Dissolution of Iron Silicides in Alkaline Electrolyte // *Protection of Metals*, **2007**. Vol. 43. No. 1. P. 54 – 58.
130. Y. Omurtag, M. Doruk. Some Investigations of the Corrosion Characteristics of Fe – Si Alloys // *Corrosion Science*, **1970**. Vol. 10. P. 225 – 231.
131. Katsuya Inoue et al. Atomic-Scale Structure and Morphology of Ferric Oxyhydroxides Formed by Corrosion of an Iron–Silicon Alloy // *Materials Transactions*, **2006**. Vol. 47. No. 2. P. 243 – 246.
132. G. H. Kelsall and R. A. Williams. Electrochemical Behavior of Ferrosilicides (Fe_xSi) in Neutral and Alkaline Aqueous Electrolytes. II. The Nature of Passive Films on Fe_xSi Electrodes // *Journal of the Electrochemical Society*, **1991**. Vol. 138. No. 4. P. 951 – 957.
133. Shigeru Suzuki et al. *Ex-situ* and *in-situ* X-ray diffractions of corrosion products freshly formed on the surface of an iron–silicon alloy // *Corrosion Science*, **2007**. Vol. 49. P. 1081 – 1096.
134. H. Busse et al. Metastable iron silicide phase stabilized by surface segregation on Fe_3Si (100) // *Surface Science*, **1997**. Vol. 381. P. 133 – 141.
135. A. Viswanathan et al. Formation of WC-iron silicide (Fe_5Si_3) composite clad layer on AISI 316L stainless steel by high power (CO_2) laser // *Surface & Coatings Technology*, **2009**. Vol. 203. P. 1618 – 1623.
136. Yutaka Shimada and Hiroshi Kojima. Magnetic properties of amorphous FeSi thin films // *Journal of Applied Physics*, **1976**. Vol. 47. No. 9. P. 4156 – 4159.
137. Seiji Motojima. Vapour-Phase Siliconizing of Iron Plate and Crystal Growth of $FeSi_2$ Using Si_2Cl_6 as a Source of Silicon // *Journal of Crystal Growth*, **1987**. Vol. 85. P. 309 – 317.
138. J. S. Armijo and B. E. Wilde. Influence of Si content on the corrosion resistance of the austenitic Fe – Cr – Ni alloys in oxidizing acids // *Corrosion Science*, **1968**. Vol. 8. P. 649 – 664.
139. M. Naka, K. Hashimoto and T. Nasumoto. Effect of Metalloidal Elements on Corrosion Resistance of Amorphous Iron-Chromium Alloys // *Journal of Non-Crystalline Solids*, **1978**. Vol. 28. P. 403 – 413.
140. G. Rife et al. Corrosion of Iron-, Nickel- and Cobalt-base Metallic Glasses Containing Boron and Silicon Metalloids // *Materials Science and Engineering*, **1981**. Vol. 48. P. 73 – 79.

12. Fe – Ge system

12.1. Iron germanides

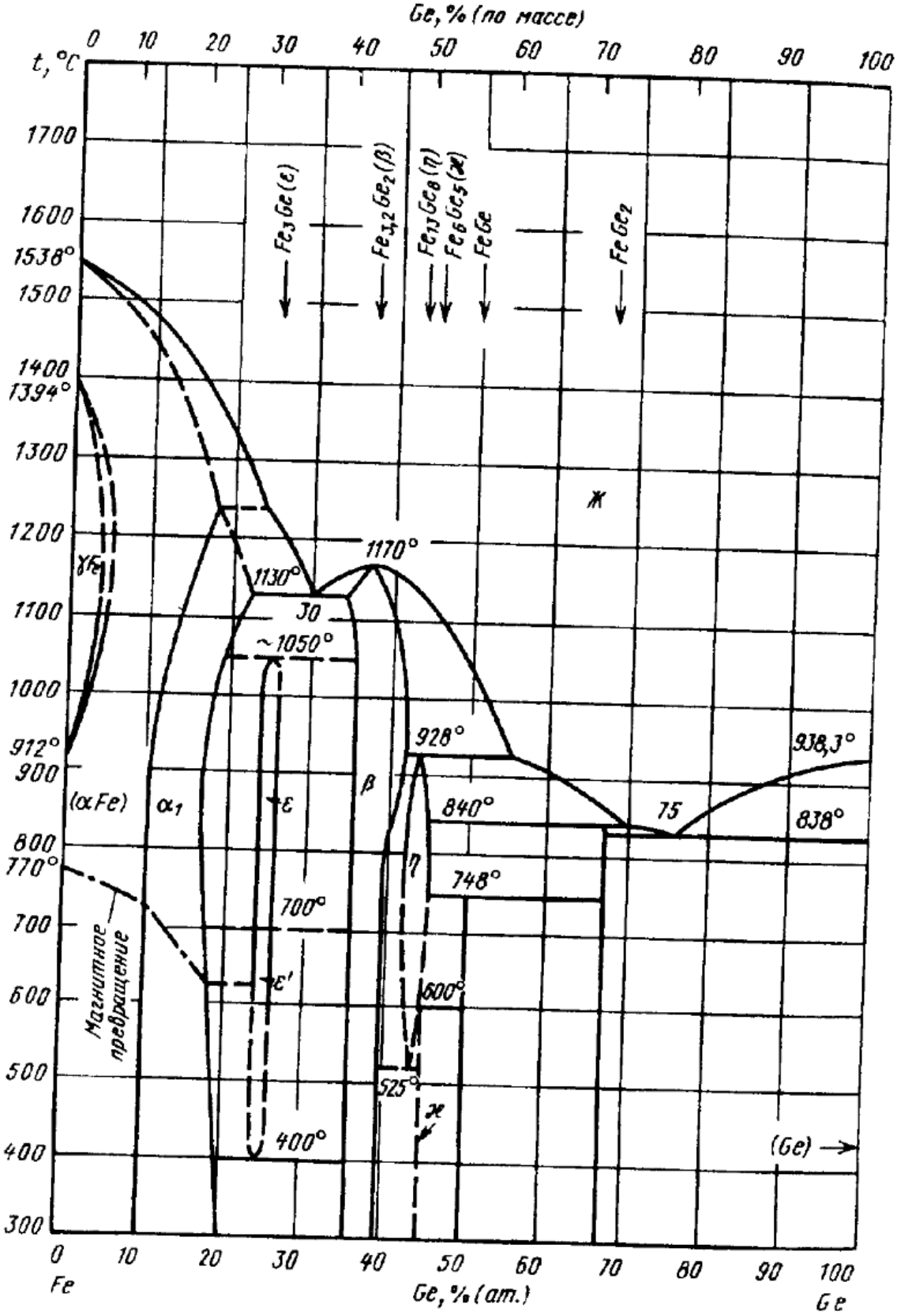

Fig. 53. The phase diagram of the Fe – Ge system [Диаграммы состояния двойных металлических систем: справочник, 2001].

Iron germanides have unusual magnetic and electric properties [Adelson, Austin, 1965; Fatséas, 1976; Häggström et al., 1975; Власенко, Однодворець, Проценко, 2013] and are widely used in nano- and quantum electronics [Tang et al., 2012; Tuan, Lee, Korgel, 2006; Vaughn et al., 2013; Yoon et al., 2012]. Iron – germanium alloys find their application in industry. Therefore, the analysis of a corrosion-electrochemical behaviour of Fe – Ge system is of practical importance.

The phase diagram of Fe – Ge system is presented in Figure 53. Three stoichiometric compounds, namely, $FeGe_2$, FeGe and Fe_6Ge_5 (χ-phase), and two solid solutions, namely, α-phase with the bcc lattice and β-phase with the hcp lattice, exist in the system at 25 °C [Richardson et al., 1967]. The solid solubility of germanium in α-phase is ~10 atomic %. The solid solubility of iron in (diamond-Ge) is vanishingly small.

The excess Gibbs energies of the solid solutions were described in terms of substitution solution model. The standard Gibbs energy of formation of the compound Fe_3G_e was estimated by the Kireev's method, and those of FeGe and $FeGe_2$ were estimated by the Gorichev's method. More details are provided in the attached publication.

12.2. Equilibira in Fe – Ge – O system

The oxides of iron were previously discussed in Section 11.2, and the oxides of germanium – in Section 10.2. There is a single ternary compound in the system, and it is iron germanate Fe_2GeO_4 [Dede, Russ, 1928; Welch, Cooper, Hawthorne, 2001], its standard Gibbs energy of formation was taken from [Chase Jr. et al., 1985].

There is a miscibility gap between Fe_3O_4 and Fe_2GeO_4 at elevated temperatures [Shtin, Lykasov, 2013; Shtin, Lykasov, 2017]. Both compounds are slightly soluble in each other, and the excess Gibbs energy of both solutions was modelled in terms of substitution solution model. The estimated solid solubility of Fe_2GeO_4 in Fe_3O_4 at 25 °C equals 0,085 atomic %, and that of Fe_3O_4 in Fe_2GeO_4 equals 0,006 atomic %.

The state diagram of Fe – Ge – O system and the list of equilibria in it are provided in the attached publication.

12.3. Potential – pH diagram of Fe – Ge – H_2O system

The potential – pH diagram of Fe – Ge – H_2O system is presented in the attached publication.

The corrosion-electrochemical behaviour of Fe – Ge system in aqueous solutions is very similar to that of Mn – Ge system. If the germanium content in the system is high enough, a continuous layer of GeO_2 would be formed on the surface; otherwise the passivation layer might consist of iron germanate Fe_2GeO_4.

Publications to chapter 12

The content of this chapter was initially published in a conference paper [Тюрин, Канатьева, Николайчук, 2013], and then the extended and revised version of this conference contribution was published in a journal paper [Тюрин, Николайчук, Канатьева, 2015]. The Russian preprint of the last paper with the title, abstract, figures and tables translated into English is presented below with the permission from *Nauka i Tehnologii*.

УДК 620.193:669.14

ТЕРМОДИНАМИКА ХИМИЧЕСКОЙ И ЭЛЕКТРОХИМИЧЕСКОЙ УСТОЙЧИВОСТИ СПЛАВОВ СИСТЕМЫ Fe – Ge

А. Г. Тюрин[1], П. А. Николайчук[1,2], И. И. Канатьева[1,3].

[1]ФГБОУ ВПО «Челябинский государственный университет», Челябинск, Россия

[2]Universität zu Köln, Köln, Deutschland

[3]Xīnjiāng Normal University, Ürümqi, Xīnjiāng, China

Определены стандартные энергии Гиббса образования интерметаллидов Fe_6Ge_5, FeGe, $FeGe_2$. Описаны термодинамические свойства α- и β- твёрдых металлических растворов системы Fe – Ge и шпинельных растворов системы Fe_3O_4 – Fe_2GeO_4. Построены фазовая диаграмма системы Fe – Ge – O и диаграмма потенциал – pH системы Fe – Ge – H_2O при 25ºC. Обсуждаются термодинамические особенности коррозионно-электрохимического поведения системы Fe – Ge.

Ключевые слова: германиды железа, система Fe – Ge, диаграмма состояния системы Fe – Ge – O, диаграмма потенциал – pH системы Fe – Ge – H_2O, химическая и электрохимическая устойчивость.

THERMODYNAMICS OF CHEMICAL AND ELECTROCHEMICAL STABILITY OF Fe – Ge SYSTEM ALLOYS

A. G. Tyurin[1], P. A. Nikolaychuk[1,2], I. I. Kanatyeva[1,3].

[1]Chelyabinsk State University, Chelyabinsk, Russia

[2]Universität zu Köln, Köln, Deutschland

[3]Xinjiang Normal University, Ürümqi, Xīnjiāng, China

The standard Gibbs energies of formation of intermatallides Fe_6Ge_5, FeGe, $FeGe_2$ were estimated. Thermodynamic properties of α- and β- solid metallic

solutions of Fe – Ge system and spinel solutions of Fe_3O_4 – Fe_2GeO_4 system were determined. The state diagram of Fe – Ge – O system and the potential – pH diagram of Fe – Ge – H_2O system at 25ºC were plotted. The thermodynamic features of the corrosion-electrochemical behaviour of Fe – Ge system was discussed.
Keywords: iron germanides, Fe – Ge system, state diagram of Fe – Ge – O system, potential – pH diagram of Fe – Ge – H_2O system, chemical and electrochemical stability.

1. ВВЕДЕНИЕ.

Одним из перспективных направлений коррозиологии является поиск новых материалов, обладающих уникальными физико-химическими свойствами и функциональными характеристиками. Примерами таких материалов могут служить металлоподобные интерметаллические соединения переходных металлов [1], в частности, силициды и германиды 3d-элементов. Германиды железа обладают необычными магнитными и электрическими свойствами [2–5] и используются в нано- и квантовой электронике [6–9]. Сплавы на основе железа и германия находят своё применение в промышленности [10, 11]. Поэтому анализ их коррозионно-электрохимических свойств является важной научно-практической задачей.

Электрохимическое поведение германидов железа в различных электролитах хорошо изучено [2]. Однако результаты теоретических исследований коррозионных свойств железогерманиевых сплавов могут существенно дополнить и расширить имеющийся материал. Цель данной работы – в рамках термодинамической теории провести описание коррозионно-электрохимического поведения сплавов системы Fe – Ge.

2. МОДЕЛИРОВАНИЕ ФАЗОВЫХ И ХИМИЧЕСКИХ РАВНОВЕСИЙ В СИСТЕМЕ Fe – Ge.

Фазовая диаграмма системы Fe – Ge представлена в работах [13–15]. В системе при 25ºС существуют три соединения стехиометрического состава – $FeGe_2$, FeGe, Fe_6Ge_5 (χ-фаза) – и два твёрдых раствора – α-фаза (Fe) с решёткой ОЦК и β-фаза с решёткой ГПУ. Растворимость германия в α-железе при 25ºС составляет около 10 ат. % [13, 14]. Растворимость железа в германии с решёткой алмаза при этой температуре пренебрежимо мала.

Значения стандартных энергий Гиббса образования германидов железа и энергий Гиббса фазовых переходов германия из решётки алмаза в кристаллические структуры α- и β-фаз в литературе отсутствуют. Поэтому, на первом этапе, методами Капустинского и Карапетьянца [16] была проведена оценка стандартной энергии Гиббса образования соединения Fe_3Ge. Для расчётов были привлечены экспериментальные данные об энергиях Гиббса образования интерметаллидов Mn_3Ge, Cr_3Ge и V_3Ge [17].

Затем методом моделирования фазовых равновесий α-фазы с Fe_3Ge и β-фазы с Fe_3Ge при температурах выше 400ºС был произведён подбор выражений (в рамках модели регулярного раствора [18]) для избыточных энергий Гиббса α- и β-фаз. При этом энергия Гиббса перехода железа из α-фазы в β-фазу взята из справочной литературы [19], а энергии Гиббса перехода германия из решётки алмаза в α- в β-фазы также были подобраны. По полученным выражениям был произведён расчёт равновесия α-фазы с β-фазой при температурах ниже 400ºС. Результаты расчётов хорошо согласуются с фазовой диаграммой [13]. Вычислены равновесные составы α- и β-фаз при 25ºС и рассчитаны термодинамические активности компонентов в них (стандартное состояние – чистый компонент с решёткой ОЦК для α-фазы и с решёткой ГПУ для β-фазы). Для обоих твёрдых растворов наблюдаются сильные отрицательные отклонения от идеальности. При моделировании фазового равновесия β-фазы с χ-фазой (Fe_6Ge_5) была

проведена оценка стандартной энергии Гиббса образования соединения Fe_6Ge_5.

Наконец, при помощи модифицированного варианта метода Горичева [20–22] по данным об энергиях Гиббса соединений Fe_3Ge и Fe_6Ge_5 была проведена оценка стандартных энергий Гиббса образования оставшихся германидов железа FeGe и $FeGe_2$.

Результаты оценки термодинамических функций фаз системы Fe – Ge обобщены в таблице 1.

Table 1. Thermodynamic functions of the phases in the Fe – Ge system.

Phase	Temperature interval, ºC	Thermodynamic fucntion, $\frac{Дж}{моль}$
α-phase (bcc)	< 700	$G^E = x_{Fe} \cdot x_{Ge} \cdot (-42{,}6 \cdot T - 98400)$
β-phase (hcp)	< 700	$G^E = x_{Fe} \cdot x_{Ge} \cdot (31{,}3 \cdot T - 148000)$
Fe_3Ge	400 – 700	$\Delta_f G_T^o = -50{,}0 \cdot T - 36000$
Fe_6Ge_5	< 500	$\Delta_f G_T^o = -96{,}36 \cdot T - 182790$
FeGe	< 500	$\Delta_f G_T^o = -14{,}3 \cdot T - 36000$
$FeGe_2$	< 500	$\Delta_f G_T^o = 78{,}4 \cdot T - 72000$
Ge (diamond)	< 800	$\Delta_{tr} G_T^o(\text{ алмаз} \rightarrow \text{ОЦК}) = -27{,}17T + 34500$ $\Delta_{tr} G_T^o(\text{ алмаз} \rightarrow \text{ГПУ}) = -25{,}3T + 40000$

3. ФАЗОВЫЕ РАВНОВЕСИЯ В СИСТЕМЕ Fe – Ge – O. ХИМИЧЕСКАЯ УСТОЙЧИВОСТЬ.

В системе Fe – Ge – O кроме простых оксидов железа и германия [14, 23] может образовываться единственное стабильное тройное соединение – германат железа, Fe_2GeO_4 [24].

Известно [25, 26], что железо (IV) может входить в состав двойных оксидов, таких как Ba_2FeO_4 или K_4FeO_4 в виде слоёв, имеющих состав FeO_2. Ранее уже высказывалась гипотеза о существовании оксида железа (IV) [27], и делались попытки создания термодинамической модели окисления железа с его участием [28]. Поэтому произведено прогнозирование термодинамических свойств гипотетического оксида железа (IV) "FeO_2". Оценка стандартной энергии Гиббса образования FeO_2 произведена с помощью методов, представленных в работах [20–22, 29]. Стандартные энергии Гиббса образования соединений обобщены в таблице 2.

Table 2. The standard Gibbs energies of formation of the compounds

Compound	$-\Delta_f G^o_{298}$, $\frac{Дж}{моль}$	Reference	Compound	$-\Delta_f G^o_{298}$, $\frac{Дж}{моль}$	Reference
$FeGe_2$	48 600	*	FeO_2	360 000	*
FeGe	40 300	*	GeO_2	495 800	[35, 36]
Fe_6Ge_5	211 500	*	Fe^{2+}	86 600	[35, 36]
Fe_3Ge	50 900	*	Fe^{3+}	12 100	[35, 36]
Fe_2GeO_4	1 104 500	[31]	Ge^{2+}	47 700	[35, 36]
Fe_3O_4	1 017 400	[34 – 36]	$HFeO_2^-$	405 800	[35, 36]
Fe_2O_3	743 500	[34 – 36]	FeO_4^{2-}	352 300	[35, 36]

* Estimated in the present study.

При температурах ниже 1375 К магнетит и германат железа ограниченно растворимы друг в друге с образованием купола расслаивания [30–33]. Для обоих шпинельных растворов наблюдаются значительные положительные отклонения от закона Рауля. Оба раствора описываются одинаковым выражением для избыточной энергии Гиббса.

Её зависимость от концентрации была рассчитана по экспериментальным данным [31, 32].

$$G^E = x_{Fe_3O_4} \cdot x_{Fe_2GeO_4} \cdot (17600 \cdot x_{Fe_3O_4} + 24400 \cdot x_{Fe_2GeO_4} + 1800 \cdot x_{Fe_3O_4} \cdot x_{Fe_2GeO_4}), \frac{Дж}{моль}$$

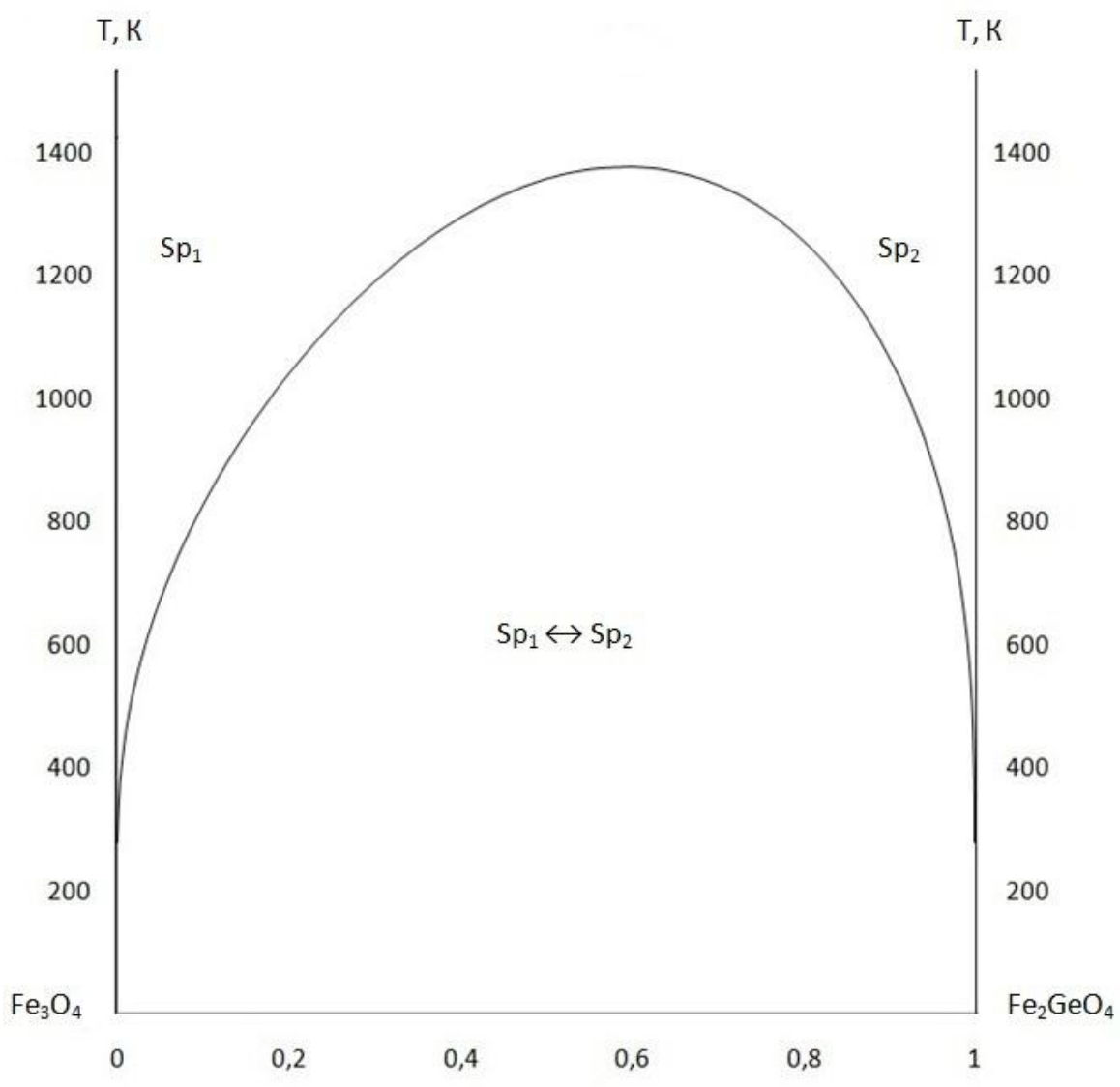

Fig. 1. The calculated miscibility gap in the Fe_3O_4 – Fe_2GeO_4 system. Sp_1 – a spinel solution based on Fe_3O_4, Sp_2 – a spinel solution based on Fe_2GeO_4.

С использованием полученной зависимости купол расслаивания был экстраполирован до стандартной температуры (см. рис. 1). Оценена максимальная взаимная растворимость компонентов шпинельного раствора. При 25ºС максимальная растворимость Fe_2GeO_4 в Fe_3O_4 составляет 0,085

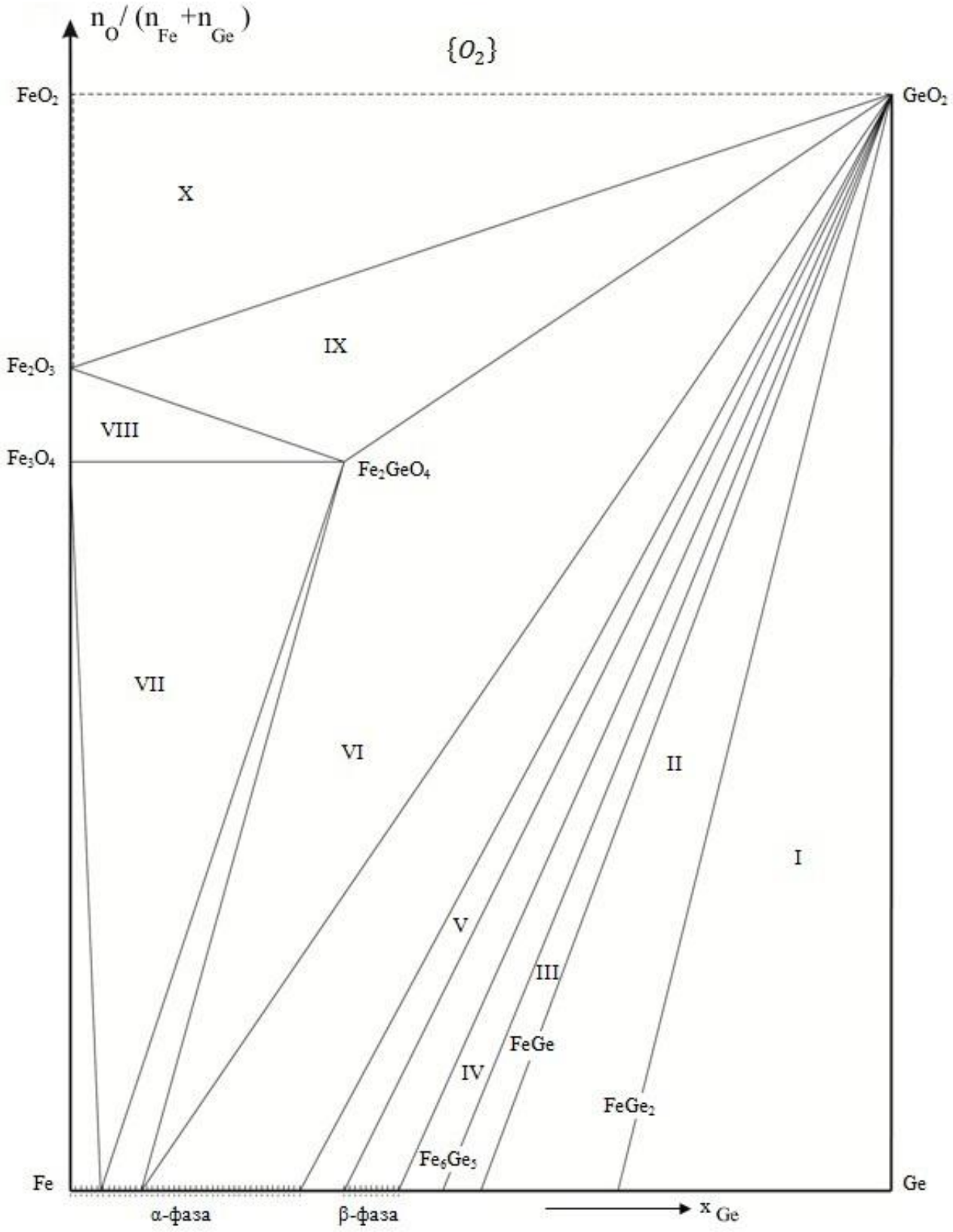

Fig. 2. The state diagram of the Fe – Ge – O system at 25ºC.

Table 3. The characteristics of the invariant states in the Fe – Ge – O system at 25ºC

No of domain in Fig. 2	Phase equilibrium	P_{O_2}, бар	Solid phases composition
I	GeO_2 – Ge – $FeGe_2$	$1{,}19\cdot10^{-103}$	$x_{Ge}=1;\ x_{FeGe_2}=1;\ x_{GeO_2}=1$
II	GeO_2 – $FeGe_2$ – FeGe	$8{,}25\cdot10^{-102}$	$x_{FeGe_2}=1;\ x_{FeGe}=1;\ x_{GeO_2}=1$
III	GeO_2 – FeGe – Fe_6Ge_5	$4{,}09\cdot10^{-101}$	$x_{FeGe}=1;\ x_{Fe_6Ge_5}=1;\ x_{GeO_2}=1$
IV	GeO_2 – β–фаза – Fe_6Ge_5	$3{,}47\cdot10^{-100}$	$x_{Fe(\beta)}=0{,}6;\ a_{Fe(\beta)}=7{,}7\cdot10^{-5};$ $x_{Ge(\beta)}=0{,}4;\ a_{Ge(\beta)}=7{,}1\cdot10^{-10};$ $x_{Fe_6Ge_5}=1;\ x_{GeO_2}=1$
V	GeO_2 – α–фаза – β–фаза	$9{,}35\cdot10^{-98}$	$x_{Fe(\beta)}=0{,}67;\ a_{Fe(\beta)}=1{,}5\cdot10^{-3};$ $x_{Ge(\beta)}=0{,}33;\ a_{Ge(\beta)}=4{,}0\cdot10^{-12};$ $x_{Fe(\alpha)}=0{,}72;\ a_{Fe(\alpha)}=2{,}2\cdot10^{-2};$ $x_{Ge(\alpha)}=0{,}28;\ a_{Ge(\alpha)}=2{,}3\cdot10^{-11};$ $x_{GeO_2}=1$
VI	GeO_2 – Fe_2GeO_4 – α–фаза	$6{,}70\cdot10^{-91}$	$x_{Fe(\alpha)}=0{,}915;\ a_{Fe(\alpha)}=0{,}662;$ $x_{Ge(\alpha)}=0{,}085;\ a_{Ge(\alpha)}=4{,}2\cdot10^{-18};$ $x_{Fe_2GeO_4}=1;\ x_{GeO_2}=1$
VII	Fe_2GeO_4 – Fe_3O_4 – α–фаза	$5{,}18\cdot10^{-90}$	$x_{Fe(\alpha)}=0{,}962;\ a_{Fe(\alpha)}=0{,}902;$ $x_{Ge(\alpha)}=0{,}038;\ a_{Ge(\alpha)}=3{,}7\cdot10^{-20};$ $x_{Fe_2GeO_4}=1;\ x_{Fe_3O_4}=1$
VIII	Fe_2GeO_4 – Fe_3O_4 – Fe_2O_3	$4{,}63\cdot10^{-88}$	$x_{Fe_2GeO_4}=1;\ x_{Fe_3O_4}=1;\ x_{Fe_2O_3}=1$
IX	GeO_2 – Fe_2GeO_4 – Fe_2O_3	$2{,}33\cdot10^{-80}$	$x_{Fe_2GeO_4}=1;\ x_{Fe_2O_3}=1;\ x_{GeO_2}=1$
X	GeO_2 – FeO_2 – Fe_2O_3	$3{,}09\cdot10^{8}$	$x_{Fe_2O_3}=1;\ x_{FeO_2}=1;\ x_{GeO_2}=1$

мольных %, а растворимость Fe_3O_4 в Fe_2GeO_4 – всего 0,006 мольных %. Поэтому и Fe_3O_4 и Fe_2GeO_4 при этой температуре можно считать

практически чистыми веществами стехиометрического состава и приравнивать их активности к единице.

Диаграмма состояния системы Fe – Ge – O при 25ºC представлена на рисунке 2. Характеристики инвариантных состояний системы приведены в таблице 3.

Как видно из полученных данных, при 25ºC химическое сродство германия к кислороду выше, чем у железа, поэтому коноды, соединяющие составы равновесных металлических фаз наклонены в область больших содержаний железа (см. рис. 2). В сплавах с содержанием германия более 8,5 мол. % единственным продуктом окисления является GeO_2. При концентрациях германия в железе от 3,8 до 8,5 мол. % реализуются равновесия с Fe_2GeO_4, а при меньших содержаниях продуктами окисления будут только оксиды железа Fe_3O_4 и Fe_2O_3. Термодинамические расчёты прогнозируют образование FeO_2 только при давлении кислорода выше $3 \cdot 10^8$ бар, что подтверждает невозможность образования этого соединения в стандартных условиях.

Table 4. The basic chemical and electrochemical equilibria in the Fe – Ge – H_2O system at 25ºC and air pressure of 1 bar

No of line in Fig. 3	Electrode reaction	Equilibrium potential, V (s. h. e.) or pH of the solution
a	$2H^+ + 2\bar{e} = H_2$(г); $P_{H_2} = 5 \cdot 10^{-7}$ бар	E = 0,186 – 0,0591pH
b	O_2(г) + $4H^+ + 4\bar{e} = 2H_2O$; $P_{O_2} = 0.21$ бар	E = 1,219 – 0,0591pH
1	$GeO_2 + 4H^+ + 4\bar{e} = Ge$ (алмаз) + $2H_2O$	E = –0,293 – 0,0591pH
2	$FeGe + GeO_2 + 4H^+ + 4\bar{e} = FeGe_2 + 2H_2O$	E = – 0,266 – 0,0591pH
3	$Fe_6Ge_5 + GeO_2 + 4H^+ + 4\bar{e} = 6FeGe + 2H_2O$	E = – 0,256 – 0,0591pH
4	$GeO_2 + 4H^+ + 4\bar{e} = Ge(\beta) + 2H_2O$ при $a_{Ge(\beta)} = 7{,}105 \cdot 10^{-10}$	E = – 0,243 – 0,0591pH
5	$GeO_2 + 4H^+ + 4\bar{e} = Ge(\beta) + 2H_2O$ при $a_{Ge(\beta)} = 4{,}047 \cdot 10^{-12}$	E = – 0,210 – 0,0591pH

6	$HFeO_2^- + 3H^+ + 2\bar{e} = Fe(\alpha) + 4H_2O$	$E = 0{,}493 - 0{,}0886pH + 0{,}0295 \lg a_{HFeO_2^-}$
7	$Fe_2GeO_4 + 4H^+ + 4\bar{e} = GeO_2 + 2Fe(\alpha) + 2H_2O$	$E = -0{,}105 - 0{,}0591pH$
8	$Fe_3O_4 + 8H^+ + 8\bar{e} = 3Fe(\alpha) + 4H_2O$	$E = -0{,}092 - 0{,}0591pH$
9	$Fe_3O_4 + 2H_2O + 2\bar{e} = 3HFeO_2^- + H^+$	$E = -1{,}819 + 0{,}0295pH - -0{,}0886 \lg a_{HFeO_2^-}$
10	$Fe_2GeO_4 + 2H_2O = GeO_2 + HFeO_2^- + 2H^+$	$pH = 20{,}22 + \lg a_{HFeO_2^-}$
11	$2Fe_3O_4 + 3GeO_2 + 4H^+ + 4\bar{e} = 3Fe_2GeO_4 + 2H_2O$	$E = -0{,}040 - 0{,}0591pH$
12	$Fe_3O_4 + 8H^+ + 2\bar{e} = 3Fe^{2+} + 4H_2O$	$E = 0{,}953 - 0{,}2364pH - -0{,}0886 \lg a_{Fe^{2+}}$
13	$Fe_2GeO_4 + 4H^+ = 2Fe^{2+} + GeO_2 + 2H_2O$	$pH = 5{,}575 - 0{,}5 \lg a_{Fe^{2+}}$
14	$Fe^{2+} + 2\bar{e} = Fe(\alpha)$, при $a_{Fe(\alpha)} = 1$	$E = -0{,}4402 + 0{,}0295 \lg a_{Fe^{2+}}$
15	$Fe^{2+} + 2\bar{e} = Fe(\alpha \leftrightarrow \beta)$, при $a_{Fe(\alpha)} = 2{,}2 \cdot 10^{-2}$	$E = -0{,}385 + 0{,}0295 \lg a_{Fe^{2+}}$
16	$Fe^{2+} + 2\bar{e} = Fe(\beta \leftrightarrow Fe_6Ge_5)$, при $a_{Fe(\beta)} = 7{,}716 \cdot 10^{-5}$	$E = -0{,}340 + 0{,}0295 \lg a_{Fe^{2+}}$
17	$5FeGe + Fe^{2+} + 2\bar{e} = Fe_6Ge_5$	$E = -0{,}317 + 0{,}0295 \lg a_{Fe^{2+}}$
18	$FeGe_2 + Fe^{2+} + 2\bar{e} = 2FeGe$	$E = -0{,}297 + 0{,}0295 \lg a_{Fe^{2+}}$
19	$2Ge(\text{алмаз}) + Fe^{2+} + 2\bar{e} = FeGe_2$	$E = -0{,}188 + 0{,}0295 \lg a_{Fe^{2+}}$
20	$Ge^{2+} + 2\bar{e} = Ge$	$E = 0{,}01 + 0{,}0295 \lg a_{Ge^{2+}}$
21	$GeO_2 + 4H^+ + 2\bar{e} = Ge^{2+} + 2H_2O$	$E = -0{,}586 - 0{,}1182pH - -0{,}0295 \lg a_{Ge^{2+}}$
22	$3Fe_2O_3 + 2H^+ + 2\bar{e} = 2Fe_3O_4 + H_2O$	$E = 0{,}234 - 0{,}0591pH$
23	$Fe_2O_3 + 6H^+ + 2\bar{e} = 2Fe^{2+} + 3H_2O$	$E = 0{,}713 - 0{,}1774pH - -0{,}0591 \lg a_{Fe^{2+}}$
24	$Fe^{3+} + \bar{e} = Fe^{2+}$	$E = 0{,}771 + 0{,}0591 \lg \frac{a_{Fe^{3+}}}{a_{Fe^{2+}}}$
25	$Fe_2O_3 + 6H^+ = 2Fe^{3+} + 3H_2O$	$pH = -0{,}32 - 0{,}33 \lg a_{Fe^{3+}}$
26	$2FeO_2 + 2H^+ + 2\bar{e} = Fe_2O_3 + H_2O$	$E = 1{,}315 - 0{,}0591pH$
27	$FeO_2 + 4H^+ + \bar{e} = Fe^{3+} + 2H_2O$	$E = 1{,}276 - 0{,}2364pH - -0{,}0591 \lg a_{Fe^{3+}}$

28	$FeO_4^{2-} + 4H^+ + 2\bar{e} = FeO_2 + 2H_2O$	$E = 2{,}673 - 0{,}1182pH + + 0{,}0295 \lg a_{FeO_4^{2-}}$

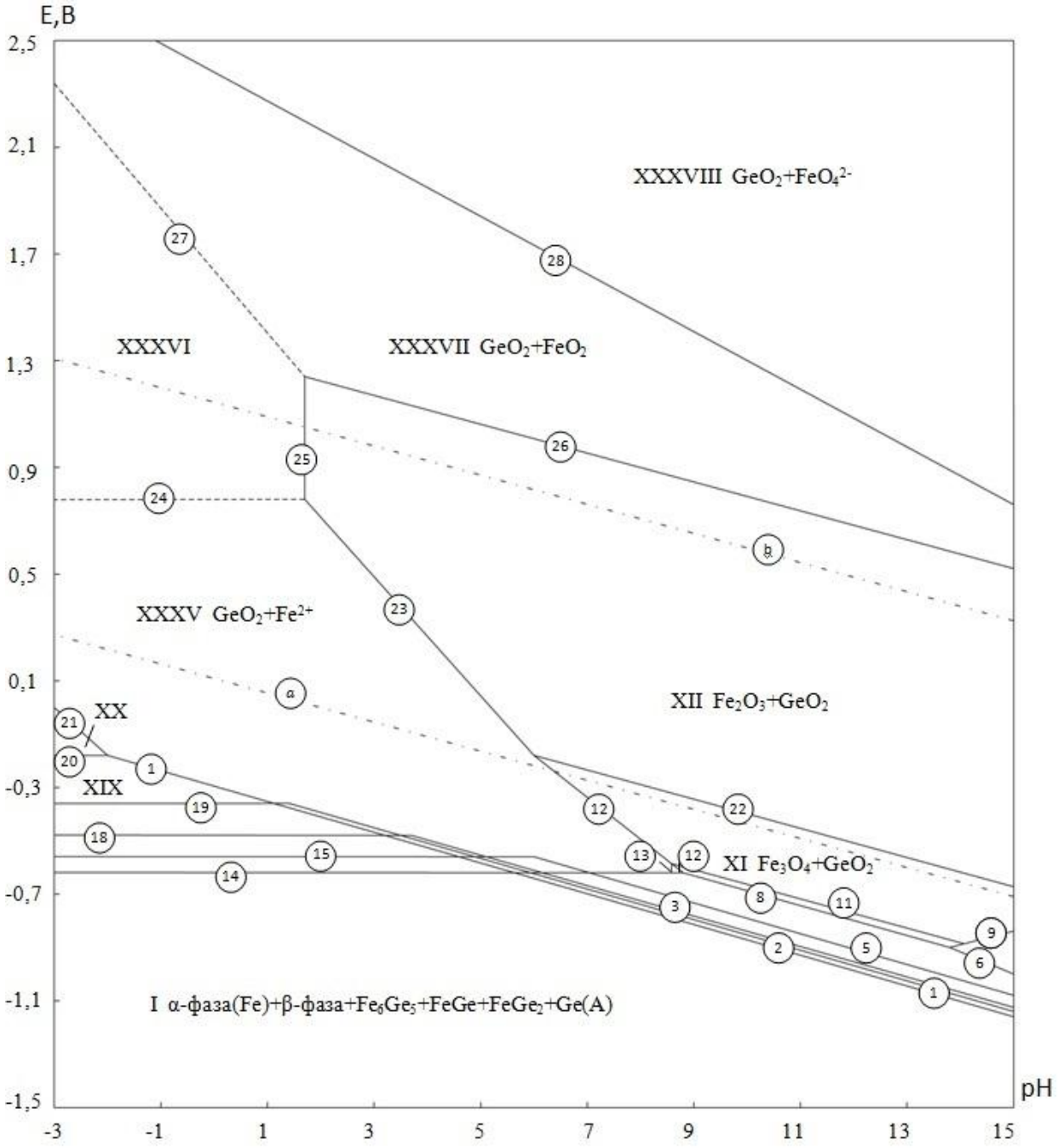

Fig. 3. The potential – pH diagram of the Fe – Ge – H_2O system at 25°C, air pressure of 1 bar and $a_i = 10^{-6}$ $\frac{\text{моль}}{\text{л}}$ (unhydrated form of the oxides).

4. ЭЛЕКТРОХИМИЧЕСКАЯ УСТОЙЧИВОСТЬ.

Термодинамические характеристики основных химических и электрохимических равновесий в системе Fe – Ge – H_2O при 25ºC и давлении воздуха 1 бар рассчитаны по результатам фазовых равновесий в системе Fe – Ge – O и данным справочной литературы [37– 41] и представлены в таблице 4. На основании этих расчётов построена диаграмма электрохимического равновесия (потенциал – pH) железогерманиевых сплавов при 25ºC, давлении 1 бар и активностях ионов в растворе, равных 10^{-6} $\frac{\text{моль}}{\text{л}}$ (стандартное состояние – гипотетический одномолярный раствор), которая изображена на рисунке 3. Рисунок 4 детализирует область активного растворения железа на диаграмме.

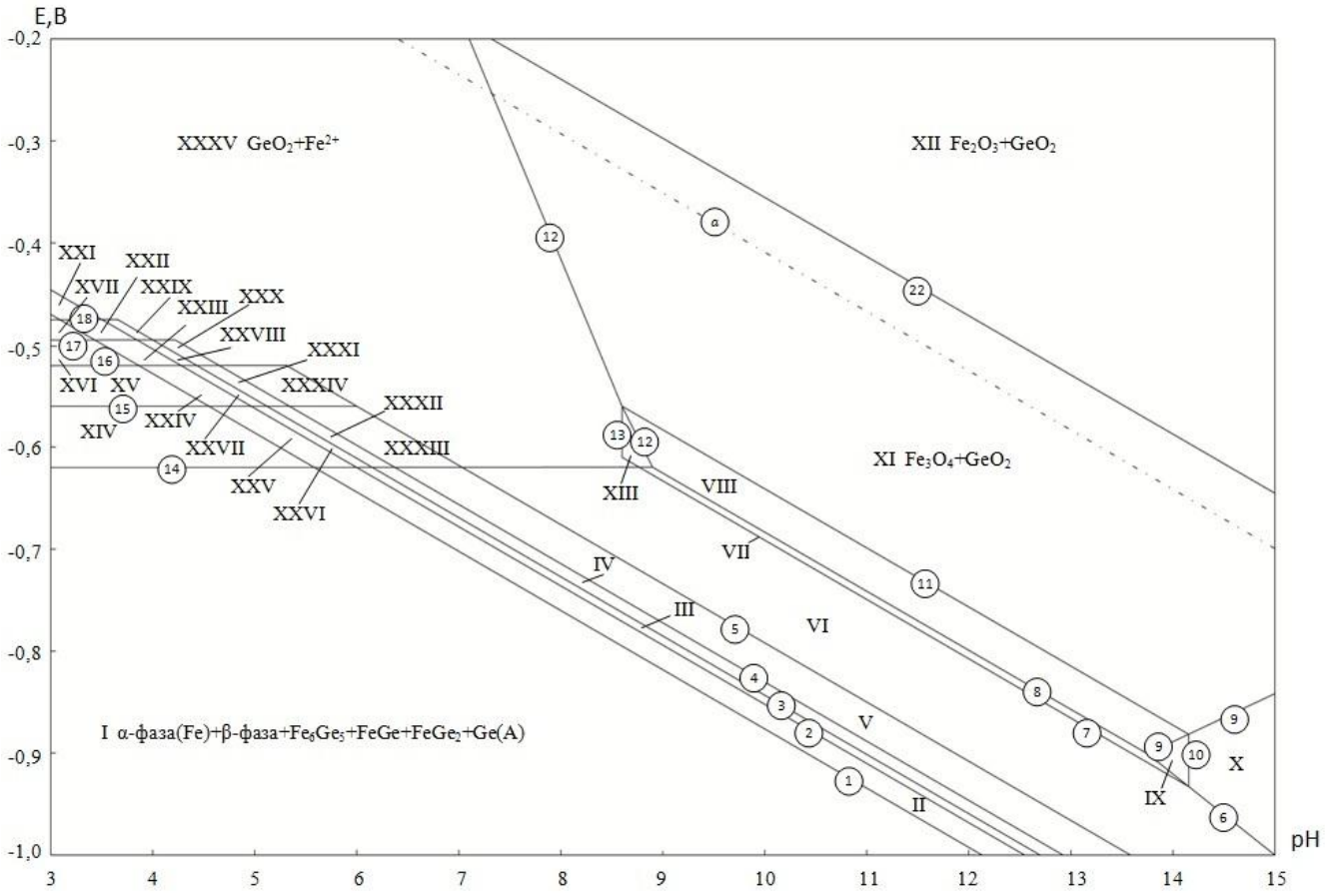

Fig. 4. The cross-section of the potential – pH diagram of the Fe – Ge – H_2O system in the domain of iron active dissolution.

На диаграмме выделяются следующие области преобладания различных фаз системы: I – α-фаза (Fe) + β-фаза + Fe_6Ge_5 + FeGe + $FeGe_2$ + Ge (алмаз); II – α-фаза (Fe) + β-фаза + Fe_6Ge_5 + FeGe + $FeGe_2$ + GeO_2; III – α-фаза (Fe) + β-фаза + Fe_6Ge_5 + FeGe + GeO_2; IV – α-фаза (Fe) + β-фаза + Fe_6Ge_5 + GeO_2; V – α-фаза (Fe) + β-фаза + GeO_2; VI – α-фаза (Fe) + GeO_2; VII – α-фаза (Fe)+Fe_2GeO_4; VIII – Fe_3O_4 + Fe_2GeO_4; IX – Fe_2GeO_4 + $HFeO_2^-$; X – GeO_2 + $HFeO_2^-$; XI – Fe_3O_4 + GeO_2; XII – Fe_2O_3 + GeO_2; XIII – Fe_2GeO_4 + Fe^{2+}; XIV – α-фаза (Fe) + β-фаза + Fe_6Ge_5 + FeGe + $FeGe_2$ + Ge (алмаз)+Fe^{2+}; XV – β-фаза + Fe_6Ge_5 + FeGe + $FeGe_2$ + Ge(алмаз) + Fe^{2+}; XVI – Fe_6Ge_5 + FeGe + $FeGe_2$ + Ge (алмаз) + Fe^{2+}; XVII – FeGe + $FeGe_2$ + Ge(алмаз) + Fe^{2+}; XVIII – $FeGe_2$ + Ge (алмаз) + Fe^{2+}; XIX – Ge (алмаз) + Fe^{2+}; XX – Ge^{2+} + Fe^{2+}; XXI – $FeGe_2$ + GeO_2 + Fe^{2+}; XXII – FeGe + $FeGe_2$ + GeO_2 + Fe^{2+}; XXIII – Fe_6Ge_5 + FeGe + $FeGe_2$ + GeO_2 + Fe^{2+}; XXIV – β-фаза + Fe_6Ge_5 + FeGe + $FeGe_2$ + GeO_2 + Fe^{2+}; XXV – α-фаза (Fe) + β-фаза + Fe_6Ge_5 + FeGe + $FeGe_2$ + GeO_2 + Fe^{2+}; XXVI – α-фаза (Fe) + β-фаза + Fe_6Ge_5 + FeGe + GeO_2 + Fe^{2+}; XXVII – β-фаза + Fe_6Ge_5 + FeGe + GeO_2 + Fe^{2+}; XXVIII – Fe_6Ge_5 + FeGe + GeO_2 + Fe^{2+}; XXIX – FeGe + GeO_2 + Fe^{2+}; XXX – Fe_6Ge_5 + GeO_2 + Fe^{2+}; XXXI – β-фаза + Fe_6Ge_5 + GeO_2 + Fe^{2+}; XXXII – α-фаза (Fe) + β-фаза + Fe_6Ge_5 + GeO_2 + Fe^{2+}; XXXIII – α-фаза (Fe) + β-фаза + GeO_2 + Fe^{2+}; XXXIV – β-фаза + GeO_2 + Fe^{2+}; XXXV – GeO_2 + Fe^{2+}; XXXVI – GeO_2 + Fe^{3+}; XXXVII – GeO_2 + FeO_2; XXXVIII – GeO_2 + FeO_4^{2-}.

Эти области можно сгруппировать следующим образом: 1) область иммунности (термодинамической устойчивости) всех возможных структурных составляющих системы Fe – Ge (область I); 2) области селективного окисления германия с образованием пассивирующей плёнки GeO_2 (области II – VI); 3) области общей коррозии сплавов с образованием пассивирующей плёнки Fe_2GeO_4 (области VII – IX, XIII); 4) области активного (Fe^{2+}) селективного растворения железа в сплавах (области XIV – XIX); 5) область общей коррозии, характеризующиеся активным растворением обоих компонентов (область XX); 6) области общей коррозии,

связанные с активным растворением железа (Fe^{2+}, Fe^{3+}, $HFeO_2^-$) и окислением германия в виде GeO_2 (области X, XXXV и XXXVI); 7) области пассивности, связанные с образованием оксидов германия и железа (области XI, XII и XXXVII); 8) область транспассивности сплавов (область XXXVIII).

ВЫВОДЫ

1. Методами практических расчётов определены стандартные энергии Гиббса образования интерметаллидов Fe_6Ge_5, FeGe и $FeGe_2$.
2. В рамках модели регулярных растворов описаны термодинамические свойства α- и β- твёрдых металлических растворов системы Fe – Ge и шпинельных растворов системы $Fe_3O_4 – Fe_2GeO_4$.
3. Рассчитаны сечения фазовых диаграмм Fe – Ge и Fe – Ge – O при 25ºC. Химическое сродство германия к кислороду при этой температуре выше, чем у железа, поэтому химическая стойкость сплавов определяется содержанием в них германия.
4. Рассчитана диаграмма потенциал – pH системы Fe – Ge – H_2O при 25ºC, 1 бар и различных активностях ионов в растворе. Рассмотрены термодинамические особенности коррозионно-электрохимического поведения германия и железа в сплавах при различных электродных потенциалах и pH растворов.

ЛИТЕРАТУРА

1. Княжева В. М., Бабич, С. Г., Колотыркин В. И. et al. Металлоподобные соединения переходных металлов – новый класс коррозионностойких материалов и покрытий // Защита металлов. 1991. Т. 27. № 4. С.603–616.
2. Fatséas G. A. Some remarks on a recent Mossbauer effect study of the p-phase iron germanide // Canadian Journal of Physics. 1976. Vol. 54. No 18. P. 1850–1853.

3. Adelson E., Austin A.E. Magnetic structures of iron germanides // Journal of Physics and Chemistry of Solids. 1965. Vol. 26. No 12. P. 1795–1804.

4. Häggström L., Ericsson T., Wappling R., Karlsson E. Mössbauer Study of Hexagonal FeGe // Physica Scripta. 1975. Vol. 11. No 1. P. 55–59.

5. Власенко А. В., Однодворець Л. В., Проценко І. Ю. Фазовий склад і магнеторезистивні властивості тришарових плівок Fe / Ge / Fe // Металлофизика и новейшие технологии. 2013. Т. 35. Т. 12. С. 1637–1644.

6. Than H.-Y., Lee D. C., Korgel B. A. Nanocrystal-Mediated Crystallization of Silicon and Germanium Nanowires in Organic Solvents: The Role of Catalysis and Solid-Phase Seeding // Angewandte Chemie. 2006. Bd. 118. H. 31. S. 5308–5311.

7. Yoon H.-N., YooY.-D., SeoK.-Y., InJ.-H., Kim B.-S. Synthesis and Applications of Noble Metal and Metal Silicide and Germanide 1-Dimensional Nanostructures // Bulletin of the Korean Chemical Society. 2012. Vol. 33. No 9. P. 2830–2844.

8. Tang J., Wang C.-Y., Hung M.-H., Jiang X., Chang L.-T., He L., Liu P.-H., Yang H.-J., Tuan H.-Y., Chen L.-J., Wang K.-L. Ferromagnetic Germanide in Ge Nanowire Transistors for Spintronics Application // ACS Nano. 2010. Vol. 6. No 6. P. 5710–5717.

9. Vaughn D. D., Sun D., Moyer J. A., Biacchi A. J., Misra R., Schiffer P., Schaak R. E. Solution-Phase Synthesis and Magnetic Properties of Single-Crystal Iron Germanide Nanostructures // Chemistry of Materials. 2013. Vol. 25. No 21. P. 4396–4401.

10. Сидорко В. Р., Буланова М. В., Мелешевич К. А. Физіко-хімічна взаємодія у системах тривалентних РЗМ із р-елементами IV групи // Порошкова металургія. 2005. Т 5, 6. С. 60–66.

11. Комаров С. М. Холодильник на фосфиде // Химия и жизнь. 2009. № 3. С. 18.

12. Шеин А. Б. Электрохимия силицидов и германидов переходных металлов: монография. Пермь: Изд-во Пермского гос. ун-та, 2009. 257 с.

13. Кубашевски О. Диаграммы состояния двойных систем на основе железа: справ. изд.; пер. с англ.; под ред. Л. А. Петровой. М.: Металлургия, 1985. 184 с.

14. Диаграммы состояния двойных металлических систем: справ. изд. В 3 т. Т. 2; под. ред. Н. П. Лякишева. М.: Машиностроение, 1997. 1024 с.

15. Richardson M. The partial equilibrium diagram of the Fe–Ge system in the range 40–72 at. % Ge, and the crystallization of some iron germanides by chemical transport reactions // Acta Chemica Scandinavica, 1967. Vol. 21. P. 2305 – 2317.

16 Киреев В. А. Методы практических расчётов в термодинамике химических реакций. М.: Химия, 1975. 537 с.

17 Физическая химия неорганических материалов. В 3 т.; под общ. ред. В. Н. Ерёменко. Киев: Наукова думка, 1988. Т. 1: Термодинамика интерметаллидов и фазовые равновесия в металлических системах / Л. В. Артюх, Ю. И. Буянов, Т. Я. Великанова et al. С. 9 – 70.

18. Hildebrand J. H. A Quantitative Treatment of Deviations from Raoult's Law // Proceedings of the National Academy of Sciences of the United States of America, 1927. Vol. 13. No. 5. P. 267 – 272.

19. Dinsdale A. T. SGTE data for pure elements // CALPHAD: Computer Coupling of Phase Diagrams and Thermochemistry, 1991. Vol. 15. No. 4. P. 317 – 425.

20. Gorichev I. G., Klyushin N. G. Dependence of standard electrode potentials and free-energies of some oxides on their stoichiometric composition // Russian Journal of Physical Chemistry. 1971. Vol. 45. No 5. P. 615.

21. Жук Н. П. Курс теории коррозии и защиты металлов: учеб. пособие. М.: ООО ТИД «Альянс», 2006. 472 с.

22. Nikolaychuk P. A., Tyurin A. G. Method of estimating the standard Gibbs energies of formation of binary compounds // Abstracts of XVIII International Conference on Chemical Thermodynamics in Russia. Vol. 2. Samara: Samara State Technical University, 2011. P. 16 – 17.

23. Dede L., Russ W. Beiträge zur Kenntnis des Germaniums, I.: Die Aufarbeitung des Germanits, Darstellung reinen Germaniumdioxyds und reinsten Germaniumtetrachlorids // Berichte der deutschen chemischen Gesellschaft (A und B Series), 1928. Bd. 61. Heft 11. S. 2451 – 2459.

24. Welch M. D., Cooper M. A., Hawthorne F. C. The crystal structure of brunogeierite, Fe_2GeO_4 spinel // Mineralogical Magazine, 2001. Vol. 65. No. 3. P. 441 – 444.

25. Cotton F. A., Wilkinson G., Murillo C. A., Bochman M. Advanced Inorganic Chemistry, 6^{th} Edition. Wiley, 1999. 1376 p.

26. Zhou Z., Liao Z. Preparation of lithium-ferrate battery and electrochemical characteristic in non-aqueous phase // Chinese Journal of Power Sources, 2003. Vol. 27. No. 6. P. 497–499.

27. Klyushin N. G., Gorichev I. G., Dukhanin V. S. Iron oxides FeO_2 // Zhurnal Neorganicheskoi Khimii. 1972. Vol. 17. No 9. P. 2329.

28. Klyushin N. G., Goichev I. G., Malov N. V. Stability regions of ferric oxides in an iron-water system // Zhurnal Fizicheskoi Khimii. 1973. Vol. 45. No 4. P. 834–837.

29. Nikolaychuk P. A., Tyurin A. G. The analysis of standard Gibbs energies of formation of MeO_2-type oxides of fourth period d-elements // Abstracts of XVIII International Conference on Chemical Thermodynamics in Russia. Vol. 2. Samara: Samara State Technical University, 2011. P. 17 – 18.

30. Hariya Yu, Wai C. M. The Stability and Phase Transition of the System Fe_2GeO_4 – Fe_2SiO_4 // Journal of the Faculty of Science, Hokkaido University. Series 4, Geology and Mineralogy, 1970. Vol. 14. No. 4. P. 355 – 363.

31. Штин С. В,, Пилипенко Е. А., Лыкасов А. А. Равновесие вюститного и металлического растворов в системе Fe – Ge – O // Вестник Южно-Уральского государственного университета. Серия: Металлургия. 2005. Т 3(43). С. 51–54.

32. Штин С. В., Лыкасов А. А. Фазовые равновесия в системе Fe – Fe_3O_4 – Fe_2GeO_4 – Ge // Вестник Южно-Уральского государственного университета. Серия: Математика, механика, физика. 2007. Т 19. С. 118–121.

33. Shtin S. V., Lykasov A. A. Investigation into the equilibrium of the wustite and spinel solutions in the Fe-Ge-O system // Russian Journal of Non-Ferrous Metals. 2013. Vol. 54. No 6. P. 429–432.

34. Chase M. W. Jr., Davies C. A., Downey J. R. Jr., Frurip D. J., McDonald R. A., Syverud A. N. JANAF – NIST Thermochemical Tables. 4th Edition // Journal of Physical and Chemical Reference Data, 1998. Monograph 9.

35. Wagman D. D., Evans W. H., Parker V. B., Schumm R. H., Halow I. B., Sylvia M., Churney K. L., Nuttal R. L. The NBS tables of chemical thermodynamic properties. Selected values for inorganic and C_1 and C_2 organic substances in SI units // Journal of Physical and Chemical Reference Data, 1982. Vol. 11. Suppl. 2.

36. Schweitzer G. K., Pesterfield L. L. The aqueous chemistry of the elements. Oxford: Oxford University Press, 2010. 433 p.

37. Справочник по электрохимии; под ред. А. М. Сухотина. Л.: Химия, 1981. 488 с.

38. Гаррелс Р. М., Крайст Ч. Л. Растворы, минералы, равновесия; пер. с англ. М.: Мир, 1968. 365 с.

39. Bard A. J., Parsons R., Jordan J. Standard potentials in aqueous solutions. New York: Marcel Dekker Inc., 1985. 848 p.

40. Speight J. Lange's Handbook of Chemistry, 16th Edition. New York: McGraw-Hill Education, 2005. 1623 p.

41. Vanýsek P. Electrochemical Series // CRC Handbook of Chemistry and Physics, 95th Edition; Ed. W. M. Haynes. CRC Press, 2014. 2704 p.

13. Co – Si system
13.1. Cobalt silicides

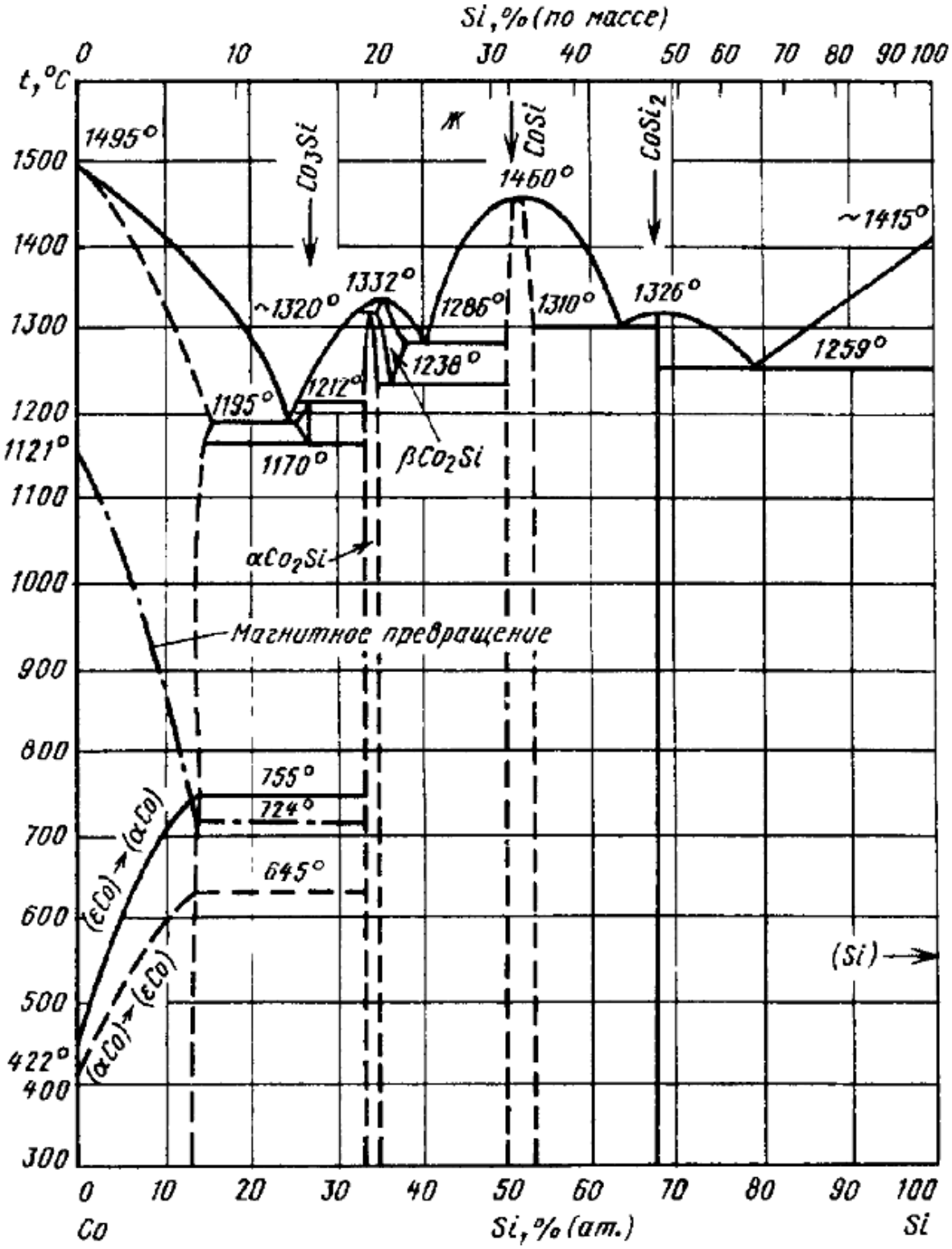

Fig. 54. The phase diagram of Co – Si system [Диаграммы состояния двойных металлических систем: справочник, 2001].

Cobalt and silicon are the basic components of cobalt-based amorphous alloys [Dark, Wei, Cantor, 1988], which are of interest to the researchers due to their unusual magnetic, mechanical, electric properties as well as high corrosion resistance. The phase diagram of Co – Si system is presented in Figure 54.

Three compounds, namely, Co_2Si, CoSi and $CoSi_2$, exist in Co – Si system at 25 °C [Soon-Don, 1992]. Another cobalt silicide, Co_3Si, is stable only at elevated temperatures. Moreover, a solid solution of Si in (hcp-Co) (ε-phase) exists in cobalt-rich region of Co – Si phase diagram. The excess Gibbs energy of this solid solution was modelled in terms of the quasiregular solution model, and the expression for it is presented in the attached publication. Calculated maximum solid solubility of silicon at 25 °C equals 10,7 atomic %; the thermodynamic activities of this saturated solid solution are equal to $a_{Co(\varepsilon)} = 0.27$, $a_{Si(\varepsilon)} = 4 \cdot 10^{-16}$. The solubility of Co in (diamond-Si) is about 10^{-17} atomic % at 1000 °C [Yoshikawa et al., 2010]. The values of standard Gibbs energies of formation of cobalt silicides were collected from [Chase Jr. et al., 1985; Kaufman, 1979; Soon-Don, 1992; Термические константы веществ, 2007].

13.2. Equilibira in Co – Si – O system

Cobalt could form a variety of oxides, namely, CoO, Co_3O_4, Co_2O_3 and CoO_2; the first two ones have a noticeable homogeneity range, which covers the compositions from CoO to $CoO_{1.07}$ for “CoO” phase and from $CoO_{1.31}$ to $CoO_{1.41}$ for “Co_3O_4” phase [Chen, Hallstedt, Gauckler, 2003]. Only one ternary compound, Co_2SiO_4, exists in Co – Si – O system [Navrotsky, Pintchovski, Akimoto, 1979]. The values of Gibbs energies of formation of cobalt oxides and silicides were obtained from [Chase Jr. et al., 1985; Chen, Hallstedt, Gauckler, 2003; Термические константы веществ, 2007]. The expression for the Gibbs energy of formation of non-stoichiometric cobalt oxides were estimated by Gorichev’s method.

The state diagram of the Co – Si – O system is presented in Figure 55. More details are provided in the attached publication.

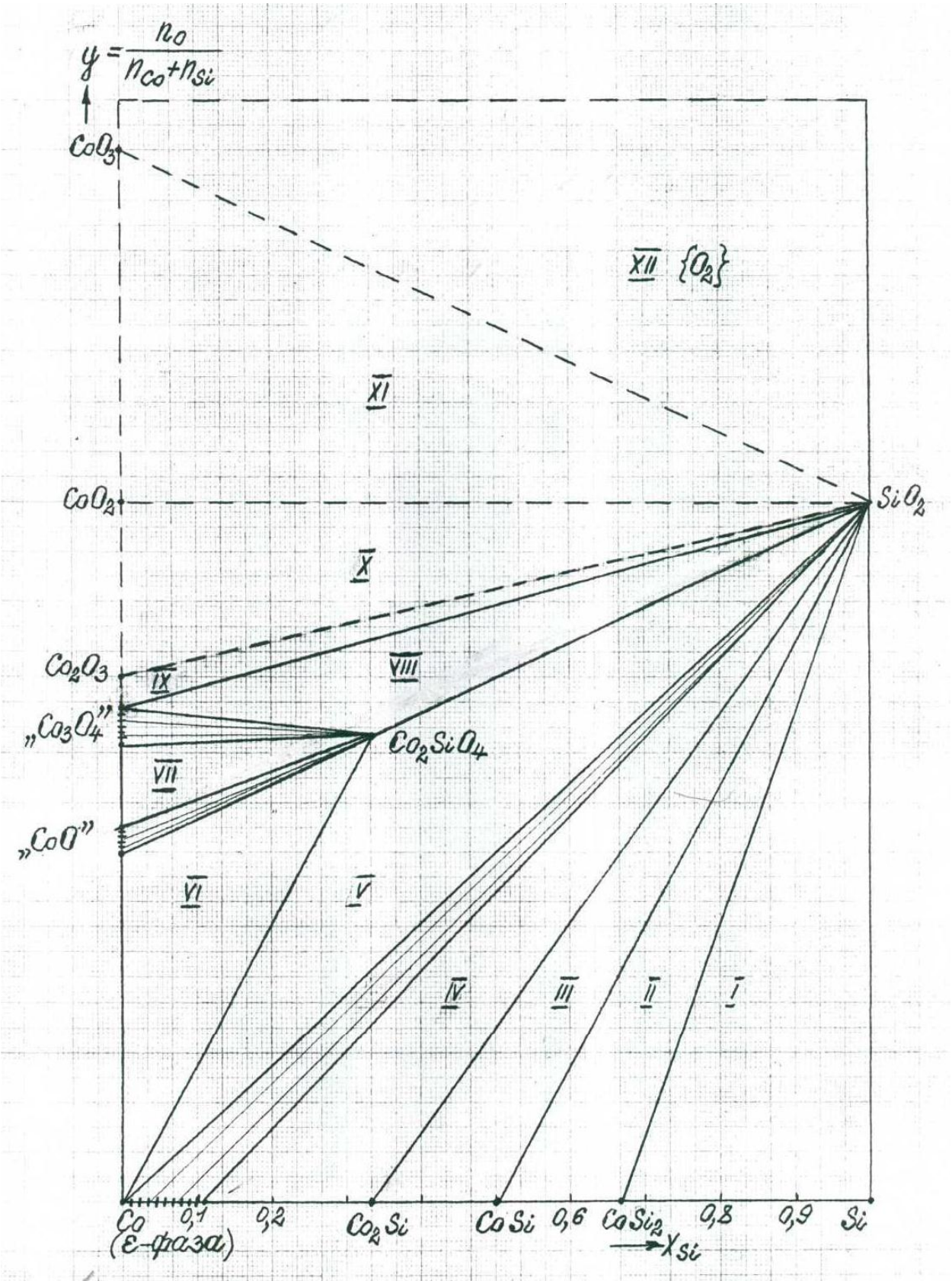

Fig. 55. The state diagram of the Co – Si – O system.

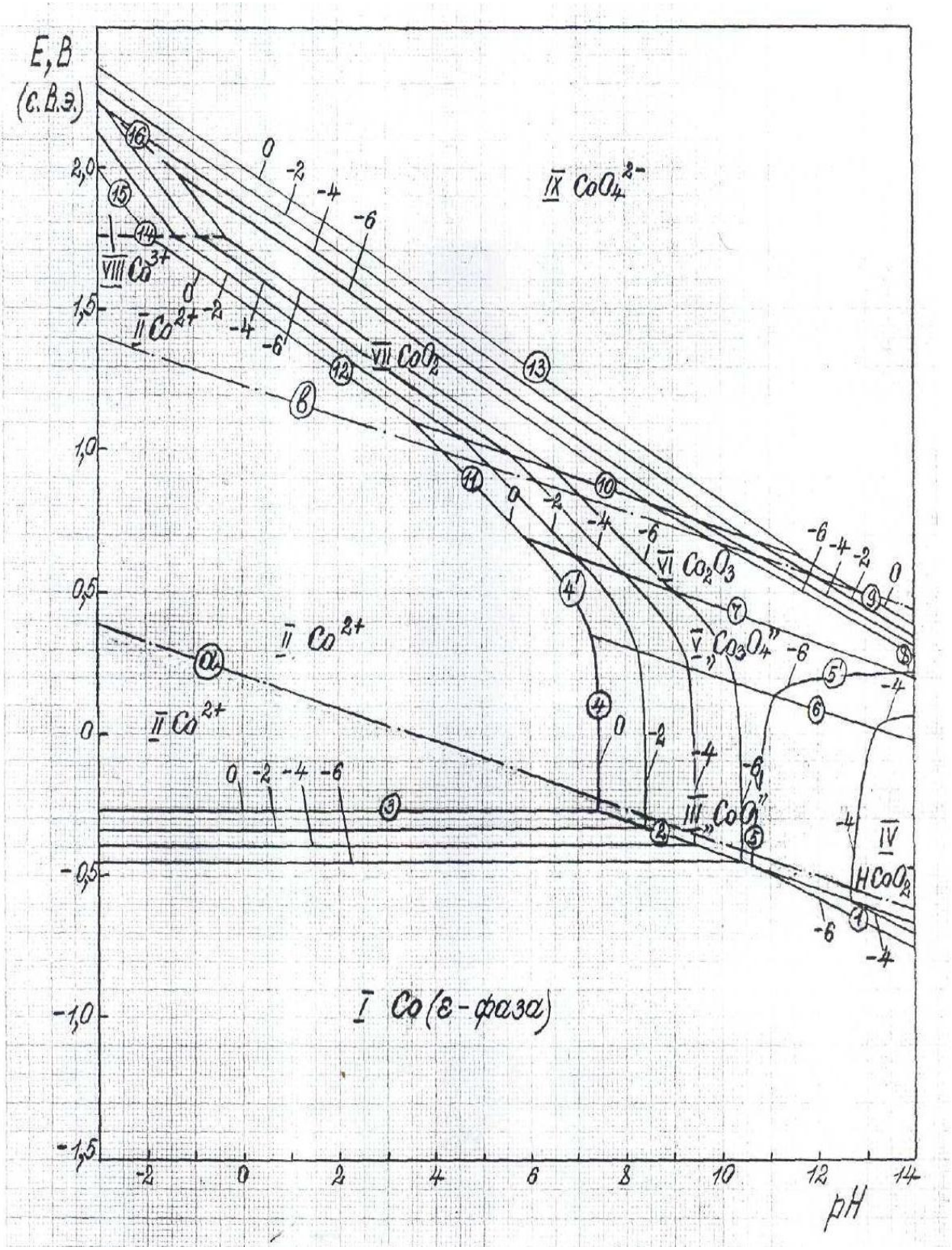

Fig. 56. The potential – pH diagram of Co – H_2O system at 25 °C, air pressure of 1 bar and the activities of cobalt species in a solution of 1, 10^{-2}, 10^{-4} and 10^{-6} M.

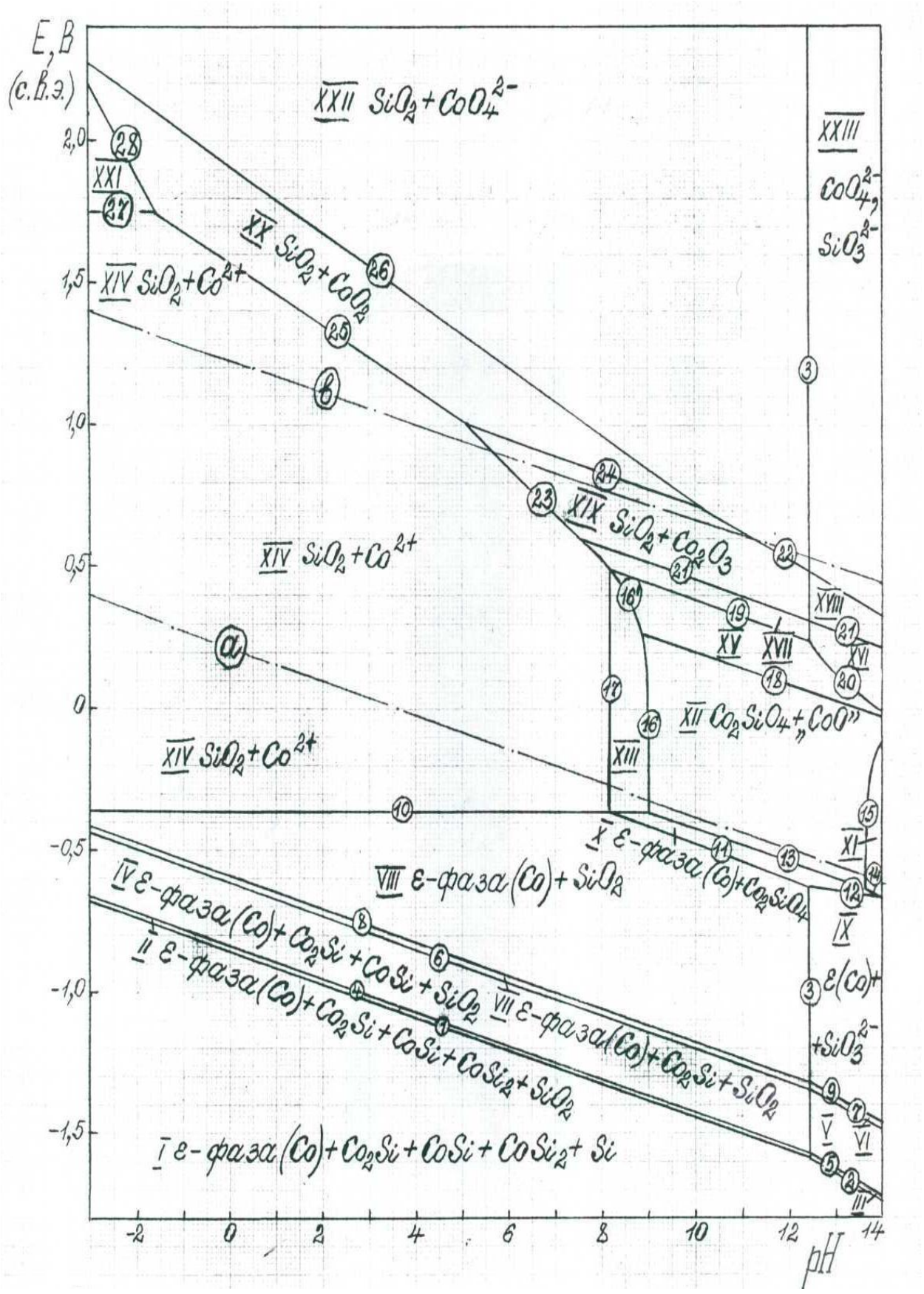

Fig. 57. The potential – pH diagram of Co – Si – H_2O system at 25 °C, air pressure of 1 bar and the activities of species in a solution of 10^{-3} M.

13.3. Potential – pH diagram of Co – H_2O system

Cobalt might form the cations Co^{2+} and Co^{3+}, and the anions $HCoO_2^-$ and CoO_4^{2-} in water solution.

The potential – pH diagram of Co – H_2O system at 25 °C, air pressure of 1 bar and the activities of cobalt species ranging from 1 to 10^{-6} $mol \cdot l^{-1}$ is presented in Figure 56.

13.4. Potential – pH diagram of Co – Si – H_2O system

The potential – pH diagram of Co – Si – H_2O system at 25 °C, air pressure of 1 bar and the activities of species in a solution of 10^{-3} $mol \cdot l^{-1}$ is presented in Figure 57. More details are provided in the attached publication.

The corrosion-electrochemical behaviour of Co – Si system alloys is very similar to that of Fe – Si system alloys. Cobalt silicate plays a minor role in the formation of a passivation film on the alloy surface. If silicon content in the system is not sufficient to form a continuous layer of H_4SiO_4, the cobalt oxides become involved in the passivation.

Publications to chapter 13

The content of this chapter was published in the paper [Тюрин, Мосунова, Николайчук, 2010]. The Russian preprint of this paper with the title, abstract, figures and tables translated into English is presented below with the permission from *Ûžno-Ural'skij gosudarstvennyj universitet (nacional'nyj issledovatel'skij universitet)*.

УДК 541.1:620.193.01:669.14

ТЕРМОДИНАМИКА ХИМИЧЕСКОЙ И ЭЛЕКТРОХИМИЧЕСКОЙ УСТОЙЧИВОСТИ СИЛИЦИДОВ КОБАЛЬТА

А. Г. Тюрин, Т. В. Мосунова, П. А. Николайчук

Построены диаграммы потенциал – pH систем Co – H_2O и Co – Si – H_2O, а также фазовая диаграмма системы Co – Si – O при 25˚C. Анализируются термодинамические особенности коррозионно-электрохимического поведения сплавов системы Co – Si различного состава.
Ключевые слова: силициды кобальта, низкотемпературное окисление, химическая устойчивость, коррозионно-электрохимическое поведение, диаграммы потенциал – pH, электрохимическая устойчивость.

THERMODYNAMICS OF CHEMICAL AND ELECTROCHEMICAL STABILITY OF COBALT SILICIDES

A. G. Tyurin, T. V. Mosunova, P. A. Nikolaychuk

The potential – pH diagrams of Co – H_2O and Co – Si – H_2O systems and phase diagram of Co – Si – O system at 25˚C are plotted. The thermodynamical features of corrosion-electrochemical behaviour of Co – Si system alloys of various composition are analysed.

Keywords: cobalt silicides, low temperature oxidation, chemical stability, corrosion-electrochemical behaviour, potential – pH diagrams, electrochemical stability.

Введение

Кобальт и кремний являются основными компонентами аморфных сплавов на основе кобальта. Состав некоторых из них представлен в табл. 1.

Table 1

The composition of some amorphous and crystallic alloys based on cobalt and silicon [1]

Alloy	Alloy index *	Comtent of components, weigth %					
		Co	Ni	Fe	Si	B	Mn
Virovac 6010	A_1, C_1	58	10	5	11	16	–
Metglas 2714A	A_2, C_2	66	1	4	15	14	–
Metglas 2705Mn	A_3, C_3	76	–	2	6	18	4

* A – amorphous, C – crystallic (annealed in a vacuum furnace at 580˚C during 10 min)

Аморфные металлические сплавы обладают комплексом необычных физико-химических свойств и являются перспективными материалами, представляющими теоретический и практический интерес. Следствием их аморфной структуры являются необычные магнитные, механические, электрические свойства и, в особенности, высокая коррозионная стойкость сплавов [2, 3]. Именно поэтому проводились и проводятся исследования коррозионного поведения системы кобальт – кремний как в воздушных, так и в водных средах. Результаты экспериментальных исследований состава и структуры пассивационных плёнок на сплавах приведены в работе [1]. Также широко исследуется [4 – 8] и электрохимическое поведение силицидов кобальта: Co_2Si [4, 8], CoSi [5, 6, 8], $CoSi_2$ [7, 8] и эвтектического сплава $CoSi_2$ – Si [7, 8] как в кислых [4 – 7], так и в щелочных [8] электролитах. В работе выполнен термодинамический

анализ химической и электрохимической устойчивости сплавов системы кобальт – кремний при 25˚С.

Из анализа фазовой диаграммы состояния системы Co – Si [9] следует, что при этой температуре в системе существуют следующие промежуточные соединения: Co_2Si, CoSi, $CoSi_2$. Предельная растворимость Si в ε-Co (с решёткой г. п. у.) лишь оценена и составляет чуть более 10 ат. %. Растворимость Co в Si если и существует, то ничтожно мала.

Избыточную энергию Гиббса G^E твёрдых растворов кремния в кобальте (ε-фаза) описывали в рамках двухпараметрического приближения обобщённой теории «регулярных» растворов [10]. Температурные зависимости энергетических параметров системы по данным [11] следующие:

$$Q_{12}^{(1)}(T) = -210455 + 32{,}01 \cdot T, \frac{\text{Дж}}{\text{моль}},$$

$$Q_{12}^{(2)}(T) = -141419 + 32{,}01 \cdot T, \frac{\text{Дж}}{\text{моль}}.$$

В литературе [11, 12] имеются различные данные о значениях энергии Гиббса образования интерметаллида Co_2Si. Однако рассчитанные на их основании значения предельной растворимости кремния в кобальте, отвечающие равновесию $2Co(\varepsilon) + Si(\varepsilon) = Co_2Si(т)$, хорошо согласуются между собой и с оценочными экспериментальными данными [9].

Химическая устойчивость

В соответствии с видом диаграмм состояния систем Co – O и Si – O [13] при 25˚С на воздухе на чистых кобальте и кремнии возможны следующие фазовые равновесия: Co | “CoO” | “Co_3O_4” | $\{O_2\}$ и Si | SiO_2 | $\{O_2\}$. Оксиды кобальта имеют весьма широкую область нестехиометрии. Так, состав фазы “CoO” может изменяться в пределах от CoO до $CoO_{1,07}$, а фазы “Co_3O_4” – от $CoO_{1,3095}$ до $CoO_{1,4096}$ [13]. Оксид Co_2O_3 может существовать только в форме гидрата $Co_2O_3 \cdot H_2O$. Кроме того, в системе Co – Si – O возможно образование соединения Co_2SiO_4.

Диаграмма состояния системы Co – Si – O при 25˚С и 1 атм. (воздух) представлена на рис. 1.

Стандартные энергии Гиббса образования оксидов взяты из справочников [12, 14] или рассчитаны с использованием интерполяционной формулы Лагранжа [10] и представлены в табл. 2. Рассчитанные характеристики трёхфазных равновесий представлены в табл. 3.

Table 2

Standard Gibbs energies of formation of compounds from elements

Oxide phase	Oxide formula	$-\Delta G^0_{298}, \frac{\text{Дж}}{\text{г–ат Co}}$	Ref.	Com-pound	$-\Delta G^0_{298}, \frac{\text{Дж}}{\text{моль}}$	Ref.
“CoO”	CoO	205126	[12]	CoO_2	233396	*
	$CoO_{1,07}$	212862	*	CoO_3	84810	*
“Co_3O_4”	$CoO_{1,3095}$	232774	*	$CoSi_2$	102260	[12]
	$CoO_{1,3333}$	234200	[12]	CoSi	98817	[12]
	$CoO_{1,4096}$	238090	*	Co_2Si	104856	[12]
Co_2O_3	$CoO_{1,5}$	241368	*	Co_2SiO_4	1233924	[12]
				SiO_2	805067	[14]

* Estimated by the authors according to Gorichev’s method.

Table 3

The characteristics of the invariant states in the Co – Si – O system at 25˚C

Equilibrium	P_{O_2}, атм	Solid phases composition
$Si – CoSi_2 – SiO_2$ (I)	$7{,}9 \cdot 10^{-142}$	$x_{Si} = 1; x_{CoSi_2} = 1; x_{SiO_2} = 1$
$CoSi_2 – CoSi – SiO_2$ (II)	$3{,}2 \cdot 10^{-141}$	$x_{CoSi_2} = 1; x_{CoSi} = 1; x_{SiO_2} = 1$

CoSi – Co_2Si – SiO_2 (III)	$2{,}8\cdot10^{-125}$	$x_{CoSi}=1; x_{Co_2Si}=1; x_{SiO_2}=1$
ε-фаза (Co) – Co_2Si – SiO_2 (IV)	$1{,}1\cdot10^{-122}$	$x_{Si(\varepsilon)}=0{,}107;\ x_{Co_2Si}=1; x_{SiO_2}=1$
ε-фаза (Co) – Co_2SiO_4 – SiO_2 (V)	$1{,}5\cdot10^{-75}$	$x_{Si(\varepsilon)}=4\cdot10^{-39};\ x_{Co_2SiO_4}=1; x_{SiO_2}=1$
ε-фаза (Co) – “CoO” – Co_2SiO_4 (VI)	$1{,}2\cdot10^{-72}$	$x_{Si(\varepsilon)}=8\cdot10^{-46};\ x_{"CoO"}=1; x_{Co_2SiO_4}=1$
“CoO” – “Co_3O_4” – Co_2SiO_4 (VII)	$7{,}1\cdot10^{-30}$	$x_{"CoO"}=1; x_{"Co_3O_4"}=1; x_{Co_2SiO_4}=1$
“Co_3O_4” – Co_2SiO_4 – SiO_2 (VIII)	$5{,}6\cdot10^{-21}$	$x_{"Co_3O_4"}=1; x_{Co_2SiO_4}=1; x_{SiO_2}=1$
“Co_3O_4” – Co_2O_3 – SiO_2 (IX)	0,79	$x_{"Co_3O_4"}=1; x_{Co_2O_3}=1; x_{SiO_2}=1$
Co_2O_3 – CoO_2 – SiO_2 (X)	$6{,}0\cdot10^{16}$	$x_{Co_2O_3}=1; x_{CoO_2}=1; x_{SiO_2}=1$
CoO_2 – CoO_3 – SiO_2 (XI)	$3{,}5\cdot10^{63}$	$x_{CoO_2}=1; x_{CoO_3}=1; x_{SiO_2}=1$

Из результатов расчёта следует, что химическое сродство кремния к кислороду намного выше, чем у кобальта. При содержании Si в ε-Co большем, чем 10^{-37} мол. % единственным продуктом окисления сплава является кремнезём. Установлено, что с ростом температуры эта пороговая концентрация кремния в сплаве возрастает. Так, при 400˚C она составляет 10^{-15} мол. %. Экспериментально изученные состав и структура оксидных слоёв на сплавах, образовавшихся на воздухе при 400˚C в течение 400 часов, представлена в табл. 4.

Table 4

Состав и структура оксидных слоёв на сплавах, образовавшихся на воздухе при температуре 400˚C в течение 400 часов [1]

Alloy index *	Oxide layer	Structural constituents of the layer
A_1	Thin	Co_2SiO_4; Co_3O_4; CoO
	Thick	Co_3O_4; Fe_3O_4; Co_2SiO_4; CoO
C_1	Thin	SiO_2 (аморф); Co_3O_4
	Thick	Co_3O_4; Co_2SiO_4; CoO
A_2	Thin	SiO_2 (аморф); Co_3O_4
	Thick	Co_3O_4; Co_2SiO_4; CoO
C_2	Thin	Co_2SiO_4; Co_3O_4; β-SiO_2
	Thick	Co_3O_4; Co_2SiO_4; CoO
A_3	Thin	Co_2SiO_4; Co_3O_4; β-SiO_2
	Thick	Co_3O_4; Co_2SiO_4; CoO
C_3	Thin	Co_3O_4; Co_2SiO_4
	Thick	Co_3O_4; Co_2SiO_4; CoO

* see Table 1

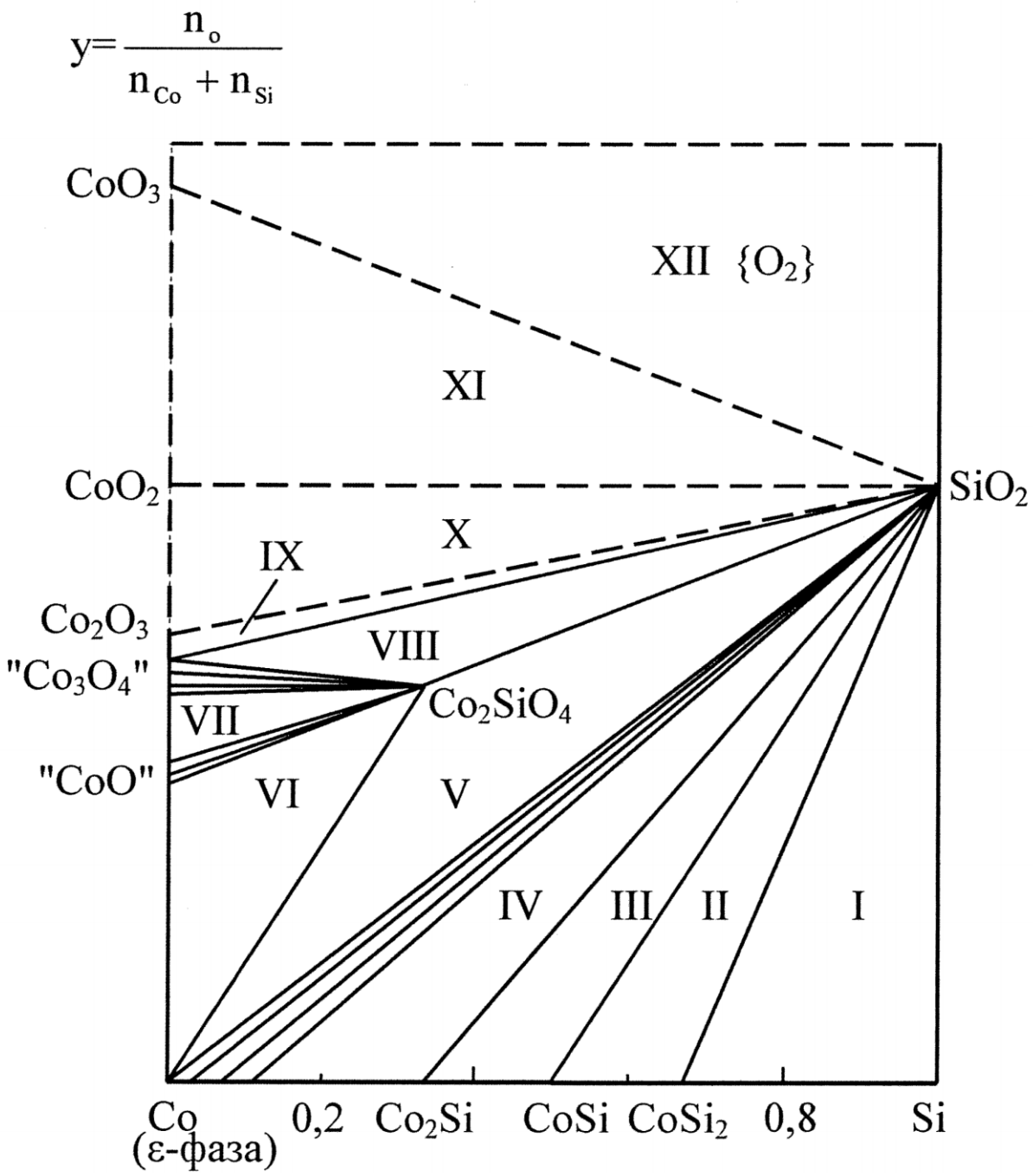

Fig. 1. The state diagram of the Co – Si – O system at 25°C.

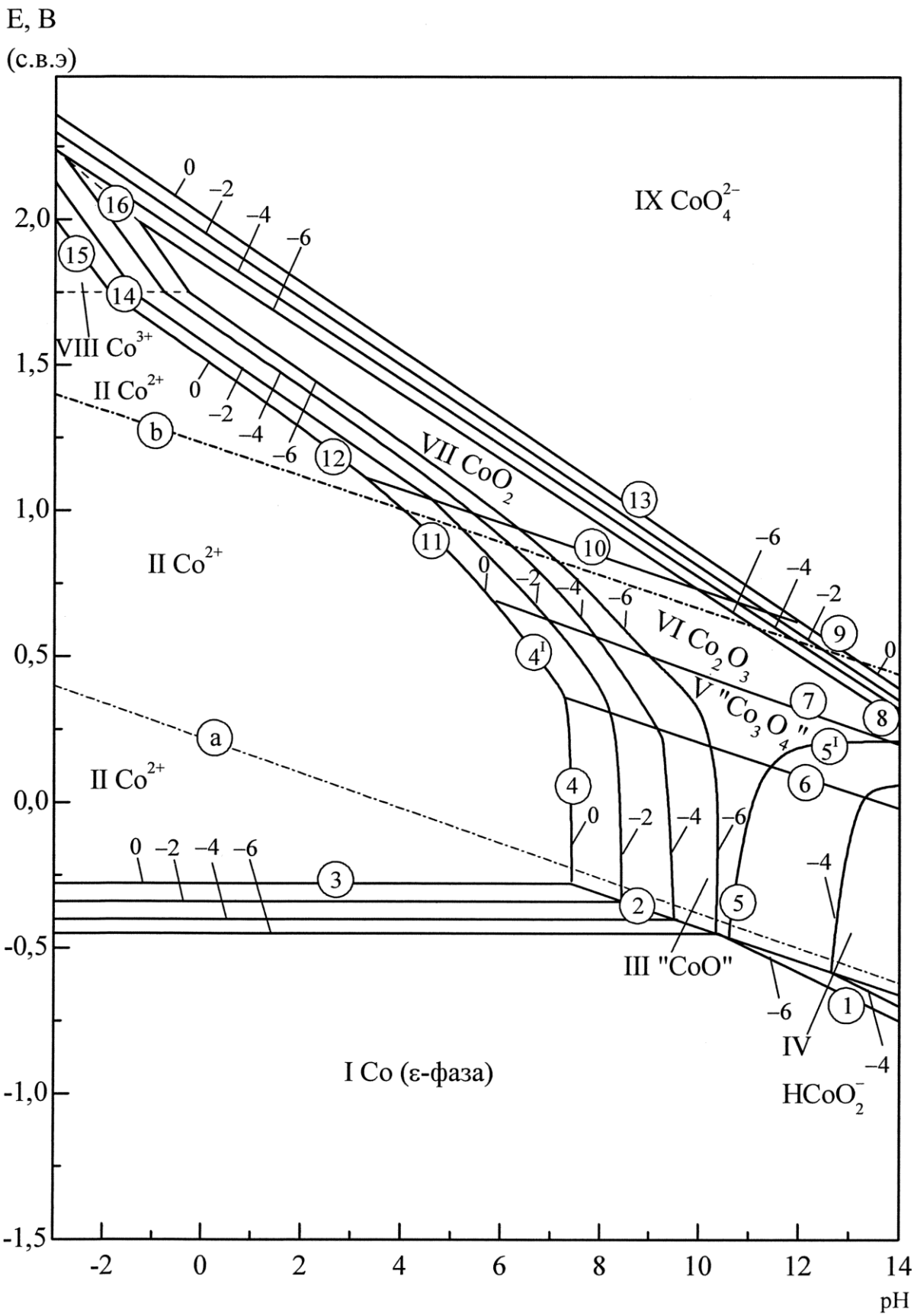

Fig. 2. The potential – pH diagram of the Co – H_2O system at 25°C, 1 bar (air) and $a_i = 10^0, 10^{-2}, 10^{-4}$ и 10^{-6} $^{mol}/_l$ (unhydrated form of oxides).

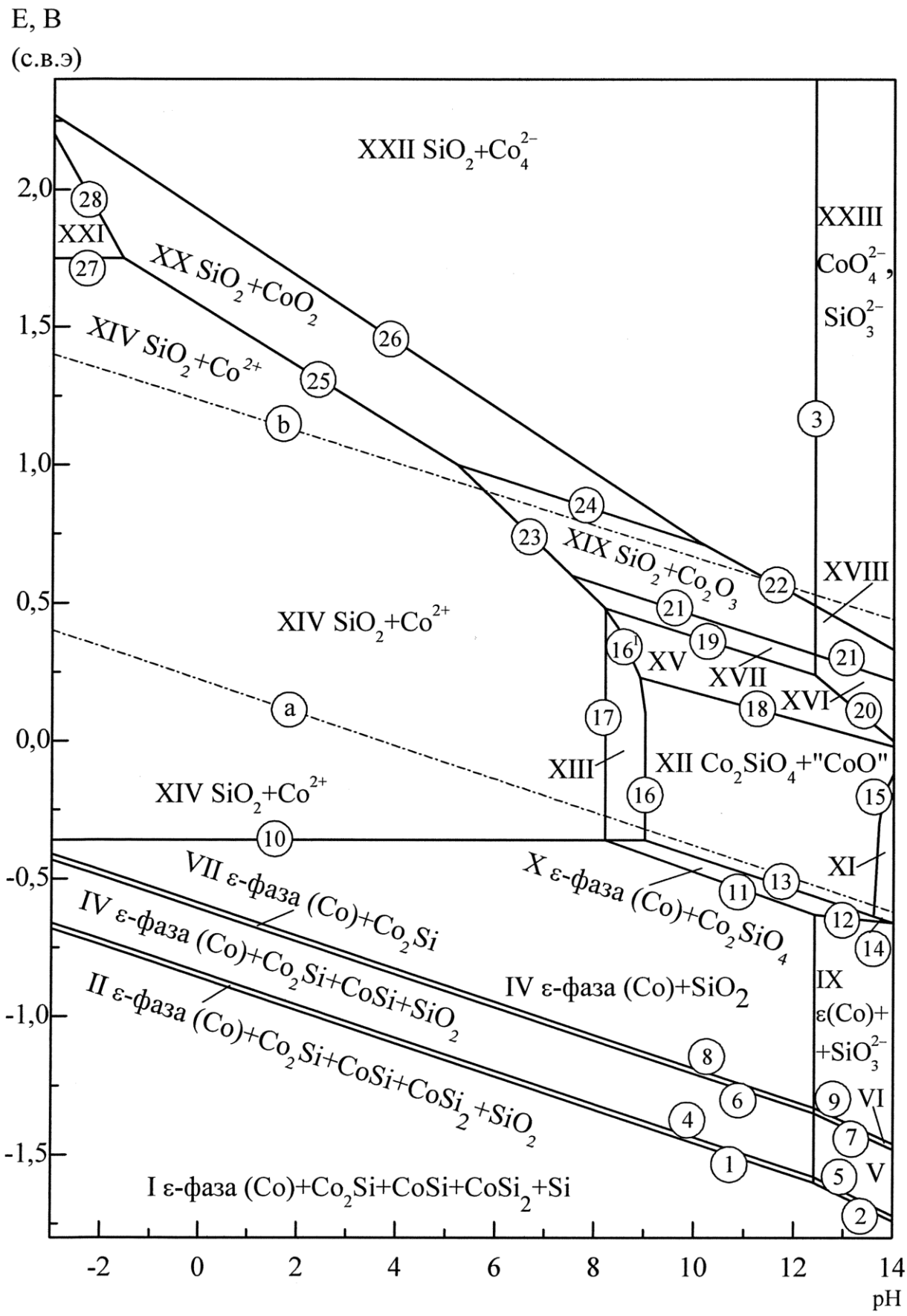

Fig. 3. The potential – pH diagram of the Co – Si – H_2O system at 25°C, 1 bar (air) and $a_i = 10^{-3}$ mol/l (unhydrated form of oxides).

Таким образом, при низких температурах (25˚С) химическая устойчивость сплавов системы кобальт – кремний определяется содержанием в них кремния. При средних (400˚С) и высоких температурах оксидная плёнка на сплавах многослойная и содержит оксиды кобальта и примесных элементов.

Электрохимическая устойчивость

Диаграммы потенциал – pH систем Co – H_2O и Co – Si – H_2O при 25˚С и 1 атм. (воздух) приведены на рис. 2 и 3. Для системы Co – H_2O она построена при активностях ионов в растворе, равных 10^0, 10^{-2}, 10^{-4}, 10^{-6} моль/л. Соответствующие линии обозначены числами 0, -2, -4, -6. Для системы Co – Si – H_2O диаграмма построена при активностях ионов, равных 10^{-3} моль/л. Результаты расчётов химических и электрохимических равновесий в системах приведены в табл. 5 и 6.

Table 5

The basic chemical and electrochemical equilibria in the Co – H_2O system at 25˚C

No of line	Electrode reaction		Equilibrium potential, V (s. h. e.) or pH of the solution
a	$2H^+ + 2e^- = H_2; P_{H_2} \approx 5\cdot10^{-7}$ атм.		$0{,}186 - 0{,}0591pH$
b	$O_2 + 4H^+ + 4e^- = 2H_2O; P_{O_2} \approx 0{,}21$атм.		$1{,}219 - 0{,}0591pH$
1	$HCoO_2^- + 3H^+ + 2e^- = Co(\text{т}) + 2H_2O$		$0{,}659 - 0{,}08865pH + 0{,}0295\lg a_{HCoO_2^-}$
2	$CoO + 2H^+ + 2e^- = Co(\text{т}) + H_2O$		$0{,}166 - 0{,}0591pH$
3	$Co^{2+} + 2e^- = Co(\text{т})$		$-0{,}277 - 0{,}0295\lg a_{Co^{2+}}$
4	$CoO_x + 2xH^+ + 2(x-1)e^- = Co^{2+} + xH_2O$		
	"CoO"	$x = 1{,}00$	$\lg a_{Co^{2+}} = 14{,}98 - 2pH$
		$1{,}00 \ge x \ge 1{,}07$	$(0{,}277 - 0{,}292x + 0{,}458x^2 - -0{,}0591x\,pH - 0{,}0591\lg a_{Co^{2+}})/(x-1)$
4’	"Co_3O_4"	$1{,}3095 \ge x \ge 1{,}4096$	
5	$CoO_x + (2-x)H_2O + 2(x-1)e^- = HCoO_2^- + (3-2x)H^+$		
	"CoO"	$x = 1{,}00$	$\lg a_{HCoO_2^-} = -16{,}67 + pH$
		$1{,}00 \ge x \ge 1{,}07$	$(-0{,}659 - 0{,}292x + 0{,}458x^2 - +0{,}0295(3-2x)\,pH - 0{,}0295\lg a_{Co^{2+}})/(x-1)$
5’	"Co_3O_4"	$1{,}3095 \ge x \ge 1{,}4096$	
6	$3CoO_{1{,}3095} + 1{,}437H^+ + 1{,}437e^- = 3CoO_{1{,}07} + 0{,}7185H_2O$		$0{,}798 - 0{,}0591pH$
7	$Co_2O_3 + 0{,}3616H^+ + 0{,}3616e^- = 2CoO_{1{,}4096} + 0{,}1808H_2O$		$1{,}041 - 0{,}0591pH$
8	$Co_2O_3 + H_2O + 2e^- = 2HCoO_2^-$		$-0{,}135 - 0{,}0591\lg a_{HCoO_2^-}$
9	$2CoO_4^{2-} + 10H^+ + 6e^- = Co_2O_3 + 5H_2O$		$1{,}770 - 0{,}0985pH + 0{,}0197\lg a_{CoO_4^{2-}}$

10	$2CoO_2 + 2H^+ + 2e^- = Co_2O_3 + H_2O$	$1{,}312 - 0{,}0591pH$
11	$Co_2O_3 + 6H^+ + 2e^- = 2Co^{2+} + 3H_2O$	$1{,}739 - 0{,}1773pH - 0{,}0591\lg a_{Co^{2+}}$
12	$CoO_2 + 4H^+ + 2e^- = Co^{2+} + 2H_2O$	$1{,}526 - 0{,}1182pH - 0{,}0295\lg a_{Co^{2+}}$
13	$CoO_4^{2-} + 4H^+ + 2e^- = CoO_2 + 2H_2O$	$1{,}999 - 0{,}1182pH + 0{,}0295\lg a_{CoO_4^{2-}}$
14	$Co^{3+} + e^- = Co^{2+}$	$1{,}754 + 0{,}0591\lg \frac{a_{Co^{3+}}}{a_{Co^{2+}}}$
15	$CoO_2 + 4H^+ + e^- = Co^{3+} + 2H_2O$	$1{,}297 - 0{,}2364pH - 0{,}0591\lg a_{Co^{3+}}$
16	$CoO_4^{2-} + 8H^+ + 3e^- = Co^{3+} + 4H_2O$	$1{,}764 - 0{,}1577pH + 0{,}0197\lg \frac{a_{CoO_4^{2-}}}{a_{Co^{3+}}}$

Table 6

The basic chemical and electrochemical equilibria in the Co – Si – H_2O system at 25°C, 1 bar (air) and $a_i = 10^{-3}$ моль/л

No of line	Electrode reaction	Equilibrium potential, V (s. h. e.) or pH of the solution
a	$2H^+ + 2e^- = H_2; P_{H_2} \approx 5 \cdot 10^{-7}$ атм.	$0{,}186 - 0{,}0591pH$
b	$O_2 + 4H^+ + 4e^- = 2H_2O; P_{O_2} \approx 0{,}21$ атм.	$1{,}219 - 0{,}0591pH$
1	$SiO_2 + 4H^+ + 4e^- = Si + 2H_2O$	$-0{,}857 - 0{,}0591pH$
2	$SiO_3^{2-} + 4H^+ + 6e^- = Si + 3H_2O$	$-0{,}499 - 0{,}0887pH$
3	$SiO_2 + H_2O = SiO_3^{2-} + 2H^+$	$pH 12{,}44$
4	$SiO_2 + CoSi + 4H^+ + 4e^- = CoSi_2 + 2H_2O$	$-0{,}848 - 0{,}0591pH$
5	$SiO_3^{2-} + CoSi + 6H^+ + 4e^- = CoSi_2 + 3H_2O$	$-0{,}480 - 0{,}0887pH$
6	$SiO_2 + Co_2Si + 4H^+ + 4e^- = 2CoSi + 2H_2O$	$-0{,}617 - 0{,}0591pH$
7	$SiO_3^{2-} + Co_2Si + 6H^+ + 4e^- = 2CoSi + 3H_2O$	$-0{,}249 - 0{,}0887pH$
8	$SiO_2 + 2Co(\text{кр}) + 4H^+ + 4e^- = Co_2Si + 2H_2O;$ $a_{Co(\text{кр})} \approx 0{,}27$	$-0{,}602 - 0{,}0591pH$
9	$SiO_3^{2-} + 2Co(\text{кр}) + 6H^+ + 4e^- = Co_2Si + 3H_2O;$ $a_{Co(\text{кр})} \approx 0{,}27$	$-0{,}237 - 0{,}0887pH$
10	$Co^{2+} + 2e^- = Co(\text{кр}); a_{Co(\text{кр})} \approx 1$	$-0{,}366$
11	$Co_2SiO_4 + 4H^+ + 4e^- = 2Co(\text{кр}) + SiO_2 +$ $+ 2H_2O; a_{Co(\text{кр})} = 1$	$0{,}118 - 0{,}0591pH$
12	$Co_2SiO_4 + 2H^+ + 4e^- = 2Co(\text{кр}) + SiO_3^{2-} +$ $+ H_2O; a_{Co(\text{кр})} = 1$	$-0{,}250 - 0{,}0295pH$
13	$CoO + 2H^+ + 2e^- = Co(\text{кр}) + H_2O; a_{Co(\text{кр})} \approx 1$	$0{,}166 - 0{,}0591pH$
14	$HCoO_2^- + 3H^+ + 2e^- = Co(\text{кр}) + 2H_2O; a_{Co(\text{кр})} \approx 1$	$0{,}571 - 0{,}0887pH$

15	$CoO_x + (2 - x)H_2O + 2(x-1)e^- =$ $= HCoO_2^- + (3-2x)H^+;$ $1{,}00 \le x \le 1{,}07$ ("CoO")	$(-0{,}571 - 0{,}292x + 0{,}458x^2 -$ $+ 0{,}0295(3-2x)\,pH)/(x-1)$
16 16'	$CoO_x + 2xH^+ + 2(x-1)e^- = Co^{2+} + xH_2O;$ $1{,}00 \le x \le 1{,}07$ ("CoO") $1{,}3095 \le x \le 1{,}4096$ ("Co_3O_4")	$(0{,}454 - 0{,}292x + 0{,}458x^2 -$ $- 0{,}0591x\,pH)/(x-1)$
17	$Co_2SiO_4 + 4H^+ = SiO_2 + 2Co^{2+} + 2H_2O$	pH8,18
18	$3CoO_{1{,}3095} + 1{,}437H^+ + 1{,}437e^- =$ $= 3CoO_{1{,}07} + 0{,}7185H_2O$	$0{,}798 - 0{,}0591pH$
19	$2CoO_{1{,}367} + SiO_2 + 1{,}468H^+ + 1{,}468e^- =$ $= Co_2SiO_4 + 0{,}734H_2O$	$0{,}972 - 0{,}0591pH$
20	$2CoO_x + SiO_3^{2-} + 2(2x-1)H^+ + 4(x-1)e^- =$ $= Co_2SiO_4 + (2x-1)H_2O;\ 1{,}3095 \le x \le 1{,}367$	$(2{,}158 - 0{,}0295(2x-1)pH)/(x-1)$
21	$Co_2O_3 + 0{,}3616H^+ + 0{,}3616e^- =$ $= 2CoO_{1{,}4096} + 0{,}1808H_2O$	$1{,}041 - 0{,}0591pH$
22	$2CoO_4^{2-} + 10H^+ + 6e^- = Co_2O_3 + 5H_2O$	$1{,}711 - 0{,}0985pH$
23	$Co_2O_3 + 6H^+ + 2e^- = 2Co^{2+} + 3H_2O$	$1{,}916 - 0{,}1773pH$
24	$2CoO_2 + 2H^+ + 2e^- = Co_2O_3 + H_2O$	$1{,}312 - 0{,}0591pH$
25	$CoO_2 + 4H^+ + 2e^- = Co^{2+} + 2H_2O$	$1{,}615 - 0{,}1182pH$
26	$CoO_4^{2-} + 4H^+ + 2e^- = CoO_2 + 2H_2O$	$1{,}911 - 0{,}1182pH$
27	$Co^{3+} + e^- = Co^{2+}$	1,754
28	$CoO_2 + 4H^+ + e^- = Co^{3+} + 2H_2O$	$1{,}474 - 0{,}2364pH$

На диаграмме потенциал – pH системы Co – H_2O можно выделить 9 областей преобладания различных фаз: I – Co(ε); II – Co^{2+}; III – "CoO"; IV – $HCoO_2^-$; V – "Co_3O_4"; VI – Co_2O_3; VII – CoO_2; VIII – Co^{3+}; IX – CoO_4^{2-}.

На диаграмме потенциал – pH системы Co – Si – H_2O можно выделить 23 области преобладания различных фаз: I – ε-фаза(Co) + Co_2Si + CoSi + $CoSi_2$ + Si; II – ε-фаза(Co) + Co_2Si + CoSi + $CoSi_2$ + SiO_2; III – ε-фаза(Co) + Co_2Si + CoSi + $CoSi_2$ + SiO_3^{2-}; IV – ε-фаза(Co) + Co_2Si + CoSi + SiO_2; V – ε-фаза(Co) + Co_2Si + CoSi + SiO_3^{2-}; VI – ε-фаза(Co) + Co_2Si + SiO_3^{2-}; VII – ε-фаза(Co) + Co_2Si + SiO_2; VIII - IV – ε-фаза(Co) + SiO_2; IX – ε-фаза(Co) + SiO_3^{2-}; X – ε-фаза(Co) + Co_2SiO_4; XI – Co_2SiO_4 + $HCoO_2^-$; XII – Co_2SiO_4 + "CoO"; XIII – Co_2SiO_4 + Co^{2+}; XIV – SiO_2 + Co^{2+}; XV – Co_2SiO_4 + "Co_3O_4"; XVI – "Co_3O_4" + SiO_3^{2-}; XVII – "Co_3O_4" + SiO_2; XVIII – Co_2O_3 + SiO_3^{2-}; XIX – Co_2O_3 + SiO_2; XX – CoO_2 + SiO_2; XXI – SiO_2 + Co^{3+}; XXII – SiO_2 + CoO_4^{2-}; XXIII – CoO_4^{2-}, SiO_3^{2-}.

Как показывают расчёты, в кислых средах пассивационная плёнка на сплавах системы Co – Si будет представлять собой чистый SiO_2, при условии отсутствия в растворе ионов F^-. Если кремния в сплаве недостаточно для образования сплошной плёнки (его содержание не превышает 15 мас. %), то будет наблюдаться селективное растворение кобальта из сплавов с образованием в растворе ионов Co^{2+}. Эти выводы подтверждаются и экспериментальными исследованиями [4 – 7]. В нейтральных и щелочных средах схема первичной пассивации сплавов системы Co – Si следующая:

$$\underset{\text{I}}{\text{сплав} + SiO_2 \rightarrow} \underset{\text{II}}{\rightarrow \text{сплав} + Co_2SiO_4 \rightarrow} \underset{\text{III}}{\rightarrow \text{сплав} + CoO.}$$

По аналогии с пассивацией силицидов железа [15] можно выделить три режима процесса. Если концентрация кремния в сплаве превышает 15 мас. %, то его достаточно для образования сплошной пассивирующей плёнки SiO_2. В этом случае процесс завершается на первой стадии. При концентрации кремния в сплаве, меньшей 15 мас. %, но большей 3 мас. %, кремния в сплаве хватает лишь для образования сплошной плёнки Co_2SiO_4, и процесс завершается на второй стадии. Если концентрация кремния ниже 3 мас. %, то процесс завершится на третьей стадии, а защитная плёнка, как и на чистом кобальте, будет состоять из CoO, а кремний в виде локальных включений Co_2SiO_4 будет входить в её внутренний подслой. Зависимость структуры пассивирующей плёнки от содержания кремния в сплаве подтверждена и экспериментально [8].

Таким образом, и электрохимическая устойчивость сплавов системы кобальт – кремний целиком определяется содержанием в них кремния.

Выводы

1. Построена фазовая диаграмма состояния системы Co – Si – O при 25˚C и 1 атм. (воздух). Показано, что химическая устойчивость сплавов Co – Si при низких температурах определяется только кремнием.
2. Построены диаграммы потенциал – pH систем Co – H_2O и Co – Si – H_2O при 25˚C, 1 атм. (воздух) и различных активностях ионов в растворе. Показано, что в кислых средах первичная пассивационная плёнка на сплавах Co – Si представляет собой чистый кремнезём. В нейтральных и щелочных средах она по мере снижения содержания кремния в сплавах может состоять из SiO_2, Co_2SiO_4 или CoO.

Литература

1. The Oxidation Behaviour of Some Cobalt-Based Amorphous Alloys / A. M. Dark, G. Wei, B. Cantor // Mater. Sci. Eng. – 1988. – P. 533 – 537.
2. Аллотропные металлические сплавы / под ред. Ф. Е. Люборского. – пер. с англ. – М.: Металлургия, 1987. – 584 с.
3. Глезер, А. М. Структура и механические свойства аморфных сплавов / А. М. Глезер, Б. В. Молотилов. – М.: Металлургия, 1992. – 206 с.
4. Шеин, А. Б. Электрохимическое поведение силицида кобальта Co_2Si в кислотах // Защита металлов. – 2000. – Т. 36. – № 2. – С. 190 – 194.
5. Шеин, А. Б. Коррозионно-электрохимическое поведение моносилицида кобальта в кислых растворах // Защита металлов. – 1989. – Т. 25. – № 1. – С. 112 – 114.

6. Шеин, А. Б. Выделение водорода на моносилициде кобальта в сернокислом электролите, содержащем поверхностно-активные вещества // Электрохимия. – 1988. – Т. 24. – Вып. 10. – С. 1335 – 1338.
7. Шеин, А. Б. Электрохимическое поведение эвтектических сплавов силицидов и германидов металлов подгруппы железа с кремнием и германием // Защита металлов. – 1998. – Т. 34. – № 1. – С. 25 – 28.
8. Шеин, А. Б. Анодное растворение силицидов кобальта в щелочном электролите / А. Б. Шеин, И. Л. Сергеева // Защита металлов. – 2004. – Т. 40. – № 6. – С. 624 – 628.
9. Диаграммы состояния двойных металлических систем: справочник / под ред. Н. П. Лякишева – М.: Машиностроение, 1997. – Т. 1. – С. 80 – 82.
10. Тюрин, А. Г. Термодинамика химической и электрохимической устойчивости сплавов: учеб. пособие: Ч. 1. Общие принципы. Высокотемпературное окисление. – Челябинск: Изд-во Челяб. гос. ун-та, 2004. – 86 с.
11. Термодинамика сплавов железа / Б. М Могутнов, И. А. Томилин, Л. А. Шварцман. – М.: Металлургия, 1984. – 208 с.
12. Рузинов, Л. П. Равновесные превращения металлургических реакций / Л. П. Рузинов, Б. С. Гуляницкий. – М.: Металлургия, 1975. – 416 с.
13. Физико-химические свойства окислов: справочник / под ред. Г. В. Самсонова – М.: Металлургия, 1978. – 472 с.
14. Справочник по электрохимии / под ред. А. М. Сухотина. – Л.: Химия, 1981. – 488 с.
15. Тюрин, А. Г. Термодинамическая оценка влияния кремния на химическую и электрохимическую устойчивость железохромистых сплавов // Защита металлов. – 2004. – Т. 40. – № 1. – С. 19 – 27.

14. Ni – Si system
14.1. Nickel silicides

According to the Ni – Si phase diagram [Lindholm, Sundman, 1996] (see Figure 58), several phases exist in system at standard conditions.

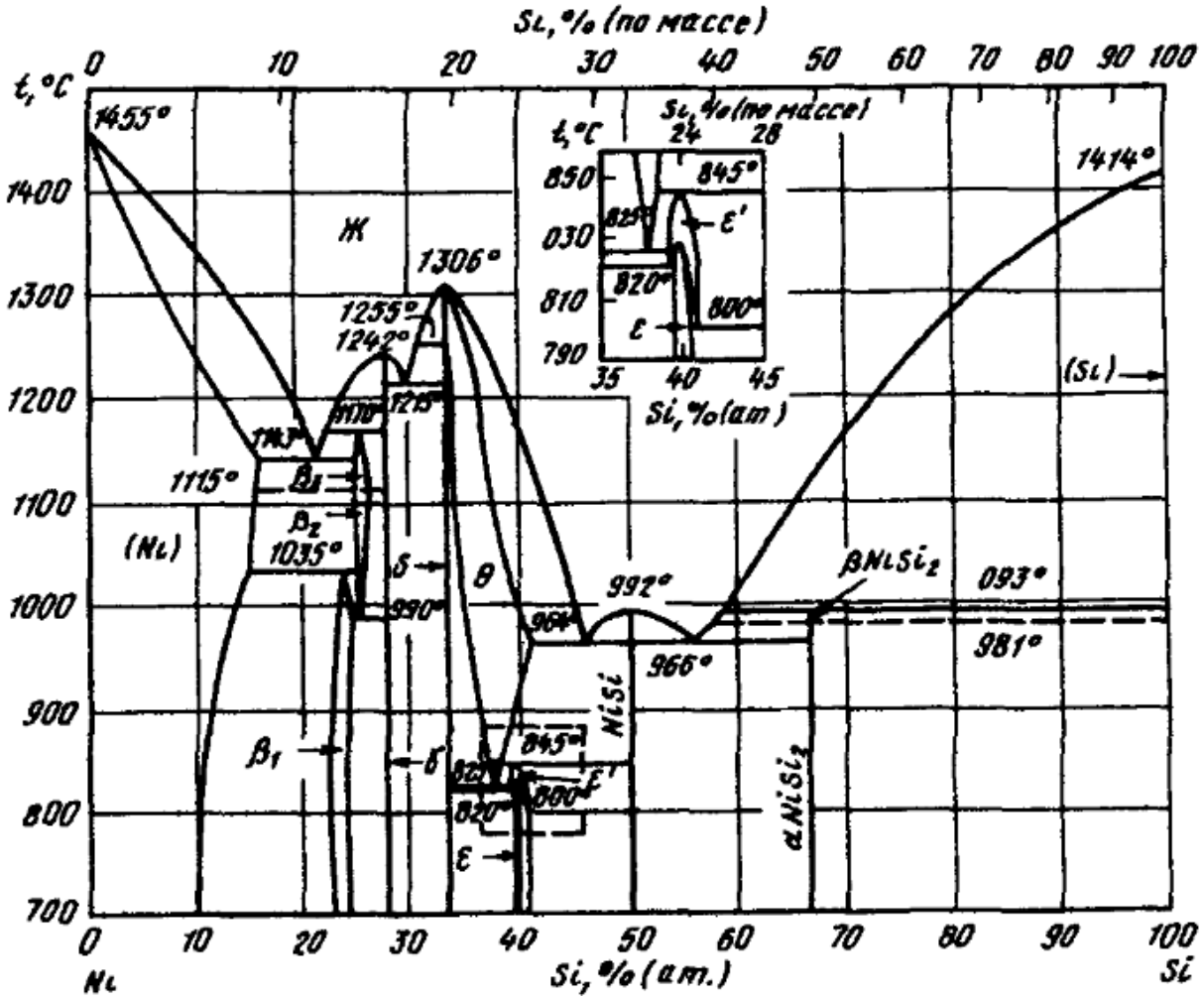

Fig. 58. The phase diagram of Ni – Si system [Диаграммы состояния двойных металлических систем: справочник, 2001].

There are six intermediate phases: β_1-phase (Ni_3Si), γ-phase (Ni_5Si_2 or $Ni_{31}Si_{12}$ [Lee et al., 2000]), δ-phase (Ni_2Si), ε-phase (Ni_3Si_2), NiSi and $NiSi_2$ [Chandrasekharaiah, Margrave, O'Hare, 1993]. Although almost all nickel silicides have a narrow homogeneity ranges at 800˚C [Lindholm, Sundman, 1996], they can be treated as stoichiometric phases at standard temperature. The solubility of Ni in (diamond-Si) do not exceeds 10^{-16} atomic % at 800˚C [Yoshikawa et al., 2010]. At the nickel-rich part of the system, the solid solution of Si in (fcc-Ni) can be formed (α-phase). There is no published information about silicon maximum solid solubility at 25˚C,

but it is relatively high (more that 10 atomic percent) at 1000 ˚C. Most CALPHAD assessments of Ni – Si system [Acker et al., 1999a; Acker, Bohmhammel, 1999; Connétable, Thomas, 2011; Lindholm, Sundman, 1996; Tokunaga et al., 2003; Yuan et al., 2012] consider β_1-phase as an ordered solid solution and use an order-disorder contribution model [Ansara et al., 1997; Ansara, Sundman, Willemin, 1988] for its Gibbs energy function. Moreover, they use sublattice model [Hillert, Staffansson, 1970; Sundman, Ågren, 1981] for Gibbs energy function of α-phase. But, since β_1-phase could be assumed as stoichiometric and composition invariant at standard temperature, there is no necessity to pay attention on order-disorder transformations in it and use such complicated thermodynamic models. Therefore, the simple quasiregular solution model was used to describe the excess Gibbs energy of α-phase. The dependence of the model parameter Q_{12} on temperature is shown in Figure 59.

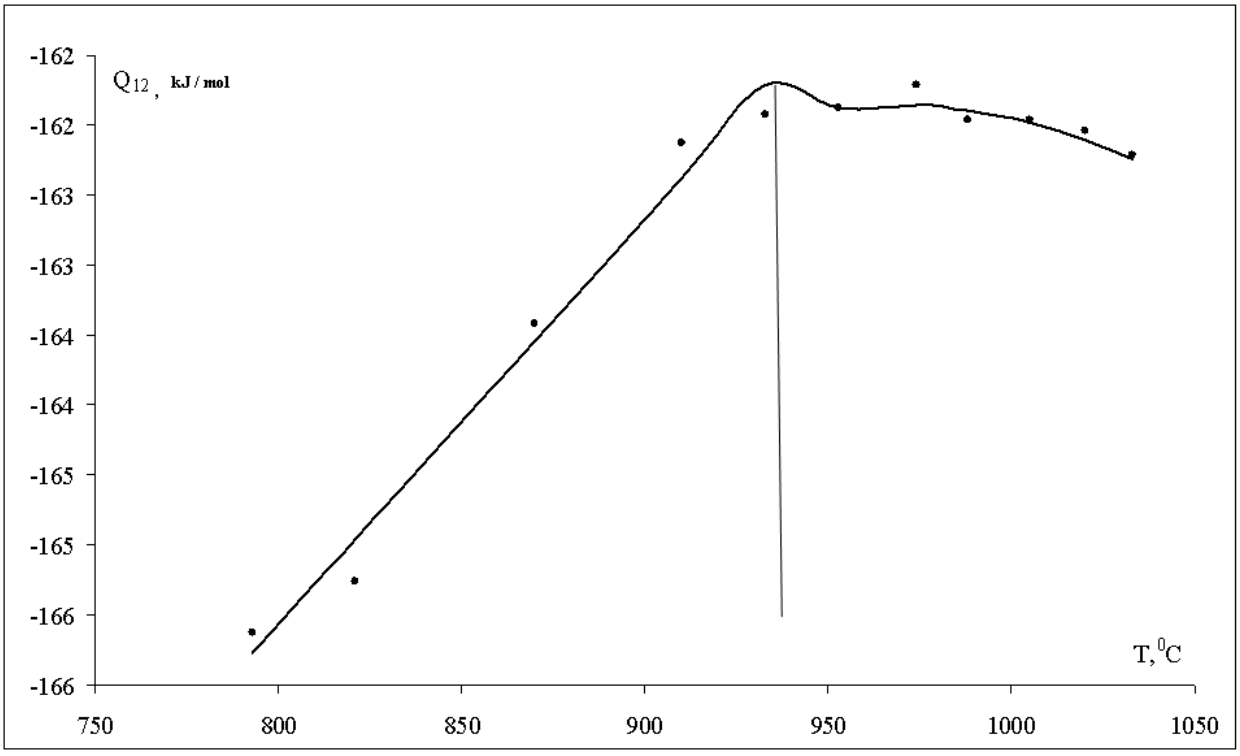

Fig. 59. The dependency of the quasiregular solution model parameter Q_{12} for the solid solution of Si in (fcc-Ni) on temperature.

Calculated solid solubility of Si in (fcc-Ni) at 25˚C equals 2,5 atomic %. The activities of solid solution components are the following: $a_{\mathrm{Ni}(\alpha)} = 0.927$, $a_{\mathrm{Si}(\alpha)} = 9 \cdot 10^{-36}$. More details are provided in the attached publication.

14.2. Equilibira in Ni – Si – O system

It is well known, that nickel monoxide (NiO) and higher nickel oxides (Ni_2O_3, NiO_2) could form a continuous series of solid solutions, which corresponds to a variable composition phase NiO_x [Морачевский, Цемехман, Цымбулов, 2008].

A single ternary compound exist in Ni – Si – O system, it is nickel orthosilicate Ni_2SiO_4 [Fedorova, Tsymbulov, Tsemekhman, 2003; Jacob et al., 1986; Jacob, Shukla, 1987; Navrotsky, 1971; Robie et al., 1984; Róg, Borchardt, 1984; Wolfenstine, Dimos, Kohlstedt, 1985]. The values of standard Gibbs energies of formation of nickel silicides and nickel silicate were collected from various sources. The expression for the standard Gibbs energy of formation of phase NiO_x was estimated according to Gorichev's method.

The state diagram of Ni – Si – O system and the list of equilibria in this system are presented in the attached publication.

14.3. Potential – pH diagram of Ni – H_2O system

Nickel can form the following ions in an aqueous solution: Ni^{2+}, $HNiO_2^-$ and NiO_4^{2-} [Тюрин, 2012]. In addition nickel can form the hydride Ni_2H [Zeng et al., 1999]. The possibilities of electrochemical reduction of nickel to its hydride are discussed in [Markos'yan, Sirota, Pchel'nikov, 2005]. The information about the Gibbs energy of formation for nickel hydride Ni_2H was taken from paper [Baranowski, Bocheńska, 1965].

The potential – pH diagram of Ni – H_2O system at 25 °C, air pressure of 1 bar and the activities of nickel species of 1 $mol \cdot l^{-1}$ is presented in Figure 60.

In very diluted solutions the formation of hydrolysed species $NiOH^+$ (aq) becomes possible. The activity – pH diagram for Ni (II) species and the potential – pH diagram of Ni – H_2O system at 25 °C, air pressure of 1 bar and the activities of nickel species of 10^{-8} $mol \cdot l^{-1}$ taking into account the formation of $NiOH^+$ (aq) is presented in the attached publication.

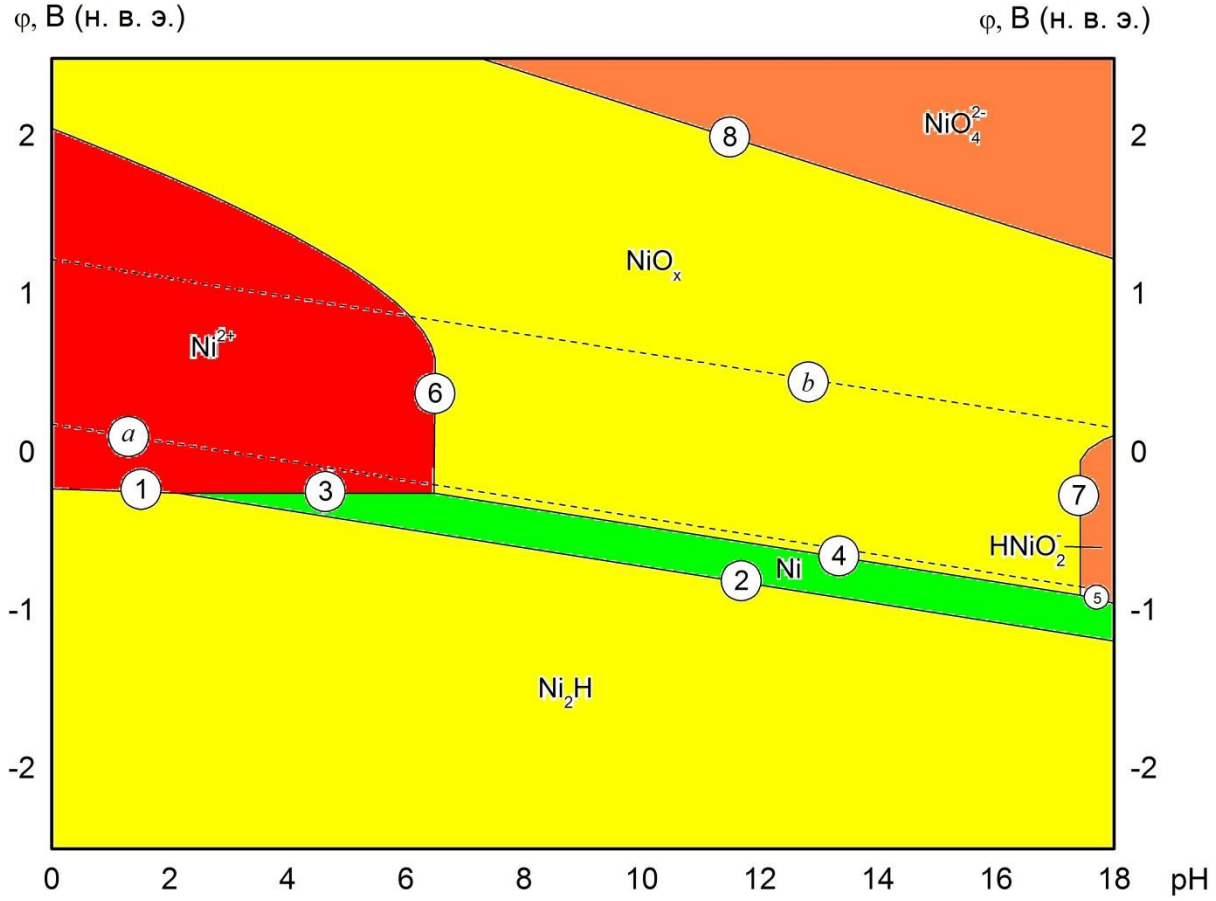

Fig. 60. The potential – pH diagram of Ni – H_2O system at 25 °C, air pressure of 1 bar and the activities of nickel species in a solution of 1 M.

14.4. Potential – pH diagram of Ni – Si – H_2O system

The potential – pH diagram of Ni – Si – H_2O system is presented in the attached publication.

In presence of nickel hydride orthosilicic acid becomes thermodynamically unstable and the mechanism of nickel silicides decomposition slightly changes.

Generally, the corrosion-electrochemical behaviour of iron, cobalt and nickel silicides is very similar. In acidic environments the passivation layer on Fe – Si, Co – Si и Ni – Si system alloys will consist of pure H_4SiO_4, if there will be no F^-ions in solution, and metal from alloys will form the cations Fe^{2+}, Co^{2+} and Ni^{2+}, respectively. In neutral and alkaline environments three cases can be considered. If silicon content in alloys is high, it will be sufficient to form a persistent passivation layer of $SiO_2 \cdot 2H_2O$on the surface. At lower silicon content in alloy it will be sufficient only to form a persistent layer of silicates Fe_2SiO_4, Co_2SiO_4 or

Ni_2SiO_4. If silicon content in alloy is very low, the protective film will consist from corresponding metal oxides, and silicon in form of local inclusions of silicates will be present in its inner layer.

Publications to chapter 14

The potential – pH diagram for Ni – H2O system was published in the form of preprint at the website of *Research Gate* unter DOI 10.13140/RG.2.1.2183.7529.

The potential – pH diagram for Ni – Si – H_2O system was published in the paper [Nikolaychuk, Tyurin, 2013a]. The preprint of this paper is presented with the permission from *Elsevier*.

УДК 544.653:544.016:544.313.2.031

THE POTENTIAL – pH DIAGRAM FOR Ni – H_2O SYSTEM

P. A. Nikolaychuk

Chelyabinsk State University, Chelyabinsk, Russia. E-mail: npa@csu.ru

Thermodynamic information on aqueous nickel species is systematized. The reactions between various species are discussed. The activity – pH diagram for Ni^{II} species and the revised potential – pH diagram of Ni – H_2O system at 25°C, 1 bar and $a_{[Ni]} = 10^{-8}$ mol l^{-1} are plotted.

The variants of Pourbaix diagram for nickel, available in literature [1–3], don't correspond to each other and don't reflect the nonstoichiometry of nickel oxide. This study proposes the revised version of this diagram.

Nickel oxides form a series of solid solutions, which can be treated as a continuous phase NiO_x with variable composition, $1 < x < 2$ [4].

Table 1. The standard Gibbs energies of formation of nickel species.

Compound	$\Delta_f G^o_{298}$, J mol^{-1}	Reference
NiO_x (s)	$155\,912 \cdot x^2 - 367\,342 \cdot x$	[4–6]
Ni_2H (s)	11 800	[8]
Ni^{2+} (aq)	–46 400	[3,9]
$NiOH^+$ (aq)	–226 300	[3,9]
$HNiO_2^-$ (aq)	–350 000	[3,9]
NiO_4^{2-} (aq)	62 900	[4]

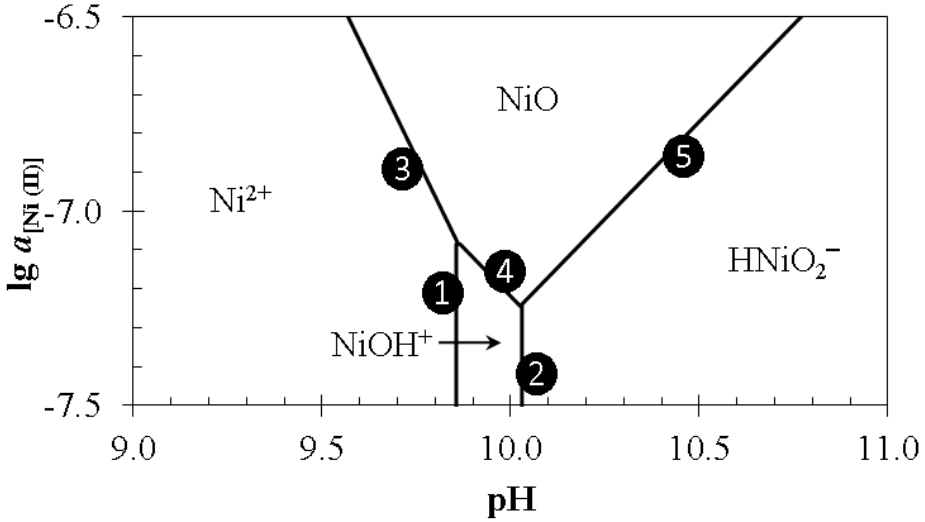

Figure 1. The activity – pH diagram for Ni^{II} species.

Table 2. The basic chemical and electrochemical equilibria in Ni – H_2O system.

Electrode reaction	E, V (s. h. e.) or pH of the solution
❶ $NiOH^+ + H^+ \rightleftharpoons Ni^{2+} + H_2O$	$pH = 9{,}856 + \lg \frac{a_{NiOH^+}}{a_{Ni^{2+}}}$
❷ $HNiO_2^- + 2H^+ \rightleftharpoons NiOH^+ + H_2O$	$pH = 10{,}030 + 0{,}5 \cdot \lg \frac{a_{HNiO_2^-}}{a_{NiOH^+}}$
❸ $NiO + 2H^+ \rightleftharpoons Ni^{2+} + H_2O$	$pH = 6{,}319 - 0{,}5 \cdot \lg a_{Ni^{2+}}$
❹ $NiO + H^+ \rightleftharpoons NiOH^+$	$pH = 2{,}781 - \lg a_{NiOH^+}$
❺ $HNiO_2^- + H^+ \rightleftharpoons NiO + H_2O$	$pH = 17{,}270 + \lg a_{HNiO_2^-}$
❻ $Ni^{2+} + 2e^- \rightleftharpoons Ni\ (fcc)$	$E = -0{,}240 + 0{,}0295 \cdot \lg a_{Ni^{2+}}$
❼ $NiOH^+ + H^+ + 2e^- \rightleftharpoons Ni\ (fcc) + H_2O$	$E = 0{,}095 - 0{,}0295 \cdot pH + 0{,}0295 \cdot \lg a_{NiOH^+}$
❽ $HNiO_2^- + 3H^+ + 2e^- \rightleftharpoons Ni\ (fcc) + 2H_2O$	$E = 0{,}644 - 0{,}0887 \cdot pH + 0{,}0295 \cdot \lg a_{HNiO_2^-}$
❾ $NiO_x + 2xH^+ + 2(x-1)e^- \rightleftharpoons Ni^{2+} + xH_2O$	$E = \frac{0{,}808 \cdot x^2 - 0{,}674 \cdot x + 0{,}240}{x - 1} - \frac{0{,}0591 \cdot x}{x-1} \cdot pH - \frac{0{,}0295}{x-1} \cdot \lg a_{Ni^{2+}}$
❿ $NiO_x + (2x-1)H^+ + 2(x-1)e^- \rightleftharpoons NiOH^+ + (x-1)H_2O$	$E = \frac{0{,}808 \cdot x^2 - 0{,}674 \cdot x - 0{,}051}{x - 1} - \frac{0{,}0295 \cdot (2x-1)}{x-1} \cdot pH - \frac{0{,}0295}{x-1} \cdot \lg a_{NiOH^+}$
⓫ $HNiO_2^- + (3-2x)H^+ + 2(1-x)e^- \rightleftharpoons NiO_x + (2-x)H_2O$	$E = \frac{-0{,}808 \cdot x^2 + 0{,}674 \cdot x + 0{,}648}{1 - x} - \frac{0{,}0295 \cdot (3 - 2 \cdot x)}{1-x} \cdot pH + \frac{0{,}0295}{1-x} \cdot \lg a_{HNiO_2^-}$
⓬ $NiO_4^{2-} + 2(4-x)H^+ + 2(3-x)e^- \rightleftharpoons NiO_x + (4-x)H_2O$	$E = \frac{-0{,}808 \cdot x^2 + 0{,}674 \cdot x + 5{,}240}{3 - x} - \frac{0{,}0591 \cdot (4-x)}{3-x} \cdot pH + \frac{0{,}0295}{3-x} \cdot \lg a_{NiO_4^{2-}}$
⓭ $2Ni\ (fcc) + H^+ + e^- \rightleftharpoons Ni_2H$	$E = -0{,}122 - 0{,}0591 \cdot pH$

The standard Gibbs energies of formation of nickel species are listed in Table 1. The expression for $\Delta_f G^o_{298}(NiO_x)$ was estimated using the modified Gorichev's method [4–7]. Thermodynamic properties of basic chemical and electrochemical equilibria in system are summarized in Table 2. Figure 1 presents the predominance diagram of Ni^{II} species.

Calculations show that in diluted solutions, when $a_{[Ni]} < 10^{-7}$ mol l^{-1}, nickel monoxide NiO isn't formed and nickel has no passivity domain in the area of electrochemical stability of water. A phase NiO_x becomes thermodynamically stable above the potentials of oxygen electrode. The following order of oxidation is possible depending on ion activities:

lg $a_{[Ni]} > -7{,}085$: $Ni^{2+}(aq) \rightarrow NiO(s) \rightarrow HNiO_2^-(aq)$;

$-7{,}085 >$ lg $a_{[Ni]} > -7{,}244$: $Ni^{2+}(aq) \rightarrow NiOH^+(aq) \rightarrow NiO(s) \rightarrow \rightarrow HNiO_2^-(aq)$;

lg $a_{[Ni]} < -7{,}244$: $Ni^{2+}(aq) \rightarrow NiOH^+(aq) \rightarrow HNiO_2^-(aq)$.

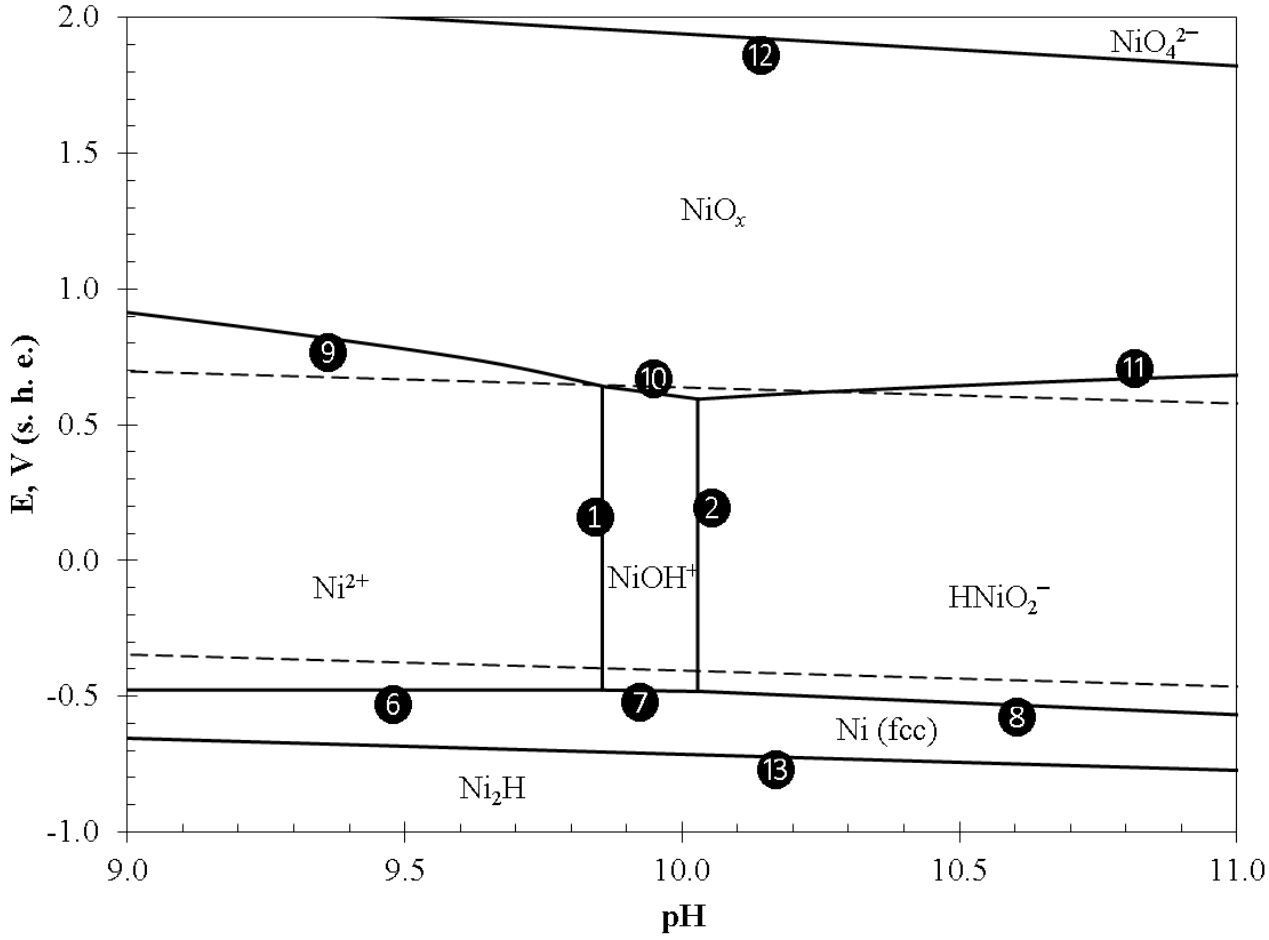

Figure 2. The potential – pH diagram for Ni – H_2O system.

The revised potential – pH diagram of Ni – H_2O system at 25ºC, 1 bar and $a_{[Ni]} = 10^{-8}$ mol l^{-1} is presented at Figure 2. Dashed lines represent the hydrogen and oxygen electrodes and border the domain of electrochemical stability of water at atmospheric conditions.

Nickel can be electrochemically reduced to nickel hydride Ni_2H [6], however, the domain of its thermodynamic stability lies outside the area of electrochemical stability of water.

The corrosion properties of nickel are strongly determined by the concentration of ionic speices in solution. In concentrated solutions nickel can be passivated by formation of nickel monoxide and higher nickel oxides. Contrary, in diluted solutions the domain of stability of the oxide phases vanishes and nickel becomes very vulnerable to corrosion.

REFERENCES:

1. Atlas of Eh-pH diagrams: Intercomparison of thermodynamic databases. Open file report № 419. National Institute of Advanced Industrial Science and Technology, 2005.

2. Brookins, D. G. Eh-pH diagrams for geochemistry. Berlin: Springer, 1987.

3. Schweitzer, G. K., Pesterfield, L. L. The aqueous chemistry of the elements. Oxford: Oxford University Press, 2010.

4. Tyurin, A. G. Termodinamika khimicheskoy I elektrokhimicheskoy ustoychivisti tvyordykh splavov zheleza, khroma i nikelya [Thermodynamics of chemical and electrochemical stability of solid alloys of iron, chromium and nickel]. Chelyabinsk: Publishing House of Chelyabinsk State University, 2011 [In Russian].

5. Nikolaychuk, P. A., Tyurin, A. G. Thermodynamics of chemical and electrochemical stability of copper-nickel alloys. Physical Chemistry of Surfaces and Protection of Metals, 2012. Vol. 48. No. 4. P. 462 – 476.

6. Nikolaychuk, P. A., Tyurin, A. G. Thermodynamic assessment of chemical and electrochemical stability of nickel – silicon system alloys. Corrosion Science, 2013. Vol. 73. P. 237 – 244.

7. Nikolaychuk, P. A., Tyurin, A. G. Method of estimating the standard Gibbs energies of formation of binary compounds. Abstracts of the XVIII International Conference on Chemical Thermodynamics in Russia (RCCT-2011). Vol. 2. Samara: Samara State Technical University, 2011. P. 16 – 17.

8. Baranowski, B., Bocheńska, K. The Free Energy and Entropy of Formation of Nickel Hydride. Zeitschrift für Physikalishe Chemie Neue Folge, 1965. Bd. 45. Heft 3 – 4. S. 140 – 152.

9. Wagman, D. D. et al. The NBS tables of chemical thermodynamic properties. Selected values for inorganic and C_1 and C_2 organic substances in SI units. Journal of Physical and Chemical Reference Data, 1982. Vol. 11. Suppl. 2.

THERMODYNAMIC ASSESSMENT OF CHEMICAL AND ELECTROCHEMICAL STABILITY OF NICKEL – SILICON SYSTEM ALLOYS

Pavel Anatolyevich Nikolaychuk and Aleksandr Georgievich Tyurin
Chelyabinsk State University, Brat'ev Kashirinykh Street, 129, Chelyabinsk, Russian Federation.
E-mail: npa@csu.ru, tag@csu.ru

Highlights:
* Phase and chemical euqilibria in Ni – Si system at 298 K are considered.
* Thermodynamic properties of nonstoichiometric NiO_x phase are estimated.
* The Ni – Si – O state diagram at 298 K is plotted.
* The potential – pH diagram of Ni – Si – H_2O system at 298 K is plotted.
* The corrosion-electrochemical behaviour of Ni – Si system is determined by silicon content in it.

Abstract:
Phase and chemical euqilibria in Ni – Si system at 298 K are considered. The possible maximum solid solubility of Si in fcc-Ni at 298 K is estimated.
The Ni – Si – O state diagram at 298 K is plotted. The Ni – Si – O system invariant conditions are calculated. The potential – pH diagram of the Ni – Si – H_2O system at 298 K, air pressure of 1 bar and activities of ions in solution, equal to 1 mol/l is plotted. Basic chemical and electrochemical equilibria in Ni – Si – H_2O system are considered.

Keywords:
A. Alloy;
B. electrochemical calculation;
B. modelling studies;
C. oxidation;
C. Pourbaix diagram;
C. thermodynamic diagrams.

1. Introduction.

In recent years there is growing evidence, indicating the perspectives of using transition metals silicides as new corrosion-resistant materials and coatings. There is currently no systematic studies of their corrosion-electrochemical behaviour, the available data are fragmentary and do not cover all the variety of compounds and corrosion-active environments. There is no single theory that can explain the chemical resistance to corrosion of the existing materials and predict such properties for the new ones [1]. One of the methods to describe the oxidation of silicides both in oxygen-containing gaseous environments (chemical stability) and in water environments (electrochemical stability) is the thermodynamic modelling.
Nickel – silicon is an important binary system, and it has been modelled many times. Moreover, many ternary systems, containing these two elements, such as C – Ni – Si [2], Mo – Ni – Si [3], Ni – Si – V [4], Mn – Ni – Si [5], Ni – Si – O [6], Fe – Ni – Si [7], Cr – Ni – Si [8], Cu – Ni – Si [9], Ni – Si – B [10] and others, are of interest to the researchers. However, almost all published materials correspond to high temperatures. The present study is devoted to thermodynamic description of Ni – Si system at standard temperature only.

2. Phase and chemical equilibria in Ni – Si system at the temperature of 298 K.

According to the Ni – Si phase diagram [11 – 13], several phases exist in system at standard conditions. There are six intermediate phases: β_1 (Ni_3Si), γ (Ni_5Si_2 or $Ni_{31}Si_{12}$ [6]), δ (Ni_2Si), ε (Ni_3Si_2), NiSi and $NiSi_2$. Pure silicon exists in diamond modification, and it seems, that nickel is insoluble in it. At the nickel-rich part of the system, the solid solution of face-centered cubic nickel can be formed. There is no published information about silicon maximum solid solubility at 298 K, but it is relatively high (more that 10 atomic percent) at 1000 K [11].

Although almost all nickel silicides have a narrow homogeneity ranges at 800˚C [13], they can be treated as stoichiometric phases at standard temperature. The standard Gibbs energies of formation of these compounds are summarized in table 1. Values, presented in [6, 10, 13 – 16], are obtained from various CALPHAD assessments of Ni – Si system, while values, presented in [17 – 21], are either experimentally measured or calculated from experimentally measured standard enthalpy of formation and calculated standard entropy of formation from [16]. As can be seen from table 1, there are no convergence between the results, and the differences are often significant. Thus the problem reveals of choosing the correct values of standard Gibbs energies of formation for further calculations. The possible solution of this problem and the principles of such choice are discussed below in section 3.

There is no available data on maximum solid solubility of silicon in fcc-nickel at 298 K. It can be estimated by considering a two-phase equilibrium of α-phase (fcc solid solution) and β_1-phase (Ni_3Si):

$$3\mathrm{Ni}\ (\alpha) + \mathrm{Si}\ (\alpha) = \mathrm{Ni_3Si}\ (\beta_1) \qquad (1).$$

The equation of chemical reaction isotherm for reaction (1) can be written as follows:

$$\Delta_r G_T^o = -RT\ \ln\ K_p = -RT\ \ln\ \frac{1}{a_{\mathrm{Ni}(\alpha)}^3 \cdot a_{\mathrm{Si}(\alpha)}} = 3RT \ln a_{\mathrm{Ni}(\alpha)} + RT \ln\ a_{\mathrm{Si}(\alpha)} \qquad (2).$$

Where T is the temperature in Kelvins, R is the universal gas constant, a are the thermodynamic activities is nickel and silicon in α-phase, referred to the standard state of pure component with fcc lattice. The value of Gibbs energy change in reaction (1) can be calculated according to Hess' law from the Gibbs energy of formation of Ni_3Si from elements, referred to their standard reference state and the Gibbs energy of phase transition of silicon from diamond lattice to the fcc one:

$$3\mathrm{Ni}\ (\gamma) + \mathrm{Si}\ (\text{diamond}) = \mathrm{Ni_3Si}\ (\beta_1) \qquad (3),$$

$$\mathrm{Si}\ (\text{diamond}) = \mathrm{Si}\ (\text{fcc}) \qquad (4),$$

$$\Delta_r G_T^o\ (1) = \Delta_r G_T^o\ (3) - \Delta_r G_T^o\ (4) = \Delta_f G_T^o\ (\mathrm{Ni_3Si}) - \Delta_{tr} G_T^o\ (\mathrm{Si}_{\text{diamond}\rightarrow\text{fcc}}) \qquad (5).$$

The value of Gibbs energy of silicon phase transition is taken from SGTE [22]. The analytical expressions of thermodynamic activities of α-phase components are linked with expression for the excess Gibbs energy G^E [23] of this phase:

$$RT\ \ln a_{i(\alpha)} = RT\ \ln\ x_{i(\alpha)} + \mu_{i(\alpha)}^{\mathrm{E}} \qquad (6),$$

where $i(\alpha)$ denotes any α-phase component (Ni or Si), x is the mole fraction of the component and $\mu_{i(\alpha)}^{\mathrm{E}}$ is an excess chemical potential of the component, that can be determined as the partial derivative of excess Gibbs energy G^E by number of moles of this component. Thus, the analytical expression of $G_\alpha^E = f\,(x_{\mathrm{Ni}(\alpha)}, x_{\mathrm{Si}(\alpha)}, T)$ is needed to perform necessary calculation.

Most variants of Ni – Si system CALPHAD assessments [13 – 16] propose treating β_1-phase as an ordered solid solution and using an order-disorder contribution model, developed by authors of [24] to describe it. They also propose using sublattice model [25] to describe α-phase properties. But, since β_1-phase can be assumed as stoichiometric and composition invariant at standard temperature, there is no necessity to use such complicated thermodynamic models. Therefore, simpler variants of thermodynamic description are considered.

The author of [26] proposes the following concentration and temperature dependences for the above-mentioned parameters (all Gibbs energies values are presented in J/mol):

Table 1. The standard Gibbs energies of formation of nickel silicides ($-\Delta_f G^o_{298}$, J/mol).

Reference / Compound	[2]	[6]	[13]	[14]	[15]	[16]	[17]	[18]	[19]	[20]	[21]	Chosen ones
Ni_3Si	–	149100[c]	–	–	161588[b]	156944[b]	150800[a]	148010[c]	148415[c]	–	148100[c]	156024
Ni_5Si_2	302796[b]	278000[c]	303613[b]	345653[b]	323645[b]	296175[b]	296100[a]	313200[c]	301040[c]	–	300825[c]	301000
Ni_2Si	129883[b]	125325[c]	130344[b]	146691[b]	141718[b]	143028[b]	143100[a]	140520[c]	140507[c]	139997[a]	140185[c]	143000
Ni_3Si_2	211696[b]	217585[c]	217796[b]	232610[b]	234579[b]	228785[b]	232000[a]	222450[c]	–	–	222575[c]	228800
NiSi	76926[b]	81680[c]	79137[b]	85631[b]	89214[b]	84478[b]	89600[a]	85256[a]	84805[a]	85650[a]	85500[c]	84500
$NiSi_2$	91175[b]	90145[c]	98598[b]	92333[b]	95122[b]	86154[b]	94200[a]	86180[a]	86265[a]	88935[a]	–	86200

[a] Experimental

[b] Calculated by CALPHAD technique

[c] Calculated from standard enthalpy of formation, given in cited study, and standard entropy of formation, taken from [16]

$$G_{\alpha}^{E} = x_{\mathrm{Ni}(\alpha)} x_{\mathrm{Si}(\alpha)} (x_{\mathrm{Ni}(\alpha)} (62,01T - 264345) + x_{\mathrm{Si}(\alpha)} (22,01T - 138239)) \quad (7),$$

$$\Delta_f G_T^o (\mathrm{Ni_3Si}) = -7,563T - 148546 \quad (8),$$

$$\Delta_{tr} G_T^o (\mathrm{Si_{diamond \to fcc}}) = -17,87T + 50626 \quad (9).$$

Another set of parameters values was determined by authors of [10]:

$$G_{\alpha}^{E} = x_{\mathrm{Ni}(\alpha)} x_{\mathrm{Si}(\alpha)} (39,31T - 205320 - 81520(x_{\mathrm{Ni}(\alpha)} - x_{\mathrm{Si}(\alpha)})) \quad (10),$$

$$\Delta_f G_T^o (\mathrm{Ni_3Si}) = 4,4T - 157300 \quad (11),$$

$$\Delta_{tr} G_T^o (\mathrm{Si_{diamond \to fcc}}) = -21,8T + 51000 \quad (12).$$

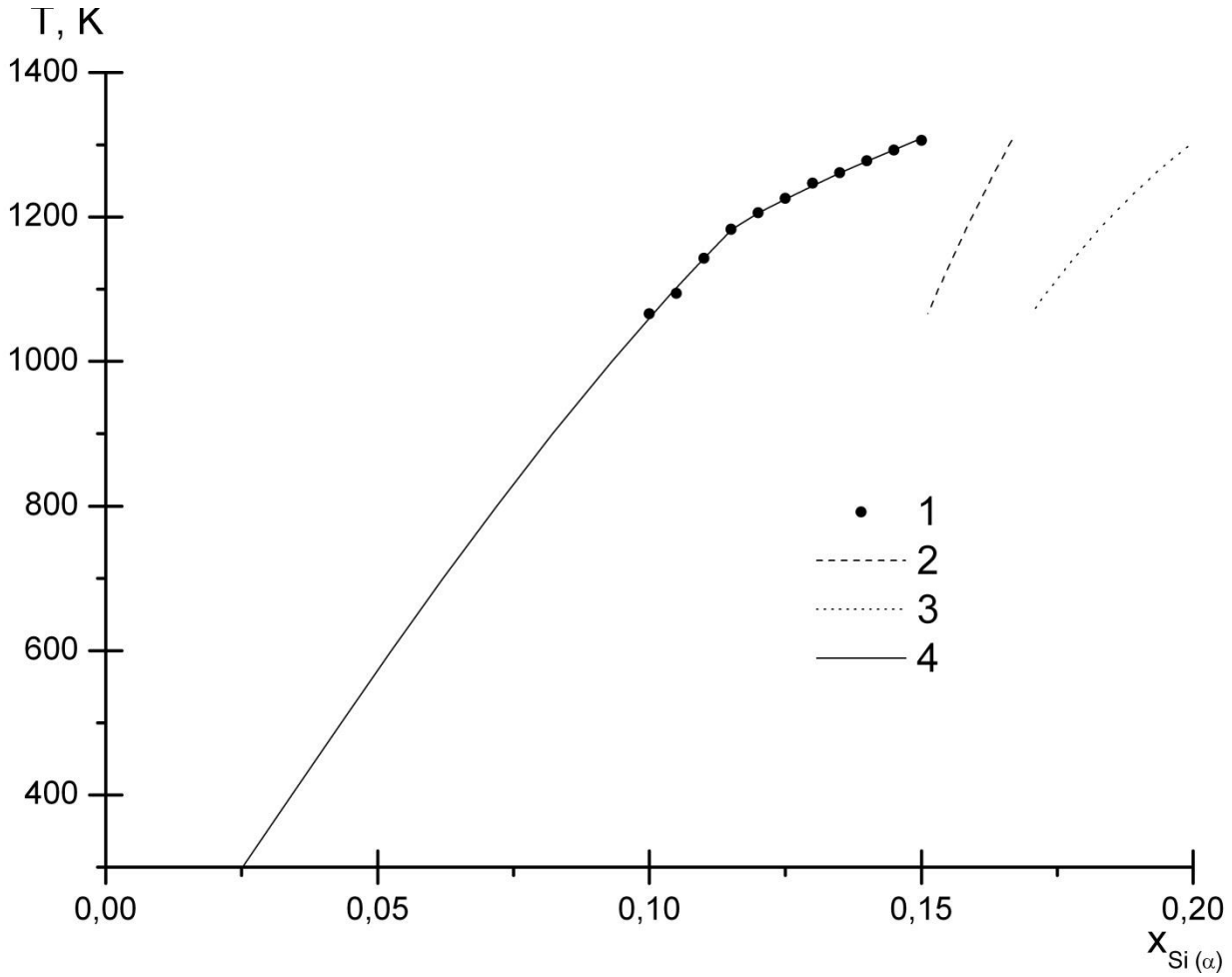

Figure 1. Maximum solid solubility of silicon in fcc-nickel at various temperatures: 1 – experimental values, obtained from Ni – Si phase diagram; 2 – calculated according to data of [26]; 3 – calculated according to data of [10]; 4 – calculated in present study.

The comparison between the experimental relationship between silicon maximum solid solubility and temperature, obtained from Ni – Si phase diagram [11] and the relationships, calculated, according to above-presented data [10, 26], is presented at figure 1. As can be seen, there is no satisfactory convergence at lower temperatures. It can be explained in a such way: the expressions of $G_{\alpha}^{E} = f(x_{\mathrm{Ni}(\alpha)}, x_{\mathrm{Si}(\alpha)}, T)$ are estimated, concerning all possible equilibria with α-phase involved, especially in high-temperature region. The estimated parameters values provide minimal deviations of calculated whole Ni – Si phase diagram from the experimental one, but these deviations are still significant, when only one single equilibrium is taken into account. Therefore, in the present study, the decision is made to borrow the temperature dependences of $\Delta_f G_T^o (\mathrm{Ni_3Si})$ and $\Delta_{tr} G_T^o (\mathrm{Si_{diamond \to fcc}})$ from paper [10], but re-estimate the expression of

$G_\alpha^E = f(x_{\mathrm{Ni}(\alpha)}, x_{\mathrm{Si}(\alpha)}, T)$ so, that it would describe the single equilibrium of β_1-phase with α-phase correctly. The results of such estimation are as follows:

$$G_\alpha^E = \begin{cases} x_{\mathrm{Ni}(\alpha)}\, x_{\mathrm{Si}(\alpha)}(17,414T - 205894), \text{ if } T < 1200\,\mathrm{K} \\ x_{\mathrm{Ni}(\alpha)}\, x_{\mathrm{Si}(\alpha)}(-19,253T - 162214), \text{ if } T > 1200\,\mathrm{K} \end{cases} \qquad (13).$$

The calculated silicon maximum solubility as function of temperature is also shown at figure 1. It is well compatible with the accepted phase diagram [11], which allows extrapolating it outside the interval, where experimental data are available and estimate the conditions of studying equilibrium at standard temperature. Calculations show, that the point of equilibrium of β_1-phase with α-phase at 298 K, correspond to $x_{\mathrm{Si}\ (\alpha)}$ = 0,025. Thermodynamic activities of the components in this "saturated" solid solution are equal to a_{Ni} = 0,927 and a_{Si} = 9,04 · 10^{-36} (standard reference state – pure component with fcc lattice).

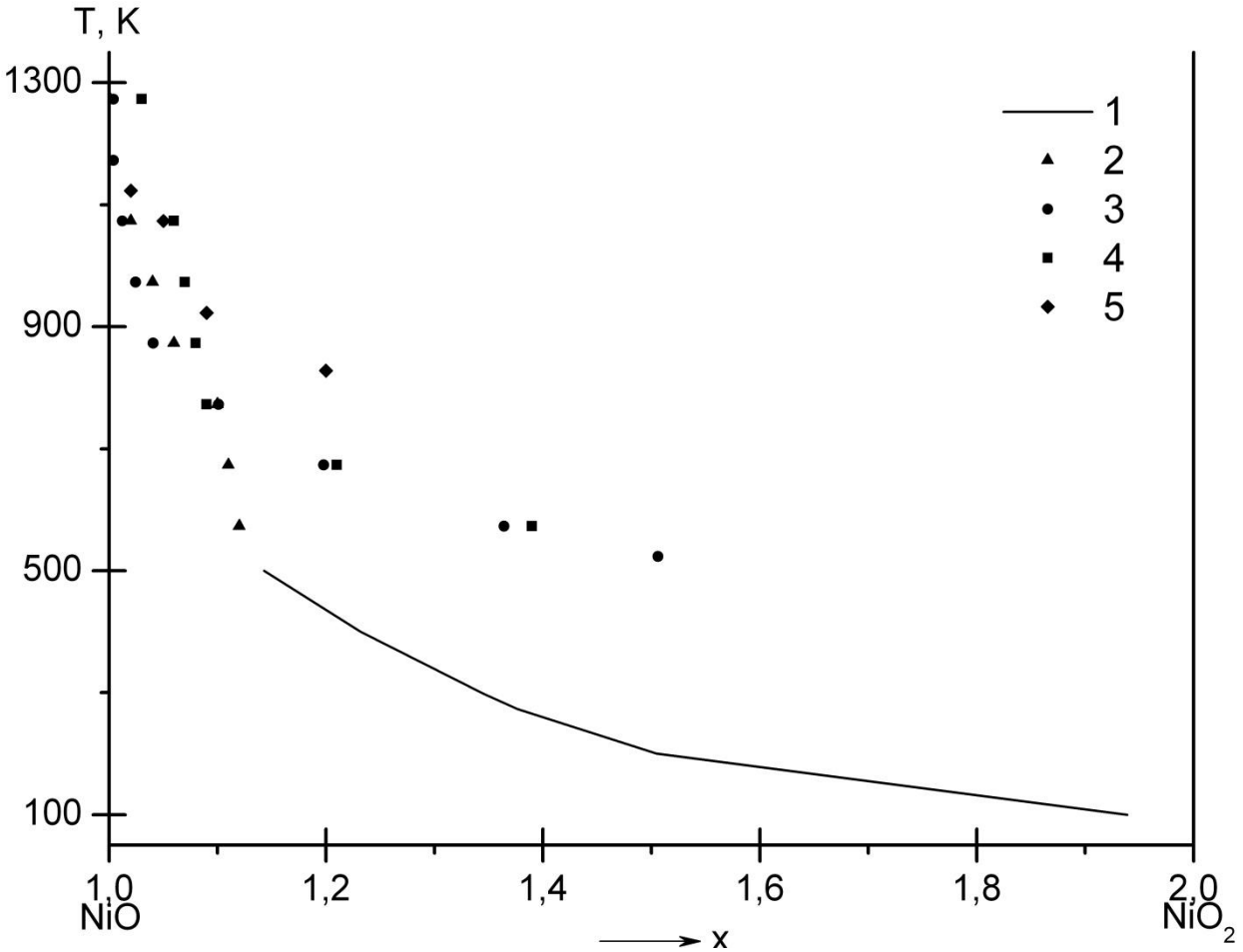

Figure 2. Area of possible nonstoichometry of the NiO_x phase at different temperatures in equilibrium with atmospheric air (at P_{O_2} = 0,21 bar): 1 – calculated in present study according to formula (14); 2 – data of [30], calculated according to radiographic measurements; 3 – data of [31], the sample is prepared from $2NiCO_3 \cdot 3Ni(OH)_2 \cdot 4H_2O$; 4 – data of [31], the sample is prepared from $Ni(NO_3)_2 \cdot 6H_2O$; 5 – data of [32], the sample is prepared from $Ni(NO_3)_2 \cdot 6H_2O$.

3. Chemical stability.

In order to plot the Ni – Si – O system phase diagram, the primary information about possible oxides in binary Ni – O and Si – O [11] systems, as well as about possible ternary compounds [27], must be taken into consideration. Formerly, the Ni – Si – O phase diagram was

plotted by the authors of [6], but it was assumed, that only nickel monoxide can be formed during oxidation of nickel. It is well known, that nickel monoxide and higher nickel oxides can form a continuous series of solid solutions, which corresponds to a variable composition phase NiO_x [28, 29]. It is shown in different studies [28, 30 – 32], that excessive oxygen content in nonstoichiomenric nickel oxide depends considerably on method and temperature of its synthesis. All known results of experimental determination of the index "x" in the formula NiO_x as temperature function are presented at figure 2.

All necessary information about the standard Gibbs energies of formation of nickel oxides was summarized earlier [33]. Thermodynamic description of NiO_x phase is performed according to Gorichev's method [34], modified by authors of [35]. It leads to a following expression [33]:

$$\Delta_f G^o_{298}(NiO_x) = 155912x^2 - 367342x,\ J/mol \quad (14).$$

The dependence of the index "x" on temperature at air pressure (P_{O_2} = 0,21 bar) is estimated, the results are also represented at figure 2. As follows from calculations, the phase with composition of $NiO_{1,344}$ is in equilibrium with atmospheric oxygen at 25˚C. It is not possible to verify this value, since there are no experimental data at such low temperatures.

Only one stable oxide – SiO_2 – exist in Si – O system. There are also many values of its Gibbs energy of formation available in literature [18 – 21]. However, since electrochemical formation of silicon dioxide is to be considered (see section 4), the value is chosen, that corresponds to experimentally determined potential of the silicon electrode [36]:

$$SiO_2 + 4H^+ + 4e^- = Si\,(diamond) + 2H_2O;\ \varphi^o_{298} = -0{,}857\,V \quad (15),$$

which leads to a following equation:

$$Si\,(diamond) + O_2 = SiO_2;\ \Delta_r G^o_{298} = -805067\ J/mol \quad (16).$$

A single ternary compound exist in Ni – Si – O system, it is nickel orthosilicate Ni_2SiO_4 [27]. Its stability was studied many times [37 – 41], but most of these studies refer to temperatures, up to 950ºC. Available information about the standard Gibbs energy of formation of Ni_2SiO_4 is listed in table 2. Data, presented in [18 – 20, 40], are obtained from experimental measurements at standard temperature, while data from [37, 39] are obtained by extrapolating the most recent high temperature values from 950ºC down to 25ºC by using heat capacity temperature dependency, measured in [40] with respect to low temperature calorimetry.

Table 2. The standard Gibbs energies of formation of nickel silicate ($-\Delta_f G^o_{298}$, J/mol).

Compound \ Reference	[18]	[19]	[20]	[37]	[39]	[40]
Ni_2SiO_4	1317270[a]	1317132[a]	1292193[a]	1282000[b]	1291215[b]	1289000[a]

[a] Experimental

[b] Extrapolated from high temperatures down to 298 K, using heat capacity from [40].

In order to plot the Ni – Si – O phase diagram, the correct sequence of equilibria of Ni – Si system alloys with oxygen is to be determined and the correct thermodynamic parameters are to be chosen. This can be done in the following way.

At first stage in order to improve reliability of further calculation, it is useful to take all values of standard Gibbs energies from one source. So, Gibbs energies of formation, predicted by CALPHAD assessments [13 – 16], are more useful, because experimentally measured values from textbooks [17 – 21] are obtained from different sources. However, CALPHAD assessments usually correspond to elevated temperatures, and extrapolating their dependencies to standard temperature leads to possible uncertainties. Particularly, calculated standard Gibbs energies of formation are much lower, than experimentally measured (see table 1). We consider the values of standard Gibbs energies of formation, taken from [16], are the best, because they stay most closely to experiments.

At second stage the following issue is to be considered. According to Gibbs phase rule, all equilibria take place in multiple stages, one after the other. Since the chemical affinity of silicon to oxygen in much higher, than that of nickel [42], silicon from nickel silicides has to be oxidized in the first order, and the consecutive formation of phases, more and more rich of nickel has to be observed. Along with this, the equilibrium oxygen pressure is to increase from the previous equilibrium to the next one. Calculation shows, that Gibbs energies, taken from [16] cannot pass this criterion, therefore value of standard Gibbs energy of formation for Ni_5Si_2 was changed to the nearest available experimental data in order to correct this. The standard Gibbs energies of formation of nickel silicides, chosen for further calculations, are also presented in table 1. Also, the standard Gibbs energy of formation of Ni_2SiO_4 from reference [40] was chosen.

The characteristics of the variable composition phases, involved in oxidation process, are calculated according to the laws of chemical equilibrium. Then, the calculated sequence of equilibria is presented in graphical form as the Ni – Si – O phase diagram. It is shown at figure 3. The appropriate characteristics of system invariant conditions are represented in table 3.

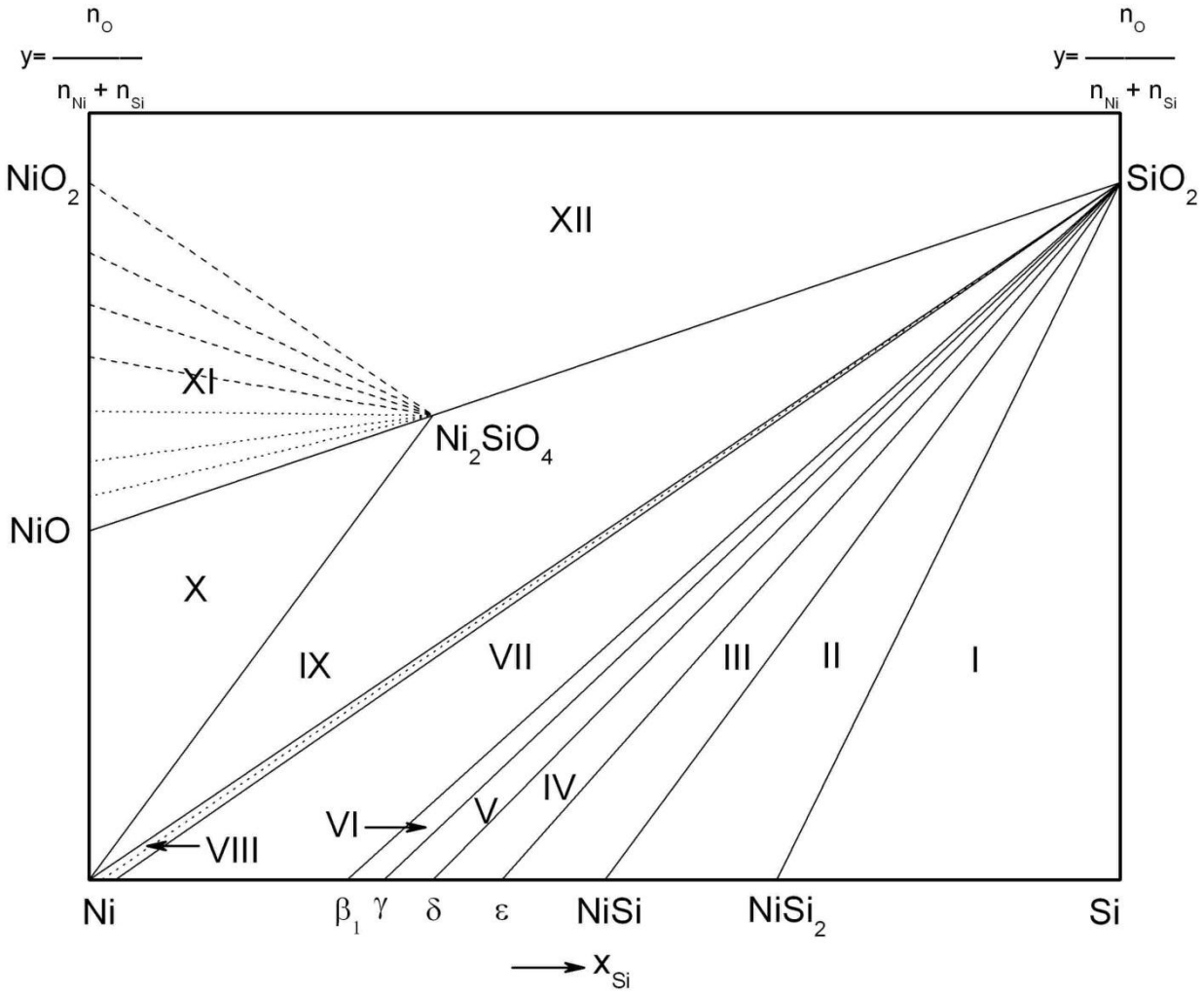

Figure 3. The Ni – Si – O state diagram at standard temperature.

Table 3. The characteristics of the Ni – Si – O system invariant conditions at standard temperature.

No. of domain	System condition	Reaction equation	P_{O_2}, bar
I	$NiSi_2 – Si – SiO_2$	$Si + O_2 = SiO_2$	$7{,}7 \cdot 10^{-142}$

II	$NiSi – NiSi_2 – SiO_2$	$NiSi_2 + O_2 = NiSi + SiO_2$	$1{,}5 \cdot 10^{-141}$
III	$Ni_3Si_2 – NiSi – SiO_2$	$3NiSi + O_2 = Ni_3Si_2 + SiO_2$	$1{,}6 \cdot 10^{-137}$
IV	$Ni_2Si – Ni_3Si_2 – SiO_2$	$2Ni_3Si_2 + O_2 = 3Ni_2Si + SiO_2$	$7{,}6 \cdot 10^{-137}$
V	$Ni_5Si_2 – Ni_2Si – SiO_2$	$5Ni_2Si + O_2 = 2Ni_5Si_2 + SiO_2$	$5{,}1 \cdot 10^{-122}$
VI	$Ni_3Si – Ni_5Si_2 – SiO_2$	$3Ni_5Si_2 + O_2 = 5Ni_3Si + SiO_2$	$2{,}8 \cdot 10^{-120}$
VII	α-phase (Ni) – Ni_3Si – SiO_2	$Ni_3Si + O_2 = 3Ni\ (\alpha) + SiO_2$ $x_{Si(\alpha)} = 0{,}025$; $a_{Si} = 9{,}04 \cdot 10^{-36}; a_{Ni} = 0{,}927$	$1{,}4 \cdot 10^{-114}$
VIII	α-phase (Ni) – SiO_2	$Si\ (\alpha) + O_2 = SiO_2$	–
IX	α-phase (Ni) – Ni_2SiO_4 – SiO_2	$2Ni\ (\alpha) + Si\ (\alpha) + 2O_2 = Ni_2SiO_4$ $Si\ (\alpha) + O_2 = SiO_2$ $x_{Si(\alpha)} = 1{,}11 \cdot 10^{-24}$; $a_{Si} = 7{,}34 \cdot 10^{-60}; a_{Ni} \approx 1$	$1{,}7 \cdot 10^{-90}$
X	α-phase (Ni) – NiO – Ni_2SiO_4	$2Ni\ (\alpha) + O_2 = 2NiO$ $2Ni\ (\alpha) + Si\ (\alpha) + 2O_2 = Ni_2SiO_4$ $x_{Si(\alpha)} = 6{,}98 \cdot 10^{-56}$; $a_{Si} = 4{,}62 \cdot 10^{-91}; a_{Ni} \approx 1$	$6{,}6 \cdot 10^{-75}$
XI	$NiO_x\ (1 \le x \le 2)$ – Ni_2SiO_4	$2NiO + (x–1)O_2 = 2NiO_x$	$\ln P_{O_2}[\text{bar}] =$ $= 125{,}79 \cdot (x+1) – 296{,}37$
	a) x = 1,344 b) x = 2		0,21 $1{,}5 \cdot 10^{35}$
XII	$NiO_x – Ni_2SiO_4$ or $Ni_2SiO_4 – SiO_2$	–	–

4. Electrochemical stability.

In order to develop thermodynamic model of nickel - silicon alloys oxidation in liquid environments, it is convenient to use the diagrams of electrochemical equilibrium diagrams (potential – pH) [43 – 45], that most clearly show the possible chemical and electrochemical equilibria in system. Method of plotting such diagrams was in detail described several times [42 – 45]. The primary information about the Ni – H_2O and Si – H_2O potential – pH diagrams and the thermodynamic properties of the electrochemical reactions, involving ions, can be obtained from textbooks [36, 45], papers [46, 47] and databases [48 – 56]. Along the above mentioned oxides, the possible ions, which can be formed in solution, have to be considered as the oxidation products. These ions are Ni^{2+}, $HNiO_2^-$, NiO_4^{2-} and SiO_3^{2-}. Any oxides or oxygen-containing ions in solution can exist in unhydrated or in hydrated form. The transition from the first form to the second one proceeds through the series of intermediate conditions. The unhydrated form is most thermodynamically stable, therefore metal hydroxides and other particles like $NiOH^+$, $NiOOH$, $Ni(OH)_3^-$, $Ni(OH)_4^{2-}$, Ni_2OH^{3+}, $Ni_4(OH)_4^{4+}$, H_4SiO_4, H_8SiO_6, $H_2Si_2O_5$, $H_6Si_2O_7$, $HSi(OH)_6^-$, $H_2SiO_4^{2-}$, $H_3SiO_4^-$, $H_4(H_2SiO_4)_4^{4-}$, $H_6(H_2SiO_4)_4^{2-}$, $SiO_2(OH)^{2-}$, $SiO(OH)_3^-$, $Si_2O_3(OH)_4^{2-}$ and others, noticed in [19, 36, 45, 48 – 56], are not taken into consideration.

The potential – pH diagram of Ni – Si – H_2O system at 25°C, air pressure of 1 bar and activities of ions in solutions (standard reference state – the hypothetical one-molar solution), equal to 1 mole/l is represented at figure 4. The characteristics of basic chemical and

electrochemical equilibria are summarized in table 4, the variable activities of ions correspond to the reference state of the hypothetical one-molar solution.

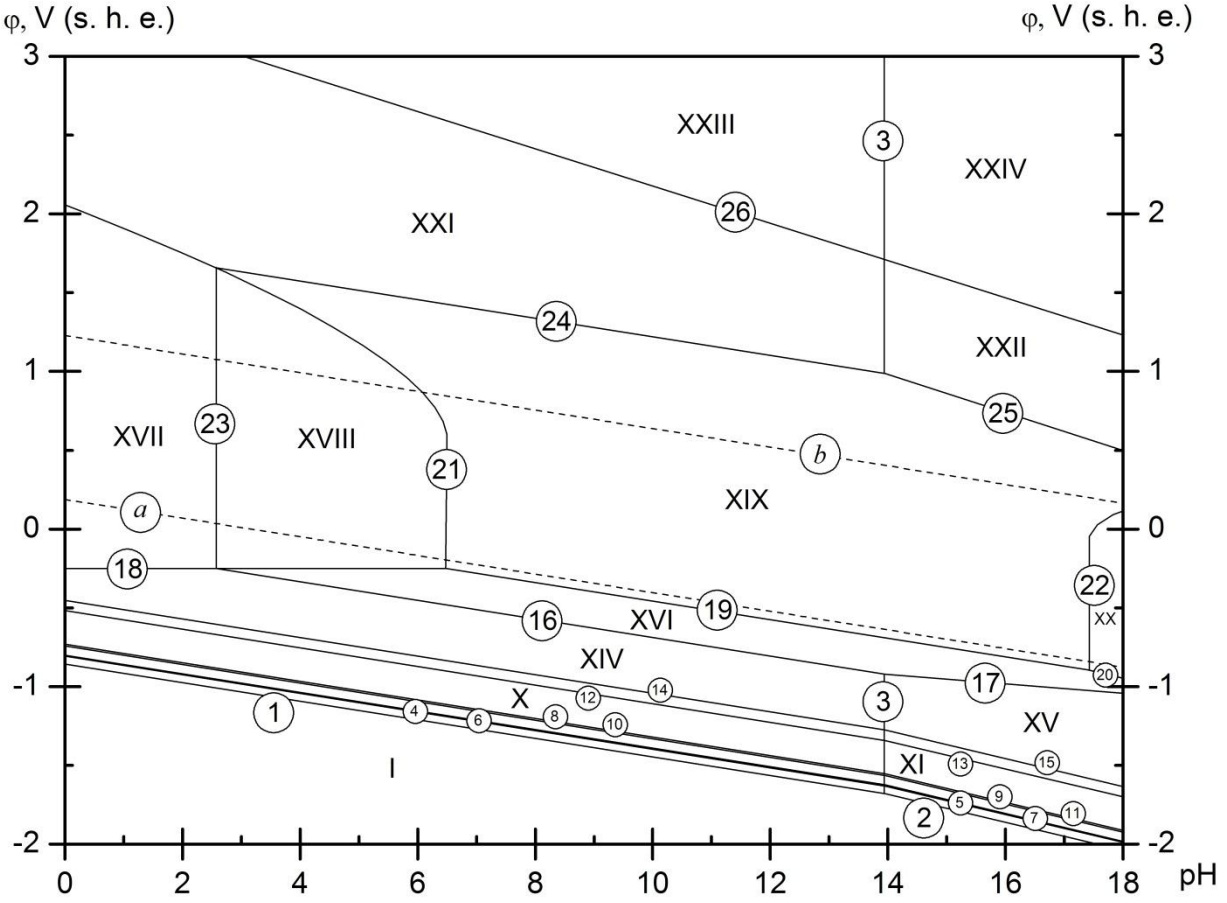

Figure 4. The potential – pH diagram of the Ni – Si – H_2O system at 298 K, air pressure of 1 bar and activities of ions in solutions, equal to 1 mole/l (unhydrated form of oxides, without nickel hydride consideration).

Table 4. Basic chemical and electrochemical equilibria in the Ni – Si – H_2O system at 298 K and air pressure of 1 bar, without nickel hydride consideration.

No. of line at figure 4	Electrode reaction	Equilibrium potential, V (s. h. e.) or solution pH
a	$2H^+ + 2e^- = H_2; P_{H_2} = 5\cdot10^{-7}$ bar	$0{,}186 - 0{,}0591\cdot pH$
b	$O_2 + 4H^+ + 4e^- = 2H_2O; P_{O_2} = 0{,}21$ bar	$1{,}219 - 0{,}0591\cdot pH$
1	$SiO_2 + 4H^+ + 4e^- = Si\ (diamond) + 2H_2O$	$-0{,}857 - 0{,}0591\cdot pH$
2	$SiO_3^{2-} + 6H^+ + 4e^- = Si(diamond) + 3H_2O$	$-0{,}444 - 0{,}0887\cdot pH + 0{,}0148\cdot \lg a_{SiO_3^{2-}}$
3	$SiO_3^{2-} + 2H^+ = SiO_2 + 2H_2O$	$pH = 13{,}94 + 0{,}5\cdot \lg a_{SiO_3^{2-}}$
4	$NiSi + SiO_2 + 4H^+ + 4e^- = NiSi_2 + 2H_2O$	$-0{,}852 - 0{,}0591\cdot pH$
5	$NiSi + SiO_3^{2-} + 6H^+ + 4e^- = NiSi_2 + 3H_2O$	$-0{,}440 - 0{,}0887\cdot pH + 0{,}0148\cdot \lg a_{SiO_3^{2-}}$
6	$Ni_3Si_2 + SiO_2 + 4H^+ + 4e^- = 3NiSi + 2H_2O$	$-0{,}793 - 0{,}0591\cdot pH$
7	$Ni_3Si_2 + SiO_3^{2-} + 6H^+ + 4e^- = 3NiSi + 3H_2O$	$-0{,}380 - 0{,}0887\cdot pH + 0{,}0148\cdot \lg a_{SiO_3^{2-}}$

8	$3Ni_2Si + SiO_2 + 4H^+ + 4e^- = 2Ni_3Si_2 + 2H_2O$	$-0,783 - 0,0591 \cdot pH$
9	$3Ni_2Si + SiO_3^{2-} + 6H^+ + 4e^- = 2Ni_3Si_2 + 3H_2O$	$-0,371 - 0,0887 \cdot pH + 0,0148 \cdot \lg a_{SiO_3^{2-}}$
10	$2Ni_5Si_2 + SiO_2 + 4H^+ + 4e^- = 5Ni_2Si + 2H_2O$	$-0,564 - 0,0591 \cdot pH$
11	$2Ni_5Si_2 + SiO_3^{2-} + 6H^+ + 4e^- = 5Ni_2Si + 3H_2O$	$-0,151 - 0,0887 \cdot pH + 0,0148 \cdot \lg a_{SiO_3^{2-}}$
12	$5Ni_3Si + SiO_2 + 4H^+ + 4e^- = 3Ni_5Si_2 + 2H_2O$	$-0,538 - 0,0591 \cdot pH$
13	$5Ni_3Si + SiO_3^{2-} + 6H^+ + 4e^- = 3Ni_5Si_2 + 3H_2O$	$-0,126 - 0,0887 \cdot pH + 0,0148 \cdot \lg a_{SiO_3^{2-}}$
14	$3Ni(\alpha) + SiO_2 + 4H^+ + 4e^- = Ni_3Si + 2H_2O$; $a_{Ni(\alpha)} = 0,927$	$-0,451 - 0,0591 \cdot pH$
15	$3Ni(\alpha) + SiO_3^{2-} + 6H^+ + 4e^- = Ni_3Si + 3H_2O$; $a_{Ni(\alpha)} = 0,927$	$-0,039 - 0,0887 \cdot pH + 0,0148 \cdot \lg a_{SiO_3^{2-}}$
16	$Ni_2SiO_4 + 4H^+ + 4e^- = 2Ni(\alpha) + SiO_2 + 2H_2O$; $a_{Ni(\alpha)} = 0,927$	$-0,098 - 0,0591 \cdot pH$
17	$Ni_2SiO_4 + 2H^+ + 4e^- = 2Ni(\alpha) + SiO_3^{2-} + H_2O$; $a_{Ni(\alpha)} = 0,927$	$-0,510 - 0,0295 \cdot pH - 0,0148 \cdot \lg a_{SiO_3^{2-}}$
18	$Ni^{2+} + 2e^- = Ni(\alpha); a_{Ni(\alpha)} = 0,927$	$-0,249 + 0,0295 \cdot \lg a_{Ni^{2+}}$
19	$NiO + 2H^+ + 2e^- = Ni(\alpha) + H_2O; a_{Ni(\alpha)} = 0,927$	$0,135 - 0,0591 \cdot pH$
20	$HNiO_2^- + 3H^+ + 2e^- = Ni(\alpha) + 2H_2O$; $a_{Ni(\alpha)} = 0,927$	$0,649 - 0,0887 \cdot pH + 0,0295 \cdot \lg a_{HNiO_2^-}$
21	$NiO_x + 2xH^+ + 2(x-1)e^- = Ni^{2+} + xH_2O$	$\frac{0,808 \cdot x^2 - 0,674 \cdot x + 0,250}{x-1} - \frac{0,0591 \cdot x}{x-1} \cdot pH - \frac{0,0295}{x-1} \cdot \lg a_{Ni^{2+}}$
22	$HNiO_2^- + (3-2x)H^+ + 2(1-x)e^- = NiO_x + (2-x)H_2O$	$\frac{-0,808 \cdot x^2 + 0,674 \cdot x + 0,648}{1-x} - \frac{0,0295 \cdot (3-2 \cdot x)}{1-x} \cdot pH + \frac{0,0295}{1-x} \cdot \lg a_{HNiO_2^-}$
23	$Ni_2SiO_4 + 4H^+ = 2Ni^{2+} + SiO_2 + 2H_2O$	$pH = 2,575 - 0,5 \cdot \lg a_{Ni^{2+}}$
24	$2NiO_{1,482} + SiO_2 + 1,928H^+ + 1,928e^- = Ni_2SiO_4 + 0,964H_2O$	$1,811 - 0,0591 \cdot pH$
25	$2NiO_{1,482} + SiO_3^{2-} + 3,928H^+ + 1,928e^- = Ni_2SiO_4 + 1,964H_2O$	$2,667 - 0,1204 \cdot pH + 0,0307 \cdot \lg a_{SiO_3^{2-}}$
26	$NiO_4^{2-} + 4H^+ + 2e^- = NiO_2 + 2H_2O$	$3,360 - 0,1182 \cdot pH + 0,0295 \cdot \lg a_{NiO_4^{2-}}$

24 domains of thermodynamic stability of certain phases can be depicted at the presented diagram (figure 4):

I – α-phase (Ni) + Ni_3Si + Ni_5Si_2 + Ni_2Si + Ni_3Si_2 + NiSi + $NiSi_2$ + Si (diamond);

II – α-phase (Ni) + Ni_3Si + Ni_5Si_2 + Ni_2Si + Ni_3Si_2 + NiSi + $NiSi_2$ + SiO_2;

III – α-phase (Ni) + Ni_3Si + Ni_5Si_2 + Ni_2Si + Ni_3Si_2 + NiSi + $NiSi_2$ + SiO_3^{2-};

IV – α-phase (Ni) + Ni_3Si + Ni_5Si_2 + Ni_2Si + Ni_3Si_2 + NiSi + SiO_2;

V – α-phase (Ni) + Ni_3Si + Ni_5Si_2 + Ni_2Si + Ni_3Si_2 + NiSi + SiO_3^{2-};

VI – α-phase (Ni) + Ni_3Si + Ni_5Si_2 + Ni_2Si + Ni_3Si_2 + SiO_2;
VII – α-phase (Ni) + Ni_3Si + Ni_5Si_2 + Ni_2Si + Ni_3Si_2 + SiO_3^{2-};
VIII – α-phase (Ni) + Ni_3Si + Ni_5Si_2 + Ni_2Si + SiO_2;
IX – α-phase (Ni) + Ni_3Si + Ni_5Si_2 + Ni_2Si + SiO_3^{2-}; X – α-phase (Ni) + Ni_3Si + Ni_5Si_2 + SiO_2;
XI – α-phase (Ni) + Ni_3Si + Ni_5Si_2 + SiO_3^{2-}; XII – α-phase (Ni) + Ni_3Si + SiO_2;
XIII – α-phase (Ni) + Ni_3Si + SiO_3^{2-}; XIV – α-phase (Ni) + SiO_2; XV – α-phase (Ni) + SiO_3^{2-};
XVI – α-phase (Ni) + Ni_2SiO_4; XVII – Ni^{2+} + SiO_2; XVIII – Ni^{2+} + Ni_2SiO_4;
XIX – NiO_x + Ni_2SiO_4; XX – $HNiO_2^-$ + Ni_2SiO_4; XXI – NiO_x + SiO_2; XXII – NiO_x + SiO_3^{2-};
XXIII – NiO_4^{2-} + SiO_2; XXIV – NiO_4^{2-} + SiO_3^{2-}.

Domain I is the domain of thermodynamic stability, where all components of Ni – Si system are immune to corrosion. At the domains II – XV the consecutive decomposition of nickel silicides takes place. Domains XVII and XVIII are the domains of active corrosion, where nickel dissolves from alloys and passes into solution in form of Ni^{2+} cations. Domains II, IV, VI, VIII, X, XII, XIV, XVI, XIX, XXI and XXII are the domains of passivity, where the protective oxide film, consisting of NiO_x, SiO_2 or Ni_2SiO_4, is formed on the alloy surface and prevent further oxidation. Domains III, V, VII, IX, XI, XIII, XV, XX, XXIII and XXIV are the domains of transpassivity, where the oxides from passivation layer oxidize further and pass into solution in form of anions, which violates the integrity of the protective film.

Although the diagram, presented at figure 4, completely corresponds to the Ni – Si – O state diagram, it is hypothetical and does not reflect the whole picture of Ni – Si alloys electrochemical corrosion. It is known, that nickel can form the hydride Ni_2H [57, 58]. It cannot be synthesized at standard conditions, since thermodynamic calculations, performed by the authors of [59], show that the equilibrium hydrogen pressure, needed for such synthesis is equal to 3420 bar. But nickel can be reduced to its hydride in electrochemical way [60 – 62]. In order to involve nickel hydride into analysis of the Ni – Si system electrochemical behaviour, the potential – pH diagram of Ni – Si – H_2O system was reassessed. The information about the Gibbs energy of formation for nickel hydride Ni_2H was taken from paper [59]. The reassessed potential – pH diagram of Ni – Si – H_2O system at 25˚C, air pressure of 1 bar and activities of ions in solutions, equal to 1 mole/l with consideration of nickel hydride is represented at figure 5. The characteristics of basic chemical and electrochemical equilibria are summarized in table 5, the activities of ions correspond to the reference state of the hypothetical one-molar solution.
17 domains of thermodynamic stability of certain phases can be depicted at modified variant of the diagram (figure 5):
I – Ni_2H + Ni_3Si + Ni_5Si_2 + Ni_2Si + Ni_3Si_2 + NiSi + $NiSi_2$ + Si (diamond);
II – Ni_2H + Ni_3Si + Ni_5Si_2 + Ni_2Si + Ni_3Si_2 + NiSi + $NiSi_2$;
III – Ni_2H + Ni_3Si + Ni_5Si_2 + Ni_2Si + Ni_3Si_2 + NiSi;
IV – Ni_2H + Ni_3Si + Ni_5Si_2 + Ni_2Si + Ni_3Si_2; V – Ni_2H + Ni_3Si + Ni_5Si_2 + Ni_2Si;
VI – Ni_2H + Ni_3Si + Ni_5Si_2; VII – Ni_2H + Ni_3Si; VIII – Ni_2H + Ni_2SiO_4;
IX – Ni (fcc) + Ni_2SiO_4; X – Ni^{2+} + SiO_2; XI – Ni^{2+} + Ni_2SiO_4; XII – NiO_x + Ni_2SiO_4;
XIII – $HNiO_2^-$ + Ni_2SiO_4; XIV – NiO_x + SiO_2; XV – NiO_x + SiO_3^{2-}; XVI – NiO_4^{2-} + SiO_2;
XVII – NiO_4^{2-} + SiO_3^{2-};

Calculation shows that silicon dioxide becomes thermodynamically unstable in presence of nickel hydride. The mechanism of nickel silicides decomposition slightly changes. SiO_2 remains stable only in strongly acidic environments in presence of Ni^{2+} cations (domain X on figure 5).

Domains I – VII are the domains of hydride passivation, where nickel reduces to Ni_2H and the hydride protective film forms. Domains X and XI are the domains of active dissolution (like the domains XVII and XVIII at figure 4). Domains VIII, IX, XII, XIV and XV are the

domains of oxide passivation and domains XIII, XVI and XVII are the domains of transpassivity.

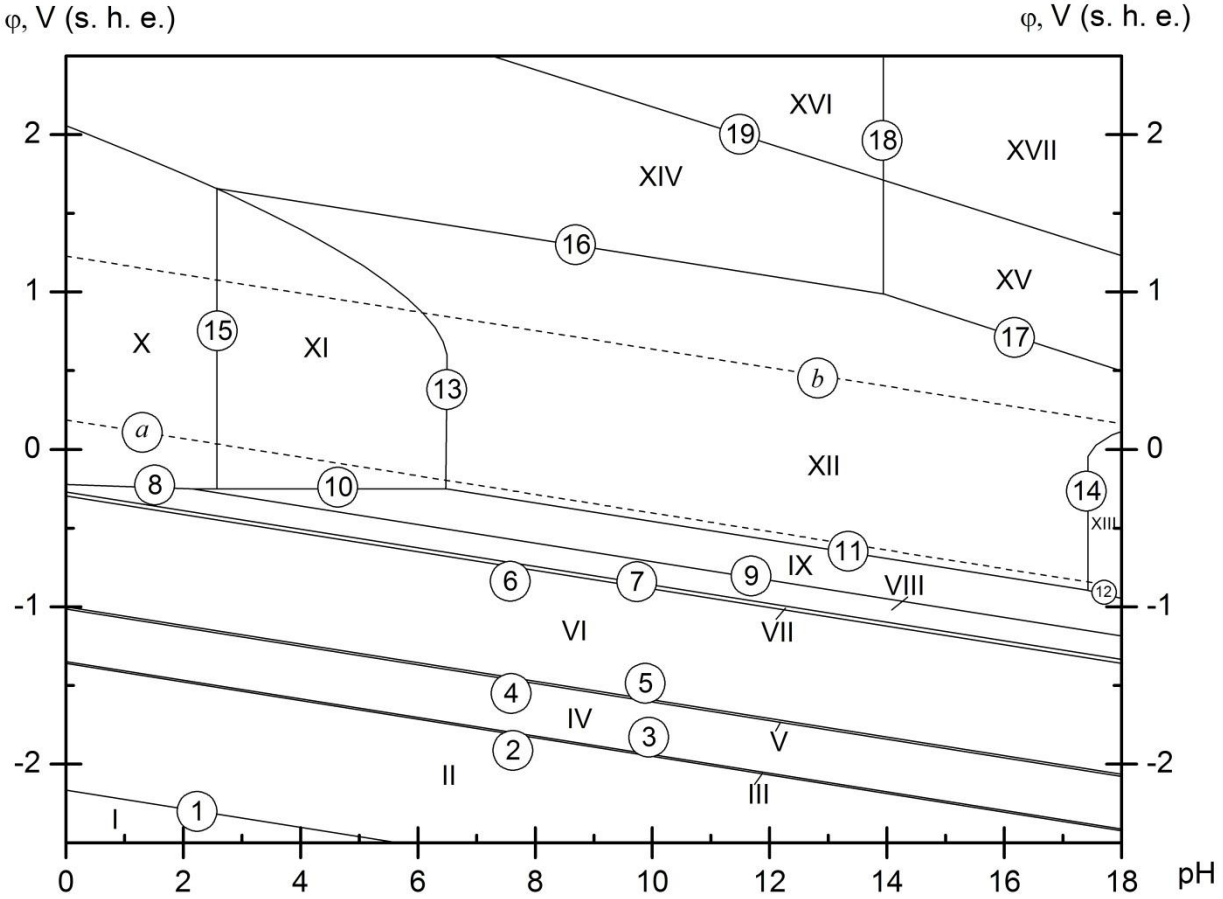

Figure 5. The potential – pH diagram of the Ni – Si – H_2O system at 298 K, air pressure of 1 bar and activities of ions in solutions, equal to 1 mol/l (unhydrated form of oxides, with consideration of nickel hydride).

Table 5. Basic chemical and electrochemical equilibria in the Ni – Si – H_2O system at 298 K and air pressure of 1 bar, with consideration of nickel hydride.

No. of line at figure 5	Electrode reaction	Equilibrium potential, V (s. h. e.) or solution pH
a	$2H^+ + 2e^- = H_2; P_{H_2} = 5 \cdot 10^{-7}$ bar	$0{,}186 - 0{,}0591 \cdot pH$
b	$O_2 + 4H^+ + 4e^- = 2H_2O; P_{O_2} = 0{,}21$ bar	$1{,}219 - 0{,}0591 \cdot pH$
1	$2NiSi_2 + H^+ + e^- = Ni_2H + 4Si$ (diamond)	$-1{,}908 - 0{,}0591 \cdot pH$
2	$4NiSi + H^+ + e^- = Ni_2H + 2NiSi_2$	$-1{,}389 - 0{,}0591 \cdot pH$
3	$2Ni_3Si_2 + H^+ + e^- = Ni_2H + 4NiSi$	$-1{,}362 - 0{,}0591 \cdot pH$
4	$4Ni_2Si + H^+ + e^- = Ni_2H + 2Ni_3Si_2$	$-1{,}309 - 0{,}0591 \cdot pH$
5	$2Ni_5Si_2 + H^+ + e^- = Ni_2H + 4Ni_2Si$	$-1{,}010 - 0{,}0591 \cdot pH$
6	$4Ni_3Si + H^+ + e^- = Ni_2H + 2Ni_5Si_2$	$-0{,}350 - 0{,}0591 \cdot pH$
7	$2Ni_2SiO_4 + Ni_2H + 15H^+ + 15e^- = 2Ni_3Si + 8H_2O$	$-0{,}285 - 0{,}0591 \cdot pH$

8	$2Ni^{2+} + H^+ + 5e^- = Ni_2H$	$-0{,}224 - 0{,}0118 \cdot pH + 0{,}0236 \cdot \lg a_{Ni^{2+}}$
9	$2Ni + H^+ + e^- = Ni_2H$	$-0{,}122 - 0{,}0591 \cdot pH$
10	$Ni^{2+} + 2e^- = Ni\ (fcc)$	$-0{,}250 + 0{,}0295 \cdot \lg a_{Ni^{2+}}$
11	$NiO + 2H^+ + 2e^- = Ni(fcc) + H_2O$	$0{,}134 - 0{,}0591 \cdot pH$
12	$HNiO_2^- + 3H^+ + 2e^- = Ni\ (fcc) + 2H_2O$	$0{,}648 - 0{,}0887 \cdot pH + 0{,}0295 \cdot \lg a_{HNiO_2^-}$
13	$NiO_x + 2xH^+ + 2(x-1)e^- = Ni^{2+} + xH_2O$	$\frac{0{,}808 \cdot x^2 - 0{,}674 \cdot x + 0{,}250}{x-1} - \frac{0{,}0591 \cdot x}{x-1} \cdot pH - \frac{0{,}0295}{x-1} \cdot lg\, a_{Ni^{2+}}$
14	$HNiO_2^- + (3-2x)H^+ + 2(1-x)e^- = NiO_x + (2-x)H_2O$	$\frac{-0{,}808 \cdot x^2 + 0{,}674 \cdot x + 0{,}648}{1-x} - \frac{0{,}0295 \cdot (3-2 \cdot x)}{1-x} \cdot pH + \frac{0{,}0295}{1-x} \cdot lg\, a_{HNiO_2^-}$
15	$Ni_2SiO_4 + 4H^+ = 2Ni^{2+} + SiO_2 + 2H_2O$	$pH = 2{,}575 - 0{,}5 \cdot \lg a_{Ni^{2+}}$
16	$2NiO_{1,482} + SiO_2 + 1{,}928H^+ + 1{,}928e^- = Ni_2SiO_4 + 0{,}964H_2O$	$1{,}811 - 0{,}0591 \cdot pH$
17	$2NiO_{1,482} + SiO_3^{2-} + 3{,}928H^+ + 1{,}928e^- = Ni_2SiO_4 + 1{,}964H_2O$	$2{,}667 - 0{,}1204 \cdot pH + 0{,}0307 \cdot \lg a_{SiO_3^{2-}}$
18	$SiO_3^{2-} + 2H^+ = SiO_2 + 2H_2O$	$pH = 13{,}94 + 0{,}5 \cdot \lg a_{SiO_3^{2-}}$
19	$NiO_4^{2-} + 4H^+ + 2e^- = NiO_2 + 2H_2O$	$3{,}360 - 0{,}1182 \cdot pH + 0{,}0295 \cdot \lg a_{NiO_4^{2-}}$

5. Results and discussion.

As can be shown from calculation, the oxidation of Ni – Si system alloys in air at standard conditions is ended by forming Ni_2SiO_4 and NiO_x. The estimated composition of this phase is $NiO_{1,344}$. It seems, that nickel orthosilicate is much thermodynamically stable, than simple oxides of nickel and silicon. For the reaction of its possible decomposition:

$$Ni_2SiO_4 + (x-1)O_2 = 2NiO_x + SiO_2 \qquad (17),$$

the Gibbs energy of reaction is always positive, regardless of the "x" value in NiO_x formula:

$$\Delta_r G^o_{298} = 311824x^2 - 734684x + 512203 > 0,\ Дж/моль \qquad (18).$$

The composition of passivation layer on Ni – Si alloys depends on silicon content in system. If it exceeds $1{,}1 \cdot 10^{-22}$ atomic percent, a continuous layer of SiO_2 + Ni_2SiO_4 can be formed. Otherwise, SiO_2 cannot be formed, and passivation layer consists of NiO_x + Ni_2SiO_4.

Silicon also plays a major role in the corrosion-electrochemical behaviour of Ni – Si system alloys. Calculation shows, that passivation film, consisting of nickel orthosilicate is much resistant in chemical and electrochemical terms, than simple oxides of nickel or silicon, because its further oxidation to anions SiO_3^{2-} or $HNiO_2^-$ is hampered. The domain of active corrosion is very low, and Ni^{2+} cations can be formed only in strongly acidic environments.

There are several publications, concerning the corrosion-electrochemical behaviour of various nickel silicides [1, 63 – 70], Ni – Si system solid solutions [71] and more complicated materials, based on them [72 – 75]. Thermodyanmic calculations, performed in present study, do not contradict to experimental data, presented in these papers. In alkaline environments [63, 64] the formation of NiO_x + $Ni(OH)_2$ takes place, and there are no silicate-ions since silicon is bound into Ni_2SiO_4. Silicon content in all nickel silicides is enough to form a persistent passivation layer from silicon dioxide in acidic environments under condition of F^- ions absence in solutions.

[68 – 70]. For the Ni – Si system solid solutions, however, silicon content up to 8% is not enough to form persistent SiO_2 layer [71], and there is no passivity region on the anodic polarization curves. In all cases the corrosion resistance of materials, based on Ni – Si binary system is very high [72 – 75] For example, the resistance of the nickel silicides coating is several times higher than that of the austenitic stainless steel 1Cr18Ni9Ti [75].

Therefore, the chemical and electrochemical stability of Ni – Si system alloys is completely determined by silicon percentage in alloys.

Conclusions

1. The Ni – Si – O state diagram and the potential – pH diagrams of Ni – Si – H_2O system at 298 K, air pressure of 1 bar and activities of ions in solution, equal to 1 mol/l with and without consideration of nickel hydride are plotted. The invariant conditions of Ni – Si – O system and basic chemical and electrochemical equilibria in Ni – Si – H_2O system are calculated.

2. Thermodynamic analysis of chemical and electrochemical stability of nickel – silicon system alloys is performed. The positive influence of silicon on nickel corrosion properties is revealed.

References:

[1]. A. B. Shein. Electrochimija silicidov i germanidov perehodnykh metallov [In Russian] (Electrochemistry of transition metals silicides and germanides). Perm: Publishing House of Perm State University, 2009.

[2]. Y. Du, J. C. Schuster. Experimental Investigations and Thermodynamic Descriptions of the Ni-Si and C-Ni-Si Systems. Metallurgical and Materials Transactions A. 30A (1999). 2409 – 2418.

[3]. K. P. Gupta. The Mo-Ni-Si (Molybdenum-Nickel-Silicon) System. Journal of Phase Equilibria and Diffusion. 26 (2006). 379 – 384.

[4]. K. P. Gupta. The Ni-Si-V (Nickel-Silicon-Vanadium) System. Journal of Phase Equilibria and Diffusion. 26 (2006). 385 – 389.

[5]. B. Hu, H. Xu, S. Liu, Y. Du, C. He, C. Sha, D. Zhao, Y. Peng. Experimental investigation and thermodynamic modeling of the Mn–Ni–Si system. CA.LPHAD: Computer Coupling of Phase Diagrams and Thermochemistry. 35 (2011). 346 – 354.

[6]. P. S. Lee, D. Mangelinck, K. L. Pey, J. Ding, J. Y. Dai, C. S. Ho, A. See. On the Ni–Si phase transformation with/without native oxide. Microelectronic Engineering. 51 – 52 (2000). 583 – 594.

[7]. V. Raghavan. Fe-Ni-Si (Iron-Nickel-Silicon). Journal of Phase Equilibria. 24 (2003). 269 – 271.

[8]. J. C. Schuster, Y. Du. Experimental Investigation and Thermodynamic Modeling of the Cr-Ni-Si System. Metallurgical and Materials Transactions A. 31A (2000). 1795 – 1803.

[9]. W. Sun, H. Xu, S. Liu, Y. Du, Z. Yuan, B. Huang, Phase equilibria of the Cu-Ni-Si system at 700˚C. Journal of Alloys and Compounds, 509 (2011). 9776 – 9781.

[10]. T. Tokunaga, K. Nishio, M. Hasebe. Thermodynamic Study of Phase Equilibria in the Ni-Si-B System. Journal of Phase Equilibria, 22 (2001). 291 – 299.

[11]. Diagrammy sostoyaniya dvoinykh metallicheskikh sistem. Spravochnik [In Russian] (Phase Diagrams of Binary Metallic Systems), N. P. Lyakishev, Ed. Moscow: Mashinostroenie, 1997. Vol. 3. Book 1. pp. 641 – 643.

[12]. Phase diagram – Web. FactSage Database. – URL: <http://www.crct.polymtl.ca/fact/documentation> (Access Date – 22. VI. 2012).

[13]. M. Lindholm, B. Sundman. A Thermodynamic Evaluation of the Nickel-Silicon System. Metallurgical and Materials Transactions A, 27A (1996). 2897 – 2903.

[14]. T. Tokunaga, K. Nishio, H. Ohtani, M. Hasebe. Thermodynamic assessment of the Ni–Si system by incorporating ab initio energetic calculations into the CALPHAD approach. Si system. CA.LPHAD: Computer Coupling of Phase Diagrams and Thermochemistry. 27 (2003). 161 – 168.

[15]. X. Yuan, L. Zhang, Y. Du, W. Xiong, Y. Tang, A. Wang, S. Liu. A new approach to establish both stable and metastable phase equilibria for fcc ordered/disordered phase transition: application to the Al-Ni and Ni-Si systems. Materials Chemistry and Physics. 135 (2012). 94 – 105.

[16]. J. Acker, K. Bohmhammel. Optimization of thermodynamic data of the Ni – Si system. Thermochimica Acta, 337 (1999). 187 – 193.

[17]. B. M. Mogutnov, I. A. Tomilin, L. A. Shvarzman. Termodinamika splavov zheleza [In Russian] (Thermodynamics of Iron Alloys). Moscow: Metallurgiya, 1984.

[18]. L. P. Ruzinov, B. S. Gulyanitskii. Ravnovesnye prevrashcheniya metallurgicheskikh reaktsii: spravochnik [In Russian] (Equilibrium Transformations in Metallurgical Reactions: Handbook). Moscow: Metallurgiya, 1975.
[19]. Thermal Constants of Substances: Database. – URL: <http://www.chem.msu.su/cgi-bin/tkv.pl?show=welcome.html> (Access Date – 22. VI. 2012).
[20]. L. B. Pankratz, J. M. Stuve, M. A. Gokcen. Thermodynamic Data for Mineral Technology: Handbook, Bureau of Mines, USA, 1984.
[21]. U. D. Veryagin et al. Termodinamicheskie svoistva neorganicheskikh veshchestv: spravochnik [In Russian] (Thermodynamic Properties of Inorganic Substances: Handbook), Zefirov, A. P., Ed. Moscow: Atomizdat, 1965.
[22]. A. T. Dinsdale. SGTE Data for Pure Elements. CALPHAD, 15 (1991). 317 – 425.
[23]. D. M. Laptev. Termodinamika metallurgicheskikh rastvorov [In Russian] (Thermodynamics of Metallurgical Solutions). Chelyabinsk: Metallurgija, 1992.
[24]. I. Ansara, B. Sundman, P. Willemin. Thermodynamic Modeling of Ordered Phases in Ni-Al System. Acta Metallurgica, 36 (1988). 977 – 982.
[25]. B. Sundman, J. Ågren. A regular solution model for phases with several components and sublattices suitable for computer applications. Journal of Physical Chemistry of Solids, 42 (1981). 297 – 301.
[26]. L. Kaufman. Coupled Phase Diagrams and Thermochemical Data for Transition Metal Binary System – VI. CALPHAD, 3 (1979). 45 – 76.
[27]. N. A. Toropov, V. P. Borzakovskiy. Diagrammy sostoyaniya silikatnykh system [In Russian] (Phase Diagrams of Silicate Systems). Vol. 2. Leningrad: Khimiya, 1965.
[28]. Yu. D. Tret'yakov. Khimiya nestekhiometricheskikh okislov [In Russian] (The Chemistry of Nonstoichiometric Oxides). Moscow: Izd. Mosk. Gos. Univ., 1974.
[29]. A. G. Morachevskii. Termodinamika sistemy nikel' – kislorod (Thermodynamics of Nickel – Oxygen System): in Morachevskii, A.G., Tsemekhman, L.Sh., and Tsymbulov, L.B., Termodinamika sistem i protsessov v metallurgii nikelya i medi [In Russian] (Thermodynamics of Systems and Processes in the Metallurgy of Nickel and Copper). St. Petersburg: Izd. Politekhn. Univ., 2008. Issue 12.
[30]. D. P. Bogatskii, I. A Mineeva. Fiziko-khimicheskoye issledovaniye struktury i svoistv kislorodnykh soyedineniy nikelya [In Russian] (Physical and Chemical Investigation of Structure and Properties of Oxygen Compounds of Nickel). Russian Journal of General Chemistry. 29 (1959). 1382 – 1390.
[31]. Yu. G. Shirokov, I. P. Kirillov. Nekotoryye magnitnyye svoistva zakisi nikelya [In Russian] (Some Magnetic Properties of Nickel Monoxide) Izvestiya Vysshykh Uchebnykh Zavedeniy, Khimiya i Khimicheskaya. Tekhnologiya, 4 (1961). 599 – 603.
[32]. Gmelins Handbuch der anorganischen Chemie [In German]. 8 Auflage. Nickel. Teil B. Lieferung 2. Vienheim: Verlag Chemie, 1966. pp. 376 – 389.
[33]. P. A. Nikolaychuk, A. G. Tyurin Thermodynamics of Chemical and Electrochemical Stability of Copper-Nickel Alloys. Protection of Metals and Physical Chemistry of Surfaces, 48 (2012). 462 – 476.
[34]. N. P. Zhuk. Kurs teorii korrozii i zashchity metallov: uchebnoye posobie dlya vuzov [In Russian] (Textbook on the Theory of Corrosion and Metal Protection. University Course), Moscow: Al'yans, 2006.
[35]. P. A. Nikolaychuk, A. G. Tyurin Method of estimating the standard Gibbs energies of formation of binary compounds. Abstracts of the XVIII International Conference on Chemical Thermodynamics in Russia (RCCT-2011). Samara, 2011. Vol. 2. pp. 17 – 18.
[36]. Spravochnik po elektrokhimii [In Russian] (Handbook of Electrochemistry), A. M. Sukhotin Ed. Leningrad: Khimiya, 1981.
[37]. K. T. Jacob, A. K. Shukla. Kinetic decomposition of Ni_2SiO_4 in oxygen potential gradients. Journal of Materials Research, 2 (1987). 338 – 344.
[38]. A. Navrotsky. Thermodynamics of Formation of the Silicates and Germanates of some Divalent Transition Metals and of Magnesium. Journal of Inorganic and Nuclear Chemistry, 33 (1971). 4035 – 4050.
[39]. G. Róg, G. Borchard. Thermodynamics of nickel orthosilicate. Journal of Chemical Thermodynamics, 16 (1984). 1103 – 1105.
[40]. R. A. Robie, B. S. Hemingway, J. Ito, K. N. Krupka. Heat capacity and entropy of Ni_2SiO_4-olivine from 5 to 1000 K and heat capacity of Co_2SiO_4 from 360 to 1000 K. American Mineralogist, 69 (1984). 1096 – 1101.
[41]. J. Wolfenstine, D. Dimos, D. L. Kohlstedt. Decomposition of Ni_2SiO_4 in an Oxygen Potential Gradient. Journal of the American Ceramic Society, 68 (1985). C-117 – C-118.

[42]. A. G. Tyurin. Termodinamika khimicheskoi i elektrokhimicheskoi ustoichivosti tverdykh splavov zheleza, khroma i nikelya [In Russian] (Thermodynamics of Chemical and Electrochemical Stability of Solid Iron, Chromium, and Nickel Alloys). Chelyabinsk: Publishing House of Chelyabinsk State University, 2011.
[43]. L. Kish. Kinetics of Electrochemical Metal Dissolution. Budapest: Akademiai Kiado, 1988.
[44]. Pourbaix diagrams / Substances & Technologies. – URL: <http://www.substech.com/dokuwiki/doku.php?id=pourbaix_diagrams> (Access Date – 22. VI. 2012).
[45]. Spravochnik khimika [In Russian] (Chemist's Handbook). B. P. Nikol'skii. Ed. Moscow: Khimiya, 1964. Vol. 3.
[46]. J. W. Ball, D. K. Nordstrom. User's manual for WATEQ4F with revised thermodynamic data base and test cases for calculating speciation of major, trace and redox elements in natural waters US geological survey. Open-file report 91-183. – URL: <http://wwwbrr.cr.usgs.gov/projects/GWC_chemtherm/pubs/wq4fdoc.pdf> (Access Date – 22. VI. 2012).
[47]. J. W. Johnson, E. H. Oelkers, H. C. Helgeson. SUPCRT92: A software package for calculating the standard molal thermodynamic properties of minerals, gases, aqueous species, and reactions from 1 to 5000 bar and 0 to 1000°C. Computers & Geosciences, 16 (1992). 899 – 947.
[48]. FactSage EpH-Web. – URL: <http://www.sgte.org/ephweb.php> (Access Date – 22. VI. 2012).
[49]. THERMEXPERT – Potential – pH diagram generator / Argentum Solutions, Inc. – URL: <http://www.argentumsolutions.com/cgi-bin/thermexpert> (Access Date – 22. VI. 2012).
[50]. SUPCRT / Prediction Central. – URL: <http://www.predcent.org/download/supcrt.html> (Access Date – 22. VI. 2012).
[51]. The Geochemist's Workbench (GWB). – Rockware: Earth Science and GIS Software. – URL: <http://www.rockware.com/product/overview.php?id=132> (Access Date – 22. VI. 2012).
[52]. JNC-TDB. – Japan Nuclear Cycle Organization. – URL: <http://migrationdb.jnc.go.jp> (Access Date – 18. XII. 2011).
[53]. ZZ-HATCHES 19: Database for radiochemical modeling / Nuclear Energy Agency. – URL: <http://www.oecd-nea.org/tools/abstract/detail/nea-1210> (Access Date – 22. VI. 2012).
[54]. PHREEQC-2: A Computer Program for speciation, batch-reaction, one-dimensional transport, and inverse geochemical calculations / USGS. – URL: <http://wwwbrr.cr.usgs.gov/projects/GWC_coupled/phreeqc> (Access Date – 22. VI. 2012).
[55]. SOLGASWATER program. – URL: <http://158.227.5.164/Chemical_Diagrams/html/ISP_Solgaswater.htm> (Access Date – 22. VI. 2012).
[56]. Atlas of Eh-pH diagrams: Intercomparison of thermodynamic databases. Geological survey of Japan. Open file report № 419. National Institute of Advanced Industrial Science and Technology, 2005. – URL: <www.gsj.jp/GDB/openfile/files/no0419/openfile419e.pdf> (Access Date – 22. VI. 2012).
[57]. K. Zeng, T. Klassen, W. Oelerich, R. Bormann. Thermodynamics of the Ni–H system. Journal of Alloys and Compounds, 283 (1999). 151 – 161.
[58]. K. Zeng, T. Klassen, W. Oelerich, R. Bormann. Thermodynamic analysis of the hydriding process of Mg–Ni alloys. Journal of Alloys and Compounds, 283 (1999). 213 – 224.
[59]. B. Baranowski, K. Bocheńska. The Tree Energy and Entropy of Formation of Nickel Hydride. Zeitschrift für Physikalishe Chemie Neue Folge, 45 (1965). 140 – 152.
[60]. G. N. Markos'yan, D. S. Sirota, A. P. Pchel'nikov. Corrosion of Hydrides of Nickel and Cu30Ni Alloy in Oxygen Containing Solutions. Protection of Metals, 41 (2005). 358 – 362.
[61]. D. S. Sirota, A. P. Pchel'nikov. Electrochemical Behavior of α-Phase of the Cu30Ni System in Sodium Hydroxide Solutions. Protection of Metals, 41 (2005). 603 – 606.
[62]. D. S. Sirota, A. P. Pchel'nikov. Electrochemical Behavior of β-Phase of the Cu30Ni System in Sodium Hydroxide Solutions. Protection of Metals, 41 (2005). 553 – 556.
[63]. A. B. Shein, I. L. Sergeeva. Corrosion-Electrochemical Behavior of Nickel Monosilicide in Alkaline Electrolyte. Protection of Metals, 40 (2004). 556 – 561.
[64]. I. L. Rakityanskaya, A. B. Shein. Anodic Behavior of Iron, Cobalt, and Nickel Silicides in Alkaline Electrolytes. Russian Journal of Electrochemistry, 42 (2006). 1208 – 1212.
[65]. A. B. Shein, O. S. Ivanova, R. N. Minkh. The Effect of Anions on the Anodic Dissolution of Nickel Silicide in Sulfate Electrolytes. Protection of Metals, 44 (2008). 32 – 38.
[66]. A. B. Shein. Effect of the Metal Component on Anodic Dissolvability of Iron, Cobalt, and Nickel Silicides. Protection of Metals, 37 (2001). 281 – 283.
[67]. A. B. Shein, O. V. Kanaeva. Peculiarities of the Anodic Dissolution of a Powder NiSi Electrode. Protection of Metals, 37 (2001). 385 – 388.

[68]. R. G. Aitov, A. B. Shein. Elektrokhimicheskoye povedeniye monosilicida nikelya v sernoy kislote [In Russian].(Electrochemical Behaviour of Nickel Monosilicide in Sulphuric Acid). Elektrokhimiya. 29 (1993). 611-615.
[69]. R. G. Aitov, A. B. Shein. Vliyaniye ftorid-ionov na anodnoye povedeniye silicidov zheleza, nikelya i kobal'ta [In Russian] (Influence of Anions on Anodic Behaviour of Iron, Nickel and Cobalt Silicides). Zashchita Metallov, 30 (1994). 439-440.
[70]. A. B. Shein. Elektrokhimicheskoye povedeniye monosilicida nikelya v sernokislom elektrolite, soderzhashchem ftorid-iony [In Russian] (Electrochemical Behaviour of Nickel Monosilicide in Sulphuric Acid Electrolyte Containing Fluoride-Ions). Elektrokhimiya. 34 (1998). 900-903.
[71]. T. E. Evans, A. C. Hart. Corrosion and Passivation of a Nickel-Silicon-Base Alloy in Sulphuric Acid Solutions. Electrochimica Acta, 16 (1971). 1955 – 1970.
[72]. X. B. Liu, L. G. Yu, H. M. Wang. Synthesis of a nickel silicide-base composite coating on austenitic steel by laser cladding. Journal of Materials Science Letters, 20 (2001). 1489 – 1492.
[73]. G. Rife, P. C. C. Chan, K. T. Aust, Y. Waseda. Corrosion of Iron-, Nickel- and Cobalt-base Metallic Glasses Containing Boron and Silicon Metalloids. Materials Science and Engineering, 48 (1981). 73 – 79.
[74]. J. Daimer, E. Fitzer, J. Schlichting. New Results and the Oxidation and Hot Corrosion of Silicide Overlay Coatings on Nickel-Base Alloys. Thin Solid Films, 84 (1981). 119 – 125.
[75]. H. M. Wang, C. M. Wang, L. X. Cai. Wear and corrosion resistance of laser clad Ni_2Si / NiSi composite coatings. Surface and Coatings Technology, 168 (2003). 202 – 208.

15. Cu – Si system

Alloying of copper alloys with silicon allows increasing their durability, plasticity, improving their mechanical, foundry and anticorrosive properties. Siliceous bronzes and brasses are very cheap substitutes for tin bronzes. In addition, silicon can be included in other copper-based alloys with aluminium, nickel, manganese. Therefore, Cu – Si system is a very important binary system for the metallurgy and chemical technology. The chemical and electrochemical stability of the Cu – Si system was already assessed earlier [Tyurin, 2008]. However, that study did not take into account all features of the system and relied on the outdated thermodynamic information. Therefore, a new assessment was performed.

15.1. Copper silicides

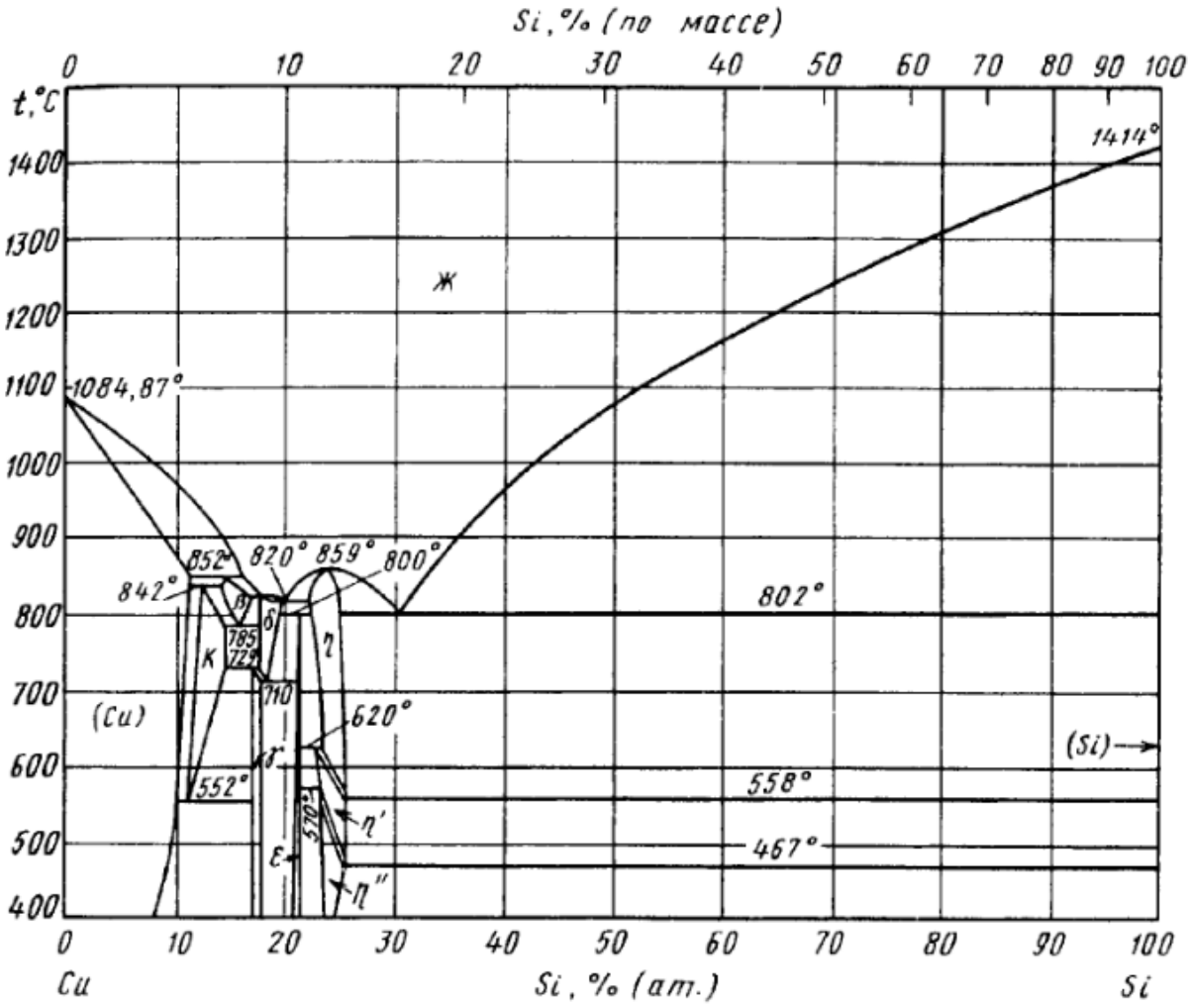

Fig. 61. The phase diagram of Cu – Si system [Диаграммы состояния двойных металлических систем: справочник, 2001].

The phase diagram of Cu – Si system is presented in Figure 61. In the system at 25˚C the existence of the following copper silicides was approved [Yan, Chang, 2000]: $Cu_{56}Si_{11}$ (γ-phase), $Cu_{15}Si_4$ (ε-phase) and $Cu_{19}Si_6$ (η”-phase). Despite all copper silicides have, in greater or lesser degree, the homogeneity range, it is negligibly small at the standard temperature, and the silicides can be assumed as daltonides. Additionally, a solid solution of Si in (fcc-Cu) (α-phase) exist in copper-rich copper of system. The expression for the excess Gibbs energy of α-phase was taken from [Yan, Chang, 2000]. The calculated silicon maximum solid solubility in α-phase at standard temperature slightly exceeds 4 atomic %. Thermodynamic activities of the components of saturated solid solution are the following: $a_{Cu(\alpha)} = 0.92, a_{Si(\alpha)} = 5.6 \cdot 10^{-8}$. The standard Gibbs energies of formation of copper silicides were estimated using the Gorichev's method. More details are presented in the attached publication.

15.2. Equilibira in Cu – Si – O system

In addition to well-known oxides Cu_2O and CuO copper can also form a Cu_2O_3 compound [Moiseev, Vatolin, 1997]. Only one ternary compound exists in Cu – Si – O ternary system, it is copper silicate $CuSiO_3$ [Navrotsky, 1971]. The standard Gibbs energies of formation of copper oxides and silicate were collected from [Chase Jr. et al., 1985; Moiseev, Vatolin, 1997; Термические константы веществ, 2007].

The state diagram of Cu – Si – O system and the list of equilibria in this system are presented in the attached publication.

15.3. Potential – pH diagram of Cu – H_2O system

Copper in an aqueous solution could form the cations Cu^+ and Cu^{2+} and the anions $HCuO_2^-$ and CuO_2^{2-}. However, aqueous Cu^+ and $HCuO_2^-$ are stable only at very low copper concentrations.

Despite copper hydride $CuH_{0,8}$ is not stable in air, it was shown [Funk, Reinstrom, 1966; Korzhavyi et al., 2011; Vaškelis, Juškėnas, Jačiauskienė, 1998], that it can be obtained during copper electrochemical reduction. The value of standard Gibbs energy of formation for copper hydride was determined by [Andreasen, 2004; Burtovyy et al., 2003; Tkacz, Burtovyy, 2004].

The potential – pH diagram of Cu – H_2O system at 25 °C, air pressure of 1 bar and the activities of copper species ranging from 1 to 10^{-6} mol·l^{-1} is presented in the attached publication.

15.4. Potential – pH diagram of Cu – Si – H_2O system

The potential – pH diagram of Cu – Si – H_2O system is presented in the attached publication.

The corrosion behaviour of Cu – Si system differs strongly depending on the composition of both the system and the solution. Several compounds, including copper oxides, silicic acids and copper silicate, as well as various aqueous species, have the domains of prevalence in the area of electrochemical stability of water. The composition of the protective passivation layer on the Cu – Si system alloys would vary depending on environmental conditions.

Publications to chapter 15

The potential – pH diagram for Cu – H_2O sysetm was presented in the conference paper [Николайчук, Канатьева, Тюрин, 2010]. The preprint is presented here with figures and tables translated into English.

The potential – pH diagram for Cu – Si – H_2O system was published in the paper [Николайчук, Тюрин, 2011d]. The paper was translated into English with the permission of *Butlerovskoe Nasledie* and posted as a preprint at the website of *Research Gate* (DOI 10.13140/2.1.2410.7201). This English version is presented below.

УТОЧНЁННАЯ ДИАГРАММА ПУРБЕ ДЛЯ МЕДИ

Николайчук П. А., Тюрин А. Г., Канатьева И. И.

ГОУ ВПО “Челябинский государственный университет”,
454021, г. Челябинск, ул. Братьев Кашириных, 129
npa@csu.ru

Одним из наиболее значительных достижений электрохимии 60-х годов XX века является построение диаграмм электрохимического равновесия (диаграмм потенциал – pH), названных в честь автора диаграммами Пурбе, для всех важных металлов [1]. Однако, с учётом данных последних лет, многие из них нуждаются в принципиальной корректировке. Так, в диссертации [2] уточнены диаграммы Пурбе для хрома, титана, никеля и молибдена. В настоящей работе уточняется диаграмма Пурбе для меди.

Диаграмма потенциал – pH для системы Cu – H_2O, построенная М. Пурбе [1], предполагает существование твёрдых фаз (Cu, Cu_2O, CuO или $Cu(OH)_2$) и ионов (Cu^{2+}, $HCuO_2^-$, CuO_2^{2-}) в растворе. В диссертации [3] обобщены работы предшественников и получены собственные экспериментальные данные, свидетельствующие о том, что анодные процессы на медном электроде в 4М растворе KOH, соответствующие анодному пику в области 0,7 – 0,8 В (н. в. э.), соответствуют образованию сексвиоксида меди Cu_2O_3. Авторами работы [4] при выполнении равновесных компьютерных экспериментов были рассчитаны термодинамические характеристики для Cu_2O_3: $\Delta_f H^o_{298} = -355$ $^{кДж}/_{моль}$, $S^o_{298} = 100 \pm 11{,}7$ $^{Дж}/_{моль\cdot K}$. Расчёты показывают, что температура разложения Cu_2O_3 по реакции Cu_2O_3(т) → 2CuO(т) + 0,5O_2(г) на воздухе при давлении 1 атм. составляет 350 К. Это согласуется с данными [5, 6] (~ 373 К).

Для того, чтобы включить Cu_2O_3 в диаграмму потенциал – pH для меди, рассчитаны характеристики основных химических и электрохимических равновесий в системе Cu – H_2O при 25°C и 1 атм. (воздух). В расчётах использованы данные [4, 7 – 9]. Результаты расчётов представлены в таблице. Диаграмма потенциал – pH системы Cu – H_2O при активностях ионов в растворе 1 $^{моль}/_{л}$ (линия 0), 10^{-2} $^{моль}/_{л}$ (линия –2) и 10^{-4} $^{моль}/_{л}$ (линия –4) представлена на рисунке 1, а при активностях ионов в растворе 10^{-6} $^{моль}/_{л}$ – на рисунке 2.

Table. The basic chemical and electrochemical equilbiria in the Cu – H_2O system at 25°C and ari pressure of 1 bar.

No of line	Electrode reaction	Equilibrium potential, V (s. h. e.) or pH of the solution
a	$2H^+ + 2e^- = H_2; P_{H_2} \approx 5 \cdot 10^{-7}$ атм.	$0{,}186 - 0{,}0591 \cdot pH$
b	$O_2 + 4H^+ + 4e^- = 2H_2O; P_{O_2} \approx 0{,}21$ атм.	$1{,}219 - 0{,}0591 \cdot pH$
1	$Cu^{2+} + 2e^- = Cu$	$0{,}337 + 0{,}0295 \cdot \lg a_{Cu^{2+}}$
2	$Cu_2O + 2H^+ + 2e^- = 2Cu + H_2O$	$0{,}439 - 0{,}0591 \cdot pH$
3	$CuO_2^{2-} + 4H^+ + 2e^- = Cu + 2H_2O$	$1{,}494 - 0{,}1182 \cdot pH + 0{,}0295 \cdot \lg a_{CuO_2^{2-}}$
4	$2Cu^{2+} + H_2O + 2e^- = Cu_2O + 2H^+$	$0{,}235 + 0{,}0591 \cdot pH + 0{,}0591 \cdot \lg a_{Cu^{2+}}$
5	$2CuO + 2H^+ + 2e^- = Cu_2O + H_2O$	$0{,}658 - 0{,}0591 \cdot pH$
6	$2HCuO_2^- + 4H^+ + 2e^- = Cu_2O + 3H_2O$	$1{,}771 - 0{,}1182 \cdot pH + 0{,}0591 \cdot \lg a_{HCuO_2^-}$
7	$2CuO_2^{2-} + 6H^+ + 2e^- = Cu_2O + 3H_2O$	$2{,}549 - 0{,}1773 \cdot pH + 0{,}0591 \cdot \lg a_{CuO_2^{2-}}$
8	$CuO + 2H^+ = Cu^{2+} + H_2O$	$pH = 3{,}58 - 0{,}5 \cdot \lg a_{Cu^{2+}}$
9	$HCuO_2^- + H^+ = CuO + H_2O$	$pH = 18{,}83 + \lg a_{HCuO_2^-}$
10	$CuO_2^{2-} + H^+ = HCuO_2^-$	$pH = 13{,}16 + \lg \frac{a_{CuO_2^{2-}}}{a_{HCuO_2^-}}$
11	$CuO_2^{2-} + 2H^+ = CuO + H_2O$	$pH = 15{,}99 + 0{,}5 \cdot \lg a_{CuO_2^{2-}}$
12	$Cu_2O_3 + 6H^+ + 2e^- = 2Cu^{2+} + 3H_2O$	$1{,}566 - 0{,}1773 \cdot pH - 0{,}0591 \cdot \lg a_{Cu^{2+}}$
13	$Cu_2O_3 + 2H^+ + 2e^- = 2CuO + H_2O$	$1{,}143 - 0{,}0591 \cdot pH$
14	$Cu_2O_3 + H_2O + 2e^- = 2HCuO_2^-$	$0{,}030 - 0{,}0591 \cdot \lg a_{HCuO_2^-}$
15	$Cu_2O_3 + H_2O + 2e^- = 2CuO_2^{2-} + 2H^+$	$-0{,}748 + 0{,}0591 \cdot pH - 0{,}0591 \cdot \lg a_{CuO_2^{2-}}$

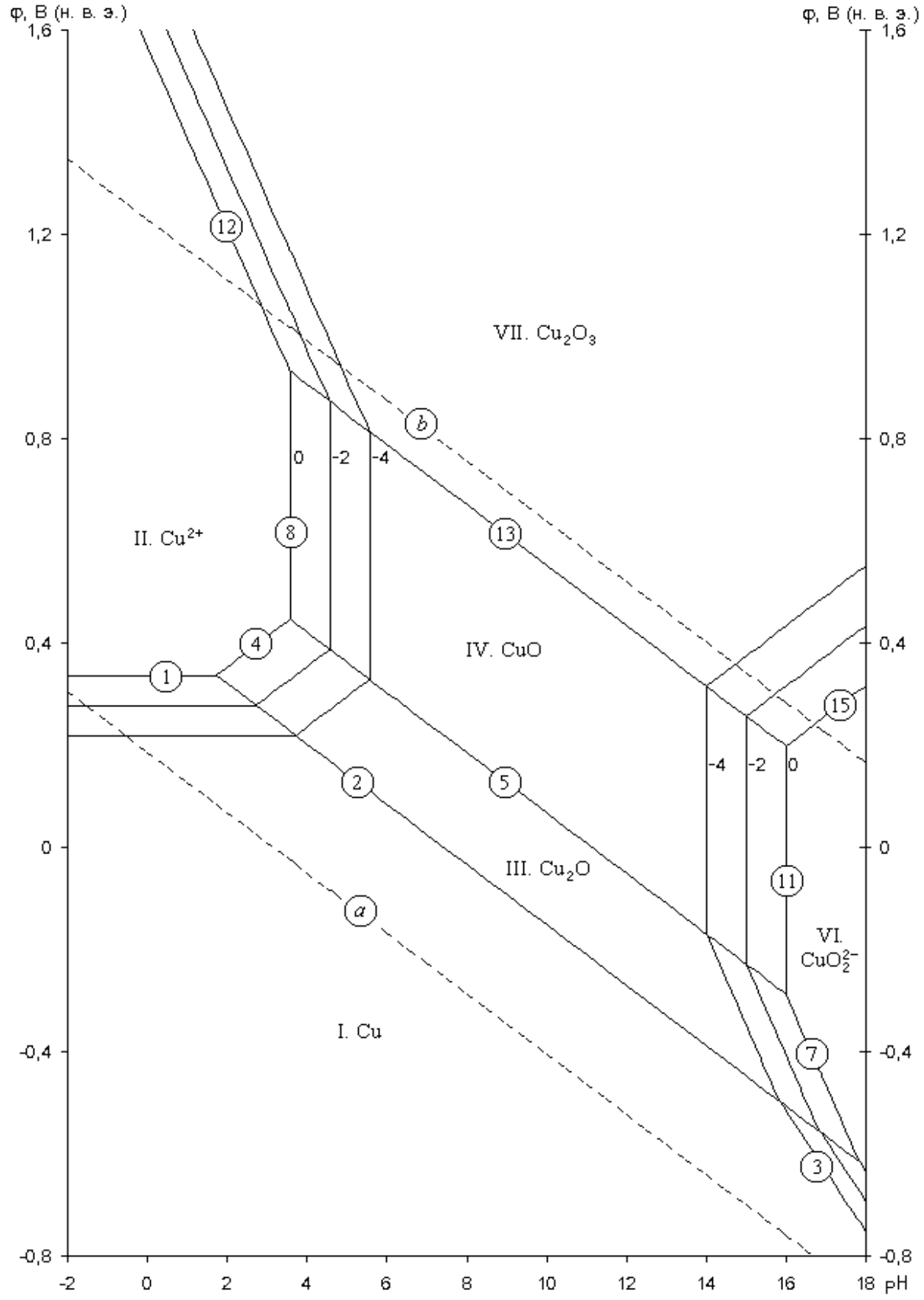

Fig. 1. The potential – pH diagram of the Cu – H_2O system
at 25˚C, air pressure of 1 bar and $a_i = 1 - 10^{-4}$ моль/л (unhydrated form of oxides).

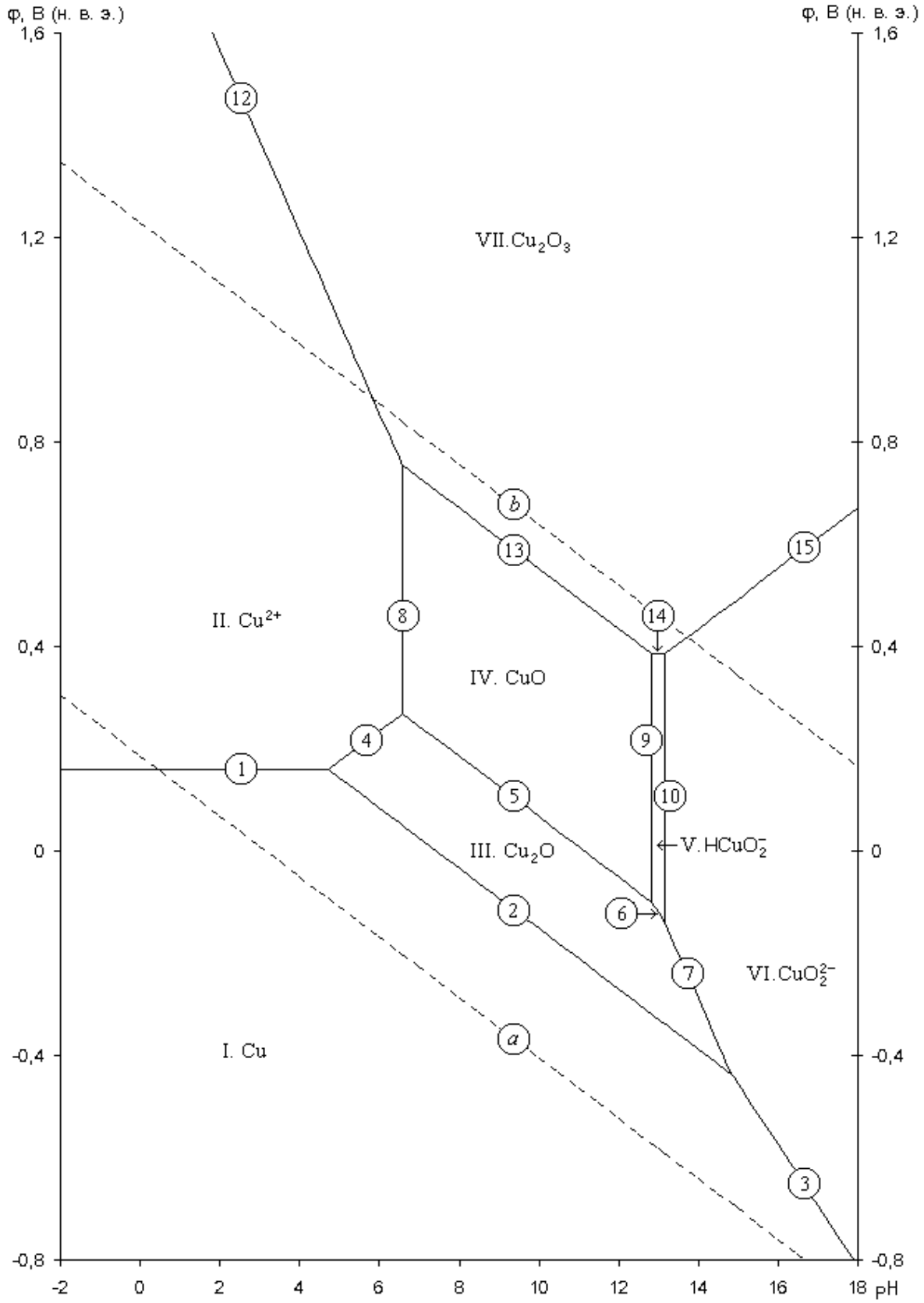

Fig. 2. The potential – pH diagram of the Cu – H_2O system
at 25°C, air pressure of 1 bar and $a_i = 10^{-6}$ моль/л (undydrated form of oxides).

Различия в виде диаграмм при различных активностях связаны со следующим обстоятельством. Как показывают расчёты, ион $HCuO_2^-$ термодинамически устойчив лишь при очень малых активностях ионов в растворе ($\lg a_i < -5{,}68$). В этом случае реализуется следующая последовательность равновесий: $CuO|HCuO_2^-|CuO_2^{2-}$ (см. рис. 2, линии 9 и 10). В более концентрированных растворах ион $HCuO_2^-$ становится неустойчивым, и окисление протекает по схеме $CuO|CuO_2^{2-}$ (см. рис. 1, линия 11).

При построении диаграммы рассмотрена только негидратированная форма оксидов, как наиболее устойчивая. Переход от негидратированной формы оксидов (Cu_2O, CuO) к гидратированной форме ($CuOH$, $Cu(OH)_2$) происходит последовательно, через метастабильные промежуточные состояния, которые не принимаются во внимание.

Результаты расчётов части диаграммы, содержащей равновесия с участием Cu_2O_3, хорошо согласуются с экспериментальными данными работы [3].

В общем случае на диаграмме потенциал – pH системы Cu – H_2O можно выделить 7 областей преобладания различных фаз. Область I – область иммунности меди, при данных значениях равновесных потенциалов и pH медь коррозии не подвергается. Область II – область активной коррозии, в которой медь переходит в раствор в виде катионов Cu^{2+}. Области III, IV и VII – области пассивности. При данных значениях потенциалов и pH на поверхности меди образуется защитная пассивирующая плёнка, состоящая из оксидов Cu_2O (область III) и CuO (область IV), которая препятствует дальнейшему окислению металла. Области V и VI – области транспассивности, в которых оксидная плёнка на металле переходит в раствор в виде анионов $HCuO_2^-$ или CuO_2^{2-}. Оксид Cu_2O_3 (область VII) не образует отдельную фазу, а входит в состав пассивирующей плёнки в виде локальных включений.

Линии *a* и *b* соответствуют водородному и кислородному электродам и определяют область электрохимической устойчивости воды.

Список использованной литературы:

1. Справочник химика [Текст] / под ред. Б. П. Никольского. – М. – Л.: Химия, 1964. – Т. 3. – 1008 с.
2. Тюрин, А. Г. Термодинамика химической и электрохимической устойчивости сплавов: автореф. дисс… док. хим. наук [Текст] / А. Г. Тюрин. – Челябинск: изд-во ЧелГУ, 2008. – 40 с.
3. Шарлай, Е. В. Особенности электрохимического поведения системы медь – раствор гидроксида калия в области температур 295 – 320 К: автореф. дисс. канд. хим. наук [Текст] / Е. В. Шарлай. – Челябинск: изд-во ЮУрГУ, 2008. – 19 с.
4. Моисеев, Г. К. Температурные зависимости приведённой энергии Гиббса некоторых неорганических веществ: альтернативный банк данных ASTRA. OWN [Текст] / Г. К. Моисеев, Н. А. Ватолин, Л. А. Маршук, Н. И. Ильиных. – Екатеринбург: УрОРАН, 1997. – 230 с.
5. Краткая химическая энциклопедия [Текст] / под ред. И. Л. Кнунянца. – М.: Сов. энциклопедия, 1964. – Т. 3. – С. 68.
6. Физико-химические свойства окислов: справочник [Текст] / под ред. Г. В. Самсонова. – М.: Металлургия, 1978. – 472 с.
7. Рузинов, Л. П. Равновесные превращения металлургических реакций [Текст] / Л. П. Рузинов, Б. С. Гуляницкий. – М.: Металлургия, 1975. – 460 с.
8. Справочник по электрохимии [Текст] / под ред. А. М. Сухотина. – Л.: Химия, 1981. – 448 с.
9. Термические константы веществ: база данных [Электронный ресурс] / руководители проекта В. С. Иориш, В. С. Юнгман. – URL: <http://www.chem.msu.su/cgi-bin/tkv.pl?show=welcome.html> (дата обращения – 05. 05. 2010 г.)

Публикация доступна для обсуждения в интернет как материал "Всероссийской рабочей химической конференции "*Бутлеровское наследие-2011*". http://butlerov.com/bh-2011/
УДК 541.1:620.193.01:669.14. Поступила в редакцию 13 января 2011 г.

Thermodynamics of Chemical and Electrochemical Stability of Cu–Si System Alloys

© **Pavel Anatolyevich Nikolaychuk** [+] and **Aleksandr Georgievich Tyurin***
Department of Analytical and Physical Chemistry. Chelyabinsk State University. Brat'ev Kashirinykh Street, 129,Chelyabinks, 454026, Russia. Phone:+7 (351)799-70-69.
E-mail:npa@csu.ru, tag@csu.ru.

*Supervisor; [+]Corresponding author

Keywords: *copper silicides, low temperature oxidation, chemical stability, diagram of electrochemical equilibrium, electrochemical stability.*

Abstract

The state diagram of Cu–Si–O system and the potential – pH diagram of Cu–Si–H_2O system at 25 ^oC, air pressure of 1 bar and activities of ions in solution, equal to 1 and 10^{-6} mole/l are plotted. A corrosion – electrochemical behaviour of Cu–Si system alloys in aqueous solutions is considered from the thermodynamical point of view.

Introduction

Alloying of copper alloys with silicon allows increasing their durability, plasticity, improving their mechanical, foundry and anticorrosive properties. Siliceous bronzes and brasses are very cheap substitutes for tin bronzes. In addition, silicon can be included in other copper-based alloys – with aluminium, nickel, manganese [1]. Therefore, the "copper – silicon" system is a very important binary system for the metallurgy and chemical technology.

There are no direct experimental data on corrosion – electrochemical behaviour of the Cu – Si system alloys available in the literature. Therefore, the theoretical description of the behaviour of this system in gaseous environments, containing oxygen, and also in aqueous environments is important scientific task. Moreover, thermodynamical analysis of this binary system will allow further using of its results while describing such technologically important ternary systems, as Cu–Zn–Si, Cu–Al–Si, Cu–Ni–Si and Cu–Mn–Si. Earlier [2] the attempt was made to describe the chemical and electrochemical stability of the Cu–Si system alloys, but that work isn't based on the latest version of the Cu–Si phase diagram, and also, doesn't account for all possible equilibria in Cu–H_2O system. The purpose of this study is to revise and complement the Cu–Si–O system state diagram, as well as the diagram of electrochemical equilibrium of the Cu–Si–H_2O system.

Experimental Procedure

The first step towards solving the problem of Cu–Si–O system thermodynamic modelling is the consideration of binary subsystems of this system.

The Cu–Si system phase diagram was investigated and complemented several times. Its latest variant is shown in handbook [3] and in paper [4], the authors of which were generalized and systematized all the available literature data. The following phases exist in copper – silicon system at 25

^{o}C: α-phase (the solid solution, based on fcc-Cu), γ-, ε- and η''-phases, which are the intermediate compounds. Despite all copper silicides have, in greater or lesser degree, the homogeneity range, it is negligibly small at the standard temperature, and the silicides can be assumed as daltonides. According to [4], they have the composition of $Cu_{56}Si_{11}$ (γ), $Cu_{15}Si_4$ (ε) and $Cu_{19}Si_6$ (η'') at low temperature.

There is no published reliable information about the standard Gibbs energies of formation of copper silicides. The authors of [4] make the attempt to estimate these values, but the results of their evaluation is unsatisfactory, because, according to their data, the stability of silicides rises with increasing in temperature, which contradicts the physical meaning. The reference data, which are available [5], correspond to a outdated version of the phase diagram, which refers to the incorrect silicides composition.

Therefore, the decision was made, to evaluate the Gibbs energies of formation of silicides by the Gorichev's method [6], using the modified variant of calculation formula [7], based on the available data from [5]. The source data, as well as the results of calculations, are presented in table 1.

Table 1. The calculation of the standard Gibbs energies of formation of copper silicides from elements.

Reference data [5]		Calculation results	
Compound	$-\Delta_f G^o_{298}$, J/mol)	Compound	($-\Delta_f G^o_{298}$, J/mol)
$Cu_{33}Si_7$	2711960	$Cu_{56}Si_{11}$ (γ)	4266560
$Cu_{15}Si_4$	1513610	$Cu_{15}Si_4$ (ε)	1513610
Cu_3Si	351640	$Cu_{19}Si_6$ (η'')	2162250

The excessive Gibbs energy of α-phase (fcc-Cu solid solution) is described by the authous of [4] by the two-parameter variant of Redlich – Kister power series:

$$G^E = x_{Cu} \cdot x_{Si} \cdot \sum_{i=0}^{1} (L^{(i)}_{Cu,Si} \cdot (x_{Cu} - x_{Si})^i) \qquad (1),$$

where the model parameters have a following dependence on the temperature:

$$L^{(0)}_{Cu,Si} = -42203.5 + 13.89137 \cdot T \qquad (2),$$

$$L^{(1)}_{Cu,Si} = -1102.2 - 18.177912 \cdot T \qquad (3).$$

Only one oxide – SiO_2 – exist in Si – O system at 25°C [3]. The value of $\Delta_f G^o_{298}(SiO_2) = -805067\ ^{J}/_{mole}$ is taken from [8], because this value is compatible with the experimentally measured standard potential of the silicon electrode ($SiO_2 + 4H^+ + 4e^- = Si(diamond) + 2H_2O$, $\varphi^o_{298} = -0{,}857\,B$).

Two oxides – Cu_2O and CuO – are widely known in the Cu – O system [3]. Their thermodynamical characteristics, taken from [9-11], are summarized in table 2. However, it is currently known, that copper (III) oxide can be formed during copper oxidation. The authors of [12] have performed evaluation of its thermodynamical properties: $\Delta_f H^o_{298} = -355\ ^{kJ}/_{mole}$; $S^o_{298} = 100\ ^{J}/_{mole \cdot K}$.

Moreover, the intermediate compound $CuSiO_3$ (copper silicate) can be formed between CuO and SiO_2 [13]. The value of its standard Gibbs energy of formation is also presented in table 2.

Table 2. The values of the standard Gibbs energies of formation of the compounds from elements $-\Delta_f G^o_{298}$, J/mol

Compound \ Reference	[9]	[10]	[11]
Cu_2O	147848	150548	147886
CuO	127890	129365	128292
$CuSiO_3$	949240	–	–

Silicon dioxide can be oxidized to SiO_3^{2-} in aqueous solutions, and copper can form the CuO_2^{2-} and $HCuO_2^-$ ions. All information about chemical and electrochemical equilibria, involving copper, is summarized in study [14], where also the refined potential – pH diagram for pure copper is plotted.

Method of calculating and plotting the Cu – Si – O state diagram and potential – pH diagram of Cu – Si – H_2O system is described in [15].

Results and Discussion

While considering the equilibrium of the α-phase with the γ-phase, the maximum solid solubility of silicon in fcc-Cu at 25 ^oC is calculated. It is slightly more than 4 atomic %. At the same time, the solid solution of Si in (Cu) is characterized by considerable negative deviations from ideal behaviour.

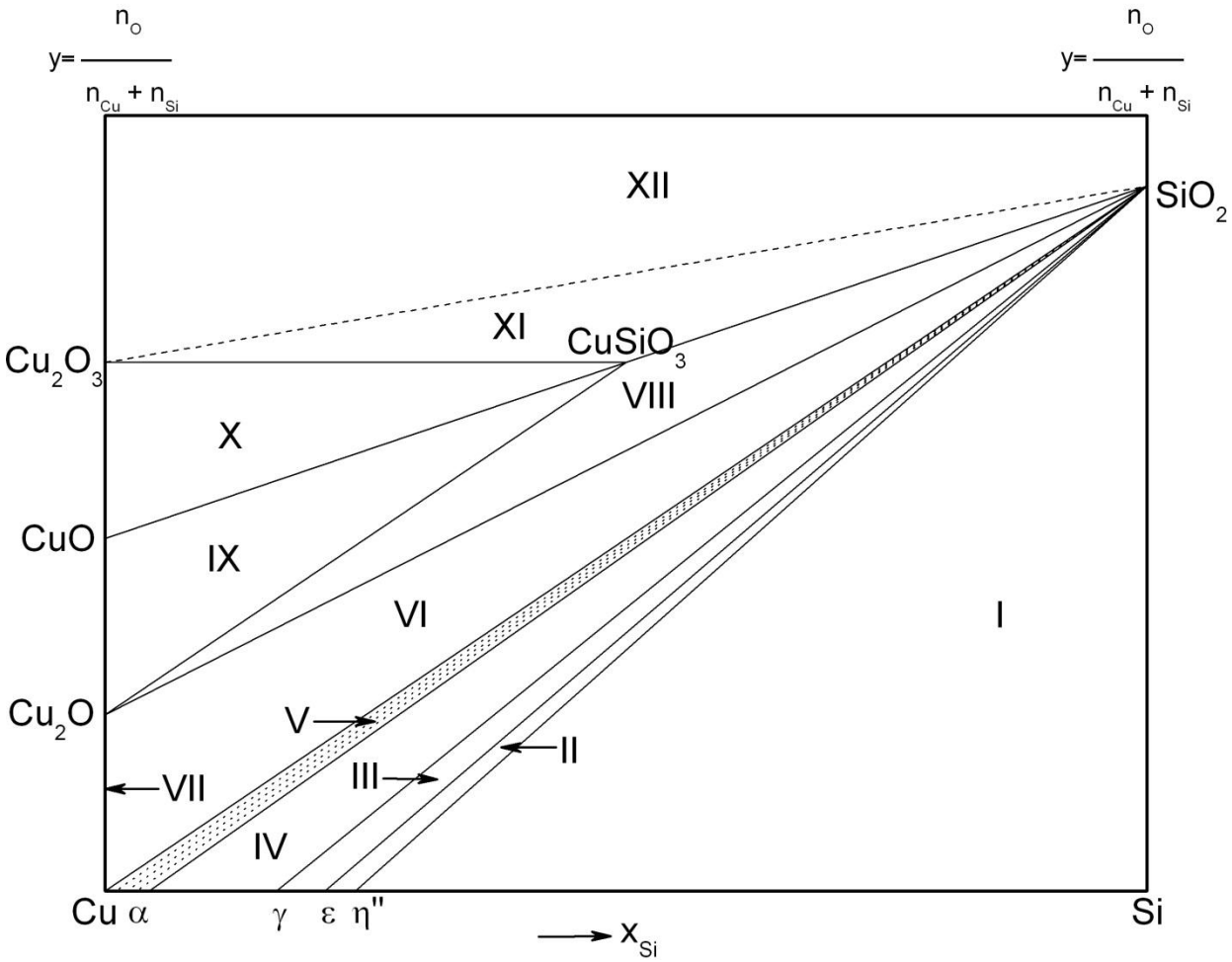

Figure 1. The state diagram of the Cu–Si–O system at 25 oC

The state diagram of the Cu–Si–O system at 25 °C is shown at figure 1. Characteristics of system conditions, referring to certain equilibria, are presented in table 3. If the components, involved in equilibria, aren't pure, their mole fractions and calculated activities are given.

As can be seen from the diagram, the chemical affinity of silicon to oxygen is much greater, than that of copper. Silicon, containing in the Cu – Si alloys, will be the only oxidation product, if its content is more than 10^{-78} atomic %. However, if its percentage in the alloy isn't sufficient to form the continuous film of SiO_2 on the surface, then the copper doesn't remain passivated, and various copper oxides, as well as $CuSiO_3$ will be included into oxide layer.

Basic chemical and electrochemical equilibria in Cu–Si–H_2O system at standard conditions are shown in table 4.

Table 3. The characteristics of the equilibria conditions in the Cu–Si–O system at 25 °C

№ of domain	System condition	Reaction equation	P_{O_2}, bar
I	$Cu_{19}Si_6$–Si–SiO_2	$Si + O_2 = SiO_2$	$7.7 \cdot 10^{-142}$
II	$Cu_{15}Si_4$–$Cu_{19}Si_6$–SiO_2	$15Cu_{19}Si_6 + 4O_2 = 19Cu_{15}Si_4 + 14SiO_2$	$8.3 \cdot 10^{-96}$
III	$Cu_{56}Si_{11}$–$Cu_{15}Si_4$–SiO_2	$56Cu_{15}Si_4 + 59O_2 = 15Cu_{56}Si_{11} + 59SiO_2$	$3.6 \cdot 10^{-80}$
IV	Cu(α)–$Cu_{56}Si_{11}$–SiO_2	$Cu_{56}Si_{11} + 11O_2 = 56Cu(\alpha) + 11SiO_2$ $x_{Si(\alpha)} = 0.042$; $a_{Cu(\alpha)} = 0.92$	$7.0 \cdot 10^{-76}$
V	Cu(α)–SiO_2	$Si(\alpha) + O_2 = SiO_2$	—
VI	Cu(α)–Cu_2O–SiO_2	$4Cu(\alpha) + O_2 = 2Cu_2O$; $Si(\alpha) + O_2 = SiO_2$ $x_{Si(\alpha)} = 1.5 \cdot 10^{-80}$; $a_{Si(\alpha)} = 2.3 \cdot 10^{-88}$; $a_{Cu(\alpha)} \approx 1$	$3.4 \cdot 10^{-54}$
VII	Cu(α)–Cu_2O	$4Cu(\alpha) + O_2 = 2Cu_2O$	—
VIII	Cu_2O–$CuSiO_3$–SiO_2	$2Cu_2O + 4SiO_2 + O_2 = 4CuSiO_3$	$2.4 \cdot 10^{-48}$
IX	Cu_2O–CuO–$CuSiO_3$	$2Cu_2O + O_2 = 4CuO$	$2.2 \cdot 10^{-39}$
X	CuO–Cu_2O_3–$CuSiO_3$	$4CuO + O_2 = 2Cu_2O_3$	$1.4 \cdot 10^{-6}$
XI	Cu_2O_3–$CuSiO_3$–SiO_2	$4CuSiO_3 + O_2 = 2Cu_2O_3 + 4SiO_2$	1282.62
XII	Cu_2O_3–SiO_2–{O_2}	—	—

The potential – pH diagram of the Cu – Si – H_2O system at activities of the ions in solution, equal to 1 mole/l, is shown at figure 2, and at activities of 10^{-6} mole/l – at the figure 3.

21 domains of the thermodynamic stability of certain phased can be depicted at the diagram (see figures. 2 and 3): I – α-phase (Cu) + γ-phase ($Cu_{56}Si_{11}$) + ε-phase ($Cu_{15}Si_4$) + η''-phase ($Cu_{19}Si_6$) + Si; II – α-phase (Cu) + γ-phase ($Cu_{51}Si_{14}$) + ε-phase ($Cu_{15}Si_4$) + η''-phase ($Cu_{19}Si_6$) + SiO_2;

Table 4. Basic chemical and electrochemical equilibria
In the Cu–Si–H_2O system at temperature 25 °C and air pressure of 1 bar

№ of line	Electrode reaction	Equilibrium potential, V (s. h. e.) or solution pH
a	$2H^+ + 2e^- = H_2$; $P_{H_2} \approx 5 \cdot 10^{-7}$ bar	$0.186 - 0.0591 \cdot pH$
b	$O_2 + 4H^+ + 4e^- = 2H_2O$; $P_{O_2} \approx 0{,}21$ bar	$1.219 - 0.0591 \cdot pH$
1	$SiO_2 + 4H^+ + 4e^- = Si + 2H_2O$	$-0.857 - 0.0591 \cdot pH$
2	$SiO_3^{2-} + 6H^+ + 4e^- = Si + 3H_2O$	$-0.444 - 0.0887 \cdot pH + 0.0148 \cdot \lg a_{SiO_3^{2-}}$

3	$14SiO_2 + 19Cu_{15}Si_4 + 56H^+ + 56e^- =$ $= 15Cu_{19}Si_6 + 28H_2O$	$-0.176 - 0.0591 \cdot pH$
4	$14SiO_3^{2-} + 19Cu_{15}Si_4 + 84H^+ + 56e^- =$ $= 15Cu_{19}Si_6 + 42H_2O$	$0.236 - 0.0887 \cdot pH + 0.0148 \cdot \lg a_{SiO_3^{2-}}$
5	$59SiO_2 + 15Cu_{56}Si_{11} + 236H^+ + 236e^- =$ $= 56Cu_{15}Si_4 + 118H_2O$	$0.055 - 0.0591 \cdot pH$
6	$59SiO_3^{2-} + 15Cu_{56}Si_{11} + 354H^+ + 236e^- =$ $= 56Cu_{15}Si_4 + 177H_2O$	$0.467 - 0.0887 \cdot pH + 0.0148 \cdot \lg a_{SiO_3^{2-}}$
7	$11SiO_2 + 56Cu(\alpha) + 44H^+ + 44e^- =$ $= Cu_{56}Si_{11} + 22H_2O;\ a_{Cu(\alpha)} = 0{,}92$	$0.151 - 0.0591 \cdot pH$
8	$11SiO_3^{2-} + 56Cu(\alpha) + 66H^+ + 44e^- =$ $= Cu_{56}Si_{11} + 33H_2O;\ a_{Cu(\alpha)} = 0.92$	$0.563 - 0.0887 \cdot pH + 0.0148 \cdot \lg a_{SiO_3^{2-}}$
9	$SiO_3^{2-} + 2H^+ = SiO_2 + 2H_2O$	$pH = 13.94 + 0.5 \cdot \lg a_{SiO_3^{2-}}$
10	$Cu^{2+} + 2e^- = Cu(\alpha);\ a_{Cu(\alpha)} \approx 1$	$0.337 + 0.0295 \cdot \lg a_{Cu^{2+}}$
11	$Cu_2O + 2H^+ + 2e^- = 2Cu(\alpha) + H_2O;\ a_{Cu(\alpha)} \approx 1$	$0.439 - 0.0591 \cdot pH$
12	$CuO_2^{2-} + 4H^+ + 2e^- = Cu(\alpha) + 2H_2O;\ a_{Cu(\alpha)} \approx 1$	$1.494 - 0.1182 \cdot pH + 0.0295 \cdot \lg a_{CuO_2^{2-}}$
13	$CuSiO_3 + 2H^+ = Cu^{2+} + SiO_2 + H_2O$	$pH = 2.46 - 0.5 \cdot \lg a_{Cu^{2+}}$
14	$2CuSiO_3 + 2H^+ + 2e^- = Cu_2O + 2SiO_2 + H_2O$	$0.526 - 0.0591 \cdot pH$
15	$2CuSiO_3 + H_2O + 2e^- = Cu_2O + 2SiO_3^{2-} + 2H^+$	$-1.123 + 0.0591 \cdot pH - 0.0591 \cdot \lg a_{SiO_3^{2-}}$
16	$CuO + SiO_3^{2-} + 2H^+ = CuSiO_3 + 2H_2O$	$pH = 15.06 + 0.5 \cdot \lg a_{SiO_3^{2-}}$
17	$2Cu^{2+} + H_2O + 2e^- = Cu_2O + 2H^+$	$0.235 + 0.0591 \cdot pH + 0.0591 \cdot \lg a_{Cu^{2+}}$
18	$2CuO + 2H^+ + 2e^- = Cu_2O + H_2O$	$0.658 - 0.0591 \cdot pH$
19	$2HCuO_2^- + 4H^+ + 2e^- = Cu_2O + 3H_2O$	$1.771 - 0.1182 \cdot pH + 0.0591 \cdot \lg a_{HCuO_2^-}$
20	$2CuO_2^{2-} + 6H^+ + 2e^- = Cu_2O + 3H_2O$	$2.549 - 0.1773 \cdot pH + 0.0591 \cdot \lg a_{CuO_2^{2-}}$
21	$CuO + 2H^+ = Cu^{2+} + H_2O$	$pH = 3.58 - 0.5 \cdot \lg a_{Cu^{2+}}$
22	$HCuO_2^- + H^+ = CuO + H_2O$	$pH = 18.83 + \lg a_{HCuO_2^-}$
23	$CuO_2^{2-} + H^+ = HCuO_2^-$	$pH = 13.16 + \lg \dfrac{a_{CuO_2^{2-}}}{a_{HCuO_2^-}}$
24	$CuO_2^{2-} + 2H^+ = CuO + H_2O$	$pH = 15.99 + 0.5 \cdot \lg a_{CuO_2^{2-}}$
25	$Cu_2O_3 + 6H^+ + 2e^- = 2Cu^{2+} + 3H_2O$	$1.566 - 0.1773 \cdot pH - 0.0591 \cdot \lg a_{Cu^{2+}}$
26	$Cu_2O_3 + 2H^+ + 2e^- = 2CuO + H_2O$	$1.143 - 0.0591 \cdot pH$
27	$Cu_2O_3 + H_2O + 2e^- = 2HCuO_2^-$	$0.030 - 0.0591 \cdot \lg a_{HCuO_2^-}$
28	$Cu_2O_3 + H_2O + 2e^- = 2CuO_2^{2-} + 2H^+$	$-0.748 + 0.0591 \cdot pH - 0.0591 \cdot \lg a_{CuO_2^{2-}}$
29	$Cu_2O_3 + 2SiO_2 + 2H^+ + 2e^- = 2CuSiO_3 + H_2O$	$1.275 - 0.0591 \cdot pH$
30	$Cu_2O_3 + 2SiO_3^{2-} + 6H^+ + 2e^- = 2CuSiO_3 + 3H_2O$	$2.924 - 0.1773 \cdot pH + 0.0591 \cdot \lg a_{SiO_3^{2-}}$

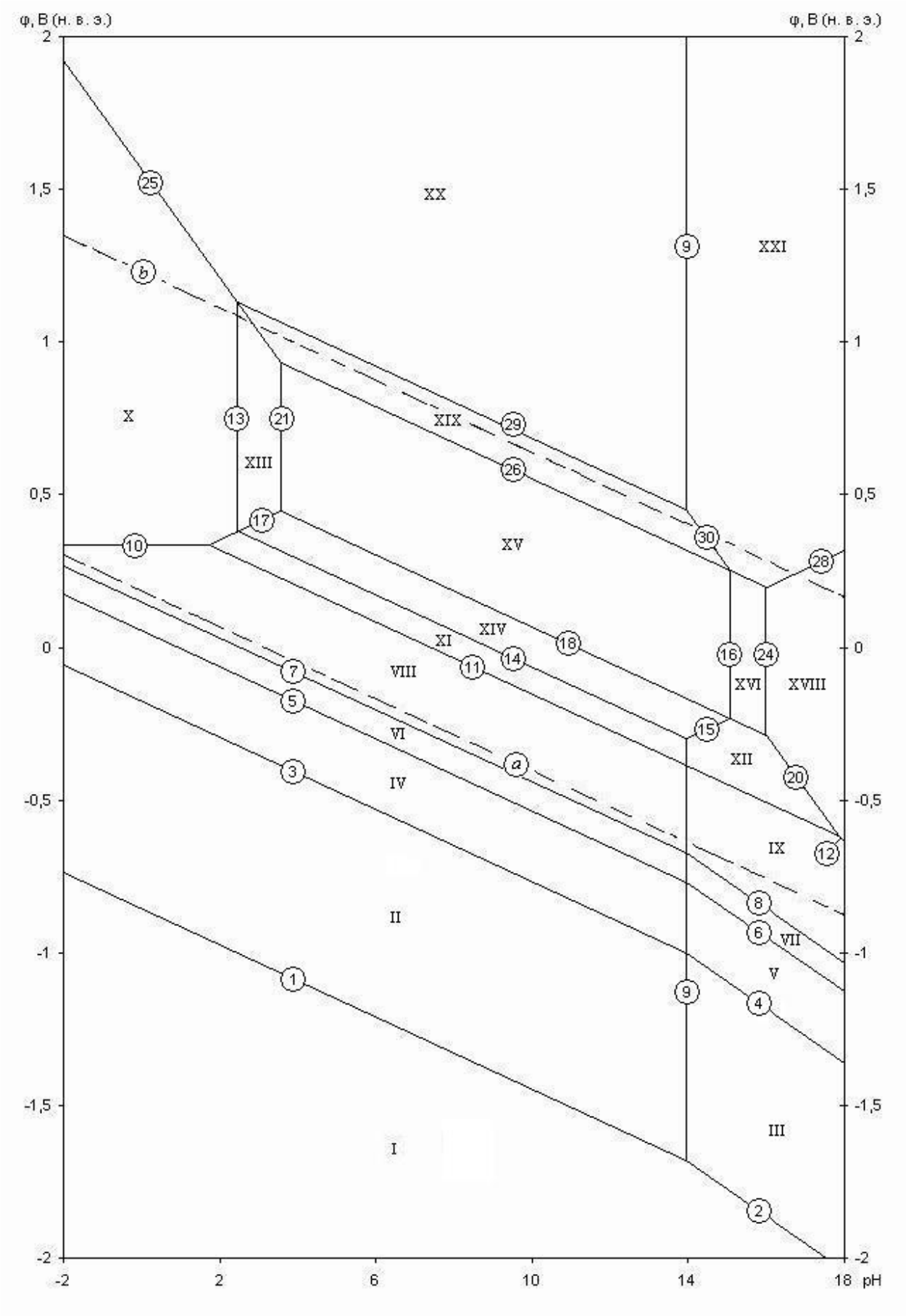

Figure 2. The potential – pH diagram of the Cu–Si–H_2O system at 25 ^oC, air pressure of 1 bar and $a_i = 1$ mole/l (unhydrated form of oxides)

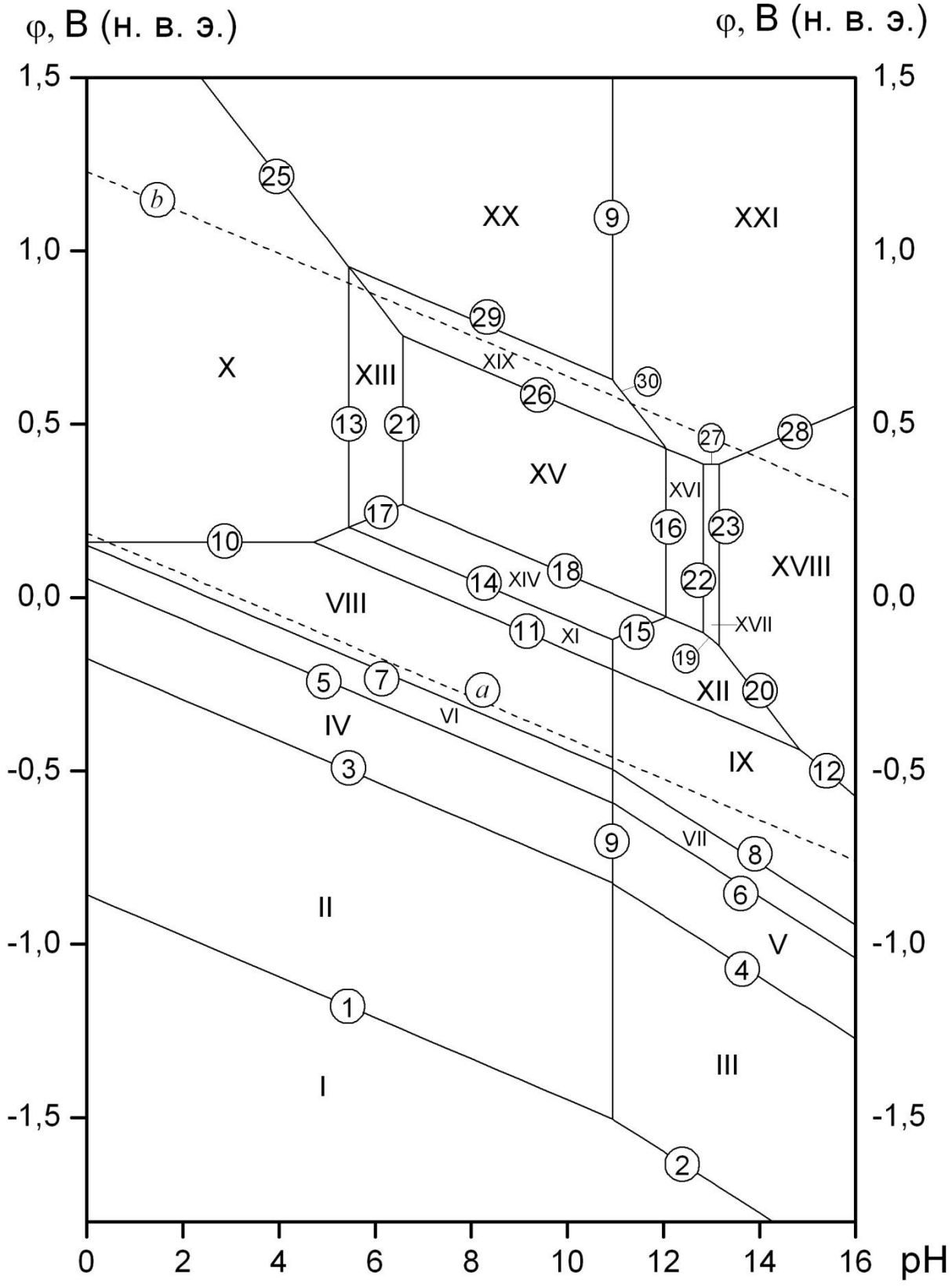

Figure 3. The potential – pH diagram of the Cu–Si–H_2O system at 25 °C, air pressure of 1 bar and $a_i = 10^{-6}$ mole/l (unhydrated form of oxides)

III – α-phase (Cu) + γ-phase ($Cu_{51}Si_{14}$) + ε-phase ($Cu_{15}Si_4$) + η''-phase ($Cu_{19}Si_6$) + SiO_3^{2-}; IV – α-phase (Cu) + γ-phase ($Cu_{51}Si_{14}$) + ε-phase ($Cu_{15}Si_4$) + SiO_2; V – α-phase (Cu) + γ-phase ($Cu_{51}Si_{14}$) + ε-phase ($Cu_{15}Si_4$) + SiO_3^{2-}; VI – α-phase (Cu) + γ-phase ($Cu_{51}Si_{14}$) + SiO_2; VII – α-phase (Cu) + γ-phase ($Cu_{51}Si_14$) + SiO_3^{2-}; VIII – α-phase (Cu) + SiO_2; IX – α-phase (Cu) + SiO_3^{2-}; X – Cu^{2+} + SiO_2; XI – Cu_2O + SiO_2; XII – Cu_2O + SiO_3^{2-}; XIII – Cu^{2+} + $CuSiO_3$; XIV – Cu_2O + $CuSiO_3$; XV – CuO + $CuSiO_3$; XVI – CuO + SiO_3^{2-}; XVII – $HCuO_2^-$, SiO_3^{2-}; XVIII – CuO_2^{2-}, SiO_3^{2-}; XIX – Cu_2O_3 + $CuSiO_3$; XX – Cu_2O_3 + SiO_2; XXI – Cu_2O_3 + SiO_3^{2-}.

Domain I corresponds to system immunity (or thermodynamic stability), all system components should not corrode at these solution pH and equilibrium potentials. The selective oxidation of silicon from alloy occurs at domains II – IX. This results in consecutive formation of phases, increasingly rich in copper, up to almost pure metal, and the excess silicon oxidizes to silica (at domains II, IV, VI, VIII) or, in highly alkaline environments, to metasilicate ions.Domains X and XIII correspond to copper selective corrosion, in which it actively passes into solution in form of Cu^{2+} cations.

All other domains, except domains XVII and XVIII, correspond to passivation of copper–silicon alloys. One of the copper oxides or copper silicate $CuSiO_3$ is the thermodynamically stable phase in these domains. However, the conditions are established in domains XVII and XVIII, at which both alloy components – both copper and silicon – pass into solution in form of ions, that violates the integrity of the oxide film. There are domains of transpassive state of the system.

Lines *a* and *b* in the diagram correspond to the work of the hydrogen and oxygen electrodes, respectively. Domain of potentials and pH, which lies between them, corresponds to the electrochemical stability of water.

Generally, chemical and electrochemical stability of copper-silicon alloys depends entirely on silicon percentage in it.

Conclusions

A state diagram of Cu–Si–O system and the potential – pH diagrams of Cu–Si–H_2O system at 25 ^oC, air pressure of 1 bar and activities of ions in solution, equal to 1 and 10^{-6} mole/l are calculated and plotted.

The thermodynamic analysis of chemical and electrochemical stability of copper-slilcon alloys is performed. It is proved, that the stability is determined by silicon content in alloys.

References

[1] Yu. M. Lakhtin, V. P. Leont'yeva. Materialovedeniye [In Russian] (Material Science). *Moscow: Masshinostroyeniye*. **1990**. 527p.

[2] A. G. Tyurin. Thermodynamics of chemical and electrochemical stability of aluminum, silicon, and tin bronzes. *Protection of Metals*. **2008**. Vol.44. No.3. P.292-300.

[3] N. P. Lyakishev. Diagrammy sostoyaniya dvoynykh metallicheskikh sistem: spravochnik [In Russian] (Phase diagrams of binary metallic systems: textbook). *Moscow: Mashinostroyeniye*. **2000**. Vol.3. Book No.1. P.449-452.

[4] Xinyan Yan, Y.A. Chang. A thermodynamic analysis of the Cu–Si system. *Journal of Alloys and Compounds*. **2000**. No.308. P.221-229.

[5] K. J. Smittlz Metally [In Russian] (Metals). *Moscow: Metallurgiya*. **1975**. 416p.

[6] N. P. Zhuk. Kurs teorii korrozii i zashchity metallov [In Russian] (The course of corrosion theory and metals protection). *Moscov: OOO TID "Alyans"*. **2006**. 472p.
[7] P. A. Nikolaychuk [et al.] Termodinamika khimicheskoy i elektrokhimicheskoy ustoychivosti splavov sistemy Mn – Si [In Russian] (Thermodynamics of chemical and electrochemical stability of Mn – Si system alloys).*Bulletin of South Ural State University. Chemistry*. **2010**. Vol. 31 (207). No.4. P.72-82.
[8] Spravochnik po elektrokhimii [In Russian] (Textbook on Electrochemistry). Editor A. M. Sukhotin. *Leningrad: Khimiya.* **1981**. 488p.
[9] L. P. Ruzinov, B. S. Gulyanitckiy. Ravnovesnyye prevrashcheniya metallurgicheskikh reaktciy [In Russian] (Equilibrium transformations in metallurgical reactions) *Moscow: Metallurgiya.* **1975**. 416p.
[10] Termicheskiye konstanty veshchestv: database [In Russian] (Thermal constants of the substances). URL: <http://www.chem.msu.su/cgi-bin/tkv.pl?show=welcome.html>
[11] JANAF Thermochemical Tables. Third Edition. *J. Phys. Chem. Ref. Data*. **1985**. Vol.14. No.1.
[12] G. K. Moiseev [et al.] Temperaturnyye zavisimosti privedyonnoy energii Gibbsa nekotorykh neorganicheskikh veshchestv:al'ternativnyy bank dannykh ASTRA. OWN [In Russian] (Temperature dependencies of the reduced Gibbs energies of some inorganic substances: ASTRA. OWN alternative databank). *Yekaterinburg: UroRAN*. **1997**. 230p.
[13] N. A. Toropov, V. P. Borzakovskiy [et al.] Diagrammy sostoyaniya silikatnykh sistem: spravochnik [In Russian] (Phase diagrams of silicate systems). *Moscow-Leningrad.: Nauka*. **1965**. Issue No.2. 372p.
[14] P. A. Nikolaychuk, A. G. Tyurin, I. I. Kanat'eva. Utochnyonnaya diagramma Purbe dlya medi [In Russian] (The revised Pourbaix diagram for copper): In Contemporary problems of theoretical and experimental chemistry. Proceedings of VII All-Russian Conference of Young Scientists. *Saratov: Publishing House "KUBiK".* **2010**. P.287-291.
[15] A. G. Tyurin. Termodinamika khimicheskoy i elektrokhimicheskoy ustoychivosti splavov [In Russian] (Thermodynamics of the chemical and electrochemical stability of alloys). In 2 parts. Part. 2. *Chelyabinsk:Publishing center of Chelyabinsk State University*. **2004**. 91p.

16. Zn – Si system
16.1. Zinc silicides

The phase diagram of Zn – Si system is presented in Figure 62. There are no intermediate compounds in Zn – Si system. Moreover, hcp-Zn and diamond-Si are insoluble in each other and form only a mechanical mixture at ambient temperature.

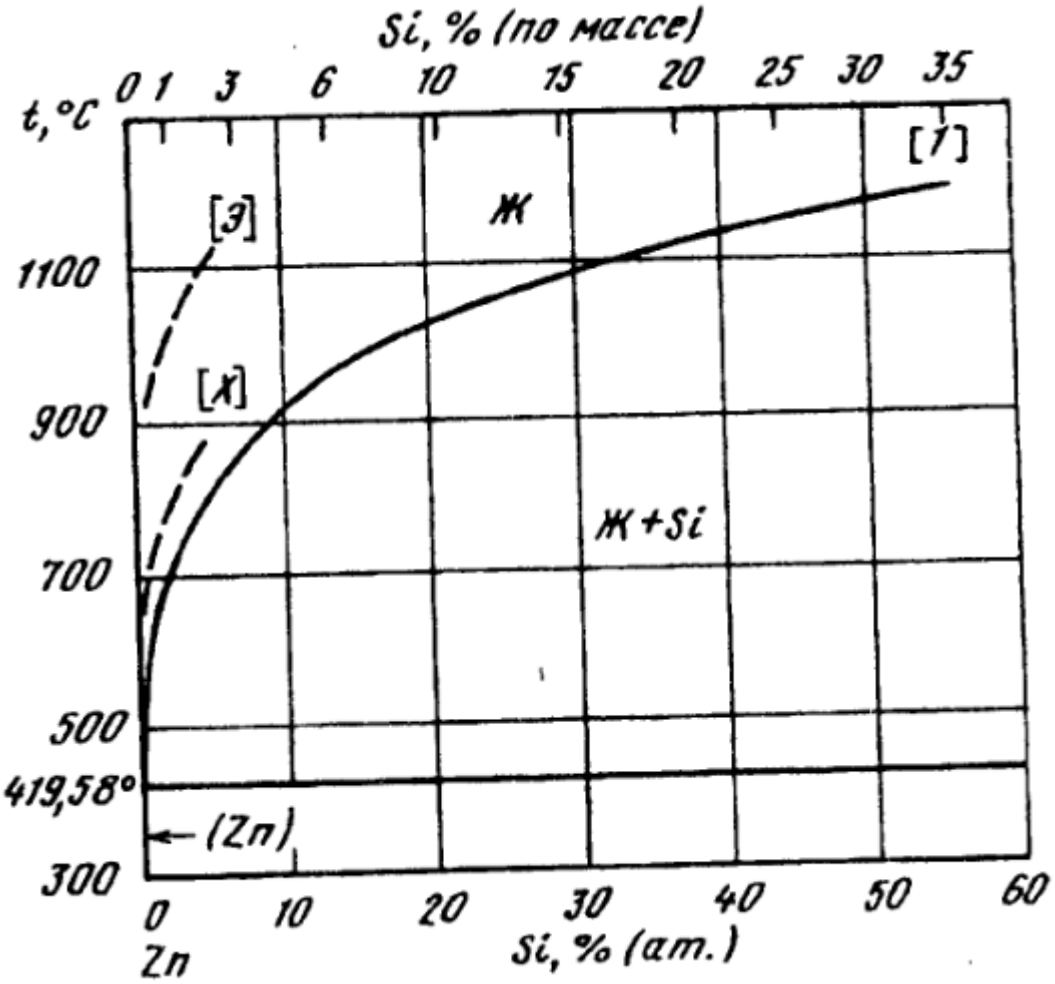

Fig. 62. The phase diagram of Zn – Si system [Диаграммы состояния двойных металлических систем: справочник, 2001].

16.2. Equilibira in Zn – Si – O system

Zinc could form two oxides, namely, ZnO and ZnO_2 [Secco, 1960; Wriedt, 1987]. One zinc silicate, $ZnSiO_3$ could be formed in Zn – Si – O system [Jak et al., 1997]. Another compound, willemite (Zn_2SiO_4), might be formed only at high temperatures or high pressures [Navrotsky, 1971]. The standard Gibbs energies of formation of zinc oxides and silicate were collected from [Chase Jr. et al., 1985; Pankratz, Stuve, Gokcen, 1984;

Термические константы веществ, 2007]. The standard Gibbs energy of formation of ZnO_2 was estimated according to Kireev's and Gorichev's methods.

The state diagram of Zn – Si – O system and the list of equilibria in this system are presented in the publication, attached to Chapter 17. Calculations show that the compound ZnO_2 is not thermodynamically stable at the atmospheric conditions.

16.3. Potential – pH diagram of Zn – H_2O system

Zinc in an aqueous solution could form the cation Zn^{2+} and the anions $HZnO_2^-$ and ZnO_2^{2-}. However, $HZnO_2^-$ is stable only at low zinc concentrations.

The potential – pH diagram of Zn – H_2O system at 25 °C, air pressure of 1 bar and the activities of zinc species of 1 $mol \cdot l^{-1}$ is presented in Figure 63, and the diagram at the activities of 10^{-6} $mol \cdot l^{-1}$ is presented in Figure 64. More details are provided in the attached publication.

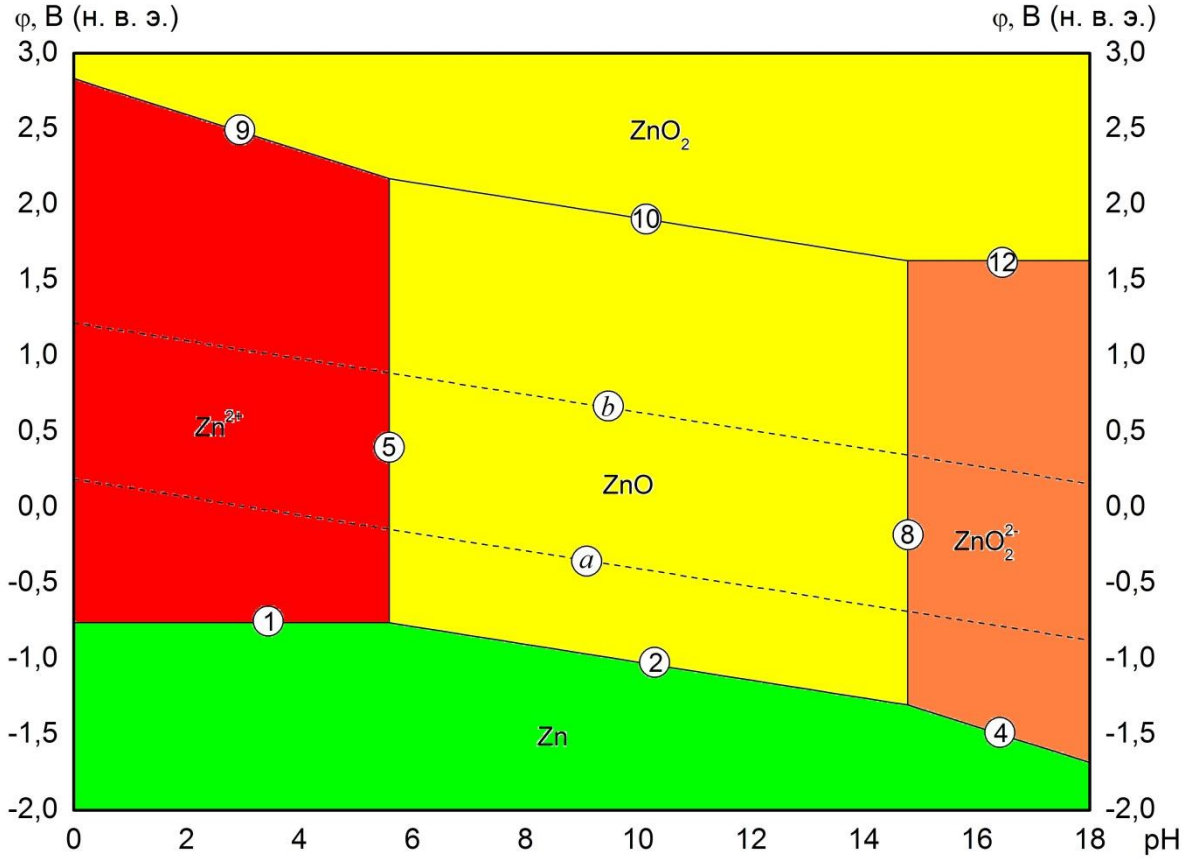

Fig. 63. The potential – pH diagram of Zn – H_2O system at 25 °C, air pressure of 1 bar and the activities of zinc species in a solution of 1 M.

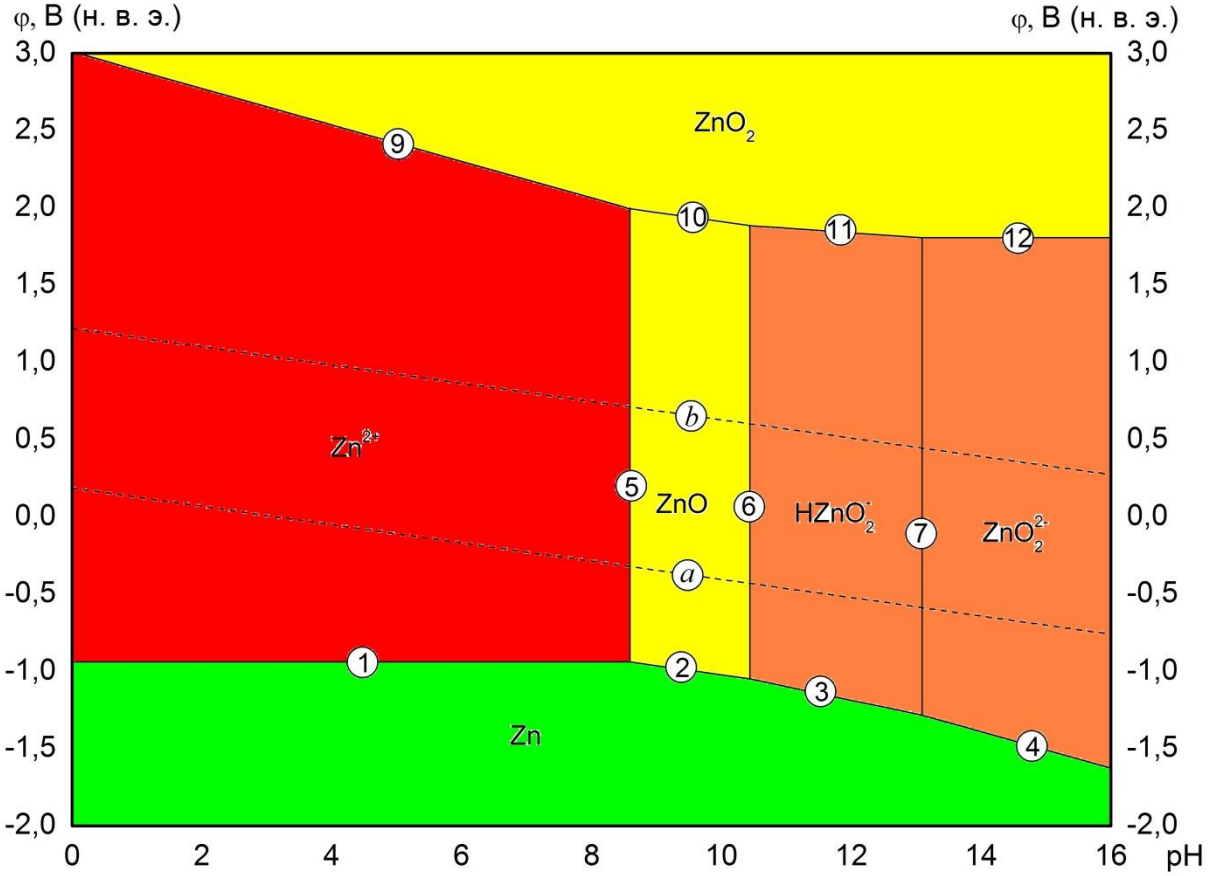

Fig. 64. The potential – pH diagram of Zn – H_2O system at 25 °C, air pressure of 1 bar and the activities of zinc species in a solution of 10^{-6} M.

16.4. Potential – pH diagram of Zn – Si – H_2O system

The potential – pH diagram of Zn – Si – H_2O system at 25 °C, air pressure of 1 bar and the activities of 1 $mol \cdot l^{-1}$ is presented in Figure 65, and the diagram at the activities of 10^{-6} $mol \cdot l^{-1}$ is presented in Figure 66. More details are provided in the publication, attached to Chapter 17.

Zinc silicate $ZnSiO_3$ has a very wide domain of thermodynamic stability and determines the corrosion behaviour of the Zn – Si system alloys. If the silicon content is not sufficient to form a continuous layer of zinc silicate on the surface, then the passivation films consists of zinc (II) oxide. The compound ZnO_2 is not thermodynamically stable in the domain of water electrochemical stability.

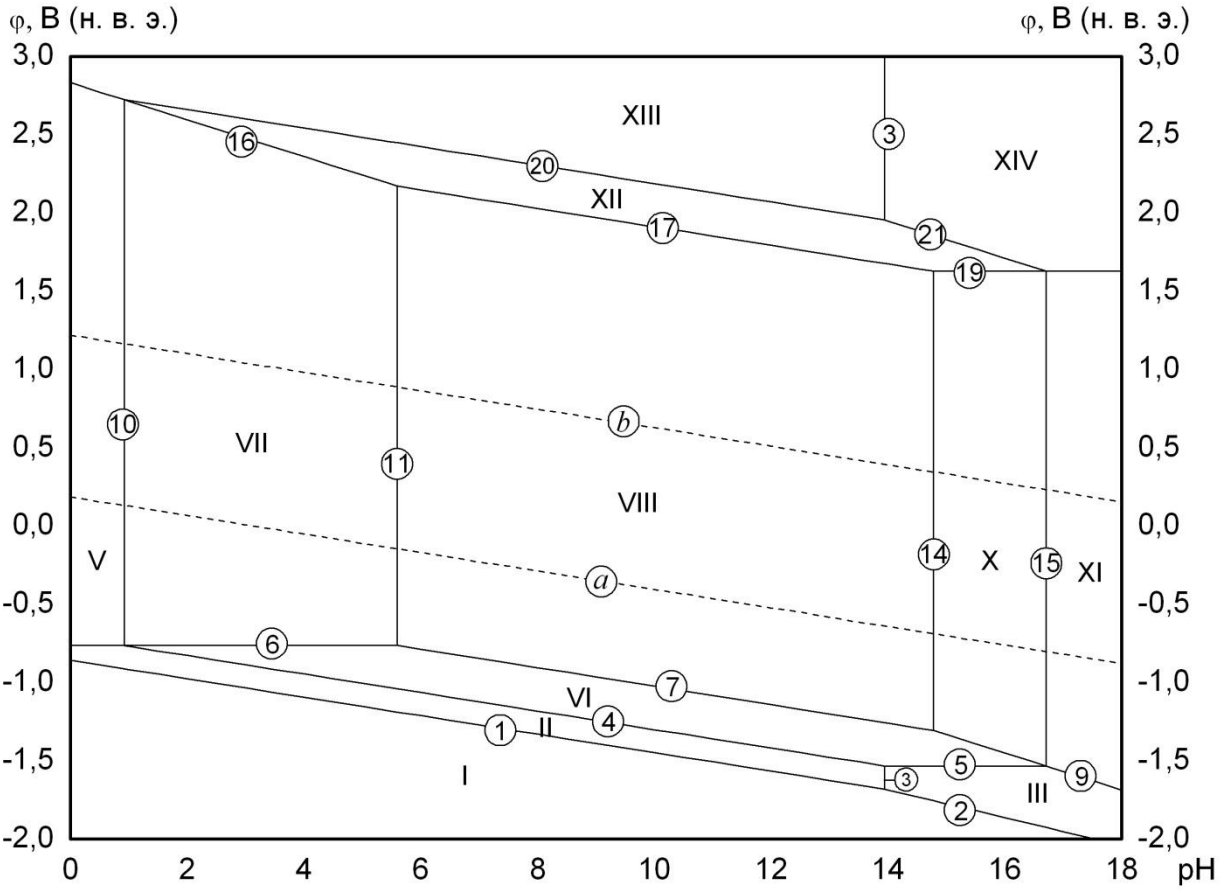

Fig. 65. The potential – pH diagram of Zn – Si – H_2O system at 25 °C, air pressure of 1 bar and the activities of 1 M.

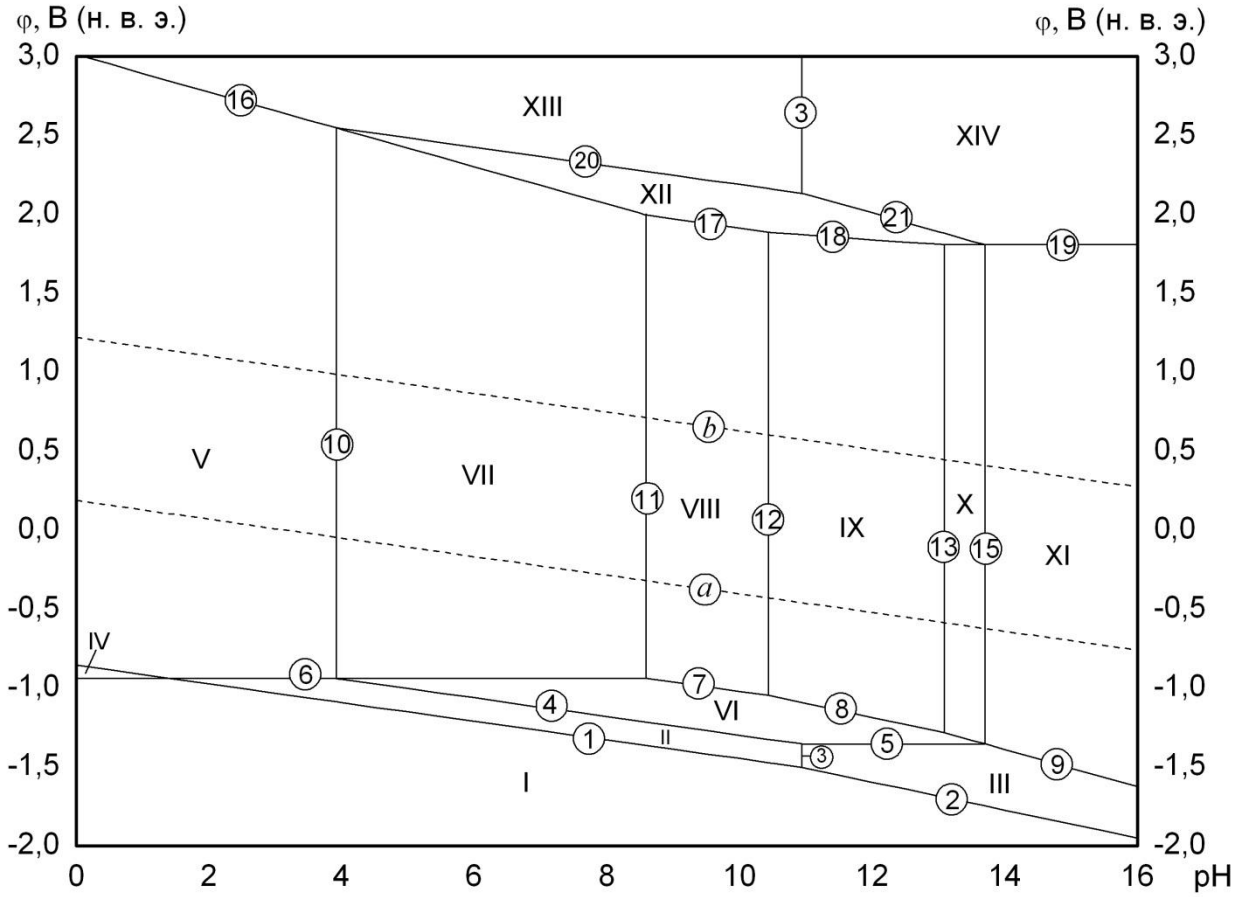

Fig. 66. The potential – pH diagram of Zn – Si – H_2O system at 25 °C, air pressure of 1 bar and the activities of 10^{-6} M.

Publications to chapter 16

The potential – pH diagram of Zn – H_2O system was published in the conference paper [Николайчук, Тюрин, 2011e]. The Russian preprint of this paper with figures and tables translated into English is presented below.

The potential – pH diagram of Zn – Si – H2O system is presented in the publication attached to Chapter 17.

УТОЧНЁННАЯ ДИАГРАММА ПУРБЕ ДЛЯ ЦИНКА

Николайчук П. А., Тюрин А. Г.

ГОУ ВПО “Челябинский государственный университет”,
454021, г. Челябинск, ул. Братьев Кашириных, 129
npa@csu.ru

Диаграмма потенциал – pH для системы Zn – H_2O, построенная М. Пурбе [1], предполагает, что цинк в растворе может окисляться до оксида (ZnO) или до ионов (Zn^{2+}, $HZnO_2^-$, ZnO_2^{2-}). Имеются сведения о том, что цинк в сильноокислительных средах может образовывать и ещё один оксид – ZnO_2 [2, 3]. Однако какая-либо справочная термодинамическая информация для этого соединения отсутствует.

Известно [4], что термодинамические характеристики различных однотипных соединений изменяются периодически с изменением порядкового номера элемента. Поэтому, для оценки $\Delta_f G^o_{298}(ZnO_2)$ была проанализирована зависимость стандартных энергий Гиббса образования оксидов типа MeO_2 d-элементов 4 периода от заряда ядра элементов. Установлено, что лучше всего для аппроксимации этой зависимости подходят следующие уравнения:

$$\lg(-\Delta_f G^o_{298}(MeO_2)) = -0{,}1472 \cdot z + 9{,}2569;\ R^2 = 0{,}9448 \quad (1),$$

$$\lg(-\Delta_f G^o_{298}(MeO_2)) = -8{,}5173 \cdot \lg z + 17{,}4776;\ R^2 = 0{,}9280 \quad (2).$$

Рассчитанные на основании уравнений (1) и (2) значения стандартных энергий Гиббса образования диоксида цинка близки между собой, и составляют $\Delta_f G^o_{298}(ZnO_2) = -75000\ {}^{Дж}/_{моль}$.

Для того, чтобы включить ZnO_2 в диаграмму потенциал – pH для цинка, рассчитаны характеристики основных химических и электрохимических равновесий в системе Zn – H_2O при 25°C и давлении воздуха 1 бар. В расчётах использованы данные [1, 5 – 7]. Результаты расчётов представлены в таблице. Диаграмма потенциал – pH системы Zn – H_2O при активностях ионов в растворе, равных 1 ${}^{моль}/_{л}$ и 10^{-6} ${}^{моль}/_{л}$ представлена на рисунке. На диаграмме активностям, равным 1 ${}^{моль}/_{л}$, соответствуют сплошные линии, на которых нумерация равновесий проведена обычным образом, а активностям ионов, равным 10^{-6} ${}^{моль}/_{л}$, соответствуют пунктирные линии, на которых номер соответствующего равновесия указан со штрихом.

Table. The basic chemical and electrochemical equilibria in the Zn – H_2O system at 25°C and air pressure of 1 bar.

No of line	Electrode reaction	Equilibrium potential, V (s. h. e.) or pH of the solution
a	$2H^+ + 2e^- = H_2; P_{H_2} \approx 5 \cdot 10^{-7}$ бар	$0{,}186 - 0{,}0591 \cdot pH$
b	$O_2 + 4H^+ + 4e^- = 2H_2O; P_{O_2} \approx 0{,}21$бар	$1{,}219 - 0{,}0591 \cdot pH$
1	$Zn^{2+} + 2e^- = Zn$	$-0{,}763 + 0{,}0295 \cdot \lg a_{Zn^{2+}}$
2	$ZnO + 2H^+ + 2e^- = Zn + H_2O$	$-0{,}432 - 0{,}0591 \cdot pH$
3	$HZnO_2^- + 3H^+ + 2e^- = Zn + 2H_2O$	$0{,}054 - 0{,}0887 \cdot pH + 0{,}0295 \cdot \lg a_{HZnO_2^-}$
4	$ZnO_2^{2-} + 4H^+ + 2e^- = Zn + 2H_2O$	$0{,}441 - 0{,}1182 \cdot pH + 0{,}0295 \cdot \lg a_{ZnO_2^{2-}}$
5	$ZnO + 2H^+ = Zn^{2+} + H_2O$	$pH = 5{,}59 - 0{,}5 \cdot \lg a_{Zn^{2+}}$
6	$HZnO_2^- + H^+ = ZnO + H_2O$	$pH = 16{,}44 + \lg a_{HZnO_2^-}$
7	$ZnO_2^{2-} + H^+ = HZnO_2^-$	$pH = 13{,}09 + \lg \frac{a_{ZnO_2^{2-}}}{a_{HZnO_2^-}}$
8	$ZnO_2^{2-} + 2H^+ = ZnO + H_2O$	$pH = 14{,}77 + 0{,}5 \cdot \lg a_{ZnO_2^{2-}}$
9	$ZnO_2 + 4H^+ + 2e^- = Zn^{2+} + H_2O$	$2{,}833 - 0{,}1182 \cdot pH - 0{,}0295 \cdot \lg a_{Zn^{2+}}$
10	$ZnO_2 + 2H^+ + 2e^- = ZnO + H_2O$	$2{,}502 - 0{,}0591 \cdot pH$
11	$ZnO_2 + H^+ + 2e^- = HZnO_2^-$	$2{,}016 - 0{,}0295 \cdot pH - 0{,}0295 \cdot \lg a_{HZnO_2^-}$
12	$ZnO_2 + 2e^- = ZnO_2^{2-}$	$1{,}629 - 0{,}0295 \cdot \lg a_{ZnO_2^{2-}}$

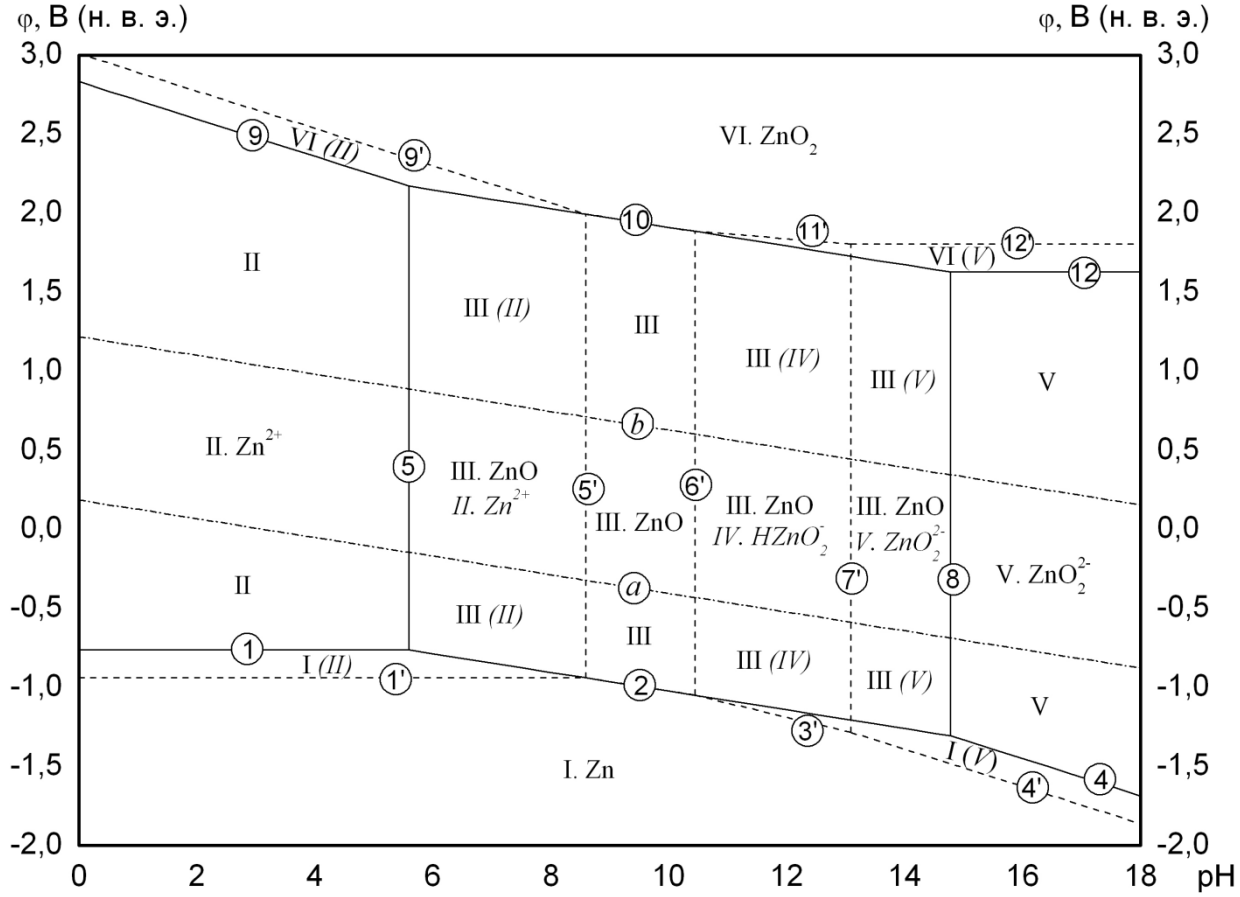

Fig. The potential – pH diagram of the Zn – H_2O system at 25˚C, air pressure of 1 bar, $a_i = 1$ моль/л и $a_i = 10^{-6}$ моль/л (undydrated form of the oxides).

Различия в виде диаграмм при различных активностях связаны с тем, что ион $HZnO_2^-$, по данным расчётов, термодинамически устойчив лишь при очень малых активностях ионов в растворе ($\lg a_i < -3{,}34$).В этом случае для различных форм цинка (II) с увеличением pH реализуется следующая последовательность равновесий: $Zn^{2+} | ZnO | HZnO_2^- | ZnO_2^{2-}$ (на рисунке – линии 5’, 6’ и 7’). В более концентрированных растворах ион $HZnO_2^-$ становится неустойчивым, и превращение осуществляется по схеме $Zn^{2+} | ZnO | ZnO_2^{2-}$ (на рисунке – линии 5 и 8).

При построении диаграммы рассмотрена только негидратированная форма оксидов, как наиболее устойчивая. Переход от негидратированной формы оксидов (ZnO, ZnO_2) к гидратированной форме ($Zn(OH)_2$) происходит через ряд промежуточных состояний.

На диаграмме потенциал – pH системы Zn – H_2O можно выделить 6 областей преобладания различных фаз. При этом (см. рисунок) положение областей при $a_i = 1$ моль/л указано обычным шрифтом, а при $a_i = 10^{-6}$ моль/л (если они не совпадают с таковыми при $a_i = 1$ моль/л) – выделено курсивом.

Область I – область иммунности цинка, при данных значениях равновесных потенциалов и pH металл коррозии не подвергается. Область II – область активной коррозии, в которой цинк переходит в раствор в виде катионов Zn^{2+}. Область III – область пассивности. При данных значениях потенциалов и pH на поверхности цинка образуется защитная пассивирующая плёнка, состоящая из оксида ZnO, которая препятствует дальнейшему окислению металла. Области IV и V – области транспассивности, в которых оксидная плёнка на металле переходит в раствор в виде анионов $HZnO_2^-$ или ZnO_2^{2-}.

Оксид ZnO_2 (область VI) не образует отдельную фазу, поскольку равновесное давление кислорода, необходимое для протекания реакции $2ZnO + O_2 \rightarrow 2ZnO_2$, составляет $1{,}3 \cdot 10^{86}$ бар. Получение диоксида цинка электрохимическим путём также практически невозможно, поскольку соответствующие реакции реализуются при потенциалах, намного превышающих потенциал выделения из воды кислорода.

Линии *a* и *b* (на диаграмме нанесены штрих-пунктиром) соответствуют работе водородного и кислородного электродов, соответственно. Область, лежащая между ними, соответствует электрохимической устойчивости воды.

Список использованной литературы:

10. Справочник химика [Текст] / под ред. Б. П. Никольского. – М. – Л.: Химия, 1964. – Т. 3. – 1008 с.
11. Физико-химические свойства окислов: справочник [Текст] / под ред. Г. В. Самсонова. – М.: Металлургия, 1978. – 472 с.
12. Диаграммы состояния двойных металлических систем: справочник [Текст] / под ред. Н. П. Лякишева. – М.: Машиностроение, 2000. – Т. 3. – Кн. 2. – 448 с.
13. Киреев, В. А. Методы практических расчётов в термодинамике химических реакций [Текст]. – М.: Химия, 1970. – С. 520.
14. Рузинов, Л. П. Равновесные превращения металлургических реакций [Текст] / Л. П. Рузинов, Б. С. Гуляницкий. – М.: Металлургия, 1975. – 460 с.
15. Справочник по электрохимии [Текст] / под ред. А. М. Сухотина. – Л.: Химия, 1981. – 448 с.
16. Термические константы веществ: база данных [Электронный ресурс] / руководители проекта В. С. Иориш, В. С. Юнгман. – URL: <http://www.chem.msu.su/cgi-bin/tkv.pl?show=welcome.html> (дата обращения – 05. 05. 2010 г.)

17. Cu – Zn – Si system

17.1. Siliceous brasses

Siliceous brasses are the alloys containing copper, zinc and silicon. They have low melting temperature, good fluidity and resistance to oxidation in molten state. They are more stable to corrosion in atmospheric conditions and sea water, than other bronzes and brasses. Studying of their stability to chemical and electrochemical corrosion from the point of view of chemical thermodynamics has wide scientific and practical importance.

Several marks of siliceous brasses with different compositions are produced in the chemical industry. The composition of some of them, determined according to the Russian State Standards and the UNS and ASTM classifications, is collected in Table 14.

Table 14. The composition of various marks of siliceous brasses according to the Russian State Standards and the UNS and ASTM classifications.

Brass	Content of the element, weight %		
	Cu	Zn	Si
ЛК80–3	80	17	3
ЛК2	78,5	19	2,5
ЛЦ16К4	80	16	4
C69400, C69430	83	12,5	4,5
C69710	77,5	19	3,5
C65550	94,8	3,8	1,4

The content of zinc and silicon in these brasses is such that the system remains one-phase and represents a three-component solid solution, based on (fcc-Cu).

17.2. Thermodynamic activities of Cu – Zn – Si system components

The expression for the excess Gibbs energy of the ternary Cu – Zn – Si system was proposed by [Miettinen, 2007] and based on the thermodynamic descriptions of the boundary binary systems Cu – Zn [Liang, Chang, 1998], Cu – Si [Yan, Chang, 2000] and Zn – Si [Jacobs, Spencer, 1996]. The data of these studies were consistent with each other. The solid solution of zinc and silicon in fcc-copper was modelled in terms of

the substitution solution model. The activities of the components for all brasses from Table 14 were calculated using the expressions proposed by. The results of these calculations are presented in Table 15.

Table 15. Thermodynamic activities of the siliceous brasses components.

Brass	Thermodynamic activity		
	Cu	Zn	Si
ЛК80–3	0,339	$3{,}8\cdot10^{-5}$	$9{,}5\cdot10^{-6}$
ЛК2	0,324	$4{,}1\cdot10^{-5}$	$1{,}2\cdot10^{-5}$
ЛЦ16К4	0,290	$6{,}1\cdot10^{-5}$	$1{,}7\cdot10^{-5}$
С69400, С69430	0,347	$4{,}0\cdot10^{-5}$	$7{,}2\cdot10^{-6}$
С69710	0,249	$8{,}3\cdot10^{-5}$	$3{,}4\cdot10^{-5}$
С65550	0,868	$5{,}6\cdot10^{-7}$	$7{,}6\cdot10^{-9}$

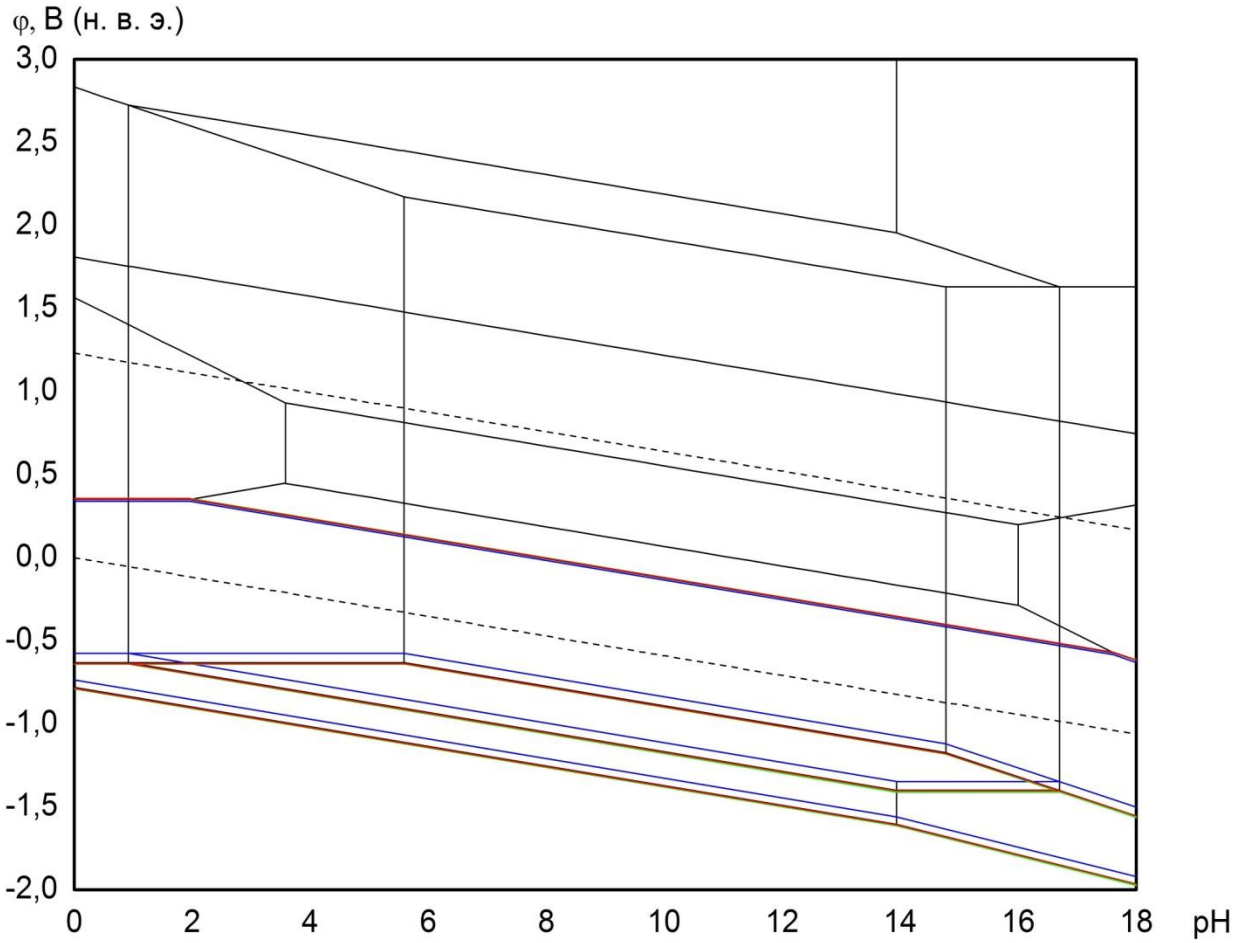

Fig. 67. The difference between the potential – pH diagrams of various siliceous brasses.

The calculations show that the solid solution of zinc and silicon in fcc-copper exhibits significant negative deviations from ideal behaviour.

17.3. Potential – pH diagram of Cu – Zn – Si – H_2O system

The potential – pH diagram of the Cu – Zn – Si – H_2O system is a superposition of the diagrams for Cu – Si – H_2O and Zn – Si – H_2O systems, discussed in Chapters 15 and 16. The diagram for the siliceous brass ЛК80–3 is presented in the attached publication. The diagrams for other brasses differ from it only in the position of a few lines denoting the equilibria involving elements in the oxidation state 0, as it is illustrated by the coloured lines in Figure 67.

The calculations show that zinc silicate $ZnSiO_3$ is thermodynamically stable in a wide range of potentials and pH, and it determines the corrosion behaviour of the siliceous brasses.

Publications to chapter 17

The content of this chapter was published in the paper [Николайчук, Тюрин, 2013]. English version of this paper [Nikolaychuk, Tyurin, 2013b] is presented in form of the preprint with the permission from *Springer*.

THERMODYNAMIC EVALUATION OF CORROSION-ELECTROCHEMICAL BEHAVIOUR OF SILICON BRASS CuZn17Si3

P. A. Nikolaychuk, A. G. Tyurin
Chelyabinsk State University
E-mail: npa@csu.ru, tag@csu.ru

Thermodynamic activities of brass CuZn17Si3 components are calculated. The potential – pH diagrams for system "brass CuZn17Si3 – H_2O" at 25°C, total air pressure of 1 bar and various activities of ions in solution are plotted. Thermodynamic features of brass CuZn17Si3 chemical and electrochemical stability are analyzed. It is shown, that high corrosion resistance of brass is achieved with respect to formation of protective film of $ZnSiO_3$ on its surface.

Introduction

Silicon brasses have low melting temperature, good fluidity and resistance to oxidation in molten state [1]. They are more stable to corrosion in atmospheric conditions and sea water, than other bronzes and brasses [2, 3]. Siliceous brass CuZn17Si3 ("ЛК80-3" in Russian classification; there is no such alloy in UNS or ASTM classifications) is most widely used in Russia [3, 4]. Studying of its stability to chemical and electrochemical corrosion from the point of view of chemical thermodynamics has wide scientific and practical importance. The method of thermodynamic modeling of multicomponent alloys chemical and electrochemical stability, which is used in present study, is proposed in monograph [5].

The purpose of this study is to make modeling of the siliceous brass CuZn17Si3 chemical and electrochemical stability.

Phase equilibria in Cu – Zn – Si system

The averaged composition of siliceous brass CuZn17Si3 [4] is presented in table 1. Zinc and silicon content is chosen in such a way, that system should remain one-phase and represent three-component solid solution, based on fcc-lattice copper [1, 6].

Table 1

The composition of brass CuZn17Si3 and thermodynamic activities (a_s) of its components

Component	Concentration		a_s
	weight %	mole fraction	
Cu	80	0,774	0,339
Zn	17	0,160	$3{,}8 \cdot 10^{-5}$
Si	3	0,066	$9{,}5 \cdot 10^{-6}$

The Cu – Zn system is characterized by formation of variety of phases with wide homogeneity ranges. The solid solution with fcc lattice (α-phase) is formed at high copper content is system [7 – 10].

The state diagram for Cu – Si system is presented in [9 – 11]. Phase equilibria in system at 25ºC are considered in study [12].

The state diagram for Zn – Si system [9, 10, 13] is characterized by absence of both intermediate compounds and significant mutual solubility of components in solid state.

The isothermal cross-sections of copper-rich part of Cu – Zn – Si system diagram are plotted by the authors of [14]. In the same study thermodynamic information is gathered (according to data of references [11, 13, 15]), which allows to perform the modeling of phase equilibria in system. Also, the variants of thermodynamic description of boundary binary systems from ternary Cu – Zn – Si system are available in studies [7, 8, 16], however, the data in these studies are not matched with each other, so than they cannot be used for ternary system thermodynamic modeling.

In order to describe the excess Gibbs energy G^E [17] of three-component solid solution in terms of substitutional solution model [18], Redlich-Kister power series [19] are used:

$$G^E = x_{Cu} \cdot x_{Zn} \cdot L_{Cu,Zn} + x_{Cu} \cdot x_{Si} \cdot L_{Cu,Si} + x_{Zn} \cdot x_{Si} \cdot L_{Zn,Si} + x_{Cu} \cdot x_{Zn} \cdot x_{Si} \cdot L_{Cu,Zn,Si} ,$$

in which each of the parameters $L_{Cu,Zn}$, $L_{Cu,Si}$, $L_{Zn,Si}$ and $L_{Cu,Zn,Si}$ can be a function of solid solution composition (x_{Cu}, x_{Zn}, x_{Si}) and temperature. According to data of [14], these parameters for fcc solid solution are the following:

$$L_{Cu,Zn} = L^{(0)}_{Cu,Zn} + L^{(1)}_{Cu,Zn} \cdot (x_{Cu} - x_{Zn}) + L^{(2)}_{Cu,Zn} \cdot (x_{Cu} - x_{Zn})^2 ,$$

$$L^{(0)}_{Cu,Zn} = 10{,}023 \cdot T - 42804 \ \mathrm{J \cdot mol^{-1}} ,$$

$$L^{(1)}_{Cu,Zn} = -3{,}053 \cdot T + 2936 \ \mathrm{J \cdot mol^{-1}} ,$$

$$L^{(2)}_{Cu,Zn} = -5{,}393 \cdot T + 9034 \ \mathrm{J \cdot mol^{-1}} ,$$

$$L_{Cu,Si} = L^{(0)}_{Cu,Si} + L^{(1)}_{Cu,Si} \cdot (x_{Cu} - x_{Si}) ,$$

$$L^{(0)}_{Cu,Si} = 13{,}891 \cdot T - 42204 \ \mathrm{J \cdot mol^{-1}} ,$$

$$L^{(1)}_{Cu,Si} = -18{,}178 \cdot T - 1102 \ \text{J} \cdot \text{mol}^{-1} ,$$

$$L_{Zn,Si} = 50000 \ \text{J} \cdot \text{mol}^{-1} ,$$

$$L_{Cu,Zn,Si} = -25 \cdot T - 24000 \ \text{J} \cdot \text{mol}^{-1} .$$

Thermodynamic activities of brass components (a_s) are calculated with respect to the following equation:

$$R \cdot T \cdot \ln a_s = R \cdot T \cdot \ln x_s + \mu_s^E ,$$

where T is temperature in Kelvins, $R = 8{,}3144 \ \text{J} \cdot \text{mol}^{-1} \cdot \text{K}^{-1}$ is a universal gas constant, μ_s^E is the excess chemical potential of component "s" [17, 18]. The expressions for calculation of the excess chemical potentials of ternary system components are taken from study [19].

The calculated brass components activities at 25ºC (reference state – a pure solid component with fcc lattice) are presented in table 1. Strong negative deviations from ideal behaviour are observed for all solid solution components.

Chemical stability

In order to develop thermodynamic model for brass oxidation processes, it is necessary at first to consider the equilibria of its individual compounds with oxygen.

Silicon forms only one stable oxide – SiO_2 [9, 10]. The value of $\Delta_f G(SiO_2, 298\,\text{K})$ is taken from textbook [20], because exactly this value corresponds to experimentally measured silicon electrode standard potential ($SiO_2 + 4H^+ + 4e^- = Si\ (diamond) + 2H_2O$; $\varphi^{o}_{298\,K} = 0{,}857\,V$).

In Cu – O system two oxides are known – Cu_2O and CuO [9, 10]. However, it is shown at present time, that copper can also form a Cu_2O_3 compound [21, 22]. Moreover, there are numerous evidences, indicating a possibility of forming complex oxides of several metals, which structure involves CuO_2-containing layers [23 – 30]. Therefore, the prediction of pure copper dioxide thermodynamic properties is also performed.

In addition to ZnO a zinc dioxide (ZnO_2) can also be formed in Zn – O system [8, 31]. However, thermodynamic characteristics of copper and zinc higher oxides at standard temperature are unavailable in literature. In order to estimate them the assumption is used, that thermodynamic properties of one-type compounds change monotonically within one period [32]. The approximate functional relationship between 4^{th} period d-element atomic number and the standard Gibbs energy of formation of its MO_2-type oxide [33] is revealed.

Between the oxides CuO and SiO_2 one intermediate compound can be formed – it is copper silicate $CuSiO_3$. Similarly, between ZnO and SiO_2 a compound $ZnSiO_3$ can be formed [34].

Another zinc silicate – Zn_2SiO_4 – can be formed only at high temperatures or high pressures and is not stable at standard conditions [35].

The information about standard Gibbs energies of formation for oxygen-containing compounds of brass CuZn17Si3 components are summarized in table 2.

Table 2

The standard Gibbs energies of formation of compounds from elements

Compound / Reference	$-\Delta_f G\,(298\,K),\ J\cdot mol^{-1}$								
	[20]	[21]	[37]	[38]	[39]	[40]	[41]	[50]	[33]*
SiO_2	805067	–	–	–	–	–	–	–	–
$CuH_{0,8}$	–	–	–	–	–	–	–	–32200	–
Cu_2O	–	–	147848	150548	147886	144340	147935	–	–
CuO	–	–	127890	129365	128292	127750	127920	–	–
Cu_2O_3	–	279480	–	–	–	–	–	–	–
CuO_2	–	–	–	–	–	–	–	–	90000
$CuSiO_3$	–	–	949240	–	–	–	–	–	–
ZnO	–	–	320706	320660	–	318150	320525	–	–
ZnO_2	–	–	–	–	–	–	–	–	75000
$ZnSiO_3$	–	–	–	1179040	–	1148612	–	–	–

* The result of estimation according to dependency $-\Delta_f G^{o}_{298}(MeO_2) = f(z)$.

The Cu – Si – O system state diagram is plotted in [12], and in the same study the thermodynamic characteristics of system conditions are presented, except equilirbia involving CuO_2. The state diagram of Cu – Zn – O system (which also does not include equilibria, involving CuO_2 and ZnO_2) is plotted in study [7].

The state diagram for Zn – Si – O system, which is the missing part of quaternary system Cu – Zn – Si – O, is plotted in present study at the temperature of 25˚C (see figure 1). This diagram is plotted in orthogonal coordinates, rather than in barycentric ones, because, as is shown in researches [5, 36], such kind of view is the most convenient for oxygen-containing systems. The characteristics of invariant system conditions are listed in table 3.

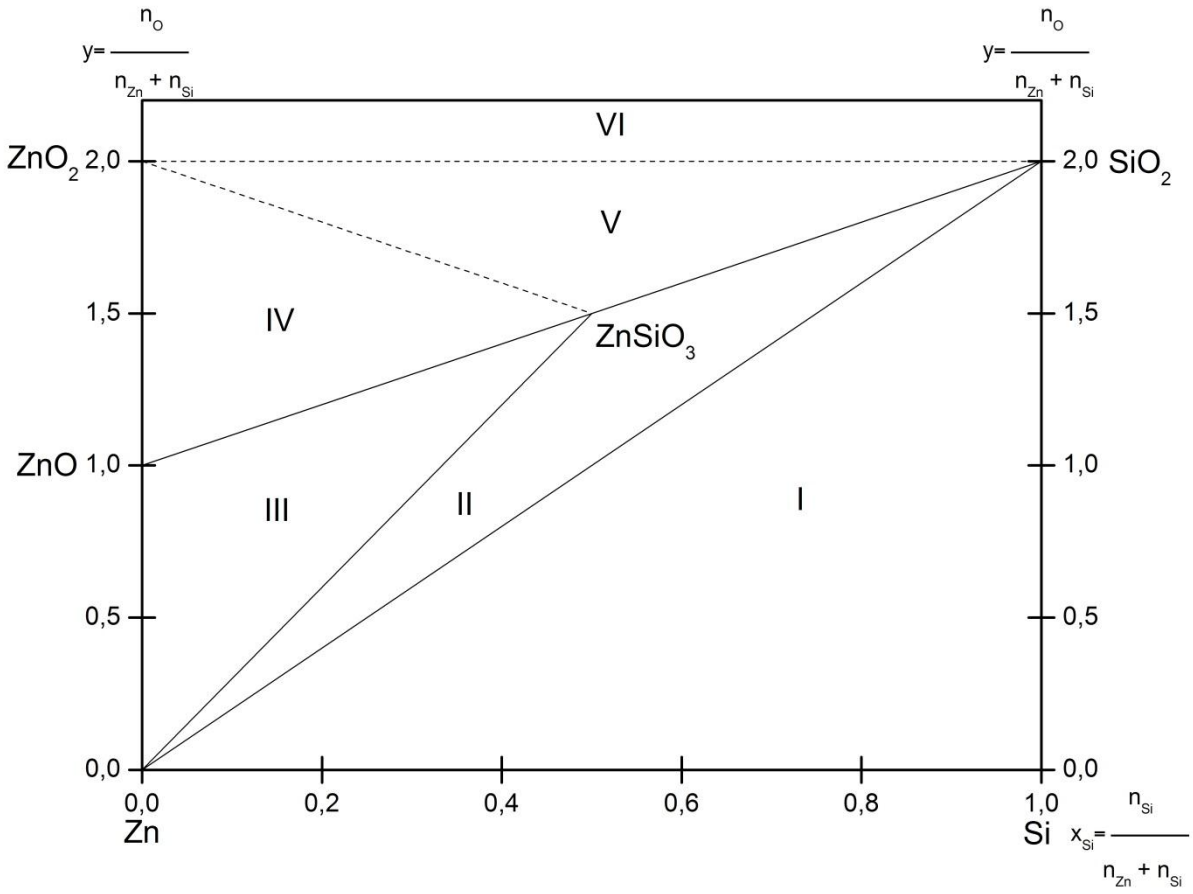

Figure 1. The state diagram for Zn – Si – O system at 25˚C

Table 3

The characteristics of invariant conditions for system Zn – Si – O at 25˚C

№ of domain	System condition	Reaction equation	p (O_2), bar
I	Si – Zn – SiO_2	Si + O_2 = SiO_2	$7{,}7 \cdot 10^{-142}$
II	Zn – $ZnSiO_3$ – SiO_2	2Zn + 2SiO_2 + O_2 = 2$ZnSiO_3$	$7{,}9 \cdot 10^{-132}$
III	Zn – ZnO – $ZnSiO_3$	2Zn + O_2 = 2ZnO	$3{,}9 \cdot 10^{-113}$
IV	ZnO – ZnO_2 – $ZnSiO_3$	2ZnO + O_2 = 2ZnO_2	$1{,}3 \cdot 10^{86}$
V	ZnO_2 – $ZnSiO_3$ – SiO_2	2$ZnSiO_3$ + O_2 = 2ZnO_2 + 2SiO_2	$6{,}4 \cdot 10^{104}$
VI	ZnO_2 – SiO_2 – O_2	—	—

Basing on calculation results for equilibria in systems Cu – Zn – O [7], Cu – Si – O [12] and Zn – Si – O (table 3), thermodynamic picture of brass CuZn17Si3 oxidation in oxygen-containing environments is created. All the equilibria, which are implemented during oxidation process, are summarized in table 4. In should be noted that, unless it is stated otherwise, the participants of all equilibria in tables 3 and 4 are treated as pure substances, and their activities are set equal to unity.

Table 4

The equilibria, occurring during brass CuZn17Si3 oxidation in oxygen-containing environments at 25˚C

	Reaction equation	$p\,(O_2)$, bar
	$Si(\alpha) + O_2 = SiO_2$; $a_{Si(\alpha)} = 9{,}5 \cdot 10^{-6}$	$8{,}1 \cdot 10^{-137}$
	$2Zn(\alpha) + 2SiO_2 + O_2 = 2ZnSiO_3$; $a_{Zn(\alpha)} = 3{,}8 \cdot 10^{-5}$	$5{,}5 \cdot 10^{-123}$
	$2Zn(\alpha) + O_2 = 2ZnO$; $a_{Zn(\alpha)} = 3{,}8 \cdot 10^{-5}$	$2{,}7 \cdot 10^{-104}$
	$4Cu(\alpha) + O_2 = 2Cu_2O$; $a_{Cu(\alpha)} = 0{,}339$	$2{,}6 \cdot 10^{-52}$
*	$2Cu_2O + 4SiO_2 + O_2 = 4CuSiO_3$	$2{,}4 \cdot 10^{-48}$
	$2Cu_2O + O_2 = 4CuO$	$2{,}2 \cdot 10^{-39}$
	$4CuO + O_2 = 2Cu_2O_3$	$1{,}4 \cdot 10^{-6}$
*	$4CuSiO_3 + O_2 = 2Cu_2O_3 + 4SiO_2$	1282,62
	$2Cu_2O_3 + O_2 = 4CuO_2$	$1{,}5 \cdot 10^{39}$
	$2ZnO + O_2 = 2ZnO_2$	$1{,}3 \cdot 10^{86}$
	$2ZnSiO_3 + O_2 = 2ZnO_2 + 2SiO_2$	$6{,}4 \cdot 10^{104}$

* These equilibria do not occur because of small silicon content in brass (see explanation in text)

The calculations show, that the compound $CuSiO_3$ is not formed during brass oxidation, despite this process is thermodynamically possible. However, since silicon content in brass is less than zinc content in it, and equilibrium oxygen pressure in system, which is necessary for zinc silicate formation, is 10^{75} times lower, than oxygen pressure, necessary for copper silicate formation, therefore all formed SiO_2 should react with zinc and be bound in $ZnSiO_3$ earlier, than even the thermodynamic conditions for $CuSiO_3$ formation will be created. Copper is unable to displace zinc from its silicate. Thus the equilibria, marked by * in table 4, do not occur.

The oxygen pressure at atmospheric air at normal conditions amounts ~0,21 bar, and all equilibria, which require higher $p(O_2)$ value, do not take place in air. Consequently, the oxidation of brass CuZn17Si3 in air should end by formation of $ZnSiO_3$ and Cu_2O_3. However, a copper (III) oxide does not form an individual phase [22], therefore the oxide layer on brass surface should consist of CuO and $ZnSiO_3$.

Electrochemical stability

In order to develop thermodynamic model for brass CuZn17Si3 oxidation in water environments, it is convenient to use diagrams of electrochemical equilibria (potential – pH) [42 – 44], which show most clearly possible chemical and electrochemical equilibria in system. A method of plotting and analyzing such kind a diagrams is set out amply in [5, 43 – 45].

Thermodynamic characteristics from table 2 as well as the data from textbook [20] (for equilibria, involving ions) are used to calculate equilibrium potentials.

The brass in water environments may be subjected not only oxide, but also hydride passivation [5]. Therefore, taking into account possible equilibria of brass components with hydrogen is important. Despite copper hydride $CuH_{0,8}$ is not stable in air, it is shown [46 – 48], that it can be obtained during copper electrochemical reduction. The electrochemical characteristics of this process are missing in literature, however the standard Gibbs energy of formation for hydride is determined basing on calorimetric measurements [49, 50] and by hydrogen equilibrium pressure in hydride thermal decomposition reaction [51]. Its value, used for further calculations, is included into table 2. No compounds are formed in Zn – H system [10], and silicon hydrides SiH_2, SiH_4 and Si_2H_6 could not be obtained in electrochemical way [52].

The diagrams of electrochemical equilibria for systems Cu – H_2O [53] and Cu – Si – H_2O [12] are plotted earlier; they, however, do not include equilibria, involving hydride $CuH_{0,8}$ and oxide CuO_2. The potential – pH diagram of Zn – H_2O system is revised in study [54].

The potential – pH diagram for Zn – Si – H_2O system, which is plotted at 25˚C, pressure of 1 bar and activities of ions in solutions, equal to 1 and 10^{-6} mole l^{-1} (reference state – a hypothetical one-molar solution) is presented at figure 2. The equilibria, related to $a_i = 1\ \text{mol}\cdot\text{l}^{-1}$, are shown with solid lines and depicted by common numbers, and equilibria, related to $a_i = 10^{-6}\,\text{mol}\cdot\text{l}^{-1}$, are shown with dashed lines and depicted by numbers with strokes..

14 domains of predominance of certain phases can be depicted at the Zn – Si – H_2O system potential – pH diagram: I – Zn + Si; II – Zn + SiO_2; III – Zn + SiO_3^{2-}; IV – Zn^{2+} + Si; V – Zn^{2+} + SiO_2; VI – Zn + $ZnSiO_3$; VII – Zn^{2+} + $ZnSiO_3$; VIII – ZnO + $ZnSiO_3$; IX – $HZnO_2^-$ + $ZnSiO_3$; X – ZnO_2^{2-} + $ZnSiO_3$; XI – ZnO_2^{2-}, SiO_3^{2-}; XII – ZnO_2 + $ZnSiO_3$; XIII – ZnO_2 + SiO_2; XIV – ZnO_2 + SiO_3^{2-}.

Domain I is the domain of thermodynamic stability of Zn – Si system. Domains IV, V and VIII correspond to zinc selective corrosion. At values of potentials and pH, corresponding to domains II, VI, VII, a stable passivation film forms on the surface, which consists of silicon dioxide (domain II), zinc silicate (domain VI), or zinc oxide (domain VIII). Domain III corresponds to system transpassivity with respect to silicon, and domains X and XI – to system transpassivity with respect to zinc. The domains, which arise only at $a_i = 10^{-6}\,\text{mol}\cdot\text{l}^{-1}$, are enclosed in parentheses at the diagram.

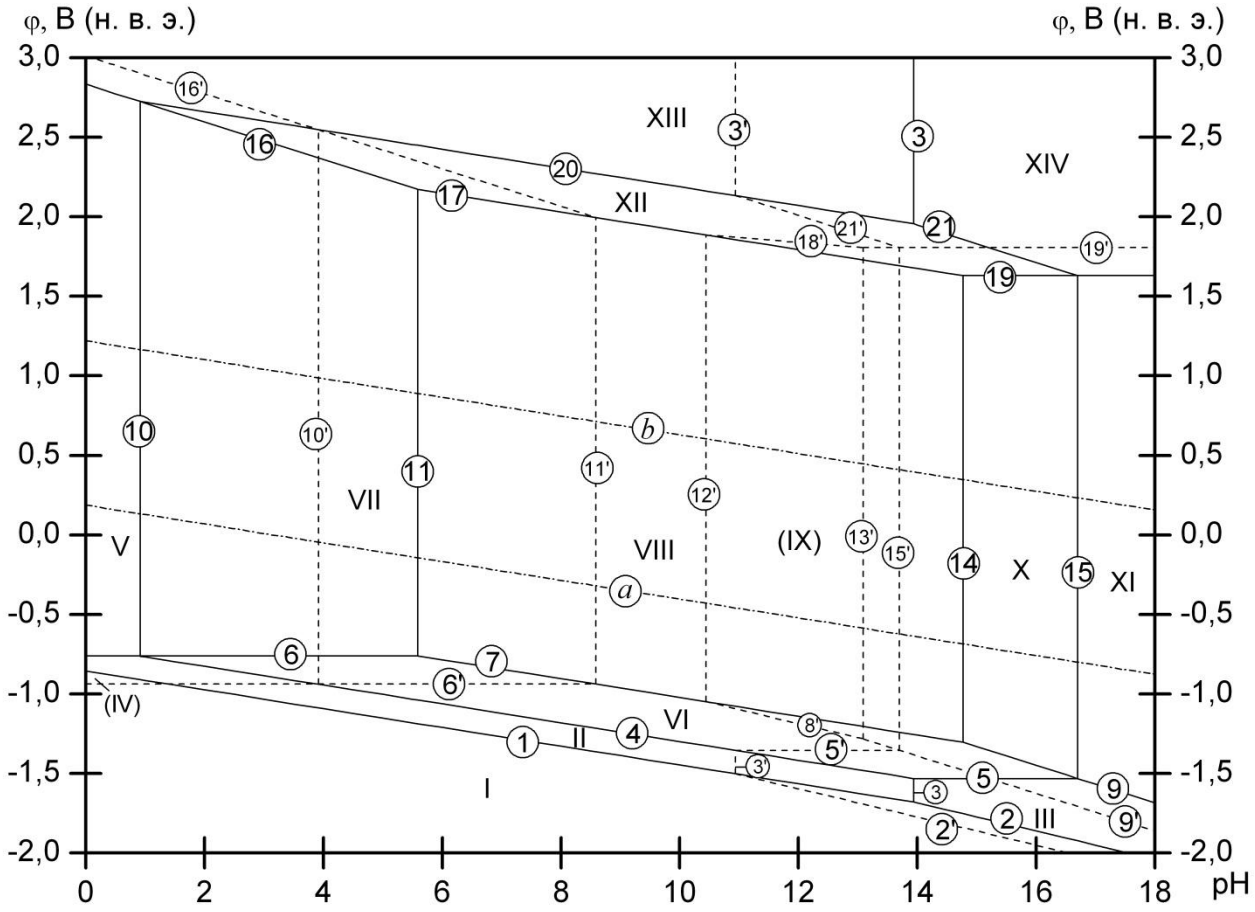

Figure 2. The potential – pH diagram of Zn – Si – H_2O system at 25˚C and pressure of 1 bar (unhydrated form of oxides): solid lines – equilibria, corresponding to a_i = 1 mol l^{-1}, dashed lines – equilibria, corresponding to $a_i = 10^{-6}$ mol l^{-1} (numbers marked by strokes).

Basing on analysis of potential – pH diagrams for systems Cu – Si – H_2O [12] and Zn – Si – H_2O (figure 2), the potential – pH diagram for system "siliceous brass CuZn17Si3 – H_2O" is plotted at 25ºC, pressure of 1 bar and activities of ions in solutions, equal to 1 (figure 3) and 10^{-6} mol l^{-1} (figure 4). Basic chemical and electrochemical equilibria in systems Zn – Si – H_2O and "brass CuZn17Si3 – H_2O" are summarized in table 5.

The differences between the diagrams, plotted at various activities of ions in solution, are related with that, as the calculations show, ions $HCuO_2^-$ and $HZnO_2^-$ are thermodynamically stable only at low concentrations of ions in solution ($\lg a_i < -5{,}68$ for $HCuO_2^-$ [53] and $\lg a_i < -3{,}34$ for $HZnO_2^-$ [54]). Therefore, different sequence of equilibria occurs at various activities of ions in solutions for various forms of copper (II) and zinc (II) [53, 54]. The results of calculations of equilibria, involving aforementioned ions, agree well with information, provided in potential – pH diagrams databases [55 – 63].

Lines *a* and *b* at the diagrams (which are shown by "dash-dot" lines at figures 2 – 4) correspond to work of hydrogen and oxygen electrodes, respectively. The area, which lies

between them, corresponds to water electrochemical stability and is most interesting for studying brass corrosion-electrochemical behaviour.

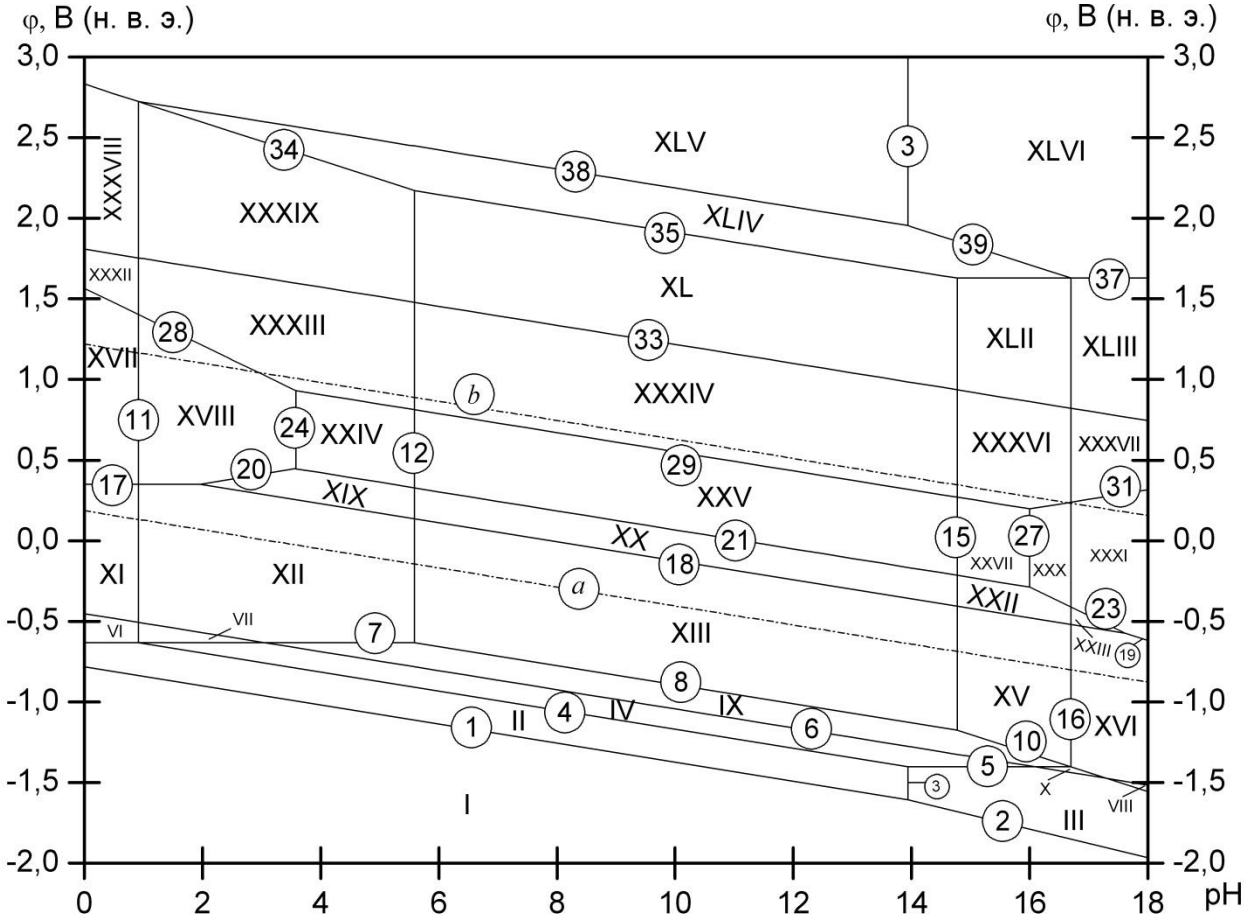

Figure 3. The potential – pH diagram of system "brass CuZn17Si3 – H_2O" at 25˚C, pressure of 1 bar and a_i = 1 mol l^{-1} (unhydrated form of oxides)

46 domains of predominance of certain phases can be depicted at the potential – pH diagram of "brass CuZn17Si3 – H_2O" system: I – α-phase (Cu, Zn, Si) + $CuH_{0,8}$; II – α-phase + $CuH_{0,8}$ + SiO_2; III – α-phase + $CuH_{0,8}$ + SiO_3^{2-}; IV – α-phase + $CuH_{0,8}$ + $ZnSiO_3$; V – α-phase + $CuH_{0,8}$ + Zn^{2+}; VI – α-phase + $CuH_{0,8}$ + SiO_2 + Zn^{2+}; VII – α-phase + $CuH_{0,8}$ + $ZnSiO_3$ + Zn^{2+}; VIII – α-phase + $CuH_{0,8}$ + SiO_3^{2-}, ZnO_2^{2-}; IX – α-phase + $ZnSiO_3$; X – α-phase + SiO_3^{2-}; XI – α-phase + $CuH_{0,8}$ + SiO_2 + Zn^{2+}; XII – α-phase + $CuH_{0,8}$ + $ZnSiO_3$ + Zn^{2+}; XIII – α-phase + ZnO + $ZnSiO_3$; XIV – α-phase + $ZnSiO_3$ + $HZnO_2^-$; XV – α-phase + $ZnSiO_3$ + ZnO_2^{2-}; XVI – α-phase + SiO_3^{2-}, ZnO_2^{2-}; XVII – SiO_2 + Zn^{2+}, Cu^{2+}; XVIII – $ZnSiO_3$ + Zn^{2+}, Cu^{2+}; XIX – $ZnSiO_3$ + Cu_2O + Zn^{2+}; XX – $ZnSiO_3$ + ZnO + Cu_2O; XXI – $ZnSiO_3$ + Cu_2O + $HZnO_2^-$; XXII – $ZnSiO_3$ + Cu_2O + ZnO_2^{2-}; XXIII – Cu_2O + SiO_3^{2-}, ZnO_2^{2-}; XXIV – $ZnSiO_3$ + CuO + Zn^{2+}; XXV – $ZnSiO_3$

+ ZnO + CuO; XXVI – $ZnSiO_3$ + CuO + $HZnO_2^-$; XXVII – $ZnSiO_3$ + CuO + ZnO_2^{2-}; XXVIII – $ZnSiO_3$ + $HZnO_2^-$, $HCuO_2^-$; XXIX – $ZnSiO_3$ + ZnO_2^{2-}, $HCuO_2^-$; XXX – $ZnSiO_3$ + ZnO_2^{2-}, CuO_2^{2-}; XXXI – ZnO_2^{2-}, CuO_2^{2-}, SiO_3^{2-}; XXXII – Cu_2O_3 + SiO_2 + Zn^{2+}; XXXIII – $ZnSiO_3$ + Cu_2O_3 + Zn^{2+}; XXXIV – $ZnSiO_3$ + ZnO + Cu_2O_3; XXXV – Cu_2O_3 + $ZnSiO_3$ + $HZnO_2^-$; XXXVI – Cu_2O_3 + $ZnSiO_3$ + ZnO_2^{2-}; XXXVII – Cu_2O_3 + SiO_3^{2-}, ZnO_2^{2-}; XXXVIII – CuO_2 + SiO_2 + Zn^{2+}; XXXIX – $ZnSiO_3$ + CuO_2 + Zn^{2+}; XL – $ZnSiO_3$ + ZnO + CuO_2; XLI – CuO_2 + $ZnSiO_3$ + $HZnO_2^-$; XLII – CuO_2 + $ZnSiO_3$ + ZnO_2^{2-}; XLIII – CuO_2 + SiO_3^{2-}, ZnO_2^{2-}; XLIV – CuO_2 + ZnO_2 + $ZnSiO_3$; XLV – CuO_2 + ZnO_2 + SiO_2; XLVI – CuO_2 + ZnO_2 + SiO_3^{2-}.

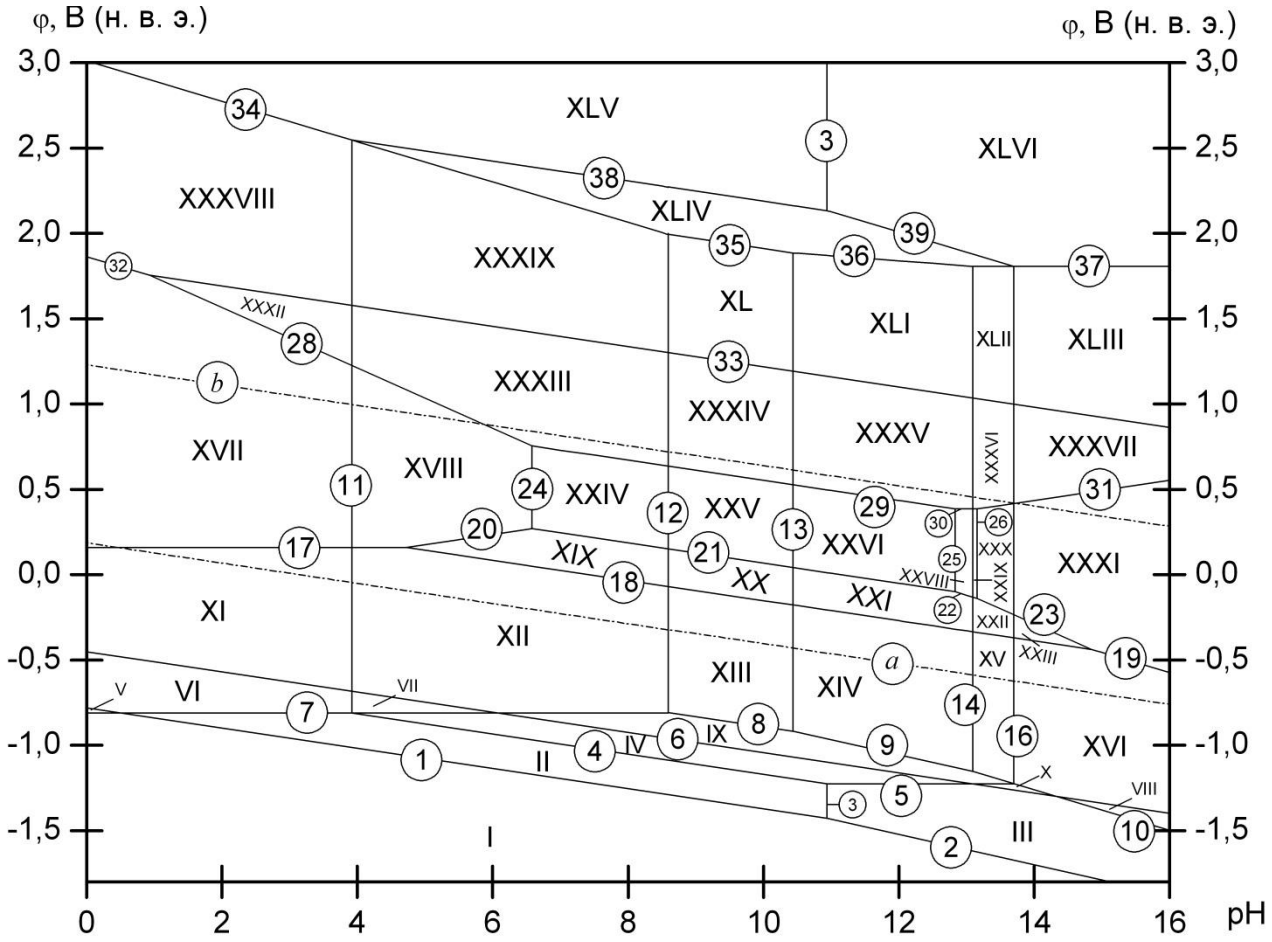

Figure 4. The potential – pH diagram of system "brass CuZn17Si3 – H_2O" at 25˚C, pressure of 1 bar and $a_i = 10^{-6}$ mol l^{-1} (unhydrated form of oxides)

Table 5

Basic chemical and electrochemical equilibria in systems "Zn – Si – H_2O" (figure 2) and "brass CuZn17Si3 – H_2O" (figures 3, 4) at 25˚C and total pressure of 10^5 Pas

Line number at fig. 2	Line number at fig. 3	Line number at fig. 4	Electrode reaction	Equilibrium potential, V (s. h. e.) or solution pH
a			$2H^+ + 2e^- = H_2$	$0{,}000 - 0{,}0591 \cdot pH - 0{,}0295 \cdot \lg p_{H_2}$
b			$O_2 + 4H^+ + 4e^- = 2H_2O$	$1{,}229 - 0{,}0591 \cdot pH + 0{,}0148 \cdot \lg p_{O_2}$
1			$SiO_2 + 4H^+ + 4e^- = Si + 2H_2O$;	
			fig. 2: $a_{Si} = 1$	$-0{,}857 - 0{,}0591 \cdot pH$
			fig. 3, 4: $a_{Si(\alpha)} = 9{,}5 \cdot 10^{-6}$	$-0{,}782 - 0{,}0591 \cdot pH$
2, 2'	2		$SiO_3^{2-} + 6H^+ + 4e^- = Si + 3H_2O$;	
			fig. 2: $a_{Si} = 1$	$-0{,}444 - 0{,}0887 \cdot pH + 0{,}0148 \cdot \lg a_{SiO_3^{2-}}$
			fig. 3, 4: $a_{Si(\alpha)} = 9{,}5 \cdot 10^{-6}$	$-0{,}370 - 0{,}0887 \cdot pH + 0{,}0148 \cdot \lg a_{SiO_3^{2-}}$
3, 3'	3		$SiO_3^{2-} + 2H^+ = SiO_2 + 2H_2O$	$pH = 13{,}94 + 0{,}5 \cdot \lg a_{SiO_3^{2-}}$
4			$ZnSiO_3 + 2H^+ + 2e^- = Zn + SiO_2 + H_2O$;	
			fig. 2: $a_{Zn} = 1$	$-0{,}709 - 0{,}0591 \cdot pH$
			fig. 3, 4: $a_{Zn(\alpha)} = 3{,}8 \cdot 10^{-5}$	$-0{,}578 - 0{,}0591 \cdot pH$
5, 5'	5		$ZnSiO_3 + 2e^- = Zn + SiO_3^{2-}$;	
			fig. 2: $a_{Zn} = 1$	$-1{,}533 - 0{,}0295 \cdot \lg a_{SiO_3^{2-}}$
			fig. 3, 4: $a_{Zn(\alpha)} = 3{,}8 \cdot 10^{-5}$	$-1{,}402 - 0{,}0295 \cdot \lg a_{SiO_3^{2-}}$
–	6		$Cu(\alpha) + 0{,}8H^+ + 0{,}8e^- = CuH_{0,8}$; $a_{Cu(\alpha)} = 0{,}339$	$-0{,}452 - 0{,}0591 \cdot pH$
6, 6'	7		$Zn^{2+} + 2e^- = Zn(\alpha)$; $a_{Zn(\alpha)} = 3{,}8 \cdot 10^{-5}$	
			fig. 2: $a_{Zn} = 1$	$-0{,}763 + 0{,}0295 \cdot \lg a_{Zn^{2+}}$
			fig. 3, 4: $a_{Zn(\alpha)} = 3{,}8 \cdot 10^{-5}$	$-0{,}632 + 0{,}0295 \cdot \lg a_{Zn^{2+}}$
7	8		$ZnO + 2H^+ + 2e^- = Zn + H_2O$;	
			fig. 2: $a_{Zn} = 1$	$-0{,}432 - 0{,}0591 \cdot pH$
			fig. 3, 4: $a_{Zn(\alpha)} = 3{,}8 \cdot 10^{-5}$	$-0{,}302 - 0{,}0591 \cdot pH$
8'	–	9	$HZnO_2^- + 3H^+ + 2e^- = Zn + 2H_2O$;	
			fig. 2: $a_{Zn} = 1$	$0{,}054 - 0{,}0887 \cdot pH + 0{,}0295 \cdot \lg a_{HZnO_2^-}$
			fig. 3, 4: $a_{Zn(\alpha)} = 3{,}8 \cdot 10^{-5}$	$0{,}185 - 0{,}0887 \cdot pH + 0{,}0295 \cdot \lg a_{HZnO_2^-}$
9, 9'	10		$ZnO_2^{2-} + 4H^+ + 2e^- = Zn + 2H_2O$;	
			fig. 2: $a_{Zn} = 1$	$0{,}441 - 0{,}1182 \cdot pH + 0{,}0295 \cdot \lg a_{ZnO_2^{2-}}$
			fig. 3, 4: $a_{Zn(\alpha)} = 3{,}8 \cdot 10^{-5}$	$0{,}572 - 0{,}1182 \cdot pH + 0{,}0295 \cdot \lg a_{ZnO_2^{2-}}$
10, 10'	11		$ZnSiO_3 + 2H^+ = Zn^{2+} + SiO_2 + H_2O$	$pH = 0{,}92 - 0{,}5 \cdot \lg a_{Zn^{2+}}$
11, 11'	12		$ZnO + 2H^+ = Zn^{2+} + H_2O$	$pH = 5{,}59 - 0{,}5 \cdot \lg a_{Zn^{2+}}$

12’	–	13	$HZnO_2^- + H^+ = ZnO + H_2O$	$pH = 16{,}44 + \lg a_{HZnO_2^-}$
13’	–	14	$ZnO_2^{2-} + H^+ = HZnO_2^-$	$pH = 13{,}09 + \lg \frac{a_{ZnO_2^{2-}}}{a_{HZnO_2^-}}$
14	15	–	$ZnO_2^{2-} + 2H^+ = ZnO + H_2O$	$pH = 14{,}77 + 0{,}5 \cdot \lg a_{ZnO_2^{2-}}$
15, 15’	16		$ZnO_2^{2-} + SiO_3^{2-} + 4H^+ = ZnSiO_3 + 2H_2O$	$pH = 16{,}70 + 0{,}25 \cdot \lg (a_{ZnO_2^{2-}} \cdot a_{SiO_3^{2-}})$
–	17		$Cu^{2+} + 2e^- = Cu;\ a_{Cu(\alpha)} = 0{,}339$	$0{,}351 + 0{,}0295 \cdot \lg a_{Cu^{2+}}$
–	18		$Cu_2O + 2H^+ + 2e^- = 2Cu + H_2O;$ $a_{Cu(\alpha)} = 0{,}339$	$0{,}467 - 0{,}0591 \cdot pH$
–	19		$CuO_2^{2-} + 4H^+ + 2e^- = Cu + 2H_2O;$ $a_{Cu(\alpha)} = 0{,}339$	$1{,}508 - 0{,}1182 \cdot pH + 0{,}0295 \cdot \lg a_{CuO_2^{2-}}$
–	20		$2Cu^{2+} + H_2O + 2e^- = Cu_2O + 2H^+$	$0{,}235 + 0{,}0591 \cdot pH + 0{,}0591 \cdot \lg a_{Cu^{2+}}$
–	21		$2CuO + 2H^+ + 2e^- = Cu_2O + H_2O$	$0{,}658 - 0{,}0591 \cdot pH$
–		22	$2HCuO_2^- + 4H^+ + 2e^- = Cu_2O + 3H_2O$	$1{,}771 - 0{,}1182 \cdot pH + 0{,}0591 \cdot \lg a_{HCuO_2^-}$
–	23		$2CuO_2^{2-} + 6H^+ + 2e^- = Cu_2O + 3H_2O$	$2{,}549 - 0{,}1773 \cdot pH + 0{,}0591 \cdot \lg a_{CuO_2^{2-}}$
–	24		$CuO + 2H^+ = Cu^{2+} + H_2O$	$pH = 3{,}58 - 0{,}5 \cdot \lg a_{Cu^{2+}}$
–		25	$HCuO_2^- + H^+ = CuO + H_2O$	$pH = 18{,}83 + \lg a_{HCuO_2^-}$
–		26	$CuO_2^{2-} + H^+ = HCuO_2^-$	$pH = 13{,}16 + \lg \frac{a_{CuO_2^{2-}}}{a_{HCuO_2^-}}$
–	27	–	$CuO_2^{2-} + 2H^+ = CuO + H_2O$	$pH = 15{,}99 + 0{,}5 \cdot \lg a_{CuO_2^{2-}}$
–	28		$Cu_2O_3 + 6H^+ + 2e^- = 2Cu^{2+} + 3H_2O$	$1{,}566 - 0{,}1773 \cdot pH - 0{,}0591 \cdot \lg a_{Cu^{2+}}$
–	29		$Cu_2O_3 + 2H^+ + 2e^- = 2CuO + H_2O$	$1{,}143 - 0{,}0591 \cdot pH$
–		30	$Cu_2O_3 + H_2O + 2e^- = 2HCuO_2^-$	$0{,}030 - 0{,}0591 \cdot \lg a_{HCuO_2^-}$
–	31		$Cu_2O_3 + H_2O + 2e^- = 2CuO_2^{2-} + 2H^+$	$-0{,}748 + 0{,}0591 \cdot pH - 0{,}0591 \cdot \lg a_{CuO_2^{2-}}$
–		32	$CuO_2 + 4H^+ + 2e^- = Cu^{2+} + 2H_2O$	$1{,}687 - 0{,}1182 \cdot pH - 0{,}0295 \cdot \lg a_{Cu^{2+}}$
–	33		$2CuO_2 + 2H^+ + 2e^- = Cu_2O_3 + H_2O$	$1{,}809 - 0{,}0591 \cdot pH$
16, 16’	34		$ZnO_2 + 4H^+ + 2e^- = Zn^{2+} + 2H_2O$	$2{,}833 - 0{,}1182 \cdot pH - 0{,}0295 \cdot \lg a_{Zn^{2+}}$
17	35		$ZnO_2 + 2H^+ + 2e^- = ZnO + H_2O$	$2{,}502 - 0{,}0591 \cdot pH$
18’	–	36	$ZnO_2 + H^+ + 2e^- = HZnO_2^-$	$2{,}016 - 0{,}0295 \cdot pH - 0{,}0295 \cdot \lg a_{HZnO_2^-}$
19, 19’	37		$ZnO_2 + 2e^- = ZnO_2^{2-}$	$1{,}629 - 0{,}0295 \cdot \lg a_{ZnO_2^{2-}}$
20	38		$ZnO_2 + SiO_2 + 2H^+ + 2e^- = ZnSiO_3 + H_2O$	$2{,}779 - 0{,}0591 \cdot pH$
21, 21’	39		$ZnO_2 + SiO_3^{2-} + 4H^+ + 2e^- = ZnSiO_3 + 2H_2O$	$3{,}603 - 0{,}1182 \cdot pH + 0{,}0295 \cdot \lg a_{SiO_3^{2-}}$

This maximum possible number of domains is characteristic for $a_i = 10^{-6}\ \text{mol} \cdot \text{l}^{-1}$ (figure 4). At the unity values of ions activities (figure 3) some domains (XIV, XXI, XXVI, XXVII, XXIX, XXXV, XLI) are missing due to thermodynamic instability of corresponding ions.

As calculations show, brass CuZn17Si3 is affected by hydride or oxide passivation almost at all values of pH and potentials. A huge domain, enclosed between the lines 4, 5, 11, 16, 38 and 39, corresponds to zinc silicate $ZnSiO_3$. Zinc and silicon content in alloy is sufficient to form a continuous $ZnSiO_3$ layer on its surface. The other zinc and copper oxides could be locally included into inner sublayer of this passivation film. Zinc silicate is much stable in chemical and electrochemical term, than zinc and copper oxides. It decomposes only within strongly acidic (left of the line 11 at figures 3 and 4), strongly alkaline (right of the line 16) and strongly oxidizing (above the lines 38 and 39) environments. This is a reason of silicon beneficial influence on corrosion-electrochemical properties of copper-zinc alloys.

Conclusions

The state diagram for Zn – Si – O system and potential – pH diagram for Zn – Si – H_2O system (which are the missing in literature parts of quaternary Cu – Zn – Si – O system) are calculated and plotted at 25˚C, air pressure of 1 bar and activities of ions in solutions, equal to 1 and 10^{-6} mol l^{-1}.

The potential – pH diagram of system “brass CuZn17Si3 – H_2O” is plotted at 25˚C, air pressure of 1 bar and activities of ions in solutions, equal to 1 and 10^{-6} mol l^{-1}.

Thermodynamic analysis of siliceous brass CuZn17Si3 oxidation processes in oxygen-containing environments, as well as the analysis of its corrosion-electrochemical behavior in water environments are performed. It is shown that high corrosion resistance of brass is achieved with respect to formation of protective layer from $ZnSiO_3$ on its surface.

References

1. Кремнистая латунь / Большая энциклопедия нефти и газа. – URL: <http://www.ngpedia.ru/id125195p3.html>.
2. Кремнистая латунь / Строительная энциклопедия. – URL: <http://www.bibliotekar.ru/spravochnik-181-2/163.htm>.
3. Некоторые виды латуней / ЦветМетТорг. – URL: <http://www.cmtorg.ru/news/2010_08_10>.
4. И. И. Новиков. Меди сплавы // Краткая химическая энциклопедия / под ред. И. Л. Кнунянц. – М.: Советская энциклопедия, 1964. – Т. 3. – С. 70.

5. А. Г. Тюрин Термодинамика химической и электрохимической устойчивости твёрдых сплавов железа, хрома и никеля. – Челябинск: Изд-во ЧелГУ, 2011. – 241 с.
6. Нормис: фазовый состав и структура сплавов. – URL: <http://normis.com.ua/index.php?option=com_content&view=article&id=28&Itemid=35>.
7. А. Г. Тюрин, А. А. Шрейнер. Термодинамика химической и электрохимической устойчивости латуней // Защита металлов, 2007. – Т. 43. – № 3. – С. 313 – 319.
8. Ulrika Borggren, Malin Selleby. A thermodynamic database for special brass // Journal of Phase Equilibria, 2003. – Vol. 24. – № 2. – P. 110 – 121.
9. Диаграммы состояния двойных металлических систем: справочник. В 3 томах / под ред. Н. П. Лякишева: Т. 1. – М.: Машиностроение, 1996 – 992 с; Т. 1. – М.: Машиностроение, 1996 – 992 с; Т. 2. – М.: Машиностроение, 1997 – 1024 с; Т. 3. Кн. 1. – М.: Машиностроение, 2001 – 872 с; Т. 3. Кн. 2. – М.: Машиностроение, 2000 – 448 с.
10. Phase diagram – Web // FactSage Database. – URL: <http://www.crct.polymtl.ca/fact/documentation>.
11. Xinyan Yan, Y. A. Chang. A thermodynamic analysis of the Cu–Si system // Journal of Alloys and Compounds, 2000. – № 308. – P. 221 – 229.
12. П. А. Николайчук, А. Г. Тюрин. Термодинамика химической и электрохимической устойчивости сплавов системы Cu – Si // Бутлеровские сообщения, 2011. – Т. 24. – № 4. – С. 88 – 94.
13. M. H. G. Jacobs and P. J. Spencer. A critical thermodynamic evaluation of the systems Si – Zn and Al – Si – Zn // CALPHAD, 1996. – Vol. 20. – № 3. – P. 307 – 320.
14. Jyrki Miettinen. Thermodynamic description of the Cu–Si–Zn system in the copper-rich corner // CALPHAD, 2007. – Vol. 31. – № 4 – P. 422 – 427.
15. H. Liang and Y.A. Chang. A thermodynamic description for the Al – Cu – Zn system // Journal of Phase Equilibria, 1998. – Vol. 19. – № 1. – P. 25 – 37.
16. А. Г. Тюрин. Термодинамика химической и электрохимической устойчивости алюминиевых, кремнистых и оловянных бронз // Защита металлов, 2008. – Т. 44. – № 2. – С. 1 – 9.
17. Д. М. Лаптев Термодинамика металлургических растворов: монография. – Челябинск: Металлургия, 1992. – 352 с.

18. Г. Г. Михайлов, Б. И. Леонович, Ю. С. Кузнецов. Термодинамика металлургических процессов и систем: монография. – М.: Изд. Дом МИСиС, 2009. – 520 с.
19. Otto Redlich and A. T. Kister. Algebraic representation of thermodynamic properties and the classification of solutions // Industrial and Engineering Chemistry, 1948. – Vol. 40. – № 2. – P. 345 – 348.
20. Справочник по электрохимии / под ред. А. М. Сухотина. – Л.: Химия, 1981. – 488 с.
21. Г. К. Моисеев, Н. А. Ватолин, Л. А. Маршук, Н. И. Ильиных. Температурные зависимости приведённой энергии Гиббса некоторых неорганических веществ: альтернативный банк данных ASTRA. OWN. – Екатеринбург: УрОРАН, 1997. – 230 с.
22. Е. В. Шарлай Особенности электрохимического поведения системы медь–раствор гидроксида калия в области температур 295 – 320 К: автореф. дисс. канд. хим. наук. – Челябинск: Изд-во ЮурГУ, 2008. – 19 с.
23. Gernot Goll. Metal-oxide superconductors // Springer Tracts in Modern Physics, 2006. – Vol. 214/2006. Unconventional superconductors. – P. 121 – 151.
24. А. Ю. Захаров, В. Я. Митрофанов, А. Е. Никифоров. Барическая зависимость температуры Нееля T_N в $LaCu_2O_4$ // Оксиды. Физико-химические свойства. Сборник трудов V Всероссийской научной конференции. – Екатеринбург, 2000. – С. 181 – 184.
25. Ю. Д. Панов, Е. В. Зенков, А. С. Москвин. Локальные эффекты анизотропного давления в сверхпроводящих CuO_2-плоскостях // Оксиды. Физико-химические свойства. Сборник трудов V Всероссийской научной конференции. – Екатеринбург, 2000. – С. 366 – 369.
26. Xu Gaojie, Pu Qirong, Zhang Zengming, Ding Zejun. Effect of oxygen-deficiency of CuO_2 plane on the structure, magnetism, and transport properties // Journal of Superconductivity, 2001. – Vol. 14. – № 4. – P. 509 – 517.
27. M. A. Teplov, O. N. Bakharev, A. V. Dooglav, A. V. Egorov, I. R. Mukhamedshin, et al. Inhomogeneity of charge and spin distribution in CuO_2 layers of high-T_c superconductors: NQR/NMR studies of 1-2-3 compounds // Journal of Superconductivity, 1999. – Vol. 12. – № 1. – P. 113 – 115.
28. Y. A. El-Tantawy, A. E. El-Kholy, T. S. E. Kasem. The passivation of dilute Cu(Hg) in alkaline solutions // Corrosion Science, 1978. – Vol. 18. – № 12. – P. 1065 – 1073.

29. Michihito Muroi, Robert Street. Charge distribution in triple-layered copper oxide superconductors // Physica C: Superconductivity, 1995. – Vol. 248. – № 3 – 4. – P. 290 – 310.
30. Y. Tokura. Material overview of high-T_c oxides // Physica C: Superconductivity, 1991. – Vol. 185 – 189. – Part 1, 1. – P. 174 – 179.
31. H. A. Wriedt. The O – Zn (oxygen – zinc) system // Bulletin of Alloy Phase Diagrams, 1987. – Vol. 8. – № 2. – P. 166 – 176, 192 – 200.
32. В. А. Киреев Методы практических расчётов в термодинамике химических реакций. – М.: Химия, 1970. – 520 с.
33. P. A. Nikolaychuk, A. G. Tyurin. The analysis of standard Gibbs energies of formation of MeO_2 type oxides of fourth period d-elements // Abstracts of the XVIII International Conference on Chemical Thermodynamics in Russia: Vol. 2. – Samara: Samara State Technical University, 2011. – P. 17 – 18.
34. Диаграммы состояния силикатных систем: справочник / Н. А. Торопов, В. П. Борзаковский [et al.]. – М.–Л.: Наука, 1965. – Вып. 2. – 372 с.
35. A. Navrotsky. Thermodynamics of Formation of the Silicates and Germanates of some Divalent Transition Metals and of Magnesium // Journal of Inorganic and Nuclear Chemistry, 1971. – Vol. 33. – P. 4035 – 4050.
36. Ю. Д. Третьяков. Термодинамика ферритов. –Л.: Химия, 1967. –305 с.
37. Л. П. Рузинов, Б. С Гуляницкий.. Равновесные превращения металлургических реакций. – М.: Металлургия, 1975. – 416 с.
38. Термические константы веществ: база данных – URL: <http://www.chem.msu.su/cgi-bin/tkv.pl?show=welcome.html>.
39. JANAF Thermochemical Tables. Third Edition // Journal of Physical and Chemical Reference Data, 1985. – Vol. 14. – Suppl. 1.
40. У. Д. Верягин [et al.] Термодинамические свойства неорганических веществ: справочник / Под ред. Зефирова А. П. – М.: Атомиздат, 1965. – 461 с.
41. L. B. Pankratz, J. M. Stuve, M. A. Gokcen Thermodynamic data for mineral technology: handbook. – Bureau of Mines USA, 1984. – 355 p.
42. Справочник химика / под ред. Б. П. Никольского. – М.–Л.: Химия, 1964. – Т. 3. – 1008 с.
43. Л. Киш Кинетика электрохимического растворения металлов / пер. с англ. Е. В. Овсянниковой; под ред. А. М. Скундина. – М: Мир, 1990. – 272 с.
44. Pourbaix diagrams / Substances & Technologies. – URL: <http://www.substech.com/dokuwiki/doku.php?id=pourbaix_diagrams>.

45. R. M. Garrels, C. L. Christ. Solutions, Minerals and Equilibria. New York : Harper & Row, 1965. – 368 p.
46. J. E. Funk, R. M. Reinstrom. Energy requirements in the production of hydrogen from water // I & EC Process Design and Development, 1966. – Vol. 5. – № 3. – P. 336 – 342.
47. A. Vaškelis, R. Juškėnas, J. Jačiauskienė. Copper hydride formation in the electroless copper plating process: in situ X-ray diffraction evidence and electrochemical study // Electrochimica Acta, 1998. – Vol. 43. – № 9. – P. 1061 – 1066.
48. Pavel Korzhavyi, Inna Soroka, Mats Boman and Börje Johansson. Thermodynamics of Stable and Metastable Cu-O-H Compounds // Solid State Phenomena, 2011. – Vols. 172 – 174. – P. 973 – 978.
49. R. Burtovyy, E. Utzig, M. Tkacz. Studies of the thermal decomposition of copper hydride // Thermochimica Acta, 2000. – Vol. 363. – P. 157 – 163.
50. R. Burtovyy, D. Włosewicz, A. Czopnik, M. Tkacz. Heat capacity of copper hydride // Thermochimica Acta, 2003. – Vol. 400. – P. 121 – 129.
51. M. Tkacz, R. Burtovyy. Decomposition of the hexagonal copper hydride at high pressure // Solid State Communications, 2004. – Vol. 132. – P. 37 – 41.
52. F. Cotton, G. Wilkinson Advanced Inorganic Chemistry. New York – London – Sydney – Toronto: John Wiley & Sons, 1972. – 1147 p.
53. П. А. Николайчук, А. Г. Тюрин, И. И. Канатьева. Уточнённая диаграмма Пурбе для меди // Современные проблемы теоретической и экспериментальной химии: Межвузовский сборник научных трудов VII Всероссийской конференции молодых учёных с международным участием. Саратов: ООО Издательство “КУБиК”, 2010. – С. 287 – 291.
54. П. А. Николайчук, А. Г. Тюрин. Уточнённая диаграмма Пурбе для цинка // Современные проблемы теоретической и экспериментальной химии: Межвузовский сборник научных трудов VIII Всероссийской конференции молодых учёных с международным участием. Саратов: ООО Издательство “КУБиК”, 2011. – С. 226 – 230.
55. FactSage EpH-Web. – URL: <http://www.sgte.org/ephweb.php>.
56. THERMEXPERT – Potential – pH diagram generator / Argentum Solutions, Inc. – URL: <http://www.argentumsolutions.com/cgi-bin/thermexpert>.
57. SUPCRT / Prediction Central. – URL: <http://www.predcent.org/download/supcrt>.
58. The Geochemist’s Workbench (GWB). – Rockware: Earth Science and GIS Software. – URL: <http://www.rockware.com/product/overview.php?id=132>.
59. JNC-TDB. – Japan Nuclear Cycle Organization. – URL: <http://migrationdb.jnc.go.jp>.

60. ZZ-HATCHES 19: Database for radiochemical modeling / Nuclear Energy Agency. – URL: <http://www.oecd-nea.org/tools/abstract/detail/nea-1210>.
61. PHREEQC-2: A Computer Program for speciation, batch-reaction, one-dimensional transport, and inverse geochemical calculations / USGS. – URL: <http://wwwbrr.cr.usgs.gov/projects/GWC_coupled/phreeqc>.
62. SOLGASWATER program. – URL: <http://158.227.5.164/Chemical_Diagrams/html/ISP_Solgaswater.htm>.
63. Atlas of Eh-pH diagrams: Intercomparison of thermodynamic databases / Geological survey of Japan. Open file report № 419. – National Institute of Advanced Industrial Science and Technology, 2005. – URL: <www.gsj.jp/GDB/openfile/files/no0419/openfile419e.pdf>.

18. Cu – Ni – Mn – Si system

18.1. Siliceous bronzes

Siliceous bronzes are copper alloys containing nickel and / or manganese and silicon.

The composition of two the most widely known siliceous brasses determined according to the Russian State Standards and the UNS and ASTM classifications is collected in Table 16.

Table 16. The composition of various marks of siliceous bronzes according to the Russian State Standards and the UNS and ASTM classifications.

Bronze	Content of the element, weight %			
	Cu	Mn	Ni	Si
БрКМц3–1, C65500	96	1	–	3
БрКН1–3, C70320	95,6	0,4	3	1

The content of the elements in these bronzes is such that the system remains one-phase and represents a three- or four-component solid solution, based on (fcc-Cu).

Table 17. Thermodynamic activities of the siliceous bronzes components.

Bronze	Thermodynamic activity			
	Cu	Mn	Ni	Si
БрКМц3–1, C65500	0,917	$9{,}4\cdot10^{-4}$	–	$3{,}6\cdot10^{-7}$
БрКН1–3, C70320	0,976	$1{,}1\cdot10^{-3}$	$3{,}0\cdot10^{-5}$	$6{,}7\cdot10^{-9}$

18.2. Thermodynamic activities of Cu – Ni – Mn – Si system components

The expression for the excess Gibbs energy of the ternary Cu – Mn – Si system and of the quarternary Cu – Ni – Mn – Si system was proposed by Miettinen and based on the thermodynamic descriptions of the boundary binary and ternary systems [Miettinen, 2003a; Miettinen, 2003b; Miettinen, 2005]. The data of these studies were consistent with each other. The solid solution of the alloying elements in fcc-copper was modelled in

terms of the substitution solution model. The activities of the components for all bronzes from Table 16 were calculated using the expressions proposed by. The results of these calculations are presented in Table 17.

The calculations show that the solid solution of manganese, nickel and silicon in fcc-copper exhibits slight negative deviations from ideal behaviour.

18.3. Potential – pH diagram of Cu – Ni – Mn – Si – H_2O system

The potential – pH diagram for the siliceous bronze БрКМц3–1 (C65500) at 25 °C, air pressure of 1 bar and the activities of 10^{-4} mol·l^{-1} is presented in Figure 68. The scheme, illustrating the domains of immunity, active dissolution, passivity and trans passivity of the bronze, as well as the probable compound that could form the protective layer on the surface, is presented in Figure 70. Figures 69 and 71 present the same, but for the bronze БрКН1–3 (C70320).

The calculations show that in the domain of electrochemical stability of water neither nickel, nor manganese silicates play a major role in the formation of the passivation layer on the brass surface. Most probably, the passivation layer might consist of copper silicate and manganese and nickel oxides.

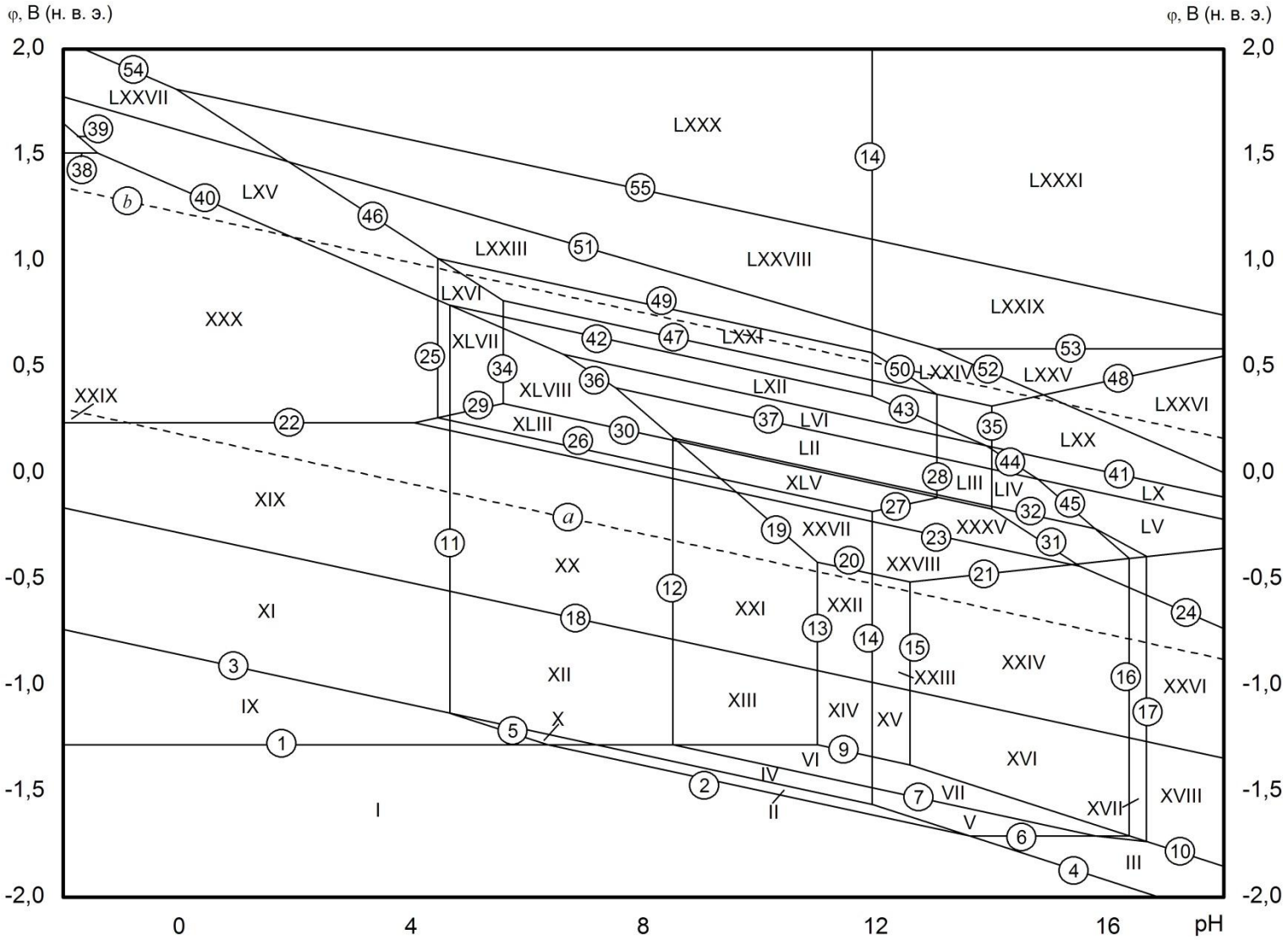

Fig. 68. The potential – pH diagram for the siliceous bronze БрКМц3–1 (C65500) at 25 °C, air pressure of 1 bar and the activities of 10^{-4} M.

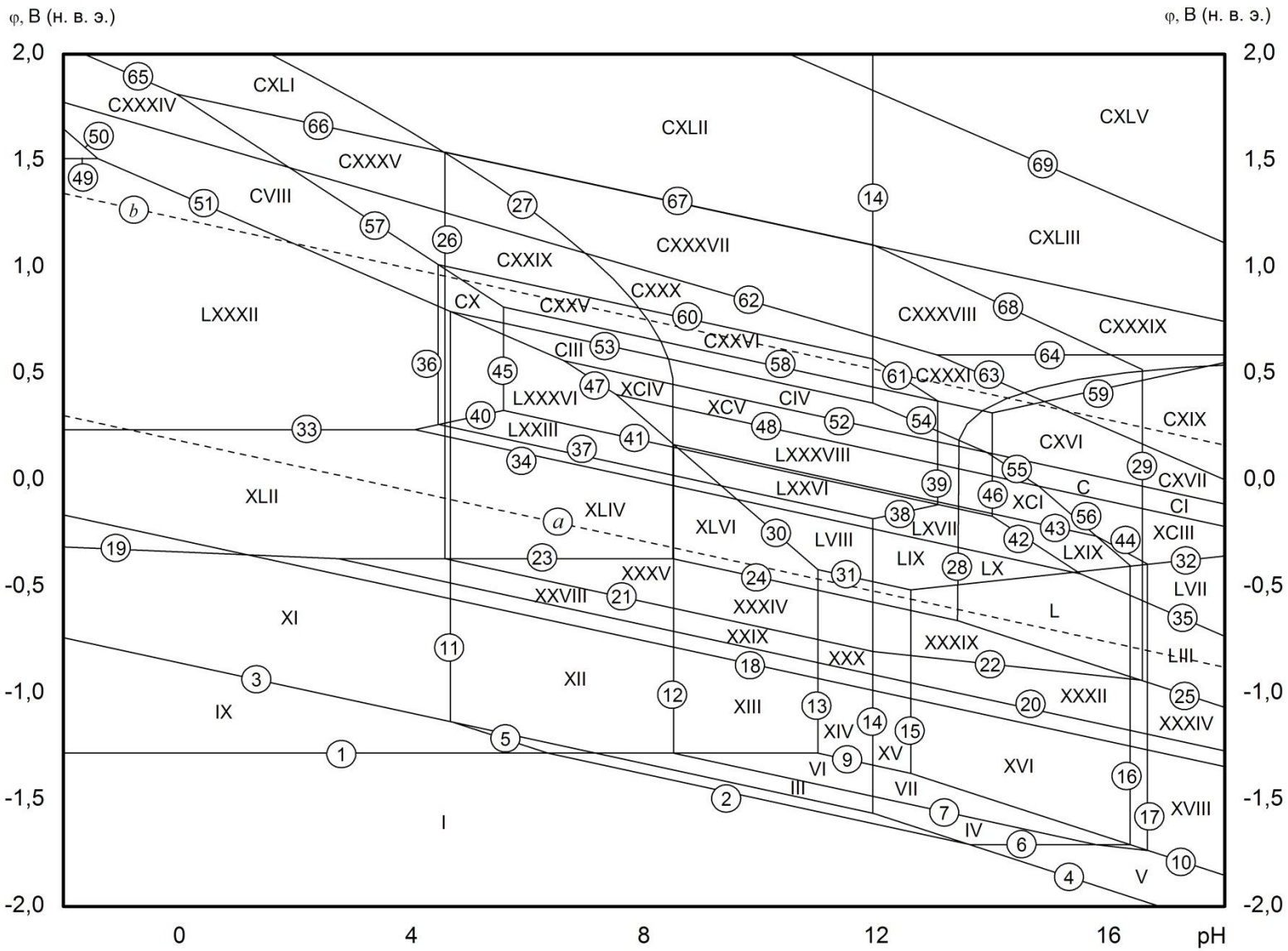

Fig. 69. The potential – pH diagram for the siliceous bronze БрКН1–3 (C70320) at 25 °C, air pressure of 1 bar and the activities of 10^{-4} M.

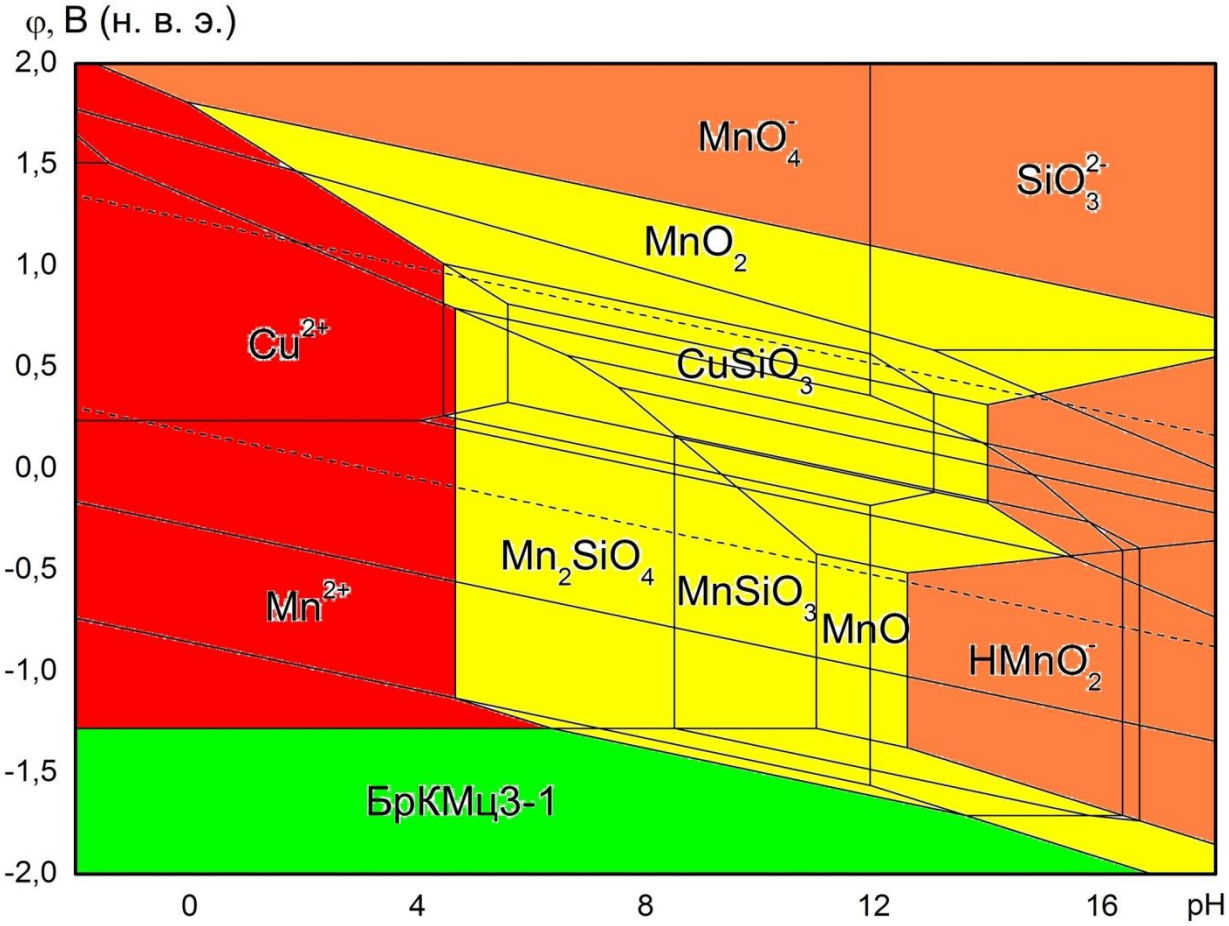

Fig. 70. The domains of various corrosion-electrochemical behaviour of the bronze БрКМц3–1 (C65500), and the probable compounds that form the passivation layer.

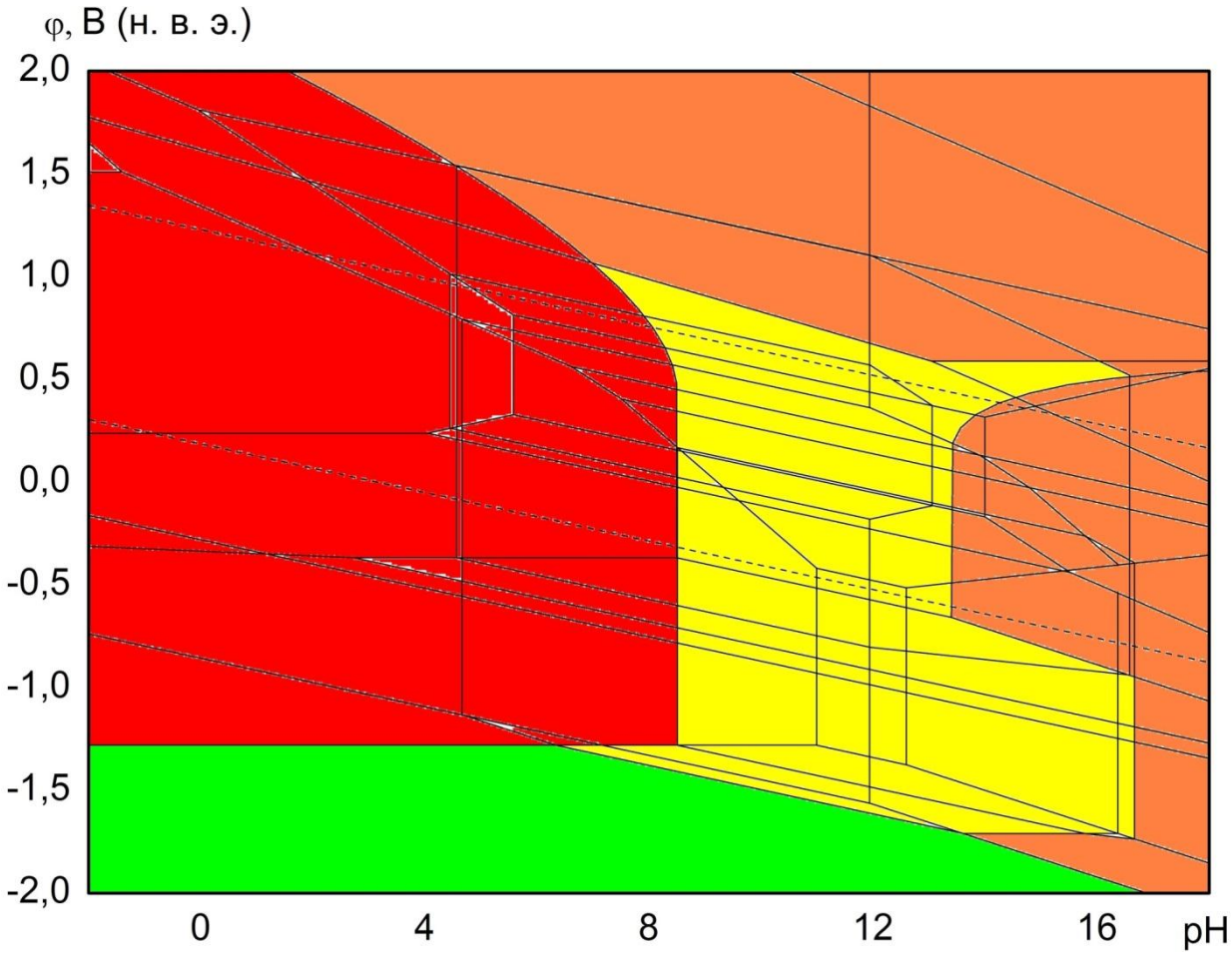

Fig. 71. The domains of various corrosion-electrochemical behaviour of the bronze БрКН1–3 (C70320).

Publications to chapter 18

The content of this chapter was not published yet.

19. Polarisation curves and polarisation potential – pH diagrams

The rate of any electrochemical reaction (which is always a heterogeneous process [Levenspiel, 1999]) is defined as:

$$r = \pm \frac{1}{S} \cdot \frac{dn_i}{dt}, \tag{106}$$

where S, m^2 is the reaction surface (which usually is determined by the surface of the corresponding electrode, at which the reaction occurs), $\frac{dn_i}{dt}, \frac{mol}{s}$ is the first derivative of the amount of substance of the reagent or the product with respect to time, *id est*, the rate of change of the amount of substance with time. The dimension units for the electrochemical reaction rate is $\frac{mol}{m^2 \cdot s}$.

However, the rate of electrochemical reaction is proportional to the density of the current passing through the electrode:

$$i = \nu_{e^-} \cdot F \cdot r = \pm \frac{\nu_{e^-} \cdot F}{S} \cdot \frac{dn_i}{dt}, \tag{107}$$

where ν_{e^-} is the number of electrons, involved in the electrochemical process, F is the Faraday constant, and i is the current density. It follows from the equation (107) that the dimension unit of the current density is $\frac{mol}{m^2 \cdot s} \cdot \frac{Cl}{mol} = \frac{Cl}{m^2 \cdot s} = \frac{A}{m^2}$.

When the surface of the electrode is known, the measure of the electrochemical reaction rate is possible by measuring the current passing through it. The rates of electrochemical reaction usually depend on electrode potentials. The plot of i = i(E) (or of lg i versus E) for the electrochemical reaction is called a *polarisation curve*.

The rates of the electrochemical processes corresponding to the various corrosion behaviours of metals and alloys are evidently different. If the system changes its corrosion-electrochemical behaviour, the slope at the polarisation curve also changes. By plotting the polarisation curves for a given sample at the different constant pH values and combining these special points in the polarisation curves, where their slope changes, the so called *polarisation potential – pH diagram* might be produced. The method of plotting such a diagram is illustrated by Figure 72.

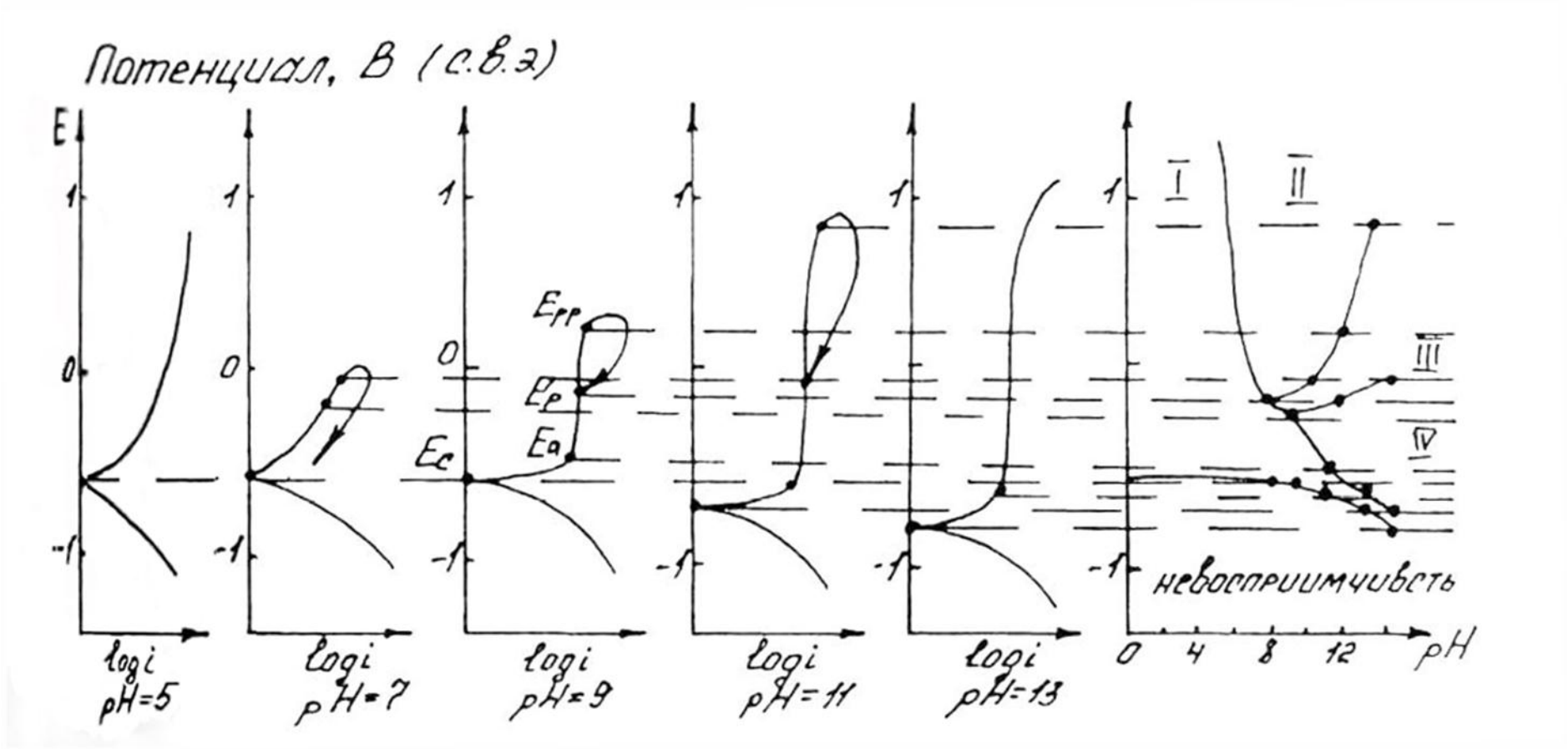

Fig. 72. The method of construction of the polarisation potential – pH diagram using the polarisation curves plotted at different pH values.

The polarisation potential – pH diagram depicts the experimental conditions of immunity, general corrosion, perfect and imperfect passivity as functions of potential and pH and shows the electrode potentials related with formation of new phases and phase transitions on alloy surface, depicting the borders of phase transformations.

Evidently, the experimentally determined potentials corresponding to the phase transitions do not match the equilibrium potentials calculated on the basis of Nerst equation due to various effects of overpotential. The nature of these effects might be related to the diffusion of the electrolyte to the electrode surface, surface effects at the electrode, the formation of phases with different crystal structures, the irreversibility of the electrode reaction *et cetera*. Moreover, the $I \cdot R$ drop caused by the electrical resistance of the solution could be minimised but not completely supressed. Consequently, the polarisation potential – pH diagrams do not match the equilibrium potential – pH diagrams perfectly. However, these two diagram types, when plotted together, could complement each other and provide more information about the phase transformations in the system during the electrochemical reactions.

19.1. Equilibrium and polarisation potential – pH diagrams of the strictural stailness steel 20KT

The structural stainless steel 20KT is manufactured according to the Russian State Standard. The main alloying elements are copper, manganese, carbon and silicon.

The procedure of constructing both the equilibrium and polarisation potential – pH diagrams for the steel 20KT is presented in the attached publication.

Publications to chapter 19

The content of this chapter was published in the paper [Tyurin et al., 2016]. The preprint of this paper is presented below with the permission from *Emerald*.

Method of estimation of corrosion stability of multicomponent alloys using equilibrium and polarization potential – pH diagrams

Tyurin, Aleksandr Georgievich
Department of Analytical and Physical Chemistry, Chelyabinsk State University, Chelyabinsk, Russian Federation;

Manannikov, Dmitriy Andreevich and Parshukov , Vladimir Pavlovich
Department of Analytical and Physical Chemistry, Chelyabinsk State University, Chelyabinsk, Russian Federation and Laboratory of Corrosion Testing, Russian Scientific-Research Institute of Pipe Industry, Chelyabinsk, Russian Federation;

Antonova, Anna Valeryevna
Department of Analytical and Physical Chemistry, Chelyabinsk State University, Chelyabinsk, Russian Federation; and

Nikolaychuk, Pavel Anatolyevich*
Department of Analytical and Physical Chemistry, Chelyabinsk State University, Chelyabinsk, Russian Federation and Institute of Physical Chemistry, Universität zu Köln, Cologne, Germany

*Corresponding Author's Email: npa@csu.ru

Structured Abstract:
Purpose: The purpose of this study is to develop a method of thermodynamic and kinetic evaluation of corrosion properties of alloys.
Design/methodology/approach: Method of estimation of corrosion-electrochemical behaviour of multicomponent alloys is proposed. Method takes into account both thermodynamic and kinetic data and is based on mutual construction of equilibrium and polarization potential – pH diagrams. The usage of the proposed method is illustrated on the example of the structural steel 20KT.
Findings: Passivation of steel 20KT is determined by formation of oxide film based on magnetite (Fe_3O_4); silicon, manganese and copper oxides as well as manganese sulphides can be locally included into inner side of passivation layer. An experimental potential – pH diagram of steel 20KT is constructed. Interpreting the results of polarization measurements revealed good agreement between equilibrium and polarization potential – pH diagrams.
Originality/value: It is shown on the example of structural steel 20KT that in for interpretation of experimental potential – pH diagrams one should compare them with corresponding equilibrium diagrams for multicomponent alloys rather than with Pourbaix diagrams for pure metals. The corrosion properties of steel 20KT are estimated using equilibrium and polarization potential – pH diagrams.

Keywords: Thermodynamic and kinetic evaluation of corrosion properties, Equilibrium potential – pH diagram, Polarization potential – pH diagram, Structural steel 20KT.

1. Introduction.

The studying of the corrosion properties of materials includes consideration of both thermodynamics and kinetics of corrosion processes (Revie and Uhlig, 2008). Thermodynamic calculations are the excellent starting point for any corrosion studies (Revie and Uhlig, 2008; Thompson et al., 2011). Pourbaix (1990) proposed a compact method of displaying thermodynamic information in form of E – pH diagrams, which are called Pourbaix diagrams (or

equilibrium potential – pH diagrams). Currently Pourbaix diagrams are constructed for the large number of systems. However any thermodynamic predictions always require experimental verification (Revie and Uhlig, 2008; Thompson et al., 2011). For the experimental study of the corrosion properties of metals and determination of the kinetic characteristics of corrosion processes polarization diagrams are usually used (Revie and Uhlig, 2008). From the other side, any polarization diagram describes the corrosion properties of studying system only in one particular environment.

The possibility of combining these two approaches was firstly shown by Nagel et al. (1957), this method was developed further by Pourbaix (1970 and 1972) and used by many researchers. By plotting the polarization diagrams for the same sample in multiple environments with different pH values, they used them to construct experimental E – pH dependencies (which are called *polarization* potential – pH diagrams). However, such studies are either devoted to constructing polarization potential – pH diagrams for pure metals (Nagel et al., 1957; Pourbaix, 1970 and 1972; Lange and Ohse, 1958; Lange and Weidinger, 1958; Ohse, 1959 and 1960; Perrault, 1979; Gimenez et al., 1981; Reymond et al. 1996; Chuan et al., 1996) or the authors compare experimental diagrams for complex alloys only with Pourbaix diagrams for pure metals (Mattsson, 1961; Horvath and Hackl, 1965; Vernik Jr and Pourbaix, 1971; Efird, 1975; Efird and Vernik Jr, 1977; Lennon and Robinson, 1986; Jingyi et al., 1989; Shih et al., 1994; Bai et al., 1995; Kurov, 1998; Tamilmani et al., 2002; Chen et al., 2005 and 2006; Xu et al., 2011; Sun et al., 2012).

The present study proposes a new approach: the experimental potential – pH diagram for multicomponent alloy has to be compared directly with equilibrium potential – pH diagram for this alloy. This is much more rational and allows to interpret correctly the results of polarization measurements and to establish the relation with thermodynamic calculations and experiment. The usage of this method is illustrated on the example of estimation of corrosion behaviour of structural steel 20KT.

2. Plotting the equilibrium E – pH diagram for steel 20KT.

2.1. Basic principles.

The procedure of construction of Pourbaix diagram for multicomponent alloys consists of three stages. In the first place, one needs to consider all phase and chemical equilibria in studied system at desired conditions, review the concordance among reference data and calculate thermodynamic properties of metallic system. At the next step it is necessary to collect information about all possible simple and mixed oxides that can be formed in system and to create thermodynamic model of oxidation of alloy in oxygen-containing environments. Finally, one needs to add to consideration the ionic species that can be formed during oxidation of alloy component in water environments, write possible reactions with their participation, calculate thermodynamic properties of these reactions and plot Pourbaix diagram (Thompson et al., 2011).

2.2. Phase equilibria in steel 20KT at standard temperature.

Chemical composition of steel 20KT according to GOST 633-80 (Russian State standard) is presented in Table 1.

Table 1. Chemical composition of the structural steel 20KT / wt-%

C	Si	Mn	P	S	Cr	Ni	Cu	Al
0.16	0.29	0.47	0.006	0.003	0.06	0.15	0.16	0.01

However, it was taken into account during modeling of phase equilibria in steel 20KT that only carbon, silicon, manganese and copper are present in alloy with iron. Traces of chromium and nickel have practically no effect on the corrosion-electrochemical behaviour of

steel (Tyurin, 2011); aluminum and sulphur, together with finishing treatment of melt with synthetic slags, specify the number and composition of the corrosion-active nonmetallic inclusions remaining in metal (Tyurin et al., 2007).

Carbon is present in steel in form of the carbides $(Fe,Mn)_3C$ and forms cementite phase. Iron, manganese and silicon form ferrite phase (a solid solution of Mn and Si in α-Fe) (Tyurin, 2011). The solubility of copper in solid iron was experimentally measured only for temperatures exceeding 450ºC (Perez et al., 2005a and 2005b; Toyama et al., 2014; Salje and Feller-Kniepmeier, 1977), therefore the solubility limit at 25ºC was estimated by CALPHAD method according to data of Chen and Jin (1995). The calculated maximum solubility of Cu in α-Fe at 25°C is ~10^{-5} mol.-%, and the excessive content is present in steel 20KT in form of distributed inclusions of pure copper (ε-Cu). Thermodynamic activities of components of ferrite phase (α-Fe) were calculated in terms of substitution solution model. The model parameters for boundary binary systems were estimated by Kaufman (1978 and 1979). The calculated values of activities of components of ferrite at 25ºC are the following: $a_{Fe(\alpha)}$=0.985; $a_{Mn(\alpha)}$=0.025; $a_{Si(\alpha)}$=$4.0\cdot10^{-26}$ (reference state – pure component with bcc lattice). The Gibbs energies of phase transition of pure manganese and silicon from their standard states to α-phase (bcc-Fe) are taken from Dinscale (1991). The standard Gibbs energies of formation of iron and manganese carbides were taken from Tyurin (2011) and listed in Table 2.

Table 2. The standard Gibbs energies of formation of compounds from elements at 25°C

Compound	$-\Delta_f G^o_{298}$ / kJ mol^{-1}	Compound	$-\Delta_f G^o_{298}$ / kJ mol^{-1}
Fe_3O_4	1020.20	$CuFeO_2$	478.3
Fe_2O_3	744.20	$CuFe_2O_4$	887.48
MnO	36.30	SiO_2	805.1
Mn_3O_4	1282.0	Fe_2SiO_4	1376.0
Mn_2O_3	88.0	$MnSiO_3$	1240.83
MnO_2	465.37	Mn_2SiO_4	1539.82
Cu_2O	147.88	$CuSiO_3$	494.24
CuO	127.89	Fe_3C	–18.80
Cu_2O_3	273.30	Mn_3C	–5.31

2.3. Thermodynamic model of oxidation of steel 20KT.

In system Fe–O at 25ºC exist the oxides Fe_3O_4 and Fe_2O_3, in system Mn–O – the oxides MnO, Mn_3O_4, Mn_2O_3 and MnO_2, in system Cu–O – the oxides Cu_2O, CuO and Cu_2O_3, and in system Si–O only one oxide SiO_2 exists. In addition, during oxidation of steel 20KT the formation of copper ferrites $CuFeO_2$ and $CuFe_2O_4$ is possible, as well as iron, manganese and copper silicides Fe_2SiO_4, $MnSiO_3$, Mn_2SiO_4 and $CuSiO_3$. The compounds Fe_3O_4, Mn_3O_4 and $CuFe_2O_4$ can form a spinel-type solid solution between each other. The silicides Fe_2SiO_4 and Mn_2SiO_4 can form olivine-type solid solution. In addition, a solid solution between the oxides Fe_2O_3 and Mn_2O_3 can be formed (Nikolaychuk and Tyurin, 2012). The standard Gibbs energies of formation of possible products of electrochemical oxidation of steel 20KT are listed in Table 2 (Tyurin, 2011; Nikolaychuk and Tyurin, 2012 and 2013; JANAF, 1985; Nikolaychuk et al., 2010).

General equilibrium potential – pH diagram of steel 20KT includes Pourbaix diagrams of steel's metallic matrix (α-phase (ferrite) + ε-phase (Cu)), cementite $(Fe,Mn)_3C$ and non-metallic inclusions. The potential – pH diagram of system (α-phase (ferrite) + ε-phase (Cu))–H_2O at 25ºC, air pressure of 1 bar and activities of ions in solution a_i =10^{-6} mol L^{-1} (reference state – hypothetical one-molar solution) is presented at Figure 1, and the potential – pH diagram of system $(Fe,Mn)_3C$ – H_2O at the same conditions is presented at Figure 2. Diagrams for non-

metallic inclusions and ε-phase (Cu) were discussed by Tyurin et al. (2007), Nikolaychuk and Tyurin (2013) and Nikolaychuk et al. (2010). Thermodynamic characteristics of basic chemical and electrochemical equilibria in system are listed in Table 3 and the description of domains of thermodynamic stability of certain phases at Figures 1 and 2 is given in Table 4.

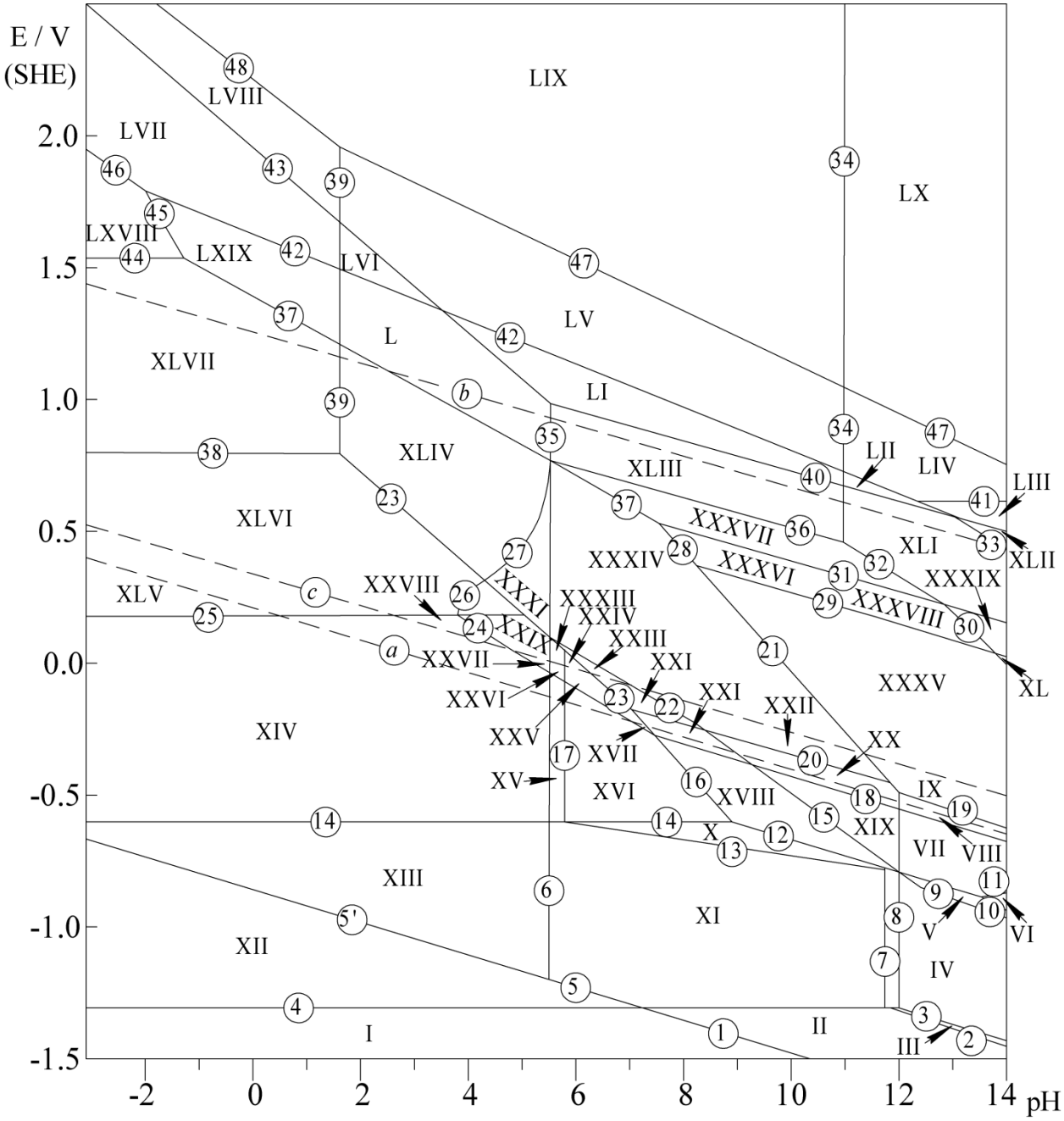

Figure 1. Equilibrium potential – pH diagram of system (α-phase (ferrite) + ε-phase (Cu))–H_2O at 25ºC, air pressure of 1 bar and activities of ions in solution $a_i = 10^{-6}$ mol L^{-1}

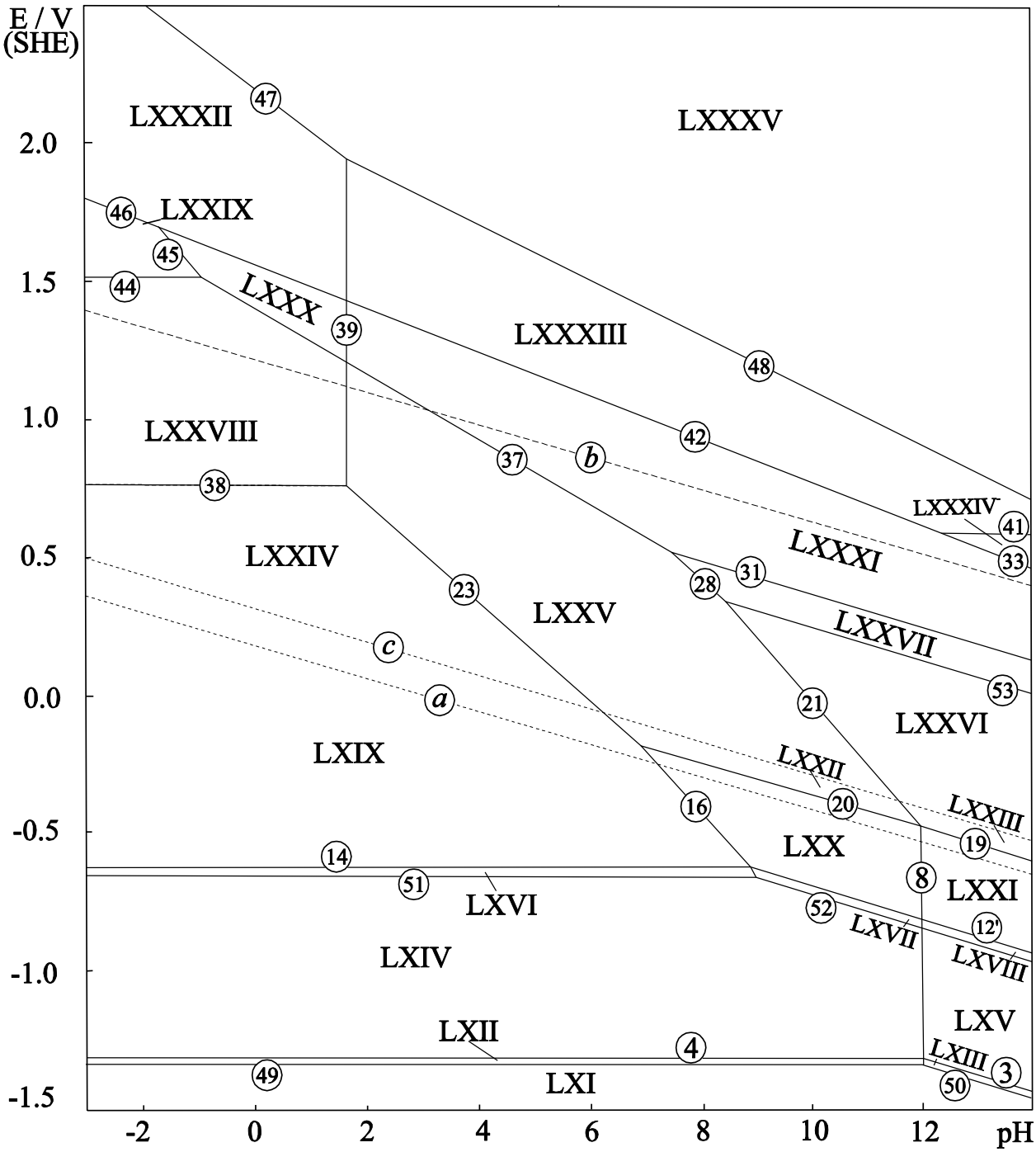

Figure 2. Equilibrium potential – pH diagram of system cementite–H_2O at 25ºC, air pressure of 1 bar and activities of ions in solution $a_i = 10^{-6}$ mol L^{-1}

Table 3. Basic chemical and electrochemical equilibria in system steel 20KT – H_2O at 25°C and air pressure of 1 bar

No	Electrode reaction	E / V (SHE) or pH of the solution
1	$MnSiO_3 + 6H^+ + 6e^- = Si(\alpha) + Mn(\alpha) + 3H_2O$ $a_{Si(\alpha)} = 4.0 \cdot 10^{-26}; a_{Mn(\alpha)} = 0.025$	$E = -0.888 - 0.0591pH$
2	$(Mn_2SiO_4)_{sln} + 2H^+ + 2e^- = Mn(\alpha) + MnSiO_3 + H_2O$ $a_{Mn(\alpha)} = 0.025;\ a_{Mn_2SiO_4} \approx 1$	$E = -0.616 - 0.0591pH$
3	$MnO + 2H^+ + 2e^- = Mn(\alpha) + H_2O$: $a_{Mn(\alpha)} = 0.025$ $a_{Mn(\alpha)} = 1$	$E = -0.602 - 0.0591pH$ $E = -0.651 - 0.0591pH$
4	$Mn^{2+} + 2e^- = Mn(\alpha)$: $a_{Mn(\alpha)} = 0.025$ $a_{Mn(\alpha)} = 1$	$E = -1.133 + 0.0295\log a_{Mn^{2+}}$ $E = -1.180 + 0.0295\log a_{Mn^{2+}}$
5	$MnSiO_3 + 6H^+ + 4e^- = Si(\alpha) + Mn^{2+} + 3H_2O;\ a_{Si(\alpha)} = 4.0 \cdot 10^{-26}$	$E = -0.722 - 0.0886pH$
5’	$SiO_2 + 4H^+ + 4e^- = Si(\alpha) + 2H_2O;\ a_{Si(\alpha)} = 4.0 \cdot 10^{-26}$	$E = -0.841 - 0.0591pH$
6	$MnSiO_3 + 2H^+ = Mn^{2+} + SiO_2 + H_2O$	$\log a_{Mn^{2+}} = 5.1 - 2pH$
7	$(Mn_2SiO_4)_{sln} + 2H^+ + 4e^- = MnSiO_3 + Mn^{2+} + H_2O;\ a_{Mn_2SiO_4} \approx 1$	$\log a_{Mn^{2+}} = 17.48 - 2pH$
8	$MnO + 2H^+ = Mn^{2+} + 2H_2O$	$\log a_{Mn^{2+}} = 17.94 - 2pH$
9	$(Mn_2SiO_4)_{sln} + (FeSiO_4)_{sln} + 4H^+ + 4e^- =$ $= 2MnSiO_3 + 2Fe(\alpha) + 2H_2O;\ a_{Fe(\alpha)} = 0.985$	$E = -0.083 - 0.0591pH +$ $+0.01478\log (a_{Mn_2SiO_4} \cdot a_{Fe_2SiO_4})$
10	$HFeO_2^- + 3H^+ + 2e^- = Fe(\alpha) + 2H_2O;\ a_{Fe(\alpha)} = 0.985$	$E = 0.483 - 0.0886pH +$ $+0.0295\log a_{HFeO_2^-}$
11	$Fe_3O_4 + 2H_2O + 2e^- = 3HFeO_2^- + H^+$	$E = -1.819 + 0.0295pH -$ $-0.0886\log a_{HFeO_2^-}$
12	$(Fe_3O_4)_{sln} + 8H^+ + 8e^- = 3Fe(\alpha) + 4H_2O$ $a_{Fe(\alpha)} = 0,985;\ a_{Fe_3O_4} \approx 1$	$E = -0.092 - 0.0591pH$
12’	$Fe_3O_4 + 8H^+ + 8e^- = 3Fe(\alpha) + 4H_2O;\ a_{Fe(\alpha)} = 1$	$E = -0.093 - 0.0591pH$
13	$(Fe_2SiO_4)_{sln} + Mn^{2+} + 2H^+ + 4e^- =$ $= 2Fe(\alpha) + MnSiO_3 + H_2O;\ a_{Fe(\alpha)} = 0.985$	$E = -0.356 - 0.0295pH +$ $+0.0148\log (a_{Mn^{2+}} \cdot a_{Fe_2SiO_4})$
14	$Fe^{2+} + 2e^- = Fe(\alpha)$: $a_{Fe(\alpha)} = 0.985$ $a_{Fe(\alpha)} = 1$	$E = -0.440 + 0.0295\log a_{Fe^{2+}}$ $E = -0.441 + 0.0295\log a_{Fe^{2+}}$
15	$2Fe_3O_4 + 3MnSiO_3 + 10H^+ + 4e^- = 3Fe_2SiO_4 + 3Mn^{2+} + 5H_2O$	$E = 0.700 - 0.1478pH -$ $-0.044\log a_{Mn^{2+}}$
16	$(Fe_3O_4)_{sln} + 8H^+ + 2e^- = 3Fe^{2+} + 4H_2O;\ a_{Fe_3O_4} \approx 1$	$E = 0.953 - 0.2364pH -$ $-0.0886\log a_{Fe^{2+}}$

17	$Fe_2SiO_4 + Mn^{2+} + 2H^+ = 2Fe^{2+} + MnSiO_3 + H_2O$	$\log(\frac{a^2_{Fe^{2+}}}{a_{Mn^{2+}}}) = 5.69 - 2pH$
18	$3CuFeO_2 + 4H^+ + 4e^- = Fe_3O_4 + 3Cu(\varepsilon) + 2H_2O;\ a_{Cu(\varepsilon)} \approx 1$	$E = 0.155 - 0.0591pH$
18'	$3(CuFe_2O_4)_{sln} + 4H^+ + 4e^- = 3CuFeO_2 + (Fe_3O_4)_{sln} + 2H_2O$	$E = 0.692 - 0.0591pH - -0.0148\log(\frac{a_{Fe_3O_4}}{a^3_{CuFe_2O_4}})$
19	$Mn_3O_4 + 2H^+ + 2e^- = 3MnO + H_2O$	$E = 0.225 - 0.0591pH$
20	$3Fe_2O_3 + 2H^+ + 2e^- = Fe_3O_4 + H_2O$	$E = 0.234 - 0.0591pH$
21	$Mn_3O_4 + 8H^+ + 2e^- = 3Mn^{2+} + 4H_2O$	$E = 1.813 - 0.2364pH - -0.0886\log a_{Mn^{2+}}$
22	$Fe_2O_3 + MnSiO_3 + 4H^+ + 2e^- = Fe_2SiO_4 + Mn^{2+} + 2H_2O$	$E = 0.545 - 0.1182pH - -0.0295\log a_{Mn^{2+}}$
23	$Fe_2O_3 + 6H^+ + 2e^- = 2Fe^{2+} + 3H_2O$	$E = 0.713 - 0.1773pH - -0.0591\log a_{Fe^{2+}}$
24	$CuFeO_2 + 4H^+ + 2e^- = Fe^{2+} + Cu(\varepsilon) + 2H_2O;\ a_{Cu(\varepsilon)} \approx 1$	$E = 0.420 - 0.1182pH - -0.0295\log a_{Fe^{2+}}$
25	$Cu^{2+} + 2e^- = Cu(\varepsilon);\ a_{Cu(\varepsilon)} = 1$	$E = 0.337 + 0.0295\log a_{Cu^{2+}}$
26	$(CuFe_2O_4)_{sln} + 8H^+ + 2e^- = Cu^{2+} + 2Fe^{2+} + 4H_2O$	$E = 0.860 - 0.2364pH + + 0.0295\ \log a_{CuFe_2O_4} - - 0.0295\ \log(a_{Cu^{2+}} \cdot a^2_{Fe^{2+}})$
27	$(CuFe_2O_4)_{sln} + 2H^+ = Cu^{2+} + Fe_2O_3 + H_2O$	$\log(\frac{a_{Cu^{2+}}}{a^3_{CuFe_2O_4}}) = 5.06 - 2pH$
28	$Mn_2O_3 + 6H^+ + 2e^- = 2Mn^{2+} + 3H_2O$	$E = 1.490 - 0.1773pH - -0.0591\log a_{Mn^{2+}}$
29	$Mn_3O_4 + 3SiO_3^{2-} + 8H^+ + 2e^- = 3MnSiO_3 + 4H_2O$	$E = 3.830 - 0.2364pH + + 0.08865\log a_{SiO_3^{2-}}$
30	$Mn_2O_3 + 2SiO_3^{2-} + 6H^+ + 2e^- = 2MnSiO_3 + 3H_2O$	$E = 2.835 - 0.1773pH + + 0.0591\log a_{SiO_3^{2-}}$
31	$2MnO_2 + 2H^+ + 2e^- = 3Mn_2O_3 + H_2O$	$E = 0.962 - 0.0591pH$
32	$MnO_2 + SiO_3^{2-} + 4H^+ + 2e^- = MnSiO_3 + 2H_2O$	$E = 1.899 - 0.1182pH + + 0.0295\log a_{SiO_3^{2-}}$
33	$MnO_4^{2-} + 4H^+ + 2e^- = MnO_2 + 2H_2O$	$E = 2.254 - 0.1182pH + + 0.0295\log a_{MnO_4^{2-}}$
34	$SiO_3^{2-} + 2H^+ = SiO_2 + H_2O$	$\log a_{SiO_3^{2-}} = -27.88 + 2pH$
35	$CuFe_2O_4 + 2H^+ = Cu^{2+} + Fe_2O_3 + H_2O$	$\log a_{Cu^{2+}} = 5.06 - 2pH$
36	$SiO_2 + MnO_2 + 2H^+ + 2e^- = MnSiO_3 + H_2O$	$E = 1.075 - 0.0591pH$

37	$MnO_2 + 4H^+ + 2e^- = Mn^{2+} + 2H_2O$	$E = 1.226 - 0.1182pH - -0.0295\log a_{Mn^{2+}}$
38	$Fe^{3+} + e^- = Fe^{2+}$	$E = 0.771 + 0.0591\log(\frac{a_{Fe^{3+}}}{a_{Fe^{2+}}})$
39	$Fe_2O_3 + 6H^+ = 2Fe^{3+} + 3H_2O$	$\log a_{Fe^{3+}} = -0.96 - 3pH$
40	$Cu_2O_3 + 2Fe_2O_3 + 2H^+ + 2e^- = 2CuFe_2O_4 + H_2O$	$E = 1.297 - 0.0591pH$
41	$MnO_4^- + e^- = MnO_4^{2-}$	$E = 0.558 + 0.0591\log(\frac{a_{MnO_4^-}}{a_{MnO_4^{2-}}})$
42	$MnO_4^- + 4H^+ + 3e^- = MnO_2 + 2H_2O$	$E = 1.695 - 0.0788pH + + 0.0197\log a_{MnO_4^-}$
43	$Cu_2O_3 + 6H^+ + 2e^- = Cu^{2+} + 3H_2O$	$E = 1.596 - 0.1773pH - -0.0591\log a_{Cu^{2+}}$
44	$Mn^{3+} + e^- = Mn^{2+}$	$E = 1.510 + 0.0591\log(\frac{a_{Mn^{3+}}}{a_{Mn^{2+}}})$
45	$MnO_2 + 4H^+ + e^- = Mn^{3+} + 2H_2O$	$E = 0.940 - 0.2364pH - -0.0591\log a_{Mn^{3+}}$
46	$MnO_4^- + 8H^+ + 4e^- = Mn^{3+} + 4H_2O$	$E = 1.505 - 0.1182pH + +0.0148\log(\frac{a_{MnO_4^-}}{a_{Mn^{3+}}})$
47	$2FeO_4^{2-} + 10H^+ + 6e^- = Fe_2O_3 + 5H_2O$	$E = 2.220 - 0.0985pH + +0.0197\log a_{FeO_4^{2-}}$
48	$FeO_4^{2-} + 8H^+ + 3e^- = Fe^{3+} + 4H_2O$	$E = 2.200 - 0.1577pH + +0.0197\log(\frac{a_{FeO_4^{2-}}}{a_{Fe^{3+}}})$
49	$3Mn^{2+} + C(gr) + 6e^- = Mn_3C$	$E = -1.189 - 0.0295\log a_{Mn^{2+}}$
50	$3MnO + C(gr) + 6H^+ + 6e^- = Mn_3C + H_2O$	$E = -0.660 - 0.0591pH$
51	$3Fe^{2+} + C(gr) + 6e^- = Fe_3C$	$E = -0.472 + 0.0295\log a_{Fe^{2+}}$
52	$Fe_3O_4 + C(gr) + 8H^+ + 8e^- = Fe_3C + 4H_2O$	$E = -0.1157 - 0.0591pH$
53	$3Mn_2O_3 + 2H^+ + 2e^- = 2Mn_3O_4 + H_2O$	$E = 0.846 - 0.0591pH$
54	$Cu_2O + 2H^+ + 2e^- = 2Cu(\varepsilon) + H_2O;\ a_{Cu(\varepsilon)} \approx 1$	$E = 0.439 - 0.0591pH$
55	$MnS + 2H^+ = Mn^{2+} + H_2S\ (aq)$	$\log a_{Mn^{2+}} = 11.008 - 2pH$
56	$MnS_2 + 4H^+ + 2e^- = Mn^{2+} + 2H_2S\ (aq)$	$E = 0.491 - 0.1182pH + + 0.0295\log a_{Mn^{2+}}$
57	$MnS_2 + Mn^{2+} + 2e^- = 2MnS$	$E = -0.160 - 0.0295\log a_{Mn^{2+}}$
58	$S_2O_3^{2-} + 10H^+ + 8e^- = 2H_2S\ (aq) + 3H_2O$	$E = 0.349 - 0.0739pH - - 0.0074\log a_{S_2O_3^{2-}}$

59	$S_2O_3^{2-} + Mn^{2+} + 6H^+ + 6e^- = MnS_2 + 3H_2O$	$E = 0.302 - 0.0591pH - $ $- 0.0099\log(a_{S_2O_3^{2-}} \cdot a_{Mn^{2+}})$
60	$S_2O_3^{2-} + 2Mn^{2+} + 6H^+ + 8e^- = 2MnS + 3H_2O$	$E = 0.186 - 0.0443pH - $ $- 0.0074\log(a_{S_2O_3^{2-}} \cdot a_{Mn^{2+}}^2)$
61	$3S_2O_3^{2-} + 2Mn_3O_4 + 34H^+ + 28e^- = 6MnS + 17H_2O$	$E = 0.343 - 0.0718pH - $ $- 0.0063\log a_{S_2O_3^{2-}}$
a	$2H^+ + 2e^- = H_2(g);\ P_{H_2} = 5.0 \cdot 10^{-7}$ bar	$E = 0.186 - 0.0591pH$
b	$O_2(g) + 2H^+ + 4e^- = 2H_2O;\ P_{O_2} = 0.21$ bar	$E = 1.219 - 0.0591pH$
c	$C(gr.) + 4H^+ + 4e^- = CH_4(g);\ P_{CH_4} = 5.0 \cdot 10^{-7}$ bar	$E = 0.318 - 0.0591pH$

Table 4. Domains of thermodynamic stability of certain phases in equilibrium potential – pH diagrams for steel 20KT

No of domain	Thermodynamically stable phases
I	α-phase (ferrite) + ε-phase (Cu)
II	α-phase (ferrite) + ε-phase (Cu) + $MnSiO_3$
III	α-phase (Fe) + ε-phase (Cu) + Mn_2SiO_4
IV	α-phase (Fe) + ε-phase (Cu) + $[(Mn,Fe)_2SiO_4]_{sln}$ + MnO
V	α-phase (Fe) + ε-phase (Cu) + $MnSiO_3$ + MnO
VI	ε-phase (Cu) + C(gr.) + $MnSiO_3$ + MnO + $HFeO_2^-$
VII	ε-phase (Cu) + C(gr.) + $MnSiO_3$ + Fe_3O_4 + MnO
VIII	ε-phase (Cu) + C(gr.) + $CuFeO_2$ + $[(Fe,Cu)Fe_2O_4]_{sln}$ + $MnSiO_3$ + MnO
IX	C(gr.) + $[(Fe,Cu,Mn)_3O_4]_{sln}$ + $MnSiO_3$ + Fe_2O_3
X	α-phase (Fe) + ε-phase (Cu) + $[(Mn,Fe)_2SiO_4]_{sln}$ + Mn^{2+}
XI	α-phase (Fe) + ε-phase (Cu) + $MnSiO_3$ + Mn^{2+}
XII	α-phase (Fe) + ε-phase (Cu) + Mn^{2+}
XIII	α-phase (Fe) + ε-phase (Cu) + SiO_2 + Mn^{2+}
XIV	ε-phase (Cu) + C(gr.) + SiO_2 + Mn^{2+}, Fe^{2+}
XV	ε-phase (Cu) + C(gr.) + $MnSiO_3$ + Mn^{2+}, Fe^{2+}
XVI	ε-phase (Cu) + C(gr.) + Fe_2SiO_4 + Mn^{2+}, Fe^{2+}
XVII	ε-phase (Cu) + C(gr.) + $CuFeO_2$ + Fe_2SiO_4 + Mn^{2+}, Fe^{2+}
XVIII	ε-phase (Cu) + C(gr.) + Fe_3O_4 + $[(Mn,Fe)_2SiO_4]_{sln}$ + Mn^{2+}
XIX	ε-phase (Cu) + C(gr.) + Fe_3O_4 + $MnSiO_3$ + Mn^{2+}
XX	ε-phase (Cu) + C(gr.) + $CuFeO_2$ + $[(Fe,Cu)Fe_2O_4]_{sln}$ + $MnSiO_3$ + Mn^{2+}
XXI	ε-phase (Cu) + C(gr.) + $CuFeO_2$ + $[(Fe,Cu)Fe_2O_4]_{sln}$ + $[(Mn,Fe)_2SiO_4]$ Mn^{2+}
XXII	C(gr.) + $[(Fe,Cu)Fe_2O_4]_{sln}$ + Fe_2O_3 + $MnSiO_3$ + Mn^{2+}
XXIII	C(gr.) + $[(Fe,Cu)Fe_2O_4]_{sln}$ + Fe_2SiO_4 + Mn^{2+}
XXIV	$[(Fe,Cu)Fe_2O_4]_{sln}$ + Fe_2SiO_4 + Mn^{2+}
XXV	ε-phase (Cu) + C(gr.) + $CuFeO_2$ + Fe_2SiO_4 + Mn^{2+}, Fe^{2+}
XXVI	ε-phase (Cu) + C(gr.) + $CuFeO_2$ + $MnSiO_3$ + Mn^{2+}, Fe^{2+}
XXVII	ε-phase (Cu) + C(gr.) + $CuFeO_2$ + SiO_2 + Mn^{2+}, Fe^{2+}
XXVIII	ε-phase (Cu) + SiO_2 + Mn^{2+}, Fe^{2+}
XXIX	ε-phase (Cu) + $CuFeO_2$ + SiO_2 + Mn^{2+}, Fe^{2+}
XXX	$[(Fe,Cu)Fe_2O_4]_{sln}$ + SiO_2 + Mn^{2+}, Fe^{2+}
XXXI	$[(Fe,Cu)Fe_2O_4]_{sln}$ + SiO_2 + Fe_2O_3 + Mn^{2+}

XXXII	ε-phase (Cu) + $CuFeO_2$ + $MnSiO_3$ + Mn^{2+}, Fe^{2+}
XXXIII	ε-phase (Cu) + $CuFeO_2$ + Fe_2SiO_4 + Mn^{2+}, Fe^{2+}
XXXIV	$[(Fe,Cu)Fe_2O_4]_{sln}$ + Fe_2O_3 + $MnSiO_3$ + Mn^{2+}
XXXV	$[(Fe,Cu,Mn)_3O_4]_{sln}$ + $MnSiO_3$ + Fe_2O_3
XXXVI	$[(Fe,Cu)Fe_2O_4]_{sln}$ + $(Fe,Mn)_2O_3$ + $MnSiO_3$
XXXVII	$[(Fe,Cu)Fe_2O_4]_{sln}$ + Fe_2O_3 + $MnSiO_3$ + MnO_2
XXXVIII	$[(Fe,Cu)Fe_2O_4]_{sln}$ + $(Fe,Mn)_2O_3$ + $MnSiO_3$
XXXIX	$[(Fe,Cu)Fe_2O_4]_{sln}$ + $(Fe,Mn)_2O_3$ + SiO_3^{2-}
XL	$[(Fe,Cu,Mn)_3O_4]_{sln}$ + Fe_2O_3 + SiO_3^{2-}
XLI	$CuFe_2O_4$ + Fe_2O_3 + MnO_2 + SiO_3^{2-}
XLII	$CuFe_2O_4$ + Fe_2O_3 + SiO_3^{2-}, MnO_4^{2-}
XLIII	$CuFe_2O_4$ + SiO_2 + Fe_2O_3 + MnO_2
XLIV	SiO_2 + Fe_2O_3 + Mn^{2+}, Cu^{2+}
XLV	C(gr.) + SiO_2 + Mn^{2+}, Cu^{2+}, Fe^{2+}
XLVI	SiO_2 + Mn^{2+}, Cu^{2+}, Fe^{2+}
XLVII	SiO_2 + Mn^{2+}, Cu^{2+}, Fe^{3+}
XLVIII	SiO_2 + Mn^{3+}, Cu^{2+}, Fe^{3+}
XLIX	SiO_2 + MnO_2 + Cu^{2+}, Fe^{3+}
L	SiO_2 + MnO_2 + Fe_2O_3 + Cu^{2+}
LI	SiO_2 + MnO_2 + Fe_2O_3 + Cu_2O_3
LII	MnO_2 + Fe_2O_3 + Cu_2O_3 + SiO_3^{2-}
LIII	Fe_2O_3 + Cu_2O_3 + SiO_3^{2-}, MnO_4^{2-}
LIV	Fe_2O_3 + Cu_2O_3 + SiO_3^{2-}, MnO_4^-
LV	SiO_2 + Fe_2O_3 + Cu_2O_3 + MnO_4^-
LVI	SiO_2 + Fe_2O_3 + Cu^{2+}, MnO_4^-
LVII	SiO_2 + Fe^{3+}, Cu^{2+}, MnO_4^-
LVIII	SiO_2 + Cu_2O_3 + Fe^{3+},
LIX	SiO_2 + Cu_2O_3 + MnO_4^-, FeO_4^{2-}
LX	Cu_2O_3 + SiO_3^{2-}, MnO_4^-, FeO_4^{2-}
LXI	$(Fe, Mn)_3C$ (cementite)
LXII	Mn(α) + $(Fe,Mn)_3C$ (cementite) + C(gr.) + Mn^{2+}
LXIII	Mn(α) + MnO + $(Fe,Mn)_3C$ (cementite) + C(gr.)
LXIV	$(Fe,Mn)_3C$ (cementite) + C(gr.) + Mn^{2+}
LXV	MnO + $(Fe,Mn)_3C$ (cementite) + C(gr.)
LXVI	Fe(α) + C(gr.) + Mn^{2+}, Fe^{2+}
LXVII	Fe_3O_4 + Fe(α) + C(gr.) + Mn^{2+}
LXVIII	MnO + Fe_3O_4 + Fe(α) + C(gr.)
LXIX	C(gr.) + Mn^{2+}, Fe^{2+}
LXX	Fe_3O_4 + C(gr.) + Mn^{2+}
LXXI	MnO + Fe_3O_4 + C(gr.)
LXXII	Fe_2O_3 + C(gr.) + Mn^{2+}
LXXIII	Mn_3O_4 + Fe_2O_3 + C(gr.)
LXXIV	Mn^{2+}, Fe^{2+}
LXXV	Fe_2O_3 + Mn^{2+}
LXXVI	Mn_3O_4 + Fe_2O_3

LXXVII	$[(Fe,Mn)_2O_3]_{sln}$
LXXVIII	Mn^{2+}, Fe^{3+}
LXXIX	Mn^{3+}, Fe^{3+}
LXXX	$MnO_2 + Fe^{3+}$
LXXXI	$MnO_2 + Fe_2O_3$
LXXXII	MnO_4^-, Fe^{3+}
LXXXIII	$Fe_2O_3 + MnO_4^-$
LXXXIV	$Fe_2O_3 + MnO_4^{2-}$
LXXXV	MnO_4^-, FeO_4^{2-}

The content of copper, manganese and silicon in steel 20KT is not sufficient to form a continuous layer of oxides of these elements on the surface. Corresponding oxides may be locally distributed at inner side of passivation layer consisting of iron oxides (Tyurin, 2011). Phase equilibria involving mixed carbide $(Fe,Mn)_3C$ are metastable, since its components Fe_3C and Mn_3C are thermodynamically unstable at standard temperature (see Table 2). Therefore equilibrium potentials of dissolution of carbides Fe_3C and Mn_3C are more negative than that of iron and manganese. Potentials of dissolution of ε-phase (Cu) and graphite (line *c* at Figures 1 and 2) are more positive than potentials of corrosion of ferrite and cementite. Consequently, in the structure of steel 20KT ε-phase (Cu) and graphite as the product of electrochemical oxidation of cementite, act as cathodic additives facilitating passivation of steel. As can be seen from the equilibrium potential – pH diagram for steel 20KT, perfect passivity can be achieved through the formation of an oxide film based on magnetite (Fe_3O_4). This is thermodynamically possible only in week acidic, neutral and alkaline environments at the potentials more positive than equilibrium potential of dissolution of iron. Thermodynamic stability of basic phases of steel 20KT decreases practically in the entire range of pH in the following sequence: ε-phase (Cu) → cementite $(Fe,Mn)_3C$ → α-phase (ferrite).

3. Plotting the polarization E – pH diagram for steel 20KT.

3.1. Basic principles.

Experimental determination of coordinates on polarization potential – pH diagram for studying alloy can be performed according to method proposed by Pourbaix (1970 and 1972). One should obtain potentiodynamic polarization curves for sample in studying solution at various fixed values of pH. Then the special points on these curves should be depicted, for example, corrosion potential (E_{corr}), passivation potential (E_p), potential of pitting formation (E_{pit}). By combining these special points at various curves one can plot the polarization diagram, which depicts the experimental conditions of immunity, general corrosion, perfect and imperfect passivity as functions of potential and pH.

Polarization potential – pH diagram shows the electrode potentials related with formation of new phases and phase transitions on alloy surface, depicting the borders of phase transformations. Therefore, such diagram has all attributes of phase diagram, and in order to correctly interpret the phase transformations it is important to compare polarization diagram with corresponding equilibrium potential – pH diagram for studying alloy.

3.2. Experimental procedure.

According to NACE/ASTM TM0169 G0031 12A Standard Guide for Laboratory Immersion Corrosion Testing of Metals, the solution for polarization measurements was prepared in the following way:

– 1L of 5 wt-% aqueous solution of NaCl was prepared;

– Solution was saturated by carbon dioxide (CO_2) during 30-40 minutes at P_{CO_2}=0.1MPa, solution pH after saturation was equal to 4.1±0.1;
– 100 mL of 100 g L^{-1} solution of Na_2CO_3 was added, after that pH was equal to 6.8±0.1;
– Solution pH was adjusted to necessary value by addition of 1M solution of NaOH or HCl respectively.

Reagents of analytical quality were used. Analytical balance with maximum uncertainty of ±0.0001 g was used for taking weights. pH-meter with maximum uncertainty of ±0.01 pH unit was used to control solution pH. Steel samples of cylindrical form with height of 12.0±0.1 mm, diameter of 6.0±0.1 mm and work surface equal to approximately 2.7 cm^2 were used. Work surface was polished and degreased by acetone. Polarization curves were measured in potentiodynamic mode using potentiostat Gamry Series G750 and the standard three-electrode thermostated cell, which is shown at Figure 3. The temperature of solution was maintained at 25±1ºC. IR drop was minimized by using and accurately positioning the Luggin capillary.

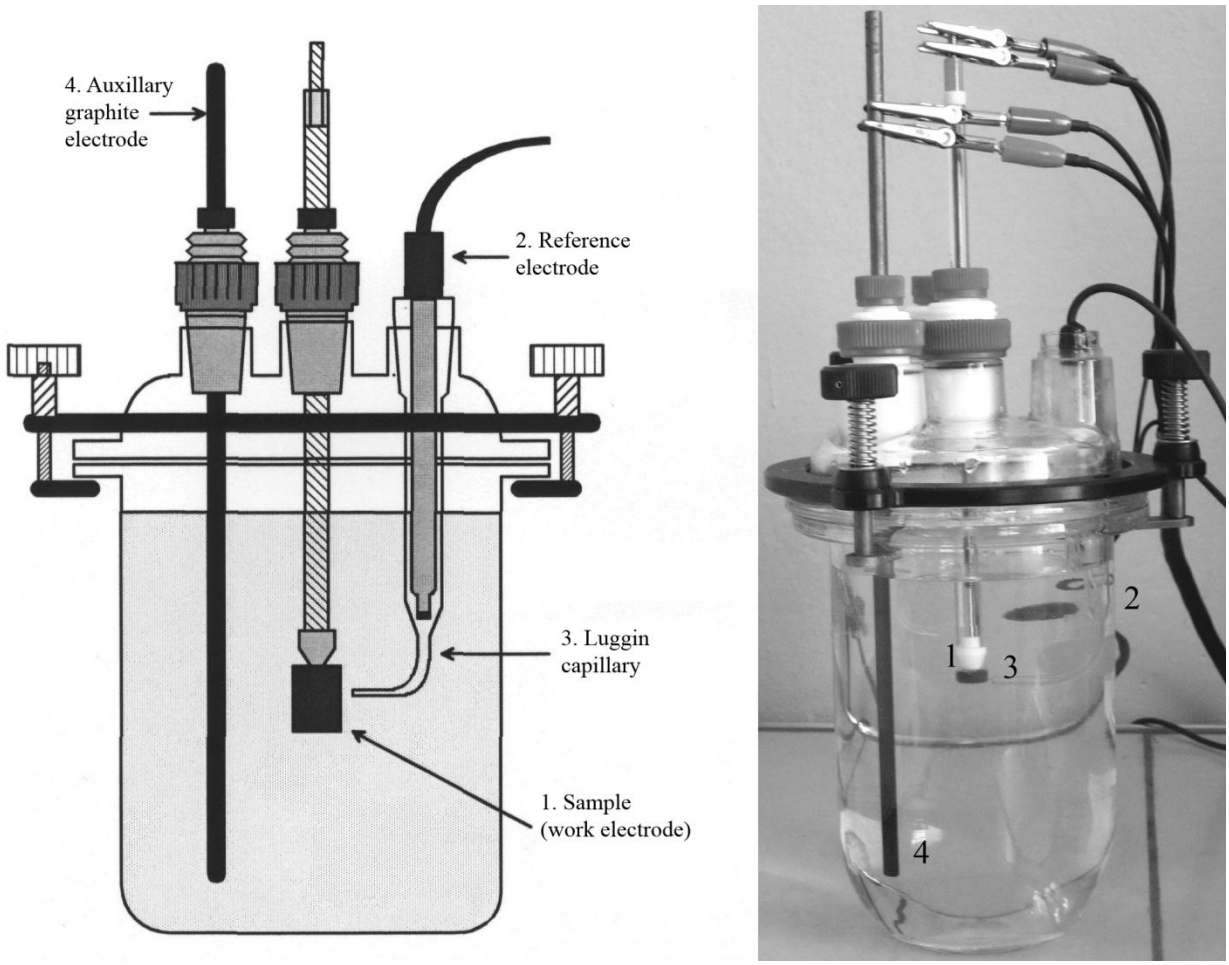

Figure 3. Construction of three-electrode electrochemical cell

The potential of dissolution of steel 20KT was preliminary determined. For this the potential on steel was measured without external polarization during at least one hour, taking E_{corr} as the potential at the end of exposure with the condition that potential change in the last 30 minutes was no more than ±30 mV. After that the sample was cathodically polarized at the potential of –1.1 V (SHE) for 10 minutes and potentiodynamic curve was registered with potential sweep rate of 0.1 mV s^{-1}. The experiment was repeated until three polarization curves compatible with each other were obtained for each solution. Visual inspection of the samples after the measurements showed that all the samples were affected by pittings, with samples tested at pH 9 and 10 have the greater number of them.

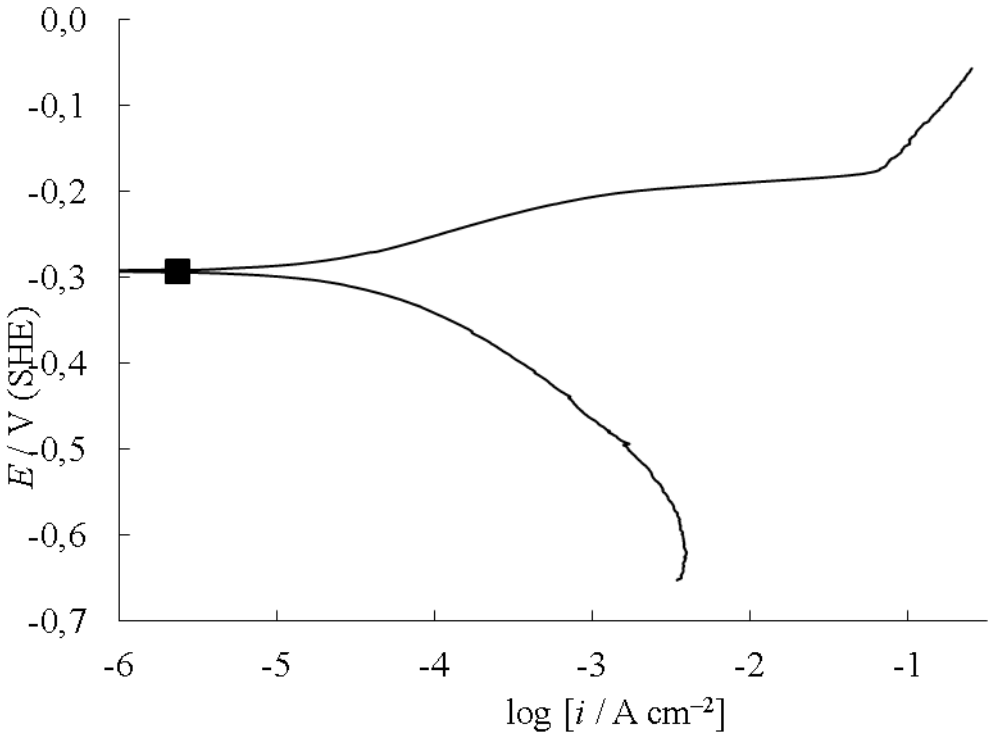

Figure 4a. Polarization curve of steel 20KT at pH 1.85 and 25ºC

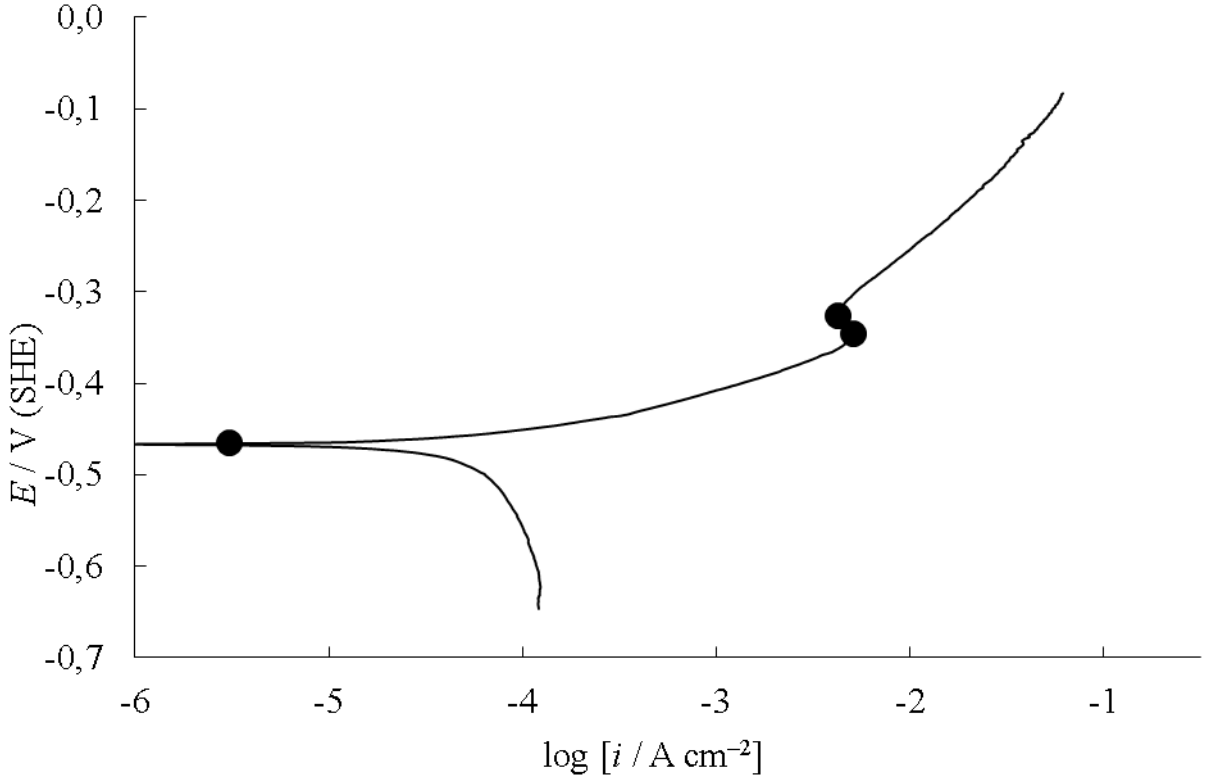

Figure 4b. Polarization curve of steel 20KT at pH 5.0 and 25ºC

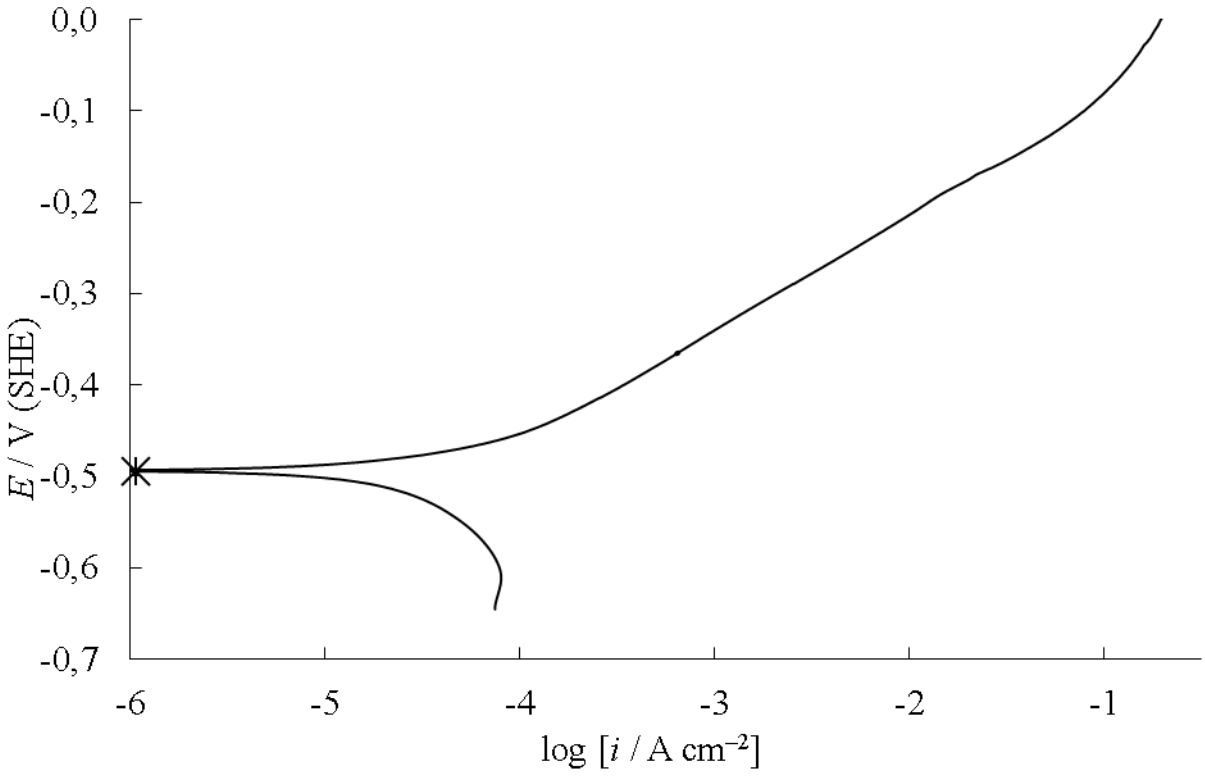

Figure 4c. Polarization curve of steel 20KT at pH 7.0 and 25ºC

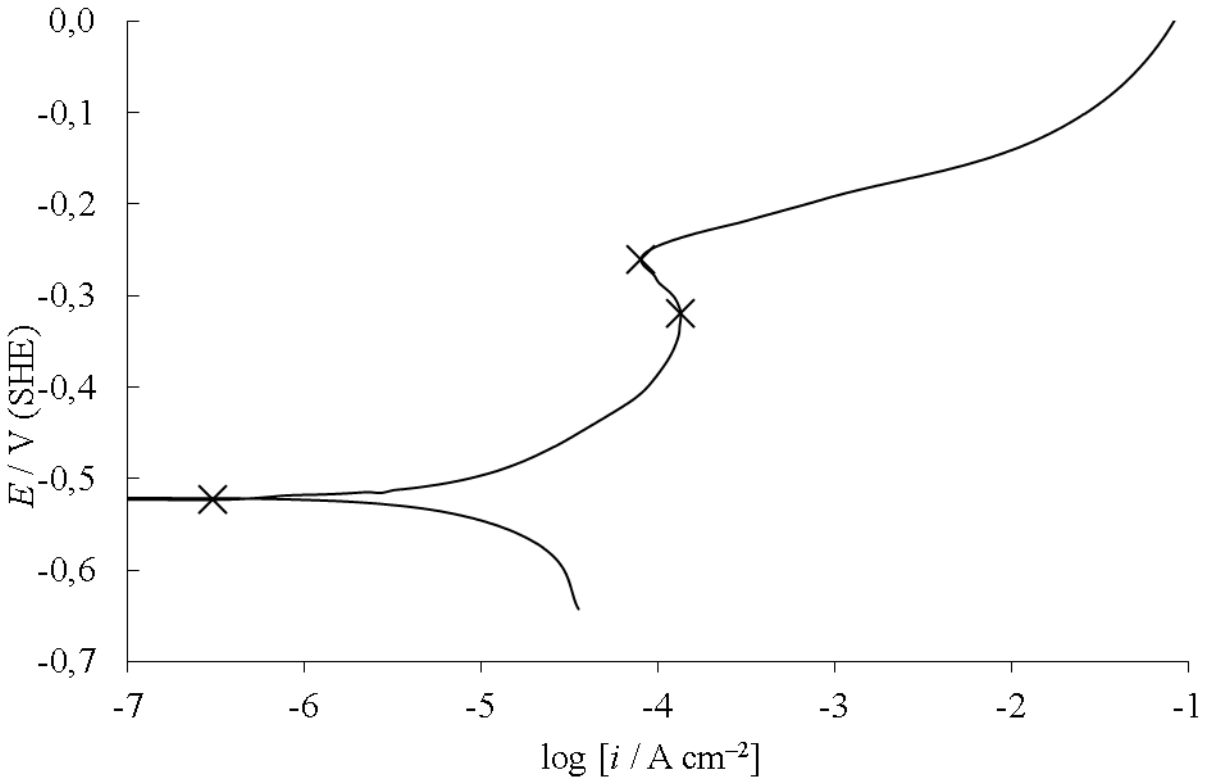

Figure 4d. Polarization curve of steel 20KT at pH 8.0 and 25ºC

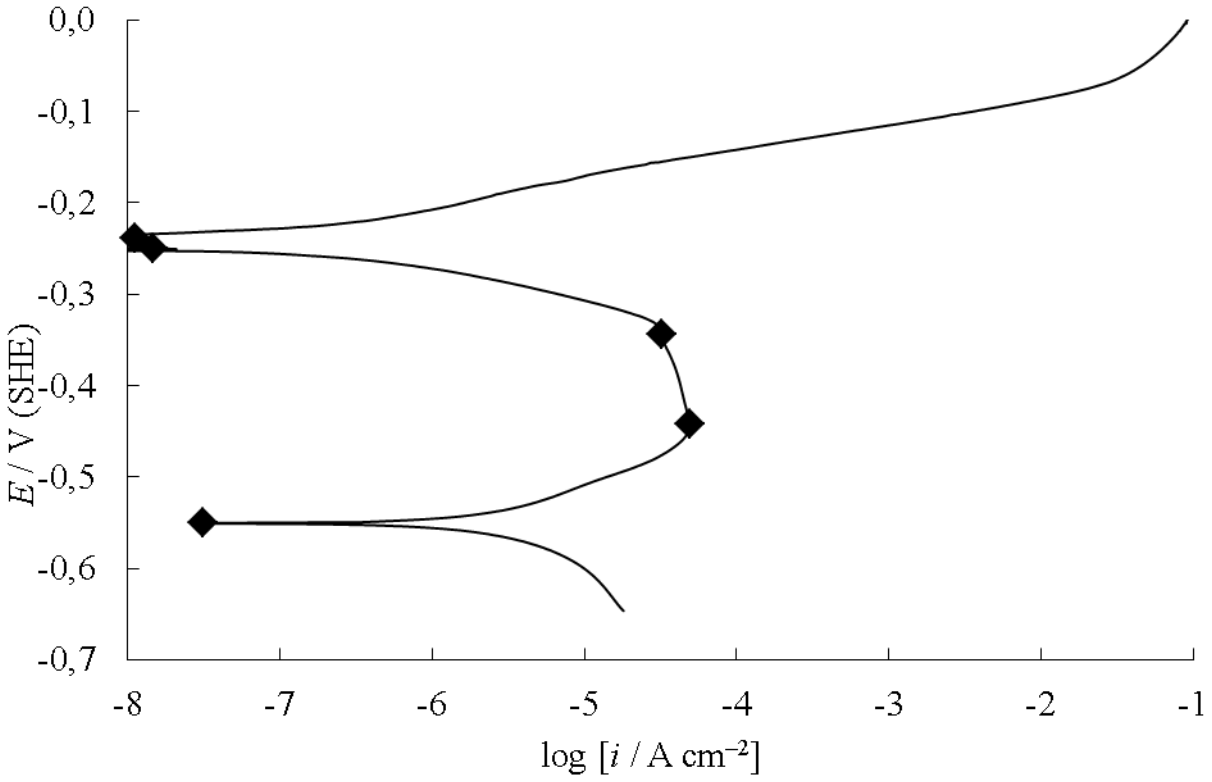

Figure 4e. Polarization curve of steel 20KT at pH 9.0 and 25ºC

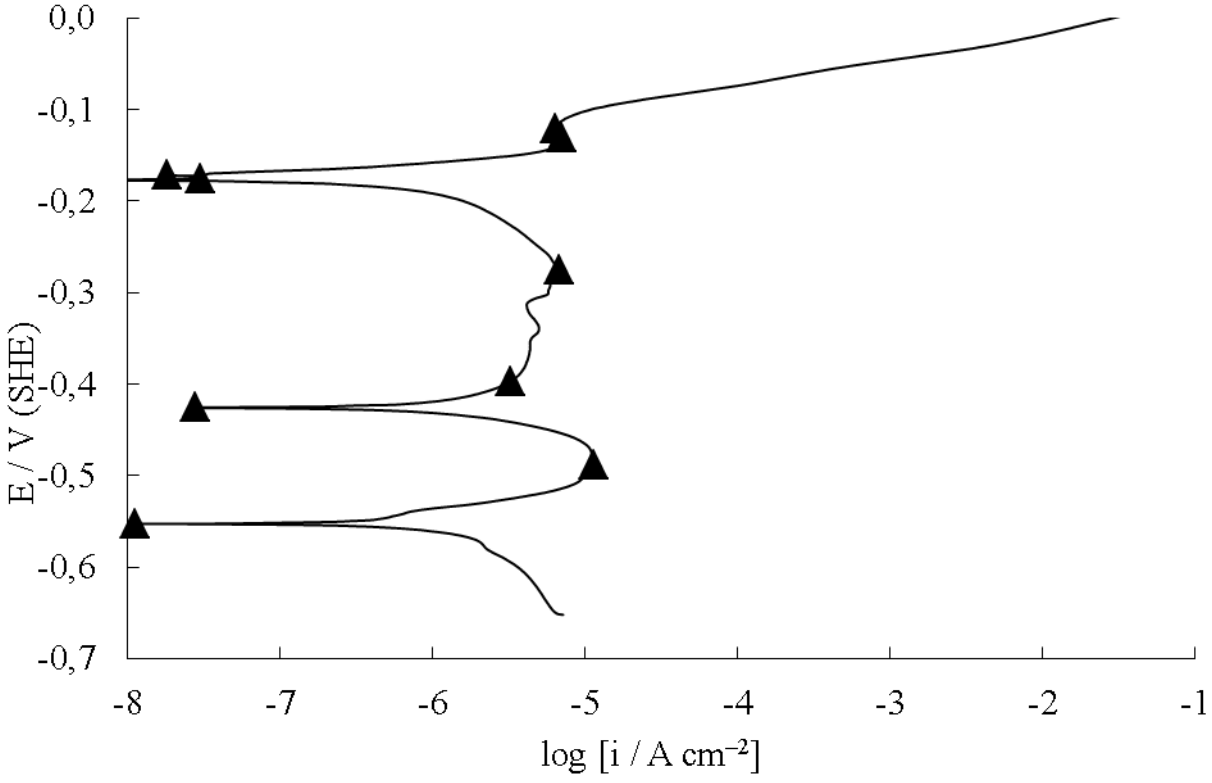

Figure 4f. Polarization curve of steel 20KT at pH 10.0 and 25ºC

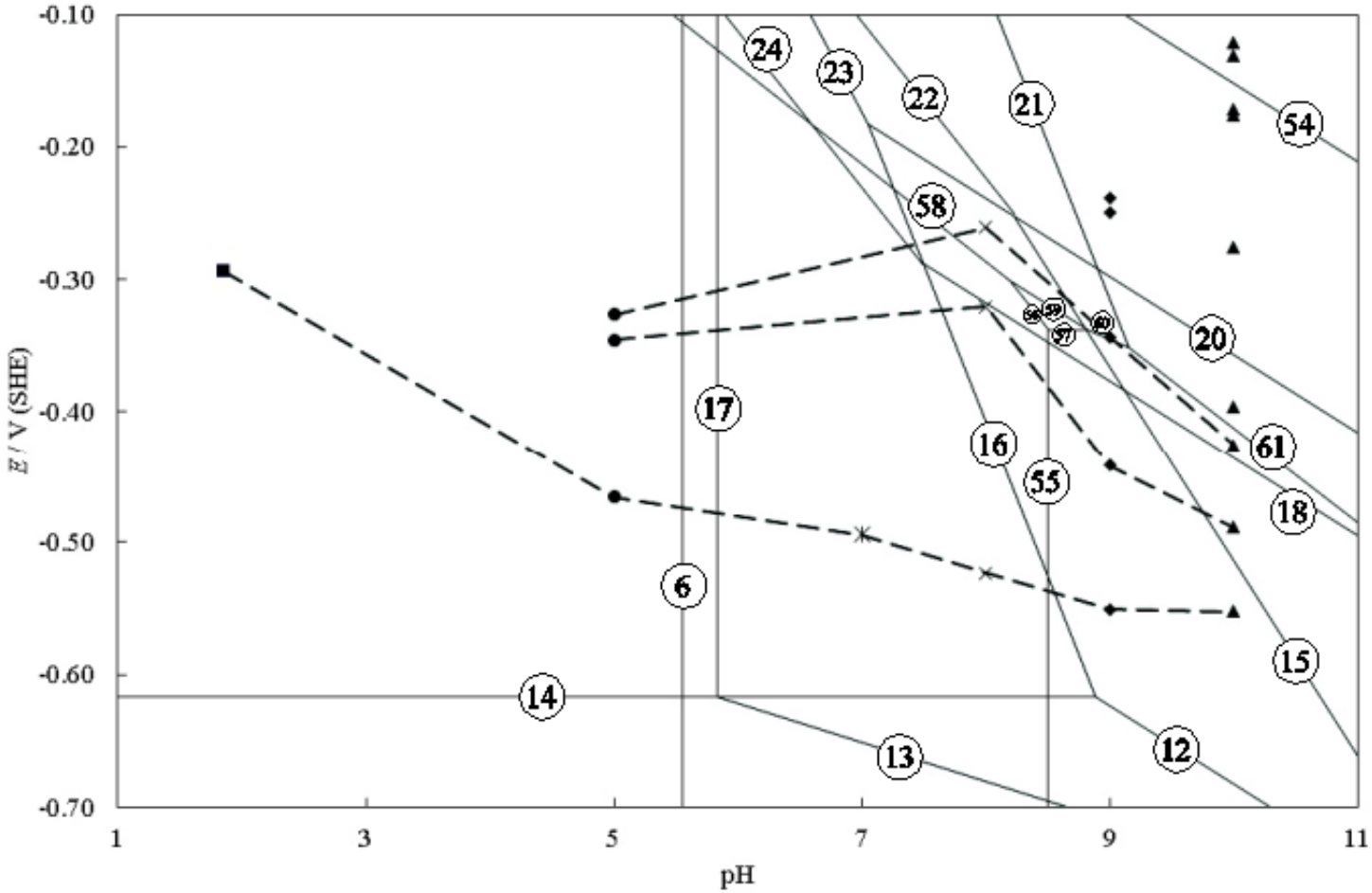

Figure 5. Polarization potential – pH diagram of steel 20KT at 25ºC

3.3. Plotting the diagram.

Figures 4a through 4f show the polarization curves of steel 20KT in solution with pH equal to 1.85, 5.0, 7.0, 8.0, 9.0 and 10.0 respectively. Special points corresponding to phase transitions were depicted on these curves. By combining these special points a polarization potential – pH diagram of steel 20KT is constructed. It characterizes the actual behaviour of steel in corrosive environments under study. To determine the nature of the processes causing the anomalies in the potentiodynamic curves at special points, polarization diagram is aligned with the corresponding equilibrium potential – pH diagram of steel. It is presented at Figure 5.

Generally, a good agreement between equilibrium and polarization diagrams is observed. The differences are related with the fact that equilibrium diagram was plotted in assumption that thermodynamic activities of all ions in solution are fixed and equal to 10^{-6} mol L^{-1}, which cannot be achieved under the experimental conditions. Analysis of obtained data indicates that most special points on polarization curves are related on dissolution of steel's ferrite matrix. However, equilibria involving cementite, ε-phase (Cu), oxide and sulphide inclusions are also clearly present in the diagram, especially at high values of pH, therefore it is insufficient to use data only from Pourbaix diagrams for pure metals to interpret all special points at polarization diagram. Method of plotting and analyzing experimental potential – pH diagrams for multicomponent alloys requires their comparison with equilibrium diagrams, which take into account all possible reactions during oxidation of these alloys.

4. Conclusions.

Method of estimation the corrosion stability of multicomponent alloys using construction of equilibrium and polarization potential – pH diagrams is proposed. It is shown that in for interpretation of experimental potential – pH diagrams one should compare them with corresponding equilibrium diagrams for multicomponent alloys rather than with Pourbaix diagrams for pure metals.

A diagram of electrochemical equilibrium of steel 20KT at 25ºC, air pressure of 1 bar and activities of ions in solution equal to 10^{-6} mol L^{-1} is constructed. Passivation of steel is determined by formation of oxide film based on magnetite (Fe_3O_4); silicon, manganese and copper oxides as well as manganese sulphides can be locally included into inner side of passivation layer.

The corrosion-electrochemical behaviour of steel 20KT in aqueous solution containing 5 wt-% NaCl + CO_2 + Na_2CO_3 (P_{CO_2} =0.1MPa) at 25ºC in pH ranging from 1.85 to 10 is studied by potentiodynamic method. An experimental potential – pH diagram of steel 20KT is constructed. Interpreting the results of polarization measurements revealed good agreement between equilibrium and polarization potential – pH diagrams.

References:

"JANAF Thermochemical tables", *Journal of Physical and Chemical Reference Data*, 1985, Suppl. 1.

Bai, X. D., Zhu, D. H. and Liu, B. X. (1995), "The establishment of a potential-pH diagram for phosphorous implanted iron in aqueous solutions", *Nuclear Instruments and Methods in Physics Research Section B: Beam Interactions with Materials and Atoms*, Vol. 103, No. 4, pp. 440 – 445.

Chen, Q. and Jin, Z. (1995), "The Fe – Cu system: a thermodynamic evaluation", *Metallurgical and Materials Transactions A*, Vol. 26, No. 2, pp. 417 – 426.

Chen, Y. Y., Chou, L. B. and Shih, H. C. (2005), "Effect of solution pH on the electrochemical polarization and stress corrosion cracking of Alloy 690 in 5 M NaCl at room temperature", *Materials Science and Engineering A*, Vol. 396, No. 1 – 2, pp. 129 – 137.

Chen, Y. Y., Chou, L. B. and Shih, H. C. (2006), "Factors affecting the electrochemical behaviour and stress corrosion cracking of Alloy 690 in chloride environments", *Materials Chemistry and Physics*, Vol. 97, No. 1, pp. 37 – 49.
Chuan, M. C., Shu, G. Y. and Liu, J. C. (1996), "Solubility of heavy metals in a contaminated soil: effects of redox potential and pH", *Water, Air, & Soil Pollution*, Vol. 90, No. 3 – 4, pp. 543 – 546.
Dinscale, A. T. (1991), "SGTE data for pure elements", *CALPHAD*, Vol. 15, No. 4, pp. 317 – 425.
Efird, K. D. (1975), "Potential-pH diagrams for 90-10 and 70-30 Cu-Ni in sea water", *Corrosion*, Vol. 31, No. 3, pp. 77 – 83.
Efird, K. D. and Vernik Jr, E. D. (1977), "The crevice protection potential for 90-10 copper nickel", *Corrosion*, Vol. 33, No. 9, pp. 128 – 131.
Gimenez, P., Rameau, J. J. and Reboul, M. C. (1981), "Experimental pH potential diagram of aluminum for sea water", *Corrosion*, Vol. 37, No. 12, pp. 673 – 682.
Horvath, J and Hackl, L. (1965), "Check of the potential/ph equilibriumdiagrams of different metal-sulphur-water ternary systems by intermittent galvanostatic polarization method", *Corrosion Science*, Vol. 5, No. 8, pp. 525 – 538.
Jingyi, Z., Pourbaix, M., Chunchun, X. and Youping, L. (1989), "Kinetic and thermodynamic behaviour inside occluded corrosion cells interpreted by potential/pH diagrams", *Corrosion Science*, Vol. 29, No. 5, pp. 557 - 566.
Kaufman, L. (1978), "Coupled phase diagrams and thermochemical data for transition metal binary systems–III", *CALPHAD*, Vol. 2, No. 2, pp. 117 – 146.
Kaufman, L. (1979), "Coupled phase diagrams and thermochemical data for transition metal binary systems–VI", *CALPHAD*, Vol. 3, No. 1, pp. 45 – 76.
Kurov, O. V. (1998), "To the Identification of Surface Chemical Compounds on Corroding Alloys", *Protection of Metals*, Vol. 34, No. 3, pp. 204 – 210.
Lange, E. and Ohse, R. (1958), "Bestimmung von Elektrodenreaktionen am Stoffsystem Cadmium/wäßrige Lösung auf Grund von intermittierten Ladekurven", *Naturwissenschaften*, Vol. 43, No. 18, pp. 437 – 438.
Lange, E. and Weidinger, H. (1958), "Aufklärung von Halbzellreaktionen am System Eisen/wäßrige Lösung mittels intermittierter Ladekurven", *Naturwissenschaften*, Vol. 43, No. 16, pp. 383 – 384.
Lennon, S. J. and Robinson, F. P. A. (1986), "The experimental determination of potential – pH diagrams for the Ni – H_2O and the low alloy steel – H_2O systems", *Corrosion Science*, Vol. 26, No. 12, pp. 995 – 1007.
Mattsson, E. (1961), "Stress corrosion in brass considered against the background of potential/pH diagrams", *Electrochimica Acta*, Vol. 3, No. 4, pp. 279 – 291.
Nagel, K., Ohse, R. and Lange, E. (1957), "Galvanostatische Aufklärung von Elektrodenreaktionen durch Ladekurven U_h $(t)_J$ mit intermittierter Belastung", *Zeitschrift für Elektrochemie, Berichte der Bunsengesellschaft für physikalische Chemie*, Vol. 61, No. 7, pp. 795 – 803.
Nikolaychuk, P. A. and Tyurin, A. G. (2012), "Thermodynamics of Chemical and Electrochemical Stability of Copper–Nickel Alloys", *Protection of Metals and Physical Chemistry of Surfaces*, Vol. 48, No. 4, pp. 462 – 476.
Nikolaychuk, P. A. and Tyurin, A. G. (2013), "Thermodynamic Evaluation of CorrosionElectrochemical Behaviour of Silicon Brass CuZn17Si3", *Inorganic Materials.*, Vol. 49, No. 5, pp. 457 – 467.
Nikolaychuk, P. A., Shalyapina, T. I., Tyurin, A. G. and Mosunova, T. V. (2010), "Termodinamika khimicheskoi i elektrokhimicheskoi ustoichivosti splavov sistemy Mn – Si", *Vestnik YuUrGU. Seriya Khimiya*, No. 3(207), pp. 72 – 82.

Nikolaychuk, P. A., Tyurin, A. G. and Kanatyeva, I. I. (2010), "Utochnyonnaya diagramma Purbe dlya medi", in *Sovremennye problemy teoreticheskoi i eksperimental»noi khimii: Mezhvuzovskii sbornik nauchnykh trudov VII Vserossiiskoi konferentsii molodykh uchenykh s mezhdunarodnym uchastiem*, KUBiK, Saratov, pp. 289 – 291.
Ohse, R. (1959), "Schabversuche an einer rotierenden Silberelektrode in alkalischer Lösung und Messung der Niveauladung bei intermittiert galvanostatischer Belastung", *Zeitschrift für Elektrochemie, Berichte der Bunsengesellschaft für physikalische Chemie*, Vol. 63. No. 9 – 10, pp. 1063 – 1068.
Ohse, R. (1960), "Eine oszillographische Untersuchung der Elektrodenreaktionen am Stoffsystem Cd/wäßrige Lösung mit der intermittiert galvanostatischen Meßmethode", *Zeitschrift für Elektrochemie, Berichte der Bunsengesellschaft für physikalische Chemie*, Vol. 64, No. 10, pp. 1171 – 1179.
Perez, M., Perrard, F., Massardier, V., Kleber, X., Deschamps, A., de Monestrol, H., Pareige, P. and Covarel, G. (2005a), "Low-temperature solubility of copper in iron: experimental study using thermoelectric power, small angle X-ray scattering and tomographic atom probe", *Philosophical Magazine*, Vol. 85, No. 20, pp. 2195 – 2210.
Perez, M., Perrard, F., Massardier-Jourdan, V., Kleber, X., Schmitt, V. and Deschamps, A. (2005b), "Low temperature solubility limit of copper in iron", *Material Science Forum*, Vol. 500 – 501, pp. 631 – 638.
Perrault, G. G. (1979), "The role of hydrides in the equilibrium of aluminum in aqueous systems", *Journal of Electrochemical Society*, Vol. 126, No. 2, pp. 199 – 204.
Pourbaix, M (1990), "Thermodynamics and corrosion", *Corrosion Science*, Vol. 30, No. 10, pp. 963 – 988.
Pourbaix, M. (1970), "Significance of protection potential in pitting and intergranular corrosion", *Corrosion*, Vol. 26, No. 10, pp. 431 – 438.
Pourbaix, M. (1972), "Theoretical and experimental considerations in corrosion testing", *Corrosion Science*, Vol. 12, No. 2, pp. 161 – 190.
Revie, R and Uhlig, H (2008), *Corrosion and corrosion control. An introduction to corrosion science and engineering*, Wiley.
Reymond, F., Steyaert, G., Carrupt, P. A., Testa, B. and Girault, H. (1996), "Ionic partition diagrams: a potential-pH representation", *Journal of the American Chemical Society*, Vol. 118, No. 47, pp. 11951 – 11957.
Russian State Standard 633-80, "Tubing pipes and couplings for them. Specifications", available at http://www.gosthelp.ru/gost/gost14250.html (accessed 31 December 2014).
Salje, G. and Feller-Kniepmeier, M. (1977) "The diffusion and solubility of copper in iron", *Journal of Applied Physics*, Vol. 48, No. 5, pp. 1833 – 1839.
Shih, H. C., Oung, J. C., Hsu, J. T., Wu, J. Y. and Wei, F. I. (1994), "Applications of electrochemical hysteresis for constructing the experimental potential-pH diagram for steels in seawater", *Materials Chemistry and Physics*, Vol. 37, No. 3, pp. 230 - 236.
Sun, H., Wu, X., Han, E. H. and Wei, Y. (2012), "Effects of pH and dissolved oxygen on electrochemical behaviour and oxide films of 304SS in borated and lithiated high temperature water", *Corrosion Science*, Vol. 59, pp. 334 – 342.
Tamilmani, S., Huang, W., Raghavan, S. and Small, R. (2002), "Potential-pH diagrams of interest to chemical mechanical planarization of copper", *Journal of Electrochemical Society*, Vol. 149, No. 12, pp. G638 – G642.
Thompson, W. T., Kaye, M. H., Bale, C. W. and Pelton, A. D. (2011), "Pourbaix Diagrams for Multielement Systems", in *Uhlig's corrosion handbook*, Wiley, pp. 103 – 110.
Toyama, T., Takahama, F., Kuramoto, A., Takamizawa, H., Nozawa, Y., Ebisawa, N., Shimodaira, M., Shimizu, Y., Inoue, K. and Nagai, Y. (2014), "The diffusivity and solubility

of copper in ferromagnetic iron at lower temperatures studied by atom probe tomography", *Scripta Materialia*, Vol. 83, pp. 5 – 8.
Tyurin, A. G. (2011), *Termodinamika khimicheskoi i elektrokhimicheskoi ustoichivosti tvyordykh splavov zheleza, khroma i nikelya*, ChelGU, Chelyabinsk.
Tyurin, A. G., Pyshmintsev, I. Yu., Kostitsyna, I. V. and Zubkova, I. M. (2007), "Thermodynamics of chemical and electrochemical stability of corrosion active nonmetal inclusions", *Protection of Metals*, Vol. 43, No. 1, pp. 34 – 44.
Vernik Jr, E. D. and Pourbaix, M (1971), "Use of electrochemical hysteresis techniques in developing alloys for saline exposures", *Corrosion*, Vol. 27, No. 12, pp. 495 – 505.
Xu, J., Wu, X. and Han, E. H. (2011), "Acoustic emission during the electrochemical corrosion of 304 stainless steel in H_2SO_4 solutions", *Corrosion Science*, Vol. 53, No. 1, pp. 448 – 457.

20. Review publications by the applicant

Two review papers, which summarise the content of this study, were published. The first one [Николайчук, Тюрин, 2012b] is the conference paper written in Russian. An extended and revised version of it was later presented as the journal paper [Nikolaychuk, 2015c] in English. The preprint of this paper is presented below with the permission from *Sibirskij federal'nyj universitet*.

П. А. Николайчук, А. Г. Тюрин

ФГБОУ ВПО “Челябинский государственный университет” (г. Челябинск)

ТЕРМОДИНАМИКА ХИМИЧЕСКОЙ И ЭЛЕКТРОХИМИЧЕСКОЙ УСТОЙЧИВОСТИ СИСТЕМ Me – Si (Me = Ti, Mo, Mn, Fe, Co, Ni, Cu, Zn)

Силициды переходных 3d-металлов отличаются весьма большим разнообразием свойств и исключительно широкой областью применения в технике. Среди этих соединений встречаются проводники с высокой электропроводностью, полупроводники и полуметаллы, сверхпроводники и т. п. В числе прочего эти соединения обладают очень высокой коррозионной стойкостью, их термодинамические и электрохимические характеристики весьма разнообразны. Широко проводятся экспериментальные исследования электрохимических свойств силицидов 3d-металлов [1]. Однако, наряду с этим, не менее важной научной и практической задачей является описание коррозионно-электрохимического поведения данных систем с позиций теории, что позволяет дополнить и расширить экспериментальную картину. Целью настоящей работы является изучение электрохимических свойств двойных систем металл – кремний для d-элементов, а также некоторых многокомпонентных сплавов на их основе с точки зрения химической термодинамики.

Все методы, приёмы и подходы, используемые при решении данной задачи, подробно изложены в [2]. Лучшим носителем термодинамической информации о возможных химических и электрохимических реакциях, протекающих в водных средах, является диаграмма электрохимического равновесия (диаграммы потенциал – pH), которая позволяет наглядно отобразить области термодинамической устойчивости всех возможных фаз и определить тип коррозионно-электрохимического поведения системы при конкретных значениях pH и равновесных потенциалов.

Диаграммы потенциал – pH для простых веществ при 25˚C впервые были построены М. Пурбе [3]. Диаграммы для систем Mn – H_2O, и Si – H_2O с тех пор не подвергались уточнениям. Диаграмма Fe – H_2O [2] была дополнена областью существования FeO_2. Диаграмма Ni – H_2O была уточнена в связи с тем обстоятельством, что вместо дискретного ряда оксидов никеля в системе образуется непрерывный ряд твёрдых растворов на основе этих оксидов (фаза нестехиометрического состава NiO_x) [4], также на диаграмму нанесена область существования гидрида никеля NiH_2. На диаграмму Co – H_2O [5] была нанесена область нестехиометрии оксидов CoO и Co_3O_4. Диаграмма Zn – H_2O [6] была дополнена областью существования ZnO_2. На диаграмме системы Cu – H_2O [7] были дополнительно введены области существования оксидов Cu_2O_3 и CuO_2, а также гидрида меди $CuH_{0,8}$. В системе Ti – H_2O [2] существует большое

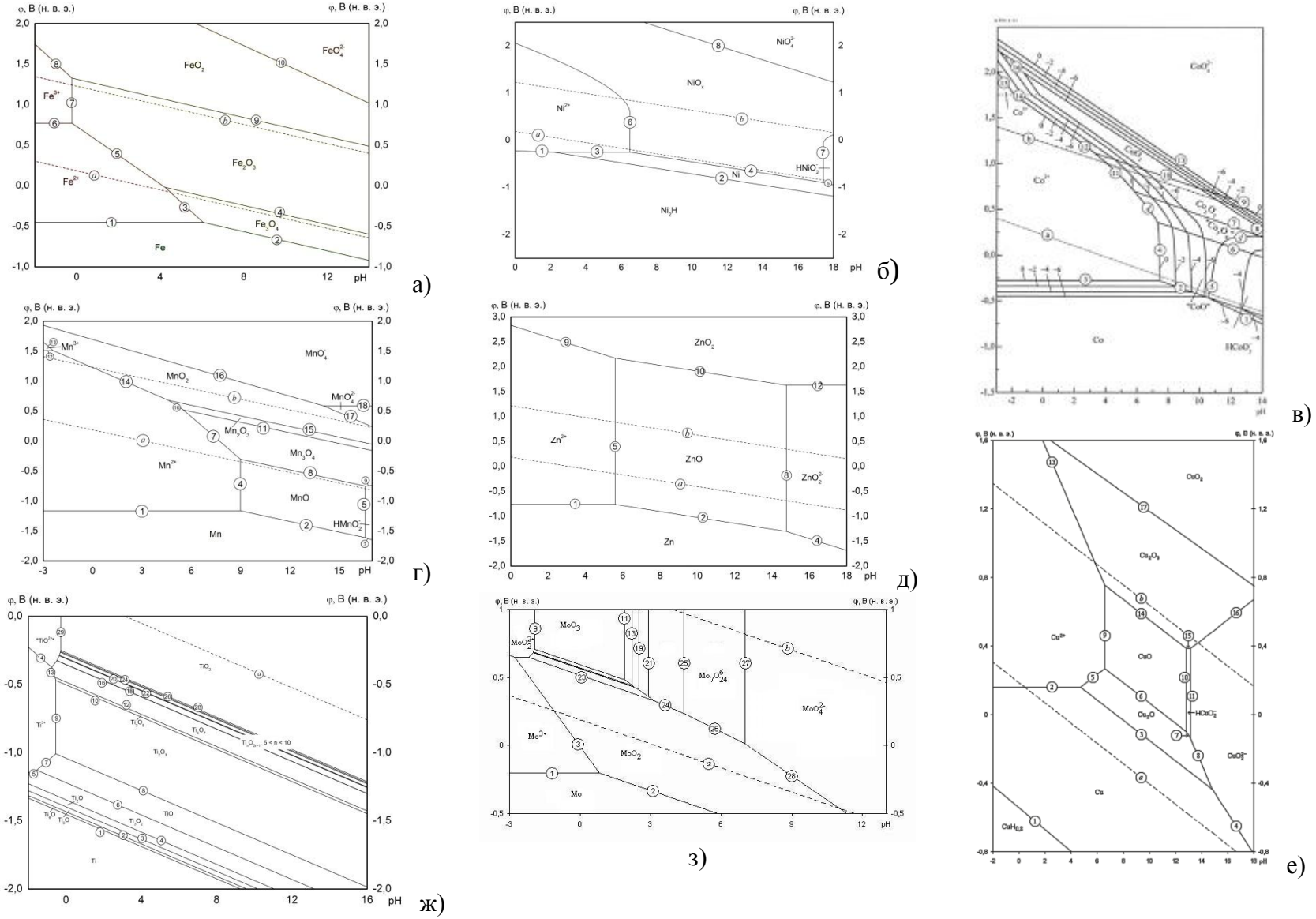

Рис. 1. Диаграммы Пурбе для Fe (а), Ni (б), Co (в), Mn (г), Zn (д), Cu (е), Ti (ж) и Mo (з).

количество оксидов и субоксидов, от Ti_6O до TiO_2, все они были нанесены на диаграмму, кроме того добавлена область устойчивости титанил-ионов. Диаграмма системы Mo – H_2O [8] дополнена областями существования всех оксидов молибдена, ионов молибденила, а также на ней учтены взаимные превращения изополимолибдат-ионов в растворе. Диаграммы потенциал – pH для перечисленных выше систем при 25˚C, давлении воздуха p = 1 бар и заданных активностях ионов в растворе представлены на рис. 1. Диаграммы на рис. 1а), 1б), 1г), 1д), 1ж) и 1з) построены при a_i = 1 моль/л, на рис. 1е) – при $a_i = 10^{-6}$ моль/л, на рис. 1в) – при $a_i = 1 - 10^{-6}$ моль/л.

Решение задачи построения диаграммы электрохимического равновесия для многокомпонентной системы Me – Si – H_2O состоит из трёх этапов. В первую очередь нужно, основываясь на диаграммах состояния бинарной системы Me – Si [9], изучить все фазовые и химические равновесия при 25˚C в ней, провести согласование справочных данных [10] и рассчитать термодинамические характеристики компонентов системы. На втором этапе нужно собрать информацию обо всех возможных оксидах и силикатах, которые могут образоваться в системе, создать термодинамическую модель окисления системы в кислородсодержащих средах и построить диаграмму состояния Me – Si – O [2]. Наконец, на завершающем этапе нужно добавить к рассмотрению ионы, которые могут образоваться при окислении компонентов системы в растворе, записать возможные реакции с их участием [11], вычислить термодинамические характеристики этих реакций и построить диаграмму потенциал – pH. Именно в таком порядке данная задача будет решаться для всех исследуемых систем.

Стоит отметить, что для многих оксидов и силицидов переходных металлов надёжные данные об их стандартных энергиях Гиббса образования в литературе отсутствуют. В этом случае для их оценки были использованы модифицированный метод Горичева [12] и в некоторых случаях наличие приближённой функциональной зависимости между термодинамической функцией образования оксида и зарядом ядра металла [13].

В системе Ti – Si при 25˚C существуют следующие соединения [9]: Ti_3Si, Ti_5Si_3, Ti_5Si_4, TiSi и $TiSi_2$, не имеющие областей гомогенности. Предельная растворимость Si в Ti с решёткой г. ц. к. составляет ~3,3 ат. % при 1000˚C и всего лишь ~0,7 ат. % при 800˚C, поэтому при стандартной температуре взаимной растворимостью титана и кремния в твёрдом состоянии можно пренебречь. В системе Si – O образуется лишь один устойчивый оксид (SiO_2), а диаграмма состояния Ti – O [9] предполагает наличие в системе при 298 K большого количества оксидов и субоксидов – Ti_6O, Ti_3O, Ti_2O, TiO, Ti_2O_3, Ti_3O_5, фаз Магнелли Ti_nO_{2n-1} ($4 \le n \le 10$), TiO_2. Между оксидами TiO_2 и SiO_2 никаких промежуточных соединений (силикатов) не образуется [14]. В водных растворах титан может

образовывать ионы Ti^{3+} и TiO^{2+}, а образования титанат-анионов не происходит. Кремний в растворе может окисляться до ионов SiO_3^{2-}.

Диаграмма потенциал – pH системы Ti – Si – H_2O, построенная [15] в соответствии с диаграммой Ti – Si – O, приведена на рис. 2а). Она разграничивает 42 области устойчивости различных фаз: I – Ti + Ti_3Si + Ti_5Si_3 + Ti_5Si_4 + TiSi + $TiSi_2$ + Si; II – Ti_6O + Ti_3Si + Ti_5Si_3 + Ti_5Si_4 + TiSi + $TiSi_2$ + Si; III – Ti_3O + Ti_3Si + Ti_5Si_3 + Ti_5Si_4 + TiSi + $TiSi_2$ + Si; IV – Ti_2O + Ti_3Si + Ti_5Si_3 + Ti_5Si_4 + TiSi + $TiSi_2$ + Si; V – Ti^{3+} + Ti_3Si + Ti_5Si_3 + Ti_5Si_4 + TiSi + $TiSi_2$ + Si; VI – TiO + Ti_3Si + Ti_5Si_3 + Ti_5Si_4 + TiSi + $TiSi_2$ + Si; VII – Ti^{3+} + Ti_5Si_3 + Ti_5Si_4 + TiSi + $TiSi_2$ + Si; VIII – TiO + Ti_5Si_3 + Ti_5Si_4 + TiSi + $TiSi_2$ + Si; IX – Ti_2O_3 + Ti_5Si_3 + Ti_5Si_4 + TiSi + $TiSi_2$ + Si; X – Ti^{3+} + Ti_5Si_4 + TiSi + $TiSi_2$ + Si; XI – Ti_2O_3 + Ti_5Si_4 + TiSi + $TiSi_2$ + Si; XII – Ti_2O_3 + Ti_5Si_4 + TiSi + $TiSi_2$ + SiO_3^{2-}; XIII – Ti^{3+} + TiSi + $TiSi_2$ + Si; XIV – Ti_2O_3 + TiSi + $TiSi_2$ + Si; XV – Ti_2O_3 + TiSi + $TiSi_2$ + SiO_3^{2-}; XVI – Ti^{3+} + $TiSi_2$ + Si; XVII – Ti_2O_3 + $TiSi_2$ + Si; XVIII – Ti^{3+} + $TiSi_2$ + SiO_2; XIX – Ti_2O_3 + $TiSi_2$ + SiO_2; XX – Ti_2O_3 + $TiSi_2$ + SiO_3^{2-}; XXI – Ti^{3+} + SiO_2; XXII – Ti_2O_3 + SiO_2; XXIII – Ti_2O_3 + SiO_3^{2-}; XXIV – Ti_3O_5 + SiO_2; XXV – Ti_3O_5 + SiO_3^{2-}; XXVI – "TiO^{2+}" + SiO_2; XXVII – Ti_4O_7 + SiO_2; XXVIII – Ti_4O_7 + SiO_3^{2-}; XXIX – Ti_5O_9 + SiO_2; XXX – Ti_5O_9 + SiO_3^{2-}; XXXI – Ti_6O_{11} + SiO_2; XXXII – Ti_6O_{11} + SiO_3^{2-}; XXXIII – Ti_7O_{13} + SiO_2; XXXIV – Ti_7O_{13} + SiO_3^{2-}; XXXV – Ti_8O_{15} + SiO_2; XXXVI – Ti_8O_{15} + SiO_3^{2-}; XXXVII – Ti_9O_{17} + SiO_2; XXXVIII – Ti_9O_{17} + SiO_3^{2-}; XXXIX – $Ti_{10}O_{19}$ + SiO_2; XL – $Ti_{10}O_{19}$ + SiO_3^{2-}; XLI – TiO_2 + SiO_2; XLII – TiO_2 + SiO_3^{2-}. Однако, титан обладает высоким химическим сродством не только к кислороду, но также к водороду и азоту, поэтому необходимо учитывать электрохимическое образование гидрида титана TiH_2 и нитрида TiN. Диаграмма, учитывающая эти особенности, приведена на рис. 2б), на ней можно выделить 16 областей преобладания различных фаз: I – TiH_2 + Ti_3Si + Ti_5Si_3 + Ti_5Si_4 + TiSi + $TiSi_2$ + Si; II – TiN + Ti_3Si + Ti_5Si_3 + Ti_5Si_4 + TiSi + $TiSi_2$ + Si; III – TiN + Ti_3Si + Ti_5Si_3 + Ti_5Si_4 + TiSi + $TiSi_2$ + SiO_2; IV – TiN + Ti_3Si + Ti_5Si_3 + Ti_5Si_4 + TiSi + $TiSi_2$ + SiO_3^{2-}; V – TiN + Ti_3Si + Ti_5Si_3 + Ti_5Si_4 + TiSi + SiO_2; VI – TiN + Ti_3Si + Ti_5Si_3 + Ti_5Si_4 + TiSi + SiO_3^{2-}; VII – TiN + Ti_3Si + Ti_5Si_3 + Ti_5Si_4 + SiO_2; VIII – TiN + Ti_3Si + Ti_5Si_3 + Ti_5Si_4 + SiO_3^{2-}; IX – TiN + Ti_3Si + Ti_5Si_3 + SiO_2; X – TiN + Ti_3Si + Ti_5Si_3 + SiO_3^{2-}; XI – TiN + Ti_3Si + SiO_2; XII – TiN + Ti_3Si + SiO_3^{2-}; XIII – Ti^{3+} + Ti_3Si + SiO_2; XIV – "TiO^{2+}" + Ti_3Si + SiO_2; XV – TiO_2 + Ti_3Si + SiO_2; XVI – TiO_2 + Ti_3Si + SiO_3^{2-}. В присутствии гидрида и нитрида титана все его оксиды, кроме высшего, становятся термодинамически неустойчивыми. Отсутствует область термодинамической устойчивости металлического титана.

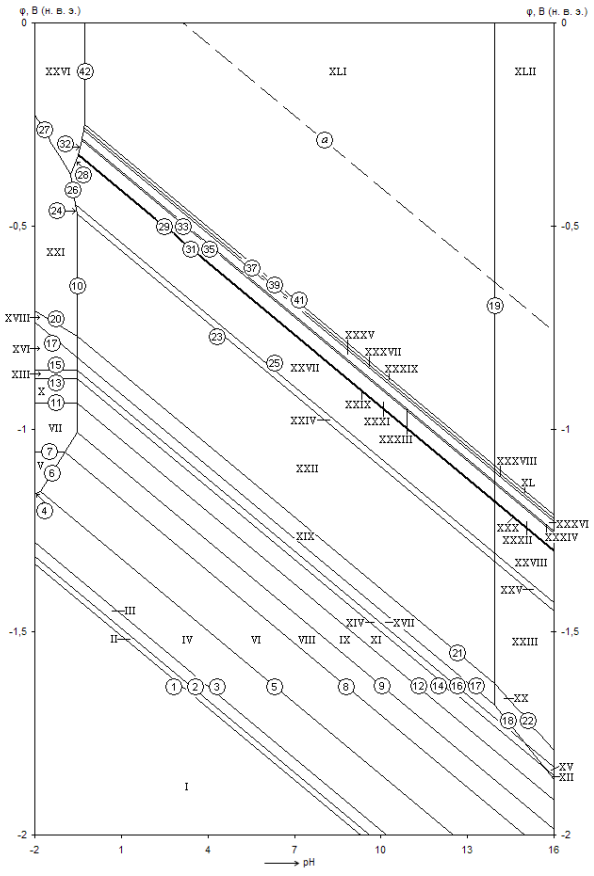

а)

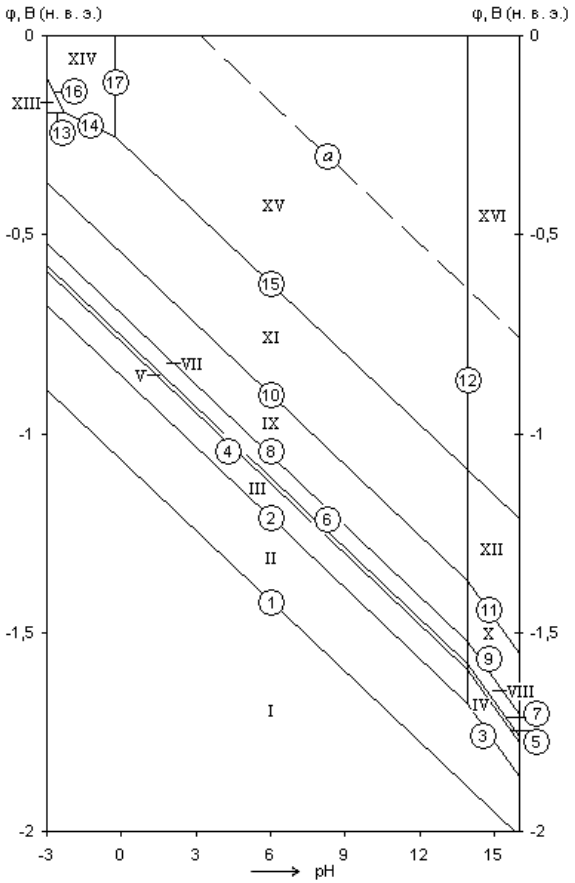

б)

Рис. 2. Диаграмма потенциал – pH системы Ti – Si – H_2O при T = 25˚C, p = 1 бар и a_i = 1 моль/л.
а) без учёта гидрида и нитрида титана;
б) с учётом гидрида и нитрида титана.

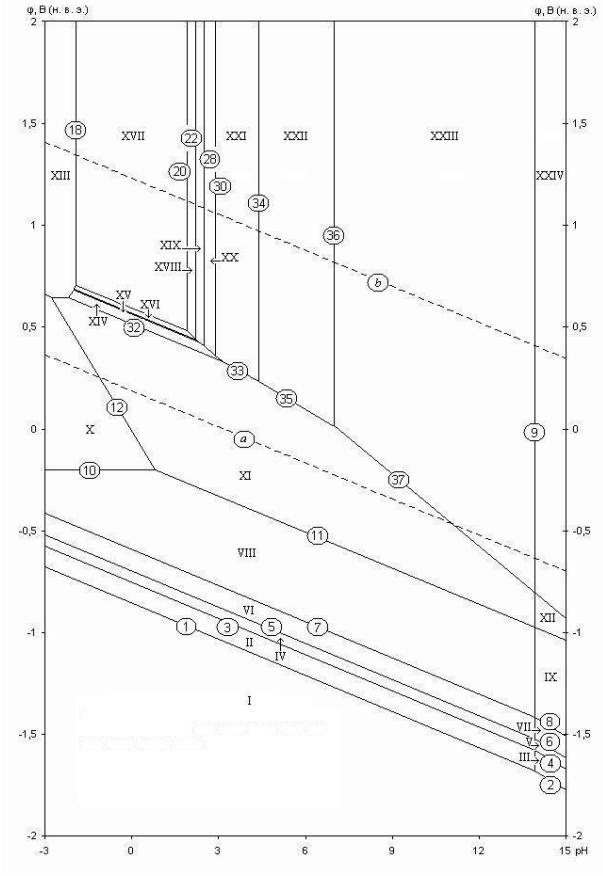

Рис. 3. Диаграмма потенциал – pH системы Mo – Si – H_2O при T = 25˚C, p = 1 бар и a_i = 1 моль/л.

Кроме того, наличие в системе гидрида и нитрида титана существенно влияет на механизм и порядок окисления его силицидов. Как видно из рис. 2б), полное разложение силицидов титана на компоненты – термодинамически невыгодный процесс. Наличие кремния в системе способно стабилизировать титан и удержать его от образования гидрида и последующего окисления. Этот факт можно связать с высокой прочностью ковалентных связей Ti – Si.

В системе Mo – Si устойчивы силициды Mo_3Si, Mo_5Si_3 и $MoSi_2$. Молибден и кремний при 25˚C взаимно нерастворимы друг в друге. Молибден образует стабильные оксиды MoO_2, Mo_4O_{11}, Mo_8O_{23}, Mo_9O_{26}, MoO_3 и ряд метастабильных фаз, которые при термодинамическом моделировании не учитываются [9]. О существовании силикатов молибдена данных в литературе нет [14]. В водном растворе молибден может существовать в виде катионов Mo^{3+} и MoO_2^{2+} и может окисляться до различных форм изополимолибдатов (VI): $H_2Mo_8O_{26}^{2-}$, $HMo_8O_{26}^{3-}$, $Mo_8O_{26}^{4-}$, $H_2Mo_7O_{24}^{4-}$, $Mo_7O_{24}^{6-}$ и MoO_4^{2-}. Диаграмма потенциал – pH системы Mo – Si – H_2O [16] приведена на рис. 3, на ней можно выделить 24 области термодинамической устойчивости различных фаз: I – Mo + Mo_3Si + Mo_5Si_3 + $MoSi_2$ + Si ; II – Mo + Mo_3Si + Mo_5Si_3 + $MoSi_2$ + SiO_2 ; III – Mo + Mo_3Si + Mo_5Si_3 + $MoSi_2$ + SiO_3^{2-} ; IV – Mo + Mo_3Si + Mo_5Si_3 + SiO_2 ; V – Mo + Mo_3Si + Mo_5Si_3 + SiO_3^{2-} ; VI – Mo + Mo_3Si + SiO_2 ; VII – Mo + Mo_3Si + SiO_3^{2-} ; VIII – Mo + SiO_2 ; IX – Mo + SiO_3^{2-} ; X – Mo^{3+} + SiO_2 ; XI – MoO_2 + SiO_2 ; XII – MoO_2 + SiO_3^{2-} ; XIII – MoO_2^{2+} + SiO_2 ; XIV – Mo_4O_{11} + SiO_2 ; XV – Mo_8O_{23} + SiO_2 ; XVI – Mo_9O_{26} + SiO_2 ; XVII – MoO_3 + SiO_2 ; XVIII – $H_2Mo_8O_{26}^{2-}$ + SiO_2 ; XIX – $HMo_8O_{26}^{3-}$ + SiO_2 ; XX – $Mo_8O_{26}^{4-}$ + SiO_2 ; XXI – $H_2Mo_7O_{24}^{4-}$ + SiO_2 ; XXII – $Mo_7O_{24}^{6-}$ + SiO_2 ; XXIII – MoO_4^{2-} + SiO_2 ; XXIV – MoO_4^{2-}, SiO_3^{2-}. Как видно из рис. 1з), молибден обладает очень узкой областью активного растворения, поскольку катионы Mo^{3+} и MoO_2^{2+} существуют только в сильнокислых средах. Однако, область его оксидной пассивации по потенциалам также довольно мала, и чем более щелочной является среда, тем шире становится область транспассивности (к ней относятся все возможные формы изополимолибдатов). В целом, электрохимическая устойчивость молибден-кремниевых сплавов (рис. 3) также целиком определяется содержанием в них кремния: оксидная плёнка SiO_2 является гораздо более стойкой в химическом и электрохимическом плане, чем плёнки из оксидов молибдена. Если кремния в сплаве достаточно для того, чтобы образовать на его поверхности сплошную плёнку кремнезёма, то активное окисление молибдена практически прекращается.

В системе Mn – Si [9] существует семь интерметаллических фаз: $Mn_{11}Si_{19}$, MnSi, Mn_5Si_3, Mn_5Si_2, Mn_3Si, Mn_9Si_2 и $Mn_{0,85}Si_{0,15}$. Растворимость

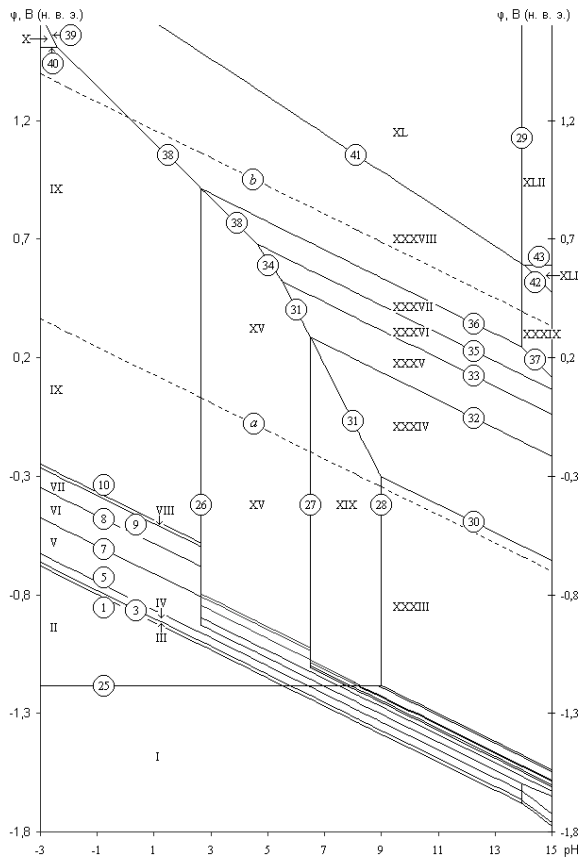

Рис. 4. Диаграмма потенциал – pH системы Mn – Si – H_2O при T = 25˚C, p = 1 бар и a_i = 1 моль/л.

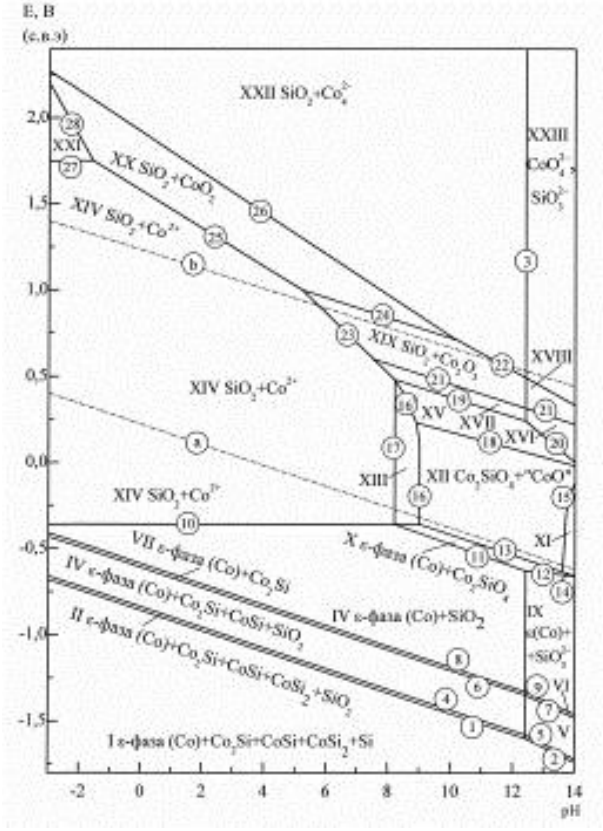

Рис. 5. Диаграмма потенциал – pH системы Co – Si – H_2O при T = 25˚C, p = 1 бар и a_i = 1 моль/л.

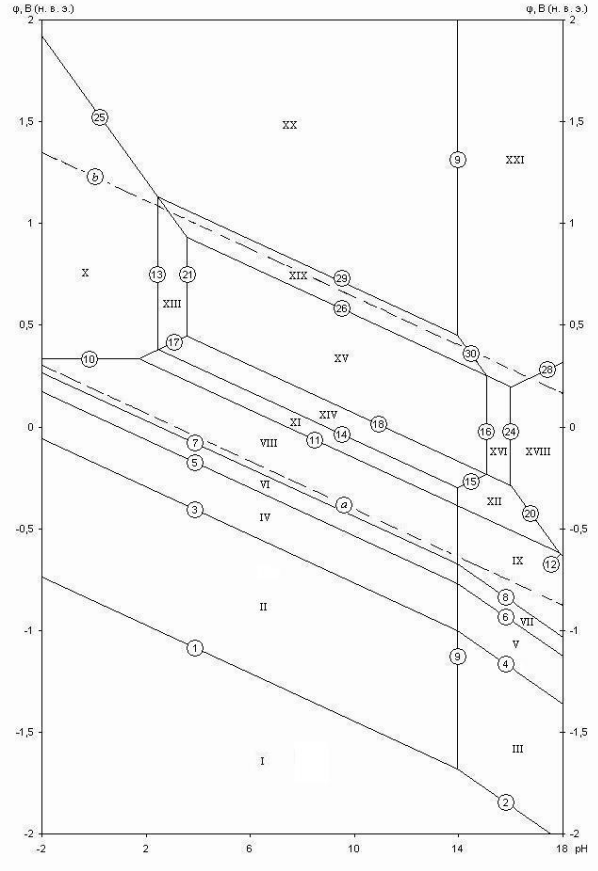

Рис. 6. Диаграмма потенциал – pH системы Cu – Si – H_2O при T = 25˚C, p = 1 бар и a_i = 1 моль/л.

Si в α-Mn при 25˚С по данным [17] составляет 4,56 мол. %. Активности компонентов твёрдого раствора следующие: $a_{\mathrm{Mn}(\alpha)} = 0{,}83$, $a_{\mathrm{Si}(\alpha)} = 3{,}8 \cdot 10^{-28}$.

Марганец образует оксиды MnO, Mn_3O_4, Mn_2O_3, MnO_2 и Mn_2O_7, хотя последний в водных растворах нестабилен [11]. Существует два силиката марганца, $MnSiO_3$ и Mn_2SiO_4 [14]. В водных средах возможно существование ионов Mn^{2+}, Mn^{3+}, MnO_4^{2-} и MnO_4^-. Диаграмма потенциал – pH системы Mn – Si – H_2O [17] приведена на рис. 4, на ней можно выделить 42 области термодинамической устойчивости различных фаз: I – α-фаза (Mn) + R-фаза ($Mn_{0,85}Si_{0,15}$) + ν-фаза (Mn_9Si_2) + Mn_3Si + Mn_5Si_2 + Mn_5Si_3 + MnSi + $Mn_{11}Si_{19}$ + Si; II – Mn^{2+} + $Mn_{0,85}Si_{0,15}$ + Mn_9Si_2 + Mn_3Si + Mn_5Si_2 + Mn_5Si_3 + MnSi + $Mn_{11}Si_{19}$ + Si; III – Mn^{2+} + $Mn_{0,85}Si_{0,15}$ + Mn_9Si_2 + Mn_3Si + Mn_5Si_2 + Mn_5Si_3 + MnSi + $Mn_{11}Si_{19}$ + SiO_2; IV – Mn^{2+} + $Mn_{0,85}Si_{0,15}$ + Mn_9Si_2 + Mn_3Si + Mn_5Si_2 + Mn_5Si_3 + MnSi + SiO_2; V – Mn^{2+} + $Mn_{0,85}Si_{0,15}$ + Mn_9Si_2 + Mn_3Si + Mn_5Si_2 + Mn_5Si_3 + SiO_2; VI – Mn^{2+} + $Mn_{0,85}Si_{0,15}$ + Mn_9Si_2 + Mn_3Si + Mn_5Si_2 + SiO_2; VII – Mn^{2+} + $Mn_{0,85}Si_{0,15}$ + Mn_9Si_2 + Mn_3Si + SiO_2; VIII – Mn^{2+} + $Mn_{0,85}Si_{0,15}$ + Mn_9Si_2 + SiO_2; IX – Mn^{2+} + $Mn_{0,85}Si_{0,15}$ + SiO_2; X – Mn^{3+} + $Mn_{0,85}Si_{0,15}$ + SiO_2; XI – Mn^{2+} + $Mn_{0,85}Si_{0,15}$ + Mn_9Si_2 + Mn_3Si + Mn_5Si_2 + Mn_5Si_3 + $MnSiO_3$; XII – Mn^{2+} + $Mn_{0,85}Si_{0,15}$ + Mn_9Si_2 + Mn_3Si + Mn_5Si_2 + $MnSiO_3$; XIII – Mn^{2+} + $Mn_{0,85}Si_{0,15}$ + Mn_9Si_2 + Mn_3Si + $MnSiO_3$; XIV – Mn^{2+} + $Mn_{0,85}Si_{0,15}$ + Mn_9Si_2 + $MnSiO_3$; XV – Mn^{2+} + $Mn_{0,85}Si_{0,15}$ + $MnSiO_3$; XVI – Mn^{2+} + $Mn_{0,85}Si_{0,15}$ + Mn_9Si_2 + Mn_3Si + Mn_5Si_2 + Mn_2SiO_4; XVII – Mn^{2+} + $Mn_{0,85}Si_{0,15}$ + Mn_9Si_2 + Mn_3Si + Mn_2SiO_4; XVIII – Mn^{2+} + $Mn_{0,85}Si_{0,15}$ + Mn_9Si_2 + Mn_2SiO_4; XIX – Mn^{2+} + $Mn_{0,85}Si_{0,15}$ + Mn_2SiO_4; XX – α + $Mn_{0,85}Si_{0,15}$ + Mn_9Si_2 + Mn_3Si + Mn_5Si_2 + Mn_5Si_3 + MnSi + $Mn_{11}Si_{19}$ + SiO_2; XXI – α + $Mn_{0,85}Si_{0,15}$ + Mn_9Si_2 + Mn_3Si + Mn_5Si_2 + Mn_5Si_3 + MnSi + $Mn_{11}Si_{19}$ + SiO_3^{2-}; XXII – α + $Mn_{0,85}Si_{0,15}$ + Mn_9Si_2 + Mn_3Si + Mn_5Si_2 + Mn_5Si_3 + MnSi + SiO_2; XXIII – α + $Mn_{0,85}Si_{0,15}$ + Mn_9Si_2 + Mn_3Si + Mn_5Si_2 + Mn_5Si_3 + MnSi + SiO_3^{2-}; XXIV – α + $Mn_{0,85}Si_{0,15}$ + Mn_9Si_2 + Mn_3Si + Mn_5Si_2 + Mn_5Si_3 + SiO_2; XXV – α + $Mn_{0,85}Si_{0,15}$ + Mn_9Si_2 + Mn_3Si + Mn_5Si_2 + Mn_5Si_3 + SiO_3^{2-}; XXVI – α + $Mn_{0,85}Si_{0,15}$ + Mn_9Si_2 + Mn_3Si + Mn_5Si_2 + Mn_5Si_3 + $MnSiO_3$; XXVII – α + $Mn_{0,85}Si_{0,15}$ + Mn_9Si_2 + Mn_3Si + Mn_5Si_2 + $MnSiO_3$; XXVIII – α + $Mn_{0,85}Si_{0,15}$ + Mn_9Si_2 + Mn_3Si + Mn_5Si_2 + Mn_2SiO_4; XXIX – α + $Mn_{0,85}Si_{0,15}$ + Mn_9Si_2 + Mn_3Si + Mn_2SiO_4; XXX – α + $Mn_{0,85}Si_{0,15}$ + Mn_9Si_2 + Mn_3Si + Mn_2SiO_4 + MnO; XXXI – α + $Mn_{0,85}Si_{0,15}$ + Mn_9Si_2 + Mn_2SiO_4 + MnO; XXXII – α + $Mn_{0,85}Si_{0,15}$ + Mn_2SiO_4 + MnO; XXXIII – $Mn_{0,85}Si_{0,15}$ + Mn_2SiO_4 + MnO; XXXIV – $Mn_{0,85}Si_{0,15}$ + Mn_2SiO_4 + Mn_3O_4; XXXV – $Mn_{0,85}Si_{0,15}$ + $MnSiO_3$ + Mn_3O_4; XXXVI – $Mn_{0,85}Si_{0,15}$ + $MnSiO_3$ + Mn_2O_3; XXXVII – $Mn_{0,85}Si_{0,15}$ + $MnSiO_3$ + MnO_2; XXXVIII – $Mn_{0,85}Si_{0,15}$ + MnO_2 + SiO_2; XXXIX – $Mn_{0,85}Si_{0,15}$ + MnO_2 + SiO_3^{2-}; XL – $Mn_{0,85}Si_{0,15}$ + SiO_2 + MnO_4^-; XLI – $Mn_{0,85}Si_{0,15}$ + MnO_4^{2-}, SiO_3^{2-}; XLII – $Mn_{0,85}Si_{0,15}$ + MnO_4^-, SiO_3^{2-}. Коррозионно-электрохимическое поведение марганец-кремниевых сплавов будет определяться кислотностью среды и установившимся в ней значением стационарного потенциала. В кислых средах будет наблюдаться селективная коррозия марганца, и переход его в раствор в виде катионов Mn^{2+}, а кремниевая составляющая сплава будет

окисляться до SiO_2. В нейтральных и щелочных средах, в зависимости от содержания кремния в системе и конкретных условий, окисление может заканчиваться образованием силикатов Mn_2SiO_4 или $MnSiO_3$. Защитная плёнка из этих силикатов является более стойкой в химическом и электрохимическом плане, нежели SiO_2, поскольку она не окисляется до SiO_3^{2-}.

В системе Co – Si при 298 К устойчивы соединения Co_2Si, CoSi и $CoSi_2$. Предельная растворимость Si в ε-Co по оценкам [5] составляет 10,7 мол. %, активности компонентов этого раствора $a_{Co(\varepsilon)} = 0,27$, $a_{Si(\varepsilon)} = 4 \cdot 10^{-16}$. Кобальт образует ряд оксидов – CoO, Co_3O_4, Co_2O_3 и CoO_2, первые два из них имеют заметную область нестехиометрии, которая простирается от CoO до $CoO_{1,07}$ и от $CoO_{1,31}$ до $CoO_{1,41}$ [9]. Известно [14] о существовании силиката кобальта Co_2SiO_4. Кобальт в растворе образует катион Co^{2+} и анионы $HCoO_2^-$, CoO_4^{2-}. Диаграмма потенциал – pH системы Co – Si – H_2O [5] приведена на рис. 5, на ней можно выделить 23 области преобладания различных фаз: I – ε-фаза(Co) + Co_2Si + CoSi + $CoSi_2$ + Si; II – ε-фаза(Co) + Co_2Si + CoSi + $CoSi_2$ + SiO_2; III – ε-фаза(Co) + Co_2Si + CoSi + $CoSi_2$ + SiO_3^{2-}; IV – ε-фаза(Co) + Co_2Si + CoSi + SiO_2; V – ε-фаза(Co) + Co_2Si + CoSi + SiO_3^{2-}; VI – ε-фаза(Co) + Co_2Si + SiO_3^{2-}; VII – ε-фаза(Co) + Co_2Si + SiO_2; VIII - IV – ε-фаза(Co) + SiO_2; IX – ε-фаза(Co) + SiO_3^{2-}; X – ε-фаза(Co) + Co_2SiO_4; XI – Co_2SiO_4 + $HCoO_2^-$; XII – Co_2SiO_4 + “CoO”; XIII – Co_2SiO_4 + Co^{2+}; XIV – SiO_2 + Co^{2+}; XV – Co_2SiO_4 + “Co_3O_4”; XVI – “Co_3O_4” + SiO_3^{2-}; XVII – “Co_3O_4” + SiO_2; XVIII – Co_2O_3 + SiO_3^{2-}; XIX – Co_2O_3 + SiO_2; XX – CoO_2 + SiO_2; XXI – SiO_2 + Co^{3+}; XXII – SiO_2 + CoO_4^{2-}; XXIII – CoO_4^{2-}, SiO_3^{2-}.

В системе Cu – Si [9] при 298 К установлено наличие силицидов меди $Cu_{56}Si_{11}$ (γ), $Cu_{15}Si_4$ (ε) и $Cu_{19}Si_6$ (η’’). Предельная растворимость Si в α-Cu при этой температуре оценена по данным о равновесии α-фазы с γ-фазой и составляет чуть больше 4 ат. %. Активности компонентов “насыщенного” твёрдого раствора таковы: $a_{Cu(\alpha)} = 0,92$, $a_{Si(\alpha)} = 5,6 \cdot 10^{-8}$. Наряду с широко известными оксидами Cu_2O и CuO медь может образовывать и высшие оксиды Cu_2O_3 и CuO_2 [4, 18], также включённые в термодинамическое описание системы. Между оксидами меди и кремния образуется одно промежуточное соединение – силикат меди $CuSiO_3$ [14]. В водном растворе медь может формировать катион Cu^{2+} и анионы $HCuO_2^-$ и CuO_2^{2-}, причём последовательность взаимных превращений различных форм меди (II) зависит от активностей ионов в растворе [7]. Также электрохимическим путём может быть получен гидрид меди $CuH_{0,8}$. Диаграмма потенциал – pH системы Cu – Si – H_2O [18] приведена на рис. 6, она определяет 21 область стабильности различных фаз: I – α-фаза (Cu) + γ-фаза ($Cu_{56}Si_{11}$) + ε-фаза ($Cu_{15}Si_4$) + η’’-фаза ($Cu_{19}Si_6$) + Si; II – α-фаза (Cu) + γ-фаза ($Cu_{51}Si_{14}$) + ε-фаза ($Cu_{15}Si_4$) + η’’-фаза ($Cu_{19}Si_6$) + SiO_2; III – α-фаза (Cu) + γ-фаза ($Cu_{51}Si_{14}$) + ε-

фаза ($Cu_{15}Si_4$) + η’’-фаза ($Cu_{19}Si_6$) + SiO_3^{2-}; IV – α- фаза (Cu) + γ-фаза ($Cu_{51}Si_{14}$) + ε-фаза ($Cu_{15}Si_4$) + SiO_2; V – α-фаза (Cu) + γ-фаза ($Cu_{51}Si_{14}$) + ε-фаза ($Cu_{15}Si_4$) + SiO_3^{2-}; VI – α-фаза (Cu) + γ-фаза ($Cu_{51}Si_{14}$) + SiO_2; VII – α-фаза (Cu) + γ-фаза ($Cu_{51}Si_14$) + SiO_3^{2-}; VIII – α-фаза (Cu) + SiO_2; IX – α-фаза (Cu) + SiO_3^{2-}; X – Cu^{2+} + SiO_2; XI – Cu_2O + SiO_2; XII – Cu_2O + SiO_3^{2-}; XIII – Cu^{2+} + $CuSiO_3$; XIV – Cu_2O + $CuSiO_3$; XV – CuO + $CuSiO_3$; XVI – CuO + SiO_3^{2-}; XVII – $HCuO_2^-$, SiO_3^{2-}; XVIII – CuO_2^{2-}, SiO_3^{2-}; XIX – Cu_2O_3 + $CuSiO_3$; XX – Cu_2O_3 + SiO_2; XXI – Cu_2O_3 + SiO_3^{2-}. Область I – это область иммунности (или термодинамической устойчивости) системы. В областях II – IX происходит селективное окисление кремния из сплава. При этом происходит последовательное образование всё более богатых медью фаз. Области X и XIII соответствуют селективной коррозии меди, при которой она переходит в раствор в виде ионов Cu^{2+}. Все другие области, кроме областей XVII и XVIII, соответствуют пассивации медно-кремниевых сплавов. Здесь термодинамически устойчивой фазой является один из оксидов меди или же соединение $CuSiO_3$. Однако, в областях XVII и XVIII создаются условия, при которых оба компонента сплава – и медь, и кремний – переходят в раствор в виде ионов, при этом целостность оксидной плёнки нарушается. Это области транспассивного состояния сплава. В целом, химическая и электрохимическая устойчивость медно-кремниевых сплавов целиком зависит от содержания в них кремния.

В системе Ni – Si [9] существует 6 интерметаллических фаз – β_1 (Ni_3Si), γ (Ni_5Si_2 или $Ni_{31}Si_{12}$), δ (Ni_2Si), ε (Ni_3Si_2), NiSi и $NiSi_2$. Растворимость Si в α-Ni при стандартной температуре невелика (около 2,5 ат. %), активности компонентов в таком растворе равны $a_{Ni(\alpha)} = 0{,}93$, $a_{Si(\alpha)} = 9 \cdot 10^{-36}$. Между оксидами никеля [4] образуется непрерывный ряд твёрдых растворов (фаза NiO_x), а силикат никеля Ni_2SiO_4 [14] оказывается термодинамически более устойчивым, чем простые оксиды никеля и кремния. В водных средах никель образует ионы Ni^{2+}, $HNiO_2^-$, NiO_4^{2-} [2, 11]. Кроме того, никель образует гидрид NiH_2. Диаграмма потенциал – pH системы Ni – Si – H_2O, построенная с учётом всех вышеперечисленных особенностей, приведена на рис. 7, на ней можно выделить 17 фаз: I–Ni_2H + Ni_3Si + Ni_5Si_2 + Ni_2Si + Ni_3Si_2 + NiSi + $NiSi_2$ + Si; II – Ni_2H + Ni_3Si + Ni_5Si_2 + Ni_2Si + Ni_3Si_2 + NiSi + $NiSi_2$; III – Ni_2H + Ni_3Si + Ni_5Si_2 + Ni_2Si + Ni_3Si_2 + NiSi; IV – Ni_2H + Ni_3Si + Ni_5Si_2 + Ni_2Si + Ni_3Si_2; V – Ni_2H + Ni_3Si + Ni_5Si_2 + Ni_2Si; VI – Ni_2H + Ni_3Si + Ni_5Si_2; VII – Ni_2H + Ni_3Si; VIII – Ni_2H + Ni_2SiO_4; IX – Ni (α) + Ni_2SiO_4; X – Ni^{2+} + SiO_2; XI – Ni^{2+} + Ni_2SiO_4; XII – NiO_x + Ni_2SiO_4; XIII – $HNiO_2^-$ + Ni_2SiO_4; XIV – NiO_x + SiO_2; XV – NiO_x + SiO_3^{2-}; XVI – NiO_4^{2-} + SiO_2; XVII– NiO_4^{2-} + SiO_3^{2-}.

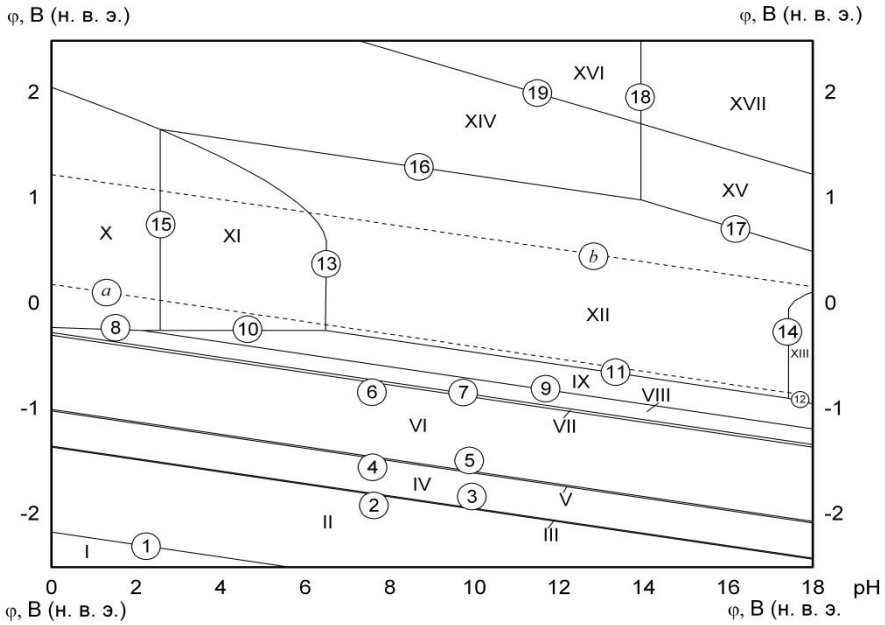

Рис. 7. Диаграмма потенциал – pH системы Ni – Si – H_2O при T = 25˚C, p = 1 бар и a_i = 1 моль/л.

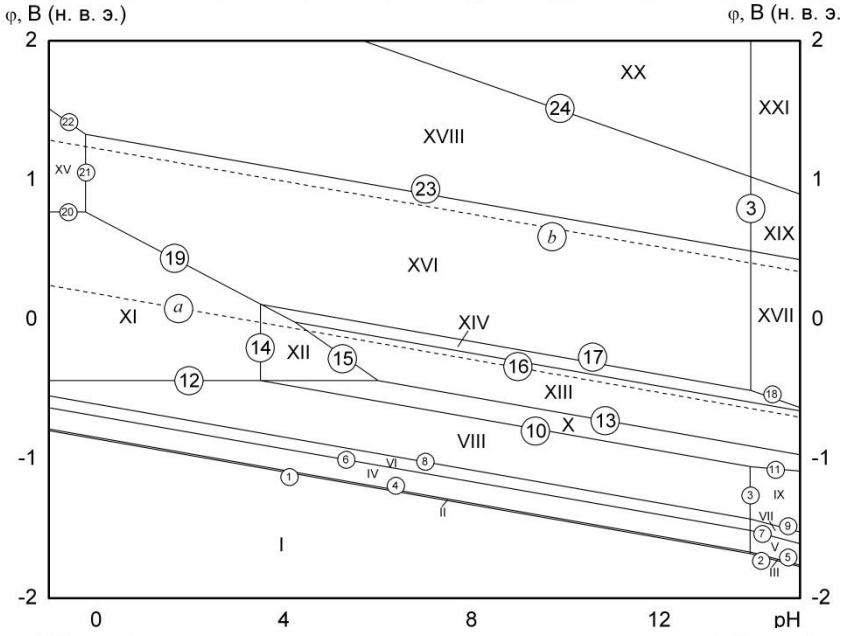

Рис. 8. Диаграмма потенциал – pH системы Fe – Si – H_2O при T = 25˚C, p = 1 бар и a_i = 1 моль/л.

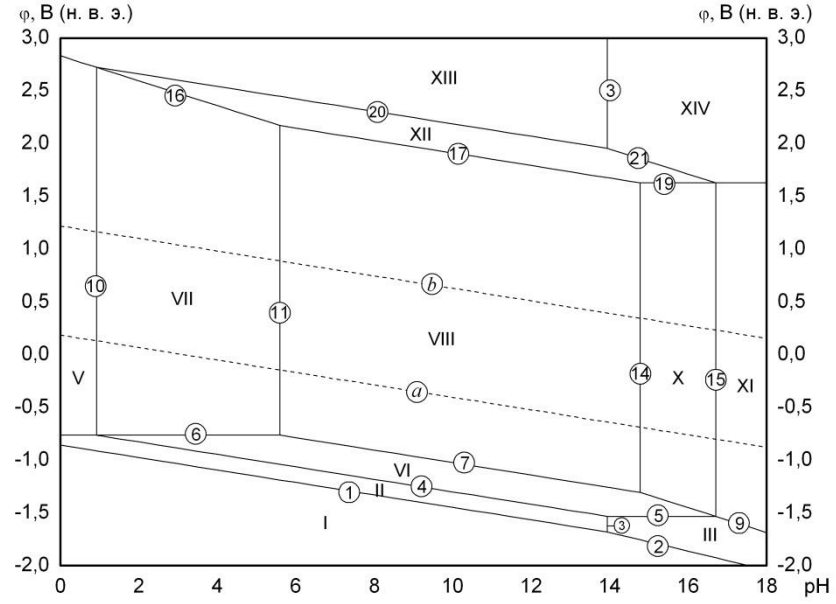

Рис. 9. Диаграмма потенциал – pH системы Zn – Si – H_2O при T = 25˚C, p = 1 бар и a_i = 1 моль/л.

В системе Fe – Si из множества силицидов при 25˚C устойчивы только FeSi, имеющий узкую область гомогенности (от $FeSi_{0,96}$ до $FeSi_{1,03}$) и $FeSi_2$. Твёрдый раствор Si в α-Fe может существовать в виде неупорядоченной фазы (α) и упорядоченных фаз (α_1 и α_2) [9]. Однако, фаза α_2, в которой достигается полное упорядочение, соответствует содержанию кремния, равному точно 25 ат. %, поэтому её часто интерпретируют как субсилицид "Fe_3Si". Предельная растворимость Si в неупорядоченной α-фазе составляет ~11 ат. %. Активности компонентов в таком растворе составляют $a_{Fe(\alpha)} = 0{,}13$, $a_{Si(\alpha)} = 5 \cdot 10^{-20}$. Поскольку FeO при стандартной температуре термодинамически неустойчив [9], то окисление железа приводит к образованию Fe_3O_4, затем Fe_2O_3 и метастабильного FeO_2. Кроме того, в системе Fe – Si – O устойчив силикат Fe_2SiO_4 [14], в котором при 25˚C растворяется [19] до $6{,}85 \cdot 10^{-5}$ ат. % Fe_3O_4. Вдобавок к этому в Fe_2O_3 растворяется до $1{,}54 \cdot 10^{-3}$ ат. % SiO_2. Железо в водном растворе может формировать ионы Fe^{2+}, Fe^{3+}, FeO_4^{2-}. Диаграмма потенциал – pH системы Fe – Si – H_2O приведена на рис. 8, и в системе можно разграничить 21 область стабильности различных фаз: I – α-фаза (Fe) + "Fe_3Si" + $FeSi_x$ + $FeSi_2$ + Si; II – α-фаза (Fe) + "Fe_3Si" + $FeSi_x$ + $FeSi_2$ + SiO_2; III – α-фаза (Fe) + "Fe_3Si" + $FeSi_x$ + $FeSi_2$ + SiO_3^{2-}; IV – α-фаза (Fe) + "Fe_3Si" + $FeSi_x$ + SiO_2; V – α-фаза (Fe) + "Fe_3Si" + $FeSi_x$ + SiO_3^{2-}; VI – α-фаза (Fe) + "Fe_3Si" + SiO_2; VII – α-фаза (Fe) + "Fe_3Si" + SiO_3^{2-}; VIII – α-фаза (Fe) + SiO_2; IX – α-фаза (Fe) + SiO_3^{2-}; X – α-фаза (Fe) + Fe_2SiO_4; XI – Fe^{2+} + SiO_2; XII – Fe^{2+} + Fe_2SiO_4; XIII – [Fe_2(Fe, Si)O_4] + Fe_2SiO_4; XIV – Fe_2O_3 + Fe_2SiO_4; XV – Fe^{3+} + SiO_2; XVI – Fe_2O_3 + [Fe_2O_3, SiO_2]; XVII – Fe_2O_3 + SiO_3^{2-}; XVIII – FeO_2 + SiO_2; XIX – FeO_2 + SiO_3^{2-}; XX – FeO_4^{2-} + SiO_2; XXI – FeO_4^{2-}, SiO_3^{2-}.

В целом, коррозионно-электрохимическое поведение силицидов железа, кобальта и никеля очень похоже. В кислых средах пассивационная плёнка на сплавах системы Fe – Si, Co – Si и Ni – Si будет представлять собой чистый SiO_2, при условии отсутствия в растворе ионов F^-, а металл из сплава образует ионы Fe^{2+}, Co^{2+} или Ni^{2+}. В нейтральных и щелочных средах можно выделить три режима процесса. Если концентрация кремния в довольно велика, то его достаточно для образования сплошной пассивирующей плёнки SiO_2.

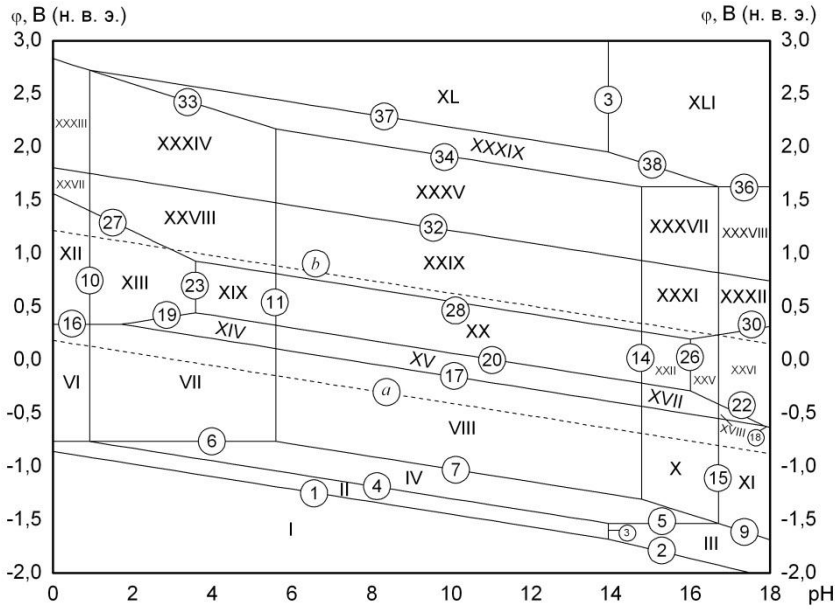

Рис. 10. Диаграмма потенциал – pH системы латунь ЛК80-3 – H_2O при T = 25˚C, p = 1 бар и a_i = 1 моль/л.

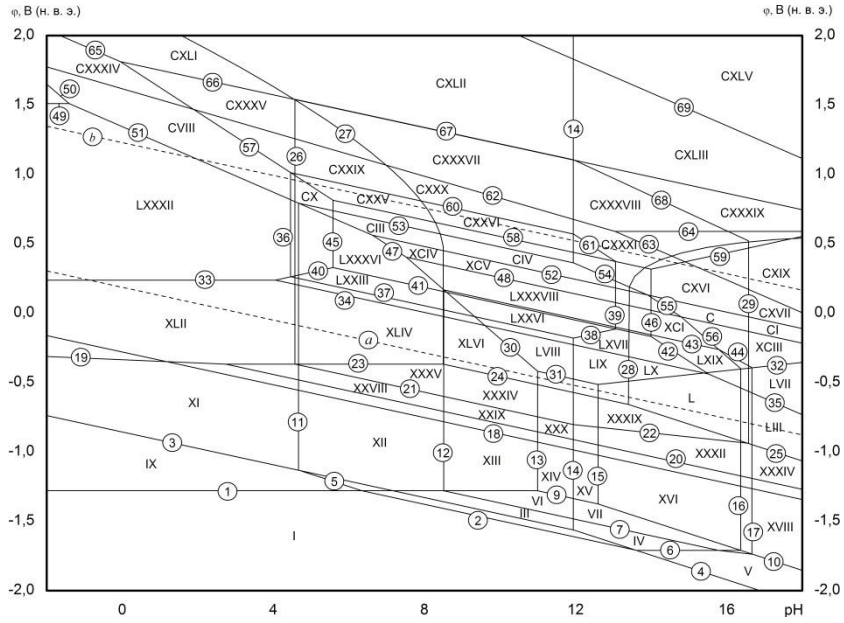

Рис. 11. Диаграмма потенциал – pH системы бронза БрКН1-3 – H_2O при T = 25˚C, p = 1 бар и a_i = 1 моль/л.

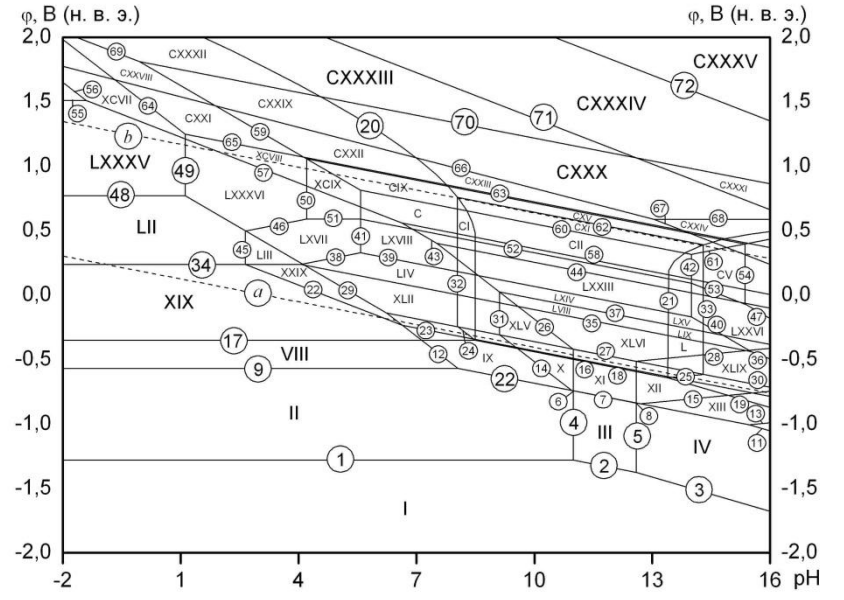
φ, В (н. в. э.)
pH
I
II
III
IV
VIII
XIX
LII
LXXXV
CXXXIII
CXXXIV
CXXXV
CXXXX
CXXXII
CXXXIII
CXXXIV
CXXXVI
CXXXVII
CXXXVIII
CXXXIX
CXL
CXLI
CXLII
CXLIII
CXLIV
CXLV
CXLVI
CXLVII
CXLVIII
CXLIX
CL
CLI
CLII
CLIII
CLIV
CLV
CLVI
CLVII
CLVIII
CLIX
CLX
CLXI
CLXII
CLXIII
CLXIV
CLXV
CLXVI
CLXVII
CLXVIII
CLXIX
CLXX
CLXXI
CLXXII
CLXXIII
CLXXIV
CLXXV
CLXXVI
CLXXVII
CLXXVIII
CLXXIX
CLXXX
CLXXXI
CLXXXII
CLXXXIII
CLXXXIV
CLXXXV
CLXXXVI
CLXXXVII
CLXXXVIII
CLXXXIX
CXC
CXCI
CXCII
CXCIII
CXCIV
CXCV
CXCVI
CXCVII
CXCVIII
CXCIX
CC
CCI
CCII
CCIII
CCIV
CCV
CCVI
CCVII
CCVIII
CCIX
CCX
CCXI
CCXII
CCXIII
CCXIV
CCXV
CCXVI
CCXVII
CCXVIII
CCXIX
CCXX
CCXXI
CCXXII
CCXXIII
CCXXIV
CCXXV
CCXXVI
CCXXVII
CCXXVIII
CCXXIX
CCXXX
CCXXXI
CCXXXII
CCXXXIII
CCXXXIV
CCXXXV
CCXXXVI
CCXXXVII
CCXXXVIII
CCXXXIX
CCXL
CCXLI
CCXLII
CCXLIII
CCXLIV
CCXLV
CCXLVI
CCXLVII
CCXLVIII
CCXLIX
CCL
CCLI
CCLII
CCLIII
CCLIV
CCLV
CCLVI
CCLVII
CCLVIII
CCLIX
CCLX
CCLXI
CCLXII
CCLXIII
CCLXIV
CCLXV
CCLXVI
CCLXVII
CCLXVIII
CCLXIX
CCLXX
CCLXXI
CCLXXII
CCLXXIII
CCLXXIV
CCLXXV
CCLXXVI
CCLXXVII
CCLXXVIII
CCLXXIX
CCLXXX
CCLXXXI
CCLXXXII
CCLXXXIII
CCLXXXIV
CCLXXXV
CCLXXXVI
CCLXXXVII
CCLXXXVIII
CCLXXXIX
CCXC
CCXCI
CCXCII
CCXCIII
CCXCIV
CCXCV
CCXCVI
CCXCVII
CCXCVIII
CCXCIX
CCC
CCCI
CCCII
CCCIII
CCCIV
CCCV
CCCVI
CCCVII
CCCVIII
CCCIX
CCCX
CCCXI
CCCXII
CCCXIII
CCCXIV
CCCXV
CCCXVI
CCCXVII
CCCXVIII
CCCXIX
CCCXX
CCCXXI
CCCXXII
CCCXXIII
CCCXXIV
CCCXXV
CCCXXVI
CCCXXVII
CCCXXVIII
CCCXXIX
CCCXXX
CCCXXXI
CCCXXXII
CCCXXXIII
CCCXXXIV
CCCXXXV
CCCXXXVI
CCCXXXVII
CCCXXXVIII
CCCXXXIX
CCCXL
CCCXLI
CCCXLII
CCCXLIII
CCCXLIV
CCCXLV
CCCXLVI
CCCXLVII
CCCXLVIII
CCCXLIX
CCCL
CCCLI
CCCLII
CCCLIII
CCCLIV
CCCLV
CCCLVI
CCCLVII
CCCLVIII
CCCLIX
CCCLX
CCCLXI
CCCLXII
CCCLXIII
CCCLXIV
CCCLXV
CCCLXVI
CCCLXVII
CCCLXVIII
CCCLXIX
CCCLXX
CCCLXXI
CCCLXXII
CCCLXXIII
CCCLXXIV
CCCLXXV
CCCLXXVI
CCCLXXVII
CCCLXXVIII
CCCLXXIX
CCCLXXX
CCCLXXXI
CCCLXXXII
CCCLXXXIII
CCCLXXXIV
CCCLXXXV
CCCLXXXVI
CCCLXXXVII
CCCLXXXVIII
CCCLXXXIX
CCCXC
CCCXCI
CCCXCII
CCCXCIII
CCCXCIV
CCCXCV
CCCXCVI
CCCXCVII
CCCXCVIII
CCCXCIX
CD
CDI
CDII
CDIII
CDIV
CDV
CDVI
CDVII
CDVIII
CDIX
CDX
CDXI
CDXII
CDXIII
CDXIV
CDXV
CDXVI
CDXVII
CDXVIII
CDXIX
CDXX
CDXXI
CDXXII
CDXXIII
CDXXIV
CDXXV
CDXXVI
CDXXVII
CDXXVIII
CDXXIX
CDXXX
CDXXXI
CDXXXII
CDXXXIII
CDXXXIV
CDXXXV
CDXXXVI
CDXXXVII
CDXXXVIII
CDXXXIX
CDXL
CDXLI
CDXLII
CDXLIII
CDXLIV
CDXLV
CDXLVI
CDXLVII
CDXLVIII
CDXLIX
CDL
CDLI
CDLII
CDLIII
CDLIV
CDLV
CDLVI
CDLVII
CDLVIII
CDLIX
CDLX
CDLXI
CDLXII
CDLXIII
CDLXIV
CDLXV
CDLXVI
CDLXVII
CDLXVIII
CDLXIX
CDLXX
CDLXXI
CDLXXII
CDLXXIII
CDLXXIV
CDLXXV
CDLXXVI
CDLXXVII
CDLXXVIII
CDLXXIX
CDLXXX
CDLXXXI
CDLXXXII
CDLXXXIII
CDLXXXIV
CDLXXXV
CDLXXXVI
CDLXXXVII
CDLXXXVIII
CDLXXXIX
CDXC
CDXCI
CDXCII
CDXCIII
CDXCIV
CDXCV
CDXCVI
CDXCVII
CDXCVIII
CDXCIX
D
DI
DII
DIII
DIV
DV
DVI
DVII
DVIII
DIX
DX
DXI
DXII
DXIII
DXIV
DXV
DXVI
DXVII
DXVIII
DXIX
DXX
DXXI
DXXII
DXXIII
DXXIV
DXXV
DXXVI
DXXVII
DXXVIII
DXXIX
DXXX
DXXXI
DXXXII
DXXXIII
DXXXIV
DXXXV
DXXXVI
DXXXVII
DXXXVIII
DXXXIX
DXL
DXLI
DXLII
DXLIII
DXLIV
DXLV
DXLVI
DXLVII
DXLVIII
DXLIX
DL
DLI
DLII
DLIII
DLIV
DLV
DLVI
DLVII
DLVIII
DLIX
DLX
DLXI
DLXII
DLXIII
DLXIV
DLXV
DLXVI
DLXVII
DLXVIII
DLXIX
DLXX
DLXXI
DLXXII
DLXXIII
DLXXIV
DLXXV
DLXXVI
DLXXVII
DLXXVIII
DLXXIX
DLXXX
DLXXXI
DLXXXII
DLXXXIII
DLXXXIV
DLXXXV
DLXXXVI
DLXXXVII
DLXXXVIII
DLXXXIX
DXC
DXCI
DXCII
DXCIII
DXCIV
DXCV
DXCVI
DXCVII
DXCVIII
DXCIX
DC
DCI
DCII
DCIII
DCIV
DCV
DCVI
DCVII
DCVIII
DCIX
DCX
DCXI
DCXII
DCXIII
DCXIV
DCXV
DCXVI
DCXVII
DCXVIII
DCXIX
DCXX
DCXXI
DCXXII
DCXXIII
DCXXIV
DCXXV
DCXXVI
DCXXVII
DCXXVIII
DCXXIX
DCXXX
DCXXXI
DCXXXII
DCXXXIII
DCXXXIV
DCXXXV
DCXXXVI
DCXXXVII
DCXXXVIII
DCXXXIX
DCXL
DCXLI
DCXLII
DCXLIII
DCXLIV
DCXLV
DCXLVI
DCXLVII
DCXLVIII
DCXLIX
DCL
DCLI
DCLII
DCLIII
DCLIV
DCLV
DCLVI
DCLVII
DCLVIII
DCLIX
DCLX
DCLXI
DCLXII
DCLXIII
DCLXIV
DCLXV
DCLXVI
DCLXVII
DCLXVIII
DCLXIX
DCLXX
DCLXXI
DCLXXII
DCLXXIII
DCLXXIV
DCLXXV
DCLXXVI
DCLXXVII
DCLXXVIII
DCLXXIX
DCLXXX
DCLXXXI
DCLXXXII
DCLXXXIII
DCLXXXIV
DCLXXXV
DCLXXXVI
DCLXXXVII
DCLXXXVIII
DCLXXXIX
DCXC
DCXCI
DCXCII
DCXCIII
DCXCIV
DCXCV
DCXCVI
DCXCVII
DCXCVIII
DCXCIX
DCC
DCCI
DCCII
DCCIII
DCCIV
DCCV
DCCVI
DCCVII
DCCVIII
DCCIX
DCCX
DCCXI
DCCXII
DCCXIII
DCCXIV
DCCXV
DCCXVI
DCCXVII
DCCXVIII
DCCXIX
DCCXX
DCCXXI
DCCXXII
DCCXXIII
DCCXXIV
DCCXXV
DCCXXVI
DCCXXVII
DCCXXVIII
DCCXXIX
DCCXXX
DCCXXXI
DCCXXXII
DCCXXXIII
DCCXXXIV
DCCXXXV
DCCXXXVI
DCCXXXVII
DCCXXXVIII
DCCXXXIX
DCCXL
DCCXLI
DCCXLII
DCCXLIII
DCCXLIV
DCCXLV
DCCXLVI
DCCXLVII
DCCXLVIII
DCCXLIX
DCCL
DCCLI
DCCLII
DCCLIII
DCCLIV
DCCLV
DCCLVI
DCCLVII
DCCLVIII
DCCLIX
DCCLX
DCCLXI
DCCLXII
DCCLXIII
DCCLXIV
DCCLXV
DCCLXVI
DCCLXVII
DCCLXVIII
DCCLXIX
DCCLXX
DCCLXXI
DCCLXXII
DCCLXXIII
DCCLXXIV
DCCLXXV
DCCLXXVI
DCCLXXVII
DCCLXXVIII
DCCLXXIX
DCCLXXX
DCCLXXXI
DCCLXXXII
DCCLXXXIII
DCCLXXXIV
DCCLXXXV
DCCLXXXVI
DCCLXXXVII
DCCLXXXVIII
DCCLXXXIX
DCCXC
DCCXCI
DCCXCII
DCCXCIII
DCCXCIV
DCCXCV
DCCXCVI
DCCXCVII
DCCXCVIII
DCCXCIX
DCCC
DCCCI
DCCCII
DCCCIII
DCCCIV
DCCCV
DCCCVI
DCCCVII
DCCCVIII
DCCCIX
DCCCX
DCCCXI
DCCCXII
DCCCXIII
DCCCXIV
DCCCXV
DCCCXVI
DCCCXVII
DCCCXVIII
DCCCXIX
DCCCXX
DCCCXXI
DCCCXXII
DCCCXXIII
DCCCXXIV
DCCCXXV
DCCCXXVI
DCCCXXVII
DCCCXXVIII
DCCCXXIX
DCCCXXX
DCCCXXXI
DCCCXXXII
DCCCXXXIII
DCCCXXXIV
DCCCXXXV
DCCCXXXVI
DCCCXXXVII
DCCCXXXVIII
DCCCXXXIX
DCCCXL
DCCCXLI
DCCCXLII
DCCCXLIII
DCCCXLIV
DCCCXLV
DCCCXLVI
DCCCXLVII
DCCCXLVIII
DCCCXLIX
DCCCL
DCCCLI
DCCCLII
DCCCLIII
DCCCLIV
DCCCLV
DCCCLVI
DCCCLVII
DCCCLVIII
DCCCLIX
DCCCLX
DCCCLXI
DCCCLXII
DCCCLXIII
DCCCLXIV
DCCCLXV
DCCCLXVI
DCCCLXVII
DCCCLXVIII
DCCCLXIX
DCCCLXX
DCCCLXXI
DCCCLXXII
DCCCLXXIII
DCCCLXXIV
DCCCLXXV
DCCCLXXVI
DCCCLXXVII
DCCCLXXVIII
DCCCLXXIX
DCCCLXXX
DCCCLXXXI
DCCCLXXXII
DCCCLXXXIII
DCCCLXXXIV
DCCCLXXXV
DCCCLXXXVI
DCCCLXXXVII
DCCCLXXXVIII
DCCCLXXXIX
DCCCXC
DCCCXCI
DCCCXCII
DCCCXCIII
DCCCXCIV
DCCCXCV
DCCCXCVI
DCCCXCVII
DCCCXCVIII
DCCCXCIX
CM
CMI
CMII
CMIII
CMIV
CMV
CMVI
CMVII
CMVIII
CMIX
CMX
CMXI
CMXII
CMXIII
CMXIV
CMXV
CMXVI
CMXVII
CMXVIII
CMXIX
CMXX
CMXXI
CMXXII
CMXXIII
CMXXIV
CMXXV
CMXXVI
CMXXVII
CMXXVIII
CMXXIX
CMXXX
CMXXXI
CMXXXII
CMXXXIII
CMXXXIV
CMXXXV
CMXXXVI
CMXXXVII
CMXXXVIII
CMXXXIX
CMXL
CMXLI
CMXLII
CMXLIII
CMXLIV
CMXLV
CMXLVI
CMXLVII
CMXLVIII
CMXLIX
CML
CMLI
CMLII
CMLIII
CMLIV
CMLV
CMLVI
CMLVII
CMLVIII
CMLIX
CMLX
CMLXI
CMLXII
CMLXIII
CMLXIV
CMLXV
CMLXVI
CMLXVII
CMLXVIII
CMLXIX
CMLXX
CMLXXI
CMLXXII
CMLXXIII
CMLXXIV
CMLXXV
CMLXXVI
CMLXXVII
CMLXXVIII
CMLXXIX
CMLXXX
CMLXXXI
CMLXXXII
CMLXXXIII
CMLXXXIV
CMLXXXV
CMLXXXVI
CMLXXXVII
CMLXXXVIII
CMLXXXIX
CMXC
CMXCI
CMXCII
CMXCIII
CMXCIV
CMXCV
CMXCVI
CMXCVII
CMXCVIII
CM

При меньших концентрациях кремния в сплаве его хватает лишь для образования сплошной плёнки силиката Fe_2SiO_4, Co_2SiO_4 или Ni_2SiO_4. Если же кремния в системе совсем мало, то защитная плёнка, как и на чистом металле, будет состоять из его простых оксидов, а кремний в виде локальных включений силикатов будет входить в её внутренний подслой.

В системе Zn – Si не образуется каких-либо силицидов, кроме того, при стандартной температуре цинк и кремний взаимно нерастворимы друг в друге [9]. Цинк образует два оксида – ZnO и ZnO_2 – и один силикат, $ZnSiO_3$ [14]. В водном растворе цинк может существовать в виде катиона Zn^{2+} и анионов $HZnO_2^-$ и ZnO_2^{2-}, причём последовательность взаимных превращений различных форм цинка (II) зависит от активностей ионов в растворе [6]. Диаграмма потенциал – pH системы Zn – Si – H_2O приведена на рис. 9, имеется 14 областей преобладания различных фаз: I – Zn + Si; II – Zn + SiO_2; III – Zn + SiO_3^{2-}; IV – Zn^{2+} + Si; V – Zn^{2+} + SiO_2; VI – Zn + $ZnSiO_3$; VII – Zn^{2+} + $ZnSiO_3$; VIII – ZnO + $ZnSiO_3$; IX – $HZnO_2^-$ + $ZnSiO_3$; X – ZnO_2^{2-} + $ZnSiO_3$; XI – ZnO_2^{2-}, SiO_3^{2-}; XII – ZnO_2 + $ZnSiO_3$; XIII – ZnO_2 + SiO_2; XIV – ZnO_2 + SiO_3^{2-}.

Применение термодинамического моделирования коррозионных свойств не ограничивается только бинарными системами. Данный подход может быть обобщён и на многокомпонентные сплавы. Для примера, основываясь на полученных данных, были построены диаграммы потенциал – pH для таких важных для цветной металлургии сплавов как кремнистая латунь ЛК80-3 (рис. 10) и кремнистая бронза БрКН1-3 (рис. 11). Для сравнения, была построена диаграмма для похожего по составу мельхиора МНЖМц30-1-1 [4], не содержащего кремний (рис. 12). Показано благотворное влияние кремния на коррозионные свойства двойных и многокомпонентных систем. Диаграммы потенциал – pH представляют собой термодинамическую модель учёта взаимного влияния компонентов сплавов на их коррозионные свойства и являются научной основой, позволяющей регулировать технологические процессы.

ЛИТЕРАТУРА

1. Шеин А. Б. Электрохимия силицидов и германидов переходных металлов: монография. – Пермь: Издательство Пермского государственного университета, 2009. – 269 с.
2. Тюрин А. Г. Термодинамика химической и электрохимической устойчивости твёрдых сплавов железа, хрома и никеля: монография. – Челябинск: Издательство Челябинского государственного университета, 2011. – 241 с.
3. Справочник химика / под ред. Б. П. Никольского. – М.–Л.: Химия, 1964. – Т. 3. – 1008 с.
4. Николайчук П. А., Тюрин А. Г. Термодинамика химической и электрохимической устойчивости медно-никелевых сплавов // Физикохимия поверхности и защита материалов, 2012. – Т. 48. – № 4. – С. 398 – 412.

5. Тюрин А. Г., Мосунова Т. В., Николайчук П. А. Термодинамика химической и электрохимической устойчивости силицидов кобальта // Вестник ЮУрГУ, серия “Химия”, 2010. – № 11 (187). – Вып. 3. – С. 52 – 60.
6. Николайчук П. А., Тюрин А. Г. Уточнённая диаграмма Пурбе для цинка // Современные проблемы теоретической и экспериментальной химии: межвузовский сборник научных трудов VIII Всероссийской конференции молодых учёных с международным участием. Саратов: ООО Издательство “КУБиК”, 2011. – С. 227 – 230.
7. Николайчук П. А., Канатьева И. И., Тюрин А. Г. Уточнённая диаграмма Пурбе для меди // Современные проблемы теоретической и экспериментальной химии: межвузовский сборник научных трудов VII Всероссийской конференции молодых учёных с международным участием. Саратов: ООО Издательство “КУБиК”, 2010. – С. 287 – 291.
8. Николайчук П. А., Тюрин А. Г. Уточнённая диаграмма Пурбе для молибдена // Бутлеровские сообщения, 2011. – Т. 24. – № 2. – С. 101 – 105.
9. Диаграммы состояния двойных металлических систем: справочник. В 3 томах / Под ред. Лякишева Н. П. – М.: Машиностроение, 1996 – 2000.
10. Термические константы веществ: база данных – URL: <http://www.chem.msu.su/cgi-bin/tkv.pl?show=welcome.html>.
11. Справочник по электрохимии / под ред. А. М. Сухотина. – Л.: Химия, 1981. – 488 с.
12. Nikolaychuk P. A., Tyurin A. G. Method of estimating the standard Gibbs energies of formation of binary compounds // Abstracts of the XVIII International Conference on Chemical Thermodynamics in Russia (RCCT-2011). Vol. 2. – Samara: Samara State Technical University, 2011. – P. 16 – 17.
13. Nikolaychuk P. A., Tyurin A. G. The analysis of standard Gibbs energies of formation of MeO_2 type oxides of fourth period d-elements // Abstracts of the XVIII International Conference on Chemical Thermodynamics in Russia (RCCT-2011). Vol. 2. – Samara: Samara State Technical University, 2011. – P. 17 – 18.
14. Диаграммы состояния силикатных систем: справочник / Торопов Н. А., Борзаковский В. П. [et al.]. – М. – Л.: Наука, 1965. – Вып. 2. – 372 с.
15. Николайчук П. А., Тюрин А. Г. Термодинамика химической и электрохимической устойчивости сплавов системы Ti – Si // Бутлеровские сообщения, 2011. – Т. 24. – № 2. – С. 77 – 87.
16. Николайчук П. А., Тюрин А. Г. Термодинамика химической и электрохимической устойчивости сплавов системы Mo – Si // Бутлеровские сообщения, 2011. – Т. 24. – № 2. – С. 95 – 100.
17. Николайчук П. А., Шаляпина Т. И., Тюрин А. Г., Мосунова Т. В. Термодинамика химической и электрохимической устойчивости сплавов системы Mn – Si // Вестник ЮУрГУ, серия “Химия”, 2010. – № 31 (207). – Вып. 4. – С. 72 – 82.
18. Николайчук П. А., Тюрин А. Г. Термодинамика химической и электрохимической устойчивости сплавов системы Cu – Si // Бутлеровские сообщения, 2011. – Т. 24. – № 2. – С. 88 – 94.
19. Кимяшов А. А. Фазовые равновесия в системах Fe – Al – O и Fe – Si – O в интервале температур 1100 – 1300 К / Дисс. канд. хим. наук. Челябинск, 2010. – 139 с.

Thermodynamic evaluation of electrochemical stability of Me – Si systems (Me = 4th row transition metal)

Pavel Anatolyevich Nikolaychuk

Department of Analytical and Physical Chemistry,

Chelyabinsk State University, Bratyev Kashirinykh street 129, Chelyabinsk, 454001, Russian Federation.

E-mail: npa@csu.ru

Abstract

This paper aims to review the studies of electrochemical properties of Me – Si binary systems for scandium, titanium, molybdenum, manganese, iron, cobalt, nickel, copper and zinc from the point of view of chemical thermodynamics. The binary phase diagrams of Me – Si and Me – O systems were considered and thermodynamic properties of metals silicides and oxides at standard conditions were collected. The potential – pH diagrams of Me – Si – H_2O systems at 25ºC, air pressure of 1 bar and activities of ions in solution equal to 1 mol l^{-1} were plotted. The corrosion-electrochemical behaviour of studying systems was discussed.

Keywords: Transition metals, silicides, oxides, chemical and electrochemical stability, potential – pH diagram, corrosion-electrochemical behaviour.

Introduction

The silicides of transition 3d-metals are characterized by a very wide variety of physical and chemical properties and an exceptionally wide range of applications in technology. There are conductors with high electroconductivity, semiconductors, metalloids, superconductors among them. In addition to other things, these compounds have high corrosion resistance; their thermodynamic and electrochemical properties are quite different. The experimental investigations of electrochemical properties of 3d-metals silicides are widely performed [1]. Hovewer along with it, a theoretical studying of corrosion-electrochemical behaviour of these systems is also important because it allows complementing and extending experimental data. This paper aims to review the studies of electrochemical properties of Me – Si binary systems for some 4th row d-metals from the point of view of chemical thermodynamics.

All the methods, techniques and approaches used in solving this problem were detailed in [2]. The best carrier of thermodynamic information about possible chemical and electrochemical reactions proceeding in water environments is the diagram of electrochemical equilibrium

(electrode potential vs. pH relationship), which allows one to clearly depict the domains of thermodynamical stability of all possible phases and determine the type of system corrosion-electrochemical behaviour in certain environmental conditions.

The potential – pH diagrams for pure elements at 25˚C were introduced by M. Pourbaix [3] and are now well known. The task of plotting potential – pH diagrams for Me – Si – H_2O systems consists from three steps. At the first step one should study all phase and chemical equilibria in binary Me – Si system at 25˚C basing on its phase diagram, look for reference thermodynamic data, check they are matched to each other and calculate thermodynamic properties of system components. At the second step one should collect information about all possible oxides and silicates that can be formed during system oxidation, develop the consequence on oxidation processes in oxygen environments and plot the state diagram for Me – Si – O system [2]. At the last step one should consider the ions that can be formed during system oxidation in solutions, possible chemical and electrochemical reactions involving these ions, calculate their electrode potentials and plot the potential – pH diagram. For all systems under consideration this task will be solved exactly in this order.

It is to be noticed that there are no reliable thermodynamic data on the standard Gibbs energies of formation of some transition metals oxides and silicides. In this case some empirical relationships were used in order to estimate them.

Sc – Si system

According to Sc – Si system phase diagram [4], two scandium silicides – Sc_5Si_3 and ScSi – exist is system at standard conditions. The third silicide, Sc_2Si_3, exists only at elevated temperatures. All silicides are stoichiometric compounds without any noticeable homogeneity ranges. There are no data on solid solubility of Si in (hcp-Sc) and Sc in (diamond-Si); it is vanishingly small and the components can be treated as insoluble in each other. The standard Gibbs energies of formation of scandium silicides were taken from [5].

Scandium can form only one oxide, Sc_2O_3. Its standard Gibbs energy of formation was obtained from [6]. Some scandium silicides exist at elevated temperatures [7] but only thorvertite ($Sc_2Si_2O_7$) remains stable at 298 K. The standard Gibbs energy of formation of this compound was estimated according to ΔO^{2-} method, proposed by the authors of [8, 9]. It seems that chemical affinity of scandium to oxygen is greater, than that of silicon, and it oxidizes more easily. The oxidation of Sc – Si system in air environments ends with formation of Sc_2O_3 and $Sc_2Si_2O_7$ in scandium-rich region and of $Sc_2Si_2O_7$ and SiO_2 in silicon-rich region.

In water environments, scandium can form only Sc^{3+} cations [10], and silicon can simultaneously exist in form of SiO_2, H_2SiO_3 and H_4SiO_4. However, only orthosilicic acid was considered by means of convenience.

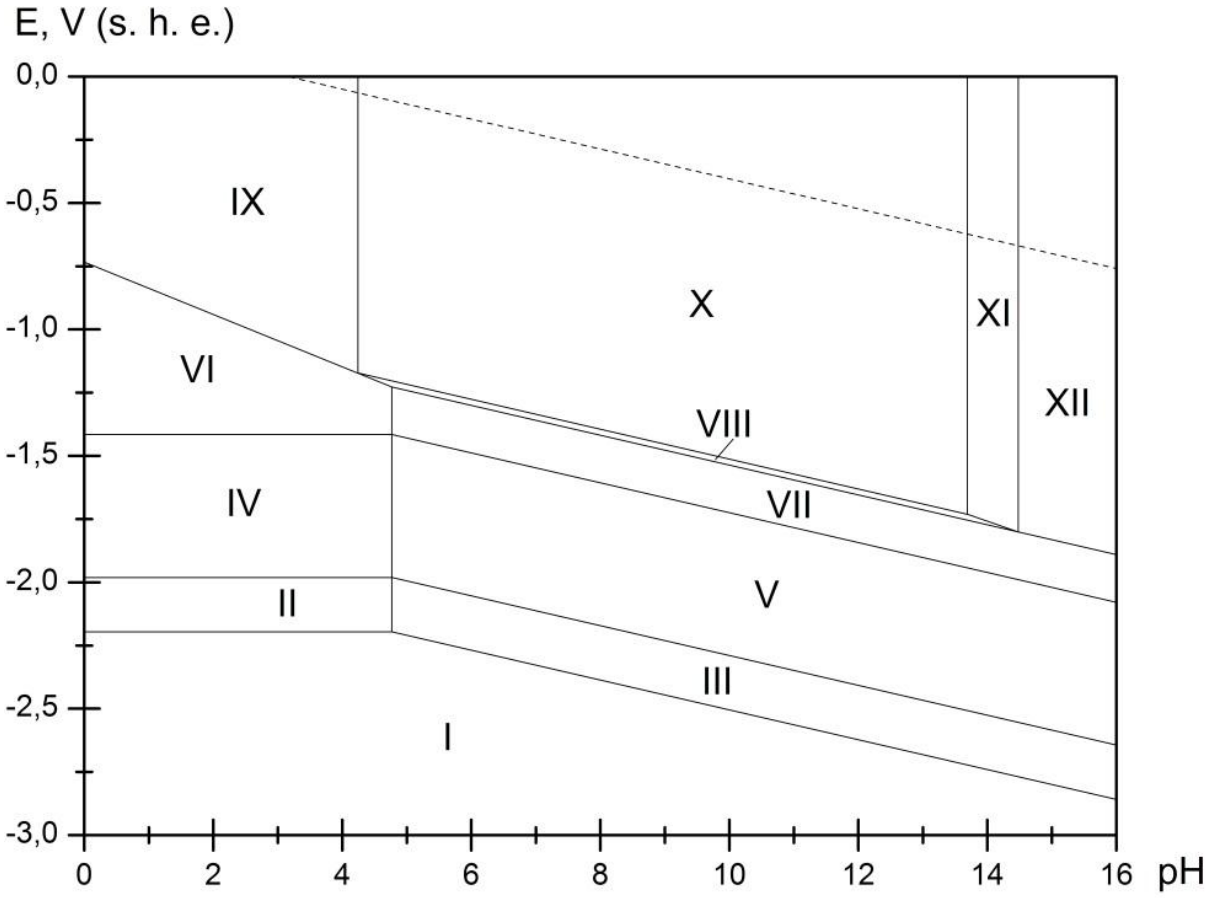

Figure 1. The potential – pH diagram of Sc – Si – H_2O system at 298 K, air pressure of 1 bar and a_i = 1 mol l^{-1}.

The potential – pH diagram of Sc – Si – H_2O system is plotted at temperature of 298 K, air pressure of 1 bar and activities of ions in solutions, equal to 1 mol l^{-1} and presented at **Figure 1**. 12 domains of prevalence of certain phases can be depicted in it: I – Sc (hcp) + Sc_5Si_3 + ScSi + Si (dia); II – Sc^{3+} + Sc_5Si_3 + ScSi + Si (dia); III – Sc_2O_3 + Sc_5Si_3 + ScSi + Si (dia); IV – Sc^{3+} + ScSi + Si (dia); V – Sc_2O_3 + ScSi + Si (dia); VI – Sc^{3+} + Si (dia); VII – Sc_2O_3 + Si (dia); VIII – $Sc_2Si_2O_7$ + Si (dia); IX – Sc^{3+} + $Sc_2Si_2O_7$ + Si (dia); X – $Sc_2Si_2O_7$ + H_4SiO_4; XI – $Sc_2Si_2O_7$ + $H_2SiO_4^{2-}$; XII – Sc_2O_3 + $Sc_2Si_2O_7$ + Si (dia).

Thermodynamic stability of Sc – Si system in air and water environments is determined by the composition of the system.

Ti – Si system

Titanium silicides are used as catodes in vacuum arc during the synthesis of superhard nanocrystal coatings [11]. They reveal high corrosion resistance in both reducing and oxidizing environments and can be characterized by stability of the passive state [12].

The following silicides exist in Ti – Si system at 25˚C [4]: Ti_3Si, Ti_5Si_3, Ti_5Si_4, TiSi and $TiSi_2$. It was reported [13] about the compounds Ti_3Si_4 and Ti_6Si_5, however, there are no confirmations of their existence in other literature. The silicide Ti_5Si_3 have wide homogeneity range at elevated temperature, but it can be considered as stoichiometric compound at 25˚C; other silicides do not have any homogeneity ranges. The maximum solid solubility of Si in (hcp-Ti) equals ~3.3 atomic percents at 1000˚C and only ~0.7 at. % at 800˚C [4], therefore it is vanishingly small at standard temperature and thus can be neglected. The solubility of Ti in (diamond-Si) is about 10^{-17} at. % at 1100˚C [14]. The values of standard Gibbs energies of formation of titanium silicides were taken from [15].

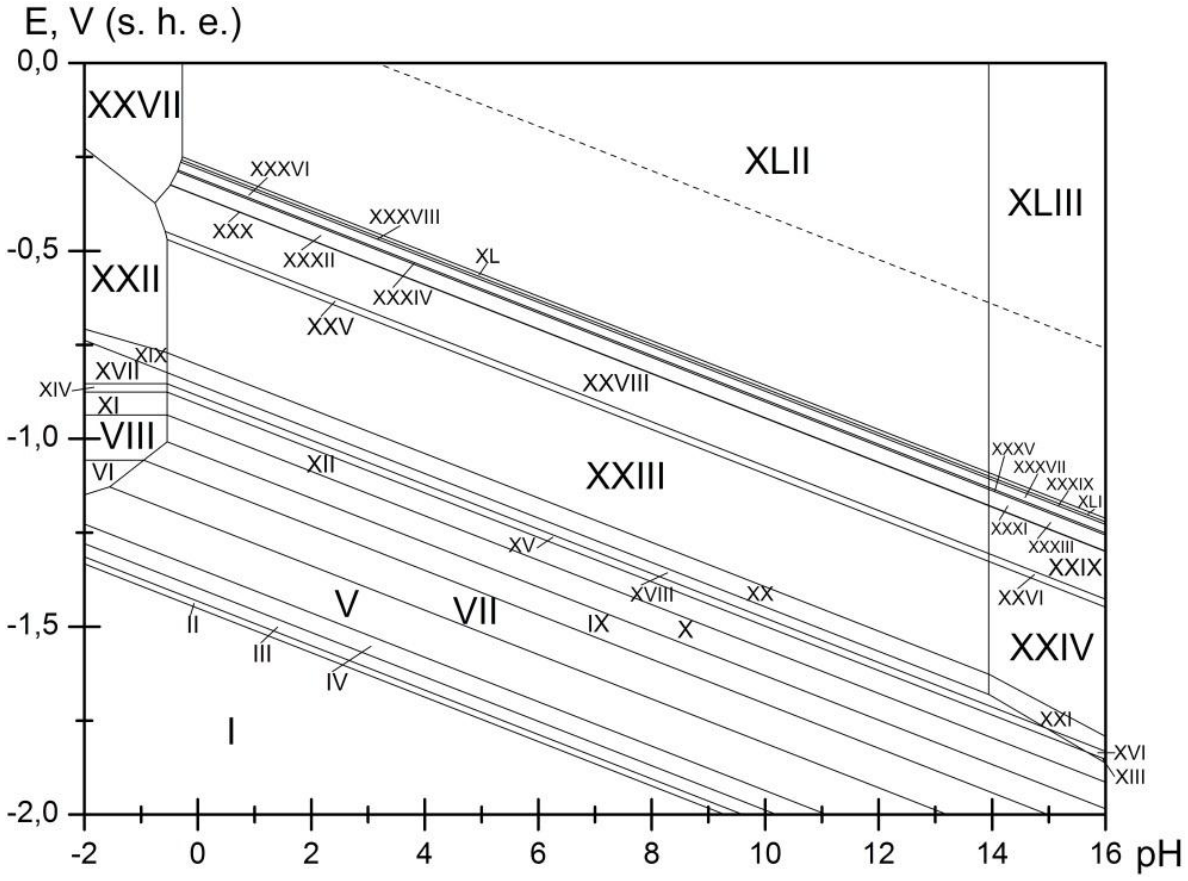

Figure 2a. The potential – pH diagram of Ti – Si – H_2O system at 298 K, air pressure of 1 bar and a_i = 1 mol l^{-1} without consideration of titanium hydride and nitride.

The phase diagram of Ti – O system [4] reveals a big number of titanium oxides and suboxides at 298 K – Ti_6O, Ti_3O, Ti_2O, Ti_3O_2, TiO, Ti_2O_3, Ti_3O_5, Magnelli phases Ti_nO_{2n-1} (

$4 \le n \le 10$), TiO_2. There are no compounds in binary TiO_2 – SiO_2 system [16]. The standard Gibbs energies of formation of titanium oxides were taken from [17]. Titanium can form anions Ti^{3+} and TiO^{2+} in water solution. No titanate-anions can be formed [18].

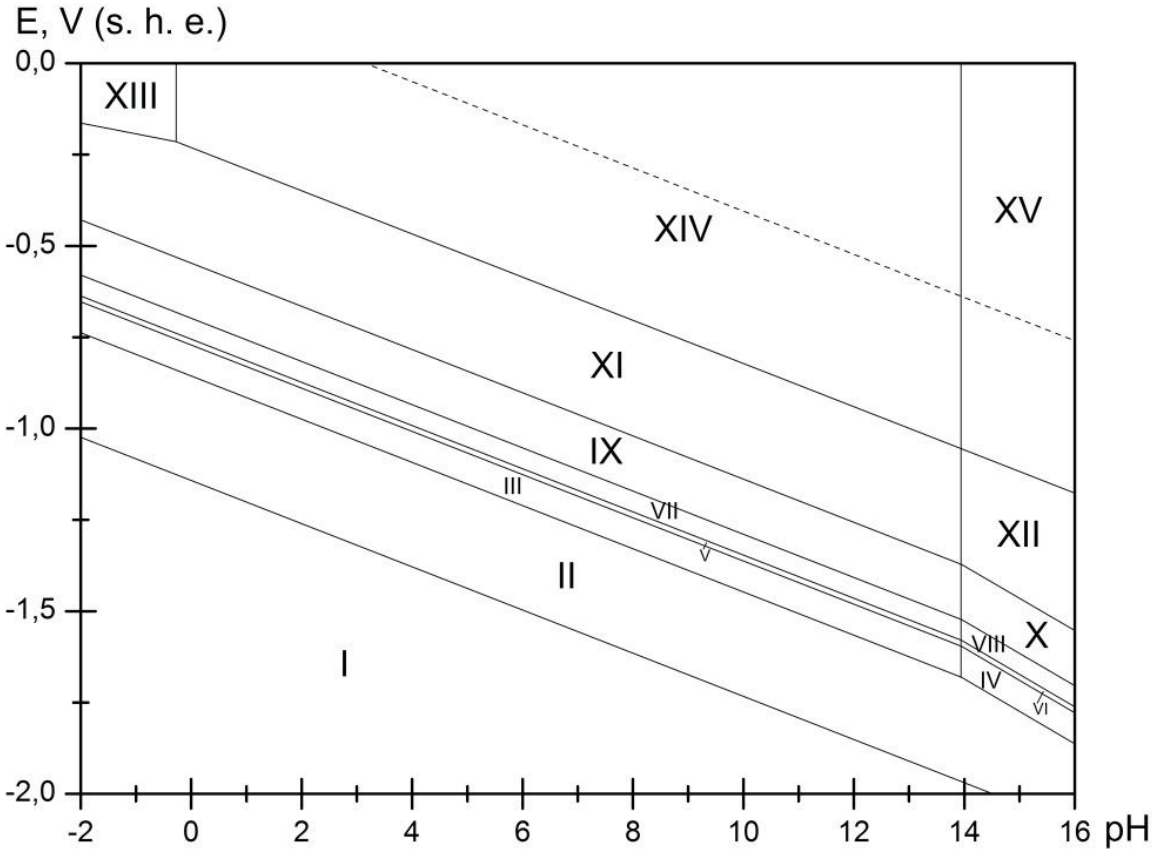

Figure 2b. The potential – pH diagram of Ti – Si – H_2O system at 298 K, air pressure of 1 bar and a_i = 1 mol l^{-1} with consideration of titanium hydride and nitride.

The potential – pH diagram of Ti – Si – H_2O system plotted in accordance with Ti – Si – O state diagram [19] is presented at **Figure 2a**. It determines 42 domains of thermodynamic stability of certain phases: I – Ti (hcp) + Ti_3Si + Ti_5Si_3 + Ti_5Si_4 + TiSi + $TiSi_2$ + Si (dia); II – Ti_6O + Ti_3Si + Ti_5Si_3 + Ti_5Si_4 + TiSi + $TiSi_2$ + Si (dia); III – Ti_3O + Ti_3Si + Ti_5Si_3 + Ti_5Si_4 + TiSi + $TiSi_2$ + Si (dia); IV – Ti_2O + Ti_3Si + Ti_5Si_3 + Ti_5Si_4 + TiSi + $TiSi_2$ + Si (dia); V – Ti_3O_2 + Ti_3Si + Ti_5Si_3 + Ti_5Si_4 + TiSi + $TiSi_2$ + Si (dia);VI – Ti^{3+} + Ti_3Si + Ti_5Si_3 + Ti_5Si_4 + TiSi + $TiSi_2$ + Si (dia); VII – TiO + Ti_3Si + Ti_5Si_3 + Ti_5Si_4 + TiSi + $TiSi_2$ + Si (dia); VIII – Ti^{3+} + Ti_5Si_3 + Ti_5Si_4 + TiSi + $TiSi_2$ + Si (dia); IX – TiO + Ti_5Si_3 + Ti_5Si_4 + TiSi + $TiSi_2$ + Si (dia); X – Ti_2O_3 + Ti_5Si_3 + Ti_5Si_4 + TiSi + $TiSi_2$ + Si (dia); XI – Ti^{3+} + Ti_5Si_4 + TiSi + $TiSi_2$ + Si (dia); XII – Ti_2O_3 + Ti_5Si_4 + TiSi + $TiSi_2$ + Si (dia); XIII – Ti_2O_3 + Ti_5Si_4 + TiSi + $TiSi_2$ + $H_2SiO_4^{2-}$; XIV – Ti^{3+} + TiSi + $TiSi_2$ + Si (dia); XV – Ti_2O_3 + TiSi + $TiSi_2$ + Si (dia); XVI – Ti_2O_3 + TiSi + $TiSi_2$ + $H_2SiO_4^{2-}$; XVII – Ti^{3+} + $TiSi_2$ + Si (dia); XVIII – Ti_2O_3 + $TiSi_2$ + Si (dia); XIX – Ti^{3+} + $TiSi_2$ +

H_4SiO_4; XX – Ti_2O_3 + $TiSi_2$ + H_4SiO_4; XXI – Ti_2O_3 + $TiSi_2$ + $H_2SiO_4^{2-}$; XXII – Ti^{3+} + H_4SiO_4; XXIII – Ti_2O_3 + H_4SiO_4; XXIV – Ti_2O_3 + $H_2SiO_4^{2-}$; XXV – Ti_3O_5 + H_4SiO_4; XXVI – Ti_3O_5 + $H_2SiO_4^{2-}$; XXVII – TiO^{2+} + H_4SiO_4; XXVIII – Ti_4O_7 + H_4SiO_4; XXIX – Ti_4O_7 + $H_2SiO_4^{2-}$; XXX – Ti_5O_9 + H_4SiO_4; XXXI – Ti_5O_9 + $H_2SiO_4^{2-}$; XXXII – Ti_6O_{11} + H_4SiO_4; XXXIII – Ti_6O_{11} + $H_2SiO_4^{2-}$; XXXIV – Ti_7O_{13} + H_4SiO_4; XXXV – Ti_7O_{13} + $H_2SiO_4^{2-}$; XXXVI – Ti_8O_{15} + H_4SiO_4; XXXVII – Ti_8O_{15} + $H_2SiO_4^{2-}$; XXXVIII – Ti_9O_{17} + H_4SiO_4; XXXIX – Ti_9O_{17} + $H_2SiO_4^{2-}$; XL – $Ti_{10}O_{19}$ + H_4SiO_4; XLI – $Ti_{10}O_{19}$ + $H_2SiO_4^{2-}$; XLII – TiO_2 + H_4SiO_4; XLIII – TiO_2 + $H_2SiO_4^{2-}$.

Hovewer, titanium has high chemical affinity not only to oxygen but also to hydrogen and nitrogen, therefore electrochemical formation of titanium hydride TiH_2 and nitride TiN have to be considered. The diagram taking into account these compounds is presented at **Figure 2b**, there are 15 domains of stability of certain phases: I – TiH_2 + Ti_3Si + Ti_5Si_3 + Ti_5Si_4 + TiSi + $TiSi_2$ + Si (dia); II – TiN + Ti_3Si + Ti_5Si_3 + Ti_5Si_4 + TiSi + $TiSi_2$ + Si (dia); III – TiN + Ti_3Si + Ti_5Si_3 + Ti_5Si_4 + TiSi + $TiSi_2$ + H_4SiO_4; IV – TiN + Ti_3Si + Ti_5Si_3 + Ti_5Si_4 + TiSi + $TiSi_2$ + $H_2SiO_4^{2-}$; V – TiN + Ti_3Si + Ti_5Si_3 + Ti_5Si_4 + TiSi + H_4SiO_4; VI – TiN + Ti_3Si + Ti_5Si_3 + Ti_5Si_4 + TiSi + $H_2SiO_4^{2-}$; VII – TiN + Ti_3Si + Ti_5Si_3 + Ti_5Si_4 + H_4SiO_4; VIII – TiN + Ti_3Si + Ti_5Si_3 + Ti_5Si_4 + $H_2SiO_4^{2-}$; IX – TiN + Ti_3Si + Ti_5Si_3 + H_4SiO_4; X – TiN + Ti_3Si + Ti_5Si_3 + $H_2SiO_4^{2-}$; XI – TiN + Ti_3Si + H_4SiO_4; XII – TiN + Ti_3Si + $H_2SiO_4^{2-}$; XIII – TiO^{2+} + Ti_3Si + H_4SiO_4; XIV – TiO_2 + Ti_3Si + H_4SiO_4; XV – TiO_2 + Ti_3Si + $H_2SiO_4^{2-}$.

In presence of titanium hydride and nitride all its oxides except TiO_2 become thermodynamically unstable. There is no domain of stability of metallic titanium. Moreover, presence of hydride and nitride changes the mechanism and order of titanium silicides oxidation. As can be seen from **Figure 2b**, full decomposition of titanium silicides to components is thermodynamically unprofitable process. The presence of silicon in system can stabilize titanium and and prevent it from formation of hydride and further oxidation. This can be explained by high strength of Ti – Si covalent bonds [12].

Mo – Si system

Molybdenum does not belong to 3d-metals. However, it is the only one metal amongst all 4d-metals that has big importance in metallurgy. Molybdenum silicides are used for making high-temperature thermocouples for measuring temperatures in air up to 1700˚C, electric resistance heaters, working without protective atmosphere, for creating materials to be used in oxidizing environments. Therefore, this system was included into consideration.

The phase diagram of Mo – Si system [4, 20] assumes the existence of molybdenum silicides Mo_3Si, Mo_5Si_3 and $MoSi_2$. All these compounds do not have any ranges of nonstoichiometry. The maximum solid solubility of Si in (fcc-Mo) equals ~2.5 atomic percents at 1500˚C and do not exceeds 1 at. % at 1300˚C [4], therefore it is vanishingly small at standard temperature and thus can be neglected. The values of standard Gibbs energies of formation of molybdenum silicides were taken from [15, 20].

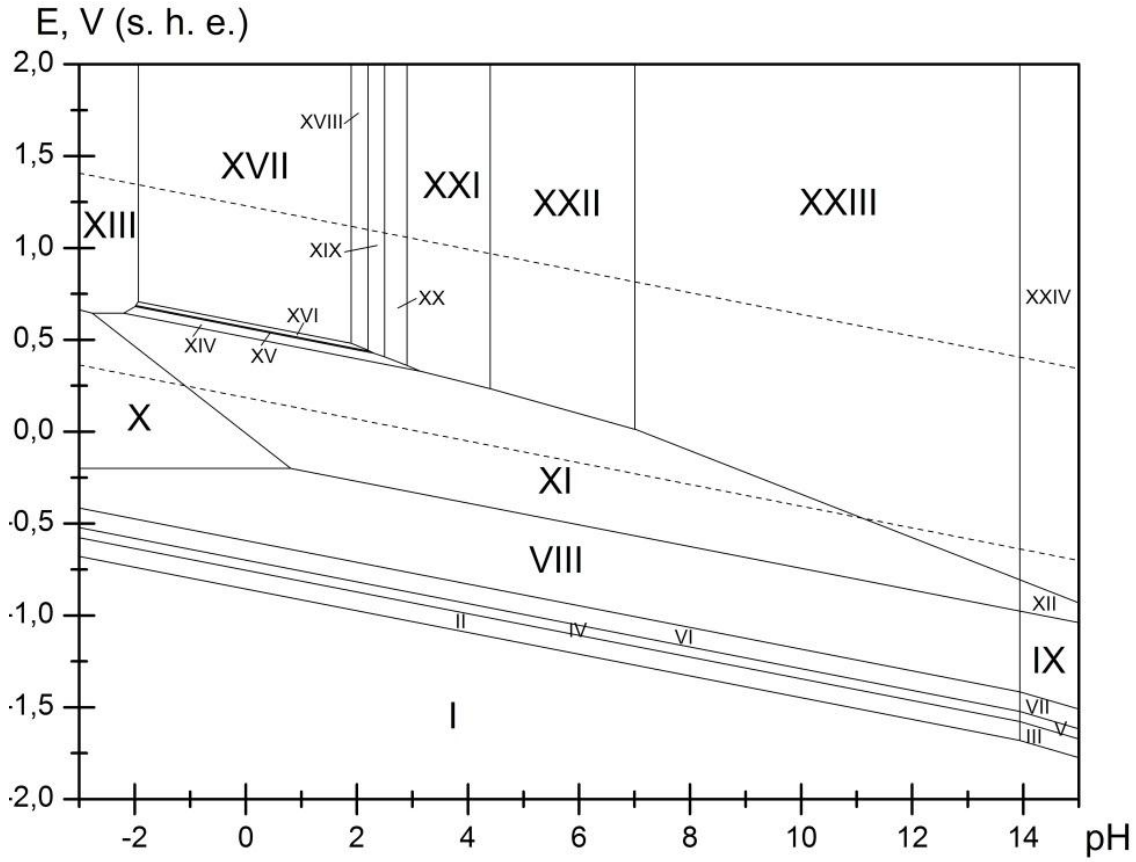

Figure 3. The potential – pH diagram of Mo – Si – H_2O system at 298 K, air pressure of 1 bar and a_i = 1 mol l^{-1}.

Molybdenum forms stable oxides MoO_2, Mo_4O_{11}, Mo_8O_{23}, Mo_9O_{26}, MoO_3 and a variety of metastable phases ($Mo_{17}O_{47}$, Mo_5O_{14}, $Mo_{18}O_{52}$) [4]. Metastable compounds were not taken into account in thermodynamic calculations. There is no data about the existence of molybdenum silicates. In water solution molybdenium forms the cations Mo^{3+} and MoO_2^{2+} and can be oxidized to various isopolymolybdate-anions with oxidation degree +6 [18, 21 – 23]. According to [24], the following anions are most stable in solution: $H_2Mo_8O_{26}^{2-}$, $HMo_8O_{26}^{3-}$, $Mo_8O_{26}^{4-}$, $H_2Mo_7O_{24}^{4-}$, $Mo_7O_{24}^{6-}$ and MoO_4^{2-}. The values of standard Gibbs energies of formation for

molybdenum oxides are taken from [25] and the values for molybdate anions are calculated according to data from Pourbaix diagram for molybdenum [26, 27].

The potential – pH diagram of Mo – Si – H_2O system [28] is presented at **Figure 3**; 24 domains of predominance of certain phases can be depicted in it: I – Mo (bcc) + Mo_3Si + Mo_5Si_3 + $MoSi_2$ + Si (dia) ; II – Mo (bcc) + Mo_3Si + Mo_5Si_3 + $MoSi_2$ + H_4SiO_4 ; III – Mo (bcc) + Mo_3Si + Mo_5Si_3 + $MoSi_2$ + $H_2SiO_4^{2-}$; IV – Mo (bcc) + Mo_3Si + Mo_5Si_3 + H_4SiO_4 ; V – Mo (bcc) + Mo_3Si + Mo_5Si_3 + $H_2SiO_4^{2-}$; VI – Mo (bcc) + Mo_3Si + H_4SiO_4 ; VII – Mo (bcc) + Mo_3Si + $H_2SiO_4^{2-}$; VIII – Mo (bcc) + H_4SiO_4 ; IX – Mo (bcc) + $H_2SiO_4^{2-}$; X – Mo^{3+} + H_4SiO_4 ; XI – MoO_2 + H_4SiO_4 ; XII – MoO_2 + $H_2SiO_4^{2-}$; XIII – MoO_2^{2+} + H_4SiO_4 ; XIV – Mo_4O_{11} + H_4SiO_4 ; XV – Mo_8O_{23} + H_4SiO_4 ; XVI – Mo_9O_{26} + H_4SiO_4 ; XVII – MoO_3 + H_4SiO_4 ; XVIII – $H_2Mo_8O_{26}^{2-}$ + H_4SiO_4 ; XIX – $HMo_8O_{26}^{3-}$ + H_4SiO_4 ; XX – $Mo_8O_{26}^{4-}$ + H_4SiO_4 ; XXI – $H_2Mo_7O_{24}^{4-}$ + H_4SiO_4 ; XXII – $Mo_7O_{24}^{6-}$ + H_4SiO_4 ; XXIII – MoO_4^{2-} + H_4SiO_4 ; XXIV – MoO_4^{2-}, $H_2SiO_4^{2-}$.

As can be seen from **Figure 3**, molybdenum has very narrow domain of active dissolution, because the cations Mo^{3+} and MoO_2^{2+} exist only in strongly acidic environments. However, the domain of the oxide passivation of molybdenum is also quiet small, and if the environment becomes more and more alkaline, then the domain of transpassivity (which contains all possible isopolymolybdate forms) becomes more and more broad. Generally, electrochemical stability of molybdenum-silicon alloys is completely determined by silicon content in them. If it is enough to form a continuous passivation film from H_4SiO_4 on alloy surface, then the active oxidation of molybdenium stops.

Mn – Si system

Manganese doped by silicon is used in manufacturing of rail and sttuctural steels, in metallurgy as the deoxidizer, as the dopant to alloys based on aluminum, magnesium and copper. There are seven intermetallic phases in Mn – Si system [4]: $Mn_{11}Si_{19}$, MnSi, Mn_5Si_3, Mn_5Si_2, Mn_3Si, ν-phase (Mn_9Si_2) and R-phase (Mn_6Si). The first five silicides are stoichiometric phases. ν-phase has a narrow homogeneity range at elevated temperatures but can be considered as stoichiometric compound at standard conditions. R-phase has a noticeable homogeneity range at 25˚C. Moreover, a solid solution of Si in (cubic-Mn) can be formed (α-phase). According to [29], R-phase in equilibrium with α-phase has the composition of $Mn_{0.85}Si_{0.15}$.

The equation for the excess Gibbs energy of α-phase was taken from [30]. Calculated solid solubility of Si in (cubic-Mn) at 25˚C equals 4.56 at. % [30]. Thermodynamic activities of solid solution compontnts are the following: $a_{\mathrm{Mn}(\alpha)} = 0.83$, $a_{\mathrm{Si}(\alpha)} = 3.8 \cdot 10^{-28}$. The solid solubility

of Mn in (diamond-Si) is about 10^{-14} at. % at 1100˚C [14]. The standard Gibbs energies of formation of manganese silicides were collected from various sources [17, 29, 31 – 33].

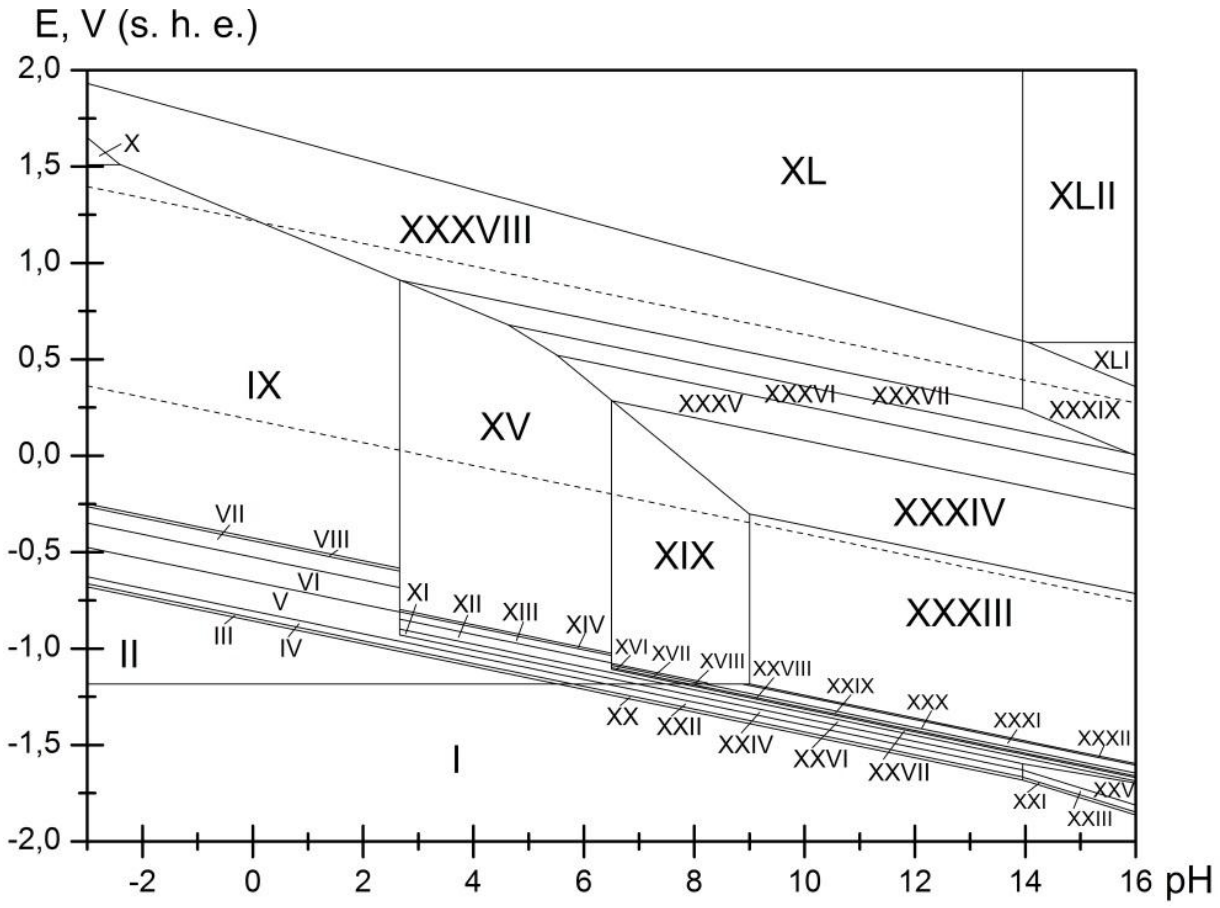

Figure 4. The potential – pH diagram of Mn – Si – H_2O system at 298 K, air pressure of 1 bar and a_i = 1 mol l^{-1}.

Manganese forms the oxides MnO, Mn_3O_4, Mn_2O_3, MnO_2 and Mn_2O_7 though the last one is not stable in water solutions. There are two manganese silicates at 25˚C – $MnSiO_3$ and Mn_2SiO_4 [34]. The compound Mn_7SiO_{12} exist only at elevated temperatures [35]. The ions Mn^{2+}, Mn^{3+}, MnO_4^{2-} and MnO_4^- exist in water solutions. The standard Gibbs energies of formation of manganese oxides, silicates and ions were taken from [17].

The potential – pH diagram of Mn – Si – H_2O system [30] is presented at **Figure 4**. 42 domains of thermodynamic stability of certain phases can be depicted in the diagram: I – α-phase (Mn) + R-phase ($Mn_{0.85}Si_{0.15}$) + ν-phase (Mn_9Si_2) + Mn_3Si + Mn_5Si_2 + Mn_5Si_3 + MnSi + $Mn_{11}Si_{19}$ + Si (dia); II – Mn^{2+} + $Mn_{0.85}Si_{0.15}$ + Mn_9Si_2 + Mn_3Si + Mn_5Si_2 + Mn_5Si_3 + MnSi + $Mn_{11}Si_{19}$ + Si (dia); III – Mn^{2+} + $Mn_{0.85}Si_{0.15}$ + Mn_9Si_2 + Mn_3Si + Mn_5Si_2 + Mn_5Si_3 + MnSi + $Mn_{11}Si_{19}$ + H_4SiO_4; IV – Mn^{2+} + $Mn_{0.85}Si_{0.15}$ + Mn_9Si_2 + Mn_3Si + Mn_5Si_2 + Mn_5Si_3 + MnSi + H_4SiO_4; V – Mn^{2+} + $Mn_{0.85}Si_{0.15}$ + Mn_9Si_2 + Mn_3Si + Mn_5Si_2 + Mn_5Si_3 + H_4SiO_4; VI – Mn^{2+} +

$Mn_{0.85}Si_{0.15}$ + Mn_9Si_2 + Mn_3Si + Mn_5Si_2 + H_4SiO_4; VII – Mn^{2+} + $Mn_{0.85}Si_{0.15}$ + Mn_9Si_2 + Mn_3Si + H_4SiO_4; VIII – Mn^{2+} + $Mn_{0.85}Si_{0.15}$ + Mn_9Si_2 + H_4SiO_4; IX – Mn^{2+} + $Mn_{0.85}Si_{0.15}$ + H_4SiO_4; X – Mn^{3+} + $Mn_{0.85}Si_{0.15}$ + H_4SiO_4; XI – Mn^{2+} + $Mn_{0.85}Si_{0.15}$ + Mn_9Si_2 + Mn_3Si + Mn_5Si_2 + Mn_5Si_3 + $MnSiO_3$; XII – Mn^{2+} + $Mn_{0.85}Si_{0.15}$ + Mn_9Si_2 + Mn_3Si + Mn_5Si_2 + $MnSiO_3$; XIII – Mn^{2+} + $Mn_{0.85}Si_{0.15}$ + Mn_9Si_2 + Mn_3Si + $MnSiO_3$; XIV – Mn^{2+} + $Mn_{0.85}Si_{0.15}$ + Mn_9Si_2 + $MnSiO_3$; XV – Mn^{2+} + $Mn_{0.85}Si_{0.15}$ + $MnSiO_3$; XVI – Mn^{2+} + $Mn_{0.85}Si_{0.15}$ + Mn_9Si_2 + Mn_3Si + Mn_5Si_2 + Mn_2SiO_4; XVII – Mn^{2+} + $Mn_{0.85}Si_{0.15}$ + Mn_9Si_2 + Mn_3Si + Mn_2SiO_4; XVIII – Mn^{2+} + $Mn_{0.85}Si_{0.15}$ + Mn_9Si_2 + Mn_2SiO_4; XIX – Mn^{2+} + $Mn_{0.85}Si_{0.15}$ + Mn_2SiO_4; XX – α + $Mn_{0.85}Si_{0.15}$ + Mn_9Si_2 + Mn_3Si + Mn_5Si_2 + Mn_5Si_3 + $MnSi$ + $Mn_{11}Si_{19}$ + H_4SiO_4; XXI – α + $Mn_{0.85}Si_{0.15}$ + Mn_9Si_2 + Mn_3Si + Mn_5Si_2 + Mn_5Si_3 + $MnSi$ + $Mn_{11}Si_{19}$ + $H_2SiO_4^{2-}$; XXII – α + $Mn_{0.85}Si_{0.15}$ + Mn_9Si_2 + Mn_3Si + Mn_5Si_2 + Mn_5Si_3 + $MnSi$ + H_4SiO_4; XXIII – α + $Mn_{0.85}Si_{0.15}$ + Mn_9Si_2 + Mn_3Si + Mn_5Si_2 + Mn_5Si_3 + $MnSi$ + $H_2SiO_4^{2-}$; XXIV – α + $Mn_{0.85}Si_{0.15}$ + Mn_9Si_2 + Mn_3Si + Mn_5Si_2 + Mn_5Si_3 + H_4SiO_4; XXV – α + $Mn_{0.85}Si_{0.15}$ + Mn_9Si_2 + Mn_3Si + Mn_5Si_2 + Mn_5Si_3 + $H_2SiO_4^{2-}$; XXVI – α + $Mn_{0.85}Si_{0.15}$ + Mn_9Si_2 + Mn_3Si + Mn_5Si_2 + Mn_5Si_3 + $MnSiO_3$; XXVII – α + $Mn_{0.85}Si_{0.15}$ + Mn_9Si_2 + Mn_3Si + Mn_5Si_2 + $MnSiO_3$; XXVIII – α + $Mn_{0.85}Si_{0.15}$ + Mn_9Si_2 + Mn_3Si + Mn_5Si_2 + Mn_2SiO_4; XXIX – α + $Mn_{0.85}Si_{0.15}$ + Mn_9Si_2 + Mn_3Si + Mn_2SiO_4; XXX – α + $Mn_{0.85}Si_{0.15}$ + Mn_9Si_2 + Mn_3Si + Mn_2SiO_4 + MnO; XXXI – α + $Mn_{0.85}Si_{0.15}$ + Mn_9Si_2 + Mn_2SiO_4 + MnO; XXXII – α + $Mn_{0.85}Si_{0.15}$ + Mn_2SiO_4 + MnO; XXXIII – $Mn_{0.85}Si_{0.15}$ + Mn_2SiO_4 + MnO; XXXIV – $Mn_{0.85}Si_{0.15}$ + Mn_2SiO_4 + Mn_3O_4; XXXV – $Mn_{0.85}Si_{0.15}$ + $MnSiO_3$ + Mn_3O_4; XXXVI – $Mn_{0.85}Si_{0.15}$ + $MnSiO_3$ + Mn_2O_3; XXXVII – $Mn_{0.85}Si_{0.15}$ + $MnSiO_3$ + MnO_2; XXXVIII – $Mn_{0.85}Si_{0.15}$ + MnO_2 + H_4SiO_4; XXXIX – $Mn_{0.85}Si_{0.15}$ + MnO_2 + $H_2SiO_4^{2-}$; XL – $Mn_{0.85}Si_{0.15}$ + H_4SiO_4 + MnO_4^-; XLI – $Mn_{0.85}Si_{0.15}$ + MnO_4^{2-}, $H_2SiO_4^{2-}$; XLII – $Mn_{0.85}Si_{0.15}$ + MnO_4^-, $H_2SiO_4^{2-}$.

The corrosion-electrochemical behavior of manganese-silicon alloys is determined by the acidity of environment and the value of equilibrium potential. In acidic environments the selective corrosion of manganese takes place and it forms the cations Mn^{2+} and silicon from alloy is oxidized to silicic acid. In neutral and alkaline environments oxidation can end with formation of passivation film consisting of silicates Mn_2SiO_4 or $MnSiO_3$.

Fe – Si system

Iron–silicon is a very important binary system for metallurgy. Iron silicides are perspective materials, they are well-known for their unusual magnetic, optical and thermodynamic properties [36]. Iron-silicon alloys can be found in Earth's core [37], they are using in technology as thin films [38] and nanowires [39]. Moreover, many important ternary

and multicomponent systems, including Fe – Si binary system are of great interest to the researches.

According to the Fe – Si phase diagram [4], several intermetallic phases exist in system: Fe_3Si_7, $FeSi_2$, FeSi, Fe_5Si_3 and Fe_2Si. But only $FeSi_2$ and FeSi are thermodynamically stable at standard conditions. FeSi has a narrow homogeneity range [4, 40], from $FeSi_{0.961}$ to $FeSi_{1.033}$, which does not depend on temperature. The solid solubility of Si in (bcc-Fe) is equal to about 25 atomic percent at ambient temperatures and silicon can form three types of solutions. The first one is the disordered phase, in which only short range ordering exist (α-phase), two others have long range atomic ordering – α_2-phase and α_1-phase. Additionally, a miscibility gap exists between α_2 and α_1 phases. Moreover, a fully ordered α_1-phase is often treated as independent compound Fe_3Si [41]. The expression for the excess Gibbs energy of α-phase was taken from [42].

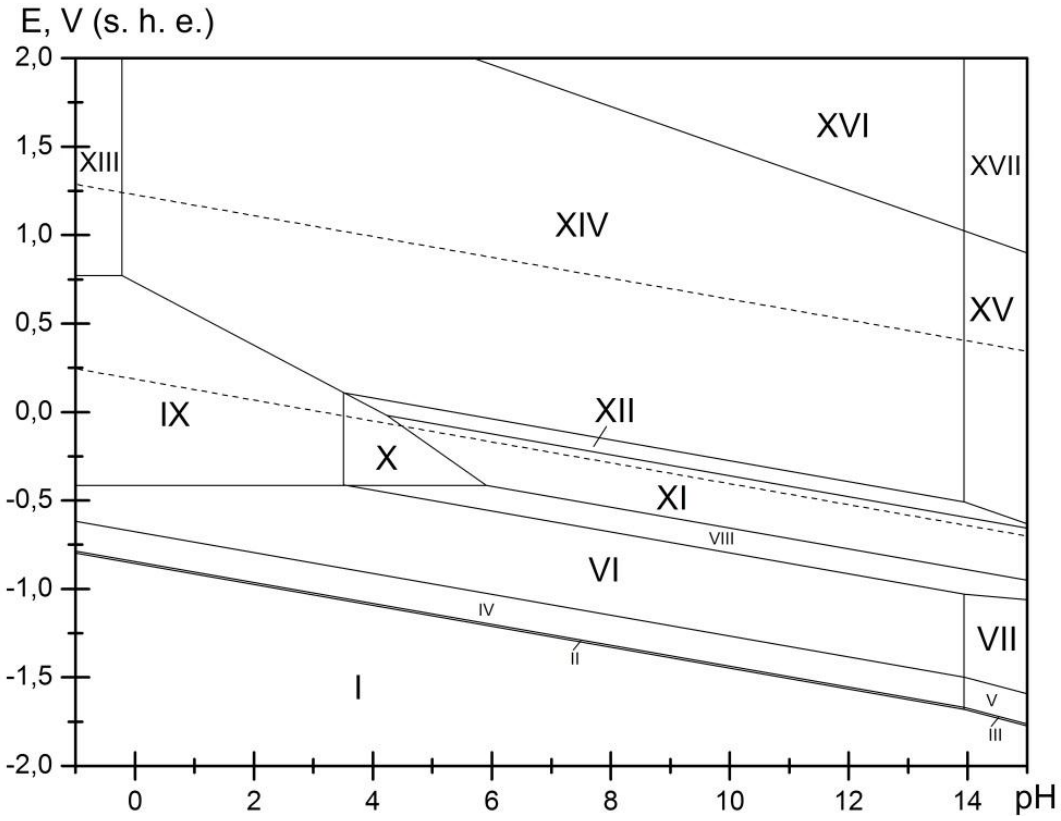

Figure 5. The potential – pH diagram of Fe – Si – H_2O system at 298 K, air pressure of 1 bar and a_i = 1 mol l^{-1}.

The activities of the components of solid solution corresponding to maximum silicon solubility in α_1-phase are the following: $a_{\mathrm{Fe}(\alpha_1)} = 0.473$ and $a_{\mathrm{Si}(\alpha_1)} = 5.5 \cdot 10^{-20}$ meaning strong negative deviations from ideal behaviour. The solid solubility of silicon in disordered α-phase at 25˚C is

about ~11 at. %. The activities of the components in this solution are equal to $a_{\mathrm{Fe}(\alpha)} = 0.13$, $a_{\mathrm{Si}(\alpha)} = 5.0 \cdot 10^{-20}$. The solubility of Fe in (diamond-Si) is about 10^{-17} at. % at 1100˚C [14]. The standard Gibbs energies of formation of iron silicides were collected from [17, 42 – 45].

Iron can form the following oxides: FeO, Fe_3O_4 and Fe_2O_3. However, FeO is not thermodynamically stable at temperatures below 570˚C [9]. Fe_3O_4 and Fe_2O_3 have noticeable homogeneity ranges at elevated temperatures but they are stoichiometric compounds at 25˚C. Only one ternary compound exist in Fe – Si – O system, it is Fe_2SiO_4 [46]. Another compound, $FeSiO_3$, exist only at elevated temperatures and pressures [47]. A solid solution of Fe_3O_4 in Fe_2SiO_4 can be formed [48] and its maximum solubility at 25˚C equals $6.85 \cdot 10^{-5}$ at. %. In addition, up to $1.54 \cdot 10^{-3}$ at. % of SiO_2 can be dissolved in Fe_2O_3 [48]. The values of standard Gibbs energies of formation of iron oxides were obtained from [17, 25, 49], the values for Fe_2SiO_4 – from [46, 50, 51].

The following ions of iron can be formed in water solution: Fe^{2+}, Fe^{3+}, FeO_4^{2-}. The potential – pH diagram of Fe – Si – H_2O is presented at **Figure 5**, and 17 domains of stability of certain phases can be depicted in it: I – α-phase (Fe) + $FeSi_x$ + $FeSi_2$ + Si (dia); II – α + $FeSi_x$ + $FeSi_2$ + H_4SiO_4; III – α + $FeSi_x$ + $FeSi_2$ + $H_2SiO_4^{2-}$; IV – α + $FeSi_x$ + H_4SiO_4; V – α + $FeSi_x$ + $H_2SiO_4^{2-}$; VI – α + H_4SiO_4; VII – α + $H_2SiO_4^{2-}$; VIII – α + Fe_2SiO_4; IX – Fe^{2+} + H_4SiO_4; X – Fe^{2+} + Fe_2SiO_4; XI – [Fe_2(Fe, Si)O_4] + Fe_2SiO_4; XII – Fe_2O_3 + Fe_2SiO_4; XIII – Fe^{3+} + H_4SiO_4; XIV – Fe_2O_3 + H_4SiO_4; XV – Fe_2O_3 + $H_2SiO_4^{2-}$; XVI – FeO_4^{2-} + H_4SiO_4; XVII – FeO_4^{2-}, $H_2SiO_4^{2-}$.

Co – Si system

Cobalt and silicon are the basic components of cobalt-based amorphous alloys [52], which are of interest to the researchers due to their unusual magnetic, mechanical, electric properties as well as high corrosion resistance.

The compounds Co_2Si, CoSi and $CoSi_2$ exist in Co – Si system at 25˚C [4, 53]. Moreover, a solid solution of Si in (hcp-Co) (ε-phase) exist in cobalt-rich region of Co – Si phase diagram. The expression for the excess Gibbs energy of this phase was provided in paper [42]. Calculated maximum solid solubility of silicon at 25˚C [54] equals 10.7 at. %, thermodynamic activities of this saturated solid solution are the following: $a_{\mathrm{Co}(\varepsilon)} = 0.27$, $a_{\mathrm{Si}(\varepsilon)} = 4 \cdot 10^{-16}$. The solubility of Co in (diamond-Si) is about 10^{-17} at. % at 1000˚C [14]. The values of standard Gibbs energies of formation of cobalt silicides were collected from [17, 25, 42, 53].

Cobalt can form a variety of oxides – CoO, Co_3O_4, Co_2O_3 and CoO_2; the first two ones have a noticeable homogeneity range, which covers the compositions from CoO to $CoO_{1.07}$ for "CoO" phase and from $CoO_{1.31}$ to $CoO_{1.41}$ for "Co_3O_4" phase [4, 55]. Only one ternary compound, Co_2SiO_4, exists in Co – Si – O system [56]. The values of Gibbs energies of formation of cobalt oxides and silicides were obtained from [17, 25, 55].

Cobalt can form a cations Co^{2+} and the anions $HCoO_2^-$ and CoO_4^{2-} in water solution. The potential – pH diagram of Co – Si – H_2O system [54] is presented at **Figure 6**.

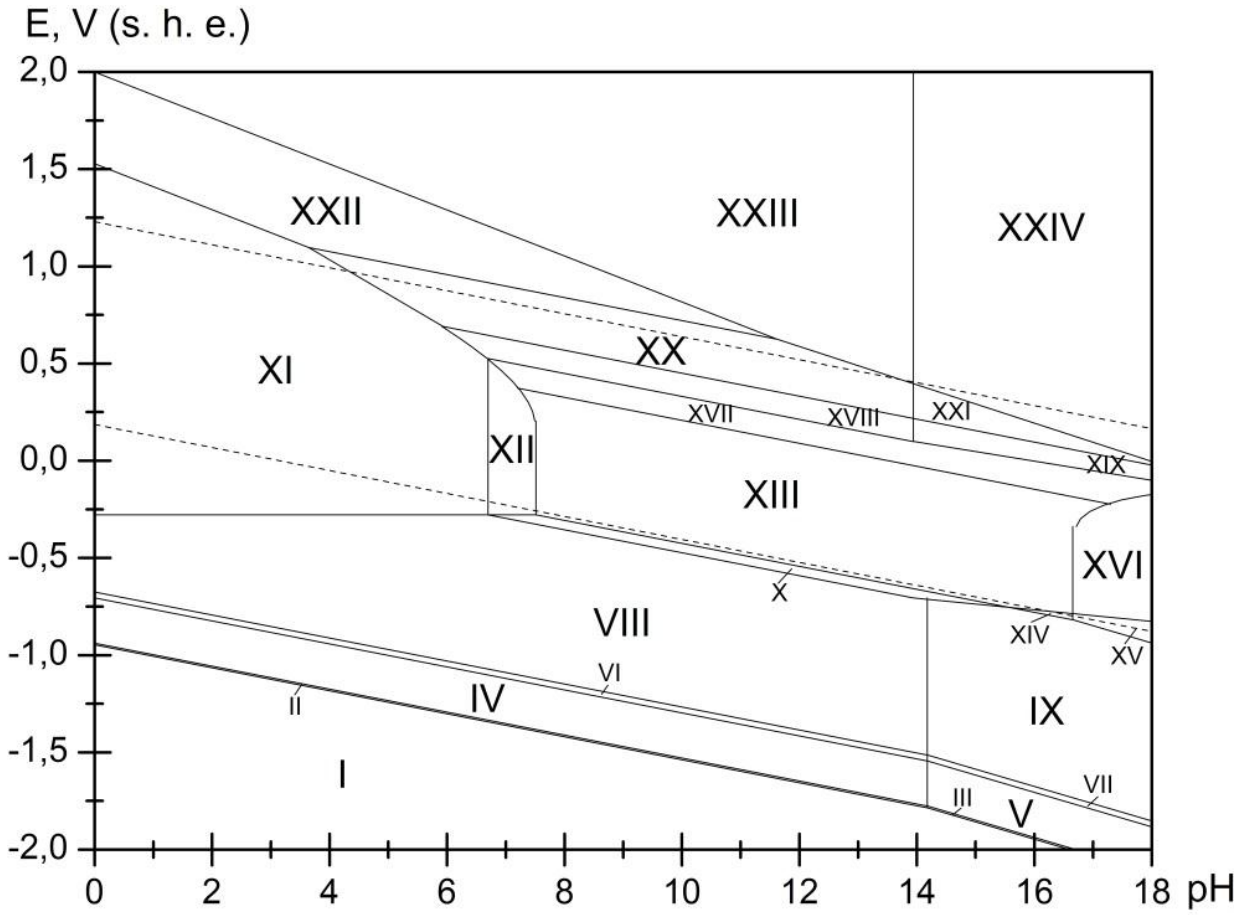

Figure 6. The potential – pH diagram of Co – Si – H_2O system at 298 K, air pressure of 1 bar and a_i = 1 mol l^{-1}.

24 domains of stability of certain phases can be depicted at the diagram: I – ε-phase (Co) + Co_2Si + CoSi + $CoSi_2$ + Si (dia); II – ε + Co_2Si + CoSi + $CoSi_2$ + H_4SiO_4; III – ε-фаза(Co) + Co_2Si + CoSi + $CoSi_2$ + $H_2SiO_4^{2-}$; IV – ε + Co_2Si + CoSi + H_4SiO_4; V – ε + Co_2Si + CoSi + $H_2SiO_4^{2-}$; VI – ε + Co_2Si + H_4SiO_4; VII – ε + Co_2Si + $H_2SiO_4^{2-}$; VIII – ε + H_4SiO_4; IX – ε + $H_2SiO_4^{2-}$; X – ε + Co_2SiO_4; XI – H_4SiO_4 + Co^{2+}; XII – Co_2SiO_4 + Co^{2+}; XIII – Co_2SiO_4 + "CoO"; XIV – "CoO" + $H_2SiO_4^{2-}$; XV – $HCoO_2^-$, $H_2SiO_4^{2-}$; XVI – Co_2SiO_4 + $HCoO_2^-$; XVII –

Co_2SiO_4 + "Co_3O_4"; XVIII – "Co_3O_4" + H_4SiO_4; XIX – "Co_3O_4" + $H_2SiO_4^{2-}$; XX – Co_2O_3 + H_4SiO_4; XXI – Co_2O_3 + $H_2SiO_4^{2-}$; XXII – CoO_2 + H_4SiO_4; XXIII – H_4SiO_4 + CoO_4^{2-}; XXIV – CoO_4^{2-}, $H_2SiO_4^{2-}$.

Ni – Si system

According to the Ni – Si phase diagram [4, 57], several phases exist in system at standard conditions. There are six intermediate phases: β_1-phase (Ni_3Si), γ-phase (Ni_5Si_2 or $Ni_{31}Si_{12}$ [58]), δ-phase (Ni_2Si), ε-phase (Ni_3Si_2), NiSi and $NiSi_2$. Although almost all nickel silicides have a narrow homogeneity ranges at 800˚C [57], they can be treated as stoichiometric phases at standard temperature. The solubility of Ni in (diamond-Si) do not exceeds 10^{-16} at. % at 800˚C [14]. At the nickel-rich part of the system, the solid solution of Si in (fcc-Ni) can be formed (α-phase). There is no published information about silicon maximum solid solubility at 25˚C, but it is relatively high (more that 10 atomic percent) at 1000 ˚C [4]. Most CALPHAD assessments of Ni – Si system [57, 59 – 61] consider β_1-phase as an ordered solid solution and use an order-disorder contribution model [62] for its Gibbs energy function. Moreover, they use sublattice model [63] for Gibbs energy function of α-phase. But, since β_1-phase can be assumed as stoichiometric and composition invariant at standard temperature, there is no necessity to pay attention on order-disorder transformations in it and use such complicated thermodynamic models. Therefore, simpler thermodynamics model was used to describe the excess Gibbs energy of α-phase [64]. Calculated solid solubility of Si in (fcc-Ni) at 25˚C equals 2.5 at. %. The activities of solid solution components are the following: $a_{\mathrm{Ni}(\alpha)} = 0.927$, $a_{\mathrm{Si}(\alpha)} = 9 \cdot 10^{-36}$.

It is well known, that nickel monoxide (NiO) and higher nickel oxides (Ni_2O_3, NiO_2) can form a continuous series of solid solutions, which corresponds to a variable composition phase NiO_x [65].

A single ternary compound exist in Ni – Si – O system, it is nickel orthosilicate Ni_2SiO_4 [46]. The values of standard Gibbs energies of formation of nickel silicides and nickel silicate were collected from various sources and analyzed by the authors of [64]. The expression for the standard Gibbs energy of formation of phase NiO_x was also proposed in [64].

Nickel can form the following ions in water solutions: Ni^{2+}, $HNiO_2^-$ and NiO_4^{2-} [2]. The potential – pH diagram of Ni – Si – H_2O system [64] is presented at **Figure 7a**. 24 domains of thermodynamic stability of certain phases can be depicted at the diagram: I – α-phase (Ni) + Ni_3Si + Ni_5Si_2 + Ni_2Si + Ni_3Si_2 + NiSi + $NiSi_2$ + Si (dia); II – α + Ni_3Si + Ni_5Si_2 + Ni_2Si + Ni_3Si_2 + NiSi + $NiSi_2$ + H_4SiO_4; III – α + Ni_3Si + Ni_5Si_2 + Ni_2Si + Ni_3Si_2 + NiSi + $NiSi_2$ + $H_2SiO_4^{2-}$; IV – α + Ni_3Si + Ni_5Si_2 + Ni_2Si + Ni_3Si_2 + NiSi + H_4SiO_4; V – α + Ni_3Si + Ni_5Si_2 +

$Ni_2Si + Ni_3Si_2 + NiSi + H_2SiO_4^{2-}$; VI – α + $Ni_3Si + Ni_5Si_2 + Ni_2Si + Ni_3Si_2 + H_4SiO_4$; VII – α + $Ni_3Si + Ni_5Si_2 + Ni_2Si + Ni_3Si_2 + H_2SiO_4^{2-}$; VIII – α + $Ni_3Si + Ni_5Si_2 + Ni_2Si + H_4SiO_4$; IX – α + $Ni_3Si + Ni_5Si_2 + Ni_2Si + H_2SiO_4^{2-}$; X – α + $Ni_3Si + Ni_5Si_2 + H_4SiO_4$; XI – α + $Ni_3Si + Ni_5Si_2 + H_2SiO_4^{2-}$; XII – α + $Ni_3Si + H_4SiO_4$; XIII – α + $Ni_3Si + H_2SiO_4^{2-}$; XIV – α + H_4SiO_4; XV – α + $H_2SiO_4^{2-}$; XVI – α + Ni_2SiO_4; XVII – $Ni^{2+} + H_4SiO_4$; XVIII – $Ni^{2+} + Ni_2SiO_4$; XIX – $NiO_x + Ni_2SiO_4$; XX – $HNiO_2^- + Ni_2SiO_4$; XXI – $NiO_x + H_4SiO_4$; XXII – $NiO_x + H_2SiO_4^{2-}$; XXIII – $NiO_4^{2-} + H_4SiO_4$; XXIV – NiO_4^{2-}, $H_2SiO_4^{2-}$.

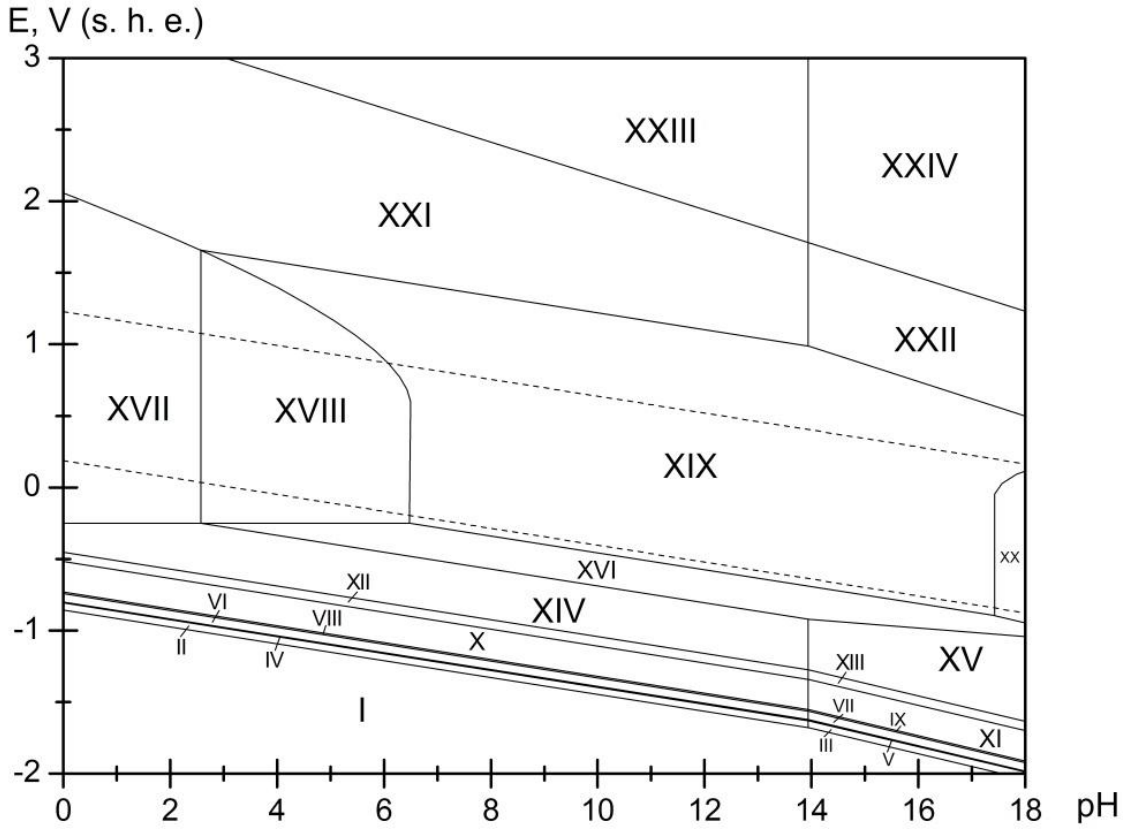

Figure 7a. The potential – pH diagram of Ni – Si – H_2O system at 298 K, air pressure of 1 bar and a_i = 1 mol l^{-1} without consideration of nickel hydride.

In addition nickel can form the hydride Ni_2H [66]. The possibilities of electrochemical reduction of nickel to its hydride are discussed in [67]. The information about the Gibbs energy of formation for nickel hydride Ni_2H was taken from paper [68]. The potential – pH diagram of Ni – Si – H_2O system with consideration of nickel hydride is presented at **Figure 7b**.

17 domains of thermodynamic stability of certain phases can be depicted at the diagram: I – $Ni_2H + Ni_3Si + Ni_5Si_2 + Ni_2Si + Ni_3Si_2 + NiSi + NiSi_2 + Si$ (dia); II – $Ni_2H + Ni_3Si + Ni_5Si_2 + Ni_2Si + Ni_3Si_2 + NiSi + NiSi_2$; III – $Ni_2H + Ni_3Si + Ni_5Si_2 + Ni_2Si + Ni_3Si_2 + NiSi$; IV – Ni_2H +

$Ni_3Si + Ni_5Si_2 + Ni_2Si + Ni_3Si_2$; V – $Ni_2H + Ni_3Si + Ni_5Si_2 + Ni_2Si$; VI – $Ni_2H + Ni_3Si + Ni_5Si_2$; VII – $Ni_2H + Ni_3Si$; VIII – $Ni_2H + Ni_2SiO_4$; IX – Ni (α) + Ni_2SiO_4; X – $Ni^{2+} + H_4SiO_4$; XI – $Ni^{2+} + Ni_2SiO_4$; XII – $NiO_x + Ni_2SiO_4$; XIII – $HNiO_2^- + Ni_2SiO_4$; XIV – $NiO_x + H_4SiO_4$; XV – $NiO_x + H_2SiO_4^{2-}$; XVI – $NiO_4^{2-} + H_4SiO_4$; XVII – $NiO_4^{2-} + H_2SiO_4^{2-}$.

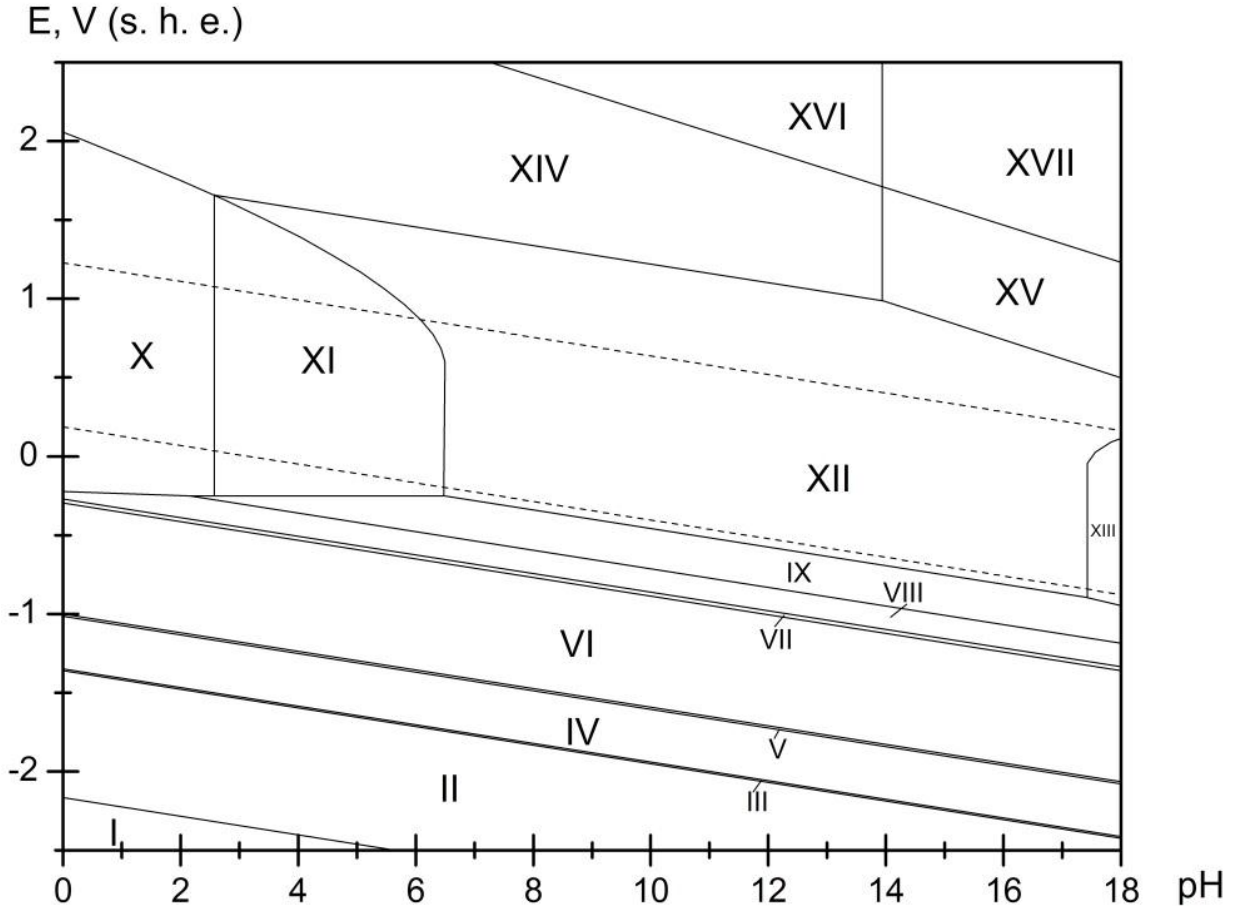

Figure 7b. The potential – pH diagram of Ni – Si – H_2O system at 298 K, air pressure of 1 bar and a_i = 1 mol l^{-1} with consideration of nickel hydride.

In presence of nickel hydride orthosilicic acid becomes thermodynamically unstable and the mechanism of nickel silicides decomposition slightly changes.

Generally, the corrosion-electrochemical behaviour of iron, cobalt and nickel silicides is very similar. In acidic environments the passivation layer on Fe – Si, Co – Si и Ni – Si system alloys will consist of pure H_4SiO_4, if there will be no F^- ions in solution, and metal from alloys will form the cations Fe^{2+}, Co^{2+} and Ni^{2+}, respectively. In neutral and alkaline environments three cases can be considered. If silicon content in alloys is high, it will be sufficient to form a persistent passivation layer of $SiO_2 \cdot 2H_2O$ on the surface. At lower silicon content in alloy it will be sufficient only to form a persistent layer of silicates Fe_2SiO_4, Co_2SiO_4 or Ni_2SiO_4. If

silicon content in alloy is very low, the protective film will consist from corresponding metal oxides, and silicon in form of local inclusions of silicates will be present in its inner layer.

Cu – Si system

Alloying of copper alloys with silicon allows increasing their durability, plasticity, improving their mechanical, foundry and anticorrosive properties. Siliceous bronzes and brasses are very cheap substitutes for tin bronzes. In addition, silicon can be included in other copper-based alloys with aluminium, nickel, manganese. Therefore, Cu – Si system is a very important binary system for the metallurgy and chemical technology.

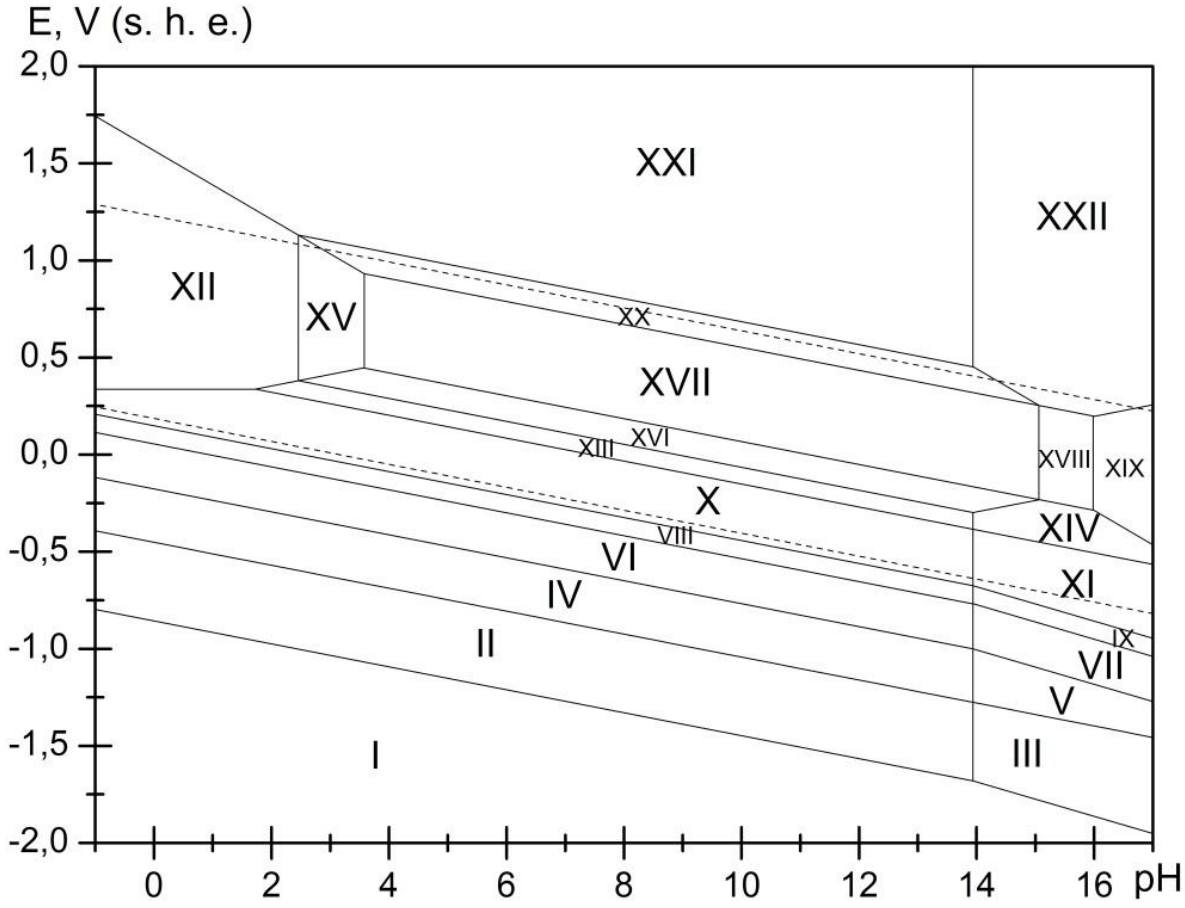

Figure 8. The potential – pH diagram of Cu – Si – H_2O system at 298 K, air pressure of 1 bar and a_i = 1 mol l^{-1}.

In Cu – Si system 25˚C the existence of the following copper silicides was aproved [4, 69]: $Cu_{56}Si_{11}$ (γ-phase), $Cu_{15}Si_4$ (ε-phase) and $Cu_{19}Si_6$ (η’’-phase). Despite all copper silicides have, in greater or lesser degree, the homogeneity range, it is negligibly small at the standard temperature, and the silicides can be assumed as daltonides. Additionally, a solid solution of Si in (fcc-Cu) (α-phase) exist in copper-rich copper of system. The expression for the excess Gibbs

energy of α-phase was taken from [69]. The calculated silicon maximum solid solubility in α-phase at standard temperature slightly exceeds 4 at. %. Thermodynamic activities of the components of saturated solid solution are the following: $a_{\mathrm{Cu}(\alpha)} = 0.92$, $a_{\mathrm{Si}(\alpha)} = 5.6 \cdot 10^{-8}$. The standard Gibbs energies of formation of copper silicides were estimated in [70].

In addition to well known oxides Cu_2O and CuO copper can also form a Cu_2O_3 compound [71]. Only one ternary compound exists in Cu – Si – O ternary system, it is $CuSiO_3$ [46]. The standard Gibbs energies of formation of copper oxides and silicate were collected from [17, 25, 71].

Copper in water solution can form the cations Cu^{2+} and the anions $HCuO_2^-$ and CuO_2^{2-}, however $HCuO_2^-$ is stable only at low concentrations of copper species in solution [70]. Despite copper hydride $CuH_{0.8}$ is not stable in air, it was shown [72 – 74], that it can be obtained during copper electrochemical reduction. The value of standard Gibbs energy of formation for copper hydride was determined by the authors of [75, 76].

The potential – pH diagram of Cu – Si – H_2O system [70] is presented at **Figure 8** and it determines 22 domains of prevalence of certain phases: I – $CuH_{0.8}$ + γ-phase ($Cu_{56}Si_{11}$) + ε-phase ($Cu_{15}Si_4$) + η''-phase ($Cu_{19}Si_6$) + Si (dia); II – $CuH_{0.8}$ + γ + ε + η'' + H_4SiO_4; III – $CuH_{0.8}$ + γ + ε + η'' + $H_2SiO_4^{2-}$; IV – α-phase (Cu) + γ + ε + η'' + H_4SiO_4; V – α + γ + ε + η'' + $H_2SiO_4^{2-}$; VI – α + γ + ε + H_4SiO_4; VII – α + γ + ε + $H_2SiO_4^{2-}$; VIII – α + γ + H_4SiO_4; IX – α + γ + $H_2SiO_4^{2-}$; X – α + H_4SiO_4; XI – α + $H_2SiO_4^{2-}$; XII – Cu^{2+} + H_4SiO_4; XIII – Cu_2O + H_4SiO_4; XIV – Cu_2O + $H_2SiO_4^{2-}$; XV – Cu^{2+} + $CuSiO_3$; XVI – Cu_2O + $CuSiO_3$; XVII – CuO + $CuSiO_3$; XVIII – CuO + $H_2SiO_4^{2-}$; XIX – CuO_2^{2-} + $H_2SiO_4^{2-}$; XX – Cu_2O_3 + $CuSiO_3$; XXI – Cu_2O_3 + H_4SiO_4; XXII – Cu_2O_3 + $H_2SiO_4^{2-}$.

Zn – Si system

There are no intermediate compounds in Zn – Si system. Moreover, hcp-Zn and diamond-Si are insoluble in each other and form only mechanical mixture at ambient temperature [4].
Zinc can form two oxides, ZnO and ZnO_2 [77]. One zinc silicate, $ZnSiO_3$ can be formed in Zn – Si – O system [78]. Another compound, willemite (Zn_2SiO_4) can be formed only at high temperatures or high pressures [46]. The standard Gibbs energies of formation of zinc oxides and silicate were collected from [17, 25, 79]. Zinc in water solution can form the cations Zn^{2+} and the anions $HZnO_2^-$ and ZnO_2^{2-}, however $HZnO_2^-$ is stable only at low concentrations of zinc species in solution [80].

The potential – pH diagram of Zn – Si – H_2O system is presented at Figure 9. There are 12 domains corresponding to stability of certain phases: I – Zn (hcp) + Si (dia); II – Zn (hcp) + H_4SiO_4; III – Zn (hcp) + $H_2SiO_4^{2-}$; IV – Zn (hcp) + $ZnSiO_3$; V – Zn^{2+} + H_4SiO_4; VI – Zn^{2+} + $ZnSiO_3$; VII – ZnO + $ZnSiO_3$; VIII – ZnO_2^{2-} + $ZnSiO_3$; XI – ZnO_2^{2-}, $H_2SiO_4^{2-}$; X – ZnO_2 + $ZnSiO_3$; XI – ZnO_2 + H_4SiO_4; XII – ZnO_2 + $H_2SiO_4^{2-}$.

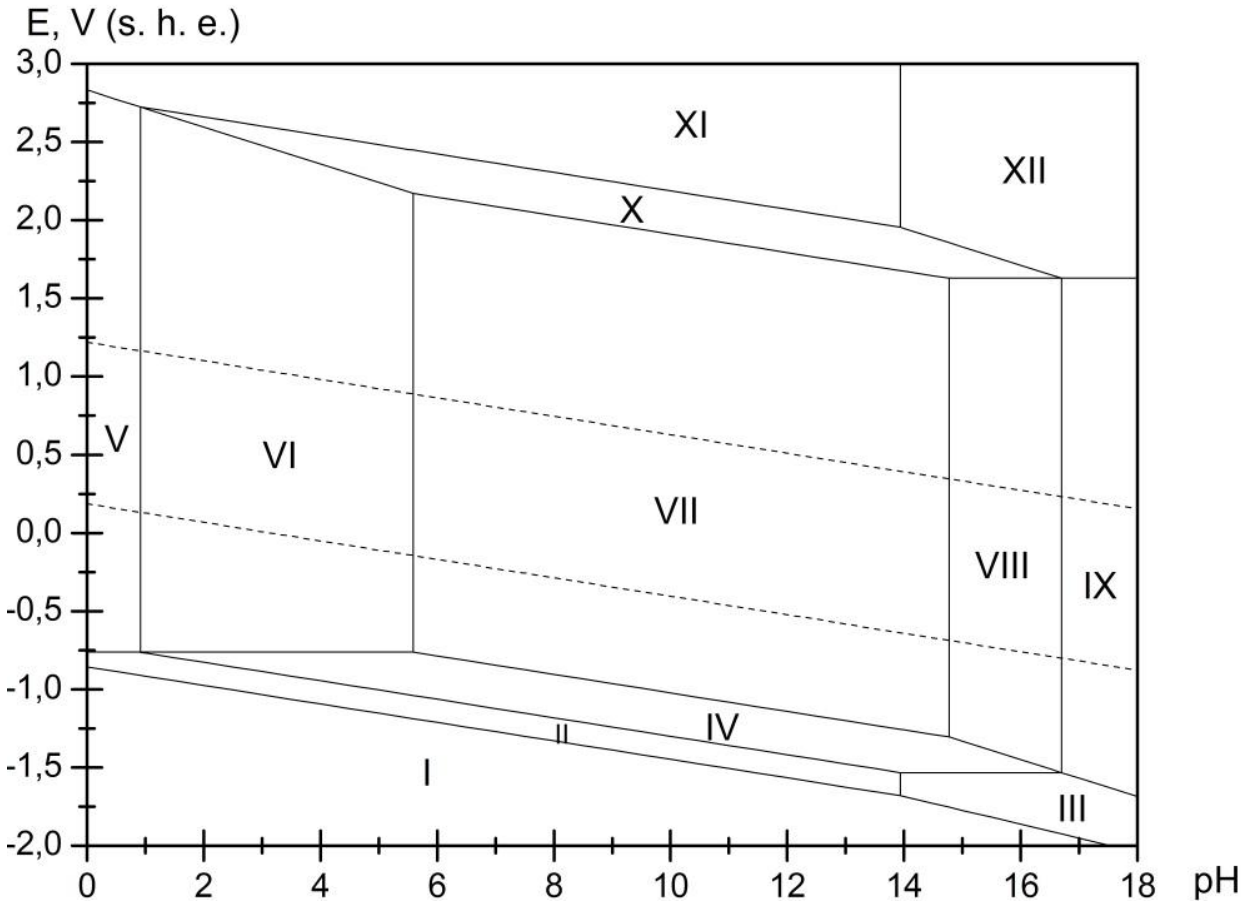

Figure 9. The potential – pH diagram of Zn – Si – H_2O system at 298 K, air pressure of 1 bar and a_i = 1 mol l^{-1}.

Conclusions

The dotted lines on the diagrams (Figures 1 through 9) mark the potentials of hydrogen and oxygen electrodes. The area between these lines depict the domain of electrochemical stability of water, which is of most interest to researchers. Thermodynamic calculations show that high corrosion resistance of transition metals silicides and metal-silicon alloys in this area is related with formation of the protective films consisting of metals silicates on their surface. This films are much stable in chemical and electrochemical term than films from simple metal oxides. Therefore, silicon reveals good influence on the corrosion resistance of 3d-metals.

The usage of thermodynamic modelling of corrosion properties is not limited to binary systems. It is the powerful instrument that can complement the results of experiments and broaden the knowledge about corrosion-electrochemical behaviour of multicomponent silicon-containing alloys like siliceous bronzes and brasses.

References

1. A. B. Shein. *Elektrokhimiya silitcidov i germanidov perekhodnykh metallov* [Electrochemistry of silicides and germanides of transition metals], Perm State University, *2009*.

2. A. G. Tyurin. *Termodimamika khimicheskoi i elektrokhimicheskoi ustoichivosti tverdykh splavov zheleza, khroma i nikelya* [Thermodynamics of chemical and electrochemical stability of solid alloys of iron, chromium and nickel], Chelyabinsk State University, *2011*.

3. M. Pourbaix. *Atlas of Electrochemical Equilibria in Aqueous Solutions*. Pergamon Press Ltd., Oxford, *1966*.

4. *Diagrammy sostoyaniya dvoinykh metallicheskikh sistem* [Phase diagrams of binary metallic systems]. In 3 volumes. Edited by Lyakishev N. P., Mashinostroyeniye, Moscow, *1996 – 2000*.

5. G. M. Lukashenko, R. I. Polotskaya, V. R. Sidorko. Thermodynamic properties of scandium, lanthanum, neodymium and gadolinium silicides and germanides. *Journal of Alloys and Compounds*, *1992*, 179(1 – 2), 299 – 305.

6. C. T. Horovitz. *Scandium. Its Occurrence, Chemistry, Physics, Metallurgy, Biology and Technology*. Elsevier, *1975*.

7. Z. Hong, L. Cheng, L. Zhang, Y. Wang. Water Vapor Corrosion Behavior of Scandium Silicates at 1400°C. *Journal of American Ceramic Society*, 2009, 92(1), 193 – 196.

8. Y. Tardy, R. M. Garrels. Prediction of Gibbs energies of formation—I. Relationships among Gibbs energies of formation of hydroxides, oxides and aqueous ions. *Geochimica et Cosmochimica Acta*, *1976*, 40(9), 1051 – 1056.

9. Y. Tardy, R. M. Garrels. Prediction of Gibbs energies of formation of compounds from the elements—II. Monovalent and divalent metal silicates. *Geochimica et Cosmochimica Acta*, *1977*, 41(1), 87 – 92.

10. J. G. Travers, I. Dellien, L. G. Hepler. Scandium: Thermodynamic properties, chemical equilibria, and standard potentials. *Thermochimica Acta*, *1976*, 15(1), 89 – 104.

11. E. N. Korosteleva, G. A. Pribytkov, A. V. Gurskikh. Bulk changes and structurization in solid-phase sintering of titanium–silicon powder mixtures. *Powder Metallurgy and Metal Ceramics*, *2009*, 48(1 – 2), 8 – 12.

12. Z. Liang, X. Dai, H. Middleton. Effect of silicon on corrosion resistance of Ti–Si alloys. *Materials Science and Engineering B*, *2011*, 176(1), 79 – 86.

13. D. Bandyopadhyay. The Ti-Si-C system (Titanium-Silicon-Carbon). *Journal of Phase Equilibria and Diffusion*, *2004*, 25(5), 415 – 420.

14. T. Yoshikawa, K. Morita, S. Kawanishi, T. Tanaka. Thermodynamics of impurity elements in solid silicon. *Journal of Alloys and Compounds*, *2010*, 490(1 – 2), 31 – 41.

15. C. Vahlas, P. Y. Shevalier, E. Blanquet. A thermodynamic evaluation of four Si-M (M = Mo, Ta, Ti, W) binary systems. *CALPHAD*, *1989*, 13(3), 273 – 292.

16. R. W. Ricker, F. A. Hummel. Reactions in the System TiO_2–SiO_2; Revision of the Phase Diagram. *Journal of the American Ceramic Society*, *1951*, 34(9), 271 – 279.

17. Thermal Constants of Substances: database. URL: < http://www.chem.msu.su/cgibin/tkv.pl?show=welcome.html >.

18. F. Cotton, G Wilkinson. *Advanced Inorganic Chemistry. Third Edition*. New York – London – Sydney–Toronto: John Wiley & Sons. *1972*.

19. P. A. Nikolaychuk, A. G. Tyurin. Termodinamika khimicheskoy i elektrokhimicheskoy ustoychivosti splavov sistemy Ti – Si [Thermodynamics of chemical and electrochemical stability of Ti – Si system alloys]. *Butlerovski*ye *Soobshcheniya*, *2011*, 24(2), 77 – 87.

20. A. B. Gokhale, G. J. Abbaschian. The Mo-Si (Molybdenum-Silicon) system. *Journal of Phase Equilibria*, *1991*, 12(4), 493 – 498.

21. K.-H. Tytko, O. Glemser. Isopolymolybdates and Isopolytungstates. *Advances in Inorganic Chemistry and Radiochemistry*, *1976*, 19, 239 – 315.

22. N. Mahadevaiah, B. Venkataramani, B. S. Jai Prakash. Restrictive Entry of Aqueous Molybdate Species into Surfactant Modified Montmorillonite – A Breakthrough Curve Study. *Chemistry of Materials*, *2007*, 19(18), 4606 – 4612.

23. G. W. Keullks, J. L. Hall, D. Chellian, K. Suzuki. The catalytic oxidation of propylene: IV. Preparation and characterization of α-bismuth molybdate. *Journal of Catalysis*, *1974*, 34(1), 79 – 97.

24. A. A. Sibirkin, O. A. Zamyatin, M. F. Churbanov. Vzaimnoye prevrashcheniye izopolisoyedineniy molibdena (VI) v vodnom rastvore [Mutual transformation of isopolycompounds of molybdenum (VI) in aqueous solution]. *Vestnik Nizhegorodskogo universiteta imeni N. I. Lobachevskogo*, *2008,* 5, 45 – 51.

25. JANAF Thermochemical Tables. Third Edition. *Journal of Physical and Chemical Reference Data*, *1985*, 14, Supplement. 1.

26. J. B. Lee. Elevated Temperature Potential-pH Diagrams for the Cr-H_2O, Ti-H_2O, Mo-H_2O, and Pt-H_2O Systems. *Corrosion*, **1981**, 37(8), 467 – 481.

27. P. A. Nikolaychuk, A. G. Tyurin. Utochnyonnaya diagramma Purbe dlya molibdena [The revised Pourbaix diagram for molybdenum]. *Butlerovski*ye *Soobshcheniya, 2011*, 24(2), 101 – 105.

28. P. A. Nikolaychuk, A. G. Tyurin. Termodinamika khimicheskoy i elektrokhimicheskoy ustoychivosti splavov sistemy Mo – Si [Thermodynamics of chemical and electrochemical stability of Mo – Si system alloys]. *Butlerovski*ye *Soobshcheniya, 2011*, 24(2), 95 – 100.

29. V. N. Eremenko et al. *Fizicheskaya khimiya neorganicheskikh materialov* [Physical chemistry of inorganic materials]: in 3 volumes. Vol. 1. *Termodinamika intermetallidov i fazovye ravnovesiya v metallicheskikh sistemakh* [Thermodynamics of intermetallides and phase equilibria in metallic systems], Naukova Dumka, Kiev, *1988*.

30. P. A. Nikolaychuk, T. I. Shalyapina, A. G. Tyurin, T. V. Mosunova. Termodinamika khimicheskoy i elektrokhimicheskoy ustoychivosti splavov sistemy Mn – Si [Thermodynamics of chemical and electrochemical stability of Mn – Si system alloys]. *Vestnik Yuzhno-Ural'skogo gosudarstvennogo universiteta. Seriya "Khimiya", 2010*, 4, 31(207), 72 – 82.

31. N. Chakraborti, H. L. Lukas. Calculation and optimization of the Mn-Si phase diagram. *CALPHAD*, *1989*, 13(3), 293 – 300.

32. P.-Y. Chevalier, E. Fisher, A. Rivet. A Thermodynamic Evolution of the Mn–Si System. *CALPHAD*, *1995*, 19(1), 57 – 68.

33. J. Miettinen. Thermodynamic description of the Cu–Mn–Si system in the copper-rich corner. *CALPHAD, 2003*, 27(4), 395 – 401.

34. F. P. Glasser. The system MnO-SiO_2. *American Journal of Science*, **1958**, 256(6), 398 – 412.

35. J. - H. Huang, E. Rosén. Determination of Gibbs free energies of formation for the silicates $MnSiO_3$, Mn_2SiO_4 and Mn_7SiO_{12} in the temperature range 1000–1350 K by solid state emf measurements. *Physics and Chemistry of Minerals, 1994*, 21(4), 228 – 233.

36. S. Paschen, E. Felder, M. A. Chernikov, L. Degiorgi, H. Schwer, H. R. Ott, D. P. Young, J. L. Sarrao, Z. Fisk. Low-temperature transport, thermodynamic, and optical properties of FeSi. *Physical Review B, 1997*, 56(20), 12916 – 12930.

37. J. - F. Lin, D. L. Heinz, A. J. Campbell, J. M. Devine, G. Shen. Iron-Silicon Alloy in Earth's Core? *Science*, **2002**, 295(5553), 313 – 315.

38. S. S. Lau, J. S.-Y. Feng, J. O. Olowolafe, M.-A. Nicolet. Iron silicide thin film formation at low temperatures. *Thin Solid Films, 1975***,** 25(2), 415 – 422.

39. J. Hu, T. W. Odom and C. M. Lieber. Chemistry and Physics in One Dimension: Synthesis and Properties of Nanowires and Nanotubes. *Accounts of Chemical Research, 1999*, 32(5), 435 – 445.

40. G. S. Patrin, V. V. Beletskiĭ, D. A. Velikanov, O. A. Bayukov, V. V. Vershinin, O. V. Zakieva, T. N. Isaeva. Nonstoichiometry and low-temperature magnetic properties of FeSi crystals. *Physics of the Solid State, 2006*, 48(4), 700 – 704.

41. A. Gude, H. Mehrer. Diffusion in the $D0_3$-type intermetallic phase Fe_3Si. *Philosophical Magazine A, 1997*, 76(1), 1 – 29.

42. L. Kaufman. Coupled phase diagrams and thermochemical data for transition metal binary systems-VI. *CALPHAD, 1979*, 3(1), 45 – 76.

43. J. Lacaze, B. Sundman. An assessment of the Fe-C-Si system. *Metallurgical and Materials Transactions A, 1991*, 22(10), 2211 – 2223.

44. B. - J. Lee, S. K. Lee, D. N. Lee. Formulation of the A2/B2/D03 atomic ordering energy and a thermodynamic analysis of the Fe-Si system. *CALPHAD, 1987*, 11(3), 253 – 270.

45. J. Acker, K. Bohmhammel, G. J. K. van der Berg, J. C. van Miltenburg, C. Kloc. Thermodynamic properties of iron silicides FeSi and α-$FeSi_2$. *Journal of Chemical Termodynamics, 1999*, 31(12), 1523 – 1536.

46. A. Navrotsky. Thermodynamics of formation of the silicates and germanates of some divalent transition metals and of magnesium. *Journal of Inorganic and Nuclear Chemistry, 1971*, 33, 4035.

47. O. B. Fabrichnaya, B. Sundman. The assessment of thermodynamic parameters in the Fe・O and Fe・Si・O systems. *Geochimica et Cosmochimica Acta, 1997***,** 61(21), 4539 – 4555.

48. A. A. Lykasov, A. A. Kimyashov. Usloviya fazovykh ravnovesiy v sisteme Fe – Si – O v interval temperature 1100 – 1300 K [The features of phase equilibria in Fe – Si – O system in temperature range of 1100 – 1300 K]. *Butlerovskiye Soobshcheniya, 2010*, 21(7), 42 – 49.

49. G. G. Charette, S. N. Flengas. Thermodynamic Properties of the Oxides of Fe, Ni, Pb, Cu, and Mn, by EMF Measurements. *Journal of Electrochemical Society, 1968*, 115(8), 796 – 804.

50. M. H. G. Jacobs, B. H. W. S. de Jong, H. A. J. Oonk. The Gibbs energy formulation of α, γ, and liquid Fe_2SiO_4 using Grover, Getting, and Kennedy's empirical relation between volume and bulk modulus. *Geochimica et Cosmochimica Acta, 2001*, 65(22), 4231 – 4242.

51. W. Yong, E. Dachs, A. C. Withers, E. J. Essene. Heat capacity of γ-Fe_2SiO_4 between 5 and 303 K and derived thermodynamic properties. *Physical Chemistry of Minerals, 2007*, 34(2), 121 – 127.

52. A. M. Dark, G. Wei, B. Cantor. The oxidation behaviour of some cobalt-based amorphous alloys. *Materials Science and Engineering B, 1988*, 99(1 – 2), 533 – 537.

53. C. Soon-Don. Thermodynamic analysis of the Co-Si system. *CALPHAD, 1992*, 16(2), 151 – 159.

54. A. G. Tyurin, T. V. Mosunova, P. A. Nikolaychuk. Termodinamika khimicheskoy i elektrokhimicheskoy ustoychivosti silitcidov kobal'ta [Thermodynamics of chemical and electrochemical stability of cobalt silicides]. *Vestnik Yuzhno-Ural's.kogo gosudarstvennogo universiteta. Seriya "Khimiya", 2010*, 3, 11(187), 52 – 60.

55. M. Chen, B. Hallstedt, L. J. Gauckler. Thermodynamic assessment of the Co-O system. *Journal of Phase Equilibria, 2003*, 24(3), 212 – 227.

56. A. Navrotsky, F. S. Pinchovski, S. - I. Akimoto. Calorimetric study of the stability of high pressure phases in the systems CoO・SiO2 and "FeO"・SiO2, and calculation of phase diagrams in MO・SiO2 systems. *Physics of the Earth and Planetary Interiors, 1979*, 19(4), 275 – 292.

57. M. Lindholm, B. Sundman. A thermodynamic evaluation of the nickel-silicon system. *Metallurgical and Materials Transactions A, 1996*, 27(10), 2897 – 2903.

58. P. S. Lee, D. Mangelinck, K. L. Pey, J. Ding, J. Y. Dai, C. S. Ho, A. See. On the Ni–Si phase transformation with/without native oxide. *Microelectronic Engineering, 2000*, 51 – 52, 583 – 594.

59. T. Tokunaga, K. Nishio, H. Ohtani, M. Hasebe. Thermodynamic assessment of the Ni–Si system by incorporating ab initio energetic calculations into the CALPHAD approach. *CALPHAD, 2003*, 27(2), 161 – 168.

60. X. Yuan, L. Zhang, Y. Du, W. Xiong, Y. Tang, A. Wang, S. Liu. A new approach to establish both stable and metastable phase equilibria for fcc ordered/disordered phase transition: application to the Al–Ni and Ni–Si systems. *Materials Chemistry and Physics, 2012*, 135(1), 94 – 105.

61. J. Acker, K. Bohmhammel. Optimization of thermodynamic data of the Ni–Si system. *Thermochimica Acta, 1999*, 337(1 – 2), 187 – 193.

62. I. Ansara, B. Sundman, P. Willemin. Thermodynamic modeling of ordered phases in the Ni・Al system. *Acta Metallurgica, 1988*, 36(4), 977 – 982.

63. B. Sundman, J. Ågren. A regular solution model for phases with several components and sublattices, suitable for computer applications. *Journal of Physical Chemistry of Solids, 1981*, 42(4), 297 – 301.

64. P. A. Nikolaychuk, A. G. Tyurin. Thermodynamic assessment of chemical and electrochemical stability of nickel–silicon system alloys. *Corrosion Science, 2013*, 73, 237 – 244.

65. A. G. Morachevskiy. *Termodinamika sistemy nikel' – kislorod* [Thermodynamics of nickel-oxygen system]: in Morachevskiy, A. G., Tsemekhman, L. Sh., Tsymbulov, L.B. *Termodinamika sistem i protsessov v metallurgii nikelya i medi* [Thermodynamics of systems

and processes in metallurgy of nickel and copper]. St. Petersburg: Izdatel'stvo Politekhnicheskogo Universiteta, *2008*. Issue 12.

66. K. Zeng , T. Klassen, W. Oelerich, R. Bormann. Thermodynamics of the Ni–H system. *Journal of Alloys and Compounds*, *1999*, 283(1 – 2), 151 – 161.

67. G. N. Markos'yan, D. S. Sirota, A. P. Pchel'nikov. Corrosion of Hydrides of Nickel and Cu30Ni Alloy in Oxygen Containing Solutions. *Protection of Metals*, *2005*, 41(4), 358 – 362.

68. B. Baranowski, K. Bocheńska. The Free Energy and Entropy of Formation of Nickel hydride. *Zeitschrift für Physikalishe Chemie. Neue Folge*, *1965*, 45(3 – 4), 140 – 152.

69. X. Yan, Y. A. Chang. A thermodynamic analysis of the Cu–Si system. *Journal of Alloys and Compounds*, *2000*, 308(1 – 2), 221 – 229.

70. P. A. Nikolaychuk, A. G. Tyurin. Termodinamika khimicheskoy i elektrokhimicheskoy ustoychivosti splavov sistemy Cu – Si [Thermodynamics of chemical and electrochemical stability of Cu – Si system alloys]. *Butlerovskiy*e *Soobshcheniya*, *2011*, 24(2), 88 – 94.

71. G. K. Moiseev, N. A. Vatolin. Estimation of the thermochemical properties and stability of Cu_2O_3. *Russian Journal of Physical Chemistry A*, *1997*, 71(3), 335 – 337.

72. J. E. Funk, R. M. Reinstrom. Energy Requirements in Production of Hydrogen from Water. *Industrial & Engineering Chemistry. Process Design and Development*, *1966*, 5(3), 336 – 342.

73. A. Vaškelis, R. Juškėnas, J. Jačiauskienė. Copper hydride formation in the electroless copper plating process: *in situ* X-ray diffraction evidence and electrochemical study. *Electrochimica Acta*, *1998*, 43(9), 1061 – 1066.

74. P. Korzhavyi, I. Soroka, M. Boman, B. Johansson. Thermodynamics of Stable and Metastable Cu-O-H Compounds. *Solid State Phenomena*, *2011*, 172 – 174, 973 – 978.

75. R. Burtovyy, D. Włosewicz, A. Czopnik, M. Tkacz. Heat capacity of copper hydride. *Thermochimica Acta*, *2003*, 400(1 – 2), 121 – 129.

76. M. Tkacz, R. Burtovyy. Decomposition of the hexagonal copper hydride at high pressure. *Solid State Communications*, *2004*, 132(1), 37 – 41.

77. H. A. Wriedt. The O−Zn (Oxygen-Zinc) system. *Bulletin of Alloy Phase Diagrams*, *1987*, 8(2), 166 – 176.

78. E. Jak, P. C. Hayes, S. Degterov, A. D. Pelton, P. Wu. Thermodynamic optimization of the systems PbO-SiO_2, PbO-ZnO, ZnO-SiO_2 and PbO-ZnO-SiO_2. *Metallurgical and Materials Transaction B*, *1997*, 28(6), 1011 – 1018.

79. L. B. Pankratz, J. M. Stuve, M. A. Gokcen. *Thermodynamic data for mineral technology: handbook.* Bureau of Mines USA, *1984*.

80. P. A. Nikolaychuk, A. G. Tyurin. Thermodynamic evaluation of corrosion-electrochemical behaviour of silicon brass CuZn17Si3. *Inorganic Materials*, *2013*, 49(5), 457 – 467.

Conclusions

1. The phase and chemical equilibria in binary systems Me – Si (where Me is the 4th-period transition metal) as well as Mo – Si, Mn – Ge and Fe – Ge at low temperatures were considered. There is no solid solubility of the components in the systems Sc – Si, Ti – Si, Mo – Si and Zn – Si. The solid solubility of silicon in vanadium, chromium, manganese, iron, nickel, cobalt and copper and that of germanium in manganese and iron was estimated using the thermodynamic models for the excess Gibbs energy of these solid solutions. The silicon solubility in vanadium and chromium at 25 °C is vanishingly small, whereas the solubility in manganese, iron, cobalt, nickel and copper is significant. Germanium also has a noticeable solubility in manganese and iron. The thermodynamic activities of the solid solutions components at the standard conditions were calculated. All solid solutions of silicon in 4th period transition metals are characterised by the significant negative deviations from the ideal behaviour. The standard Gibbs energies of formation of scandium, titanium, vanadium, chromium, molybdenum, manganese, iron, cobalt and nickel silicides were collected from reference sources, those of copper silicides and manganese and iron germanides were estimated.

2. The phase equilibria in Me – Si – O, Mo – Si – O, Mn – Ge – O and Fe – Ge – O ternary systems at standard conditions were considered from a thermodynamic viewpoint. The state diagrams for these systems were constructed, and the thermodynamic characteristics of these equilibria were calculated. Figure 73 compares the chemical affinities of considered transition elements (as the oxygen partial pressures necessary to oxidise the elements to their lower oxides) with those of silicon and germanium. The lower the oxygen partial pressure is, the easier the corresponding element forms its oxide. It might be seen that generally the chemical affinity of the transition metal to oxygen decreases while moving from group III towards groups XII of the fourth period, except the anomalously high chemical affinity to oxygen of zinc. The atmospheric corrosion of transition metals silicides and manganese and iron germanides was discussed. The chemical affinities of scandium and titanium to oxygen are much higher than that of silicon, which implies that these metals oxidise more readily, and the silicates oxidise in order from the lowest to the highest with formation of transition metals oxides. The chemical affinities of vanadium, chromium and manganese to oxygen are comparable with

that of silicon, and the oxidation of the lowest silicides with formation of transition metals oxides takes place in the equal extent with the oxidation of highest silicides with formation of silicon dioxide. The chemical affinities to oxygen of molybdenum, iron, cobalt, nickel and copper are much lower that that of silicon, and the silicates oxidise in the order from highest to lowest with formation of silicon dioxide. Manganese and iron also have the chemical affinities to oxygen comparable to that of germanium.

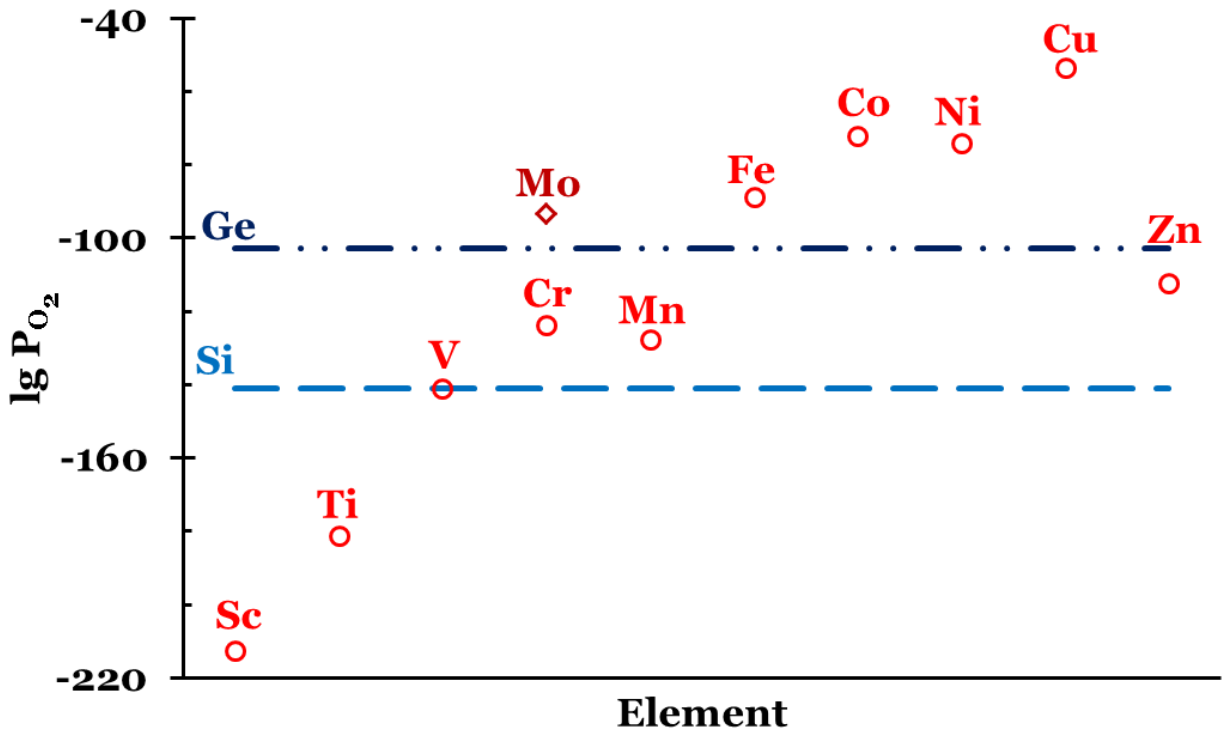

Fig. 73. The chemical affinities of various elements to oxygen.

Moreover, the silicates of transition metals and manganese and iron germanate also influence the oxidation processes.

3. The chemical and electrochemical equilibria in Me – Si – H_2O, Mo – Si – H_2O, Mn – Ge – H_2O and Fe – Ge – H_2O systems were considered from a thermodynamic viewpoint. Pourbaix diagrams for some 4th-period transition metals, as well as for silicon, were revised. The potential – pH diagrams for Me – Si – H_2O, Mo – Si – H_2O, Mn – Ge – H_2O and Fe – Ge – H_2O systems were plotted in the first time. The different corrosion-electrochemical behaviour of transition metals silicides and manganese and iron germanides in aqueous media was discussed. Silicates have the different effect on the corrosion properties of various metals. Scandium, manganese and zinc silicates might be the basis of the protective films

forming on the alloy surface, whereas chromium, iron, cobalt, nickel and copper silicates have a not thermodynamically stable in the whole range of potentials and pH in the area of water electrochemical stability and have a little effect on the formation of the protective film. The potential – pH diagrams for some siliceous brasses and bronzes were plotted, and the corrosion of these alloys in aqueous media was discussed.

4. Method of estimation of corrosion-electrochemical behaviour of multicomponent alloys, which takes into account both thermodynamic and kinetic data and is based on mutual construction of equilibrium and polarisation potential – pH diagrams, was described. Its usage was illustrated in the example of the structural steel 20KT.

References

This list contains only in-text references. The references from attached publications are not included. Each attached publication has its own reference list.

Abbruzzese C. Percolation leaching of manganese ore by aqueous sulfur dioxide // Hydrometallurgy. 1990. Vol. 25. No 1. P. 85–97.

Abreli N.M., Brearley A.J. Carbonates in Vigarano: Terrestrial, preterrestrial, or both? // Meteoritics & Planetary Science. 2005. Vol. 40. No 4. P. 609–625.

Acker J. et al. Thermodynamic properties of the nickel silicide NiSi between 8 and 400K // Thermochimica Acta. 1999a. Vol. 339. No 1–2. P. 29–33.

Acker J. et al. Thermodynamic properties of iron silicides FeSi andα-$FeSi_2$ // The Journal of Chemical Thermodynamics. 1999b. Vol. 31. No 12. P. 1523–1536.

Acker J., Bohmhammel K. Optimization of thermodynamic data of the Ni–Si system // Thermochimica Acta. 1999. Vol. 337. No 1–2. P. 187–193.

Acree W.E. Mathematical representation of thermodynamic properties: Part 2. Derivation of the combined nearly ideal binary solvent (NIBS)/Redlich-Kister mathematical representation from a two-body and three-body interactional mixing model // Thermochimica Acta. 1992. Vol. 198. No 1. P. 71–79.

Adelson E., Austin A.E. Magnetic structures of iron germanides // Journal of Physics and Chemistry of Solids. 1965. Vol. 26. No 12. P. 1795–1804.

Adrain R. Research concerning the probabilities of the errors which happen in making observations, &c // The Analyst; or Mathematical Museum. 1808. Vol. 1. No 4. P. 93–109.

Akalin S., Özer U.Y. Hydrolysis of Sc_{aq}^{3+} and the stabilities of scandium (III)-Tiron chelates in aqueous solution // Journal of Inorganic and Nuclear Chemistry. 1971. Vol. 33. No 12. P. 4171–4180.

Aksel'rud N. V. Hydroxide chlorides and hydroxides of elements of the scandium subgroup and of the lanthanides // Russian Chemical Reviews. 1963. Vol. 32. No 7. P. 353–366.

Akyol A., Can O.T., Bayramoglu M. Treatment of hydroquinone by photochemical oxidation and electrocoagulation combined process // Journal of Water Process Engineering. 2015. Vol. 8. P. 45–54.

Alimarin I.P., Yung-Schaing T. Separation and determination of scandium using N-benzoylphenylhydroxylamine // Talanta. 1961. Vol. 8. No 5. P. 317–321.

Anderko A. Modeling of Aqueous Corrosion // Shreir's Corrosion. Volume 2: Corrosion in Liquids, Corrosion Evaluation. Amsterdam: Elsevier, 2010. P.

1585–1629.
Anderko A., Sanders S.J., Young R.D. Real-Solution Stability Diagrams: A Thermodynamic Tool for Modeling Corrosion in Wide Temperature and Concentration Ranges // Corrosion. 1997. Vol. 53. No 1. P. 43–53.
Anderko A., Shuler P. A computational approach to predicting the formation of iron sulfide species using stability diagrams // Computers & Geosciences. 1997. Vol. 23. No 6. P. 647–658.
Anderson C.G., Twidwell L.G. The alkaline sulfide hydrometallurgical separation, recovery andfixation of tin, arsenic, antimony and gold // Lead and Zinc 2008. The Southern Africa Insitute of Mining and Metallurgy, 2008. P. 121–132.
Anderson G.M. Is there alkali-aluminum complexing at high temperatures and pressures? // Geochimica et Cosmochimica Acta. 1995. Vol. 59. No 11. P. 2155–2161.
Andersson J.-O. et al. Thermo-Calc & DICTRA, computational tools for materials science // Calphad: Computer Coupling of Phase Diagrams and Thermochemistry. 2002. Vol. 26. No 2. P. 273–312.
Andersson S., Magnéli A. Diskrete Titanoxydphasen im Zusammensetzungsbereich $TiO_{1,75}$-$TiO_{1,90}$ // Die Naturwissenschaften. 1956. Bd. 43. H. 21. S. 495–496.
Andreasen A. Predicting formation enthalpies of metal hydrides. Roskilde: Risø National Laboratory, 2004. 36 p.
Ang X., Zhang Y., Bao S. Extraction of vanadium from sulfuric acid leaching solution of stone coal by ion exchange // Bulgarian Chemical Communications. 2015. No D. P. 99–104.
Angelis A. de et al. New method for H_2S removal in acid solutions. // ChemSusChem. 2010. Vol. 3. No 7. P. 829–833.
Angus J.C.., Angus C.T. Computation of Pourbaix Diagrams Using Virtual Species: Implementation on Personal Computers // Journal of The Electrochemical Society. 1985. Vol. 132. No 5. P. 1014–1019.
Angus J.C., Zappia M.J. Electron Number Diagrams: A New Phase Diagram for Complex Redox Systems // Journal of The Electrochemical Society. 1987. Vol. 134. No 6. P. 1374–1383.
Ansara I. et al. Thermodynamic assessment of the Al–Ni system // Journal of Alloys and Compounds. 1997. Vol. 247. No 1–2. P. 20–30.
Ansara I., Sundman B., Willemin P. Thermodynamic modeling of ordered phases in the Ni–Al system // Acta Metallurgica. 1988. Vol. 36. No 4. P. 977–982.
Antonovich V.P., Nazarenko V.A. Spectrophotometric determination of the hydrolysis constants of scandium ions // Russian Journal of Inorganic

Chemistry. 1968. Vol. 13. No 7. P. 940–941.
Aoudj S. et al. Electrocoagulation process applied to wastewater containing dyes from textile industry // Chemical Engineering and Processing: Process Intensification. 2010. Vol. 49. No 11. P. 1176–1182.
Aoudj S. et al. Removal of fluoride and turbidity from semiconductor industry wastewater by combined coagulation and electroflotation // Desalination and Water Treatment. 2016. Vol. 57. No 39. P. 18398–18405.
Aoyama I. et al. Effects of Ge Doping on Micromorphology of MnSi in $MnSi_{\sim 1.7}$ and on Their Thermoelectric Transport Properties // Japanese Journal of Applied Physics. 2005. Vol. 44. No 12. P. 8562–8570.
Arif A.F. et al. Highly conductive nano-sized Magnéli phases titanium oxide (TiO_x) // Scientific Reports. 2017. Vol. 7. No 1. P. 3646.
Arkharov V.I., Kichigina Z.P. // Surface Interactions between Metals and Gases. New York: Consultants Bureau, 1966. C. 101–103.
Arras E. et al. Phase diagram, structure, and magnetic properties of the Ge-Mn system: A first-principles study // Physical Review B. 2011. Vol. 83. No 17. P. 174103.
Ateya B.G., AlKharafi F.M., Al-Azab A. S. Electrodeposition of Sulfur from Sulfide Contaminated Brines // Electrochemical and Solid-State Letters. 2003. Vol. 6. No 9. P. C137–C140.
Atkins P.W. et al. Shriver and Atkins' Inorganic Chemistry, Fifth Edition. New York: W. H. Freeman and Company, 2010. 851 p.
Aveston J. Hydrolysis of scandium(III): ultracentrifugation and acidity measurements // Journal of the Chemical Society A: Inorganic, Physical, Theoretical. 1966. P. 1599–1601.
Baes Jr. C.F., Mesmer R.E. The Hydrolysis of Cations. New York: Wiley, 1976. 254 p.
Baes Jr. C.F., Mesmer R.E. The thermodynamics of cation hydrolysis // American Journal of Science. 1981. Vol. 281. No 7. P. 935–962.
Baker M.., Castle J.. The initiation of pitting corrosion of stainless steels at oxide inclusions // Corrosion Science. 1992. Vol. 33. No 8. P. 1295–1312.
Bale C.W., Pelton A.D. Mathematical representation of thermodynamic properties in binary systems and solution of Gibbs-Duhem Equation // Metallurgical Transactions. 1974. Vol. 5. No 11. P. 2323–2337.
Ball J.W., Nordstrom D.K. Critical Evaluation and Selection of Standard State Thermodynamic Properties for Chromium Metal and Its Aqueous Ions, Hydrolysis Species, Oxides, and Hydroxides // Journal of Chemical & Engineering Data. 1998. Vol. 43. No 6. P. 895–918.
Banaś J. et al. Effect of CO_2 and H_2S on the composition and stability of passive

film on iron alloys in geothermal water // Electrochimica Acta. 2007. Vol. 52. No 18. P. 5704–5714.
Bandyopadhyay D. The Ti-Si-C system (Titanium-Silicon-Carbon) // Journal of Phase Equilibria and Diffusion. 2004. Vol. 25. No 5. P. 415–420.
Baranowski B. Thermodynamics of metal/hydrogen systems at high pressures // Berichte der Bunsengesellschaft für physikalische Chemie. 1972. Bd. 76. H. 8. S. 714–724.
Baranowski B., Bocheńska K. The Free Energy and Entropy of Formation of Nickel hydride // Zeitschrift für Physikalische Chemie. Neue Folge. 1965. Bd. 45. H. 3–4. S. 140–152.
Bard A.J., Parsons R., Jordan J. Standard Potentials in Aqueous Solution. : CRC Press, 1985.
Barnes H., Kullerud G. Equilibria in sulfur-containing aqueous solutions, in the system Fe-S-O, and their correlation during ore deposition // Economic Geology. 1961. Vol. 56. No 4. P. 648–688.
Bashkin I.O., Ponyatovskii E.G., Kost M.E. Phase Transformations in Hydrides of Rare-Earth Metals under Pressure. II. The Sc-H and Yb-H Systems under High Hydrogen Pressure // Physica Status Solidi (b). 1978. Vol. 87. No 1. P. 369–372.
Berche A., Tedenac J.C., Jund P. Thermodynamic modeling of the germanium–manganese system // Intermetallics. 2014. Vol. 47. P. 23–30.
Bertrand G.L., Acree W.E., Burchfield T.E. Thermochemical excess properties of multicomponent systems: Representation and estimation from binary mixing data // Journal of Solution Chemistry. 1983. Vol. 12. No 5. P. 327–346.
Bethune A.J. de, Licht T.S., Swendeman N. The Temperature Coefficients of Electrode Potentials: The Isothermal and Thermal Coefficients—The Standard Ionic Entropy of Electrochemical Transport of the Hydrogen Ion // Journal of The Electrochemical Society. 1959. Vol. 106. No 7. P. 616.
Beverskog B., Puigdomenech I. Revised pourbaix diagrams for chromium at 25–300 °C // Corrosion Science. 1997. Vol. 39. No 1. P. 43–57.
Biedermann G. et al. Studies on the Hydrolysis of Metal Ions. 18. The Scandium Ion, Sc^{3+}. // Acta Chemica Scandinavica. 1956. Vol. 10. P. 1327–1339.
Biernat R., Robins R. High temperature potential/pH diagrams for the sulphur-water system // Electrochimica Acta. 1969. Vol. 14. No 9. P. 809–820.
Biernat R., Robins R. High-temperature potential/pH diagrams for the iron—water and iron—water—sulphur systems // Electrochimica Acta. 1972. Vol. 17. No 7. P. 1261–1283.
Binder G., Graff M. Mikrobiell verursachte Korrosion an Stahlbauteilen //

Materials and Corrosion. 1995. Vol. 46. No 11. P. 639–648.
Blackman A., Gahan L. Aylward and Findlay's SI Chemical Data. 7th ed. New York: Wiley, 2014. 240 p.
Blander M., Pelton A.D. Thermodynamic analysis of binary liquid silicates and prediction of ternary solution properties by modified quasichemical equations // Geochimica et Cosmochimica Acta. 1987. Vol. 51. No 1. P. 85–95.
Bohn H. Arsenic Eh-pH diagram and comparisons to the soil chemistry of phosphorus. // Soil Science. 1976. Vol. 121. No 2. P. 125–127.
Bohn H.L., Fenn D.B., Moore W.J. Electrode potentials of nitrogen and sulfur half-reactions // Soil Science. 1969. Vol. 108. No 2. P. 95–101.
Bombara G., Baudo G., Tamba A. Thermodynamics of corrosion in fused sulphates // Corrosion Science. 1968. Vol. 8. No 6. P. 393–404.
Bommer H., Hohmann E. Zur Thermochemie der seltenen Erden. I. Die Lösungswärmen der Metalle der seltenen Erden // Zeitschrift für anorganische und allgemeine Chemie. 1941. Bd. 248. H. 4. S. 357–372.
Bouet J., Brenet J. Contribution a l'etude du diagramme tension/pH du fer en milieux sulfures // Corrosion Science. 1963. T. 3. N. 1. P. 51–63.
Bouroushian M. Electrochemistry of metal chalcogenides. Berlin: Springer, 2010.
Boxall C., Kelsall G.H. Photoelectrophoresis of colloidal semiconductors. Part 1.—The technique and its applications // Journal of the Chemical Society, Faraday Transactions. 1991. Vol. 87. No 21. P. 3537–3545.
Brahmi K. et al. Use of Electrocoagulation with Aluminum Electrodes to Reduce Hardness in Tunisian Phosphate Mining Process Water // Mine Water and the Environment. 2015.
Brahmi K. et al. Highly Cost-Effective and Reuse-Oriented Treatment of Cadmium-Polluted Mining Wastewater by Electrocoagulation Process // Journal of Environmental Engineering. 2016. P. 04016061.
Brandon N.P. et al. Thermodynamics and electrochemical behaviour of Hg–S–Cl–H_2O systems // Journal of Electroanalytical Chemistry. 2001. Vol. 497. No 1–2. P. 18–32.
Brandon N.P. et al. Simultaneous recovery of Pb and PbO_2 from battery plant effluents. Part II // Journal of Applied Electrochemistry. 2003. Vol. 33. No 10. P. 853–862.
Bratsch S.G. Standard Electrode Potentials and Temperature Coefficients in Water at 298.15 K // Journal of Physical and Chemical Reference Data. 1989. Vol. 18. No 1. P. 1–21.
Brent Hiskey J., Atluri V.P. Dissolution Chemistry of Gold and Silver in Different Lixiviants // Mineral Processing and Extractive Metallurgy Review. 2007.

Vol. 4. No 1–2. P. 95–134.
Brookins D. Geochemical behavior of antimony, arsenic, cadmium and thallium: Eh_pH diagrams for 25°C, 1-bar pressure // Chemical Geology. 1986. Vol. 54. No 3–4. P. 271–278.
Brookins D.G. Eh - pH Diagrams for Geochemistry. Berlin, Heidelberg: Springer-Verlag, 1988. 183 p.
Bryzgalin O. V. Electrostatic-model estimates of electrolyte dissociation constants up to 800 °C and 5 kbar // Geochemistry International. 1989. Vol. 26. No 10. P. 63–70.
Buckley A., Hamilton I., Woods R. An investigation of the sulphur (– II)/sulphur (0) system on gold electrodes // Journal of electroanalytical chemistry and interfacial electrochemistry. 1987. Vol. 216. No 1–2. P. 213–227.
Burgot J.-L. Ionic Equilibria in Analytical Chemistry. New York: Springer New York, 2012. 729 p.
Burtovyy R. et al. Heat capacity of copper hydride // Thermochimica Acta. 2003. Vol. 400. No 1–2. P. 121–129.
Campbell F.C. Phase Diagrams: Understanding the Basics. Ohio: ASM International, 2012. 470 p.
Campbell J., Whiteker R. A periodic table based on potential-pH diagrams // Journal of Chemical Education. 1969. Vol. 46. No 2. P. 90.
Campbell S.W. An expression for G^E for use in the reduction of ternary vapor-liquid equilibrium data // Fluid Phase Equilibria. 1992. Vol. 74. P. 35–46.
Can B.Z. et al. Arsenic and Boron Removal by Electrocoagulation with Aluminum Electrodes // Arabian Journal for Science and Engineering. 2016. Vol. 41. No 6. P. 2229–2237.
Canut J.-M. Le, Maximovitch S., Dalard F. Electrochemical characterisation of nickel-based alloys in sulphate solutions at 320 °C // Journal of Nuclear Materials. 2004. Vol. 334. No 1. P. 13–27.
Carvalho H.P. de et al. Improvement of Methylene Blue removal by electrocoagulation/banana peel adsorption coupling in a batch system // Alexandria Engineering Journal. 2015. Vol. 54. No 3. P. 777–786.
Chakraborti N., Lukas H.L. Calculation and optimization of the Mn-Si phase diagram // Calphad: Computer Coupling of Phase Diagrams and Thermochemistry. 1989. Vol. 13. No 3. P. 293–300.
Chamberland B.L. The chemical and physical properties of CrO_2 and tetravalent chromium oxide derivatives // Critical Reviews in Solid State and Materials Sciences. 1977. Vol. 7. No 1. P. 1–31.
Chandrasekharaiah M.S., Margrave J.L., O'Hare P.A.G. The Disilicides of Tungsten, Molybdenum, Tantalum, Titanium, Cobalt, and Nickel, and

Platinum Monosilicide: A Survey of Their Thermodynamic Properties // Journal of Physical and Chemical Reference Data. 1993. Vol. 22. No 6. P. 1459–1468.

Chaparro A. Thermodynamic analysis of the deposition of zinc oxide and chalcogenides from aqueous solutions // Chemistry of materials. 2005. Vol. 17. No 16. P. 4118–4124.

Charette G.G., Flengas S.N. Thermodynamic Properties of the Oxides of Fe, Ni, Pb, Cu, and Mn, by EMF Measurements // Journal of The Electrochemical Society. 1968. Vol. 115. No 8. P. 796–804.

Charlot G., Collumeau A., Marchon M.J.C. Selected Constants: Oxidation-Reduction Potentials of Inorganic Substances in Aqueous Solution. Oxford: Butterworths, 1971. 73 p.

Chase Jr. M.W. et al. JANAF Thermochemical Tables Third Edition // Journal of Physical and Chemical Reference Data. 1985. Vol. 14. Supplement 1.

Chen H., Du Y., Schuster J.C. On the melting of Cr_5Si_3 and update of the thermodynamic description of Cr–Si // Calphad: Computer Coupling of Phase Diagrams and Thermochemistry. 2009. Vol. 33. No 1. P. 211–214.

Chen K. et al. Crystal structures of ferredoxin variants exhibiting large changes in [Fe-S] reduction potential // Nature structural biology. 2002. Vol. 9. No 3. P. 188–192.

Chen L.J. Metal silicides: An integral part of microelectronics // The Journal of The Minerals, Metals & Materials Society. 2005. Vol. 57. No 9. P. 24–30.

Chen M., Hallstedt B., Gauckler L.J. Thermodynamic assessment of the Co-O system // Journal of Phase Equilibria. 2003. Vol. 24. No 3. P. 212–227.

Chen S.-L., Kao C.R., Chang Y.A. A generalized quasi-chemical model for ordered multi-component, multi-sublattice intermetallic compounds with anti-structure defects // Intermetallics. 1995. Vol. 3. No 3. P. 233–242.

Cheng C.Y., Kelsall G.H. Models of Hypochlorite production in electrochemical reactors with plate and porous anodes // Journal of Applied Electrochemistry. 2007. Vol. 37. No 11. P. 1203–1217.

Cheng W., Ganguly J. Some aspects of multicomponent excess free energy models with subregular binaries // Geochimica et Cosmochimica Acta. 1994. Vol. 58. No 18. P. 3763–3767.

Cheraghi A. et al. Thermodynamics of vanadium (V) solvent extraction by mixture of D_2EHPA and TBP // International Journal of Mineral Processing. 2015. Vol. 138. P. 49–54.

Chesworth W., Martínez Cortizas A., García-Rodeja E.. The redox–pH approach to the geochemistry of the Earth's land surface, with application to peatlands // Developments in Earth Surface Processes Developments in

Earth Surface Processes. Elsevier, 2006. P. 175–195.
Chevalier P.-Y., Fischer E., Rivet A. A thermodynamic evaluation of the Mn-Si system // Calphad: Computer Coupling of Phase Diagrams and Thermochemistry. 1995. Vol. 19. No 1. P. 57–68.
Cho S. et al. Ferromagnetism in Mn-doped Ge // Physical Review B. 2002. Vol. 66. No 3. P. 033303.
Clark W.M. The determination of hydrogen ions; an elementary treatise on the hydrogen electrode, indicator and supplementary methods, with an indexed bibliography on applications. Baltimore: Williams and Wilkens, 1920. 762 p.
Clark W.M. Studies on Oxidation-Reduction. I. Introduction // Public Health Reports. 1923. Vol. 38. No 10. P. 443–455.
Clark W.M., Cohen B. Studies on Oxidation-Reduction. II. An Analysis of the Theoretical Relations between Reduction Potentials and pH // Public Health Reports. 1923. Vol. 38. No 13. P. 666–683.
Cole D.L. et al. Kinetics of aqueous scandium(III) perchlorate hydrolysis and dimerization // Inorganic Chemistry. 1969. Vol. 8. No 3. P. 682–685.
Connétable D., Thomas O. First-principles study of nickel-silicides ordered phases // Journal of Alloys and Compounds. 2011. Vol. 509. No 6. P. 2639–2644.
Cook W.G., Olive R.P. Pourbaix diagrams for chromium, aluminum and titanium extended to high-subcritical and low-supercritical conditions // Corrosion Science. 2012. Vol. 58. P. 291–298.
Córdoba E.M. et al. Leaching of chalcopyrite with ferric ion. Part I: General aspects // Hydrometallurgy. 2008. Vol. 93. No 3–4. P. 81–87.
Corry C.E. Spontaneous polarization associated with porphyry sulfide mineralization // Geophysics. 1985. Vol. 50. No 6. P. 1020–1034.
Costa M.C. et al. Wine wastes as carbon source for biological treatment of acid mine drainage. // Chemosphere. 2009. Vol. 75. No 6. P. 831–836.
Cotton F., Wilkinson G. Advanced Inorganic Chemistry. New York – London – Sydney – Toronto: John Wiley & Sons, 1971. 1171 p.
Coughanowr C.A., Ansara I., Lukas H.L. Assessment of the Cr–Si System // Calphad: Computer Coupling of Phase Diagrams and Thermochemistry. 1994. Vol. 18. No 2. P. 125–140.
Couture R.-M., Cappellen P. Van. Reassessing the role of sulfur geochemistry on arsenic speciation in reducing environments. // Journal of hazardous materials. 2011. Vol. 189. No 3. P. 647–652.
Craig B.D. Fundamental Aspects of Corrosion Films in Corrosion Science. Berlin/Heidelberg: Springer, 2013. 200 p.

Cui S., Jung I.-H. Thermodynamic assessments of the Cr-Si and Al-Cr-Si systems // Journal of Alloys and Compounds. 2017. Vol. 708. P. 887–902.
Dark A.M., Wei G., Cantor B. The oxidation behaviour of some cobalt-based amorphous alloys // Materials Science and Engineering. 1988. Vol. 99. No 1–2. P. 533–537.
Davoodi A. et al. A comparative H_2S corrosion study of 304L and 316L stainless steels in acidic media // Corrosion Science. 2011. Vol. 53. No 1. P. 399–408.
Davoodi A., Babaiee M., Pakshir M. Imitating seasonal temperature fluctuations for the H_2S corrosion of 304L and 316L austenitic stainless steels // Metals and Materials International. 2013. Vol. 19. No 4. P. 731–740.
Dean J.A. Lange's Handbook of Chemistry. 12th ed. New York: McGraw-Hill, 1979.
Dean J.A. Lange's Handbook of Chemistry. 15th edn. New York: McGraw-Hill, 1999.
Debski A., Debski R., Gasior W. New Features of Entall Database: Comparison of Experimental and Model Formation Enthalpies/ Nowe Funkcje Bazy Danych Entall: Porównanie Doświadczalnych I Modelowych Entalpii Tworzenia // Archives of Metallurgy and Materials. 2014. Vol. 59. No 4. P. 1337–1343.
Dede L., Russ W. Beiträge zur Kenntnis des Germaniums, I.: Die Aufarbeitung des Germanits, Darstellung reinen Germaniumdioxyds und reinsten Germaniumtetrachlorids // Berichte der deutschen chemischen Gesellschaft (A und B Serien). 1928. Bd. 61. H. 11. S. 2451–2459.
Delahay P., Pourbaix M., Rysselberghe P. Van. Potential-pH diagrams // Journal of Chemical Education. 1950. Vol. 27. No 12. P. 683–688.
Delahay P., Pourbaix M., Rysselberghe P. Van. Potential-pH Diagram of Lead and its Applications to the Study of Lead Corrosion and to the Lead Storage Battery // Journal of The Electrochemical Society. 1951. Vol. 98. No 2. P. 57–64.
Demir-Cakan R. et al. An aqueous electrolyte rechargeable Li-ion/polysulfide battery // Journal of Materials Chemistry A. 2014. Vol. 2. No 24. P. 9025–9029.
Deschênes G., Ghali E. L'électrodissolution d'une poudre de galène en milieu d'acétate d'ammonium et d'acide chlorhydrique // Journal of applied electrochemistry. 1988. Vol. 18. No 2. P. 304–311.
Detournay J. et al. The region of stability of green rust II in the electrochemical potential-pH equilibrium diagram of iron in sulphate medium // Corrosion Science. 1975. Vol. 15. No 5. P. 295–306.
Dewitt R., Mesmaeker A.K. Capacitance characteristics of the polycrystalline

CdS/NaOH and CdS/cysteine interfaces // Journal of the Electrochemical Society. 1983. Vol. 130. No 10. P. 1995–1998.
Dhawale S. Thiosulfate: An Interesting Sulfur Oxoanion that is Useful in Both Medicine and Industry-But is Implicated in Corrosion // Journal of Chemical Education. 1993. Vol. 70. No 1. P. 12.
Dinsdale A.T. SGTE data for pure elements // Calphad. 1991. Vol. 15. No 4. P. 317–425.
Djamali E., Cobble J.W. A Unified Theory of the Thermodynamic Properties of Aqueous Electrolytes to Extreme Temperatures and Pressures // The Journal of Physical Chemistry B. 2009. Vol. 113. No 8. P. 2398–2403.
Dolejs D. Thermodynamics of Aqueous Species at High Temperatures and Pressures: Equations of State and Transport Theory // Reviews in Mineralogy and Geochemistry. 2013. Vol. 76. No 1. P. 35–79.
Dollase W.A., Seifert F., O'Neill H.S.C. Structure of Cr_2SiO_4 and possible metal-metal interactions in crystal and melt // Physics and Chemistry of Minerals. 1994. Vol. 21. No 1–2. P. 104–109.
Du A., Zhang H., Pourbaix M. Thermodynamic equilibrium diagrams of sulphur-chromium system // Rare Metals. 2001. Vol. 20. No 4. P. 236–239.
Du Y. et al. Experimental Investigation and Thermodynamic Calculation of the Titanium–Silicon–Carbon System // Journal of the American Ceramic Society. 2000. Vol. 83. No 1. P. 197–203.
Du Y. et al. A thermodynamic description of the Al-Mn-Si system over the entire composition and temperature ranges // Metallurgical and Materials Transactions A. 2004. Vol. 35. No 5. P. 1613–1628.
Du Y., Schuster J.C. Experimental reinvestigation of the CrSi-Si partial system and update of the thermodynamic description of the entire Cr-Si system // Journal of Phase Equilibria. 2000. Vol. 21. No 3. P. 281–286.
Dufek V., Brožek V., Petrů F. Zur Existenz des Seandiummonoxides // Monatshefte für Chemie. 1969. Bd. 100. H. 5. S. 1628–1630.
Dufek V., Petrů F., Brožek V. Über Sauerstoff-haltige Verbindungen vom Strukturtyp B_1 der ersten vier Übergangsmetalle // Monatshefte für Chemie. 1967. Bd. 98. H. 6. S. 2424–2430.
Duman E. et al. Competing magnetic interactions in rare-earth manganese silicides and germanides // Journal of Magnetism and Magnetic Materials. 2007. Vol. 309. No 1. P. 40–53.
Dutta P.K. et al. Role of Sulfur during Acetate Oxidation in Biological Anodes // Environmental Science & Technology. 2009a. Vol. 43. No 10. P. 3839–3845.
Dutta P.K. et al. Electrochemical regeneration of sulfur loaded electrodes //

Electrochemistry Communications. 2009b. Vol. 11. No 7. P. 1437–1440.
Eastman E.D. The mass effect in the entropy of substances // Journal of the American Chemical Society. 1923. Vol. 45. No 1. P. 80–83.
Eggert G., Weichert M. Some news about «black spots» // Proceedings of the International Conference on Metals Conservation. 2004. P. 142–148.
Eklund G. Initiation of pitting at sulfide inclusions in stainless steel // Journal of the Electrochemical Society. 1974. Vol. 121. No 4. P. 467–473.
El-Raghy S., El-Demerdash M. Computation of EH-pH Diagrams for M-S-H_2O Systems: A New Approach // Journal of the Electrochemical Society. 1989. Vol. 136. No 12. P. 3647–3654.
Elliott J.F., Gleiser M. Thermochemistry for steelmaking. Boston: Addison-Wesley Pub. Co, 1960. 296 p.
Eriksson G. An algorithm for the computation of aqueous multi-component, multiphase equilibria // Analytica Chimica Acta. 1979. Vol. 112. No 4. P. 375–383.
Escudero R., Espinoza E., Tavera F.J. Precipitation of Lead Species in a Pb – H_2O System // Research Journal of Recent Sciences. 2013. Vol. 2. No 9. P. 1–4.
Espinoza E., Escudero R., Tavera F.. Waste Water Treatment by Precipitating Copper, Lead and Nickel Species // Research Journal of Recent Sciences. 2012. Vol. 1. No 10. P. 1–6.
Evans H.T., Garrels R.M. Thermodynamic equilibria of vanadium in aqueous systems as applied to the interpretation of the Colorado Plateau ore deposits // Geochimica et Cosmochimica Acta. 1958. Vol. 15. No 1–2. P. 131–149.
Fabrichnaya O.B., Sundman B. The assessment of thermodynamic parameters in the Fe–O and Fe–Si–O systems // Geochimica et Cosmochimica Acta. 1997. Vol. 61. No 21. P. 4539–4555.
Faraday M. Experimental Researches in Electricity. Third Series // Philosophical Transactions of the Royal Society of London. 1833. Vol. 123. P. 23–54.
Faraday M. Experimental Researches in Electricity. Seventh Series // Philosophical Transactions of the Royal Society of London. 1834. Vol. 124. P. 55–123.
Fatséas G.A. Some remarks on a recent Mössbauer effect study of the β-phase iron germanide // Canadian Journal of Physics. 1976. Vol. 54. No 18. P. 1850–1853.
Fedorova N.A., Tsymbulov L.B., Tsemekhman L.S. Influence of SiO_2 on the Equilibrium in the Cu-Ni-Cu_2O-NiO System // Russian Journal of Applied Chemistry. 2003. Vol. 76. No 4. P. 526–530.
Fei Y., Saxena S.K., Eriksson G. Some binary and ternary silicate solution models

// Contributions to Mineralogy and Petrology. 1986. Vol. 94. No 2. P. 221–229.
Feitknecht W., Schindler P. Solubility constants of metal oxides, metal hydroxides and metal hydroxide salts in aqueous solution // Pure and Applied Chemistry. 1963. Vol. 6. No 2. P. 125–206.
Finetti B. de. Considerazioni matematiche sull'ereditarietà mendeliana // Metron. 1926. Vol. 6. N. 1. P. 3–41.
Firer D., Friedler E., Lahav O. Control of sulfide in sewer systems by dosage of iron salts: comparison between theoretical and experimental results, and practical implications. // The Science of the total environment. 2008. Vol. 392. No 1. P. 145–156.
Fishtik I. Thermodynamic Stability Relations in Redox Systems // Environmental Science & Technology. 2006. Vol. 40. No 6. P. 1902–1910.
Fomchenko N. V., Muravyov M.I. Thermodynamic and XRD analysis of arsenopyrite biooxidation and enhancement of oxidation efficiency of gold-bearing concentrates // International Journal of Mineral Processing. 2014. Vol. 133. P. 112–118.
Forsén O., Aromaa J. the Use of Hydrometallurgy in Treatment of Secondary Raw Materials and Low – Grade Ores // Acta Metallurgica Slovaca. 2013. Vol. 19. No 3. P. 184–195.
Fränzle S., Markert B., Wünschmann S. Technische Umweltchemie: innovative Verfahren der Reinigung verschiedener Umweltkompartimente. 2005.
Fukunaga O., Saito S. Phase Equilibrium in the System CrO_2 - Cr_2O_3 // Journal of the American Ceramic Society. 1968. Vol. 51. No 7. P. 362–363.
Funk J.E., Reinstrom R.M. Energy Requirements in Production of Hydrogen from Water // Industrial & Engineering Chemistry Process Design and Development. 1966. Vol. 5. No 3. P. 336–342.
Ganguly J. Thermodynamic modelling of solid solutions // EMU Notes in Mineralogy. Jena: European Mineralogical Union, 2001. P. 37–69.
Garrels R., Naeser C. Equilibrium distribution of dissolved sulphur species in water at 25 C and 1 atm total pressure // Geochimica et Cosmochimica Acta. 1958. Vol. 15. No 1–2. P. 113–130.
Génin J.-M.R. et al. Preparation and Eh--pH diagrams of Fe(II)-Fe(III) green rust compounds; hyperfine interaction characteristics and stoichiometry of hydroxy-chloride, -sulphate and -carbonate // Hyperfine interactions. 1998. Vol. 111. No 1–4. P. 313–318.
Génin J.-M.R. et al. Synthesis of green rusts by oxidation of $Fe(OH)_2$, their products of oxidation and reduction of ferric oxyhydroxides; –pH Pourbaix diagrams // Comptes Rendus Geoscience. 2006. T. 338. N. 6–7. P. 433–

446.
Génin J. et al. On the stoichiometry and pourbaix diagram of Fe (II)-Fe (III) hydroxy-sulphate or sulphate-containing green rust 2: An electrochemical and Mössbauer spectroscopy // Corrosion Science. 1996. Vol. 38. No 10. P. 1751–1762.
Gerstein B.C. Heat Capacity of Scandium from 6 to 350°K // The Journal of Chemical Physics. 1971. Vol. 54. No 11. P. 4723–4737.
Ghali E., Toedtemeier M., Dandapani B. Electrodissolution de la galène en milieu suifamique // Journal of applied electrochemistry. 1984. Vol. 14. No 2. P. 151–164.
Gibbs J.W. On the Equilibrium of Heterogeneous Substances. First Part // Transactions of the Connecticut Academy of Arts and Sciences. 1876a. Vol. 3. P. 108–248.
Gibbs J.W. On the Equilibrium of Heterogeneous Substances (concluded) // Transactions of the Connecticut Academy of Arts and Sciences. 1876b. Vol. 3. P. 343–524.
Gibbs J.W. Zur elektrochemischen Thermodynamik // Zeitschrift für Physikalische Chemie. Stöchiometrie und Verwandtschaftslehre. 1889. Bd. 3. H. 3. S. 159–163.
Glasser F.P. The system MnO-SiO_2 // American Journal of Science. 1958. Vol. 256. No 6. P. 398–412.
Gök Ö. Catalytic production of antimonate through alkaline leaching of stibnite concentrate // Hydrometallurgy. 2014. Vol. 149. P. 23–30.
Gokhale A.B., Abbaschian G.J. The Cr–Si (Chromium-Silicon) system // Journal of Phase Equilibria. 1987. Vol. 8. No 5. P. 474–484.
Gokhale A.B., Abbaschian G.J. The Mo-Si (Molybdenum-Silicon) system // Journal of Phase Equilibria. 1991. Vol. 12. No 4. P. 493–498.
Gokhale A.B., Abbaschian R. The Ge-Mn (Germanium-Manganese) system // Journal of Phase Equilibria. 1990. Vol. 11. No 5. P. 460–468.
Gorichev I.G., Klyushin N.G. Dependence of standard electrode potentials and free-energies of some oxides on their stoichiometric composition // Russian Journal of Physical Chemistry A. Focus on Chemistry. 1971. Vol. 45. No 5. P. 615.
Goto Y., Kitamura T. On the Phase Diagram of the Cr-O System at High Pressure of Oxygen and Some Properties of the Compound CrO_{2+X} // 粉体および粉末冶金. 1962. Vol. 9. No 3. P. 109–113.
Graedel T. Corrosion mechanisms for silver exposed to the atmosphere // Journal of the Electrochemical Society. 1992. Vol. 139. No 7. P. 1963–1970.
Griffiths R., Pryde J.A., Righini-Brand A. Phase diagram and thermodynamic

data for the hydrogen/vanadium system // Journal of the Chemical Society, Faraday Transactions 1: Physical Chemistry in Condensed Phases. 1972. Vol. 68. P. 2344–2349.

Gschneider Jr. K.A. Rare Earth Alloys: A Critical Review of the Alloy Systems of the Rare Earth, Scandium, and Yttrium Metals. New Jersey: Van Nostrand, 1961. 449 p.

Gude A., Mehrer H. Diffusion in the DO_3 -type intermetallic phase Fe_3Si // Philosophical Magazine A. 1997. Vol. 76. No 1. P. 1–29.

Gudyanga F.. et al. Reductive-oxidative pretreatment of a stibnite flotation concentrate: Thermodynamic and kinetic considerations // Minerals Engineering. 1998. Vol. 11. No 6. P. 563–580.

Guggenheim E.A. The Conceptions of Electrical Potential Difference between Two Phases and the Individual Activities of Ions // The Journal of Physical Chemistry. 1928. Vol. 33. No 6. P. 842–849.

Guggenheim E.A. The Statistical Mechanics of Regular Solutions // Proceedings of the Royal Society A: Mathematical, Physical and Engineering Sciences. 1935. Vol. 148. No 864. P. 304–312.

Haas J.R., Shock E.L., Sassani D.C. Rare earth elements in hydrothermal systems: Estimates of standard partial molal thermodynamic properties of aqueous complexes of the rare earth elements at high pressures and temperatures // Geochimica et Cosmochimica Acta. 1995. Vol. 59. No 21. P. 4329–4350.

Häggström L. et al. Mössbauer Study of Hexagonal FeGe // Physica Scripta. 1975. Vol. 11. No 1. P. 55–59.

Hamilton I., Woods R. An investigation of surface oxidation of pyrite and pyrrhotite by linear potential sweep voltammetry // Journal of Electroanalytical Chemistry and Interfacial Electrochemistry. 1981. Vol. 118. P. 327–343.

Hamilton I., Woods R. An investigation of the deposition and reactions of sulphur on gold electrodes // Journal of applied electrochemistry. 1983. Vol. 13. No 6. P. 783–794.

Harvig H. et al. An Extended Version of the Regular Solution Model for Stoichiometric Phases and Ionic Melts // Acta Chemica Scandinavica. 1971. Vol. 25. P. 3199–3204.

Hasab M., Rashchi F., Raygan S. Chloride–hypochlorite oxidation and leaching of refractory sulfide gold concentrate // Physicochemical Problems of Mineral Processing. 2013. Vol. 49. No 1. P. 61–70.

Hasselbalch K.A. Die Berechnung der Wasserstoffzahl des Blutes aus der freien und gebundenen Kohlensäure desselben, und die Sauerstoffbindung des

Blutes als Funktion der Wasserstoffzahl // Biochemische Zeitschrift. Beiträge zur chemischen Physiologie und Pathologie. 1917. Bd. 78. S. 112–144.
Hayes P.C., Algie S.H. Process Principles in Minerals and Materials Production. Brisbane: Hayes Publishing Co, 1993.
Hazlewood P.E., Singh P.M., Hsieh J.S. Corrosion Behavior of Carbon Steels in Sulfide-Containing Caustic Solutions // Industrial & Engineering Chemistry Research. 2006. Vol. 45. No 23. P. 7789–7794.
Helffrich G., Wood B.J. Subregular model for multicomponent solutions // American Mineralogist. 1989. Vol. 74. No 9–10. P. 1016–1022.
Helgeson H.C. Thermodynamics of hydrothermal systems at elevated temperatures and pressures // American Journal of Science. 1969. Vol. 267. No 7. P. 729–804.
Helgeson H.C., Kirkham D.H. Theoretical prediction of the thermodynamic behavior of aqueous electrolytes at high pressures and temperatures; I, Summary of the thermodynamic/electrostatic properties of the solvent // American Journal of Science. 1974a. Vol. 274. No 10. P. 1089–1198.
Helgeson H.C., Kirkham D.H. Theoretical prediction of the thermodynamic behavior of aqueous electrolytes at high pressures and temperatures; II, Debye-Huckel parameters for activity coefficients and relative partial molal properties // American Journal of Science. 1974b. Vol. 274. No 10. P. 1199–1261.
Helgeson H.C., Kirkham D.H. Theoretical prediction of the thermodynamic properties of aqueous electrolytes at high pressures and temperatures. III. Equation of state for aqueous species at infinite dilution // American Journal of Science. 1976. Vol. 276. No 2. P. 97–240.
Helgeson H.C., Kirkham D.H., Flowers G.C. Theoretical prediction of the thermodynamic behavior of aqueous electrolytes by high pressures and temperatures; IV, Calculation of activity coefficients, osmotic coefficients, and apparent molal and standard and relative partial molal properties to 600 d // American Journal of Science. 1981. Vol. 281. No 10. P. 1249–1516.
Helmholtz H. von. Zur Thermodynamik chemicher Vorgänge. Dritter Beitrag. // Sitzungsberichte der Königlich Preussischen Akademie der Wissenschaften zu Berlin. 1883. H. Jan-Mai. S. 647–665.
Hem J. Chemistry and occurrence of cadmium and zinc in surface water and groundwater // Water Resources Research. 1972. Vol. 8. No 3. P. 661–679.
Hem J., Durum W. Solubility and occurrence of lead in surface water // Journal (American Water Works Association). 1973. Vol. 65. No 8. P. 562–568.
Hem J., Stumm W. Stability Field Diagrams as Aids in Iron Chemistry Studies //

Journal (American Water Works Association). 1961. Vol. 53. No 2. P. 211–232.
Hemmingsen T. The electrochemical reaction of sulphur—oxygen compounds—part I. A review of literature on the electrochemical properties of sulphur/sulphur—oxygen compounds // Electrochimica acta. 1992. Vol. 37. No 15. P. 2775–2784.
Hemmingsen T., Fusek F., Skavås E. Monitoring of the corrosion process on sulphide film formation with electrochemical and optical measurements // Electrochimica Acta. 2006. Vol. 51. No 14. P. 2919–2925.
Hemmingsen T., Lima H. Electrochemical and optical studies of sulphide film formation on carbon steel // Electrochimica Acta. 1998. Vol. 43. No 1–2. P. 35–40.
Henderson L.J. Concerning the relationship between the strength of acids and their capacity to preserve neutrality // American Journal of Physiology. 1908a. Vol. 21. No 2. P. 173–179.
Henderson L.J. The theory of neutrality regulation in the animal organism // American Journal of Physiology. 1908b. Vol. 21. No 4. P. 427–448.
Henríquez E. Corrosion and Scaling Deposits in the Berlín Geothermal Field // Proceedings World Geothermal Congress. 2005. P. 1–4.
Herman P. et al. Chloride monitoring apparatus. Patent, 1997.
Hermansson H. The stability of magnetite and its significance as a passivating film in the repository environment. Stockholm, 2004.
Hildebrand J.H. A Quantitative Treatment of Deviations from Raoult's Law // Proceedings of the National Academy of Sciences of the United States of America. 1927. Vol. 13. No 5. P. 267–272.
Hildebrand J.H. Solubility. XII. Regular solutions[1] // Journal of the American Chemical Society. 1929. Vol. 51. No 1. P. 66–80.
Hillert M., Staffansson L.-I. The Regular Solution Model for Stoichiometric Phases and Ionic Melts // Acta Chemica Scandinavica. 1970. Vol. 24. No 10. P. 3618–3626.
Holland T.J.B., Powell R. An internally consistent thermodynamic data set for phases of petrological interest // Journal of Metamorphic Geology. 1998. Vol. 16. No 3. P. 309–343.
Holland T.J.B., Powell R. An improved and extended internally consistent thermodynamic dataset for phases of petrological interest, involving a new equation of state for solids // Journal of Metamorphic Geology. 2011. Vol. 29. No 3. P. 333–383.
Holleman A.F., Wiberg E., Wiberg N. Holleman-Wiberg's Inorganic Chemistry. Amsterdam: Elsevier, 2001. 1924 p.

Holton O.T., Stevenson J.W. The Role of Platinum in Proton Exchange Membrane Fuel Cells // Platinum Metals Review. 2013. Vol. 57. No 4. P. 259–271.

Hong Z. et al. Water Vapor Corrosion Behavior of Scandium Silicates at 1400°C // Journal of the American Ceramic Society. 2009. Vol. 92. No 1. P. 193–196.

Hongyu C. pb-h_2so_4-h_2o ti xi dian wei -ph tu de zuo yong // Chinese Labat Man. 1995. Vol. 4. P. 22–26.

Horovitz C.T. et al. Scandium Its Occurrence, Chemistry Physics, Metallurgy, Biology and Technology. London: Academic Press, 1975. 614 p.

Horstmann A. Theorie der Dissociation // Justus Liebig's Annalen der Chemie und Pharmacie. 1873. Bd. 170. H. 1–2. S. 192–210.

Horvath J., Hackl L. Check of the potential/ph equilibriumdiagrams of different metal-sulphur-water ternary systems by intermittent galvanostatic polarization method // Corrosion Science. 1965. Vol. 5. No 8. P. 525–538.

Horváth J., Novák M. Potential/pH equilibrium diagrams of some Me–S–H2O ternary systems and their interpretation from the point of view of metallic corrosion // Corrosion Science. 1964. Vol. 4. No 1–4. P. 159–178.

Hu J., Odom T.W., Lieber C.M. Chemistry and Physics in One Dimension: Synthesis and Properties of Nanowires and Nanotubes // Accounts of Chemical Research. 1999. Vol. 32. No 5. P. 435–445.

Huang H.-H. The Eh-pH Diagram and Its Advances // Metals. 2016. Vol. 6. No 1. Article No 23.

Huang J.-H., Rosén E. Determination of Gibbs free energies of formation for the silicates $MnSiO_3$, Mn_2SiO_4 and Mn_7SiO_{12} in the temperature range 1000–1350 K by solid state emf measurements // Physics and Chemistry of Minerals. 1994. Vol. 21. No 4. P. 228–233.

Hubbard K.J., Schlom D.G. Thermodynamic stability of binary oxides in contact with silicon // Journal of Materials Research. 1996. Vol. 11. No 11. P. 2757–2776.

Huber E.J. et al. The heat of formation of scandium oxide // The Journal of Physical Chemistry. 1963. Vol. 67. No 8. P. 1731–1733.

Huber N. The environmental control of sedimentary iron minerals // Economic Geology. 1958. Vol. 53. No 2. P. 123–140.

Hundal H.S. et al. Arsenic mobilization in alluvial soils of Punjab, North–West India under flood irrigation practices // Environmental Earth Sciences. 2012. Vol. 69. No 5. P. 1637–1648.

Hwang C.-A. et al. A simple relation to predict or to correlate the excess functions of multicomponent mixtures // Fluid Phase Equilibria. 1991. Vol. 62. No 3.

P. 173–189.
Inczedy J., Lengye T., Ure A.M. Compendium of Analytical Nomenclature (Definite Rules 1997): The Orange Book. Hoboken: Blackwell Science, 1998. No 3. 964 p.
Ingri N. et al. High-speed computers as a supplement to graphical methods—V1Haltafall, a general program for calculating the composition of equilibrium mixtures // Talanta. 1967. Vol. 14. No 11. P. 1261–1286.
Jackson S.L. Extension of Wohl's ternary asymmetric solution model to four and n components // American Mineralogist. 1989. Vol. 74. No 1–2. P. 14–17.
Jacob K.T. et al. Gibbs' Energy of Formation of Nickel Orthosilicate (Ni_2SiO_4) // High Temperature Materials and Processes. 1986. Vol. 7. No 2–3. P. 141–148.
Jacob K.T., Shukla A.K. Kinetic decomposition of Ni_2SiO_4 in oxygen potential gradients // Journal of Materials Research. 1987. Vol. 2. No 03. P. 338–344.
Jacobs M.H.G., Jong B.H.W.S. de, Oonk H.A.J. The Gibbs energy formulation of α, γ, and liquid Fe_2SiO_4 using Grover, Getting, and Kennedy's empirical relation between volume and bulk modulus // Geochimica et Cosmochimica Acta. 2001. Vol. 65. No 22. P. 4231–4242.
Jacobs M.H.G., Spencer P.J. A critical thermodynamic evaluation of the systems Si–Zn and Al–Si–Zn // Calphad: Computer Coupling of Phase Diagrams and Thermochemistry. 1996. Vol. 20. No 3. P. 307–320.
Jak E. et al. Thermodynamic optimization of the systems PbO-SiO_2, PbO-ZnO, ZnO-SiO_2 and PbO-ZnO-SiO_2 // Metallurgical and Materials Transactions B. 1997. Vol. 28. No 6. P. 1011–1018.
Janeczek J. et al. Chemical composition and Raman spectroscopy of cornubite and its relation to cornwallite in Miedzianka, the Sudety Mts., Poland // Neues Jahrbuch für Mineralogie - Abhandlungen: Journal of Mineralogy and Geochemistry. 2016. Vol. 193. No 3. P. 265–274.
Jerosch-Herold M., Torgeson D.., Barnes R.. Systematics of the anomalous high-temperature ^{45}Sc spin–lattice relaxation in scandium hydrides and deuterides // Journal of Alloys and Compounds. 1997. Vol. 253–254. P. 441–444.
Jiang J.-Q. et al. Laboratory study of electro-coagulation–flotation for water treatment // Water Research. 2002. Vol. 36. No 16. P. 4064–4078.
Jiang Z., Dai X., Middleton H. Effect of silicon on corrosion resistance of Ti–Si alloys // Materials Science and Engineering: B. 2011. Vol. 176. No 1. P. 79–86.
Jichang B., Ke'ren H. shi er wan ji liu suan na cun zai xia zuo duo yuan luo he wu

xian se fan ying de yan jiu // Hua xue shi ji. 1984. Vol. 6. No 2. P. 118–119.
Johansson L., Vannerberg N. The corrosion of unprotected steel in an inert-gas atmosphere containing water vapour, oxygen, nitrogen and different amounts of sulphur dioxide and carbon dioxide // Corrosion Science. 1981. Vol. 21. No 12. P. 863–876.
Johnson J.W., Norton D. Critical phenomena in hydrothermal systems; state, thermodynamic, electrostatic, and transport properties of H_2O in the critical region // American Journal of Science. 1991. Vol. 291. No 6. P. 541–648.
Johnson J.W., Oelkers E.H., Helgeson H.C. SUPCRT92: A software package for calculating the standard molal thermodynamic properties of minerals, gases, aqueous species, and reactions from 1 to 5000 bar and 0 to 1000°C // Computers & Geosciences. 1992. Vol. 18. No 7. P. 899–947.
Jones D.A., Amy P.S. Related Electrochemical Characteristics of Microbial Metabolism and Iron Corrosion // Industrial & Engineering Chemistry Research. 2000. Vol. 39. No 3. P. 575–582.
Jones D., Amy P. A thermodynamic interpretation of microbiologically influenced corrosion // Corrosion. 2002. Vol. 58. No 8. P. 638–645.
Kaesche H. Corrosion of Metals. Berlin, Heidelberg: Springer Berlin Heidelberg, 2003. 594 p.
Kalinkin A. et al. Surface oxidation of synthetic pyrrhotite during wetting-drying treatment // Environmental Engineering Science. 2000. Vol. 17. No 6. P. 329–336.
Kanibolotskii D.S., Lesnyak V. V. Thermodynamic properties of Mn-Si alloys // Russian Metallurgy (Metally). 2006. Vol. 2006. No 3. P. 199–205.
Karakas Z.K. et al. The Effect of the pH of the Solution in the Boron Removal using Polyaluminium Chloride (PAC) Coagulant with Chemical Coagulation Method // Journal of Selçuk University Natural and Applied Science. 2013. Vol. 2. ICOEST Conference 2013 (Part 2). P. 339–346.
Katsura M. Thermodynamics of nitride and hydride formation by the reaction of metals with flowing NH_3 // Journal of Alloys and Compounds. 1992. Vol. 182. No 1. P. 91–102.
Kattner U.R. The thermodynamic modeling of multicomponent phase equilibria // The Journal of The Minerals, Metals & Materials Society. 1997. Vol. 49. No 12. P. 14–19.
Kaufman L. Coupled phase diagrams and thermochemical data for transition metal binary systems-VI // Calphad: Computer Coupling of Phase Diagrams and Thermochemistry. 1979. Vol. 3. No 1. P. 45–76.
Kaufman L. et al. Transformation, stability and Pourbaix diagrams of high

performance corrosion resistant (HPCRM) alloys // Calphad: Computer Coupling of Phase Diagrams and Thermochemistry. 2009. Vol. 33. No 1. P. 89–99.
Kaufman L., Bernstein H. Computer Calculation of Phase Diagrams with Special Reference to Refractory Metals. New York: Academic Press, 1970. 334 p.
Keller L.M., Capitani C. De, Abart R. A Quaternary Solution Model for White Micas Based on Natural Coexisting Phengite–Paragonite Pairs // Journal of Petrology. 2005. Vol. 46. No 10. P. 2129–2144.
Kelsall G., Thompson I. Redox chemistry of H_2S oxidation in the British Gas Stretford Process Part I: Thermodynamics of sulphur-water systems at 298 K // Journal of applied electrochemistry. 1993. Vol. 23. No 4. P. 279–286.
Kelsall G., Thompson I., Francis P. Redox chemistry of H_2S oxidation by the British Gas Stretford process part IV: V-S-H_2O thermodynamics and aqueous vanadium (v) reduction in alkaline solutions // Journal of applied electrochemistry. 1993. Vol. 23. No 5. P. 417–426.
Kelsall G.H. Electrochemical Behavior of Ferrosilicides (Fe_xSi) in Neutral and Alkaline Aqueous Electrolytes // Journal of The Electrochemical Society. 1991a. Vol. 138. No 4. P. 931–940.
Kelsall G.H. Cyanide Oxidation at Nickel Anodes. I . Thermodynamics of CN - H_2O and Ni - CN - H_2O Systems at 298 K // Journal of The Electrochemical Society. 1991b. Vol. 138. No 1. P. 108–116.
Kelsall G.H., Robbins D.J. Thermodynamics of Ti-H_2O-F(-Fe) systems at 298 K // Journal of Electroanalytical Chemistry and Interfacial Electrochemistry. 1990. Vol. 283. No 1–2. P. 135–157.
Keulks G.W. et al. The catalytic oxidation of propylene IV. Preparation and characterization of $alpha;-bismuth molybdate // Journal of Catalysis. 1974. Vol. 34. No 1. P. 79–97.
Kilpatrick M., Pokras L. Acid Dissociation of the Aquoscandium Ions // Journal of The Electrochemical Society. 1953. Vol. 100. No 2. P. 85–92.
Kilpatrick M., Pokras L. The Acid Dissociation of the Aquoscandium Ions // Journal of The Electrochemical Society. 1954. Vol. 101. No 1. P. 39–43.
Kirchhoff G. Ueber einen Satz der mechanischen Wärmetheorie, und einige Anwendungen desselben // Poggendorf's Annalen der Physik und Chemie. 1858. Bd. 103. H. 2. S. 177–206.
Kirchhoff G. Gesammelte Abhandlungen. Leipzig: J. A. Barth, 1882. 641 s.
Kishimoto H. et al. Sulfur Poisoning on SOFC Ni Anodes: Thermodynamic Analyses within Local Equilibrium Anode Reaction Model // Journal of The Electrochemical Society. 2010. Vol. 157. No 6. P. B802.
Kiss L. Kinetics of Electrochemical Metal Dissolution. Budapest: Akademiai

Kiado, 1988.
Klyushin N.G., Gorichev I.G., Malov N. V. Stability regions of ferric oxides in an iron - water system // Zhurnal Fizicheskoi Khimii. 1973. Vol. 45. No 4. P. 834–837.
Ko M., Lichti K. Corrosion of Cu-Base Alloys in Geothermal Condensates // Proceedings World Geothermal Congress, 2010. P. 1–10.
Kobayashi T., Takei H. Chemical vapor deposition of scandium hydride // Journal of Crystal Growth. 1978. Vol. 45. P. 29–36.
Kobayashi T., Takei H. Chemical vapour deposition of scandium metal // Journal of the Less Common Metals. 1980. Vol. 70. No 2. P. 243–252.
KocabaĞ D. Sülfür Cevherlerinin Flotasyonu 1: Sülfür Minerallerinin Özellikleri ve Flotasyona Etkileri // Madencilik. 1992. Vol. 31. No 3. P. 33–50.
Koch D.F.A. Electrochemisty of sulfide minerals // Modern aspects of electrochemistry / ed. J.O. Bockris, B.E. Conway, R.E. White. New York: Plenum, 1975. P. 211–238.
Komissarova L.N., Prutkova N.M., Pushkina G.Y. Stability of hydroxo-ions of scandium in aqueous solution // Russian Journal of Inorganic Chemistry. 1971. Vol. 16. No 7. P. 954–956.
Korosteleva E.N., Pribytkov G.A., Gurskikh A. V. Bulk changes and structurization in solid-phase sintering of titanium–silicon powder mixtures // Powder Metallurgy and Metal Ceramics. 2009. Vol. 48. No 1–2. P. 8–12.
Korzhavyi P.A. et al. Thermodynamics of Stable and Metastable Cu-O-H Compounds // Solid State Phenomena. 2011. Vol. 172–174. P. 973–978.
Kounde B., Raharinaivo A., Olowe A. Mössbauer characterization of the corrossion products of steels in civil works: Suspension bridge and reinforced concrete // Hyperfine Interactions. 1989. Vol. 46. No 1–4. P. 421–428.
Krupp R.E., Weiser T. On the stability of gold-silver alloys in the weathering environment // Mineralium Deposita. 1992. Vol. 27. No 4. P. 268–275.
Kubal M., Panacek F. Potential-pH diagram for Fe–H_2O–citric acid system // British Corrosion Journal. 1995. Vol. 30. No 4. P. 309–311.
Kubota B. Decomposition of Higher Oxides of Chromium Under Various Pressures of Oxygen // Journal of the American Ceramic Society. 1961. Vol. 44. No 5. P. 239–248.
Kuprashvili I.S., Naumkin O.P., Savitskii E.M. Phase diagram of the Scandium - Oxygen system // Inorganic Materisla. 1969. Vol. 5. No 12. P. 1809–1813.
Kurov O. V. Plotting Alloy Corrosion State Diagrams // Corrosion. 2001. Vol. 57. No 6. P. 502–507.

Kurov O. V. Experimental corrosion diagrams of metals // Corrosion Engineering, Science and Technology. 2013. Vol. 48. No 1. P. 55–64.
Kurov O.V. Experimental plotting of metal corrosion diagrams // Materials and Corrosion. 2007. Vol. 58. No 7. P. 533–540.
Laar J.J. van. Die Schmelz- oder Erstarrungkurven bei binären Systemen, wenn die feste Phase ein Gemisch (amorphe feste Lösung oder Mischkristalle) bei beiden Komponenten ist. Erster Teil. Mit 19 Figuren im Text // Zeitschrift für Physikalische Chemie. Stöchiometrie und verwandtschaftslehre. 1908a. Bd. 63. H. 2. S. 216–253.
Laar J.J. van. Die Schmelz- oder Erstarrungkurven bei binären Systemen, wenn die feste Phase ein Gemisch (amorphe feste Lösung oder Mischkristalle) bei beiden Komponenten ist. Zweiter Teil. Mit 34 Figuren im Text // Zeitschrift für Physikalische Chemie. Stöchiometrie und verwandtschaftslehre. 1908b. Bd. 64. H. 3. S. 257–297.
Laar J.J. van. Beschouwingen over eenige fundamenteele eigenschappen von den thermodynamischen potentiaal // Chemisch Weekblad. 1908c. Bd. 6. S. 1027–1041.
Laar J.J. van. Über Dampfspannungen von binären Gemischen. Mit 6 Figuren im Text // Zeitschrift für Physikalische Chemie. Stöchiometrie und verwandtschaftslehre. 1910. Bd. 72. H. 6. S. 723–751.
Laar J.J. van. Zur Theorie der Dampfspannungen von binären Gemischen. Erwiderung an Herrn F. Dolezalek // Zeitschrift für Physikalische Chemie. Stöchiometrie und verwandtschaftslehre. 1913. Bd. 83. H. 5. S. 599–608.
Lacaze J., Sundman B. An assessment of the Fe-C-Si system // Metallurgical Transactions A. 1991. Vol. 22. No 10. P. 2211–2223.
Lagrange J.L. de. Leçons élémentaires sur les mathématiques données à l'École Normale en 1795 // Journal de l'École polytechnique / publié par le Conseil d'instruction de cet établissement. 1812. T. 2. P. 173–278.
Larsen D., Linkson P. Thermodynamics of the zinc-sulfur dioxide-water system // Metallurgical Transactions B. 1993. Vol. 24. No 3. P. 409–417.
Larsen J., Oil M., Hilbert L. Investigation into Under Deposit Corrosion in Halfdan Production Tubulars // CORROSION 2014: NACE International, 2014. P. 1–16.
Lasebikan B.A. et al. The effect of hydrogen sulphide on ammonium bisulphite when used as an oxygen scavenger in aqueous solutions // Corrosion Science. 2011. Vol. 53. No 12. P. 4014–4025.
Lau S.S. et al. Iron silicide thin film formation at low temperatures // Thin Solid Films. 1975. Vol. 25. No 2. P. 415–422.
Lee B., Lee S.K., Lee D.N. Formulation of the $A_2/B_2/DO_3$ atomic ordering energy

and a thermodynamic analysis of the Fe-Si system // Calphad: Computer Coupling of Phase Diagrams and Thermochemistry. 1987. Vol. 11. No 3. P. 253–270.

Lee J.B. Elevated Temperature Potential-pH Diagrams for the Cr-H_2O, Ti-H_2O, Mo-H_2O, and Pt-H_2O Systems // Corrosion. 1981. Vol. 37. No 8. P. 467–481.

Lee P.S. et al. On the Ni–Si phase transformation with/without native oxide // Microelectronic Engineering. 2000. Vol. 51–52. P. 583–594.

Levenspiel O. Chemical Reaction Engineering. New York: Wiley, 1999. 668 p.

Lewis D. Some aspects of electrochemical thermodynamics and equilibrium diagrams for aqueous systems at elevated temperatures and for simple molten salt systems // Journal of Inorganic and Nuclear Chemistry. 1971a. Vol. 33. No 7. P. 2121–2140.

Lewis G.N. The Development and Application of a General Equation for Free Energy and Physico-chemical Equilibrium. // Proceedings of the American Academy of Arts and Sciences. 1899. Vol. 35. No 1. P. 1–38.

Lewis G.N. VIII. Outlines of a New System of Thermodynamic Chemistry // Proceedings of the American Academy of Arts and Sciences. 1907. Vol. 43. P. 257–294.

Lewis G.N. The Osmotic Pressure of Concentrated Solutions, and the Laws of the Perfect Solution // Journal of the American Chemical Society. 1908. Vol. 30. No 5. P. 668–683.

Lewis G.N., Randall M. Thermodynamics and the free energy of chemical substances. New York: McGraw-Hill, 1923. 653 p.

Liang H., Chang Y.A. A Thermodynamic Description for the Al-Cu-Zn System // Journal of Phase Equilibria. 1998. Vol. 19. No 1. P. 25–37.

Liborio L., Harrison N. Thermodynamics of oxygen defective Magnéli phases in rutile: A first-principles study // Physical Review B. 2008. Vol. 77. No 10. P. 104104.

Lichti K.A. Forgotten phenomenon of materials selection and use in geothermal energy applications // Materials at High Temperatures. 2007. Vol. 24. No 4. P. 351–363.

Lieberman M.L., Wahlbeck P.G. The Thermodynamics of the Scandium-Hydrogen System[1,2] // The Journal of Physical Chemistry. 1965. Vol. 69. No 10. P. 3514–3519.

Lin J.-F. Iron-Silicon Alloy in Earth's Core? // Science. 2002. Vol. 295. No 5553. P. 313–315.

Lindholm M., Sundman B. A thermodynamic evaluation of the nickel-silicon system // Metallurgical and Materials Transactions A. 1996. Vol. 27. No 10.

P. 2897–2903.
Lindqvist-Reis P., Persson I., Sandström M. The hydration of the scandium(iii) ion in aqueous solution and crystalline hydrates studied by XAFS spectroscopy, large-angle X-ray scattering and crystallography // Dalton Transactions. 2006. No 32. P. 3868–3878.
Lisak G. et al. A study on lowering the detection limit with solid-state lead-selective electrodes. // Talanta. 2010. Vol. 83. No 2. P. 436–440.
Liu H., Zhang C. Computation of multi-component E-pH predominance diagrams // Calphad: Computer Coupling of Phase Diagrams and Thermochemistry. 2001. Vol. 25. No 3. P. 363–380.
Livingston R. A. Influence of the environment on the patina of the Statue of Liberty // Environmental Science & Technology. 1991. Vol. 25. No 8. P. 1400–1408.
Lukas H.L., Fries S.G., Sundman B. Computational Thermodynamics: The Calphad Method. Cambridge: Cambridge University Press, 2007. 323 p.
Lukashenko G.., Polotskaya R.., Sidorko V.. Thermodynamic properties of scandium, lanthanum, neodymium and gadolinium silicides and germanides // Journal of Alloys and Compounds. 1992. Vol. 179. No 1–2. P. 299–305.
Macdonald D., Hyne J. The thermodynamics of the iron/sulphur/water system. Pinawa, Manitoba, 1979. Report No. AECL-5811 p.
Magnéli A. Structure of β-Tungsten Oxide // Nature. 1950. Vol. 165. No 4192. P. 356–357.
Magnéli A. et al. Identification of Molybdenum and Tungsten Oxides by X-Ray Powder Patterns // Analytical Chemistry. 1952. Vol. 24. No 12. P. 1998–2000.
Magnéli A. Non-stoichiometry and structural disorder in some families of inorganic compounds // Pure and Applied Chemistry. 1978. Vol. 50. No 11–12. P. 1261–1271.
Mahadevaiah N., Venkataramani B., Jai Prakash B.S. Restrictive Entry of Aqueous Molybdate Species into Surfactant Modified Montmorillonite: A Breakthrough Curve Study // Chemistry of Materials. 2007. Vol. 19. No 18. P. 4606–4612.
Majer V., Sedlbauer J., Wood R.H. Calculation of standard thermodynamic properties of aqueous electrolytes and nonelectrolytes // Aqueous Systems at Elevated Temperatures and Pressures. Amsterdam: Elsevier, 2004. P. 99–147.
Majima H. How oxidation affects selective flotation of complex sulphide ores // Canadian Metallurgical Quarterly. 1969. Vol. 8. No 3. P. 269–273.

Makgamatha K., Mulaba-Bafubiandi A., Adams F. Potentiodynamic Polarisation and Chronopotentiometric Studies of Cobalt-Copper Oxidised Ore in Sulphuric Acid // International Journal of Research in Chemical, Metallurgical and Civil Engineering. 2014. Vol. 1. No 1. P. 54–60.

Malmberg C.G., Maryott A.A. Dielectric constant of water from 0 to 100 C // Journal of Research of the National Bureau of Standards. 1956. Vol. 56. No 1. P. 1–8.

Marcus P. Surface science approach of corrosion phenomena // Electrochimica Acta. 1998. Vol. 43. No 1–2. P. 109–118.

Marcus P. Corrosion mechanisms in theory and practice. 3rd ed. Taylor & Francis, 2011.

Marcus P., Protopopoff E. Potential-pH Diagrams for Adsorbed Species Application to Sulfur Adsorbed on Iron in Water at 25° and 300° C // Journal of The Electrochemical Society. 1990. Vol. 137. No 9. P. 2709–2712.

Marcus P., Protopopoff E. Potential pH diagrams for sulfur and oxygen adsorbed on nickel in water at 25 and 300 C // Journal of The Electrochemical Society. 1993. Vol. 140. No 6. P. 1571–1575.

Marcus P., Protopopoff E. Potential-pH Diagrams for Sulfur and Oxygen Adsorbed on Chromium in Water // Journal of The Electrochemical Society. 1997a. Vol. 144. No 5. P. 1586–1590.

Marcus P., Protopopoff E. Thermodynamics of thiosulfate reduction on surfaces of iron, nickel and chromium in water at 25 and 300 °C // Corrosion Science. 1997b. Vol. 39. No 9. P. 1741–1752.

Margules M. Über die Zusammensetzung der gesättigten Dämpfe von Mischungen // Sitzungsberichte der Kaiserlichen Akademie der Wissenschaften. Mathematisch-Naturwissenschaftliche Classe. Abtheilung 2. Mathematik, Physik, Chemie, Physiologie, Meteorologie, physische Geographie und Astronomie. 1895. Bd. 104. S. 1243–1278.

Marinakis K.I., Kelsall G.H. The surface chemical properties of scheelite ($CaWO_4$). I. The scheelite/water interface and $CaWO_4$ solubility // Colloids and Surfaces. 1987. Vol. 25. No 2–4. P. 369–385.

Markos'yan G.N., Sirota D.S., Pchel'nikov A.P. Corrosion of Hydrides of Nickel and Cu30Ni Alloy in Oxygen Containing Solutions // Protection of Metals. 2005. Vol. 41. No 4. P. 358–362.

Marques R.N. et al. Complexation of some trivalent lanthanides, scandium(III) and thorium(IV) by benzylidenepyruvates in aqueous solution // Journal of Alloys and Compounds. 1997. Vol. 249. No 1–2. P. 102–105.

Marsh K.N. A general method for calculating the excess Gibbs free energy from isothermal vapour-liquid equilibria // The Journal of Chemical

Thermodynamics. 1977. Vol. 9. No 8. P. 719–724.
Mattsson E. Stress corrosion in brass considered against the background of potential/pH diagrams // Electrochimica Acta. 1961. Vol. 3. No 4. P. 279–291.
McCafferty E. Thermodynamics of Corrosion: Pourbaix Diagrams // Introduction to Corrosion Science. New York, NY: Springer New York, 2010. P. 95–117.
McCarty C.G., Vitz E. pH Paradoxes: Demonstrating That It Is Not True That pH ≡ -log[H^+] // Journal of Chemical Education. 2006. Vol. 83. No 5. P. 752.
McCormick S., Dayananda M., Grace R. Diffusion-limited sulfidation of wustite // Metallurgical and Materials Transactions B. 1975. Vol. 6. No 1. P. 55–61.
McNaught A.D., Wilkinson A. Compendium of Chemical Terminology: The Gold Book. 2nd ed. Hoboken: Blackwell Science, 1997. 464 p.
McNeil M., Jones J., Little B. Production of sulfide minerals by sulfate-reducing bacteria during microbiologically influenced corrosion of copper // Corrosion. 1991. Vol. 47. No 9. P. 674–677.
McNeil M., Little B. The use of mineralogical data in interpretation of long-term microbiological corrosion processes: sulfiding reactions // Journal of the American Institute for Conservation. 1999. Vol. 38. No 2. P. 186–199.
McNeil M.B., Mohr D.W. Sulfate Formation During Corrosion of Copper Alloy Objects // MRS Proceedings. 1992. Vol. 267. P. 1047.
McNeil M.B., Mohr D.W. Formation of copper—iron sulfide minerals during corrosion of artifacts and possible implications for pseudogilding // Geoarchaeology. 1993. Vol. 8. No 1. P. 23–33.
Meijering E. A chronology of interpolation: from ancient astronomy to modern signal and image processing // Proceedings of the Institute of Electrical and Electronics Engineers. 2002. Vol. 90. No 3. P. 319–342.
Meyer F.H. et al. Corrosion Products of Mild Steel In Hydrogen Sulfide Environments // Corrosion. 1958. Vol. 14. No 2. P. 69–75.
Michaelis L. Oxidation-Reduction Potentials. Philadelphia: J. B. Lippincott Company, 1930. 199 p.
Michałowska-Kaczmarczyk A.M. et al. “Why Not Stoichiometry” Versus “Stoichiometry—Why Not?” Part II: GATES in Context with Redox Systems // Critical Reviews in Analytical Chemistry. 2015. Vol. 45. No 3. P. 241–269.
Michałowska-Kaczmarczyk A.M., Toporek M., Michałowski T. Speciation Diagrams in Dynamic Iodide + Dichromate System // Electrochimica Acta. 2015. Vol. 155. P. 217–227.
Miedema A.R. A simple model for alloys. Il, The influence of ionicity on the stability and other physical properties of alloys // Philips Technical Review.

1973a. Vol. 33. P. 196–202.
Miedema A.R. A simple model for alloys. Il, The influence of ionicity on the stability and other physical properties of alloys // Philips Technical Review. 1973b. Vol. 33. P. 149–160.
Miettinen J. Thermodynamic description of the Cu–Mn–Ni system at the Cu–Ni side // Calphad: Computer Coupling of Phase Diagrams and Thermochemistry. 2003a. Vol. 27. No 2. P. 147–152.
Miettinen J. Thermodynamic description of the Cu–Mn–Si system in the copper-rich corner // Calphad: Computer Coupling of Phase Diagrams and Thermochemistry. 2003b. Vol. 27. No 4. P. 395–401.
Miettinen J. Thermodynamic description of the Cu–Ni–Si system in the copper-rich corner above 700 ∘C // Calphad: Computer Coupling of Phase Diagrams and Thermochemistry. 2005. Vol. 29. No 3. P. 212–221.
Miettinen J. Thermodynamic description of the Cu–Si–Zn system in the copper-rich corner // Calphad: Computer Coupling of Phase Diagrams and Thermochemistry. 2007. Vol. 31. No 4. P. 422–427.
Miki T., Morita K., Sano N. Thermodynamic properties of titanium and iron in molten silicon // Metallurgical and Materials Transactions B. 1997. Vol. 28. No 5. P. 861–867.
Miletich R. et al. High-pressure crystal chemistry of chromous orthosilicate, Cr_2SiO_4. A single-crystal X-ray diffraction and electronic absorption spectroscopy study // Physics and Chemistry of Minerals. 1999. Vol. 26. No 6. P. 446–459.
Minzari D. et al. Morphological study of silver corrosion in highly aggressive sulfur environments // Engineering Failure Analysis. 2011. Vol. 18. No 8. P. 2126–2136.
Mishra K. Electrodeposition and Characterization of SnS Thin Films // Journal of The Electrochemical Society. 1989. Vol. 136. No 7. P. 1915–1923.
Missaoui K. et al. Boron Removal by Electrocoagulation Using Full Factorial Design // Journal of Water Resource and Protection. 2013. Vol. 5. No 9. P. 867–875.
Mittal A. et al. Some Thermodynamic Aspects of the Oxides of Chromium // Metallurgical and Materials Transactions B. 2014. Vol. 45. No 2. P. 338–344.
Moeller T., Kremers H.E. The Basicity Characteristics of Scandium, Yttrium, and the Rare Earth Elements. // Chemical Reviews. 1945. Vol. 37. No 1. P. 97–159.
Moiseev G.K., Vatolin N.A. Estimation of the thermochemical properties and stability of Cu_2O_3 // Russian Journal of Physical Chemistry A. Focus on

Chemistry. 1997. Vol. 71. No 3. P. 335–337.
Molinero J., Samper J. Large-scale modeling of reactive solute transport in fracture zones of granitic bedrocks. // Journal of contaminant hydrology. 2006. Vol. 82. No 3–4. P. 293–318.
Morita K., Miki T. Thermodynamics of solar-grade-silicon refining // Intermetallics. 2003. Vol. 11. No 11–12. P. 1111–1117.
Mortimer R. Mathematics for Physical Chemistry. Amsterdam: Elsevier, 2013. 272 p.
Mukhopadhyay B., Basu S., Holdaway M.J. A discussion of Margules-type formulations for multicomponent solutions with a generalized approach // Geochimica et Cosmochimica Acta. 1993. Vol. 57. No 2. P. 277–283.
Mulaudzi N., Mahlangu T. Oxidative precipitation of Mn (II) from cobalt leach solutions using dilute SO_2/air gas mixture // The Journal of The Southern African Institute of Mining and Metallurgy. 2009. Vol. 109. P. 375–382.
Murarka S.P. Transition Metal Silicides // Annual Review of Materials Science. 1983. Vol. 13. No 1. P. 117–137.
Murray R.C.J., Cubicciotti D. Thermodynamics of Aqueous Sulfur Species to 300°C and Potential-pH Diagrams // Journal of The Electrochemical Society. 1983. Vol. 130. No 4. P. 866–869.
Mycroft J.R. et al. Detection of sulphur and polysulphides on electrochemically oxidized pyrite surfaces by X-ray photoelectron spectroscopy and Raman spectroscopy // Journal of Electroanalytical Chemistry and Interfacial Electrochemistry. 1990. Vol. 292. No 1–2. P. 139–152.
Naje A.S. et al. Treatment performance of textile wastewater using electrocoagulation (EC) process under combined electrical connection of electrodes // International Journal of Electrochemical Science. 2015. Vol. 10. No 7. P. 5924–5941.
Navrotsky A. Thermodynamics of formation of the silicates and germanates of some divalent transition metals and of magnesium // Journal of Inorganic and Nuclear Chemistry. 1971. Vol. 33. No 12. P. 4035–4050.
Navrotsky A., Pintchovski F.S., Akimoto S.-I. Calorimetric study of the stability of high pressure phases in the systems CoO–SiO_2 and "FeO"–SiO_2, and calculation of phase diagrams in MO–SiO_2 systems // Physics of the Earth and Planetary Interiors. 1979. Vol. 19. No 4. P. 275–292.
Nernst W. Ueber die electromotorischen Kräfte, welche durch den Magnetismus in von einem Wärmestrome durchflossenen Metallplatten geweckt werden // Wiedermann's Annalen der Physik und Chemie. 1887. Bd. 31. H. 8. S. 760–789.
Nernst W. Die elektromotorische Wirksamkeit der Ionen // Zeitschrift für

Physikalische Chemie. Stöchiometrie und Verwandtschaftslehre. 1889a. Bd. 4. H. 2. S. 129–181.
Nernst W. Zur Theorie umkehrbarer galvanischer Elemente // Sitzungsberichte der Königlich Preusßichen Akademie der Wissenschaften zu Berlin. 1889b. Bd. 1889. H. 1. S. 83–98.
Ness P. Gegenwärtiger stand der forschungsarbeiten an positiven elektroden in bleiakkumulatoren // Electrochimica Acta. 1967. Vol. 12. No 2. P. 161–178.
Niessen A.K. et al. Model predictions for the enthalpy of formation of transition metal alloys II // Calphad: Computer Coupling of Phase Diagrams and Thermochemistry. 1983. Vol. 7. No 1. P. 51–70.
Nila C., González I. Thermodynamics of Cu - H_2SO_4 -Cl^- and Cu-NH_4Cl-H_2O based on predominance-existence diagrams and Pourbaix-type diagrams // Hydrometallurgy. 1995. Vol. 42. No 1. P. 63–82.
Ning J. et al. A Thermodynamic Study of Hydrogen Sulfide Corrosion of Mild Steel // Corrosion. 2014. Vol. 70. No 4. P. 375–389.
Nunes C.A., Coelho G.C., Ramos A.S. On the invariant reactions in the Mo-rich portion of the Mo-Si system // Journal of Phase Equilibria. 2001. Vol. 22. No 5. P. 556–559.
Oelkers E.H. et al. Summary of the Apparent Standard Partial Molal Gibbs Free Energies of Formation of Aqueous Species, Minerals, and Gases at Pressures 1 to 5000 Bars and Temperatures 25 to 1000 °C // Journal of Physical and Chemical Reference Data. 1995. Vol. 24. No 4. P. 1401–1560.
Ohoyama T. X-ray and Magnetic Studies of the Manganese-Germanium System // Journal of the Physical Society of Japan. 1961. Vol. 16. No 10. P. 1995–2002.
Oka Y. Studies of the Fundamental Reactions in Analytical Chemistry. I // Nippon Kagaku Kaishi. 1938. Vol. 59. No 8. P. 971–1013.
Okamoto H. Cr-Si (Chromium-Silicon) // Journal of Phase Equilibria. 1997. Vol. 18. No 2. P. 222.
Okamoto H. Cr-Si (Chromium-Silicon) // Journal of Phase Equilibria. 2001. Vol. 22. No 5. P. 593.
Okamoto H. Si-V (Silicon-Vanadium) // Journal of Phase Equilibria and Diffusion. 2010. Vol. 31. No 4. P. 409–410.
Okamoto H. Mo-Si (Molybdenum-Silicon) // Journal of Phase Equilibria and Diffusion. 2011. Vol. 32. No 2. P. 176–176.
Padilha A.C.M. et al. Ti_nO_{2n-1} Magnéli phases studied using density functional theory // Physical Review B. 2014. Vol. 90. No 3. P. 035213.
Pandit V., Keswani M. Removal of gold particles from chromium oxynitride surface with dilute sulfuric acid solutions // ECS Transactions. 2007. Vol.

11. No 2. P. 471–478.
Pankratz L.B., Stuve J.M., Gokcen M.A. Thermodynamic Data for Mineral Technology. USA: Bureau of Mines, 1984. 360 p.
Parent A.R., Crabtree R.H., Brudvig G.W. Comparison of primary oxidants for water-oxidation catalysis. // Chemical Society reviews. 2013. Vol. 42. No 6. P. 2247–2252.
Parsa J.B. et al. Removal of Acid Brown 14 in aqueous media by electrocoagulation: Optimization parameters and minimizing of energy consumption // Desalination. 2011. Vol. 278. No 1–3. P. 295–302.
Paschen S. et al. Low-temperature transport, thermodynamic, and optical properties of FeSi // Physical Review B. 1997. Vol. 56. No 20. P. 12916–12930.
Patrin G.S. et al. Nonstoichiometry and low-temperature magnetic properties of FeSi crystals // Physics of the Solid State. 2006. Vol. 48. No 4. P. 700–704.
Paul A.D. The chloride and bromide complexing of scandium (III) and yttrium (III) in aqueous solution // The Journal of Physical Chemistry. 1962. Vol. 66. No 7. P. 1248–1252.
Pavlov D. Lead-Acid Batteries: Science and Technology. : Elsevier, 2011. 29-114 p.
Peng D.-Y. Extending the Van Laar Model to Multicomponent Systems // The Open Thermodynamics Journal. 2010. Vol. 4. No 1. P. 129–140.
Pesterfield L.L. et al. Pourbaix (E –pH-M) Diagrams in Three Dimensions // Journal of Chemical Education. 2012. Vol. 89. No 7. P. 891–899.
Peters E. Direct leaching of sulfides: chemistry and applications // Metallurgical Transactions B. 1976. Vol. 7. No 4. P. 505–517.
Peters R. Ueber Oxydations- und Reduktionsketten und den Einfluss komplexer Ionen auf ihre elektromotorische Kraft // Zeitschrift für Physikalische Chemie. Stöchiometrie und verwandtschaftslehre. 1898. Bd. 26. H. 2. S. 193–236.
Petrů F., Brožek V., Dufek V. Contribution to the chemistry of the rarer elements. LXI. Contribution to the study of the structure of scandium monoxide // Collection of Czechoslovak Chemical Communications. 1970. Vol. 35. No 4. P. 1041–1046.
Phillipson S.., Romberger S.. Volcanic stratigraphy, structural controls, and mineralization in the san cristobal Ag–Zn–Pb deposit, southern bolivia // Journal of South American Earth Sciences. 2004. Vol. 16. No 8. P. 667–683.
Piet Lens P.N.L.L.L.H.P. Environmental Technologies to Treat Sulfur Pollution: Principles and Engineering. IWA Publishing, 2000.
Plyasunov A. V., Shock E.L. Correlation strategy for determining the parameters

of the revised Helgeson-Kirkham-Flowers model for aqueous nonelectrolytes // Geochimica et Cosmochimica Acta. 2001. Vol. 65. No 21. P. 3879–3900.

Poisot-Díaz M.E., González I., Lapidus G.T. Electrodeposition of a Silver-Gold Alloy (DORÉ) from Thiourea Solutions in the Presence of Other Metallic Ion Impurities // Hydrometallurgy. 2008. Vol. 93. No 1–2. P. 23–29.

Pokrovskii V.A., Helgeson H.C. Calculation of the standard partial molal thermodynamic properties of KCl^{o} and activity coefficients of aqueous KCl at temperatures and pressures to 1000°C and 5 kbar // Geochimica et Cosmochimica Acta. 1997. Vol. 61. No 11. P. 2175–2183.

Pope M.T., Dale B.W. Isopoly-vanadates, -niobates, and -tantalates // Quarterly Reviews, Chemical Society. 1968. Vol. 22. No 4. P. 527–548.

Post K., Robins R.G. Thermodynamic diagrams for the vanadium-water system at 298·15K // Electrochimica Acta. 1976. Vol. 21. No 6. P. 401–405.

Pourbaix A., Aguiar L., Clarinval A. Local corrosion processes in the presence of sulphate-reducing bacteria: measurements under biofilms // Corrosion science. 1993. Vol. 35. No 1–4. P. 693–698.

Pourbaix A., Marquez Jacone M. The Enhancement of Reaction Kinetics by Bacteria // Microbial Corrosion 1: Proceedings of the 1. European Federation of Corrosion Workshop on Microbial Corrosion. Sintra: Springer Science & Business Media, 1988. P. 29–39.

Pourbaix M. Atlas of Electrochemical Equilibria in Aqueous Solutions. Oxford: Pergamon Press Ltd, 1966.

Pourbaix M. Diagrams of Chemical and Electrochemical Equilibria in the Presence of Oxygen and Sulphur. 1984.

Pourbaix M. et al. Some oxidation equilibria: towards the setting-up of atlases of chemical and electrochemical equilibria in the presence of a gaseous phase // Corrosion science. 1986. Vol. 26. No I. P. 873–917.

Pourbaix M. Thermochemical diagrams: Some applications to the study of high temperature corrosion // Materials Science and Engineering. 1987. Vol. 87. P. 303–317.

Pourbaix M., Pourbaix A. Potential-pH equilibrium diagrams for the system S-H_2O from 25 to 150 ° C : Influence of access of oxygen in sulphide solutions // Geochimica et Cosmochimica Acta. 1992. Vol. 56. No 8. P. 3157–3178.

Pourbaix M., Zhang H. Equilibrium diagrams of systems O-S, O-Al, O-Cr, O-Fe, O-S-Al, O-S-Cr and O-S-Fe. Towards a thermodynamic predetermination of the circumstances of dry // Werkstoffe und Korrosion. 1988. Bd. 39. H. 11. S. 504–511.

Pourbaix M.J.N. Thermodynamique des solutions aqueuses diluées:

représentation graphique du rôle du pH et du potentiel. Dissertation. 1945.
Predel B. Cr-Cs ... Cu-Zr. Berlin, Heidelberg: Springer, 1994. 354 p.
Predel B. Ge-Mn (Germanium-Manganese) // Ga-Gd – Hf-Zr. Landolt-Börnstein - Group IV Physical Chemistry (Numerical Data and Functional Relationships in Science and Technology), vol. 5f. Berlin/Heidelberg: Springer-Verlag, 1996. P. 1–5.
Predel B. O-Sc (Oxygen-Scandium) // Ni-Np – Pt-Zr. Berlin/Heidelberg: Springer-Verlag, 1998. P. 1–2.
Prengaman R.D. New low-antimony alloy for straps and cycling service in lead–acid batteries // Journal of Power Sources. 2006. Vol. 158. No 2. P. 1110–1116.
Protopopoff E., Marcus P. Potential–pH diagrams for sulfur and hydroxyl adsorbed on copper surfaces in water containing sulfides, sulfites or thiosulfates // Corrosion Science. 2003. Vol. 45. No 6. P. 1191–1201.
Protopopoff E., Marcus P. Potential–pH diagram for sulfur and hydroxyl adsorbed on silver in water containing sulfides // Electrochimica Acta. 2012. Vol. 63. P. 22–27.
Puente-Siller D.M., Fuentes-Aceituno J.C., Nava-Alonso F. A kinetic–thermodynamic study of silver leaching in thiosulfate–copper–ammonia–EDTA solutions // Hydrometallurgy. 2013. Vol. 134–135. P. 124–131.
Puigdomenech I., Taxen C. Thermodynamic data for copperImplications for the corrosion ofcopper under repository conditions. Stockholm, 2000.
Qingfeng Y. et al. Thermodynamic analyses for S-H_2O system at 25 C // Transactions of Nonferrous Metals Society of China. 1997. Vol. 7. No 1. P. 27–32.
Qingfeng Y., Xiaoping L., Xiulin Z. Thermodynamic analysis for a new process of electrochemical decomposition of aqueous hydrogen sulfide solution into sulfur and hydrogen gas // Journal of Hunan University of Science & Technology (Natural Science Edition). 2004. Vol. 4. P. 83–87.
Racault C., Langlais F., Bernard C. On the chemical vapour deposition of Ti_3SiC_2 from $TiCl_4$-$SiCl_4$-CH_4-H_2 gas mixtures // Journal of Materials Science. 1994. Vol. 29. No 19. P. 5023–5040.
Rahmel A. Thermodynamische Gesichtspunkte der Korrosion in Sulfatschmelzen: Die Konstruktion und Anwendung von E/log p so_3 Diagrammen // Electrochimica Acta. 1968. Vol. 13. No 3. P. 495–505.
Rayner-Canham G. Periodic patterns: the Group (n) and Group (n + 10) linkage // Foundations of Chemistry. 2013. Vol. 15. No 2. P. 229–237.
Reader A.H. et al. Transition metal silicides in silicon technology // Reports on Progress in Physics. 1993. Vol. 56. No 11. P. 1397–1467.

Redlich O., Kister A.T. Algebraic representation of thermodynamic properties and the classification of solutions // Industrial and Engineering Chemistry. 1948. Vol. 40. No 2. P. 345–348.

Refait P. et al. Green rusts in electrochemical and microbially influenced corrosion of steel // Comptes Rendus Geoscience. 2006. T. 338. N. 6–7. P. 476–487.

Renon H., Prausnitz J.M. Local compositions in thermodynamic excess functions for liquid mixtures // AIChE Journal. 1968. Vol. 14. No 1. P. 135–144.

Revie R.W., Uhlig H.H. Corrosion and Corrosion Control: An Introduction to Corrosion Science and Engineering. 4th ed.Hoboken, NJ, USA: John Wiley & Sons, Inc., 2008. 513 p.

Richardson M. et al. The Partial Equilibrium Diagram of the Fe-Ge System in the Range 40-72 at. % Ge, and the Crystallisation of some Iron Germanides by Chemical Transport Reactions. // Acta Chemica Scandinavica. 1967. Vol. 21. P. 2305–2317.

Ricker R.W., Hummel F.A. Reactions in the System TiO_2-SiO_2; Revision of the Phase Diagram // Journal of the American Ceramic Society. 1951. Vol. 34. No 9. P. 271–279.

Robie R.A. et al. Heat capacity and entropy of Ni_2SiO_4 -olivine from 5 to 1000 K and heat capacity of Co_2SiO_4 from 360 to 1000 K // American Mineralogist. 1984. Vol. 69. No 11–12. P. 1096–1101.

Robie R.A., Hemingway B.S., Fisher J.R. Thermodynamic Properties of Minerals and Related Substances at 298.15 K and 1 Bar (10^5 Pascals) Pressure and at Higher Temperatures. 2nd ed.Washington: U. S. Government Printing Office, 1979. 464 p.

Robinson R.A., Stokes R.H. Electrolyte Solutions. The Measurement and Interpretation of Conductance, Chemical Potential and Diffusion in Solutions of Simple Electrolytes. 2nd ed. London: Butterworths Scientific Publication, 1959. 559 p.

Robozerov V., Zykov V., Gavrikova T. Chemical etching of lead chalcogenides // Inorganic materials. 2000. Vol. 36. No 2. P. 177–181.

Rodriguez-Freire L. et al. Biomineralization of arsenate to arsenic sulfides is greatly enhanced at mildly acidic conditions. // Water research. 2014. Vol. 66. P. 242–253.

Róg G., Borchardt G. Thermodynamics of nickel orthosilicate // The Journal of Chemical Thermodynamics. 1984. Vol. 16. No 12. P. 1103–1105.

Rojas-Hernández A. et al. Construction of Multicomponent Pourbaix Diagrams Using Generalized Species // Journal of The Electrochemical Society. 1991. Vol. 138. No 2. P. 365–371.

Roozeboom H.W.B. Sur les différentes formes de l'équilibre chimique hétérogène // Recueil des Travaux Chimiques des Pays-Bas. 1887. T. 6. N. 9. P. 262–303.

Roozeboom H.W.B. Erstarrungspunkte der Mischkrystalle Zweier Stoffe. Umwandlungspunkte vei Mischkrystallen // Zeitschrift für physikalische Chemie, Stöchiometrie und Verwandtschaftslehre. 1899. Bd. 30. S. 385–412.

Ropp R.C., Carroll B. Precipitation of rare earth vanadates from aqueous solution // Journal of Inorganic and Nuclear Chemistry. 1977. Vol. 39. No 8. P. 1303–1307.

Rumpold R., Antrekowitsch J. Recycling of platinum group metals from automotive catalysts by an acidic leaching process // Fifth International Platinum Conference. 2012. P. 695–714.

Sadiq M. Thermodynamic solubility relationships of inorganic vanadium in the marine environment // Marine Chemistry. 1988. Vol. 23. No 1–2. P. 87–96.

Salesse A. et al. Surface passivation of GaInAsSb photodiodes with thioacetamide // Physica status solidi (c). 2007. Vol. 4. No 4. P. 1508–1512.

Salhi R. A Rigorous Calculation Method for Determining Potential-pH Diagrams Part I: Copper in Aqueous Solutions of Various Complexing Agents // Iranian Journal of Chemistry and Chemical Engineering. 2005. Vol. 24. No 3. P. 29–39.

Salvi G.R., Bethune A.J. De. The Temperature Coefficients of Electrode Potentials: II . The Second Isothermal Temperature Coefficient // Journal of The Electrochemical Society. 1961. Vol. 108. No 7. P. 672.

Sandström M., Jalilehvand F., Persson I. Deterioration of the seventeenth-century warship Vasa by internal formation of sulphuric acid // Nature. 2002. Vol. 415. P. 893–897.

Sanlı A.E., Aytaç A., Mat M. Investigation of the electro-oxidation of artificial Black Sea water by cyclic voltammetry on molybdenum (II) // International Journal of Hydrogen Energy. 2014. Vol. 39. No 17. P. 9221–9229.

Santamaria M., Muratore F., Quarto F. Di. Growth and Characterization of Anodic Films on Scandium // Journal of the Electrochemical Society. 2013. Vol. 161. No 1. P. C36–C41.

Sassani D.C., Shock E.L. Speciation and solubility of palladium in aqueous magmatic-hydrothermal solutions // Geology. 1990. Vol. 18. No 10. P. 925–928.

Sassani D.C., Shock E.L. Estimation of standard partial molal entropies of aqueous ions at 25°C and 1 bar // Geochimica et Cosmochimica Acta. 1992. Vol. 56. No 11. P. 3895–3908.

Sato M. Persistency-field Eh-pH diagrams for sulfides and their application to supergene oxidation and enrichment of sulfide ore bodies // Geochimica et Cosmochimica Acta. 1992. Vol. 56. No 8. P. 3133–3156.

Saulov D. On the multicomponent polynomial solution models // Calphad: Computer Coupling of Phase Diagrams and Thermochemistry. 2006. Vol. 30. No 4. P. 405–414.

Scatchard G. Equilibria in Non-electrolyte Solutions in Relation to the Vapor Pressures and Densities of the Components. // Chemical Reviews. 1931. Vol. 8. No 2. P. 321–333.

Scatchard G. Equilibrium in Non-Electrolyte Mixtures. // Chemical Reviews. 1949. Vol. 44. No 1. P. 7–35.

Scatchard G. Excess free energy and related properties of solutions containing electrolytes // Journal of the American Chemical Society. 1968. Vol. 90. No 12. P. 3124–3127.

Scatchard G., Raymond C.L. Vapor—Liquid Equilibrium. II. Chloroform—Ethanol Mixtures at 35, 45 and 55° // Journal of the American Chemical Society. 1938. Vol. 60. No 6. P. 1278–1287.

Schlesinger M.E. Thermodynamics of solid transition-metal silicides // Chemical Reviews. 1990. Vol. 90. No 4. P. 607–628.

Schmitt G. Effect of Elemental Sulfur on Corrosion in Sour Gas Systems // Corrosion. 1991. Vol. 47. No 4. P. 285–308.

Scholz F. Thermodynamics of Electrochemical Reactions // Electroanalytical Methods. Berlin, Heidelberg: Springer Berlin Heidelberg, 2010. P. 11–31.

Schon T., Heidendael M. Wasserstoffbildung durch Metallkorrosion. Jülich: Forschungszentrum Jülich, 1998. 86 s.

Schulte M.D., Shock E.L. Aldehydes in hydrothermal solution: Standard partial molal thermodynamic properties and relative stabilities at high temperatures and pressures // Geochimica et Cosmochimica Acta. 1993. Vol. 57. No 16. P. 3835–3846.

Schweitzer G.K., Pesterfield L.L. The Aqueous Chemistry of the Elements. Oxford: Oxford University Press, 2010. 447 p.

Schwingenschlögl U., Eyert V. The vanadium Magnéli phases V_nO_{2n-1} // Annalen der Physik. 2004. Bd. 13. H. 9. S. 475–510.

Secco E.A. Decomposition of zinc oxide // Canadian Journal of Chemistry. 1960. Vol. 38. No 4. P. 596–601.

Sedlbauer J., O'Connell J.P., Wood R.H. A new equation of state for correlation and prediction of standard molal thermodynamic properties of aqueous species at high temperatures and pressures // Chemical Geology. 2000. Vol. 163. No 1–4. P. 43–63.

Sekine T., Hasegawa Y. Studies of Scandium in Various Solutions. I. An Ion-Exchange Study of Scandium(III) Chloride and Nitrate Complexes // Bulletin of the Chemical Society of Japan. 1966. Vol. 39. No 2. P. 240–243.

Sequeira C.A.C., Hocking M.G. E-po2– Diagram for Nickel Corrosion in Na_2SO_4 at 1173 K // British Corrosion Journal. 1977. Vol. 12. No 3. P. 158–162.

Sergeev G.M., Shlyapunova E. V., Pozdnyakova M. a. Selective extraction-photometric redox determination of low concentrations of sulfur(IV), selenium(IV), tellurium(IV), and arsenic(III) // Journal of Analytical Chemistry. 2007. Vol. 62. No 5. P. 416–423.

Seward T. Equilibrium and oxidation potential in geothermal waters at Broadlands, New Zealand // American Journal of Science. 1974. Vol. 274. No 2. P. 190–192.

Sgambato F. et al. Il centenario del pH (1909-2009). Ma in medicina, è proprio indispensabile utilizzare i logaritmi negativi per misurare gli idrogenioni? Parte I // Italian Journal of Medicine. 2011a. Vol. 5. No 3. P. 147–155.

Sgambato F. et al. Il centenario del pH (1909-2009) - Parte seconda. Ma era proprio necessario sostituire l'equazione di Henderson con quella di Henderson-Hasselbalch? // Italian Journal of Medicine. 2011b. Vol. 5. No 4. P. 215–226.

Sheets W.C. et al. Facile synthesis of BiCuOS by hydrothermal methods. // Inorganic chemistry. 2007. Vol. 46. No 25. P. 10741–10748.

Shock E.L. et al. Calculation of the thermodynamic properties of aqueous species at high pressures and temperatures. Effective electrostatic radii, dissociation constants and standard partial molal properties to 1000 °C and 5 kbar // Journal of the Chemical Society, Faraday Transactions. 1992. Vol. 88. No 6. P. 803–826.

Shock E.L. et al. Inorganic species in geologic fluids: Correlations among standard molal thermodynamic properties of aqueous ions and hydroxide complexes // Geochimica et Cosmochimica Acta. 1997a. Vol. 61. No 5. P. 907–950.

Shock E.L. et al. Inorganic species in geologic fluids: Correlations among standard molal thermodynamic properties of aqueous ions and hydroxide complexes // Geochimica et Cosmochimica Acta. 1997b. Vol. 61. No 5. P. 907–950.

Shock E.L., Helgeson H.C. Calculation of the thermodynamic and transport properties of aqueous species at high pressures and temperatures: Correlation algorithms for ionic species and equation of state predictions to 5 kb and 1000°C // Geochimica et Cosmochimica Acta. 1988. Vol. 52. No 8. P. 2009–2036.

Shock E.L., Helgeson H.C. Erratum to Geochim. Cosmochim.: E. L. Shock and H. C. Helgeson: Cosmochimica Acta 52, pp. 2009–2036 // Geochimica et Cosmochimica Acta. 1989. Vol. 53. No 1. P. 215.

Shock E.L., Helgeson H.C. Calculation of the thermodynamic and transport properties of aqueous species at high pressures and temperatures: Standard partial molal properties of organic species // Geochimica et Cosmochimica Acta. 1990. Vol. 54. No 4. P. 915–945.

Shock E.L., Helgeson H.C., Sverjensky D.A. Calculation of the thermodynamic and transport properties of aqueous species at high pressures and temperatures: Standard partial molal properties of inorganic neutral species // Geochimica et Cosmochimica Acta. 1989. Vol. 53. No 9. P. 2157–2183.

Shock E.L., Koretsky C.M. Metal-organic complexes in geochemical processes: Calculation of standard partial molal thermodynamic properties of aqueous acetate complexes at high pressures and temperatures // Geochimica et Cosmochimica Acta. 1993. Vol. 57. No 20. P. 4899–4922.

Shock E.L., McKinnon W.B. Hydrothermal Processing of Cometary Volatiles—Applications to Triton // Icarus. 1993. Vol. 106. No 2. P. 464–477.

Shtin S. V., Lykasov A.A. Investigation into the equilibrium of the wustite and spinel solutions in the Fe-Ge-O system // Russian Journal of Non-Ferrous Metals. 2013. Vol. 54. No 6. P. 429–432.

Shtin S.V., Lykasov A.A. Investigation of the Equilibrium Germanium-Substituted Wustite with Metal and Spinel Solutions in the Fe-Ge-O System // Solid State Phenomena. 2017. Vol. 265. P. 827–833.

Sillen L.G. Redox diagrams // Journal of Chemical Education. 1952. Vol. 29. No 12. P. 600–608.

Simon L., Génin J., Refait P. Standard free enthalpy of formation of Fe (II) – Fe (III) hydroxysulphite green rust one and its oxidation into hydroxysulphate green rust two // Corrosion science. 1997. Vol. 39. No 9. P. 1673–1685.

Siqueira O.S. et al. Complexation of some trivalent lanthanides, scandium(III) and thorium(IV) by benzylidenepyruvates and cinnamylidenepyruvate in aqueous solution // Journal of Alloys and Compounds. 1995. Vol. 225. No 1–2. P. 267–270.

Sluys W.A. Van Der, Emanuelson R.H. Cyclic Crack Growth Behavior of Reactor Pressure Vessel Steels in Light Water Reactor Environments // Journal of Engineering Materials and Technology. 1986. Vol. 108. No 1. P. 26.

Smith J.F. The Si–V (Silicon-Vanadium) system // Bulletin of Alloy Phase Diagrams. 1981. Vol. 2. No 1. P. 42–48.

Smith J.F. The Si–V (Silicon-Vanadium) system: Addendum // Bulletin of Alloy

Phase Diagrams. 1985. Vol. 6. No 3. P. 266–271.
Smith J.S., Miller J.D.A. Nature of Sulphides and their Corrosive Effect on Ferrous Metals: A Review // British Corrosion Journal. 1975. Vol. 10. No 3. P. 136–143.
Smith R.M., Martell A.E. Critical Stability Constants. Volume 4. Inorganic Complexes. Springer, 1976.
Song W.M., Ziyuan Y.O. Thermodynamic Analysis of the Mineral Assemblages of Shell Fossils // Acta Sedimentologica Sinica. 1991. Vol. 9. No 1. P. 129–135.
Soon-Don C. Thermodynamic analysis of the Co-Si system // Calphad: Computer Coupling of Phase Diagrams and Thermochemistry. 1992. Vol. 16. No 2. P. 151–159.
Sörensen S.P.L. Enzymstudien. II: Mitteilung. Über die Messung und die Bedeutung der Wasserstoffionenkoncentration bei enzymatischen Prozessen // Biochemische Zeitschrift. 1909. Bd. 21. S. 131–304.
Sørensen S.P.L. Études enzymatiques. II. Sur la mesure et l'importance de la concentration des ions hydrogène dans les réactions enzymatiques // Comptes rendus des travaux du laboratoire Carlsberg. 1909a. T. 8. P. 1–162.
Sørensen S.P.L. Enzymstudier II. Om Maalingen og Betydningen af Brintionkoncentrationen ved enzymatiske Processer // Meddelelser fra Carlsberg Laboratoriet. 1909b. T. 8. P. 1–153, 313–317.
Sourisseau T., Chauveau E., Baroux B. Mechanism of copper action on pitting phenomena observed on stainless steels in chloride media // Corrosion Science. 2005. Vol. 47. No 5. P. 1097–1117.
Soustelle M. Thermodynamic Modeling of Solid Phases. New York: Wiley, 2015. 264 p.
Spear K.E., Gilles P.W., Schäfer H. Chemical transport reactions in the vanadium-silicon-oxygen system and the ternary phase diagram // Journal of the Less Common Metals. 1968. Vol. 14. No 1. P. 69–75.
Speight J.G. Lange's Handbook of Chemistry. 16th ed. McGraw-Hill, 2005.
Stampler E.S. et al. Temperature driven reactant solubilization synthesis of BiCuOSe. // Inorganic chemistry. 2008. Vol. 47. No 21. P. 10009–10016.
Storms E., Myers C.E. Thermodynamics and Phase Equilibria in the Vanadium–Silicon System. Binghamton, 1984. 24 p.
Struthers J.D. Solubility and Diffusivity of Gold, Iron, and Copper in Silicon // Journal of Applied Physics. 1956. Vol. 27. No 12. P. 1560–1560.
Sundman B., Ågren J. A regular solution model for phases with several components and sublattices, suitable for computer applications // Journal of Physics and Chemistry of Solids. 1981. Vol. 42. No 4. P. 297–301.

Sverjensky D.A., Shock E.L., Helgeson H.C. Prediction of the thermodynamic properties of aqueous metal complexes to 1000 degrees C and 5 kb. // Geochimica et Cosmochimica Acta. 1997. Vol. 61. No 7. P. 1359–1412.

Switendick A.C. Electronic Structure and Properties of Scandium, Titanium, and Yttrium Hydride Systems* // Zeitschrift für Physikalische Chemie. 1989. Bd. 163. H. Teil 2. S. 527.

Takayama E. The system GeO_2–MnO–Mn_2O_3 at 900°C // Journal of Solid State Chemistry. 1981. Vol. 39. No 1. P. 133–134.

Takeno N. Atlas of Eh–pH Diagrams. Intercomparison of Thermodynamic Databases. , 2005. Open File Report No. 419 p.

Tan K.G., Rolia E. Chemical Oxidation Methods for the Treatment of Thiosalt-Containing Mill Effluents // Canadian Metallurgical Quarterly. 1985. Vol. 24. No 4. P. 303–310.

Tang C., Zhou D., Zhang Q. Synthesis and characterization of Magneli phases: Reduction of TiO_2 in a decomposed NH_3 atmosphere // Materials Letters. 2012. Vol. 79. P. 42–44.

Tang J. et al. Ferromagnetic Germanide in Ge Nanowire Transistors for Spintronics Application // ACS Nano. 2012. Vol. 6. No 6. P. 5710–5717.

Tanger J.C. Calculation of the Standard Partial Molal Thermodynamic Properties of Aqueous Ions and Electrolytes at High Pressures and Temperatures. Berkeley: University of California, 1986. 264 p.

Tanger J.C., Helgeson H.C. Calculation of the thermodynamic and transport properties of aqueous species at high pressures and temperatures; revised equations of state for the standard partial molal properties of ions and electrolytes // American Journal of Science. 1988. Vol. 288. No 1. P. 19–98.

Tardy Y., Garrels K.M. A method of estimating the Gibbs energies of formation of layer silicates // Geochimica et Cosmochimica Acta. 1974. Vol. 38. No 7. P. 1101–1116.

Tardy Y., Garrels R.M. Prediction of Gibbs energies of formation—I. Relationships among Gibbs energies of formation of hydroxides, oxides and aqueous ions // Geochimica et Cosmochimica Acta. 1976. Vol. 40. No 9. P. 1051–1056.

Tardy Y., Garrels R.M. Prediction of Gibbs energies of formation of compounds from the elements—II. Monovalent and divalent metal silicates // Geochimica et Cosmochimica Acta. 1977. Vol. 41. No 1. P. 87–92.

Thiry M., Galbois J., Schmitt J.-M. Unusual Phosphate Concretions Related to Groundwater Flow in a Continental Environment // Journal of Sedimentary Research (SEPM). 2006. Vol. 76. No 5. P. 866–870.

Thompson W.T. et al. Pourbaix Diagrams for Multielement Systems // Uhlig's

corrosion handbook. Wiley, 2011. P. 103–110.
Thomson W. On an Absolute Thermometric Scale founded on Carnot's Theory of the Motive Power of Heat, and calculated from Regnault's Observations // Proceedings of the Cambridge Philosophical Society, Mathematical and physical sciences. 1843. Vol. 1. P. 66–71.
Thornber M. Supergene alteration of sulphides, II. A chemical study of the Kambalda nickel deposits // Chemical Geology. 1975. Vol. 15. No 2. P. 117–144.
Tkacz M., Burtovyy R. Decomposition of the hexagonal copper hydride at high pressure // Solid State Communications. 2004. Vol. 132. No 1. P. 37–41.
Toedtemeir M., Dandapani B., Ghali E. La Corrosion Et Le Diagramme E –pH De Sulfure De Plomb // Canadian Metallurgical Quarterly. 1992. Vol. 31. No 2. P. 95–104.
Tokunaga T. et al. Thermodynamic assessment of the Ni–Si system by incorporating ab initio energetic calculations into the CALPHAD approach // Calphad: Computer Coupling of Phase Diagrams and Thermochemistry. 2003. Vol. 27. No 2. P. 161–168.
Tomio A. et al. Role of alloyed copper on corrosion resistance of austenitic stainless steel in H_2S–Cl^- environment // Corrosion Science. 2014. Vol. 81. P. 144–151.
Travers J.G., Dellien I., Hepler L.G. Scandium: Thermodynamic properties, chemical equilibria, and standard potentials // Thermochimica Acta. 1976. Vol. 15. No 1. P. 89–104.
Trefall H., Nordö J. On Systematic Errors in the Least Squares Regression Analysis, with Application to the Atmospheric Effects on the Cosmic Radiation // Tellus. 1959. Vol. 11. No 4. P. 467–477.
Tuan H.-Y., Lee D.C., Korgel B.A. Nanocrystal-Mediated Crystallization of Silicon and Germanium Nanowires in Organic Solvents: The Role of Catalysis and Solid-Phase Seeding // Angewandte Chemie. 2006. Bd. 118. H. 31. S. 5308–5311.
Tukel C., Kelebek S., Yalcin E. Eh-pH Stability Diagrams for Analysis of Polyamine Interaction with Chalcopyrite and Deactivation of Cu-Activated Pyrrhotite // Canadian Metallurgical Quarterly. 2010. Vol. 49. No 4. P. 411–418.
Tunnicliffe M., Mohammadi F., Alfantazi A. Polarization Behavior of Lead-Silver Anodes in Zinc Electrowinning Electrolytes // Journal of The Electrochemical Society. 2012. Vol. 159. No 4. P. C170–C180.
Türkel N., Aydin R., Özer U. Stabilities of complexes of Scandium (III) and Yttrium (III) with salicylic acid // Turkish Journal of Chemistry. 1999. Vol.

23. No 3. P. 249–256.
Tytko K.-H., Glemser O. Isopolymolybdates and Isopolytungstates // Advances in Inorganic Chemistry and Radiochemistry. 1976. P. 239–315.
Tyurin A., Biryukov A. Diagramma elektrokhimicheskogo ravnovesiza stali St. 3 v silnokislykh sulfatnykh rastvorakh // Vestnik Kazanskogo tekhnologicheskogo universiteta. 2012. T. 15. № 16. C. 74–77.
Tyurin A., Biryukov A. Vliyaniye anionov na korrozionno-elektrokhimicheskoye povedeniye stali St.3 v sulfatnykh sredakh. Soobshcheniye 1. Termodinamika // Vestnik Yuzhno-Uralskogo gosudarstvennogo universiteta. Seriya Khimija. 2013a. T. 5. № 3. C. 36–44.
Tyurin A., Biryukov A. Diagramma E-pH sistemy Cu - H_2SO_4 - H_2O // X International Kurnakov Reading on Physical-Chemical Analysis. Samara: Samara State Technical University, 2013b. P. 82–85.
Tyurin A.G. Thermodynamics of molecular and ionic-solutions // Russian Metallurgy (Metally). 1993. No 2. P. 39–47.
Tyurin A.G. Thermodynamic analysis of the silicon effect on chemical and electrochemical stability of iron-chromium alloys // Protection of Metals. 2004. Vol. 40. No 1. P. 14–22.
Tyurin A.G. Thermodynamics of chemical and electrochemical stability of aluminum, silicon, and tin bronzes // Protection of Metals. 2008. Vol. 44. No 3. P. 292–300.
Tyurin A.G. et al. Thermodynamics of chemical and electrochemical stability of corrosion active nonmetal inclusions // Protection of Metals. 2007. Vol. 43. No 1. P. 34–44.
Tzvetkoff T., Gencheva P. Mechanism of formation of corrosion layers on nickel and nickel-based alloys in melts containing oxyanions—a review // Materials Chemistry and Physics. 2003. Vol. 82. No 3. P. 897–904.
Uematsu M., Frank E.U. Static Dielectric Constant of Water and Steam // Journal of Physical and Chemical Reference Data. 1980. Vol. 9. No 4. P. 1291–1306.
Vahlas C., Chevalier P.Y., Blanquet E. A thermodynamic evaluation of four Si-M (M = Mo, Ta, Ti, W) binary systems // Calphad: Computer Coupling of Phase Diagrams and Thermochemistry. 1989. Vol. 13. No 3. P. 273–292.
Valenzuela A., Valenzuela J., Parga J. Effect of Pretreatment of Sulfide Refractory Concentrate with Sodium Hypochlorite, Followed by Extraction of Gold by Pressure Cyanidation, on Gold Removal // Advances in Chemical Engineering and Science. 2013. Vol. 3. No 3. P. 171–177.
Vanýsek P. Electrochemical Series // CRC Handbook on Chemistry and Physics. 93rd ed. Chemical Rubber Company, 2012.

Vaškelis A., Juškėnas R., Jačiauskienė J. Copper hydride formation in the electroless copper plating process: in situ X-ray diffraction evidence and electrochemical study // Electrochimica Acta. 1998. Vol. 43. No 9. P. 1061–1066.

Vaughn D.D. et al. Solution-Phase Synthesis and Magnetic Properties of Single-Crystal Iron Germanide Nanostructures // Chemistry of Materials. 2013. Vol. 25. No 21. P. 4396–4401.

Venkatraman M., Neumann J.. The Cr-H (Chromium-Hydrogen) system // Journal of Phase Equilibria. 1991. Vol. 12. No 6. P. 672–677.

Vernik E.D. Simplified Procedure for Constructing Pourbaix Diagrams // Corrosion. 1967. Vol. 23. No 12. P. 371–373.

Visco S.J. et al. Aqueous electrolyte lithium sulphur batteries. Dissertation, 2014.

Vitorge P. et al. Estimating the stabilities of actinide aqueous species. Influence of sulfoxy-anions on uranium(IV) geochemistry and discussion of Pa(V) first hydrolysis // Comptes Rendus Chimie. 2007. T. 10. N. 10–11. P. 978–993.

Wadsley M. Stoichiometric considerations in multicomponent aqueous stability diagrams // Hydrometallurgy. 1992. Vol. 29. No 1–3. P. 91–108.

Wagman D.D. et al. The NBS tables of chemical thermodynamic properties. Selected values for inorganic and C_1 and C_2 organic substances in SI units // Journal of Physical and Chemical Reference Data. 1982. Vol. 11. Supplement 2.

Walther J. V. Ionic association in H_2O–CO_2 fluids at mid-crustal conditions // Journal of Metamorphic Geology. 1992. Vol. 10. No 6. P. 789–797.

Wang W. et al. $[Sc_2(\mu\text{-}OH)_2(H_2O)_6(NO_3)_2](NO_3)_2$: Aqueous Synthesis and Characterization // Inorganic Chemistry. 2013. Vol. 52. No 4. P. 1807–1811.

Wang X., Forssberg E., Bolin N.J. The Aqueous and Surface Chemistry of Activation in the Flotation of Sulphide Minerals—A Review. Part I: An Electrochemical Model // Mineral Processing and Extractive Metallurgy Review. 1989. Vol. 4. No 3–4. P. 135–165.

Waring E. Problems concerning Interpolations. By Edward Waring, M. D. F. R. S. and of the Institute of Bononia, Lucasian Professor of Mathematics in the University of Cambridge // Philosophical Transactions of the Royal Society of London. 1779. Vol. 69. P. 59–67.

Warner T.E., Rice N.M., Taylor N. Thermodynamic stability of pentlandite and violarite and new EH -pH diagrams for the iron-nickel sulphur aqueous system // Hydrometallurgy. 1996. Vol. 41. No 2–3. P. 107–118.

Warren G., Drouven B., Price D. Relationships between the Pourbaix Diagram for Ag-S-H_2O and electrochemical oxidation and reduction of Ag_2S //

Metallurgical Transactions B. 1984. Vol. 15. No 2. P. 235–242.
Wasserman E., Wood B., Brodhol J. The static dielectric constant of water at pressures up to 20 kbar and temperatures to 1273 K: Experiment, simulations, and empirical equations // Geochimica et Cosmochimica Acta. 1995. Vol. 59. No 1. P. 1–6.
Wasserman E., Wood B., Davies A. Equation of state for aqueous silica species at pressures from 1 bar to 20 kbar and temperatures from 25° to 900°C based on simulated values of the dielectric constant // Chemical Geology. 1995. Vol. 121. No 1–4. P. 3–9.
Welch M.D., Cooper M.A., Hawthorne F.C. The crystal structure of brunogeierite, Fe_2GeO_4 spinel // Mineralogical Magazine. 2001. Vol. 65. No 3. P. 441–444.
White S., Lichti K., Bacon L. Application of chemical and wellbore modeling to the corrosion and scaling properties of OHAAKI deep wells // Proceedings of the World Geothermal Congress. 2000. P. 3963–3968.
White W.B., Roy R. The system chromium-oxygen at high oxygen pressures // Geochimica et Cosmochimica Acta. 1975. Vol. 39. No 6–7. P. 803–817.
Wiener M.S. et al. Effect of H_2S on corrosion in polluted waters: a review // Corrosion Engineering, Science and Technology. 2006. Vol. 41. No 3. P. 221–227.
Wilhelmi K.-A. et al. Formation of Chromium Oxides in the Cr_2O_3-CrO_3 Region at Elevated Pressures up to 4 Kilobar. // Acta Chemica Scandinavica. 1968. Vol. 22. No 8. P. 2565–2573.
Wloka J., Virtanen S. Influence of scandium on the pitting behaviour of Al–Zn–Mg–Cu alloys // Acta Materialia. 2007. Vol. 55. No 19. P. 6666–6672.
Wohl K. Thermodynamic evaluation of binary and ternary liquid systems // Transactions of the American Institute of Chemical Engineers. 1946. Vol. 42. P. 215–249.
Wohl K. Thermodynamic Evaluation of Binary and Ternary Liquid Systems // Chemical Engineering Progress. 1953. Vol. 49. P. 218–219.
Wolfenstine J., Dimos D., Kohlstedt D.L. Decomposition of Ni_2SiO_4 in an Oxygen Potential Gradient // Journal of the American Ceramic Society. 1985. Vol. 68. No 5. P. C-117-C-118.
Wong G.T.F. The oxidation state diagram — a potential tool for studying redox chemistry in seawater // Marine Chemistry. 1980. Vol. 9. No 1. P. 1–12.
Wood S.A., Samson I.M. The aqueous geochemistry of gallium, germanium, indium and scandium // Ore Geology Reviews. 2006. Vol. 28. No 1. P. 57–102.
Woods R., Young C., Yoon R. Ethyl xanthate chemisorption isotherms and E h-pH diagrams for the copper/water/xanthate and chalcocite/water/xanthate

systems // International journal of mineral processing. 1990. Vol. 30. No 1–2. P. 17–33.
Woods R.Y.R.H.. Y.C.A. Eh-pH Diagrams for Stable and Metastable Phases in the Copper - Sulfur - Water System // International journal of mineral processing. 1987. Vol. 20. No 1–2. P. 109–120.
Work D.E., Eick H.A. On the preparation of condensed ScO // Journal of the Less Common Metals. 1972. Vol. 26. No 3. P. 413–416.
Wriedt H.A. The O–Zn (Oxygen-Zinc) system // Journal of Phase Equilibria. 1987. Vol. 8. No 2. P. 166–176.
Wu D. et al. Solvent extraction of scandium(III), yttrium(III), lanthanum(III) and gadolinium(III) using Cyanex 302 in heptane from hydrochloric acid solutions // Journal of Alloys and Compounds. 2004. Vol. 374. No 1–2. P. 442–446.
Yagi S. Potential-pH Diagrams for Oxidation-State Control of Nanoparticles Synthesized via Chemical Reduction // Thermodynamics - Physical Chemistry of Aqueous Systems. London: InTech, 2011. P. 223–240.
Yan X., Chang Y.. A thermodynamic analysis of the Cu–Si system // Journal of Alloys and Compounds. 2000. Vol. 308. No 1–2. P. 221–229.
Yaws C.L. Handbook of Thermodynamic Diagrams, Volume 4: Inorganic Compounds and Elements. Texas: Gulf Professional Publishin, 1996. 384 p.
Yilmaz A.E. et al. The investigation of parameters affecting boron removal by electrocoagulation method // Journal of Hazardous Materials. 2005. Vol. 125. No 1–3. P. 160–165.
Yilmaz A.E. et al. Boron removal from geothermal waters by electrocoagulation // Journal of Hazardous Materials. 2008. Vol. 153. No 1–2. P. 146–151.
Yilmaz A.E., Boncukcuoğlu R., Kocakerim M.M. A quantitative comparison between electrocoagulation and chemical coagulation for boron removal from boron-containing solution // Journal of Hazardous Materials. 2007. Vol. 149. No 2. P. 475–481.
Yokokawa H. et al. Generalized Ellingham Diagrams for Utilization in Solid Oxide Fuel Cells with an Emphasis on Interactions of Nickel Cermet Anode with Impurities in Coal Synthesis // ECS Transactions. 2009. Vol. 25. No 2. P. 2131–2140.
Yokokawa H., Kawada T., Makajuki D. Construction of Chemical Potential Diagrams for Metal-Metal-Nonmetal Systems: Applications to the Decomposition of Double Oxides // Journal of the American Ceramic Society. 1989. Vol. 72. No 11. P. 2104–2110.
Yokokawa H., Sakai N. Generalized Electrochemical Potential Diagrams for Complex Aqueous (M-X-H-O-e^-) Systems // Journal of The

Electrochemical Society. 1990. Vol. 137. No 2. P. 388–398.
Yong W. et al. Heat capacity of γ-Fe_2SiO_4 between 5 and 303 K and derived thermodynamic properties // Physics and Chemistry of Minerals. 2007. Vol. 34. No 2. P. 121–127.
Yoon H.-N. et al. Synthesis and Applications of Noble Metal and Metal Silicide and Germanide 1-Dimensional Nanostructures // Bulletin of the Korean Chemical Society. 2012. Vol. 33. No 9. P. 2830–2844.
Yoshikawa T. et al. Thermodynamics of impurity elements in solid silicon // Journal of Alloys and Compounds. 2010. Vol. 490. No 1–2. P. 31–41.
You H.-X. et al. Potential—pH diagrams of Cr-H_2O system at elevated temperatures // 中国有色金属学报. 2010. Vol. 20. Supplement 1. P. s26–s31.
Young C. A., Dahlgren E.J., Robins R.G. The solubility of copper sulfides under reducing conditions // Hydrometallurgy. 2003. Vol. 68. No 1–3. P. 23–31.
Young Jr. J.E., Sienko M.J. Plasma-synthesized substoichiometric scandium oxide // Solid State Chemistry. Proceedings of the 5th Materials Research Symposium / ed. R.S. Roth, S.J. Schneider. National Bureau of Standards (U.S.), 1972. P. 385–395.
Yuan X. et al. A new approach to establish both stable and metastable phase equilibria for fcc ordered/disordered phase transition: application to the Al–Ni and Ni–Si systems // Materials Chemistry and Physics. 2012. Vol. 135. No 1. P. 94–105.
Zappia M.J. Electrochemical phase diagrams for aqueous redox systems. Dissertation, 1990.
Zappia M.J., Angus J.C., Yung R.C. Electrochemical Phase Diagrams for Aqueous Redox Systems. Case Western Reserve University, 1989.
Zeng K. et al. Thermodynamics of the Ni–H system // Journal of Alloys and Compounds. 1999. Vol. 283. No 1–2. P. 151–161.
Zhang C. et al. Thermodynamic modeling of the V–Si system supported by key experiments // Calphad: Computer Coupling of Phase Diagrams and Thermochemistry. 2008. Vol. 32. No 2. P. 320–325.
Zhang F., Huang W., Chang Y.A. Equivalence of the generalized bond-energy model, the Wagner-Schottky-type model and the compound-energy model for ordered phases // Calphad: Computer Coupling of Phase Diagrams and Thermochemistry. 1997. Vol. 21. No 3. P. 337–348.
Zhang L. Electrochemical equilibrium diagrams for sulphidization of oxide copper minerals // Minerals engineering. 1994. Vol. 7. No 7. P. 927–932.
Zhang R.F. et al. Miedema Calculator: A thermodynamic platform for predicting formation enthalpies of alloys within framework of Miedema's Theory //

Computer Physics Communications. 2016. Vol. 209. P. 58–69.
Zhang R.F. et al. An informatics guided classification of miscible and immiscible binary alloy systems // Scientific Reports. 2017. Vol. 7. No 1. P. 9577.
Zhang W., Singh P., Muir D. Oxidative precipitation of manganese with SO_2/O_2 and separation from cobalt and nickel // Hydrometallurgy. 2002. Vol. 63. No 2. P. 127–135.
Zhijian Wang et al. Research on a Novel Technology of Interactive Roast of Complex Low-grade Bismuth Sulfide Ore and Pyrolusite // Characterization of Minerals, Metals, and Materials 2013 / ed. Jiann-Yang Hwang et al. Wiley, 2013. P. 415–422.
Zhou X. et al. Thermodynamics of vanadium–sulfur–water systems at 298K // Hydrometallurgy. 2011a. Vol. 106. No 1–2. P. 104–112.
Zhou X. et al. Thermodynamics of vanadium–sulfur–water systems at 298K // Hydrometallurgy. 2011b. Vol. 106. No 1–2. P. 104–112.
Zotov N., Keppler H. Silica speciation in aqueous fluids at high pressures and high temperatures // Chemical Geology. 2002. Vol. 184. No 1–2. P. 71–82.
Акимов Е.Н., Сенин А.В., Рощин В.Е. Термодинамический анализ получения низкоуглеродистого феррохрома с применением модели ассоциированных растворов // Вестник Южно-Уральского государственного университета. Серия „Металлургия“. 2013. Т. 13. № 1. С. 182–185.
Алымовъ И.П. Научныя выводы относительно водяного пара // Морской сборникъ. Неоффиціальная часть. 1865. Т. 77. № 3. С. 86–113.
Аплатов А.В., Падерин С.Н. Термодинамические модели жидких многокомпонентных металлических растворов // Электрометаллургия. 2009. № 9. С. 28–36.
Артюх Л.В. и др. Физическая химия неорганических материалов. В 3 т. Т. 1. Термодинамика интерметаллидов и фазовые равновесия в металлических системах. Киев: Наукова Думка, 1988. 365 с.
Бережной А.С. Кремний и его бинарные системы. Киев: Издательство Академии Наук УССР, 1958. 252 с.
Верягин У.Д. и др. Термодинамические свойства неорганических веществ: справочник / ed. А.П. Зефирова. Москва: Атомиздат, 1965. 461 с.
Власенко О.В., Однодворець Л.В., Проценко І.Ю. Фазовий склад і магнеторезистивні властивості тришарових плівок Fe/Ge/Fe // Металлофизика и Новейшие Технологии. 2013. Т. 35. № 12. С. 1637–1644.
Гельд П.В., Сидоренко Ф.А. Силициды переходных металлов четвёртого периода. Москва: Металлургия, 1971. 581 с.

Гиббс Д.В. Термодинамические работы. Москва, Ленинград: Государственное издательство технико-теоретической литературы, 1950. 495 с.

Жук Н.П. // Журнал физической химии. 1954. Т. 38. № 11. С. 1523–1527.

Жук Н.П. Курс теории коррозии и защиты металлов: учебное пособие для вузов. Москва: ООО ТИД «Альянс», 2006. 372 с.

Карапетьянц М.Х. Химическая термодинамика. 3 изд. Москва: Химия, 1975. 584 с.

Киреев В.А. Методы практических расчётов в термодинамике химических реакций. Москва: Химия, 1970. 520 с.

Комиссарова Л.Н. Неорганическая и аналитическая химия скандия. Москва: Эдиториал УРСС, 2001. 512 с.

Купрашвили И.С., Наумкин О.П., Савицкий Е.М. Фазовая диаграмма системы скандий - кислород // Известия Академии Наук СССР. Неорганические материалы. 1969. Т. 5. № 12. С. 2123–2127.

Лаптев Д.М. Термодинамика металлургических растворов. Челябинск: Металлургия, 1992. 352 с.

Лурье Ю.Ю. Справочник по аналитической химии. 7 изд. Москва: Альянс, 2007. 447 с.

Лыкасов А.А., Кимяшов А.А. Условия фазовых равновесий в системе Fe–Si–O в интервале температур 1100–1300 К // Бутлеровские сообщения. 2010. Т. 21. № 7. С. 42–49.

Менделѣевъ Д.И. Объ общей формулѣ для газовъ // Журналъ Русскаго Физико-Химическаго Общества при Императорскомъ Петроградскомъ университетѣ. Часть Физическая. 1874a. Т. 6. № 7. С. 121–122.

Менделѣевъ Д.И. Объ общей формулѣ для газовъ // Журналъ Русскаго Физико-Химическаго Общества при Императорскомъ Петроградскомъ университетѣ. Часть Химическая. 1874b. Т. 6. № 7. С. 208–209.

Менделѣевъ Д.И. Основы химіи. 8–е изд. Санктпетербургъ: Типографія М. П. Фроловой, 1906.

Моисеев Г.К. и др. Температурные зависимости приведённой энергии Гиббса некоторых неорганических веществ: альтернативный банк данных ASTRA.OWN. Екатеринбург: УрО РАН, 1997. 230 с.

Морачевский А.Г. Термодинамика расплавленных металлических и солевых систем. Москва: Металлургия, 1987. 240 с.

Морачевский А.Г., Цемехман Л.Ш., Цымбулов Л.Б. Термодинамика системы никель – кислород // Термодинамика систем и процессов в металлургии никеля и меди. Выпуск 12. Санкт-Петербург: Издательство Политехнического университета, 2008. 149 с.

Музгин В.Н. и др. Аналитическая химия ванадия. Москва: Наука, 1981. 216 с.

Парфёнова С.И., Гаркушин И.К., Медовщикова Л.А. Анализ термодинамических свойств элементов на группы периодической системы // Оксиды. Физико-химические свойства: сборник трудов V Всероссийской научной конференции. Екатеринбург. 2000. С. 374–377.

Рузинов Л.П., Гуляницкий Б.С. Равновесные превращения металлургических реакций. Москва: Металлургия, 1975. 417 с.

Рябин В.А., Остроумов М.А., Свит Т.Ф. Термодинамические свойства веществ. Справочник. Ленинград: Химия, 1977. 392 с.

Самсонов Г.В., Дворина Л.А., Рудь Б.М. Силициды. Москва: Металлургия, 1979. 272 с.

Свечников В.Н., Кочержинский Ю.А., Юлко Л.М. Диаграмма хром – кремний // Сборник научных трудов института металлофизики АН УССР. 1964. № 19. С. 212–218.

Сибиркин А.А., Замятин О.А., Чурбанов М.Ф. Взаимное превращение изополисоединений молибдена (VI) в водном растворе // Вестник Нижегородского университета им. Н. И. Лобачевского. 2008. № 5. С. 45–51.

Смитлз К.Д. Металлы. Москва: Металлургия, 1980. 447 с.

Сорокина О.В., Зыкова Е.С. Современные формы представления окислительно-восстановительных процессов с помощью диаграмм Латимера, Фроста и Пурбе // Вестник Московского института тонких химических технологий имени М. В. Ломоносова. 2006. № 3. С. 50–55.

Третьяков Ю.Д. Термодинамика ферритов. Ленинград: Химия, 1967. 305 с.

Тюрин А.Г. Термодинамика химической и электрохимической устойчивости твёрдых сплавов железа, хрома и никеля. Челябинск: Издательство Челябинского государственного университета, 2012. 241 с.

Храпко С.А. Анализ и сравнение формул субрегулярных растворов для многокомпонентных систем // Металл и литьё Украины. 2006. № 3–4. С. 35–39.

Храпко С.А. Выбор вида формул теории субрегулярных растворов // Наукові праці Донецького Національного технічного університету. Серія «Металургія». 2011. № 12 (177). С. 16–26.

Юдин Б.Ф. и др. // Журнал прикладной химии. 1976. Т. 49. С. 776–780.

周震涛, 廖宗友. 非水性锂-高铁酸盐电池的制备及其电化学性能 // 电源技术. 2003. Vol. 27. No 6. P. 497–499.

夏大海, Luo J.-L. 690合金在300 ℃含硫模拟碱性水化学中的腐蚀行为 // 物理化学学报. 2015. Vol. 31. No 3. P. 467–475.

曾英, 马旻锐. 高浓度V-H_2O体系的溶解组分优势区域图和Pourbaix图 // 物理化学学报. 2009. Vol. 25. No 5. P. 953–957.

SUPCRT / Prediction Central [Electronic resource]. URL: http://www.predcent.org/download/supcrt.

Japan Nuclear Cycle Organization Thermodynamic Database [Electronic resource]. URL: http://migrationdb.jnc.go.jp.

ChemEQL [Electronic resource]. URL: http://www.eawag.ch/research_e/surf/Researchgroups/sensors_and_analytic/chemeql.html.

SGTE E-pH Web [Electronic resource]. URL: http://www.sgte.org/ephweb.php.

The Geochemist's Workbench (GWB) [Electronic resource]. URL: http://www.gwb.com/thermo.php.

PhreePlot [Electronic resource]. URL: http://www.phreeplot.org/.

ZZ HATCHES-20, Database for radiochemical modelling [Electronic resource]. URL: http://www.oecd-nea.org/tools/abstract/detail/nea-1210.

THERMEXPERT – Potential – pH diagram generator [Electronic resource]. URL: http://www.argentumsolutions.com/cgi-bin/thermexpert.

Materials Project Pourbaix Diagrams [Electronic resource]. URL: https://materialsproject.org/#apps/pourbaixdiagram.

Chemical Equilibrium Diagrams [Electronic resource]. URL: https://sites.google.com/site/chemdiagr/.

Справочник химика. Том третий. Химическое равновесие и кинетика. Свойства растворов. Электродные процессы / ed. Б.П. Никольского и др. 2 изд. Москва, Ленинград: Химия, 1965. 1008 с.

Modern Aspects of Electrochemistry No 10 / ed. J.O. Bockris, B.E. Conway. Boston, MA: Springer US, 1975. 460 p.

Thermodynamics in Geology / ed. D.G. Fraser. Dordrecht: Springer Netherlands, 1977. 407 p.

Справочник по электрохимии / ed. А.М. Сухотина. Ленинград: Химия, 1981. 488 с.

Comprehensive Treatise of Electrochemistry. Volume 4: Electrochemical Materials Science / ed. J.O. Bockris et al. Boston, MA: Springer US, 1981. 579 p.

Диаграммы состояния двойных металлических систем: справочник / ed. Н.П. Лякишева. Москва: Машиностроение, 2001. 872 с.

Краткий справочник физико-химических величин / ed. А.А. Равделя, А.М. Пономарёвой. 10 изд. Санкт-Петербург: Иван Фёдоров, 2003. 240 с.

Термические константы веществ [Electronic resource]. URL: http://www.chem.msu.ru/cgi-bin/tkv.pl?show=welcome.html.
Uhlig's Corrosion Handbook / ed. R.W. Revie. Hoboken, NJ, USA: John Wiley & Sons, Inc., 2011. 1227 p.
Progress in the Science and Technology of the Rare Earths / ed. L. Eyring. Amsterdam: Elsevier, 2013. 540 p.

Applicant publications list

Journal papers

Manannikov D.A., Parshukov V.P., Nikolaychuk P.A. Experimental and theoretical investigation of the corrosion properties of steel X13 in the acetic acid at 20 and 80 °c // Periódico Tchê Química. 2017. Vol. 14. No 27. P. 19–29.

Nikolaychuk P.A. The revised Pourbaix diagram for silicon // Silicon. 2014a. Vol. 6. No 2. P. 109–116.

Nikolaychuk P.A. The Third Dimension in Pourbaix Diagrams: A Further Extension // Journal of Chemical Education. 2014b. Vol. 91. No 5. P. 763–765.

Nikolaychuk P.A. Thermodynamic evaluation of electrochemical stability of Me – Si systems (Me = 4th row transition metal) // Журнал Сибирского федерального университета. Серия Химия. 2015c. Т. 8. № 2. С. 160–180.

Nikolaychuk P.A. The revised potential – pH diagram of Sc – H_2O system // Научные ведомости Белгородского государственного университета. Серия: Естественные науки. 2016a. №. 25 (246). Вып. 37. С. 70–87.

Nikolaychuk P.A. Aleksandr Georgievich Tyurin (1953–2015) and his research in corrosion science // Journal of Solid State Electrochemistry. 2017. Vol. 21. No 1. P. 1–8.

Nikolaychuk P.A., Tyurin A.G. Thermodynamics of chemical and electrochemical stability of copper-nickel alloys // Protection of Metals and Physical Chemistry of Surfaces. 2012a. Vol. 48. No 4. P. 462–476.

Nikolaychuk P.A., Tyurin A.G. Thermodynamic assessment of chemical and electrochemical stability of nickel – silicon system alloys // Corrosion Science. 2013a. Vol. 73. P. 237–244.

Nikolaychuk P.A., Tyurin A.G. Thermodynamic Evaluation of Corrosion-Electrochemical Behaviour of Silicon Brass CuZn17Si3 // Inorganic Materials. 2013b. Vol. 49. No 5. P. 457–467.

Nikolaychuk P.A. Is calomel truly a poison and what happens when it enters the human stomach? A study from the thermodynamic viewpoint // Main Group Metal Chemistry. 2016b. Vol. 39. No 1–2. P. 41–47.

Tyurin A.G., Manannikov D.A., Parshukov V.P., Antonova A. V., Nikolaychuk P.A. Method of estimation of corrosion stability of

multicomponent alloys using equilibrium and polarization potential – pH diagrams // Anti-Corrosion Methods and Materials. 2016. Vol. 63. No 5. P. 386–397.

Николайчук П.А., Шаляпина Т.И., Тюрин А.Г., Мосунова Т.В. Термодинамика химической и электрохимической устойчивости сплавов системы Mn – Si // Вестник Южно-Уральского государственного университета. Серия „Химия“. 2010. №. 4. Вып. 31(207). С. 72–82.

Николайчук П.А., Бирюков А.И., Працкова С.Е. Жизнь и научный путь Александра Георгиевича Тюрина // Бутлеровские сообщения. 2016. Т. 48. С. 39A–48A.

Николайчук П.А., Тюрин А.Г. Термодинамика химической и электрохимической устойчивости сплавов системы Ti – Si // Бутлеровские сообщения. 2011a. Т. 24. № 2. С. 77–87.

Николайчук П.А., Тюрин А.Г. Уточнённая диаграмма Пурбе для молибдена // Бутлеровские сообщения. 2011b. Т. 24. № 2. С. 101–105.

Николайчук П.А., Тюрин А.Г. Термодинамика химической и электрохимической устойчивости сплавов системы Mo – Si // Бутлеровские сообщения. 2011c. Т. 24. № 2. С. 95–100.

Николайчук П.А., Тюрин А.Г. Термодинамика химической и электрохимической устойчивости сплавов системы Cu – Si // Бутлеровские сообщения. 2011d. Т. 24. № 2. С. 88–94.

Николайчук П.А., Тюрин А.Г. Термодинамика химической и электрохимической устойчивости медно-никелевых сплавов // Физикохимия поверхности и защита материалов. 2012a. Т. 48. № 4. С. 398–412.

Николайчук П.А., Тюрин А.Г. Термодинамическая оценка коррозионно-электрохимических свойств кремнистой латуни ЛК80-3 // Неорганические материалы. 2013. Т. 49. № 5. С. 480–490.

Тюрин А.Г., Мананников Д.А., Паршуков В.П., Николайчук П.А. Коррозионно-электрохимическое поведение стали Х1310 в растворе 5% NaCl + 0,5% CH_3COOH + CH_3COONa + CO_2 // Journal of Corrosion Science and Engineering. 2016. Vol. 19. Preprint No 27. P. 1–12.

Тюрин А.Г., Мосунова Т.В., Николайчук П.А. Термодинамика химической и электрохимической устойчивости силицидов кобальта // Вестник Южно-Уральского государственного

университета. Серия „Химия“. 2010. №. 3. Вып. 11(187). С. 52–60.
Тюрин А.Г., Николайчук П.А., Кабардин А.М. Термодинамическая оценка коррозионно-электрохимического поведения сплавов системы марганец-германий // Journal of Corrosion Science and Engineering. 2016. Vol. 19. Preprint No 20. P. 1–38.
Тюрин А.Г., Николайчук П.А., Канатьева И.И. Термодинамика химической и электрохимической устойчивости сплавов системы Fe – Ge // Коррозия: материалы, защита. 2015. № 12. С. 1–9.

Conference papers

Nikolaychuk P.A. The potential – pH diagram for Mn – H_2O system // Фундаментальные и прикладные исследования в области химии и экологии: материалы международной научно-практической конференции студентов, аспирантов и молодых учёных. Курск: ЗАО “Университетская книга”, 2015a. С. 120–123.
Nikolaychuk P.A. The potential – pH diagram for Fe – H_2O system // Фундаментальные и прикладные исследования в области химии и экологии: материалы международной научно-практической конференции студентов, аспирантов и молодых учёных. Курск: ЗАО “Университетская книга”, 2015b. С. 80–83.
Nikolaychuk P.A., Tyurin A.G. The analysis of standard Gibbs energies of formation of MeO_2 type oxides of fourth period d-elements // Abstracts of the XVIII International Conference on Chemical Thermodynamics in Russia (RCCT-2011). Vol. 2. Samara: Samara State Technical University, 2011a. С. 17–18.
Nikolaychuk P.A., Tyurin A.G. Method of estimating the standard Gibbs energies of formation of binary compounds // Abstracts of the XVIII International Conference on Chemical Thermodynamics in Russia (RCCT-2011). Vol. 2. Samara: Samara State Technical University, 2011b. С. 16–17.
Nikolaychuk P.A., Tyurin A.G. The estimation of Fe – Si system oxidation at 298 K in air and water environments // Physical Chemistry 2012: proceedings of the 11th International Conference on Fundamental and Applied Aspects of Physical Chemistry. Vol. 1. Belgrade: Society of Physical Chemists of Serbia, 2012b. С. 37–39.
Николайчук П.А. О методах расчёта зависимости энергии Гиббса образования ионов в водных средах от давления и температуры // Физико-химические процессы в конденсированных средах и на межфазных границах (ФАГРАН—2015): материалы VII

Всероссийской конференции (г. Воронеж, 10—13 ноября 2015 г.). Воронеж: Издательско-полиграфический центр «Научная книга», 2015. С. 377–380.

Николайчук П.А., Канатьева И.И., Тюрин А.Г. Уточнённая диаграмма Пурбе для меди // Современные проблемы теоретической и экспериментальной химии: межвузовский сборник научных трудов VII Всероссийской конференции молодых учёных с международным участием. Саратов: ООО Издательство «КУБиК», 2010. С. 287–291.

Николайчук П.А., Тюрин А.Г. Уточнённая диаграмма Пурбе для цинка // Современные проблемы теоретической и экспериментальной химии: межвузовский сборник научных трудов VIII Всероссийской конференции молодых учёных с международным участием. Саратов: ООО Издательство «КУБиК», 2011е. С. 227–230.

Николайчук П.А., Тюрин А.Г. Термодинамика химичекой и электрохимической устойчивости систем Me – Si (Me = Ti, Mo, Mn, Fe, Co, Ni, Cu, Zn) // Итоги диссертационных исследований: Материалы IV Всероссийского конкурса молодых ученых. Том 1. Москва: РАН, 2012b. С. 54–68.

Тюрин А.Г., Канатьева И.И., Николайчук П.А. Диаграммы химической и электрохимической устойчивости сплавов системы Fe – Ge // X Международное Курнаковское совещание по физико-химическому анализу: сборник трудов. Том 2.. Самара: Издательство Самарского государственного технического университета, 2013. С. 85–90.

Appendices
A. Software „EpHDiagrPlot“ for calculating and plotting potential – pH diagrams

A software „EpHDiagrPlot” is written on *Visual Basic for Applicatons* (VBA) incorporated into *Microsoft Excel*™ software. It is an Excel spreadsheet designed for calculations of the oxygen partial pressures for the equilibria of the metals with oxygen and of the potentials and pH for the equilibria in aqueous media, and for plotting the potential – pH diagrams. The starting screen of the program is presented in Figure 74.

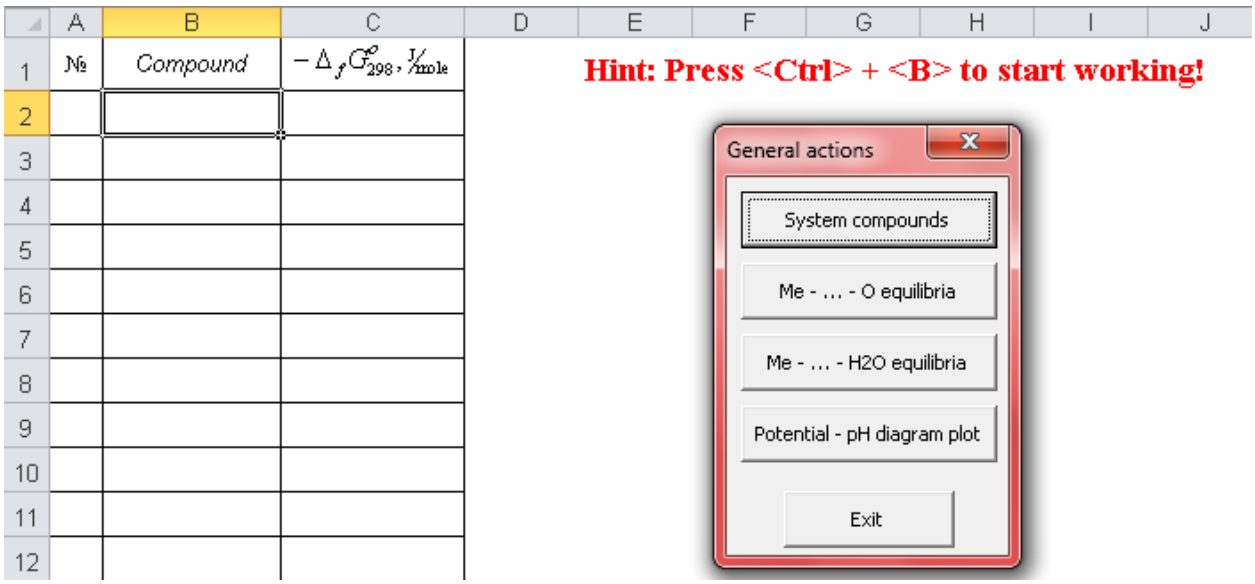

Fig. 74. The starting screen of the program „EpHDiagrPlot”.

The spreadsheet consists of four modules. The first one collects initial data needed for all further calculations (the chemical formulae of the compounds and their values of the Gibbs energies of formation). Up to 100 species might be present in a spreadsheet. The Gibbs free energies of formation multiplied by –1 should be entered. Figure 75 shows the example of the first module work.

The second module helps to calculate partial oxygen pressures for the equilibria of the system compounds with oxygen using the equation (20). User might select the reactants and the products from the dropping lists containing the compounds entered into the first module. After that the program calculates the oxygen partial pressure for the given equilibrium and places it into the table. Figure 76 shows the example of the second module work.

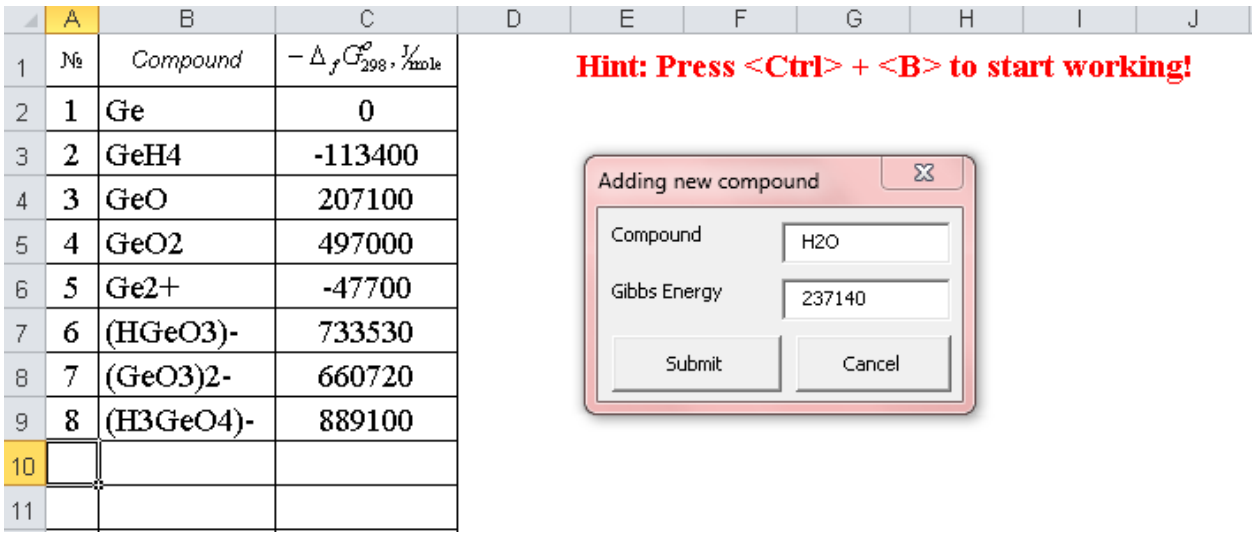

Fig. 75. The first module of the program „EpHDiagrPlot" that collects the initial data.

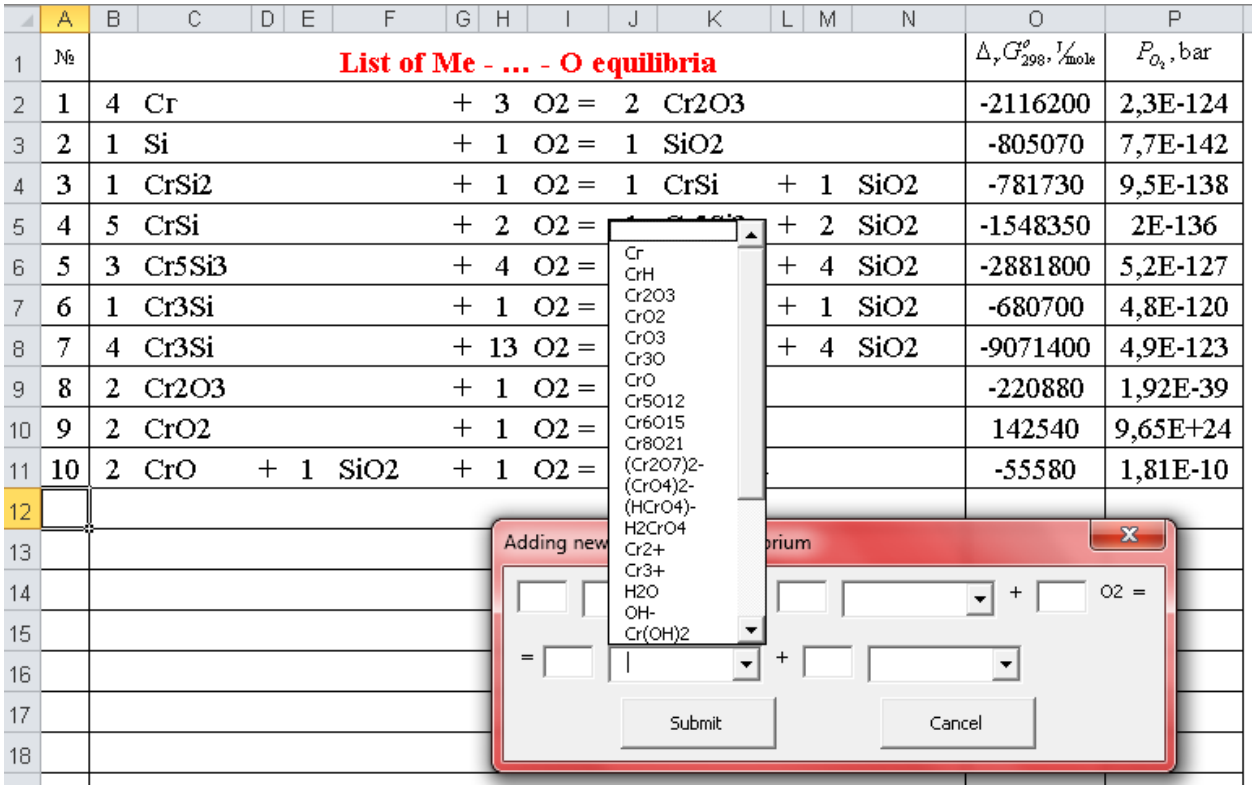

Fig. 76. The second module of the program „EpHDiagrPlot" for the equilibria of the compounds with oxygen.

The third module helps to calculate equations for the lines on potential – pH diagram for the equilibria of the system compounds in aqueous media using the equations (27) and (28). User might select the reactants and the products from the dropping lists containing the compounds entered into the first module. After that the program determines the equilibrium type and calculates einther the potential at pH

= 0 and the slope of the line for horizontal and sloped lines, or the pH value for vertical lines, and places them into the table. Figure 77 shows the example of the third module work.

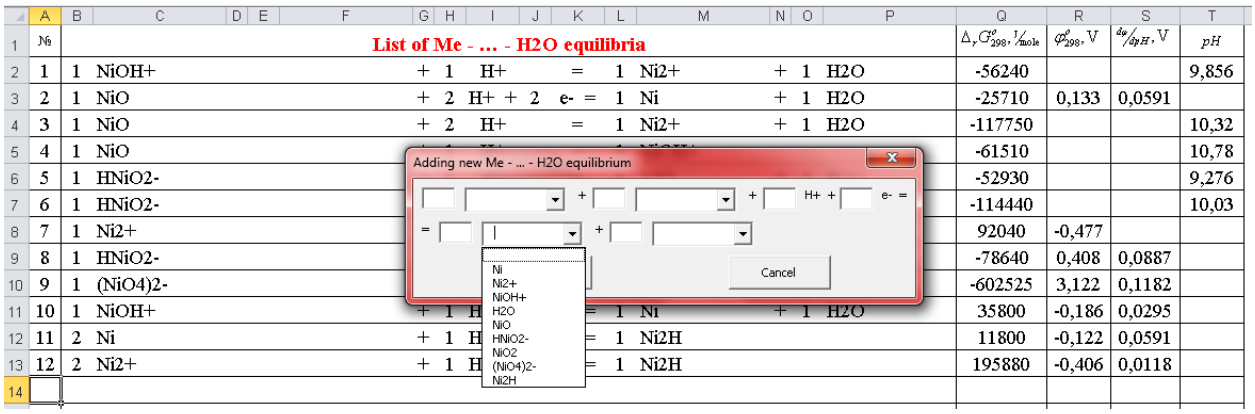

Fig. 77. The third module of the program „EpHDiagrPlot" for the equilibria in aqueous media.

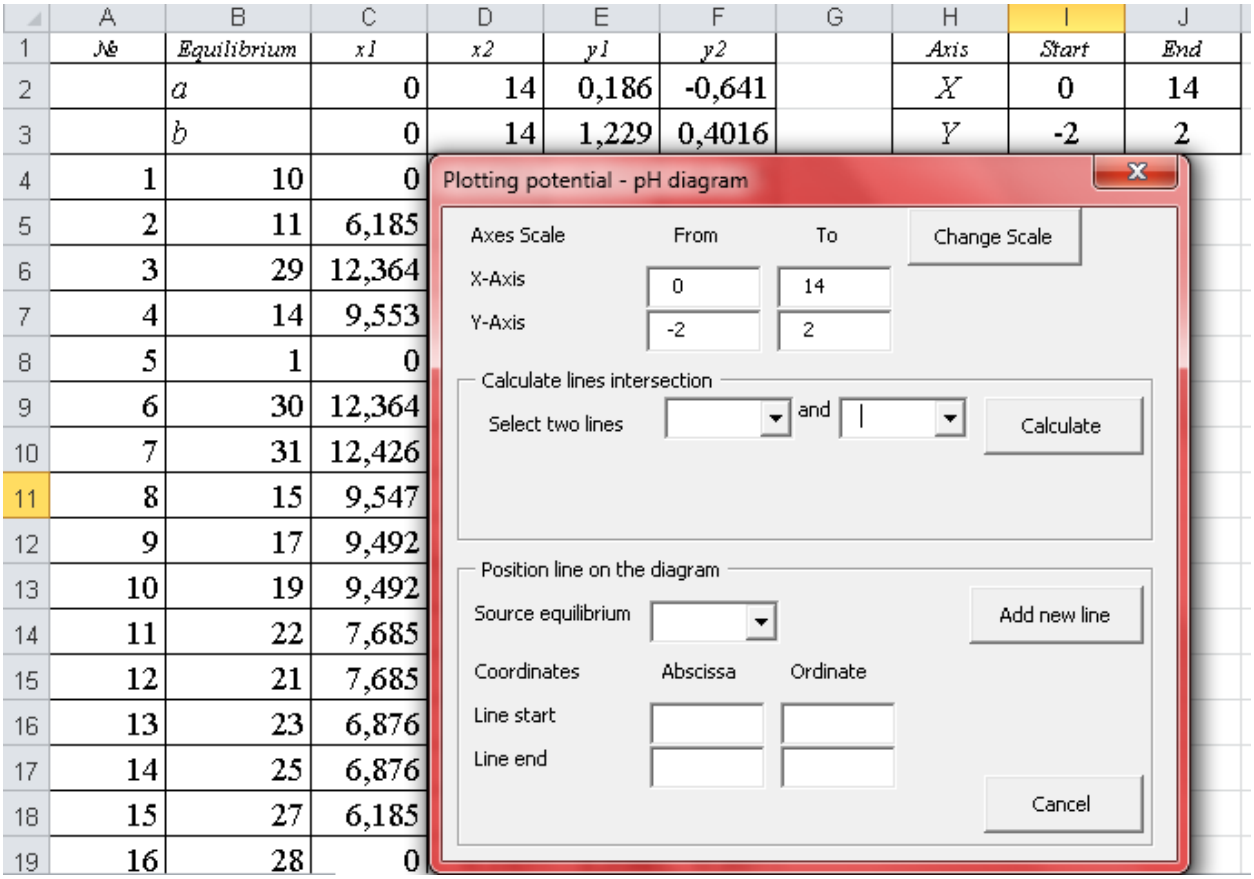

Fig. 78. The fourth module of the program „EpHDiagrPlot" that plots the potential – pH diagram.

The last module plots the potential – pH diagram using the equilibria calculated by the third module. User might calculate the coordinates of the possible intersection point for lines corresponding to any two selected

equilibria, change the scale on the axes or add new lines to the plot. Figure 78 shows the example of the fourth module work.

The VBA code of the software is listed below.

```
Public a(1 To 100) As Integer, d(1 To 50) As Integer, f(1 To 100) As Integer,
g(1 To 100, 1 To 2) As Integer
Public b(1 To 100) As String, R(1 To 50) As String, RR(1 To 50) As String,
RRR(1 To 50) As String, RRRR(1 To 50) As String
Public c(1 To 100) As Single, T(1 To 50) As Single, TT(1 To 50) As Single,
TTT(1 To 50) As Single, TTTT(1 To 50) As Single, TOxx(1 To 50) As Single
Public S(1 To 100) As String, SS(1 To 100) As String, SSS(1 To 100) As
String, SSSS(1 To 100) As String
Public U(1 To 100) As Single, UU(1 To 100) As Single, UUU(1 To 100) As
Single, UUUU(1 To 100) As Single, Uh(1 To 100) As Single, Ue(1 To 100) As
Single, x(1 To 100) As Single, xx(1 To 100) As Single, y(1 To 100) As Single,
yy(1 To 100) As Single
Public resG1(1 To 50) As Single, resP(1 To 50) As Double
Public resG2(1 To 100) As Single, resF(1 To 100) As Single, resFF(1 To 100)
As Single, resPH(1 To 100) As Single
Public i As Integer, j As Integer, k As Integer, l As Integer, m As Integer,
ax As Integer, axx As Integer, ay As Integer, ayy As Integer
Public in1 As Integer, in2 As Integer, in3 As Integer
Public datarange As Range, equ1range As Range, equ2range As Range, linerange
As Range

Rem a - data counter, b - compound name, c - Gibbs energy
Rem d, f - equilibrium counters, g - line counter, R, RR; S, SS - reactants,
RRR, RRRR; SSS, SSSS - products, T, TT, TTT, TTTT, TOxx; U, UU, UUU, UUUU,
Uh, Ue - coefficients
Rem x,y - lines start coordinates, xx, yy - lines end coordinates,ax,axx,
ay,ayy - plot scale borders
Rem resG1 - results for dG values of Me - ...  - O equilibria, resP - results
for P(O2) of its.
Rem resG2 - results for dG values of Me - ...  - H2O equilibria, resF - line
ordinates, resFF - line angles, resPH - values of pH
Rem datarange is a sheet, containing primary data
Rem equ1range is a sheet, containing Me - ...  - O equilibria
Rem equ2range is a sheet, containing Me - ...  - H2O equilibria
Rem linerange is a sheet, containing lines on a diagram
Rem in1, in2, in3 - indices of selected lines on a diagram
Rem i, j, k, l, m - counters

Sub begin()
Set datarange = Data.Range("A2")
Set equ1range = O2.Range("A2")
Set equ2range = H2O.Range("A2")
Set linerange = Lines.Range("A2")
Call Indices
Call Evaluate
Actions.Show
End Sub

Sub Evaluate()
Reactions1.R1.Clear
```

```
Reactions1.R2.Clear
Reactions1.R3.Clear
Reactions1.R4.Clear
Reactions1.R1.AddItem ""
Reactions1.R2.AddItem ""
Reactions1.R3.AddItem ""
Reactions1.R4.AddItem ""
Reactions2.R1.Clear
Reactions2.R2.Clear
Reactions2.R3.Clear
Reactions2.R4.Clear
Reactions2.R1.AddItem ""
Reactions2.R2.AddItem ""
Reactions2.R3.AddItem ""
Reactions2.R4.AddItem ""
Data.Activate
datarange.Range("B1").Activate
Let i = 1
Let j = 1
Let l = 1
Let m = 1
Do Until ActiveCell.Value = ""
Let a(i) = i
Let b(i) = ActiveCell.Text
Let c(i) = ActiveCell.Offset(0, 1).Value
ActiveCell.Offset(0, -1).Value = a(i)
ActiveCell.Offset(1, 0).Activate
Reactions1.R1.AddItem b(i)
Reactions1.R2.AddItem b(i)
Reactions1.R3.AddItem b(i)
Reactions1.R4.AddItem b(i)
Reactions2.R1.AddItem b(i)
Reactions2.R2.AddItem b(i)
Reactions2.R3.AddItem b(i)
Reactions2.R4.AddItem b(i)
Let i = i + 1
Loop
O2.Activate
equ1range.Range("A1").Activate
Do Until ActiveCell.Value = ""
Let d(j) = ActiveCell.Value
Let T(j) = ActiveCell.Offset(0, 1).Value
Let R(j) = ActiveCell.Offset(0, 2).Value
For k = 1 To i - 1
If R(j) = b(k) Then
ActiveCell.Offset(50, 2).Value = a(k)
Exit For
End If
Next k
If R(j) = "" Then ActiveCell.Offset(50, 2).Value = 50
Let TT(j) = ActiveCell.Offset(0, 4).Value
Let RR(j) = ActiveCell.Offset(0, 5).Value
For k = 1 To i - 1
If RR(j) = b(k) Then
ActiveCell.Offset(50, 5).Value = a(k)
Exit For
```

```
End If
Next k
If RR(j) = "" Then ActiveCell.Offset(50, 5).Value = 50
Let TOxx(j) = ActiveCell.Offset(0, 7).Value
Let TTT(j) = ActiveCell.Offset(0, 9).Value
Let RRR(j) = ActiveCell.Offset(0, 10).Value
For k = 1 To i - 1
If RRR(j) = b(k) Then
ActiveCell.Offset(50, 10).Value = a(k)
Exit For
End If
Next k
If RRR(j) = "" Then ActiveCell.Offset(50, 10).Value = 50
Let TTTT(j) = ActiveCell.Offset(0, 12).Value
Let RRRR(j) = ActiveCell.Offset(0, 13).Value
For k = 1 To i - 1
If RRRR(j) = b(k) Then
ActiveCell.Offset(50, 13).Value = a(k)
Exit For
End If
Next k
If RRRR(j) = "" Then ActiveCell.Offset(50, 13).Value = 50
Let resG1(j) = T(j) * ActiveCell.Offset(100, 2).Value + TT(j) *
ActiveCell.Offset(100, 5).Value - TTT(j) * ActiveCell.Offset(100, 10).Value -
TTTT(j) * ActiveCell.Offset(100, 13).Value
ActiveCell.Offset(0, 14).Value = resG1(j)
Let resP(j) = 1 / (Exp(-resG1(j) / (TOxx(j) * 8.3144 * 298)))
ActiveCell.Offset(0, 15).Value = resP(j)
ActiveCell.Offset(1, 0).Activate
Let j = j + 1
Loop
For k = j To 49
ActiveCell.Offset(k - j + 50, 2).Value = 50
ActiveCell.Offset(k - j + 50, 5).Value = 50
ActiveCell.Offset(k - j + 50, 10).Value = 50
ActiveCell.Offset(k - j + 50, 13).Value = 50
Next k
H2O.Activate
equ2range.Range("A1").Activate
Do Until ActiveCell.Value = ""
Let f(l) = ActiveCell.Value
Let U(l) = ActiveCell.Offset(0, 1).Value
Let S(l) = ActiveCell.Offset(0, 2).Value
For k = 1 To i - 1
If S(l) = b(k) Then
ActiveCell.Offset(100, 2).Value = c(k)
Exit For
End If
Next k
Let UU(l) = ActiveCell.Offset(0, 4).Value
Let SS(l) = ActiveCell.Offset(0, 5).Value
For k = 1 To i - 1
If SS(l) = b(k) Then
ActiveCell.Offset(100, 5).Value = c(k)
Exit For
End If
```

```
Next k
Let Uh(l) = ActiveCell.Offset(0, 7).Value
Let Ue(l) = ActiveCell.Offset(0, 9).Value
Let UUU(l) = ActiveCell.Offset(0, 11).Value
Let SSS(l) = ActiveCell.Offset(0, 12).Value
For k = 1 To i - 1
If SSS(l) = b(k) Then
ActiveCell.Offset(100, 12).Value = c(k)
Exit For
End If
Next k
Let UUUU(l) = ActiveCell.Offset(0, 14).Value
Let SSSS(l) = ActiveCell.Offset(0, 15).Value
For k = 1 To i - 1
If SSSS(l) = b(k) Then
ActiveCell.Offset(100, 15).Value = c(k)
Exit For
End If
Next k
Let resG2(l) = U(l) * ActiveCell.Offset(100, 2).Value + UU(l) *
ActiveCell.Offset(100, 5).Value - UUU(l) * ActiveCell.Offset(100, 12).Value -
UUUU(l) * ActiveCell.Offset(100, 15).Value
ActiveCell.Offset(0, 16).Value = resG2(l)
If Ue(l) <> 0 Then
Let resF(l) = -resG2(l) / (Ue(l) * 96485)
Let resFF(l) = 0.0591 * Uh(l) / Ue(l)
ActiveCell.Offset(0, 17).Value = resF(l)
If resFF(l) <> 0 Then ActiveCell.Offset(0, 18).Value = resFF(l)
End If
If Ue(l) = 0 Then Let resPH(l) = -resG2(l) / (2.303 * 8.3144 * 298 * Uh(l)):
ActiveCell.Offset(0, 19).Value = resPH(l)
ActiveCell.Offset(1, 0).Activate
l = l + 1
Loop
For k = l To 99
ActiveCell.Offset(k - j + 100, 2).Value = ""
ActiveCell.Offset(k - j + 100, 5).Value = ""
ActiveCell.Offset(k - j + 100, 12).Value = ""
ActiveCell.Offset(k - j + 100, 15).Value = ""
Next k
Data.Activate
End Sub

Sub Indices()
O2.Activate
Range("C102").Select
ActiveCell.FormulaR1C1 = "=INDEX(Data!R2C3:R100C3,'O2'!R[-50]C)"
Selection.AutoFill Destination:=Range("C102:C150"), Type:=xlFillDefault
Range("C102").Select
Selection.Copy
Range("F102:F150").Select
ActiveSheet.Paste
Range("K102:K150").Select
ActiveSheet.Paste
Range("N102:N150").Select
ActiveSheet.Paste
```

```
End Sub

Sub dia()
Lines.Activate
linerange.Range("I1").Activate
Let ax = ActiveCell.Value
Let axx = ActiveCell.Offset(0, 1).Value
Let ay = ActiveCell.Offset(1, 0).Value
Let ayy = ActiveCell.Offset(1, 1).Value
Diagramma.xs.Value = Str(ax)
Diagramma.xe.Value = Str(axx)
Diagramma.ys.Value = Str(ay)
Diagramma.ye.Value = Str(ayy)
Diagramma.Line1.Clear
Diagramma.Line2.Clear
Diagramma.Line.Clear
For k = 1 To l - 1
Diagramma.Line1.AddItem (k)
Diagramma.Line2.AddItem (k)
Diagramma.Line.AddItem (k)
Next k
Diagramma.x1.Value = ""
Diagramma.x2.Value = ""
Diagramma.y1.Value = ""
Diagramma.y2.Value = ""
Diagramma.x1.Locked = False
Diagramma.x2.Locked = False
Diagramma.y1.Locked = False
Diagramma.y2.Locked = False
linerange.Range("B1").Value = "a"
linerange.Range("B2").Value = "b"
linerange.Range("C1").Value = ax
linerange.Range("C2").Value = ax
linerange.Range("D1").Value = axx
linerange.Range("D2").Value = axx
linerange.Range("E1").Value = 0.186 - 0.0591 * ax
linerange.Range("E2").Value = 1.229 - 0.0591 * ax
linerange.Range("F1").Value = 0.186 - 0.0591 * axx
linerange.Range("F2").Value = 1.229 - 0.0591 * axx
If Diagr.SeriesCollection.Count > 1 Then
For k = 1 To Diagr.SeriesCollection.Count - 1
Diagr.SeriesCollection(1).Delete
Next k
End If
Diagr.SeriesCollection(1).Border.ColorIndex = 2
Diagr.SeriesCollection(1).MarkerStyle = xlNone
Diagr.SeriesCollection.NewSeries
Diagr.SeriesCollection(2).XValues = linerange.Range("C1:D1")
Diagr.SeriesCollection(2).Values = linerange.Range("E1:F1")
Diagr.SeriesCollection(2).AxisGroup = 2
Diagr.SeriesCollection.NewSeries
Diagr.SeriesCollection(3).XValues = linerange.Range("C2:D2")
Diagr.SeriesCollection(3).Values = linerange.Range("E2:F2")
Diagr.SeriesCollection(3).AxisGroup = 2
With Diagr.Axes(xlCategory)
.MinimumScale = ax
```

```
.MaximumScale = axx
.MajorUnit = Int((axx - ax) / 5)
.Crosses = xlCustom
.CrossesAt = ax
End With
With Diagr.Axes(xlValue)
.MinimumScale = ay
.MaximumScale = ayy
.Crosses = xlCustom
.CrossesAt = ay
End With
With Diagr.Axes(xlValue, xlSecondary)
.MinimumScale = ay
.MaximumScale = ayy
.Crosses = xlCustom
.CrossesAt = ay
End With
With Diagr.SeriesCollection(2).Border
.ColorIndex = 1
.Weight = xlThin
.LineStyle = xlDash
End With
Diagr.SeriesCollection(2).MarkerStyle = xlNone
With Diagr.SeriesCollection(3).Border
.ColorIndex = 1
.Weight = xlThin
.LineStyle = xlDash
End With
Diagr.SeriesCollection(3).MarkerStyle = xlNone
linerange.Range("A3").Activate
Do Until ActiveCell.Value = ""
Let g(m, 1) = ActiveCell.Value
Let g(m, 2) = ActiveCell.Offset(0, 1).Value
Let x(m) = ActiveCell.Offset(0, 2).Value
Let xx(m) = ActiveCell.Offset(0, 3).Value
Let y(m) = ActiveCell.Offset(0, 4).Value
Let yy(m) = ActiveCell.Offset(0, 5).Value
Diagr.SeriesCollection.NewSeries
Diagr.SeriesCollection(m + 3).XValues = linerange.Range(Cells(m + 2, 3),
Cells(m + 2, 4))
Diagr.SeriesCollection(m + 3).Values = linerange.Range(Cells(m + 2, 5),
Cells(m + 2, 6))
Diagr.SeriesCollection(m + 3).Border.ColorIndex = 1
Diagr.SeriesCollection(m + 3).MarkerStyle = xlNone

m = m + 1
ActiveCell.Offset(1, 0).Activate
Loop
Diagramma.Show
End Sub

Private Sub CommandButton1_Click()
Actions.Hide
Compounds.Show
End Sub
```

```
Private Sub CommandButton2_Click()
Actions.Hide
End Sub

Private Sub CommandButton3_Click()
Actions.Hide
O2.Activate
Reactions1.Show
End Sub

Private Sub CommandButton4_Click()
Actions.Hide
H2O.Activate
Reactions2.Show
End Sub

Private Sub Diagram_Click()
Actions.Hide
Call dia
End Sub

Private Sub Done_Click()
Compounds.Hide
Actions.Show
End Sub

Private Sub Label2_Click()

End Sub

Private Sub Submit_Click()
GoTo Beg
Ers: MsgBox ("Invalid data!"): GoTo fin
Beg: On Error GoTo Ers
Let a(i) = i
Let b(i) = Compounds.Compound.Text
Let c(i) = Compounds.Energy.Value
Data.Activate
datarange.Range("A" + LTrim(Str(i))) = a(i)
datarange.Range("B" + LTrim(Str(i))) = b(i)
datarange.Range("C" + LTrim(Str(i))) = c(i)
Let i = i + 1
fin: Compounds.Hide
Actions.Show
End Sub

Private Sub Calculate_Click()
Let in1 = Diagramma.Line1.Value
Let in2 = Diagramma.Line2.Value
If resFF(in1) = resFF(in2) Or (Ue(in1) = 0 And Ue(in2) = 0) Then
Diagramma.Result.Caption = "Parallel lines do not intersect!"
If Ue(in1) = 0 And Ue(in2) <> 0 Then Diagramma.Result.Caption = "Potential: "
+ FormatNumber(resF(in2) - resFF(in2) * resPH(in1), 3) + "; pH: " +
FormatNumber(resPH(in1), 3)
```

```
If Ue(in2) = 0 And Ue(in1) <> 0 Then Diagramma.Result.Caption = "Potential: "
+ FormatNumber(resF(in1) - resFF(in1) * resPH(in2), 3) + "; pH: " +
FormatNumber(resPH(in2), 3)
If Ue(in1) <> 0 And Ue(in2) <> 0 And resFF(in1) <> resFF(in2) Then
Diagramma.Result.Caption = "Potential: " + FormatNumber(resF(in1) -
resFF(in1) * (resF(in1) - resF(in2)) / (resFF(in1) - resFF(in2)), 3) + " | "
+ FormatNumber(resF(in2) - resFF(in2) * (resF(in1) - resF(in2)) / (resFF(in1)
- resFF(in2)), 3) + "; pH: " + FormatNumber((resF(in1) - resF(in2)) /
(resFF(in1) - resFF(in2)), 3)
End Sub


Private Sub ChangeScale_Click()
Lines.Activate
linerange.Range("I1").Activate
Let ax = Val(Diagramma.xs.Value)
Let axx = Val(Diagramma.xe.Value)
Let ay = Val(Diagramma.ys.Value)
Let ayy = Val(Diagramma.ye.Value)
ActiveCell.Value = ax
ActiveCell.Offset(0, 1).Value = axx
ActiveCell.Offset(1, 0).Value = ay
ActiveCell.Offset(1, 1).Value = ayy
End Sub

Private Sub Done_Click()
Diagramma.Hide
Data.Activate
Actions.Show
End Sub


Private Sub Line_Change()
If Diagramma.Visible = False Then GoTo fin
Diagramma.x1.Value = ax
Diagramma.x2.Value = axx
Diagramma.y1.Value = ay
Diagramma.y2.Value = ayy
Let in3 = Diagramma.Line.Value
If Ue(in3) <> 0 Then
Diagramma.x1.Locked = False
Diagramma.x2.Locked = False
Diagramma.y1.Locked = True
Diagramma.y2.Locked = True
Diagramma.y1.Value = FormatNumber(resF(in3) - resFF(in3) *
Diagramma.x1.Value, 3)
Diagramma.y2.Value = FormatNumber(resF(in3) - resFF(in3) *
Diagramma.x2.Value, 3)
End If
If Ue(in3) = 0 Then
Diagramma.x1.Locked = True
Diagramma.x2.Locked = True
Diagramma.y1.Locked = False
Diagramma.y2.Locked = False
Diagramma.x1.Value = FormatNumber(resPH(in3), 3)
Diagramma.x2.Value = FormatNumber(resPH(in3), 3)
```

```
End If
fin:
End Sub

Private Sub Line1_Change()
Diagramma.Result.Caption = ""
End Sub

Private Sub Line2_Change()
Diagramma.Result.Caption = ""
End Sub


Private Sub Place_Click()
Lines.Activate
Let g(m, 1) = m
Let g(m, 2) = Diagramma.Line.Value
Let x(m) = Diagramma.x1.Value
Let xx(m) = Diagramma.x2.Value
Let y(m) = Diagramma.y1.Value
Let yy(m) = Diagramma.y2.Value
linerange.Range("A" + LTrim(Str(m + 2))) = g(m, 1)
linerange.Range("B" + LTrim(Str(m + 2))) = g(m, 2)
linerange.Range("C" + LTrim(Str(m + 2))) = x(m)
linerange.Range("D" + LTrim(Str(m + 2))) = xx(m)
linerange.Range("E" + LTrim(Str(m + 2))) = y(m)
linerange.Range("F" + LTrim(Str(m + 2))) = yy(m)
Diagr.SeriesCollection.NewSeries
Diagr.SeriesCollection(m + 3).XValues = linerange.Range(Cells(m + 2, 3),
Cells(m + 2, 4))
Diagr.SeriesCollection(m + 3).Values = linerange.Range(Cells(m + 2, 5),
Cells(m + 2, 6))
Diagr.SeriesCollection(m + 3).Border.ColorIndex = 1
Diagr.SeriesCollection(m + 3).MarkerStyle = xlNone
Let m = m + 1
End Sub

Private Sub Result_Click()

End Sub

Private Sub x1_Change()
If Diagramma.Visible = False Then GoTo fin
If IsNumeric(Diagramma.x1.Value) = False Then GoTo fin
Let in3 = Diagramma.Line.Value
If Ue(in3) <> 0 Then
Diagramma.x1.Locked = False
Diagramma.y1.Locked = True
Diagramma.y1.Value = FormatNumber(resF(in3) - resFF(in3) *
Diagramma.x1.Value, 3)
End If
fin:
End Sub

Private Sub x2_Change()
If Diagramma.Visible = False Then GoTo fin
```

```
If IsNumeric(Diagramma.x2.Value) = False Then GoTo fin
Let in3 = Diagramma.Line.Value
If Ue(in3) <> 0 Then
Diagramma.x2.Locked = False
Diagramma.y2.Locked = True
Diagramma.y2.Value     =     FormatNumber(resF(in3)     -     resFF(in3)     *
Diagramma.x2.Value, 3)
End If
fin:
End Sub

Private Sub Done_Click()
Reactions1.Hide
Data.Activate
Actions.Show
End Sub

Private Sub Submit_Click()
GoTo Beg
Ers: MsgBox ("Invalid data!"): GoTo fin
Beg: On Error GoTo Ers
Let d(j) = j
Let R(j) = Reactions1.R1.Text
Let RR(j) = Reactions1.R2.Text
Let RRR(j) = Reactions1.R3.Text
Let RRRR(j) = Reactions1.R4.Text
Let T(j) = Val(Reactions1.T1.Value)
Let TT(j) = Val(Reactions1.T2.Value)
Let TTT(j) = Val(Reactions1.T3.Value)
Let TTTT(j) = Val(Reactions1.T4.Value)
Let TOxx(j) = Val(Reactions1.TOx.Value)
O2.Activate
equ1range.Range("A" + LTrim(Str(j))) = j
If T(j) <> 0 Then equ1range.Range("B" + LTrim(Str(j))) = T(j)
equ1range.Range("C" + LTrim(Str(j))) = R(j)
If R(j) <> "" And RR(j) <> "" Then equ1range.Range("D" + LTrim(Str(j))) = "+"
If TT(j) <> 0 Then equ1range.Range("E" + LTrim(Str(j))) = TT(j)
equ1range.Range("F" + LTrim(Str(j))) = RR(j)
equ1range.Range("G" + LTrim(Str(j))) = "+"
If TOxx(j) <> 0 Then equ1range.Range("H" + LTrim(Str(j))) = TOxx(j)
equ1range.Range("I" + LTrim(Str(j))) = "O2 ="
If TTT(j) <> 0 Then equ1range.Range("J" + LTrim(Str(j))) = TTT(j)
equ1range.Range("K" + LTrim(Str(j))) = RRR(j)
If RRR(j) <> "" And RRRR(j) <> "" Then equ1range.Range("L" + LTrim(Str(j))) =
"+"
If TTTT(j) <> 0 Then equ1range.Range("M" + LTrim(Str(j))) = TTTT(j)
equ1range.Range("N" + LTrim(Str(j))) = RRRR(j)
If Reactions1.R1.Text <> "" Then equ1range.Range("C" + LTrim(Str(j + 50))) =
Reactions1.R1.ListIndex Else equ1range.Range("C" + LTrim(Str(j + 50))) = 50
If Reactions1.R2.Text <> "" Then equ1range.Range("F" + LTrim(Str(j + 50))) =
Reactions1.R2.ListIndex Else equ1range.Range("F" + LTrim(Str(j + 50))) = 50
If Reactions1.R3.Text <> "" Then equ1range.Range("K" + LTrim(Str(j + 50))) =
Reactions1.R3.ListIndex Else equ1range.Range("K" + LTrim(Str(j + 50))) = 50
If Reactions1.R4.Text <> "" Then equ1range.Range("N" + LTrim(Str(j + 50))) =
Reactions1.R4.ListIndex Else equ1range.Range("N" + LTrim(Str(j + 50))) = 50
```

```
Let resG1(j) = T(j) * equ1range.Range("C" + LTrim(Str(j + 100))).Value +
TT(j) * equ1range.Range("F" + LTrim(Str(j + 100))).Value - TTT(j) *
equ1range.Range("K" + LTrim(Str(j + 100))).Value - TTTT(j) *
equ1range.Range("N" + LTrim(Str(j + 100))).Value
Let resP(j) = 1 / Exp(-resG1(j) / (TOxx(j) * 8.3144 * 298))
equ1range.Range("O" + LTrim(Str(j))) = resG1(j)
equ1range.Range("P" + LTrim(Str(j))) = resP(j)
Let j = j + 1
fin:
End Sub

Private Sub Done_Click()
Reactions2.Hide
Data.Activate
Actions.Show
End Sub

Private Sub Submit_Click()
GoTo Beg
Ers: MsgBox ("Invalid data!"): GoTo fin
Beg: On Error GoTo Ers
Let f(l) = l
Let S(l) = Reactions2.R1.Text
Let SS(l) = Reactions2.R2.Text
Let SSS(l) = Reactions2.R3.Text
Let SSSS(l) = Reactions2.R4.Text
Let U(l) = Val(Reactions2.T1.Value)
Let UU(l) = Val(Reactions2.T2.Value)
Let UUU(l) = Val(Reactions2.T3.Value)
Let UUUU(l) = Val(Reactions2.T4.Value)
Let Uh(l) = Val(Reactions2.TH.Value)
Let Ue(l) = Val(Reactions2.Te.Value)
H2O.Activate
equ2range.Range("A" + LTrim(Str(l))) = l
If U(l) <> 0 Then equ2range.Range("B" + LTrim(Str(l))) = U(l)
equ2range.Range("C" + LTrim(Str(l))) = S(l)
If S(l) <> "" And SS(l) <> "" Then equ2range.Range("D" + LTrim(Str(l))) = "+"
If UU(l) <> 0 Then equ2range.Range("E" + LTrim(Str(l))) = UU(l)
equ2range.Range("F" + LTrim(Str(l))) = SS(l)
If Uh(l) <> 0 Then
equ2range.Range("G" + LTrim(Str(l))) = "+"
equ2range.Range("H" + LTrim(Str(l))) = Uh(l)
End If
If Uh(l) <> 0 And Ue(l) <> 0 Then equ2range.Range("I" + LTrim(Str(l))) = "H+
+"
If Uh(l) <> 0 And Ue(l) = 0 Then equ2range.Range("I" + LTrim(Str(l))) = "H+"
If Uh(l) = 0 And Ue(l) <> 0 Then equ2range.Range("I" + LTrim(Str(l))) = "+"
If Ue(l) <> 0 Then equ2range.Range("J" + LTrim(Str(l))) = Ue(l)
equ2range.Range("K" + LTrim(Str(l))) = IIf(Ue(l) <> 0, "e-  =", "=")
If UUU(l) <> 0 Then equ2range.Range("L" + LTrim(Str(l))) = UUU(l)
equ2range.Range("M" + LTrim(Str(l))) = SSS(l)
If SSS(l) <> "" And SSSS(l) <> "" Then equ2range.Range("N" + LTrim(Str(l))) =
"+"
If UUUU(l) <> 0 Then equ2range.Range("O" + LTrim(Str(l))) = UUUU(l)
equ2range.Range("P" + LTrim(Str(l))) = SSSS(l)
For k = 1 To i - 1
```

```
If S(l) = b(k) Then equ2range.Range("C" + LTrim(Str(l + 100))) = c(k)
If SS(l) = b(k) Then equ2range.Range("F" + LTrim(Str(l + 100))) = c(k)
If SSS(l) = b(k) Then equ2range.Range("M" + LTrim(Str(l + 100))) = c(k)
If SSSS(l) = b(k) Then equ2range.Range("P" + LTrim(Str(l + 100))) = c(k)
Next k
Let resG2(l) = U(l) * equ2range.Range("C" + LTrim(Str(l + 100))) + UU(l) *
equ2range.Range("F" + LTrim(Str(l + 100))) - UUU(l) * equ2range.Range("M" +
LTrim(Str(l + 100))) - UUUU(l) * equ2range.Range("P" + LTrim(Str(l + 100)))
equ2range.Range("Q" + LTrim(Str(l))) = resG2(l)
If Ue(l) <> 0 Then
Let resF(l) = -resG2(l) / (Ue(l) * 96485)
Let resFF(l) = 0.0591 * Uh(l) / Ue(l)
equ2range.Range("R" + LTrim(Str(l))) = resF(l)
If resFF(l) <> 0 Then equ2range.Range("S" + LTrim(Str(l))) = resFF(l)
End If
If Ue(l) = 0 Then Let resPH(l) = -resG2(l) / (2.303 * 8.3144 * 298 * Uh(l)):
equ2range.Range("T" + LTrim(Str(l))) = resPH(l)
l = l + 1
fin:
End Sub
```

The software is registered in the *Federal Service of Intellectual Property of the Russian Federation* (in Russian: *Федеральная Служба по Интеллектуальной Собственности*), registration number 2015617603. The registration certificate is presented below.

РОССИЙСКАЯ ФЕДЕРАЦИЯ

СВИДЕТЕЛЬСТВО

о государственной регистрации программы для ЭВМ

№ 2015617603

EpHDiagramPlot

Правообладатель: ***Николайчук Павел Анатольевич (RU)***

Автор: ***Николайчук Павел Анатольевич (RU)***

Заявка № **2015614495**
Дата поступления **29 мая 2015 г.**
Дата государственной регистрации
в Реестре программ для ЭВМ ***15 июля 2015 г.***

Врио руководителя Федеральной службы
по интеллектуальной собственности

Л.Л. Кирий

B. List of attended scientific conferences

№	Conference Title		Status	Dates	Place	Participation form	Involved system
	Original	Translated					
1	XVII International Conference of Chemical Thermodynamics in Russia (RCCT-2009)		International	29 June – 3 July 2009	Kazan, Russia	Poster Report	Co – Si
2	Современные проблемы теоретической и экспериментальной химии: VII Всероссийская конференция молодых учёных с международным участием	Contemporary Problems of Theoretical and Experimental Chemistry: VII All-Russian Conference of Young Scientists with International Participation	National with International Participation	3 – 9 July 2010	Saratov, Russia	Vitrual participation	Cu – H_2O
3	Всероссийская конференция «Современные проблемы коррозионно-электрохимической науки»	All-Russian Conference “The Contemporary Problems of Corrosion and Electrochemical	National	18 – 22 October 2010	Moscow, Russia	4 Oral Reports	Ti – Si, Mo – Si, Ni – Si, Cu – H_2O

		Sciences”					
4	Всероссийская рабочая конференция «Бутлеровское наследие – 2011»	All-Russian Working Conference “Butlerov Heritage – 2011”	National	15 – 20 May 2011	Kazan, Russia	Plenary Report	All
5	Современные проблемы теоретической и экспериментальной химии: VIII Всероссийская конференция молодых учёных с международным участием	Contemporary Problems of Theoretical and Experimental Chemistry: VIII All-Russian Conference of Young Scientists with International Participation	National with International Participation	14 – 20 June 2011	Saratov, Russia	Vitrual participation	Zn – H_2O
6	XIX Mendeleyev Congress on General and Applied Chemistry		International	24 – 29 September 2011	Volgograd, Russia	Oral Report	Siliceous brasses
7	XVIII International Conference of Chemical Thermodynamics in Russia (RCCT-2011)		International	3 – 7 October 2011	Samara, Russia	1 Oral Report and 2 Poster Reports	Mn – Si, Sections 3.4 and 3.5

8	Всероссийская конференция «Химия твёрдого тела и функциональные материалы»	All-Russian Conference “Chemistry of the Solid State and Functional Materials – 2012”	National	6 – 10 February 2012	Yekaterinburg, Russia	Poster Report	Ni – Si
9	VI Всероссийская конференция молодых учёных, аспирантов и студентов с международным участием «Менделеев-2012»	VI All-Russian Conference of Young Scientists, Aspirants and Students with International Participation “Mendeleev-2012”	National with International Participation	3 – 7 April 2012	Saint-Petersburg, Russia	Oral Report	Me – H_2O
10	Свиридовские чтения 2012: Шестая Международная конференция по химии и химическому образованию	Sviridov Readings 2012: 6th International Conference on Chemistry and Chemical Education	International	9 – 13 April 2012	Minsk, Belarus	Oral Report	Siliceous bronzes

11	11th International Conference on Fundamental and Applied Aspects of Physical Chemistry		International	24 – 28 September 2012	Belgrade, Serbia	Oral Report	Fe – Si
12	VI Всероссийская конференция «Физико-химические процессы в конденсированных средах и на межфазных границах» (ФАГРАН – 2012)	VI All-Russian Conference “Physical and Chemical Processes in Condensed Media and on Phase Boundaries” (FAGRAN – 2012)	National	15 – 18 October 2012	Voronezh, Russia	Plenary Report	All
13	IV Всероссийский конкурс молодых учёных	IV All-Russian Competition of the Young Scientists	National	16 – 18 October 2012	Miass, Russia	Vitrual participation	All
14	VI Всероссийская конференция молодых учёных, аспирантов и студентов с международным участием по химии	VII All-Russian Conference of Young Scientists, Aspirants and Students with International	National with International Participation	2 – 6 April 2013	Saint-Petersburg, Russia	Poster Report	Si – H_2O

	и наноматериалам «Менделеев-2012»	Participation on Chemistry and Nano-Materials “Mendeleev-2013”|					
15	XIX International Conference of Chemical Thermodynamics in Russia (RCCT-2013)		International	24 – 28 June 2013	Moscow, Russia	Oral Report	Sc – Si
16	X Международное Курнаковское совещание по физико-химическому анализу	X International Kurnakov Meeting on Physical and Chemical Analysis	International	3 – 7 July 2013	Samara, Russia	Oral Report	Fe – Ge
17	Школа – конференция молодых учёных «Неорганические соединения и функциональные материалы»	School – Conference of the Young Scientists “Inorganic Compounds and Functional Materials”	National	30 September – 4 October 2013	Novosibirsk, Russia	Oral Report	Siliceous brasses and bronzes
18	Достижения молодых учёных: химические науки	The Achievements of the Young	National with International	24 – 27 May 2015	Ufa, Russia	Vitrual participation	Sc – H_2O

		Scientists: Chemical Sciences	Participation				
19	Фундаментальные и прикладные исследования в области химии и экологии: международная научно-практическая конференция студентов, аспирантов и молодых учёных	The fundamental and applied researches in the field of chemistry and ecology: The international scientific-practical conference of students, aspirants and young scientists	International	23 – 26 September 2015	Kursk, Russia	Vitrual participation	Fe – H_2O, Mn – H_2O
20	VII Всероссийская конференция «Физико-химические процессы в конденсированных средах и на межфазных	VII All-Russian Conference “Physical and Chemical Processes in Condensed Media and on Phase	National	10 – 13 November 2015	Voronezh, Russia	Oral Report	Section 3.8

	границах» (ФАГРАН – 2012)	Boundaries" (FAGRAN – 2012)					
21	XI Международное Курнаковское совещание по физико-химическому анализу в рамках XX Менделеевского съезда по общей и прикладной химии	XI International Kurnakov Meeting on Physical and Chemical Analysis within the framework of XX Mendeleev Congress on Pure and Applied Chemistry	International	27 – 30 June 2016	Voronezh, Russia	Vitrual participation	Mn – Ge

Lebenslauf

Letzte Ausgabe: 15. März 2018

Persönliche Daten

Name	Pawel Anatoljewitsch Nikolajtschuk
Staatgehörigkeit	Russe
Familienstand	ledig
Anschrift	Martenowskaja, 16 – 66, Tscheljabinsk 454025, Russische Föderation
Geburtsdatum	17. Oktober 1985
Geburtsort	Kurgan, Union der Sozialistischen Sowjetrepubliken
Sprachen	russisch (Muttersprache), englisch (B2), deutsch (B2)

Ausbildung

1991 – 2002 Gymnasium Nr. 27, Kurgan, Russische Föderation

2002 – 2007 Staatuniversität Tscheljabinsk, Tscheljabinsk, Russische Föderation
Abschlussgrad: Spezialist
Fachbereich: Chemie

2008 – 2011 Staatuniversität Tscheljabinsk, Tscheljabinsk, Russische Föderation
Abschlussgrad: Aspirant
Forschungsinteresse: Thermodynamik von Mehrkomponentensystemen

Berufslaufbahn

2007 – heute **Oberlaborant**
Lehrstuhl für analytische und physikalische Chemie, Fakultät für Chemie, Staatuniversität Tscheljabinsk

2008 – 2010, 2012 – 2013, 2015 – 2016 **Hochschullehrer**
Lehrstuhl für analytische und physikalische Chemie, Fakultät für Chemie, Staatuniversität Tscheljabinsk

Unterrichtete Fächer: Analytische Chemie, Physikalische Chemie, Chemische Methoden der Trennung und Konzentration, Thermodynamik von Lösungen und Verbindungen, Thermodynamik der chemischen und elektrochemischen Stabilität von Legierungen

2014 – 2015 **Gastwissenschaftler**
Institut für physikalische Chemie, Department für Chemie, Mathematisch-Naturwissenschaftliche Fakultät, Universität zu Köln

2016 – 2018 **Gastwissenschaftler**
Lehrstuhl für Thermodynamik und Energietechnik, Fakultät für Maschinenbau, Universität Paderborn

2018 **Wissenschaftliche Hilfskraft**
Lehrstuhl für Thermodynamik und Energietechnik, Fakultät für Maschinenbau, Universität Paderborn

Computerkenntnisse

Textverarbeitungssoftware	Microsoft Word, OpenOffice Writer, LibreOffice Writer
Wissenschaftliche Grafik-software	Microsoft Excel, Origin Pro, Igor Pro, DataScene, SigmaPlot, CorelDraw, Photoshop
Programmierung	VBA

Pawel Anatoljewitsch Nikolajtschuk
18. Mai 2018

Eigenständigkeitserklärung

Hiermit erkläre ich, dass diese Arbeit bisher von mir weder an der Mathematisch-Naturwissenschaftlichen Fakultät der Ernst-Moritz-Arndt-Universität Greifswald noch einer anderen wissenschaftlichen Einrichtung zum Zwecke der Promotion eingereicht wurde.

Ferner erkläre ich, dass ich diese Arbeit selbstständig verfasst und keine anderen als die darin angegebenen Hilfsmittel und Hilfen benutzt und keine Textabschnitte eines Dritten ohne Kennzeichnung übernommen habe.

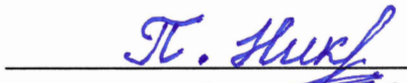

Pawel Anatoljewitsch Nikolajtschuk

Danksagung

Als erstes, möchte ich meinem wissenschaftlichen Betreuer Prof. Dr. Aleksandr Georgiewitsch Türin danken. Als er verstarb, war meine Dissertation noch weit von der Fertigstellung entfernt. Ich bedauere es sehr, dass er den Abschluss dieser Dissertation nicht mehr erleben kann. Ich widme diese Arbeit seinem Gedenken, vor allem auch, weil er es war, der mir den Weg in die Wissenschaft gebahnt hat.

Ich bin auch meinen Studenten sehr dankbar, die zu verschiedenen Zeiten meiner Karriere mit mir zusammengearbeitet haben und zu zu den Forschungsergebnissen beigetragen haben:

Tatjana Wladimirowna Stepanowa (Татьяна Владимировна Степанова), Absolventin der Staatsuniversität Tscheljabinsk 2009, hat geholfen, die Potenzial – pH-Diagramme für die Systeme Ni – H_2O und Ni – Si – H_2O zu plotten.

Tatjana Igorewna Schaljapina (Татьяна Игоревна Шаляпина), Absolventin der Staatsuniversität Tscheljabinsk 2010, hat geholfen, die Potenzial – pH-Diagramme für die Systeme Mn – H_2O und Mn – Si – H_2O zu plotten.

Tatjana Nikolaewna Aschtscheulowa (Татьяна Николаевна Ащеулова), Absolventin der Staatsuniversität Tscheljabinsk 2011, hat geholfen, die Potenzial – pH-Diagramme für die Systeme Fe – H_2O und Fe – Si – H_2O zu plotten.

Irina Igorewna Kanatjewa (Ирина Игоревна Канатьева), Absolventin der Staatsuniversität Tscheljabinsk 2012, hat zur Überarbeitung des Potenzial – pH-Diagramms des Systems Cu – H_2O beigetragen und auch das Diagramm des Systems Fe – Ge – H_2O geplottet.

Anastasija Sergeewna Kolpakowa (Анастасия Сергеевна Колпакова), Absolventin der Staatsuniversität Tscheljabinsk 2012, hat für mich die Informationen über die Übergangsmetalle und deren Verbindungen mit Silizium gesammelt und so zum ersten Kapitel dieser Arbeit beigetragen.

Zum Schluss möchte ich mich für die Unterstützung durch meine Eltern, Freunde und Kollegen bedanken, die immer an den Erfolg meiner Arbeit geglaubt haben, und mir nicht erlaubt haben aufzuhören.